INVESTIGATIONS OF THRESHOLD EFFECTS IN SOIL DEFORMATIONS

by

David Richardson

A thesis submitted for the degree of

Doctor of Philosophy

at the City University

Department of Civil Engineering

Geotechnical Engineering Research Centre

April 1988

....Fellwalking is a pastime for life.

But—and this is the reason for the appearance of this book—physical and other disabilities may develop in later years. Bodily ailments may occur in spite of healthy exercise: legs tend to become rickety and bones brittle; or a half-century of pipe smoking may play havoc with the wind; or a street accident may curtail freedom to walk and climb in comfort; or over-indulgence in sexual activities may have robbed the limbs of energy (perish the thought, but it had to be mentioned).

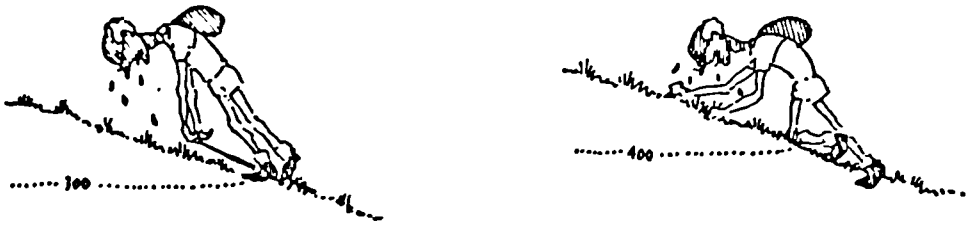

But remember..... you are not as young as you used to be.

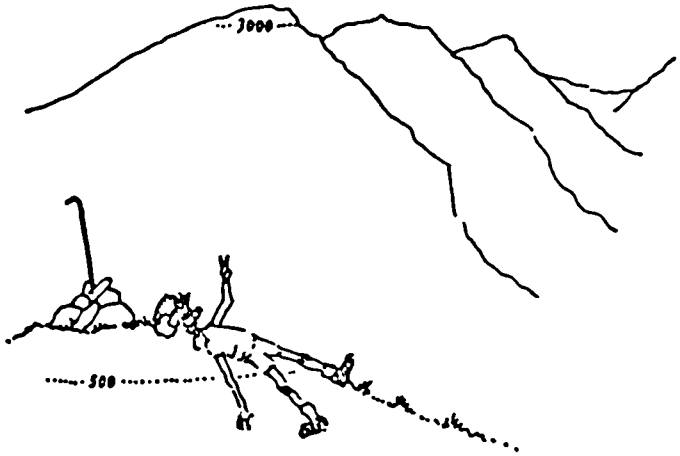

You might come across me on Orrest Head someday, gazing over the lake to the Langdales. Or, more likely, halfway up, resting and having a pipe....and wishing I was fifty years less old.

aw

November 1973

awainwright

Wainwright,A.(1973). The Outlying Fells. Westmorland Gazette.

CONTENTS.

		Page No.
Plates.		7
Tables.		7
Figures.		10
Acknowledgements.		30
Declaration.		31
Synopsis.		31
List of Symbols.		32
CHAPTER 1. Introduction.		39
1.1	Introduction to Soil Deformation.	40
1.2	Previous Research.	41
1.3	Objectives of Research.	42
1.4	Outline of Thesis.	42
CHAPTER 2. Review of Factors Affecting Soil Stiffness.		44
2.1	Introduction.	45
2.2	Methods of Determining Soil Deformations.	45
2.2.1	Classical Elastic Analyses.	45
2.2.2	Stress Path Methods.	46
2.2.3	Computer Methods.	48
2.2.4	Problems in Deformation Analyses.	50
2.3	Factors Affecting the Measured Soil Stiffness.	50
2.3.1	Sample Se ection	51
2.3.2	Sample Disturbance.	52
2.3.2.1	Stress Relief.	52
2.3.2.2	Mechanical Disturbance.	53
2.3.2.3	Temperature.	54
2.3.2.4	Discussion on the Effect of Disturbance.	55
2.3.3	Initial Consolidation History.	56
2.3.4	Current State of the Sample.	57
2.3.5	Stress Path Followed.	59
2.3.6	Temperature.	60
2.3.7	Rate of Test.	61
2.3.8	Apparatus Flexibility and System Errors.	62
2.3.8.1	Apparatus Flexibility.	63

2.3.8.2 Other System Errors. 65
2.3.8.3 Discussion. 67
2.3.9 Definition of Stiffness Moduli. 68
2.3.9.1 Choice of Secant or Tangent Stiffness Moduli. 69
2.3.9.2 Choice of Defining Moduli with respect to Stresses or Strains. 69
2.3.9.3 Selection of Normalising Parameters. 70
2.3.9.4 Discussion. 71
2.4 Threshold Effects. 72
2.4.1 Time Effects. 73
2.4.2 Stress Path Effects. 76
2.4.2.1 Introduction. 76
2.4.2.2 Previous Observations. 77
2.4.3 Effect of Sampling on Threshold Effects. 80
2.5 Comparison of Laboratory and Field Data. 81
2.5.1 Introduction. 81
2.5.2 Comparison of Data from In-Situ Tests. 82
2.5.3 Comparison of Data for London Clay. 83
2.5.4 Comparison of Data for Other Clays. 84
2.6 Discussion. 85

CHAPTER 3. Mathematical Models for Soils. 89

3.1 Introduction. 90
3.2 General Requirements of Soil Models. 90
3.3 Definition of Parameters. 91
3.4 The Elastic Model. 92
3.4.1 Properties of the Elastic Model. 94
3.4.2 Equations of Elastic Behaviour. 95
3.4.3 Limitations on Values of Elastic Parameters. 98
3.4.4 Discussion of the Elastic Model. 99
3.5 Critical State Soil Mechanics. 100
3.5.1 The State Boundary Surface. 100
3.5.2 Behaviour of Soil Below the State Boundary Surface. 103
3.5.3 Behaviour of Soil on the State Boundary Surface. 104
3.5.4 Failure. 108
3.5.5 Problems in Applying the Critical State Model. 109
3.6 Pender's Model. 111
3.6.1 Model for Overconsolidated Behaviour. 111
3.6.2 Model for Normally Consolidated Behaviour. 112
3.7 A Model Incorporating Kinematic Hardening. 113
3.7.1 Description of Model Behaviour. 113
3.7.2 Determination of Model Parameters. 113

3.7.3 Discussion. 114
3.8 Models for Threshold Effects. 115
3.8.1 Models for Time Effects. 115
3.8.2 Model L.C. 116
3.8.2.1 Elastic Strains (Threshold Range). 117
3.8.2.2 Intermediate Strains. 117
3.8.2.3 Plastic Strains. 118
3.8.2.4 Application of the Model. 118
3.8.3 Bi-Linear Threshold Models. 119
3.9 Discussion of Soil Models. 121

CHAPTER 4. Test Program. 124

4.1 Scope and Objectives. 125
4.2 General Test Requirements. 125
4.3 Tests for Range of Threshold Effects. 126
4.4 Tests to Assess the Effect of Changes in Direction of Effective Stress Paths. 127
4.5 Tests for Path Dependence. 127
4.6 Tests to Study the Effect of Varying the Total Stress Approach Paths. 128
4.7 Tests to Failure. 128
4.8 Variation of Test Procedures. 129

CHAPTER 5. The Triaxial Stress Path Apparatus. 130

5.1 Introduction. 131
5.2 Power Supply to System Components. 131
5.3 Pressure Supply. 132
5.4 System Components. 132
5.4.1 The Triaxial Cell. 133
5.4.2 Instrumentation. 133
5.4.3 Pressure Control. 134
5.4.4 Axial Strain Control. 135
5.4.5 Spectra and Epson Hardware. 135
5.4.6 Functions of the Spectra System. 136
5.4.7 Functions of the Epson System. 138
5.4.8 Spectra Software. 138
5.4.8.1 The Main Loop. 139
5.4.8.2 Time Dependent Operations. 139
5.4.8.3 The Option List. 139
5.4.8.4 Calculation of Stresses and Strains. 140
5.4.8.5 Computation of Required State. 142
5.4.9 Epson Software. 142

5.4.9.1 Epson "Link" Program. 142
5.4.9.2 Analysis of Data. 143
5.5 Discussion of the Design and Performance of the Spectra-Epson System. 144

CHAPTER 6. Calibration of Apparatus and Routine Testing of Equipment. 146

6.1 Introduction. 147
6.2 Calibration Procedures. 148
6.2.1 The Load Cell. 148
6.2.2 Cell and Pore Pressure Transducers. 148
6.2.3 Axial Displacement Transducers. 148
6.2.4 Volume Gauge. 149
6.3 Selection of Calibration Constants. 149
6.4 Hysteresis of the Instrumentation. 150
6.5 Drift and Noise of Instrumentation. 150
6.6 Compliance of System. 151
6.6.1 The Pore Pressure and Volume Gauge. 151
6.6.2 The Axial Displacement. 152
6.6.3 Discussion of the Apparatus Compliance. 153
6.7 System Testing. 154
6.8 Discussion. 154

CHAPTER 7. Experimental Details. 157

7.1 Introduction. 158
7.2 Requirements of Soils for Testing. 158
7.3 Details of Soils for Testing. 158
7.4 Compression and Swelling Properties of Soils. 159
7.5 Sample Preparation. 160
7.5.1 Soil Preparation. 160
7.5.2 Water Absorption by Dry Soil. 160
7.5.3 Preparation of the Soil Slurry. 161
7.5.4 Description of Sample Presses. 161
7.5.5 Setting up of Mix in Presses. 161
7.5.6 Loading of Slurry. 162
7.5.7 General Comments on Samples from Presses. 162
7.5.8 Alternative Method of Sample Preparation. 163
7.5.9 Comments on Samples Produced by Alternative Method. 163
7.6 Setting up of a Test. 164
7.6.1 Introduction. 164
7.6.2 Preparations for a Test. 165
7.6.3 Measurement of Initial Sample Dimensions. 165

7.6.4 Sample Mounting. 165
7.6.5 Initial Test Stages. 166
7.6.5.1 Method A 166
7.6.5.2 Saturation Test. 166
7.6.5.3 Connection of Top Cap to Load Cell. 167
7.6.5.4 Method B. 167
7.6.5.5 Method C. 168
7.7 Conducting a Test. 168
7.7.1 Rates of Test. 169
7.7.2 Selection of Control Limits. 170
7.7.3 Compression and Swelling Stages. 170
7.7.4 Definition of End of a Test Stage. 171
7.7.5 Intermediate Test Stages. 171
7.7.6 Tests to Examine Changes in Direction of Total Stress Paths. 172
7.7.7 Test Stages to Failure. 173
7.8 After Final Tests Stage. 173

CHAPTER 8. Calculations and Results. 174

8.1 Introduction. 175
8.2 Corrections to Tests Data. 175
8.2.1 Load Cell Compliance. 175
8.2.2 Volume Gauge Compliance. 176
8.2.3 Corrections for the Stiffness of Membrane and Side Drains. 176
8.2.4 Volume Changes of Filter Papers. 178
8.3 Calculation of Strains. 178
8.4 Calculation of Stresses. 178
8.5 Calculation of Specific Volume. 179
8.6 Calculation of Stiffness. 180
8.7 Results. 180
8.7.1 Compression and Swelling Stages. 181
8.7.2 Effect of Changes in Direction of Stress Path. 181
8.7.3 Tests for the Range of Threshold Effects. 181
8.7.4 Tests for Path Dependence. 181
8.7.5 Tests to Failure. 181
8.7.6 Special Tests. 182

CHAPTER 9. Discussion of Experimental Results. 183

9.1 Introduction. 184
9.2 Specific Volume of Samples and Leakage. 184
9.3 Compression and Swelling Stages. 184

9.3.1 Results Plotted as specific volume against Log_e p'. 184
9.3.2 Strain Paths. 185
9.3.3 Stress Paths. 186
9.3.4 Accuracy of control. 187
9.4 Effect of a Change in Direction of Effective Stress Path. 188
9.4.1 Main Test Series. 189
9.4.1.1 Stiffness of Samples. 189
9.4.1.2 The Strain Increment Ratio. 190
9.4.1.3 The Stress Path Threshold Effect on Different Stress Paths. 191
9.4.2 The Effect of Initial Stress History. 192
9.4.3 The Effect of Overconsolidation Ratio. 193
9.5 Tests for the Range of Stress Path Effects. 194
9.6 Effect of Rest Periods. 196
9.7 Effect of a Change in Direction of Total Stress Path. 197
9.8 Path Dependence. 197
9.8.1 Type 1 tests. 198
9.8.2 Type 2 tests. 200
9.8.3 Type 3 tests. 201
9.8.4 Discussion of Path Dependence Tests. 204
9.9 Tests to Failure. 204
9.9.1 Threshold Tests to Failure. 205
9.9.1.1 Tests on Various Soils. 205
9.9.1.2 Special London Clay Tests. 206
9.9.2 Tests to Establish the State Boundary Surface for London Clay. 209
9.10 Normalising of Test Results. 212
9.10.1 The Normalising of Stiffness Data. 212
9.10.2 The Normalising of Stress-Strain Curves. 212
9.10.3 The Normalising of Stress Paths. 213
9.11 Comparison of Material Parameters. 214
9.12 Errors in Test Results. 216
9.13 Mathematical Modelling of the Tests Results. 217
9.13.1 Principle Features of Threshold Tests. 217
9.13.2 Path Dependence Tests. 218
9.13.3 A Simple Model for Stress Path Threshold Effects. 218
9.13.4 A Model Including the Effects on Strain Increment Directions. 220
9.14 Discussion. 220

CHAPTER 10. Conclusions and Recommendations for Further Research. 223

10.1 Introduction. 224
10.2 The Critical State Model. 224
10.2.1 Compression and Swelling Data. 224

10.2.2 Stress-Strain Curves and Failure. 225
10.2.3 Uniqueness of the State Boundary Surface. 225
10.3 Threshold Test Data. 225
10.3.1 Stress Path Effects. 225
10.3.2 Time Effects. 226
10.3.3 Tests to Failure. 226
10.4 Tests for Path Dependence. 226
10.5 Evidence of Plastic Behaviour below the State Boundary Surface. 227
10.6 Evidence of Total Stress Path on Stress Path Threshold Effects. 227
10.7 Recommendations for Laboratory Testing of Soils. 227
10.8 Recommendations for Further Research. 228

APPENDIX 1. Rate of Loading in Triaxial Tests. 230

A.1.1 Introduction. 231
A.1.2 Basic Theoretical Considerations. 231
A.1.3 Bishop and Henkel (1962) Calculations. 234
A.1.4 Atkinson (1984b) Calculations. 235
A.1.5 Discussion. 236

APPENDIX 2. Effect of Errors in Water Content on Compression and Swelling Parameters. 240

A.2.1 Introduction. 241
A.2.2 Factors Affecting Errors in the Measurement of Compression and Swelling Parameters. 241
A.2.2.1 Water Content of Slurry. 241
A.2.2.2 Initial Sample Water Content. 241
A.2.2.3 Measurement of Volume Strain During a Test. 242
A.2.2.4 Measurement of Stresses During A Test. 244
A.2.2.5 Measurement of Final Water Content and Calculation of Specific Volume. 246
A.2.3 Typical Test Data. 246
A.2.4 Discussion. 247

References. 248
Plates. 271
Tables. 274
Figures. 302

PLATES.

Plate 5.1 General view of the Bishop and Wesley triaxial cell.

Plate 5.2 The Spectra-Epson system.

Plate 7.1 Sample set up in the Bishop and Wesley triaxial cell.

TABLES.

Table 2.1 Effect of disturbance on sample stiffness (Hight, Gens and Jardine, 1985).

Table 2.2 Summary of stiffness parameters for reconstituted London Clay (Richardson 1984a).

Table 2.3 Summary of tests by Jardine et al (1984).

Table 4.1 Abbreviations of test types.

Table 5.1 Summary of the resolution of instrumentation in the Bishop and Wesley triaxial cell.

Table 6.1 Results from a typical instrument calibration check.

Table 6.2 Summary of the accuracy of instrumentation in the Bishop and Wesley triaxial cell.

Table 7.1 Summary of soil index properties.

Table 7.2 Summary of compression and swelling parameters for soils under test.

Table 7.3 Target slurry water content and mix quantities.

Table 7.4 Water content, mass and dimensions of samples produced from slurry.

Table 7.5 Water content, mass and dimensions of remoulded samples.

Table 7.6a General test data for samples tested by Method A.

Table 7.6b General test data for samples tested by Method B.

Table 7.6c General test data for samples tested by Method C.

Table 7.7 Summary of rates of testing used and excess pore pressures observed.

Table 7.8 Summary of tests conducted.

Table 8.1 System Compliance Data.

Table 8.2 Specific volumes, at the start and finish of tests, and calculated from the normal compression line.

Table 9.1 Critical State Soil Parameters for all Soils.

Table 9.2 Values of swelling parameters κ_0, κ_1, $\Delta p'/p'_0$ and p'_0.

Table 9.3 The effect of periods of rest on the stiffness of London clay samples.

Table 9.4 Summary of failure states in threshold tests for all isotropically compressed soils.

Table 9.5 Summary of failure states in threshold tests for London Clay compressed with anisotropic stress histories.

Table 9.6 Summary of failure states in tests to establish the state boundary surface for London Clay.

Table 9.7 Values of the total strain increment ratio predicted from the state boundary surface and that observed during anisotropic compression for London Clay.

Table A.1.1 Drainage Parameters for various drainage conditions (Bishop and Henkel, 1962).

Table A.1.2 Effect of filter paper efficiency on drainage times (Bishop and Henkel, 1962).

Table A.1.3 Effect of filter paper permeability on the efficiency of side drains for soils under test.

FIGURES.

Fig 2.1 Effect of mechanical disturbance on Weald Clay (Skempton and Sowa, 1963).

Fig 2.2 Effect of disturbance on normally consolidated Lower Cromer till (Hight, Gens and Jardine, 1985).

Fig 2.3 Effect of disturbance on over-consolidated Lower Cromer till (Hight, Gens and Jardine, 1985).

Fig 2.4 Variation of normalised stiffness for drained and undrained tests on Lower Cromer till (Gens, 1982).

Fig 2.5 Stress-strain curves for isotropically and anisotropically compressed samples of undisturbed London Clay (Costa-Filho, 1979).

Fig 2.6 Variation of sample stiffness with state (Wroth, 1971).

Fig 2.7 Plot of τ against axial strain for undrained tests on isotropically compressed samples of Lower Cromer till at large strains (Gens, 1982).

Fig 2.8 Plot of τ against axial strain for undrained tests on isotropically compressed samples of Lower Cromer till at small strains (Gens, 1982).

Fig 2.9 Plot of τ against axial strain for undrained extension tests on isotropically compressed samples of Lower Cromer till at large strains (Gens, 1982).

Fig 2.10 Plot of τ against axial strain for undrained extension tests on isotropically compressed samples of Lower Cromer till at small strains (Gens, 1982).

Fig 2.11 Plot of t against axial strain for undrained compression tests on anisotropically (K_o) compressed samples of Lower Cromer till at large strains (Gens, 1982).

Fig 2.12 Plot of t against axial strain for undrained compression tests on anisotropically (K_o) compressed samples of Lower Cromer till at small strains (Gens, 1982).

Fig 2.13 Plot of t against axial strain for undrained extension tests on anisotropically (K_o) compressed samples of Lower Cromer till at large strains (Gens, 1982).

Fig 2.14 Plot of t against axial strain for undrained extension tests on anisotropically (K_o) compressed samples of Lower Cromer till at small strains (Gens, 1982).

Fig 2.15 Plot of t and ε_v against axial strain for drained compression tests on isotropically compressed samples of Lower Cromer till (Gens, 1982).

Fig 2.16 Plots of t and ε_v against axial strain for drained compression tests on anisotropically (K_o) compressed samples of Lower Cromer till at large strains (Gens, 1982).

Fig 2.17 Plots of t and ε_v against axial strain for drained compression tests on anisotropically (K_o) compressed samples of Lower Cromer till at small strains (Gens, 1982).

Fig 2.18 Total stress paths followed by London Clay samples (Richardson, 1984a).

Fig 2.19 Step loading and smooth loading paths.

Fig 2.20 Effect of temperature on the voids ratio against $\log_e p'$ plot for saturated Illite (Plum and Esrig, 1969).

Fig 2.21 Effect of rate of loading on the radial variation of water content in triaxial samples (Atkinson, Evans and Ho, 1984).

Fig 2.22 Definition of random (Δ P) and systematic (Δ A) errors.

Fig 2.23 Stiffnesses and Compliances.

Fig 2.24 Tangent Stiffness Moduli.
a) Defined at the origin.
b) Defined at a stress level.
c) Defined at a strain level.
d) Effect of bedding errors on tangent moduli.

Fig 2.25 Secant Stiffness Moduli.
a) Defined at the origin over a stress interval.
b) Defined at the origin over a strain interval.
c) Defined at a stress level over a stress interval.
d) Defined at a strain level over a strain interval.
e) Effect of bedding errors on secant moduli.

Fig 2.26 Values of secant E_u/c_u derived from model L.C. at various shear strain levels (Simpson et al, 1980).

Fig 2.27 Results of tests by Jardine, Symes and Burland (1984).

Fig 2.28 Results of tests by Jardine, Symes and Burland (1984).

Fig 2.29 Results of tests by Jardine, Symes and Burland (1984).

Fig 2.30 Collected normalised secant stiffness moduli for various soils (Jardine, Symes and Burland,1984).

Fig 2.31 Collected normalised secant stiffness moduli (Jardine, Symes and Burland,1984).
a) Normalised with respect to c_u.
b) Normalised with respect to p'_o.

Fig 2.32 Effect on sample stiffness of a cycle of temperature change. (Plum and Esrig, 1969).

Fig 2.33 Results of oedometer tests on undisturbed London Clay with a rest period of 93 days (Som,1968).

Fig 2.34 Results of œdometer tests on undisturbed London Clay with a rest period of 7 days (Som, 1968).

Fig 2.35 Results of œdometer tests on undisturbed London Clay with a rest period of 93 days (Som, 1968).

Fig 2.36 Results of œdometer tests on undisturbed London Clay with no rest period (Som, 1968).

Fig 2.37 Effect of a period of rest on the voids ratio against $\log_{10} \sigma'_v$ plot for Drammen clay (Bjerrum, 1967).

Fig 2.38 a) Effect of adding sodium chloride to Drammen clay on the voids ratio against $\log_{10} \sigma'_v$ plot (Bjerrum,1967).
b) Effect of cementation of soil grains (Bjerrum, 1967).

Fig 2.39 Stress ratio and volumetric strain plotted against axial strain for Ham River Sand (Daramola, 1979).

Fig 2.40 Stiffness moduli for Ham River Sand (Daramola, 1979).
a) Tangent moduli.
b) Secant moduli.

Fig 2.41 Types of stress probe tests.
a) Same initial stress history, different final paths.
b) Different initial stress history, same final paths.
c) Same initial stress history, different recent stress history, same final paths.

Fig 2.42 Effect of varying size of stress probe on Slate dust (Lewin, 1970).

Fig 2.43 Plot of λ / κ against overconsolidation ratio for Ware till (Little, 1985).

Fig 2.44 Small strain stiff zones in Lower Cromer till (Hight et al, 1985).

Fig 2.45 Plots of q' against ε_s and ε_v against ε_s for reconstituted speswhite kaolin, positive values of θ (Tests by Atkinson, 1983a).

Fig 2.46 Plots of q' against ε_s and ε_v against ε_s for reconstituted speswhite kaolin, negative values of θ (Tests by Atkinson, 1983a).

Fig 2.47 Plots of shear and bulk moduli against θ for reconstituted speswhite kaolin (Tests by Atkinson, 1983a).

Fig 2.48 Laboratory and field secant stiffness moduli for London Clay (St.John, 1975).

Fig 2.49 Results of a typical plate bearing test conducted by Marsland (1971a) (Simpson et al, 1979).

Fig 2.50 Distribution of shear strain behind a retaining wall (Simpson et al, 1979).

Fig 2.51 Results of unconsolidated undrained tests on undisturbed London Clay from an initial isotropic stress state (Costa-Filho, 1978a).

Fig 2.52 Results of consolidated anisotropically undrained tests on undisturbed London Clay (Costa-Filho, 1978a).

Fig 2.53 Laboratory and field stiffness moduli for London Clay including stiffness data from Figs 2.51 and 2.52 (Simpson et at, 1979).

Fig 2.54 Laboratory and field stiffness moduli for London Clay (Jardine et al, 1985).

Fig 3.1 Limits on the admissible values of elastic parameters (Pickering, 1970).

Fig 3.2 Three dimensional view of a state boundary surface for an isotropically compressed soil (Atkinson and Bransby, 1978).

Fig 3.3 The state boundary surface (Atkinson and Bransby, 1978).
a) ln q', p' space.
b) ln v , lnp' space.

Fig 3.4 Definitions of critical state model constants.
a) ln q', p' space.
b) ln v , lnp' space.

Fig 3.5 A state boundary surface for a soil anisotropically consolidated with a stress ratio of η'_o.

Fig 3.6 a) Rotational hardening of the state boundary surface.
b) Kinematic hardening of the state boundary surface.

Fig 3.7 Drained failure of soil samples.
a) Normally consolidated.
b) Overconsolidated.

Fig 3.8 Variation of stiffness moduli (Houlsby, 1981).
a) Shear modulus, $G' \alpha p'$.
b) Shear modulus, $G' \alpha p'_c$.

Fig 3.9 a) Yield locus in Pender's model (Pender, 1978).
b) Anisotropic yield locus in Pender's model (Pender, 1977).
c) Changing shape of yield locus with loading (Pender, 1977).

Fig 3.10 A model incorporating kinematic hardening (Mroz et al, 1979).
a) Position of K.Y.S. while state is on the consolidation surface at A.
b) State at P_1 moving off the consolidation surface into the K.Y.S.
c) Initial movement of the K.Y.S. (State point P_2).
d) Effect of change in direction of loading (to P_3) below the consolidation surface.
e) Definition of size of the kinematic yield surface.

Fig 3.11 Effect of time on the position of the consolidation surface.
a) Effect on the q', p' plot.
b) Effect on v, p' plot.

Fig 3.12 The use of the kinematic yield surface in model L.C. (Simpson et al, 1979).

Fig 3.13 Bi-linear elastic models (Leach, 1984).
a) Bi-linear elastic perfectly plastic model.
b) Modified Cam Clay including a threshold range.

Fig 3.14 Data for the threshold range in London Clay (Leach, 1986).

Fig 4.1 Test paths to assess the effect of changes in direction of effective stress path.

Fig 4.2 Test paths to assess the effect of changes in direction of total stress path.

Fig 5.1 General arrangement of the Bishop and Wesley Spectra / Epson control system.

Fig 5.2 Diagrammatic view of sample and instrumentation in the Bishop and Wesley cell.

Fig 5.3 Axial strain control system.

Fig 5.4 Spctra control program main loop.

Fig 5.5 The Spctra option list.

Fig 5.6 Specimen Spctra data sheet.

Fig 5.7 Specimen Spctra transducer calibration data sheet.

Fig 6.1 Typical load cell calibration.
a) At low stress levels.
b) At high stress levels.

Fig 6.2 Typical calibration curve for the cell pressure transducer.

Fig 6.3 Typical calibration curve for the pore pressure transducer.

Fig 6.4 Typical calibration curve for the axial strain transducer.

Fig 6.5 Typical calibration curve for the volume gauge.

Fig 6.6 Exaggerated diagram of calibration errors.

Fig 6.7 Calibration of the volume gauge expansion.

Fig 6.8 Calibration of the load cell compressibility, cell 5.

Fig 6.9 Calibration of the load cell compressibility, cell 6.

Fig 6.10 Precision of control in the Spectra system.

Fig 7.1 Plot of volumetric strain against square root of time.
a) Unsuitable soil for testing.
b) Suitable soil for testing.

Fig 7.2 Diagram of sample presses.

Fig 7.3 Initial water content profile in London Clay samples.

Fig 7.4 Initial water content profile in Ware till samples.

Fig 7.5 Initial water content profile in Cowden till samples.

Fig 7.6 Initial water content profile in Speswhite kaolin samples.

Fig 7.7 Initial water content profile in Slate dust samples.

Fig 7.8 Diagrammatic view of sample set up in the triaxial cell.

Fig 7.9 ε_v against $\sqrt{t}$ for London Clay, initial compression by Method A.

Fig 7.10 ε_v against $\sqrt{t}$ for Ware till, initial compression by Method A.

Fig 7.11 ε_v against $\sqrt{t}$ for Speswhite kaolin, initial compression by Method A.

Fig 7.12 ε_v against $\sqrt{t}$ for Cowden till, initial compression by Method A.

Fig 7.13 ε_v against $\sqrt{t}$ for Slate dust, initial compression by Method A.

Fig 7.14 Final water content profile at the end of tests on London Clay samples.

Fig 7.15 Final water content profile at the end of tests on Ware till samples.

Fig 7.16 Final water content profile at the end of tests on Cowden till samples.

Fig 7.17 Final water content profile at the end of tests on Speswhite kaolin samples.

Fig 7.18 Final water content profile at the end of tests on Slate dust samples.

Fig 8.1 Selection of stiffness definition.

Fig 8.2 Plot of specific volume, v, against $\log_e p'$. Speswhite kaolin, isotropic compression and swelling.

Fig 8.3 Plot of specific volume, v, against $\log_e p'$. Ware till, isotropic compression and swelling.

Fig 8.4 Plot of specific volume, v, against $\log_e p'$. Cowden till, isotropic compression and swelling.

Fig 8.5 Plot of specific volume, v, against $\log_e p'$. Slate dust, isotropic compression and swelling.

Fig 8.6a Plot of specific volume, v, against $\log_e p'$. London Clay. Isotropic compression and swelling.

Fig 8.6b Plot of specific volume, v, against $\log_e$ p'. London Clay. Isotropic compression and swelling.

Fig 8.6c Plot of specific volume, v, against $\log_e$ p'. London Clay. Isotropic compression and swelling.

Fig 8.7 Plot of shear strain, ε_s , against volumetric strain, ε_v .Speswhite kaolin. Isotropic compression and swelling.

Fig 8.8 Plot of shear strain, ε_s , against volumetric strain, ε_v .Ware till. Isotropic compression and swelling.

Fig 8.9 Plot of shear strain, ε_s , against volumetric strain, ε_v. Cowden till. Isotropic compression and swelling.

Fig 8.10 Plot of shear strain, ε_s, against volumetric strain, ε_v . Slate dust. Isotropic compression and swelling.

Fig 8.11a Plot of shear strain, ε_s , against volumetric strain, ε_v . London Clay , isotropic compression and swelling.

Fig 8.11b Plot of shear strain, ε_s , against volumetric strain, ε_v. London Clay. Isotropic compression and swelling.

Fig 8.12 Plot of specific volume, v , against $\log_e$ p'. All stress histories (excluding isotropic) London Clay.

Fig 8.13 Plot of shear strain, ε_s , against volumetric strain, ε_v . London Clay compression and swelling , $\eta'_o = 0.25$.

Fig 8.14 Plot of shear strain, ε_s , against volumetric strain, ε_v . London Clay one-dimensional compression and swelling.

Fig 8.15 Plot of shear strain, ε_s , against volumetric strain, ε_v . London Clay. Compression and swelling ,$\eta'_o = 0.75$.

Fig 8.16 Plot of shear strain , ε_s, against volumetric strain, ε_v . London Clay .Two - dimensional compression and swelling.

Fig 8.17 Stress paths,q' against p', for one-dimensionally compressed London Clay.

Fig 8.18 Stress paths, q' against p', for London clay. $\eta'_o = 0.25$ and 0.75 . Compression and swelling.

Fig 8.19 Stress paths , q' against p', for two dimensionally compressed London clay.

Fig 8.20 Plots of q' against ε_s and ε_v against ε_s .Speswhite kaolin, isotropically compressed, OCR = 2, p' = 200kPa, constant p' path.

Fig 8.21a Plots of q' against ε_s and ε_v against ε_s . Positive deviations of stress path Ware till, isotropically compressed, OCR = 2, p' = 200kPa, constant p' path.

Fig 8.21b Plots of q' against ε_s and ε_v against ε_s . Negative deviations of stress path Ware till, isotropically compressed, OCR = 2, p' = 200kPa, constant p' path.

Fig 8.22 Plots of q' against ε_s and ε_v against ε_s .Cowden till, isotropically compressed,

Fig 8.23 Plots of q' against ε_s and ε_v against ε_s. Slate dust, isotropically compressed, OCR = 2, p' = 200kPa, constant p' path.

Fig 8.24a Plots of q' against ε_s and ε_v against ε_s. Positive deviations of stress path London clay isotropically compressed, OCR = 2, p' = 200kPa, constant p' path

Fig 8.24b Plots of q' against ε_s and ε_v against ε_s. Negative deviations of stress path London clay, isotropically compressed, OCR = 2, p' = 200kPa, constant p' path.

Fig 8.25 Plots of q' against ε_s and ε_v against ε_s. London clay, isotropically compressed, OCR = 1.5, p' = 267kPa, constant p' path.

Fig 8.26 Plots of q' against ε_s and ε_v against ε_s. London clay, isotropically compressed, OCR = 4.0, p' = 100kPa, constant p' path.

Fig 8.27 Plots of q' against ε_s and ε_v against ε_s. London clay, isotropically compressed, OCR = 8.0, p' = 50kPa, constant p' path.

Fig 8.28 Plots of q' against ε_s and ε_v against ε_s. London clay, compressed with $\eta'_o = 0.25$, OCR = 2.0, p' = 200kPa, q'_o = 5kPa, constant p' path.

Fig 8.29 Plots of q' against ε_s and ε_v against ε_s. London clay, compressed with $\eta'_o = 0.75$, OCR = 2.0, p' = 200kPa, q'_o = 7kPa, constant p' path.

Fig 8.30 Plots of q' against ε_s and ε_v against ε_s. London clay, one dimensionally compressed, OCR = 2.0, p' = 200kPa, q'_o = -12kPa, constant p' path.

Fig 8.31 Plots of q' against ε_s and ε_v against ε_s. London clay, one dimensionally compressed, OCR = 1.5, p' = 267kPa, q'_o = 85kPa, constant p' path.

Fig 8.32 Plots of q' against ε_s and ε_v against ε_s. London clay, one dimensionally compressed, OCR = 2.0, p' = 200kPa, q'_o = 36kPa, constant p' path.

Fig 8.33 Plots of q' against ε_s and ε_v against ε_s. London clay, one dimensionally compressed, OCR = 4.0, p' = 100kPa, q'_o = -5kPa, constant p' path.

Fig 8.34 Plots of q' against ε_s and ε_v against ε_s. London clay, one dimensionally compressed, OCR = 8.0, p' = 50kPa, q'_o = -24kPa, constant p' path.

Fig 8.35 Plots of q' / p' against ε_s for London clay at various overconsolidation ratios. constant p' paths.
a) Isotropically compressed.
b) one dimensionally compressed.

Fig 8.36 Plots of q' against p' and ε_s against ε_v. Isotropically compressed Ware till,various stress paths.

Fig 8.37 Plots of q' against ε_s and p' against ε_s. Isotropically compressed Ware till, various paths.

Fig 8.38 Plots of q' against p' and ε_s against ε_v. Isotropically compressed London clay, various stress paths.

Fig 8.39 Plot of p' against ε_v. Isotropically compressed London clay, various paths.

Fig 8.40 Plots of q' against p' and ε_s against ε_v . Isotropically compressed London clay various stress paths. OCR = 2.0 , p' = 200kPa.

Fig 8.41 Plots of q' against ε_s and p' against ε_s . Isotropically compressed London clay, various stress paths. OCR = 2.0 ,p' =200kPa.

Fig 8.42 Plots of q' against ε_s and p' against ε_s . Isotropically compressed London clay. OCR = 2.0 ,p' =200kPa, constant p' paths. Various approach path lengths.

Fig 8.43 Plot of q' against p'. Stress paths followed during path dependence type one tests. $\eta'_o = 0$, OCR = 2.0. All data Figs 8.44 - 8.53.

Fig 8.44 Plot of strain paths, ε_s against ε_v for type one path dependence tests on speswhite kaolin.

Fig 8.45 Plot of strain paths, ε_s against ε_v for type one path dependence tests on Ware till.

Fig 8.46 Plot of strain paths, ε_s against ε_v for type one path dependence tests on Cowden till.

Fig 8.47 Plot of strain paths, ε_s against ε_v for type one path dependence tests on slate dust.

Fig 8.48 Plot of strain paths, ε_s against ε_v for type one path dependence tests on London clay.

Fig 8.49 Plots of q' against ε_s and p' against ε_v for type one path dependence tests on speswhite kaolin.

Fig 8.50 Plots of q' against ε_s and p' against ε_v for type one path dependence tests on Ware till.

Fig 8.51 Plots of q' against ε_s and p' against ε_v for type one path dependence tests on Cowden till.

Fig 8.52 Plots of q' against ε_s and p' against ε_v for type one path dependence tests on slate dust.

Fig 8.53 Plots of q' against ε_s and p' against ε_v for type one path dependence tests on London clay.

Fig 8.54 Plot of q' against p'. Stress paths followed during path dependence type one tests. $\eta'_o = 0$, various OCR's, London clay. All data Figs 8.55 - 8.60.

Fig 8.55 Plot of strain paths, ε_s against ε_v for type one path dependence tests on London clay, OCR = 1.5.

Fig 8.56 Plot of strain paths, ε_s against ε_v for type one path dependence tests on London clay, OCR = 4.0.

Fig 8.57 Plot of strain paths, ε_s against ε_v for type one path dependence tests on London clay, OCR = 8.

Fig 8.58 Plots of q' against ε_s and p' against ε_v for type one path dependence tests on London clay, OCR = 1.5.

Fig 8.59 Plots of q' against ε_s and p' against ε_v for type one path dependence tests on London clay, OCR = 4.0.

Fig 8.60 Plots of q' against ε_s and p' against ε_v for type one path dependence tests on London clay, OCR = 8.0.

Fig 8.61 Plot of q' against p'. Stress paths followed during type one path dependence tests. Various stress histories, OCR = 2.0, p' = 200kPa. London clay . All data Figs 8.62 - 8.67.

Fig 8.62 Plot of strain paths, ε_s against ε_v for type one path dependence tests on London clay, $\eta'_o = 0.25$.

Fig 8.63 Plot of strain paths, ε_s against ε_v for type one path dependence tests on London clay, $\eta'_o = 0.75$.

Fig 8.64 Plot of strain paths, ε_s against ε_v for type one path dependence tests on London clay, two dimensionally compressed.

Fig 8.65 Plot of q' against ε_s for type one path dependence tests on London clay, $\eta'_o = 0.25$.

Fig 8.66 Plot of q' against ε_s for type one path dependence tests on London clay, $\eta'_o = 0.75$.

Fig 8.67 Plot of q' against ε_s for type one path dependence tests on London clay, two dimensionally compressed .

Fig 8.68 Plot of q' against p'. Stress paths followed during type one path dependence tests on one dimensionally compressed London clay, various OCR's. All data Figs 8.69 - 8.76.

Fig 8.69 Plot of strain paths, ε_s against ε_v for type one path dependence tests on one dimensionally compressed London clay, OCR = 1.5.

Fig 8.70 Plot of strain paths, ε_s against ε_v for type one path dependence tests on one dimensionally compressed London clay, OCR = 2.0.

Fig 8.71 Plot of strain paths, ε_s against ε_v for type one path dependence tests on one dimensionally compressed London clay, OCR = 4.0.

Fig 8.72 Plot of strain paths, ε_s against ε_v for type one path dependence tests on one dimensionally compressed London clay, OCR = 8.0.

Fig 8.73 Plot of q' against ε_s for type one path dependence tests on one dimensionally compressed London clay, OCR = 1.5.

Fig 8.74 Plot of q' against ε_s for type one path dependence tests on one dimensionally compressed London clay, OCR = 2.0.

Fig 8.75 Plot of q' against ε_s for type one path dependence tests on one dimensionally compressed London clay, OCR = 4.0.

Fig 8.76 Plot of q' against ε_s for type one path dependence tests on one dimensionally compressed London clay, OCR = 8.0.

Fig 8.77 Plot of q' against p'. Stress paths followed during type one path dependence tests on London clay, $\eta'_o = 0$, OCR = 2.0, various p'. All data Figs 8.78 - 8.81.

Fig 8.78 Plot of strain paths, ε_s against ε_v for type one path dependence tests on London clay, OCR = 2.0, p' = 100 kPa.

Fig 8.79 Plot of strain paths, ε_s against ε_v for type one path dependence tests on London clay, OCR = 2.0, p' = 300 kPa.

Fig 8.80 Plot of q' against ε_s for type one path dependence tests on London clay, OCR = 2.0, p' = 100kPa.

Fig 8.81 Plot of q' against ε_s for type one path dependence tests on London clay, OCR = 2.0, p' = 300kPa.

Fig 8.82 Plot of q' against p'. Stress paths followed during path dependence type two tests. $\eta'_o = 0$, OCR = 2.0. All data Figs 8.83 - 8.92.

Fig 8.83 Plot of strain paths, ε_s against ε_v for type two path dependence tests on speswhite kaolin.

Fig 8.84 Plot of strain paths, ε_s against ε_v for type two path dependence tests on Ware till.

Fig 8.85 Plot of strain paths, ε_s against ε_v for type two path dependence tests on Cowden till.

Fig 8.86 Plot of strain paths, ε_s against ε_v for type two path dependence tests on slate dust.

Fig 8.87a Plot of strain paths, ε_s against ε_v for type two path dependence tests on London clay.

Fig 8.87b Plot of stress paths, q' against p', and strain paths followed during path dependence type two tests on London clay. $\eta'_o = 0$, OCR = 2.0, p' = 200kPa, q'=-90kPa. Data in Fig 8.92a.

Fig 8.88 Plots of q' against ε_s and p' against ε_v for type two path dependence tests on speswhite kaolin.

Fig 8.89 Plots of q' against ε_s and p' against ε_v for type two path dependence tests on Ware till.

Fig 8.90 Plots of q' against ε_s and p' against ε_v for type two path dependence tests on Cowden till.

Fig 8.91 Plots of q' against ε_s and p' against ε_v for type two path dependence tests on slate dust.

Fig 8.92a Plots of q' against ε_s and p' against ε_v for type two path dependence tests on London clay.

Fig 8.92b Plots of q' against ε_s and p' against ε_v for type two path dependence tests on London clay.

Fig 8.93 Plot of q' against p'. Stress paths followed during path dependence type two tests. $\eta'_o = 0$, various OCR's, London clay. All data Figs 8.94 - 8.99.

Fig 8.94 Plot of strain paths, ε_s against ε_v for type two path dependence tests on London clay, OCR = 1.5.

Fig 8.95 Plot of strain paths, ε_s against ε_v for type two path dependence tests on London clay, OCR = 4.0.

Fig 8.96 Plot of strain paths, ε_s against ε_v for type two path dependence tests on London clay, OCR = 8.

Fig 8.97 Plots of q' against ε_s and p' against ε_v for type two path dependence tests on London clay, OCR = 1.5.

Fig 8.98 Plots of q' against ε_s and p' against ε_v for type two path dependence tests on London clay, OCR = 4.0.

Fig 8.99 Plots of q' against ε_s and p' against ε_v for type two path dependence tests on London clay, OCR = 8.0.

Fig 8.100 Plot of q' against p' and ε_s against ε_v for type two path dependence tests on London clay . η'_o = 0.25, OCR = 2.0.

Fig 8.101 Plot of q' against ε_s and p' against ε_v for type two path dependence tests on London clay, η'_o = 0.25, OCR = 2.0.

Fig 8.102 Plot of q' against p' and ε_s against ε_v for type two path dependence tests on London clay . η'_o = 0.75, OCR = 2.0.

Fig 8.103 Plot of q' against ε_s and p' against ε_v for type two path dependence tests on London clay, η'_o = 0.75, OCR = 2.0.

Fig 8.104 Plot of q' against p' and ε_s against ε_v for type two path dependence tests on London clay, two dimensionaly compressed, OCR = 2.0.

Fig 8.105 Plot of q' against ε_s and p' against ε_v for type two path dependence tests on London clay, two dimensionaly compressed, OCR = 2.0.

Fig 8.106 Plot of q' against p'. Stress paths followed during type two path dependence tests on London clay, one dimensionally compressed, various OCR's. All data Figs 8.107 - 8.114.

Fig 8.107 Plot of strain paths, ε_s against ε_v for type two path dependence tests on one dimensionally compressed London clay, OCR = 1.5.

Fig 8.108 Plot of strain paths, ε_s against ε_v for type two path dependence tests on one dimensionally compressed London clay, OCR = 2.0.

Fig 8.109 Plot of strain paths, ε_s against ε_v for type two path dependence tests on one dimensionally compressed London clay, OCR = 4.0.

Fig 8.110 Plot of strain paths, ε_s against ε_v for type two path dependence tests on one dimensionally compressed London clay, OCR = 8.0.

Fig 8.111 Plots of q' against ε_s and p` against ε_v for type one path dependence tests on one dimensionally compressed London clay, OCR = 1.5.

Fig 8.112 Plots of q' against ε_s and p` against ε_v for type two path dependence tests on one dimensionally compressed London clay, OCR = 2.0.

Fig 8.113 Plots of q' against ε_s and p` against ε_v for type two path dependence tests on one dimensionally compressed London clay, OCR = 4.0.

Fig 8.114 Plots of q' against ε_s and p` against ε_v for type two path dependence tests on one dimensionally compressed London clay, OCR = 8.0.

Fig 8.115 Plot of q' against p'. Stress paths followed during type two path dependence tests on London clay, η'_o = 0, OCR = 2.0, various p'. All data Figs 8.116 - 8.119.

Fig 8.116 Plot of strain paths, ε_s against ε_v for type two path dependence tests on London clay, OCR = 2.0, p' = 100 kPa.

Fig 8.117 Plot of strain paths, ε_s against ε_v for type two path dependence tests on London clay, OCR = 2.0, p' = 300 kPa.

Fig 8.118 Plots of q' against ε_s and p` against ε_v for type two path dependence tests on London clay, OCR = 2.0, p' = 100kPa.

Fig 8.119 Plots of q' against ε_s and p' against ε_v for type two path dependence tests on London clay, OCR = 2.0, p' = 300kPa.

Fig 8.120 Plot of q' against p'. Stress paths followed during path dependence type three tests. $\eta'_o = 0$, OCR = 2.0. All data Figs 8.121 - 8.130b.

Fig 8.121 Plot of strain paths, ε_s against ε_v for type three path dependence tests on speswhite kaolin.

Fig 8.122 Plot of strain paths, ε_s against ε_v for type three path dependence tests on Ware till.

Fig 8.123 Plot of strain paths, ε_s against ε_v for type three path dependence tests on Cowden till.

Fig 8.124 Plot of strain paths, ε_s against ε_v for type three path dependence tests on slate dust.

Fig 8.125a Plot of strain paths, ε_s against ε_v for type three path dependence tests on London clay.

Fig 8.125b Plot of stress paths, q' against p', and strain paths followed during path dependence type three tests on London clay. $\eta'_o = 0$, OCR = 2.0, p' = 200kPa. Data in Fig 8.130b.

Fig 8.126 Plots of q' against ε_s and p' against ε_v for type three path dependence tests on speswhite kaolin.

Fig 8.127 Plots of q' against ε_s and p' against ε_v for type three path dependence tests on Ware till.

Fig 8.128 Plots of q' against ε_s and p' against ε_v for type three path dependence tests on Cowden till.

Fig 8.129 Plots of q' against ε_s and p' against ε_v for type three path dependence tests on slate dust.

Fig 8.130a Plots of q' against ε_s and p' against ε_v for type three path dependence tests on London clay.

Fig 8.130b Plots of q' against ε_s and p' against ε_v for type three path dependence tests on London clay.

Fig 8.131 Plot of q' against p'. Stress paths followed during path dependence type three tests. $\eta'_o = 0$, various OCR's, London clay. All data Figs 8.132 -137.

Fig 8.132 Plot of strain paths, ε_s against ε_v for type three path dependence tests on London clay, OCR = 1.5.

Fig 8.133 Plot of strain paths, ε_s against ε_v for type three path dependence tests on London clay, OCR = 4.0.

Fig 8.134 Plot of strain paths, ε_s against ε_v for type three path dependence tests on London clay, OCR = 8.

Fig 8.135 Plots of q' against ε_s and p' against ε_v for type three path dependence tests on London clay, OCR = 1.5.

Fig 8.136 Plots of q' against ε_s and p' against ε_v for type three path dependence tests on London clay, OCR = 4.0.

Fig 8.137 Plots of q' against ε_s and p' against ε_v for type three path dependence tests on London clay, OCR = 8.0.

Fig 8.138 Plot of q' against p' and ε_s against ε_v for type three path dependence tests on London clay . η'_o = 0.25, OCR = 2.0.

Fig 8.139 Plot of q' against ε_s and p' against ε_v for type three path dependence tests on London clay, η'_o = 0.25, OCR = 2.0.

Fig 8.140 Plot of q' against p' and ε_s against ε_v for type three path dependence tests on London clay . η'_o = 0.75, OCR = 2.0.

Fig 8.141 Plot of q' against ε_s and p' against ε_v for type three path dependence tests on London clay, η'_o = 0.75, OCR = 2.0.

Fig 8.142 Plot of q' against p' and ε_s against ε_v for type three path dependence tests on London clay, two dimensionaly compressed, OCR = 2.0.

Fig 8.143 Plot of q' against ε_s and p' against ε_v for type three path dependence tests on London clay, two dimensionaly compressed, OCR = 2.0.

Fig 8.144 Plot of q' against p'. Stress paths followed during type three path dependence tests on London clay, one dimensionally compressed, various OCR's. All data Figs 8.145 - 8.152.

Fig 8.145 Plot of strain paths, ε_s against ε_v for type three path dependence tests on one dimensionally compressed London clay, OCR = 1.5.

Fig 8.146 Plot of strain paths, ε_s against ε_v for type three path dependence tests on one dimensionally compressed London clay, OCR = 2.0.

Fig 8.147 Plot of strain paths, ε_s against ε_v for type three path dependence tests on one dimensionally compressed London clay, OCR = 4.0.

Fig 8.148 Plot of strain paths, ε_s against ε_v for type three path dependence tests on one dimensionally compressed London clay, OCR = 8.0.

Fig 8.149 Plots of q' against ε_s and p` against ε_v for type three path dependence tests on one dimensionally compressed London clay, OCR = 1.5.

Fig 8.150 Plots of q' against ε_s and p` against ε_v for type three path dependence tests on one dimensionally compressed London clay, OCR = 2.0.

Fig 8.151 Plots of q' against ε_s and p` against ε_v for type three path dependence tests on one dimensionally compressed London clay, OCR = 4.0.

Fig 8.152 Plots of q' against ε_s and p` against ε_v for type three path dependence tests on one dimensionally compressed London clay, OCR = 8.0.

Fig 8.153 Plot of q' against p'. Stress paths followed during type three path dependence tests on London clay, η'_o = 0, OCR = 2.0, various p'. All data Figs 8.154 - 8.157.

Fig 8.154 Plot of strain paths, ε_s against ε_v for type three path dependence tests on London clay, OCR = 2.0, p' = 100 kPa.

Fig 8.155 Plot of strain paths, ε_s against ε_v for type three path dependence tests on London clay, OCR = 2.0, p' = 300 kPa.

Fig 8.156 Plots of q' against ε_s and p` against ε_v for type three path dependence tests on London clay, OCR = 2.0, p' = 100kPa.

Fig 8.157 Plots of q' against ε_s and p' against ε_v for type three path dependence tests on London clay, OCR = 2.0, p' = 300kPa.

Fig 8.158 Plots of q' against ε_s ,q'/p' against ε_s and ε_v against ε_s. Threshold tests to failure. Isotropically compressed speswhite kaolin. OCR = 2.0, p' =200kPa, constant p' paths.

Fig 8.159 Plot of v against $\log_e$ p' for threshold tests to failure. Isotropically compressed speswhite kaolin. OCR = 2.0, p' = 200kPa, constant p' paths.

Fig 8.160 Plot of q' / p' against v_λ . Threshold tests to failure. Isotropically compressed speswhite kaolin. OCR = 2.0, p' = 200kPa, constant p' paths.

Fig 8.161 Plot of q' / p'_e against p' / p'_e . Threshold tests to failure. Isotropically compressed speswhite kaolin. OCR = 2.0, p' = 200kPa, constant p' paths.

Fig 8.162 Plots of q' against ε_s ,q'/p' against ε_s and ε_v against ε_s. Threshold tests to failure. Isotropically compressed Ware till. OCR = 2.0, p' =200kPa, constant p' paths.

Fig 8.163 Plot of v against $\log_e$ p' for threshold tests to failure. Isotropically compressed Ware till. OCR = 2.0, p' = 200kPa, constant p' paths.

Fig 8.164 Plot of q' / p' against v_λ . Threshold tests to failure. Isotropically compressed Ware till. OCR = 2.0, p' = 200kPa, constant p' paths.

Fig 8.165 Plot of q' / p'_e against p' / p'_e . Threshold tests to failure. Isotropically compressed Ware till. OCR = 2.0, p' = 200kPa, constant p' paths.

Fig 8.166 Plots of q' against ε_s ,q'/p' against ε_s and ε_v against ε_s. Threshold tests to failure. Isotropically compressed Cowden till. OCR = 2.0, p' =200kPa, constant p' paths.

Fig 8.167 Plot of v against $\log_e$ p' for threshold tests to failure. Isotropically compressed Cowden till. OCR = 2.0, p' = 200kPa, constant p' paths.

Fig 8.168 Plot of q' / p' against v_λ . Threshold tests to failure. Isotropically compressed Cowden till. OCR = 2.0, p' = 200kPa, constant p' paths.

Fig 8.169 Plot of q' / p'_e against p' / p'_e . Threshold tests to failure. Isotropically compressed Cowden till. OCR = 2.0, p' = 200kPa, constant p' paths.

Fig 8.170 Plots of q' against ε_s ,q'/p' against ε_s and ε_v against ε_s. Threshold tests to failure. Isotropically compressed slate dust. OCR = 2.0, p' =200kPa, constant p' paths.

Fig 8.171 Plot of v against $\log_e$ p' for threshold tests to failure. Isotropically compressed slate dust. OCR = 2.0, p' = 200kPa, constant p' paths.

Fig 8.172 Plot of q' / p' against v_λ . Threshold tests to failure. Isotropically compressed slate dust. OCR = 2.0, p' = 200kPa, constant p' paths.

Fig 8.173 Plot of q' / p'_e against p' / p'_e . Threshold tests to failure. Isotropically compressed slate dust. OCR = 2.0, p' = 200kPa, constant p' paths.

Fig 8.174 Plots of q' against ε_s ,q'/p' against ε_s and ε_v against ε_s. Threshold tests to failure. Isotropically compressed London clay. OCR = 2.0, p' =200kPa, constant p' paths.

Fig 8.175 Plots of q' against $\varepsilon_s$and ε_v against ε_s for threshold tests to failure. Isotropically compressed London clay. OCR = 2.0, various p', constant p' paths.

Fig 8.176 Plots of q' against ε_s and ε_v against ε_s for threshold tests to failure. Isotropically compressed London clay. various OCR's, $\theta = 180^o$. constant p' paths.

Fig 8.177 Plot of q' / p' against ε_s for threshold tests to failure. Isotropically compressed London clay. various OCR's, $\theta = 180^o$. constant p' paths.

Fig 8.178 Plot of v against $\log_e p'$ for threshold tests to failure. Isotropically compressed London clay. various OCR's. constant p' paths.

Fig 8.179 Plot of q' / p' against v_λ . Threshold tests to failure. Isotropically compressed London clay. Various OCR's, constant p' paths.

Fig 8.180 Plot of q' / p'_e against p' / p'_e . Threshold tests to failure. Isotropically compressed London clay. Various OCR's, constant p' paths.

Fig 8.181 Plots of q' against ε_s ,q'/p' against ε_s , ε_v against ε_s and v against $\log_e p'$. Threshold tests to failure on London clay. $\eta'_o = 0.25$, OCR = 2.0, p' =200kPa, constant p' paths.

Fig 8.182 Plot of q' / p' against v_λ . Threshold tests to failure on London clay. $\eta'_o = 0.25$,OCR = 2.0, p' = 200kPa, constant p' paths.

Fig 8.183 Plot of q' / p'_e against p' / p'_e . Threshold tests to failure.London clay. $\eta'_o = 0.25$, OCR = 2.0, p' = 200kPa,constant p' paths.

Fig 8.184 Plots of q' against ε_s ,q'/p' against ε_s , ε_v against ε_s and v against $\log_e p'$. Threshold tests to failure on London clay. One dimensionally compressed, OCR = 2.0, p' =200kPa, constant p' paths .

Fig 8.185 Plots of q' against $\varepsilon_s$and ε_v against ε_s for threshold tests to failure. One dimensionally compressed London clay. various OCR's, $\theta = 180^o$. constant p' paths

Fig 8.186 Plot of v against $\log_e p'$ for threshold tests to failure. One dimensionally compressed London clay. various OCR's. constant p' paths.

Fig 8.187 Plot of q' against p'. Stress paths to failure of one dimensionally compressed London clay. Various OCR's, constant p'.

Fig 8.188 Plot of q' / p' against ε_s for threshold tests to failure. One dimensionally compressed London clay. various OCR's, $\theta = 180^o$. constant p' paths.

Fig 8.189 Plot of q' / p' against v_λ . Threshold tests to failure. One dimensionally compressed London clay. Various OCR's, constant p' paths.

Fig 8.190 Plot of q' / p'_e against p' / p'_e . Threshold tests to failure. One dimensionally compressed London clay. Various OCR's, constant p' path.

Fig 8.191 Plots of q' against ε_s ,q'/p' against ε_s , ε_v against ε_s and v against $\log_e p'$. Threshold tests to failure on London clay. $\eta'_o = 0.75$, OCR = 2.0, p' =200kPa, constant p' paths.

Fig 8.192 Plot of q' / p' against v_λ . Threshold tests to failure on London clay. $\eta'_o = 0.75$,OCR = 2.0, p' = 200kPa, constant p' paths.

Fig 8.193 Plot of q' / p'_e against p' / p'_e . Threshold tests to failure. Isotropically compressed London clay. $\eta'_o = 0.75$, OCR = 2.0, p' = 200kPa,constant p' paths.

Fig 8.194 Plots of q' against ε_s ,q'/p' against ε_s , ε_v against ε_s and v against $\log_e p'$. Threshold tests to failure on London clay. Two dimensionally compressed, OCR = 2.0, p' =200kPa, constant p' paths .

Fig 8.195 Plot of q' / p' against v_λ . Threshold tests to failure on London clay. Two dimensionally compressed , OCR = 2.0, p' = 200kPa, constant p' paths.

Fig 8.196 Plot of q' / p'_e against p' / p'_e . Threshold tests to failure. London clay. Two dimensionally compressed, OCR = 2.0, p' = 200kPa,constant p' paths.

Fig 8.197a Plot of q' against p'. Drained stress paths to failure of normally consolidated London clay ($\eta'_o = 0$).

Fig 8.197b Plot of q' against p'. Undrained stress paths to failure of normally consolidated London clay ($\eta'_o = 0$).

Fig 8.197c Plot of q' against p'. Undrained stress paths to failure of overconsolidated London clay ($\eta'_o = 0$).

Fig 8.197d Plot of q' against p' for states at failure . Normally and overconsolidated London clay ($\eta'_o = 0$).

Fig 8.198 Plots of q' against ε_s and ε_v against ε_s for drained normally consolidated tests to failure on London clay ($\eta'_o = 0$).

Fig 8.199 Plots of q' against ε_s and u against ε_s for undrained tests to failure on London clay ($\eta'_o = 0$).
a) Normally consolidated.
b) Overconsolidated.

Fig 8.200 Results of extension tests to failure on isotropically compressed London clay. Drained and undrained . Plotted as q' against ε_s , ε_v against ε_s ,q' / p' against ε_s and u against ε_s.

Fig 8.201 Drained tests to failure on normally consolidated London clay ($\eta'_o = 0$).
a) q' / p' against ε_s.
b) q' / p' against $v\varepsilon_s$.

Fig 8.202 Undrained tests to failure on London clay ($\eta'_o = 0$).
a) q' / p' against ε_s.
b) q' / p' against $v\varepsilon_s$.

Fig 8.203 Plot of v against $\log_e p'$ all London clay tests to failure ($\eta'_o = 0$).

Fig 8.204 Plot of q' / p' against v_λ . For all compression tests to failure on London clay. ($\eta'_o = 0$).

Fig 8.205 Plot of q' / p'_e against p' / p'_e .For all compression tests to failure on London clay. ($\eta'_o = 0$).

Fig 8.206 Plot of q' / p' against v_λ . For all compression and extension tests to failure on London clay. ($\eta'_o = 0$).

Fig 8.207 Plot of q' / p'_e against p' / p'_e .For all compression and extension tests to failure on London clay. ($\eta'_o = 0$).

Fig 8.208 Plots of q' against ε_s and ε_v against ε_s .The effect of varying the rest periods for isotropically compressed samples of London clay. OCR = 2.0, p' = 200kPa, constant p' paths.

Fig 8.209 Plot of ε_v against square root of time elapsed, $\sqrt{t}$ for rest periods for London clay.

Fig 8.210 Plots of q' against ε_s and ε_v against ε_s for isotropically compressed samples of London clay. OCR = 2.0, p' = 100kPa, constant p' paths.

Fig 8.211 Plots of q' against ε_s and ε_v against ε_s for isotropically compressed samples of London clay. OCR = 2.0, p' = 300kPa, constant p' paths.

Fig 8.212 Plot of q' / p' against ε_s for isotropically compressed London clay. OCR = 2.0, various p', constant p' paths.
a) At low stress levels.
b) To failure.

Fig 8.213 Total, q against p, and effective, q' against p', stress paths for London clay for total stress path threshold tests. $\eta'_o = 0$, OCR = 2.0.

Fig 8.214 Plots of q' against ε_s and ε_v against ε_s for London clay for total stress path threshold tests. $\eta'_o = 0$, OCR = 2.0.

Fig 8.215 Total, q against p, and effective, q' against p', stress paths for London clay for total stress path threshold tests. $\eta'_o = 0$, OCR = 2.0.

Fig 8.216 Plots of q' against ε_s and ε_v against ε_s for London clay for total stress path threshold tests. $\eta'_o = 0$, OCR = 2.0.

Fig 9.1 Hysteresis loops in swelling and recompression data. definitions of κ_o and κ_1.

Fig 9.2 Plot of stress increment ratio, dq' / dp' against strain increment ratio $d\varepsilon_s / d\varepsilon_v$ for London clay during anisotropic compression stages.

Fig 9.3 Variation of $K_o = \sigma'_r / \sigma'_a$ during one dimensional compression and swelling of London clay with overconsolidation ratio.

Fig 9.4 Variation of $K = \sigma'_r / \sigma'_a$ during anisotropic compression and swelling of London clay .

Fig 9.5 Effect of errors in control during two dimensional compression and swelling tests on London clay.

Fig 9.6 Plot of normalised stiffness $\delta q' / vp'\delta\varepsilon_s$ against $\log_e \Delta\eta'$. Speswhite kaolin isotropically compressed, OCR = 2.0, p' = 200 kPa, constant p' paths.

Fig 9.7 Plot of normalised stiffness $\delta q' / vp'\delta\varepsilon_s$ against deviation of stress path, θ . Speswhite kaolin isotropically compressed, OCR = 2.0, p' = 200 kPa, constant p' paths.

Fig 9.8 Plot of total strain increment ratio, $d\varepsilon_v / d\varepsilon_s$, against $\log\Delta\eta'$. Speswhite kaolin, isotropically compressed, OCR = 2.0, p' = 200kPa, constant p' paths.

Fig 9.9 Plot of total strain increment ratio, $d\varepsilon_v / d\varepsilon_s$, against deviation of stress path, θ. Speswhite kaolin, isotropically compressed, OCR = 2.0, p' = 200kPa, constant p' paths.

Fig 9.10 Plot of normalised stiffness $\delta q' / vp'\delta\varepsilon_s$ against $\log_e \Delta\eta'$. Ware till isotropically

compressed, OCR = 2.0, p' = 200 kPa, constant p' paths.

Fig 9.11 Plot of normalised stiffness $\delta q' / vp'\delta\varepsilon_s$ against deviation of stress path, θ. Ware till isotropically compressed, OCR = 2.0, p' = 200 kPa, constant p' paths.

Fig 9.12 Plot of total strain increment ratio, $d\varepsilon_v / d\varepsilon_s$, against $\log\Delta\eta'$. Ware till, isotropically compressed, OCR = 2.0, p' = 200kPa, constant p' paths.

Fig 9.13 Plot of total strain increment ratio, $d\varepsilon_v / d\varepsilon_s$, against deviation of stress path, θ. Ware till, isotropically compressed, OCR = 2.0, p' = 200kPa, constant p' paths.

Fig 9.14 Plot of normalised stiffness $\delta q' / vp'\delta\varepsilon_s$ against $\log_e\Delta\eta'$. Cowden till isotropically compressed, OCR = 2.0, p' = 200 kPa, constant p' paths.

Fig 9.15 Plot of normalised stiffness $\delta q' / vp'\delta\varepsilon_s$ against deviation of stress path, θ. Cowden till isotropically compressed, OCR = 2.0, p' = 200 kPa, constant p' paths.

Fig 9.16 Plot of total strain increment ratio, $d\varepsilon_v / d\varepsilon_s$, against $\log\Delta\eta'$. Cowden till, isotropically compressed, OCR = 2.0, p' = 200kPa, constant p' paths.

Fig 9.17 Plot of total strain increment ratio, $d\varepsilon_v / d\varepsilon_s$, against deviation of stress path, θ. Cowden till, isotropically compressed, OCR = 2.0, p' = 200kPa, constant p' paths.

Fig 9.18 Plot of normalised stiffness $\delta q' / vp'\delta\varepsilon_s$ against $\log_e\Delta\eta'$. Slate dust isotropically compressed, OCR = 2.0, p' = 200 kPa, constant p' paths.

Fig 9.19 Plot of normalised stiffness $\delta q' / vp'\delta\varepsilon_s$ against deviation of stress path, θ. Slate dust isotropically compressed, OCR = 2.0, p' = 200 kPa, constant p' paths.

Fig 9.20 Plot of total strain increment ratio, $d\varepsilon_v / d\varepsilon_s$, against $\log\Delta\eta'$. Slate dust, isotropically compressed, OCR = 2.0, p' = 200kPa, constant p' paths.

Fig 9.21 Plot of total strain increment ratio, $d\varepsilon_v / d\varepsilon_s$, against deviation of stress path, θ. Slate dust, isotropically compressed, OCR = 2.0, p' = 200kPa, constant p' paths.

Fig 9.22 Plot of normalised stiffness $\delta q' / vp'\delta\varepsilon_s$ against $\log_e\Delta\eta'$. London clay isotropically compressed, OCR = 2.0, p' = 200 kPa, constant p' paths.

Fig 9.23 Plot of normalised stiffness $\delta q' / vp'\delta\varepsilon_s$ against deviation of stress path, θ. London clay isotropically compressed, OCR = 2.0, p' = 200 kPa, constant p' paths.

Fig 9.24 Plot of total strain increment ratio, $d\varepsilon_v / d\varepsilon_s$, against $\log\Delta\eta'$. London clay, isotropically compressed, OCR = 2.0, p' = 200kPa, constant p' paths.

Fig 9.25 Plot of total strain increment ratio, $d\varepsilon_v / d\varepsilon_s$, against deviation of stress path, θ. London clay, isotropically compressed, OCR = 2.0, p' = 200kPa, constant p' paths.

Fig 9.26 Plot showing range of stiffness, R, against plasticity index, PI, for $\Delta\eta'$ = 0.40 and $\Delta\eta'$ = 0.05.

Fig 9.27 Plot of normalised stiffness $\delta q' / vp'\delta\varepsilon_s$ against $\log_e\Delta\eta'$. London clay isotropically compressed, OCR = 1.5, p' = 267 kPa, constant p' paths.

Fig 9.28 Plot of normalised stiffness $\delta q' / vp'\delta\varepsilon_s$ against deviation of stress path, θ. London clay isotropically compressed, OCR = 1.5, p' = 267 kPa, constant p' paths.

Fig 9.29 Plot of total strain increment ratio, $d\varepsilon_v / d\varepsilon_s$, against $\log\Delta\eta'$. London clay, isotropically compressed, OCR = 1.5, p' = 267kPa, constant p' paths.

Fig 9.30 Plot of total strain increment ratio, $d\varepsilon_v / d\varepsilon_s$, against deviation of stress path, θ.

London clay , isotropically compressed, OCR = 1.5, p' = 267kPa, constant p' paths.

Fig 9.31 Plot of normalised stiffness $\delta q' / vp'\delta\varepsilon_s$ against $\log_e\Delta\eta'$. London clay isotropically compressed, OCR = 4.0, p' = 100 kPa, constant p' paths.

Fig 9.32 Plot of normalised stiffness $\delta q' / vp'\delta\varepsilon_s$ against deviation of stress path, θ . London clay isotropically compressed, OCR = 4.0, p' = 100 kPa, constant p' paths.

Fig 9.33 Plot of total strain increment ratio, $d\varepsilon_v / d\varepsilon_s$, against $\log\Delta\eta'$. London clay , isotropically compressed, OCR = 4.0, p' = 100kPa, constant p' paths.

Fig 9.34 Plot of total strain increment ratio, $d\varepsilon_v / d\varepsilon_s$, against deviation of stress path, θ. London clay , isotropically compressed, OCR = 4.0, p' = 100kPa, constant p' paths.

Fig 9.35 Plot of normalised stiffness $\delta q' / vp'\delta\varepsilon_s$ against $\log_e\Delta\eta'$. London clay isotropically compressed, OCR = 8.0, p' = 50 kPa, constant p' paths.

Fig 9.36 Plot of normalised stiffness $\delta q' / vp'\delta\varepsilon_s$ against deviation of stress path, θ . London clay isotropically compressed, OCR = 8.0, p' = 50 kPa, constant p' paths.

Fig 9.37 Plot of total strain increment ratio, $d\varepsilon_v / d\varepsilon_s$, against $\log\Delta\eta'$. London clay , isotropically compressed, OCR = 8.0, p' = 50kPa, constant p' paths.

Fig 9.38 Plot of total strain increment ratio, $d\varepsilon_v / d\varepsilon_s$, against deviation of stress path, θ. London clay , isotropically compressed, OCR = 8.0, p' = 50kPa, constant p' paths.

Fig 9.39 Plot of normalised stiffness $\delta q' / vp'\delta\varepsilon_s$ against $\log_e\Delta\eta'$. London clay, $\eta'_o = 0.25$, OCR = 2.0, p' = 200 kPa, constant p' paths.

Fig 9.40 Plot of normalised stiffness $\delta q' / vp'\delta\varepsilon_s$ against deviation of stress path, θ . London clay, $\eta'_o = 0.25$, OCR = 2.0, p' = 200 kPa, constant p' paths.

Fig 9.41 Plot of total strain increment ratio, $d\varepsilon_v / d\varepsilon_s$, against $\log\Delta\eta'$. London clay, $\eta'_o = 0.25$, OCR = 2.0, p' = 200kPa, constant p' paths.

Fig 9.42 Plot of total strain increment ratio, $d\varepsilon_v / d\varepsilon_s$, against deviation of stress path, θ. London clay, $\eta'_o = 0.25$, OCR = 2.0, p' = 200kPa, constant p' paths.

Fig 9.43 Plot of normalised stiffness $\delta q' / vp'\delta\varepsilon_s$ against $\log_e\Delta\eta'$. London clay one dimensionally compressed, OCR = 1.5, p' = 267 kPa, constant p' paths.

Fig 9.44 Plot of normalised stiffness $\delta q' / vp'\delta\varepsilon_s$ against deviation of stress path, θ . London clay one dimensionally compressed, OCR = 1.5, p' = 267kPa, constant p' paths.

Fig 9.45 Plot of total strain increment ratio, $d\varepsilon_v / d\varepsilon_s$, against $\log\Delta\eta'$. London clay , one dimensionally compressed, OCR = 1.5, p' = 267kPa, constant p' paths.

Fig 9.46 Plot of total strain increment ratio, $d\varepsilon_v / d\varepsilon_s$, against deviation of stress path, θ. London clay , isotropically compressed, OCR = 1.5, p' = 267kPa, constant p' paths.

Fig 9.47 Plot of normalised stiffness $\delta q' / vp'\delta\varepsilon_s$ against $\log_e\Delta\eta'$. London clay one dimensionally compressed, OCR = 2.0, p' = 200 kPa, constant p' paths.

Fig 9.48 Plot of normalised stiffness $\delta q' / vp'\delta\varepsilon_s$ against deviation of stress path, θ . London clay one dimensionally compressed, OCR = 2.0, p' = 200kPa, constant p' paths.

Fig 9.49 Plot of total strain increment ratio, $d\varepsilon_v / d\varepsilon_s$, against $\log\Delta\eta'$. London clay, one dimensionally compressed, OCR = 2.0, p' = 200kPa, constant p' paths.

Fig 9.50 Plot of total strain increment ratio, $d\varepsilon_v / d\varepsilon_s$, against deviation of stress path, θ. London clay, isotropically compressed, OCR = 2.0, p' = 200kPa, constant p' paths.

Fig 9.51 Plot of normalised stiffness $\delta q' / vp'\delta\varepsilon_s$ against $\log_e\Delta\eta'$. London clay one dimensionally compressed, OCR = 4.0, p' = 100 kPa, constant p' paths.

Fig 9.52 Plot of normalised stiffness $\delta q' / vp'\delta\varepsilon_s$ against deviation of stress path, θ. London clay one dimensionally compressed, OCR = 4.0, p' = 100kPa, constant p' paths.

Fig 9.53 Plot of total strain increment ratio, $d\varepsilon_v / d\varepsilon_s$, against $\log\Delta\eta'$. London clay, one dimensionally compressed, OCR = 4.0, p' = 100kPa, constant p' paths.

Fig 9.54 Plot of total strain increment ratio, $d\varepsilon_v / d\varepsilon_s$, against deviation of stress path, θ. London clay, isotropically compressed, OCR = 4.0, p' = 100kPa, constant p' paths.

Fig 9.55 Plot of normalised stiffness $\delta q' / vp'\delta\varepsilon_s$ against $\log_e\Delta\eta'$. London clay one dimensionally compressed, OCR = 8.0, p' = 50kPa, constant p' paths.

Fig 9.56 Plot of normalised stiffness $\delta q' / vp'\delta\varepsilon_s$ against deviation of stress path, θ. London clay one dimensionally compressed, OCR = 8.0, p' = 50kPa, constant p' paths.

Fig 9.57 Plot of total strain increment ratio, $d\varepsilon_v / d\varepsilon_s$, against $\log\Delta\eta'$. London clay, one dimensionally compressed, OCR = 8.0, p' = 50kPa, constant p' paths.

Fig 9.58 Plot of total strain increment ratio, $d\varepsilon_v / d\varepsilon_s$, against deviation of stress path, θ. London clay, isotropically compressed, OCR = 8.0, p' = 50kPa, constant p' paths.

Fig 9.59 Plot of normalised stiffness $\delta q' / vp'\delta\varepsilon_s$ against $\log_e\Delta\eta'$. London clay, $\eta'_o = 0.75$, OCR = 2.0, p' = 200kPa, constant p' paths.

Fig 9.60 Plot of normalised stiffness $\delta q' / vp'\delta\varepsilon_s$ against deviation of stress path, θ. London clay, $\eta'_o = 0.75$, OCR = 2.0, p' = 200kPa, constant p' paths.

Fig 9.61 Plot of total strain increment ratio, $d\varepsilon_v / d\varepsilon_s$, against $\log\Delta\eta'$. London clay, $\eta'_o = 0.25$, OCR = 2.0, p' = 200kPa, constant p' paths.

Fig 9.62 Plot of total strain increment ratio, $d\varepsilon_v / d\varepsilon_s$, against deviation of stress path, θ. London clay, $\eta'_o = 0.75$, OCR = 2.0, p' = 200kPa, constant p' paths.

Fig 9.63 Plot of normalised stiffness $\delta q' / vp'\delta\varepsilon_s$ against $\log_e\Delta\eta'$. London clay two dimensionally compressed, OCR = 2.0, p' = 200 kPa, constant p' paths.

Fig 9.64 Plot of normalised stiffness $\delta q' / vp'\delta\varepsilon_s$ against deviation of stress path, θ. London clay two dimensionally compressed, OCR = 2.0, p' = 200 kPa, constant p' paths.

Fig 9.65 Plot of total strain increment ratio, $d\varepsilon_v / d\varepsilon_s$, against $\log\Delta\eta'$. London clay two dimensionally compressed, OCR = 2.0, p' = 200 kPa, constant p' paths.

Fig 9.66 Plot of total strain increment ratio, $d\varepsilon_v / d\varepsilon_s$, against deviation of stress path, θ. London clay two dimensionally compressed, OCR = 2.0, p' = 200 kPa, constant p' paths.

Fig 9.67 a) Plot of normalised stiffness, $\delta q' / vp'\delta\varepsilon_s$, against stress ratio (during initial

compression, $\eta'_{o)}$, for London clay, OCR = 2.0.
b) Plot of range of stiffness observed, R, against initial stress ratio during compression, η'_o.

Fig 9.68 Plot of normalised stiffness, $\delta q' / vp'\delta\varepsilon_s$, against overconsolidation ratio for isotropically compressed London clay.
a) For a given stress level.
b) For a given strain level.

Fig 9.69 Plot of normalised stiffness, $\delta q' / vp'\delta\varepsilon_s$, against overconsolidation ratio for one dimensionally compressed London clay.
a) For a given stress level.
b) For a given strain level.

Fig 9.70 Range of stiffness, R, plotted against overconsolidation ratio for both isotropically and one dimensionally compressed London clay.

Fig 9.71 Idealised plot of normalised stiffness against $\log_e \Delta\pi'$.

Fig 9.72 Plot of q' / p' against v_λ for samples of London clay from all initial compression histories.

Fig 9.73 Plot of q' / p'_e against p' / p'_e for samples of London clay from all initial compression histories using a value of N from isotropic compression data.

Fig 9.74 Effect of local drainage on the stress strain behaviour and failure states of samples.

Fig 9.75 Plots of v against $\log_e p'$ and ε_s against ε_v for speswhite kaolin samples produced by the alternative method. Isotropic compression and swelling.

Fig 9.76 Plots of v against $\log_e p'$ and ε_s against ε_v for London clay samples produced by the alternative method. Isotropic compression and swelling.

Fig 9.77 Typical form of data obtained from tests plotted as normalised stiffness against deviation of stress path.
a) Constant p' paths.
b) Constant q' paths.

Fig 9.78 Effect of a kinematic yield surface on the behaviour of samples due to different approach paths.

Fig 9.79 Growth of the threshold zone due to rest periods.

Fig A 1.1 Plot of volumetric strain against square root of time.

Fig A 1.2 Plot of specific volume against $\log_e p'$.

Fig A 1.3 Dissipation of excess pore pressures at the end of loading for London clay.

Fig A 1.4 Dissipation of excess pore pressures at the end of loading for Ware till.

Fig A 1.5 Dissipation of excess pore pressures at the end of loading for Cowden till.

Fig A 1.6 Dissipation of excess pore pressures at the end of loading for Speswhite kaolin.

Fig A 1.7 Dissipation of excess pore pressures at the end of loading for Slate dust.

Fig A 2.1 Plot of volumetric strain against lnp' for filter paper side drains.

Fig A 2.2 Plot of specific volume against lnp' for isotropically compressed London clay. Initial water contents unadjusted.

Fig A 2.3 Error in specific volume between initial and final values against duration of test.

ACKNOWLEDGEMENTS.

The work described in this thesis was conducted in the Geotechnical Engineering Research Centre at The City University, London. During this period I was supported by a CASE studentship from the Science and Engineering Research Council in co-operation with Ove Arup and Partners.

Many members of the Geotechnical Engineering Research Centre and The City University have been of assistance to me throughout the period of this work only some of whom are mentioned here. Firstly I am very grateful to Professor J.H. Atkinson of the City University and Dr B. Simpson of Ove Arup and Partners for suggesting the subject of the research and for supervising this work. The guidance which they have given has been invaluable. Professor J.H. Atkinson supervised the work at The City University, provided data for threshold tests on speswhite kaolin and also gave advice on the writing up of the experimental work and the analysis of the test data.

The Spectra triaxial testing system was developed and tested by members of the Geotechnical Engineering Research Centre before this research commenced by Professor J.H. Atkinson, Mr J.S. Evans, and Mr C.R. Scott. The SPCTRA control program was developed and tested by Mr C.R. Scott.

Thanks are due to Mr K. Osbourne and the technicians of the department who were of great help with the experimental work. They maintained equipment and assisted whenever faults developed. I am also grateful to Mr J. Hooker of the surveying department for printing the photographs which appear in this thesis. The staff and students of the research centre were also of great help throughout this work for the many helpful discussions and advice regarding this research.

I am also grateful to those who have assisted either directly or indirectly in the production of this thesis. Firstly I must thank Mrs Judy Chamberlain for typing from an often unintelligible manuscript. The typing was done on a Macintosh computer owned by the Britannia Inn at Elterwater in Cumbria and I am most grateful to Mr David Fry for allowing me the use of the system. The printing was done on an Apple / Macintosh Laser writer system at Lakeland Computer Services, Ambleside. I am very grateful to the owners Paul and Rick Fry for the use of various software , the Laserwriter, and the Macintosh computer in order to complete and print this thesis. I am also grateful to my mother and father, Mrs G.R. Richardson and Mr E.E. Richardson for assistance in producing the necessary copies of the thesis and for their support and encouragement during this research.

I would like to thank those who have put up with the disturbance caused by this work during the last four years, my mother and father and in particular Diane my wife.

DECLARATION.

I grant the powers of discretion to the University Librarian to allow this thesis to be copied in whole or part without further reference to me. This permission covers only single copies made for study purposes, subject to normal conditions of acknowledgement.

SYNOPSIS.

Some of the methods used in deformation analyses are briefly reviewed. It is observed that often there is a large difference between data quoted from laboratory tests and that obtained from the back analysis of either field tests or back analysed structures. Some of the factors which affect soil stiffness are reviewed. The major factors affecting soil stiffness are identified as the stress history of samples, the current stress state and the current stress path. The effect of sample disturbance is to reduce measured stiffnesses, opinion has in the past attributed the differences in stiffness to this factor. However this is not supported by the results of high quality laboratory tests in which field and laboratory data agree well. The importance of care when defining stiffness moduli and the need for the definition to be given at appropriate points on the stress-strain curve are emphasised. Some indication of the significance of recent stress history in the form of threshold effects is discussed, although this is based on limited evidence in the case of stress path effects.

The soils to be tested and the equipment to be used for the soil test program are discussed. Particular emphasis is placed on the calibration of the apparatus and system compliance. Details of the tests conducted are briefly given with details of the method of preparation of soil and soil samples for testing.

The results of these tests indicate that as the deviation of the current stress path from that immediately preceding increases so the stiffness on a given stress path increases. In addition it is observed that the strain increment ratio is non-unique. These effects are observed to be most important for high plasticity soils. Further tests indicate the independence of time and stress path threshold effects. The variation of these effects with stress history and overconsolidation ratio are investigated. It is found that these effects are most significant for soils which have been isotropically compressed and swelled to have an overconsolidation ratio of two. The results of these tests indicate some of the reasons for difficulties in tests to examine path dependence in earlier research.

Finally some conclusions from this experimental work are drawn together and topics for further research suggested. The importance of considering the complete stress history of samples including recent stress paths and periods of rest are emphasised for inclusion in the stress path method.

List of Symbols

A	Area.
A	Compliance parameter.
A	Parameter in Pender's model (Chapter 3).
A	Skempton's pore pressure parameter.
A_d	Cross sectional area of side drains.
A_m	Current cross sectional area of membrane.
A_o	Initial area of sample.
A_{om}	Initial cross sectional area of membrane.
A_{os}	Initial area of sample.
A_s	Current area of sample.
B	Compliance parameter.
B	Skempton's pore pressure parameter.
C	Compliance parameter.
C	Volumetric compliance of soil under drained conditions.
C	Volumetric compliance of soil under undrained conditions.
C_c	Compression index.
C_s	Swelling index.
C_s	Volumetric compliance of soil grains.
C_w	Volumetric compliance of water.
C_α	Secondary compression index.
D	Compliance parameter.
D	Current area of sample.
D_m	Current average diameter of membrane.
D_{mo}	Initial average diameter of membrane.
D_o	Initial diameter of sample.
D_s	Current diameter of sample.
E	Young's modulus.
E'	Young's modulus in terms of effective stress.
E_{fp}	Young's modulus for filter paper.
E_m	Young's modulus for rubber membrane.
E_u	Young's modulus for undrained loading in terms of total stress.
E'_v	Non-dimensional vertical stiffness modulus (Simpson et al, 1979; Chapter 3).
F	Flow rule.
F	Fraction of sample surface area covered by filter paper side drains.
F	Ratio of stiffness $(\delta q'/vp'\delta\varepsilon)^\theta / (\delta q'/vp'\delta\varepsilon)^{\theta=0}$ after change of stress state π'_a
$[F_{ijkl}]$	Elastic compliance matrix.
G'	Elastic shear modulus in terms of effective stress.
G'	Stiffness modulus.
G_1	Shear modulus in threshold range.
G_e	Elastic shear modulus.
G_f	$[(p' - \alpha_p)^2 + (q' - \alpha_q)/n^2)^2]^{1/2}$.

G_F	$[(p'-c)^2+(q'/n^2)^2]^{1/2}$.
G_s	Specific Gravity.
H	Height.
K	Bulk modulus.
K'	Bulk modulus in terms of effective stress.
K_o	Coefficient of earth pressure at rest.
K_p	Plastic hardening modulus.
K_{po}	Value of K at initial yielding.
K_{pr}	Value of K on boundary surface.
K_s	Elastic bulk modulus.
L	Length.
L_m	Current length membrane.
L_{mo}	Initial length of membrane.
L_o	Initial length.
LL	Liquid limit.
LI	Liquidity Index.
M	Modulus of rigidity of membrane ($E_m t_m$).
M	Slope of critical state line.
M_c	Slope of critical state line in compression.
M_e	Slope of critical state line in extension.
$[M_{ijkl}]$	Plastic compliance matrix.
N	Specific volume on the normal compression line at p'= 1.0 kPa (v vs lnp').
N*	Specific volume on the normal compression line at p' = 1.0 kPa (ln v vs lnp').
P	Total axial force.
P_d	Axial force on filter paper side drains.
P_m	Axial force on membrane.
P_s	Axial force on sample.
PL	Plastic limit.
PI	Plasticity index.
Q	Rate of flow.
R	Range of stiffness $((\delta q'/vp'\delta\varepsilon)_{\theta = 0^o}/(\delta q'/vp'\delta\varepsilon)_{\theta = 180^o})$.
R_f	Failure ratio.
R_{os}	Initial radius of sample.
R_p	Overconsolidation ratio with reference to p' (p'_m/p').
T	Time factor.
U	Average degree of consolidation.
U	Excess pore pressure.
U_f	Degree of equalisation of pore pressure.
U_o	Excess pore pressure without pore pressure redistribution.
V	Volume.
V_o	Initial volume.
W_s	Distortional work.

W_v	Volumetric work.
a	Semi-diameter of bounding ellipse.
a	Parameter in hyperbolic model.
a	Sample radius.
a_o	Semi-diameter of kinematic yield surface (K.Y.S).
b	Parameter in hyperbolic model.
b	$(\sigma'_2 - \sigma'_3) / (\sigma'_1 - \sigma'_3)$.
c	p' co-ordinate of the centre of the bounding surface.
c'	Cohesion.
c_u	Undrained shear strength.
c_v	Coefficient of consolidation.
c_{vt}	True coefficient of consolidation.
d	Differential operator.
d	Small change of.
e	Voids ratio.
h	2h = sample height.
i	Hydraulic gradient.
k	Coefficient of permeability.
k_c	Permeability of soil in the radial direction.
k_p	Permeability of filter paper.
ln	Natural logarithm.
m_v	Coefficient of volume compressibility.
n	Porosity.
n'	Ratio of stiffnesses in cross-anisotropic soil (E'_1 / E'_3).
n	Ratio of minor to major axes of ellipse.
p'	Mean effective stress $^1/_3(\sigma_1' + \sigma_2' + \sigma_3')$.
Δ p'	Correction to mean effective stress.
p'_c	Pre-consolidation pressure.
p'_{cs}	Value of p' at critical state on the current yield curve.
p'_e	Equivalent pressure.
p'_f	Value of p' at failure.
p'_m	Maximum value of p'.
p'_o	Initial value of p'.
p'_u	Ultimate value of p'.
q'	Deviator stress $(^1/_2((\sigma'_1 - \sigma'_2)^2 + (\sigma'_2 - \sigma'_3)^2 + (\sigma'_3 - \sigma'_1)^2))^{1/2}$.
Δ q'	Correction to q'.
q'	Value of q' at failure.
q'	Ultimate value of q'.
s'	$^1/_2(\sigma'_1 + \sigma'_3)$.
t = t'	$^1/_2(\sigma'_1 - \sigma'_3)$.

t	Time elapsed.
t_{100}	Time for 100% consolidation.
t_d	Current thickness of filter paper side drains.
t_f	Time to failure or first significant reading.
t_f	Thickness of filter paper side drains.
t_{ft}	True time to failure of first significant reading.
t_m	Current thickness of membrane.
t_o	Initial thickness of filter paper side drains.
t_{om}	Initial thickness of membrane.
u	Pore pressure.
u_o	Initial pore pressure.
v	Specific volume.
v_o	Initial specific volume.
v_o	Plastic volumetric strain.
v_f	Final specific volume.
v_p	Plastic volumetric strain.
v_κ	Specific volume on a swelling line at p' = 1.0 kPa (v , lnp').
v^*_κ	Specific volume on a swelling line at p' = 1.0 kPa (lnv, lnp').
v_λ	Specific volume reference section (lnv , lnp').
w	Water content.
Γ	Specific volume on the critical state line at p' = 1.0 kPa (v , lnp').
Γ^*	Specific volume on the critical state line at p' = 1.0 kPa (lnv, lnp').
Δ	Large increment of.
Σ	Sum of.
α	Current slope of stress path ($\delta q'/\delta p'$).
α	$\Delta q' / \Delta p'$.
α	Slope of undrained stress path.
α	Orientation of σ'_1 , relative to the vertical (Symes, 1984).
α_G	Shear stiffness parameter in K-G model.
α_K	Volumetric parameter in K-G model.
α_q	q' co-ordinate of centre of kinematic yield surface.
α_p	p' co-ordinate of centre of kinematic yield surface.
β_G	Shear stiffness parameter in K-G model.
γ	Plastic hardening modulus.
γ	Unit weight.

γ_{oct}	Octahedral shear strain, $^2/_3[(\varepsilon_1-\varepsilon_2)^2+(\varepsilon_2-\varepsilon_3)^2+(\varepsilon_3-\varepsilon_1)^2)^{1/2}$.
γ_p	Plastic shear strain.
γ_w	Unit weight of water.
δ	Small increment of.
δ	Filter paper thickness.
δ	Distance between conjugate stress points on bounding surface and kinematic yield surface.
δ_o	Maximum value of δ for current value of 'a', $\delta = 2(a-a_o)$.
ε	Strain.
ε_a	Axial strain in sample.
ε_{am}	Axial strain in membrane.
ε_{ao}	Axial strain in membrane before testing.
ε_{fp}	Axial strain in filter paper side drains.
ε_h	Hoop strain in membrane.
ε_m	Axial strain in membrane.
ε_r	Radial strain in sample.
ε_{ro}	Radial strain in membrane before testing.
ε_{rm}	Radial strain in membrane.
ε_s	Shear strain $[^2/_9((\varepsilon_1-\varepsilon_2)^2+(\varepsilon_2-\varepsilon_3)^2+(\varepsilon_3-\varepsilon_1)^2))^{1/2}$.
ε_v	Volumetric strain $(\varepsilon_1+\varepsilon_2+\varepsilon_3)$.
η'	Stress ratio q'/p'.
η'_o	Initial stress ratio.
η	Drainage parameter.
η	Relative bulk density (1/v).
η_p	Plastic component of η (1/v).
θ	Angle between effective stress paths.
θ^T	Angle between total stress paths.
κ	Slope of swelling curve (negative) (v , lnp').
κ^*	Slope of swelling curve (negative) (ln v , lnp').
κ_1	Initial slope of swelling curve (negative).
κ_2	Final slope of swelling curve (negative).
λ	Slope of normal compression line (negative) (v,lnp').
λ^*	Slope of normal compression line (negative) (ln v , lnp').

π'	Natural stress change $\sqrt{(1+\alpha^2)}\log_e(1+\Delta p'/p'_o)$
μ	Drainage condition parameter.
ν'	Poissons ratio defined with respect to effective stresses.
ν_m	Poissons ratio for membrane.
ν_u	Poissons ratio for undrained conditions.
ρ	Drainage condition parameter.
σ	Total normal stress.
σ_a	Axial stress.
$\Delta\sigma_a$	Correction to axial stress.
$\Delta\sigma_{ac}$	Corrected value of axial stress.
$\Delta\sigma_{am}$	Correction to axial stress due to membrane.
$\Delta\sigma_{afp}$	Correction to axial stress due to filter paper side drains.
σ_h	Hoop stress in membrane.
σ_l	Longitudinal stress in membrane.
σ_r	Radial stress.
$\Delta\sigma_r$	Correction to radial stress.
$\Delta\sigma_{rc}$	Corrected value of radial stress.
$\Delta\sigma_{rm}$	Correction to radial stress due to membrane.
$\Delta\sigma_1$	Correction to axial stress.
$\Delta\sigma_3$	Correction to radial stress.
$\tau = \tau'$	$^1/_2(\sigma_1 - \sigma_3)$.
ϕ'	Angle of internal friction.

Subscripts.

1, 2, 3	Principal directions.
a	Axial.
cs	Critical state.
f	Failure.
h	Horizontal.
o	Initial.
r	Radial.
u	Ultimate.
v	Vertical.
x, y, z	Co-ordinate axes.

τ_{xy} Shear stress between x and y plane.

ν_{xy} Poissons ratio for strain in the y direction due to stress in the x direction.

Superscripts.

' Effective stress e.g. σ'.

e Elastic.

p Plastic.

t Total.

CHAPTER 1

INTRODUCTION

Haystacks 10

THE SUMMIT

AWainwright

Wainwright,A.(1965). The Western Fells, Book 7. Westmorland Gazette.

CHAPTER 1 INTRODUCTION.

1.1 Introduction.

The object of soil testing in the laboratory and field is to provide data for the design of earth structures. Designs may be based on the experience of the performance of similar structures or by the use of mathematical models derived from and calibrated by the data obtained from such tests. In many cases data obtained in laboratory and field tests was modified according to experience of the behaviour of similar structures where performance had been monitored and back analysed using similar mathematical models. This had often proved necessary in deformation analyses due to discrepancies between data obtained in the laboratory and observations in the field. The mathematical models used are only an idealisation of soil behaviour which are considered to be sufficiently accurate over the range of conditions of interest (Scott, 1963). Hence, when extrapolating data obtained from small samples in the laboratory to a natural undisturbed soil in the field some differences may be observed.

Despite extensive research into the mechanical behaviour of soils, this subject is still far from being fully understood even for the case of the simplest type of soil samples, laboratory reconstituted soils. In particular large discrepancies have often been reported in stiffness data obtained from laboratory tests, field tests, and back analysed structures (St.John, 1975). Advances in testing technology and greater care in the analysis of test results have resolved some of these differences, but detailed questions regarding soil behaviour remain, in particular the effects of recent loading history on soil samples.

In the study of theoretical soil mechanics two main divisions may be observed, the characterisation of the soil (i.e the study of constitutive relations), and the solution of boundary value problems (Houlsby, 1981). The present research deals with the former. Within the heading of constitutive relations three main regions of study may be identified. The first is the study of the behaviour and properties of real soils either in the field or in the laboratory. Secondly there is the study of the applicability of a particular mathematical model to a soil or group of soils. Finally there is the study of the model itself e.g. the fundamental theoretical conditions which apply to a given model. In general the procedure followed during research is that a model (with restrictions and limitations defined) is proposed, assessed against test data, and then the relevant soil properties determined. The subject of the present research relates to the stiffness of soils and in particular those effects due to recent stress history termed threshold effects by Atkinson (1973). This study deals with the behaviour of reconstituted soils as observed in laboratory tests and the relationship of these results to a number of stress-strain theories.

The selection of the mathematical models for study needs careful consideration and those finally selected may not be so solely for accuracy. Models which are very accurate tend also to be highly complex. A simple model may offer advantages despite the loss of accuracy, for example the use of standard solutions in the case of linear elasticity. Furthermore the parameters contained in

complex models for the calibration of the model are often poorly defined and difficult to determine, perhaps also needing highly specialised testing equipment and procedures. The values of such parameters may be suspect if loading conditions and the stress system differ by a large degree from those in the testing apparatus, i.e. such parameters may not be fundamental parameters and so are not soil "constants". These problems may be overlooked due to the powerful computational methods available which allow the application of models to highly complex loading situations , the solutions from which cannot readily be checked by a simple calculation or from previous experience. Such computer methods are far in advance of the understanding of soil behaviour and of the ability to measure fundamental soil properties in either the laboratory or the field, (Costa Filho, 1979). However in order to model the results of tests conducted on complex stress paths some degree of complexity must be introduced to a model. Mathematical models which can model such behaviour with the minimum of complexity and a minimum number of soil parameters are therefore to be favoured.

1.2 Previous Research.

There has been much previous research into the stiffness of soils and path dependence in particular. However there are very little previous data relating to threshold effects and in particular stress path threshold effects. A complete review of some of these data will be given in Chapter 2, this section will only summarise the areas of previous research.

In general tests have concentrated on isotropically consolidated samples of reconstituted soils. The types of test conducted for path dependence generally involve "probing" tests. These tests typically involve loading a number of samples to a common stress state before a variety of stress paths are followed away from that point. This is performed in such a manner that all samples initially have the same loading history before either all arriving at the common stress point on one common approach path or arrive on a variety of stress paths all passing through the common stress point. These types of tests are analysed in terms of stiffnesses at or close to the common stress point and any departures from a common set of stiffness data are interpreted as either variability of samples or due to the influence of the different stress paths followed after the common stress state. Such tests do not yield data which may readily be interpreted for stress path threshold tests since the effects of stress path and different changes of direction of stress path are confused.

Tests conducted by Atkinson (1983a) differ from the above test types. In these tests samples having the same initial loading history reached a common stress state via different stress paths. A common loading path was then followed for all samples. The differences in stiffness observed were attributed to the direction of the previous loading path and hence the change in direction of loading before the common loading path. While other data exist these data provide the most direct evidence of stress path threshold effects. In the case of time threshold effects much data are available but generally only relating to isotropic or one-dimensional compression and swelling. The evidence indicates however that periods of up to 100 days may be sufficient to cause significant changes in sample stiffness for laboratory samples.

1.3 Objectives of the Present Research.

This research dealt with the threshold effect in soil deformation. The object was to study these effects by a series of laboratory tests using a computer controlled stress path triaxial apparatus. In view of the time required to develop significant time effects only stress path effects were studied in detail.

Initially the object of the testing program was to confirm that such effects do occur as a result of soil behaviour and not due to various equipment effects. The type of tests conducted were identical to those of Atkinson (1983a) which are described in chapter 2. Tests then examined these effects for a number of soils in order to determine which soil types are most susceptible to these effects. Using one particular soil, tests were conducted to determine the effect of consolidation history , overconsolidation ratio and also to determine if it is the total or effective stress deviations of path which are responsible for causing these effects. All these data were analysed with the object of determining the size of a threshold zone and the effects if any on sample stiffness, strain increment ratio, and failure states with varying deviations of stress path. Finally a limited number of tests on samples subjected to both deviations of stress path and short periods of rest were conducted with the object of determining if these effects are additive to produce an effect greater than either acting alone. The form which mathematical models may take will also be indicated although these models were not implemented.

In addition to the main test series these data provided much data of the form normally acquired in the course of tests for path dependence. These data were analysed and reviewed in the light of the data provided by the threshold tests.

1.4 Outline of Thesis.

This thesis is divided into a total of ten chapters and two appendices. Chapter 2 divides into three sections. The first section reviews some of the general methods used in deformation analyses and the type of stiffness data required. The second section reviews some of the factors known to affect soil stiffness. This chapter concludes with a review of the evidence available for both stress path and time threshold effects. Chapter 3 reviews some commonly used soil models and the assumptions made regarding values of stiffness with varying state and stress path. This chapter continues with a review of models describing threshold effects and those describing similar effects.

The proposed test program and the general test types to be conducted are discussed in Chapter 4. Chapter 5 gives details of the equipment used for the soil tests and Chapter 6 the calibration of the apparatus including the calibration for system compliance. Chapter 7 gives details of the preparation of soil samples and a detailed account of how the tests proposed in Chapter 4 were conducted.

The analysis of the results and the presentation of the basic test data are given in Chapter 8. These results are discussed in Chapter 9 with further analyses of the basic results are given. In addition two soil models are proposed which reproduce some features of the test results.

In Chapter 10 some conclusions from Chapter 9 are drawn together and suggestions are made for further research. Finally some additional material is presented in appendices 1 and 2 which discuss the rate of test in triaxial tests and some of the factors which influence the accuracy of measurement of the specific volumes of samples.

CHAPTER 2

REVIEW OF FACTORS AFFECTING SOIL STIFFNESS

"A young fellow in the office had a saying he repeated whenever the subject of the opposite sex was mentioned: "Women are all alike with a blanket over their heads": no need to be selective."

"If there are any young fellows reading these lines, my advice is to shop around for someone with similar interests and aspirations. Women may all seem alike with a blanket over their heads, but they are not."

Wainwright,A.(1987). Ex-Fellwanderer. Westmorland Gazette.

CHAPTER 2 REVIEW OF FACTORS AFFECTING SOIL STIFFNESS.

2.1 Introduction.

The purpose of soil mechanics and soil testing is to provide parameters for the design of earth structures. For any structure there are two main requirements; firstly there must be an adequate factor of safety against collapse and secondly, at working loads deformations must be such that the structure remains serviceable and deformations acceptable. Until recently it had been normal practice to deal with these two problems in separate analyses.

It has been found that while strength parameters may be determined reasonably accurately, the stiffness parameters required in the deformation analysis are much less reliable as determined from standard laboratory tests.

In this chapter some of the reasons for the problems of obtaining reliable stiffness data will be discussed with particular reference to threshold effects. This discussion will include the effects of sampling and the methods used in performing tests and calculations which are relevant to both undisturbed soils and laboratory produced reconstituted soils.

This chapter divides into three sections. The first deals with some of the general methods used to assess the deformations in earth structures. The second section deals with the factors which affect the stiffness parameters required in those calculations. The third and final section deals with the evidence for the existence of threshold effects and a review and comparison of some laboratory and field data.

2.2 Methods of Determining Soil Deformations.

This section will deal briefly with the general methods used to determine soil deformations. Specific details of soil models will not be given, these are discussed in Chapter 3. The methods covered include elastic calculations, stress path methods and computer methods. Empirical methods will not be considered.

Some references to and examples of soil models used will be given in this section. For a full discussion of these models and the definition of parameters the reader is referred to Chapter 3.

2.2.1 Classical Elastic Analyses.

The first stage of most deformation analyses is to assess the state of stress in the ground and the changes of stress caused by the imposed loading. For many situations in practice an elastic model is used. Standard solutions have been developed from Boussinesq's expression for the stress distribution below a point load (Boussinesqu , 1876). These include various shapes of applied load and distributions of loading (e.g. Jurgenson , 1934; Newmark, 1935; Fadum, 1948;

Poulos and Davis, 1974). These solutions assume the soil to be a layer of infinite thickness, and to behave as an ideal isotropic, homogeneous, linear-elastic continuum. Alternatively influence charts may be used to simplify analyses (Newmark, 1942). In these solutions only the Poisson's ratio for the soil influences the stress distribution. Since Poisson's ratio varies very little for most soils, the stress distributions can be assessed quite easily, hence the sensitivity of these solutions to the elastic properties is small (Morgenstern and Phukan, 1968; Atkinson, 1981). By using superposition of solutions almost any shape of loaded area can be accommodated. In practice the idealisation of the soil as an isotropic, homogeneous, linear elastic continuum can often represent an unacceptable approximation of the behavior of a real soil. Solutions for layers of finite thickness with a rigid base have been developed by Biot (1935) and Burmister (1945). Tables and charts have also been developed for multiple horizontally layered media (Acum and Fox, 1951). Anisotropy has been included by Hooper (1970) and Gibson (1974). This has been shown to have a significant effect in some cases on the stress distribution below a foundation. Finally solutions have been given for the case of an inhomogeneous soil (Gibson, 1967; Brown and Gibson, 1973). The variation of properties chosen was that of a stiffness modulus varying with depth linearly from an initial value of depth zero. This is of particular significance since from the data from back analysed structures this appears to be the typical stiffness variation in natural soils. Some of the more complex solutions above are more easily implemented by computerised methods.

Once the stress changes have been calculated the strains in the soil may be computed. For this purpose a Youngs modulus, E, and Poissons ratio ν , are required. Calculations may be performed either for drained or undrained conditions by use of suitable parameters. In the case of rapid loading where an undrained calculation is performed, this may be followed by consolidation. It is then normal to use the coefficient of volume compressibility, m_v , as determined from an oedometer test to determine strains during the consolidation stage.

In practice these calculations may be performed in a single stage without computing the stress distribution in the soil by use of charts and influence factors relating surface loads and deformations. Charts are given in many text books (e.g. Terzaghi and Peck, 1967); Scott, 1980; Atkinson, 1981) and are usually based on the work of Steinbrenner (1934) and Newmark (1942). The advantage of computing the stress distribution is however that it allows the selection of a suitable secant stiffness modulus to be made for soils which have a non-linear stress-strain response. Where the parameter m_v , is used in drainage calculations, various modifications and corrections may be applied to allow for the deviation of conditions from those observed in the oedometer (Skempton and Bjerrum, 1957) and for loads which are applied at some depth below the surface in the soil mass (Fox, 1948).

2.2.2 Stress Path Methods.

As will be discussed in detail later in this chapter soils are often highly path dependent in their behaviour. In an effort to overcome these problems various stress path methods of determining soil

parameters have been proposed (Lambe, 1964, 1967; Davis and Poulos, 1963, 1968; Simons and Som, 1970). The stress path method described by Lambe (1964, 1967) requires special loading paths as does the stress path method of Davis and Poulos (1963, 1968) but the method due to Simons and Som (1970) does not. This final method only requires the accurate determination of the material parameters (isotropic or anisotropic) and then these parameters to be applied to the correct stress paths followed by soil elements. The assumption is therefore made that these parameters are independent of path followed.

The stress path method described by Lambe (1964, 1967) proposed the use of special stress path tests to predict soil deformation. The triaxial test is used to simulate the stress changes predicted for representative points in the ground beneath the loaded area. A sample is first brought to the initial stress state predicted in the ground. The sample is then subject to the changes of stress anticipated at that point either drained, undrained or partially drained, and the strains observed. Generally these stress changes will be those predicted by elastic theory as described in section 2.2.1. Using these strains the field deformations may then be predicted. This method does not require the determination of elastic parameters for the design process.

The stress path method of Davis and Poulos (1963, 1968) used triaxial tests in the same way as that of Lambe but the results are not used directly. They are instead expressed as elastic moduli for use in expressions similar to those of section 2.2.1. The only difference is therefore, that this method determines the appropriate elastic parameters for a given predicted path and so accounts for path dependence of these parameters.

The method proposed by Simons (1970) calculated surface settlements from a method similar to that proposed by Skempton and Bjerrum (1957). It was observed from tests conducted by Som (1970) on undisturbed London clay that while the volumetric compressibility, m_v, was relatively independent of stress path, the ratio of strains $\varepsilon_1 / \varepsilon_v$ was not. It was proposed that this ratio should be determined either from a stress path approach or with little loss of precision by appropriate elastic theory (anisotropic in the case of London Clay).

Ladd and Foott (1974) proposed a stress path method which differs in some important details from those described above. This method was termed SHANSEP. It was proposed that undisturbed samples should be loaded to stresses in a triaxial cell exceeding the pre-consolidation pressure and then swelled to a range of overconsolidation ratios. Standard drained or undrained tests were then performed and the soil parameters obtained normalised with respect to suitable parameters e.g. the maximum vertical stress, for use in design calculations. The method was intended for use with soft soils, the objectives of this approach being to reduce the effects of disturbance by reconsolidating samples. Tavenas and Leroueil (1979) have indicated that this method may in fact destroy the in-situ structure of some soils by use of this consolidation stage.

The disadvantage of these methods is that they generally require specialised testing equipment in order to apply the special loading paths. Indeed in some cases where the loading path does not

correspond to one of axisymmetric conditions , the triaxial test cannot follow the correct path and so a three-dimensional testing apparatus would be needed. A further point was noted by Simons (1984), which may make the interpretation of stiffness data from such tests difficult. It is observed that if a sample is reconsolidated to its pre-consolidation pressure some consolidation of the sample is observed compared to when the sample last attained that state. As a result the sample must be consolidated well past its previous maximum pressure to ensure that the normally consolidated state has been reached.

2.2.3 Computer Methods.

All of the above methods may be implemented on a computer if required. For complex problems this will often be necessary. The use of a computer however allows more advanced analysis techniques to be used such as the finite element method which is considered here. The operation of the finite element method and the selection of suitable elements and numbers of elements will not be discussed here. For such details see for example Naylor et al (1981), Gunn and Britto (1982), Woods (1986a).

This method differs from those described above in that the stages of calculating the stress distribution and of the deformation analyses are combined into one. For this reason such programs are often used in order to determine the stress distribution in cases which are either very complex or difficult to analyse by methods described above. This method may be implemented using any incremental stress-strain relationship desired, elastic or elasto-plastic.

Some of the soil models which have been used in finite element analyses and the problems encountered with them have been discussed by Ko (1980), Naylor et al (1981), and Woods (1986a). For each element of soil or surrounding structure, behaviour is described by constitutive relationships which may be different for different elements, hence layering and variation of properties with depth may readily be accommodated. Typical models used include elastic (e.g. linear, hyperbolic or K-G), elasto-plastic (e.g. Cam clay) or elasto-visco-plastic.

Elastic models may be of two types, those which are differential, and those which are non-differential. Those which fall into the category of non-differential models usually fit a curve to the stress-strain data such as the hyperbolic model (Ladd and Foott, 1974). Some adjustments are often necessary to ensure that these curves include the required failure point (for example in the case of the hyperbolic model see Duncan and Chang (1970). In the case of this model behaviour is determined from the equation,

$$\sigma'_1 - \sigma'_3 = \varepsilon_a / (a + b\varepsilon_a) \qquad 2.1$$

where a and b are constants. This model is non-differential since it relates the stress state to the accumulated strains rather than increments of stress to increments of strain. In practice it has proved necessary to allow the "constants" a and b to vary according to test path and sample state.

In the formulation of this approach used by Seed et al (1975) up to nine parameters are needed to define the values of a and b.

Differential elastic models are described by incremental relationships linking increments of stress and strain. Any set of elastic parameters may be chosen (see Chapter 3 for details), however many models are expressed in terms of invariants p', q', ε_v and ε_s so that suitable parameters may be the bulk and shear moduli, K' and G', respectively to give the equations,

$$\delta q' = 3G'\delta\varepsilon_s \qquad 2.2$$

$$\delta p' = K'\delta\varepsilon_v \qquad 2.3$$

for an isotropic soil. The parameters G' and K' may be constant or may vary in some prescribed manner for example in the K-G model (Naylor et al, 1981) these parameters are given by,

$$G' = G'_1 + \alpha_G p' + \beta_G q' \qquad 2.4$$

$$K' = K'_1 + \alpha_K p' \qquad 2.5$$

where α_G, α_K, β_G, G'_1, and K'_1 are all constants. It should be noted that these equations may not fully satisfy conditions required for elasticity as defined in Chapter 3. Further details are required in this model in order to define yielding and failure.

The use of elasto-plastic models such as Cam clay, in finite element calculations is increasing. The model may be expressed incrementally and then used in a similar way to the K-G model above. Details of the specific forms of these equations are given in Chapter 3. The implementation of these models is discussed by Gunn and Britto (1982) and Woods (1986a). Similar models of this type have been developed e.g. Simpson et al (1979).

The attraction of the finite element method is that the soil response need not be modelled as linear, in practice any desired set of equations could be used. The method can handle very complex geometries of loading and very complex loading paths but relies for its accuracy on the soil model used. If required the method can include coupled consolidation analyses (Biot, 1941) in a constitutive model. It should be noted that the finite element method is normally applied incrementally, that is in small steps of applied load or small steps in time. The accuracy of calculations is very sensitive to the number of elements used to model the soil under load. While increasing the number of increments and elements may improve accuracy it will also greatly increase the time and cost of such solutions. The stiffness moduli appropriate to such calculations are tangent moduli which may be contrasted with the secant approach described in section 2.2.1 of the classical methods of deformation analysis.

2.2.4 Problems in Deformation Analyses.

It is found that the stress distribution in the ground can be reasonably accurately determined. Even using an elastic model the errors are relatively small. This is due to the equations given for stress distributions (e.g. Poulos and Davis, 1974) being insensitive to the magnitudes of stiffness moduli, only the Poisson's ratio and in the case of the anisotropic model the ratio of the vertical to horizontal stiffness are required in calculations. The difficulties arise when trying to determine the ground movements from these stress changes. The ground movements are highly dependent on the stiffness moduli and it is these moduli which prove difficult to determine. Reviews of deformation parameters for soils are normally given in terms of the undrained Young's modulus E_u, the coefficient of volume compressibility m_v, and the drained Young's modulus E'. Such reviews have been given by Butler (1975) and Ladd et al (1977).

In many cases the precise definitions of moduli are not given which makes comparison difficult. Often they are simply termed deformation moduli. In all but a very few cases they are secant moduli quoted at a given percentage of deviator stress at failure (normally 20%, 33% or 50%) or at a given strain level (normally ε_a = 1%). Where unload / reload loops are used the values of such moduli are highly sensitive to the size of such loops and the stress levels at which they occur. Often these important factors are not given.

The analyses performed based on laboratory data are rarely within 20% of the field values and in some cases errors of up to 50% or more are observed. These errors are partly due to the model of soil behavior used, partly the inhomogeneity of soil, and partly due to modelling of the behaviour of the structure. For example the modelling of soil consolidation by use of a coefficient of volume compressibility m_v from oedometer tests introduces errors due to the greatly reduced lateral restraint observed in the field compared to the oedometer. The evidence appears to indicate that improved understanding of soil stiffness would most improve deformation predictions.

It is generally found (Ward et al, 1959) that routinely determined laboratory measurements of stiffness greatly underestimate the field values of such moduli. It is the object of the remainder of this chapter and this research in general to examine some of the reasons for the discrepancies observed.

2.3 Factors Affecting the Measured Soil Stiffness.

The measurement of soil stiffness has proved to be very difficult judging from a comparison of typical field and laboratory data. In this section some of the factors affecting the measured stiffness will be discussed for both laboratory produced samples and undisturbed samples of soil. The areas which will be considered include,

a) sample selection,
b) sample disturbance,

c) initial consolidation history,
d) current state of sample,
e) stress path followed,
f) temperature,
g) rate of test,
h) apparatus flexibility,
i) definition of stiffness moduli,
j) threshold effects.

These sections have been arranged in the order that these factors may be encountered in a typical laboratory investigation i.e. starting with sampling and finishing with interpretation of the results. In general each point is discussed with particular reference to the triaxial test although data relating to other types of laboratory test apparatus are referred to where relevant. Finally threshold effects are discussed. It will be seen that some of the features of threshold effects would appear to overlap with some of the other factors considered e.g. sample stress history and stress path threshold effects. However, the factors significant to threshold effects are not considered in standard laboratory testing practice even if design parameters are determined from a stress path approach as described in section 2.2.3.

2.3.1 Sample Selection.

In obtaining parameters for design only a limited number of tests may be conducted. In deciding which tests should be conducted two factors must be considered. Firstly those stress paths which can be considered as representative of the soil mass should be followed, and secondly samples must be large enough to contain a representative sample of the soil fabric.

The first factor may be dealt with by conducting tests on a sufficient number of appropriate stress paths. This is rarely done since "standard" triaxial tests and laboratory tests in general allow for only a very limited number of stress paths to be followed. Specialised equipment is required to follow complex and varied stress paths. Often this is unavailable.

The second factor however depends on the soil being tested. For intact uniform homogeneous soils there is little advantage or disadvantage in varying the sample size. For laboratory prepared samples it is likely therefore that unless the grain size is very large that 38mm diameter samples will be adequate. For undisturbed samples however a representative sample of the soil fabric must be included. Samples should contain fissures if they are found in the soil since failure to do so would result in the stiffness of the soil being overestimated. Data for undisturbed London Clay presented by Marsland (1971a) showed that the stiffness of 38mm samples is greater than that for 100mm samples. This was due to the 38mm samples containing less fissures per unit volume than the 100mm samples. Data from Costa-Filho (1984) also for undisturbed London Clay showed a similar trend, however Costa-Filho noted that it was important to differentiate between those fissures which are closed and those which are open. Closed fissures may result in only a 10%

reduction in stiffness but open fissures may have a greater effect as noted by Marsland (1971a). In a similar way in soils with a significant stone content e.g. glacial tills (Anderson and McKinlay, 1975); McKinlay et al, 1975), a representative sample of such stone content should be included in the sample. Failure to do so may result in a stiffness much lower than that of the whole soil.

These factors dictate the size of sample which should be tested; in general the smallest size possible is chosen in order to minimise testing times. The sample size must remain large enough to be of the same scale as the fabric of the soil, this has resulted in samples up to 250mm in diameter for some glacial soils. In both the cases discussed above the scatter in results is also reduced by the use of larger samples due to the reduction in the variability of samples. It should be noted that the effect of sample size may increase or reduce stiffness depending on the type of fabric present. Even when testing large samples however, the heterogeneous nature of deposits results in some scatter in the stress-strain curves obtained.

2.3.2 Sample Disturbance.

The subject of sample disturbance is very complex. Only a few general aspects will be considered here. Disturbance may be divided into a number of headings for example, mechanical, stress relief and temperature. Probably due to the complexity of the subject and the difficulties in assessing the true effect of these factors this has often been given as the main reason for the lack of correspondence of laboratory and field data. Each of these factors will be briefly discussed below.

Extensive reviews of the effects of sampling have been given by Terzaghi and Peck (1967), Hvorslev (1949), Clayton (1984) and Simpson et al (1980). Most of this work has concentrated on the effects of disturbance on the strength of samples rather than the sample stiffness. The degree of disturbance determines the use to which samples may be put. Those subject to the greatest disturbance may only be used for classification purposes while those used to determine stiffness data must be of the highest quality e.g. block samples where possible.

2.3.2.1 Stress Relief.

Total stress relief is unavoidable in the process of sampling. The important factor is the magnitude of negative pore pressures which a soil may sustain in order to prevent swelling. If sufficient negative pore pressure cannot develop the sample may swell and so could be changed irreversibly. In addition gasses may come out of solution from the pore water due to reduction of total stresses.

In the case of intact clays these pressures may be very high (Bishop et al, 1975). However if the clay is fissured these pore pressures may be greatly reduced and so allow fissures to open. As a result there may be a limiting depth from which samples may be recovered if they are not to suffer a severe loss of stress memory. This has been discussed in detail by Wallays (1980) who has shown that the critical depth may be quite shallow (in the case of Boom Clay, 3m to 5m for samples from

above the water table or 6m to 10m if the water table co-incides with the ground surface). Costa Filho (1984) noted the effect of fissures opening was to greatly reduce the stiffness of undisturbed London Clay.

The effect of stress relief has been examined by Skempton and Sowa (1963), and Hight, Gens and Jardine (1985). Skempton and Sowa (1963) observed that by reducing the axial stress to the value of the radial stress and commencing an unconsolidated undrained test a large reduction in stiffness was observed for a normally consolidated sample of Weald Clay. Hight, Gens and Jardine (1985) observed similar behaviour for a North Sea clay when normally consolidated but for overconsolidated samples there was very little effect on stiffness. It should be noted however that due to reductions of effective stress in the sample the normalised stiffnesses increase and do not reduce.

Kirkpatrick and Khan (1984) investigated the effect of storage time on samples subject to stress relief using reconstituted kaolin and illite. They observed very large drops in the shear strength of unconsolidated undrained samples, approximately 50% after 50 days, and even larger reductions in the stiffness of samples, up to 86% reductions (undrained stiffness at half q_{max}). Much of these losses were regained on reconsolidation of samples. The samples showed a rapid loss of suctions and appeared to behave as if heavily overconsolidated after periods of storage. Such behaviour would appear to indicate swelling of samples, however details of water contents were not given. Since these results are at variance with those discussed above and other data discussed later regarding blocks of London Clay stored for long periods (up to 2 years) these data should be treated cautiously.

2.3.2.2 Mechanical Disturbance.

Mechanical disturbance has been the subject of a large amount of research which has been reviewed by Simpson et al (1980). In general it has been found that block samples are required in order to obtain reliable results especially in soils with unusual characteristics e.g. McManis and Arman (1979) testing a cemented clay found tube samples destroyed the cemented fabric. It is generally observed that higher stiffnesses are recorded for block samples when compared to tube samples and the pre-consolidation pressure is better defined in a specific volume, against log pressure plot. The reason given for these observations is the reduced disturbance experienced by samples.

Unconsolidated undrained tests conducted by Skempton and Sowa (1963) on normally consolidated Weald Clay indicate that where a large degree of mechanical disturbance occurs the strength and stiffness of a sample may be greatly reduced reflecting the greatly reduced suctions in the sample. In effect the sample behaves as if heavily overconsolidated, Fig 2.1. Similar conclusions have been reached by Hight, Gens and Jardine (1985) testing a North Sea clay. For an overconsolidated sample a similar reduction in strength and stiffness was also observed. Data from Hight, Gens and Jardine (1985) show a progressive reduction of stiffness of samples in

unconsolidated undrained tests as disturbance increases from "perfect" (stress relief only) to gross disturbance (i.e. major remoulding of samples), Fig 2.2 and table 2.1. The reduction is most significant in normally consolidated samples while for overconsolidated samples the effect reduces with increasing overconsolidation ratio. It is also noticeable that the stress paths are changed less in the case of the overconsolidated samples than those of the normally consolidated samples as a result of disturbance. The changes which occur may be explained in terms of the different strain paths (Baligh, 1984) and hence the stress paths followed by various elements of the soil during sampling which result in changes in sample suctions before testing (Hight, Gens and Jardine, 1985). For cases where samples have not been subject to gross disturbance and where the original soil structure is not significantly affected by ageing or cementing the use of the SHANSEP method (Ladd and Foott, 1974) may be used to recover in-situ stress-strain behavior.

2.3.2.3 Temperature.

The effect of temperature is referred to here in the context of sample disturbance. Some of the effects of temperature on tests in progress will be discussed in section 2.3.6. The effect of temperature on the negative pore pressures generated in a sample has been considered by Hight (1983). In general the conditions in the laboratory are much warmer than those existing in the ground, as a result the negative pore pressures in a sample may be reduced. The result is a loss of stress memory. In practice it proves very difficult to compute the effect of temperature on the negative pore pressures due to difficulties in the determination of constants required for the calculations. Sandroni (1977) suggests that the change in suction may be as much as 5 kPa / ^{0}C for London clay, while for illite Campanella and Mitchell (1968) observed a change of approximately 1 kPa / ^{0}C. Other data presented by Mitchell (1969) indicated for a range of soils the change in pore pressures lay in the range of 0.7 kPa / ^{0}C for Weald clay to 7 kPa / ^{0}C for saturated sandstone. Such changes depend on the mineralogy, the structure and the water content of the soil in question. These changes were also observed to be not completely reversible over cycles of temperature change.

Further changes may occur due to the drying of the surface of the sample during preparation for testing. This may be of particular significance when preparing triaxial samples from blocks. Although it will generally be the surface which is affected (Costa Filho, 1978a) it is very important that samples are prepared and installed in the apparatus and protected from further drying as rapidly as possible. This drying of the sample surface results in an increase of sample suctions. Further changes may occur however once the sample has been placed in the triaxial cell. If side drains are used any free water may be absorbed by the sample causing loss of suction. Water may also be taken from wet membranes surrounding the sample. Dry membranes may have the reverse effect and cause a drying of the sample surface with increase of suctions. Changes may also occur due to water in the porous stone at the end of the sample, the amount depending on the coarseness of the stone. Clearly these factors make assessment of the suctions measured in the laboratory very complex, these effects have been summarised by Clayton (1984).

2.3.2.4 Discussion of the Effect of Disturbance.

The determination of the effect of sampling on sample behaviour in the laboratory is very complex. It has been found that where carefully prepared block samples have been used e.g. Atkinson (1973), Costa-Filho (1978a) consistent results may be obtained even where storage periods have been over two years. This is not what would be expected however, since the opening of fissures would be expected to produce much more random results which may be significantly affected by the period of storage. In comparing data from both block and tube samples Costa-Filho (1978a, 1984) concluded that the blocks generally produced slightly higher stiffnesses with less scatter, however this was not conclusive within the general scatter of the results. The difference in behaviour of tube and block samples has been explained by Hight, Gens and Jardine (1985) for a North Sea clay by the stress paths applied to the sample and the effective stress changes which occur as a result in the sample during the process of sampling. It is possible therefore that by careful sampling and correct laboratory procedures i.e. temperature control and careful setting up of samples, that the effects of sampling may be minimised. The precise effect of disturbance depends on both the state of the sample (normally or overconsolidated) and on the plasticity in the case of clays (Hight, 1984). In each case however it has been shown by Hight (1984) that the d screpancies in data from unconsolidated undrained tests may be reduced by reconsolidating samples by following a suitable stress history. If for example an isotropic reconsolidation path is used as opposed to an anisotropic path on an anisotropic soil then errors may remain in the measurement of strength but also to a much greater degree in stiffness.

It is notable however that Wesley (1975) testing the same London clay as Atkinson (1973) did not obtain the same regular consistent results from block samples. This may be due to the high degree of fissuring observed in these blocks. The success of tests by Costa-Filho (1978a) in reproducing high stiffnesses observed in the field in laboratory samples is encouraging. It is confirmed by the observations of Hight, Gens and Jardine, (1985) that for soils of high overconsolidation ratio stress relief alone is not very significant, although the reconsolidation of samples in an anisotropic state may produce further improvements in agreement with field data (Costa-Filho,1978a). The results of comparative tests appear to show that so long as good samples are obtained and are not allowed to deteriorate during storage e.g. by changes in water content , they will yield moduli which are little affected by the process of sampling, provided that the samples can sustain the negative pore pressures resulting from stress relief. This discussion of disturbance has been restricted. Many other categories may be defined (Clayton, 1984). Each stage of the drilling, sampling, storage and sample preparation procedures causes some disturbance. Of those factors not considered the effects of chemical interaction of the soil and sampling tube and drying out due to poor sealing of samples are probably most significant. It should be noted however (Clayton, 1984) that all tests including field tests are subject to some degree of disturbance which is caused in the process of drilling a borehole. Parry (1979) stated that the difference in laboratory and field measured stiffness moduli could not in his opinion be accounted for as solely due to disturbance. Although samples are subjected to large cycles of stress during the sampling process sample disturbance may not be such a significant factor as has

previously been considered. In all but very sensitive soils or those with special fabric features which may be destroyed by stress relief, it is likely that samples of sufficiently good quality can be obtained for laboratory measurements of stiffness. In cases where this cannot be done even field data should be treated with extreme caution due to the inevitable disturbance caused during field testing. In tests conducted by Jardine et al (1985) on London Clay it was found that normalised field stiffnesses were approximately the same as those obtained from reconsolidated tube samples and about 20% higher than those from unconsolidated tests. These data illustrate that disturbance may not be significant in heavily overconsolidated clays. In general it is found that disturbance reduces the measured stiffness and so where it is suspected that this could be a significant factor higher values of stiffness are favoured.

2.3.3 Initial Consolidation History.

The effect of the initial consolidation history refers to the stress changes applied to the soil during compression and swelling from a slurry state or from natural deposition. This does not include small changes in stress which have subsequently been applied. In the case of natural soils compression generally takes place under conditions of approximately zero lateral strain i.e. one-dimensional or K_o compression. In standard triaxial laboratory tests however samples are prepared isotropically and all testing commences from an isotropic state. Natural samples may therefore show the features of structural or stress induced anisotropy (Wong and Arthur, 1985).

Investigations of the shape of the state boundary surface for anisotropically compressed soils have been made by Lewin (1970), Gens (1983), Robinson (1984), Koustofas (1980), Atkinson, Richardson and Robinson (1986) and many others (see Gens (1983) for others). In the case of tests by Lewin (1970) and Gens (1983) various consolidation histories were investigated. In the case of Robinson (1984) work was restricted to those of K_o conditions and normally compressed samples, while Koustofas (1980) also investigated K_o conditions only but for various overconsolidation ratios. It is observed from these data that with increasing η'_o, the stress ratio during consolidation (q'/p'), the stiffness in compression and extension increases compared with isotropically compressed samples, although by a greater amount in compression than extension for normally compressed and lightly overconsolidated samples. Similar results are observed as η'_o reduces (i.e. negative q'/p'), except that the stiffness in extension increases by more than the stiffness in compression. Data from Gens (1983) has been reproduced in Fig 2.4 to illustrate the change in stiffness with η'_o on strandard triaxial drained and undrained stress paths (these data were derived from plots shown in Figs 2.7 to 2.17 discussed in section 2.3.4). Costa-Filho (1978a), Costa-Filho (1979) and Hight and Gens (1979) have commented on the behaviour of K_o compressed overconsolidated undisturbed samples of London Clay and Lower Cromer till respectively, as compared to that of isotropically prepared samples. Hight and Gens (1979) observed that the section of the stress-strain curve for the one-dimensionally compressed sample above the isotropic axis was very similar in shape to that of the isotropic samples, Fig 2.5. However, the initial portion of the stress-strain curve of the one-dimensionally compressed

samples was steeper than for the isotropic samples by 10 - 15% in the case of undisturbed London Clay.

Changes in sample behaviour due to loading past the previous maximum stresses applied on a different constant stress ratio path to that originally followed may produce significant changes in sample behavior due to stress induced anisotropy. These effects probably commence as soon as the state boundary surface (see chapter 3) starts to expand. Tests conducted by Balasubramaniam (1969), Lewin (1978) and Gens (1983) all indicate a transitional region until a stress of about 2 - 3 times the previous maximum is reached, at which behaviour has changed so as to be indistinguishable from that of samples not subjected to the original consolidation stage. In the field these effects may not be as significant as for laboratory samples since structural anisotropy probably dominates behaviour to a much greater degree (Arthur and Menzies, 1972).

In the case of laboratory samples significant changes in behaviour have also been observed due to variations in the initial water contents of samples. Hight et al (1979) testing samples reconstituted from a slurry and remoulded samples of Lower Cromer till and Balasubramaniam (1969) testing Spestone kaolin compressed from slurries of different initial water contents, observed such behaviour. It was found that the slopes of the normal compression line and swelling lines reduced and the "equilibrium voids ratio" (the voids ratio at which the excess pore pressures are zero) reduced as initial water content of sample reduced. The samples therefore showed an increase of stiffness which was also reflected in shear tests to failure which followed.

These tests and others indicate that the correct stress path must be followed when consolidating samples in the triaxial apparatus for testing. Normal practice of following an isotropic stress history will produce an underestimate of the stiffness of the soil in compression tests. This feature is very significant for laboratory compressed soils in which in general structural anisotropy is not a major feature and also in lightly overconsolidated and normally consolidated natural soils.

2.3.4 Current State of the Sample.

The state of a soil sample may be described by the variables of the critical state model (see chapter 3). For the axisymmetric triaxial test these are, the specific volume v, the mean effective stress p', and the shear stress q'. The sample itself may be normally or overconsolidated. For general loading conditions an extra parameter is required to describe the value of the intermediate effective stress, σ'_2.

In general it is found that the shear stiffness of samples increases with increasing p' and reduces with increasing q'. Further it is found that the stiffness of an overconsolidated sample is greater than that for a normally consolidated sample at the same value of p'. These factors have been examined by Wroth (1971) for London clay, By plotting stress ratio η' ($\eta' = q'/p'$) against strain a series of curves were produced one each for each overconsolidation ratio. This suggests the normalisation of data with respect to p'. Furthermore by assuming that the equation of a swelling

line was linear, Wroth demonstrated that the bulk stiffness normalised with respect to p' may be expected to vary linearly with the logarithm of overconsolidation ratio. By using isotropic elastic theory similar arguments were made for both the uniaxial stiffness, E', and the shear stiffness G'. Data from undrained triaxial tests on samples from Ashford Common shaft (Bishop, Webb and Lewin, 1965) were replotted as E'/p' on a plot of specific volume against log p' (stiffness taken as secants at ε_a = 1%), Fig 2.6. The trend of data plotted as G'/p' and K'/p' also appeared to be linear with overconsolidation ratio and indicated a constant Poisson's ratio. Similar data for a number of soils were presented by Wroth and Houlsby (1985). This work is limited by two factors. Firstly the requirement of constant Poisson's ratio is found to be inadmissible under these conditions for elastic theory (Zytinski et al, 1978). Secondly the assumption of linearity of swelling and recompression curves is unrealistic. In practice not only is the variation of slope significant, but there is a difference in water contents of samples which have swelled and re-compressed to reach a given overconsolidation ratio at a given p'. It is interesting to note from this diagram that while E'_z in the field may be expected to increase with increasing depth due to increasing p', the normalised stiffness E'_z/p' reduces, since the overconsolidation ratio reduces with depth.

The effect of sample state is well illustrated by data from Gens (1983). Figs 2.7 to 2.17 show the stress-strain curves for anisotropicand isotropic samples of Lower Cromer till tested in compression and extension at various overconsolidation ratios. It can be seen that the stiffness generally reduces with overconsolidation ratio. However when normalised with respect to the axial stress at the end of consolidation, σ'_{ac} , a plot as in Fig 2.4 results. It should be noted that the data have been normalised with respect to σ'_{ac}, and not the current value of p' as by Wroth (1971), Figs 2.4 and 2.6 are therefore not directly comparable. Significant differences in the variation of stiffness of anisotropic and isotropic samples can however be seen.

Similar efforts at correlating data have been made by Wroth et al (1979) and Houlsby (1985). Wroth et al (1979) found that for a range of soils stiffnesses could be normalised with respect to p' while Houlsby (1985) found that data for sands could be normalised with similar accuracy with respect to either current p' of the pre-consolidation pressure, p'_c. Houlsby (1985) concluded that neither method was likely to be entirely correct and that the sample stiffness probably depended on both p' and p'_c. Data for Ware till (Atkinson and Little, 1986) shows the trend indicated by Wroth (1971) for both remoulded and undisturbed samples, the linearity of G'/p' against log OCR observed was probably due to the small variation of the slope of the swelling curve for Ware till.

In this section data has been normalised with respect to p' or in some cases σ'_a. It is common practice however to normalise data with respect to the undrained shear strength c_u . Due to difficulties in defining the precise value of c_u due to localised drainage in overconsolidated samples (Atkinson and Richardson, 1985b) and variation of c_u with stress path (Wroth, 1984), normalising with respect of p' is to be preferred. Some problems do occur in the field however since p' may prove difficult to estimate (Simpson et al, 1980) while a value of c_u may be available. This point regarding the selection of suitable normalising parameters will be discussed further in section 2.3.9.3.

2.3.5 Stress Path Followed.

The stiffness of a sample is highly dependent on the stress path followed. In standard triaxial tests it is observed that compression tests show a higher stiffness than extension tests on isotropically and one dimensionally compressed samples (Gens, 1983; Jardine et al, 1985). For the case of reconstituted London Clay from Bell Common stiffnesses in compression (E_u /p'_o .) exceed those in extension by about 50% (Jardine et al, 1985). In order to obtain the correct stiffness for use in calculations the correct stress path must therefore be followed. This is the purpose of the stress path methods described by Davis and Poulos (1968), Lambe (1964) and the SHANSEP method of Ladd and Foott (1974). It is important however to distinguish true stress path effects from those which occur due to a deficiency of the mathematical model used, i.e. those due to differing sample behaviour. In general mathematical models can be written incrementally as,

$$\delta\varepsilon_s = A\,\delta q' + B\,\delta p' \qquad 2.6$$
$$\delta\varepsilon_v = C\,\delta q' + D\,\delta p'$$

The precise meanings of these parameters will be discussed in Chapter 3. A true stress path effect would occur where different values of the parameters A, B, C and D are required to describe behaviour on different stress paths at a single stress state. In cases where an inappropriate model is used to describe behaviour e.g. use of the isotropic elastic model where the anisotropic model is needed, it may appear that the soil is path dependent when in fact a unique set of parameters could describe behaviour in an alternative model. Path dependence should also be expected where significant changes of sample state occur e.g. the comparison of paths for a normally compressed soil where some paths are directed outwards from the yield curve while others pass inwards to the overconsolidated region.

Cairncross and James (1979) observed that in general extension and compression behaviour of samples was different and so argued that an elastic model was inappropriate to exclusively describe any soil behaviour. Graham and Houlsby (1981) conducted a large number of different stress path tests on lightly overconsolidated samples of Lake Agassiz Clay (from Canada). They found that while significant path dependence would be predicted from use of an isotropic elastic model, by use of an anisotropic model a consistent set of parameters could be derived. The stress-strain response was however reasonably linear so there were few problems in determining elastic parameters.

Tests conducted by Richardson (1984a) on remoulded London Clay and Atkinson (1983b) testing Speswhite kaolin showed large differences in sample stiffness with stress path. In the tests by Richardson (1984a) samples were one-dimensionally compressed and swelled before being loaded undrained along the total stress paths shown in Fig 2.18. The values of the secant undrained stiffness, $E_u = \Delta\sigma'_a / \Delta\varepsilon_a$, at ε_a = 1%, shown in table 2.2 from Atkinson, Evans and Richardson (1984), show that the undrained stiffness varied by a factor of 3 for tests 5101, 6100 and 6102, all of which started from the same initial state. Similar results for sands have been derived by Lade and Duncan (1976). Others however, for example Varadarajan and Mishra (1980) (testing Badarpur Sand), have noted that the path dependence of stress-strain behaviour of sandy soils appears to be less than that for clay soils.

The stiffness of samples is also observed to vary with the intermediate effective stress σ'_2. Tests on Ham River sand by Symes (1983), Symes et al (1984) and Hight et al (1983) using a hollow shear apparatus, have shown that sample stiffness also depends on the value of σ'_2 and also on the orientation of the principal stresses with respect to the sample. Samples were anisotropic with the horizontal directions in the sample having similar properties, the orientation of the principal axes of loading was measured as the angle α^0, between the maximum principle stress and the vertical axis of the sample and the relative magnitude of σ'_2 by the parameter b (where $b = (\sigma'_2 - \sigma'_3) / (\sigma'_1 - \sigma'_3)$). The data showed that the stiffnesses of samples were greatest for $\alpha = 0^0$ i.e. triaxial compression and a minimum for $\alpha = 45^0$. In general it was found that the behaviour of samples as α varied was fully described by tests in which α was constant and only q' and p' varied.

These factors are particularly important when comparing results from different types of apparatus and from back analysed field data (Wroth, 1984). Different types of testing apparatus impose different restrictions on the test sample. As a result the different imposed stress and strain paths for similar types of tests (eg undrained) give different stiffness moduli. In order to compare laboratory data to conditions in the ground the stress path applied should be considered and in addition the effect of principal stress rotation on elements of soil. Certain types of laboratory test may be appropriate to certain cases of field loading due to the similarity of restrictions on the deformation of the sample under test.

The effect of stress path may also be considered significant to test procedures. In many stress path tests conducted in the past it has been standard procedure to apply loads incrementally. The procedure has been to apply a load increment with the drainage valve closed. The drainage valve has then been opened and the sample allowed to drain against a back pressure to reach equilibrium in a similar manner to oedometer tests, Fig 2.19. The effect of the load increment ratio may be significant where large increments are used. Clearly the two paths shown in Fig 2.19 are different and so if soils are path dependent the behaviour resulting from the the two paths, direct, and that of undrained loading followed by consolidation, will be different. Balasubramaniam (1969) studied this factor and showed that an increase in step size from 4.9 kPa (0.7 lb/in^2) to 180 kPa (26 lb/in^2) produced a decrease of sample stiffness by a factor of 2.3. It is therefore preferable to use an apparatus which can apply a continuous smooth loading path or one in which the steps are very small so that a continuous smooth loading may be applied to follow a stress path closely as intended.

2.3.6 Temperature.

The temperature at which a test is run at a given stress state may have a significant effect on the test results.

The results of consolidation tests in oedometers reported by Campanella and Mitchell (1968) for illite Fig 2.20, indicate a reduction of compressibility at a given pressure as temperature increases. It is observed that the normal consolidation lines are parallel but as temperature increases the voids ratio reduces at a given pressure (Fig 2.20). Similar results have been reported by Plum and Esrig (1969) for Newfield clay and illite, and by Laguros (1969) for a number of other clays. The effect of temperature on undisturbed samples was discussed in section 2.3.2.3.

In assessing the effects of temperature on the results of tests the effects on the soil sample itself and on the apparatus being used to conduct the tests should be considered separately. The apparatus may expand with rising temperature and so may record strains not occurring in the sample. Further errors may occur in the readings of stress and strain recorded from the instrumentation. Due to changes in temperature the calibration of instruments and of data logging equipment may change. In the sample expansion may occur, but more importantly due to the difference in thermal expansivities of the pore water and the solid part of the soil, changes in pore pressure will occur in undrained samples while in drained tests volume changes (as discussed above) will be observed. Ting (1968) indicates that for Spestone kaolin the pore water in a sample (not including drainage leads and volume gauge) will change in volume by about 0.022 cc / °C (for a 76mm x 38mm sample) which is equivalent to 0.026 % / °C. For these reasons it is very important that all tests are conducted in a laboratory with temperature control.

2.3.7 Rate of Test.

The rate of test selected in drained tests is such that the excess pore pressures developed in the sample may be considered negligible while in an undrained test the requirement is that the pore pressures have equalised throughout the sample to a degree which is considered acceptable. The selection of suitable values of excess pore pressure or degree of equalisation should be such that effects due to these errors should be negligible, this can either be done from experience or methods given by various authors e.g. Bishop and Henkel (1962), Atkinson (1984b). Balasubramaniam (1969) has demonstrated that provided sufficient time is allowed for dissipation of excess pore pressures there is negligible difference in behaviour for decreasing rate of test provided that the creep rate for the soil is not very high.

In practice high rates of test may lead to problems in samples with radial drainage. Atkinson, Evans and Ho, (1985) have examined this problem. A series of tests on Speswhite kaolin were conducted in which loads were applied isotropically at increasing rates and finally in one large increment to give a range of test rates of dp'/dt = 4 to 2560 kPa / hr plus single step loading of 200 kPa. Samples showed an increasing variation of water content as the test rate rose up to a maximum of about 1.5 %, Fig 2.21. These tests were modelled using a coupled consolidation model (Biot consolidation, Biot, 1941) by Woods, (1986b) who reproduced similar data using a finite element programme. The data in Fig 2.21 and from the finite element analysis also showed another interesting feature. Even at very low rates of test some non-uniformity of samples was observed (about 0.5 % water content in 38mm diameter samples). This was explained as being

due to the radial strains causing hoop stresses which resulted ,even in slow tests ,in a non uniformity of stress distribution across the sample. In one-dimensional compression tests modelled in the same way the effect did not occur. This variation of water content produces non-uniform samples which in the case of the kaolin tested, indicated a variation of effective stress of p' = 44 kPa, at an average stress of p' = 225 kPa, across the diameter of the sample. Clearly this represents a large variation of stiffness across the diameter of the sample (about 13%). Atkinson, Evans and Ho (1985) recommended that either very low rates of tests should be used to reduce the effect, or the radial drainage should not be used so as to minimise the effect further. This is therefore a further objection to incrementally loaded stress path tests discussed in section 2.3.5.

In tests conducted by Hight (1983) the time to failure in undrained triaxial tests was varied from 2 to 547,200 seconds. It was observed that the fastest tests tended to give the highest values of stiffness. However the difference in stiffness was small , and due to the small strains measured and high rate of test the results were not conclusive since stiffness moduli were not accurately determined.

The rate of test may not therefore be very significant, provided test procedures are followed which ensure that samples remain sufficiently uniform both due to case hardening effects (Atkinson, Evans and Ho, 1985), and non-uniformity due to incomplete drainage.

2.3.8 Apparatus Flexibility and System Errors.

Errors in the testing system occur due to a number of factors. They may be classified into three types of error,

a) random,

b) systematic,

c) gross errors.

Random errors are those which occur due to the precision of the measuring system i.e. the transducer and data logger , and system noise. They tend to be randomly scattered about a mean and are just as likely to be negative as positive in any given reading. They may be assessed by quoting a standard deviation about the mean.

Systematic errors occur due to the methods of measurement used. Such factors as system flexibility and drift fall into this category. It is most important to eliminate these types of errors since they affect the accuracy of recorded readings. Gross errors are those which occur mainly due to operator error e.g. inputting incorrect data, errors in control or recording of incorrect instrument zeros. Gross errors can be avoided by care when conducting a test, those due to random and systematic errors must be reduced to an acceptable level.

The difference between random and systematic errors is illustrated in Fig 2.22 which shows a number of readings which are displaced by an error in the accuracy of ΔA and are spread about a mean with a standard deviation of ΔP, the precision. It should be the main objective to eliminate systematic errors since these represent an otherwise undetected error. e.g. compressibility of system components registered as sample displacements. Although random errors are important since they should not swamp the readings taken, it is not such a critical factor since the mean of these readings is still correct and may be deduced if a sufficient number of readings are taken over a short period or integration time. This section will concentrate on the errors relevant to the triaxial test.

2.3.8.1 Apparatus Flexibility.

The effect of apparatus flexibility when determining strains cannot be overlooked. It is of great importance to determine accurately the displacements and stresses in the the sample alone as opposed to those in the measuring system as a whole.

Flexibility in the system occurs due to the way in which measurements of sample deformations are made. It is observed that generally where measurements are made a long way from the sample flexibility is of much greater significance than if measurements are made very close to or on the sample itself.

There are two approaches to the problem, firstly equipment may be calibrated in order to eliminate or reduce the errors due to flexibility or secondly, equipment may be designed in such a way that flexibility of the system is not significant. While in principle it is possible to calibrate for such errors it is often very difficult to do so, due to the fact that these corrections are often path dependent and dependent on procedures used to set up the apparatus. It is much better to eliminate such errors by design where possible.

In most triaxial testing systems the measurement of stresses is relatively free from errors due to flexibility but it is the strains which are not. The exception is in the measurement of the pore pressure in tests where the pore pressure varies, where deformations of the pore pressure transducer and pore water may affect readings taken. Typical errors include axial strains in the Bishop and Wesley triaxial cell due to,

a) compression of filter papers at ends of sample;

b) deformation of load cell strain gauges;

c) deformation of top and bottom platens and bending in the cell top plate;

d) movement of the threaded rod carrying the load cell;

and volumetric strains recorded due to,

e) changes in effective cell pressure causing expansion or compression of drainage leads;

f) expansion or contraction of belloframs in the volume gauge due to changes of pore pressure.

Since radial strains are normally computed from these quantities they are therefore similarly affected.

The problems of volume change measurement are relatively small provided precautions are taken to ensure drainage leads are a short as possible, stiff, the system filled with de-aired water, and provided that tests are conducted at constant back pressure (undrained tests do not require volume change measurements and so changes of pore pressure in such tests are not significant. Only in the case of coarse grained soils do errors become significant due to problems caused by membrane penetration (Molenkamp and Luger, 1981) where the membrane flexibility may cause false volume and pore pressure changes as the cell pressure varies. Such effects are not significant for clay soils.

Further errors also occur due to bedding, seating and tilting of the end platens and end restraint caused by friction between end platens and the sample. Errors due to bedding and seating are very significant in tests on concrete and rocks due to the non-uniform stress distributions which are set up in the sample. Jardine et al (1984) argued that for very stiff clays and sands similar effects were significant in triaxial tests and demonstrated the use of strain measuring devices mounted on the sample to eliminate these errors. These errors may alternatively be eliminated or reduced by careful test procedures as described by Atkinson and Evans (1985). It was suggested that by connecting the top cap at an early stage of the test i.e. during the consolidation stage, errors due to bedding could be eliminated in all but very stiff samples. Errors due to tilting and seating would be apparent in the early stages of the application of deviator stress and so could readily be corrected once the results had been plotted. Data from Gens (1983) appears to confirm these findings. The result of these types of error is to greatly reduce the measured stiffnesses of samples. It was observed by Jardine et al (1985) testing undisturbed London Clay, that even with corrections applied for load cell compliance the stiffness of samples was much less using external strain measurement than internal. In addition the stress-strain curves derived from devices on the sample membrane showed much greater non-linearity than those obtained from external strain measurements. The reason for this difference is unclear. The flexibility of the whole system in use must be considered, the above arguments strictly only apply to the Bishop and Wesley stress path triaxial cell. It should be noted that with soils of relatively low stiffness or where soils are compressed from a slurry state of high water content difficulties may occur with devices such as those of Jardine et al (1984) due to large strains developing which may allow relative movement of sample and membrane.

In such cases devices could be mounted directly on the sample with mountings penetrating the membrane surrounding the sample (see Costa Filho, 1978a for example). This system however suffers from the disadvantages of more complex and time consuming setting up techniques required and the possibility of some effects on sample behaviour if the devices penetrate the sample surface (Hight, 1983).

2.3.8.2 Other System Errors.

Other errors may occur in the system due to various factors. These include such factors as, errors in the measured stresses due to the stiffness of the rubber membrane and filter paper side drains and sample non-uniformities.

Errors due to the stiffness of the membrane and side drains result in an overestimate of the stresses applied to the sample and as a result an overestimate of the samples stiffness. For very stiff soils the effects are likely to be small, however for soft soils there may be a need for a relatively large correction to be applied to the measured stresses. This factor will be discussed further in Chapter 8 when considering the corrections to be applied to test data. Errors due to non-uniformities in samples occur due to a number of reasons, these include errors due to end restraint of samples, variation of pore pressure through a sample and the formation of slip planes.

Pore pressures are generally measured at sample boundaries and so will not necessarily reflect the pore pressures in the centre of samples. During drained tests the sample cannot be fully drained while drainage is taking place since excess pore pressures are required to cause the flow of water from the sample. By use of slow rates of test the magnitude of excess pore pressures may be reduced to an acceptable level.

End restraint results from the friction between the soil sample and the end platens. The result is non-uniformities of strain throughout the length of the sample, this has been the subject of much research (Roscoe, Schofield and Thuraijajah, 1963b; Balasubramaniam, 1969; Daramola, 1978). Compression samples tend to "barrel" so that the central part of the sample is of greater cross-sectional area than the ends while for extension samples "necking" occurs so that the sample area is smaller. Errors of up to 40% have been observed in strain measurements at failure (Roscoe, Schofield and Thurairajah, 1963b) if overall strain measurements are used. It is found that strains measured over the middle third of samples are reasonably uniform for triaxial samples with a height to diameter ratio of two but that the uniformity of strain distribution may be improved by the use of "free ends". Rowe and Barden (1964) described a typical system in which greased rubber discs are placed on the end platens above and below the sample. Due to instability of samples of a height to diameter ratio of two on such platens, samples are used with a height to diameter ratio of one. Tests indicate that samples deform more uniformly, are less likely to form slip planes at failure, and show a reduction of ϕ' by approximately 2 - 3°. The improvement of uniformity of samples is shown by the variation of water content of samples at failure which is better than $\pm 0.2\%$ compared to $\pm$ 0.75% for samples tested with fixed frictional ends. It was noted however that there were no

significant differences in stiffnesses and stress-strain behaviour at low stress levels (approx 50% of failure stress ratio). The use of free ends was therefore recommended in tests to failure and in particular those where slip planes may form.

While this improves the strain uniformity until immediately before failure, (Balasubramaniam, 1969), it contributes to the system flexibility as the rubber and grease layers may compress. It is found that the errors involved may be very large and may exceed the magnitude of the true strains in some cases if overall strain measurements are used (Sarsby et al, 1980). Furthermore the compressibility of free ends is difficult to calibrate due to the slow squeezing out of the grease.

The use of free ends with very stiff soils may lead to some difficulties. In concrete and rock testing it was observed that the use of free or rubber ends during testing caused a very large reduction in both strength and stiffness of samples. This was found to occur since the rubber ends had a much greater compressibility than that of the sample. Instead of samples being restrained by rough ends, tensile shear stresses were being developed at the sample surfaces causing the cross sectional area of the sample to increase at the ends at a greater rate than at mid height. Balla (1960) has investigated the stress distributions in samples subject to various degrees of end restraint using elastic theory. It is found that only the central portion of a sample may contain a region of reasonably uniform strains and stresses. Testing rock samples Hawkes and Mellor (1970) observed that even using very thin layers of compressible materials over the end platens could reduce strength by up to 12%, while for fully flexible platens e.g. made of rubber, the reductions of strength and stiffness were much greater. This occurred even though strains due to the free ends deforming had been accounted for in these analyses. They concluded that due to these problems the elimination of platen restraint or of "negative" restraint may be undesirable. Jaeger and Cook (1976) concluded that in order to minimise the effects of either restraint or of "negative" restraint that the lateral stiffness of platen and sample should be matched, so that for an isotropic elastic material the ratio of platen stiffness, E_p, to the sample stiffness, E_s, is given by;

$$\frac{E_p}{E_s} = \frac{\delta\sigma_3(1-\nu_p)-\delta\sigma_1\nu_p}{\delta\sigma_3(1-\nu_s)-\delta\sigma_1\nu_s} \qquad 2.7$$

If the cell pressure remains constant then this reduces to the condition, given by Jaeger and Cook (1976), $(\nu_p / E_p) = (\nu_s / E_s)$. This is not always possible due to the vast range of stiffnesses which must be catered for. In rock mechanics this has led in many cases to the use of platens made of the same material as is under test or the use of long samples with a height to diameter ratio of at least two. It therefore seems that a similar method would be appropriate for soils, that is either use platens matched to the initial stiffness of samples or use long samples as is standard practice already with rigid end platens. Although negative restraint does not appear to have been observed in soils it is a factor to be borne in mind. If free ends are used it is essential that internal strain measurements are made in order to eliminate errors due to the compressibility of the ends.

Finally a small error may occur in volume change measurements due to compression and swelling

of the filter paper of the side drains and discs at the ends of samples (Shimizu, 1981). Although the error is small it may be very significant in determining compression and swelling parameters for stiff overconsolidated soils. Clearly the use of side drains should be avoided wherever possible. Volume strains will also occur due to the membrane either absorbing water if dry or possibly releasing water if soaked during the first 48 hours of a test (Lewin, 1985). While these volumes are small they may be significant where the sample is very stiff. By far the greatest errors in recorded strains occur however if the pore water pressure system contains air. Bubbles will change volume under pressure and with changes of pressure. Throughout this discussion it has been assumed that the system is saturated. Due to the errors which may occur it is of the greatest importance to reduce the volume of air in the system to a minimum.

2.3.8.3 Discussion.

Many of the difficulties of axial strain measurement can only be overcome by placing devices on the sample (Burland and Symes, 1982; Symes and Burland (1984). This technique has been used successfully and extensively by Symes (1983) in the hollow shear apparatus and by Jardine (1986) and Jardine, Symes and Burland (1984) in the axisymmetric triaxial apparatus. These devices placed on the middle third of the specimen also eliminate many of the errors due to non-uniform straining of the sample. Devices can also be designed for the measurement of radial strain on the sample, these may help to reduce errors which occur due to bulging and necking of samples in compression and extension tests respectively. However it is not possible to measure directly the volume strains occurring in this same portion of the sample. Such devices prove extremely accurate up to the point at which the sample and membrane start to deform independently which appears to be at axial strains of about 5 - 6 % (Symes et al, 1984). While this limit is satisfactory for very stiff samples it may not be satisfactory for soft soils where these strains may be been attained before shear loading to failure commences, this is most likely to be attained in cases where long stages of one dimensional compression have been followed. Difficulties may also occur where the effective cell pressure is very low since independent deformation of sample and membrane may commence at much lower strain levels (Henkel and Gilbert, 1952). It has been shown however by Gens (1983) that by very careful calibration of the apparatus flexibility there may be little advantage in using internally mounted devices, the main advantage however is to eliminate the need for this calibration stage.

All these errors become especially serious when samples cease to deform homogeneously and slip planes start to develop as in heavily overconsolidated clays. Once this occurs relative displacements on the slip plane may be very large while the surrounding material essentially acts as rigid blocks, and localised drainage may take place (Atkinson and Richardson, 1986). Measurements made on the sample boundary may then not be truely representative of the state of stress and strain on the shear plane where deformations are concentrated (Roscoe, 1970). In such cases the calculation of the true current area of the sample and corrections for the stiffness of membrane and side drains becomes very complicated, as yet no satisfactory solution has been presented.

For good quality undisturbed samples and laboratory samples the factors discussed in this section are amongst the most important when attempting to accurately determine soil stiffness. The effect on sample stiffness is often neglected or not considered in standard laboratory practice.

2.3.9 Definition of Stiffness Moduli.

Once tests have been conducted on soil samples and the data corrected for various factors it is necessary to obtain stiffness parameters for design purposes. The stress-strain response of soils is in general highly non-linear. The stiffness relates the ratio of stress to strain under specified conditions but does not imply that any particular type of deformation is taking place e.g. elastic or elasto-plastic behaviour. The selection of stiffnesses to represent the response of the soil on a particular loading path is therefore very difficult and may appear to be somewhat arbitrary. It is likely that the selection of a single stiffness parameter as in the case of linear elasticity will not be sufficient.

The types of stiffness moduli which may be defined may be classified into those which are;

a) tangent or secant modulus;

b) defined with respect to stresses or strains;

c) for drained or undrained conditions.

It should be noted that while undrained conditions define a specific group of effective stress paths the drained condition does not. There are an infinite number of possible drained paths, that which is normally considered i.e. in the triaxial test with $\Delta\sigma_r = 0$ and σ_a increasing or reducing, is only one of those possible. Due to the path dependent nature of soils (as defined in section 2.3.5) moduli from different drained paths may not correspond. By use of the constitutive model for the soil those effects due to soil alone may be isolated. If the constitutive model for the soil were known then drained and undrained moduli may also be related, this has been shown by Atkinson and Bransby (1978) for the case of the isotropic elastic soil.

The choice of relating stress and strain via a stiffness also needs to be considered . The use of a stiffness rather than a compliance would appear to be historical. Although the value of the compliance may simply be expressed as the reciprocal of the stiffness, the compliance would prove more convenient for plotting purposes in the area of rapid changes of large stiffnesses at the start of loading. Fig 2.23 shows an example to illustrate the point. Close to $\eta' = 0$ the rate of change of stiffness is so great that it is difficult to appreciate the changes taking place or the precise value which should be used at a particular stress level Fig 2.23a. In the case of the compliances however it can be seen that the variation is much clearer Fig 2.23b. Although there are rapid changes of compliance as failure is approached this region is of little interest in deformation analyses. Many constitutive models are normally expressed incrementally in terms of

compliances e.g. the Critical State Models (Schofield and Wroth, 1968). Most finite element programs are written however in terms of stiffnesses and so for those purposes it is more convenient to use stiffnesses.

For the remainder of this section arguments are applied only to stiffnesses although they could apply equally well to compliances. It should be noted that no distinction will be made between drained and undrained moduli since these arguments apply only to the description of the shape of a non-linear curve.

2.3.9.1 Choice of Secant or Tangent Stiffness Moduli.

The selection of secant of tangent moduli should be appropriate to the type of calculation to be performed. When using a secant modulus the type of calculation will be one in which loading is applied either in a single step or in a number of very large steps. Boussinesqu type settlement calculations fall into this category. Clearly in such calculations the moduli must be carefully selected to correspond to the state of the soil in the ground at the end of loading and be defined over the loading increment applied i.e. the points between which moduli are taken must be defined. Due to the variation of state of the soil after loading a number of moduli may be required for different sections of the soil mass or alternatively a single modulus which gives a good average for the range of states below the loaded area.

Many modern soil models are applied incrementally in finite element calculations. In these types of calculations the loading is applied in a large number of very small steps and the soil state updated for the next increment of load due to changes occurring in the current increment. Such theories may generally be expressed in the form of equation 2.6 (page 59). The parameters A, B, C and D depend on the theory selected and the current state of the sample. The values of these parameters must therefore be continuously changing with the changing state of the sample. Expressed in the form of equation 2.6 these parameters are compliances however stiffnesses may be used if desired. For such incremental theories it is therefore appropriate to use tangent moduli defined at the appropriate state and not secant moduli. In all cases except where a linear stress-strain response is observed the tangent and secant moduli will differ in value. In the case of a shear test conducted to failure the secant modulus at a given point always exceeds the tangent modulus.

Most literature continues to quote values of secant moduli. The only explanation of this continued practice can be the ease with which such moduli can be derived from stress-strain data. However by use of a simple spline fitting computer program (Woods, 1985b) tangent moduli may readily be obtained from data. The advantages of using stiffness data when describing the shape of stress-strain curves has been discussed by Atkinson, Richardson and Woods (1986).

2.3.9.2 Choice of Defining Moduli with Respect to Stresses or Strains.

Once the decision has been made as to whether to use a secant or tangent modulus, the

appropriate method of definition must be selected. Data may be analysed either in terms of stresses or strains. Some of the possibilities for moduli are shown in Figs 2.24 and 2.25. In the case of tangent moduli, the modulus may be quoted at the origin, Fig 2.24a, or at a specified stress or strain level, Figs 2.24b and 2.24c respectively. In the case of secant moduli there are more choices. Firstly it may be defined from the start of a test stage over either a specified stress interval Fig 2.25a, of a specified strain interval Fig 2.25b. Alternatively the modulus may be defined over a specified stress or strain interval but at a particular stress or strain interval after the start of the test, Figs 2.25c and 2.25d respectively. In the case of isotropically compressed soils moduli are normally defined from the isotropic axis It must therefore be decided whether to take moduli from the start of the test or from the isotropic axis (Costa-Filho, 1978a).

It may therefore appear that the decision of whether to define moduli with respect to stresses or strains is of little importance since it is clearly possible to derive the same modulus in both cases. It is preferable however that stresses are used rather than strains. If the solutions for stress distributions below a loaded area are examined it is found that they are not highly dependent on the soil stiffness (Atkinson, 1981). Solutions given by Poulos and Davis (1974) for isotropic and anisotropic elastic soils indicate only a small dependence on stiffness parameters but a major dependence on the values of Poisson's ratios in all cases (see also section 2.2.1). The most accurate method of solution of boundary value problems is to first compute the stress distribution in the soil mass using estimated stiffness parameters and to use these stresses to select appropriate stiffness moduli to compute the strains. By a process of iteration using the stiffness moduli the computed stress distribution may be refined. In the case of finite element calculations in which this process is completed in a single stage, stiffness moduli are continuously updated by reference to the sample state in terms of q', p' and v (see Chapter 3 for definitions) and not the accumulated strains. This is reasonable since the state of a sample is defined with respect to a known fixed datum in terms of stresses, i.e. all measurements are absolute, whereas strains are defined relative to an arbitrary datum and so cannot be used to describe the current sample behaviour.

2.3.9.3 Selection of Normalising Parameters.

For the purposes of comparing stiffness data for a given soil at a number of states and stress conditions data is normalised with respect to an appropriate parameter. In section 2.3.4 the variation of sample stiffness with state was discussed. Using this information suitable normalising parameters may be defined.

In soil mechanics it is common practice to use the undrained strength, c_u , for normalising. However as discussed by Atkinson (1985b) there are often problems in defining the undrained strength and in particular for heavily over consolidated soils. Such soils often show the effects of localised drainage on slip planes , and so do not exhibit truly undrained behaviour. As a result the strength indicated by the sample is less than the true undrained shear strength. It is also difficult to relate the strength measured to the average water content of the sample. Further difficulties may

also come in relating data from various general stress paths (Wroth, 1984) due to the variation of undrained shear strength with the value of the magnitude of the intermediate effective stress, σ'_2. The undrained strength is therefore a poor choice of normalising parameter.

A much better choice would be to select the parameter vp' or p', where v is the specific volume and p' the mean effective stress. This choice is appropriate since as is shown in Chapter 3 many incremental stress-strain theories contain such parameters to normalise stiffness data. Such parameters may readily be determined in the laboratory for these purposes. In the field however these parameters are not so easily determined, especially p', and so the use of c_u continues. Despite the theoretical objections of normalising with respect to these parameters for elastic behaviour (Houlsby, 1981), it has been shown that such normalising parameters produce good results (Houlsby, 1985; Wroth et al, 1979).

In attempting to correlate data from different states one point is often overlooked. Data should be compared over similar ranges of similar types of behaviour e.g. over similar ranges of elastic or elasto-plastic behaviour. If this is not done then moduli cannot be expected to form a consistent pattern.

2.3.9.4 Discussion.

Some of the definitions used by various authors have been reviewed by Souto Silveira (1967), Atkinson (1973) and Costa-Filho (1978a). The non-linearity of stress-strain curves has been suggested by Simpson et al (1980) and Hight (1984) as a reason for the lack of correspondence between laboratory and field data. Typical laboratory test data is quoted at either a stress level of half the deviator stress at failure or at a strain level of 1%. Since such strain levels are greatly in excess of those observed in the field, the stiffnesses quoted are much less than those which may be expected in the field. The effect of strain level on the quoted moduli is illustrated by Fig 2.53 for London Clay showing data for laboratory and field cases. Data for London Clay derived from Model L.C. (Simpson et al, 1979) has been given by Simpson et al (1980) in terms of E_u / c_u against shear strain to illustrate the different secant moduli typically derived from various soil tests Fig 2.26.

The great differences in both drained and undrained moduli which could be quoted for any particular test are well illustrated by data presented from tests by Gens (1983), Figs 2.7 to 2.17. In particular Figs 2.8, 2.10, 2.12, 2.14 and 2.17 which illustrate the small strain behaviour of Lower Cromer Till. In data from Jardine et al (1984) stress-strain curves are given for a number of soils including a North Sea clay, Ham River sand, London Clay and Upper Chalk (see table 2.3 for summary). These tests illustrate the high secant stiffness of soils at low strains or stress levels, see Figs 2.27 to 2.29, and plotted as E_u / c_u against log axial strain show the variation of stiffness with strain level. Finally this data may be collected in normalised stiffness plots (E_u / c_u) in Figs 2.30 and 2.31. Fig 2.30 illustrates the effect of increasing strain level while Fig 2.31 illustrates the effect of overconsolidation ratio at a specified strain level on the normalised stiffnesses E_u / c_u and

E_u/c_u. This data does not however reveal the shape of stress strain curve in the same way that tangent moduli would.

It would therefore appear that for most purposes the use of tangent moduli is to be preferred, defined with respect to stresses. The reluctance of engineers to use tangent moduli rather than secant moduli may at least partially be explained by the fact that more effort is needed to extract such data from stress strain curves. Only in cases where an equation is known or assumed for the shape of such curves may tangents easily be determined (section 2.2.3). In other cases a numerical spline fitting technique could be used (Woods, 1985a). Tangent moduli have the further advantage of eliminating bedding and seating errors in calculated moduli. If plotted against strains these errors still appear in comparing different tests since it displaces data along the strain axis. By plotting against stresses this error may also be removed and hence give a true illustration of the shape of stress-strain curves. The use of secant moduli results in errors in the stiffness for all stiffnesses which reduces the measured stiffness (Fig 2.25e). Only in cases where the input to a constitutive model requires secant moduli should such moduli be used.

Due to the great variations in values of moduli which can be obtained from a single curve the definitions used must be clearly defined (Van Wambeke, 1980). In particular great care should be exercised when using terms such as Young's modulus, bulk modulus, and shear modulus since they have specific meanings in materials science.

2.4 Threshold Effects.

The term "threshhold effect" has been used to describe various factors of soil behaviour which do not conform to an expected pattern. For the purposes of this report however the definition outlined by Atkinson (1973) is used.

From observation of various test data Atkinson (1973) noted that,

> "Where a delay at constant stress state is involved or where the direction of the stress probe differs from the previous stress path the strains produced by a small stress increment may be very much smaller than the strains produced by a large increment or those where there was no rest period or where the direction of the stress probe did not deviate much from the previous loading path."

It should be noted however that the observation of a high stiffness or of non-linear behaviour does not necessarily imply threshold effects. This can only be established where data exist for either different rest periods or for different deviations of stress path before passing along the same stress path.

If these restrictions on the definitions of threshold effects are relaxed so as to include any effect on the soil which produces a change in sample stiffness on subsequent loading on a given path,

there are a number of other threshold effects which can be observed. For example where a sample is subject to an increase of temperature followed by a decrease to the initial temperature (Fig 2.32) . On continued loading the sample stiffness is observed to have increased in a similar way to that due to a period of rest at constant effective stress (Mitchell, 1969; Plum and Esrig, 1969). At least part of this effect may be due to accelerated secondary compression during the period in which the temperature was raised, and continuing secondary compression when the temperature is reduced again. Such effect may therefore be predominantly time effects (i.e. due to creep), although the cycle of temperature, may modify these time effects as compared to a sample held at both constant effective stress and at a constant temperature. Bjerrum (1967) also described a process which had the reverse effect of the other effects described here. In Norwegian clays it was observed that if leaching of salts took place the stiffness of the clay was substantially reduced. Such effects may be termed chemical effects.

There are therefore two principle types of threshold effect which will be discussed here, time effects and stress path threshold effects. These will be discussed separately below, although it should be noted that these are not necessarily separable effects. It is possible that a prolonged period at constant effective stress followed by a different stress path may produce a much more significant effect than that due to either factor individually. At present however there is insufficient data to draw any firm conclusions on this point.

2.4.1 Time Effects.

The influence of time refers to the effect of a rest period at constant effective stress before continued loading. It has long been known that the effect of a period of rest is to produce a stiffer response of the material on subsequent loading. Such behaviour has been attributed to creep of the soil.

One of the earliest references to such effects was by Langer (1936) who observed that the position of the plot of voids ratio against logarithm of effective vertical stress was dependent on the load increment ratio and the time between load increments. This was quantified by Taylor (1941, 1948) who proposed a series of "time lines". It was suggested that the small strains which were observed to continue after the end of primary consolidation resulted in a stiffer structure. Terzaghi (1941) observed a similar phenomenon below the foundations of the Charity Hospital, New Orleans. It was noted that significant settlement did not occur at a point 100 feet down although there had been an increase in stress. This Terzaghi (1941) attributed to the development of a rigid bond in the soil structure during the long period at rest before continued loading. Laboratory tests conducted by Moretto(1946) and Bjerrum and Lo (1963), showed that after long periods of rest significant increases of stiffness occurred.

More direct experimental evidence is given by oedometer tests conducted by Leonards and Ramiah (1959) and Leonards and Altschaefll (1964). Loading increments were maintained on a medium plasticity clay for up to 100 days and the strains observed during this period. After this

period they found that the magnitude of the stiffness in subsequent loading increments was critically dependent on the size of the loading increment. This was also found in cases where the volume changes due to creep were prevented. Similar observations were made by Som (1968) testing samples of undisturbed London clay in oedometers. In these tests samples were held at constant effective stress for periods of 1, 7 and 90 days. For rest periods of 1 and 7 days there was no significant effect on subsequent behaviour, but for a rest period of 90 days these results were much different. In order to achieve comparable stiffnesses to those observed in conventional tests the load increment ratio had to be much greater than one. If the load increment ratio was reduced to 0.1 or less then the observed strains during the first few increments were very small. Som (1968) explained this behaviour by suggesting that during the period of rest the sample developed a more stable structural arrangement which was not broken down until the load increment exceeded a certain value. Only with the tests of small load increment ratio could this region be observed and plotted. Data is shown in Fig 2.36 for tests involving a one day rest period, Fig 2.34 for a 7 day rest period and in Figs 2.33 and 2.35 for 90 day rest periods. It was suggested that the threshold range extended for a change of stress of 10% of the current mean effective stress. Clearly this range is time dependent and depends on the duration of the period of rest.

Further evidence that changes in fabric of the clay may be important in such cases comes from tests conducted by Schumattmann (1981). Evidence was produced to suggest that clays which possess a dispersed structure exhibit a quasi pre-consolidation pressure. A dispersed structure is one in which the clay particles all lie in approximately the same direction, as opposed to a random structure in which case particles are randomly orientated with many edge to face contacts of particles in the soil matrix. It was suggested that a dispersed structure could develop during periods of rest. In laboratory tests conducted on kaolinite with various periods of rest from 2 hours to 25 days, the stiffness of a sample could be increased by a factor of ten for the longest rest periods. Schumattmann (1981) argued that it was unlikely that structural bonding would occur in laboratory ageing periods, it would only be significant generally in much longer periods i.e. significant geological periods of time.

The stiffening due to long periods of rest has been discussed by Bjerrum (1967) with reference to soft Norwegian Clays and in particular Drammen Clay. In the case of these clays a large amount of secondary compression may accumulate in relatively short periods of time. The effect of this secondary compression was illustrated by the diagram shown in Fig 2.37a. This illustrates that as the period of rest increases the volume change increase (due to creep) and so the region of high stiffness on reloading increases. This stiff behaviour was termed a reserve resistance against compression by Bjerrum (1967). These effects only became important where the age of the deposit is large compared with the age of the structure. Field data for various Norwegian clays has been collected by Bjerrum and Wu (1960) and Keinonen (1963).

In order to explain these effects Bjerrum (1967) discussed the following factors,

a) cold welding of mineral contact points between particles;

b) exchange of cations;

c) precipitation of cementing agents.

Cold welding of contact points probably occurs in all clays to some extent and so may not be significant in explaining the increase resistance to continued loading. The process of exchange of cations was considered to be the most important effect in the case of Norweglan clays. Such changes occur due to the changes in the chemistry of the pore water following deposition in a marine environment and subsequent uplift with exposure to rainwater and weathering. In the case of the Drammen clays leaching due to artesian ground water conditions was also considered to be significant. This effect was demonstrated experimentally by treating a clay with sodium chloride. The results shown in Fig 2.38 show a larger stiff portion of stress-strain response than would normally be expected from time effects due to a shift of the position of the normal consolidation line. The last factor concerning the precipitation of cementing agents is probably only of importance in very long periods of rest (Fig 2.37b). None of these factors however are likely to explain the changes which occur in laboratory tests which take place over relatively short periods of time. Chemical effects are unlikely to occur especially in reconstituted soils. In these shorter periods it seems that another mechanism must operate, probably that the sample takes up a more stable structure at almost the same water content which provides an increased resistance to straining on continued loading (Som, 1968). The change in state of sample may be interpreted as the state of the sample falling below the state boundary surface (Chapter 3) as the surface continues to expand with passing time.

Further reports of similar effects have been given by Ladd et al (1977), Buri (1978), Egeli (1978) and Mesri et al (1978). Most of these tests concentrate on oedometer samples. In triaxial tests conducted by El Ghamrawy (1978) it was noted that ageing had a less significant effect in anisotropically compressed samples as compared to those isotropically compressed. However, due to the short periods of rest, up to 9 days, these results may not be conclusive. Data from Som (1968) indicates that periods of up to 90-100 days may be required for significant effects to develop.

The above observations indicate that for a wide range of clays from soft to stiff, whether normally or overconsolidated, on a variety of stress paths, a period of rest will result in a stiffening of the response of the soil when compared to that of a sample without a period of rest. There is limited evidence to suggest however, that the effect may not be restricted to clay soils. Daramola (1978) conducted tests on Ham River sand with varying periods of rest during the tests and observed an increase in stiffness as the period of ageing increased. Fig 2.39 shows the results of four tests on samples ranging age from 0 to 152 days, before drained shearing (data from Daramola, 1980). The strain ratio, $\varepsilon_a / \varepsilon_v$ remained approximately the same for all tests but the sample tangent stiffness, $M_t = \delta\sigma'_a / \delta\varepsilon'_a$ increased, Fig 2.40a. The secant stiffness taken between stress levels of 10% and

50% of maximum deviator stress increased by a factor of about two, Fig 2.40b, for a rest period of 152 days , and demonstrates an increase of stiffness of about 50% per log cycle of time. It is noticeable however that the effect is greatly reduced from that observed in clays. Similar data for sands has been reported by Vrymoed et al (1980) testing a silty-sandy clay from the Perris Dam, California. For rest periods of up to 1000 days the soil stiffness was observed to increase linearly with the log of the duration of the rest period. The increase in stiffness was about 15% per log cycle of time elapsed. A more rapid increase of stiffness was observed by Bishop, Green and Skinner (1973) who reported one test on Ham River sand conducted in a hydraulic oedometer (designed and used by Som, (1968) for tests on London clay). During continuous loading immediately before reaching a pressure of σ'_v = 8826 kPa (σ'_v = 1280 lb / in^2) the compressibility was recorded as 3.39 x 10^{-6}/ kPa (2.34 x 10^{-5}/lb in^{-2}). On continued loading after a rest period of approximately 15 days the compressibility fell to 1.38 x 10^{-6}/kPa (0.95 x 10^{-5}/lb in^{-2}) before rising again to 3.58 x 10^{-6}/kPa 2.47 x 10^{-5}/lb in^{-2}) at σ'_v = 10,343 kPa (1500 lb/in^2). This represents an increase of about 2.5 times in the stiffness due to a period of rest of only 15 days. This increase in stiffness appears to be greater than that observed by Daramola (1978) but this modulus was quoted after only a 10 kPa change in stress which corresponds to much lower strains than the moduli quoted by Daramola (1978).

This review of previous test data is by no means complete, such observations are in fact very common. All of the above are due to creep effects and so longer periods of rest have a more significant effect. Only where very long periods of time are involved may structural bonding and cementation of particles cause further increases in sample stiffness. Tests of this type require extremely careful laboratory procedures in order to eliminate errors due to leakage which could become very significant due to the long test periods involved.

2.4.2 Stress Path Effects.

2.4.2.1 Introduction.

In this section of the effects of changes of direction of stress path on stress-strain behaviour of soils will be discussed. In this case however, data is much more limited than in the case of time effects. This is largely due to the limited number of stress paths followed in most programs of laboratory testing. In the case of the triaxial apparatus these have usually been restricted to tests on isotropically compressed samples tested in extension and compression under drained or undrained conditions with constant cell pressure. In a few cases anisotropic samples have been prepared but again it is normal only to follow the same very restricted number of stress paths. Such a limited variety of stress paths and stress histories does not give much indication of the significance of stress path threshold effects.

There are a number of types of test which are of interest. Firstly there are those tests in which samples all have the same stress history and are loaded from the same state along a number of different paths or stress probes (Lewin, 1970). From this type of test some indication of the range

over which threshold effects may extend may be gained provided that sample behaviour along all probes is of the same type e.g. elastic or elasto-plastic. There are difficulties in analysing such data since each of the paths may be associated with a different set of stiffness parameters (section 2.3.5). Most probing type test programs which have been conducted are of this type , Fig 2.41a. The second type of test of interest is that in which a number of samples all having different stress histories are loaded from a common stress state along a common loading path. This may further be subdivided into two cases, that in which samples have different general stress histories e.g. isotropic or one-dimensional compression but the same recent loading history, Fig 2.41b, and that in which the general stress history is the same but the details of recent loading history vary 2.41c. In the first case (Figs 2.41a, 2.41b) the general importance of stress history effects on samples will be indicated as discussed in section 2.3.3. In the second case (Fig 2.41c) the effects of recent stress history will be indicated. Since this case includes the effects of the approach stress path these are the type of test data which are significant to stress path threshold effects. In the field such changes may be brought about by a number of factors e.g. draw down of the water table due to pumping, or the construction of a nearby earth structure. This case is likely to be of greater significance than the other cases considered above in geotechnical engineering since most soils have stress histories which approximate to either one dimensional compression or isotropic compression conditions, with differences only in recent loading history.

The lack of suitable test data in the past is probably due to the lack of suitable testing apparatus which can readily apply a great variety of stress and strain paths. For triaxial testing a suitable apparatus is the Bishop and Wesley triaxial stress path cell (Bishop and Wesley, 1975), when equipped with automatic feedback computer control (Atkinson, 1985a).

2.4.2.2 Previous Observations.

Tests conducted by Lewin (1970) consisted of loading samples of kaolin and Llyn Brianne slate dust to a number of stress states before following a number of stress probes from those basic stress states. In particular on one path tests were conducted to assess the effect on strains of varying the magnitude of the applied stress probe. The stress probe lay at about 57° to the initial compression path (plotted as q' against p') and the magnitude of the probe varied from 0.7% to 10.3% of the basic stress state. For a probe of about 1.7% the stiffness of the sample was observed to be seven times that of a 5% stress increment or larger, Fig 2.42. It should be noted that this data has been replotted from the original data given in terms of σ'_1 , σ'_3 , ε_a and ε_v (Lewin, 1970). Similar tests conducted by Tamai and Namura (1973) on Yokosuka clay came to very similar conclusions. These tests were also reported by Karube (1977). In both cases samples were left for a period at the basic stress state before applying the stress probes, 2 days in the case of Lewin (1970) and 12 hours in the case of Tamai and Namura (1973). It is therefore unclear how much of the increase in stiffness is due to the time delay and how much due to the change in stress path. In the case of tests by Lewin (1970) other samples were tested which experienced no change in direction of stress path. For these samples the combined effect of the two day rest period and similar sized stress increments reduced strains by about 50% as compared to continuous tests

without the rest period. It is therefore likely that the change of stress path, 57° in this case, caused a stiffening of the sample by a factor of three to four times. In the tests by Tamai and Namura (1973) such comparative data was not available, however using values of the compression and swelling indices it is possible to estimate that the sample stiffness increased by about double for a similar deviation of stress path.

Increased sample stiffness is often observed during unload and reload cycles. Mesri et al (1978) conducted oedometer tests on four reconstituted stiff clays. In each case results suggested that the response of soil during swelling was very stiff initially before reaching a more constant steady stiffness when results are plotted as voids ratio against logarithm of mean effective stress, p'. This range of very stiff behaviour corresponded to about 20% of the initial stress state, p'_o. This is in fact a common feature of most oedometer tests but due to the size of load increments used it is not often clearly seen. Similar observations were made by Little (1985) testing Ware till. Characteristic curves of the slope of the swelling curves show a very stiff region initially. Typical data plotted as λ/κ against overconsolidation ratio is shown in Fig 2.43. It should be noted that the values of κ used were taken as secants from the pre-consolidation pressure to the current overconsolidation ratio and not as tangents at that point. In shear tests cycles of stress are also observed to produce similar regions of stiff behaviour (e.g. Louden, 1967; Ting, 1968; Gens, 1983).

Probe tests of a similar type to those of Lewin (1970) have been described by Clinton (1985), conducted on undisturbed Gault clay. These tests were intended to examine the variation of the anisotropic elastic parameters with stress path for this material. It was found that in general where large deviations of path occurred a stiffer sample response was observed (by a factor of up to 1.5 times). A consistent set of data should only be attained by analysing tests in which samples had been subject to similar changes in direction of stress path. These effects were attributed to stress path threshold effects. In a series of undrained tests a notable feature emerged. In each test samples were subjected to different total stress paths. It was observed that each sample produced the same pore pressure response and the same stress-strain response. It may therefore be concluded that it is the change in direction of the effective stress path which is of importance in this consideration and not the change in direction of the total stress path.

A stiff small strain region was observed by Hight, Gens and Jardine (1985) in both London clay and a glacial clay from the North Sea in consolidated undrained triaxial tests. The stiff region observed was non-linear and extended to a principal strain contour of about 0.1%. Similar behaviour was observed in a number of other soils by Jardine et al (1984). The factor of E_u/p'_o (where E_u = the undrained stiffness, and p'_o = the initial mean effective stress), was used to estimate the size of the stiff region. This showed that with increasing overconsolidation ratio the region reduced in size and also the shape of the region distorted as the state boundary surface is approached, Fig 2.44. Hight et al (1985) also anticipated that the size of the region would vary in size with the rate of shearing and the period of rest for the sample. On the limited evidence it was suggested that the region would increase in size with period of rest. It was suggested that the stiff zone would be

carried around stress space as the sample state changed. As a result of a change of stress path the sample stiffness on the new stress path would depend not only on the current stress state but also on the direction of the immediately preceding stress path. This would occur since for different cases different portions of the region are traversed. The boundary of this region set at 0.1% strain is similar to the kinematic yield surface included in Model L.C. (Simpson et al, 1979), a mathematical model for threshold effects, in which the boundary of the kinematic yield surface is set at 200με or 0.02%. A similar region is included in a model by Mroz et al (1979), these two mathematical models are described in Chapter 3. The shape of the stiff region would appear to have been established from a series of probe tests (although details were not given in the paper). This method of investigating threshold effects is not entirely satisfactory due to the variation of stiffness along each path. However this method does give an indication of the shape of the stiff region in stress space.

The most direct evidence of threshold effects is provided by Atkinson (1983a). These tests were conducted on Speswhite kaolin which was isotropically compressed and swelled to a state of p' = 200 kPa with an overconsolidation ratio of two, all stages were conducted drained. Various approach paths were followed before following a single unique path for the comparison of data. The path chosen for comparison was a drained stress path with constant cell pressure. Figs 2.45 and 2.46 illustrate the results as q' plotted against shear strain, ε_s and volumetric strain, ε_v, plotted against shear strain, ε_s. A plot of normalised stiffness against change in direction of stress path (stiffnesses taken at q' = 20 kPa, η' = 0.10) is shown in Fig 2.47. It can be seen that an increase of stiffness occurs as the angle of rotation of stress path increases up to a maximum of a factor of five. This data illustrates that there is an increase in both the shear and volumetric stiffness of samples due to the change in direction of stress paths. In addition this data appears to indicate that the strain increment ratio along a given path for an overconsolidated soil may not be unique.

So far all of the observations discussed have been for overconsolidated soils. Observations of threshold effects in a normally consolidated soil due to changes of stress path are much more difficult to make with any certainty.

It may be expected that some kind of threshold effect would occur since the yield surface would be crossed at different points as the path progressed. Also some effects due to rotational hardening of the yield surface would be observed. However in tests conducted by Hambly (1972) after following one consolidation path a change in direction of stress path was made. On this new path it was observed that while the strain increment direction was as expected, the actual magnitudes of strains were much smaller. In tests by Lewin (1978) a path at constant q'/p' was followed, then a stage at constant p', and then a path at a new constant q'/p' value followed. In this case on the new constant q'/p' path, initially only very small strains were observed, however after larger increments of stress had been applied much larger strains developed at a rate and in a ratio compatible with that for a sample which had continuously followed the new q'/p' path from the start of the test. Wood (1975) conducted tests on isotropically compressed spestone kaolin in the Cambridge true

triaxial apparatus. Two particular series of tests showed the effect of stress path threshold effects. In one series a number of samples were subjected to right angled changes in direction of stress path. The results of these tests were compared to those of samples following the same final loading path but not subjected to a change in direction of stress path. The samples appeared to be stiffer as a result of the change in direction of path and furthermore the strain increment ratio was different, being rotated towards its direction on the preceding loading path. After some distance along the common stress path behaviour of the two sets of samples became essentially identical. In the second series of tests the magnitude of the change in direction was varied. The effect was shown to be greater for larger changes in direction of loading path. Summarising these data Wood (1974) commented "the sample remembers which way the stress path was heading before the turn". In practice due to the complications of defining the yield surface during the period of changing between paths and in passing along the new path it is very difficult to decide which effects are due to the new paths, which are due to changes in shape of the yield surface, and which are due to the change in direction of the stress path for normally consolidated soils.

2.4.3 Effect of Sampling on Threshold Effects.

The general effects of sampling on stiffness measurements in soils have been discussed, in this section the effect of sampling will be considered with particular reference to threshold effects.

In the process of sampling the state of stress of the sample is changed from that existing in-situ as the overburden pressures are removed, In addition further mechanical disturbance occurs due to the actual process of sampling. As a result of such cycles of stress it is unlikely that the laboratory sample can be expected to behave in exactly the same way as an element in the ground. This is of particular importance when considering time effects. These effects (section 2.4.1) are by definition the changes in stress-strain behaviour immediately following a period at constant effective stress. Due to changes of stress in sampling any influence of such a period of rest in the ground is unlikely to be observed in the laboratory sample. In order to model such an effect laboratory samples would need to be held at a state equivalent to that existing in the ground for an equivalent period of time to allow for ageing to occur (Schumattmann, 1981). Such a process may not be practical due to the long periods of time which may be involved. It is of interest to note that in many cases where block samples have been stored for up to two years before testing, Atkinson (1973), Wesley (1975), Costa-Filho (1978a), that significant differences have not been observed in stress-strain behaviour as a result of the storage period. These authors commenting on the lack of difference in behaviour which had been observed due to these rest-periods stated that if threshold effects were significant they would have expected some changes to occur during this period. However, this is not surprising since the samples taken from such blocks would have been subject to large changes of stress during preparation. These large cycles of stress would have destroyed any time effects which may have developed during the storage period and therefore time effects would not be observed in these samples. It is therefore likely that it is not possible to observe the significance of time effects directly on samples extracted from the ground due to the stress history imposed in the ground. Instead tests must be conducted with appropriate periods of

rest as indicated by Schumattmann (1981).

The effect of sampling in the case of stress path effects is much more difficult to assess. There are the general effects of disturbance (section 2.3.1) and in addition there are those due to following the incorrect stress history to the start of the test. In principle it should be possible to take a perfect undisturbed sample (which is free from mechanical disturbance) and place it in a testing apparatus which then mimics not only the general features of the stress history of the sample e.g. one dimensional compression and swelling if appropriate, but also the features of recent stress history such as the last unload-reload cycle applied to the element. It should be possible if the appropriate test stress paths are followed to produce results which are free from the effects of sample disturbance due to changes in stress and so the results should be subject to the same threshold effects as would be significant in the field. This is essentially the stress path method as described by Davis and Poulos (1968), Lambe (1964).

2.5 Comparison of Laboratory and Field Data.

2.5.1 Introduction.

The stiffness of soil for the purposes of calculations may be derived from laboratory tests, in-situ tests or past experience based on the back analysis of similar structures. In many cases calculations assume isotropic linear elastic behaviour i.e. only one stiffness modulus is used. Stress-strain behaviour is normally highly non-linear making selection of this single modulus difficult.

In the previous sections many of the factors affecting the stiffness of samples have been discussed. The effect of most of these could be reduced in the laboratory with correct testing procedures, involving very complex stress paths in many cases. However the in-situ state of the sample and its precise consolidation history are often difficult to determine. The process of stress relief during sampling involves large cycles of stress (Hight et al, 1985) and so may cause irreversible straining and opening of fissures both pre-existing and due to the stress relief. It may therefore prove very difficult in such cases to obtain useful data from these samples.

In-situ tests have therefore been used in an effort to eliminate the need for sampling (Marsland 1971a) and to calibrate laboratory tests. Similar data may be obtained from the monitoring of actual structures during and after construction. However it is very difficult to analyse such tests to produce stiffness moduli since soil behaviour is non-linear and may be in-elastic. Despite these difficulties many authors e.g. Marsland (1972) have claimed good agreement between in-situ field tests and back analysed structures. This agreement may be fortuitous and may only be due to the similarity of the methods of analysis used for each case. Others e.g. Jardine et al (1985) have found that in-situ tests yield lower moduli than back analysed structures. Even where in-situ tests have been used to determine the soil stiffness the distribution of soil movements may not be accurately predicted (Burland et al, 1979). Jardine et al (1985) have discussed the reliability of

moduli derived in the field from boundary measurements of soil movements. Due to areas of high stress and large strains locally, such moduli may underestimate the true soil stiffness at small strains. Only where local measurements of soil movements are made can such data be considered reliable. Some of these examples of comparison between laboratory and field data will now be discussed with particular reference to the factors highlighted in the preceding sections. Much of the discussion will centre on London Clay but this is only due to the great amount of data which is available. The arguments apply equally to other clays.

2.5.2 Comparison of Data from In-situ Tests.

Two types of in-situ test will be considered here, the plate bearing test and the pressuremeter test. In the plate bearing the stress-strain behaviour of the soil is derived from the deflection of the plate under known applied loads. The data is found to be dependent on the size of the plate to some degree but is also greatly dependent on the cleaning of the excavation into which the plate is placed and the time that the ground surface is left exposed (allowing swelling and drying of the surface) before the plate is installed. In the pressuremeter tests data are derived from the pressure of fluid in a bag and the change in volume of that bag. In both cases a factor often ignored is that the soil in the region of the test site is subject to intense disturbance (Clayton, 1984). This includes mechanical disturbance, stress relief (especially of importance if tests are performed in deep boreholes), temperature changes, swelling of surrounding soil and drying of the surface of the borehole. In order to interpret the results an estimate of the in-situ state of stress is required, this may prove very difficult (Simpson et al, 1980; Fahey and Randolph, 1984). In boreholes, tests must be performed within a short period of opening the hole in order to reduce the effect of swelling due to stress relief. In soils of very high permeability this may be difficult.

In general it has been observed that the data from pressuremeter tests gives lower values of stiffness than the plate bearing test (Marsland and Randolph, 1977). However Eisenstein and Morrison (1973) and Burgess and Eisenstein (1977) have claimed good agreement between pressuremeter tests and back analysed results from structures founded on a stiff glacial till. The effect of a disturbance on the results of pressuremeter tests has been discussed by Fahey and Randolph (1984) and Clarke and Wroth (1985). Fahey and Randolph (1984) conducted a series of tests in sand and made measurements of the strength of the sand and the stiffness using a variety of drilling shoes, each causing a different degree of disturbance. The results indicated large variations in the estimated strength and a slightly smaller variation of stiffness measurements. It was found that measurements of initial soil stiffness were highly variable, varying by a factor of up to four while those obtained from an unload reload loop varied by a factor of about1.5. The lower values were obtained in tests where the greatest degree of disturbance occurred. Clarke and Wroth (1985) discussing these results indicated that the initial modulus was a poor measure of stiffness since this was highly susceptible to disturbance during drilling and that values obtained from unload-reload loops should be more reliable. Similar conclusions were reached by Jamiolkawski et al (1985) for a number of different soil types. By plotting the results against mean effective stress, p', rather than depth improved agreement of results could be obtained. These

results clearly indicate that great care is needed if reliable results for stiffness are to be obtained from the pressuremeter test.

The differences between different field tests may therefore partly be attributed to varying degrees of disturbance, although in the case of results from carefully conducted tests using the self boring pressuremeter (Wroth and Hughes, 1973; Windle and Wroth, 1977) good agreement is indicated with plate bearing tests. In such cases it is likely that the different stress paths followed, the different stress or strain levels at which moduli are quoted, and the different stress states during the tests are significant when interpreting the results. In the plate bearing tests stresses are increased by increasing the vertical load but in the pressuremeter test this is done by increasing horizontal loads (Parry, 1979). These tests therefore perform compression and extension tests respectively (with reference to vertical triaxial samples), which are generally not observed to yield identical stress-strain behaviour for field samples. The interpretation of the results may be further complicated if tests are conducted at different depths since samples will have been subjected to different amounts of stress relief and so will lie on different unload-reload cycles of stress.

2.5.3 Comparison of Data for London Clay.

A good illustration of the typical differences in stiffness data from laboratory and field data may be given by data in Fig 2.48 from St John (1975). The diagram shows that laboratory tests appear to yield much lower values of stiffness than those derived from field tests for both horizontal and vertical directions. The laboratory data quoted is that from the Ashfield Common Shaft (Ward, Marsland and Samuels, 1965) for unconsolidated undrained tests, while the field data comes from a number of sources indicated in the diagram. All the moduli quoted in this diagram are undrained secant stiffness moduli, the field data is quoted so as to give the best fit to observed structural movements while the laboratory data is quoted over a range of axial strain of ε_a = 0 to1%. These differences may be accounted for by the factors discussed in section 2.3.

In comparing data reference should be made to the strain levels at which moduli are taken. In laboratory tests moduli are typically quoted at any axial strain up to about 1%. This probably occurs due to convenience for calculations and provides a standard which is compared between different soils, however due to non-linearity of stress-strain behaviour this is not satisfactory (section 2.3.9). Atkinson (1973) quotes figures at 0.25% axial strain while Gens (1983) and Jardine et al (1984) have quoted moduli at strains as low as 0.001%. In typical laboratory tests this yields values of normalised stiffness of E_u / c_u = 100-150, while for the tests of Gens (1983) and Jardine et al (1984) testing London clay values as high as E_u / c_u = 2500 have been given in Fig 2.23. The results of a typical plate bearing test conducted by Marsland (1971a, b) are shown in Fig 2.49. It can be seen that at strains below 0.1% the tangent modulus may be approximated by E_u / c_u = 1000. At higher shear strain values however the modulus falls to a value of E_u / c_u $\cong$ 200-300 which is comparable to that from laboratory tests. St John (1975) studied a number of excavations and taking a limit for wall movement of 0.02% of the wall height (Peck, 1969), computed the shear strain distribution in the ground, see Fig 2.49 (diagram taken from Simpson et al, 1980). Only

locally do shear strains exceed 0.1%, values of E_u / c_u back analysed from such structures are of the order of 1000, which is close to those for field tests. Butler (1975) conducted a similar review of structures where strains were generally larger than those studied by St John (1975). There was a larger zone of material with strains of the order of 0.1% to 0.2% and these yielded stiffnesses of E_u / c_u in the range of 500 - 1000. In this review similar differences were noted for other clays when comparing laboratory and field data.

The data would appear to show that where moduli at similar strain levels are compared the values obtained are very similar. Simpson et al (1980) superimposed moduli derived from data by Costa-Filho (1978a) for undisturbed London clay (see Figs 2.51 and 2.52) at various strain levels on St John's diagram Fig 2.53. The data shows improved agreement using definitions of moduli at small strains while at half maximum deviator stress values compare well with those of the Ashford Common Shaft. The improved agreement of results may also be attributed to using the correct initial anisotropic state for samples and the correct stress history for those which had been reconsolidated. In addition the use of internally mounted strain devices eliminated many of the errors observed in previous test data. A similar comparison of data by Jardine at al (1985) for London clay quoted at small strains also shows very good agreement between field and laboratory stiffness results. Abbiss (1981) used a geophysical method to determine stiffnesses at strain levels comparable to those of the tests by Gens (1983) and Jardine et al (1984). The data gives good agreement with these tests and with plate bearing test results by Marsland and Eason (1973).

Data for London clay from Cannon's Park and Bell Common shows a similar agreement between field and laboratory moduli when laboratory stiffness parameters from low strain levels are used, Fig 2.54. The field data given by Jardine et al (1985) was derived from tests where local measurements of soil movement were made. Good agreement of stiffnesses was also obtained in comparisons made to samples produced in the laboratory by one-dimensionally compressing and swelling samples formed from a slurry. In is notable however that in-situ tests greatly underestimated the soil stiffness due to the large influence of regions of high stress close to the in-situ test.

2.5.4 Comparison of Data for Other Clays.

Similar problems to those discussed for London clay have been observed on other clays.

Plate bearing tests conducted by Feda (1979) on Furonian Sandstone at various depths demonstrated that the stiffness of the soil was dependent on the stress increment applied. For small stress increments the strains were very small and so yielded high stiffnesses. It is unclear however as to what degree this was due to path dependent deformations of the material, cementing of the sandstone or threshold effects due to changes in direction of stress path.

The effects of stress reversals have been observed to have a significant effect on subsequent loading behaviour. In oedometer tests and triaxial tests the early parts of stress-strain curves

following a reversal of stress are always observed to indicate a higher stiffness than on subsequent loading or than would have occurred on the same path had there not been a reversal of path. Data from Parry (1979) for plate tests on Gault clay and pressuremeter tests show a similar increase in stiffness and improved agreement between the tests when stiffnesses from unload-reload cycles are compared. Similar conclusions were reached by Hight and Gens (1979) in tests on Lower Cromer Till.

The above would appear to suggest that the effect of changes in direction of the applied stress path may initially produce a very stiff response. This is the threshold effect which results due to stress path effects. It is therefore necessary to consider the following factors when planning a series of laboratory tests to determine stiffness data.

a) The stress history of the sample.

b) The modulus must be of the correct type and defined at the correct stress or strain level.

c) The correct stress path must be followed.

d) Recent stress history and rest period details should be considered due to the existence of threshold effects.

By these methods a better correspondence between laboratory and field data may be possible.

2.6 Discussion.

In this chapter some of the methods used to analyse boundary value problems have been discussed. The problems in calculating ground movements are largely due to the difficulties encountered when trying to measure the stiffness of soils. For a wide range of soils there appear to be considerable differences in the moduli derived from field data and laboratory data. Since the stress distributions in the ground are found to be relatively insensitive to the soil stiffness they can be predicted with reasonable confidence, however it is the deformations of the soil mass under these stresses which is the problem. For an ideal soil the parameters, A, B, C and D in equation 2.1 could be determined using any apparatus which can apply two different effective stress paths. This method has been used on anisotropic overconsolidated soils by Clinton (1984) testing undisturbed Gault clay, Houlsby (1981) testing Leighton Buzzard sand, Graham and Houlsby (1983) testing Agassiz clay and Atkinson (1973) testing London clay. In practice this does not appear to be sufficient even for overconsolidated soils due to the path and stress history dependance of soil deformations. It is therefore necessary to use an apparatus which can apply a wide range of stress paths to samples in order to investigate these effects.

In general it is assumed that the soil grains and the pore water are incompressible, that is the

stiffness of the soil structure is much less than that of the soil grains or pore water. Hence the values of stiffness measured are assumed to be mainly dependent on the stiffness of the soil structure. The bulk modulus of water is of the order of 2×10^3 MPa (Vennard and Street, 1976) and that of the soil grains 7.5×10^4 MPa (for calcite) to 3.8×10^4 MPa (for quartz) (Bishop and Hight, 1977). For the very high values of stiffness measured at the start of some tests it is clear that these components represent a significant part of the strains measured where changes in direction of loading path occur (the precise definitions of these stiffnesses i.e. strain level and type of moduli, are unknown). Bishop and Hight (1977) showed that the undrained Young's modulus, E_u and Poisson's ratio ν_u, may be significantly affected by these factors since the assumption that volume strains are zero (or $K_u = \infty$, $\nu_u = 1/2$) is theoretically and practically impossible. The effect on E_u is of little consequence since the stiffness of all components is measured and used, however a value of $\nu_u = 1/2$ is normally assumed.

The lack of agreement generally observed between laboratory and field data may not be so large as is generally believed. Simply by considering similar stress or strain levels in the field and laboratory when quoting moduli very significant improvements may be gained (Simpson et al, 1980). Other factors known to affect the stiffness of samples should also be considered in the laboratory so as to model field conditions as closely as possible. This will include following the correct consolidation history for the sample and following the correct stress paths for typical elements of the soil in the ground. Such procedures are necessary since while overconsolidated soils may behave elastically when relatively small loads are applied monotonically, the behaviour itself is often path dependent and generally strains irrecoverable. Details of measuring systems also need to be considered carefully so as to ensure that they are not excessively flexible and record only strains occurring in the sample or may be corrected for flexibility. In general this means placing devices close to or actually on samples, however such systems may bring new problems as discussed in section 2.3.8. This is of particular significance when testing very stiff soils.

It is notable that nearly all of the factors considered in this chapter have the effect of reducing the measured soil stiffness by some amount. If careful laboratory procedures are followed and the results analysed carefully then more realistic parameters may be obtained. In particular the stress path methods proposed (e.g. Davis and Poulos, 1967; Lambe, 1964) should be extended to include the effects of recent stress history which at present they do not. In this way the general effects of stress path and those of stress path threshold effects may be reduced. With improved procedures it would be anticipated that given high quality sampling the results of laboratory tests should be more reliable than those of field tests, since in the laboratory a much greater degree of control and much more accurate measurements may be made of soil deformations. As discussed by Jardine et al (1985) unless local measurements of ground movements are made during in-situ tests the data derived may be unreliable and produce an underestimate of the soil stiffness.

The effect of sample disturbance has often been quoted as the reason for the discrepancy between laboratory data but careful tests conducted by Atkinson (1973) give consistent results,

which appear to indicate that disturbance due to stress relief may not be as significant a factor as previously considered. Tests by Skempton and Sowa (1963), Hight et al (1985) and Jardine et al (1985) appear to confirm these findings for heavily overconsolidated soils. For normally consolidated soils the effects are reduced to a minimum by reconsolidating samples to the initial states in-situ. Only the cases of highly sensitive soils, sands, and those soils with a fabric which may be destroyed during sampling and reconsolidation, may prove unsuitable for routine laboratory testing. It is particularly important to remember that in field tests the soil is also subject to some degree of disturbance both stress relief and mechanical and therefore disturbance alone is unlikely to account for the major differences existing between field and laboratory data. In both cases the effect of disturbance is interpreted as producing a reduction of measured stiffness and so higher values of stiffness obtained in all tests are generally favoured for analysis.

In field observations it is notable that in many cases despite using stiffnesses derived from field data correspondence between field and predicted movements it is not as good as would be hoped. Typically the magnitudes of maximum movements are predicted quite well but the extent of the area of measurable movements is normally overestimated. This has been observed both in the ground movements above tunnels and the settlement troughs behind retaining walls (Burland et al, 1979). Similar observations have been made in the laboratory where samples have been subjected to a change in direction of stress path or period at constant effective stress. For some threshold stress, strains are very small compared to those which would have resulted on the same path without either the change in stress path or the period of rest. The two effects appear to be entirely separate phenomena but it is unclear as to whether the effects are cumulative or only operate individually. The magnitude of this threshold range has variously been suggested at between 10% and 30% of the mean effective stress or in terms of strains between 0.02% and 0.01%. The evidence is unclear since in most tests both types of threshold effect may be significant due to long periods of rest often allowed in step loaded tests. In any case the selection of a range for these effects is likely to be a somewhat arbitrary factor since the range is unlikely to be clearly defined. The threshold stress in the case of time effects is time dependent as illustrated by Bjerrum (1967) but those due to stress path probably depend on the magnitude of the change in direction of stress path (Atkinson, 1983a). The significance of such effects in the laboratory is clear since in tests by Atkinson (1983a) and Lewin (1970) the stiffness of samples immediately following a change in direction of loading was increased by a factor of up to 9 times. It is unclear as to whether such a region should be defined in terms of stresses or strains but it is thought that since the stress state is a true measure of the sample state that it is more likely that this definition will prove satisfactory. The conditions under which a change in stress state or a change of strains for defining such a region are the same will be discussed in chapter 3. In the field few cases have been analysed by models incorporating threshold effects as opposed to non-linearity of stress-strain curves. Data from Simpson et al (1979) suggests that this may have a very significant effect in the case of the movements around deep excavations. The use of a threshold zone in model L.C. (see Chapter 3) greatly improved the predictions of ground movements around such excavations.

It is not clear as to which soils are most sensitive to threshold effects. For time effects it would appear that high plasticity clays are most affected while sands are least affected. Increases of stiffness of clays may be up to 9 or 10 times while for similar periods of rest sands may only increase in stiffness by about 50%. For stress path effects no such comparative data has been found.

It would therefore appear that the stress path method should be extended to cover periods of rest during loading sequences, and the recent stress history of soil elements in the ground.

CHAPTER 3

MATHEMATICAL MODELS FOR SOILS

CHAPTER 3 MATHEMATICAL MODELS FOR SOILS.

3.1 Introduction.

The purpose of soil models is to provide a mathematical relationship between stresses and strains i.e. a constitutive law, for the material involved. Soils are an unusual material in that they are in general a three phase material consisting of solid soil grains, water and gases. In general soils are treated only as a two phase material, either fully saturated (no gases present) or dry (no free water present). Throughout the following discussion it is assumed that the soil is fully saturated.

There are two basic approaches to theories in soil mechanics. The soil may be considered to be a continuum where all elements merge into one, or it may be considered as a body made up of individual particles. The majority of models in use are of the continuum type e.g. the critical state model (Schofield and Wroth, 1968). An example of a particulate model would be the stress dilatancy model (Rowe, 1963, 1969, 1971). In this work only models of the critical state type or which are associated with the critical state model will be considered. It should be noted that these models are rate independent and do not include viscous effects or account for creep in soils.

Whatever type of model is selected for analysis it should not be postulated that the soil behaves in an identical manner to the ideal substance from which the model was developed. Instead the behaviour of soil may be approximated to the behaviour of the ideal substance for a range of conditions over which the results are considered to be of sufficient accuracy (Scott, 1963).

A central feature of critical state soil theories is the principle of effective stress. Terzaghi (1936) stated the importance of the principle as "all measurable effects of a change in stress such as compression , distortion and a change in shearing resistance are exclusively due to changes in effective stress". The effective stress σ' is defined as:

$$\sigma' = \sigma - u \qquad 3.1$$

Where σ is the total stress and u is the pore pressure.

More extensive reviews of soil models in current use have been given by Ko (1981), Ng (1982), Ladd et al (1977) and Woods (1986a).

3.2 General Requirements of Soil Models.

A model should allow deformation and stresses to be calculated in the solution of boundary value problems and should contain a criterion which defines a maximum shear stress allowable for the soil. Ideally models should be sufficiently general to consider any stress or strain path but also give accurate results and remain simple with easily obtainable, well defined material parameters which

have a physical meaning.

These requirements to some extent conflict. For a model to apply to general loading cases and give results of high precision, a single model may become unacceptably complex. This may be overcome by use of a series of models all of which may incorporate increasing levels of complexity e.g. Anisotropy, as the problem investigated requires. In such a way qualitative results indicating the type of behaviour to be expected may be obtained before using a more complex model. The use of a simple theory in this manner has much to recommend it provided the loss of precision is not too great.

The requirement that the parameters in the model should be well defined is very important. The actual numerical values should be easily determined from simple graphs of stress-strain data or normalised plots rather than by a process of trial and error. It is also preferable that the number of tests required to determine this data should be reduced to a minimum and the tests themselves made as simple as possible so as to eliminate the need for specialised testing equipment and procedures.

Finally parameters should be independent of the tests conducted i.e. they should be truely fundamental material parameters. It should therefore be possible to model the results of one test using results from another (Roscoe, 1970). For soils this proves a very difficult requirement to satisfy since soils are path dependent and due to the different restrictions applied by various pieces of test equipment they may apparently give different results for the same parameters unless due account is taken of the different applied stress paths (Wroth, 1984). Most models require that co-axiality applies to the material, that is the property which requires coincidence of principal stress and principal strain directions. It should further be noted that most test data used in the development and calibration of these models are derived from tests in which the axes of principal stress remain fixed or in certain cases e.g. simple shear tests, rotate in a specified manner. Only in very sophisticated pieces of equipment e.g. the hollow shear apparatus, can the rotation of axes be prescribed and controlled. In the field axes rotate in most loading situations and hence it is assumed that soil behaviour is not significantly affected by such rotations.

3.3 Definition of Parameters.

In classical theories the stress state of the sample is defined in terms of the principal stresses σ_1, σ_2, σ_3 and the pore pressure u. The strains observed in the sample are the principal strains ε_1, ε_2, ε_3, the volume of the sample is defined by the voids ratio e given by:-

$$e = wG_S \qquad 3.2$$

where w = water content of the sample and G_S = the specific gravity of the soil grains. These parameters are sufficient to fully describe the soil state and deformations for the case where co-

axiality applies. The principal stresses and strains are invariants i.e. the values of these parameters are independent of the orientation of the reference co-ordinate axes. It is more convenient to use the stress and strain invariants in terms of which critical state theories are formulated. In general three invariants are required, however for the cylindrical triaxial test only two are required. The stress invariants used are given by:

$$p' = 1/3\,(\sigma_1' + \sigma_2' + \sigma_3') \qquad 3.3$$

$$q' = [1/2\,[(\sigma_1' - \sigma_2')^2 + (\sigma_2' - \sigma_3')^2 + (\sigma_3' - \sigma_1')^2]]^{1/2} \qquad 3.4$$

where p' is the mean effective stress and q' the deviator stress. In place of the voids ratio, the specific volume , v, is normally used where,

$$v = 1 + wG_s \qquad 3.5$$

or $$v = 1 + e \qquad 3.6$$

In the case of the triaxial test where $\sigma_2' = \sigma_3'$ it is convenient to re-write the stress invariants as:-

$$p' = 1/3\,(\sigma_a' + 2\sigma_r') \qquad 3.7$$

$$q' = (\sigma_a' - \sigma_r') \qquad 3.8$$

where σ_a' = the effective axial stress and σ_r' = the effective radial stress.

For strain invariants to be correctly associated with these stress invariants they should satisfy certain criteria. For an isotropic elastic material, changes in shear strain should be due solely to the changes of shear stress, and the changes of volumetric strain should be due only to changes of the mean normal stress i.e. the constitutive equations should decouple in such a case (Atkinson and Bransby, 1978). Suitable invariants are found to be:-

$$\varepsilon_v = \varepsilon_1 + \varepsilon_2 + \varepsilon_3 \qquad 3.9$$

$$\varepsilon_s = [2/9\,[(\varepsilon_1 - \varepsilon_2)^2 + (\varepsilon_2 - \varepsilon_3)^2 + (\varepsilon_3 - \varepsilon_1)^2]]^{1/2} \qquad 3.10$$

which for the case of the triaxial test for a sample with the same properties in both horizontal directions become,

$$\varepsilon_v = \varepsilon_a + 2\varepsilon_r \qquad 3.11$$

$$\varepsilon_s = 2/3 (\varepsilon_a - \varepsilon_r) \qquad 3.12$$

While these parameters are adequate for isotropic soils some care is required for anisotropic materials e.g. horizontal samples. These equations have further advantages shown by Wood (1984) that the increments of volumetric work, δW_v , and distortional work, δW_s , for the above case are given by equations 3.13 and 3.14 respectively.

$$\delta W_v = \delta p' \delta \varepsilon_v \qquad 3.13$$

$$\delta W_s = \delta q' \delta \varepsilon_s \qquad 3.14$$

It should be noted at this point that while all stresses used in calculations are measured relative to an absolute datum i.e. atmospheric pressure, strains are only measured relative to an arbitrary datum. Strains cannot therefore be used to describe the state of a sample. Furthermore equations 3.10 and 3.12 are strictly only correct for small strains and so these equations should only be applied incrementaly. Where large strains occur natural strains should be used. Throughout this thesis all the terms defined in this section are taken as positive for compression and negative for extension states.

3.4 The Elastic Model.

The elastic model has been used for many years in soil mechanics to predict the stress-strain behaviour of soils. For example, the movements around deep excavations in London Clay have been analysed using a linear elastic model by a number of workers (Cole and Burland, 1972; St John, 1975; Burland and Hancock, 1977).

Various definitions of elastic behaviour have been given by research workers e.g. Love (1942), Atkinson (1973), Costa Filho (1978a), often with the object of identifying ranges of elastic behaviour in soils in laboratory or field tests. These definitions include,

a) linear relationship between stresses and strains (Wroth, 1971);
b) no energy dissipation in a cycle of loading and unloading (Drucker, 1964);
c) the strain increment ratio is a unique function of the stress increment ratio (Atkinson, 1973);
d) recoverability of strains on unloading and reloading (Rowe, 1971);
e) independence of stress path.

Clearly linearity is not necessary for elasticity but condition c) alone is not sufficient to define elasticity during cycles of loading. The thermodynamic definition of elasticity requires that no energy is dissipated during loading i.e. any strains observed are fully recoverable. The problem of such a definition is that where stress paths are not cyclic full recoverability cannot be checked. It

should be noted that hysteresis is not acceptable within the theory of elasticity since the area of the hysteresis loop represents energy dissipated On monotonic tests it therefore becomes difficult to define ranges of elastic behaviour.

For soils definitions of elasticity using as a criteria the recoverability of strains during cycles of loading (Rowe, 1971) may be too restrictive (Atkinson, 1973; Houlsby, 1981). It has been shown by Atkinson (1973) that a more flexible definition based on the mathematical theory of elasticity (Love, 1942) may successfully be used to define a range of behaviour which is elastic in character for monotonic loading. This method will be described in section 3.4.1. The range of true elastic behaviour is probably restricted to small stress changes of the order of 10 - 20 kPa with only very small strains occurring (Lambe and Whitman, 1979). Although the range of behaviour which is elastic in character for monotonic loading may extend further, up to strains of 1% for undisturbed London Clay (Atkinson, 1973), before the soil yields and elasto-plastic strains develop. This range is limited by the point at which large numbers of soil grains start to slide over each other. Balasubramaniam (1969) noted that for spestone kaolin elastic strains appeared to be limited by changes of stress corresponding to about 30% of the initial value of the mean effective stress.

3.4.1 Properties of the Elastic Model.

The general equations describing elastic behaviour may be written as:-

$$[d\varepsilon_{ij}] = \pm [F_{ijkl}][d\sigma'_{kl}] \qquad 3.15$$

where i, j, k and l = 1 to 3. The matrix $[d\sigma'_{kl}]$ represents the stress increments applied to the soil while $[F_{ijkl}]$ contains a number of elastic parameters, and matrix $[d\varepsilon_{ij}]$ is the matrix of strain increments which result from the stress increments $(d\sigma'_{kl})$. For the special case of linearity the matrix $[F_{ijkl}]$ is constant in value. The maximum requirements of stiffness parameters would appear to be 81 for a material which was anisotropic in all three orthogonal directions. However there are only six independent components of stress and strain so this requirement reduces to 36 and from considerations of equilibrium for a homogeneous material the maximum number of parameters is reduced to 21 (Love, 1942; Jaeger, 1969; Houlsby, 1981). For the case of a cross anisotropic soil (one axis of symmetry of soil properties) only five independent parameters are needed. This case is of particular importance since many natural soils deposited and compressed under conditions under of approximately zero lateral strain fall into this category. Further simplification to a homogeneous isotropic elastic soil reduces the requirement to that of two parameters. Specific forms of the equations of elasticity are given in section 3.4.2.

For all homogeneous elastic materials the elastic equations remain symmetrical about the leading diagonal of the stiffness matrix if the stress and strain invariants are correctly associated, i.e. in the equations below $B^e = C^e$.

$$\delta\varepsilon_s = A^e\delta q' + B^e\delta p' \qquad 3.16$$

$$\delta\varepsilon_v = C^e\delta q' + D^e\delta p' \qquad 3.17$$

For the special case of isotropy $B^e = C^e = 0$ i.e. equations 3.16 and 3.17 are decoupled. The form of the parameters A^e, B^e, C^e and D^e given in section 3.4.2 are only for the cases of isotropy and cross-anisotropy where the axes of loading co-incide with the axes of anisotropy.

It should be noted that equations 3.16 and 3.17 only require three elastic constants to describe behaviour of the soil in the axi-symmetric triaxial test. This shows that the requirement of the number of elastic parameters is reduced for certain cases of symmetry of loading, although if the sample were re-orientated horizontally a further parameter would be required.

The fifth elastic parameter is only needed where principal axes of applied loading do not co-incide with the axes of anisotropy.

A method of defining the range of elastic behaviour has been described by Atkinson (1973). For elastic behaviour the strain increment ratio is a function of the stress increment ratio and not related to the stress state, (equation 3.15). Therefore if a linear stress path is applied to the soil a linear strain path should be observed, similar arguments apply if a straight strain path is applied, then a straight stress path should be observed. The relative slopes of the stress and strain paths give a measure of the degree of anisotropy of samples (Atkinson, 1973).

It should be noted that while this method allows variable horizontal and vertical stiffnesses it assumes that the degree of anisotropy and the values of Poisson's ratio remain unchanged. Equations 3.15 may be contrasted with the general equation of plasticity (Hill, 1950) which may be written as:

$$d\varepsilon_{ij} = [\,M_{ijkl}\,][\,\sigma'_{kl}\,] \qquad 3.18$$

In this case the strain increment ratio can be seen to be a function of stress state rather than of the stress increments applied (Atkinson, 1973) and only for special cases e.g. constant q'/p', tests will linear strain paths result for linear stress paths.

3.4.2 Equations of Elastic Behaviour.

The equations of stress-strain behaviour for an isotropic soil may be written as (see Atkinson and Bransby (1978) for example):-

$$\delta\varepsilon_1 = \frac{1}{E'}(\delta\sigma_1 - \nu'\delta\sigma_2 - \nu'\delta\sigma_3)$$

$$\delta\varepsilon_2 = \frac{1}{E'}(\delta\sigma_2 - \nu'\delta\sigma_1 - \nu'\delta\sigma_3) \qquad 3.19$$

$$\delta\varepsilon_3 = \frac{1}{E'}(\delta\sigma_3 - \nu'\delta\sigma_1 - \nu'\delta\sigma_2)$$

Where E' is the Youngs modulus and ν' the Poissons ratio, both defined with respect to effective stress. In terms of machine axes equation 3.19 may be written as:-

$$\delta\varepsilon_a = \frac{1}{E'}(\delta\sigma'_a - 2\nu'\delta\sigma'_r)$$

$$3.20$$

$$\delta\varepsilon_r = \frac{1}{E'}(\delta\sigma'_r - \nu'(\delta\sigma'_a + \delta\sigma'_r))$$

These equations may be re-written in terms of the stress and strain invariants given in section 3.3:-

$$\delta\varepsilon_s = \frac{2(1+\nu')}{3E'}\delta q'$$

$$\delta\varepsilon_v = \frac{3(1-2\nu')}{E'}\delta p'$$

or re-written as:-

$$\delta\varepsilon_s = \frac{1}{3G'}\delta q' \qquad 3.22$$

$$\delta\varepsilon_v = \frac{1}{K'}\delta p'$$

where G' and K' are the elastic shear and bulk moduli respectively. These equations are decoupled as discussed in section 3.3.

It is unlikely for an anisotropic soil the simple isotropic model will be sufficient. In such cases the anisotropic elastic model should be used. The use of the anisotropic model causes a major increase in complexity. For this case the equations of elasticity may be written as:-

$$\begin{bmatrix} \delta\varepsilon_x \\ \delta\varepsilon_y \\ \delta\varepsilon_z \\ \delta\gamma_{xy} \\ \delta\gamma_{yx} \\ \delta\gamma_{zx} \end{bmatrix} = \begin{bmatrix} \frac{1}{E'_x} & -\frac{\nu'_{xx}}{E'_x} & -\frac{\nu'_{yx}}{E'_x} & & & \\ -\frac{\nu'_{xy}}{E'_x} & \frac{1}{E'_y} & -\frac{\nu'_{xy}}{E'_x} & & & \\ -\frac{\nu'_{xx}}{E'_x} & -\frac{\nu'_{xy}}{E'_x} & \frac{1}{E'_x} & & & \\ & & & \frac{1}{G'_{xy}} & & \\ & & & & \frac{1}{G'_{xy}} & \\ & & & & & \frac{2(1+\nu'_{xx})}{E'_x} \end{bmatrix} \begin{bmatrix} \delta\sigma'_x \\ \delta\sigma'_y \\ \delta\sigma'_z \\ \delta\tau'_{xy} \\ \delta\tau'_{yx} \\ \delta\tau'_{zx} \end{bmatrix} \qquad 3.23$$

or if directions z, y and x correspond to principal directions 1, 2 and 3 with the stiffness in directions 2 and 3 the same, these equations may be re-written as:-

$$\delta\varepsilon_1 = \frac{\delta\sigma'_1}{E'_1} - \nu'_{13}\frac{\delta\sigma'_2}{E'_3} - \nu'_{13}\frac{\delta\sigma'_3}{E'_3}$$

$$\delta\varepsilon_2 = -\nu'_{31}\frac{\delta\sigma'_1}{E'_1} - \frac{\delta\sigma'_2}{E'_3} - \nu'_{33}\frac{\delta\sigma'_3}{E'_3} \qquad 3.24$$

$$\delta\varepsilon_3 = -\nu'_{31}\frac{\delta\sigma'_1}{E'_1} - \nu'_{33}\frac{\delta\sigma'_2}{E'_3} - \frac{\delta\sigma'_3}{E'_3}$$

where the parameters have the meanings given on page 32. It should be noted that only four parameters are defined in equations 3.23, the fifth independent shear modulus may not be determined from the triaxial test unless diagonal samples are used. There are however some difficulties with this method of determination discussed by Atkinson (1973) and Costa-Filho (1978a). If direction one represents the vertical or axial direction and the axis of symmetry, then directions two and three are horizontal and have the same properties. With the parameters redefined, with definitions given on page 32 the incremental equations may be written in terms of the stress and strain invariants as:-

$$\delta\varepsilon_v = \frac{(1+2n'(1-\nu'_{hh})-4\nu'_{ha})}{E'_a}\delta p' + \frac{2(1+n'(1-\nu'_{hh})-\nu'_{ha})}{E'_a}\delta q'$$

$$\delta\varepsilon_s = \frac{2(1+n'(1-\nu'_{hh})-\nu'_{ha})}{E'_a}\delta p' + \frac{2(2+4\nu'_{ha}+n'(1-\nu'_{hh}))}{E'_a}\delta q' \qquad 3.25$$

These equations apply only for a vertical sample. For a horizontal sample due to differing sample stiffnesses in the radial directions of the apparatus the sample no longer deforms in a circular section. A distinction must therefore be made between $\delta\varepsilon_2$ and $\delta\varepsilon_3$ and a more complete equation used for $\delta\varepsilon_s$ (equation 3.10) , this results in a very complex expression which allows determination of the fourth elastic parameter. These equations are clearly no longer decoupled.

In order to determine four of the elastic parameters two tests only are required, one on a horizontal sample and one on a vertical sample. Such tests are described by Atkinson (1973).

Difficulties with the non-uniform deformation of horizontal samples have already been noted, if a third test is conducted on a diagonally cut sample to determine G'_{xy} similar problems of non-uniform deformation will occur.

Although certain elastic parameters have been used in the above discussion there are many alternative sets which may be used to describe behaviour, For example Clinton (1985).

3.4.3 Limitations on Values of Elastic Parameters.

The elastic parameters used in section 3.4.2 must have values lying within certain limits. Additionally the manner in which they vary with state is controlled by thermodynamic limitations. The variation of these parameters has been discussed by Pickering (1970), Gibson (1974), Hooper (1975), Zytinski et al (1978) and Houlsby (1981). In general, hysteresis loops must not be developed i.e. the system is conservative, dilation is not permitted and stiffnesses must be positive.

For an isotropic material the limitations on the value of Poissons ratio are that it must lie in the range of -1 to 0.5 and the stiffness, E, must be positive. This arises from the thermodynamic requirements that the strain energy function remains positive (Pickering, 1970). It should be noted that materials appear to take values of Poissons ratio in the range 0 to 0.5, the author is unaware of any elastic material for which $\nu' < 0$.

In the case of an anisotropic material the conditions are more complex and are best described as follows. All stiffnesses E'_x, E'_y and G'_{xy} must all be positive while the parameters $n' = E'_y/E'_x$, ν'_{xx} and ν'_{xy} must all lie within limits given by Pickering (1970) and shown diagrammatically in Fig 3.1. the surface shown forms a boundary enclosing all thermodynamically acceptable values of the parameters. Pickering (1970) and Hooper (1975) discussed some interesting properties of the elastic model which may be observed from this Figure.

The value of n' ($n'=E'_x/E'_z$) may be expected to vary with consolidation history. For isotropic samples it takes the value of one while for samples compressed with $\eta'_o>0$ $n'>1$ and for samples compressed with $\eta'_o<0$, $n'<1$. It should be noted however that even if $n'=1$ this is not sufficient for isotropy since there remain a further three independent parameters. It has been assumed throughout that the soil grains themselves are incompressible and the soil is fully saturated, the effect of these factors has been considered by Bishop and Hight (1977). Where the compressibility of the soil grains and the pore water is taken into account, the value of the bulk modulus is no longer infinite for undrained loading and hence $\nu_u \neq 1/2$.

In practice the elastic moduli vary with sample state and so it is also of interest to know in what manner these parameters may vary. Some of the experimental observations were discussed in chapter 2, there is however no guarantee that the data from such tests includes only elastic behaviour. Only the isotropic model with bulk and shear moduli will be considered here. The bulk and shear moduli are commonly considered to increase with p' in the manner outlined in section 3.5.2. Zytinski et al (1978) have shown that if this is so then the Poissons ratio cannot be constant due to the implications on the variation of the shear modulus again from thermodynamic considerations. If the shear modulus is allowed to vary with p' then the bulk modulus must also vary with q' (Zytinski et al, 1978). Although there is evidence to suggest that the shear modulus may depend on p' there is none to illustrate the dependence of bulk modulus on q'. Finally it is acceptable for the shear modulus to take a constant value. Some alternative models which do not obey the full thermodynamic requirements will be discussed in section 3.5.2.

3.4.4 Discussion of the Elastic Model.

The attraction of the elastic model for analysis has been the simplicity of the model. Often in calculations the soil is taken to be isotropic linear elastic, but the importance of using the anisotropic model where appropriate has been demonstrated by Hooper (1975). Significant changes in stress distributions in a soil mass are predicted as a result of anisotropy. Despite the simplicity of the model many more sophisticated models incorporate isotropic elastic regions to describe the behaviour of overconsolidated samples.

Since soils are generally highly non-linear in the overconsolidated state, it proves difficult to select appropriate elastic parameters for design from laboratory tests. It is generally observed, as discussed in chapter 2, that field and laboratory parameters do not agree very well. Even where field derived moduli are used (based on back analysed structures) a number of problems detailed by Simpson et al (1979) exist when analysing deep excavations :

a) separate analyses are required for predictions of the wall movement and ground movements around the excavation;

b) much higher stiffness moduli are required than those typically quoted from laboratory tests;

c) material inside diaphragm walls progressively yields as excavations progress;

d) non-linearity makes definition of stiffness moduli very difficult: the prediction of long term movements when the material has drained is particularly difficult.

For these reasons the authors presented a non-linear elasto-plastic computer model for London clay (described in section 3.7.2).

Although the elastic model may be used for the prediction of behaviour in monotonic loading tests (Atkinson, 1973) it seems that the model is limited when applied to boundary value problems. Some of the predictions which have been claimed to be very close to observed behaviour may be fortuitous since in reality the soil behaviour differs significantly from that of an ideal elastic material.

3.5 Critical State Soil Mechanics.

The critical state models are strain hardening plasticity models. Precise details of the features very according to which version of these models is considered. The model considered below will generally be the Cam clay model (Schofield and Wroth, 1968), but features of more recent formulations will be indicated where relevant. These models and the critical state concept were based on the generalised principle of effective stress proposed by Rendulic (1937).

These models are particularly attractive for analysis since they incorporate many features of classical soil mechanics in one model and allow both deformation and stability analyses to be performed using the one model. The models developed from the work of Roscoe et al (1958), who combined the concept of a unique surface in p', q', v space for normally consolidated clays (Rendulic, 1937), the normalisation of clay behaviour with respect to pre-cconsolidation pressure (Hvorslev, 1936) and an extension of the concept of a critical voids ratio (Casagrande 1936) to that of a critical state line in q', p', v space. A work equation proposed by Roscoe et al (1963a) allowed the derivation of a plastic potential and yield curve using Drucker's stability hypothesis (Drucker, 1959). The model is fully described by Schofield and Wroth (1968). Alternative models have also developed along similar lines including an incremental theory by Roscoe and Poorooshasb (1963) and the modified cam clay theory (Roscoe and Burland, 1968) which makes use of the modified work equation to develop the flow rule

The models include isotropic elastic behaviour for overconsolidated soils and either a Mohr Coulomb failure criterion (Roscoe and Burland, 1968) or the extended Von-Mises criterion (Schofield and Wroth, 1968) The relationship of these criteria has been discussed by Atkinson and Bransby (1978 A review of critical state type models and the variations of each has been presented by Woods (1986a)

3.5.1 The State Boundary Surface.

In critical state theory the state boundary surface is of major importance. This surface limits the states which may be attained by a given soil both normally and overconsolidated. The shape of the surface is normally defined in p', q', v space. In Fig 3.2 a typical surface for an isotropically compressed soil is shown. It should be noted that this surface need not be symmetrical about the q' = 0 axis for extension states as shown by Fig 3.3. The state boundary surface is also a yield curve and so separates regions of elastic behaviour below the surface for overconsolidated soils from elasto plastic behaviour which occurs on the surface.

In most formulations of the critical state models the shape of the surface remains constant and independent of the size of any sections. Hence by use of simple normalising procedures discussed by Atkinson (1984a) dimensionless curves may be produced.

The precise shape of the various parts of the model vary according to which version is being used. For the normally consolidated region the Cam clay model uses a log spiral for the bounding curve while the modified Cam clay model (Roscoe and Burland, 1968) uses an ellipse. In most recent models developments appear to have been based on the elliptical surface e.g. Wei (1981), Mroz et al (1979). In the Cam clay model the complete three dimensional equation of the surface is given by:-

$$| q' | = \frac{Mp'(\Gamma + \lambda - \kappa - v - \lambda \ln p')}{(\lambda - \kappa)} \qquad 3.26$$

For modified Cam clay the surface is described by:-

$$q' = Mp' \left[\exp\left(\frac{N - v - \lambda \ln p'}{(\lambda - \kappa)} \right) - 1 \right]^{1/2} \qquad 3.27$$

The definitions of the various constants in these equations are given in Figs 3.4a and b. The region below the surface divides into regions described as being wet of critical for all states to the right of critical state (lightly overconsolidated) and dry of critical for all states to the left of critical state (heavily overconsolidated, Fig 3.4b. The shape of the surface on the dry side of critical i.e. heavily overconsolidated samples, is less well defined due to the relatively small amount of research conducted in this area

Various alternatives on the dry side of critical have been proposed combined with a normally consolidated (Roscoe) surface of either Cam clay of modified Cam clay. One of the alternatives is discussed by Atkinson (1978). In this case Cam clay is combined with a linear Hvorslev surface limited by a 1:3 sloping no tension cut off. Tests conducted during the period of this research by the author to examine the shape of the state boundary surface at low effective stresses have been reported by Atkinson (1984c) for Gault clay from Cambridge and Atkinson and Farrar (1984) for London clay from Denham, Buckinghamshire. These tests indicated a bounding surface which had a slope of less than 1 3 which was non-linear and appeared to be merging into an approximately linear Hvorslev surface which had been established from tests at higher stress levels.

From Figs 3.4a and 3.3b it can be seen that the critical state line is defined by the equations;

$$q' = Mp' \qquad 3.28$$

and

$$v = \Gamma - \lambda \ln p' \qquad 3.29$$

and the normal consolidation line by the equation;

$$v = N - \lambda \ln p' \qquad 3.30$$

alternative formulations (Butterfield, 1979 and Houlsby, 1981) suggest that some improvement in linearity of the critical state and normal compression lines may be gained by plotting data in lnv , lnp' space i.e. the equations of the critical state and normal compression lines respectively are given by:-

$$\ln v = \Gamma^* - \lambda^* \ln p' \qquad 3.31$$

and,

$$\ln v = N^* - \lambda^* \ln p' \qquad 3.32$$

The implications of this change are to change the shape of the state boundary surface. In the case of the modified Cam clay model this becomes:-

$$q' = Mp' \left[\exp \left[\frac{\ln N^* - \ln v - \lambda^* \ln p'}{(\lambda^* - \kappa^*)} \right] - 1 \right] \qquad 3.33$$

It should be noted that the statement by Butterfield (1979) that an advantage of using these equations was that a negative voids ratio (a specific volume less than one) could never be attained is false since clearly in the case of the normal compression line this will occur when:-

$$p' = \exp (N^* / \lambda^*) \qquad 3.34$$

It is clear from equation 3.34 that this does not occur however until very high pressures. Some of the other implications of this change will be discussed in later sections.

In this section discussion has been restricted to that of formulations of critical state theory for isotropically compressed soils. There is evidence however that where soils have not followed an isotropic stress history that the shape of the state boundary surface may differ considerably. This is of particular significance since most sedimented soils occurring naturally are not isotropically compressed but are one-dimensionally compressed i.e. under conditions of zero lateral strain. In such cases it has been observed that for reconstituted soils the state boundary surface is orientated about the consolidation path in q', p' space as shown in Fig 3.5, (Koustofas, 1980; Gens, 1983; Rao et al, 1983; Robinson, 1984; Atkinson, Richardson and Robinson, 1986). Similar observations have been made using carefully sampled undisturbed soils (Mitchell, 1970; Pender, Parry and George, 1975). The same principles apply to these anisotropic models but the mathematical models differ to the isotropic models in that they depend on the consolidation stress ratio (η'_o). In addition there are those cases to consider where "rotational" hardening of the state

boundary surface may take place. Rotational hardening may be interpreted as stress induced anisotropy (Wong and Arthur, 1985) and occurs where a sample after following one consolidation history changes path and continues on a new consolidation path for a considerable distance. In such cases the state boundary surface slowly rotates from its original position to orientate about the new stress path (Hashiguchi, 1977). This is a form of kinematic hardening of the yield surface. Tests conducted by Lewin (1978) on Slate dusts show this type of behaviour. Other forms of kinematic hardening of the surface may also occur and are a feature of some of the models described later. This describes the movement of the axis of the surface relative to the q' and p' axes (Fig 3.6) without rotation. In both cases the shape of the yield surface may distort.

The significance of rotational and kinematic hardening is uncertain but may provide a better fit to experimental data than the standard critical state model although at sacrifice of complexity.

3.5.2 Behaviour of Soil Below the State Boundary Surface.

When the state of the soil falls below the state boundary surface the soil behaviour is assumed to be isotropic elastic. The equations defining such behaviour were given in section 3.4 (equations 3.22). It should be noted however that in the original cam clay model (Schofield and Wroth, 1968) the elastic shear strains were neglected. Simpson (1973) included an elastic shear modulus due to difficulties caused in finite element calculations by the assumption that $G = \infty$ in the Cam clay model. Samples unloaded by reducing p' while q' = o are assumed to follow a log spiral on a v:p' plot as shown in Fig 3 4 and defined by the equation:

$$v = v_\kappa - \kappa \ln p' \qquad 3.35$$

from equations 3 21 and 3 22 it may be shown that,

$$K' = vp' \kappa \qquad 3.36$$

and,

$$G' = \frac{vp' 3(1-2\nu')}{\kappa \quad 2(1+\nu')} \qquad 3.37$$

Some of these conditions regarding the variation of these parameters have been discussed in section 3.4. These equations correctly apply only to homogeneous, isotropic although not necessarily linear elastic soils. As a result of the assumption of isotropic elastic behaviour with the equations de-coupled (3.21, 3.22) elastic behaviour is restricted to the vertical planes known as elastic walls. These elastic walls also pass into the state boundary surface for negative values of q'. If the anisotropic elastic equations were used as a result of the lack of decoupling the elastic walls would no longer be vertical. From the equation 3.36 it can be seen that if κ is constant then K' and hence E' and G' depend on current values of p' and v . This also highlights the different meanings

of linearity in various models. In critical state models linearity is interpreted as log linearity. If the modification of plotting in lnv, lnp' space is applied then the equation of the swelling curve becomes;

$$\ln v = v_{\kappa^*} - \kappa^* \ln p' \qquad 3.38$$

and the dependence on v of the bulk modulus is removed to give;

$$K' = p' / \kappa^* \qquad 3.39$$

A further variation was suggested by Naylor et al (1981). In this case linearity of the swelling line was assumed in specific volume, p' space. Hence the value of K' was assumed to be a constant with κ varying. This corresponds to the normal meaning of linear elasticity.

The interpretation of the plotting therefore affects the manner in which it is predicted that stiffness data is normalised. In the standard Cam clay models all stiffnesses are normalised with respect to 1 vp' e g. K'/ vp' = constant, whereas for the modified method of plotting data, all stiffnesses are normalised with respect to 1 p' e g. K' p' = constant.

3.5.3 Behaviour of Soil on the State Boundary Surface.

When the soil moves on elast c wa s below the state boundary surface only elastic strains occur w th no plastic strains The elastic wall is limited by the state boundary surface. Once the state of the sample reaches the state boundary surface yielding occurs and hence plastic strains develop in add t on to elast c stra ns The intersection of an elast'c wall and the state boundary surface forms a yield curve There are an inf nite number of elastic wa ls so that the state boundary surface it e f a yield surface

In order to compute the pla tic stra ns result ng from load ng a hardening law, a plastic potential and a flow rule are requ red The harden ng law determines the magnitude of strains while plastic potent al and flow rule relate the increments of volumetric and shear strains to the stress state. In the ong nal cam clay model it was assumed that the flow rule was associated so that the yield curve and plastic potential co incided, hence the strain increment vector is normal to the yield surface so that normal ty may be sa d to apply. The flow rule need not be associated, it is merely an idea ation based on the the success of plasticity models us'ng an associated flow rule for the prediction of behaviour of metals. The question of the applicability of normality has been the subject of much literature (see for example Houlsby, 1981) and experimental work. The problem has recently been re examined and a new experimental method of testing for normality proposed by Atkinson and Richardson (1985a) who concluded that for the soils they tested normality was likely to be sufficiently accurate Further similar tests have been conducted by Ho (1985a). In some formulations of critical state models the concept of normality is not used or its restrictions relaxed by the use of more than one yield locus (Roscoe and Burland, 1968). In cases of multiple

yield loci the condition permits the strain increment vector to lie between the normals drawn to individual yield loci. It can therefore be seen that the strain increment ratio is a function of stress state and not the stress increments themselves (Hill, 1950). The precise form of flow rule depends on the version of model selected.

On the state boundary surface it is assumed that the total strains are the arithmetic sum of the plastic and elastic components i.e.

$$\delta\varepsilon_s = \delta\varepsilon^e_s + \delta\varepsilon^p_s \qquad 3.40$$

$$\delta\varepsilon_v = \delta\varepsilon^e_v + \delta\varepsilon^p_v \qquad 3.41$$

The elastic components may be computed as described in section 3.5.2 for an isotropic elastic material, the general approach to the computation of the plastic components will now be given. There are a number of alternative methods of approaching the derivation of these equations, two methods were outlined by Schofield and Wroth (1968) and Atkinson and Bransby (1978). An alternative thermodynamic approach has been described by Houlsby (1981).

The flow rule F relating plastic increments of shear and volumetric strain is a function of the state of stress of the sample and the shape of the plastic potential and may be written,

$$F = \delta\varepsilon^p_s / \delta\varepsilon^p_v \qquad 3.42$$

The function F may either be derived from energy considerations (Schofield and Wroth, 1968; Roscoe and Burland, 1968) or be chosen as a convenient function. Following Schofield and Wroth (1968) equation 3.42 may be integrated to derive the shape of the plastic potential and hence the yield curve if normality applies.

$$\log_e\left[\frac{p'}{p'_c}\right] = -\int_0^{\eta} \frac{d\eta'}{((1/F)+\eta)} \qquad 3.43$$

where the definitions of the parameters are given in Fig 3.3. The incremental strains may be computed by considering the specific volume changes which occur in moving between two yield curves so that the increment of volumetric strain may be derived as,

$$\delta\varepsilon_v = \frac{\lambda}{v}\left[\frac{\delta p'}{p'} + \left[\frac{1-\kappa}{\lambda}\right]\left[\frac{\delta\eta'}{(1F)+\eta'}\right]\right] \qquad 3.44$$

By considering only the plastic part of equation 3.44 the increment of shear strain may be derived as,

$$\delta\varepsilon_s = \frac{(\lambda-\kappa)}{v}\left[\frac{\delta p'}{p'} + \frac{\delta\eta'}{(1F)+\eta'}\right]F + \frac{\delta q'}{3G'} \qquad 3.45$$

The equation of the state boundary surface may then be obtained by integrating equation 3.44 to get,

$$\log_e\left[\frac{p'_e}{p'}\right] = \left[\frac{1-\kappa}{\lambda}\right]\int_0^{\eta'} \frac{\delta\eta'}{(1/F)+\eta'} \qquad 3.46$$

where p'_e is the equivalent mean effective pressure (Schofield and Wroth, 1968) given by,

$$p'_e = \exp((N-v)/\lambda) \qquad 3.47$$

and shown in Fig 3.3. This together with p'_c the pre-consolidation pressure,

$$p'_c = \exp((N-v-\kappa \ln p')/(\lambda-\kappa) \qquad 3.48$$

are very important normalising parameters. Note that the use of lnv, lnp' axes changes the value of these parameters, for example the equation for p'_e becomes

$$p'_e = \exp((\ln N^* - \ln v)/\lambda^*) \qquad 3.49$$

Hence if the flow rule is known the constitutive equations may easily be derived.

An alternative approach is to make use of the expression,

$$\delta\eta' = \frac{\delta q'}{p'} - \eta'\frac{\delta p'}{p'} \qquad 3.50$$

in equation 3.44. This equation may then be written in the form,

$$\delta\varepsilon_v = (C^e + C^p)\,\delta q' + (D^e + D^p)\,\delta p' \qquad 3.51$$

where C^p and D^p are hardening parameters which depend on the state of stress and the shape of the yield surface. From equations 3.51 and 3.42 the increment of shear strain may be written as,

$$\delta\varepsilon_s = (A^e + FC^p)\,\delta q' + (B^e + FD^p)\,\delta p' \qquad 3.52$$

From section 3.4 for an isotropic soil $C^e = B^e = 0$ and so the total strains may be written as,

$$\delta\varepsilon_s = (FC^p + 1/3G')\,\delta q' + FD^p\,\delta p' \qquad 3.53$$

$$\delta\varepsilon_v = C^p\,\delta q' + (D^p + 1/K')\,\delta p' \qquad 3.54$$

These equations further simplify as normality and co-axiality apply so that (Naylor et al, 1981),

$$C^p = FD^p \qquad 3.55$$

Equations 3.53 and 3.54 may therefore be written in matrix form as,

$$\begin{bmatrix}\delta\varepsilon_s\\ \delta\varepsilon_v\end{bmatrix} = \begin{bmatrix}FC^p + 1/3G' & C^p\\ C^p & (C^p/F) + 1/K'\end{bmatrix}\begin{bmatrix}\delta q'\\ \delta p'\end{bmatrix} \qquad 3.56$$

This method follows that of Atkinson and Bransby (1978). If the equation of the state boundary surface were known, by expressing the equation in terms of specific volume and differentiating, the terms C^p and D^p and hence F may be derived to arrive at the constitutive equations. This method was used by Robinson (1985) to derive an anisotropic Cam clay type model.

For the Cam clay model the equations 3 56 , may be written as,

$$\begin{bmatrix}\delta\varepsilon_s\\ \delta\varepsilon_v\end{bmatrix} = \begin{bmatrix}\dfrac{\lambda-\kappa}{(M-\eta')vMp'} + \dfrac{1}{3G'} & \dfrac{\lambda-\kappa}{vMp'}\\ \dfrac{\lambda-\kappa}{vMp'} & \dfrac{(M-\eta')(\lambda-\kappa)}{vMp'} + \dfrac{1}{K'}\end{bmatrix}\begin{bmatrix}\delta q'\\ \delta p'\end{bmatrix} \qquad 3.57$$

using the modified theory of Roscoe and Burland (1968) these equations become,

$$\begin{bmatrix}\delta\varepsilon_s\\ \delta\varepsilon_v\end{bmatrix} \begin{bmatrix}\dfrac{4\eta^2(\lambda-\kappa)}{(M^2-\eta^2)(M^2+\eta'^2)vp'} + \dfrac{1}{3G'} & \dfrac{2\eta'(\lambda-\kappa)}{vp'(M^2+\eta^2)}\\ \dfrac{2\eta'(\lambda-\kappa)}{vp'(M^2+\eta^2)} & \dfrac{(\lambda-\kappa)(M^2-\eta^2)}{vp'(M^2+\eta^2)} + \dfrac{1}{K'}\end{bmatrix}\begin{bmatrix}\delta q'\\ \delta p'\end{bmatrix} \qquad 3.58$$

Both of these equations show the feature d scussed in section 3 4. The stiffnesses both elastic and p astic are norma sed w th respect to the parameter 1 vp'. This is as a consequence of a um ng lineanty of the normal compression and swe ng l nes in v , lnp' space. By using the assumption of l nearity in lnv , lnp' space Hou sby (1981 has der ved the equation of the state boundary surface for the mod f ed Cam clay model as

$$\ln v \quad \ln N^* - \lambda^* \ln p' + (\lambda^* - \kappa^*)\ln(M^2\ (M^2+\eta^2\ ) \qquad 3.59$$

The flow rule for th s model is unchanged from that of the modified Cam clay model. The incremental equations may then be derived as,

$$\begin{bmatrix}\delta\varepsilon_s\\ \delta\varepsilon_v\end{bmatrix} = \begin{bmatrix}\dfrac{4\eta'^2(\lambda^*-\kappa^*)}{p'(M^2-\eta'^2)(M^2+\eta'^2)} + \dfrac{1}{3G'} & \dfrac{2\eta'(\lambda^*-\kappa^*)}{p'(M^2+\eta^2)}\\ \dfrac{2\eta'(\lambda^*-\kappa^*)}{p'(M^2+\eta'^2)} & \dfrac{(M^2-\eta^2)(\lambda^*-\kappa^*)}{p'(M^2+\eta'^2)} + \dfrac{1}{K'}\end{bmatrix}\begin{bmatrix}\delta q'\\ \delta p'\end{bmatrix} \qquad 3\,60$$

These equations show that stiffnesses are now normalised only with respect to the parameter 1/p', the dependence on specific volume being removed. Note that K' in equation 3.60 is given by equation 3.39.

3.5.4 Failure.

The definition of failure for a normally consolidated sample is relatively simple, however for an overconsolidated sample it is not so clear.

Typically normally consolidated samples do not show a peak strength, the stress strain curve rises to reach a maximum (ultimate) value at which failure may be said to occur. At very large strains reductions in strength are observed as the soil strength approaches its residual value (Skempton, 1964). For an overconsolidated soil there is often a peak strength before a rapid reduction of strength at modest strains before a very slow reduction to residual strength at very large strains. This is shown in Fig 3.7b for a drained sample. The peak strength proves to be of little use in correlating data since its magnitude above the ultimate value is dependent on overconsolidation ratio, similarly except where pre-existing shear planes exist the residual strength is unlikely to be of interest due to the large strains required to attain this strength.

The strength which is of interest is the ultimate strength which corresponds to the critical state. It is characterised by a number of features At the critical state the shear strains may become very large without further changes in the stresses q' and p' or the stress ratio $\eta' = q'/p'$. In addition changes in volume of the sample will tend to zero, so that in undrained tests the pore pressures reach a constant value while in drained tests the change in volumetric strain tends to zero. For the normally consolidated sample this corresponds to the maximum strength observed, while for overconsolidated samples it is the strength indicated immediately before the long slow reduction to residual strength, Fig 3.7b

It is the ultimate strengths which should be correlated in the critical state framework. The choice of failure criterion is normally either Von Mises or Mohr Coulomb. The relationship between these criteria and some of the other alternatives has been discussed by Atkinson and Bransby (1978) and Houlsby (1981) These criteria generally indicate (except Von-Mises) a different maximum shear stress q' on different paths to failure due to the influence of the intermediate effective principal stress σ'_2 This leads to difficulties when comparing strength data from difference types of tests e.g. triaxial compression and extension tests, simple shear tests etc. In order to correlate this data account must be taken of the intermediate stress σ'_2 (Wroth, 1984). Some alternative failure criteria are discussed by Roscoe, Schofield and Thurairajah (1963b), Houlsby and Wroth (1984) In the case of the critical state models, failure is normally considered to occur with a constant value of M for all paths ie an extended Von-Mises failure criterion, (Schofield and Wroth,

1968). However in some cases ,eg Roscoe and Burland (1968) , a Mohr-Coulomb failure criterion has been iincorporated . In this case for triaxial extension and compression the values of M_c and ϕ'_c , M_e and ϕ'_e may be related (ie $M_c = 6 \sin \phi'_c / (3 - \sin \phi'_c)$, $M_e = 6 \sin \phi'_e / (3 + \sin \phi'_e)$,Atkinson and Bransby, (1978)).

3.5.5 Problems in Applying the Critical State Model.

The critical state model provides a very powerful conceptual model of soil behaviour and requires only four soil constants in order to calibrate the model for a given soil. However, it can prove difficult to apply in some cases. The model was developed using normally consolidated and lightly overconsolidated samples of reconstituted soils and has been successfully applied only to these materials. Some difficulties have been associated with the anisotropy of real soils, these difficulties are being overcome through specialised testing techniques and new analytical models. Furthermore both of the models outlined above in common with most other critical state models fix the ratio of p'_{cs} / p'_o. This factor appears to vary widely for real soils (see for example Bishop, 1970 and Little, 1985), Fig 3 3a, and may vary with such factors as the plasticity of the soil and its particle size distribution A more flex ble model would allow this easily determined factor to be fixed as an input parameter, examples of such models are those by Mroz et al (1979), Wei (1981), Woods (1986c)

The main d fficult es often ie in determining the va ue of the soil constants. The slope (λ) and intercept N) of the normal consolidation l ne are usually well defined, it is the remaining parameters which prove e easy to determine The critical state is often poorly defined making the determination of the critical state intercept (Γ) difficult. This is especially true of many und sturbed soils and in particu ar those which are heavi y overconsolidated and soils which tend to fail on well defined shear planes rather than by plastic fa lure. In such cases the critical state may have been atta ned on the shear plane but not in the rema nder of the soil. This, combined with loca sed dra nage around the shear plane (Atk nson, 1985b , can cause great difficulty in defining the cri cal state Tests conducted on London clay by Atkinson and Richardson (1985b) tend to conf rm that th s occurs Th s is not therefore a fa ng of the model but is due to difficulties in determ n ng the sample state Roscoe (1970) d scussed s m lar problems when interpreting data from the s mple shear apparatus and noted that such s p p anes were typically observed (by X-ray techniques) to be of the order of 10 grains in thickness. These s p planes were observed to form after peak stress ratio had been reached The degree of non-uniformity of samples then increased unt l at critical state the water content on the slip plane was approximately 3.5% greater than that of the average for the samp e Atkinson and Richardson (1985b) observed errors of a similar magnitude indirectly in triax al tests on overconsolidated reconstituted London Clay.

Problems also occur in defining the slope of a swelling curve, κ, in a v , lnp' plot (equation 3.35). The assumption of linearity does not prove very accurate over large changes of stress, nor does the change to lnv, lnp' co-ord nates make much improvement. The slope of the swelling curve (κ)

is observed to increase from very small values on stress reversal to considerably greater values after some change of stress. Little (1985) has plotted characteristic curves for Ware till to illustrate this effect. Evidence presented by Parry and Amerasighe (1973) suggests that values of κ close to stress reversal i.e. low values of κ , should be used in analysis in critical state models. The reasons given were that after large changes of stress, "reverse" plastic strains were occurring and the observed response below the state boundary surface was not entirely elastic.

This observation is confirmed by the presence of hysteresis loops seen in isotropic compression and swelling curves below the state boundary surface. Some plastic strains must occur since an abrupt yield point is not observed in practice for overconsolidated samples. A number of models do allow such plastic strains, two of which will be described in sections 3.6 and 3.7 below. Other models have allowed some plastic strains only for increasing stress levels below the state boundary surface e g a revised version of the modified Cam clay model (Roscoe and Burland, 1968) or a more complex model incorporating a retracting yield locus (or bounding surface) by Dafalias and Herrmann (1980) In these models plastic strains develop progressively until the largest previously encountered yield locus is reached at which point the material develops the strains associated with a normally consolidated material

An alternative approach has been to use ranges of pseudo-elastic behaviour in which stiffness moduli are allowed to vary in a manner which has some of the characteristics of elastic behaviour but may not satisfy the conditions required thermodynamically. Nova and Hueckel (1981) and Nova (1982 developed a model for which the stiffness below the state boundary surface depended on the state of the sample and also on the distance along the stress path since last stress reversal relative to the distance from the reversal point to the state boundary surface. This behaviour was termed "Paraelastic" and reproduced hysteresis loops. Two models were developed by Houlsby (1981 one in which the shear modulus was proportional to p' and the other in which the shear modulus was proportional to the pre-consolidation pressure, p'_c. In the model with G' proportional to p' , contours of constant volume become parabolic in shape and are limited by a maximum stress ratio line (Fig 3 8a . It has already been indicated that this model is unacceptable thermodynamically but Fig 3 8a shows a further objection in that lines of constant volume may cross for samples of high overconsolidation ratio It was indicated that this model is only acceptable thermodynamically if v' vanes or if the bulk modulus depends on q'. Evidence from anisotropic compression and swelling tests suggests this is not the case since the initial value of κ does not vary with p'_c and hence is also independent of the value q' (Namy, 1970; Gens, 1983 Variation of slope on a single swelling line depends only on the overconsolidation ratio of samples, p'_c/p' and appears to be independent of stress history (isotropic or anisotropic). Since this variation is independent of p'_c and also of q' the value of K' does not depend on q'.

In the model with $G' \propto p'_c$ elastic plastic coupling occurs since the elastic strains depend on the plastic strains accumulated This requires a slight modification to the shape of the yield locus below which G' is constant (Fig 3 8b) This model has other drawbacks such as the constant value

of G' below the yield locus, which are fully discussed by Houlsby (1981). Evidence presented by Houlsby (1985) suggested that the precision of fit to laboratory data for a sand for both models was similar, the conclusion was that the true behaviour was a combination of these two factors. Further data presented by Wroth et al (1979) confirms this pressure dependence for a variety of soils. Graham and Houlsby (1983) presented data for Winnepeg clay which gave a good fit to a pressure dependent set of anisotropic stiffness moduli. Despite the theoretical objections to this method a good fit is provided to a variety of soil test data.

3.6 Pender's Model.

The critical state models were originally developed for normally consolidated soils. A model for overconsolidated soils with the critical state framework was developed by Pender (1977, 1978). This model allowed for plastic strains below the state boundary surface and could be applied to both isotropic and anisotropic soils. With some modifications some kinematic hardening effects could also be allowed for. The version of the model described here is the anisotropic model which can be reduced to the isotropic model if required. The same model parameters as for the Cam clay models were used and the assumption of zero elastic shear strain was retained.

In this model yield loci are lines of constant stress ratio and a shape for the undrained stress path is assumed. This together with a non-associated flow rule allows the development of the model.

3.6.1 Model for Overconsolidated Behaviour.

The yield locus is shown in Fig 3.9a. These are lines of constant stress ratio and it is assumed that these follow the state path so that plastic strains may develop under both increasing and decreasing stresses for all paths except those of constant stress ratio, η'. The shape for the undrained stress path was assumed to be,

$$\left[\frac{\eta'-\eta'_o}{AM-\eta'_o}\right]^2 = \frac{p'_{cs}}{p'}\left[\frac{1-(p'_o/p')}{1-(p'_o/p'_{cs})}\right] \qquad 3.61$$

and the flow rule was assumed to be given by,

$$\frac{d\varepsilon^p_s}{d\varepsilon^p_v}_{oc} = \frac{(AM-\eta'_o)^2}{(AM)^2 v(p'_o/p'_{cs})-1)((AM-\eta'_o)-(\eta'-\eta'_o)(p'/p'_{cs}))} \qquad 3.62$$

Hence the incremental equations could be obtained (Pender, 1978),

$$d\varepsilon^p_{s\,oc} = \frac{2\kappa(p'/p'_{cs})(\eta'-\eta'_o)\,d\eta'}{(AM)^2 v((2p'_o/p')-1)((AM-\eta'_o)-(\eta'-\eta'_o)(p'/p'_{cs}))} \qquad 3.63$$

$$d\varepsilon^p_{v\,oc} = \frac{2\kappa((p'_o/p'_{cs})-1)(p'/p'_{cs})(\eta'-\eta'_o)\,d\eta'}{v(AM-\eta'_o)^2((2p'_o/p')-1)} \qquad 3.64$$

$$d\varepsilon^e_v = \frac{\kappa dp'}{vp'} \qquad 3.65$$

where the parameters are defined on page 32. Using this model many of the features of overconsolidated behaviour of soils could be reproduced both for anisotropic and isotropic cases (with $\eta'_o = o$). It should be noted that although plastic strains may develop for any unloading or reloading path in which η' changes, on constant η' paths only elastic strains develop, hence the hysteresis loops observed in isotropic compression and swelling tests are not reproduced.

3.6.2 Model for Normally Consolidated Behaviour.

The model was extended to that of normally consolidated soils by Pender (1977). The overconsolidated behaviour was retained as described in section 3.6.1 but a second yield locus was introduced to describe normally consolidated behaviour. Plastic strains for normally consolidated states were assumed to be the sum of those for both normally and overconsolidated states together. The additional yield locus was taken as being equation 3.61 for the normally consolidated soil. However this locus was allowed to change shape as it expanded with varying η' (η'_o is taken as the value of η' at the end of the previous increment). For reducing stresses when the state passes inside the surface it does not change shape until it is met again on a later path Figs 3 9b and 3.9c. The flow rule for the normally consolidated state was taken as,

$$\frac{d\varepsilon^p_s \text{ nc}}{d\varepsilon^p_v \text{ nc}} = \frac{\eta'}{AM - \eta'} \qquad 3.66$$

Hence the incremental strains for the normally consolidated yield surface only were derived as,

$$d\varepsilon^p_v \text{ nc} = \frac{(\lambda - \kappa)}{v}\left[\frac{dp'}{p'} + \frac{2(p'/p'_{cs})((p'_o/p'_{cs}) - 1)(\eta' - \eta'_o)\,d\eta'}{(AM - \eta'_o)^2(2p'_o\ p') - 1)}\right] \qquad 3.67$$

$$d\varepsilon^p_s \text{ nc} = \frac{\eta'}{AM - \eta'}\, d\varepsilon^p_v \text{ nc} \qquad 3.68$$

The total strains occurring for a normally consolidated soil could then be computed from,

$$d\varepsilon_v = d\varepsilon^p_v \text{ nc} + d\varepsilon^p_v \text{ oc} + d\varepsilon^e_v$$
$$d\varepsilon_s = d\varepsilon^p_s \text{ nc} + d\varepsilon^p_s \text{ oc} \qquad 3.69$$

This model reproduces many of the effects observed in both normally and overconsolidated soils. For normally consolidated soils it models a non-uniqueness of the direction of the strain increment vector and also models some effects of stress induced anisotropy. It does not however reproduce the hysteresis loops observed in tests conducted on constant η' paths. It should also be noted that although plastic strains do occur below the state boundary surface this model produces a unique strain increment ratio for a given stress path after following a given initial consolidation history, regardless of the loading history in its overconsolidated state.

3.7 A Model Incorporating Kinematic Hardening.

The model described here was developed by Mroz et al (1979). It uses an isotropic state boundary surface (consolidation surface in this model) and a kinematic yield surface the function of which will be described. The model will only be described in principle.

3.7.1 Description of Model Behaviour.

The consolidation surface expands as in the Cam clay models as loading progresses in a normally consolidated state. The strains during this phase are described by equations similar to those of modified Cam clay. During this phase the kinematic surface remains in contact with the consolidation surface at the current state point, Fig 3.10a. If the state moves inside the consolidation surface then the kinematic yield surface is entered. While within the kinematic yield surface strains are only elastic. Once the edge of the kinematic yield surface is reached plastic strains start to develop below the consolidation surface and the kinematic yield surface moves with the state point in a prescribed manner (Fig 3.10b). The movement is such that on the present loading path the kinematic yield surface and the consolidation surface will engage at a point of equal slope. As loading progresses the motion of the kinematic yield surface is directed along P_1R_1 and P_2R_2 in Figs 3.10c and d respectively so that the ratio of shear and volumetric strains varies as loading moves towards the consolidation surface. It is assumed that the motion of the K.Y.S. is directed along linear paths P_1R_1 and P_2R_2 towards the consolidation surface. The plastic strains which develop are in proportion to the current distance, δ , from the consolidation surface related to the distance when the kinematic yield surface was last engaged, δ_0 . A power law is used in order to compute the current plastic stiffness moduli using this data. In this way a smooth transition is provided between the regions of elastic and plastic behaviour on the state boundary surface, the behaviour of the model may be interpreted as progressive yielding.

3.7.2 Determination of Model Parameters.

The above causes a major increase in complexity of equations below the state boundary surface and requires three additional parameters compared to the Cam clay models, these are the size of the kinematic yield surface, a_0 , the initial plastic hardening modulus, K_{po} and the power, γ , of the power law for interpolating the plastic behaviour. If desired the elastic region can be reduced to a point, i.e. $a_0 = 0$, in which case there will be no zone of exclusively elastic behaviour although elastic strains would occur continuously on all paths with simultaneous plastic strains. The method suggested for interpreting these new constants was to observe the specific volume, lnp' plot for an isotropic compression a swelling test. The initial stiff portion of the swelling and recompression curves could be interpreted as providing the parameter κ and also the range of the kinematic yield surface in terms of the ratio a/a_0 as defined in Fig 3.10e. All strains occurring in excess of those predicted by the swelling line i.e. equation 3.35, would be interpreted as plastic and so used to derive the power of the power law for the interpolation rule, Fig 3.10e. The plastic volumetric

strains then calculated are plotted as log of plastic volumetric strain against log of mean effective stress p'. The slope of the plot gives the parameter γ, and the initial hardening modulus, K_{po} is defined as the modulus at the edge of the K.Y.S. i.e. at B in Fig 3.9d.. Further fine tuning of these parameters could then be done using data from other tests involving stress cycles. If a further change in direction of stress path occurs then for small changes of direction the path will not re-enter the kinematic yield surface. If however the change in direction is large, Figs 3.10c and d, then the kinematic yield surface will be entered, and on reaching the edge a new distance of δ_o set. Continued loading may result in the kinematic yield surface reaching the consolidation surface, in which case the two surfaces engage at a point of equal slope i.e. along a common normal, and then move together with the state point, without crossing. The behaviour is then as for a material moving on the state boundary surface of the modified Cam clay model.

3.7.3 Discussion.

The model was compared to data from various types of test and the comparison proved very favourable in the case of isotropically compressed soils. In the case of one-dimensionally compressed soils the comparison was not so good but this was explained by the shape of the state boundary surface chosen. This method could simply be applied in principle to any shape of y eld curve or state boundary surface so the extens on to anisotropic models may be made.

Many of the features of the model however have little justification from data observed in laboratory te ts No data exists to conf rm that the shape of the kinematic yield surface is the same as that of the consolidation surface nor is there any data to confirm the relative motion of these surfaces or the form of the interpolation rule for regions between the two surfaces. The model does however reproduce many features of s l behaviour . There is no requirement for a sharp yield point, plastic stra ns develop progres ve y unt l the conso dation surface is reached, a feature which may be anticipated in a real so l Furthermore the elastic stra ns have been restricted to much smaller reg ons of stress space which is l ke y to be more reasonable (Lambe and Whitman, 1979; Parry and Amersingha, 1973 The model can reproduce hysteresis loops even for isotropic compression and swe ng tests It can also reproduce many of the features of undrained compression tests includ ng the characteristic pattern of shear strain contours observed by Louden (1967) While the parameters a_o and γ prove quite easy to define two defects should be noted Firstly the behaviour is sens tive to the values of the elastic stiffnesses. From parametric stud es (Mroz et al, 1979) it would appear that higher values are to be favoured which results in small values of a_o i e small ranges of stiff elastic behaviour. The second problem is rather greater, the model is very sens tive to the shape selected for the consolidation surface including the overconsolidation reg on Although for the comparisons given by Mroz et al (1979) the fit to data was quite good this is clearly an area where improvements could be made if good quality data was available.

Naylor et al (1981) noted that this type of model had major advantages in finite element calculations

as compared with the ordinary critical state models. In such models there is a sudden jump in stiffness between elastic and plastic regions which may cause some numerical problems. However by use of progressive yielding as with this model no such sudden jump occurs and so these numerical problems are avoided.

Finally the most important feature of this model is the non-uniqueness of behaviour which it predicts. All the models described so far in this chapter have been dependent for the soil behaviour only on the maximum past pressure (p'_c) applied i.e. the limiting yield curve, for loading at a given state along a given path regardless of loading history below the state boundary surface. In this model soil has the same limiting yield curve and the same overconsolidation ratio and even with current pressures being identical will depend totally on the recent stress history i.e. the direction of approach of the last loading path, in order to describe its behaviour. The magnitude of strains and the direction of the strain increment vector are totally dependent on the immediately preceding loading history for all states below the state boundary surface. This is as a consequence of including the kinematic yield surface. Further developments were made to this model with cyclic loading over many cycles by Mroz et al (1981).

3.8 Models for Threshold Effects.

Models developed specifica y to describe threshold effects are uncommon. For threshold effects due to time effects some models do exist although not specifically developed for the modeling of threshold effects. Mode s of th s type will not be described in detail but the general form of such models will be described Models for stress path threshold effects are even fewer.S o far as the author is aware only two such models exist at the present time, Simpson et al (1979) developed Model L C. specifically for London clay, and Leach (1984) has developed a second model. These two models will be described in detail.

3.8.1 Models for Time Effects.

Models which included time effects are time dependent models. Models of this type generally operate in the manner of the model described by Borja and Kavazanjian (1985). The yield surface is predicted to expand in a s mi ar manner to that of the cam clay models i.e. with changing sample state in terms of q', p' and spec fic volume. If loading should stop then following the dissipation of any excess pore pressures the y eld locus is observed to expand with time. This expansion of the yield surface is described by a logarithmic law relating volume strain and time so that the volume strains at time Δt after diss pation of excess pore pressures are given by,

$$\varepsilon_v = C_\alpha \log (\Delta t / t_o) \qquad 3.70$$

This equation was given by Taylor (1948). These volume strains relating the change in state from

A to A' in Fig 3.11 are interpreted as representing an increase in the size of yield locus and the development of a quasi-preconsolidation pressure of $p'_c + \Delta p'_c$. Further time elapsed may result in the state point advancing to A". The strains are interpreted as being part elastic and part plastic in the ratio of the elastic and plastic soil parameters, κ and $(\lambda - \kappa)$ respectively. For each log cycle of time a similar reduction of volume and so increase in yield locus size is observed. Shear strains during this period are often interpreted from an empirical hyperbolic relationship due to Singh and Mitchell (1968).

If after a period of time loading is continued then behaviour is assumed to be as that for an overconsolidated soil until the 'quasi' limiting yield curve is reached, thereafter behaviour is the same as that for a normally consolidated state.

These types of models reproduce the volumetric behaviour observed for many soils by use of Taylor's equation. However the description of the shear strains during the period of rest would appear to be less satisfactory. Further work is required in this area in order to provide a better model of the shear strain behaviour. Since the yield locus together with the time relationship is used to describe the volumetric behaviour it would seem logical to use the shear strain predicted from the yield locus from the same calculation to predict the shear strain behaviour. There would appear however to be insufficient data available to assess this possibility.

3.8.2 Model L.C.

Model L C. was developed by Simpson et al (1979) for the analysis of earth structures in London Clay. The object of this model was to assess the significance of using an elasto-plastic model instead of the elastic model to analyse the movements of retaining walls. The model incorporates three ranges of behaviour each of which will be described,

a) elastic strains, within the range of threshold effects;

b) intermediate strains, that range which in the laboratory conforms to monotonic elastic loading (Atkinson, 1973 ;

c) plastic strains, large strains where both plastic and intermediate strains occur together.

The model is basically an adaption of the Cam clay model with a threshold range introduced into the early stages of the elastic range.

The model was developed for the analysis of plane strain conditions but may be applied to other cases e g. axisymmetric and plane stress, with certain limitations. Although the model was developed for use with earth structures in London clay there is no reason in principle why, with suitable substitution of parameters, the model could not be used for other soils. This threshold

range together with the plastic range was designed to overcome some of the problems associated with the elastic model discussed in section 3.4.4.

3.8.2.1 Elastic Strains (Threshold Range).

The elastic range is modelled by use of a kinematic yield surface (K.Y.S.). This defines a zone of stress or strain space in which high stiffnesses apply. Inside this zone behaviour is elastic and recoverable although non-linear. On reaching the edge of the K.Y.S. continued straining moves the K.Y.S. along with the current stress state (Fig 3.12). If the direction of loading is then reversed the high stiffness range again applies until the edge of the K.Y.S. is reached. The distance for which the high stiffness range applies on a loading path can be seen to vary with the precise details of the path.

The precise shape of the K.Y.S. could not be determined from existing data. Therefore it was assumed that a spherical shape defined in terms of strains should be used. It was also assumed that the initial state of the soil lay at the centre of the K.Y.S. and the radius of the K.Y.S. was about 200 $\mu\varepsilon$. The effect of time delay and creep may be to move the position of the K.Y.S. relative to the sample state or to change the radius of the K.Y.S. These features were not modelled. Stiffnesses in this range were taken as ten times those in the intermediate range. Data for this range was selected from the values of stiffnesses obtained from back analysed structures mostly based on experience with undisturbed London Clay.

3.8.2.2 Intermediate Strains.

The intermediate strains are taken as that range which corresponds to the range over which laboratory data is normally quoted. In this range ,behaviour is of an elastic nature although not recoverable. For London Clay Atkinson (1973) concluded that over this intermediate range behaviour could be considered as being non-linear anisotropic elastic for monotonic loading tests.

Stiffness parameters for this range were selected to correspond to Atkinson's data for London Clay and from the analysis of the elastic model by Gibson (1974). The data used in the model were;

$$E'_v = \bar{E}'_v (s + c' \cot \phi') \qquad 3.71$$

where

$$s = \tfrac{1}{2}(\sigma'_x + \sigma'_y) \qquad 3.72$$

$$\bar{E}'_v = 50 \text{ (dimensionless)}$$

$$E'_h = 1.67\, E'_v$$

$$G_{hv} = 0.4\, E'_h$$

$\nu'_{hv} = 0.16$ $\nu'_{hh} = 0.2$

The above parameters are defined on page 32. The range of intermediate behaviour was taken as extending up to strains of 1%.

3.8.2.3 Plastic Strains.

For strains in excess of 1% plastic strains are assumed to occur in addition to continued intermediate strains.

The plastic strains are computed from a modified Cam clay type flow rule written as;

$$\delta v_p / \delta \gamma_p = F_o \sin\phi' (1 - (F / F_o) \qquad 3.73$$

where

v_p = Plastic volumetric strain.

γ_p = Plastic shear strain.

F_o = Constant.

$F = s + c' \cot\phi'$.

The flow rule is associated The stress levels are constrained to lie within the possible limits i.e. between active and passive failure states.

3.8.2.4 Application of the Model.

Simpson et al (1979) tested the model against a number of loading paths relevant to both the field and laboratory tests These included undrained triaxial tests , plain strain tests, oedometer tests, plate bearing tests, pressuremeter tests and back analysed excavations. It was found that the triaxial test was difficult to model but better agreement could be obtained with plane strain tests. This is not surprising since the model was designed to apply to plane strain cases and not axisymmetric loading (see equation 3.72 for example . However many features were considered to be reasonably modelled in the triaxial test up to about 2% strain. Departures from predicted behaviour were possibly also due to the sample not behaving in an axisymmetric manner at large strains e g deforming on preferred shear planes and discontinuities.

Comparisons with oedometer tests were generally quite reasonable but departures occurred as the normally consolidated state was approached. These were probably due to some plastic strains developing before the normally consolidated state was reached i.e. below the yield curve.

Plate bearing tests were modelled and compared with field data. In this case the in-situ stress state of the soil is required for predictions producing a further uncertainty in the data. It was found that a

larger KYS was required (radius = 500 με) to improve predictions. However, this problem is axisymmetric and as in the case of the triaxial test, failure and behaviour at large strains was poorly modelled. The results of a comparison with the pressuremeter test showed a similar pattern to those of the plate bearing test (Simpson et al, 1980). The importance of determining the initial stress state was demonstrated by its effect on the load displacement curve for the plate bearing test.

Comparisons with two back analysed excavations were made, New Palace Yard (Ward and Burland, 1973. Burland and Hancock, 1977) and Neasden underpass (Sills, Burland and Czechowski, 1977). In the case of the New Palace Yard excavation there was a significant improvement in predictions of ground movements as compared to predictions of the linear elastic model. The predictions of movement of the diaphragm walls were also generally very good although the prediction of pore pressure distribution proved more difficult to interpret. Finally a parametric study was conducted to assess the importance of each of the features of the model. This demonstrated the significance of the KYS in the model in reducing the magnitude of movements at large distances from the excavation to values much closer to those observed in the field.

The Neasden underpa s excavation involved the analysis of an anchored diaphragm wall. In this case similar conclusions were reached as for the New Palace Yard excavation however, there were d screpancies noted and attributed to incorrect modelling of soil properties at depth on this site.

Wh le the model can be seen to generally produce good agreement with observed behaviour one particular deficiency should be noted The expression for E'_v (equation 3.71) is found to be highly sens tive to values of c' and ϕ' Costa-Fi ho (1979) noted that if correct data for a given site were not used (i e using average data for a particu ar soil from many sites) then appreciable errors could occur Data presented by Costa Fi ho (1980 showed close agreement to the predictions of model L C and in particular to high in t al stiffnesses observed after a change in direction of stress paths. Th s data was not conc usive however s nce tests started from d fferent initial states, some isotropic and some anisotrop c and it was unclear as to the changes in direction of stress path each had f lowed

3.8.3 Bi linear Threshold Models.

Two much simpler threshold models have been developed by Leach (1984). These models do not use a kinematic yield surface and are only suitable for monotonic loading.

The first model is a bi linear elastic, perfectly plastic model. Soil behaviour is modelled by two elastic moduli E_1 and E_2 (Fig 3 13a) with the threshold range defined in terms of a threshold strain ε_{th} Fa lure is modelled by a Mohr-Coulomb fa lure criterion. This model has been used to describe the behaviour of granular soils (Leach, 1986). It is assumed that the Poissons ratio remains constant both inside and outside the threshold region. It should be noted that since this model

computes the values of bulk and shear moduli from the current youngs modulus E_1 or E_2, that the threshold effect is assumed to be significant for both shear and volumetric strains.

The second model is based on the modified Cam clay model with the behaviour below the state boundary surface modified to include a threshold range. The elastic shear modulus used is taken to vary only with p' during the loading, Fig 3.13b. The threshold range is defined by a specified change in octahedral shear strain (γ_{oct}) inside which a higher elastic shear stiffness, G, is taken to apply. In this model the elastic bulk modulus is calculated from the slope of the swelling line and the current sample state hence threshold effects are assumed only to apply to shear strains and not volumetric strains. The shear modulus is assumed to be dependent on p' as shown in Fig 3.13b. The model has been used to describe the behaviour of clay soils.

These models have been implemented in a finite element program and used in the analysis of ground movements adjacent to a trench and two tunnels, all in London Clay, (Leach, 1986). The comparison of the predictions of the models for the case of the two tunnels with that of an analysis without the threshold range is unknown, however several analyses for comparison have been made in the case of the trench.

In the analysis of the movements around the two tunnels the first model was used for sand and gravel in the upper layers at the s de and the second model for London clay in which the tunnels were to be constructed. The st ffness of the sands and gravels inside the threshold was taken as 13 t mes the stiffness outs de for a complete reversal of stress path (as measured in the laboratory), and to be l m ted by a max mum princ p e strain of 0.005%. Data for London Clay was based on data from laboratory tests from a deep trench constructed near Bracknell, details of which are given below

In the analysis of movements adjacent to an instrumented trench three models were used,

a Isotropic linear e astic,

b) Isotropic bi linear elastic (model one above),

c) Isotropic non linear elastic.

In each case moduli were taken to be pressure (p') dependent. It was found that model "a" was completely unsuitable since it not only predicted the incorrect magnitude of ground movements but also the distribution of movements were incorrect. Moduli taken at 20% and 50% of deviator stress at failure and the average modulus from an unload/reload loop were all found to greatly underestimate the soil stiffness. Model 'c' was also found to be unsatisfactory giving poor predictions of the distribut on of ground movements. Model "b" gave the best all round predictions of magnitudes of deformations and the extent of the settlement trough. If a no tension cut off was used in the yield criterion (to allow cracking near the ground surface) further

improvements were made. Data were derived from the unload/reload loops of undrained triaxial tests. It was found that the threshold stiffness, G_1, lay in the range of 10.7 Mpa to 178.4 Mpa over a range of strains from 0.047% to 0.007%. Outside of the range of stiffnesses were taken to be about one tenth of these values. It is interesting that these data indicate a steady increase of threshold range in terms of strains as the mean effective stress and the threshold stiffness reduce (Fig 3.14). If however the range is analysed in terms of the change in stress required to reach the edge of the threshold range the data from (Leach, 1986) indicates an almost constant figure of about 0.1 to 0.16 of the consolidation pressure. Unfortunately due to the high rates of testing used in the triaxial tests from which this data was derived (0.4 % / min on undisturbed London clay) pore pressure measurements were not made. It is possible that due to these high rates of test this data may not be reliable for stiffness measurements due to the lack of equalisation of pore pressures throughout the samples.

Despite the disadvantages of these models they are a great deal simpler than Model L.C. Although they may not fully reproduce all features of threshold effects they may give a better understanding of the significance of a threshold range on analyses.

3.9 Discussion of Soil Models.

The number and type of soil models has been restricted in the above sections. Many other models exist including v sco-elast c, endochron c and other forms of elasto-plastic models. All the models in this chapter make use of the concepts of crit'cal state soil mechanics or are a part of it e g the elastic model. In practice the correct model can only be selected by considering the type of soil under loading, the state of the soil and the type of loading applied e.g. monotonic, cyclic etc It is h ghly unl kely that any s ngle model could be used even for one soil type in any possible stress state following any stress path. The models se ected here have particular relevance to this research.

All the models discussed model behav our wh ch is path dependent. The constitutive equations may be written as,

$$\delta\varepsilon_s = A\,\delta q' + B\,\delta p' \qquad 3.74$$

$$\delta\varepsilon_v = C\,\delta q' + D\,\delta p'$$

where the equations may apply to elastic or elasto-plastic behaviour. If a given path of $\delta q' / \delta p' =$ constant is followed then equat ons 3 81 may be written either in terms of the increments of $\delta q'$ or $\delta p'$, for example in terms of $\delta q'$ equations 3.74 become;

$$\delta\varepsilon_s = (A + B/\alpha)\,\delta q \qquad 3.75$$

$$\delta\varepsilon_v = (C + D/\alpha) \delta q'$$

where α is a constant equal to $\delta q' / \delta p'$ over the load increment. Hence the soil will be observed to be path dependent in that the stress-strain curves of q' against ε_s and q' against ε_v are not unique. Similar arguments apply in terms of p' or for constrained behaviour where restrictions are placed on the strain path e.g. one-dimensional compression, undrained loading. However this is not path dependence in the terms discussed in chapter 2 so long as a unique set of parameters A, B, C and D at a given state can fully describe soil behaviour on any loading path. Only where equations 3.74 are decoupled e.g. for the isotropic elastic model, will no path dependence of stress-strain curves be observed.

All the models assume that the soil is homogeneous and that co-axiality applies. Although co-axiality has been shown to be a reasonable assumption (Cole, 1967; Roscoe, Basset and Cole, 1967; Balasubramaniam, 1969; Arthur and Menzies, 1972) some departures have been observed for anisotropic soils loaded along axes not co-incid'ng with the axes of anisotropy, (Symes, 1983). The assumption of homogeneity is less likely to be attained. Slip planes in triaxial samples, end restraint and radial dra nage in step loaded tests may all contribute to produce samples which are significantly in-homogeneous None of the models cons'ders the significance of particle crushing, however for most soils at normal stress levels this is not significant. Additionally all of the models assume that the rotation of and or entation of princ pal axes is not significant (Wroth, 1984).

Most of the models described make use of norma ty when describing plastic strains and all of the models rely on the concepts of yield loci, plast c potentials and the direction of the strain increment vector to describe and deve op equat ons of so l behaviour. Houlsby (1981) has shown that this is unnecessary and has developed the Cam c ay equat ons from thermodynamic considerations without call to the above concepts.

The advantages of us ng an sotropic crit cal state models as opposed to isotropic models is now generally realised. Models have been developed from tests on reconstituted samples but they are particularly relevant to natural soi s. The advantages of the anisotropic elastic model has however, been appreciated for much longer (Atkinson, 1973; Hooper, 1975). The Cam clay model developed by the Cambridge soil mechanics group was intended purely for use with isotropically consolidated soils (Schofield and Wroth, 1968). Although the limitations of these theories were realised attempts were made by many workers to correlate data from anisotropic soils with the model. More recently an sotropic models have been developed by Robinson (1984), Gens (1983), Pender (1978), Mroz et al (1979) and Ohta (1973) in an attempt to provide models which describe the behaviour of natural soils more accurately. In practice it proves relatively easy to fit curves to describe the shape of the state boundary surface but the test of the fit of the model is a comparison of the predicted and observed stiffnesses. This is a very severe test of any model. With the availability of finite element programs on computers many of the models have developed rapidly in complexity and in the requirements placed on soil test data. Many of the models are so

sophisticated that progress in laboratory test methods may not be sufficiently rapid in order to produce the required input parameters. For example the model by Mroz et al (1979) contains many features which are difficult to test experimentally e.g. the shape of the kinematic yield surface, the motion of the kinematic yield surface and the form of interpolation rule for plastic strains below the consolidation surface.

The behaviour of soils below the state boundary surface in critical state models is generally poorly modelled. Some of the alternatives for describing behaviour below the state boundary surface and in particular hysteresis have been discussed. In general this requires that the strict thermodynamic requirements for elasticity are violated or that behaviour is plastic in character. In the case of the critical state model it was observed (Parry and Amersinghe 1973) that the range of elastic behaviour in isotropic swelling and recompression i.e. the range in which κ should be determined, occurred immediately following stress reversal and so the smallest value of κ applies. In the elastic model changes of stress corresponding to 10 to 20 kPa (Lambe and Whitman, 1979) were to be expected to be the limit of elastic behaviour. In Model L.C. elastic behaviour is limited to a range of strain corresponding to a change in stress on the stress path of about 10 to 20% the current stress state, or as in the model after strains of 0.02%. All these data tend to indicate that true elastic behaviour for soils is restricted to small high stiffness regions below the state boundary surface following large changes in direction of stress path.

The most sophisticated model is that due to Mroz et al (1979) which uses a kinematic yield surface below the state boundary surface to describe progressive plastic straining. This model may be distinguished from all the other models in that the strain increment ratio and the stiffnesses for a given stress path following a given consolidation history but different stress history below the state boundary surface are non-unique. This model could be used in a similar way to Model L.C. in order to describe threshold effects due to stress path effects. If such a model were combined with one which allowed the yield surface to expand with time at constant effective stress then a complete although complex model may be developed.

In this research the soil test data will be interpreted with the above models in mind. The model by Leach (1984) is unlikely to be sufficient on its own, but is simple in application. From the test data it is hoped that it will be possible to indicate whether the threshold range should be defined in terms of a change in stress or a change in strain, or if neither is applicable. These two cases are different except for the case where data is plotted on a log-log scale of stress and strain. For this case alone the definitions of stress and strain for the size of the kinematic yield surface are the same. The data should also indicate if the stiff response for large deviations of stress path is associated with the same strain increment ratio for a given state and stress path or if the strain increment ratio may vary. This will indicate whether the strains are elastic or plastic in character and so whether a kinematic yield surface of the form described by Simpson et al (1979), Model L.C. or that by Mroz et al (1979), will best describe the data obtained.

CHAPTER 4

TEST PROGRAM

CHAPTER 4 TEST PROGRAMME.

4.1 Scope and Objectives.

In the present series of tests it is intended to study both threshold effects and path dependence of soils. The study of threshold effects will generally be limited to those of stress path effects although the effect of short periods of rest will be studied. In general the study of time effects requires very long periods of rest to allow sufficient creep to occur for measurable effects to develop (at least 90-100 days), for this reason these effects will not be studied in detail. In these tests the objectives are to assess,

a) the range over which threshold effects are significant;

b) the effect of various changes in direction of effective stress path on the initial stiffnesses of samples following the same effective stress path;

c) the variation of the threshold effect with sample state, stress history and direction of loading path,

d) the significance of threshold effects on the behaviour of a range of different clay soils

e) the effect of changes in direction of total stress path as opposed to changes in direction of effective stress path,

f) the effect of stress path on the stiffness of samples with state below the state boundary surface

The requirements of the soils selected for these tests will be given in Chapter 7 together with details of the five clay soils selected However, in order to reduce the effect of creep and time effects on the results it is desirable to choose soils with low creep rates

In order that results of tests may be compared the main series of tests will use samples which follow the same consolidation history and so have the same state and overconsolidation ratio before testing

The full programme of tests conducted will be discussed in chapter 7. The abbreviations by which some of these tests will be referred to are given in table 4.1

4.2 General Test Requirements.

There are certain requirements for the triaxial tests in order to obtain consistent results for comparison Firstly in each series of tests samples should have the same general consolidation

history. For London clay, samples will be prepared for a variety of consolidation histories all with an overconsolidation ratio of two, while for all other soils only an isotropic stress history will be followed for an overconsolidation ratio of two. In addition for London clay only, tests will be conducted on isotropic and one dimensionally compressed samples at various overconsolidation ratios.

Each series of tests will start from a common stress state e.g. for isotropic samples with overconsolidation ratio (OCR) of two all tests will start from a state;

$q' = 0$
$p' = 200\ kPa$
$OCR = 2$

The effect of stress state will be examined by conducting tests on London clay at different values of p' but still with an overconsolidation ratio of two.

Rate effects may be elim nated by conducting all test stages at the same rate for any particular soil. The selection of appropriate rates of test will be d scussed in Chapter 7.

The object of this work is to minimise the effect of creep and time effects on the results in order to examine only those effects due to changes in stress path. All soils exhibit some creep at the end of test stages, but by select ng soils for which the creep rate is low compared to the compressibility of the soil the effect may be min mised. In order to reduce the effect further the rest periods at the ends of test stages shou d be as short as poss ble and they should all be of the same duration. Results of any series of te ts w l then g ve a truer reflection of those effects due solely to recent stress h story However care must be taken to ensure that the primary consolidation at the end of a te t stage has completed so that pore pressures in samp es are in equilibrium before commencing the next test stage Th s may be done by reference to a plot of volumetric strain against square r t of time as d scussed in section 7 7 4

4.3 Tests for Range of Thresh ld Effects.

In order to examine the max mum range of thres h ld effects due to changes of stress path, test paths which involve 180^0 rotation of stress path should be used for comparison with paths involving a 0^0 rotation of path (i e no change in direction). Since there is no evidence to suggest if the range of threshold effects varies with the particular stress path followed, two different paths wil be examined for each soil for both increasing and decreasing stresses.

Isotropic compression and swe ng tests involve a rotation of 180^0 of the stress path. This type of test will be used with stages of swelling and recompression to various overconsolidation ratios to examine the change in the range of thres hold effects and so also assess the effect of the initial stress state

The second type of test will follow a constant p' path with a rotation of 180^0 of the stress path at the isotropic axis.

The results of these tests will then be compared to the general predictions of the models described in Chapter 3.

4.4 Tests to Assess the Effect of Changes in Direction of Effective Stress Paths.

Samples initially brought to a common stress state, point A in Fig 4.1, will follow more complex stress paths in order to examine the effects of various changes in direction of effective stress path. The sample at A may be loaded to a point B within a short distance of A. The path B to A is then followed. A common loading path for all loading tests AC is then followed. In the case of the main test programme a constant p' compression path will be used. However for London Clay additional paths will include constant p' extension and constant q' with p' both increasing and decreasing. Although any paths could be used for AC in such tests, for the purposes of analysis the constant p' and constant q' paths are convenient. The angle between BA and AC may then be varied for a number of tests Further tests using the same sample may then be completed by following paths CB', B'A and AC aga n so that one sample may be used for a number of angles BAC. These results may be compared to tho e of samples not subject to more than one rotation of path to check the effect of the cycles of load ng For the final stages of testing samples may be loaded along ACD to fa lure at D, to examine the effect of recent stress h story on fa lure states.

The selection of lengths of paths BA and AC needs some consideration. Firstly path BA should be long enough to pass outside the thres h ld range from A. From past results this may not be more than 30 o of the ba ic stress state or about 60 kPa for an initial state of p'=200 kPa. Secondly as d scussed in section 4 2, a spe ified rest period is required at A before following path AC. This requ res careful adjustment of the path lengths to ensure that the stress path is changed at a conven ent time It s also de rable to conduct stages BA and AC in one day so that given the perm s ble rates of test the maximum lengths of these paths may be defined. The distance to the state boundary surface must be considered in order to prevent samples from yielding and deve ping large plastic stra ns before return ng to po nt A A limiting stress ratio (q'/p') of ± 0.7 was therefore placed on these paths For tests on samples of overconsolidation ratio = 1.5 and 2 the path length selected was 90 kPa while for overconsolidat on ratios of 4 and 8 path lengths of 50 kPa and 30 kPa respect ve y were selected.

4.5 Tests for Path Dependence.

Data from the above tests wi l provide a large quantity of data on the path dependence of the stiffness of samples below the state boundary surface. At points A and C (Fig 4.1) there is a large amount of data for paths departing from these points and also arriving at point A. If behaviour below the state boundary surface were elastic then a single set of stiffness parameters should describe all the test paths. For points A and C this is unlikely since each path is subject to a

different rotation of path at these points and so each path is affected differently by threshold effects. However, at point A on paths BA, all paths arriving at A are effectively following paths which are subject to no rotation of path i.e $\theta = 0^0$. Therefore all these paths are unaffected by threshold effects and so should provide a true reflection of the effect of path dependence on stiffness parameters for overconsolidated soils. For each soil there will be at least 8 such paths for comparison.

4.6 Tests to Study the Effect of Varying the Total Stress Approach Paths.

The main series of tests have the objective of studying the effect of recent effective stress history i.e paths BA (Fig 4.1) on a common effective stress path AC. By varying the pore pressure during a test stage the effect of the total stress approach path on behaviour along path AC may be studied.

In Fig 4 2 an effective stress approach path BA is shown together with a common loading path AC as before Path B^tA represents the total stress approach path. By varying the pore pressures in a different manner in a number of tests the direction of the approach path B^tA may be varied. The change in direction of the effective stress path may be referred to as θ while that of the total stress path by θ^t. If the value of θ^t is varied while maintaining θ as constant the factor controlling stiffness, the total stress paths or the effective stress paths may be examined.

Only two values of θ will be used in these tests, $\theta = 0^0$ and $\theta = 180^0$, with θ^t varying by approximately 66^0. It would be anticipated from the principle of effective stress that the value of θ the effective stress path rotation) and not the value of θ^t (the total stress path rotation) would control the magnitude of stress path threshold effects.

Further tests of a similar nature may also be conducted in which the total stress path deviation remains unchanged but the effective stress path varies. This further isolates the significance of total or effective stress paths in recent loading history

4.7 Tests to Failure.

Except for a small number of tests in which samples are to be subject only to cycles of compression, swelling and recompression all samples will be loaded to failure. For all tests described above a constant p' path in compression will be followed. This must be completed stress controlled for the reasons outlined later in Chapters 5 and 7. As a result these tests do not yield information regarding post peak behaviour, and so ultimate states cannot be determined. These tests would however provide data regarding the effect of recent stress history on the peak failure state of samples and strains at failure. For most of the soils under test data was available for the shape of the state boundary surface so that these data from constant p' tests to failure may be interpreted. For the London clay however such data was unavailable. A series of tests will therefore

be conducted to establish the shape of the boundary surface for isotropically compressed samples using stress and strain controlled tests at a variety of stress states and overconsolidation ratios.

4.8 Variation of Test Procedures.

Some of the above test procedures are somewhat arbitrary, for example the length of approach path BA (Fig 4.1) and the period at rest at the end of each stage.

By varying the length of path BA further evidence should be provided as to the size of the threshold range. This would confirm if the length of path BA of 90 kPa selected is sufficiently long to reach the edge of threshold range before commencing path AC.

The period of rest at point A has been standardised for all tests in order to minimise the effects of creep on different recent stress histories. By varying this rest period the significance of this factor on sample stiffness may be studied, and some indication should be provided of whether threshold effects due to stress path and time effects are separate or the same phenomenon. Only relatively short periods of rest shall be considered, that is up to about 10 days. This covers two log cycles of time elapsed and so should provide some indication of the effects of time and stress path effects together.

CHAPTER 5

THE TRIAXIAL STRESS PATH APPARATUS

CHAPTER 5 THE TRIAXIAL STRESS PATH APPARATUS.

5.1 Introduction.

All the tests conducted during the period of this research were carried out using computer controlled stress path triaxial cells.

The equipment consisted of Bishop and Wesley hydraulic triaxial cells with conventional triaxial instrumentation. Pressures were provided by an air compressor and regulated by Fairchild air pressure control valves driven by small electric motors under the command of a computer. All the instruments were of the resistive type and were read using a Spectra-xb system. This system includes a microcomputer for the purposes of control of signal conditioning, for switching and data storage. In addition the microcomputer carries the basic control program for monitoring and adjusting tests, the calculation of stress and strains and storage of the data at regular intervals and so provides full feedback control to the triaxial cells. The object of this chapter is to describe this equipment in some detail and the functions and operation of the control program. Further details of the design and operation of this equipment are given by Atkinson, Evans and Scott (1983 a,b; 1985) and Intercole Systems Ltd (1977). A second microcomputer, an Epson QX10 was connected to the Spectra-xb system. This was used for data storage of readings taken by the Spectra system and dumping data to floppy disk for permanent storage. In addition various other programmes may be used on this system, for example for data analysis. The program used for data capture and storage is described by Woods (1985b) and the other software in use by Woods (1985c, 1985d), Baldwin (1985), and Micropro (1983).

The apparatus was operating in the soil mechanics research laboratory in the Geotechnical Engineering Research Centre of the City University. Since electrical measuring devices are sensitive to changes in temperature including the instrumentation and interface system, the laboratory in which the equipment is located is temperature controlled. This system has been designed, built and tested by the soil mechanics group. At the start of the period of this research, October 1983, the system had completed accuracy and reliability trials and a number of undergraduate and research projects had been successfully completed using the system.

5.2 Power Supply to System Components.

A number of power supplies are needed for the operation of the system. These include 240v mains supply for the Spectra xb and the electric motors on the air pressure control valves; 12v for the relays between the electric motors and spectra relays, and a 10v supply for the instrumentation.

The supply to the Epson and Spectra-xb systems was first filtered and smoothed to remove spikes and surges which occur from time to time in the mains supply due to large pieces of equipment being turned on and off in the University. Such events have caused the control program to 'crash'

in the past with as a consequence the loss of all running tests.

The 10v power supply for the instruments was provided directly from the Spectra system which has an output for this purpose.

The 240v electric motors were supplied direct from the mains supply since they are not sensitive to power surges. The provision of 12v relays between the Spectra relays and electric motors was designed to ensure that the 240v supply was isolated from the sensitive Spectra relays. In addition to the above a Motivair air compressor which supplies air pressures also requires a 240v mains supply.

In the event of a mains power failure an emergency generator will supply power to the system components. During the period in which the generator reaches full power a rechargeable battery pack can provide emergency power to the Epson and Spectra-xb systems. However, all other systems including the motors and compressor will cease to function until the emergency generator has reached full power. If the emergency generator should fail to operate then the emergency power pack can supply power for approximately one hour, after which time all tests will be lost.

5.3 Pressure Supply.

The pressure supplies required in the B shop and Wesley cell are cell pressure, back pressure (to the pore pressure and volume gauge system) and axial pressure for the loading ram. The arrangement is illustrated diagramatically in Fig 5.1.

The air pressures required to generate these pressures were supplied from a Motivair air compressor operating to maintain a pressure in the range of 800 - 900 kPa. The air from the compressor was cleaned and dried before passing through an air pressure control valve which allowed a maximum of 750 kPa to be supplied to the equipment. The purpose of this valve was to ensure a smooth pressure supply to the cells unaffected by the varying output of the compressor. The air supply then passed to air pressure control valves controlling the air pressures supplied to the back pressure system and the water and oil interfaces for the cell and axial pressures respectively.

The cell pressure was transmitted from the supply air pressure to the de-aired cell water by an air-water accumulator via a membrane impermeable to air. The axial pressure was transmitted by the supply air pressure acting directly on the surface of oil in a cylinder reservoir, the oil then passed to the loading ram of the triaxial cell. For extension tests, where cell pressure exceeds the ram pressure, a rubber suction cap was used to connect the load cell to the top platen(Fig 5.2). This was open to atmosphere and so held in place against the load cell by the cell pressure for such tests. The back pressure supply will be dealt with in a later section together with the volume gauge.

5.4 System Components.

The testing system may be divided into a number of principal components, these are:-

a) the triaxial cells,

b) instrumentation,

c) air pressure control valves and motors,

d) Spectra and Epson hardware,

e) Spectra and Epson software.

Each of these individual components will now be considered separately.

5.4.1 The Triaxial Cell.

The principles of the design and operation of the conventional triaxial apparatus were described by Bishop and Henkel (1962). The City University Spectra system uses hydraulically operated Bishop and Wesley stress path cells (Bishop and Wesley 1975; Wesley 1975).

The complete Spectra system consists of six Bishop and Wesley cells all controlled by one Spectra-xb logger. During the course of this research four cells have been used at various stages of the work (cells 1,3,5 and 6). Diagrams of the operating system and the cells are shown in Figs 5.1 and 5.2 respectively. The cell is also shown in Plate 5.1.

Cells 3,5 and 6 used in this work are all of a modified type. The standard cells are described in detail by Bishop and Wesley (1975) and Wesley (1975). The modified cells differ from the standard version in that details of the drainage connections have been redesigned and the perspex cell body has been enlarged to 200mm in diameter to accommodate internal instrumentation. These modifications have been described by Daramola (1978). These wide bodied cells were developed to allow the use of instruments inside the cell attached to the sample however this facility has yet to be included in the Spectra system.

5.4.2 Instrumentation.

The instrumentation provided in all the Bishop and Wesley cells comprised of standard triaxial instruments. The measurements made are the axial force, F, the cell pressure, σ_r, the pore pressure, u , axial displacements, δL, and the change of volume, δV. The general arrangement of the instruments is indicated in Fig 5.2.

All the instruments used with these cells were of the resistive type.

This avoids the difficulties which may occur when resistive and inductive devices are mixed in the same system. All the measurements were based on a full Wheatstone Bridge arrangement of strain gauges with a nominal input voltage of 10 volts. The actual bridge voltage was monitored by the Spectra system as each set of readings was taken and so the readings were corrected to allow for fluctuations in bridge voltage.

The axial force was measured using a standard 450 Kgf Imperial College load cell (designed by Dr A.E.Skinner and described by E.L-Ruwayiah (1975)). This type of load cell makes all measurements inside the cell, submersed in the cell fluid. This device is so designed as to be unaffected by changes in cell pressure and since it is placed inside the cell close to the sample it records the loads imposed on the sample without frictional losses through a piston seal in the top of the cell.

Axial displacements were measured externally as the relative displacement of the top of the cell and the crosshead below the sample on both a dial gauge and an LSC-HS25 transducer manufactured by MPE Transducers Ltd.

Both cell and pore pressures were recorded using Druck PDCR 10 transducers with a pressure range of 0-1000 kPa.

Volume changes were recorded using an Imperial College type 50 cc capacity volume gauge This device consists of a freely moving piston in a cylindrical chamber with rolling bellofram seals top and bottom Air pressure from an air pressure control valve is applied to the lower bellofram. A pressure is generated in water in the top chamber of the volume gauge which is part of the pore water system As the piston moves in the cylinder due to changes in volume of the sample an LSC-HS25 transducer mounted on the side of the volume gauge records these movements and so gives a measure of changes in the volume of the sample. This device for measuring volume strains not considered reliable for back pressure of less than approximately 50 kPa.

In the present system radial strains are not measured directly Instead they are computed from the observed axial and volumetric strains assuming the sample deforms as a right cylinder.

The range of each of these devices and the computed resolution of each device is given in table 5 1 The accuracy of these instruments will be discussed in Chapter 6.

5.4.3 Pressure Control.

The source of pressure for the Bishop and Wesley cells had already been discussed in section 5 3, and the general arrangement shown in Fig 5.1.

The control of pressures is achieved by computer controlled motors driving air pressure control valves. These motors are a direct current type and are capable of operating in either forward or

reverse direction to allow for increasing or decreasing pressures as required. Each motor drives the air pressure control valves via a gearbox, the ratio of which has been chosen such that a maximum rate of change of pressure of about 60 kPA per hour could be achieved with the motor running continuously.

This corresponds to a deviator stress rate of about 150 kPa per hour since the ratio of the area of the lower bellofram chamber to the area of a triaxial sample is approximately 2.5. Hence this choice of gearbox allows most triaxial tests to be carried out in 6 hours if required.

5.4.4 Axial Strain Control.

The system of three air pressure control valves each driven by a motor, one each to adjust axial, radial and pore pressures should in principle also be able to control tests in which strains are varied rather than pressures. In the early stages of design and testing of the system it was found that the system proved too flexible during strain controlled axial loading. Although the strain path was followed, "hunting" in the control was observed so that at any instant in time large deviations could be observed from the chosen path.

For tests involving axial strain control an alternative arrangement for control is shown in Fig 5.3; this is the system in use with the present Spectra system. When the valve is closed a fixed volume of fluid is contained in the system. The motor drives a screw jack which displaces the fluid so that the ram in the triaxial cell rises or falls according to the direction of travel of the motor. The gearbox in this system is chosen to allow a maximum strain rate of about 0.5% per hour with the motor running continuously. Higher rates of strain are not normally required for research purposes but could easily be accommodated by selecting a suitable gearbox.

Other strain controlled tests involving control of either radial or volumetric strains are also possible with this system. While tests involving radial strain control for one dimensional compression tests have been completed, no tests have been conducted involving control of volumetric strain.

5.4.5 Spectra and Epson Hardware.

The feedback control and data logging is controlled by an Intercole Spectra-xb microcomputer. In order to obtain hard copies of all data and to dump data to floppy disk for permanent storage a second system, an Epson QX10 microcomputer and Epson RX80 printer, is permanently connected to the Spectra system. The current system comprised the following,

Spectra -

1) A microcomputer with 32k words memory.

2) A VDU with keyboard used as control console.

3) A set of 48 analogue input channels.

4) A set of 48 digital output relay channels.

5) A single cartridge tape drive.

Epson :-

1) A QX10 microcomputer with 192k words memory with 2 disk drives.

2) A VDU with keyboard.

3) A Epson RX80 printer.

The system is shown in plate 5.2.

5.4.6 Functions of the Spectra System.

In the Spectra system the VDU and keyboard are used to input control and system data by the operator. The Epson system normally provides a permanent link with Spectra via an RS232 serial bus to provide hard copies of all tests performed on Spectra and temporary storage of about 14 days of Spectra test data during any single stage. The precise maximum depends on the amount of data stored from other tests also in progress. The cartridge tape drive holds the control program "SPCTRA" and operating programs for the Spectra system.

The Spectra microcomputer is used for a number of functions.

1) Selection of channel to read.

2) Control of signal conditioning and analogue to digital conversion (A to D).

3) Conversion of digital signal to engineering units through suitable calibration constants.

4) Calculation of stresses and strains.

5) Control of stresses and strains via motor controlled air pressure control valves.

6) Data capture and storage.

The 48 input channels are scanned at 10 second intervals and stresses and strains on the sample are computed from the results. Each cell is allocated six channels as follows:-

1) Load cell.

2) Pore pressure transducer.

3) Cell pressure transducer.

4) Axial displacement transducer.

5) Volume gauge.

6) Spare.

The remaining 12 channels are spare and unallocated.

In order to arrive at results for the computation of stresses and strains, readings are integrated over 300 scans during a 0.02 second period for each instrument. By integrating the readings in this way the effect of random fluctuations of instrument outputs over short periods e.g. due to noise, may be reduced.

There are 48 output channels, seven allocated to each cell.

1) Test running light.

2) motor one (hydraulic jack) or
3) motor four (a r pressure regulator to ce l pedestal) — axial strain / stress control.

4) motor two (air pressure regulator to base of volume gauge) : Pore water back pressure control.
5)

6) motor three (a r pressure regulator the a r water accumulator) : Cell pressure control.
7)

In each case there are two channels for each motor (motors one and four use the same channels, the motor in operation may be selected by a switch), one to set the motor on or off and the other to determine the direction I e. increasing or decreasing. The remaining six output channels are unallocated.

The interface unit selected is one of the most important parts of the system since it controls the accuracy and resolution of measurement of the system. The Spectra system converts the

analogue to digital signal with 16 bit accuracy or a resolution of 1 part in 32,768 of full range (one bit used for ± sign) before the signal is passed to the microcomputer. The manufacturer quotes the accuracy of the Spectra-xb in performing these tasks of 0.0015% of full scale of the channel being read (Intercole Systems Limited, 1977).

5.4.7 Functions of the Epson System.

The Epson system consists of a VDU and keyboard, an Epson RX80-FT dot matrix printer and a microcomputerwith 192k word memory. The system performs the following functions:-

1) Printing of test data including:-
   a) first page data referring to test details,
   b) hourly records printed once every 24 hours,
   c) storage of test data from the current test stage.

2) Dumping of data at the end of a test stage to floppy disk for permanent storage.

3) Analysis of floppy disk data with various programs.

4) Wordprocessor.

The Epson system is required for data storage due to the limited memory of the Spectra system which allows only twenty four sets of five readings from each of the six cells before maximum capacity is reached. The large memory in the Epson system therefore allows more data to be stored before overwriting earlier records.

Data passed to Epson from Spectra via an RS232 link. The system normally carries a continuously running program, "LINK". This program passes all data received from Spectra to the printer to provide a hard copy of all data and also opens files to store the hourly readings passed from Spectra. As had already been stated the maximum capacity of this system is about fourteen days before action must be taken by the operator to reduce the quantity of data in store. This program may be interrupted at any time (except during data transmission) in order to use the microcomputer for any other purposes such as data analysis and plotting.

This complete Epson-Spectra system allows six independent stress-path tests to be conducted at any time.

5.4.8 Spectra Software.

The Spectra software is written in BASIC computer language and is named "SPCTRA".The main control loop of the program is shown in Fig 5.4 and will now be described. Some sections of the program such as that for channel control use machine code routines.

5.4.8.1 The Main Loop.

If not performing other functions the program follows a closed loop as illustrated by Fig 5.4.

a) Test the option switch. If the switch is set display the list of options, Fig 5.5.

b) If the switch is not set or at specific points of execution of various options, the time is checked and various time dependent operations are conducted.

c) Return to step a).

5.4.8.2 Time Dependent Operations.

While operating the main loop Spectra performs a number of time dependent operations. Every 10 seconds all the transducers of each operating cell and the transducer supply voltage are scanned and the current stresses and strains computed. The control routine is then executed and the required state computed according to the stress-strain path defined by the operator. The actual and required states are then compared and action taken to make necessary corrections if any lie outside of the control limits specified by the operator.

Every ten minutes an internal function is called to check the calibration of the analogue to digital converter. Every hour on the hour the computed current state of the sample is recorded in the memory. These records may be d splayed by use of option 8 or printed by use of option 9 at any t me without erasing these records.

Every day at 6 00 hours GMT the records of the previous 24 hours are passed to the Epson computer where they are stored on image d sk and hard copy printed. These records are then cleared from the Spectra memory and are no longer avai able from Spectra. This procedure is necessary due to the limited memory of the Spectra micro-computer.

It should be noted that any of the above funct ons may be delayed by requiring the execution of any of the Spectra options Th s is most critical since it effectively leaves the cells uncontrolled except at pre-determined points in the execution of these options. Operators must always therefore be completely ready with all the data and informat on necessary to complete an option without delay in order to minimise this problem.

5.4.8.3 The Option List.

If the option switch has been depressed and the main control loop broken, the option list will be displayed, Fig 5.5. Most of these options are self-explanatory and will be discussed in Chapter 7 when describing test procedures, however a number of these options require further explanation.

Option 1, Enter test data, is used to enter all the data required to conduct a test stage. A sample data sheet is shown in Fig 5.6. Data identifying the test is required as follows; the cell number, the job title, the test and stage number. The sample dimensions required are those relating to when the strain zeroes were last recorded. Finally the control data is required. Firstly the control function must be stated;

-1 no control;
0 stress control;
1 strain control,

for each of three pairs of independent functions from; function 1, axial stress or axial strain; function 2, pore pressure or volumetric strain; function 3 cell pressure or radial strain. Secondly for each controlled function the following data must be given; start value, increment per hour, finish value and the control limits (for stresses in kPa, and strains %). The control limits represent the maximum deviation from the required path permitted by the operator, typical values being 1 kPa for stresses and 0.007% - 0.01% for strains.

Option 10, Test relays, allows each relay to be switched on and off in turn for a particular cell in order to check for correct operation.

Option 11, Calibrate transducers, allows the reading in volts of up to six input channels for any one cell and for the readings to be displayed or printed for purposes of calibration. This method of was not used for these tests; the present calibration procedure will be described in Chapter 6.

Option 12, Enter calibration data, allows the input of all calibration data for any particular cell. This includes data referring calibration constants for instruments, the channels for output and input to the Spectra system and the gain of the input channels from transducers. This data need only be input when revising constants after re-calibration or when starting up the system from a complete shutdown, a sample data sheet is shown in Fig 5.7.

The program itself has been written in such a way that options must be carried out in a particular order so as to ensure correct procedures are followed. Option 12 must be used before all others. Options 1 to 5 must then be carried out in numerical order to start the first stage. For other stages only options 1 and 5 need be executed but options 3 and 4 may be used if required depending on individual testing procedures. An error trap prevents any of these options being called for a cell which already has a test in progress e g preventing zeroing of stress readings during a test stage.

5.4.8.4 Calculation of Stresses and Strains.

The values of stresses and strains are computed every 10 seconds for each cell using the calibration constants and the transducer readings in the control program. This involves converting the digital voltage readings using the linear calibration contants input relating changes of

dimension, stress and force to the change in the digital voltage readings.

Strains were computed as:

Axial strain $\varepsilon_a = -\delta L/L_o$ 5.1

Volumetric strain $\varepsilon_v = -\delta V/V_o$ 5.2

Radial strain $\varepsilon_r = 1/2(\varepsilon_v - \varepsilon_a)$ 5.3

where L_o and V_o are the reference length and volume respectively when option 4 was last called to zero the strains. It should be noted that these strains are ordinary strains, (Richardson, 1984b) and so the computation of radial strains by equation 5.3 remains approximately correct only for small radial strains. This is of little consequence in this case since values of radial strain are not recorded or used further in cases where large errors may occur. In all further calculations for analysis the radial strains were computed by a more exact formula (see Chapter 8).

Pore pressure and cell pressure readings were computed from the readings of the pore pressure and cell pressure transducers.

Pore pressure = u (the pressure of water in the pore pressure block).

Radial stress = σ_r (the pressure of water in the cell body).

In order to calculate the axial stress the current area, A, of the sample is required. The formula used by Spectra is that given by Bishop and Henkel (1962) based on the assumption that the sample deforms as a right cylinder,

$$A = A_o \frac{(1 - \varepsilon_v)}{(1 - \varepsilon_a)} \qquad 5.4$$

where A_o = the initial area of the sample $(\pi D_o^2/4)$,

D_o = the initial diameter of the sample,

from which the axial stress, σ_a, may be computed as,

$$\sigma_a = \frac{F}{A} + \sigma_r \qquad 5.5$$

where F = force recorded by the load cell. It should be noted that due to the design of the load cell the measurements of F which it makes are unaffected by changes of cell pressure.

In all the above calculations no corrections are made for any factors other than the current area of

the sample. Corrections for the stiffness of membrane and side drains, hysteresis and non-linearity of transducers are not made in the program but left to the operator. These factors will be discussed in later chapters.

5.4.8.5 Computation of Required State.

Every ten seconds the state of the sample is assessed as described above. In order to make adjustments to maintain the desired loading path the required state must also be computed. The data input as described in section 5.4.8.3 is used for this purpose together with the time elapsed since the start of the test. Firstly the computer checks if each function in turn is controlled or not, and if so, whether stress or strain control is required. Secondly it takes the initial value and adds the increment per hour multiplied by the time elapsed to arrive at the required state. This is checked against the final state. If the final state has been reached then that state replaces the previously computed figure as the required state. Finally the required state is compared with the actual state of the sample. If the difference exceeds that specified by the control limits then suitable adjustments are made.

The present system has provision for only linear variations of the controlled parameters. It would be a simple matter however to make minor adjustments to the program to allow any form of loading path to be defined

5.4.9 Epson Software.

The purpose of th s part of the system has been stated in section 5.4.7. This section describes s me of the software which is used w th the system The "LINK" program is described in detail by Wood 1985b

5.4.9.1 Epson "LINK" Program.

Th s program is the resident program on the Epson micro-computer and runs continuously when the computer is not engaged with any other work.

The program is in a constant state of read ness for data passed from Spectra. The data is stored in memory and also printed to g ve a hard copy The data in memory may then be dumped to floppy disk for storage. The Link program must be operat ng whenever it is necessary to obtain a printout from a Spectra operation Th s occurs,

a) when a test stage is started (opt on 5 ,

b) at 06 00 hours GMT for print out of the previous 24 hours data,

c) when printing records in store (option 9),

d) when ending a test stage (option 6).

When a test stage is started the first page data is passed from Spectra to Epson and is printed on the Epson printer. This data includes the date and time, details of the job title, test and stage numbers, calibration constants and test details. Of this data only the job title, test and stage numbers are stored. These are stored on an image disk file opened in the name of the cell e.g cell 5.dat.

The process of storing each set of 24 records for each day has already been described in an earlier section. At the end of a test stage the final page data is printed and the operator is prompted to place a disk in the disk drive for all data relevant to that cell to be dumped. That section of the Epson memory is then cleared of all data records.

In practice the period of 14 days of records has proved sufficient for most tests. If the need arose to conduct longer tests this may be done in one of two ways. Firstly the stage could be stopped, data copied to disk and a new stage re-started. Alternatively it is possible to copy data from 'link' during a stage and erase these records from the Epson leaving sufficient file space for subsequent records.

5.4.9.2 Analysis of Data.

Having copied all test data to floppy d sk programs are available for the Epson system to analyse the data The 'Link' program may be stopped without affecting data stored on the image d'sk file and other programs used provided that this area of the computer memory is not used. Deta'ls of the analysis programs, 'Inspctra', 'Spectran', and 'Specp ot' are given elsewhere (Woods 1985c, 1985d, Baldwin, 1985). The 'Spectran' program produces useful stress and strain parameters for p ott ng including stress and stra n invariants, various normal sing parameters, natural strains and tangent st ffness moduli

For this research some mod fcat ons were made to the 'Spectran' analysis program which include:-

a) Error trap rout nes.

b) Various mod fcations to program operation to a ow files to be analysed more than once without the need to input all the test data a second time.

c) More options for analysis including;
   1) more normal sing parameters,
   2) calculation of incremental stresses and stra ns,
   3) calculation of secant st ffness moduli.

d) Corrections to test data including;

1) zero corrections to transducers,
2) change transducer calibration constants,
3) corrections for load cell compliance,
4) corrections for volume gauge compliance,
5) corrections for membrane and side drain stiffness to recorded axial and radial stresses (see Richardson 1986 for details).

e) The ability to store corrected data on disk together with details of the corrections made to the data, and the ability to print out a hard copy of the correction data.

The use of some of these features will be discussed in later sections.

5.5 Discussion of the Design and Performance of the Spectra-Epson System.

The equipment was designed to perform stress path triaxial tests using either stress or strain control or a combination of both. The system had to perform such tests under fully drained or fully undrained conditions or allow variation of pore pressure so as to allow any path to be followed within the limits of the triaxial system symmetry. This system had to allow relatively slow rates of loading compared to standard testing procedures (British Standards Institution, 1975), with linear increases or decreases or to hold constant any chosen parameters. The advantage of continuous loading (as opposed to step loading) is that the difficulties associated with deciding on a size of step for step loaded tests are avoided. This factor may significantly affect the behaviour of samples due to the very different effective stress paths which are followed when large steps are involved. Furthermore in cases where radial drainage is used case hardening of samples (Ho, 1984) may occur. The loading paths followed by the Spectra system are in fact step loading paths with steps so small as to be effectively continuous paths. This minor compromise avoids many of the difficulties of systems which attempt to provide truely continuous loading. The object of the design was to utilise proven equipment and testing technology (Atkinson, Evans and Scott, 1983a, 1985). Finally the system had to be simple to operate, reliable and accurately follow the chosen loading paths.

Clearly these requirements are in some cases incompatible since highly accurate systems for example are usually very complicated to operate. The system is simple to operate and is not labour intensive with only a minimum of experience necessary to conduct tests successfully. However, the simple procedures detailed in the operating manual (Atkinson, Evans and Scott, 1983b) must be adhered to in order to ensure that preparatory work for a test is conducted correctly and all data necessary input to the system. The most serious weakness in the system is that a single operator error, such as failing to return control to the computer after examining the current state in a test, can result in the loss of the tests in all six cells. Fortunately such errors are rare. The computer is not affected by power failure provided that all the back up systems function correctly which allows a good deal of certainty that tests will be completed successfully. The system is not completely flexible in the form of loading paths it may follow since although any path may be followed some are

restricted to only stress or strain control e.g a constant p' path may not be conducted using strain control. While it is simple to write routines which can follow any general stress paths under strain control, due to the limited memory of the Spectra-xb system it is not practical to implement them.

The data logging part of the system works well since it allows a test to run for long periods of time unattended. However due to the fixed record interval of one hour it can become necessary to take additional intermediate readings manually in the early parts of stages. For example in tests on stiff soils it becomes necessary to use very slow rates of stress or strain control for the initial period of loading.

The accuracy of the whole system will be discussed fully in the next chapter but it can be stated that the overall accuracy of control alone is of the order of ± 0.5 kPa for pore and cell pressures, ± 1 kPa for the axial stress and ± 0.01% for strains. These figures are to some extent dependent on the gearbox ratios on the air pressure control valves. Clearly any ratio of gearbox could allow the slow rates of test required, but gearboxes allowing faster rates of test would not be able to follow loading paths as accurately and so would in effect increase the size of the small steps in the step loading process. For the purposes of research in which very slow rates of test are normal the present system offers a good compromise.

The system itself is not responsible for errors of its own, these are either generated from erroneous input or due to outside influences such as system failure, but so long as data input is accurate a test may be expected to be performed without difficulty provided limitations of the equipment are not exceeded e.g. excessive pressures. Some regular checks are needed however to ensure that equipment does perform reliably. Transducer displacements, the condition of the air pressure control valve motor clutches (these have sheared due to the high loads, and the cell (for major leaks) should all be checked. The Epson system itself needs very little attention. It is only necessary to check if the program is running (it may crash if there is an error during data transmission, and that there is sufficient paper in the printer. Individual testers must also ensure that the quantity of data stored on Epson does not become excessive and so cause difficulties.

On the whole the system has been shown by a large number of commercial and research projects conducted to date to fulfil the objectives it was designed to meet. It provides a very flexible stress path testing facility which can conduct tests to a good degree of accuracy with minimum of attention, it is simple to set up and simple to use.

CHAPTER 6

CALIBRATION AND ROUTINE TESTING OF THE SYSTEM

CHAPTER 6 CALIBRATION OF APPARATUS AND ROUTINE TESTING OF EQUIPMENT.

6.1 Introduction.

In this chapter the calibration of the instruments and of the whole system will be discussed. The methods used and the selection of suitable calibration constants will be discussed .Tests will be described which may be used to ensure that the system is fully functioning and operating without significant system errors e.g. leakage from the drainage system. Further tests are described from which the flexibility of the measuring system may be assessed so that corrections may be applied to any test data. Finally the factors influencing the accuracy of the system will be discussed and the estimated accuracy of indervidual components stated.

The operation of the system is such that the stresses and strains recorded and subsequently output and analysed, result from changes of electrical resistance of the relevant devices on or around the triaxial cell The conversion of such signals to engineering units goes through several stages -

a) recording of an amplified analogue signal,

b conversion of the analogue to a d g tal signal,

c conversion of the dig tal signa to a pressure, force or d splacement as appropriate according to the calibration constants input

d) calculation of stress and stra n read ngs for control or storage purposes.

In th s process the operator is rea y nterested in the actual state of stress and stra n of the samp e and it relat nship to the stres es and stra ns recorded All the steps a to d) above are involved n th conversion It is theref re des rab e to ca brate the who e system with one ca ibrat on constant for each device coverng al stages a to d rather than a number of constants for each stage.

Many different procedures have been used for the ca ibration of the Spectra system. On y the method used in this research w l be descr bed here t is more ful y descnbed by Atkinson Evans and Scott (1983b , but some deta ed d fferences are discussed here t s of nterest to know how close the f nal computed values of stress and stra n are ikely to be to those ex sting in the sample and hence any correct ns which may be requ red for systemat c errors e g due to non- ineanty of transducer re ponse and of the prec ion of those results

The ca ibrat n of the apparatus and of the associated instrumentation for measurements to be made and the ca ibration for the system f exib ity due to various factors forms a very important part of any so l test ng program The qua ity of data derived from tests is dependant on the quality of the ca ibration of the system and its components . High qua ity data cannot be obtained

unless great care is taken in this work.

6.2 Calibration Procedures.

Various calibration procedures have been used with this equipment, that used during these tests will be described below.

Each instrument was calibrated by applying a known displacement, load, or pressure to the device as appropriate, such that a known stress or strain would be displayed by Spectra on the VDU screen. Using the displayed readings and the known stresses or strains which should have been displayed the present calibration factor could be adjusted. On repeating the test further fine adjustments could be made in order to reach a satisfactory value for the calibration constant.

6.2.1 The Load Cell.

The load cell measures the deviator force which may be tensile or compressive; different calibration constants were used for each range. The method of calibration used was to apply dead weights to the load cell, via a hanger for tensile calibrations and directly to the load cell for a compression calibration. A known weight was applied from which using the diameter of the sample entered on the system an equivalent axial stress may be calculated. This may then be compared with the stress displayed by the Spectra system and suitable adjustments made. At low stress levels small load increments were used while at higher stress levels large increments are used up to the maximum stress levels anticipated during the testing program. The object of the small stress increments at low levels was to examine the non-linearity of the device in this range.

The results of a typical calibration, which includes both increasing and decreasing loads are given in Figs 6.1a and 6.1b and Table 6.1.

6.2.2. Cell and Pore Pressure Transducers.

The cell and pore pressure transducers were calibrated using a Budenburg apparatus. This apparatus applies a known hydraulic pressure by supporting weights on a piston of known diameter. The piston rotates so as to minimise friction in the loading system. The transducers are mounted in a block and a zero reading is recorded, after de-airing the system, with the system open to the atmosphere, and a series of weights applied to the piston. The displayed values of stresses may then be compared with those computed from the applied loads. The results of a typical calibration are given in Figs 6.2, 6.3 and Table 6.1. The non-linearity of these devices can be seen to be considerably less than that of the load cell.

6.2.3. Axial Displacement Transducer.

The axial displacement transducer was calibrated using a block incorporating a micrometer screw

gauge. Using the screw gauge precise displacements could be applied to the transducer. Using the length of the specimen entered on the system the equivalent axial strain could be computed and compared with directly with that displayed by the Spectra system. The results of a typical calibration are given in Fig 6.4 and Table 6.1.

6.2.4. Volume Gauge.

The volume gauge was calibrated using a Bishop ram connected to the bleed valve on top of the gauge (see Fig 5.2). Each complete rotation of the ram displaces a known volume of water into or out of the volume gauge. Using the sample dimensions input to the system the equivalent volumetric strain may therefore be computed and compared with that displayed by the Spectra system. The results of a typical calibration are shown in Fig 6.5 and Table 6.1.

It should be noted that by using these methods the whole of the Spectra system is calibrated using one calibration constant i e. stages a) to d) of section 6.1 above, including all wiring and connections in the system

6.3. Selection of Calibration Constants.

As a result of these calibrat on procedures it is found that the devices were not linear over the whole range of calibrations Th s is particularly not ceable when working at low stress levels and when perating at or near the end of travel of both the axial displacement and the volume gauge.The current Spectra system a lows on y one cal bration constant for each device (except for the load ce l which uses two, one each for extension and compression), so that the system assumes that the devices are linear The magn tude of th s departure is not great but needs to be assessed to determine the magnitude of the result ng error. Data in Table 6 1 show there is a variation of ca brat on constants appropriate to each stress or stra n level for each device which demonstrates the non l nearity of each device

In the case of both the ax a d p acement transducer and the volume gauge, the problem is simply avoided by conducting tests so that these devices are on y operated over the central part of their travel The effect of non l nearity is then very hard to detect as shown by the typical, calibration curves in Figs 6 1 and 6 5

In the case of both cell and pore pressure tranducers the worst effects of non-linearity can also be reduced In a typical test these devices would be operated within a certain range of stress which would be unlikely to be close to the non linear range close to zero pressure. Therefore a suitable constant may be chosen with n th s range (centrally if poss ble) and so ensure that readings during the test were of the highest accuracy possible. In drained tests with constant back pressure, the pore pressure transducer would be cal brated at the value of back pressure chosen, if so desired. The effect is illustrated by the exaggerated diagram of a ca bration curve in Fig 6.6. The error in the recorded reading is represented as the difference between the true calibration curve and the

assumed linear calibration. The results of a typical calibration in Table 6.1 show the magnitudes of this error to be expected.

In the case of the axial load cell a similar procedure followed to that of the pore pressure and cell pressure transducers in order to select suitable calibration constants for both extension and compression. In this case however the choice is not so easy since typically in a test the force registered by the load cell (for the computation of the deviator stress) will vary from zero to some final value and so will cover the range where non-linearity is greatest. Hence more care is required in the selection of these calibration constants in order to ensure the maximum positive and negative errors (actual stress less computed stress), are approximately the same.

The errors due to non-linearity are not large and by these methods may be reduced to a minimum. They are generally only significant when working at low stress levels. In the case of the tests conducted in this research stress levels were generally sufficiently high and confined to relatively small changes in stress that these effects were ins'gnificant in magnitude. In some cases however e g. the tests conducted at an overconsolidation ratio of eight, the calibration constant for deviator stress was adjusted during analysis of test data to allow for non-linearity. A study to examine the improvements which could be made by use of more calibration constants for each device showed that the present system was adequate without producing a h'ghly complex calibration procedure.

6.4. Hysteresis of the Instrumentation.

Hysteres s may be defined as the failure of a device to return the same reading under a given load or d placement under cond t ons of both increas ng and decreasing load or displacement. During the calibration procedure some hysteresis was noted in all the devices. Such effects are of particular importance where cycles of loading or rap d changes in direction of loading path occur.

The ca ibration data of Table 6 1 shows the magn tude of the hysteresis of each device. Only the volume gauge shows hysteres s which may be of s gn f cance.

6.5. Drift and Noise of Instrumentation.

During the original proving and test ng of the system much work was conducted investigating these two factors. Each device produces a s gnal wh ch is constantly varying with time. These variations occur due to drift, noise, and creep.

Drift refers to changes in gauge res stance under no strain conditions and may therefore be assessed by changes in the zero stress readings over a period of time. This may be observed at the end of a test as the fa lure of the transducers to return to zero at the end of the test. Creep refers to changes in resistance under strain condition. This may be observed by changes in the values of the calibration constants. In these tests changes of calibration constants were observed to be very small even over long periods of time (up to approximately 35 days). It should be noted

that temperature changes have a significant effect on drift and creep of devices. However, in the Spectra system all the devices are read using a full bridge arrangement and the equipment is located in a temperature controlled laboratory so that temperature effects should be negligible.

Noise refers to any signal which is transmitted in addition to the instrument output. Noise occurs due to resistance changes in the connections and induced voltages (from magnetic fields generated by other devices e.g. transformers etc). The magnitude of the noise may be detected by turning off the bridge supply and observing the signal recorded. In the Spectra system the instruments are continuously energised when the program is running and so it is difficult to assess this error. However, the combination of noise and the precision of the reading system may be estimated by observing the short term variation of a reading when a constant pressure or displacement is applied to a device. The error due to noise and drift may be reduced by increasing the integration time for readings from a device. This may not be increased without limit since in the Spectra system there are six cells each with five devices to be read every ten seconds and appropriate control action taken.

Typical values of these errors are shown in Table 6 2. The drift measurements were assessed over a long period up to sixty days. The noise readings were checked by repeated readings over a period of one minute.

6.6. Compliance of the System.

In order to apply pressures to the soil sample, similar pressures must be generated within the apparatus. As a result of these pressures the soil sample will deform. Despite careful design of the systems for measuring stresses and strains in the sample the compliance of the Bishop and Wesley system will contribute some errors in the measurements of sample deformations. The measurement of deviator force and cell pressure are free from such errors however the remaining measurements are all affected to some degree.

6.6.1. The Pore Pressure and Volume Gauge.

The flexibility of the pore pressure and volume change measuring system is significant in three areas,

a) expansion and contraction of the volume gauge due to varying back pressure;

b) deformation of the pore pressure transducer due to varying back pressure;

c) expansion and contraction of the drainage leads due to variation of both cell and back pressure.

The expansion and contraction of the volume gauge may be significant in tests where the back

pressure is varied and occurs due to expansion or contraction of the belloframs in the volume gauge as the back pressure reduces or increases respectively. It may be assessed by closing the drainage valve (Fig 5.2) and raising and lowering the back pressure while observing the resulting volumetric strains. Fig 6.7 shows the change in volumetric strain for cells 5 and 6. This shows that the expansion is approximately linear but is of very small magnitude.

Changes in volume of the drainage leads occur due to changes in both cell and back pressures. Leads outside of the cell are affected only by the back pressure while those inside submersed in the cell fluid vary in volume according to the effective cell pressure. This may be checked by placing a porous stone on the lower pededstal and a rubber membrane sealing it immediately above and below on the top and bottom pedestals. The pore pressure transducer is then removed and replaced by a blanking plug. By holding the cell pressure constant and varying the back pressure (observed by the Bourden gauge connected to the air pressure control valves) any volume strains due to varying back pressure may be observed. It was found that no volume change was registered by Spectra in excess of that due to the volume gauge even for very large changes in pressure. It was therefore concluded that this factor was negligible.

In order to assess the deformation of the pore pressure transducer the above test was repeated with the transducer in pos tion in place of the blanking plug. The difference in volume strain reading between that described above and this test should establish the compliance of the pore pressure transducer. Aga n the volume changes recorded were fully accounted for by the variation in volume of the volume gauge, and so this factor is also considered negligible for these tests

It should be noted that in conduct ng these tests great care must be taken to de-air the system as fu ly as possible so as not to record volume changes due to the deformation of air bubbles in the sy tem Furthermore it is a sumed that the pore water is incompressible. For the pressure changes involved here the error due to th s factor is neg gible.

6.6.2 The Axial Displacement.

The f ex b l ty of the axial d p acement measuring system has been reduced in many ways by the des gn of the B shop and Wes ey cell. Changes in cell pressure and the associated change in length of the cell body do not affect stra n measurements s nce displacements are taken directly as the relative movement of the edge of the cell top plate and the crosshead below the cell (Fig 5.1) wh ch is connected d rectly to the lower platen in the cell. Errors in the axial strains do however occur due to a number of factors.

a) bending of the ce l top p ate and deformation of the top and bottom platens;

b) deformation of the stra n gauges in the load cell;

c) movements in the strain gauge seatings of the load cell.

It may be shown that for the maximum cell pressures encountered in the triaxial cell, the bending of the cell top plates and the deformation of the top and bottom platens (including the screw rod carrying load cell), is several orders of magnitude smaller than that which the present measuring system can resolve. It is therefore considered that with devices and instrumentation in use this factor is negligible.

The deformation of the load cell is very significant. Firstly there are strains observed due the deformation of the strain gauges under varying deviator stress. Secondly there is a jump in the recorded strains as the strain gauges move on their seatings when the isotropic axis is crossed from compression to extension (and vice versa). In addition a similar movement occurs in the threaded rod carrying the load cell due to the threads moving in the threaded top bush of the triaxial cell. The movement due to the threaded rod may be eliminated if the load cell is as close as possible to the cell top plate after setting up a sample. This requires great care when setting up or the axial strains which may be developed during compression will be very limited: The errors due to the deformation of the load cell may be observed by applying loads and recording the deflection of the base of the load cell. In compression th's is most readily done by using a steel sample and increasing the deviator stress while observing the axial strains. In extension, loads must be applied by a hanger and the deformations measured by a transducer placed under the load cell A typical load-deflection cal bration for two load ce ls is given in Figs 6.8 and 6.9. It can be seen that for these load cells the corrections are very sim ar in both extension and compression but sl'ghtly larger in extension. The curves are non-l near but may be approximated by a quadratic at low stress levels and linear thereafter. In cross ng the isotropic ax s a sudden jump occurs which appears to be constant for any particular load cell. Hysteres s in these ca ibration curves was observed to be very small and in practice it was decided to neglect it for the purposes of corrections to be applied. Th s method of calibration also corrects for the compression of the end platens and top plate due to changes of the deviator stress, the only error is that due to the compression of the 76mm steel dummy sample (if E = 200 x 10^6 kPa for steel (Ryder, 1978) then the error in the strain correction is 5 x 10^{-7} %/kPa or an error of 0 0005 % for a q' of 1000 kPa

6.6.3 Discussion of Apparatus Compliance.

The present version of the control program does not automat cally correct for any of the factors discussed above. The data analysis program (see sect'on 5.4.9.2) does allow for these corrections on input of suitable ca bration constants. The correction for the movement of the load cell on crossing the isotropic axis rema ns a problem, since the data must be examined carefully to decide which points require the correction applying as actual movement normally occurs just after the isotropic axis has been crossed.

Other factors which may contribute to errors in stra n measurements such as bedding and seating errors and errors due to non-homogeneous straining of samples are not discussed here since

they do not fall under the category of system compliance. They have been fully discussed however in Chapter 2 (section 2.3.8). The reduction of the errors due the factors discussed here may be accomplished by using revised instrumentation. Axial strains may be measured by devices mounted directly on the sample (subject to the restrictions discussed in section 2.3.8), and a revised type of load cell (designed at Surrey University and marketed by Wykeham Farrance Ltd) used to measure deviator force. This revised load cell has a much higher stiffness than the Skinner load cell and is not subject to the jump in strains when crossing the isotropic axis. The penalty for this greater stiffness is a much reduced output signal for the same stress range with as a consequence a reduction of resolution if using the same interface units. It should be noted that even with this improved load cell careful setting up of samples is required since the jump in strains due to the movement of the threaded rod carrying the load cell will still occur if the load cell is not as close to the top of the cell body as possible.

6.7 System Testing.

A number of tests need to be performed from time to time to assess the performance of particular parts of the system and to check for faults. The calibration procedures do this to some extent since they allow monitoring of the values of the calibration constants of the instrumentation. Wide fluctuations of these constants will generally indicate a suspect instrument or channel which should be subject to more detailed analysis and inspection.

Further to these checks option 10 (section 5.4.8.3) should be used from time to time to check the correct functioning of all relays. Checks are required to ensure that the roller bearings of the axial loading ram have not stiffened to produce excessive friction. It should be noted however, that since this is a feedback system with the load cell isolated from the frictional effects, the friction will not affect the accuracy of control or of the recorded readings of axial stress, but will affect the precision with which the chosen stress path is followed i.e. there may be "hunting" on the chosen path. Similar checks are required of the volume gauge since it is of a similar construction and friction in the roller bearing may result in increased hysteresis in volume change measurements and increased "hunting" in control of either back pressure or volumetric strain.

Checks are also required to check the drainage system for leaks. These tests must be conducted over extended periods of at least 72 hours. Any leaks may be identified by isolating sections of the system while under pressure and observing either the changes of volumetric strain recorded by the Spectra system or the variation of pore pressure. These tests are extremely important especially where individual tests are likely to be conducted over a period of weeks. These tests are described in detail by Atkinson, Evans and Scott (1983b).

6.8 Discussion.

In this chapter the methods followed in calibrating the instruments have been outlined and the accuracy and precision of these devices assessed. Of the above errors, those due to calibration

and flexibility of the apparatus are systematic errors and could be eliminated if desired by using suitable correction and calibration procedures. The remaining errors due to drift, noise, and the limiting precision of the devices and interface are all random errors and nothing can be done to reduce them except to use higher quality instrumentation and in particular a more precise interface and logging system.

Finally there are those errors due to the control system itself, i.e. the flexibility of the control system, delays in issuing commands and response times. Assessing all these errors together the accuracy of the system was estimated to lie at all times within the limits summarised in table 6.2. It can be seen that the axial stress is subject to the greatest errors. This is due to a number of factors including; the friction in the axial loading ram; the reduction in sensitivity due to the bellofram diameter to sample diameter ratio of 2.5; and the method of calculation of axial stress. The load cell only records the axial force and does so with a precision similar to that of the other instrumentation (table 5.1). In order to compute the axial stress equation 5.5 is used which requires the values of radial stress, volumetric and axial strains to be used in the calculation. As a result the axial stress displayed is subject to four sets of errors in the readings resulting in a large loss of precision.

The errors resulting in the control of stresses are therefore due to two components, firstly that due to the ability of the system to provide a controlled loading path to the stress path cell and secondly that due to the performance of the whole system in applying a required stress to the sample. This is illustrated by Fig 6.10 which shows the system diagramatically. The true stress on the sample is σ_s, this is sensed by the transducer and after applying calibration constants is recorded as a stress σ_r. The microcomputer then sends a command to apply a pressure p_c and the pressure supplied is p_s. The accuracy of the control ($p_s - p_c$) is of the order $\pm$ 0.5 kPa ($\pm$ 1 kPa for axial stress) and is only controlled by the gearing of the motors, air pressure control valves and friction in the system. The accuracy of the system ($\sigma_s - \sigma$) is that due to the instrumentation as discussed in this chapter and summarised in table 6.2. The magnitude of ($\sigma_s - \sigma_r$) is controlled by the hysteresis of devices, the linearity of devices and the corrections made for systematic errors such as system compliances. It should be noted that these errors refer to the overall accuracy of recorded parameters and not to the precision of the measurements as discussed in Chapter 5. Similar arguments may be applied to strains with control of the order $\pm$ 0.01% and accuracy as stated in table 6.2. These figures are as good as or better than those obtained in the conventional triaxial testing equipment. The errors in derived quantities e.g. effective stresses or stress invariants, may be greater due to accumulating these errors. If improved accuracy is required then special devices could be used such as differential pressure transducers to measure effective stresses directly. Errors for each individual case have not been presented since in practice it is very difficult to separate individual components in the total errors. In any case it is the total combined errors which are of significance. Even though it is desirable that the control follows the required path as closely as possible i.e. ($p_s - p_c$) is as small as possible, it is of far greater importance to know with certainty the actual stresses applied to the sample and so minimise ($\sigma_s - \sigma_r$). Further improvements in the

accuracy of measurements made of the state of the sample require significant upgrading of instrumentation and interface systems. The improved instrumentation might include differential pressure transducers, internal axial strain devices (Jardine, Symes and Burland, 1984) and use of the improved load cell. These improvements were not made for this research since differential pressure transducers were not considered necessary and the improved load cell was not available during the main part of the experimental work. The reasons for not using the internal axial strain devices with reconstituted soils were set out in section 2.3.8.

CHAPTER 7

EXPERIMENTAL DETAILS.

CHAPTER 7. EXPERIMENTAL DETAILS.

7.1 Introduction.

This chapter contains particulars of the tests which were conducted and the methods used. Details will first be given of the factors affecting the choice of soils for testing during this research. The details of the soils selected will then be given and the method of preparation of soil samples for testing. Finally the procedures followed in conducting a test will be discussed in detail including, the setting up of a sample in the apparatus, the conduct of test stages and procedures following the final test stage. The chapter concludes with full details of the tests conducted and the objectives of each of these test series.

All the tests were performed in cells 1,3, 5 and 6 of the Spectra system and were conducted by the author unless otherwise stated.

7.2 Requirements of Soils for Testing.

The scope of this program of research has been outlined in Chapter 4. The object of this research is only to analyse the effects of recent stress history on subsequent stress-strain behaviour of the soil sample. It is therefore desirable to test soils for which threshold effects due to creep are minimised. This may be done by selecting soils for testing which have reasonably high compressibilities in order to ensure that strains are measurable, but which have a very low creep rate. The present research will be restricted to clay soils.

Suitable soils may be selected by inspection of consolidation curves plotted as volumetric strain against square root of time elapsed. The two diagrams shown in Figs 7.1a and 7.1b illustrate suitable and unsuitable choices of soils. In the case of a soil with a high creep rate it would be difficult to decide when a test stage should terminate and the next start since appreciable strains may register long after the loading path had been completed. It is likely that at the chosen point a large amount of secondary compression may have occurred and hence threshold effects due to creep would influence the results as well as the change of stress path. For tests in which threshold effects due to creep were to be analysed it would be desirable to use a soil which had a relatively large creep rate, so as to get large changes in material behaviour for only modest periods of rest.

It is also desired to test a number of different soils to demonstrate the significance of threshold effects for various soil types. This test series will be restricted to clay soils only, with soils selected with a range of plasticity indices.

7.3 Details of Soils for Testing.

A number of different soils have been used in this investigation. These include London Clay, Speswhite kaolin, Cowden Till, Iate dust and Ware Till. The index properties of these soils have

been established by a number of workers and are given in table 7.1. All the test results quoted are from tests conducted in accordance with BS 1377 (British Standards Institution, 1975).

The London Clay was provided by the Building Research Establishment. The material comes from Bell Common in Essex on the site of the M25 Motorway. The soil was provided for research into the movements of retaining walls (Richardson 1984a), the data for the index properties is quoted from this work.

The Speswhite kaolin was obtained by the City University in 1980 for general research into the fundamental stress-strain properties of soils. Since this time many research projects have been conducted, the data quoted in table 7.1 comes from a selection of some of these projects.

The Cowden Till was provided by the Building Research Establishment. The soil comes from a large batch from a site near Hull on Humberside. This soil is the subject of a large research project at the City University and the Building Research Establishment. Some of the results to date are reported by Lewin and Ng (1985), Ng (1985) and Clinton (1985). It is from these reports that the data in table 7.1 is derived.

The slate dust comes from Llyn Brianne in South Wales. The material is fully described by Tombs 1969). The index properties are quoted from Lewin (1970).

The Ware Till used in this project was collected from a site near Wellwyn Garden City in Hertfordshire, Holywell Hyde plt. It was used for an undergraduate research project at the City University (Richardson ,1982 This material has been the subject of research on undisturbed and remoulded samples by Little (1985

Full descriptions of each of the soils and details of the tests conducted may be found in the references quoted above

7.4 Compression and Swelling Properties of Soils.

The values of the parameters for both isotropic and one-dimensional compression and swelling of these soils have been obtained by various workers at the City University using the Spectra stress path system. The values are summarised in table 7 2. Further data for Ware Till using different triaxial apparatus and oedometers is also given from Little (1985).

It should be noted however that these parameters appear to be very sensitive to the method used to prepare samples. Large differences in the slope of the normal compression and swelling lines may occur where the final water content of the sample prepared for testing varies. This is seen particularly in the case of Ware Till for remoulded and undisturbed samples (Little ,1985). This may be noted from the figures obtained in this research for various methods of preparation of both Speswhite kaolin and London Clay Similar observations have been made by Hight et al (1979)

testing samples reconstituted from a slurry and remoulded samples of lower Cromer till. Balasubramaniam (1969) testing Speswhite kaolin reconstituted from a slurry to various final water contents noted that the slope of the compression and swelling lines reduced and the equilibrium voids ratio (the voids ratio at which the excess pore pressures are zero) reduce as the water content of the sample before testing reduces. It is therefore very important that the method of sample preparation is consistent and similar samples can be reproduced in large numbers for research purposes.

7.5 Sample Preparation.

Two methods of sample preparation were used in the course of this research. In order that large numbers of samples could be reproduced which were all very similar for testing, the first method discussed below was used to produce samples for the main program of testing.

7.5.1 Soil Preparation.

The actual soils selected for testing were described in section 7.3. For all the soils except the Speswhite kaolin the following procedures were followed before preparing any samples.

The soil supplied was first broken down into p eces of about 25mm in size and any very coarse material such as stones removed Th s material was then placed in trays for drying in an oven at 105°C for a period of approximately 24 hours Each soil was then broken down into small pieces and again stones removed before being passed through a grinder. The material leaving the grinder was not greater than 0 425mm in size. Th s material was then placed in store until required for produc ng samples. In the case of Speswh te kaol n the material was supplied in sacks as a dry powder and so there was no need to carry out the above stages

7.5.2 Water Absorption by Dry Soil.

In the course of these investigations a check was made to see how much water was taken up by the powdered soil over a period of t me Th s is of sign ficance when it is realised that in order to produce s milar slurries of each so l, each batch of dry so l must be assumed to contain no free water, i e. a water content of zero The test was conducted on London Clay which had been prepared and stored two months previously. The resu ts ind cated that over this period the soil had taken in about 1 5 to 2% water content from the atmosphere. All other soils were stored for much shorter periods than two months before test ng so although the quantity of water absorbed may depend on the precise m neralogy of each soil, th s factor was not considered to be significant and no account was taken of absorbed water in calculat ons. The powdered soil could alternatively have been dried before producing samples but considering the small error involved it was not thought to be necessary. It should be noted that no special precautions were taken to prevent the soil from taking up water since it was only stored in a r-tight plastic bags.

7.5.3 Preparation of the Soil Slurry.

Details of the water contents of the slurry for each soil are given in Table 7.3 together with details of mix quantities of dry soil and water needed to produce a 38mm diameter sample of 76mm in length. The water contents were determined by the following criteria ;

a) it should be possible to pour the slurry smoothly without entraining air;

b) when jarred gently the slurry should be just liquid enough to allow air bubbles to rise to the surface and burst.

If these citeria were not satisfied large quantities of air could be trapped in the slurry and cause difficulties when trying to saturate samples. In all cases the water used to prepare samples was de-aired tap water from the laboratory mains water supply. The determination of the actual water contents to be used is a matter of trial and error or from past experience. The water contents used for London clay , Cowden Till, and slate dust were recommended by Lewin (1985).

In order to prepare a slurry quantities of dry soil and water were carefully weighed so as to obtain a slurry at the desired water content. These were carefully mixed by continuous mixing so as to ensure that a uniform slurry would result. This slurry was then jarred so as to allow bubbles to rise and burst. A vacuum was not used in order to de-a r the slurry. Table 7.4 gives details of the actual water contents of slurries which were achieved, it can be seen that there is a relatively sma l variation of water content compared to the mean required (Table 7.3).

7.5.4 Description of Sample Presses.

The presses are shown d agramat cal y in f g 7.2 and are identical to those used by Lewin (1970). They consist of perspex tubes 38mm in d ameter and approx mately 200mm long. At each end a p ston carrying a porous stone is free to move a ong the bore of the tube. This arrangement therefore produces one-d mensiona l y compressed samp es (i e. conditions of zero lateral strain) with drainage permitted from the ends of the samp e only. In order to prevent clogging of the porous stones at each end, filter paper d scs were p aced over the stones. A hanger loaded with suitable weights suppl ed the load for conso dat on v a a ba l bearing on the top piston. In order to reduce friction when consolidating a sample, a 20mm section of the bottom of the 38mm diameter tube may be removed at a later stage in the consol dat on process to allow the tube to float on the lower piston

7.5.5 Setting up of Mix in Presses.

The lower piston was covered with a moistened filter paper and placed in the container. The removable 20mm length of tube was placed over the top and then the main sample tube over this. The complete assembly was then weighed. The tube was then filled with the slurry to a pre-

determined level such that a sample of approximately 76mm long would remain at the end of consolidation. This was easily done by a series of pilot tests to determine the final water contents of samples of each soil from the presses under a given load such that they could handled for setting up in the triaxial cell. With a knowledge of the water content of the sample it is possible to determine the weight of slurry required in the tube. Once the correct quantity of slurry had been measured out the weight of tube and slurry was recorded. A damp filter paper and the upper piston were then placed on top of the slurry.

A final load of 6 Kg was found to be adequate for all the soils used in order to produce samples of the required water contents. The final water contents achieved for each soil are given in table 7.4.

7.5.6. Loading of Slurry.

Loads were applied to the upper piston by a hanger and ball bearing. The first increment consisted of only the hanger, approximately 0.4 Kg (equivalent to an axial stress of 3.5 kPa). The settlement of the hanger was recorded via a dial gauge so as to keep a record of the length of the sample and hence the volume of water expelled. Increments were then added at approximately one hour intervals, each increment approximately doubling the applied load to a maximum applied load of 6 Kg (51.9 kPa) on all samples. This maximum load was then left for a period of approximately 24 hours. The loading stages were as follows:

Stage 1 hanger only =	0.4Kg	equivalent to 3.5 kPa
Stage 2 add 600g =	1.0Kg	equivalent to 8.8 kPa
Stage 3 add 1.0 Kg =	2.0Kg	equivalent to 17.6 kPa
Stage 4 add 2.0 Kg =	4.0Kg	equivalent to 35.3 kPa
Stage 5 add 2.0 Kg =	6.0Kg	equivalent to 51.9 kPa

The lower 20mm ring was removed at the end of stage two. Details of the final water content of these samples and their dimensions for each soil are given in Table 7.4. The period of 24 hours was required in order to allow samples to consolidate under the applied loads. This period allowed samples to become reasonably uniform in water content over their length. At the end of this period if excess pore pressures had fully dissipated and there were no losses due to friction between the tube and the pistons and slurry, the vertical effective stress would be approximately 51.9 kPa or a value of mean effective stress, p', of 35 kPa (taking K_o as 0.5). At the end of this period samples were removed from the presses and immediately placed in the triaxial cell after the filter papers had been removed and the sample measured and weighed to provide a check on the final water content. None of the samples produced by these procedures was trimmed to length before use or placed in storage.

7.5.7 General Comments on Samples from Presses.

Samples produced by these procedures proved to be very easy to reproduce. Details of final

dimensions and water contents are summarised in Table 7.4, and show only a small spread of results. The water contents of samples produced in this way are not completely uniform over the whole length of the sample. Typical water content profiles of samples produced from these presses for each soil are shown in Figs. 7.3 to 7.7. It can be seen that, as would be expected, both ends of the sample had a very similar water content which is lower than that of the middle section of the sample. The maximum difference in water content between the ends and centre of samples can be seen to be about 1.5 to 2.0% i.e. $\pm$ 0.75 to $\pm$ 1.0% of the mean water content determined from the whole sample. Similar results have been reported by Robinson (1984) for Speswhite kaolin using a very similar technique but different presses and by Lewin (1970) using Spestone kaolin and Slate dust in the same presses as in this work. Some tests were conducted with samples in the presses for longer periods but the spread of water content remained very similar with a similar mean water content which suggests that twenty four hours was long enough for samples to reach equilibrium and that the variation of water content reflected the friction along the length of the perspex tube.

It has already been noted that samples produced by this method are one-dimensionally compressed and so will initially behave as an anisotropic sample. This is of no significance if one is interested in testing one-dimensionally compressed soils but if it is intended to conduct tests on isotropic samples then the sample must be loaded to a sufficiently high stress level so that the yield surface moves to be orientated about the $q' = 0$ axis and so the soil behaves isotropically. It is anticipated from the previous data (Balasubramaniam, 1969; Gens, 1983), that the maximum past stress must be exceeded by a factor of 2 to 3 times to ensure that this happens (i.e. a value of p' of 70 to 105 kPa). Although for the purpose of these tests this point is not of significance, since it is only desired to produce a number of similar samples, it may be an important point when analysing the results to determine an explanation of the reasons for stress path threshold effects.

7.5.8 Alternative Method of Sample Preparation.

At the start of the present program of tests a number of samples were produced by an alternative method

As before quantities of dry soil and de-aired water were carefully weighed. For these samples however the water content was much lower than that of the slurry samples. The soil and water were mixed into a thick paste and then pushed into 38mm diameter tubes. Samples were then extruded, trimmed to length and immediately placed in the triaxial cell for testing.

Details of the water content of the paste and details of the samples produced are given in Table 7.5. This method was only used for samples of Speswhite kaolin and London Clay although data was available for samples produced in a similar manner of Ware till (Richardson, 1982).

7.5.9 Comments on Samples produced by Alternative Method.

The samples produced by this method had the advantage that they could be produced very

rapidly when required. From plots of specific volume against log $_e$p' it was estimated that they had an effective stress of about p' = 40 - 50 kPa applied during the process of forming the samples, which is very similar to that of the reconstituted slurry samples. In addition as data presented later will show they behaved in a manner which was much closer to that of an isotropic sample during the early stages of loading.

This type of sample was not adopted for general use however for a number of reasons. Firstly the samples produced in this way were not fully saturated so that a period of time had to be allowed for the samples to saturate when placed on the triaxial cell. Secondly it was difficult to produce similar samples to better than about 2% to 3% average water content (although the water content profile along the length of the sample was quite uniform). Despite careful mixing of the soil paste some local random variations of water content in samples were inevitable due in part to the drying of the mix while the sample was formed and due to variations of water content in the paste itself. Finally samples produced in this way had to be trimmed and so were subject to some degree of mechanical disturbance which could vary between samples.

The final two points are of greatest significance since samples with different initial water contents are found to have significantly different stiffnesses even after following similar consolidation paths. It is also important that any degree of disturbance which can be avoided should be due to the possible effects on sample stiffness (see Chapter 2). It was therefore decided that due to the superiority of the samples produced from the presses and their consistent repeatability that it should be the method chosen for sample preparation.

7.6 Setting up of a Test.

7.6.1 Introduction.

In this section the procedures followed to set up a sample in the triaxial cell will be described. The general procedures are detailed in the Spectra system manual, Atkinson, Evans and Scott (1983b

In these tests samples were extruded from the preparation tubes and placed in the apparatus such that they existed at an isotropic state of zero total stress with negative pore pressures reflecting the magnitude of the maximum past effective stress applied in the sample presses. They were then compressed and swelled to reach an initial starting point for testing. The precise stress paths to be followed both during initial compression and swelling and during the following loading depended on the details of the test. In some tests isotropic compression, swelling and recompression were repeated over many cycles in order to establish values for compression and swelling indices. The procedures used in order to reach the start of the loading paths are described below.

7.6.2. Preparations for a Test.

In all tests filter paper side drains to the pattern of Bishop and Henkel (1962) were used. Filter paper discs were used at each end of the sample with a coarse porous stone on the lower platen below the lower filter paper disk (fig 7.8). In order to minimise leakage from sample to cell between the membrane and the pedestal during the test, despite the 'O' rings, the sides of both top cap and bottom pedestal were lightly greased with silicone grease, Evans (1983). Finally the pore water system was de-aired and the volume gauge centralised.

7.6.3 Measurement of Initial Sample Dimensions.

All measurements of strain throughout the test were based on the initial sample dimensions recorded of the extruded samples. These dimensions are therefore very important for the accurate conduct of tests. Measuring samples after extrusion from the tubes prove very difficult since the sample was soft and the calipers used to measure the sample may push into the sides and ends.

In this work the method used was to measure the sample before extrusion from the tube. In all tests the same two sample tubes were used to produce all samples. The diameter of these tubes was carefully measured and the average calculated so that the diameter of all samples was known. In order to record the length of a sample the tube containing the sample was measured overall with the pistons in place. The length of the pistons together with filter papers were then measured to establish the length of the sample. These dimensions were recorded to 0.1mm for input data for the Spectra system. All samples were also weighed and the mass recorded to 0.01g. Details of sample dimensions and masses are given in tables 7.4 and 7.5.

7.6.4 Sample Mounting.

The first stage before starting to set up the sample is to use option 2 to record the zero stress readings This option records the output readings from each of the transducers with no pressures applied In all the following calculations these readings are used to compute the change of output from transducers and so using the calibration constants the current stress state.

The saturated porous stone was then placed on the lower platen followed by the moistened lower filter paper disk, the sample, the moistened upper filter paper disk and the top cap (fig 7.8). The moistened filter paper side drains were then placed around the sample so as to overlap the porous stone at the base. A dry membrane, previously tested for leaks was then stretched over the sample In all tests only a single dry membrane was used. The membrane was then sealed top and bottom with two 'O' rings at each end Finally the rubber suction cap was placed over the top cap. Great care was required in placing the suction cap on the top cap to avoid damage to the sample. In all but the very early tests a redesigned top cap was used which consisted of the normal top cap cut in two but with a threaded screw in the middle to connect the two halves. This allowed the

rubber cap to be placed on the upper portion of the top cap which was then carefully screwed into the lower section already in place on the sample.

The cell body was placed over the sample, screwed down and filled with de-aired tap water. The initial sample dimensions and test data were then entered in Spectra in order that applied stresses would be computed correctly using option one. The sample set up with the cell body over the sample and bolted in position is shown in plate 7.1.

7.6.5 Initial Test Stages.

The initial test stages include checking the sample saturation, connecting the top cap and all stages leading to the compression and swelling stages for samples. During the period of this research three different test procedures were followed during testing, each will be described separately.

7.6.5.1 Method A.

In the initial tests the procedures described by Atkinson, Evans and Scott (1983b) were followed. The first stage was to increase the cell pressure manually to 200 kPa with drainage valves closed. The sample was then left to allow the pore pressure to come to equilibrium.

Once the samples had reached equilibnum (a period of not normally more than 15 minutes) they were allowed to consol date against a back pressure of 150 kPa. This stage was completed in a s ngle step normally with computer control but w th additional readings taken manually of radial stress, pore pressure and volumetnc stra n. A plot of volumetric strain against square root of time could then be made and so the time for 100% consolidation (t_{100}) estimated.

Deta ls of these tests are given in table 7 6a . The data given includes the initial pore pressures before initial consolidation, the water content of the sample before mounting, the bulk density of the sample and the final volumetnc strain during the consolidation stage. Figs 7.9 to 7.13 show typical ε_v against $\sqrt{t}$ plots for each soil type.

7.6.5.2 Saturation Test.

Following the initial consolidation stage the saturation test was performed. The first stage was to de-air the drainage system For this purpose a Bishop ram was used. This was first de-aired. The drainage valve to the sample was then closed and water pumped into the volume gauge via the bleed valve (fig 5 2). The Bishop ram was then connected to the bleed valve on the pore pressure transducer block, the drainage valve opened and water allowed to pass from the volume gauge across the bottom platen and out into the Bishop ram. Often during this operation air bubbles could be seen moving through and out of the system.

The drainage valve was then closed and the Bishop ram disconnected. The saturation test was then performed by raising the cell pressure in 50 kPa steps and observing the pore pressure response. In all cases the response was less than B = 1 but was never less than B = 0.95, where B = $\Delta u/\Delta\sigma_r$ (Skempton, 1954). The actual figures observed are given in table 7.6a.

7.6.5.3 Connection of Top Cap to Load Cell.

Although not required during isotropic compression and swelling test stages for the purposes of loading, the connection was always made at this stage in tests for two reasons. Firstly this allowed measurements of axial strain to be made in order to compute sample dimensions and secondly, it reduced bedding errors in any following test stages (Atkinson and Evans, 1985). The cell pressure was reduced to 200 kPa once again and the axial stress increased manually until the axial loading ram was just balanced by the oil pressure and could be moved by light pressure of the hand. The procedures outlined by Atkinson, Evans and Scott (1983b) were then followed in order to connect the top cap.

It was found that with care a deviator stress of not greater than 1 to 2 kPa was applied to the sample during connection. However during this period a small rise in pore pressure had taken place and so a further consolidation stage of a few hours was required, by re-opening the drainage valve, to reduce the pore pressures to 150 kPa before commencing the next stage.

It should be noted that up until this point all strains had to be computed on the assumption that the sample behaved isotropically i e $\Delta\varepsilon_v=3\Delta\varepsilon_a$, this is not necessarily true. However due to the relatively small magnitude of strains up to this stage this was not considered significant. These procedures were modified when using samples reconstituted from a slurry since the strains were quite large. The top cap was connected before the initial consolidation to p' = 50 kPa. Consolidation to p' = 50 kPa was then completed with control by Spectra. The saturation test was also completed by Spectra by increasing both axial and radial stresses at the maximum rate possible (about 60 kPa per hour) This method had the advantage of providing correct sample dimensions throughout testing and was also slightly quicker than the first method described. Great care was needed in order to connect the top cap at this stage since the samples had very low strength before initial compression (initial effective stress of approximately p` = 25 - 30 kPa). A further advantage of early connection of the top cap arrangement is to reduce bedding errors observed in later stages of the test (Atkinson and Evans, 1985).

7.6.5.4 Method B.

Tests by Atkinson, Evans and Ho (1985) indicate that single step consolidation stages for samples with radial drainage may cause case hardening effects that is a variation of water content across the radius of the sample. The procedures outlined in Method "A" were therefore modified to eliminate the single step consolidation stage

In Method "B" the top cap was connected as soon as the sample had been set up in the cell with an undrained isotropic stress increment of 200 kPa. The pore pressure response was then observed and the back pressure set equal to this value. The drainage valve could then be opened and no volumetric strains would be observed. The system was then de-aired and a saturation test performed as described before. With the cell and axial pressures reset to 200 kPa and the back pressure set to the pore pressure response the initial compression stage was performed with axial and cell pressures increasing and the pore pressure reducing at a constant rate to 150 kPa from its initial value.

Tests conducted by this method are listed in table 7.6b. In table 7.6b details are given of the initial pore pressures before initial consolidation, the water content of the sample, and the B value from the saturation test.

7.6.5.5 Method C.

For most of the tests conducted in the course of this research method "C" was used. While method "B" does have the advantage over method "A" of avoiding the initial single step consolidation stage it has two disadvantages which may be avoided. Firstly the variation of the back pressure means that a small correction is required to all volume strain measurements to allow for the flexibility of the volume gauge Secondly control of the back pressure means that there are three controlled functions a l vary ng in value with t me. As a result the desired test path is not f lowed w th the best precision of wh h the system is capable

n method "C" the init al undra ned otropic stress increment was applied so as to result in a pore pres ure response of 150 kPa The system was then deaired w th the back pressure set at 150 kPa and a saturation test performed The top cap was then connected as previously described bef re both ce l and ax al pres ures were readjusted in order to g've a pore pressure response of 15 kPa Th s allowed the in t al compression stage to commence with only axial and radial stresses increas ng with the pore pressure ma nta ned constant In tests which did not follow an isotropic stress history this method was varied s ght y The in t al values of cell and axial pressure were set to give a pore pres ure of 150 kPa and a so to g ve the required value of the ratio of effective pressures f r the path to be f lowed (on paths for which $\eta_0' \neq 0$).

Deta s of tests performed us ng th s method are g ven in table 7.6c. In table 7.6c details are given of the in t al isotropic pressure required to get a pore pressure response of 150 kPa, the water content of the sample, and the B va ue from the saturation test.

7.7 Conducting a Test.

The tests which have been performed generally fall into one of three types; those to examine the range over which threshold effects are observed, those to examine threshold effects due to various approach path directions, and for London clay only a series of tests to failure to establish

the shape of the state boundary surface.

In the first type of tests, stages of the isotropic compression swelling and recompression were followed. In the second type of tests most samples followed the stages described below:-

stage one: compression to p' = 400 kPa.

stage two: swelling to p' = 200 kPa ($R_p = 2$).

For all five soils such stages were followed in isotropic compression and swelling. For London Clay only, such stages were also followed for stress histories in which η'_o = 3/4, 1/4, one-dimensional and two-dimensional compression and swelling. Also for London Clay only , the effect of stress level on stress path threshold effects was examined by following isotropic compression stages in two tests to p' = 600 kPa and p' = 200 kPa followed by swelling stages to p' = 300 kPa and p' = 100 kPa respectively. Finally for London Clay only, the effect of overconsolidation ratio was examined for both isotropically and one-dimensionally compressed and swelled samples at overconsolidation ratios of 1.5, 2, 4 and 8 with a maximum pressure during stage one in each case of p' = 400 kPa.

In the third type of test, samples were compressed to various values of p' and swelled to various overconsolidation ratios before loading to failure in compression along a number of stress paths including, constant p', undrained and drained tests with constant cell pressure.

In all tests the procedures for stopping and starting stages followed those outlined in chapter 5. Option 1 is called to input test data then Option 4 is called to record the zero strain readings, followed by Option 5 to start the test stage. The stage was then terminated by use of Option 6. In most cases samples were not left uncontrolled by Spectra for more than a few minutes due to changing test stages (while one stage was stopped, the data input for the next stage and the next test stage started). Throughout these tests strains were accumulated from the time when the top cap was connected through all stages except where large deformations required re-centering and zeroing of the strain gauges.

7.7.1 Rates of Test.

The rate of test in triaxial tests has been the subject of much discussion in literature. Normal laboratory practice leads to the use of expressions due to Bishop and Henkel (1962). These however lead to very slow rates of test and can only readily be applied to strain controlled tests.

An alternative method of selecting a suitable rate of test has been proposed by Atkinson (1984b). The major difference lies in that this method uses a maximum allowable excess pore pressure, u , rather than a degree of dissipation throughout the samples in order to determine the rate of test. This method is more logical since at low stress levels the Bishop and Henkel formula may imply

excess pore pressures which may be so small that the pressures and the effects they have could not be measured by conventional instrumentation. By selection of a suitable excess pore pressure and with a knowledge of t_{100} (the time for 100% consolidation) together with details of the sample drainage, the rate of test may be computed directly in terms of a rate of change of axial and radial stresses. Details of the calculated maximum permissible rates of loading for the chosen soils are given in table 7.7, for a maximum excess pore pressure of 5kPa.

By checking the continued volumetric strains at the end of an isotropic test it is possible to check the calculations made above for the rate of test (Atkinson, 1984b). This has been done for all these tests and the computed excess pore pressures are shown in table 7.7.

In general the rate of test used has been much slower than that predicted from the above calculations. This has been done in order to limit the volume strains which occur at the end of a test stage, which even for an excess pore pressure of 5 kPa are quite large due to the relatively high compressibility of these soils. The actual rate used and the corresponding excess pore pressure are given in the above tables for each soil. This method of computing rates of test is discussed more fully in Appendix two.

7.7.2 Selection of Control Limits.

In chapter 5 it was indicated that the operator must state the limits of control required in the test i e. the maximum deviation from the specified path to be allowed.

Th s must be chosen such that the path is fo owed with sufficient accuracy but is not so small as to exceed the precision of the instrumentation If too small a tolerance figure is given then hunting w l occur due to random fluctuations in read ngs of the transducers. Also with very low rates of test about 2 kPa per hour) some hunt ng may occur w thin the control limits. Some "under" and "over shooting" of the path must be expected due to the t me delay in readings, a feature which is particularly obvious when operators are us ng the system for other functions e.g. to observe the current state, since the control of the system w ll lapse wh le these functions are performed. From previous work, experience has shown that control lim ts are best set to $\pm$ 1 kPa for stresses and not less than 0 007% for strains.

7.7.3 Compression and Swelling Stages.

All tests incorporated such stages either to reach the start point of more complex stress paths or as the test itself.

The rate of test chosen was appl ed to both the cell and axial pressures to produce a constant rate of loading along the desired path. Rates of test were in the range of 1 to 7 kPa per hour for all soils. In all tests except those conducted using method B during setting up, undrained tests and special tests with varying pore pressure (section 4 6), the pore pressure was maintained constant at 150

kPa. Both axial and volumetric strains were recorded throughout. In tests on one-dimensionally compressed samples and on two-dimensionally compressed samples control was achieved by use of both stress and strain control. In the case of one dimensionally compressed samples the radial strain was maintained at zero while the axial stress increased in compression and decreased during swelling. The Spectra system then increased or decreased the radial stress so as to maintain the condition of zero radial strain and so follow the required path For two-dimensional compression and swelling procedures were similar but in this case the axial strain was maintained at zero while the radial stress increased and decreased. The swelling stages of the tests on samples compressed with stress ratios η'_o = 3/4 and 1/4 were conducted with controlled strain ratio since it was observed that during compression both these tests followed paths in which not only was the stress ratio constant but also the strain ratio was constant (except for during the very early stages of these tests).

7.7.4 Definition of End of a Test Stage.

In practice it proves somewhat difficult to decide when a test stage should finish. Any definition which is chosen will be somewhat arbitrary. In these tests since the initial stiffness of samples is of interest it is important to ensure that all samples are subject to a similar amount of secondary compression following the end of primary compression (due to the dissipation of excess pore pressure generated during loading

By observing the shape of volumetric strain against square root of elapsed time plot, the time for 100 % consolidation may be estimated It is observed however that volumetric strains continue at a considerable rate for some time after t_{100}, before reducing to a very small constant rate (in a plot of ε_v against $\sqrt{t}$) For the soils selected here this appears to be at about a time of $4t_{100}$ or about 3 hours for the soil with the longest t_{100} time here It therefore decided that for all samples of all soils that a rest period of 3 to 4 hours would be allowed at the end of all test stages before starting the next stage During this period it is anticipated that all samples would show insignificant volumetric strains for the final three recorded readings

7.7.5 Intermediate Test Stages.

These stages followed the compression and swelling of samples and preceded loading to failure. All these stages were conducted at a constant rate of test for each soil and was generally such that the rate of movement along the stress path ($\sqrt{(q^2 + p^2)}$ was 4.5 kPa per hour. The periods of rest at the end of each path were wherever possible controlled to be the same, and in all cases before constant p' and constant q' stages to between 3 and 4 hours. The object of these stages was to examine the effect of various approach path directions on threshold effects on a number of paths, and also to examine path dependence of soils below the state boundary surface. All these stages were conducted stress controlled with the pore pressure maintained at 150 kPa throughout The lengths of these paths were such that they could be conducted conveniently in one or two days testing and in general did not reach deviator stresses exceeding 90 kPa (for

samples of overconsolidation ratios of 2 and 1.5) or exceed stress ratios of 0.7 (for samples of overconsolidation ratios of 4 and 8), in order to avoid sample being subject to large plastic strains.

7.7.6 Tests to Examine Changes in Direction of Total Stress Paths.

The tests described in section 7.7.5 were conducted so as to examine the effect of changes in direction of effective stress path θ (fig 4.1). Since the pore pressure remains constant the total and effective stress path deviations are the same i.e. $\theta = \theta^t$. It is necessary to determine the effect of θ and θ^t separately in order to determine which controls material behaviour. In order to examine the effect of changes in direction of total stress path two common effective approach stress paths were selected $\theta = 0^0$ and 180^0, before a common loading path of constant p' in compression. By varying the pore pressure changes along the effective stress approach paths, different total stress paths are followed (fig 4.2). Hence different changes in direction of total stress path, θ^t, occur before following the constant p' stage. These tests were conducted on London clay only, isotropically compressed and swelled to p' = 200 kPa, with an overconsolidation ratio of 2. Due to the large variations of pore pressure during the approach path stages corrections to the volumetric strain were required during these stages.

Similar tests involving a constant value of θ^t may also be conducted while varying θ. Hence the effect of θ alone without any variation of θ^t will be observed.

7.7.7 Test stages to Failure.

Most of the samples were taken to failure except a few which were used only to establish isotropic compression and swelling parameters for each soil.

All samples which had followed intermediate test stages as described above were loaded to failure along constant p' paths using stress control. As a result none of these tests yield any information on post peak behaviour of the soil under test Strain control of such tests was not possible since the present control program does not allow strain controlled constant p' test paths to be followed.

For London clay only, a program of tests was conducted to establish the shape of the normally and overconsolidated state boundary surfaces. This was done through a series of stress and strain controlled triaxial tests with constant cell pressure for states in extension (normally compressed only) and compression (normally and overconsolidated). For normally consolidated samples the initial stress state varied from p' = 50 kPa to p' = 500 kPa and for overconsolidated samples from p' = 15 kPa (overconsolidation ratio = 40) to p' = 300 kPa (overconsolidation ratio = 2). All tests started from an isotropic stress state and all samples were isotropically compressed and swelled from reconstituted slurry samples. It should be noted that for the extension samples only side drains were omitted due to the potentially large errors which may result in extension tests due to the stiffness of the filter paper (see section 8 2.3).

7.8 After Final Test State.

On completion of the final stage the apparatus was dismantled and the sample removed as soon as possible. On removal from the apparatus the sample was weighed, measured and the sample dried in the oven to obtain the final water content. In these tests the whole sample was used to determine the average water content. The variation of water content over the length of a typical sample is shown in fig 7.14 to 7.18 for each soil. It can be seen that although the variation is less than that at the start of the test it is of the order of ± 0.3% of the average with maximum water content near the top reducing to a minimum at the base. Tests by Atkinson, Evans and Ho, (1985) also indicated that there may be some radial variation of the water content although this was not examined in these tests. Figs 7.14 to 7.18 also show that the variation of the water content appears to be slightly less in samples which had not been loaded to failure.

In the case of samples which had been brought to failure the dimensions were not easy to determine and so current dimensions were computed from the initial dimensions using the recorded strains and checked against the measured final dimensions. In the case of the sample length this proved successful but in the case of the sample diameter this proved less successful due to barrelling in samples which had failed.

In the case of samples removed without loading to failure both final dimensions were found to correspond well with the initial dimensions . The specific volume was computed from the final water content since the sample may not have been saturated when initially placed in the apparatus.

In tables 7.6a, b and c the water content before and after tests are given and the change in water content Also the volumetric strain recorded during the test for all stages is given.

Finally the zero readings of the stress transducers were recorded from Spectra. All should read as at the start of the test when stresses were zeroed In all cases readings were found to be within ± 1 kPa of zero indicating that drift of instruments was small even for tests of one to two months duration.

Throughout the period of this research very few problems were encountered with instrumentation and equipment. Where instrument failure occurred this normally resulted in failure of samples as Spectra tried to correct the state which was not being recorded correctly. Leakage did not prove to be a problem provided regular checks on equipment were made and any minor anomalies investigated, in only one case was there found to be a leak in the drainage system, data from the preceding tests was therefore discarded as it was probably unreliable. A small number of tests were lost either due to program crashes or power failures and due to failure of the air pressure control valve to motor clutches In total 86 tests were successfully completed, details of which are summarised in table 7.8.

CHAPTER 8.

CALCULATIONS AND RESULTS.

CHAPTER 8 CALCULATIONS AND RESULTS.

8.1 Introduction.

Data from the Spectra system consisted of axial stress, pore pressure, cell pressure, axial and volumetric strains. Although some corrections were made automatically by the SPCTRA control program others need to be applied by the operator at a later stage during analysis of the test results. Some of the corrections likely to be required have been discussed in Chapter 6.

From the corrected values of the recorded data, stresses and strains may be calculated for the plotting of the results. This chapter describes the corrections applied to test data obtained in this research and the diagrams which have been plotted of those results.

8.2 Corrections to Test Data.

The current version of the SPCTRA control program makes corrections to the axial stress for the changing cross sectional area of the sample. These corrections are based on the assumption that the sample deforms as a right cylinder and were described in section 5.4.8.4.

Due to the system compliance further corrections may need to be applied to the strains for the load cell and volume gauge compliances. Other possible corrections include corrections to stresses for the stiffness of the rubber membrane and filter paper side drains, and corrections to the volumetric strains due to the compression and swelling of the filter paper side drains.

By following certain test procedures some of these corrections may be minimised e.g. by maintaining the pore pressure as constant in drained tests the need for corrections due to volume gauge compliance may be eliminated.

8.2.1 Load Cell Compliance.

The method of calibration for load cell compliance was described in section 6.6.2 and the results of typical calibrations shown in Figs 6.8 and 6.9. At low stresses these curves may be approximated by a quadratic curve of the form,

$$F = A(\Delta L) + B(\Delta L)^2 \qquad 8.1$$

At higher stress levels these curves are approximately linear and may be given by,

$$F = C(\Delta L) + F_1 \qquad 8.2$$

Using the calibration constants A, B and C the analysis program calculates where the two curves join so that they form a single smooth continuous curve. A correction for the load cell jump due to

the sudden movement of the load cell strain gauges of ΔL_o is also required for tests involving stress paths which cross the isotropic axis. The values of the constants A, B, C and ΔL_o are summarised in table 8.1 for each of the load cells used during the course of this research.

Corrections of this type have been made to all axial strain data for all tests.

8.2.2 Volume Gauge Compliance.

The method of calibration for volume gauge compliance was described in section 6.6.1 and the results of typical calibrations given in Fig 6.7. These curves may be approximated by a single straight line over the range of the calibration. The correction therefore takes the form,

$$\Delta u = D\,\Delta V \qquad 8.3$$

The values of the constant D for the equipment used in these tests are summarised in table 8.1.

These corrections have been applied in all drained tests where the pore pressure has been varied. It should be noted that corrections for the variation of the volume of the drainage leads and of the pore pressure transducer were not found to be necessary for the range of pressures encountered in these tests.

8.2.3 Corrections for the stiffness of membrane and side drains.

As the soil sample deforms under the applied loads the membrane and side drains also deform and so as a result will carry some part of the applied loadings. Corrections required to the axial and radial pressures may be computed from approximate formulae given by Bishop and Henkel (1962) of from more exact formulae as given by Richardson (1986). For the filter paper side drains of the strip type described by Bishop and Henkel (1962) the correction is only required to the axial stress and is given by,

$$\Delta\sigma_{a\,fp} = -FE_{fp}\varepsilon_{fp}\frac{((D_s \pm t_d)^2 - D_s^2)}{D_s^2} \qquad 8.4$$

where $D_s = D_o \dfrac{1-\varepsilon_v}{1-\varepsilon_a}$ the current sample diameter,

$t_d = t_o(1-\varepsilon_a)$

D_o = Initial sample diameter,

t_o = Initial filter paper thickness,

E_{fp} = Stiffness of filter paper,

F = Proportion of sample surface covered by filter paper,

ε_{fp} = Axial strain in filter paper,

ε_a = Axial strain of sample,

ε_v = Volumetric strain of sample.

In the case of the membrane, corrections are required to both the axial and radial pressures. These corrections are given by:

$$\Delta\sigma_{am} = \frac{-A_m E_m}{A_s (1 - \nu_m^2)} (\varepsilon_{am} + \nu_m \varepsilon_{rm}) \qquad 8.5$$

$$\Delta\sigma_{rm} = \frac{-2E_m t_m}{D_m (1 - \nu_m^2)} (\varepsilon_{rm} + \nu_m \varepsilon_{am}) \qquad 8.6$$

$$A_s = A_o \frac{(1 - \varepsilon_v)}{(1 - \varepsilon_a)} \quad , \quad D_s = D_o \frac{1 - \varepsilon_v}{1 - \varepsilon_a}$$

$$\varepsilon_r = 1 - \frac{1 - \varepsilon_v}{1 - \varepsilon_a} \quad , \quad D_m = D_s + t_m$$

$$A_m = \frac{\pi}{4} ((D_s + 2t_m)^2 - D_s^2)$$

$$t_m = t_{om} (1 + \varepsilon_a + \varepsilon_r)$$

A_o = Initial sample diameter ($\pi D_o^2/4$),
t_m = membrane thickness,
t_{om} = initial membrane thickness,
ε_r = radial strain of sample.

If the sample is surrounded by both membrane and filter papers then the sample diameter used in the membrane correction calculations must be increased to $D_{sfp} = D_s + 2t_d$ where t_d is the current thickness of the filter paper side drains as given before.

In both sets of formulae a distinction is made between the strains observed in the sample and those in the membrane and filter paper side drains. At some point the membrane and side drains may start to buckle and so no further load may be carried beyond some maximum value of strain. The point at which this buckling starts to occur cannot be determined accurately and so corrections for these factors have not been applied to any of the data. As a result it is estimated that there may be errors in the values of stresses quoted of up to 5 kPa at the end of consolidation (Richardson, 1986). These corrections would however only have a minor effect on the shape of stress-strain curves and so stiffnesses quoted will be in error by only very small amounts. Only in extension tests to failure would the errors become significant as shown by data from Robinson (1983) and Ng (1986) where tests were compared for samples with and without side drains on the same test path. None of these tests accumulated large strains in extension hence major errors are not anticipated since the corrections are strain level dependent and are independent of stress level. The effect on the failure states in compression will be to cause an overestimate of the stresses q' and p' and an overestimate of the stress ratio q'/p'. Since the errors in q' and p' do not vary greatly with rising consolidation stress level p'_o the effect of q'/p' at failure is greatest for tests conducted at low values of p'. At high consolidation pressures the corrections may have an insignificant effect on q'/p'. In the extension tests to failure for London clay side drains were not used.

8.2.4 Volume Changes of Filter Papers.

Filter papers are used as side drains and also at the ends of samples as filter paper discs. These filter papers will vary in volume as the mean effective stress p' on the sample varies. Details of the volume change characteristics of the filter papers used in these tests are described in appendix 2. The correction required is given by,

$$\Delta\varepsilon_v\,(\%) = 0.15\,\Delta\ln p' \qquad 8.7$$

Since these corrections may be of great importance immediately following a change in direction of loading in an isotropic compression and swelling test, these corrections have been applied to all test data.

8.3 Calculation of Strains.

The strains recorded by Spectra are axial and volumetric strains as defined by equations 5.1 and 5.2. These are ordinary strains as defined by Richardson (1984b), that is they relate the total strain accumulated to the initial sample dimension, L_o. As indicated by Richardson (1984b) the use of such a strain definition may lead to large errors in derived strain quantities e.g. radial or shear strain, when strains become large. In order that results remain consistent natural strains (Nadai, 1931) should be used. A relationship between ordinary strains, ε, and natural strains, ε_n, is given by,

$$\varepsilon_n = -\ln(1-\varepsilon) \qquad 8.8$$

In all the results except where otherwise stated all strains and strain increments quoted are natural strains.

Strain data in this report are presented in terms of the volumetric, ε_v, and the shear strain, ε_s, invariants as appropriate to the triaxial test (defined in section 3.3),

$$\varepsilon_v = \varepsilon_a + 2\varepsilon_r \qquad 8.9$$

$$\varepsilon_s = {}^2/_3(\,\varepsilon_a - \varepsilon_r\,) \qquad 8.10a$$

or $$\varepsilon_s = \varepsilon_a + \varepsilon_v/3 \qquad 8.10b$$

where ε_a is the axial strain and ε_r is the radial strain. All strains quoted are given in units of percent (%).

8.4 Calculation of Stresses.

All data for stresses are quoted in terms of the appropriate stress invariants as defined in section 3.3,

$$q' = \sigma'_a - \sigma'_r \qquad 8.11$$

$$p' = {}^1/_3(\sigma'_a + 2\sigma'_r) \qquad 8.12$$

where σ'_a and σ'_r are the effective axial and radial stresses respectively. These stresses as indicated earlier are corrected only for the current sample area and not for the effect of the stiffness of the membrane and filter paper side drains. All stresses quoted are given in units of kilopascals (kPa).

8.5 Calculation of Specific Volume.

In order to complete the description of the sample state in the critical state model the specific volume of the sample is required. This was defined in section 3.3 as,

$$v = 1 + wG_s \qquad 8.13$$

where w is the sample water content and G_s the specific gravity of the soil particles. In order to compute the specific volume a reliable measure of the sample water content is required at some stage of testing together with a complete record of volumetric strains throughout the test. The specific volume at any stage of the test may then be calculated from,

$$v = v_o\,(1 - \varepsilon_v) \qquad 8.14$$

where v is the current specific volume, v_o the initial specific volume and ε_v the ordinary volumetric strain accumulated since v_o was recorded.

Since the water content of samples is recorded both at the start and at the end of tests the specific volume could be calculated from either. For reasons stated in appendix two it is thought that the recorded water contents at the ends of tests may be more reliable for the purpose of calculating the specific volume of samples. This has been done throughout these tests; however as reported by Robinson (1984) some scatter in results appears to remain. An examination of a typical group of test data (see appendix two) shows that while the slopes of compression and swelling lines remain consistent between a number of tests, the actual position of these lines in specific volume, $\log_e p'$ plots may vary. This causes considerable difficulty when comparing the results of different tests and when normalising results Following Robinson(1984) it has been assumed that a single normal compression line should exist for samples of a given material prepared and tested in a specified manner. Test data must therefore be adjusted so that they fall onto a single unique line. This has been done by assuming that the data is scattered randomly about the true normal compression line. At a chosen value of p' the average specific volume of all tests for the soil was calculated and assumed to be the location of the normal compression line. The initial specific volumes of all the individual tests are then adjusted so as to ensure that the state of each passes

through this point during consolidation. For this work a value of p' = 400kPa was chosen for all tests for the point at which to calculate the mean value of specific volume.

8.6 Calculation of Stiffness.

Some of the alternative definitions of stiffness were discussed in section 2.3.7. All tangent stiffnesses were calculated using a curve fitting routine in the 'spectran' data analysis program (Woods,1985c). The stiffnesses quoted in the results are tangent stiffnesses and are quoted after a change in stress or stress ratio from the start of the test stage instead of with respect to strains as is normal practice.

The reasons are illustrated by Fig 8.1. If two samples are tested, one subjected to a large rotation of stress path (A), and the other subject to a small deviation of stress path (B), they may fail at similar values of q' but at very different values of strain. If secant moduli were used the two tests would not show any similarity in stiffness as the edge of the threshold zone is approached. However, if tangent moduli are used instead the point at which the threshold range is reached and hence where the stiffnesses of the two samples become similar, σ_t, will be more clearly defined. Furthermore these data must be plotted against stress level for the same reasons since plotting against strains will not show where the two samples start to behave in a similar manner.

Throughout the results all stiffnesses are normalised with respect to vp' where v is the current specific volume and p' the current mean effective stress in order to remain consistent with the critical state model. All stiffnesses quoted have the units of kilopascals (kPa).

8.7 Results.

This section describes the plots of the data for each set of tests performed. Further plots[1] of these basic data together with analysis and discussion of these data are given in Chapter 9.

8.7.1 Compression and Swelling Stages.

All samples followed compression and swelling stages in order to reach the starting point for further tests. In addition a number of samples followed only compression and swelling stages for each soil.

Data are presented in the form of specific volume, $\log_e p'$ plots and shear strain, volumetric strain plots for all isotropic compression tests. The plots of specific volume against $\log_e p'$ are shown in Figs 8.2 to 8.6c inclusive while the plots of shear strain against volumetric strain are shown in Figs 8.7 to 8.11c.

For the case of London clay only, other stress histories were followed including compression with stress ratios of 0.25, one dimensional, 0.75, and two dimensional in addition to isotropic loading.

(1) For Footnote see page 182.

A plot of specific volume against $\log_e p'$ for all these tests is shown in Fig 8.12 and shear strain plotted against volumetric strain in Figs 8.13 to 8.16. In addition the stress paths followed in compression and swelling in q',p' space are shown in Figs 8.17 to 8.19.

8.7.2 Effect of Changes in Direction of Stress Path.

All soils examined such effects along constant p' paths in compression after following stages of isotropic compression and swelling. Data are presented in the form of plots of q' against shear strain and volumetric strain against shear strain. These data are shown in Figs 8.20 to 8.24. For the case of London Clay three other overconsolidation ratios were also examined with overconsolidation ratios of 1.5, 4.0, and 8.0, data from these tests is shown in Figs 8.25 to 8.27.

Also for London Clay other stress histories were examined, these data are shown in Figs 8.28 to 8.30 and for one dimensionally compressed samples at various overconsolidation ratios in Figs 8.31 to 8.34.

For both Ware Till and London Clay further data for such effects on other stress paths are available. These are shown in the form of plots of q' against p' and shear strain against volumetric strain in Figs 8.35, 8.37, and 8.39 and as plots of q' against shear strain and p' against volumetric strain in Figs 8.36, 8.38, and 8.40.

8.7.3 Tests for the Range of Threshold Effects.

For each soil such data are available from the plots described under sections 8.7.1 and 8.7.2. However a special test series on London Clay to examine this factor was conducted. The results of these tests are shown in Fig 8.42 in the form of plots of q' against shear strain and volumetric strain against shear strain.

8.7.4 Tests for Path Dependence.

Three types of tests were conducted to investigate path dependence. These data are presented in the form of plots of q' against p', shear strain against volumetric strain, q' against shear strain, and p' against volumetric strain. For the case of paths all leaving from a common stress point after approaching from different directions these data are shown in Figs 8.43 to 8.81. For paths all leaving a common stress point after following the same stress history, these data are shown in Figs 8.82 to 8.119; and for stress paths all arriving at a common stress point in Figs 8.120 to 8.157.

8.7.5 Tests to Failure.

Tests to failure on samples subjected to threshold tests were conducted on all soils. These data are shown in plots of the following parameters:- q' against shear strain, volumetric strain against shear

strain, q' / p' against shear strain, and specific volume against $\log_e p'$. In addition data are shown normalised in plots of q' / p' against v_λ (equivalent specific volume) where v_λ is given by,

$$v_\lambda = v + \lambda \ln p' \qquad 8.15$$

and q' / p'_e against p' / p'_e where p'_e is the equivalent mean effective stress given by,

$$p'_e = \exp(N - v)/\lambda \qquad 8.16$$

These data are shown in Figs 8.158 to 8.196.

In addition to these tests further tests were conducted on London Clay in order to establish the shape of the state boundary surface and the critical state failure parameters for the London Clay being used. These data are presented as plots of the following:- q' against p' q' against shear strain, volumetric strain against shear strain, q' / p' against shear strain, u against shear strain (undrained tests only), specific volume against $\log_e p'$, q' / p' against v_λ and q' / p'_e against p' / p'_e. These plots are shown in Figs 8.197a to 8.207.

8.7.6 Special Tests.

Three sets of special test series were conducted on London Clay in addition to the above tests. These were tests involving longer than standard periods of rest, tests at the same overconsolidation ratio but at different stress states, and tests to determine the significance of total stress path deviations on threshold effects as opposed to effective stress path deviations.

Data for tests involving different rest periods are shown as q' against shear strain and volumetric strain against shear strain in Fig 8.208. In addition the volumetric strains occurring during the rest periods are shown as volumetric strain plotted against square root of time elapsed in Fig 8.209.

The results of tests conducted at different stress states at an overconsolidation ratio of two are shown as plots of q' against shear strain, volumetric strain against shear strain, and q' / p' against shear strain in Figs 8.210 to 8.212.

Data from tests to examine the significance of total stress paths on threshold effects are shown in plots of q' against p', q' against shear strain, and volumetric strain against shear strain in Figs 8.213 to 8.216.

(1) Footnote to Page 180. Due to the very large number of data points, the results are generally shown as smooth curves with data points ommited for clarity. Data points have been shown for some tests in order to illustrate typical scatter of data (Figs 8.4, 8.9, 8.22, 9.14 and 9.16). The scatter observed lies within the limits discussed in Chapter 6 and given in table 6.2.

CHAPTER 9

DISCUSSION OF EXPERIMENTAL RESULTS.

. Mountain climbing is an epitome of life, and good practice for it. You start at the bottom, the weaklings and the irresolute drop out on the way up, the determined reach the top. Life is like that.

Wainwright,A.(1972). Fellwanderer. Westmorland Gazette.

Chapter 9 DISCUSSION OF EXPERIMENTAL RESULTS.

9.1 Introduction.

This chapter discusses the results presented in Chapter 8. In addition further analyses of these basic results will be presented. The data will be compared to previously published data for soil stiffness and interpreted within the critical state model. Finally some suggestions will be made as to the mathematical modelling of such effects for finite element calculations.

9.2 Specific Volume of Samples and Leakage.

The specific volume of samples was calculated from the final water content of the sample. As a check for leakage the initial sample weight and the final dry weight of the sample were used to calculate the initial specific volume (see appendix 2). The difference in the specific volumes calculated in this manner can be seen in tables 7.6a, 7.6b and 7.6c. In general the implied error in the water content is very small typically lying within a range of $\pm$ 0.4% water content. As shown by data presented in appendix 2 these errors are approximately evenly distributed about a mean of zero and show no tendency to increase with time. This therefore indicates that leakage either through or past the membrane was not significant in these tests. This is contrary to the findings of Ting (1968) who estimated from the rate of leakage that the permeability of rubber membranes was $k = 1.1 \times 10^{-13}$, m/s which would be expected to represent leakage at a rate of $Q = 4.3 \times 10^{-10}$ m^3/day or $\varepsilon_v = 0.05\%$ for a 76mm by 38mm sample with a 100 kPa effective cell pressure. This value of permeability would appear however to include the effects of leakage due to other factors such as past the 'O' rings at the ends of the sample and through fittings and valves. Using a figure of $k = 5 \times 10^{-16}$ m/s quoted by Poulos (1964) the rate of leakage may be calculated as $Q = 2.0 \times 10^{-12} m^3$ / day / kPa of effective cell pressure or $\varepsilon_v = 2.3 \times 10^{-6}$ % / day / kPa. This magnitude is considered negligible. Tests by Evans (1983) and Poulos (1964) are in agreement with the findings in this research when the sides of the platens in contact with the membrane are highly greased.

Since the final water contents recorded appear to be more reliable than the initial water contents (see appendix 2 and section 8.5), the data were initially analysed using these water contents and then adjustments made as described in section 8.5. The calculated initial specific volumes based on this averaging procedure are shown in tables 7.6a, 7.6b and 7.6c. The adjustments made can be seen to be small and generally do not exceed $\pm$ 0.5% water content.

9.3 Compression and Swelling Stages.

9.3.1 Results plotted as Specific Volume $\log_e p'$.

After adjustment of the sample specific volumes it can be seen from Figs 8.2 to 8.6c and Fig 8.12 that all samples of a given soil tested on a given consolidation path fall close to unique

compression and swelling lines. The value of λ, the slope of the normal compression line, is well defined for each soil with slightly higher values tending to be appropriate for tests which started with larger initial specific volumes. Values of N, the intercept of the normal compression line at p' = 1 kPa also lay within a small range. The average values of N and λ are summarised in table 9.1. For the case of London Clay where samples were compressed along paths with different stress ratios, η'_o, it may be noticed that while the value of λ for each is the same, the value of N is not. The maximum value of N_λ^{was} observed for samples isotropically compressed ($\eta'_o = 0$) where a value of $N = 2.675_\lambda^{was}$ observed. The value of N_λ^{was} then found to be less both for sample compressed with $\eta'_o > 0$ and $\eta'_o < 0$. This result was also found by Gens (1983 testing lower Cromer Till, Ting (1968) and Lewin (1970).

The swelling curves for each soil are also found to coincide. Those for different initial consolidation histories for London clay are of the same shape as those for isotropic compression but are displaced due to the different values of N during virgin compression. This was also found by Namy (1970) and Gens (1983). The swelling curves are found to be non-linear in a plot of specific volume against $\log_e p'$ which does not agree with the assumptions of the critical state model where these lines are assumed to be straight and of slope κ. Although the swelling curves form a continuous curve they may be idealised by a pair of straight lines of slope κ_1 close to the start of swelling and κ_o at a later stage. On reloading a stiff response is once more observed initially before the stiffness reduces to that of a normally consolidated sample. Again these stages may be idealised by a pair of swelling lines initially of slope κ_1 and later of κ_o before the normal compression line is reached once more. This is illustrated in Fig 9.1. The formation of a hysteresis loop in this manner indicates that behaviour below the state boundary surface is not entirely elastic. However, while within the range of stresses in which κ_1 applies the sample behaviour would appear to approximate closely to that of non-linear elasticity. Values of κ_o and κ_1 together with the normalised range ($\Delta p'/p'_o$) are given in table 9.2 for each soil. The values of κ normally quoted for soils in literature correspond closely to κ_1. Evidence presented by Parry and Amersinghe (1973) suggests that low values of κ should be favoured since this more closely approximated to elastic behaviour. This corresponds to κ_o as defined here. The low initial value of κ observed here is directly attributable to the stress path threshold effects since it occurs immediately following a reversal of stress path in either direction.

9.3.2 Strain Paths.

Data in Figs 8.7 to 8.11c and 8.13 to 8.16 show plots of shear strain, ε_s, against volumetric strain, ε_v. For isotropic compression and swelling tests it would be anticipated that for isotropic samples there should be zero shear strain during these tests. All tests show some negative shear strains during the early stages of the compression stage. These generally do not exceed -1% and do not continue much after $\varepsilon_v \approx 5\%$. This corresponds to an increase in p' by a factor of 2 to 3 times the initial value of p', ie p'_o, for these soils.There is however considerable scatter in the total shear strain accumulated. Once past this stage where $\varepsilon_v \approx 5\%$ the total shear strain remains

approximately constant indicating that samples are then behaving isotropically. The reason for this departure in the early stages of loading may be due to two factors. Firstly samples initially compressed in tubes will be one-dimensionally consolidated. It will therefore require some period of loading (at least 2 - 3 times the initial p', Balasubramaniam, (1969)), before the sample behaves isotropically. In addition samples are not of uniform water content along their length at the start of testing. At the end of testing samples appear to be almost uniform in water content (see section 7.8), hence the behaviour of samples while the water content distribution becomes more uniform may not be isotropic. This corresponds to the non-linear region in the v , $\log_e p'$ plots for each soil before the virgin compression line is reached. During swelling samples are again observed to accumulate very small negative shear strains initially. This indicates that samples are again not behaving isotropically. This departure is small and is not thought to be significant for the interpretation of these results.

The compression and swelling of London clay samples with different stress ratios show a similar pattern in the results. Initially the samples show a changing strain ratio which slowly approaches a value which remains constant with continued loading. These final strain increment ratios were used to specify the loading path when swelling samples initially compressed with stress ratios of η' = 0.25 and 0.75 . Using the final total strain increment ratios observed during compression Fig 9.2 has been drawn showing the stress increment ratio dq'/dp' plotted against the total strain increment ratio $d\varepsilon_s / d\varepsilon_v$. The data appear to fall on a single unique line which is slightly curved, although it may be taken as approximately linear within a range of stress ratios of $\eta' \approx \pm 0.5$. This corresponds with the findings of Lewin (1970), (1978) testing slate dust.

9.3.3 Stress Paths.

The stress paths during compression and swelling are shown in Figs 8.17 to 8.19 for London Clay samples not compressed with a stress ratio of $\eta'_o = 0$. In all cases as swelling continues the stress ratio approaches zero as an overconsolidation ratio of two is approached. In the case of one-dimensional compression tests, the samples were swelled to overconsolidation ratios of up to eight. These samples crossed the isotropic axis at an overconsolidation ratio of about three, the stress ratio then increasing in the negative q' region. The change in stress ratio during swelling is often illustrated by the ratio of the radial effective stress to the axial effective stress, σ'_r / σ'_a . In the case of one-dimensional compression this ratio is termed the coefficient of earth pressure at rest, K_o . The variation of K_o is shown in Fig 9.3 and the variation of σ'_r / σ'_a for two-dimensional compression and other stress ratios in compression in Fig 9.4. Also shown in Fig 9.3 is the variation of K_o observed by Brooker and Ireland (1965) and Skempton (1961) testing undisturbed London Clay, and Lau (1985) testing reconstituted London clay. These results are similar to those by Lau (1985) but lie below those of both Brooker and Ireland (1965) and Skempton (1961). The tests by Lau (1985) were conducted in the same triaxial cells as these tests. The tests by Brooker and Ireland (1965) were conducted in an instrumented oedometer while the results

from Skempton (1961) are based on the investigation of the failure of an excavation. The values of K_o for the normally consolidated state are close from all sources of data. The variations at other overconsolidation ratios may be due partly to the different apparatus used in each case (in particular the accuracy of control of radial strain) and partly due to the sources of London Clay.

9.3.4 Accuracy of Control.

The accuracy of control during these test stages was affected by both random and systematic errors. The magnitude of the random errors was discussed in Chapter 6. These are concerned with the resolution of the instruments and data logger. Such errors are unlikely to have affected these results to any large degree except at very low stresses since the average of the recorded readings will lie close to the true compression and swelling lines. The systematic errors are of concern and include such factors as, the system flexibility (load cell compressibility) and the compression and swelling of side drains. These factors are not corrected in the main control program SPCTRA and so will affect the accuracy with which a path is followed when strain control is used.

These errors cause a very small error in the value of the calculated area of the sample. This however has a negligible effect on the value calculated for the axial stress. The errors considered here are those where the strain is a controlled parameter e.g. in the one-dimensional compression and swelling tests, where the radial strain is maintained constant. If strains occur from sources other than that of the sample this will represent a control error.

During compression stages only one and two-dimensionally compressed samples followed strain controlled paths. In the case of one-dimensionally compressed samples the maximum total error in the axial strain due to load cell compressibility would be approximately $\delta\varepsilon_a = + 0.2\%$ while that in the volumetric strain due to compression of the side drains would be approximately $\delta\varepsilon_v = + 0.3\%$. These tests were controlled by maintaining the radial strain as constant. Since these errors are compensating when calculating the radial strain, the error in the value of K_0 and in the stress path for normally consolidated material is very small and may be neglected. For two-dimensionally compressed samples the error in the axial strain is approximately $\delta\varepsilon_a = +0.3\%$. Since the two-dimensional compression test is controlled by maintaining the axial strain reading as constant this will cause a reduction in the measured value of η' compared with that for the true stress path. This error is however small, the measured value of being $\eta' = -0.400$ and the estimated true value being $\eta' = -0.408$.

During swelling stages all samples not following isotropic stress paths followed strain controlled paths. For samples initially compressed with a stress ratio of $\eta' = 0.75$ the error in the axial strains at the end of the test stage was approximately $\delta\varepsilon_a = -0.26\%$ while that in the volumetric strain was $\delta\varepsilon_v = - 0.15\%$. These errors produce only negligible deviations of stress path from that intended. For

one-dimensionally compressed and samples compressed with $\eta' = 0.25$ the corresponding errors at an overconsolidation ratio of two are $\delta\varepsilon_a = -0.20\%$, $\delta\varepsilon_v = -0.15\%$ and $\delta\varepsilon_a = 0.12\%$, $\delta\varepsilon_v = -0.15\%$ respectively. Again these errors represent negligible deviations from the intended stress paths. One-dimensionally compressed samples were swelled to a maximum overconsolidation ratio of eight at which point errors due to these factors remain negligible. However at an overconsolidation ratio of approximately three the stress path crosses the isotropic axis. As a result the strain gauges in the load cell move and a further error is introduced. This error is approximately $\delta\varepsilon_a = 0.10\%$ which represents an error of $\delta\varepsilon_r = +0.05\%$. As a result the value of q' is overestimated by approximately 4 kPa causing an underestimate of K_o . A sudden jump is not obvious in the results either in Fig 8.17 (q', p') or Fig 9.3 (K_o , OCR) which suggests that the effect on results was insignificant. In the case of two-dimensionally compressed samples the errors in strains during swelling to an overconsolidation ratio of two were approximately $\delta\varepsilon_a = 0.15\%$, and $\delta\varepsilon_v = -0.15\%$. The error in the axial strain causes the value of q' to be increased during loading by 5 kPa. This however is offset by the error during compression so that at an overconsolidation ratio of two the stress state is approximately correct. The errors caused for a two-dimensionally compressed sample are illustrated diagramatically in Fig 9.5.

In order to improve the accuracy of the strain controlled stage either the system flexibility must be reduced e.g by use of stiffer load cells, or strain measurements must be made locally on the sample by use of a radial strain belt for one-dimensional compression tests and local measurements of axial strain (as used by Jardine et al, 1985).

9.4 Effect of a Change in Direction of Effective Stress Path.

Some evidence for the existence of stress path threshold effects was discussed in section 9.3.1. Samples subjected to isotropic compression and swelling show on reversal of stress path a major increase in stiffness which is reflected by the low initial values of κ (κ_o) recorded. These changes in direction of stress path correspond to a complete reversal of path i.e $\theta = 180^0$. Similar behaviour is observed of samples compressed and swelled with different stress ratios; all give approximately the same values of κ_o and κ_1. These samples were not subjected to complete reversals of stress path in q', p' space but to deviations of path between $\theta = 172^0$ and 155^0 for the stress histories followed here. Since these deviations of path are still very large it may not be surprising that significant differences in the values of were not observed.

The main series of tests for stress path threshold effects followed a large number of deviations of stress path (both positive and negative as defined in Chapter 4) mostly on constant p' paths with q' increasing. Other paths were also followed for London Clay only. On the evidence of the values of κ_o and κ_1 the maximum increase in stiffness caused by stress path effect may be estimated to lie in the range of 10.6 to 5.2, values for each soil are given in table 9.2.

9.4.1 Main Test Series.

The main test series for stress path threshold effects was conducted along common loading paths OA (Fig 4.1) which were constant p' compression paths at p' = 200 kPa with an overconsolidation ratio of two. The basic results of these tests for each soil are shown in Figs 8.20 to 8.24b.

9.4.1.1 Stiffness of Samples.

It can be seen that the stiffness of samples increases as the angle of deviation of stress path increases from $\theta = 0^0$ to $\theta = 180^0$. This increase of stiffness is seen in all samples and is a steady increase of stiffness with increase in deviation of stress path. It should be noted that there is not a sudden increase of stiffness for some samples indicating that there is not a sharp boundary to the threshold region. For each soil the response of a sample to a complete reversal of path is initially an almost rigid stress-strain response. It is noticeable that samples subjected to positive angles of rotation of path appear to have a slightly higher stiffness than those subjected to the same deviation of path but with negative angles of path deviation. Stiffness plots of this data are shown in Figs 9.6, 9.10, 9.14, 9.18 and 9.22 as normalised tangent stiffness $\delta q' / vp'\delta\varepsilon_s$ plotted against $\log_e$ of change in stress ratio $\Delta\eta'$. These plots illustrate the differences between the stress-strain curves more clearly. It can be seen that while there are large differences between stiffnesses initially, these differences reduce with increasing stress ratio so that at a stress ratio of approximately 0.35 all samples have very similar stiffnesses. The data show that even after normalising with respect to the specific volume the samples subjected to positive rotations of stress path remain stiffer than those subjected to negative rotations of path. The reasons for this behaviour are unknown but it forms a consistent pattern through all these test results. It can be observed that with the stiffnesses of all samples converging at higher stress ratios the effect of the change in direction of stress path has been to greatly increase the non-linearity of the stress-strain curves. Those subjected to no deviation of path appear almost linear until the state boundary surface is approached.

The spread and non-linearity of results are well illustrated by plots of normalised stiffness, $\delta q' / vp'\delta\varepsilon_s$ against angle of rotation of stress path, θ for changes in stress ratio $d\eta'$ of 0.05 and 0.40. This is shown in Figs 9.7, 9.11, 9.15, 9.19 and 9.23. At a stress level of $\eta' = 0.05$ there is a large spread in the results with a distinct difference between positive and negative rotations of stress path. However, at a stress level of $\eta' = 0.40$ this difference has greatly reduced and the spread in results from $\theta = 0^0$ to $\theta = 180^0$ reduced. These results are repeatable as can be seen from the data for London Clay (Fig 9.23) where tests were repeated several times on different samples.

The spread of results for each soil type may be compared by a plot of range of stiffness against plasticity index for each soil. The range of stiffness R is defined as,

$$R = \frac{(\delta q' / vp' \delta \varepsilon_s)_{\theta = 180^o}}{(\delta q' / vp' \delta \varepsilon_s)_{\theta = 0^o}} \qquad 9.1$$

This has been done for changes of stress ratio of $d\eta' = 0.05$ and 0.40 and is shown in Fig 9.26. At a stress level of $\eta' = 0.05$ there is a rising trend in the data of increasing range of stiffness with increasing plasticity index. The maximum range observed being 10.14 for London Clay. At a stress level of 0.40 the range of stiffness is greatly reduced so that all samples of any soil behave similarly.

9.4.1.2 The Strain Increment Ratio.

It may also be observed from Figs 8.20 to 8.24c that the strain increment ratio is non-unique for each soil even though all tests were conducted on the same path. If the material was behaving in the idealised elastic manner assumed in the critical state model then all behaviour below the state boundary surface should correspond to non-linear isotropic elasticity. In this case it would be expected that volumetric strains would be zero since p' remains constant during the test stage. Any departure from this may be taken as anisotropic elastic behaviour or elasto-plastic behaviour. As the strain increment ratio is non-unique and the samples have only been subject to isotropic compression and swelling it seems unlikely that the behaviour is anisotropic elastic in character. This is further supported by the conditions applied by Atkinson (1973) to define elastic behaviour. These required that if a linear stress path was applied to a soil sample then a linear strain path should result. Although the stress path applied in each case is linear none of the resulting strain paths are linear. It would therefore appear that a model similar to that described by Mroz et al (1979, 1981) incorporating a kinematic yield surface would best fit these data. The variation of the strain increment ratio $d\varepsilon_v / d\varepsilon_s$ is illustrated by plots of $d\varepsilon_v / d\varepsilon_s$ against $\log_e \eta'$ in Figs 9.8, 9.12, 9.16, 9.20 and 9.24.

It can be seen that beyond a stress ratio of $\eta' = 0.35$ all the strain increment ratios lie within a small range. This is the same value of stress ratio at which the stiffness data converged to reach a single value. By plotting the strain increment ratio $d\varepsilon_v / d\varepsilon_s$ against angle of deviation of stress path θ at a stress ratio of $\eta' = 0.05$ the spread of values of $d\varepsilon_v / d\varepsilon_s$ can be seen. This is shown in Figs 9.9, 9.13, 9.17, 9.21 and 9.25. For all the soils the range of values of $d\varepsilon_v / d\varepsilon_s$ is within a range of approximately ± 1 but is not evenly placed about the line $d\varepsilon_v / d\varepsilon_s = 0$. In all cases the mean of the results lie on the positive side of the $d\varepsilon_v / d\varepsilon_s = 0$ line. The pattern of these results ,as has already been stated, cannot be described by the elastic model or the plastic model with a unique yield surface. There remains the possibility however of a model for elasticity in which the degree of anisotropy is allowed to vary. In such a model the degree of anisotropy is stress induced, depending on its value for the values of η' encountered. Such a model would therefore develop a pattern of $d\varepsilon_v / d\varepsilon_s$ for tests such as these in which values of θ from -90^o through 180^o to $+90^o$

would be associated with negative values of $d\varepsilon_v / d\varepsilon_s$ and values of θ from -90° through 0° to +90° with positive values of $d\varepsilon_v / d\varepsilon_s$ (Graham and Houlsby, 1983). This clearly does not occur here since the maximum values positive and negative of $d\varepsilon_v / d\varepsilon_s$ are not associated with approaches from the highest values of $d\varepsilon_v / d\varepsilon_s$ but are associated with approaches from the lowest values of θ i.e. $\theta = \pm 90^0$.

9.4.1.3 The Stress Path Threshold Effect on Different Stress Paths

For London Clay and Ware Till some data were obtained as to the importance of threshold effects due to changes in direction of stress path. Data for Ware Till are shown in Figs 8.36 and 8.37 and for London Clay in Figs 8.38 to 8.41 inclusive.

The additional data for Ware Till are restricted to three stress paths as shown in Figs 8.36 by a plot of q' against p'. As before the strain paths can be seen to be non-unique and samples subjected to larger deviations of path show greatly increased stiffnesses. This is more clearly seen by plots of q' against ε_s and p' against ε_v shown in Fig 8.37. This demonstrates that such effects apply to both shear and volumetric effects.

More data were obtained for London Clay. A total of five additional paths being examined. During isotropic compression and swelling stages shown in Fig 8.38 four different approach paths were followed. These show the same pattern of increasing stiffness with increasing angle of deviation of stress path and also the non-unique strain increment ratio. It is interesting to note that samples which approach these paths from areas of positive η' show slightly higher stiffnesses than those which approached from areas of negative η', (Fig 8.39).

A more complete set of data is available for London Clay with three different paths all starting from a state of q' = 0, p' = 200 kPa, OCR = 2. The paths examined were constant p', q' reducing and constant q', p' reducing and increasing (isotropic compression and swelling), Fig 8.40. Four stress path rotations for each were followed. Stress-strain plots are shown in Fig 8.41. In general the pattern of results is the same as that already described. For the case of a constant p', q' reducing path an approach of $\theta = -90^0$ shows a higher stiffness than one of $\theta = +90^0$. This indicates that it is not the direction of rotation of path which determines which is the higher stiffness but the region of stress space from which the approach path comes. For constant p' paths with q' both increasing and decreasing, approaches from regions of high p' produces higher stiffnesses than approaches from regions of low p' even if the change in angle of stress path is the same. For paths at constant q' with increasing and decreasing p' there is very little difference in the stiffnesses observed for approaches from regions of either positive or negative q' for the same deviation of stress path. These paths also show a further interesting feature. If behaving isotropically all samples following isotropic stress paths should show no shear strains during loading. The strain increment ratio is

however non-unique as before, indicating that samples are not behaving isotropically when subjected to approach paths from regions of positive or negative stress ratio. This would be in accordance with the predictions of a mathematical model using a kinematic yield surface in stress space.

9.4.2 The Effect of Initial Stress History

Samples of London Clay were compressed with five different initial stress histories before swelling to overconsolidation ratios of two at a mean effective pressure of p' = 200 kPa. The results of these tests are shown in Figs 8.24a to 8.24c, Figs 8.28 to 8.30 and Fig 8.32. The same general pattern of results is observed. Plots of stiffness against $\ln \Delta\eta'$ are shown in Figs 9.22, 9.39, 9.47, 9.59 and 9.63. All these plots show stiffness data converging after a change in stress ratio of approximately 0.30 to 0.35. It should be noted that the stress state at the end of swelling is different for each sample due to the different stress histories followed. The pattern of stiffness plotted against angle of deviation of stress path in Figs 9.23, 9.40, 9.48, 9.60 and 9.64 is similar and shows very little variation in stiffness of samples after a change in stress ratio of 0.40. This implies that the size of the threshold region is independent of the stress ratio with which samples were initially consolidated for a given stress state. The trends of the strain increment ratios may be seen to be very similar for all samples independent of stress history (Figs 9.24, 9.41, 9.49,9.61 and 9.65). This is not what would be anticipated. It would be expected that samples compressed with an initially higher stress ratio should show a larger tendency toward anisotropy with large deviations from the behaviour of isotropic samples. Although there are minor differences these do not appear to be significant. Plots of strain increment ratio against angle of deviation of stress path (Figs 9.25, 9.42, 9.50, 9.62 and 9.66) after a change in stress ratio of $\Delta\eta' = 0.05$ all show similar patterns. The maximum values of $d\varepsilon_v/d\varepsilon_s$ generally being observed for paths subjected to deviations of $\theta = \pm 90^0$ but with the average for all deviations of path lying on the positive side of the $d\varepsilon_v/d\varepsilon_s$ axis. It would have been anticipated that there may have been a trend in the movement of the mean value of $d\varepsilon_v/d\varepsilon_s$ for all paths with the largest values of $d\varepsilon_v/d\varepsilon_s$ being associated with samples compressed initially with the highest stress ratio. Even samples subjected to reversals of stress path ($\theta = 180^0$) which it may have been anticipated would be behaving elastically, do not show significant trends in the values of $d\varepsilon_v/d\varepsilon_s$. In the absence of such trends it is concluded that these samples are not behaving in a strongly anistoropic manner.

The normalised stiffness plotted against stress ratio during initial compression (Figs 9.67a) shows that samples compressed with $\eta'_o = 3/4$ have the highest stiffness initially with a reduction in stiffness for samples subjected to all rotations of stress path initially compressed with $\eta'_o < 3/4$, the lowest values recorded for two dimensionally compressed samples ($\eta'_o = -0.4$). This variation in stiffness is observed to be greatest for samples subjected to no deviation of path, $\theta = 0^0$. It can be seen that at an overconsolidation ratio of two the range of stiffnesses observed is greatest for

isotropically compressed samples but steadily reduces for any others compressed along different paths. This is illustrated in Fig 9.67b by a plot of range, R (Equation 9.1) against initial stress ratio, η'_o .

9.4.3 The Effect of Overconsolidation Ratio

Samples with initially isotropic and one-dimensional stress histories were tested at a selection of overconsolidation ratio, these were 1.5, 2, 4 and 8.

For the isotropically compressed samples the results of these tests are shown in Figs 8.24a to 8.27 inclusive. The results for each overconsolidation ratio follow the usual pattern. A plot of stress ratio q'/p' against ε_s shows how there is a general trend of increasing stiffness with overconsolidation ratio, the maximum stiffnesses in these tests being observed for OCR = 8.0 (Fig 8.35a). The stiffness data for these tests are shown in Figs 9.22, 9.27, 9.31, 9.35 as normalised stiffness plotted against $\log_e \Delta\eta'$. Once again these data converge after a similar change in stress ratio after deviations of stress path i.e. $\Delta\eta' \approx 0.35$. When data are plotted as normalised stiffness against angle of deviation of stress path (Figs 9.23, 9.28, 9.32, 9.36) it is seen that the greatest range of stiffnesses and the highest stiffnesses are observed at overconsolidation ratios of 2 and 8 respectively (Fig 9.68a). These data are of a similar form to that discussed in Chapter 2 for isotropically compressed soils. Gens (1983) testing Lower Cromer Till observed an increase of stiffness (secant) with overconsolidation ratio in both drained and undrained tests in extension and compression which was of a similar magnitude to the increase of stiffness observed here (Fig 2.4). Similar trends of increasing normalised stiffness have been reported for other soils e.g. undisturbed London Clay, Fig 2.6 (Wroth, 1971). Data illustrating the strain increment ratios observed are shown in Figs 9.24, 9.29, 9.33 and 9.37 as strain increment ration against $\log_e \Delta\eta'$ and in Figs 9.25, 9.30, 9.34 and 9.38 as strain increment ratio against deviation of stress path θ . All these data follow the normal patterns already observed and tend to converge at stress ratios of approximately $\eta' = 0.35$. It is noticable however that as the overconsolidation ratio increases the range of values of strain increment ratio $d\varepsilon_v / d\varepsilon_s$ observed at low stress levels increases. These data tend to indicate that the size of the threshold region may be dependent on the value of p' such that if the range of the threshold region was defined as $\Delta\sigma'_{th}$, ($\Delta\sigma' = \sqrt{(\Delta q')^2 + (\Delta p')^2}$) then

$$\Delta\sigma'_{th} / p' = \text{constant} \qquad 9.2$$

The variation of stiffness with overconsolidation ratio is shown in Fig 9.68a as a plot of normalised stiffness against OCR, stiffnesses defined at a given stress level $\Delta\eta' = 0.05$. For the purposes of comparison to other data shown in literature this has also been plotted with the same axes but with tangent stiffnesses taken at a strain level of $\varepsilon_s = 0.02\%$ (Fig 9.68b). These data show similar trends to that in Fig 9.68a but over a reduced range of stiffnesses due to the influence of non-linearity of

stress-strain curves.

Data for one dimensionally compressed samples are shown in a similar manner. Stress-strain curves and strain paths are shown in Figs 8.31 to 8.34. A stress ratio (q'/p') against ε_s plot shows that these data follow a different trend to that of the isotropic data. In this case samples with an overconsolidation ratio of two have the highest stiffness, Fig 8.35b. Stiffness data are shown in Figs 9.43, 9.47, 9.51 and 9.55 as normalised stiffness plotted against change in stress ratio $\Delta\eta'$. It should be noted that the start points for all of these tests lie on a one dimensional swelling line and so each sample has a different starting state in terms of q', p', and q'/p'. All stiffnesses tend to converge after changes in stress ratio of 0.35 but it is noticable that samples at higher overconsolidation ratios do not converge in stiffness so rapidly. This was not observed in the data from isotropically compressed samples and so may indicate a difference in the shape (if not in size) of the threshold region for samples compressed on different stress histories which only becomes significant at high overconsolidation ratios. Data plotted as normalised stiffness against angle of path deviation show that although the stiffnesses generally reach a maximum at an overconsolidation ratio of two the range of stiffness continues to increase with overconsolidation ratio. This is similar to the results of the isotropically compressed samples as shown in Fig 9.70. It is also noticeable that the range of stiffness observed is generally less in the case of one dimensionally compressed samples. This may indicate that stress path threshold effects are less significant for soils compressed initially in this manner. Data illustrating the strain increment ratios observed are shown in Figs 9.44, 9.48, 9.52 and 9.56 as $d\varepsilon_v / d\varepsilon_s$ against $\log_e\Delta\eta'$ and in Figs 9.45, 9.49, 9.53 and 9.57. These diagrams show a maximum range of data for samples with an overconsolidation ratio of two. The data also show a trend towards increasingly positive values of $d\varepsilon_v / d\varepsilon_s$ as the overconsolidation ratio increases. The variation in the stiffness data is illustrated as plots of normalised stiffness against OCR at a specified value of stress level ($\Delta\eta' = 0.05$), Fig 9.69a, and at a specified strain level ($\Delta\varepsilon_s = 0.02\%$), Fig 9.69b. These data show different trends to that of the isotropic test data and the recorded stiffnesses are larger for all overconsolidation ratios. This trend is similar to that observed by Gens (1983) testing Lower Cromer Till where it was also observed that one dimensionally compressed samples were stiffer than isotropically compressed samples. The difference in stiffnesses however for one dimensionally compressed and isotropically compressed samples was much larger in the tests by Gens (1983).

Similar data presented by Jardine et al (1984) for a number of soils show the stiffness of one dimensionally compressed samples. In all cases a peak stiffness was observed at overconsolidations in the range of 1.5 to 2.0 as observed in these data. The values of the stiffnesses observed here for one dimensionally compressed London Clay agree well with those quoted by Jardine et al (1985).

9.5 Tests for the Range of Stress Path Effects

Some evidence for the range of stress path threshold effects has already been discussed. The data

for compression and swelling tests on each soil provide some information on the range of threshold effects. These tests indicate that the range may extend for approximately a change of stress of 25% to 30% of the current mean effective stress p'. This appears to remain the same regardless of the state of the sample, whether swelling from a normally consolidated state or being recompressed from an overconsolidated state.

On constant p' paths stiffnesses of all samples and the observed strain increment ratio, $d\varepsilon_v$ / $d\varepsilon_s$ all become approximately constant regardless of recent stress history after a change in stress ratio of approximately 30 to 35%. Examining these data in a similar manner to the compression and swelling data (Fig 9.71) suggests that the range for the stress path effects may be similar on such paths i .e. $\delta q' = 0.25\, p'$.

Strictly the data from these two types of tests may not be compared directly. The problem is similar to that of ordinary and natural strains. In the constant q' tests the value of p' varies, but in the constant p' tests it does not. This gives rise to a small discrepancy if data are defined in terns of $\Delta\sigma'$ / p' for the range of threshold effects since the value of $\Delta\sigma'$ / p' depends on the value of p' taken. The solution is the use of a natural stress change term as used by Butterfield (1979). For the range of threshold effects on path on which $\alpha = \Delta q' / \Delta p'$, this term is given by;

$$\pi' = \sqrt{(1+\alpha^2)}\,(\log_e (1+\Delta p' / p'_0)) \qquad 9.3$$

For the case of a constant p' test equation 9.3 cannot be used ($\alpha = \infty$), but π' is given by,

$$\pi' = \Delta\eta' \qquad 9.4$$

This parameter has been used throughout for the comparison of these data (table 9.2)

In order to investigate the range more carefully on constant p' paths a series of tests on samples was conducted with varying approach path lengths BA. The path lengths were varied from 200 to 22 kPa. The results are shown in Fig 8.42 in the form of plots of q' against ε_s and ε_s against ε_v . It can be seen that for approach paths of length 200, 145 and 90 kPa there is little difference in the behaviour of samples except that due to random variations between tests. For an approach path length of 45 kPa the sample produced a much stiffer response on path AC and also a different strain path was followed. On the final path, AC was stiffer still and comparable to that of a sample subjected to a complete stress reversal both in stiffness and in strain path response. It would therefore appear from these results that the range of the threshold zone is approximately 45 kPa at p' = 200 kPa, which corresponds to a change in stress state of 22.5% of p'.

9.6 Effect of Rest Periods

In Chapter 2 the effect of rest periods on the stress-strain response of samples was discussed. The evidence suggested that creep during rest periods is responsible for "time threshold effects". Since very long rest periods would be needed to fully investigate this factor only the effect of short rest periods on stress path threshold effects were examined with the object of determining if time and stress path effects are additive or if they are independent so that a maximum increase of stiffness may be observed.

In Fig 8.209 data showing the magnitude of volume strains during the rest period at A are given as a plot of volumetric strain against square root of time. It can be seen that all samples show approximately the same value of t_{100} i.e. the time for dissipation of excess pore pressures from the previous loading stage, of approximately 96 minutes. The magnitude of the volumetric strains observed during this period is however dependent on the stress path followed in order to reach point A (Fig 4.1). During the rest period each sample showed very small volumetric strains accumulating at a rate constant with logarithm of time elapsed. All samples did so at approximately the same rate. Using a creep equation of the form of equation 3.70 i.e.

$$\varepsilon_v = C_\alpha \log_e (\Delta t / t_0) \qquad 9.5$$

all samples give a value for C_α of 0.000665% (with t_0 = 1 min).

Following these rest periods at 'A' the effect on the stress-strain response of a sample following a constant p' stress path was examined for samples subjected to deviations of path of $\theta = 0^0$, $+90^0$ and 180^0. The results are shown as q' plotted against ε_s and ε_s against ε_v in Fig 8.206. In the case of the sample subjected to a deviation of $\theta = +90^0$ rest periods of 3 hours (standard), 48 hours and 11 days were allowed. This produced an increase in stiffness of samples with the duration of rest period. The values of initial stiffness recorded are given in table 9.3. After a period of 11 days the sample stiffness had been almost doubled, the increase in stiffness through the three data points being approximately linear with the logarithm of time elapsed during the rest period. For the samples subjected to path changes of $\theta = 0^0$ and 180^0 periods of rest of only 3 hours and 11 days were examined. Both of these samples show a similar increase in stiffness to that subjected to a deviation of path of $\theta = 90^0$ and a rest period of 11 days i.e. and increase of stiffness due to the 11 day rest period of approximately two times. It would therefore appear that time and stress path effects are additive so as to produce a greater effect on sample stiffness than either acting individually. The data for strain paths for these samples shows that the pattern of strain paths for each sample is unaffected by the rest period except that the magnitude of the strains is reduced for both volumetric and shear strains.

9.7 Effect of a Change in Direction of Total Stress Path

All the test results described in the preceding sections examine the effects of changes in effective stress path. Since the pore pressure remained constant in these tests both the total and effective stress paths were subjected to the same deviation of path. In this series of tests samples were subjected to the same deviation of effective stress path while the total stress path deviation was varied.

The stress paths followed are shown in Fig 8.213 as total stress paths q against p and effective stress paths as q' against p'. Samples were subjected to changes in direction of effective stress path of 0^0 and 180^0 while the total stress path deviation varied by approximately 66^0. Stress-strain plots for these paths are shown in Fig 8.214 as q' against ε_s and ε_s against ε_v . It can be seen that for any deviation of total stress path there is little variation in the stress-strain response of samples. This is also observed in the strain path response where all results lie close to the average from tests previously described having $\theta = 0^0$ and 180^0. This tends to indicate that threshold stress path effects are due solely to changes of effective stress path and not total stress path.

In order to confirm this a further series of tests were conducted in which the total stress path remained the same for three different test paths while the effective stress paths of approach were varied. Values of $\theta = +135^0$, $+90^0$ and $+45^0$ were used (Figs 8.215). The results of these tests shown as q' against ε_s and ε_s against ε_v (Fig 8.216) again show that the effective stress path change θ was of importance and not the total stress path change θ^t . The results of these tests lie close to those given in Fig 8.24 for the same deviations of stress path. These data therefore confirm that it is the effective stress path changes which determine the magnitude of threshold stress path effects.

9.8 Path Dependence

The tests conducted for path dependence fall into three categories. Firstly there are tests in which the samples all leave the point 'A' (Fig 4.1) on different stress paths after having followed different approach paths to point A. Secondly there are those tests in which the samples all leave on different stress paths from point C but after having followed the same approach stress path, AC. Finally there are those paths which all converge on the point A from different directions i.e. on different stress paths.

The object of these tests was to examine the behaviour of samples to determine if behaviour was elastic in character and if so whether a single set of elastic parameters could be derived from the data. It should be noted that throughout these tests strains ε_s and ε_v , were observed to be recoverable at point A, ie where cycles of loading occured the strains accumulated at A remained approximately constant.

9.8.1 Type 1 Tests

Tests of this type depart from point 'A' on different paths after having arrived at 'A' also on different paths. As a result samples may be subjected to different deviations of stress path at 'A' before following these paths. The paths followed are shown diagramatically in Fig 8.43 for all the soils tested and are referred to by letters from A1 to H1.

The strain paths plotted as shear strain, ε_s , against volumetric strain ε_v are shown in Figs 8.44 to 8.48 inclusive. All the strain paths shown in these diagrams can be seen to be non-linear. According to the method proposed by Atkinson (1973) for determining regions of elastic behaviour (see Chapter 2) this implies that behaviour is not of an elastic nature. The only possibility of allowing elastic behaviour would be if it could be shown that either the Poissons ratio for the material had changed or the degree of anisotropy had changed i.e.stress induced anisotropy. The alternative that behaviour is of a plastic nature is also difficult to apply in the usual way with a single unique yield curve and plastic potential. For such a case a unique strain increment ratio would be expected for all stress paths regardless of the stress increment ratio. From an examination of these diagrams this is clearly not the case. This suggests plastic strains developed as a result of a non-unique yield curve. This will be discussed further in section 9.12 when considering mathematical modelling of these results.

It is noticeable that the results of tests on paths A1 and E1 (constant p') and C1 and G1 (constant q') indicate that samples were not behaving in an elastic isotropic manner due to volumetric and shear strains respectively observed on these paths. Although the general pattern of results for each soil can be seen to be very similar some differences may be observed for different soils in the strain paths obtained for the same stress path. This may be seen in a comparison, for example, of path A1 for each soil. Speswhite kaolin, Ware till and Slate dust all show negative volumetric strains on this path while London clay and Cowden till show positive strains. This probably results from the different approach paths followed for each soil. This type of behaviour could be predicted from the results of threshold test stages where it was observed that the strain path was non-unique, depending on the direction of the previous loading path as well as the current loading path direction.

Stress-strain data for these tests are shown in the form of plots of q' against ε_s and p' against ε_v in Figs 8.49 to 8.53. In order to eliminate the effect of changing stress state the stiffnesses should be compared at the start of loading on these test stages. If the samples were behaving in an isotropic elastic manner a unique set of stiffness data would result such that the initial shear and bulk moduli were the same for all paths. It can be seen that this does not occur in any case with the stiffnesses observed generally being higher for compression states (q' > 0) and higher values of p' . Efforts were also made to fit anisotropic elastic parameters to data at point 'A'.These however proved unsuccessful due to very large variations in the derived values depending on which paths were selected for the calculations. It was therefore decided that this form of model was unsuitable for examining these results.

The stress-strain data are clearly dependent on the deviation of path occuring at 'A' e.g. path A1 for London clay (Figs 8.48 and 8.53). Test 5117/16 was subjected to a reversal of path ($\theta = 180^0$) while all the other tests were subject to changes of path of $\theta = +90^0$. As a result it can be seen that the strains observed were of different magnitude and the strain increment ratio was also different.

Results of tests conducted on samples at overconsolidation ratios of two at p' = 100 and 300 kPa (stress paths Fig 8.77, strain paths Fig 8.78 and 8.79, and stress-strain curves Figs 8.80 and 8.81) are similar to those obtained for samples at p' = 200 kPa. These results show slightly smaller deviations fron isotropy which may be accounted for by the fact that all these paths were subject to deviations of path of $\theta = 0^0$ in both cases.

Tests conducted on samples with different intial stress histories are shown in Fig 8.61. The strain path data are shown in Figs 8.62 to 8.64 and 8.70 and the stress-strain data in Figs 8.65 to 8.66 and 8.74. It is notable that the strain path patterns do not differ markedly from those of the isotropic samples which may indicate that the strain increment ratio on a given path is more sensitive to the previous loading path direction than the stress history during consolidation. As a result the combination of the anisotropy of the sample and certain loading path approach directions may mask the true anisotropic stress-strain response of these samples.

Tests were conducted on samples at other overconsolidation ratios for the case of isotropically and one dimensionally compressed samples. For the tests on isotropically compressed samples stress path data are given in Fig 8.54, strain path data in Figs 8.48 and 8.55 to 8.57, and stress-strain data in Figs 8.53 and 8.58 to 8.60. The general pattern of results is identical to that described above with certain trends observable. The strain paths show an increasing departure from isotropy as the overconsolidation ratio increases. In particular the sample with an overconsolidation ratio of eight (Figs 8.57 and 8.60) shows strain paths totally different to those predicted from isotropic elastic theory. For path A1 (stage 3) this departure may be due to the direction of the approach stress path, $\theta = +90^0$. For path E1 however this is not the case since this sample had been subjected to no deviation of stress path $\theta = 0^0$. This may suggest that the shape of the threshold region is distorted at high overconsolidation ratios as observed by Hight et al (1985) at low overconsolidation ratios. The stress-strain data show similar trends to that of the stress path threshold data. Stiffness is seen to increase with overconsolidation ratio with maximum normalised stiffnesses occuring for samples with an overconsolidation ratio of eight. The results of tests on one dimensionally compressed samples at various overconsolidation ratios are shown in Fig 8.68 as stress paths, Figs 8.69 to 8.72 for strain paths and the stress-strain data in Figs 8.73 to 8.76. These data show similar patterns to those of the isotropic data. With increasing overconsolidation ratio the strain increment ratio on paths A1 and E1 shows an increasing tendency towards anisotropic behaviour from almost isotropic at an overconsolidation ratio of 1.5 to highly anisotropic at an overconsolidation ratio of 8. It is thought that the results from test 5137 (overconsolidation ratio = 8) reflect the true degree of anisotropy since stage 7 follows a deviation of path of $\theta = 0^0$ and stage 11 follows a deviation of $\theta = 180^0$, this was not the case with the data from isotropically compressed samples. The effect of threshold effects on the

strain increment ratio will in this case have been minimised.

In conclusion the results of these tests indicate that this type of test is unsuitable for the investigation of the stiffness and stress-strain behaviour of soils. Not only are the effects of following different stress paths observed but also the effect of varying deviations of stress path before following the present path have an effect on the results.

9.8.2 Type 2 Tests

These tests are similar to those of Type 1 in that samples depart from a given point, C in this case, on different stress paths. All samples however follow a common approach path to reach point C, as a result all samples are subject to different deviations of stress path. The paths followed are shown diagramatically in Fig 8.82 for all the soils tested and are referred to by letters A2 to P2.

The strain paths plotted as ε_s against ε_v are shown in Figs 8.83 to 8.87a inclusive. Again these paths are highly non-linear indicating similar behaviour to that observed in section 9.8.1 i.e. inelastic if the degree of anisotropy is constant or plastic with a non-unique yield surface. However those paths subject to reversals of stress path ($\theta = 180^0$) are close to linearity, although the strains are very small, which may indicate regions of elastic behaviour. All the soils show very similar patterns of behaviour.This may be due to each soil having been subject to the same deviations of path for any given stress path. For paths A2, I2 (both constant p'), E2, M2 (constant q') deviations of strain paths from elastic isotropy are obvious due to the accumulations of volumetric and shear strains respectively.

Stress-strain data for these tests are shown in the form of plots of q' against ε_s and p' against ε_v in Figs 8.88 to 8.92a. As with the type 1 tests this data should be compared at the start of stress paths in order to eliminate the effects of varying stress state. From these diagrams it can be seen that these soils do not behave in an isotropic elastic manner due to the variation of the stiffness of samples at C. In general the pattern of results shows that tests conducted with increasing p' show higher stiffnesses while those following paths of increasing q' give lower stiffnesses than those with reducing q'. This is illustrated by Fig 8.87a for London Clay where it can be seen that the strain path data although of essentially the same shape in each quadrant is much different in magnitude. Again efforts were made to derive a unique set of stress-strain parameters for these tests. This was not possible, very large variations in all the parameters being required according to which data was used to derive these parameters. This was therefore interpreted as being an indication of the selection of the wrong form of mathematical model rather than any inconsistency in the results. The consistency of the results are proven by those for London Clay where several paths were repeated many times. The reason for this lack of correspondence is thought to be due to the different deviations of stress path to which each sample has been subject so that again some samples may be within a threshold zone while others would be outside.

Similar results are recorded for London Clay on 3 test paths all starting from a stress state of q' = -90

kPa, p' = 200 kPa, OCR = 2 in Figs 8.87b and 8.92b. These tests give lower stiffnesses than on comparable paths from the main body of data which is consistent with the findings above ie stiffness is less for extension states.

Tests conducted at p' = 100 and 300 kPa (both overconsolidation ratio of two) are shown in Fig 8.115 (stress paths, Fig 8.116 and 8.117 (strain paths) and Figs 8.118 and 8.119 (stress-strain plots). These data show an almost identical strain path pattern to other isotropic tests at p' = 200 kPa (OCR = 2) but a variation of stiffness which increases in proportion to the value of p'.

The tests conducted on samples following different stress histories in addition to isotropic tests are shown in Figs 8.100, 8.102, 8.104 and 8.106. The results are shown in Figs 8.100, 8.102, 8.104 and 8.108 for strain paths and Figs 8.101, 8.103, 8.105 and 8.112 for stress-strain data. The strain path data for these tests indicate that the samples do not appear to be behaving in a highly anisotropic manner if compared to the results of tests on isotropic samples (Figs 8.87a and 8.92a) Again it would appear that the deviation of stress paths before the present loading path has had such a significant effect on the strain increment ratio as to hide the true anisotropy of the sample response.

Samples were also tested at different overconsolidation ratios after both isotropic and one dimensional compression histories. For isotropically compressed samples the stress paths followed are shown in Fig 8.93 and the strain paths in Figs 8.87a and 8.94 to 8.96. These tests show an increasing departure from the predictions of isotropic elastic theory as the overconsolidation ratio increases. This is best seen by the response to paths A2 and I2 (constant p' paths) for which increasing large volumetric strains are observed. It can be seen that on path I2 the samples which continued to a stress state of q' = -90kPa, p' = 200kPa show an increase in anisotropy of response on crossing the isotropic axis. Stress- strain data in Figs 8.92a and 8.97 to 8.99 show the path dependance of response of all these tests. The stress paths and the resulting strain paths for the one dimensionally compressed samples are shown in Figs 8.106 and 8.107 to 8.110 respectively. The stress-strain data is shown in Figs 8.111 to 8.114. These data show the same trends as those described above. Samples of high overconsolidation ratio show a greater tendency towards anisotropy and the stress strain response is observed to be both path dependent and dependent on the recent stress history. In general however, the one dimensionally compressed samples show a higher stiffness than the isotropically compressed samples for all paths and the tendency to a greater degreee of anisotropy particularly at high overconsolidation ratios.

It may be concluded that although the use of a common approach path produces a consistent pattern of data these types of test are again unsuitable for examining the stresss strain behaviour of soils. Each sample was subjected to different deviations of stress path and so when comparing data for stiffness some may lie within a threshold zone while others do not.

9.8.3 Type 3 Tests.

In the final series of tests for path dependence samples were all brought to a common stress point 'A'

along different stress paths. Effectively therefore by the time each sample reaches 'A' (provided BA is of sufficient length) all samples will have states lying outside a threshold zone and so effectively arrive at 'A' having been subject to changes in direction of stress path of $\theta = 0^0$. These tests should as a result provide data which are independent of the influence of stress path threshold effects. Data from this test series should therefore be compared at the end of the test stage not at the start as with type 1 and 2 tests. The stress paths plotted as q' against p' are shown in Fig 8.120 for all the soils tested and are refered to by letters from A3 to P3 as shown.

Strain paths are plotted as shear strain, ε_s, against volumetric strain, ε_v , in Figs 8.121 to 8.125b inclusive for each soil. Although some paths remain highly non-linear (e.g. path O3 for kaolin Fig 8.121) the paths generally show a much closer approximation to linearity as required for elastic behaviour. These diagrams all appear to be spread along the volumetric strain axis which tends to indicate a much higher shear stiffness than bulk stiffness. This may be explained by considering the paths followed before the present paths under consideration. Before following paths on which potentially large shear strains may develop i.e. paths A3, I3 and those close to them, samples had been subjected to large deviations of stress path at 'B'. Therefore stiffnesses were initially very high on these paths and so reduced the overall magnitude of strains accumulated along the whole path length.

Stress strain data for these tests are given in Figs 8.126 to 8.130b inclusive. The effect of stress state on the stiffness of samples can be seen once again. Paths approaching from regions of higher p' generally show higher stiffnesses than those approaching from lower values of p'. Also samples approaching from the compression side of the isotropic axis ($q' > 0$, $\eta' > 0$) were stiffer than those approaching from below the isotropic axis from extension states. This may be seen for example by a comparison of test paths C3, G3, K3 and O3 for kaolin (Fig 8.126). Path C3 results in the highest stiffness at A since this lies in a quadrant in which p' is higher than that at A and also q' is > 0. Tests conducted on samples of different p' (Fig 8.153, stress paths; Figs 8.154 and 8.155, strain paths; and Figs 8.156 and 8.157, stress-strain data) show similar patterns of results. The stiffness of the samples increases with p' but the overall magnitude of strains and strain increment ratios changes little as a result. Despite the improved linearity of strain paths it does not prove possible to fit a unique set of stiffness data to these results either isotropic or anisotropic. It may therefore be concluded that sample behaviour is influenced by stress induced elastic anistropy or the samples are behaving in an elasto-plastic manner with a non-unique yield surface.

In tests to study the effect of length of approach path (in order to determine the range of threshold effects, section 9.5) the length of path E3 was varied. The behaviour of samples on path E3 at p' = 200 kPa , q' = 0 kPa can be seen to vary. Samples on shorter approach paths are stiffer, ie from p' = 245 and 222 kPa, and also have different strain paths which are closer to those followed during the previous stage of testing. These results do however tend to converge as the paths proceed so that at p' = 200 , q' = 0 kPa the values of $d\varepsilon_v$ / $d\varepsilon_s$ are similar. This is consistent with the results of threshold tests discussed earlier, and results from memory of recent stress history i.e. the change in q' and p' experienced by a sample and how long previously in its loading history. Similar may be

observed on path M3 where sample M3(2) has approached from p' = 25 kPa instead of the standard p' = 110 kPa. As a result M3(2) is less stiff than the average of the results for other tests as shown by M3(1) and has a slightly different value of $d\varepsilon_v / d\varepsilon_s$. The differences at p' = 200, q' = 0 kPa are not so marked however since both samples M3(1) and M3(2) have traversed the entire threshold zone by that stage of the tests.

Data for tests on samples with different initial stress histories is shown as stress and strain paths in Figs 8.138, 8.140, 8.142, 8.144 and 8.146. Stress-strain data is shown in Figs 8.139, 8.141, 8.143 and 8.150. The strain paths show an increasing degree of anisotropy of samples as the value of η'_0 in initial compression increases. Hence the samples in which η'_0 = 0.75 show the largest departures from isotropic behaviour. These conclusions were reached from an examination of constant p' paths (A3 and I3) and constant q' paths (E3 and M3) for each case. Furthermore it is noticeable that samples compressed with higher values of η'_0 during initial compression yield lower values of stiffness on the paths examined. This is in agreement with the findings of the threshold tests described earlier. The observations of these anisotropy effects not seen in the previous two types of path dependence test may be explained by the elimination of the influence of threshold effects on these results since all samples arriving at A have been subjected to the same deviation of stress path i.e. $\theta = 0$.

Tests were conducted on samples of different overconsolidation ratio for samples following both a one dimensional and an isotropic stress history. The results of the tests on isotropically compressed samples are shown in Figs 8.120 and 8.131 (stress paths), Figs 8.125a and 8.132 to 8.134 (strain paths) and Figs 8.130a and 8.135 to 8.137 (stress-strain data). All samples show a similar departure from ideal isotropic elastic behaviour. However there is no tendency for these differences to increase with rising overconsolidation ratio as in the type one or type two tests. The usual pattern of stiffnesses is observed here again. The results for the one dimensionally compressed samples are shown in Fig 8.144 (stress paths), Figs 8.145 to 8.148 (strain paths) and Figs 8.149 to 8.152 (stress-strain data). In this case it is noticible that as the overconsolidation ratio increases the effects of anisotropy also increase. Samples compressed with an overconsolidation ratio of 1.5 show behaviour of very close to that of isotropically compressed samples; however the pattern of strain paths at an overconsolidation of 8.0 is completely different. The change in the pattern reflects the increasing anisotropy of the samples. These effects are observed since all samples approach point A after the same deviation of stress path and so are not subject to the effect of stress path threshold effects.

This type of test also proves unsuitable for the examination of the stress-strain behaviour of soils. Although the behavour of samples is generally elastic in character as shown by the linear strain paths, close analysis of the results shows that it remains impossible to fit a single set of stiffness data (isotropic or anisotropic) to these results.

9.8.4 Discussion of Path Dependence Tests.

A large amount of data has been collected for three different types of test for path dependence. In general it has been observed that in type one tests and type two tests the strains occuring do not appear to be elastic in character since the strain paths observed while folllowing linear stress paths are highly non-linear. Such behaviour could only be acceptable within the elastic model if the degree of anisotropy of a given sample was allowed to vary. While it is possible that stress induced anisotropy could affect the results, the changes required in 'n' (see chapter 3 for definition) are very large if a single set of soil data is to be obtained. It is notable that stress induced anisotropy was not a significant factor in the results of stress path threshold tests; it is therefore thought that it is not responsible for the departures from elastic behaviour observed here. Furthermore samples initially compressed with high stress ratios which would be expected to show a high degree of anisotropy do not neccesarily do so. This would appear to be due to such effects being masked by changes in strain increment ratios due to threshold effects. Both of these types of test prove unsuitable mainly due to the different deviations of path to which each sample is subjected at points A and C.

Although type three tests are generally observed to produce linear strain paths, as required for elasticity, the data again do not prove to be elastic in character. A single set of stiffness data cannot be fitted to these results. This type of test does prove more successful at demonstrating the degree of anisotropy of samples since this is not concealed by stress path threshold effects.

None of these types of test produced results which were truly elastic in character despite accumilated strains at point A remaining approximately constant. This indicates that hysteresis loops formed which is further evidence of inelastic behaviour. In addtion it was observed that these data could not be reproduced by an elasto-plastic model using a single yield surface. It was observed in Chapters 2 and 3 that the range of true elastic behaviour may be restricted to regions of stress space immediately following a reversal of stress path. It may therefore not be surprising that the above test types do not yield exclusively elastic behaviour. In order to examine the elastic behaviour of soils the following test procedure is recommended. All samples should initially follow the same consolidation history. Each sample should then be loaded to reach points B at some distance from A as in Fig 4.1. The samples then follow a path from B to A and then from A to B. The paths AB may then be compared in order to examine the elastic behaviour of the soil at point A. By following this procedure all samples are subject to a reversal of stress path ($\theta = 180^{0}$) at A and so all are equally affected by stress path threshold effects. Immediately after the point A behaviour will be exclusively elastic (if any such range exists), and so a single set of stiffness data should fit the results.

9.9 Tests to Failure

With the exception of samples used solely for compression and swelling tests all samples were brought to failure. All samples for threshold tests and path dependence tests followed constant p' paths stress controlled to failure. In addition to these for London clay only a series of tests were conducted on a number of test paths in order to establish the shape of the state boundary surface.

9.9.1 Threshold Tests to Failure

All samples used to perform threshold tests were brought to failure stress controlled on constant p' loading paths. As a result these tests do not in general give values of q' at critical state, instead peak values are given. Throughout this section when discussing failure states reference is being made to peak failure states not critical states unless otherwise stated.

9.9.1.1 Tests on Various Soils

The stress-strain data for these tests are given in the form of plots of q' against ε_s, q' / p' against ε_s and ε_v against ε_s in Figs 8.158, 8.162, 8.166, 8.170 and 8.174. These data show that the failure deviator stress q' appears to be unaffected by the angle of deviation of stress path before the loading to failure. For each soil values of failure q' lie within a small range which does not show any significant change due to deviation of path. The values of failure strain ε_s do however show a trend of increasing failure strain as the angle of deviation of stress path reduces. These data are summarised in table 9.4. The strain paths ε_v against ε_s also reflect the effect of recent stress history. Initially they follow trends similar to those described earlier in section 9.4 for the behaviour of samples after small changes of stress. In the latter stages of loading the convergence of strain paths continues so that at failure not only do all samples follow strain paths with similar strain increment ratios but also the magnitude of volumetric strains close to failure is similar. However it may be noted that although the rate of change of volumetric straining is reducing as failure approaches it does not reach zero as expected at the critical state. The convergence of strain paths may be seen in the data shown in Figs 9.8, 9.12, 9.16, 9.20 and 9.24. The specific volume of samples at failure is illustrated by plots of specific volume, v, against log p', Figs 8.159, 8.163, 8.167, 8.171 and 8.178. It can be seen that the variation of specific volume at failure for all soils is small; these values are summarised in table 9.4.

The data are also shown in normalised plots as stress ratio, q' /p' against v_λ equivalent specific volume, Figs 8.160, 8.164 8.168, 8.172 and 8.179, and as q' / p'_e against p' / p'_e , Figs 8.161, 8.165, 8.169, 8.173 and 8.180. Also shown on these diagrams are data previously established by various workers for the shape of the state boundary surface for each soil. It can be seen that the present results lie close to these surfaces at failure indicating close agreement with these results. The sources of the data for the shape of the state boundary surfaces are given on the appropriate diagrams. Contours of ε_s are shown for $\theta = +90^0$ and compare well with those for drained and undrained tests established by the sources noted on the figures. The value of $\theta = 90^0$ was selected for contour plotting since it lies close to the values of θ experienced by samples following drained and undrained paths at constant cell pressure. In general the position of these contours is non-unique being dependent on the value of θ experienced before loading to failure. It can be seen that there is little difference between the normalised results for any deviation of path either at the start of loading or at failure.

In conclusion the data for the failure states of samples show little effect due to stress path threshold effects. The effect of time effects on such data was not investigated, however due to the changes

on specific volume during the period of rest it may be anticipated that some change in the failure state may occur. Although not shown in these results, the shear strain contours shown on plots of q'_e/p'_e against p'_e/p'_e e.g. by Loudon (1967), will not be unique due to the different stiffnesses observed for different deviations of stress path.

9.9.1.2 Special London Clay Tests

Additional tests were conducted on London Clay in order to investigate the effect of stress level at a given overconsolidation ratio, the effects of initial consolidation history and the effect of overconsolidation ratio. The failure data for these tests are given in table 9.5.

Tests were conducted at two different values of p' for an overconsolidation ratio of 2, the values of p' being 100 and 300 kPa. The results are shown as q' plotted against ε_s and ε_v against ε_s in Fig 8.175 and as stress ratio q' /p' against ε_s in Fig 8.177. The results show that all samples failed at approximately the same shear strain although it is difficult to be precise due to the stress control used in these tests. The paths can however be seen to be almost identical when compared in a plot of q' / p' against ε_s . Data for the strain paths (Fig 8.175) also appear to be almost the same for all tests. Again this indicates the normalisation of stiffness data with respect to p' in order to eliminate the effects of p' on samples starting from similar states. It should be noted that the data compared here for these samples was obtained for tests in which the deviation of stress path was the same in all cases (θ = 180°). Data plotted as v against $\log_e p'$ is shown in Fig 8.178. It can been that the failure specific volume for all samples of overconsolidation ratio = 2 lie close to a single line lying parallel to the normal compression line, however for the reason stated earlier the states may not coincide with the critical state line. Normalised plots of data Figs 8.179 and 8.180 show that these samples follow paths close to others of overconsolidation ratio 2 but tested with p' = 200 kPa.

Samples were tested with four different stress histories (all OCR=2.0) in addition to those of an isotropic stress history. The stress-strain data q' against ε_s and q' / p' against ε_s and strain path data ε_s against ε_v are shown in Figs 8.181, 8.184, 8.191 and 8.194. Only one test was conducted for each stress history. The results show a trend towards rising deviatior stress at failure as the consolidation stress ratio rises. This increase is smaller for samples initially compressed with q' / p' > 0 than for those compressed with q' / p' < 0 . The two dimensionally compressed sample shows a very large increase in the maximum q' compared to isotropic samples by approximately 10% or 20 kPa. This increase in failure deviator stress for these samples may be partly accounted for by the lower equilibrium voids ratio associated with each consolidation history for a given value of p'. Since the volume strains accumulated to peak failure in each case are similar this implies that the failure line lies in a different position for each case. This would allow the samples to reach higher values of stress (q') at failure. The large increase in strength of the two dimensionally compressed sample may however also be due to a correction required for membrane and side drain stiffness. The specific volume at failure for each sample is shown in Figs 8.181, 8.184, 8.191 and 8.194. Normalised data for these tests are shown in Figs 8.182, 8.189, 8.192 and 8.195 as q' /p' against v_λ ,

and in Figs 8.183, 8.190, 8.193 and 8.196 as q' / p'_e against $p` / p`_e$. In the plots of q' /p' against v_λ it can be seen that the differences in N for each sample are reflected in the values of v_λ before loading to failure. There is a reduction in v_λ with rising consolidation stress ratio and at the same time an increase in the maximum value of q' / p' attained. The data plotted as q' / p'_e against $p` / p`_e$ shows that all samples start from similar values of p' / p'_e since this is a reflection of the overconsolidation ratio of samples. The peak state however is reached at different values of q' /p'_e. This data indicate that the state boundary surface for each of these samples is different and is dependent for its shape on the initial consolidation history followed. None of these samples are observed to show any large degree of anisotropy. This is in keeping with the earlier findings regarding threshold effects although it should be noted that these samples were not all subjected to the same deviation of stress path. The failure data for these tests is summarised in table 9.5.

For isotropically and one dimensionally compressed samples data were obtained at a total of four overconsolidation ratios for each. The stress-strain data for isotropically compressed samples, q' against ε_s and ε_v against ε_s are shown in Fig 8.176. The data show a tendency towards failure at smaller shear strains as the overconsolidation ratio rises and failure occurs at higher stress ratios (Fig 8.177). All samples were subject to a deviation of stress path of $\theta = 180^o$. The strain paths all start with a similar strain increment ratio direction before diverging so that samples with low overconsolidation ratios show compressive strains at failure while those at higher overconsolidation ratios are swelling close to failure. This is also reflected in the changes of specific volume which are shown in Fig 8.178. The data plotted as q' /p' against v_λ, and q' / p'_e against $p` / p`_e$ are shown in Figs 8.179 and 8.180. These data all lie within the state boundary surface as described before; however only the sample with an overconsolidation ratio of 1.5 reached critical state, all other samples failing at a peak state. Only this sample showed zero volumetric strain increments at failure. Although all of these samples showed departures from isotropy which increase with overconsolidation ratio, these are small and are not apparent in normalised plots of tests data.

The data for one dimensionally compressed samples is shown in Fig 8.185 as q' against ε_s and ε_s against ε_v and in Fig 8.188 as q' /p' against ε_s. These data show a different trend to that of the isotropic data. In this case the strains ε_s to failure increase with overconsolidation ratio instead of reducing. Fig 8.188 shows the reduction of normalised stiffness with overconsolidation ratio. It is noticable that all these samples reach higher stress ratios , q' / p', at a given overconsolidation ratio than isotropic samples at failure. This can be seen from Fig 8.188 and the plot of stress paths during loading to failure in Fig 8.187. Similar trends in data have been observed by Gens (1983) testing Lower Cromer Till, from Cromer, Humberside (Fig 2.11). Also the volumetric strains while initially showing similar behaviour to the isotropic samples differ as the test continues. At failure all samples have swelled from their initial states with those of lowest overconsolidation ratio (1.5) swelling the least. This is reflected in the specific volume against $\log_e p'$ plot shown in Fig 8.186. This implies that the true critical state line for one dimensionally compressed samples lies "above" all the states used here in a plot of v against $\log_e p'$ so that even the sample with an overconsolidation ratio of 1.5 may not have reached critical state. The normalised plots tend to confirm that none of the samples reached

critical state (Figs 8.189 and 8.190). All sample states rise to meet a unique line where they fail abruptly without moving to a unique critical state point. The swelling of samples towards failure is reflected by these normalised paths leaning to the right in both plots of q' /p' against v_λ ,and q' / p'$_e$ against p`/ p`$_e$. Shear strain contours are shown on the plot of q' / p'$_e$ against p`/ p`$_e$. These have been derived from the failure data which is only for samples with deviations of path $\theta = 180^o$. Although a similar pattern of countours may be expected for other deviations of path they will lie in a different position on the diagram, illustrating the non-uniqueness of these contours.

It is interesting to compare data from plots of stress ratio against v_λ for each stress history. By superimposing the data from each set of tests it is seen that a plot of data is derived which is nearly unique (Fig 9.72). While this may be fortuitous it does at least suggest that such a section taken through the state boundary surface may be of similar shape regardless of the consolidation history followed. This would appear to be worth investigating further with a series of tests on normally consolidated samples each having followed different stress histories. No such uniqueness is observed in the plots of q' / p'$_e$ against p`/ p`$_e$ where the values of N appropriate to each consolidation history have been used. However if the value of N appropriate for isotropic compression and swelling is used in all calculations of p'$_e$ a different picture emerges. The surface formed by the isotropic data then appears to form a limiting envelope which bounds the data from all tests (Fig 9.73). Samples consolidated with different histories fall on the surface so that they appear to have higher overconsolidation ratios than those isotropically compressed nominally to the same overconsolidation ratio. All the overconsolidated samples now lie on a unique surface. These data do not indicate however if the same extension could be applied to normally consolidated data. Gens (1983) also found similar results for Lower Cromer Till and suggested that the isotropic surface was a surface bounding all possible states with the exception of some deviations for normally compressed samples.

It may also be noted that the normalised stress path followed during swelling in the q' /p' against v_λ plots is approximately linear over the range of changing stress examined in these tests (Figs 8.182, 8.189, 8.192 and 8.195). Using this information it is therefore possible with the knowledge of v_λ appropriate to a given overconsolidation ratio to predict the current value of stress ratio and hence for one dimensionally compressed samples the value of K_o ($K_o = \sigma'_3 / \sigma'_1$) see Fig 8.189. While this relationship would appear to hold for low values of overconsoliation ratio (up to 8) further tests would be required to establish the limits of its application. The form that this equation takes is,

$$\eta' = \left(\frac{\eta'_{nc}}{N - v_{\lambda o}}\right)(v_\lambda - v_{\lambda o}) \qquad 9.6$$

Where $v_{\lambda o} = N - (\lambda - \kappa)\log_e R_{po}$ and R_{po} is the overconsolidation ratio at which $\eta' = 0$ i.e. where the isotropic axis is crossed. The values of K_o predicted from this equation are shown in Fig 9.3. It can be seen that the agreement is good within the range of the test results.

9.9.2 Tests to Establish the State Boundary Surface for London Clay

For all the soils, except the London Clay tested here, data was already available for the shape of the state boundary surface. Therefore a series of tests was conducted with the object of establishing the shape of the surface for isotropically compressed samples in both normally and overconsolidated states. The stress paths followed were restricted to drained and undrained compression test paths with constant cell pressure. The failure data for all these tests is given in table 9.6.

The stress paths followed are shown as q' against p' in Figs 8.197a, b and c and the stress state at failure in Fig 8.197d. Using the data in Fig 8.197d the critical state line has been established using data only from normally consolidated samples. It can be seen that all the data for normally consolidated samples, Fig 8.197a (drained tests) and 8.197b (undrained tests), falls close to this critical state line. The data for overconsolidated samples (Fig 8.197c do not, with the deviation from the critical state line increasing with overconsolidation ratio. This indicates that despite the use of strain control close to failure in order that failure should occur in a controlled manner, critical state was not attained by samples with an overconsolidation ratio in excess of approximately 5.

Stress-strain data for drained normally consolidated tests are shown in Fig 8.198. All samples show similar patterns of stress-strain response with failure occuring at strains of 18% - 25%. It is noticable that tests conducted at higher pressures tend to fail at higher strains than those at lower pressures. This suggests that normalisation of data with respect to vp' rather than p' may be appropriate. This is one of the predictions from the critical state model. The volumetric strains accumulated for each sample are similar with the rate of accumulation of strain tending to zero as failure is approached indicating that sample states are close to critical states. Data for these tests have been normalised in Figs 8.201a and b with respect to p' as q' /p' against ε_s and with respect to vp' as q' /p' against $v\varepsilon_s$. Although there is some scatter in the data in Fig 8.201a there is little improvement by normalising with respect to vp' in Fig 8.201b. This data was therefore inconclusive as to the correct normalising parameter. This is probably due to the relatively small difference in specific volume between these tests.

Stress-strain data for undrained tests in the form of plots of q' and u against ε_s are given in Figs 8.199a and b for normally and overconsolidated samples respectively. The data for undrained normally consolidated samples was of a similar form to those for the drained samples. Failure occurs at strains in the range of ε_s = 12% - 15%, again with samples compressed to low stress levels (and high specific volume) failing at lower strains than those compressed to higher stress levels. It can be seen that as failure is approached the pore pressure tends towards a constant value as may be expected at critical state. These data normalised with respect to p' are shown in Fig 8.202a. A similar spread of results can be seen as was observed in the drained test data in Fig 8.201a. Normalising data in a plot of q' /p' against $v\varepsilon_s$ in Fig 8.202b produces a slight improvement in the agreement of normally consolidated data; however the difference is small and may not be significant. The data for both drained and undrained tests for normally consolidated states in both Figs 8.201a and 8.202a show a trend towards higher failure stress ratio as the value of consolidation pressure reduces. This may

be partly accounted for by the influence of the membrane and side drain stiffness. Since the magnitude of the correction at failure remains approximately constant the influence on the value of q'/p' increases with falling p'_o .

Data for overconsolidated undrained tests show a reduction in strains to failure as the overconsolidation ratio rises (Fig 8.199b). In addition samples show a tendency towards dilation after an initial rise in pore pressure for samples with overconsolidation ratios in excess of 2. Again all samples show a tendency towards constant pore pressure as failure is approached tending to suggest that all samples reach critical state. However when the results are plotted as q'/p' against ε_s Fig 8.202a it is observed that despite the constant values of q' and u samples have not reached critical state since the stress ratio continues to change falling with increasing shear strain towards critical state. Only samples with overconsolidation ratios of up to 2 definitely reach critical state. The departure from the critical state value of stress ratio at the end of the test increases with rising overconsolidation ratio.

In the case of an overconsolidation ratio of 5 samples were tested undrained immediately following recompression and swelling stages. In all other cases tests were only conducted following swelling stages. The results indicate that the sample which was recompressed (6216) behaved in a manner as if of a lower overconsolidation ratio than the sample which was swelled. The deviator stress at failure is lower and the failure water content is higher as would be expected. The data shows that in the normalised plots the recompressed sample lies with a state to the right of the sample which had been swelled. All of these differences may be accounted for by the difference in water content of these two samples due to the cycle of swelling and recompression. This indicates that great care is required when testing the samples and comparing data to ensure that only samples with similar recent stress histories are directly compared.

Data was obtained in extension for normally consolidated states only with one drained and undrained test to failure both with constant cell pressure. The stress paths (Figs 8.197a and b) both appear to reach similar stress ratios at failure (Fig 8.197d). The value of M_e is however less than M_c but is such that $\phi'_c = \phi'_e$ indicating that a Mohr Coulomb failure criterion is appropriate rather than an extended Von Mises. Stress strain data are shown as q' against ε_s and u against ε_s (Fig 8.200). These data show that samples tested in extension were of a lower stiffness than samples tested at similar states in similar tests in compression. The strain path is shown as a plot of ε_v against ε_s (Fig 8.200) for the drained test. Both the pore pressure ,u, and the volumetric strain, ε_v, become approximately constant close to failure indicating that critical state had been reached. This is further confirmed by the plot of stress ratio q'/p' against ε_s which reaches a constant value of q'/p' at failure. It is notable that failure occurs at shear strains, ε_s, in excess of 20% which is much greater than for similar tests in compression. Data plotted in terms of v against $\log_e p'$ (Fig 8.203) fall close to the critical state line establised for compression samples

With the data plotted as v against $\log_e p'$ it can be seen that a unique critical state line may be defined from data from compression tests on samples starting from states wet of critical. Tests starting from

the dry side of critical all fail to reach the critical state line defined in this manner by an amount which increases with rising overconsolidation ratio. This failure of samples to reach a critical state when heavily overconsolidated has been discussed by Atkinson and Richardson (1986). They concluded that these samples which often develop slip planes may be affected by local drainage close to these slip planes. As the sample starts to develop a slip plane water from the immediately surrounding soil is drawn into the plane (Fig 9.74a) and so causes a reduction in the maximum value of q' and hence also p' observed at failure (from F to T, Fig 9.74d) . On measuring the sample water content after testing this difference in water content may not be observed since it is restricted to only very thin zones in the sample. The average water content of the whole sample will however remain unchanged. The difference between the measured average water content and that measured on the slip plane represents the error in the data in a plot of v against $\log_e p'$ (Fig 9.74a) . The true path followed by the zone in which failure occurs is likely to be in the form shown in Figs 9.74 as ARPT. Data from tests on heavily overconsolidated samples for specific volume may not therefore be reliable regarding failure states.

Finally this data is shown in the form of normalised plots q' / p' against v_λ and q' / p'_e against p' / p'_e , Figs 8.204 and 8.205 respectively. Data with an overconsolidation ratio of 2 or less (except for constant p' tests) can be seen to reach a critical state with the parameters already derived from plots of data as q' against p' and v against $\log_e p'$. These results fall close to a unique line with only small differences between the average normalised paths for drained and undrained samples. The data at higher overconsolidation ratios progressively fall short of the critical state as the overconsolidation ratio rises. However all data at high overconsolidation ratios do appear to fall close to unique lines representing the state boundary surface despite the comments above regarding the possible unreliability of this data. Data from undrained tests, if the sample is behaving in an isotropic elastic manner, should rise vertically to reach the state boundary surface. It can be seen that as the overconsolidation ratio increases the departures from isotropy also increase until at an overconsolidation ratio of 40 the behaviour of samples is highly anisotropic. Also shown on the diagram of q' / p'_e against p' / p'_e are contours of ε_s drawn from the results of the drained and undrained tests only. A unique set of contours results which are of a similar form to those described by Loudon (1967) and Gens (1983). It is observed that the contours appear horizontal on the wet side of critical but tend to converge towards the origin for states dry of critical. As stated earlier these contours are non-unique since they are dependent on the angle of deviation of stress path before following the current loading path. In the case of the data used here all samples were subject to similar deviations of stress path before loading to failure i.e. approximately $\theta = +90^o$ and so a consistent set of contours were obtained.

In Figs 8,206 and 8.207 normalised data for the extension tests are shown. It can be seen that the state boundary surface is not symetrical about either the v_λ or the p'/p'_e axes respectively. For extension the value of Γ is found to be slightly less than in compression ie $\Gamma_c > \Gamma_e$. The lower stiffness of extension samples is clearly seen in Fig 8.207 by the higher strains reached at low values of q'/p' compared to compression samples. It is also notable that the normalised undrained stress path lies "inside" that of the normalised drained stress path which may indicate differences in the

shape of the yield curves for such samples. Both sets of data , compression and extension, in Figs 8.204 and 8.206 plotted as q'/p' against v_λ are non-linear. This does not therefore conform to the shape of the state boundary surface predicted from the cam clay model which requires a single unique linear line to result from such a plot. In addition the differences in M and p'/p'_e at failure do not correspond to the prediction of Cam clay which requires these parameters to be equal in extension and compression. This feature is however common to many soils (eg Speswhite kaolin, Robinson;1984).

9.10 Normalising of Test Results

In order to compare data from different types of test and on different stress paths the data must be normalised in order to isolate only those factors which are controlling behaviour. Some of the procedures for normalising test data were discussed in Chapters 2 and 3. In the light of the above results some of the conclusions reached earlier will be reviewed. This section is divided into three sub-sections, firstly the normalising of stiffness data, secondly the normalising of stress-strain curves, and finally the normalising of general test data such as stress paths and stress-strain curves.

9.10.1 The Normalising of Stiffness Data

As discussed in earlier chapters it is often normal practice to normalise stiffness data with respect to the undrained strength, s_u . Some of the disadvantages were discussed and the data described in the previous section illustrated the difficulties in defining the undrained strength. Throughout these results all data had been normalised with respect to vp' in order to be consistent with the critical state model. Often data is only normalised with respect to the term p'. The difference as discussed in Chapter 3 lies in whether linearity is observed in plots which have a linear term plotted against a logarithmic term or a logarithmic term plotted on both axes. An example of this is the plotting of compression and swelling curves. If these are observed to be linear in terms of v against log p' then normalisation with respect to vp' is appropriate. If however linearity is observed in a plot of log v against log p' then normalisation with respect to p' only is appropriate.

In practice unless the volume changes observed are very large there is likely to be little difference between the two methods of plotting data so that either may be appropriate. In following normal practice data were plotted as v against log p' and as has already been stated in earlier sections linear paths were observed hence stiffness data was normalised with respect to vp'.

9.10.2 Normalising of Stress-Strain Curves

General test data referred to here are taken as stress-strain data and stress paths. Stress-strain data is often normalised with respect to the initial value of p' during a test, p'_o. This is only suitable however for the comparison of one type of test data. Comparison of drained and undrained tests for example, using this method will not yield a unique curve even for samples consolidated with the same stress history to the same stress state. Alternatively data may be normalised with respect to the current value of p'. This tends to give a single unique curve for samples on various stress paths as has been

shown by the data in this chapter in Figs 8.201a and 8.202a. It was observed however that the data showed a tendency towards failure at lower values of ε_s for lower initial consolidation pressures on both the types of loading paths investigated. The critical state model in its normal form (Cam clay) suggests the normalisation of stress-strain data in the form of q'/p' against $v\varepsilon_s$. This method of plotting was used in Figs 8.201b and 8.202b. While some improvement may be noted the differences are in fact very small due to the relatively small variation of specific volume over the range of pressures normally used in soil testing. For the purposes of these tests and most testing programmes the use of normalisation by either method may therefore be satisfactory. However for test programmes conducted over very large ranges of pressure further consideration of this factor may be required.

9.10.3 The Normalising of Stress Paths

The normalising of stress paths is often undertaken with the object of investigating the shape of the state boundary surface. Parameters commonly used include the equivalent specific volume v_λ and equivalent mean effective stress p'_e defined in Chapter 8 (equations 8.15 and 8.16) and the pre-consolidation pressure p'_c defined in equation 3.48. In practice the pre-consolidation pressure proves more difficult to define from test data than the other parameters. It requires values of N, λ and κ all to be used together with the current state of the sample or a detailed knowledge of the sample stress history. Although the values of N and λ can be defined without too much difficulty the value of κ is not constant and so will be difficult to define for calculations. If a value of κ appropriate to small changes in pressure is used (as it has been suggested is necessary in the critical state model), at higher overconsolidation ratios the value of p'_c will be underestimated, the error increasing with rising overconsolidation ratio. This is especially of importance in tests where volume changes occur causing changes in the appropriate value of p'_c to be taken. In preference therefore the parameter p'_e should be used. This requires the use only of parameters N and λ for the soil. If the proedures outlined in this report for obtaining the position of the normal compression line are followed and the data adjusted in the manner described for each sample then reliable plots of data in the form of q'/p'_e against p'/p'_e may be obtained. This method of normalising takes a view of the state boundary surface along a constant volume section and so although similar in shape to the theoretical plot of q'/p'_c against p'/p'_c the values of p'/p'_e do not correspond to the inverse of the overconsolidation ratio which the values of p'/p'_c theoretically do. The method of normalising here has been to use the parameter p'/p'_e.

An alternative view of the state boundary surface may be obtained by normalising shear strains with respect to p' and specific volumes in the form of the equivalent specific volume v_λ. This method of normalising data takes a view of the state boundary surface in a direction parallel to the normal compression line. It proves to be a very satisfactory method of normalising test data if specific volumes have been adjusted, since the only soil parameter requried to produce v_λ is the value of λ. Since this is generally known with some degree of certainty the value of v_λ can be determined reliably. This parameter has been used in the normalisation of test data throughout these results.

In the analysis of these results it was noted that the shape of the isotropic state boundary surface plotted as q' /p' against v_λ appeared to be a boundary to all possible states. The data for other consolidation histories lying on this same surface when normalised in the same manner. Data from Gens (1983) suggests that this may also be so for normally consolidated soils except in the region close to the normally consolidated state for other stress histories. This was again observed here with data points in Fig 9.72 representing the normally consolidated state for different stress histories lying just beneath the isotropic state boundary surface. This suggests that a unique surface should also exist when data is plotted in the form of q' / p'_e against p' / p'_e. This was achieved in Fig 9.73 by using the value of N appropriate to isotropic compression in all calculations of p'_e instead of the value of N associated with the normally compressed state for that particular stress history. A similar pattern of results emerged with the isotropic state boundary surface forming a boundary onto which all other data from other stress histories fell. Again the points representing the normally compressed state for each history lie slightly within the isotropic state boundary surface. The yield curves and possibly the state boundary surfaces for each history are however not the same, at least in the region of the normally compressed state for each, since the values of $d\varepsilon_v / d\varepsilon_s$ obtained during compression for each stress history are not the same as those predicted from the shape of the isotropic state boundary surface (table 9.7, Fig 9.2). The predictions of the experimentally established surface are however better than those by the other methods shown in table 9.7. All strain increments are total strain increments in table 9.7. This may be due to only local variations in the shape of these curves or may be more general for the normally compressed state. In any case data for normally compressed states in extension e.g. Robinson (1984), Gens (1983), will lie within the isotropic surface. This raises the question of the value of N to be used in calculations of p'_e. These results would appear to indicate that where data only from one stress history is to be compared the use of an N value appropriate to that stress history would give satisfactory results. Furthermore it has the advantage that in the normally compressed state value of p' / p'_e is equal to one, indicating the normally consolidated state. However where data from different stress histories is to be compared it may be more appropriate to use a value of N from isotropic compression tests. The disadvantage is that for all stress states other than isotropic the point at which samples are normally consolidated will not be indicated by p' / p'_e equal to one.

9.11 Comparison of Material Parameters

The material parameters obtained from these tests were summarised in table 9.1 for each soil and for different stress histories for London Clay. These may be compared to the previously published values of parameters for these soils as given in table 7.2.

Data for the compression and swelling properties of soils proves highly sensitive to the methods of sample preparation and methods of testing followed. For kaolin the value of λ is found to be slightly less than that obtained by Robinson (1983) but the same as that by Ng (1986). The tests conducted by both sources were using the same triaxial equipment as used in this research. For the tests by Robinson (1983) a slightly different method of sample preparation was used probably resulting in higher values of λ due to higher initial sample water contents. The results from tests by Ng are however for identical methods of sample preparation and testing. The lower values of λ are reflected

also in the lower values of N obtained when data is compared with Robinson (1983). However the data from Ng (1986) prove very close to the present results. Values of κ obtained are somewhat difficult to compare since due to the variation of the slope of the swelling line the value is sensitive to the position at which it is taken and how i.e. tangent or secant. The method of obtaining the values of κ here was described earlier, the value of κ_1 taken compares well with that quoted from previous data. Other soil parameters were not determined (M or Γ) during these tests and so cannot be compared to previous data, however the data did fall within the previously established state boundary surfaces for these soils. Differences in the data for Ware Till may almost certainly be attributed to differences in the methods of sample preparation. The tests by Little (1985) were on undisturbed and remoulded samples while those by Richardson (1983) were also conducted on remoulded samples. It is interesting to note that the shape of the state boundary surface seems little affected despite these different methods of sample preparation. Results for Cowden Till indicate higher values of λ and N for the present data compared to Ng (1985). Since the methods of sample preparation were very similar this suggests some variability between the sample tubes from which soil was taken to prepare samples. Slate dust data proved to be almost identical to that obtained by Lewin (1970). The state boundary surface obtained however can be seen to be non-unique over much of the path to failure. Initially and at the ends of tests the surfaces coincide and so do not cause difficulties for the interpretation of the present tests. This does however raise the question as to whether a further surface may exist appropriate to the present type of tests i.e. constant p' tests.

For London Clay a full set of critical state parameters were obtained for isotropic samples. The values of λ and κ are very slightly less than those quoted by Schofield and Wroth (1968) and the value of M almost identical. The values of both N and Γ however are much larger than those quoted, the differences representing an error in the sample water content of approximately 4%. The reasons for this difference are unknown. Previous data for N, λ and κ for other stress histories was not available, however the values of λ and κ are found to be unique for this particular soil for compression under all stress histories and at failure in defining the slope of the critical state line, λ. The trend in the values of N was described earlier in section 9.3 but other data was not available to confirm actual values for London Clay. The same trend was observed by Gens (1983) testing Lower Cromer Till.

In the early stages of this test programme data were obtained for London Clay and Speswhite kaolin prepared by an alternative method described in Chapter 7. The results of these tests, shown in Fig 9.75 as v plotted against $\log_e p'$ and Fig 9.76 as ε_s against ε_v, show major differences compared to samples prepared in the normal manner. In particular of interest here is the fact that both soils give much lower values of λ, κ and N than those prepared by the standard method. These differences must be attributable to the much lower water contents of the remoulded samples and the different methods of sample preparation. In addition it may be noticed that these samples behave in a manner closer to isotropy in the early stages of loading than those from the normal method of sample preparation. This may be accounted for by the more uniform general water content of samples and the method of preparation which is more likely to produce isotropic samples.

9.12 Errors in Test Results

Some of the errors in these results have been discussed in the appropriate sections of this thesis chapter such as the effect of errors in axial strain measurement due to load cell compressibility on strain controlled tests. Such errors can be corrected at a later stage during analysis in order to assess the reliability of results and produce corrected stress-strain plots of data. Also there are those errors due to instrumentation and control as discusssed in Chapters 5 and 6, the effect of these may with care be reduced to negligible proportions. The errors considered here are those which are unavoidable in the triaxial test or which require different testing procedures in order to eliminate them .

The barrelling or necking of samples is caused by friction on the end platens which restrains samples from moving radially at their ends. With the present apparatus such effects are inevitable at high strain levels, either close to failure or when testing samples along paths with high stress ratios either in compression or extension states. As a result the strain distribution and stress distribution along the length and across the diameters of samples is not uniform so that the average area calculated may not the true area over which failure may be occuring. All samples were subject to the resulting errors during loading to failure. However in general at other times the effects of these errors were small. During intial compression and swelling the radial strains were relatively small for samples following isotropic stress histories and those with $\eta'_o = 0.25$. During one dimensional compression and swelling these strains were zero. However for samples compressed with $\eta'_o = 0.75$ the radial strains were very large since this path lies close to the failure line $\eta'_o = M = 0.89$. Samples could be seen to show the effects of barrelling. However since a continuous linear strain path was followed by this sample under stress controlled compression, it is believed that the errors involved are not significant. For the purposes of comparison of test paths for threshold effects all paths are similarly affected and so the data should prove reliable. In two dimensional tests the reverse effect was observed with very large positive radial strains (compressive) being observed. However over the bulk of the length of the sample the shape was sufficiently uniform to consider the data reliable. The solution to these problems would be to use "free ends". This would improve sample uniformity until much closer to failure. However it may lead to problems of negative restraint in some cases where stiffnesses are very high (Chapter 2) and will require the use of internal instrumentation if axial strains are to be measured accurately.

The membrane and side drains both due to their stiffness cause errors in the measured stresses on samples. While the error due to membrane stiffness is quite small that due to the side drains especially for extension tests is potentially very large. On its own the membrane correction is small so that for membranes of low stiffness it may be neglected. The main difficulty with making corrections for these factors lies in deriving a reliable value of stiffness for use in calculations and in deciding precisely what the strains are occuring in the membrane and side drains. Without some direct form of measurement, slippage and buckling may not be identified leading to large errors in the corrections themselves. For these reasons these corrections were not applied to these results. Since these results compare well with those of previous data it is thought that these results are at least as reliable as previous data in this respect.

As discussed in Appendix Two both the membrane and side drains may contribute to the volumetric strains during loading. In the case of the membranes this may be avoided by using membranes already saturated before test. In the case of the side drains however the volume strains are inevitable and can only be corrected afterwards as has been done for these results.

The side drains also contribute to further testing errors. These are radial non-uniformity due to high rates of loading (Atkinson, Evans and Ho, 1985) and the reduction of suctions due to samples swelling when the side drains are placed on the sample.

In conclusion it may therefore be stated that the use of side drains of any form should be avoided except where the use is absolutely necessary. Also the use of free ends while improving the uniformity of samples may lead to other difficulties which require significant upgrading of testing equipment and instrumentation.

9.13 Mathematical Modelling of the Test Results

In order to make use of the findings in this research it is necessary to produce a mathematical model to reproduce the principal features of the results. The suggestions described here for the mathematical modelling of these results will be made within the context of the critical state model and in particular the modified Cam clay model. These modifications to the modified Cam clay have not been implemented in a finite element model. The objective throughout this section is to demonstrate how the minimum amount of additional input data and changes can produce results which are significant improvements over those of the standard modified Cam clay model.

9.13.1 Principal Features of Threshold Tests

The main features of the threshold tests were summarised in earlier sections however they will briefly be repeated here. Tests show a progressive increase in stiffness as the angle of deviation of stress path increases. The magnitude of the increase in stiffness appears to vary for different soils being greatest for those of high plasticity. This increase in stiffness is similar for different stress paths, those tested here being constant p' and constant q' paths. For the constant p' paths some difference was noted as to whether the direction of approach was from a zone of higher p' or lower p' even when samples were subjected to the same deviation of stress path. The results show that data obtained after approach paths from areas of higher p' generally have higher stiffnesses than those from areas of lower p', similarly approach directions from ares of negative q'/p' generally gave lower stiffnesses than those from positive values of q'/p'. This leads to the diagrams shown in Fig 9.77 which show the typical form of normalised stiffness data at a given stress level for constant q' and constant p' paths. The difference between the data for different deviations of path progressively reduces as the stress path proceeds until at some stress level the difference is small enough to be neglected. The typical form of data for various rotations of stress path is shown in Fig 9.71 as normalised stiffness plotted against $\log_e \pi'$. The final feature of these data was the non-uniqueness of the strain increment ratio observed. Typically for a constant p' path the value of $d\varepsilon_v$ / $d\varepsilon_s$ varied between +1 and -1 showing a distinct trend in the data as the angle of deviation of stress path

altered. In general negative values were associated with samples which had approached from higher values of p'. Furthermore these paths were non-linear which indicates that samples were behaving in an in-elastic manner as described by Atkinson (1973). Once again these data converged to a single strain increment ratio after a change in stress similar to that defining the range of threshold effects in terms of stiffness. These effects did not appear to have any effect on the failure states of samples in terms of stress state or specific volume.

On varying the consolidation history of samples these effects were found to occur over similar regions of stress space but the magnitude of the effect varied. At an overconsolidation ratio of two samples compressed with $\eta' = 0.75$ had the highest stiffness but samples compressed isotropically and with overconsolidation ratio of two showed the greatest magnitude of threshold effect ie the greatest difference in stiffness between $\theta = 0$ and $\theta = 180^0$.

The effect of overconsolidation ratio was to show a generally reducing magnitude of threshold effect with rising overconsolidation ratio but over a similar change of state in terms of π' as the tests at an overconsolidation ratio of two. The magnitudes of stiffness and the variation of stiffness with overconsolidation ratio was dependent on the initial consolidation history of samples.

The effect of a period of rest appeared to be to increase the sample stiffness. This could occur in addition to any stress path effects so that the two effects were in fact additive.

9.13.2 Path Dependence Tests

These tests conclude that none of the test types examined were suitable for the examination of the path dependence of stress-strain behaviour. However these tests did provide some very useful additional data on the behaviour of samples below the state boundary surface.

The first feature to be noticed is that despite the linear stress paths used throughout very few of the tests excepting those approaching a given point (type 3 tests) give linear strain paths. Once again this indicates that samples are not behaving in an elastic manner unless stress induced anisotropy is considered acceptable. It is found from an examination of the stress-strain data that a unique set of stiffness data cannot be fitted to the results either elastic or plastic in form. This is taken to indicate that strains may be plastic in character but may not be associated with a unique yield curve. Many of these discrepancies can be resolved by considering the deviations of stress path and the likely effect of stress path threshold effects not only on the magnitude of the strains and stiffnesses but also on the strain increment ratio.

9.13.3 A Simple Model for Stress Path Threshold Effects

In a simplified model of threshold effects, only the change in sample stiffness caused by deviations of path may be modelled. No attempt is made to introduce the changes which occur to the strain increment ratio. Furthermore the minimum of testing and analysis of data is required in order to interpret the necessary input parameters.

The model uses an identical state boundary surface to that of the modified Cam clay model. The only differences occur in behaviour below the state boundary surface. In order to define the range R (equation 9.1) of stress path effects it is first assumed that the range for shear effects, R_q (Equation 9.1), is the same as that for volumetric effects, R_p i.e.

$$R_{q'} = R_{p'} = \frac{(\delta\sigma' / vp'\delta\varepsilon)_{\theta = 180^o}}{(\delta\sigma' / vp'\delta\varepsilon)_{\theta = 0^o}} \qquad 9.7$$

In order to define the value of $R_{p'}$ an isotropic compression and swelling test must be conducted and values of κ_o and κ_1 or K'_o and K'_1 (where K'_o and K'_1 are the values of bulk moduli appropriate to κ_o and κ_1 respectively) obtained from the data. It may be easier to obtain K'_o than κ_o due to the flatness of the v , $\log_e p'$ plot close to stress reversals. The ratio of K' or of κ at the same stress state may then be used in order to define the range $R_{p'}$ and hence $R_{q'}$. In addition using the plot of v against $\log_e p'$ the size of the threshold zone $\Delta\sigma' / p'$ may be defined from Fig 9.1 as,

$$\Delta\sigma' / p' = \Delta p' / p'_o \qquad 9.8$$

where $\Delta\sigma' = \sqrt{(\Delta q')^2 + (\Delta p')^2}$. Hence the value of π' may be obtained. This is again assumed to be the same for all test paths. With these data the volumetric behaviour is fully described and the range and size of zone of stress path effects defined.

In order to define the shear modulus two options are available. Firstly one of the two methods used in the critical state model could be employed. The first used a constant value of Poissons ratio to develop a relationship between the current G' and K' (equation 3.37). This would automatically provide the necessary link so that both shear and volumetric effects were scaled in a similar manner inside the threshold zone. The alternative method was to select a single value of G' which may either be constant or p' dependent (despite theoretical objections, Chapter 3) which would represent the shear stiffness outside the threshold zone G'_1 i.e. the value of G' for $\theta = 0^o$.

Inside the threshold zone the stiffness would simply be factored by the value of a paramter F which depends on the deviation of path encountered. This parameter is given by the expression

$$F = (\delta\sigma'/vp'\delta\epsilon)/(\delta\sigma'/vp'\delta\epsilon)_1 ,$$

$$\text{or} \quad F = \left(\theta\left[\frac{R-1}{180^o}\right]+1\right) \qquad 9.9$$

where the deviation of path is given in degrees and $(\delta\sigma' / vp'\delta\varepsilon)_1$ is a stiffness associated with $\theta = 0^o$ e.g. K'_1 or G'_1. This is the idealisation of data shown in Fig 9.77 as $\delta\sigma' / vp'\delta\varepsilon$ against θ. In all the data quoted in this chapter the value of F was stated at $\pi' = 0.05$ for $\theta = 180$ i.e. R. Due to the variation of F with π' this must be stated in the results. Beyond the edge of the threshold zone i.e. at π'_b the value of F is reduced to 1 i.e. $\theta = 0^o$. In the case of option one equation 9.9 need only be applied to the bulk modulus K'_1 but for option two it must be applied to both shear and bulk

moduli separately. The model developed by Leach (1986) is of the second type but does not use a parameter such as F . Instead only two moduli are used, one inside the threshold zone and one outside. This method of calculating stiffnesses is applied only to the elastic strains, on reaching the state boundary surface the sample yields and develops plastic strains simultaneously as it moves towards failure.

The second option available in order to define the shear modulus is to make use of the idealised normalised stiffness $\delta\sigma' / vp'\delta\varepsilon$, $\log_e \pi'$ diagram Fig 9.71. The stiffness data in the threshold range may be idealised by a series of straight lines as shown, and from the point where these converge a single straight line taken up to the point at which the state boundary surface is reached. The spread of these lines along the $\delta\sigma' / vp'\delta\varepsilon$ axis may be assumed to be linear with θ from the idealised line shown in Fig 9.77. Hence the normalised shear stiffness of a sample subjected to no deviation of stress path is given by,

$$\delta\sigma' / vp'\delta\varepsilon = m \log_e \pi' + c \qquad 9.10$$

where m is the slope and c is the intercept as shown in Fig 9.71. These may readily be computed given the sample stiffness at two points on a stress path, one of which lies in the threshold zone e.g. at $\pi' = 0.05$, and the other at its boundary , B In order to calculate the stiffness for other rotations of stress path the values of m and c must be recalculated. By calculating F (equation 9.9) at the value of π' used to obtain the values of κ_o , κ_1 and R, the value of stiffness within the threshold zone may be factored for the value of θ in question, while that at the edge of the zone remains unchanged (Fig 9.71). Hence it may be shown that the values of m and c are given by,

$$m = \left[\left(\frac{\delta\sigma'}{vp'\delta\varepsilon} \right)_{\pi'b} - F \left(\frac{\delta\sigma'}{vp'\delta\varepsilon} \right) \right] / \log_e(\pi'_b / \pi') \qquad 9.11$$

$$c = \left(\frac{\delta\sigma'}{vp'\delta\varepsilon} \right)_{\pi'b} - m \log_e \pi'_b \qquad 9.12$$

As before the value of F reduces to 1 at the edge of the threshold zone and so the equations reduce to those for $\theta = 0^0$. This method has the advantage of allowing non-linear stress-strain curves but is more complex than the first if the shear modulus is also made to be pressure dependent.

While these models may reproduce the effect on stiffness of threshold effects they do not reproduce the effects on the strain increment ratio since all these models are elastic in character i.e. strain increments depend on the stress increments not the stress state.

9.13.4 A Model Including the Effects on Strain Increment Directions

In order to model the effects on the strain increment direction a major increase in complexity of the mathematical model is needed. The form of model suggested will therefore only be described in principle, not in detail.

A different type of model is required for the purpose. That selected needs to include a kinematic yield surface as used by Mroz et al (1979) and Simpson et al (1979). The model developed by Mroz et al (1979) has many of the characteristics required and will be used. On the state boundary surface strains develop in the same manner as described in the modified Cam clay model however below the state boundary surface there are some differences. The main features of the model were described in Chapter 3 where it was stated that zones of uniquely elastic behaviour were restricted to the kinematic yield surface. As the state reaches the edge of this zone plastic strains develop below the state boundary surface of a magnitude in proportion to the distance from the current stress state to the state boundary surface related to the distance when the kinematic yield surface was first engaged by the state point. The plastic strain increment ratio is determined by the current position of the kinematic yield surface which is dependent on the recent loading history of the sample. This is illustrated on Fig 9.78 for samples having experienced a variety of recent stress histories before all following a constant p' path. To these strains the elastic strain increments must be added. It can be seen that each has a different strain increment ratio. The motions of this surface as the stress point moves must be such that the two surfaces will engage along a common normal when the state point reaches the state boundary surface (Fig 3.10). Hence it would be anticipated that not only is the strain increment ratio non-unique but also a number of tests all subjected to different deviations of path before the current path will show non-linear strain paths on which the strain increment ratio converges towards a common value. The pattern of strain increment ratios observed in the model are consistent with those observed in the results described.

In order to use this model to describe the present results it would be necessary to reduce the kinematic yield surface to almost a point in size so that samples with large deviations of stress path i.e. paths which would pass within the kinematic yield surface, do not all have the same strain increment ratio on continued loading. This model may then at least reproduce the pattern of much of the threshold data but this does lead to a major increase in complexity of the model which may not be justified. It should therefore be noted that unlike model L. C. (Simpson et al 1979) the KYS does not represent a zone of threshold behaviour, but is used only to control the direction of the strain increment vector for states inside the state boundary surface.

9.14 Discussion

The principal features of the results have been discussed under the individual headings it only remains to draw together these comments.

The previously observed patterns of stress path threshold effects have been confirmed for a number of soils and using these data the type of deformations occuring identified. The results indicate that for a wide range of soil types, initial consolidation histories and overconsolidation ratios, the behaviour below the state boundary surface is not elastic in character. The strains occuring may however be described by an elasto-plastic model using a kinematic yield surface within which behaviour is exclusively elastic. Since such a model is very complex a simplified threshold model was also described which only reproduces the effect of stress path effects on the stiffness of samples. If any zone of truly exclusive elastic behaviour does exist then it only occurs for small changes in stress

close to complete stress path reversals. This is a feature identified in the past by Parry and Amerasinghe (1973), Mroz, Norris and Zienkiewicz (1979) and Simpson, O'Riorden and Croft (1979). It has been suggested that the true value of κ, the slope of a swelling line should be taken immediately following reversal of path to represent true elastic behaviour, this corresponds to κ here.

Time effects are also observed but have not been included in the models suggested here. These effects are due to creep and probably occur due to the changes of volume of samples rather than any major changes of structure due to the short periods which are needed for such effects to develop (Bjerrum, 1967). As the sample volume reduces at constant p' and q' the sample effectively behaves as if more heavily overconsolidated that is a higher pseudo pre-consolidation pressure develops (Bjerrum, 1967). This may be interpreted as an increase in the size of the threshold zone around the sample with the sample state if initially on the edge of the zone lying inside the expanded surface and so accounting for the increased stiffness even of samples subjected to changes of path of $\theta = 0^0$. This however has not been confirmed experimentally and is only a conceptual model. If this did prove to be a method of describing such effects then the growth of the pre-consolidation pressure would be linked to the sample volume changes and in turn the size of the threshold zone to the current pre-consolidation pressure. Changes in volume would be related through equation 9.3. This is illustrated by Fig 9.79.

The magnitudes of stiffness observed here compared favourably with those of previous high quality laboratory tests on both undisturbed and reconstituted samples. It is noticeable that despite the use of external instrumentation the results appear to be unaffected by such factors as bedding and seating errors. This demonstrated that for reconstituted soils where corrections are made for system compliance these methods of strain measurement may prove satisfactory unless it is necessary to resolve much smaller strain quantities.

No attempt has been made throughout this work to relate these effects to physical material behaviour. The effects observed do however seem intuitively reasonable, with changes in the conditions of loading being responded to in a manner such that there is period of change in which behaviour relates to the previous loading history before a more unique sample response is observed on the current loading path. It is factors such as these which would have appeared in the past to have contributed to considerable scatter in tests conducted to investigate the elasticity of soils as has been shown here for three such types of test.

Although the models described here had not been implemented in calculations it is thought that the modelling of these effects is of great importance. Based on the limited evidence available (Leach, 1986; Simpson et al, 1979) the inclusion of a simple very stiff zone leads to major improvements in the predictions of magnitudes and distributions of ground movements. The inclusion of such effects as, stiffness dependent on deviation of previous loading path and the effects of recent stress history on the strain increment ratio, should improve predictions further.

CHAPTER 10.

CONCLUSIONS AND RECOMMENDATIONS FOR FURTHER RESEARCH.

CHAPTER 10.
CONCLUSIONS AND RECOMMENDATIONS FOR FURTHER RESEARCH.

10.1 Introduction.

The objectives of this research were set out in chapter 4. The general aims however have been to examine some of the possible reasons for some discrepancies between laboratory and field stiffness data. In chapter 2 it was shown that soil stiffness is highly dependent on many factors including those of threshold effects. This indicates that in any soil stiffness testing in the laboratory or in the field, great care must be taken in the control of the conditions under which tests are conducted. Failure to do so may lead to considerable inconsistencies in results.

Until recently opinion generally favoured field stiffness results as being reliable and data obtained from laboratory tests as being of little use mainly due to the effects of disturbance. This explanation was offered for the major differences often observed in such data (Marsland, 1971) eg London clay (St John, 1975). However this seems unlikely with the repeatability of laboratory tests even on undisturbed material. Advances in testing techniques and instrumentation indicate that when field and laboratory data are compared over similar ranges of stress or strain the differences in such data may be very small with laboratory tests tending to give slightly higher and more consistent results. This tends to lead to the conclusion that laboratory data may be of greater reliability than field data for all but highly sensitive soils. This may be the case since even in field tests some disturbance will inevitably occur but the soil to be tested cannot be inspected prior to testing. Also the test conditions in the field cannot be controlled to the same degree as in the laboratory. As has been seen such factors as stress path and stress history are very important to stress - strain behaviour. The modulus derived in the field results only from surface measurements and so can only represent an average stiffness for the soil profile which is dependent on the assumptions made regarding the behaviour of that soil.

This research has concentrated on examining some of the effects of stress history and recent stress history on the stress - strain response of soils. The conclusions of the experimental program are summarised in this chapter.

10.2 The Critical State Model.

10.2.1 Compression and Swelling Data.

The data obtained have been analysed within the framework of the critical state model (plotted with axes of v, lnp'). For normally consolidated material the predictions fit the present data reasonably well. All virgin compression lines are found to be linear and parallel for a given soil (with a slope = λ). The intercept of the compression line on the specific volume axis, N, is also found to be unique for a given soil and compression history. Both these parameters are however highly sensitive to the methods of preparation of samples and testing procedures. The value of N is observed to be a maximum for the case of an isotropic stress history with all other stress histories giving lower values

of N, the reduction being progressively greater as departure from isotropic stress history increases. It is observed that swelling curves are all of similar shape. However they do not fit the assumption of linearity even for relatively small changes of stress state.

10.2.2 Stress - Strain curves and Failure.

The state boundary surface appears to be unique for a given stress history. However some difficulties may be found in defining the surface accurately at high overconsolidation ratios due local drainage in samples. All samples fail at a unique stress ratio and at approximately similar strains. It is noticeable that, in accordance with the critical state model normalising data as q'/p' against $v\varepsilon_s$ produces slight improvements in the agreement of data compared to the more usual axes of q'/p' against ε_s. In general the normalising of stress - strain or stiffness data with respect to either 1/p' or 1/vp' may be used since differences in v between tests are often small and so of little consequence. In order to identify the critical state, diagrams of stress path, strain path and the variation of stress ratio with shear strain must be examined. Samples tested at low overconsolidation ratios and normally consolidated all show the anticipated trend of a constant q' with no change in pore pressure or volumetric strain and constant stress ratio at critical state. Samples tested stress controlled on the dry side of critical all reach peak stress ratios before failure occurs. These stress ratios were higher than that for critical state and could be observed not to be at critical state due to non - zero volumetric strain increments. For tests on samples of high overconsolidation ratio the continuing fall of the q'/p' , ε_s plot showed that despite a constant value of q' and ε_v having been reached these samples were not at critical state.

10.2.3 Uniqueness of the State Boundary Surface.

For each stress history a unique surface could be defined in q'/p' , v_λ and q'/p'$_e$, p'/p'$_e$ plots. Using the value of N for isotropic compression the latter plot could be reduced to one single unique diagram for a given soil. This may demonstrate that the isotropic data forms a limiting boundary to the states of all samples however they have been compressed. Data for normally consolidated states for other histories were not available to confirm this, although a similar conclusion was reached by Gens (1983). The plots of q'/p' , v_λ were found to be close to unique when superimposed without further adjustment.

10.3 Threshold Test Data.

10.3.1 Stress Path Effects.

The size of the threshold zone was estimated to be of the order of 25% of the current value of p' for a variety of soils. This is the range over which stiffnesses and strain increment ratios are significantly affected by the recent loading history. This figure appears to be approximately constant with overconsolidation ratio and stress history. On the evidence of the four stress paths

followed it is further suggested that this range may be similar for all paths and so the threshold zone may be taken as circular in q' , p' space. In order to estimate the size of this zone, the use of constant p' and constant q' (isotropic compression and swelling) tests are recommended. Probably the most convenient for most cases will be the isotropic compression and swelling tests (constant q').

The magnitude of the increase in sample stiffness is observed to vary with the deviation of stress path, θ. The increases in stiffness observed are similar for various stress paths for a given soil. It is observed however that the overall range of stiffness R may vary for a given soil with consolidation stress history , and overconsolidation ratio. It is observed that the largest range occurs for samples with an overconsolidation ratio of two and after following an isotropic stress history. For all other cases the value of R is reduced. These effects also vary with soil type, high plasticity soils being affected to the greatest degree. The range of values of R observed was from a maximum of 9.6 for London Clay down to 5.3 for slate dust, all these samples with an overconsolidation ratio of two. Due to the non - linearity of the stress - strain data the value of R varies , the figures given here refer to a change of stress state of $\pi' = 0.05$ from the start of the test stage. A further feature of these results was the non - uniqueness of the strain increment ratio and non - linearity of the strain paths.

10.3.2 Time Effects.

Samples were subjected to short periods of rest at constant effective stress as well as being subjected to specified deviations of stress path. The data indicate that the effect of a rest period results in a further increase of sample stiffness which was similar for the three deviations of path examined. This suggests that for short periods of rest at least, that time and stress path effects are separate effects which may combine to produce a greater effect than either acting alone. It is thought that these effects are due to changes in volume of the sample due to creep.

10.3.3 Tests to Failure .

These tests indicated that the failure state of samples was unaffected by deviations of stress path before loading to failure. The only difference observed was that samples subject to large deviations of stress path failed at lower shear strains than those subject to small deviations of path. The precise value of recorded strain at failure may however be unreliable due to the use of stress control during these tests.

All the data lie within previously established shapes of state boundary surfaces for each soil. However contours of shear strain which are often superimposed on normalised plots, q'/p'_e against p'/p'_e are non - unique due to the varying effect of threshold effects on the stress - strain response of samples.

10.4 Tests for Path Dependence.

Three types of test for path dependance were conducted. None of these tests proved successful in producing data for the comparison of the elastic stiffness of London clay on various paths. Only type three tests produced data which was free from the influence of threshold effects. Since a single set of stiffness data cannot be fitted to the results of these tests it was concluded that a model with a kinematic yield surface would be needed to model the results. In order to examine the elastic path dependence of data it was suggested that samples should be subjected to reversals of stress path on a number of stress paths at the point where path dependence is to be examined. It was observed in type one and two tests that the influence of threshold effects on the strain increment ratio could mask the effects of anisotropy for samples initially compressed in an anisotropic manner

10.5 Evidence of Plastic Behaviour Below the State Boundary Surface.

The critical state model makes the assumption of elastic isotropic behaviour below the state boundary surface. The results of these tests suggest that there may be departures from this. Firstly it is observed that hysteresis loops occur in all data where stress path reversals occur. This is observed both in constant p' and constant q' tests (isotropic compression and swelling) and occurs due to the influence of stress path effects immediately following a reversal of stress path. Secondly it is observed that strain paths resulting from linear stress paths are non - linear. This in terms of the definitions by Atkinson (1973) indicates inelastic behaviour, the pattern of the results for stress path threshold effects discounting the possibility of stress induced anisotropy. Finally it is observed that on the same stress path and at the same stress state the strain path is non-unique. As a result it also proves impossible to fit an elasto - plastic model with a unique yield surface to this data.

10.6 Effect of Total Stress Path on Stress Path Threshold Tests.

The results of two special series of tests indicate that stress path effects are dependent on changes in effective stress path only. Tests conducted using the same deviation of effective stress path but with various deviations of total stress path yield a single stress - strain curve indicating the lack of importance of the total stress path. This was confirmed by a second series of tests in which the total stress path deviation was maintained constant while the effective stress path deviation was varied. This gave a number of stress - strain curves, one for each deviation of effective stress path which agreed with the results from the main test series for the same deviations of effective stress path.

These results therefore confirm the principal of effective stress for stress path threshold effects.

10.7 Recommendations for Laboratory Testing of Soils.

As a consequence of the above findings recommendations regarding the testing of soils for the

determination of stiffness of soils may be made.

Firstly where undisturbed samples are tested , samples must be of the highest quality possible. Although disturbance may not be as significant a factor on sample stiffness as has previously been thought, at least for heavily overconsolidated soils, it has been shown that the effect of disturbance is to cause a reduction of the measured sample stiffness.

Secondly test conditions must be carefully controlled in order to eliminate the effects of temperature change. The effects of changes in pore water chemistry may also need to be considered if it is intended to use distilled water when testing undisturbed soils (Bjerrum, 1967).

Thirdly when conducting a test the recent stress history of samples prior to following the stress path of interest must be considered. This should include considering the effect of rest periods (Schumattmann, 1981) although this factor is difficult to model in the laboratory. In addition the direction and lengths of recent loading paths should be considered since as has been shown the stiffness and strain increment ratio are heavily dependent on this factor. These two factors constitute an extension of the stress path method described by Lambe (1967).

Finally the results of these tests must be analysed in a manner appropriate to the type of calculations to be performed. This refers to the type of modulus to be taken (secant or tangent), the method of definition chosen, and the position at which it is taken on the stress - strain curve.

10.8 Recommendations for Further Research.

The present program of tests has been restricted to that of reconstituted samples of clay soils. It is therefore recommended that the present tests are extended to include other soil types. This should include tests on silts and sands for which it may be anticipated from the trends of the present results that stress path threshold effects may be of diminishing importance. In addition the testing of undisturbed soils is highly recommended. This would confirm the existence of such effects in natural soils. For this purpose London clay is recommended initialy due to the large amount of data available for the purposes of comparison including back analysed structures, field tests and laboratory tests Further testing is also required in order to establish the effects of longer rest periods combined with various deviations of stress path.

This program of testing should be combined with the development and implementation of a mathematical model in a finite element formulation. Initially this may be of the simplified type described in chapter nine to reproduce only the effects on stiffness. This may then be used in parametric analyses of various problems to identify the types of problems for which these effects are most significant. The model may then be extended to cover the effect on strain increment ratio. It is anticipated that the range of exclusively elastic behaviour represented by the kinematic yield surface may be very small, possibly reducing to a single point in stress space. Similar calculations may then be performed and again the importance of including such effects assessed. It is anticipated that similar results to those obtained by Simpson et al (1979) and Leach (1986)

would be produced indicating the significance of such regions in a mathematical model.

Finally the effects of temperature cycles should be investigated. It was indicated in chapter two that where cycles of temperature change occur similar effects as those due to time effects occur. It should be determined if these effects due to temperature changes are due to the effect of the rest period or if the cycles of temperature change represent a third type of threshold effect. This may have implications for the testing of undisturbed soil samples in the laboratory due changes of temperature experienced by samples during the sampling and testing process.

I will close by wishing you many many happy days on the fells. You will be following in my footsteps, wherever you go, and I hope you find the enjoyment I found: I am sure you will. Please be helpful to the people you meet, and please be kind to the birds and animals. Don't forget to watch where you are putting your feet, and you'll be all right.

And if you, dear reader, should get a bit of grit in your boot as you are crossing Haystacks in the years to come, please treat it with respect. It might be me.

Wainwright,A.(1972). Fellwanderer. Westmorland Gazette.

APPENDIX 1.

RATE OF LOADING IN TRIAXIAL TESTS.

A VERY SPECIAL NOTE: Arrangements have been made with the Border Hotel at Kirk Yetholm for *bona fide* Pennine Wayfarers *who have completed the walk in a single journey* to be supplied with a congratulatory pint (of beer or lemonade, NOT whisky — and one only, mind you!) at the author's expense. Just say "Charge it to Wainwright." Cheers! (P.S. You'd better have some money of your own, in case his credit has run out).

Wainwright,A.(1967). A Pennine Way Companion. Westmorland Gazette.

Now you can rest on your laurels in the Bay Hotel with a pint, but (let there be no misunderstanding about this) you do so at your own expense. It's no use saying "charge it to Wainwright" as you did at the Border Hotel at Kirk Yetholm. No, sonny. that game won't work here. Pay for your own. I'm skint.

Wainwright,A.(1970). A Coast to Coast Walk. Westmorland Gazette.

APPENDIX 1 RATE OF LOADING IN TRIAXIAL TESTS.

A 1.1 Introduction.

For any soil loading test the rate at which loading may be conducted must be considered. It is desirable that the rate of test be as rapid as possible in order to reduce the cost of testing, however the rate of loading should be such that errors due to incomplete drainage or lack of uniformity of samples are negligible. In some tests eg the oedometer test, loading is incremental, each increment of load being applied once consolidation from the previous increment has completed. The calculations described in this appendix apply to tests in which a loading path is followed at either a constant rate of application of stress or constant rate of strain.

In drained tests the requirement is that the pore pressure in the sample should be close to that measured by the transducer, whereas in an undrained test the rate of loading must be such that the pore pressures are reasonably uniform throughout the sample. Where rates of loading are very high and radial drainage is used, case hardening effects may occur (Atkinson, Evans, and Ho.,1985).

Two methods of calculating the rate of test are considered here. The method due to Bishop and Henkel (1962) is used in standard laboratory practice but may lead to very slow rates of testing. The method produces a rate of loading in terms of the time to the first significant reading for the sample from considerations of the degree of equalisation of pore pressures throughout a soil sample. Atkinson (1984b) proposed an alternative method based on an acceptable error in the pore pressure measurements, this gave a rate of loading in terms of a rate of change of stress state of the sample. This method produces rates of loading which are more rapid in the early stages of loading but which may be too fast as failure is approached. The method may readily be applied for any stress path.

A method of assessing the error in the pore pressure measurements was given by Atkinson (1984b). The method may be used to check the rates of loading calculated by either of the above methods.

A 1.2 Basic Theoretical Considerations.

As loading of a soil sample proceeds changes of total stress generate changes in pore pressures. In a drained test these pore pressures dissipate as the sample volume changes while in an undrained test these may be measured by the pore pressure transducer. The rate at which pore pressures are generated should be balanced by the rate of application of total stress, so that the remaining average excess pore pressure, u, remains within acceptable limits. The excess pore pressure represents an error since the pore pressure measured is not that in the sample, furthermore it results in a lack of homogeneity in samples. However a small excess pore pressure is necessary at all times for drainage to take place. The magnitude of the average excess pore

pressures generated and hence the rate of loading is dependent on a number of factors which include, the soil properties (in particular the pore pressure response and consolidation characteristics), the drainage conditions, the sample geometry, and the stiffness of the pore pressure transducer and drainage leads.

The rate at which excess pore pressures dissipate may be illustrated by plotting volumetric strains against square root of time elapsed since application of the loading increment. The initial section of the curve is approximately linear with an intercept on the final linear portion of t_{100}. The value of t_{100} depends on the sample geometry and the coefficient of consolidation of the soil, c_v. The value of t_{100} for various drainage conditions for cylindrical triaxial samples for a height to diameter ratio of two are given in table A 1.1. from Bishop and Henkel (1962). It should be noted that the average degree of consolidation of samples at time t_{100} is only about 90% and is not complete until a time in excess of $2t_{100}$. All these formulae also assume that the coefficient of permeability of the filter paper side drains and porous stone (below the sample) are infinite and so do not affect the consolidation characteristics of the soil. Bishop and Gibson (1963) showed that the time to first significant reading should be increased to allow for these factors. In the case of a test not using side drains the true time to first significant reading, t^*_f, is given by,

$$t^*_f = \frac{(1+4/\lambda)t_f}{(1+3/\lambda)} \qquad \text{A 1.1}$$

where $\lambda = (k_D d)/(k_c t_D)$.

k_D = Permeability of porous stone.

k_c = Permeability of soil.

d = Mean path length of drainage.

t_d = Thickness of porous stone.

The value of k_D may vary greatly a typical value would be of the order of 10^{-5}m/s but may be reduced by clogging during a test. Bishop and Green (1963) concluded that this factor was not significant unless $\lambda < 50$.

For tests on soils of low permeability filter paper side drains are often used. In most cases the filter paper side drains are found to be less than 100% efficient and so the times for t_{100} predicted by the formulae in table A 1.1 may not be achieved. The actual efficiency of the side drains depends on the ratio of the permeability of the filter paper to that of the soil and the percentage of the sample surface area covered. Often the efficiency of the side drains is not greater than about 30%, this however also includes the loss of efficiency of drainage due to the porous stone. The ratio of the effective coefficient of consolidation, c_v, for use in equations in table A 1.1 to the true coefficient of consolidation, c_{vt}, is related to the parameter ν given by the expression (from Bishop and Gibson, 1963),

$$\nu = \frac{\pi^2 k_p a \delta}{4 k_c h^2} \qquad \text{A 1.2}$$

where k_p = Permeability of filter paper.

k_c = Permeability of soil in the radial direction.

a = Sample radius.

2h = Sample hight.

δ = Filter paper thickness.

This equation does not account however for the lack of complete coverage of the sample surface. The filter papers used in this research were made of Whatman's No 54 filter paper which had a thickness of approximately 0.15mm. The permeability of this filter paper varies with effective radial pressure from approximately 1.4×10^{-5}m/s at 30kPa to 1.0×10^{-6}m/s at 690kPa according to Martin (1970) or from 1.7×10^{-5}m/s to 5.4×10^{-7}m/s over a similar range of stresses according to Webb (1966). A value of $k_p = 5 \times 10^{-6}$m/s has been used in calculations since it represents a good average value for the stress levels at which tests have been conducted. The accuracy of this factor is of relatively little consequence due to the lack of sensitivity of the factor $t_{100} / t_{100\ t}$ to the parameter ν for values of $\nu < 10$ (see table A 1.2). High values of ν indicate highly efficient drainage. From values of ν calculated for each soil used in this research a value of c_v / c_{vt} and the calculated values of t_f / t_{ft} are given in table A 1.3. The figures in the final column illustrate the error due to using an experimentally determined value of t_{100} in the theory assuming complete coverage of the sample surface, t_{ft}, to that of more exact theory. It can be seen that errors of up to 20% may occur. Values of soil permeability in table A 1.3 were determined from tests without side drains. The lack of continuity of side drains further reduces the efficiency of sample drainage. For the case of alternating strips and gaps of filter paper placed longitudinally on the sample (Bishop and Henkel (1962) pattern), Martins (1962) has shown that the efficiency of the drains may be reduced by half ie t_{100} times may be doubled. Bishop and Gibson (1963) noted that this was only true for cases where $\nu > 5$. Further reductions of efficiency may be anticipated due to clogging of the drains, hence efficiencies of the order of only 30% may not be unusual.

The rate at which pore pressures are generated depends on the sample state and the stress path followed. If undrained the average excess pore pressure is given by (Atkinson,1984b),

$$u = \delta p + \alpha \delta q \qquad \text{A 1.3}$$

Where α is a parameter similar to Skempton's pore pressure parameter, A (Skempton,1954). Atkinson(1984b) showed that the parameter α may be interpreted as the slope of the undrained stress path, dp' / dq'. Clearly the value of α may vary considerably during a test. It may therefore be necessary to assess the value of α and also the rate of loading at various stages of a test, for example at the start of loading and as failure is approached. If a sample is allowed to drain, equation A 1.3 may be used as shown in section A 1.4 to calculate the excess pore pressures generated due to a given rate of loading.

A 1.3 Bishop and Henkel (1962) Calculation.

The method of computing the rate of loading due to Bishop and Henkel (1962) relates the time to failure or first significant reading to the degree of dissipation or equalisation of pore pressures required.

For drained loading the degree of equalisation is defined as,

$$u_f = \frac{q'_f - q'_u}{q'_d - q'_u} \qquad \text{A 1.4}$$

where q'_f = Strength measured.

q'_u = Fully undrained strength.

q'_d = Fully drained strength.

The time to failure or first significant reading, t_f, is given by,

$$t_f = \mu t_{100} / (1 - u_f) \qquad \text{A 1.5}$$

Where μ is a factor depending on sample drainage conditions, see table A I.1. Hence if 95% equalisation of pore pressures is required the time to the first significant reading would become,

$$t_f = 20\mu t_{100} \qquad \text{A 1.6}$$

For undrained loading the degree of equilisation is defined as,

$$u_f = 1 - u / u_o \qquad \text{A 1.7}$$

where u_o = excess pore pressure if no redistribution of pore pressures takes place. The time to failure or first significant reading is then given by,

$$t_f = Th^2 / c_v \qquad \text{A 1.8}$$

where $2h$ = sample hight.

T = Time factor (1.65 for single end drainage, 0.071 for all round drainage).

Atkinson(1984b) showed by using these formulae that the permissible rate of loading in an undrained test with all round drainage was 7 times as fast as that for a drained test where similar degrees of equilisation are required. In both cases only a time to the first significant reading is given. If only the failure point is of interest then an estimate of the failure state will be required in order to determine the rate of test. Similarly where the complete stress strain curve is required the time to the first reading to achieve the desired degree of equilisation is given by equations A 1.6 or A 1.8. The errors implied at low stress levels may be very small and the rates of test required very

slow, it may therefore be necessary to accept a lower degree of equilisation at the start of loading in order to achieve reasonable rates of test.

A 1.4 Atkinson(1984b) Calculations.

This method considers the steady state condition of constant stress rate loading at which the rate of generation of excess pore pressures equals the rate of dissipation.

From equations A 1.3 the excess pore pressure generated in an undrained test is given by,

$$u = \left[\frac{dp}{dt} + \alpha \frac{dq}{dt} \right] t \qquad \text{A 1.9}$$

Where dp' / dt and dq' / dt are the rates of loading and t the time after the start of loading. If drained test is considered in which the degree of dissipation is u, the excess pore pressure is given by,

$$u = \left[\frac{dp}{dt} + \alpha \frac{dq}{dt} \right] (1 - u)\, t \qquad \text{A 1.10}$$

However from equation A 1.5 the rate at which pore pressures dissipate is known hence,

$$u = \mu t_{100} \left[\frac{dp}{dt} + \alpha \frac{dq}{dt} \right] t \qquad \text{A 1.11}$$

The rate of test for a given excess pore pressure may therefore be computed for any drained stress path. This analysis does not apply to undrained loading, for such tests Atkinson (1984b) suggested that loading should be conducted either at a similar rate to drained tests or in the same ratio as the rates given by Bishop and Henkel (1962) calculations (ie 7 times faster for all round drainage).

In order to check these calculations a method was proposed for determining the excess pore pressures in drained tests. At the end of a period of loading any excess pore pressures will dissipate giving rise to changes in volume. If the volumetric strain is plotted against square root of time elapsed since the end of loading then these volume strains may be estimated , Fig A 1.1. In a plot of specific volume against $\log_e p'$ these volume strains are seen as a change in specific volume, OA, at constant measured mean effective stress, p', Fig A 1.2. The exact point , A, at which the pore pressures have dissipated before the commencement of secondary compression may be found using the volume strains plotted in Fig A 1.1. The displacement of the point A at constant volume from point B on the compression line established in the test represents the excess pore pressures generated during loading, and may be calculated from the equation of the normal consolidation line,

$$v = N - \lambda \ln p' \qquad \text{A 1.12}$$

Differentiating equation A 1.12 and dividing by the specific volume gives,

$$\delta\varepsilon_v = \lambda\, \delta p' / vp' \qquad \text{A 1.13}$$

Since $\delta p' = \delta u = u$, the excess pore pore pressure, this may be re-written as,

$$u = vp'\, \delta\varepsilon_v / \lambda \qquad \text{A 1.14}$$

Using this method Atkinson (1984b) found good agreement between the calculated excess pore pressures (equation A 1.11), and those determined experimentally for speswhite kaolin.

A 1.5 Discussion.

The methods described by Atkinson (1984b) have been used throughout this research. The calculated maximum rates of loading for each soil were given in tables 7.6a, b, and c, for an excess pore pressure u of 5kPa. Also given in these tables are details of the observed and calculated excess pore pressures for the rates of test used. The agreement in the results may be observed to be quite good. An example of typical data for each soil is given in Figs A 1.3 to A 1,7 to illustrate these calculations. It is interesting to note that using data given in table A 1.3 for each of these soils, the filter paper side drains were only approximately 30% efficient.This is much greater than the loss of efficiency predicted by equation A 1.2 due to the permeability of the side drains (see table A 1.3). The further losses may be accounted for by the other factors discussed including losses due to the permeability of the porous stone and lack of continuity of the side drains.

Both sets of calculations, Bishop and Henkel (1962), and Atkinson(1984b), require the parameter t_{100} or c_v . These parameters are known to vary with stress level and sample state. The errors observed in the calculations in tables 7.7 are probably partly due to the values of t_{100} used being taken at a stress level of p' = 50 kPa rather than at a higher stress level closer to that at which the tests were conducted and due to the clogging of the filter paper side drains. A small error occurs in these calculations since the sample surface is no longer completely covered, and therefore parameters ρ and η, and hence also μ (where $\mu = 1 / \eta\rho$), are no longer strictly correct for the conditions quoted in table A 1.1. The errors in η and ρ tend to be compensating so that μ is little affected. Clinton(1984) has indicated that provided the t_{100} measured from the sample with side drains rather than that calculated using the formulae in table A 1.1, the errors in the rate of test due to the efficiency of the side drains is small. This will account for the loss in efficiency of the drains due to the factors described but not the use of a t_{100} value from low stress levels. Since much slower rates of test were used than the maximum allowable, the errors due to using a t_{100} from a stress level of p' = 50 kPa are not significant as is shown in table 7.7.

The use of stress controlled tests produces reasonable rates of loading at low stress levels where the full stress strain curve is required. Furthermore any loading path within the limitations of the triaxial apparatus may easily be followed, however close to failure in order to define peak and ultimate (critical) states accurately, strain control is necessary. A hybrid loading pattern is therefore often required. This type of loading procedure was followed in drained and undrained tests to failure, at constant cell pressure during this research. Once the strain rate reached the rate of approximately 0.2 to 0.25% per hour during the stress controlled stage the method of control was switched to strain control at the rate observed in the previous few hours of loading. This procedure was not possible in the constant p' tests to failure using the current version of the control program.

Drainage Conditions	t_{100}	ρ	η	$\mu = 1/\eta\rho$
One end	$\frac{\pi h^2}{c_v}$	π	0.75	0.424
Two ends	$\frac{\pi h^2}{4c_v}$	$\frac{\pi}{4}$	3.0	0.424
Radial only	$\frac{\pi h^2}{64c_v}$	$\frac{\pi}{64}$	32.0	0.638
Radial and one end only	$\frac{\pi h^2}{81c_v}$	$\frac{\pi}{81}$	35.8	0.721
Radial and both ends	$\frac{\pi h^2}{100c_v}$	$\frac{\pi}{100}$	40.4	0.789

Note:- 2h = Sample height and h = sample diameter.

Table A 1.1 Drainage Parameters for Various Drainage Conditions (Bishop and Henkel,1962).

ν	Drainage from one end and radially			Drainage from both ends and radially		
	η (1)	c_v / c_{vt}	t_f / t_{ft}	η (1)	c_v / c_{vt}	t_f / t_{ft}
∞	35.80	1	1	40.39	1	1
100	34.79	0.834	0.98	38.98	0.953	0.98
10	26.81	0.341	0.877	30.09	0.674	0.847
5	21.20	0.212	0.806	24.03	0.515	0.813
1	8.36	0.064	0.781	10.68	0.208	0.800
0	0.75	0.012	0.769	3.00	0.059	0.800

Notes:- c_v and t_f by exact theory

c_{vt} and t_{ft} established from consolidation stage.

(1) Effective value of η.

Table A 1.2 Effect of filter paper efficiency on drainage times (Bishop and Gibson,1963).

Soil	k (m/s)	v	c_v / c_{vt}	t_f / t_{ft}
London clay	1.2×10^{-8}	4.1	0.226	0.815
Speswhite kaolin	7.1×10^{-6}	0.07	0.020	0.770
Slate dust	9.8×10^{-7}	0.1	0.05	0.776
Ware till	1.9×10^{-8}	2.6	0.111	0.791
Cowden till	2.4×10^{-6}	0.02	0.016	0.769

Table A 1.3 Effect of filter paper permeability on the efficiency of side drains for soils under test.

APPENDIX 2

EFFECT OF ERRORS IN WATER CONTENT ON COMPRESSION AND SWELLING PARAMETERS κ, λ, and N.

APPENDIX 2 Effect of Errors in Water Content on Compression and Swelling Parameters κ, λ, and N.

A 2.1 Introduction.

Errors occur in the measurement of the water content and of the volumetric strains due to a number of factors. Some of these factors will be considered in this appendix with reference to the effect of such errors on the slopes on the normal compression and swelling lines, λ and κ respectively, and the intercept of the normal compression line N (as defined in chapter 3). It is often observed (Atkinson, 1983a) that the values of λ and κ are very similar for a large number of samples while there may be considerable variation in the value of N. Errors are also observed when comparing values of sample water content when preparing a sample, at a the start of a test, and at the end of a test.

A 2.2 Factors Affecting Errors in the Measurement of Compression and Swelling Parameters.

The variation of compression and swelling parameters between samples causes considerable problems in defining the sample water content during a test. These problems become significant when comparing data from a number of similar tests or when normalising data.

A 2.2.1 Water Content of Slurry.

The differences between the water content of samples in preparation as a slurry, and that predicted for the slurry from the sample water content when being placed in the apparatus after removal from the preparation tube may be explained mainly by losses of soil slurry during the preparation of samples. These losses are very difficult to calculate, and as a result the water contents used in all calculations should not be based on the water contents or masses measured when preparing the slurry. In general it would be anticipated that the sample at the start of the test would have a larger water content than that implied by the slurry water content. If the slurry water content is to be determined accurately either it must be ensured that the soil powder used is oven dry or, a sample of the slurry must be weighed and dried in the oven. Even taking such precautiions data showed considerable differences in water content predicted from the slurry and from the samples placed in the apparatus which would have been consistent with a loss of soil during preparation of samples in sample tubes of approximately 5 to 10g.

When the sample is placed in the apparatus it is unlikely to be fully saturated hence, the water content if measured at that stage should not be used to calculate the specific volume. When placed in the apparatus the sample would swell on saturation and so apparently give a lower value of N than might otherwise be expected. Furthermore due to the variation of water content of samples compressed in tubes, see Chapter 7, section 7.5.7, the water content of the trimmings from the ends of specimens may be expected to be considerably lower than that of the average of the sample. This would tend to produce lower values of N than the true value for the soil.

When obtaining the water content of samples dried in an oven a number of weighings are made, these include, the mass of the drying tin, the mass of the wet soil and the mass of the dry soil. The masses were recorded in this research to 0.01g. If the typical mass of wet soil used was about 20g and the water content 30% the worst likely error due to weighing is about ± 0.3%. This may cause considerable scatter in the values of N. The water content was not recorded in these tests at this stage since in general samples were not trimmed. Instead the mass of the whole sample was recorded and the water content calculated using the dry mass of soil recorded for the whole sample at the end of the test. This is likely to introduce small errors due to losses of soil on the filter papers and membrane when they are removed which will result in the initial water content being overestimated by a small amount using this method. Since such errors are likely to be very small this method was used in order to calculate the initial water contents, w_1, given in tables 7.4, 7.5 and 7.6.

A 2.2.3 Measurement of Volume Strains During a Test

The volume strains measured are used in order to check the change in water content between the beginning and end of a test. Errors in the measured volume strains are caused by,

a. Incorrect sample dimensions,
b. Calibration errors of volume gauge,
c. Changes in water content of filter paper drains and membrane,
d. Air in the drainage system,
e. Flexibility of the drainage system,
f. Leakage either into or out of the sample and drainage system
g. Lack of homogeneity of samples.

Errors due to incorrect sample dimensions will be particularly significant in tests where large volume changes take place. With volume strains of approximately 10%, if the sample dimensions, length and diameter are recorded to ± 0.1 mm then errors of up to ± 0.07% may be expected. In this research the methods used to record sample dimensions were given in Chapter 7, section 7.6.3. Dimensions were recorded to ± 0.1 mm although the calipers used to make the measurements recorded dimensions to ± 0.02 mm. After recording the sample dimensions great care must be taken to ensure that the minimum change in these dimensions occurs during setting up of the sample. However provided all changes are undrained then the effect of such changes on the volume strains will be minimal.

Errors due to incorrect calibration of equipment are unlikely to be significant. Considerable errors would be required to produce a large effect on κ, λ or N. For example if the calibration constraint is in error by +1% then at volume strains of 10% the error in the volume strain measured is 0.1% (true volume strain = 10.1%).

Both the sample membrane and the filter paper drains are observed to change volume during a

test. In the case of the membrane the effect depends on whether the membrane has been soaked previously. If the membrane has been soaked then it is likely that very little change in volume will occur. If the membrane is dry then it may be expected to take up water during approximately the first 48 hours of a test (Lewin, 1985). Dry membranes were used in all these tests. The change in mass of a membrane during a test was observed to be approximately 0.5g for the membranes used, approximately 6.0g mass and 0.2 mm thick. Presumably half of this water flows from the sample and drainage leads and half from the cell fluid. This leaves an error of 0.25 g or 0.25 cc volume of water. This is equivalent to an error of approximately 0.3% reduction of the true volumetric strains. The effect is therefore to produce a small reduction in the value of κ and λ which is likely to be insignificant for all but very stiff soils. Filter paper side drains and filter paper disks on the ends of the sample may also change volume. These are normally placed on the sample after having been soaked, any free water may either be absorbed by the sample or may contribute to an increase in the observed volumetric strains. During further stages of testing these filters may then compress and swell in a similar way to the sample (Shimizu, 1981). The magnitude of the error depends on the surface area and thickness of the filter papers. For those used in these tests the volume strains due to the filter papers was found from tests to be given by,

$$\Delta\varepsilon_v = 0.15\,\Delta\log_e p' \qquad \text{A 2.1}$$

i.e. volume strains registered of 0.15% (for a 76 mm x 38 mm sample) for every log cycle of stress change. Typical compression and swelling curves are shown in Fig A 2.1. Again these volume changes are unlikely to be significant except where testing very stiff soils, although they may be significant when determining the value of κ especially immediately following stress path reversal where κ is very small. While errors due to free water on side drains may vary between tests it is unlikely that there will be much variation of the errors due to the wetting of the membrane or the compression and swelling of the side drains. These factors will therefore produce an error in the absolute values of the parameters measured but may not cause significant variation of them.

Air in the drainage system may contribute large errors in the measured volume strains. This air may be in the drainage leads, porous stone, the soil sample or trapped between the sample and membrane. During a test this air may dissolve causing an apparent flow of water towards the sample, and so reducing the volume strains measured. The air which does not dissolve may remain in the form of bubbles which then compress and swell with varying pressure and so also give false volume changes. Every effort should therefore be made to eliminate air from the system. The volume gauge and drainage leads should be filled with de- aired water and flushed through during a test if it proves difficult to saturate the sample. Lack of saturation of the system may be tested by following the procedures described in chapter7, section 7.6.5.2. An acceptable degree of saturation must be decided on, since it will prove to be impossible to fully saturate the whole system due to air trapped in the porous stone and sample. In many cases a "B" response of 95% (as described in section 7.6.5.2) is considered acceptable.

In general all measuring systems have some flexibility which gives rise to errors in the measurements taken. By careful testing procedures these may be minimised. The flexibility of the system used in this research was considered in section 6.6, in these tests it is considered that errors due to system flexibility on the volume change measurements are negligible.

Potentially the greatest errors in the volume measurement are those due to leakage. This may occur from drainage leads, valves and connections to atmosphere outside the cell or from the cell fluid into the drainage leads and connections. Such leaks can be reduced to insignificant proportions by conducting regular leakage checks on the system (see chapter 6). Other leaks which may occur include leakage past the "o" rings which seal the membrane against the sides of the top and bottom platens or through the membrane either through small holes or due to the permeability of the rubber. Tests by Poulos (1964), Rowe and Barden (1964)and Evans (1983) suggest that by greasing the sides of the platens leakage past the membrane / "o" rings may be eliminated. This procedure was followed during these tests. Leakage through the membrane and valves was considered to be very significant by Ting (1968) and Poulos (1964). Both authors quote a typical permeability for membranes of $k = 5\times10^{-18}$m/s, which suggests a rate of in flow into the sample of $Q = 2.3\times10^{-17}m^3/s/kPa$ (an increase of volumetric strains of $\varepsilon_v = 0.00023\%$ / day for every 100kPa of effective radial pressure). This figure is very small so that even where samples remain at constant effective stress for long periods such small strains are unlikely to be observed. In this test series the average mean effective stress throughout a test was 200 kPa, with tests not exceeding 60days in duration this corresponds to a total leakage through the membrane of 0.024% of the sample volume. Such errors if present could be identified by a lack of correspondence of initial and final water contents.

Finally errors may occur in the volume strains due to the lack of homogeneity of samples. Samples may not be homogeneous due to the method of preparation of samples or due to the methods of testing used. This refers to the non - uniformity of samples produced from presses due to the variation of water content over the length of the samples and effects such as case hardening (Atkinson, Evans and Ho, 1985) due high rates of testing. The effect of errors due to these factors are unknown but should remain constant if sample preparation and test procedures do not vary in a series of tests. Difficulties also occur when samples deform along slip planes since local large variations of water content may take place (Atkinson and Richardson, 1986). This is a significant factor when considering failure, however if the sample is used only to determine the swelling and compression properties of a soil it should not be significant.

A 2.2.4 Measurement of Stresses During a Test.

An alternative view of the errors observed in N is that they occur due to errors in the measurement of stresses between indervidual tests. Errors in the measured stresses are caused by,

a. Incomplete drainage of samples,
b. lack of homogeneity of samples,

c. incorrect sample dimensions,
d. errors in the calibration of transducers,
e. stiffness of membrane and side drains.

Errors due to incomplete drainage of samples causes a displacement of the position of the compression and swelling lines by an amount μ, the excess pore pressure as discussed in appendix one. If a number of tests are conducted at the same rate this factor will represent a constant error in the value of N (an overestimate) with a very small increase in the value of λ. If the rate of test is varied however, the value of N may be expected to increase slightly with increasing rate of test although the final equilibrium specific volume , after allowing these excess pore pressures to dissipate should remain unchanged.

Samples may not be homogeneous due to the effects of end restraint. For a series of tests however all conducted by the same procedures the effects on each should be the same and so produce no variation in the values of κ, λ, or N.

Sample dimensions are not required for the calculation of cell pressure or pore pressure. However where a deviator stress is applied the cross sectional area of the sample is needed. The error in the deviator stress measured is likely to be about $\pm$ 0.5% for dimensions measured to $\pm$ 0.1mm. Such a small error is likely to be negligible. In isotropic compression and swelling tests this factor has no effect on the determination of κ, λ, or N.

The effect of calibration errors is also small. An error of 1% in the calibration constant of a device causes an error of 1% in the readings of that device i.e. 1 kPa in 100 kPa. Since at least two devices are used for all calculations eg cell pressure and pore pressure in isotropic tests, an error not exceeding 2% could be anticipated. If the calibration constant is too large the effect is to increase the values of N and λ very slightly. Typical calibration data for these tests was shown in chapter six.

Finally there are those errors due to the stiffness of the membrane and side drains. The effect is to either under or over estimate the imposed loads on the sample as discussed by Richardson (1986). For a series of tests all using similar membranes and side drains the errors are likely to be similar due to these factors. In most cases the effect is to produce an overestimate of N and a slightly smaller overestimate of λ.

It can be seen from this section that the effect of errors due to stress measurement are likely to be much smaller than those of volume measurements. Throughout sections A 2.2.3 and A 2.2.4 it has been assumed that the devices are perfectly linear and are not significantly affected by noise. Such factors while significant to the absolute measured values of κ, λ, or N are unlikely to significantly affect the scatter in values determined from a number of otherwise identical tests.

A 2.2.5 Measurement of Final Water Content and Calculation of Specific Volume.

At the end of a test a sample must be removed from the apparatus as rapidly as possible so as not to allow the sample to absorb water from the porous stone , side drains or drainage leads. The errors caused by such factors are difficult to estimate but they are likely to increase with time. The sample must then be weighed after drying any excess surface moisture and placed in an oven as soon as possible. The determination of the final water content is subject to errors due to weighing of the sample and the drying tin. These amount to ±0.04% in the water content of a sample of 30% water content with masses recorded to ± 0.01g (total sample mass ≈ 150g). Such errors are not significant, however it must be ensured that the side drains and filter paper discs on the ends of the sample are completely removed. The dry weight may then be used as discussed in section A 2.2.2 in order to calculate the initial water content of the sample before testing began. When determining these water contents care should be taken to ensure that the samples remain in the oven sufficiently long to be "oven" dry. For most soils this period needs to be at least 6 to 12 hours (Akroyd,1957; Head, 1980), while BS 1377 (1975) suggests a period of 24 hours which was used in these tests and is generally used in standard practice.

A comparison of the initial and final water contents determined by these methods may then be made using the expression,

$$v = v_o (1 - \varepsilon_v) \qquad \text{A2.2}$$

Where v_o is the initial specific volume ,

v is the specific volume after volume strains ε_v have taken place ($\varepsilon_v = \delta v / v_o$).

The specific volume is given by the expression,

$$v = 1 + wG_s \qquad \text{A2.3}$$

Where w is the water content,

G_s is the specific gravity of the soil grains.

Errors in the specific gravity of the soil grains will cause a consistent lack of correspondence of the final and initial specific volumes. The factors affecting the accuracy of the volume strains in equation A 2.2 were discussed in section A 2.2.3.

A 2.3 Typical Test Data.

The data from the tests conducted in this research was presented in chapter 8. It can be seen from Fig A 2.2 that the values of κ and λ for a large number of tests on London Clay do not vary significantly except due to variations of sample preparation procedures. It can be seen that the variation of N is much greater.

In all the data in Figs 8.2 to 8.6c inclusive, the specific volume has been back calculated using the water content measured at the end of the tests. The variation of N determined in this manner is approximately ± 0.015 or slightly greater than ± 0.5% in water content. The correspondence between the initial and final water contents is generally good although the use of water contents from the ends of tests produces less scatter in the value of N . The correspondence between initial and final water contents is approximately ± 0.4% water content, see table 8.2 (Using data from the start of the test the variation is approximately ± 0.7% water content). The reasons for this error were discussed in section A 2.2.2 and would appear to be due to difficulties in determining the initial water content.

Leakage does not appear to be a significant factor in these tests since there is no consistent and increasing error as the length of test increases. In Fig A 2.3 the error in the measured water content between the start and end of each test is plotted against duration of test. This shows a scatter which is evenly displaced about a mean of approximately zero which does not vary with duration of test. Such a trend is not consistent with the errors expected due to leakage.

A 2.4 Discussion.

In this appendix some of the factors affecting the determination of the water content of samples at the beginning and end of tests have been discussed with reference to the effect on the compression and swelling parameters κ, λ and N. It was observed that the values of κ and λ are reasonably constant for a series of identical tests although the value of N may show some scatter. This causes difficulties when normalising data or comparing the results of a number of tests all at the same stress state, although with different water contents. The discussion does not suggest that either high or low values of N should be favoured due to systematic errors. Instead it appears that errors are random and so may be expected to be equally displaced positive and negative errors about the true value. The data presented in chapter eight has been derived by taking average values of N for all tests and computing all water contents in further analyses using the calculated average value of N. In this way it has been observed that all data corresponds more closely. The final water contents computed using these values of N for each soil are given in table 8.2. It can be seen that the errors implied in the measured final water contents are small (± 0.2%). This probably reflects the precision with which the final water content of a sample may be determined by the present methods when allowances are made for the accuracy of weighing , the changes in water content at the end of a test (both increases and decreases), the non - uniformity of samples at the end of test and some variations between the indervidual samples themselves.

It is therefore recommended that the water contents of samples are determined from the final water contents . A check should then be made on the initial water content by using the recorded volumetric strains, the mass of the whole sample at the start of testing and the dry mass of the sample at the end of testing. Such a check will indicate any gross errors which may occur due to faulty instrumentation or leakage from or into the drainage system. The values of λ and κ may then easily be determined and the value of N taken as the average recorded for a number of tests.

REFERENCES.

References.

Abbiss,C.P. (1981). Shear wave measurements of the elasticity of the ground. Geotechnique Vol 31, No 1, pp 91-104.

Acum,W.A.E. and Fox,L.(1951). Computation of load stresses in a three layer elastic system. Geotechnique Vol 2, No 4, pp 293-300.

Anderson,W.F. and McKinlay,D.G.(1975). Tests to find the modulus of deformation of till. Proceedings of a Symposium on the Engineering Behaviour of Glacial Materials. Birmingham. pp165-179.

Akroyd,T.N.W.(1957). Laboratory testing in soil engineering. Marshal press.

Arthur,J.R.F. and Menzies,B.K.(1972). Inherent anisotropy in sand. Geotechnique Vol 22, No 1, pp 115-129.

Atkinson,J.H.(1973). The deformation of undisturbed London Clay. PhD thesis, University of London.

Atkinson,J.H.(1981). Foundations and slopes. McGraw - Hill.

Atkinson,J.H.(1983a). Personal communication.

Atkinson,J.H.(1983b). Effects of stress path and stress history on the stiffness of soils near trenches. The City University, Geotechnical Engineering Research Centre, research report GE/83/7.

Atkinson,J.H.(1984a). Some procedures for normalising soil test results. The City University, Geotechnical Engineering Research Centre, research report GE/84/3.

Atkinson,J.H.(1984b). Rates of loading in drained and undrained stress path and triaxial tests. The City University, Geotechnical Engineering Research Centre, research report GE/84/1.

Atkinson,J.H.(1984c). Strength of Gault clay from the A45 Cambridge by-pass at low effective stresses. A report submitted to the Transport and Road Research Laboratory, Ground Engineering Division, for contract CON/340c/16. The City University, Geotechnical Engineering Research Centre, research report GE/84/18.

Atkinson,J.H.(1985a). Simple and inexpensive pressure control equipment for conventional and stress path triaxial testing of soils. Geotechnique Vol 35, No 1, pp 61 - 63.

Atkinson,J.H.(1985b). Effect of slip planes and local drainage on the undrained strength of soil. The City University, Geotechnical Engineering Research Centre, research report GE/85/3.

Atkinson,J.H. and Bransby,P.L.(1978). The Mechanics of Soils. McGraw - Hill.

Atkinson,J.H. and Evans,J.S.(1985). Discussion on: The measurement of soil stiffness in the triaxial apparatus, by Jardine,R.J., Symes,M.J.R.P. and Burland,J.B.(1984). Geotechnique Vol35, No 3, pp 378 - 382.

Atkinson,J.H., Evans,J.S. and Ho,E.W.L.(1985). Non - uniformity of triaxial samples due to consolidation with radial drainage. Geotechnique Vol 35, No3, pp353 - 355.

Atkinson,J.H., Evans,J.S. and Richardson,D.(1984). Effects of stress path and stress history on the stiffness of reconstituted London clay. Proceedings of 20th Regional Meeting on Site Investigation Practice: Assessing BS5930. Engineering Group of the Geotechnical Society. Vol 1, pp 44 - 55.

Atkinson,J.H.,Evans,J.S. and Scott,C.R.(1983a). Development of a new microcomputer based controller for stress path testing. The City University, Geotechnical Engineering Research Centre, research report GE/83/2.

Atkinson,J.H.,Evans,J.S. and Scott,C.R.(1983b). Stress path testing equipment: Spectra system operating manual. The City University, Geotechnical Engineering Research Centre, research report GE/83/1.

Atkinson,J.H.,Evans,J.S. and Scott,C.R.(1985). Developments in stress path testing equipment for measurements of soil parameters. Ground Engineering, Vol 18, No 1, pp 15 - 22.

Atkinson,J.H. and Farrar,D.M.(1984). Stress path tests to measure soil strength parameters for shallow landslips. The City University, Geotechnical Engineering Research Centre, research report GE/84/12.

Atkinson,J.H. and Little,J.A.(1986). Undrained triaxial compressive strength of reconstituted and undisturbed samples of a till from the Vale of St Albans. In preparation.

Atkinson,J.H. and Richardson,D.(1985a). Elasticity and normality in soil - experimental examinations. Geotechnique Vol 35, No 4, pp 443 - 450.

Atkinson,J.H. and Richardson,D.(1985b). The effect of local drainage on the undrained strength of overconsolidated clay. The City University, Geotechnical Engineering Research Centre, research report GE/85/26.

Atkinson,J.H., Richardson,D. and Robinson,P.J.(1986). Compression and extension of K_o normally consolidated clay. The City University, Geotechnical Engineering Research Centre, research report GE/86/5.

Atkinson,J.H. Richardson,D. and Woods,R.I.(1986). A note on the determination of tangent stiffness parameters from soil test data. Computers and Geotechnics Journal. In press.

Balasubramaniam,A.S.(1969). Some factors influencing the stress - strain behaviour of clay. PhD thesis, Cambridge University.

Balasubramaniam,A.S. and Waheed - Uddin.(1977). Deformation characteristics of Bangkok clay in triaxial extension. Geotechnique Vol 27, No 1, pp75 - 79.

Balasubramaniam,A.S. and Waheed - Uddin.(1978). Discussion on: Deformation characteristics of Bangkok clay in triaxial extension. Geotechnique Vol 28, No 2, pp231 - 234.

Baldwin,S.R.(1985). Specplot, computer plotting of SPECTRA triaxial test data user manual (version 85.3). The City University, Geotechnical Engineering Research Centre.

Baligh,M.M.(1984). The strain path method in geotechnical engineering. MIT report No R84 - 01.

Balla,A.(1960). Stress conditions in triaxial compression. Journal of Soil Mechanics and Foundation Engineering Division, American Society of Civil Engineering Vol 87, SM6, pp57 - 84.

Barden,L.(1963). Stresses and displacements in a cross anisotropic soil. Geotechnique Vol 13, No 3, pp 198 - 210.

Biot,M.A.(1935). Effect of certain discontinuities on the pressure distribution in a loaded soil. Physics Vol 6.

Biot,M.A.(1941). General theory of three dimensional consolidation. Journal of Applied Physics Vol 12, pp155 - 164.

Bishop,A.W.(1970). Shear strength parameters for undisturbed and remoulded soil samples. Proceedings of the Roscoe Memorial Symposium on the Stress Strain Behaviour of Soils, Cambridge. Foulis. pp 3 - 58.

Bishop,A.W.,and Gibson,R.E.(1963). The influence of the provisions for boundary drainage on the strength and consolidation characteristics of soils as measured in the triaxial apparatus. Proceedings of Symposium on Laboratory Shear Testing of Soils. American Society for Testing and Materials, Special Technical Publication No 361, pp 435 - 451.

Bishop,A.W., Green,G.E., and Skinner,A.E.(1973). Strength and deformation measurements on soils. Proceedings of the 8th International Conference on Soil Mechanics and Foundation Engineering, Moscow. Vol 1.1, pp57 - 64.

Bishop,A.W. and Henkel,D.J.(1962). The measurement of soil properties in the triaxial test. Edward Arnold.

Bishop,A.W. and Hight,D.W.(1977). The value of poisson's ratio in saturated soils and rocks stressed under undrained conditions. Geotechnique Vol27, No3, pp 369 - 384.

Bishop,A.W., Kumpley,N.K., and El-Ruwayiah,A.(1975). The influence of pore water tension on the strength of clay. Phil. Trans. of the Royal Society. Vol 278, AL286, pp 511 - 554.

Bishop,A.W.,Webb,D.L., and Lewin,P.I.(1965). Undisturbed samples of London clay from the Ashford Common shaft. Geotechnique Vol 15, No 1, pp1 - 31.

Bishop,A.W., and Wesley,L.D.(1975). A hydraulic triaxial apparatus for controlled stress path testing. Geotechnique Vol 25, No 4, pp 657 - 670.

Bjerrum,L.(1967). Engineering geology of Norwegian normally consolidated marine clays as related to settlements of buildings. Seventh Rankine Lecture. Geotechnique Vol17, No 2, pp 81 - 118.

Bjerrum,L.,and Lo,K.Y.(1963). Effect of aging on the shear strength properties of a normally consolidated clay. Geotechnique Vol 13, No 2, pp 147 - 157.

Bjerrum,L. and Wu,T.H.(1960). Fundamental shear strength properties of the Lilla Edet clay. Geotechnique Vol 10, No 2, pp 101 - 109.

Boussinesq,J.V.(1876). Equilibre d'elasticitê d'un sol isotropic sans pesanteur, supportant differents poid's, Comptes Rendus Hebdomadaires, Vol16, pp1260 - 1263, Paris.

Borja,R.I. and Kavazanjian Jr,E.(1985). A constitutive model for the stress - strain - time behaviour of 'wet clays'. Geotechnique Vol35, No3, pp 283 - 298.

British Standards Institution. (1975). Methods of test for soils for civil engineering purposes. BS1377.

Brooker,E.W. and Ireland,H.O.(1965). Earth pressures at rest related to stress history. Canadian Geotechnical Journal, Vol 2, No 1, pp 1 - 15.

Brown,P.T. and Gibson,R.E.(1973). Rectangular loads on inhomogeneous elastic soil. Journal of the Soil Mechanics and Foundation Engineering Division, American Society of Civil Engineering, Vol 99, SM 10, pp 917 - 920.

Burgess,N. and Eisenstein,Z.(1977). The application of pressuremeter tests in deformation analyses. Canadian Geotechnical Journal, Vol14, No 1, pp 64 - 75.

Burland,J.B. and Hancock,P.J.R.(1977). Underground car park at the House of Commons: Geotechnical aspects. Structural Engineer, Vol 55, pp 87 - 100.

Burland,J.B.,Simpson,B. and St John,H.D.(1979). Movements around excavations in London clay. Design Parameters in Geotechnical Engineering. Proceedings of 7th European Conference on Soil Mechanics and Foundation Engineering, Brighton. Vol 1, pp 13 - 30.

Burland,J.B. and Symes,M.J.R.P.(1982). A simple displacement gauge for use in the triaxial apparatus. Geotechnique Vol 32, No 1, pp 62 - 64.

Burmister,A.(1945). The general theory of stress and displacement in layered soil systems. Journal of Applied Physics, Vol16.

Buri,P.B.(1978). Influence of secondary consolidation and overconsolidation on the behaviour of a soft alluvial clay. PhD thesis, University of London.

Butler,F.G.(1975). Heavily overconsolidated clays. Proceedings of Conference on Settlement of Structures, Cambridge, Review Paper, session 3.

Butterfield,R.(1979). A natural compression law for soils (an advance on e - log p'). Geotechnique Vol 29, No 4, pp 469 - 480.

Cairncross,A.M. and James,R.G.(1977). Anisotropy in overconsolidated clays. Geotechnique Vol 27, No 1, pp 31 - 36.

Campanella,R.G., and Mitchell,J.K.(1968). Influence of temperature variations on soil behaviour. Journal of the Soil Mechanics and Foundation Engineering Division, American Society of Civil Engineers, Vol 94, SM 3, pp 709 - 734.

Casagrande,A.(1936). Characteristics of cohesionless soils affecting the stability of slopes and earth fills. Journal of the Boston Society of Civil Engineers, January.

Clarke,B.G. and Wroth,C.P.(1985). Discussion on:- Fahey,M. and Randolph,M.F. Effect of disturbance on parameters derived from self boring pressuremeter tests in sand. Geotechnique Vol 35, No 2, pp 219 - 222.

Clayton,C.R.I.(1984). Sample disturbance and BS 5930. Proceedings of 20th Regional Meeting on Site Investigation Practice: Assessing BS5930 . Engineering Group of the Geotechnical Society. Vol 2, pp 61 - 75.

Clinton,D.B.(1984). The effect of the permeability of filter paper side drains on consolidation measurements and testing time prediction. The City University, Geotechnical Engineering Research Centre. Research report GE/84/13.

Clinton,D.B.(1985). Determination of soil parameters for design from stress path tests. Report on progress during the second year of research. The City University, Geotechnical Engineering Research Centre. Research report GE/85/29.

Cole,E.R.L.(1967). Behaviour of soils in the simple shear apparatus. PhD thesis. Cambridge University.

Cole,K.W. and Burland,J.B.(1972). Observation of retaining wall movements associated with a large excavation. Proceedings of 5th European Conference on Soil Mechanics and Foundation Engineering. Vol1, pp 445 - 453.

Costa Filho,L.M.(1978a). A laboratory investigation of the small strain behaviour of London clay. PhD thesis, University of London.

Costa Filho,L.M.(1978b). Discussion on:- Balasubramaniam,A.S. and Waheed Uddin. Deformation characteristics of Bankok clay in triaxial extension. Geotechnique Vol 28, No 2, pp 228 - 231.

Costa Filho,L.M.(1979). Discussion. Design Parameters in Geotechnical Engineering. Proceedings of 7th European Conference on Soil Mechanics and Foundation Engineering, Brighton. Vol 4, pp124 - 128.

Costa Filho,L.M.(1980). Discussion on:- Simpson,B., O'Riordan,N.J. and Croft,D.D.(1979). A computer model for the analysis of ground movements in London clay. Geotechnique Vol 30, No 3, pp 336 - 339.

Costa Filho,L.M.(1984). A note on the influence of fissures on the deformation characteristics of London clay. Geotechnique Vol 34, No 2, pp 268 - 272.

Dafalias,Y.F., and Hermann,L.R.(1980). A bounding surface soil plasticity model. Proceedings of International Symposium on Soils Under Cyclic and Transient Loading , Swansea. pp 335 - 345.

Daramola,O.(1978). The influence of stress history on the deformation of sand. PhD thesis. University of London.

Daramola,O.(1980). Effect of consolidation age on stiffness of sand. Geotechnique Vol 30, No 2, pp 211 - 215.

Davis,E.H. and Poulos,H.G.(1963). Triaxial testing and three - dimensional settlement analysis. Proceedings of the 4th Australian / New Zealand Conference on Soil Mechanics and Foundation Engineering. pp 233 - 235.

Davis,E.H. and Poulos,H.G.(1968). The use of elastic theory for settlement prediction under three - dimensional conditions. Geotechnique Vol 18, No 1, pp 67 - 91.

Drucker,D.C.(1959). A definition of a stable inelastic material. Journal of Applied Mathematics Vol14, No 1, pp 35 - 42.

Drucker,D.C.(1964). On the postulate of stability of material in the mechanics of continua. Journal de Mechanica. Vol 13, No 2, pp 235 - 249.

Duncan,J.M. and Chang,C.Y.(1970). Non- linear analysis of stress and strain in soils. Journal of the Soil Mechanics and Foundation Engineering Division, American Society of Civil Engineers, Vol 96, SM 5, pp 1629 - 1653.

Egeli,I.(1978). Pore pressures and volume changes in undrained and unsaturated clays. PhD thesis, University of London.

Eisenstein,Z. and Morrison,N.A.(1973). Prediction of foundation deformations in Edmonton using an in - situ pressure probe. Canadian Geotechnical Journal, Vol 10, No 2, pp 193 - 210.

El - Ghamrawy,M.K.(1978). A sandy clay till - some properties measured during consolidation and shear. PhD thesis, University of London.

El - Ruwayiah.(1975). Stress strain characteristics of rock fill, and of clays under high pore pressure tension. PhD thesis, University of London.

Evans,J.S.(1983). Personal communication.

Fadum,R.E.(1948). Influence values for estimating stresses in elastic foundations. Proceedings of 2nd International Conference on Soil Mechanics and Foundation Engineering.

Fahey,M and Randolph,M.F.(1984). Effect of disturbance on parameters derived from self-boring

pressuremeter tests in sand. Geotechnique Vol 34, No 1, pp 81 - 98.

Feda,J.(1979). Physical and design non - homogeneity of sub - soil. Design Parameters in Geotechnical Engineering. Proceedings of 7th European Conference on Soil Mechanics and Foundation Engineering, Brighton. Vol 1, pp 155 - 159.

Fox,E.N.(1948). The mean elastic settlement of a uniformly loaded area at a depth below the ground surface. Proceedings of the 2nd International Conference on Soil Mechanics and Foundation Engineering.

Gens,A.(1983). Stress strain and strength characteristics of a low plasticity clay. PhD thesis, University of London.

Gens,A.,and Hight ,D.W.(1979). The laboratory measurement of design parameters for a glacial till. Design Parameters in Geotechnical Engineering. Proceedings of 7th European Conference on Soil Mechanics and Foundation Engineering, Brighton. Vol 2, pp 59 - 65.

Gibson,R.E.(1967). Some results concerning displacements and stresses in a non - homogeneous elastic half space. Geotechnique Vol 17, No 1, pp 58 - 67.

Gibson,R.E.(1974). The analytical method in soil mechanics. The 14th Rankine Lecture. Geotechnique Vol24, No 1, pp 115 - 140.

Graham,J. and Houlsby,G.T.(1983). Anisotropic elasticity of a natural clay. Geotechnique Vol 33, No 2, pp 165 - 180.

Gunn,M.J. and Britto,A.(1982). CRISP - users and programmers guide, Cambridge University Engineering Department.

Hambley,E.C.(1972). Plane strain behaviour of remoulded normally consolidated kaolin. Geotechnique Vol 22, No 2, pp 301 - 318.

Hashiguchi,K.(1977). An expression of anisotropy in a plastic constitutive equation for soils. Constitutive Equations for Soils. Proceedings of Speciality Session No 9, 9th International Conference on Soil Mechanics and Foundation Engineering, Tokoyo, Vol 9, pp 302 - 305.

Hawkes,I. and Mellor,M.(1970). Uniaxial test in rock mechanics laboratories. Engineering Geology, Vol 4, pp 177 - 285.

Head,K.H.(1980). Manual of soil testing. Vol 1. Soil classification and compaction tests. Pentech Press, London.

Henkel,D.J. and Gilbert,G.D.(1952). The effect of the rubber membrane on the measured triaxial compressive strength of clay samples. Geotechnique Vol 3, No 1, pp 20 - 29.

Hight,D.W.(1983). Laboratory investigations of sea bed clays. PhD thesis, University of London.

Hight,D.W.(1984). Laboratory testing : Assessing BS 5930. Proceedings of 20th Regional Meeting on Site Investigation Practice: Assessing BS5930. Engineering Group of the Geotechnical Society. Vol 2, pp 79 - 95.

Hight,D.W.,El - Ghamrawy,M.K. and Gens,A.(1979). Some results of a laboratory study of a sandy clay and implications regarding its insitu behaviour. Proceedings of 2nd International Conference on the Behaviour of Offshore Structures, London. Vol 1, pp 133 - 150.

Hight,D.W. and Gens,A.(1979). Discussion. Design Parameters in Geotechnical Engineering. Proceedings of 7th European Conference on Soil Mechanics and Foundation Engineering, Brighton. Vol 4, pp 128 - 129.

Hight,D.W., Gens,A., De Campos,T.M.F. and Takahorshi,M.(1982). Factors influencing the interpretation of in-situ strength tests in sensitive low plasticity clays. Proceedings of 3rd International Conference on the Behaviour of Offshore Structures, MIT, Vol 2, pp 435 - 450.

Hight,D.W., Gens,A., and Jardine,R.J.(1985). Evaluation of geotechnical parameters from triaxial tests on offshore clay. Proceedings of International Conference on Offshore Site Investigation, London. pp 1 - 31.

Hight,D.W., Gens,A. and Symes,M.J.(1983). The development of a new hollow cylinder apparatus for investigating the effects of principal stress rotation in soils. Geotechnique Vol33, No 4, pp 355 - 384.

Hill,R.(1950). The mathematical theory of plasticity. Oxford University Press, London.

Ho,E.W.L.(1984). An investigation into non-uniformity of triaxial samples due to consolidation with radial drainage. The City University, Geotechnical Engineering Research Centre, research report GE/84/21.

Ho,E.W.L.(1985a). Personal communication.

Ho,E.W.L.(1985b). Undrained triaxial compression and extension tests on reconstituted speswhite kaolin consolidated under K_o conditions with particular reference to perfect sampling. The City University, Geotechnical Engineering Research Centre, research report GE/85/17.

Hooper,J.A.(1975). Elastic settlement of a circular raft in adhesive contact with a transversely isotropic medium. Geotechnique Vol 25, No 4, pp 691 - 712.

Houlsby,G.T.(1981). A study of plasticity theories and their applicability to soils. PhD thesis, University of Cambridge.

Houlsby,G.T.(1985). The use of a variable shear modulus in elastic - plastic models for clays. Computers and Geotechnics Journal, Vol1, No 1, pp 3 - 13.

Hvorslev,M.J.(1936). Condition of failure for remoulded cohesive soils. Discussion, Proceedings of 1st International Conference on Soil Mechanics and Foundation Engineering, Cambridge, Massachusetts. Vol 3, pp 51 - 53.

Hvorslev,M.J.(1949). Subsurface exploration and sampling of soils. Report on the joint research project of the American Society of Civil Engineers, the Engineering Foundation, Harvard University, and the U.S. Waterways Experimental Station. New York. Engineering Foundation.

Intercole Systems Ltd.(1977). User manual, Spectra-xb system.

Jaeger,J.C.(1969). Elasticity, fracture and flow. London, Methuen.

Jaeger,J.C. and Cook,N.G.W.(1976). Fundamentals of rock mechanics. Chapmann Hall, 2nd Edition.

Jamiolkewski,M., Ladd,C.C.,Germaine, J.T. and Lancellotta,R.(1985). New developments in field and laboratory testing of soils. Proceedings of the 11th International Conference on Soil Mechanics and Foundation Engineering, San Francisco. Vol 1, pp 57 - 133.

Jardine,R.J.(1986). Investigations of pile soil behaviour with special reference to the foundations of offshore structures. PhD thesis, University of London.

Jardine,R.J., Fourie,A., Maswoswe,J. and Burland,J.B.(1985). Field and laboratory measurements of soil stiffness. Proceedings of the 11th International Conference on Soil Mechanics and Foundation Engineering, San Francisco. Vol 2, pp 511 - 514.

Jardine,R.J., Symes,M.J.R.P. and Burland,J.B.(1984). The measurement of soil stiffness in the triaxial apparatus. Geotechnique Vol 34, No 3, pp 323 - 340.

Jurgenson,L.(1940). The application of theories of elasticity and plasticity to foundation problems. Contributions to Soil Mechanics 1925 - 1940. Boston Society of Civil Engineers.

Karube,D.(1977). A stress strain time equation of normally consolidated clay. Proceedings of Speciality Session No 9, Constitutive Equations for Soils. 9th International Conference on Soil Mechanics and Foundation Engineering, Tokoyo, Vol 9, pp 105 - 112.

Keinonen,L.(1963). On the sensitivity of water laid sediments in Finland and factors inducing sensitivity. Statens Tekniska Forkningsanstalt, Helsinki. Publikasjan. No 77, p131.

Kirkpatrick,W.M, and Khan,A.J.(1984). The reaction of clays to sampling stress relief. Geotechnique Vol 34, No 1, pp 29 - 42.

Ko,H.Y.(1980). State of the art : Data reduction and applications for analytical modelling. Laboratory Shear Strength of Soils. American Society for testing and Materials, Special Technical Publication No 740.

Koustofas,D.C.(1980). Undrained behaviour of a marine clay. Laboratory Shear Strength of Soils. American Society for testing and Materials, Special Technical Publication No 740.

Ladd,C.C. and Foott,R.(1974). New design procedure for stability of soft clays. Journal of the Geotechnical Engineering Division of the American Society of Civil Engineers. Vol 100, GT 7, pp 763 - 786.

Ladd,C.C., Foott,R., Ishihara,K., Schlosser,F. and Poulos,H.G.(1977). Stress deformation and strength characteristics, state of the art report. Proceedings of the 9th International Conference on Soil Mechanics and Foundation Engineering, Tokoyo. Vol 2, pp 421 - 494.

Lade,P.V. and Duncan,J.M.(1976). Stress path dependant behaviour of cohesionless soil. Journal of the Geotechnical Engineering Division of the American Society of Civil Engineers. Vol 102, GT 1, pp 51 - 68.

Laguros,J.G.(1969). Effect of temperature on some engineering properties of clay soils. Effects of Temperature and Heat on Engineering Behaviour of Soils, Highway Research Board Special Report 103, pp 186 - 193.

Lambe,T.W.(1964). Methods of estimating settlement. Journal of the Soil Mechanics and Foundation Engineering Division, American Society of Civil Engineering, Vol 90, SM 5, pp 43 - 67.

Lambe,T.W.(1967). Stress path method. Journal of the Soil Mechanics and Foundation Engineering Division, American Society of Civil Engineering, Vol 93, SM 6, pp 309 - 332.

Lambe,T.W. and Whitman,R.V.(1979). Soil Mechanics. Wiley, 2nd edition.

Langer,K.(1936). The influence of the speed of loading increment on the pressure void ratio diagram of undisturbed soil samples. Proceedings of the 1st International Conference on Soil Mechanics and Foundation Engineering, Cambridge, Massachusetts. Vol 2, pp 116 - 120.

Lau,W.(1985). K_o consolidation and swelling and undrained loading tests on soils using the microcomputer controlled stress path testing equipment. The City University, Geotechnical Engineering Research center, research report.

Leach,G.(1985). Personal communication.

Leach,G.(1985). Personal communication.

Leonards,G.A. and Altschaefll,A.G.(1964). Compressibility of clay. Journal of the Soil Mechanics and Foundation Engineering Division, American Society of Civil Engineering, Vol 90, SM 5, pp 133 - 156.

Leonards,G.A. and Ramiah,B.K.(1959). Time effects in the consolidation of clays. American Society for testing and Materials, Special Technical Publication No 254, pp 116 - 130.

Lewin,P.I.(1970). Stress deformation characteristics of a saturated soil. MSc. thesis. University of London.

Lewin,P.I.(1978). The deformation of a soft clay under generalised stress conditions. PhD thesis, University of London.

Lewin,P.I.(1985). Personal communication.

Lewin,P.I. and Burland,J.B.(1970). Stress probe experiments on saturated normally consolidated clay. Geotechnique Vol 20, No 1, pp 38 - 56.

Lewin,P.I. and Ng,C.L.(1985). Triaxial tests on remoulded and reconstituted Cowden till . The City University, Geotechnical Engineering Research Centre, research report GE/85/19(R).

Little,J.A.(1985). Engineering properties of glacial till in the Vale of St Albans. PhD thesis, The City University.

Loudon,P.A.(1967). Some deformation characteristics of kaolin. PhD thesis, Cambridge University.

Love,A.E.H.(1942). A treatise on the mathematical theory of elasticity. 2 Vols. Cambridge University Press.

Marsland,A.(1971a). Large in-situ tests to measure the properties of stiff fissured clays. Proceedings of the 1st Australia / New Zealand Conference on Geomechanics, Melbourne. Vol 1, pp 180 - 189.

Marsland,A.(1971b). The shear strength of stiff fissured clays. Stress Strain Behaviour of Soils, Roscoe Memorial Symposium . Cambridge, Foulis. pp 59 - 68.

Marsland,A.(1972). Laboratory and in-situ measurements of the deformation moduli of London clay. Proceedings of a Symposium on the Interaction of Structure and Foundation, Birmingham. pp 7 - 71.

Marsland,A. and Eason,B.J.(1973). Measurement of displacement in the ground below loaded plates in deep boreholes. Proceedings of British Geotechnical Society Symposium, Field Testing, London.

Marsland,A and Randolph,M.F.(1977). Comparison of the results from pressuremeter tests and large in-situ plate tests in London clay. Geotechnique Vol 27, No 2, pp 217 - 243.

Martin,P.L.(1970). The influence of boundary drainage on the duration of drained triaxial tests. MSc dissertation, University of London.

Martins,J.B.(1962). Some factors controlling the consolidation of saturated soils. MSc disseration University of London.

McKinlay,D.G., McGown,A., Radwin,A.M., and Hossain,D.(1975). Representative sampling and testing in fissured lodgement tills. Proceedings of a Symposium on the Engineering Behaviour of Glacial Materials, Birmingham, pp 129 - 141.

McMannis,K.L. and Arman,A.(1979). Evaluation of design parameters obtained by conventional sampling. Proceedings of the 7th European Conference on Soil Mechanics and Foundation Engineering, Design Parameters in Geotechnical Engineering, Brighton. Vol 2, pp 81 - 86.

Mesri,G., Ullrich,C.R., and Choi,Y.K.(1978). The rate of swelling of overconsolidated clays subjected to unloading. Geotechnique Vol 28, No 2, pp 281 - 307.

Micropro.(1983). Wordstar reference manual (release 3.3). Micropro International.

Mitchell,J.K.(1969). Temperature effects on the engineering properties and behaviour of soils. Effects of Temperature and Heat on Engineering Behaviour of Soils, Highway Research Board Special Report 103, pp 9 - 28.

Mitchell,J.K.(1970). On the yielding and strength of the Leda clays. Canadian Geotechnical Journal, Vol 7, pp 297 - 312.

Molenkamp,F. and Luger,H.J.(1981). Modelling and minimisation of membrane penetration effects in tests on granular soils. Geotechnique Vol 31, No 4, pp 471 - 486.

Morgenstern,N.R. and Phukan,A.L.T.(1968). Stresses and displacements in a homogeneous non - linear foundation. Proceedings of International Symposium on Rock Mechanics, Madrid. pp 313 - 320.

Moretto,O.(1946). An investigation of the effect of certain factors on the strength and compressibility of clays. PhD thesis, University of Illinois.

Mroz,Z., Norris,V.A. and Zienkiewicz,O.C.(1979). Application of an anisotropic hardening model in the analysis of elasto - plastic deformation of soils. Geotechnique Vol 29, No 1, pp 1 - 34.

Mroz,Z., Norris,V.A. and Zienkiewicz,O.C.(1981). An anisotropic, critical state model for soils subject to cyclic loading. Geotechnique Vol 31, No 4, pp 451 - 470.

Nadai,A.L.(1931). The flow and fracture of solids. Vol 1. McGraw - Hill.

Namy,D.(1970). An investigation into certain aspects of stress strain relationships for clay soils. PhD thesis,Cornell University.

Naylor,D.J., Pande,G.N., Simpson,B. and Tabb,R.(1981). Finite elements in geotecnical engineering. Pineridge Press, Swansea.

Newmark,N.M.(1935). Simplified computations for vertical pressure in elastic foundations. University of Illinois. Engineering Experimental Station Bulletin 429.

Newmark,N.M.(1942). Influence charts for computation of stresses and strains in elastic foundations. University of Illinois. Engineering Experimental Station Bulletin 338.

Ng,C.L.(1982). Review of constitutive models for soils, MSc dissertation , University of London.

Ng,C.L.(1984). Personal communication .

Ng,C.L.(1985). Report on progress in first year of research on strength and deformation characteristics of Cowden till. The City University, Geotechnical Engineering Research Centre, research report GE/85/7.

Ng,C.L.(1986). Personal communication.

Nova,R.(1982). A constitutive model for soil under monotonic and cyclic loading. Soil Mechanics - Transient and Cyclic Loads, Constitutive Relations and Numerical Treatment. Ed. G.N.Pande and O.C.Zienkiewicz. pp 343 - 374.

Ohta,H.(1973). An extended Cam clay model. Proceedings of a Symposium on the Role of Plasticity in Soil Mechanics, Cambridge. pp 136 - 214.

Parry,R.H.G.(1979). Discussion. Design Parameters in Geotechnical Engineering. Proceedings of 7th European Conference on Soil Mechanics and Foundation Engineering, Brighton. Vol 4, pp 129 - 131.

Parry,R.H.G. and Amersinghe,S.F.(1973). Components of deformation in clays. Proceedings of a Symposium on the Role of Plasticity in Soil Mechanics, Cambridge. pp 108 - 126.

Peck,R.B.(1969). Deep excavations and tunneling in soft ground. Proceedings of the 7th International Conference on Soil Mechanics and Foundation Engineering, Mexico. State of the Art Volume. pp 225 - 290.

Pender,M.J., Parry,R.H.G. and George,P.J.(1975). The response of a soft clay layer to embankment loading. Proceedings of the 2nd Australian / New Zealand conference on Geomechanics, Brisbane. pp 169 - 173.

Pender,M.J.(1977). A unified model for soil behaviour. Proceedings of the 9th International Conference on Soil Mechanics and Foundation Engineering, Tokoyo. Vol 2, pp 213 - 222.

Pender,M.J.(1978). A model for the behaviour of overconsolidated soil. Geotechnique Vol 28, No 1, pp 1 - 26.

Pickering,D.J.(1970). Anisotropic elastic parameters for soil. Geotechnique Vol 20, No 3, pp 271 - 276.

Plum,R.L. and Esrig,M.I.(1969). Some temperature effects on soil compressibility and pore water pressure. Effects of Temperature and Heat on Engineering Behaviour of Soils, Highway Research Board Special Report 103, pp 231 - 242.

Poulos,H.G. and Davis,E.H.(1974). Elastic solutions for soil and rock mechanics. Wiley (New York).

Poulos,S.J.(1964). Control of leakage in the triaxial test. Harvard Soil Mechanics Series No 71.

Rao,N.B.S., Yudhbir, Madhav,M.R.(1983). Influence of stress history on the experimental flow rule. Geotechnical Journal of the American Society of Testing and Materials. Vol 6, No 1, pp 42 - 45.

Raymond,G.P.(1970). Discussion on:- Barden,L. Stresses and displacements in a cross anisotropic soil. Geotechnique Vol 20, No 4, pp 456 - 458.

Rendulic,L.(1937). Ein grundgesetz der ton-mechanik und sein experimentaller bewis. Bauingenieur Vol 18, pp 459 - 467.

Richardson,D.(1982). The geotechnical properties of the Ware Till. The City University, Undergraduate final year project.

Richardson,D.(1984a). Effects of stress path on the strength and stiffness of soils near retaining walls. The City University, Geotechnical Engineering Research Centre, research report GE/84/4.

Richardson,D.(1984b). The importance of natural strains in soil mechanics. The City University, Geotechnical Engineering Research Centre, research report GE/84/23.

Richardson ,D.(1986). Effect of membrane and filter paper stiffness on the stress strain behaviour of triaxial samples. The City University, Geotechnical Engineering Research Centre, research report GE/86/4.

Robinson,P.J.(1984). Report on research work completed to date on the anisotropic stress strain properties of kaolin consolidated under conditions of zero lateral strain. The City University, Geotechnical Engineering Research Centre.

Robinson,P.J.(1985). Personal communication.

Roscoe,K.H.(1970) The influence of strains in soil mechanics. The 10th Rankine Lecture. Geotechnique Vol 20, No 2, pp 129 - 170.

Roscoe,K.H., Bassett,R.H., and Cole,E.R.L.(1967). Principal axes observed during simple shear of a sand. Proceedings of Geotechnical Conference, Oslo. Vol 1, pp 231 - 237.

Roscoe,K.H. and Burland,J.B.(1968). On the generalised stress strain behaviour of "wet clay". Engineering Plasticity, Ed. J.Heyman, F.A.Leckie. Cambridge University Press. pp 535 - 609.

Roscoe,K.H. and Poorooshasb,H.B.(1963). A theoretical and experimental study of strains in triaxial compression tests on normally consolidated clays. Geotechnique Vol 13, No 1, pp 12 - 38.

Roscoe,K.H., Schofield,A.N. and Thurairajah,A.(1963a). Yielding of clays in states wetter than critical. Geotechnique Vol 13, No 3, pp 211 - 239.

Roscoe,K.H., Schofield,A.N. and Thurairajah,A.(1963b). An evaluation of test data for selecting a yield criterion for soils. Laboratory Shear Testing of Soils, Special Technical Publication No 361, American Society for Testing and Materials. pp 111 - 128.

Roscoe,K.H., Schofield,A.N. and Wroth,C.P.(1958). On yielding of clays. Geotechnique Vol 8, No 1, pp 22 - 53.

Rowe,P.W.(1963). Stress dilatancy, earth pressures and slopes. Journal of the Soil Mechanics and Foundation Engineering Division, American Society of Civil Engineering, Vol 89, SM 3, pp 37 - 62.

Rowe,P.W.(1969). The relationship between the strength of sands in the triaxial compression, plane strain and direct shear. Geotechnique Vol 19, No 1, pp 75 - 86.

Rowe,P.W.(1971). Theoretical meaning and observed values of deformation parameters for soil. Proceedings of the Roscoe Memorial Symposium on the Stress Strain Behaviour of Soils, Cambridge. Foulis. pp 143 - 194.

Rowe,P.W. and Barden,L.(1964). Importance of free ends in triaxial testing. Journal of the Soil Mechanics and Foundation Engineering Division, American Society of Civil Engineering, Vol 90, SM 1, pp 1 - 27.

Ryder,G.H.(1978). Strength of materials. 3rd edition . MacMillan Press.

Sandroni,S.S.(1977). The undrained shear strength of London Clay in total and effective stress terms. PhD thesis, University of London.

Sarsby,R.W., Kaleziotis,N. and Haddad,E.H.(1980). Bedding error in triaxial tests on granular material. Geotechnique Vol 30, No 3, pp 302 - 309.

Seed,H.B., Duncan,J.M. and Idriss,I.M.(1975). Criteria and methods for static and dynamic analysis of earth dams. Proceedings of International Symposium on Criteria and Assumptions for Numerical Analysis of Dams,. Eds D.J. Naylor, A.Stagg, O.C.Zienkiewicz. Swansea. pp 564 - 568.

Schofield,A.N. and Wroth,C.P.(1968). Critical state soil mechanics. McGraw - Hill.

Schumattmann,J.H.(1981). A general time related soil friction increase phenomenon. American Society of Testing and Materials, Special Technical Publication 740. pp 456 - 484.

Scott,C.R.(1980). An introduction to soil mechanics and foundations. 3rd edition. Applied Science Publishers.

Scott,R.F.(1963). Principles of soil mechanics. Addison Wesley.

Shitiba,T. and Karube,D.(1965). Influence of the variation of the intermediate principal stress on the mechanical properties of normally consolidated clays. Proceedings of the 6th International Conference on Soil Mechanics and Foundation Engineering, Montreal. Vol 1, pp 359 - 363.

Shimizu,M.(1981). Factors affecting the measurement of volume change of cohesive soils in drained triaxial tests. Soils and Foundations, Journal of the Japanese Society of Soil Mechanics and Foundation Engineering, Vol21, No 2, pp 121 - 128.

Sills,G.C., Burland,J.B. and Czechowski,M.K.(1977). Behaviour of an anchored diaphragm wall in stiff clay. Proceedings of the 9th International Conference on Soil Mechanics and Foundation Engineering, Tokoyo. Vol 2, pp 147 - 155.

Simons,N.E.(1970). The stress path method of settlement analysis applied to London Clay. Proceedings of the Roscoe Memorial Symposium on the Stress Strain Behaviour of Soils, Cambridge. Foulis. pp 241 - 252.

Simons,N.E.(1984). Discussion. Proceedings of 20th Regional Meeting on Site Investigation Practice:Assesing BS5930. Engineering Group of the Geotechnical Society. Vol 2, p 103.

Simpson,B.(1973). Finite elements applied to problems of plane strain deformation in soils. PhD thesis, University of Cambridge.

Simpson ,B., Atkinson,J.H. and Richardson,D.(1986). Discussion session 1A. Proceedings of the 11th International Conference on Soil Mechanics and Foundation Engineering, San- Francisco . In Press.

Simpson,B., Calabresi,G., Sommer,H. and Wallays,M.(1980). Design parameters for stiff clays. General Report, Proceedings of 7th European Conference on Soil Mechanics and Foundation Engineering, Brighton. Vol 1, pp 91 - 125.

Simpson,B., O'Riorden,N.J. and Croft,D.D.(1979). A computer model for the analysis of ground movements in London clay. Geotechnique Vol 29, No 2, pp 149 - 175.

Singh,A. and Mitchell,J.K.(1968). General stress strain time functions for soils. Journal of the Soil Mechanics and Foundation Engineering Division, American Society of Civil Engineering, Vol 94, SM 1, pp 21 - 44.

Skempton,A.W.(1954). The pore pressure parameters A and B. Geotechnique Vol 4, No 4, pp 143 - 147.

Skempton,A.W.(1961). Horizontal stresses in an overconsolidated Eocene clay. Proceedings of the 1st International Conference on Soil Mechanics and Foundation Engineering, Cambridge, Massachusetts. Vol 1, pp 351 - 357.

Skempton,A.W.(1964). Long term stability of clay slopes. Geotechnique Vol 14, No 1, pp 77 -102.

Skempton,A.W. and Bjerrum,L.(1957). A contribution to the settlement analysis of foundations on clay. Geotechnique Vol 7, No 2, pp 168 - 178.

Skempton,A.W. and Sowa,V.A.(1963). The behaviour of saturated clays during sampling and testing. Geotechnique Vol 13, No 2, pp 269 - 290.

Som,N.N.(1968). The effect of stress path on the deformation of London Clay. PhD thesis, University of London.

Souto Silveiro,E.B.(1967). Thoughts concerning the applicability of elasticity to soils. Proceedings of the 3rd Pan - American Conference on Soil Mechanics and Foundation Engineering. Vol 1, pp 3 - 27.

Steinbrenner,W.(1934). Tafeln zur setzenberechnung. Die Strasse, Vol1.

St John,H.D.(1975). Field and theoretical studies of the behaviour of ground around deep excavations in London clay. PhD thesis, University of London.

Symes,M.J.R.P.(1983). Rotation of principal stresses in sands, PhD thesis, University of London.

Tamai,T. and Namura,K.(1973). Stress probe tests on soils. Proceedings of Annual Meeting of the Japanese Society of Civil Engineers. pp 72 - 73.

Tavenas ,F. and Leroueil,S.(1979). Clay behaviour and the selection of design parameters. Design Parameters in Geotechnical Engineering. Proceedings of 7th European Conference on Soil Mechanics and Foundation Engineering, Brighton. Vol 1, pp 281 - 291.

Taylor,D.W.(1941). Research on the consolidation of clays. MIT Department of Civil and Sanitary Engineering. Serial 82.

Taylor,D.W.(1948). Fundamentals of soil mechanics. New York.

Terzaghi,K.(1936). The shearing resistance of saturated soils and the angle between planes of shear. Proceedings of the 1st International Conference on Soil Mechanics and Foundation Engineering, Cambridge, Massachusetts. Vol 1, pp 54 - 56.

Terzaghi,K.(1941). Undisturbed clay samples and undisturbed clays. Journal of the Boston Society of Civil Engineers. Vol 28, No 3.

Terzaghi,K. and Peck,R.B.(1967). Soil mechanics in engineering practice. Wiley, New York. 2nd edition.

Ting,W.H.(1968). Some effects of history on the stress strain behaviour of kaolin. PhD thesis, Cambridge University.

Tombs,S.G.(1969). Strength and deformation characteristics of rock fill. PhD thesis, University of London.

Van-Wambeke,A.(1980). Discussion. Design Parameters in Geotechnical Engineering. Proceedings of 7th European Conference on Soil Mechanics and Foundation Engineering, Brighton. Vol 4, p141.

Varadarajan,A. and Mishra,S,C.(1980). Stress path dependent stress strain volume change behaviour of a granular soil. Proceedings of International Symposium on Soils Under Cyclic and Transient Loading. Modelling of Cyclic and Transient Behaviour in the Laboratory, Ed. G.N.Pande, O.C.Zienkiewicz. Swansea. Vol 1.1. pp 109 - 120.

Vennard,J.K. and Street,R.L.(1976). Elementary fluid mechanics. 5th edition. Wiley, New York.

Vrymoed,J., Bennett,W., Jafroudi,S. and Chen,C.K.(1980). Cyclic strength and shear modulus as a function of time. Proceedings of International Symposium on Soils Under Cyclic and Transient Loading. Modelling of Cyclic and Transient Behaviour in the Laboratory, Ed. G.N.Pande, O.C.Zienkiewicz. Swansea. Vol 1.1. pp135 - 142.

Wainwright,A.(1965). The Western Fells, Book 7. Westmorland Gazette.

Wainwright,A.(1967). A Pennine Way Companion. Westmorland Gazette.

Wainwright,A.(1970). A Coast to Coast Walk. Westmorland Gazette.

Wainwright,A.(1972). Fellwanderer. Westmorland Gazette.

Wainwright,A.(1973). The Outlying Fells. Westmorland Gazette.

Wainwright,A.(1987). Ex-Fellwanderer. Westmorland Gazette.

Ward,W.H. and Burland,J.B.(1973). The use of ground strain measurements in civil engineering. Building Research Establishment, Current paper 13 / 73.

Ward,W.H., Marsland,A. and Samuels,S.G.(1965). Properties of the London Clay at Ashford Common shaft. In-situ and undrained strength tests. Geotechnique Vol 15, No 4, pp 321 - 344.

Ward,W.H., Samuels,S.G. and Butler,M.E.(1959). Further studies of the properties of London Clay. Geotechnique Vol 9, No 2, pp 33 - 38.

Wallays,M.(1980). Discussion. Design Parameters in Geotechnical Engineering. Proceedings of 7th European Conference on Soil Mechanics and Foundation Engineering, Brighton. Vol 4, pp 121 - 125.

Webb,D.L.(1966). The mechanical properties of undisturbed samples of London Clay and Pierre shale. PhD thesis, University of London.

Wei,R.L.(1981). Constitutive laws of normally consolidated clay. Proceedings of the 10th International Conference on Soil Mechanics and Foundation Engineering, Stockholm. Vol 1, pp 269 - 272.

Wesley,L.D.(1975). Influence of stress path and anisotropy on the behaviour of a soft alluvial clay. PhD thesis, University of London.

Windle,D. and Wroth,C.P.(1977). In - situ measurements of the properties of stiff clays with a self boring instrument. Proceedings of the 9th International Conference on Soil Mechanics and Foundation Engineering, Tokoyo. Vol 1, pp 347 - 352.

Wong,R.K.S. and Arthur,J.R.F.(1985). Induced and inherent anisotropy in sand. Geotechnique Vol 35, No 4, pp 471 - 482.

Wood,D.M.(1974). Some aspects of the mechanical behaviour of kaolin under truely triaxial conditions of stress and strain. PhD thesis, Cambridge University.

Wood,D.M.(1984). On stress and strain parameters. Geotechnique Vol 34, No 2, pp 282 - 287.

Woods,R.I.(1985a). Evaluation of soil stiffness from triaxial test data. The City University, Geotechnical Engineering Research Centre, research report GE/85/12.

Woods,R.I.(1985b). Link, (version 85.5) Epson-Spectra data capture program user manual. The City University, Geotechnical Engineering Research Centre, research report GE/85/10.

Woods,R.I.(1985c). Spectran, (version 85,4) Analysis of triaxial test data user manual. The City University, Geotechnical Engineering Research Centre, research report GE/85/11.

Woods,R.I.(1985d). Inspectra (version 84.5) Input, editing and disk storage of triaxial test data user manual. The City University, Geotechnical Engineering Research Centre, research report GE/85/9.

Woods,R.I.(1986a). Applications of critical state soil mechanics : interim report. The City University, Geotechnical Engineering Research Centre, research report in preparation.

Woods,R.I.(1986b). Finite element analysis of coupled loading and consolidation. Proceedings of 2nd International Symposium on Numerical Models in Geomechanics, Ghent. In press.

Woods,R.I.(1986c). Personal communication.

Wroth,C.P.(1971). Some aspects of the elastic behaviour of overconsolidated clay. Proceedings of the Roscoe Memorial Symposium on the Stress Strain Behaviour of Soils, Cambridge. Foulis. pp 347 - 361.

Wroth,C.P.(1984). The interpretation of in- situ soil tests. The 24th Rankine Lecture. Geotechnique Vol34, No 4, pp 447 - 492.

Wroth,C.P. and Houlsby,G.T.(1985). Soil mechanics property characteristics and analysis procedures. Proceedings of the 11th International Conference on Soil Mechanics and Foundation Engineering, San Francisco. Vol 1, pp 1 - 55.

Wroth,C.P. and Hughes,J.M.(1973). An instrument for the in- situ measurement of the properties of soft clays. Proceedings of the 8th International Conference on Soil Mechanics and Foundation Engineering, Moscow. Vol 1.2, pp 487 - 494.

Wroth,C.P., Randolph,M.F., Houlsby G.T. and Fahey,M.(1979). A review of the engineering properties of soils with particular reference to the shear modulus. CUED / D - soils TR75, Cambridge.

Zytinski,M., Randolph,M.F., Nova,R. and Wroth,C.P.(1978). On modelling the unloading-reloading behaviour of soils. International Journal of Numerical and Analytical Methods in Geomechanics, Vol 2, No 1, pp 87 - 93.

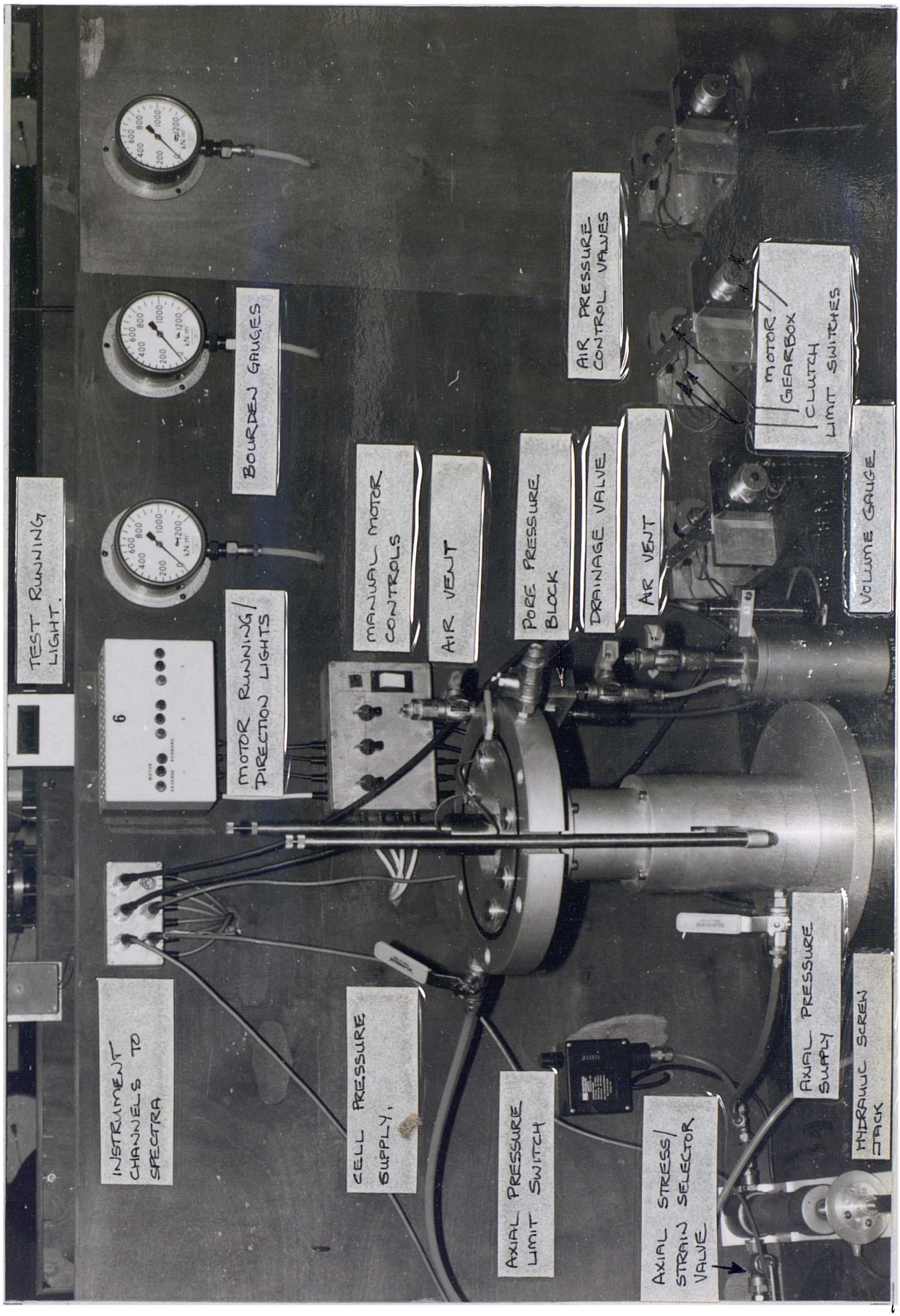

Plate 5.1 General view of the Bishop and Wesley triaxial cell.

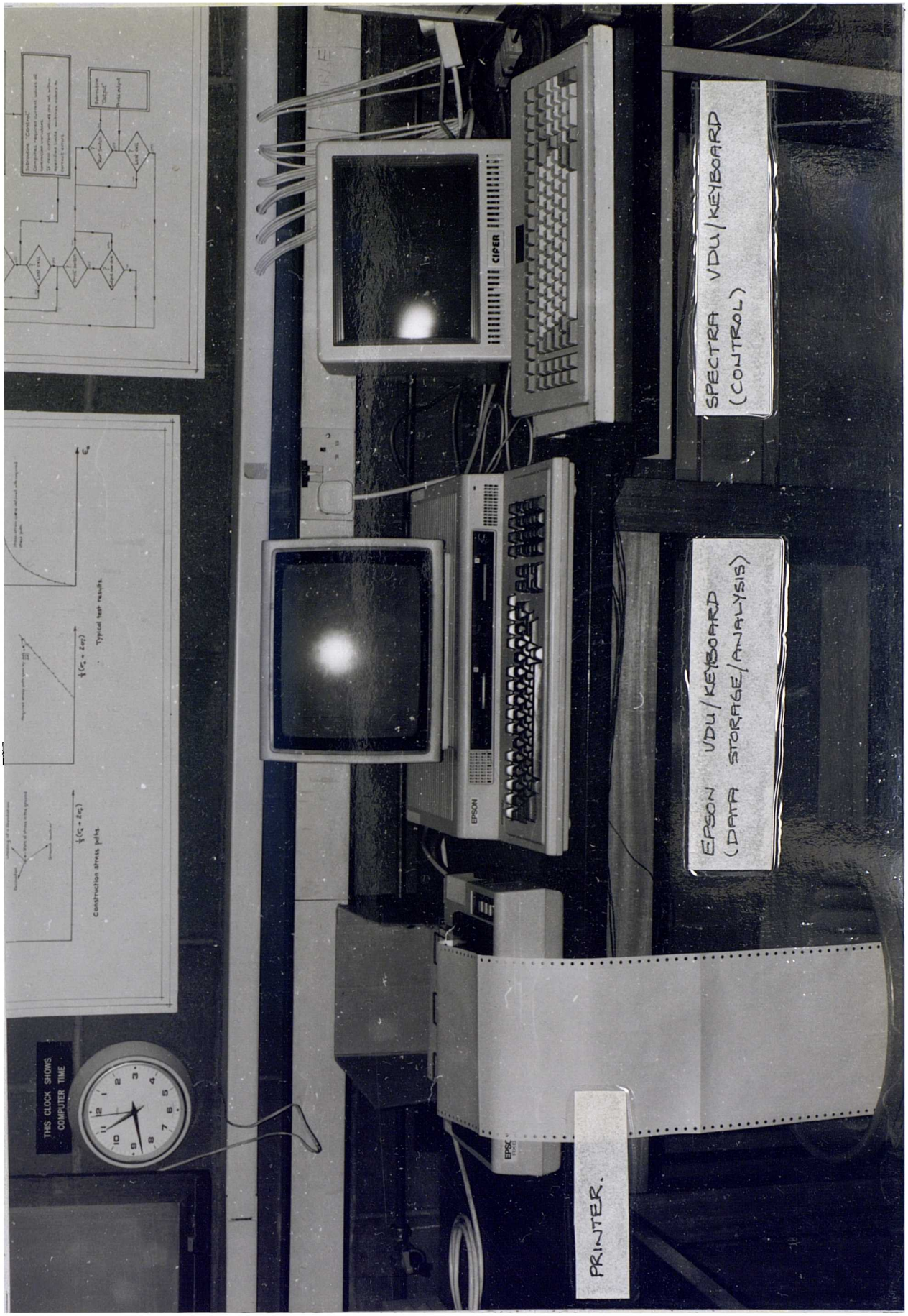

Plate 5.2 The Spectra-Epson system.

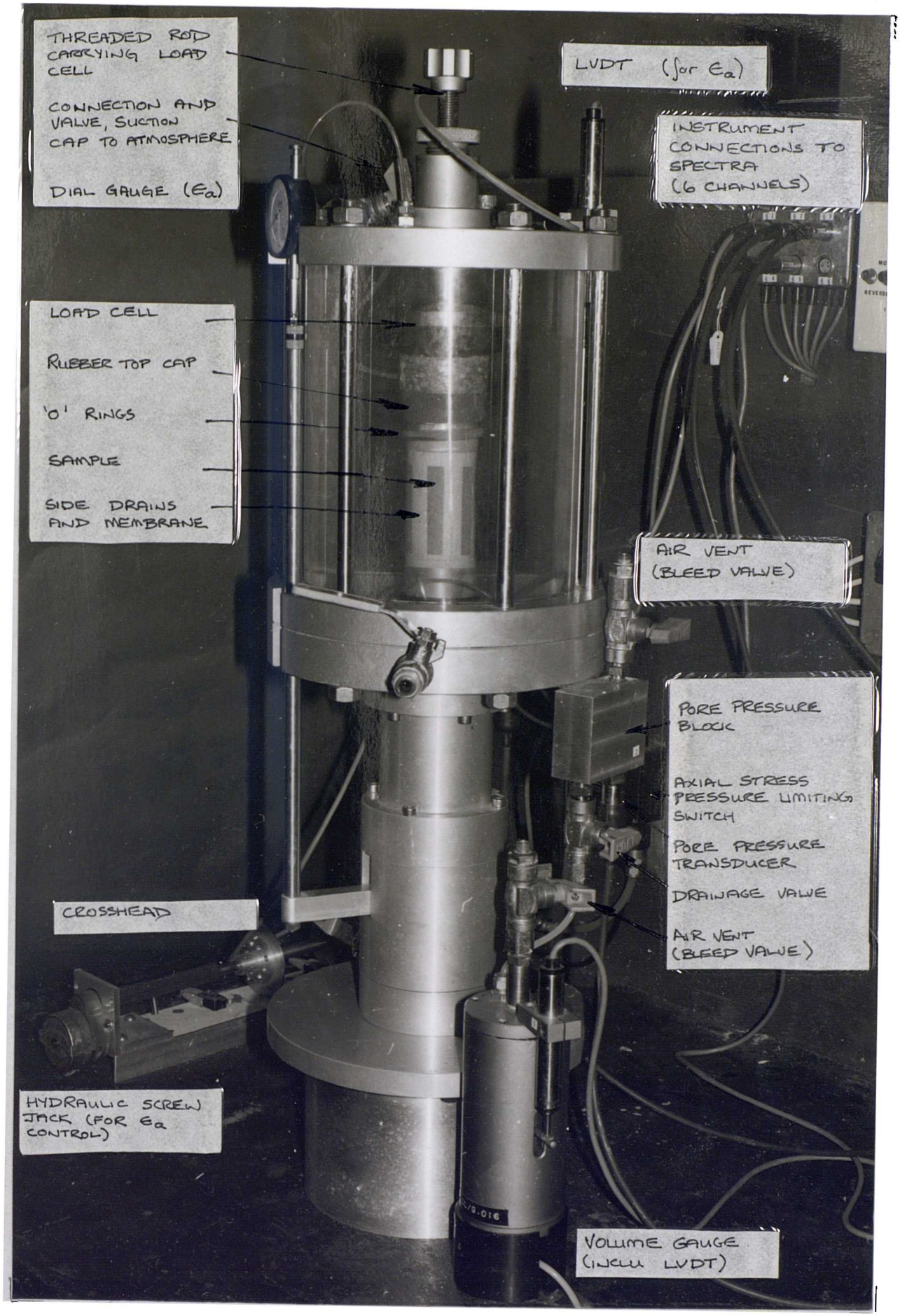

Plate 7.1 Sample set up in the Bishop and Wesley triaxial cell.

	$\frac{(E_u)_{0.01\%}}{p'_o}$	$L = \frac{E_{u(0.1)\%}}{E_{u(0.01)\%}}$	OCR	p'_o (kPa)
'In Situ'				
R1	830	0.185	1	267
R1.4	2180	0.270	1.4	206
R2	2270	0.353	2.05	158
R4	2130	0.386	3.73	106
R8	1740	0.407	7.4	65
After 'Perfect Sampling'				
PS1	1371	0.404	1*	193
PS8	852	0.58	7.4*	62
After 'Block Sampling'				
IS1	1661	0.435	2*	55
IS2	1436	0.42	2*	72
After 'Tube Sampling'				
I1 (UU)	1080	0.333	1.1^+	474
I2 (Reconsolidated)	1460	0.187	1.1^+	508
I3 (UU)	2030	0.340	$> 50^+$	46

* before sampling

\+ estimated

Table 2.1 Effect of disturbance on sample stiffness (Hight, Gens and Jardine, 1985).

Test	E_u (kPa)	p'_o (kPa)	v	c_u (kPa)	$\frac{E_u}{vp'_o}$	$\frac{E_u}{c_u}$	Notes
5102	5200	50	1.798	62.5	61.2	133	σ_r constant σ_a increasing
5101	17500	200	1.793	133	50.6	132	σ_r constant σ_a increasing
5103	13600	400	1.699	170.5	20.0	80.0	σ_r constant σ_a increasing
6100	15300	200	1.728	113	44.2	135	σ_r constant σ_a reduced
6102	6000	200	1.724	120	17.4	50	σ_r constant σ_a reduced

Notes (1) E_u defined at 1% axial strain.

(2) All tests undrained.

(3) All samples one dimensionally compressed and swelled.

Table 2.2 Summary of stiffness parameters for reconstituted London Clay (Richardson, 1984a)

Name	Material	Sample preparation	Consolidation details	OCR before shearing	p_0' (initial): kPa
R1	North Sea clay	Reconstituted	K_0 (see Fig. 6)	1·0	267
R1·4	North Sea clay	Reconstituted	K_0 (see Fig. 6)	1·4	206
R2	North Sea clay	Reconstituted	K_0 (see Fig. 6)	2·05	158
R4	North Sea clay	Reconstituted	K_0 (see Fig. 6)	3·73	106
R8	North Sea clay	Reconstituted	K_0 (see Fig. 6)	7·4	65
I1	North Sea clay	Intact	Lightly overconsolidated in situ, then sampled	≃1·1	474
I2	North Sea clay	Intact	As above, reconsolidated 'field stresses'	≃1·1	508
I3	North Sea clay	Intact	Heavily overconsolidated in field. Swelled back after sampling	>50	46
RM1	North Sea clay	Remoulded LI = 0·18	Not consolidated	—	10
RM2	North Sea clay	Remoulded LI = 0·09	Not consolidated	—	43
HRS1	Ham river sand	Pluviated R_D = 0·749	Isotropically consolidated	4	132
HRS2	Ham river sand	Pluviated R_D = 0·848	Isotropically consolidated	1	404
LC1	London clay	Intact	Overconsolidated in situ then sampled	—	226
LC2	London clay	Intact	As above	—	199
C1	Upper Chalk	Intact	Cut from quarry face isotropically consolidated	—	345
C2	Upper Chalk	Intact	As above	—	363

Table 2.3 Summary of tests by Jardine et al (1984).

TIn	Threshold test on isotropically compressed sample with overconsolidation ratio = n.
TKn	Threshold test on one dimensionally compressed sample with overconsolidation ratio = n.
TAn	Threshold test on anisotropically compressed sample (other than one dimensionally compressed), with overconsolidation ratio = n.
Sn	Test to establish state boundary surface with overconsolidation ratio = n.
C	Test involving compression and swelling only.

Table 4.1 Abbreviations of test types.

Function	Instrument	Range	Instrument number	Resolution
Axial stress σ_a	Imperial college Skinner load cell. Non - linearity ±0.5% F.R. Hysteresis ±0.5% F.R. Zero shift and temperature shift ±0.035% F.R. / °C	± 3000kPa	Cell 1 844 Cell 3 846 Cell 5 852 Cell 6 748	0.027kPa
Pore pressure u	Druck POCR 10 Non - linearity and hysteresis ±0.1% F.R. Zero shift and temperature shift ±0.5% F.R.	±1000kPa	Cell 1 57928 Cell 3 57932 Cell 5 57936 Cell 6 57929	0.049kPa
Radial stress σ_r	As above	± 1000kPa	Cell 1 57926 Cell 3 57930 Cell 5 57831 Cell 6 57937	0.049kPa
Axial strain ε_a	MPE L.V.D.T. transducer, HS25 Non - linearity ±0.1% F.R. Hysteresis ±0.02% F.R. Zero shift and temperature shift ±0.005% F.R. / °C	40% -	-	0.0008%
Volumetric strain ε_v	Imperial college 50cc volume gauge. (incorporates L.V.D.T. HS25)	40%	Cell 1 G,002 Cell 3 G,007 Cell 5 G,006 Cell 6 G,016	0.0008%
Radial strain ε_r	Calculation	-	- -	

Table 5.1 Summary of instrumentation and resolution of instrumentation in the Bishop and Wesley triaxial cell / SPECTRA system

Function	Actual Reading (A = (D +I)/2)		Required	Mean	Hysteresis
	Increasing (I)	Decreasing (D)	Reading (R)	Difference (A-R)	(D-I)
σ_a (kPa)	-0.1	-0.7	0	-0.4	0.6
Compression	3.8	3.4	4.32	-0.72	-0.4
	12.1	11.9	12.97	-0.97	-0.2
	37.8	37.8	38.92	-1.12	0
	85.2	85.6	86.0	-0.6	-0.4
	171.7	173.3	173.0	-0.5	-1.6
	260.3	258.3	259.0	0.3	-2.0
	346.7	346.4	346.0	0.6	-0.3
σ_a (kPa)	-0.4	0.1	0	-0.15	0.5
Extension	-4.7	-4.3	-4.32	-0.18	0.4
	-13.5	-12.0	-12.97	-0.22	0.5
	-39.8	-39.3	-38.92	-0.63	0.5
	-87.5	-87.0	-86.0	-1.25	0.5
	-174.8	-174.5	-173.0	-1.65	0.3
	-262.5	-262.0	-259.0	-3.2	0.4
	-347.6	-345.1	-346.0	-0.35	0.5
u (kPa)	0	0	0	0	0
	100.4	101.2	100.0	0.8	0.8
	198.9	200.2	200.0	-0.45	1.3
	301.0	300.8	300.0	0.9	0.2
	402.3	402.1	400.0	2.2	0.2
	606.0	-	600.0	6.0	-
σ_r (kPa)	0	-0.1	0	-0.05	-0.1
	100.5	101.3	100.0	0.9	0.8
	199.2	199.3	200.0	-1.75	0.1
	301.4	301.2	300.0	1.3	-0.2
	402.8	403.0	400.0	2.9	0.2
	606.8	-	600.0	6.8	-
ε_a (%)	0	0	0	0	0
	1.31	1.31	1.32	-0.01	0
	2.65	2.61	2.63	0	0.04
	6.55	6.54	6.58	-0.035	-0.01
	13.14	13.12	13.16	-0.03	-0.02
	19.45	-	19.49	-0.04	-
ε_v (%)	0	-0.01	0	-0.005	-0.01
	1.27	1.26	1.29	-0.025	-0.01
	2.56	2.54	2.58	-0.03	-0.02
	6.44	6.43	6.46	-0.025	-0.01
	12.91	12.9	12.92	-0.015	-0.01
	19.41	19.39	19.38	-0.02	-0.02
	26.05	-	26.04	0.01	-

Table 6.1 Results from a typical instrument calibration check.

Function	Observed behaviour			Comments
	Noise	Drift	Accuracy	
σ_a	± 0.5 kPa	± 3 kPa	± 5 kPa	
u	± 0.5 kPa	± 1 kPa	± 1 kPa	
σ_r	± 0.5 kPa	± 1 kPa	± 1 kPa	
ε_a	0	± 0.02 %	± 0.02 %	
ε_v	0	± 0.03 %	± 0.03 %	
ε_r	-	-	-	Calculation

Table 6.2 Summary of the accuracy of instrumentation in the Bishop and Wesley triaxial cell.

Soil	LL (%)	PL (%)	PI (%)	G_s	Reference
London clay	70	27	43	2.75	This thesis
	75	30	45	2.75	Schofield and Wroth (1968)
Cowden till	35	17	18	2.65	Ng (1984)
Speswhite kaolin	65	35	30	2.60	Robinson (1983)
Ware till	39	22	17	2.61	Richardson (1982)
	37	21	16	2.63	Little (1985)
Slate dust	29	18	11	2.78	Lewin (1970)

Table 7.1 Summary of soil index properties.

Soil	λ	κ	N	M	Γ	Reference
London clay	0.161	0.062	-	0.888	2.448	Schofield and Wroth (1968).
Cowden till	0.0845	0.013	1.875	1.26	1.810	Ng (1984).
Speswhite kaolin	0.190 0.180	0.05 -	3.26 3.22	0.95 0.97	3.16 3.10	Robinson (1985). Ng (1986).
Ware till (1) (1) (2)	0.079 0.065 0.070	0.019 0.030 0.019	2.036 1.863 1.695	1.021 0.84 0.86	1.957 1.845 1.680	Richardson (1983). Little (1985). Little (1985).
Slate dust	0.078 (3)	0.0108 (3)	-	1.044 (4)	-	Lewin (1970).

Notes:- (1) Results from remoulded samples.

(2) Results from undisturbed samples.

(3) From values of compression index (C_c) and swelling index (C_s).

(4) From value of ϕ'.

All values of M quoted are for compression states.

Table 7.2 Summary of compression and swelling parameters for the soils under test.

Soil	Mass of dry soil (g)	Mass of water (g)	Slurry water content (%)	Typical sample water content (%)
London clay	115	104	90	42
Ware till	115	98	85	32
Cowden till	115	92	80	32
Slate dust	135	108	80	30
Speswhite kaolin	100	150	150	57

Table 7.3 Target slurry water content and mix quantities.

Soil / Test Number / Test type		Water content (%) Slurry	Water content (%) Sample	Length (mm)	Diameter (mm)	γ (KN/m^3)	Mass (g)
Slate dust							
5128	C	83.48	30.17	72.50	37.90	18.81	156.83
5129	TI2	76.82	32.52	82.70	37.90	18.35	174.51
5130	TI2	81.44	29.97	79.30	37.90	18.93	172.65
5131	TI2	81.21	30.40	76.10	37.90	18.65	163.20
5132	TI2	79.64	30.43	75.30	37.90	18.77	162.58
6197	C	80.54	31.08	75.90	37.90	18.81	164.20
6198	C	79.96	30.94	76.20	37.90	19.07	167.11
6219	TI2	80.46	30.40	77.80	37.90	18.73	167.61
Ware till.							
6195	C	84.67	31.60	76.10	37.90	17.50	153.16
6196	C	84.88	32.05	74.90	38.04	17.28	149.96
6203	TI2	82.97	31.64	76.41	38.04	16.74	148.19
6204	TI2	84.76	33.08	77.40	37.90	17.97	159.92
6205	TI2	85.68	32.09	76.40	37.90	17.34	152.35
6206	TI2	84.50	31.42	72.30	37.90	17.60	146.34
6207	TI2	84.23	33.27	79.50	37.90	17.46	159.65
5120	TI2	88.59	31.74	73.80	37.90	17.74	150.58
Speswhite kaolin							
3101	C	152.10	57.84	75.20	38.04	16.39	142.80
3102	C	149.61	57.10	75.90	38.04	16.27	143.10
5123	TI2	149.95	57.91	76.40	37.90	16.25	142.74
5137	TI2	153.48	57.32	79.60	37.90	15.92	145.72
6220	TI2	151.80	57.64	76.70	37.90	15.95	140.66
6221	TI2	151.82	57.62	79.80	37.90	15.94	146.32
6224	TI2	149.58	56.13	67.40	37.90	15.79	122.41
Cowden till							
3104	C	79.64	31.61	75.00	37.90	17.35	149.61
3106	C	81.29	33.16	74.80	37.90	17.14	147.42
3252	TI2	80.76	31.41	76.10	38.04	17.15	151.20
3253	TI2	78.24	32.09	75.40	38.04	16.96	148.11
3254	TI2	80.64	32.17	75.90	37.90	17.12	149.43
3255	TI2	81.98	31.74	76.15	38.04	17.03	150.20
London clay							
1200	TI2	93.44	43.10	76.00	38.04	17.44	152.52
1201	TI2	91.07	43.30	78.62	38.04	16.60	151.18
1210	S20	89.67	42.90	78.20	37.90	17.02	153.05
3250	TI2	92.52	42.83	75.80	37.90	16.48	143.67
3251	TI2	88.76	43.18	76.10	37.90	17.40	152.30
3257	TI2	90.47	45.04	78.00	37.90	17.06	153.07
3258	TI2	91.22	42.80	74.80	37.90	16.98	146.08
3260	TI2	89.80	41.91	75.20	37.90	16.99	146.92
3261	TI2	92.47	43.56	77.60	37.90	17.13	152.88
3277	S1	90.86	43.48	76.20	37.90	17.41	152.54
3275	S1	91.21	41.62	76.40	37.90	17.43	153.09
3300	C	91.04	44.74	80.30	37.90	17.49	161.51
3301	S10	89.85	41.95	76.40	37.90	17.12	150.34
3302	S40	90.62	41.43	79.50	37.90	17.45	159.55
5112	C	91.27	44.62	76.50	37.90	17.12	150.62
5113	C	88.93	42.95	75.90	38.04	17.08	150.18

Table 7.4 Water content, mass and dimensions of samples produced from a slurry (page 1 of 2).

Soil / Test Number / Test type		Water content (%)		Length (mm)	Diameter (mm)	γ (KN/m^3)	Mass (g)
		Slurry	Sample				
5115	C	91.24	44.89	76.60	38.04	17.04	151.26
5116	C	91.46	43.50	77.10	38.04	17.07	152.51
5117	TI2	89.70	45.88	75.40	38.09	16.58	145.28
5118	TI2	90.27	40.18	72.40	38.04	17.53	147.04
5119	TI2	89.94	42.68	74.30	37.90	17.57	150.23
5121	TA2	90.01	43.45	76.30	37.90	17.21	151.00
5122	TA2	91.12	42.92	78.30	37.09	17.51	157.67
5123	S1	91.13	42.90	75.40	37.90	16.85	146.09
5124	S1	94.01	46.76	81.20	37.90	16.72	156.17
5125	S1	93.29	44.04	83.20	37.90	16.83	161.05
5126	TI4	89.96	43.93	78.60	37.90	17.05	154.10
5127	S1	87.10	43.21	77.50	37.90	17.21	153.35
5134	TI8	92.54	42.07	76.20	37.90	17.25	151.19
5135	TK8	88.03	42.55	77.20	37.90	17.50	155.37
5136	TK4	89.15	40.42	77.80	37.90	17.31	154.84
6200	TI2	91.57	43.69	72.50	38.04	16.63	139.71
6201	TI2	91.84	44.36	78.42	38.04	16.71	151.81
6202	TI2	89.41	42.95	78.10	38.04	16.90	151.46
6208	TI2	89.12	42.54	80.78	37.90	17.16	159.37
6209	S1	88.72	42.83	80.50	37.90	17.21	159.34
6210	S2	88.81	42.86	80.60	37.90	17.06	158.12
6211	TI1.5	89.70	43.88	79.50	37.90	17.01	155.60
6212	S1	89.88	45.54	79.50	37.90	17.12	156.54
6214	S20	91.60	41.26	72.00	37.90	17.41	141.42
6215	C	92.54	42.65	75.30	37.90	17.32	149.98
6216	S5	93.73	43.49	75.30	37.90	16.81	145.57
6217	C	93.35	41.40	76.40	37.90	17.21	151.24
6218	S1	91.28	40.57	75.40	37.90	17.18	148.96
6220	S5	90.47	42.13	75.90	37.90	16.85	147.04
6222	TK1.5	90.42	41.63	76.40	37.90	17.48	153.60
6223	TK2	91.24	40.28	76.60	37.90	17.64	155.40
6225	TA2	92.39	41.53	78.70	37.90	17.77	160.83

Table 7.4 Water content, mass and dimensions of samples produced from a slurry (page 2 of 2).

Soil / Test Number / Test type	Water content of paste (%)	Length (mm)	Diameter (mm)	γ (KN/m^3)	Mass (g)
Speswhite kaolin.					
5110 C	35.97	76.10	38.10	16.51	146.02
5111 C	33.21	75.90	38.20	16.47	146.00
6110 C	35.06	75.90	38.20	16.41	145.54
6111 C	36.98	73.20	38.20	16.70	142.78
London clay.					
6112 C	34.86	76.05	37.90	17.44	152.55
6113 C	32.94	76.10	37.90	17.49	153.01
6114 C	33.22	75.80	38.10	17.27	152.11
6115 C	33.76	74.90	38.10	17.42	151.65

Table 7.5 Water content, mass and dimensions of remoulded samples.

Soil / test Number / Test type.	Initial Values					1st stage	Final value	All stages
	w_o (%)	σ_r (kPa)	σ_a (kPa)	u_o (kPa)	$B = \frac{\Delta u}{\Delta \sigma_r}$	ε_v (%)	w_f (%)	ε_v (%)
Speswhite kaolin.								
5110	35.97	200	200	161	0.95	1.41	29.28	9.07
5111	33.21	200	200	164	0.94	2.06	28.94	5.96
6110	35.06	200	200	159	0.96	1.57	29.43	7.74
6111	36.98	200	200	166	0.96	1.66	29.54	9.68
London clay.								
6112	34.86	200	200	158	0.97	0.89	26.36	11.36
6113	32.94	200	200	161	0.95	1.22	25.98	9.78
6114	33.22	200	200	159	0.96	2.07	26.04	10.20
6115	33.76	200	200	165	0.98	1.54	26.57	9.96

Notes:- All strains are ordinary strains.

Table 7.6a General test data for samples tested by method A.

Soil / test Number / Test type.		Initial Values					Final value	All stages
		w_o (%)	σ_r (kPa)	σ_a (kPa)	u_o (kPa)	$B = \frac{\Delta u}{\Delta \sigma_r}$	w_f (%)	ε_v (%)
Ware till.								
6195	C	31.60	200	200	176	0.97	22.47	13.27
6196	C	32.05	200	200	174	0.95	22.58	13.74
6203	TI2	31.64	200	200	173	0.98	22.75	12.30
6204	TI2	33.08	200	200	180	0.96	23.08	14.40
5120	TI2	31.74	200	200	180	0.99	22.83	12.87
London clay.								
1200	TI2	43.10	200	200	177	0.96	28.13	18.95
1201	TI2	43.30	200	200	175	0.95	28.52	18.05
5118	TI2	40.18	200	200	182	0.97	26.40	15.79
5119	TI2	40.18	200	200	169	0.96	27.80	18.90
5121	TA2	42.68	200	200	175	0.96	29.05	17.61
6200	TI2	43.69	200	200	180	0.95	28.66	17.96
6201	TI2	44.36	200	200	186	0.97	28.11	19.84
6202	TI2	42.95	200	200	185	0.97	28.19	18.73
6214	S20	46.26	200	200	180	0.98	30.41	18.28

Notes:- All strains are ordinary strains.

Table 7.6b General test data for samples tested by method B.

Soil / test Number / Test type.		Initial Values w_o (%)	σ_r (kPa)	σ_a (kPa)	u_o (kPa)	$B = \frac{\Delta u}{\Delta \sigma_r}$	Final value w_f (%)	All stages ε_v (%)
Slate dust.								
5128	TI2	30.17	162	162	150	0.98	20.85	12.98
5129	TI2	32.52	155	155	150	0.99	22.61	13.78
5130	TI2	29.97	170	170	150	0.95	22.60	10.61
5131	TI2	30.40	164	164	150	0.98	22.86	11.35
5132	TI2	30.43	164	164	150	0.96	22.81	11.51
6197	C	31.08	161	161	150	0.97	22.74	12.20
6198	C	30.94	159	159	150	0.98	22.67	12.25
6219	TI2	30.40	169	169	150	0.97	22.77	11.43
Ware till.								
6205	TI2	32.09	178	178	150	0.96	22.98	14.22
6206	TI2	31.42	183	183	150	0.95	23.18	12.15
6207	TI2	33.27	175	175	150	0.95	22.81	14.04
Speswhite kaolin.								
3101	C	57.84	166	166	150	0.99	41.40	17.70
3102	C	57.10	172	172	150	0.96	41.82	17.12
5133	TI2	57.91	170	170	150	0.95	41.60	17.76
5137	TI2	57.32	169	169	150	0.97	41.29	16.69
6220	TI2	57.64	165	165	150	0.98	41.57	16.90
6221	TI2	57.62	168	168	150	0.96	40.89	17.84
6224	TI2	56.13	180	180	150	0.95	41.26	14.86
Cowden till.								
3104	C	31.61	171	171	150	0.95	21.42	14.52
3106	C	33.16	160	160	150	0.99	21.59	15.98
3252	TI2	31.41	165	165	150	0.96	22.08	13.74
3253	TI2	32.09	164	164	150	0.96	21.96	14.92
3254	TI2	32.17	168	168	150	0.95	22.37	14.51
3255	TI2	31.74	162	162	150	0.97	22.00	13.68
London clay.								
1210	S20	42.90	170	170	150	0.98	30.78	15.05
3250	TI2	42.83	172	172	150	0.98	28.59	17.20
3251	TI2	43.18	165	165	150	0.96	28.41	18.40
3257	TI2	45.04	169	169	150	0.97	28.20	21.10
3258	TI2	42.80	163	163	150	0.96	28.76	18.08
3260	TI2	41.91	166	166	150	0.96	32.91	11.66
3261	TI2	43.56	170	170	150	0.95	26.44	21.11
3277	S1	42.48	171	171	150	0.97	31.93	13.51
3275	S1	41.62	168	168	150	0.96	29.95	15.18
3300	C	44.74	166	166	150	0.99	29.12	19.51
3301	S10	41.95	176	176	150	0.97	30.20	15.83
3302	S40	41.43	174	174	150	0.97	31.72	12.33
5112	C	44.62	170	170	150	0.98	26.45	22.61
5113	C	42.95	171	171	150	0.95	26.18	20.87
5115	C	44.89	164	164	150	0.96	26.59	22.97
5116	C	43.50	167	167	150	0.97	25.98	22.82
5117	TI2	45.88	175	175	150	0.96	28.86	20.24
5122	TA2	42.92	162.5	175	150	0.97	25.78	21.80 (1)
5123	S1	42.09	174	174	150	0.96	27.70	20.46 (1)
5124	S1	46.76	158	158	150	0.99	23.16	30.88 (1)
5125	S1	44.04	161	161	150	0.99	26.49	22.42

Table 7.6c General test data for samples tested by method C (page 1 of 2)

Soil / test Number / Test type.		Initial Values					Final value	All stages
		w_o (%)	σ_r (kPa)	σ_a (kPa)	u_o (kPa)	$B = \frac{\Delta u}{\Delta \sigma_r}$	w_f (%)	ε_v (%)
5126	TI4	43.93	167	167	150	0.99	30.64	16.13
5127	S1	43.21	180	180	150	0.97	36.54	7.94
5134	TI8	42.07	178	178	150	0.96	33.63	11.06
5135	TK8	42.55	179	190	150	0.97	32.61	12.89
5136	TK4	40.42	170	191	150	0.96	31.11	12.02
6208	TI2	42.54	170	170	150	0.96	28.59	18.25
6209	S1	42.83	172	172	150	0.97	31.02	15.53
6210	S2	42.86	174	174	150	0.98	26.01	21.59
6211	TI1.5	43.86	170	170	150	0.98	27.31	21.39
6212	S1	45.54	170	170	150	0.97	36.15	11.95
6215	C	12.65	179	179	150	0.98	30.12	15.54
6216	S5	43.49	179	179	150	0.97	29.37	16.70
6217	C	41.40	186	186	150	0.95	30.20	14.07
6218	S1	40.57	181	181	150	0.96	35.57	6.45
6220	S5	42.13	164	164	150	0.97	29.75	15.80
6222	TK1.5	41.63	181	193	150	0.96	27.11	18.63
6223	TK2	40.28	169	183	150	0.98	28.61	14.62
6225	TA2	41.53	170	166	150	0.98	28.33	16.35

Notes:- (1) Strains accumulated from several strain zero's.

(2) All strains are ordinary strains.

Table 7.6c General test data for samples tested by method C (page 2 of 2)

Soil	t_{100} (mins)	Permissible loading rate (u = 5kPa) σ'_p (kPa / hr)	Actual loading rate σ'_A (kPa / hr)	Observed at p' = 400kPa	
				$\delta\varepsilon_v$ (%)	u (kPa)
Cowden till	42.2	9.9	4.5 (1)	0.065	3.7
Ware till	64.8	6.4	4.9 (1) 5.5 (1) 5.9 (1)	0.052 0.058 0.070	4.8 5.4 6.5
Speswhite kaolin	37.2	11.1	5.9 (1) 6.0 (1) 7.0 (1) 7.5 (1)	0.089 0.096 0.100 0.109	4.2 4.8 5.1 5.2
Slate dust	83.7	5.0	4.5 (1) 5.9 (1) 6.5 (1) 7.5 (1)	0.067 0.071 0.079 0.107	5.7 6.0 6.7 9.1
London clay	91.2 710.0	4.6 4.6 4.6 3.7 2.9 2.9 2.6 3.3 1.0	6.5 (1) 5.9 (1) 4.0 (1) 3.6 (2) 2.4 (3) 3.0 (3) 3.0 (4) 3.5 (5) 1.0 (6)	0.158 0.134 0.116 0.120 0.107 0.149 0.143 0.133 0.129	7.1 6.0 5.2 5.4 4.8 6.7 6.4 6.0 5.8

Notes:- (1) Isotropic compression and swelling.

(2) Compression with $\eta'_o = 0.25$.

(3) One dimensional compression and swelling.

(4) Compression with $\eta'_o = 0.75$.

(5) Two dimensional compression and swelling.

(6) Isotropic compression and swelling without side drains.

Table 7.7 Summary of rates of testing used during initial compression and the excess pore pressures observed.

Test type	Number of deviations of path	Soil	Number of tests
Isotropic compression and swelling only		Slate dust	3
		Ware till	2
		Speswhite kaolin	2
		Cowden till	2
		London clay	7
Stress path threshold tests.	8	Slate dust	5
Constant p', increasing q' paths.	14	Ware till	6
p' = 200kPa, overconsolidation ratio = 2.	8	Speswhite kaolin	5
Isotropically compressed.	8	Cowden till	4
	18	London clay	15
Stress path threshold tests , isotropically compressed.		London clay	
(constant p', q' increasing paths).			
Overconsolidation ratio's = 1.5, 4, 8.	4 each		3
Total stress path deviations.	4 each		2
Extended rest periods (two periods).	3		3
Length of approach path (5 lengths).	1		1
Tests with OCR = 2.0 and p' = 100,300kPa.	4		2
Stress path threshold tests , isotropically compressed.		London clay	
Constant p', q' reducing path.	4		1
Constant q', p' increasing path.	4		1
Constant q', p' reducing path.	4		1
Compressed with:- $\eta'_o = 0.25$	5	London clay	1
$\eta'_o = 0.75$	5		1
η'_o = two dimensional	5		1
One dimensionally compressed.		London clay	
Constant p', q' increasing paths with			
Overconsolidation ratios = 1.5, 2.0, 4.0, 8.0.	5 each		4

Table 7.8 Summary of tests conducted (page 1 of 2).

Tests to establish state boundary surface ,			
Compression,		London clay	
Normally consolidated			
Drained (σ'_r constant)			
p' = 50, 100, 200, 500kPa.			4
Undrained (σ_r constant)			
p' = 100 (2), 500 kPa.			3
Overconsolidated			
Undrained (σ_r constant)			
p' = 15, 30 (2), 60, 120 (2), 300 kPa.			7
(overconsolidation ratios = 40, 20, 10, 5, 2 respectively).			6
Extension, (no side drains).			
Drained (σ'_r constant)			
p' = 200kPa, normally compressed.			1
Undrained (σ_r constant)			
p' = 200kPa, normally compressed.			1

Notes:- All samples of overconsolidation ratio = 2, tested at p' = 200kPa on constant p' increasing q' paths unless otherwise stated.

Table 7.8 Summary of tests conducted (page 2 of 2).

Cell number / instrument number		Load cell				Volume gauge
		A (KN / mm)	B (KN / mm^2)	C (KN / mm)	ΔL_o (mm)	D (kPa / mm^3)
Cell 1.						
843	C	40298	21.22	104.9	0.625	
	E	40490	21.79	105.3		
G,002						2.429
Cell 3.						
846	C	42061	23.26	115.4	0.708	
	E	42436	23.72	116.9		
G,007						2.398
Cell 5.						
852	C	41138	21.89	108.8	0.623	
	E	41208	22.06	109.4		
G,006						2.275
Cell 6.						
748	C	48069	27.32	126.1	0.745	
	E	48273	28.01	126.8		
G,016						2.500

Notes:- C Compression.
E Extension.

Table 8.1 System compliance data.

Soil / test number / Test type		v_{oi} (1)	ε_v (%)	v_{ff} (2)	v_{of} (2)	$v_{oi} - v_{of}$	v_o (3)	$v_o - v_{of}$
Slate dust.								
5128	TI2	1.8387	12.98	1.5796	1.8152	0.0235	1.8277	0.0075
5129	TI2	1.9041	13.78	1.6286	1.8889	0.0152	1.8907	0.0018
5130	TI2	1.8332	10.61	1.6283	1.8216	0.0116	1.8265	0.0049
5131	TI2	1.8451	11.35	1.6355	1.8449	0.0002	1.8384	-0.0065
5132	TI2	1.8460	11.51	1.6341	1.8466	-0.0006	1.8413	-0.0053
6197	C	1.8640	12.20	1.6322	1.8590	0.0050	1.8567	-0.0023
6198	C	1.8601	12.25	1.6302	1.8578	0.0023	1.8596	0.0018
6219	TI2	1.8451	11.43	1.6330	1.8437	0.0014	1.8362	-0.0075
Ware till.								
6195	C	1.8248	13.27	1.5865	1.8292	-0.0044	1.8294	0.0002
6196	C	1.8365	13.74	1.5893	1.8425	-0.0060	1.8409	-0.0016
6203	TI2	1.8258	12.30	1.5938	1.8173	0.0085	1.8242	0.0069
6204	TI2	1.8634	14.40	1.6024	1.8720	-0.0086	1.8768	0.0048
6205	TI2	1.8375	14.22	1.5998	1.8650	-0.0275	1.8639	-0.0011
6206	TI2	1.8201	12.15	1.6050	1.8270	-0.0069	1.8224	-0.0046
6207	TI2	1.8683	14.04	1.5933	1.8559	0.0124	1.8530	-0.0029
5120	TI2	1.8284	12.87	1.5959	1.8316	-0.0032	1.8465	0.0149
Speswhite kaolin.								
3101	C	2.5038	17.70	2.0764	2.5230	-0.0192	2.5174	-0.0056
3102	C	2.4846	17.12	2.0873	2.5185	-0.0339	2.5159	-0.0026
5133	TI2	2.5057	17.76	2.0816	2.5311	-0.0254	2.5186	-0.0125
5137	TI2	2.4903	16.69	2.0735	2.4889	0.0014	2.5100	0.0211
6220	TI2	2.4986	16.90	2.0808	2.5040	-0.0054	2.5018	-0.0022
6221	TI2	2.4981	17.84	2.0631	2.5111	-0.0130	2.5256	0.0145
6224	TI2	2.4594	14.86	2.0728	2.4346	0.0248	2.4471	0.0125
Cowden till.								
3104	C	1.8377	14.52	1.5676	1.8339	0.0038	1.8361	0.0022
3106	C	1.8787	15.98	1.5721	1.8711	0.0076	1.8684	-0.0027
3252	TI2	1.8324	13.74	1.5851	1.8376	-0.0052	1.8352	-0.0024
3253	TI2	1.8504	14.92	1.5819	1.8594	-0.0090	1.8521	-0.0073
3254	TI2	1.8525	14.51	1.5928	1.8631	-0.0106	1.8698	0.0067
3255	TI2	1.8411	13.68	1.5830	1.8339	0.0072	1.8375	0.0036
London clay.								
1200	TI2	2.1853	18.95	1.7736	2.1883	-0.0030	2.1962	0.0079
1201	TI2	2.1908	18.05	1.7843	2.1773	0.0135	2.1753	-0.0020
1210	S20	2.1798	15.05	1.8465	2.1736	0.0062	2.1609	-0.0127
3250	TI2	2.1778	17.20	1.7862	2.1573	0.0205	2.1564	-0.0009
3251	TI2	2.1875	18.40	1.7813	2.1830	0.0046	2.1647	-0.0183
3257	TI2	2.2386	21.10	1.7755	2.2503	-0.0117	2.2388	-0.0165
3258	TI2	2.1770	18.08	1.7909	2.1862	-0.0092	2.1908	0.0046
3260	TI2	2.1525	11.66	1.9051	2.1565	0.0040	2.1612(b)	0.0047
3261	TI2	2.1979	21.11	1.7272	2.1894	0.0085	2.1965	0.0074
3277	S1	2.1682	13.51	1.8781	2.1715	0.0033	2.1718(c)	0.0003
3275	S1	2.1446	15.18	1.8236	2.1500	-0.0054	2.1561(c)	0.0061
3300	C	2.2304	19.51	1.8008	2.2373	-0.0069	2.2271	-0.0102
3301	S10	2.1536	15.83	1.8305	2.1748	-0.0212	2.1508	-0.0240
3302	S40	2.1393	12.33	1.8723	2.1356	0.0037	2.1387	0.0031

Table 8.2 Specific volumes, at the start and finish of tests, and calculated from the normal compression line (page 1 of 2).

Soil / test number / Test type		v_{oi} (1)	ε_v (%)	v_{ff} (2)	v_{of} (2)	$v_{oi} - v_{of}$	v_o (3)	$v_o - v_{of}$
5112	C	2.2271	22.61	1.7274	2.2320	-0.0049	2.2461	0.0141
5113	C	2.1811	20.87	1.7200	2.1736	0.0075	2.1948	0.0212
5115	C	2.2345	22.97	1.7312	2.2475	-0.0130	2.2266	-0.0209
5116	C	2.1963	22.82	1.7145	2.2214	-0.0251	2.2310	0.0096
5117	TI2	2.2617	10.14	1.7937	2.2489	0.0128	2.2270	-0.0219
5118	TI2	2.1050	15.79	1.7843	2.1189	-0.0139	2.1138	-0.0051
5119	TI2	2.1737	18.90	1.7645	2.1768	-0.0031	2.1747	-0.0021
5121	TA2	2.1948	17.61	1.7988	2.1832	0.0116	2.1832	0
5122	TA2	2.1803	21.80(4)	1.7090	2.1853	-0.0050	2.1853	0
5123	S1	2.1575	20.46(4)	1.7618	2.1636	-0.0061	2.1814(c)	0.0178
5124	S1	2.2859	30.88(4)	1.6369	2.3081	-0.0222	2.3004	-0.0077
5125	S1	2.2111	22.42	1.7285	2.2280	-0.0169	2.2324	0.0045
5126	TI4	2.2081	16.13	1.8426	2.1970	0.0111	2.2172	0.0202
5127	S1	2.1883	7.94	2.0049	2.1778	0.0105	2.1584(b)	-0.0194
5134	TI8	2.1569	11.06	1.9248	2.1642	-0.0073	2.1373	-0.0269
5135	TK8	2.1701	12.89	1.8968	2.1775	-0.0074	2.1456	-0.0319
5136	TK4	2.1116	12.02	1.8555	2.1090	0.0026	2.0762	-0.0328
6200	TI2	2.2015	17.96	1.7882	2.1796	0.0219	2.1737	-0.0059
6201	TI2	2.2199	19.84	1.7730	2.2118	-0.0128	2.2111	-0.0007
6202	TI2	2.1811	18.73	1.7752	2.1844	-0.0033	2.1926	0.0082
6208	TI2	2.1699	18.25	1.7862	2.1850	-0.0151	2.1676	-0.0174
6209	S1	2.1778	15.53	1.8531	2.1937	-0.0159	2.1732(b)	-0.0205
6210	S2	2.1787	21.59	1.7153	2.1876	-0.0089	2.1997	0.0121
6211	TI1.5	2.2062	21.39	1.7510	2.2275	-0.0213	2.2230	-0.0045
6212	S1	2.2524	11.95	1.9941	2.2648	-0.0124	2.1909(a)	-0.0739
6214	S20	2.2722	18.28	1.8363	2.2470	0.0252	2.2357	-0.0113
6215	C	2.1729	15.54	1.8283	2.1647	0.0082	2.1730	0.0083
6216	S5	2.1960	16.70	1.8077	2.1701	0.0259	2.1880	0.0179
6217	C	2.1385	14.07	1.8305	2.1302	0.0083	2.1476	0.0174
6218	S1	2.1157	6.45	1.9782	2.1146	0.0011	2.1235(b)	0.0089
6220	S5	2.1586	15.80	1.8180	2.1591	-0.0005	2.1508	-0.0083
6222	TK1.5	2.1448	18.63	1.7455	2.1452	-0.0004	2.1570	0.0118
6223	TK2	2.1077	14.62	1.7868	2.0927	0.0150	2.0952	0.0025
6225	TA2	2.1420	16.35	1.7790	2.1267	0.0153	2.1267	0

Notes:-

(1) From recorded water content (w_o) at the start of testing.

(2) From final water content (w_f) at the end of testing.

(3) Calculated from $v = N - \lambda \ln p'$ at $p' = 400$kPa except as below:-

(a) $p' = 50$kPa (end of isotropic compression).

(b) $p' = 100$kPa (end of isotropic compression).

(c) $p' = 200$kPa (end of isotropic compression).

(4) Strains accumulated from several strain zero's.

(5) All strains are ordinary strains.

(6) Volumetric strains accumulated from all stages.

Table 8.2 Specific volumes, at the start and finish of tests, and calculated from the normal compression line (page 2 of 2).

Soil	η'_o	λ	κ_1[1]	N	M_c	M_e	Γ_c	Γ_e	Notes
London clay	-0.400[2]	0.157	0.0068	2.690	-	-	-	-	2 DIMENSIONAL compression
	0	0.157	0.0068	2.710	0.890	0.692	2.620	2.615	
	0.25[2]	0.157	0.0068	2.702	-	-	-	-	
	0.575[2]	0.157	0.0068	2.680	0.890[2]	-	2.605[2]	-	1 DIMENSIONAL compression
	0.75[2]	0.157	0.0068	2.650	-	-	-	-	
Cowden till	0	0.105	0.0024	2.125	-	-	-	-	
Speswhite kaolin	0	0.180	0.0055	3.190	-	-	-	-	
Ware till	0	0.110	0.0028	2.259	-	-	-	-	
Slate dust	0	0.077	0.0021	2.092	-	-	-	-	
London clay	0	0.120	0.0037	2.475	-	-	-	-	Remoulded sample
Speswhite kaolin	0	0.069	0.0029	2.232	-	-	-	-	remoulded sample

Notes:- (1) After $\pi' = 0.05$.

(2) One test each only.

Table 9.1 Critical state soil parameters for all soils tested.

Soil	κ_1	κ_o	$\Delta p' / p'_o$	π'
London clay.				
Swelling	0.0068	0.059	-0.23	-0.26
Recompression	0.0068	0.058	0.27	0.24
Cowden till.				
Swelling	0.0024	0.015	-0.18	-0.20
Recompression	0.0023	0.014	0.22	0.20
Speswhite kaolin.				
Swelling	0.0057	0.047	-0.21	-0.24
Recompression	0.0056	0.048	0.26	0.23
Ware till.				
Swelling	0.0028	0.0171	-0.25	-0.29
Recompression	0.0028	0.0169	0.35	0.30
Slate dust.				
Swelling	0.0022	0.0110	-0.26	-0.30
Recompression	0.0019	0.0110	0.36	0.31

Table 9.2 Values of swelling parameters κ_o, κ_1, $\Delta p' / p'_o$ and π'.

Rest period (hrs)	Initial normalised stiffness of sample $\frac{\delta q'}{vp' \delta \varepsilon_s}$ ($\Delta\eta' = 0.05$)	θ^o
3	98	0
241	174	
3	412	90
48	607	
246	749	
3	765	180
242	1303	

Table 9.3 The effect of periods of rest on the stiffness of samples of London clay.

Soil / test number / test type	q'_o (kPa)	p'_o (kPa)	η'_o	v_o	q'_f (kPa)	p'_f (kPa)	η'_f	v_f	ε_{sf} (%)	θ^o
Slate dust.										
5129 TI2	0	200	0	1.643	216.5	200	1.083	1.630	16.49	180
5130 TI2	0	200	0	1.640	220.1	200	1.101	1.632	19.62	+90
5131 TI2	0	200	0	1.648	215.8	200	1.079	1.630	25.21	-90
5132 TI2	0	200	0	1.637	215.1	200	1.076	1.629	12.68	0
6219 TI2	0	200	0	1.647	214.2	200	1.071	1.629	16.35	-135
Ware till.										
6203 TI2	0	200	0	1.613	212.4	200	1.062	1.600	10.41	180
6204 TI2	0	200	0	1.617	211.2	200	1.056	1.607	22.68	0
6205 TI2	0	200	0	1.615	212.0	200	1.060	1.599	20.84	-90
6206 TI2	0	200	0	1.614	210.2	200	1.051	1.601	17.02	+45
6207 TI2	0	200	0	1.610	207.3	200	1.036	1.594	20.66	-45
6208 TI2	0	200	0	1.611	214.4	200	1.072	1.608	14.06	+90
Speswhite kaolin.										
5133 TI2	0	200	0	2.092	176.4	200	0.882	2.071	15.21	180
5137 TI2	0	200	0	2.104	170.9	200	0.855	2.091	15.96	+90
6220 TI2	0	200	0	2.100	177.3	200	0.887	2.079	19.94	0
6221 TI2	0	200	0	2.116	181.1	200	0.906	2.075	15.42	-90
6224 TI2	0	200	0	2.110	172.8	200	0.864	2.083	15.36	-90
Cowden till.										
3252 TI2	0	200	0	1.604	214.0	200	1.070	1.583	13.80	-90
3253 TI2	0	200	0	1.596	205.1	200	1.026	1.578	15.96	0
3254 TI2	0	200	0	1.606	208.9	200	1.045	1.595	11.76	+90
3255 TI2	0	200	0	1.604	210.6	200	1.053	1.586	10.28	180
London clay.										
1200 TI2	0	200	0	1.782	207.4	200	1.037	1.780	15.62	+90
1201 TI2	0	200	0	1.793	206.9	200	1.035	1.783	20.95	-90
3250 TI2	0	200	0	1.790	206.1	200	1.031	1.785	13.06	0
3251 TI2	0	200	0	1.779	208.5	200	1.043	1.776	14.26	-90
3257 TI2	0	200	0	1.774	210.4	200	1.052	1.774	15.69	0
3258 TI2	0	200	0	1.790	206.5	200	1.033	1.779	10.36	180
3260 TI2	0	100	0	1.924	105.9	100	1.059	1.905	12.28	180
3261 TI2	0	300	0	1.745	321.6	300	1.072	1.727	14.47	180
5117 TI2	0	200	0	1.792	208.1	200	1.041	1.776	17.38	180
5118 TI2	0	200	0	1.795	209.1	200	1.046	1.780	14.01	-30
5119 TI2	0	200	0	1.770	208.3	200	1.042	1.768	11.68	+45
5126 TI4	0	100	0	1.856	117.7	100	1.177	1.860	6.14	180
5134 TI8	0	50	0	1.889	76.4	50	1.528	1.901	3.98	180
6200 TI2	0	200	0	1.788	212.1	200	1.061	1.783	16.56	0
6201 TI2	0	200	0	1.774	207.3	200	1.037	1.772	8.78	180
6202 TI2	0	200	0	1.782	206.0	200	1.030	1.782	11.86	180
6208 TI2	0	200	0	1.784	210.8	200	1.054	1.773	9.97	+90
6211 TI1.5	0	267	0	1.773	272.1	200	1.019	1.748	12.31	180

Table 9.4 Summary of failure states in threshold tests for all isotropically compressed samples.

Soil / test number / test type	q'_o (kPa)	p'_o (kPa)	η'_o	v_o	q'_f (kPa)	p'_f (kPa)	η'_f	v_f	ε_{sf} (%)	θ^o
London clay.										
5121 TA2	3.1	200	0.015	1.795	212.6	200	1.063	1.799	12.12	0
5122 TA2	7.0	200	0.035	1.703	218.1	200	1.096	1.709	9.45	0
5135 TK8	-18.8	50	-0.376	1.840	83.1	50	1.662	1.869	16.83	180
5136 TK4	-6.1	100	-0.061	1.810	145.6	100	1.456	1.827	4.46	180
6222 TK1.5	85.2	267	0.319	1.750	267.5	267	1.002	1.755	3.07	180
6223 TK2	31.4	200	0.157	1.778	216.4	200	1.082	1.789	3.95	180
6225 TA2	-13.1	200	-0.066	1.775	233.2	200	1.166	1.779	11.31	180

Table 9.5 Summary of failure states in threshold tests for London clay compressed with anisotropic initial stress histories.

Soil / test number / test type	p'_o (kPa)	u_o (kPa)	OCR	v_o	q'_f (kPa)	p'_f (kPa)	u_f (kPa)	η'_f	v_f	ε_s (%)
London clay.										
1210 S20	30	150	20	1.836	112.1	93.6	123.8	1.20	1.836	16.65
3275 S1	200	150	1	1.878	-113.0	162.0	150.0	-0.69	1.823	-24.82
3277 S1	200	150	1	1.878	-76.0	108.1	217.1	-0.71	1.878	-26.61
3301 S10	60	150	10	1.810	159.0	152.1	110.9	1.05	1.810	15.82
3302 S40	15	150	40	1.875	87.2	67.6	125.8	1.29	1.875	14.38
5123 S1	200	150	1	1.878	261.6	287.2	150.0	0.91	1.735	26.96
5124 S1	500	150	1	1.734	648.1	720.1	150.0	0.90	1.590	27.84
5125 S1	500	150	1	1.732	267.0	301.0	438.7	0.89	1.732	16.18
5127 S1	100	150	1	1.987	51.9	52.6	215.2	0.99	1.987	15.34
6209 S1	100	150	1	1.987	143.6	147.9	150.0	0.96	1.836	21.58
6210 S2	300	150	2	1.729	282.3	310.1	234.0	0.91	1.729	19.90
6212 S1	50	150	1	2.096	74.0	74.6	150.0	0.99	1.929	22.80
6214 S20	30	150	20	1.827	118.2	109.1	110.3	1.08	1.827	20.86
6216 S5	120	150	5	1.823	154.1	151.2	170.4	1.02	1.823	21.20
6218 S1	100	150	1	1.987	52.6	55.4	212.1	0.95	1.987	20.67
6220 S5	120	150	5	1.811	246.1	257.5	97.8	0.96	1.811	23.14

Tables 9.6 Summary of failure states in tests to establish the state boundary surface for isotropically compressed London clay.

η'_o	$\frac{d\varepsilon_s}{d\varepsilon_v}$ (1)	$\frac{d\varepsilon_s}{d\varepsilon_v}$ (2)	$\frac{d\varepsilon_s}{d\varepsilon_v}$ (3)	$\frac{d\varepsilon_s}{d\varepsilon_v}$ (4)
-0.408	-1.230	-0.886	-0.498	-0.333
0	-	0	0	0
0.25	0.939	0.484	0.294	0.204
0.575	1.932	1.719	1.106	0.666
0.75	4.215	4.406	2.104	1.130

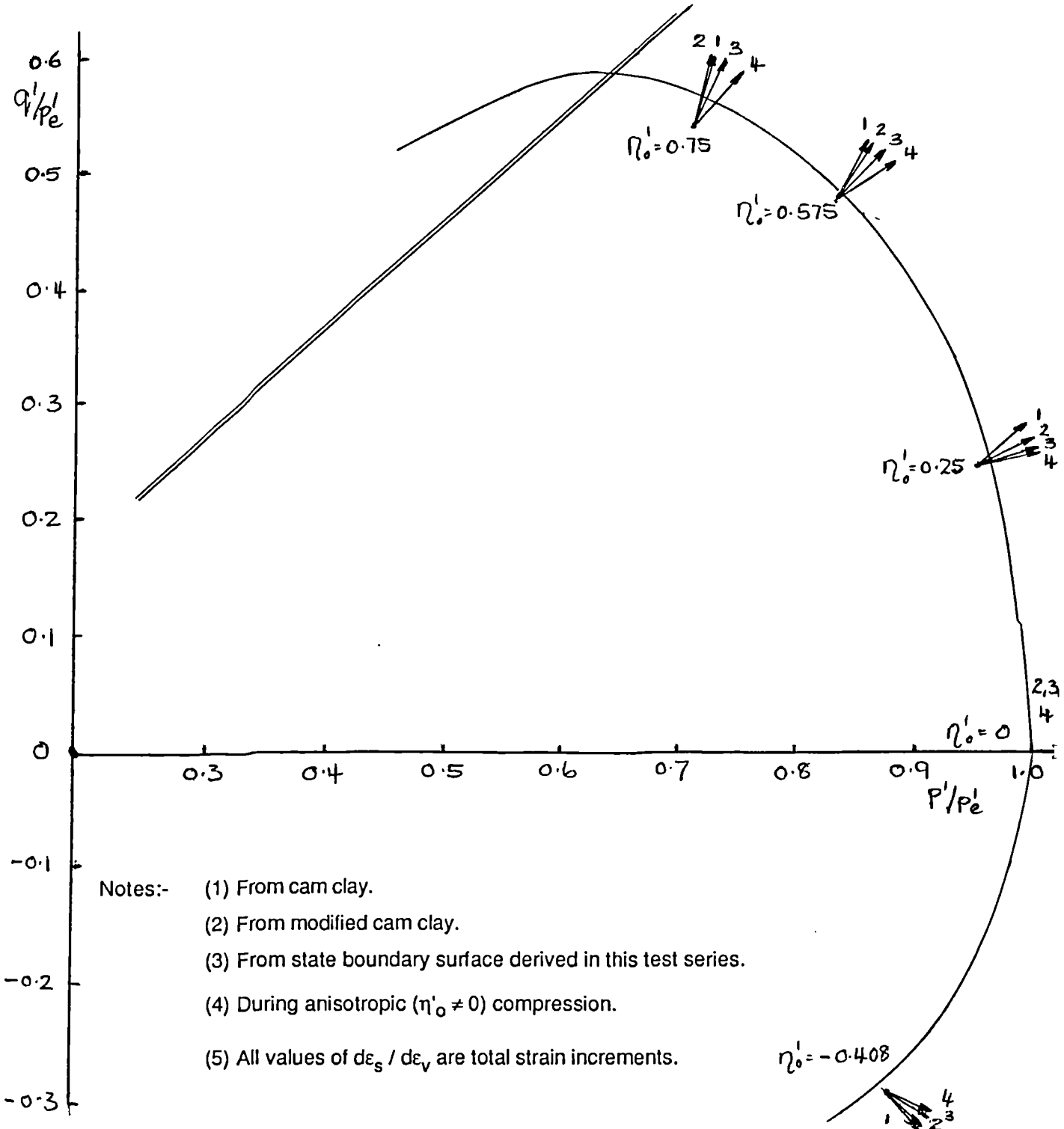

Notes:-

(1) From cam clay.

(2) From modified cam clay.

(3) From state boundary surface derived in this test series.

(4) During anisotropic ($\eta'_o \neq 0$) compression.

(5) All values of $d\varepsilon_s / d\varepsilon_v$ are total strain increments.

Table 9.7 Values of the total strain increment ratio predicted from the state boundary surface and that observed during anisotropic compression for London clay.

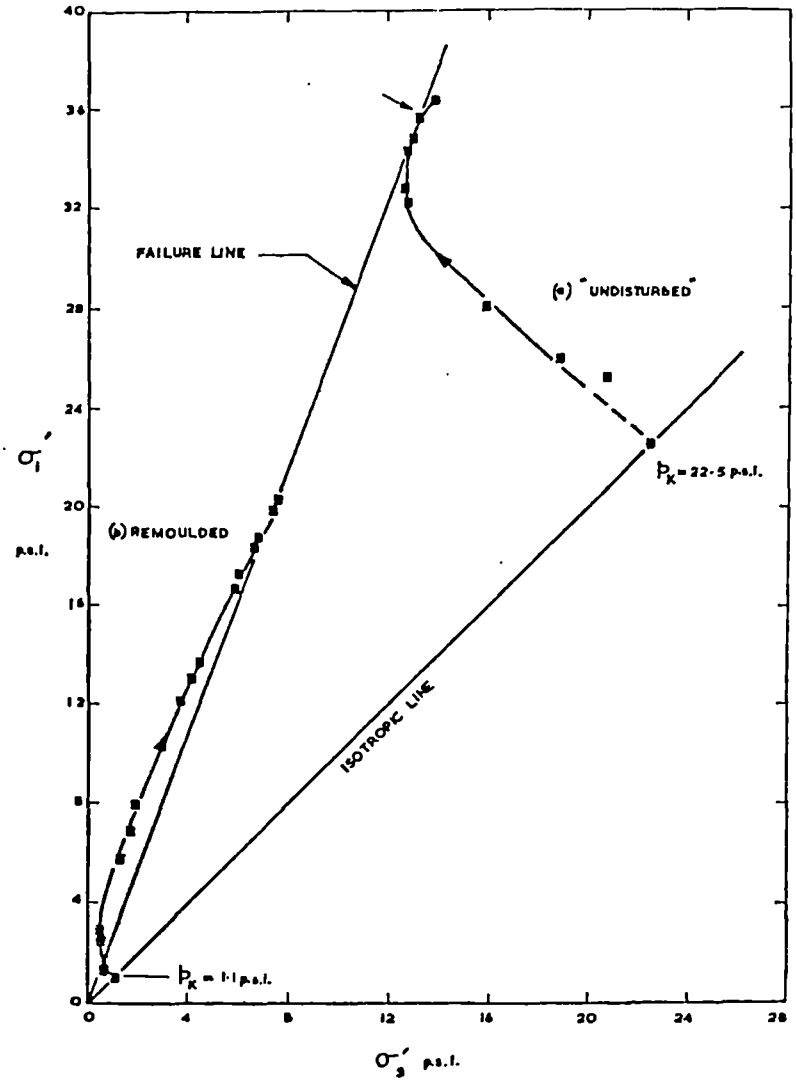

Fig 2.1 Effect of mechanical disturbance on Weald Clay (Skempton and Sowa, 1963).

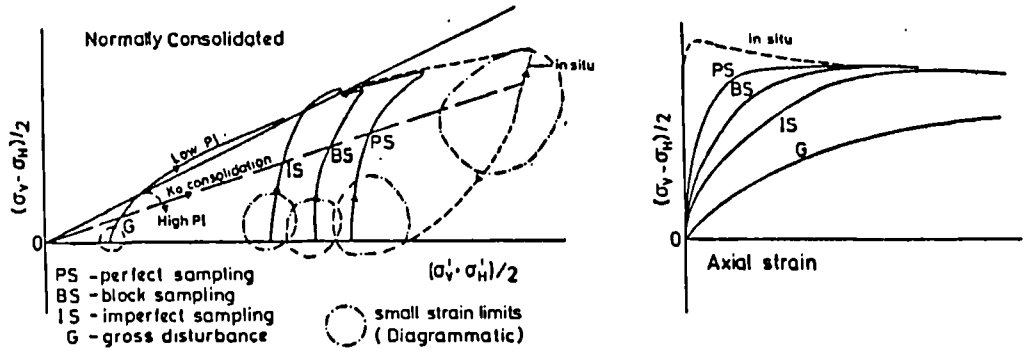

Fig 2.2 Effect of disturbance on normally consolidated Lower Cromer till (Hight, Gens and Jardine, 1985).

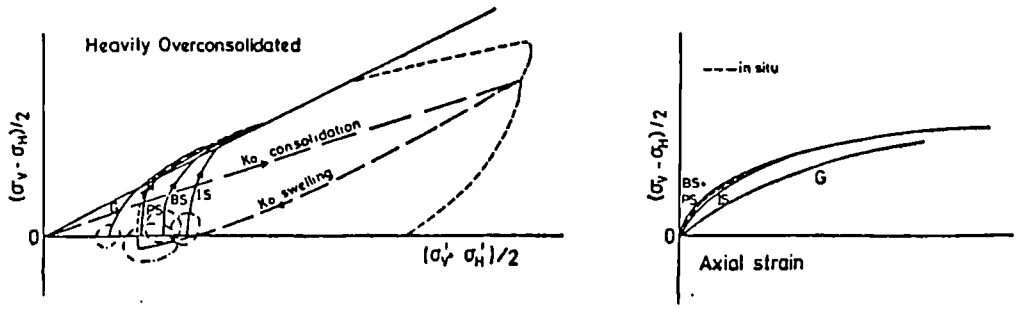

Fig 2.3 Effect of disturbance on over-consolidated Lower Cromer till (Hight, Gens and Jardine, 1985).

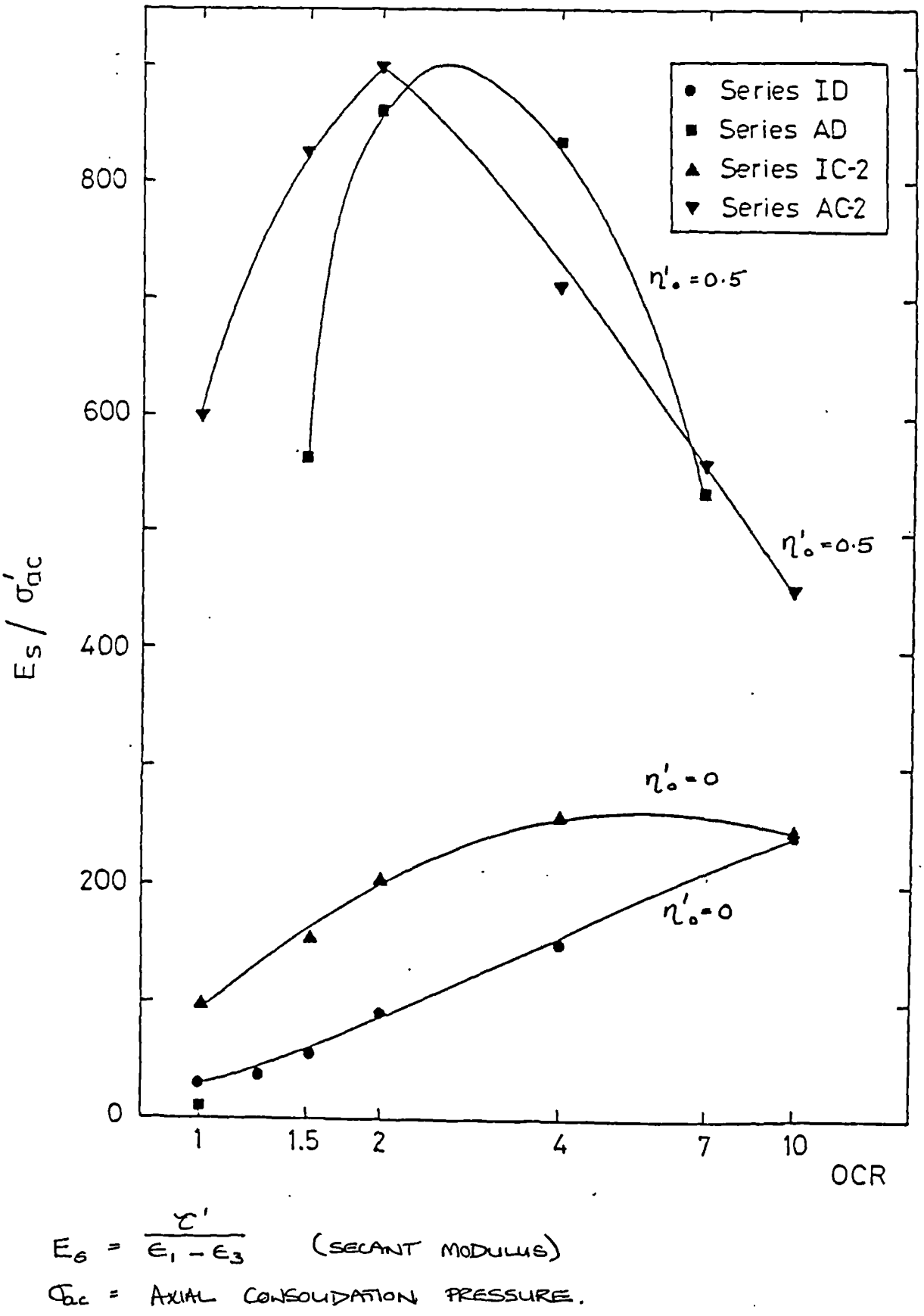

$E_s = \frac{\sigma'}{\epsilon_1 - \epsilon_3}$ (SECANT MODULUS)

σ_{ac} = AXIAL CONSOLIDATION PRESSURE.

Fig 2.4 Variation of normalised stiffness for drained and undrained tests on Lower Cromer till (Gens, 1982).

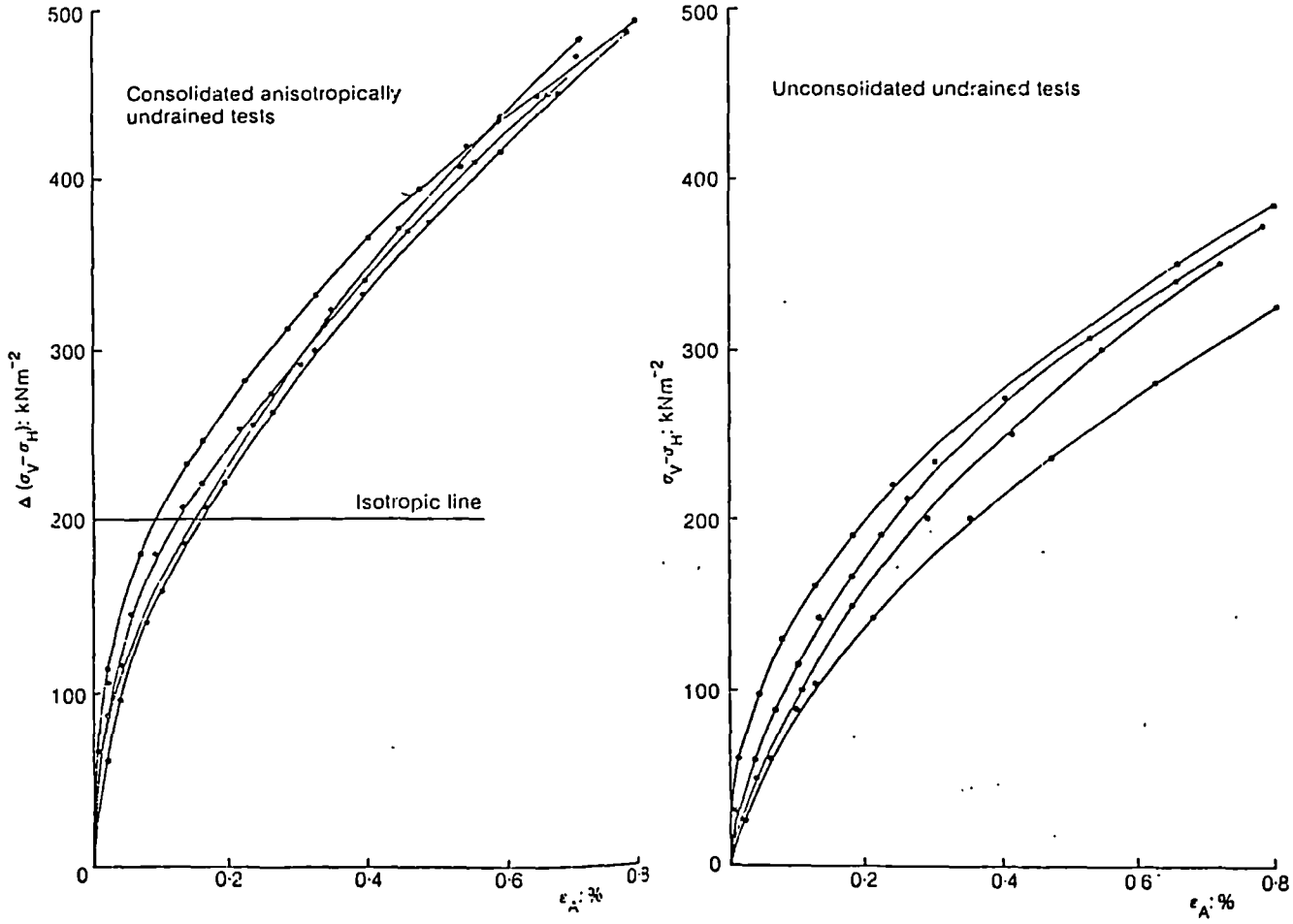

Fig 2.5 Stress-strain curves for isotropically and anisotropically compressed samples of undisturbed London Clay (Costa-Filho, 1979).

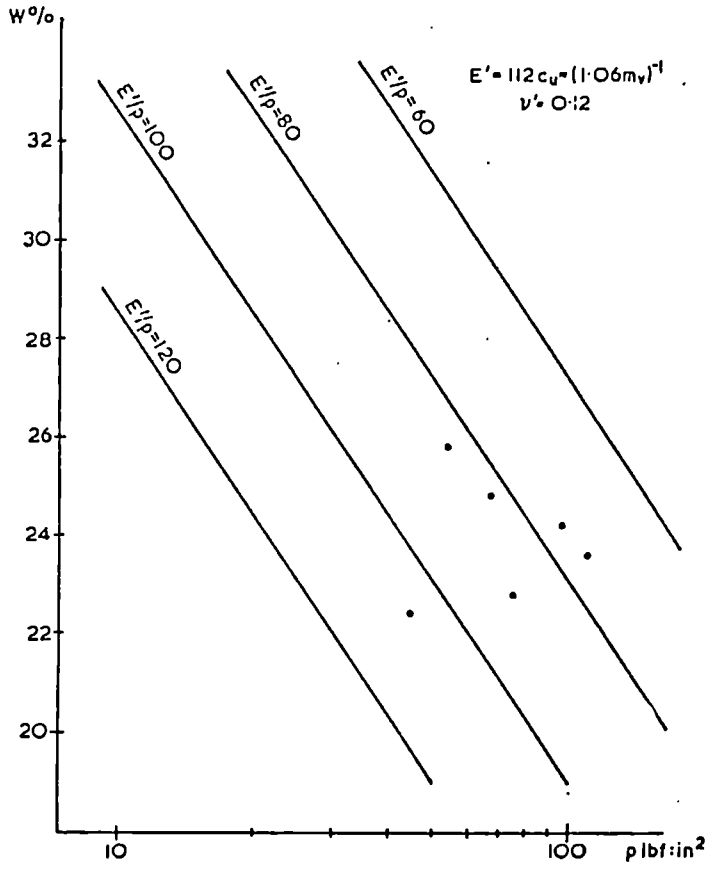

Fig 2.6 Variation of sample stiffness with state (Wroth, 1971).

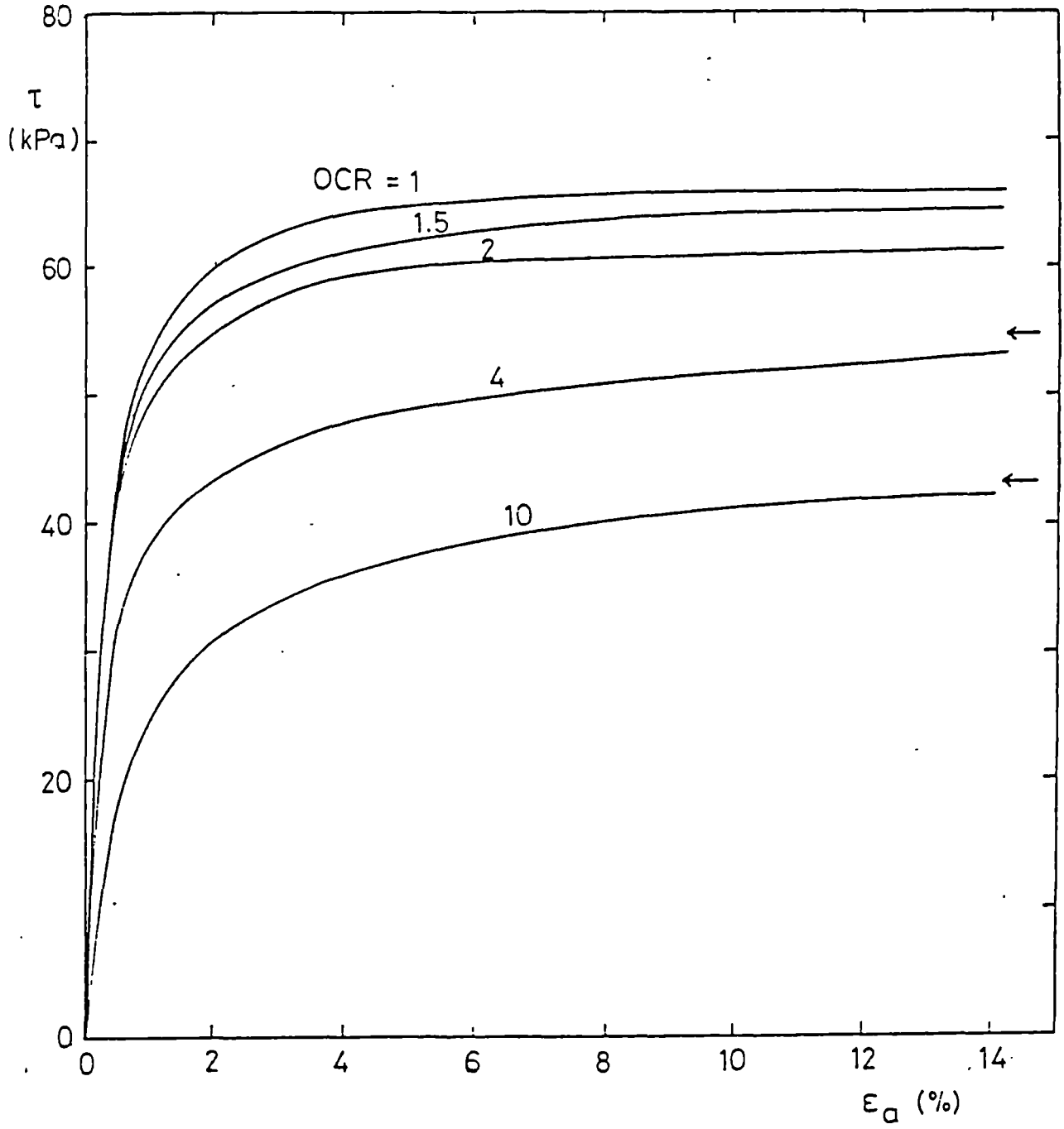

Fig 2.7 Plot of τ against axial strain for undrained tests on isotropically compressed samples of Lower Cromer till at large strains (Gens, 1982).

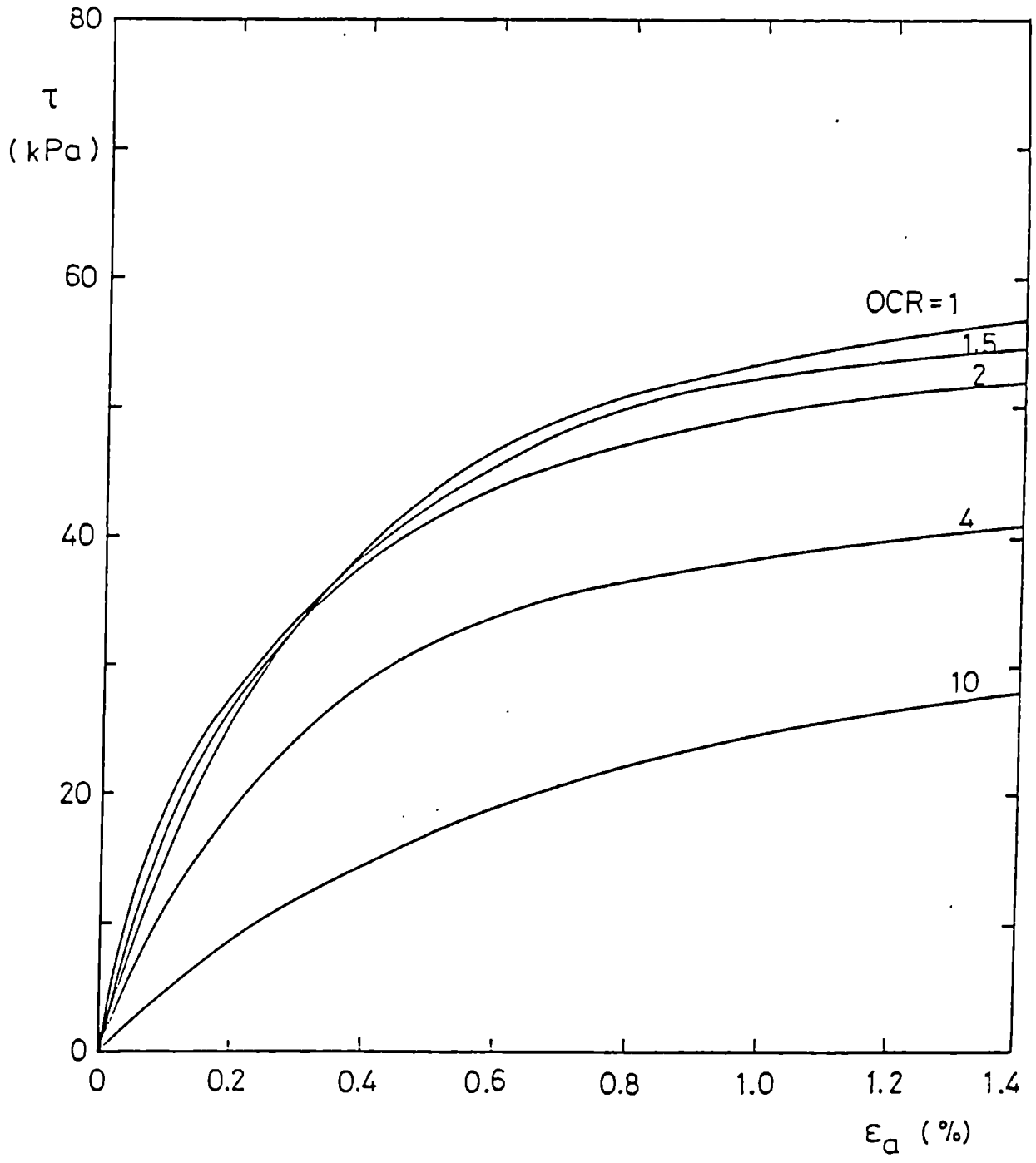

Fig 2.8 Plot of τ against axial strain for undrained tests on isotropically compressed samples of Lower Cromer till at small strains (Gens, 1982).

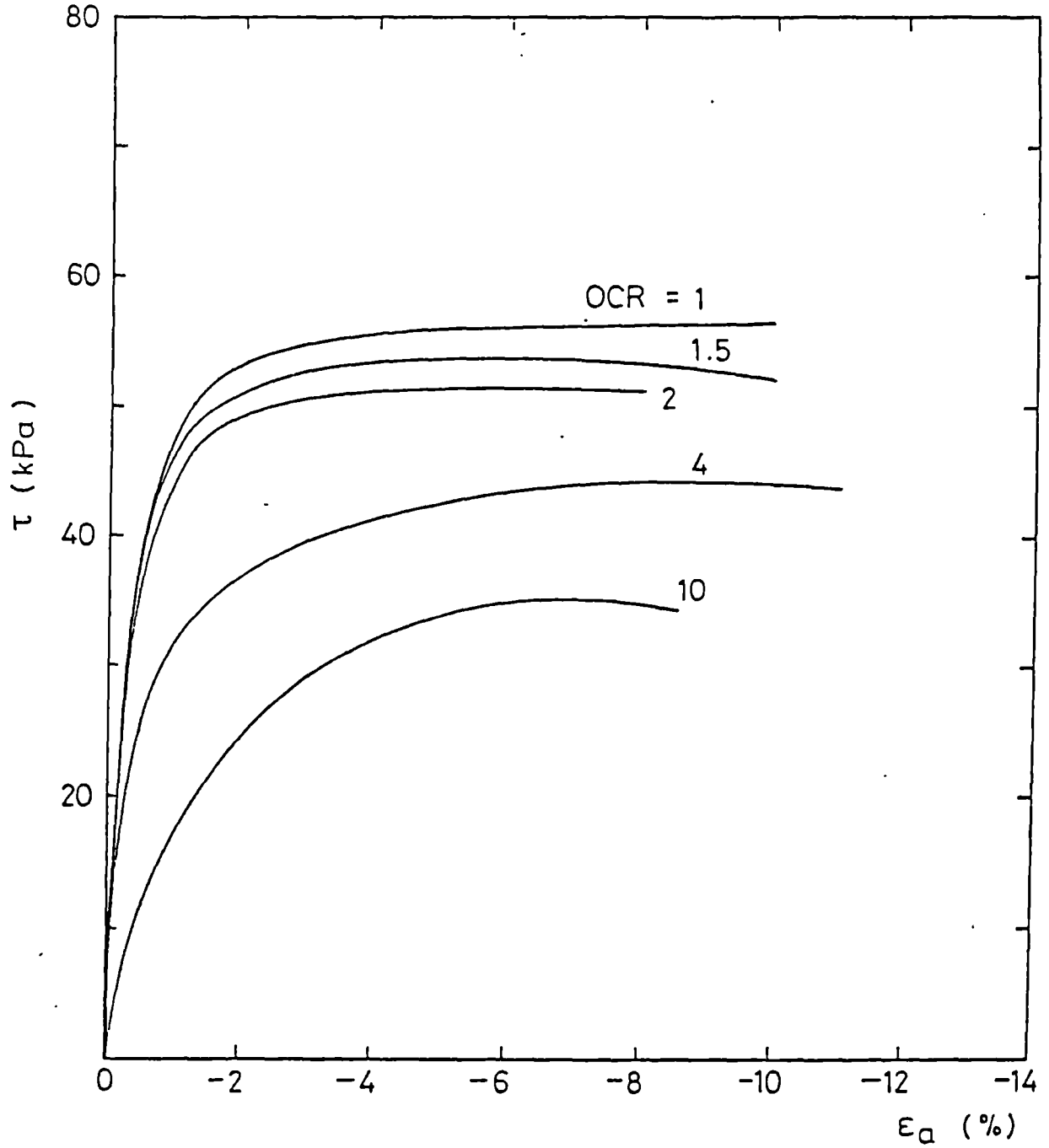

Fig 2.9 Plot of τ against axial strain for undrained extension tests on isotropically compressed samples of Lower Cromer till at large strains (Gens, 1982).

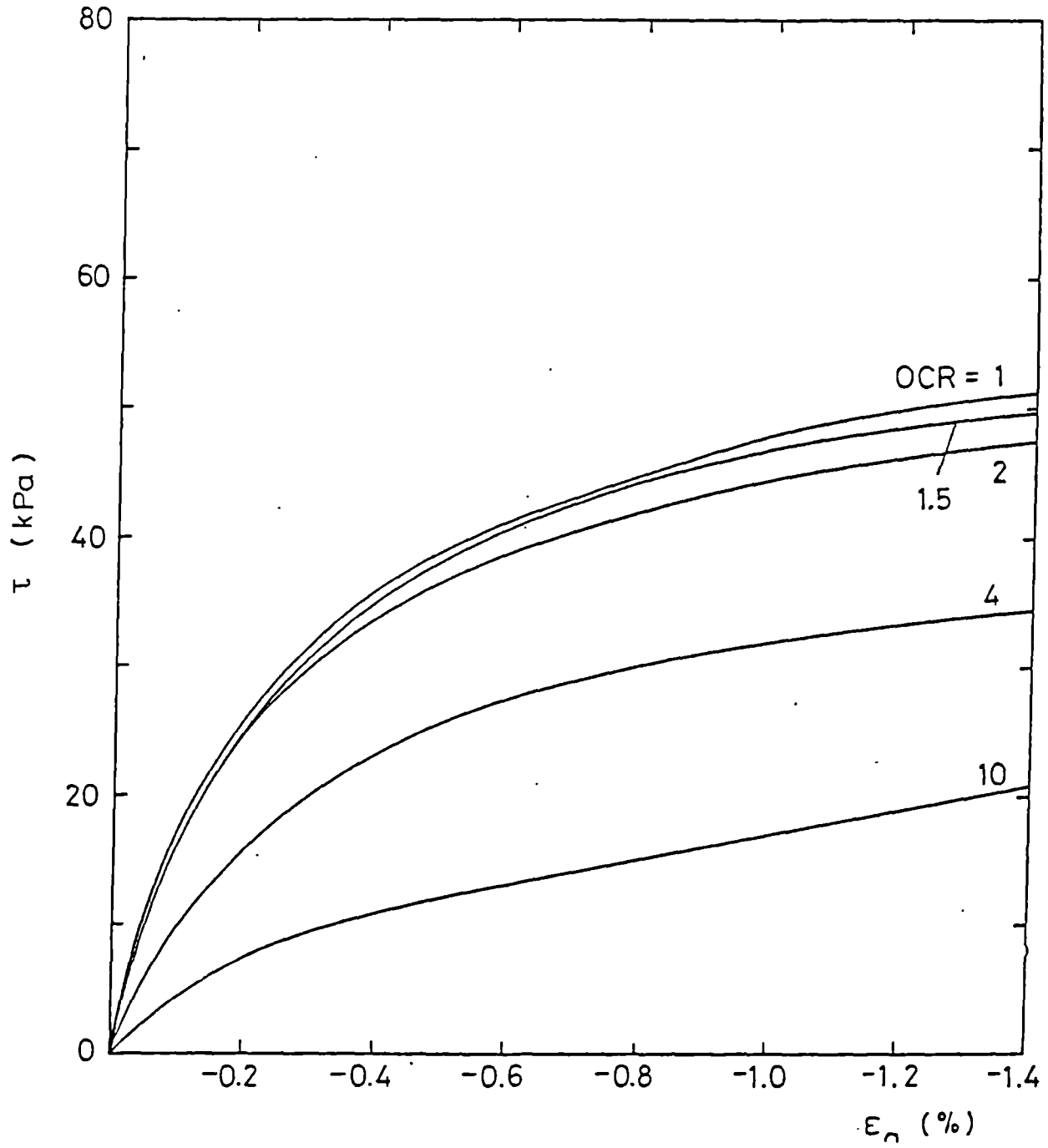

Fig 2.10 Plot of τ against axial strain for undrained extension tests on isotropically compressed samples of Lower Cromer till at small strains (Gens, 1982).

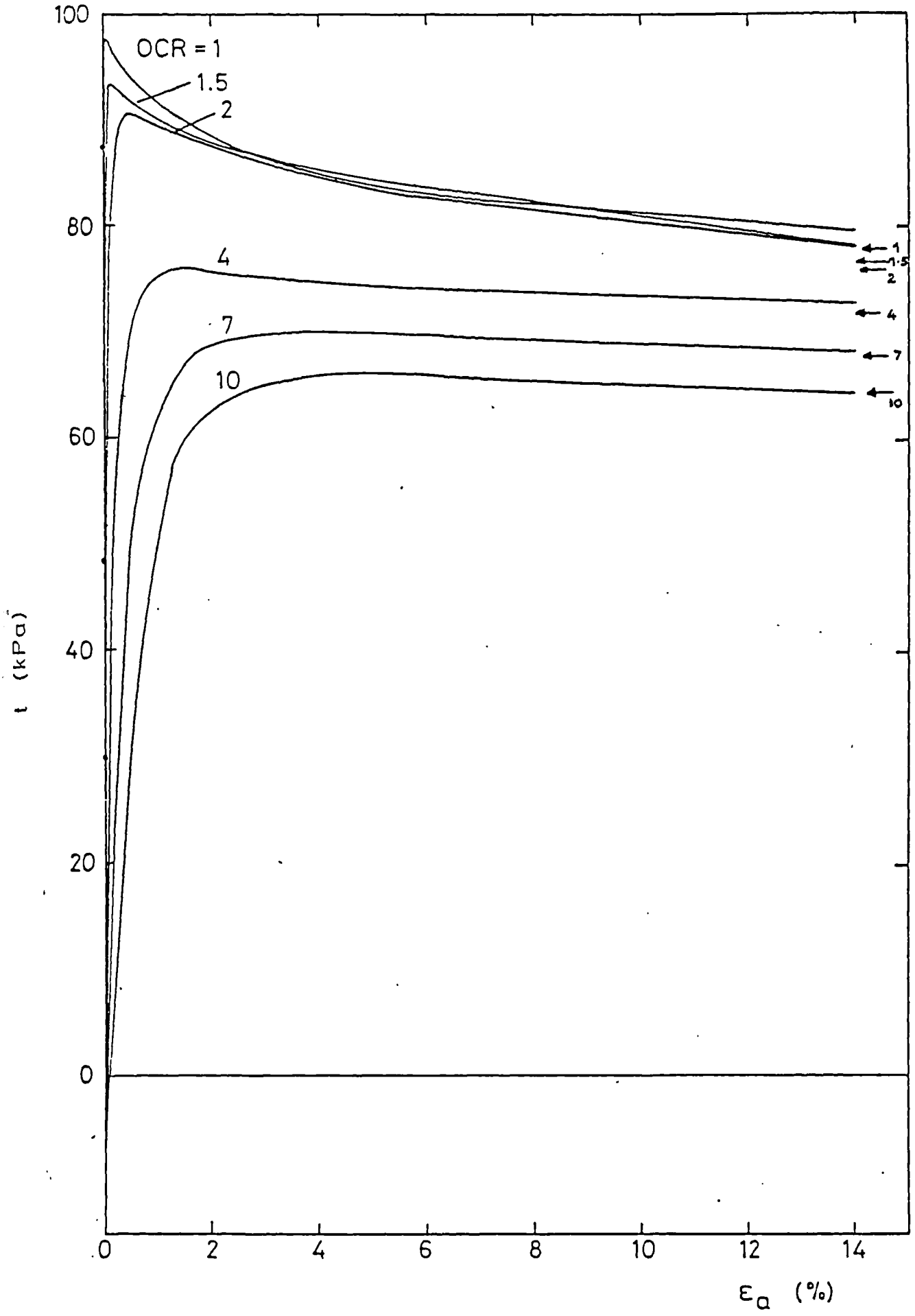

Fig 2.11 Plot of t against axial strain for undrained compression tests on anisotropically (K_o) compressed samples of Lower Cromer till at large strains (Gens, 1982).

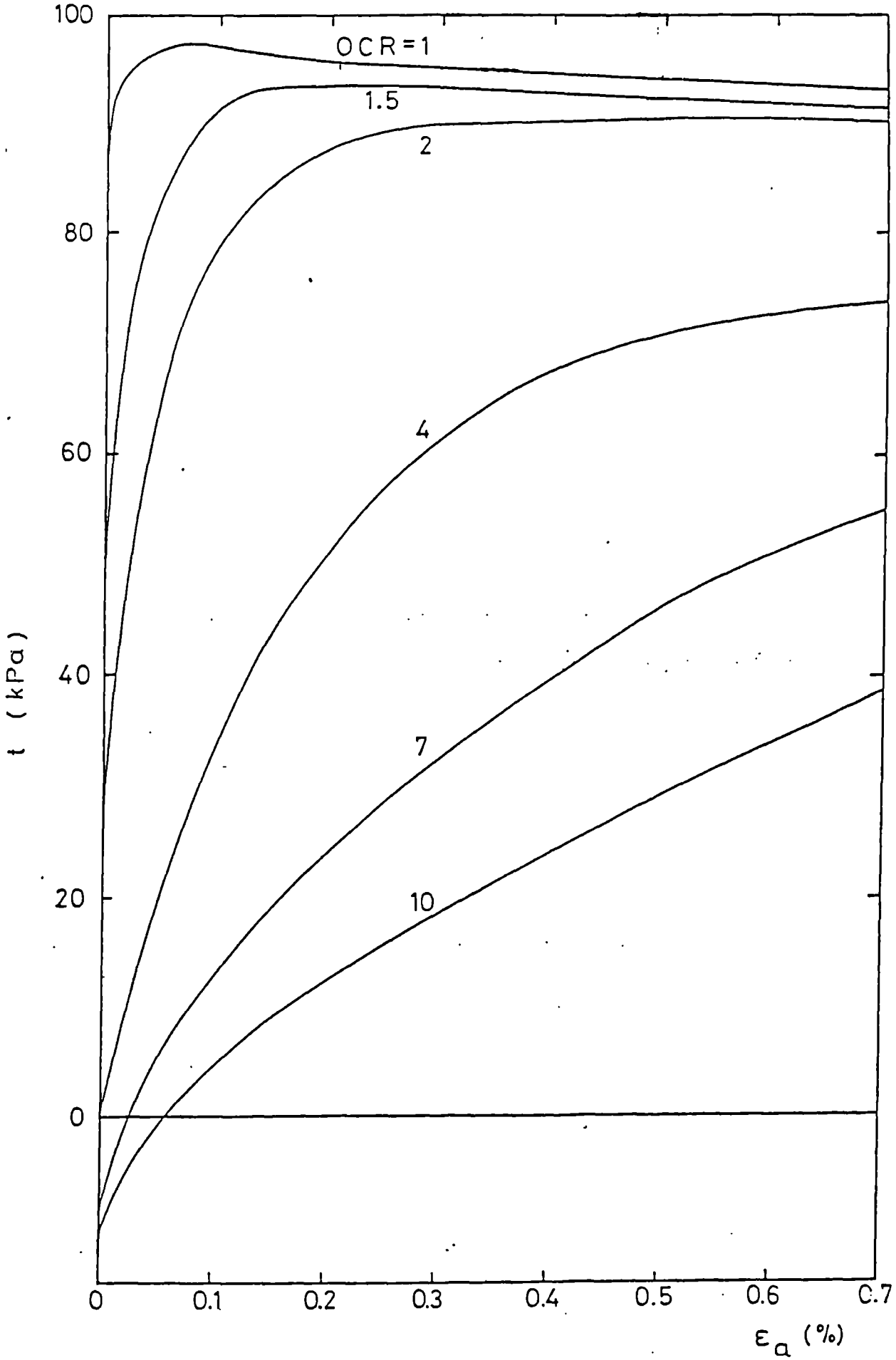

Fig 2.12 Plot of t against axial strain for undrained compression tests on anisotropically (K_o) compressed samples of Lower Cromer till at small strains (Gens, 1982).

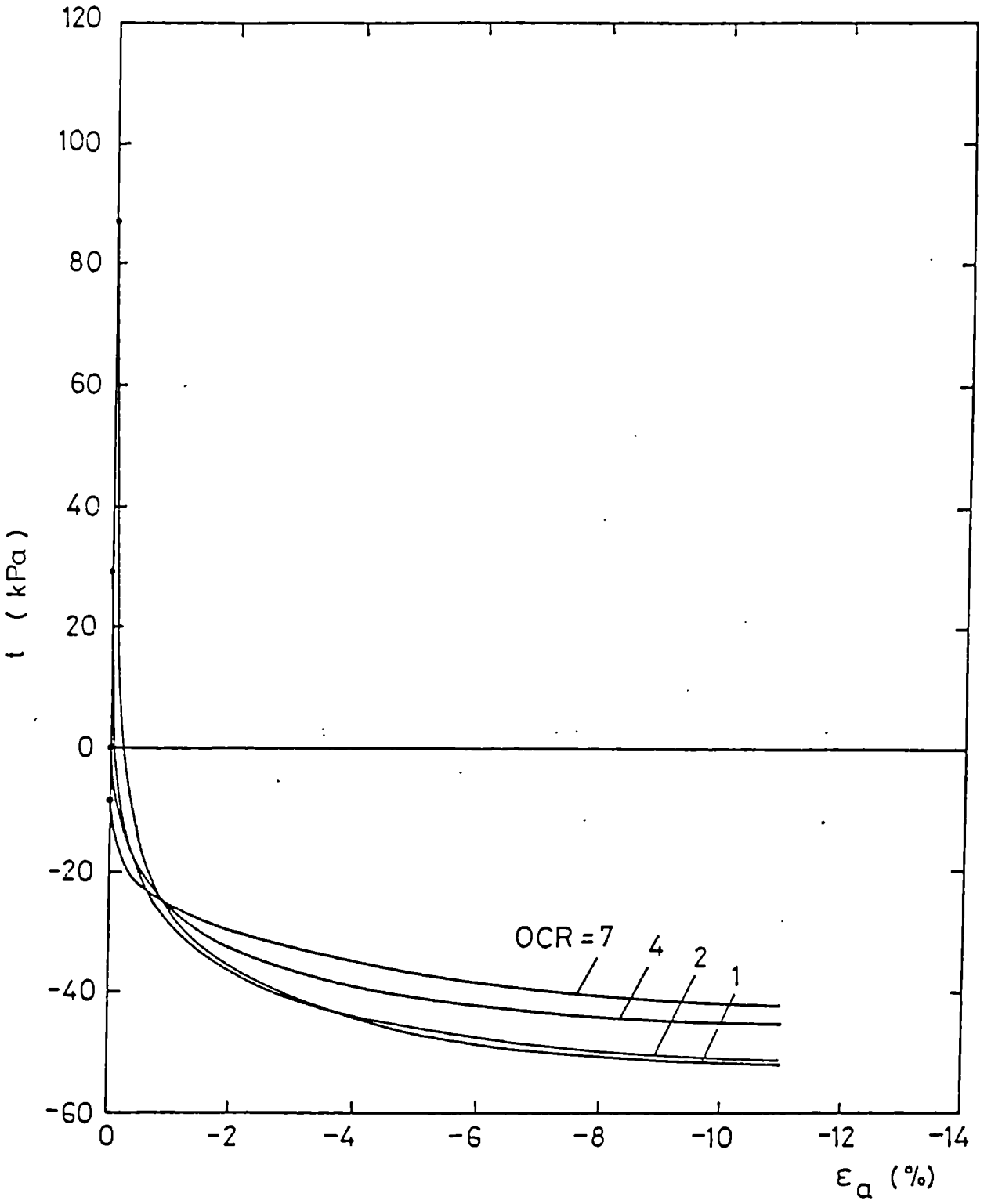

Fig 2.13 Plot of t against axial strain for undrained extension tests on anisotropically (K_o) compressed samples of Lower Cromer till at large strains (Gens, 1982).

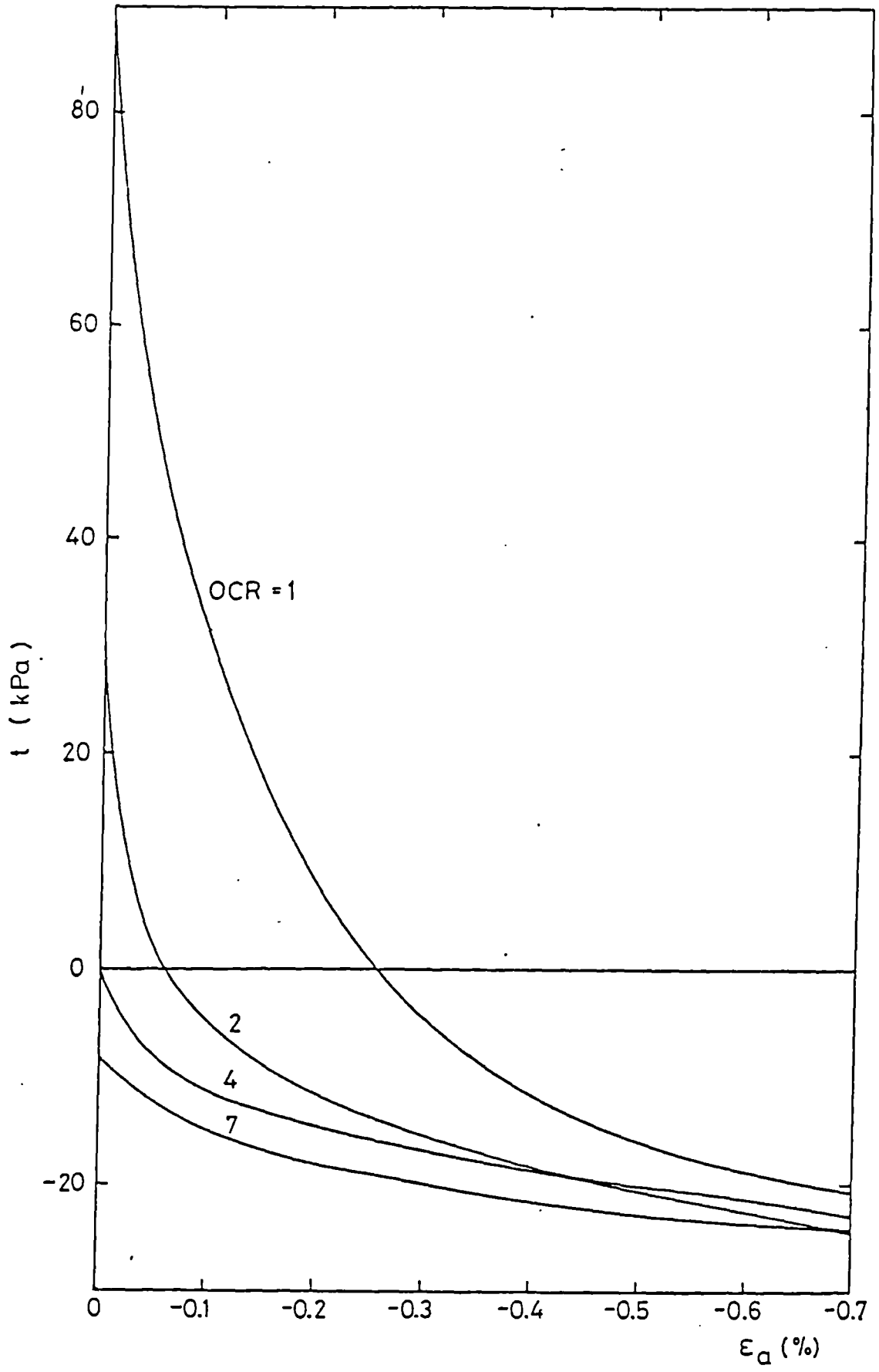

Fig 2.14 Plot of t against axial strain for undrained extension tests on anisotropically (K_o) compressed samples of Lower Cromer till at small strains (Gens, 1982).

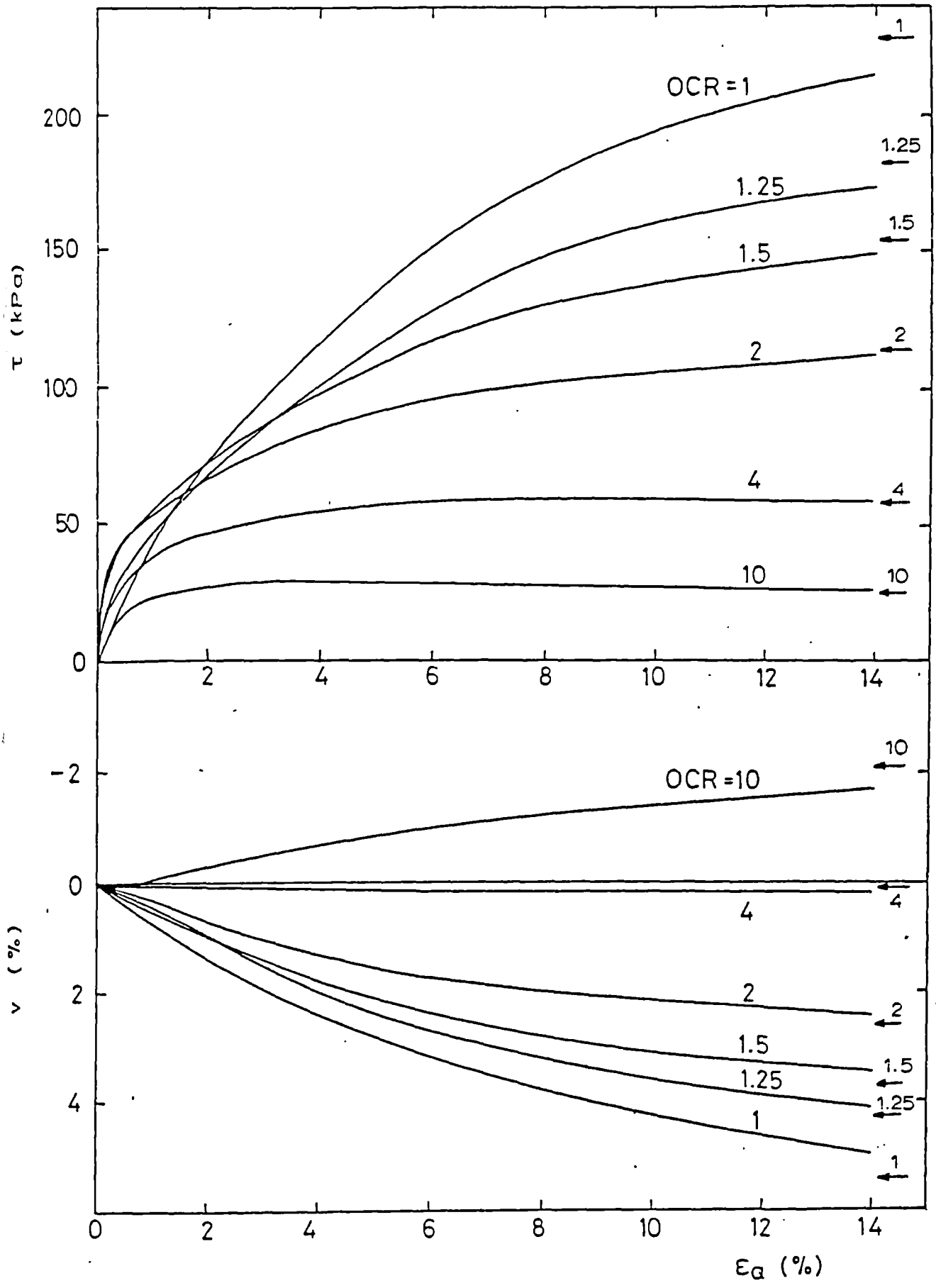

Fig 2.15 Plot of t and ε_v against axial strain for drained compression tests on isotropically compressed samples of Lower Cromer till (Gens, 1982).

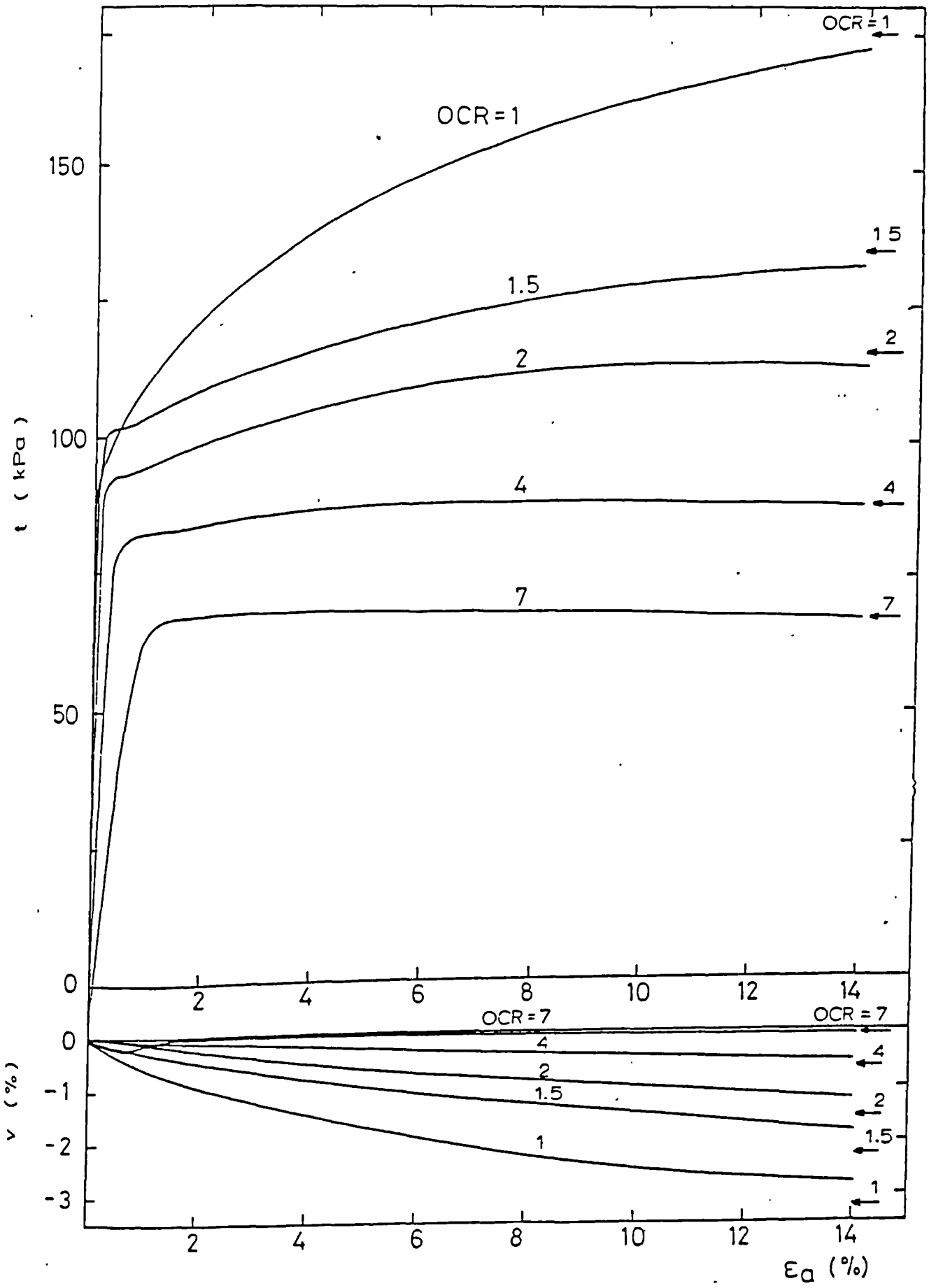

Fig 2.16 Plots of t and ε_v against axial strain for drained compression tests on anisotropically (K_0) compressed samples of Lower Cromer till at large strains (Gens, 1982).

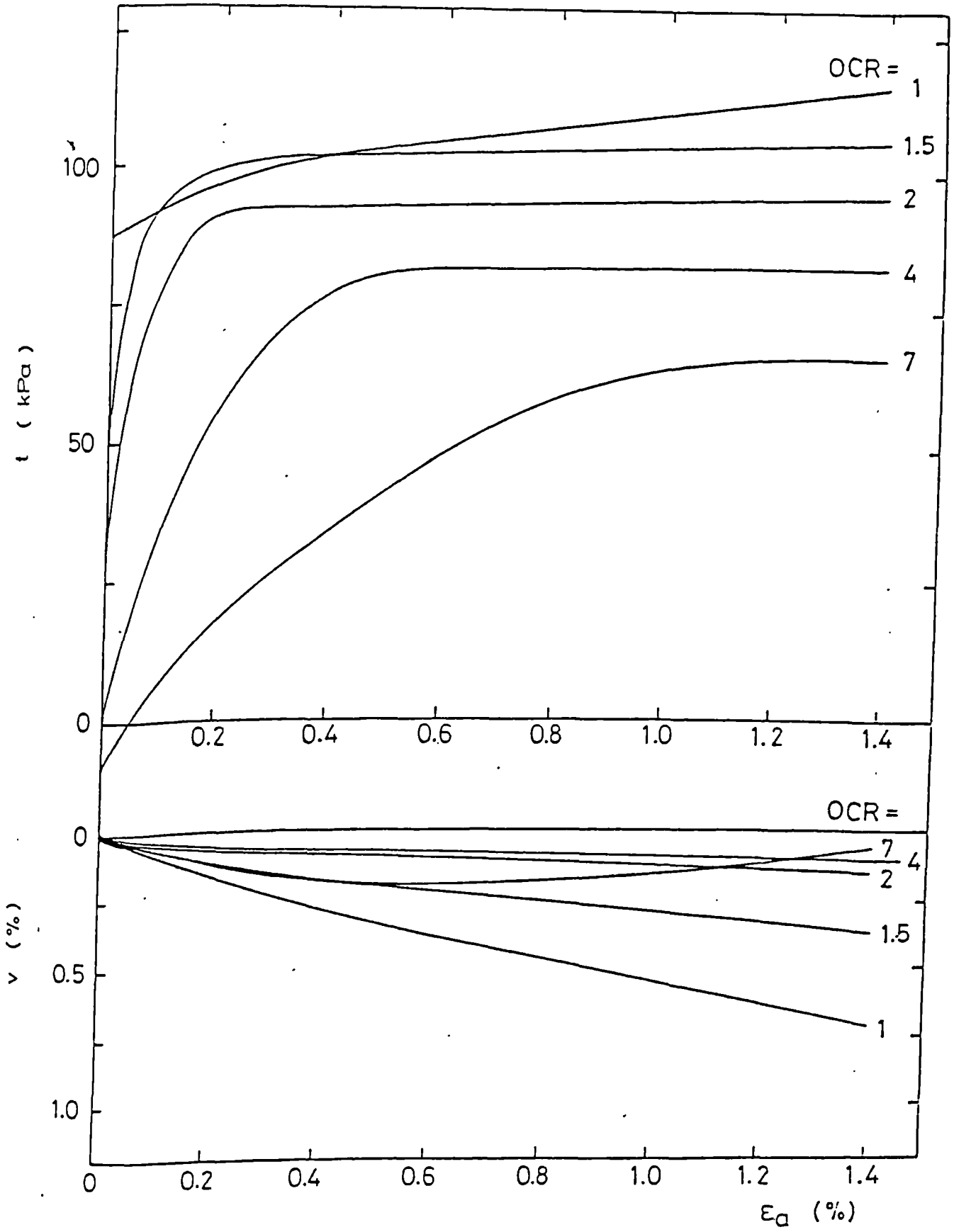

Fig 2.17 Plots of t and ε_v against axial strain for drained compression tests on anisotropically (K_o) compressed samples of Lower Cromer till at small strains (Gens, 1982).

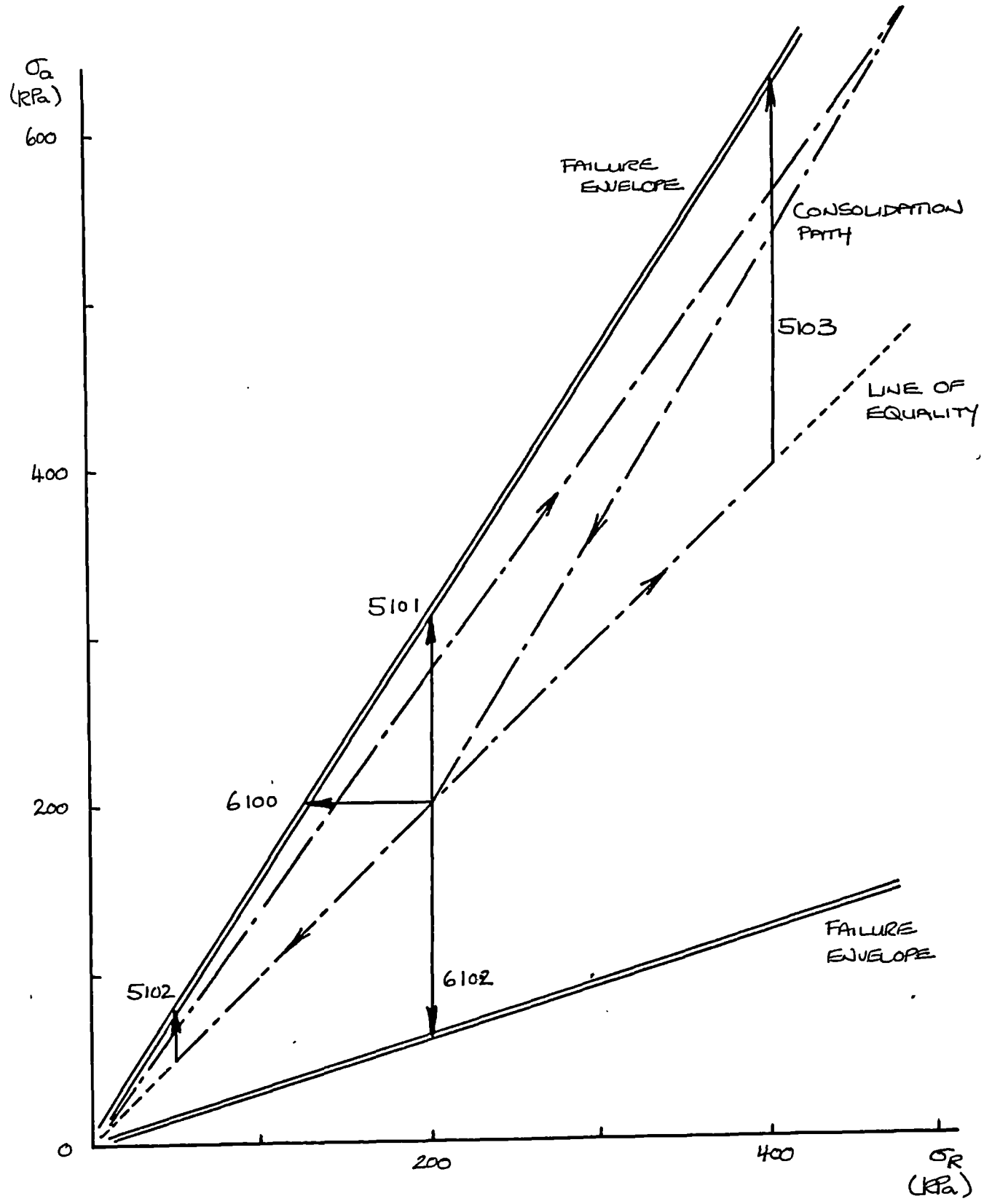

Fig 2.18 Total stress paths followed by London Clay samples (Richardson, 1984a).

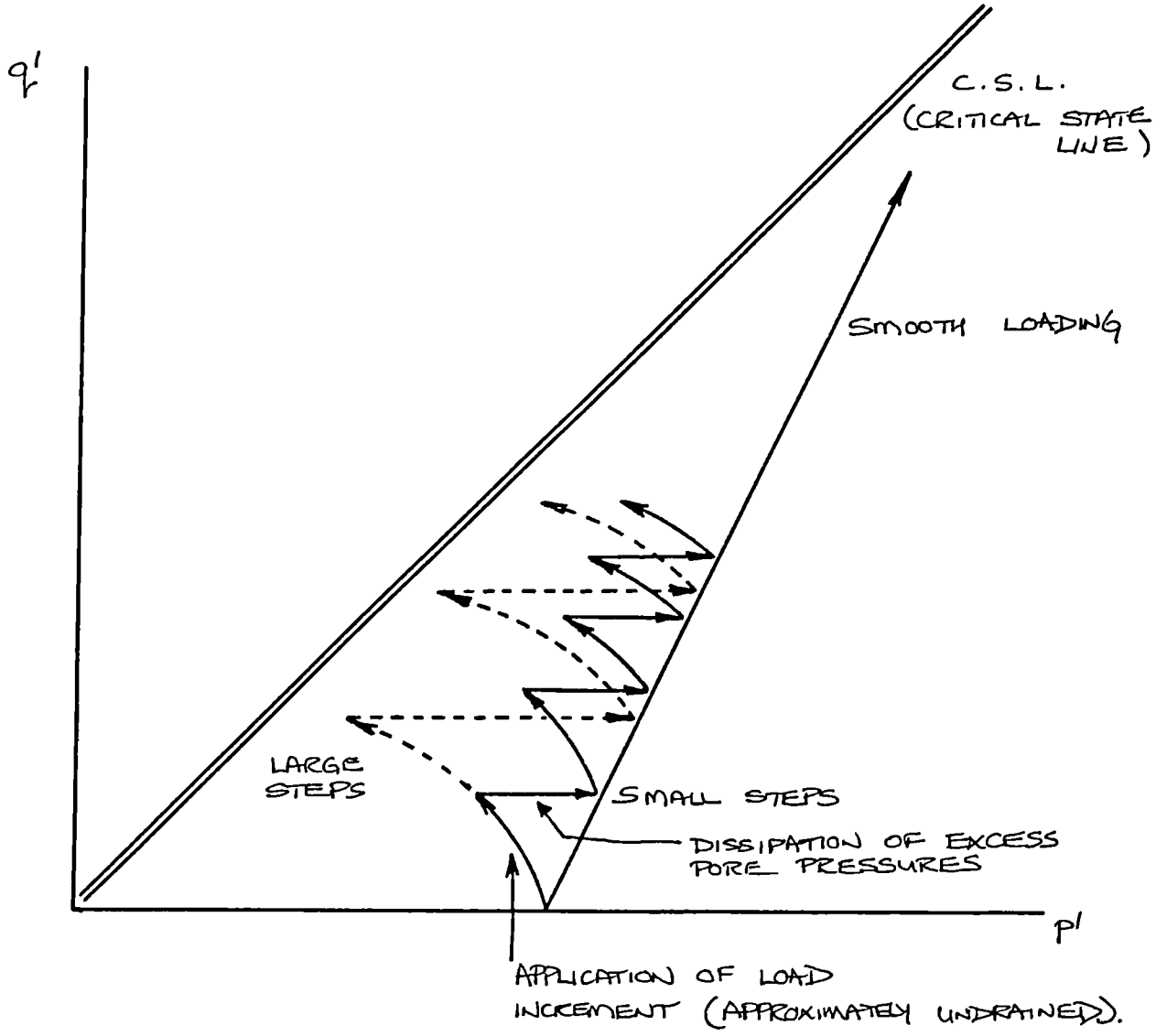

Fig 2.19 Step loading and smooth loading paths.

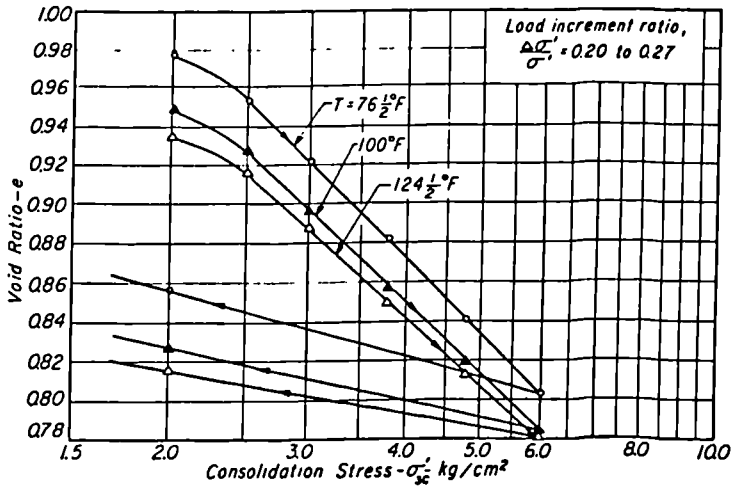

Fig 2.20 Effect of temperature on the voids ratio against $\log_e p'$ plot for saturated Illite (Plum and Esrig, 1969).

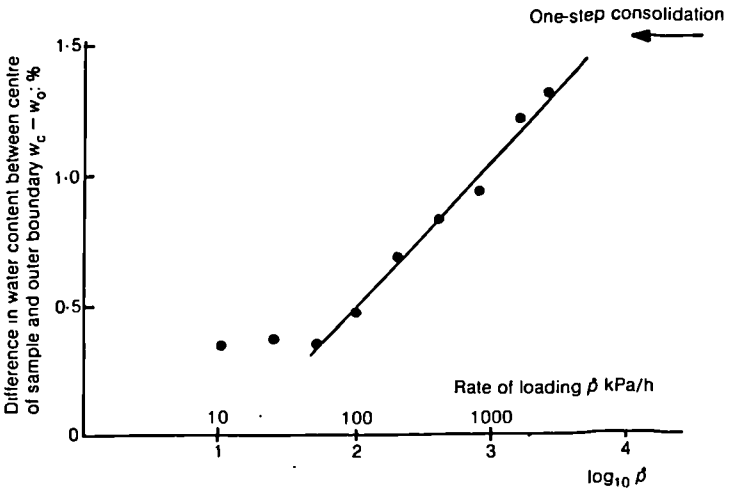

Fig 2.21 Effect of rate of loading on the radial variation of water content in triaxial samples (Atkinson, Evans and Ho, 1984).

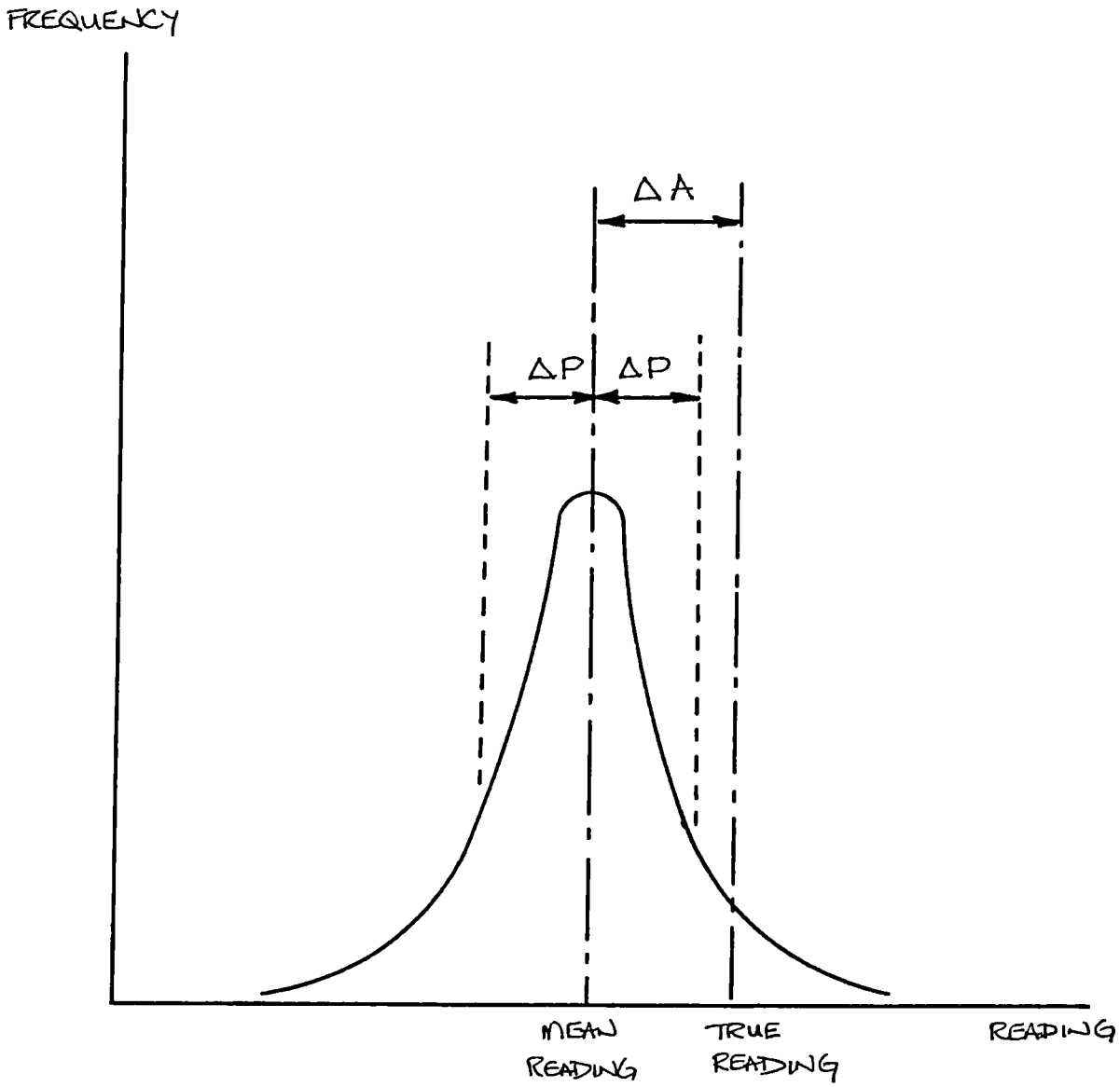

Fig 2.22 Definition of random (Δ P) and systematic (Δ A) errors.

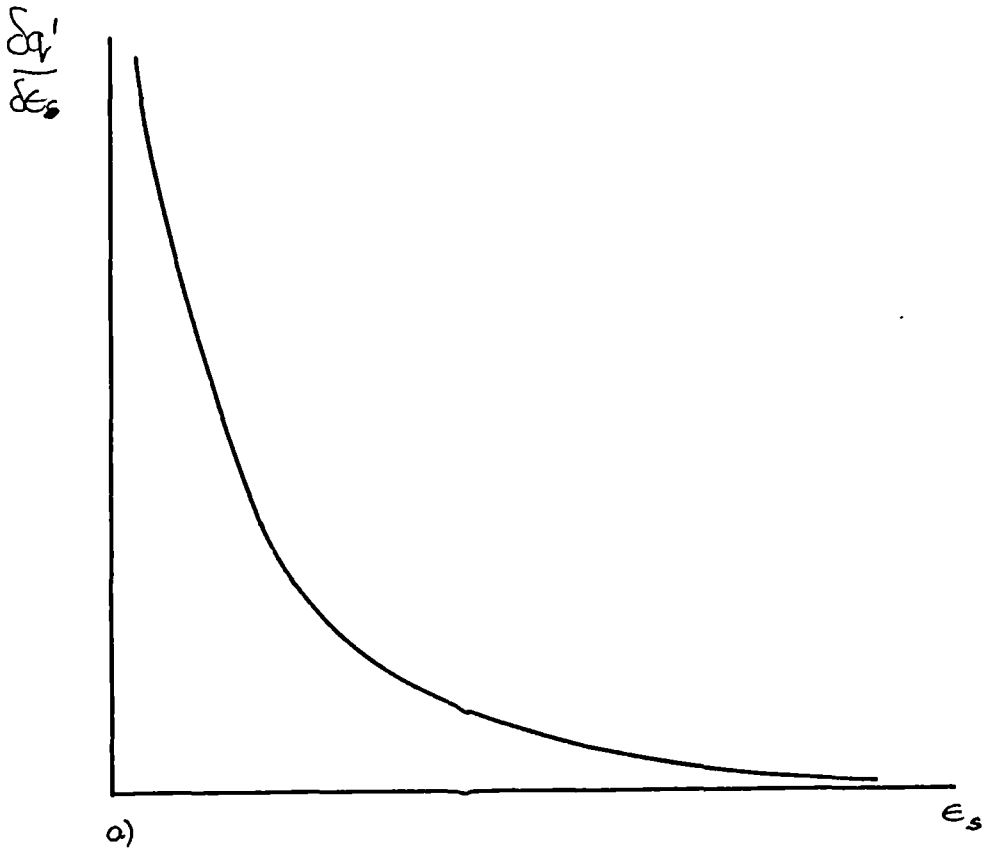

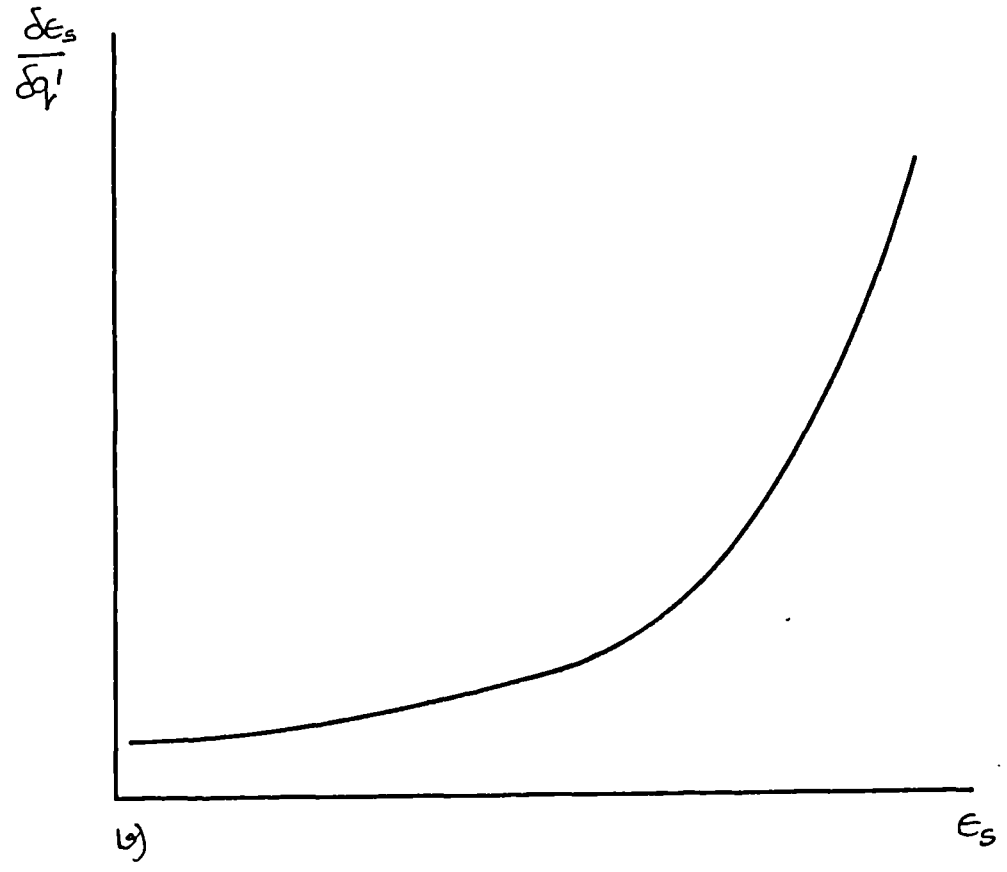

Fig 2.23 Stiffnesses and Compliances.

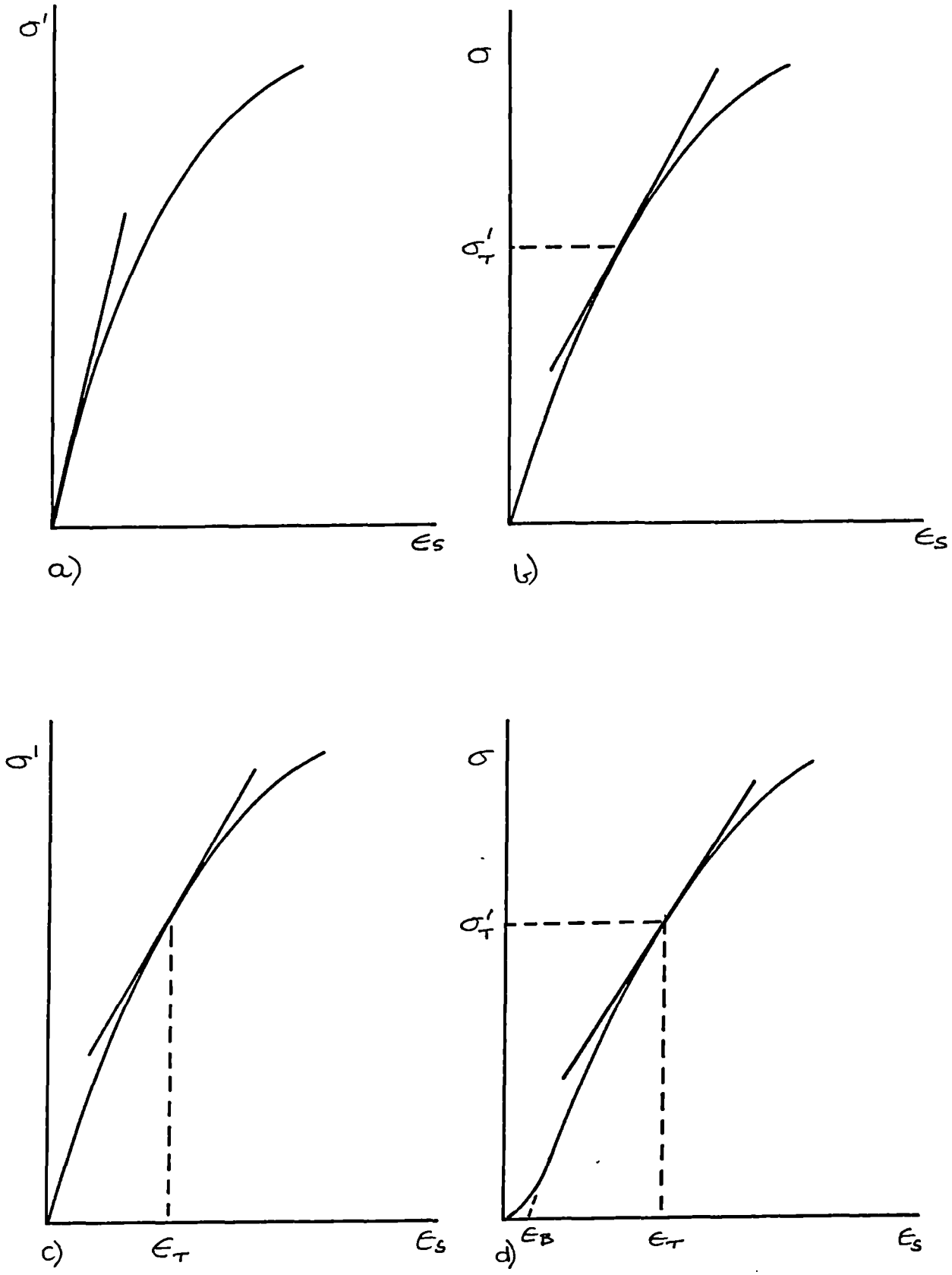

Fig 2.24 Tangent Stiffness Moduli.

a) Defined at the origin.
b) Defined at a stress level.
c) Defined at a strain level.
d) Effect of bedding errors on tangent moduli.

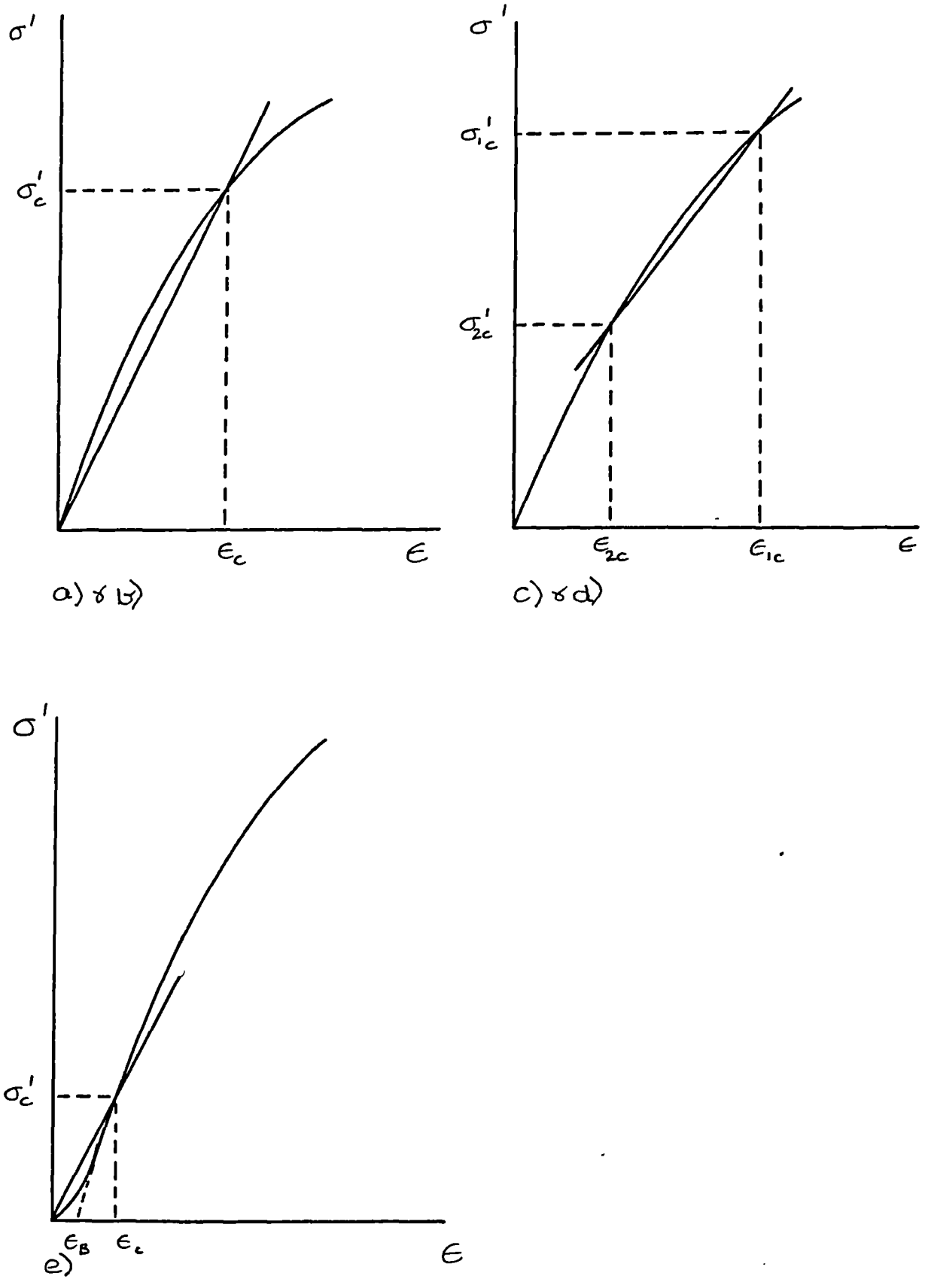

Fig 2.25 Secant Stiffness Moduli.

a) Defined at the origin over a stress interval.
b) Defined at the origin over a strain interval.
c) Defined at a stress level over a stress interval.
d) Defined at a strain level over a strain interval.
e) Effect of bedding errors on secant moduli.

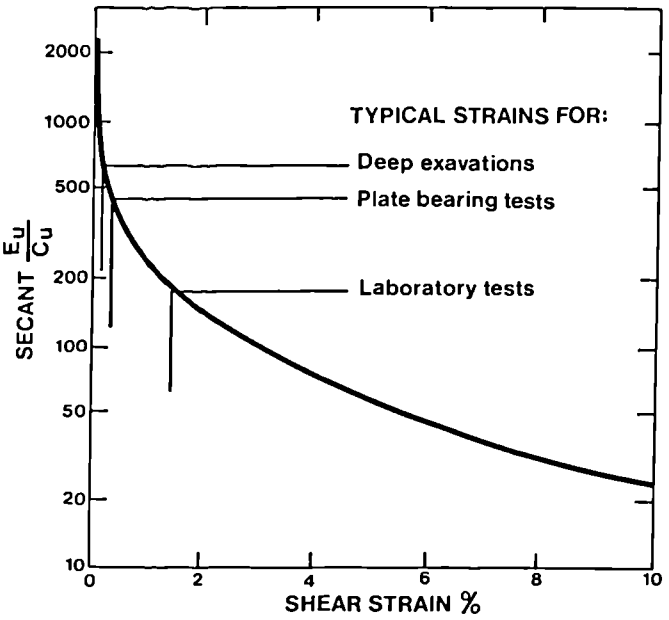

Fig 2.26 Values of secant E_u / c_u derived from model L.C. at various shear strain levels (Simpson et al, 1980).

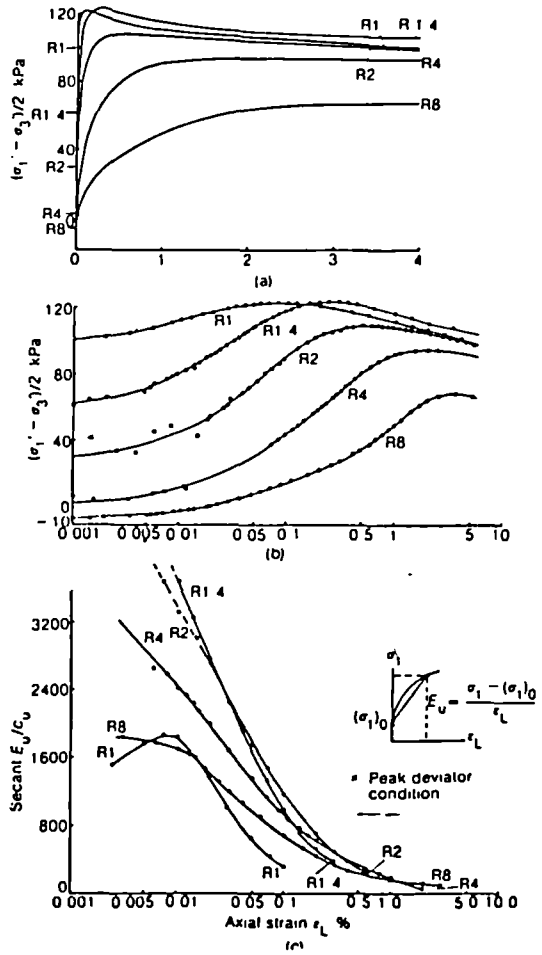

Fig 2.27 Results of tests by Jardine, Symes and Burland (1984).

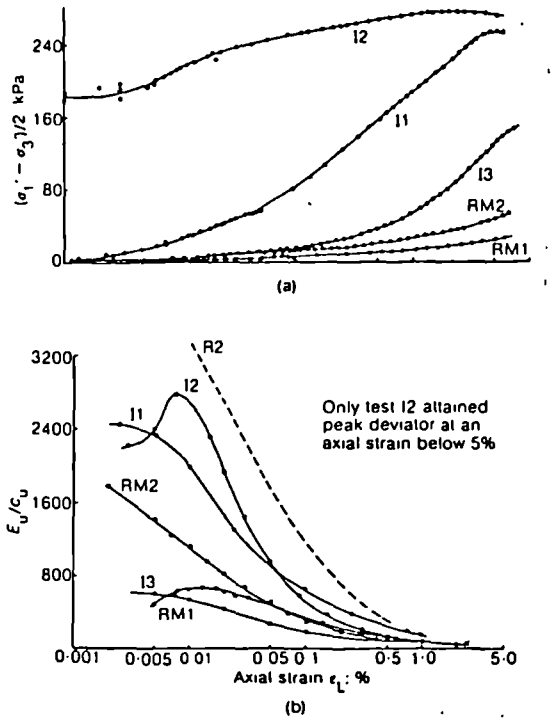

Fig 2.28 Results of tests by Jardine, Symes and Burland (1984).

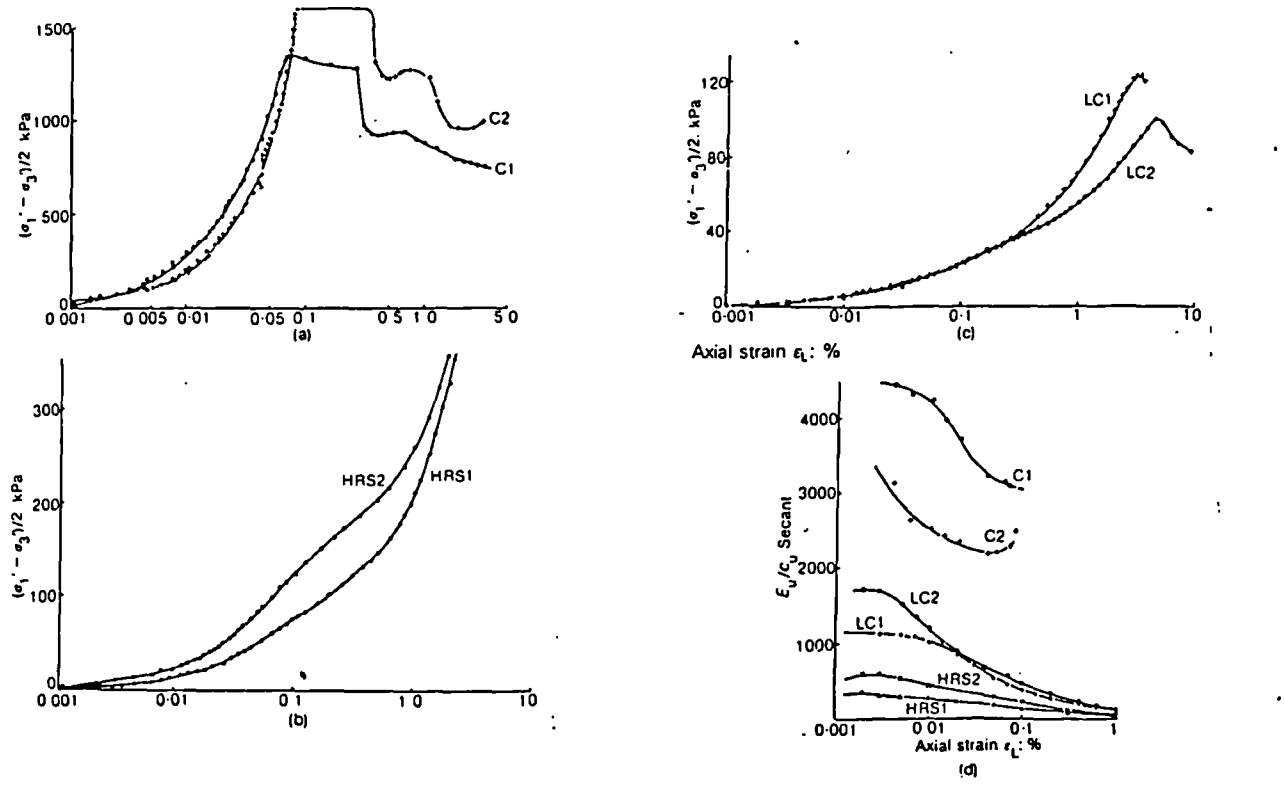

Fig 2.29 Results of tests by Jardine, Symes and Burland (1984).

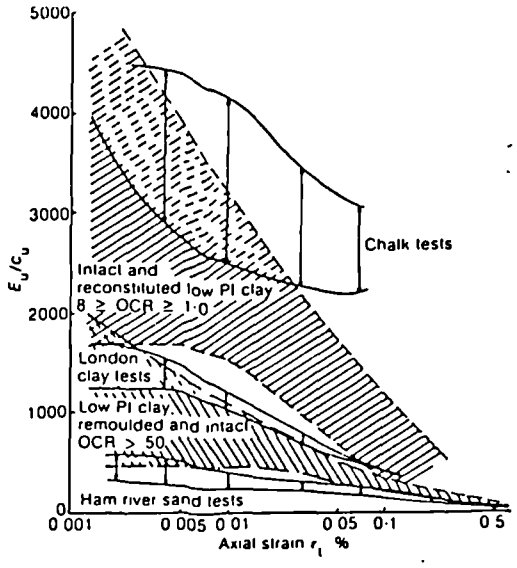

Fig 2.30 Collected normalised secant stiffness moduli for various soils (Jardine, Symes and Burland,1984).

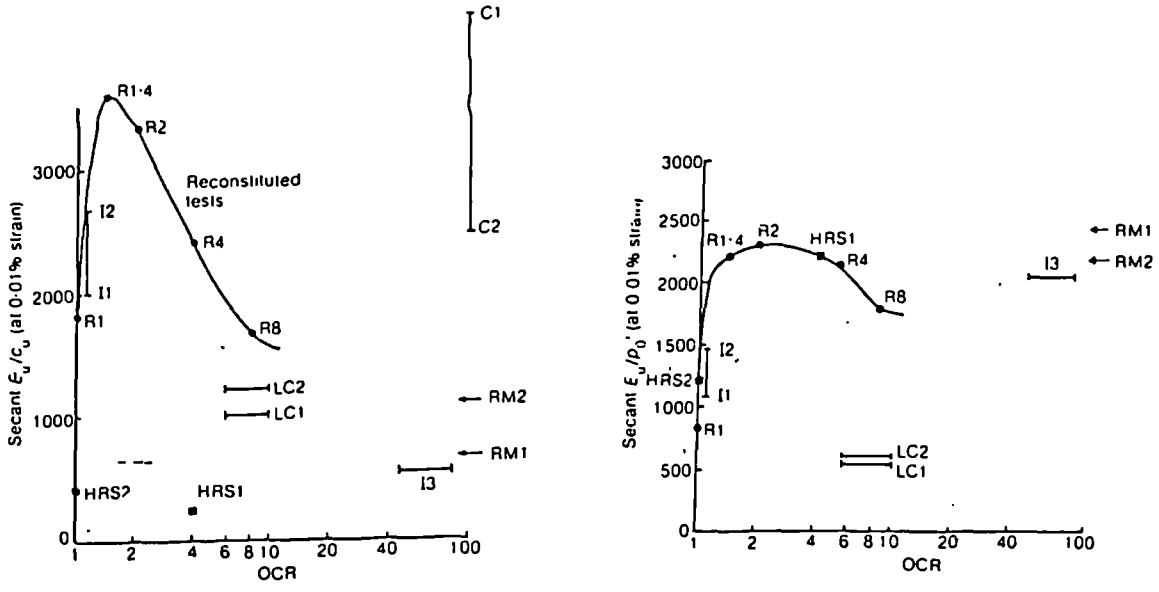

Fig 2.31 Collected normalised secant stiffness moduli (Jardine, Symes and Burland,1984).
a) Normalised with respect to c_u.
b) Normalised with respect to p'_o.

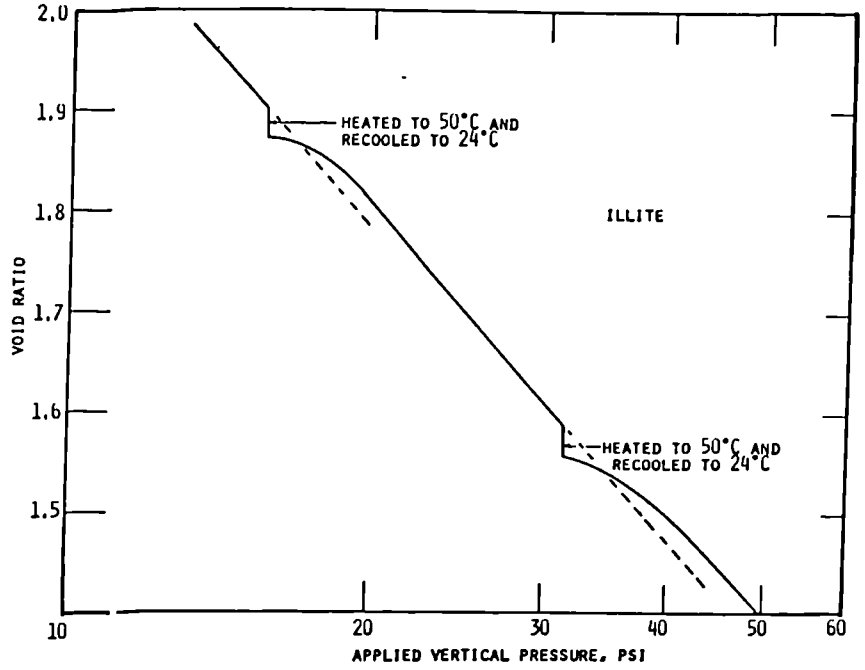

Figure 3. Effect on stress-strain behavior in consolidometer of heating and cooling illite.

Fig 2.32 Effect on sample stiffness of a cycle of temperature change. (Plum and Esrig, 1969).

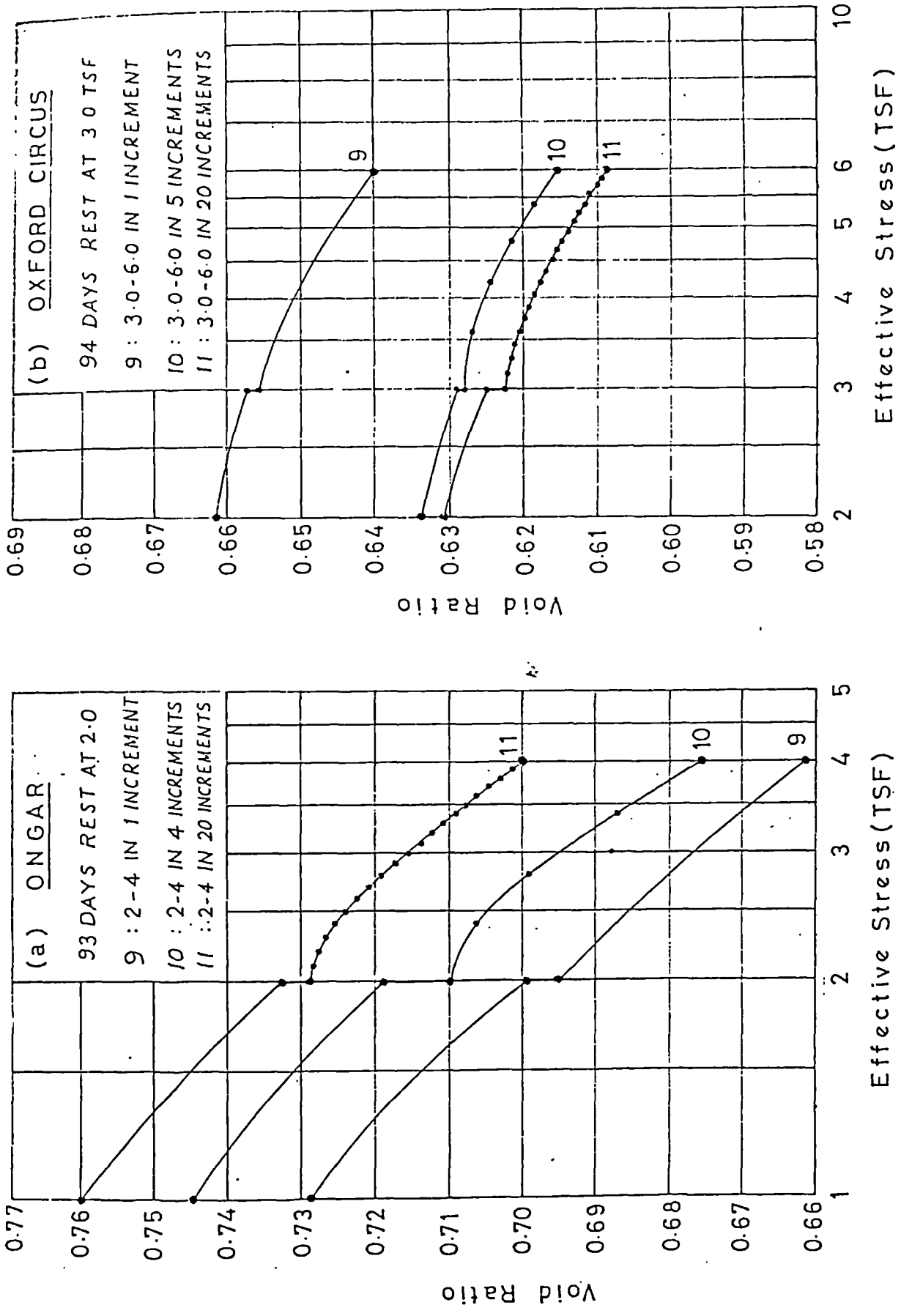

Fig 2.33 Results of oedometer tests on undisturbed London Clay with a rest period of 93 days (Som,1968).

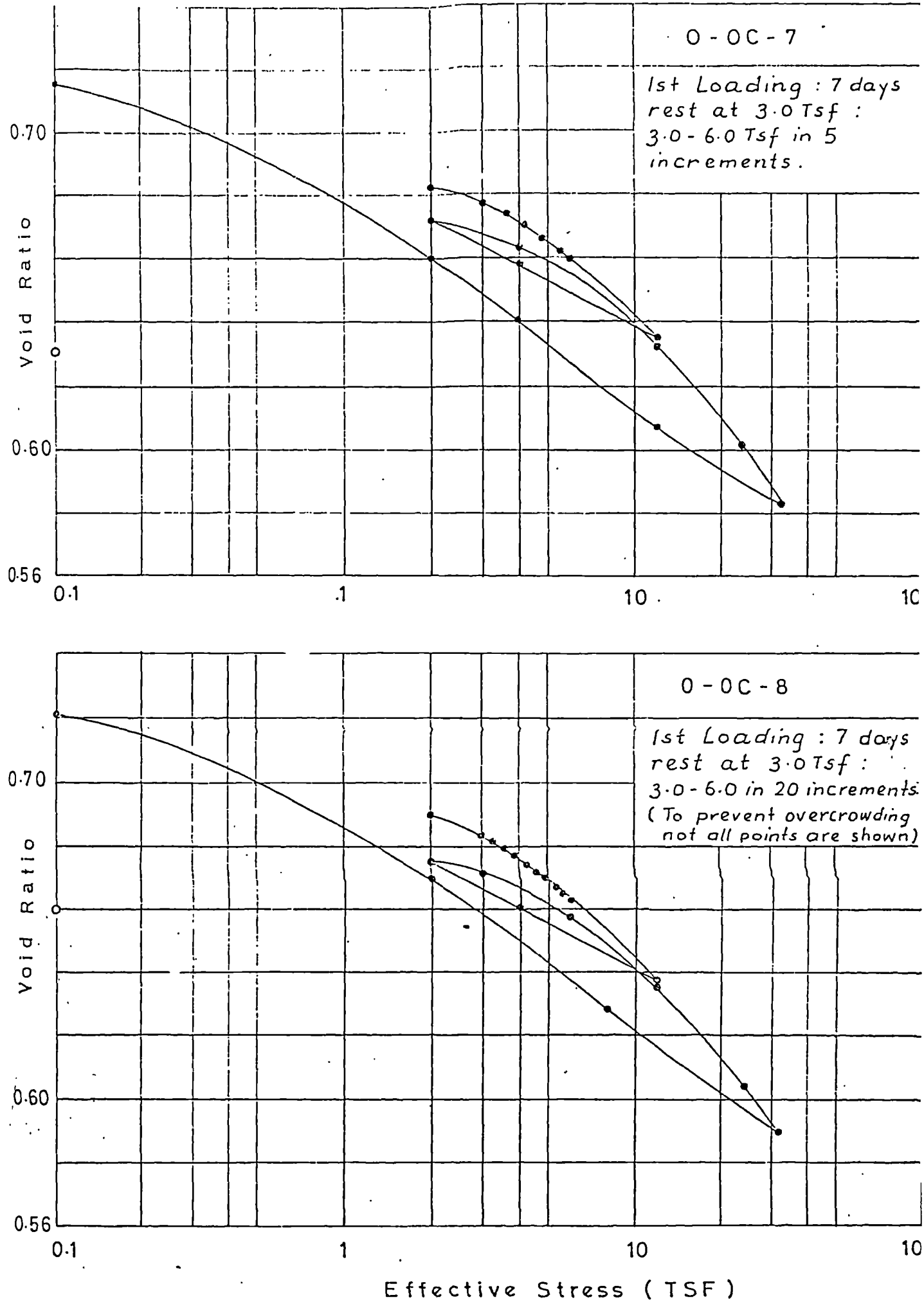

1 TSF = 107·4 KPa.

Fig 2.34 Results of œdometer tests on undisturbed London Clay with a rest period of 7 days (Som, 1968).

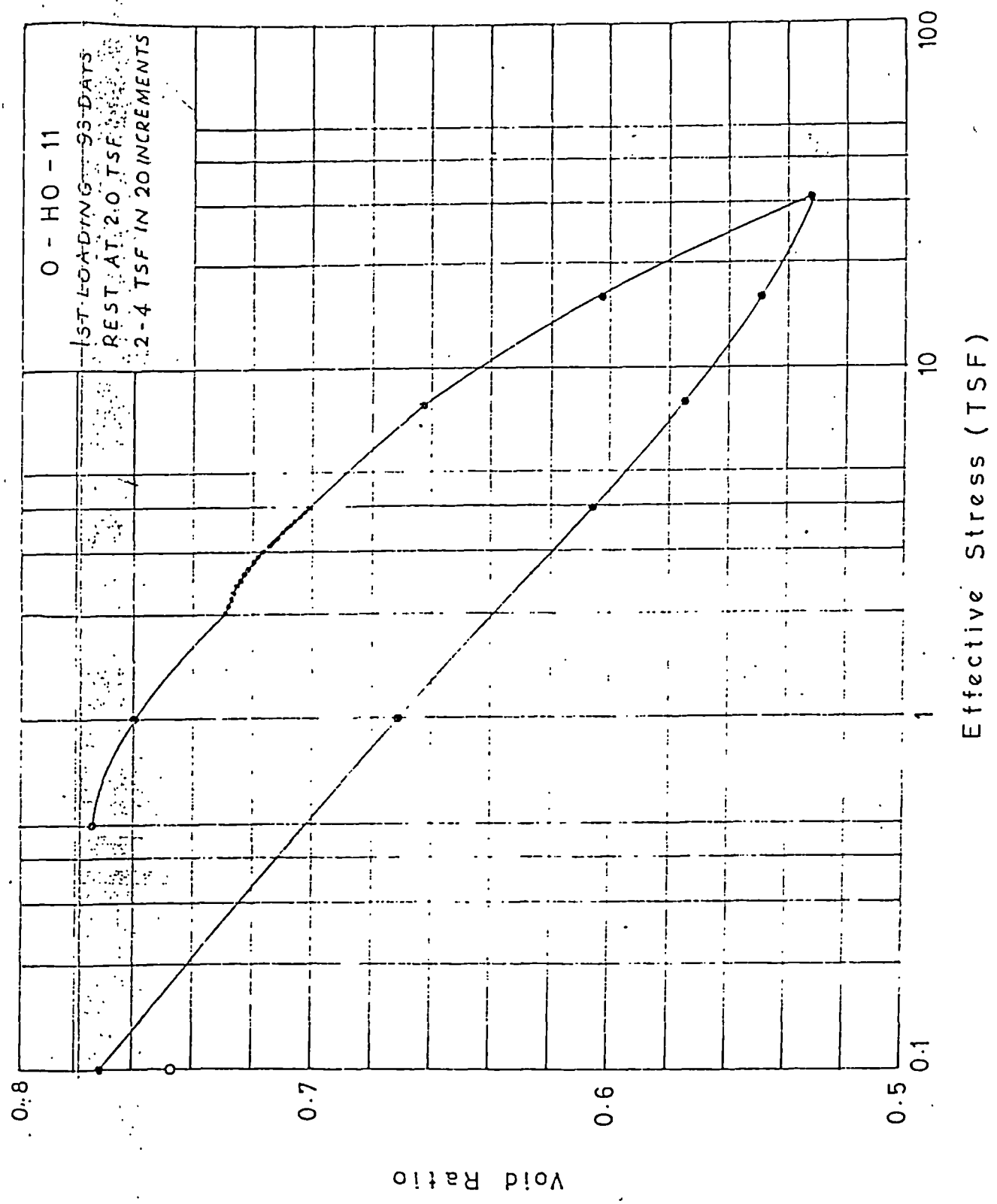

1 TSF ≡ 107.4 kPa.

Fig 2.35 Results of œdometer tests on undisturbed London Clay with a rest period of 93 days (Som, 1968).

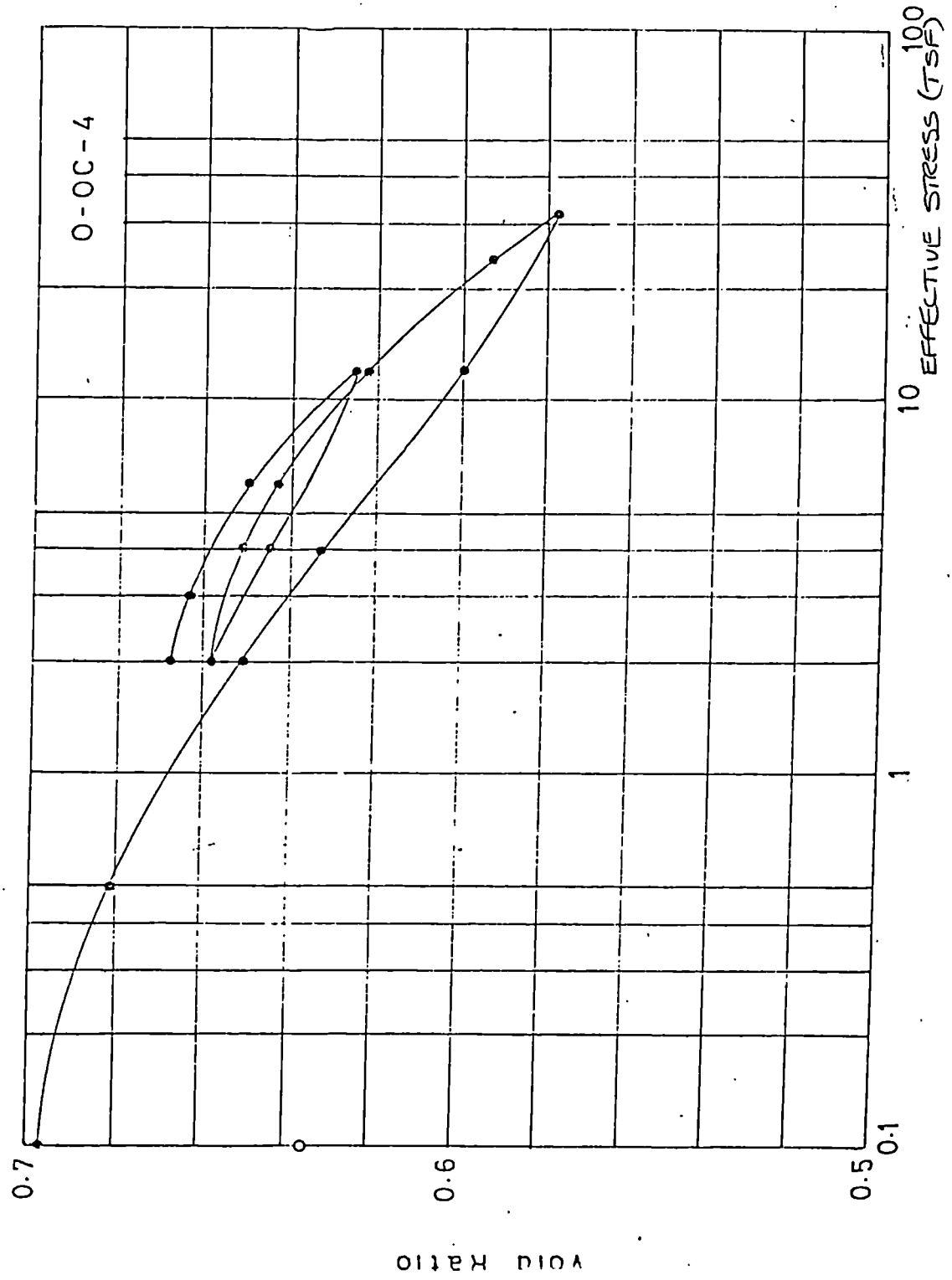

1 TSF = 107.4 KPa.

Fig 2.36 Results of œdometer tests on undisturbed London Clay with no rest period (Som, 1968).

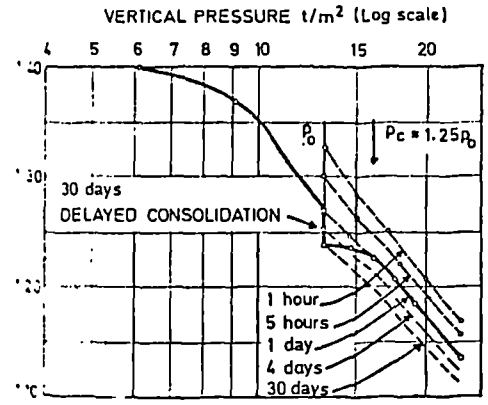

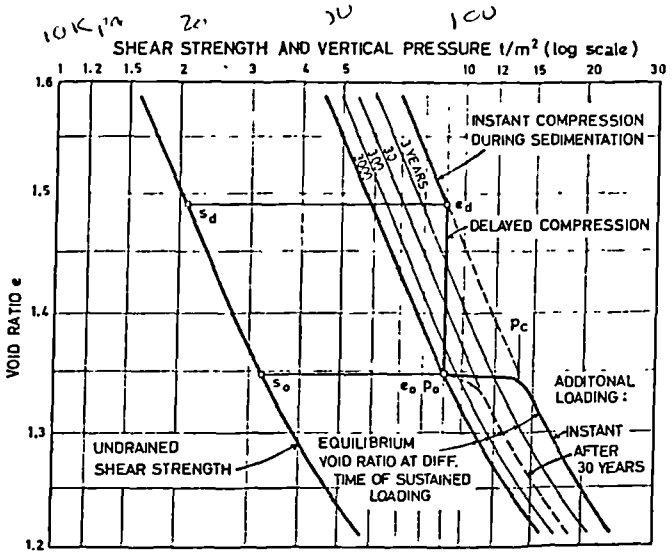

Fig 2.37 Effect of a period of rest on the voids ratio against $\log_{10} \sigma'_v$ plot for Drammen clay (Bjerrum, 1967).

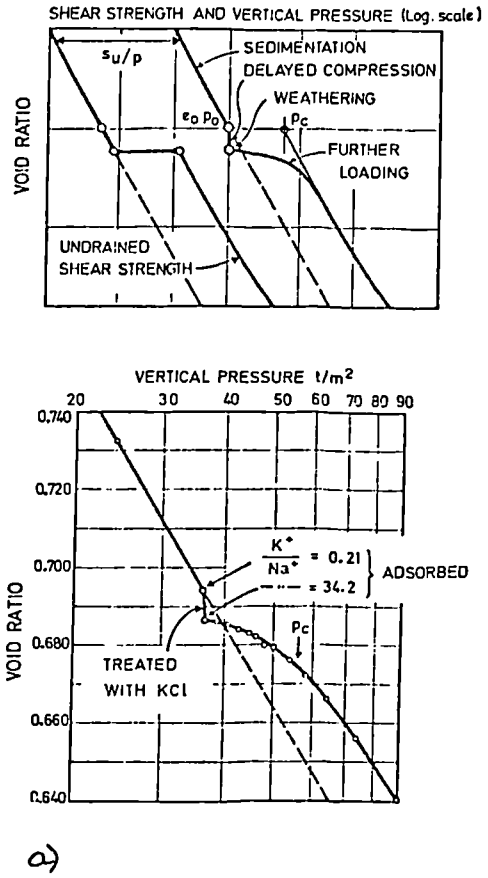

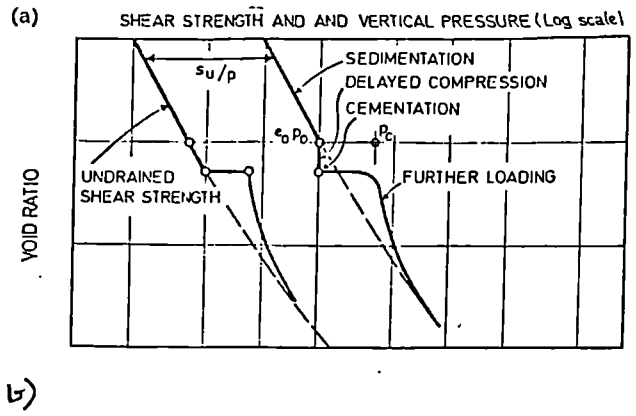

Fig 2.38 a) Effect of adding sodium chloride to Drammen clay on the voids ratio against $\log_{10} \sigma'_v$ plot (Bjerrum,1967).
b) Effect of cementation of soil grains (Bjerrum, 1967).

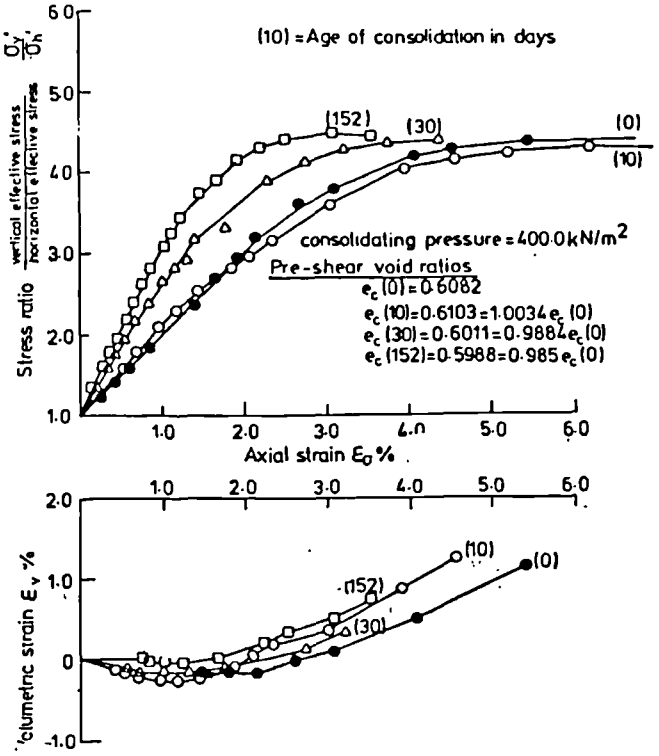

Fig 2.39 Stress ratio and volumetric strain plotted against axial strain for Ham River Sand (Daramola, 1979).

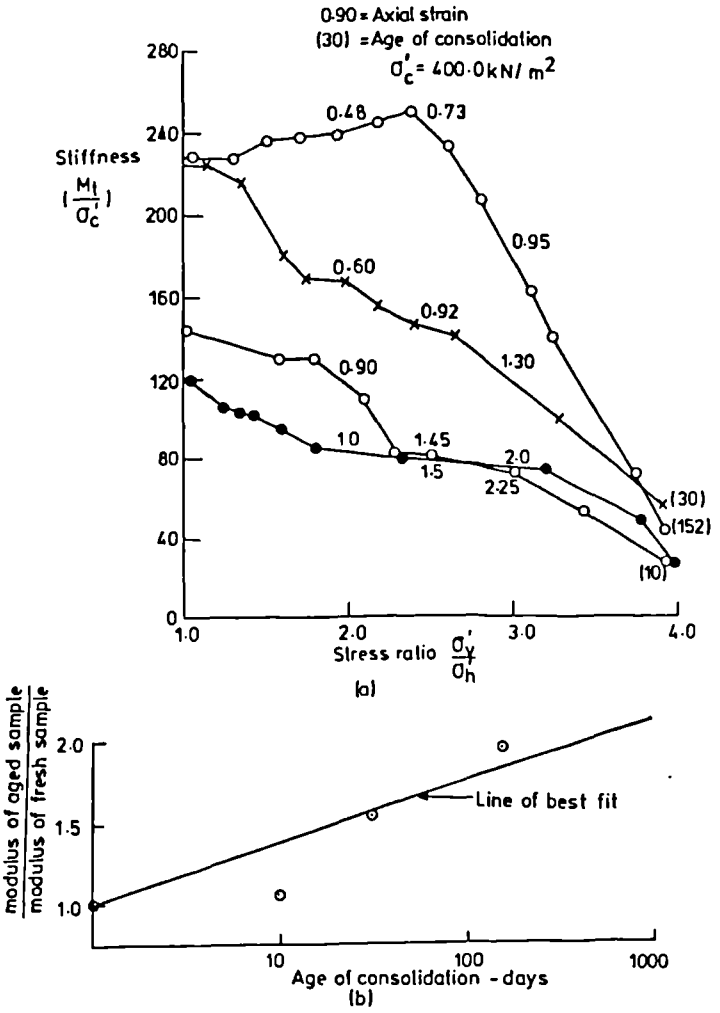

Fig 2.40 Stiffness moduli for Ham River Sand (Daramola, 1979).
a) Tangent moduli.
b) Secant moduli.

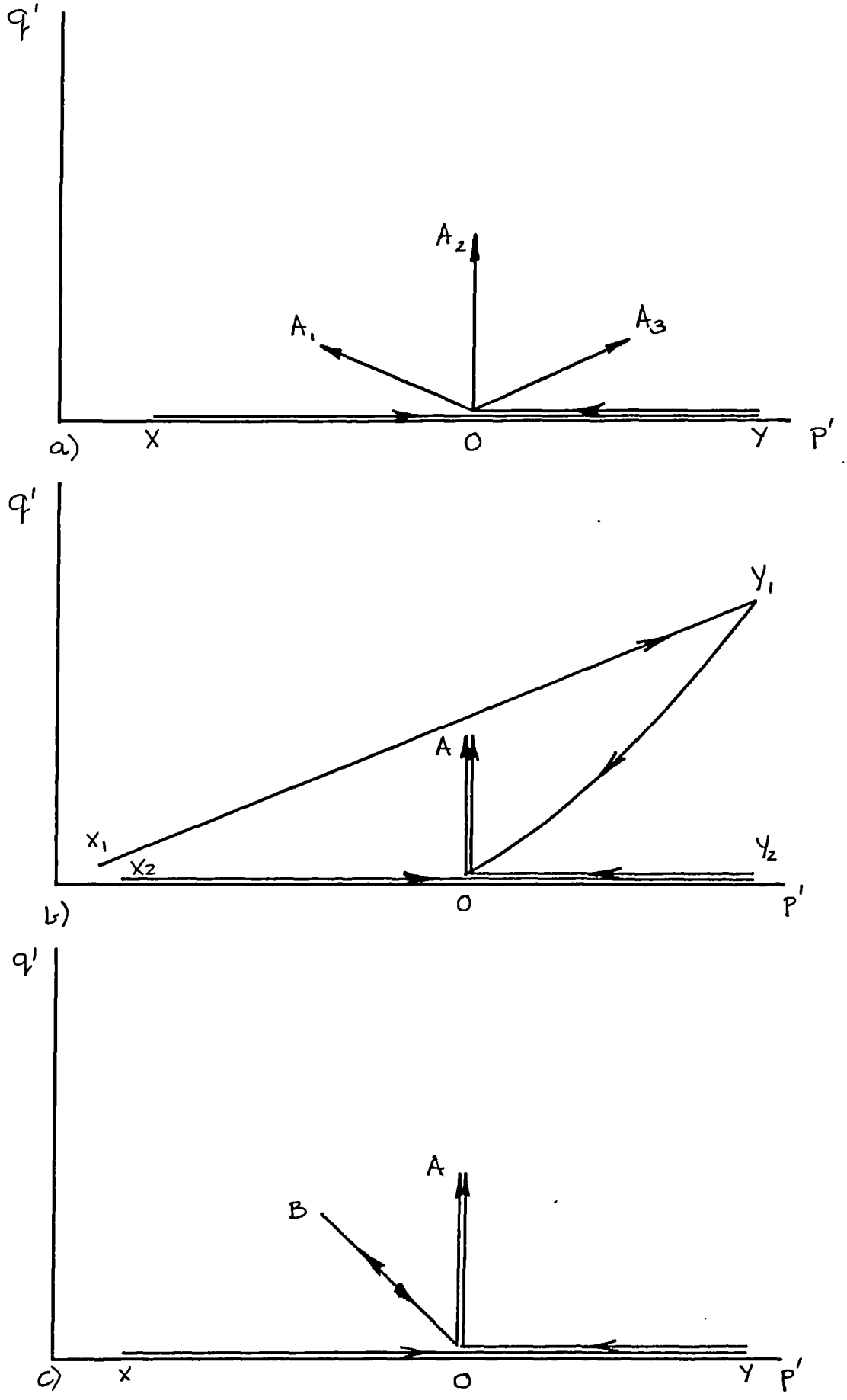

Fig 2.41 Types of stress probe tests.

a) Same initial stress history, different final paths.
b) Different initial stress history, same final paths.
c) Same initial stress history, different recent stress history, same final paths.

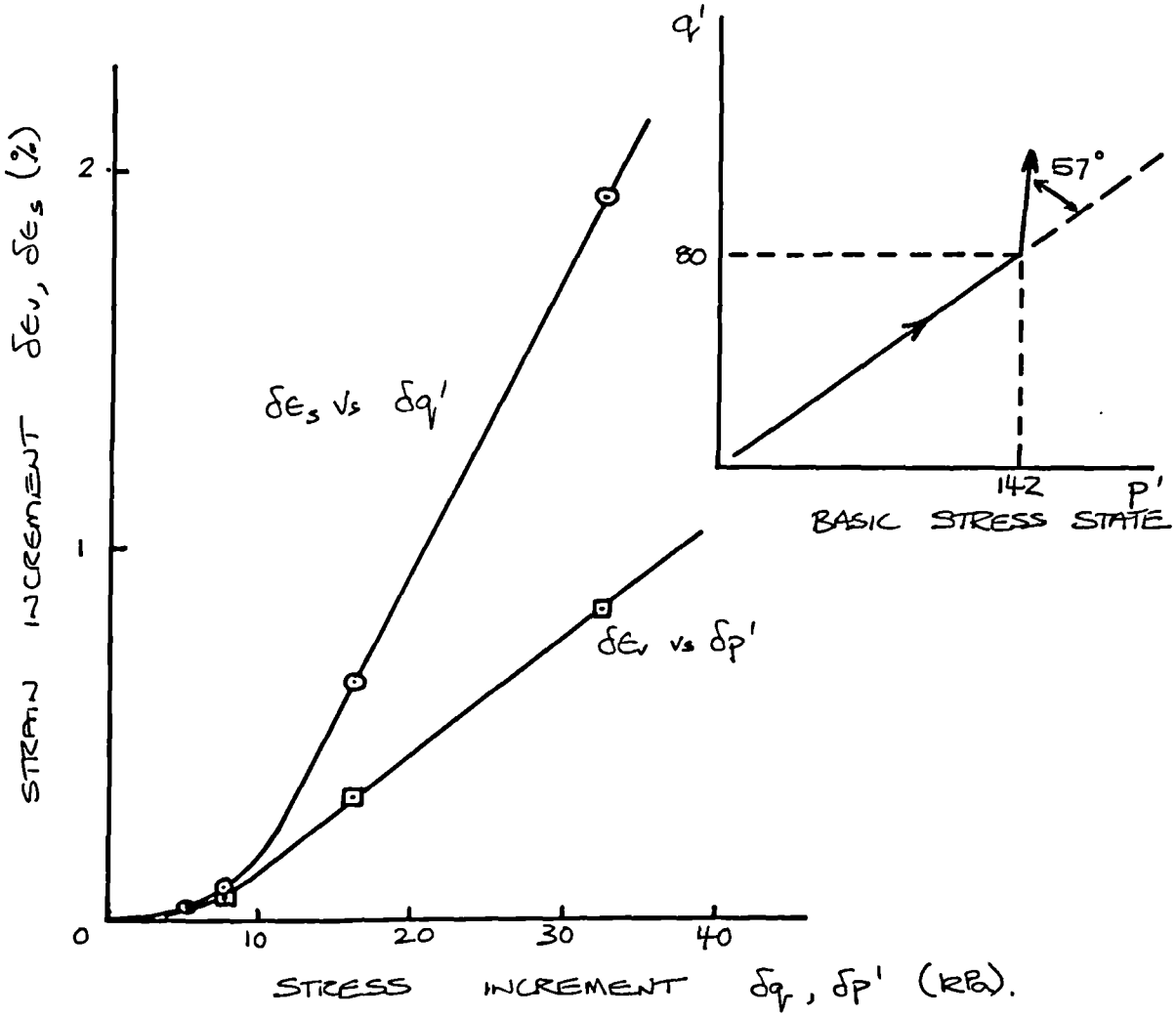

Test	$\Delta\sigma'_1$ kPa	$\Delta\sigma'_3$ kPa	$\Delta q'$ kPa	$\Delta p'$ kPa	$\Delta\varepsilon_1$ %	$\Delta\varepsilon_v$ %	$\Delta\varepsilon_s$ %	$\frac{\Delta q'}{\Delta\varepsilon_s}$ MPa	$\frac{\Delta p'}{\Delta\varepsilon_v}$ MPa
RF1 2 days at 1/3 normal	3.9	-1.5	5.4	0.9	0.035	0.011	0.031	17.4	3.2
RF1 2 days at 1/3 normal 1 day at 2/3 normal	7.9	-2.9	10.8	2.1	0.124	0.061	0.104	10.4	3.4
RF2 2 days at 2x normal	23.6	-8.8	32.4	6	2.189	0.826	1.914	1.7	0.7
RF 2 days at normal	11.8	-4.4	16.2	3	0.756	0.331	0.646	2.5	0.9

Fig 2.42 Effect of varying size of stress probe on Slate dust (Lewin, 1970).

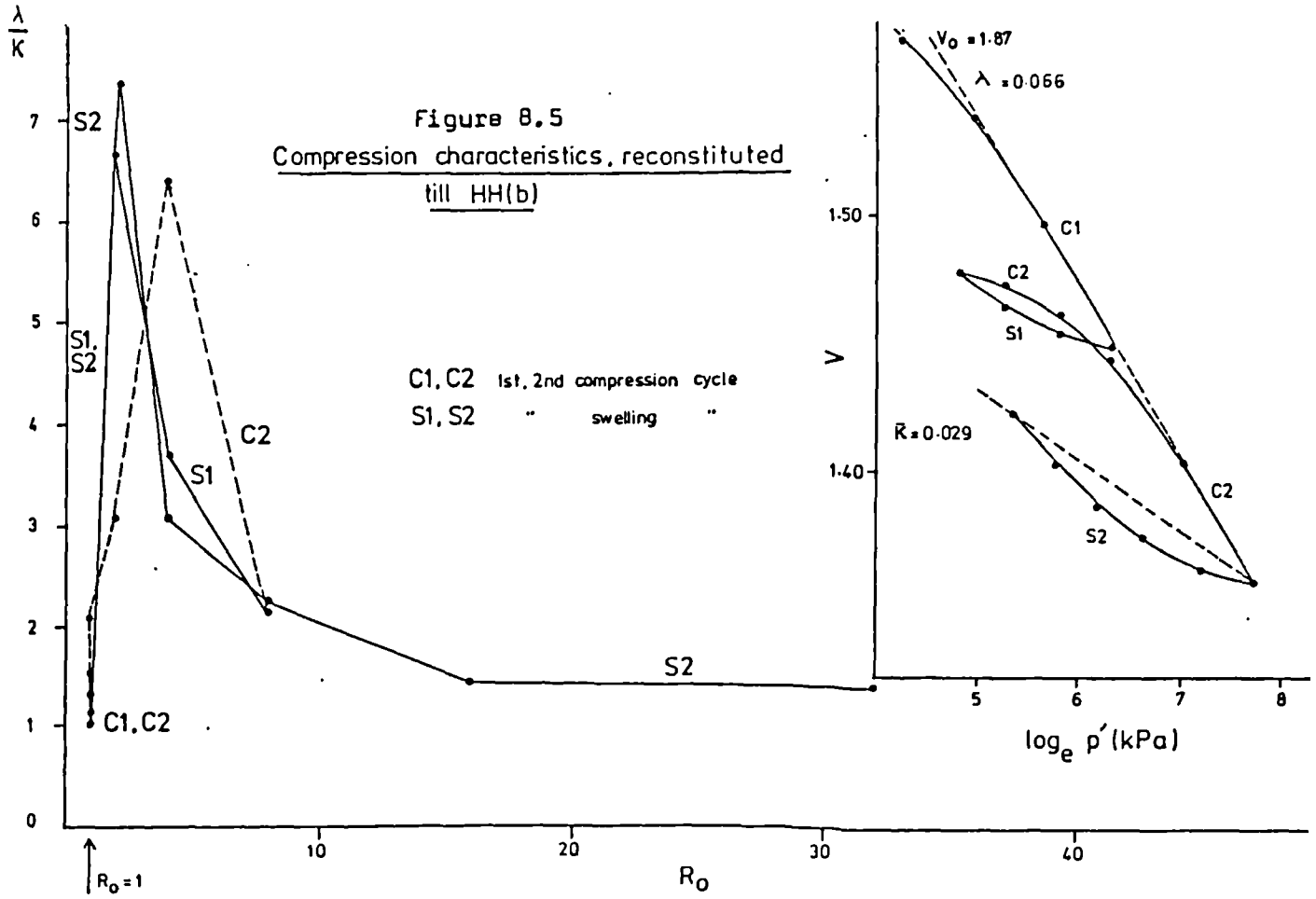

Fig 2.43 Plot of λ / κ against overconsolidation ratio for Ware till (Little, 1985).

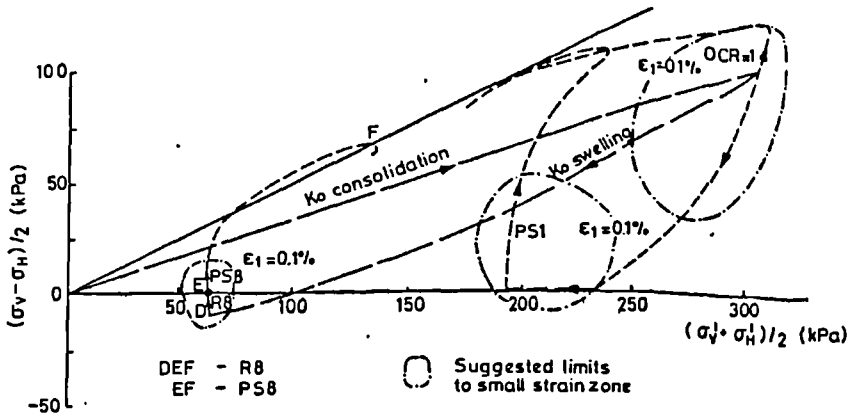

Fig 2.44 Small strain stiff zones in Lower Cromer till (Hight et al, 1985).

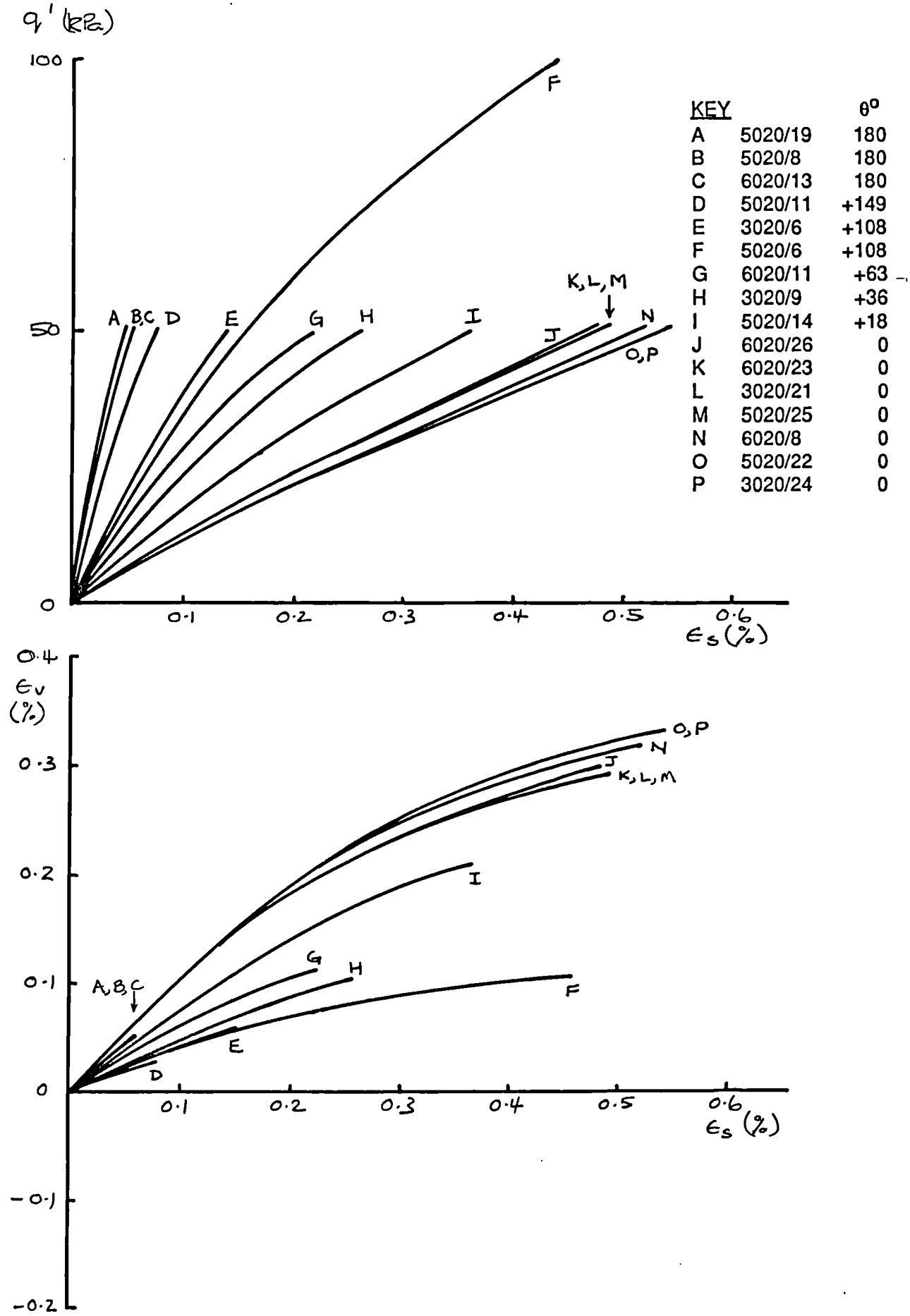

Fig 2.45 Plots of q' against ε_s and ε_v against ε_s for reconstituted speswhite kaolin, positive values of θ (Tests by Atkinson, 1983a).

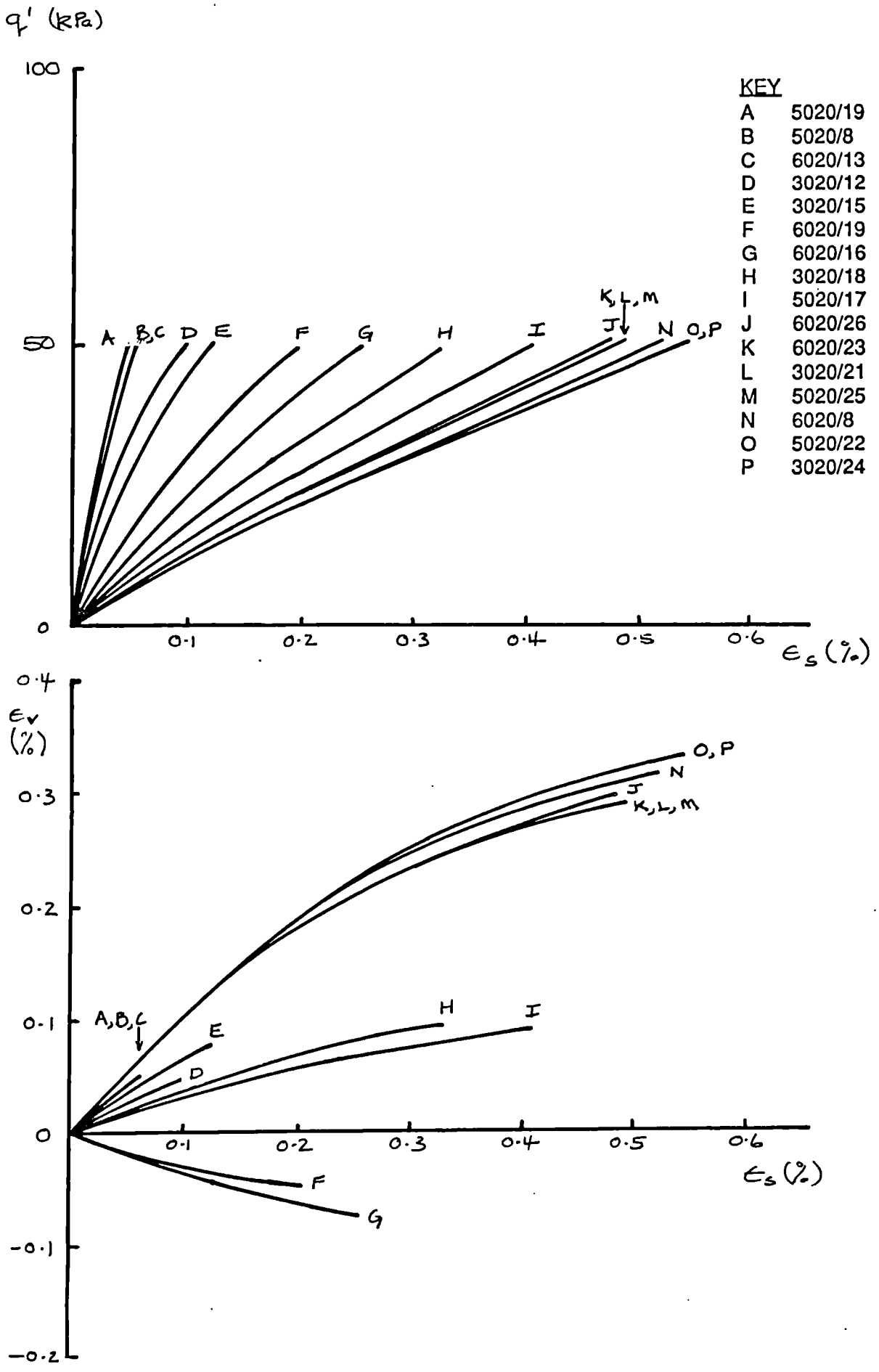

Fig 2.46 Plots of q' against ε_s and ε_v against ε_s for reconstituted speswhite kaolin, negative values of θ (Tests by Atkinson, 1983a).

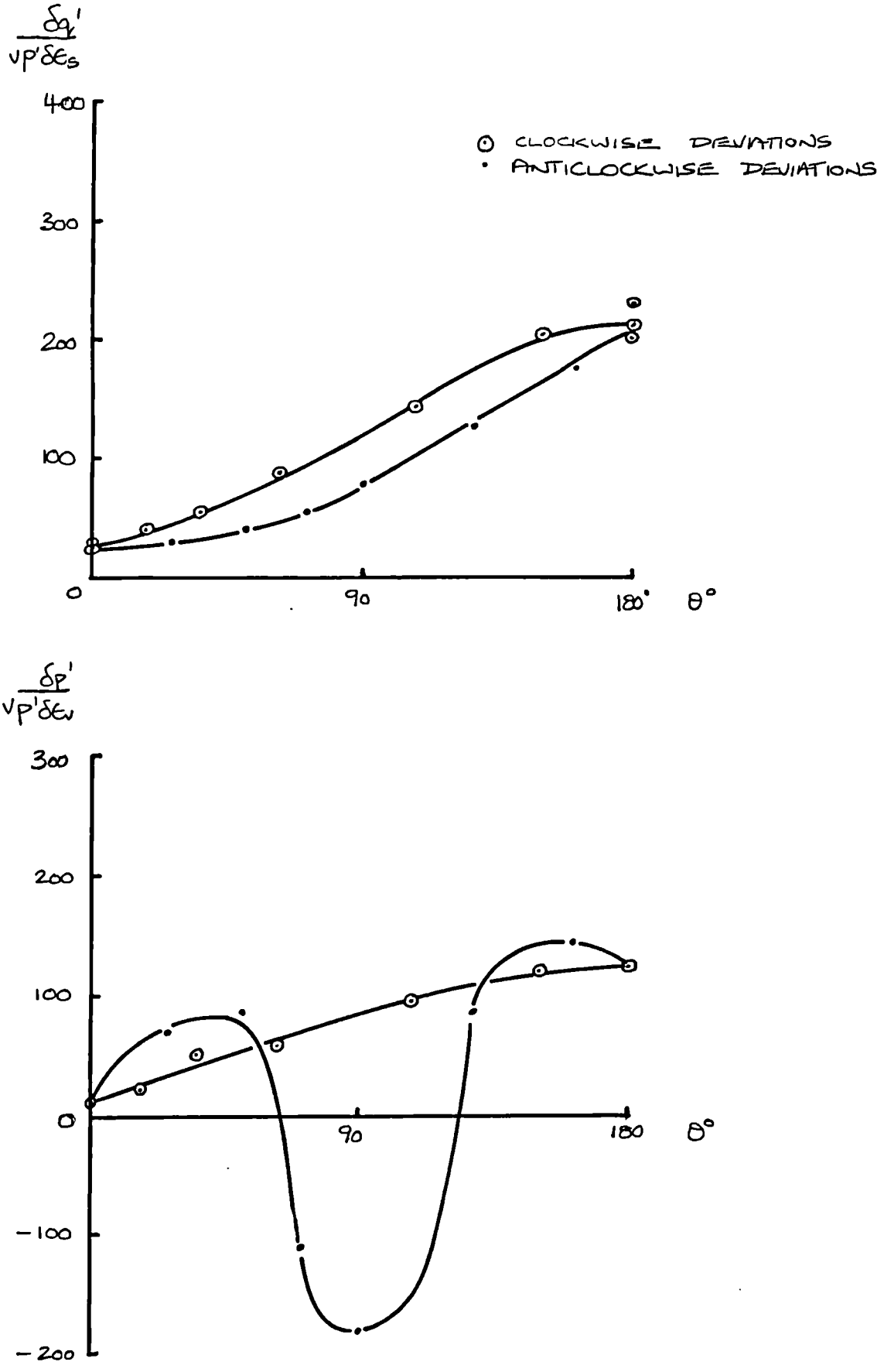

Fig 2.47 Plots of shear and bulk moduli against θ for reconstituted speswhite kaolin (Tests by Atkinson, 1983a).

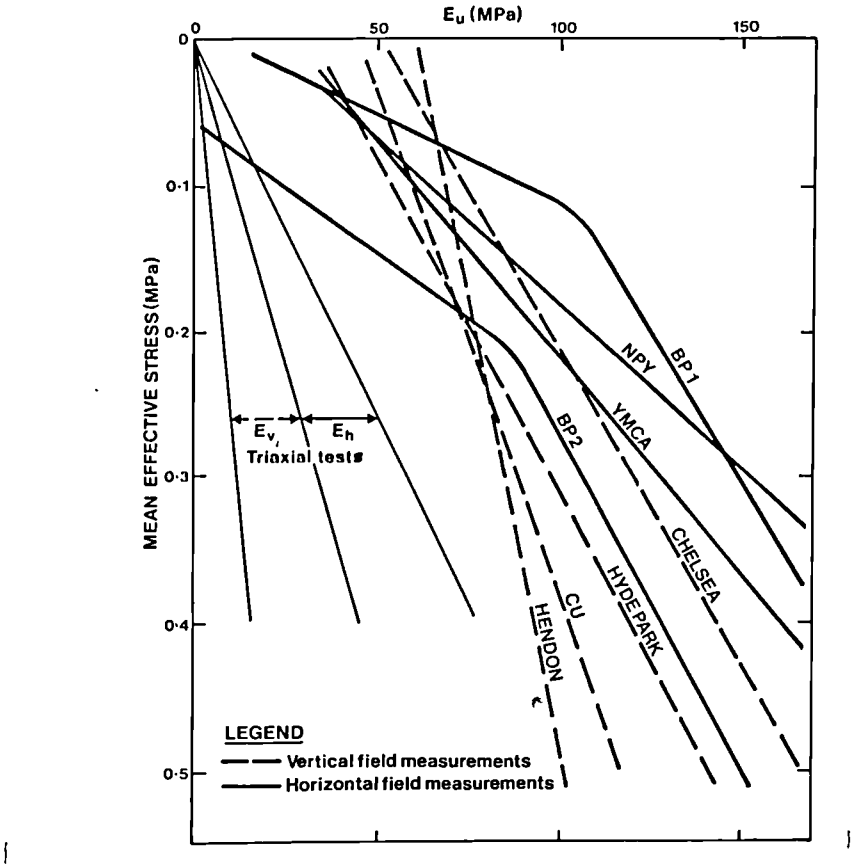

Fig 2.48 Laboratory and field secant stiffness moduli for London Clay (St.John, 1975).

KEY As Fig 2·53
BP - BRITANIC HOUSE
NPY - NEW PALACE YARD
YMCA
CHELSEA
HYDE PARK
CU - COMMERCIAL UNION
HENDON
TRIAXIAL TESTS FROM ASHFORD COMMON SHAFT

FOR REFERENCES FOR ABOVE DATA SEE
ST JOHN (1975) OR COSTA FILHO (1978)

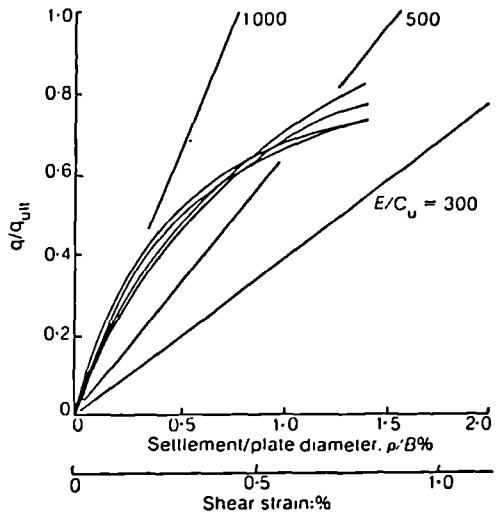

Fig 2.49 Results of a typical plate bearing test conducted by Marsland (1971a) (Simpson et al, 1979).

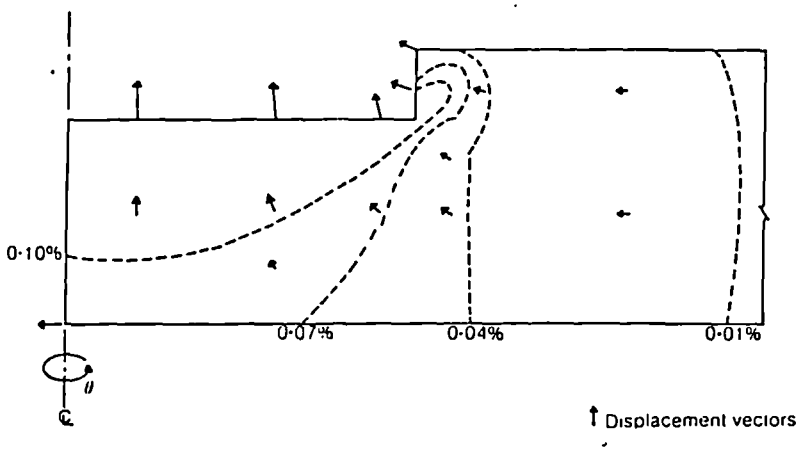

Fig 2.50 Distribution of shear strain behind a retaining wall (Simpson et al, 1979).

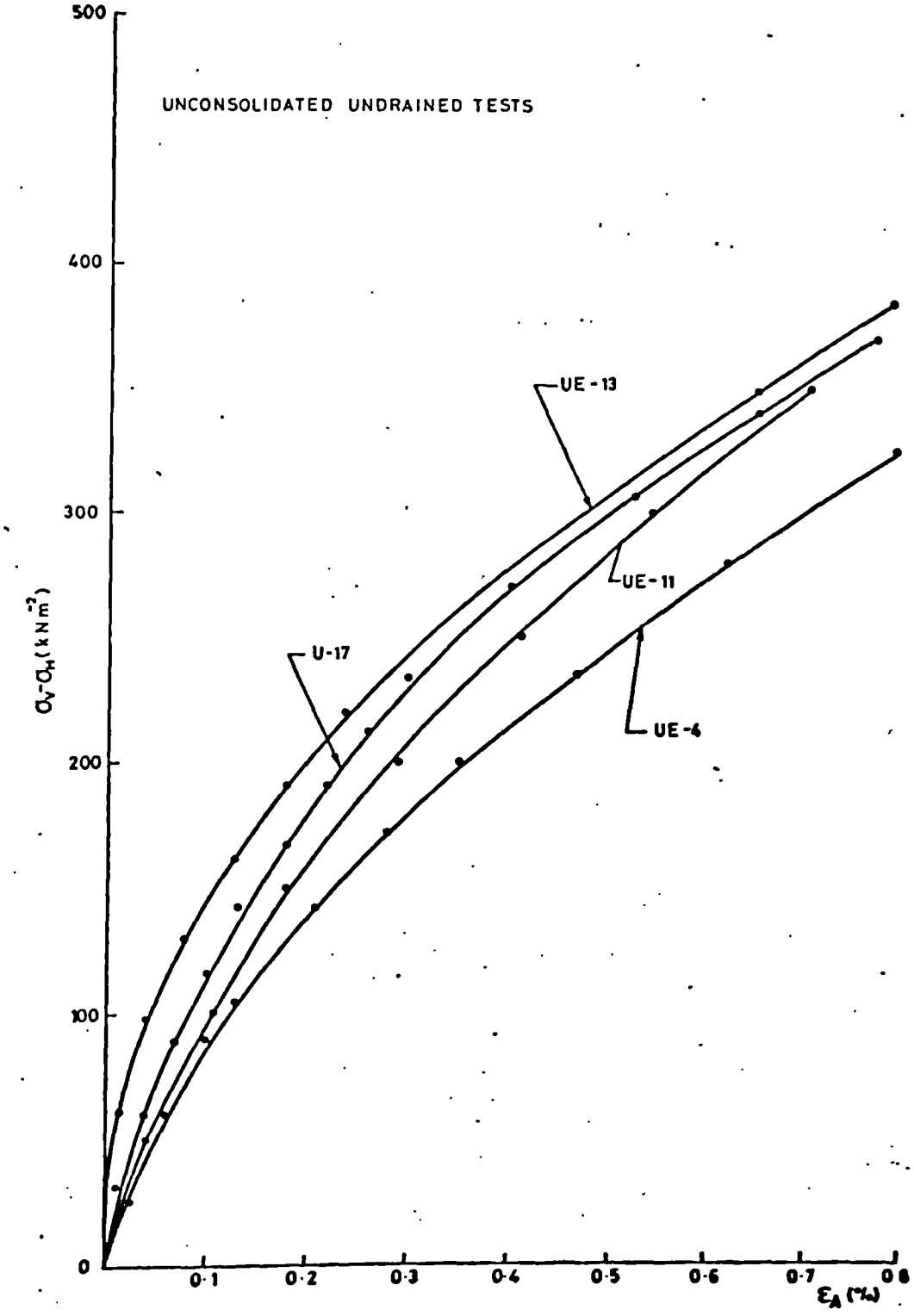

Fig 2.51 Results of unconsolidated undrained tests on undisturbed London Clay from an initial isotropic stress state (Costa-Filho, 1978a).

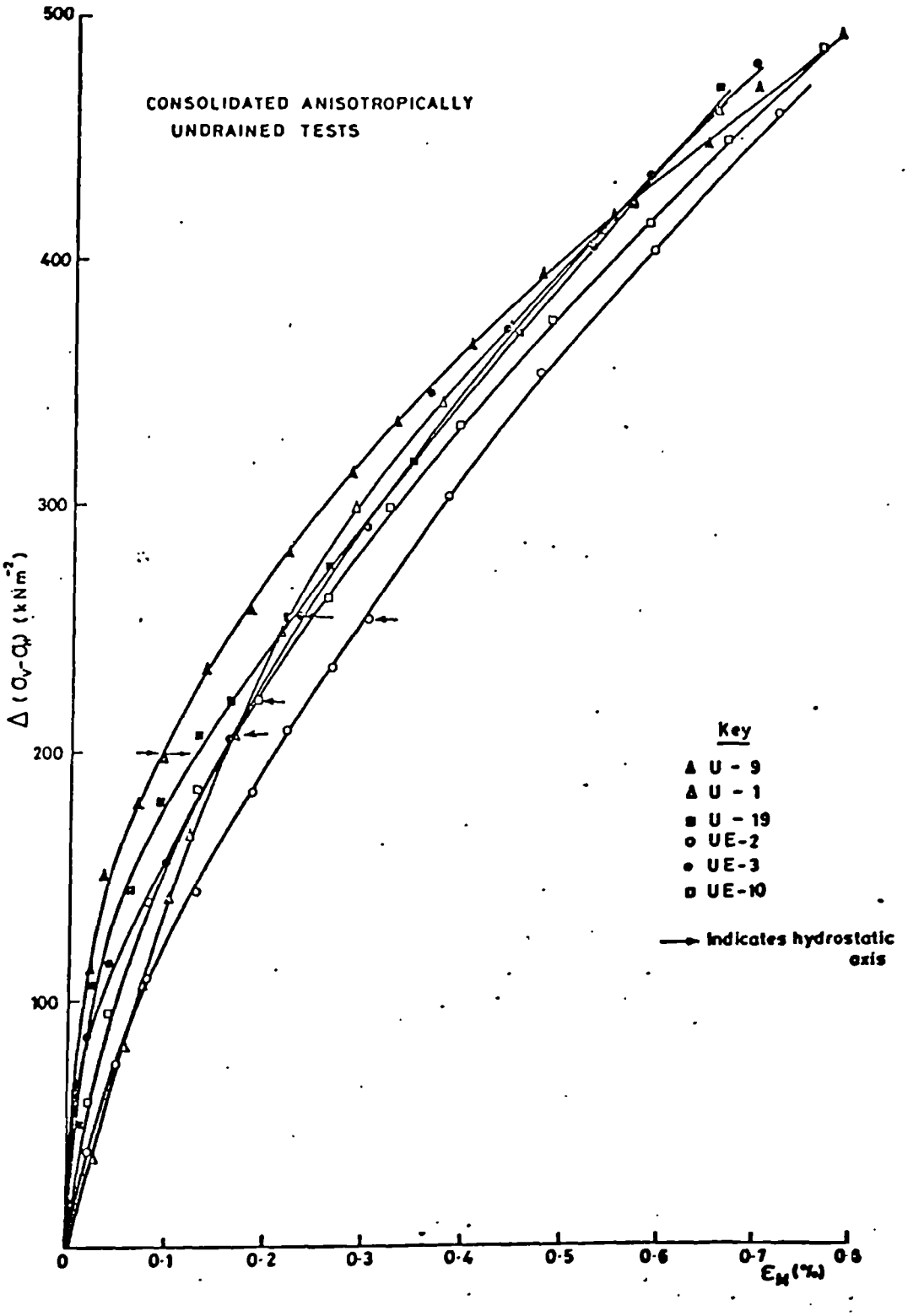

Fig 2.52 Results of consolidated anisotropically undrained tests on undisturbed London Clay (Costa-Filho, 1978a).

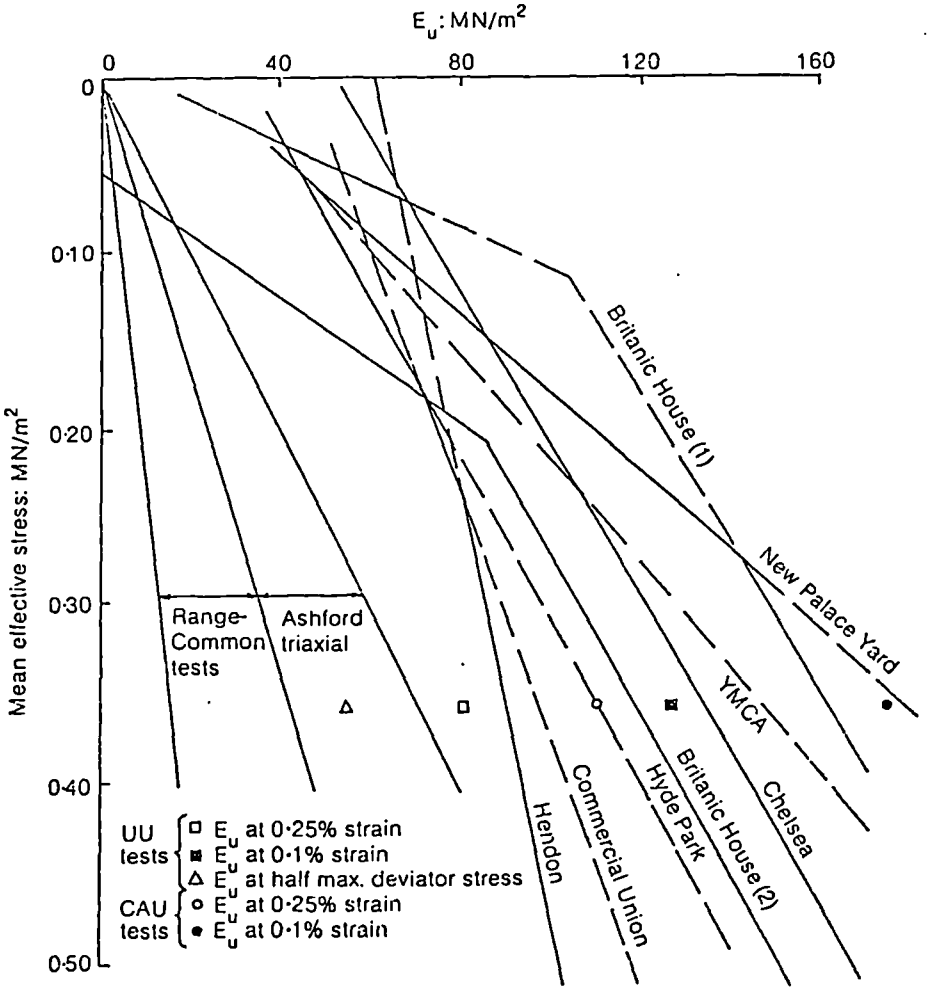

DATA FOR UU AND CAU TESTS FROM FIGS 2.51 AND 2.52 COSTA FILHO (1978)

Fig 2.53 Laboratory and field stiffness moduli for London Clay including stiffness data from Figs 2.51 and 2.52 (Simpson et at, 1979).

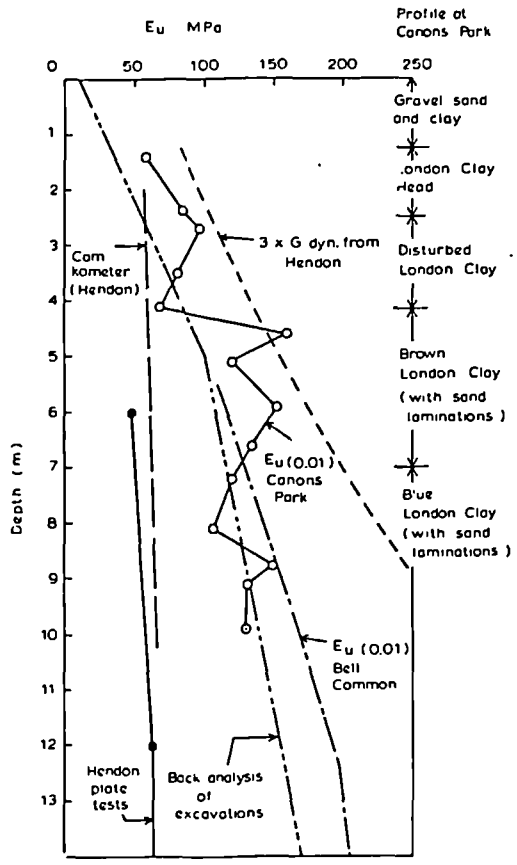

Fig 2.54 Laboratory and field stiffness moduli for London Clay (Jardine et al, 1985).

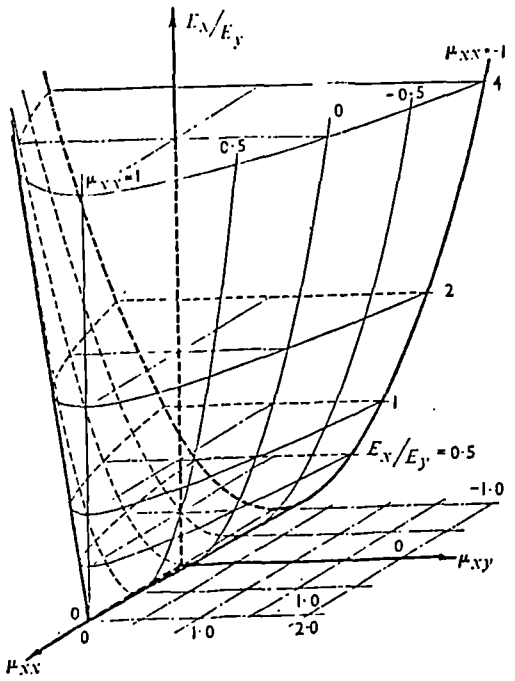

Fig 3.1 Limits on the admissible values of elastic parameters (Pickering, 1970).

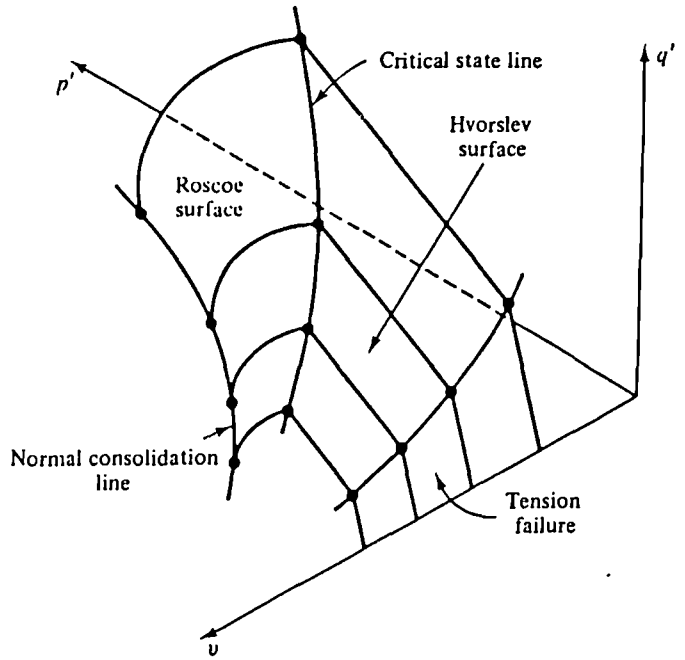

Fig 3.2 Three dimensional view of a state boundary surface for an isotropically compressed soil (Atkinson and Bransby, 1978).

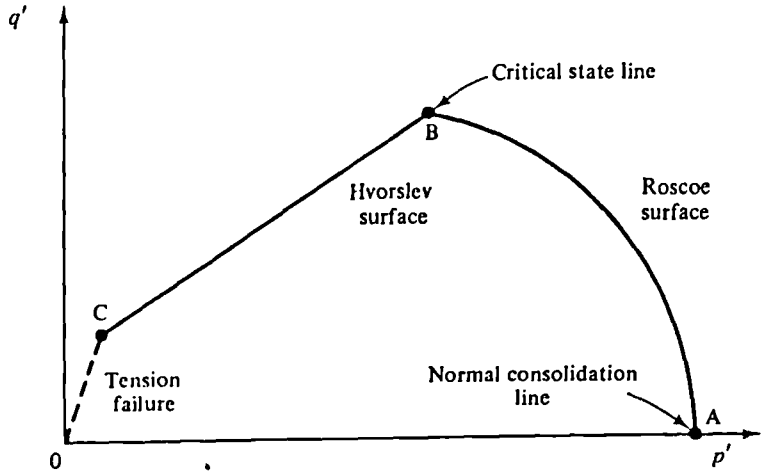

a)

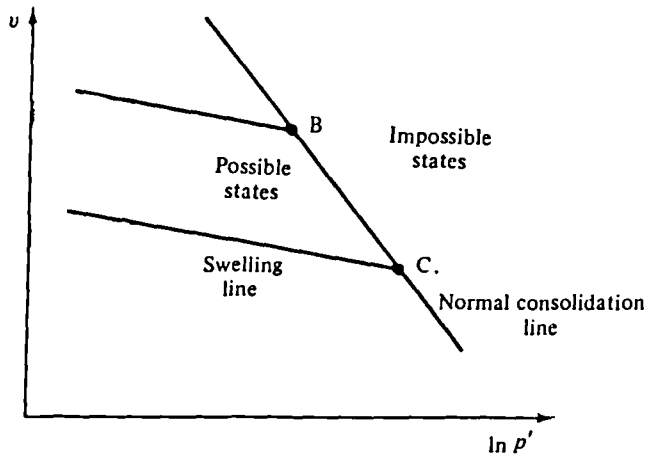

b)

Fig 3.3 The state boundary surface (Atkinson and Bransby, 1978).
a) ln q', p' space.
b) ln v , lnp' space.

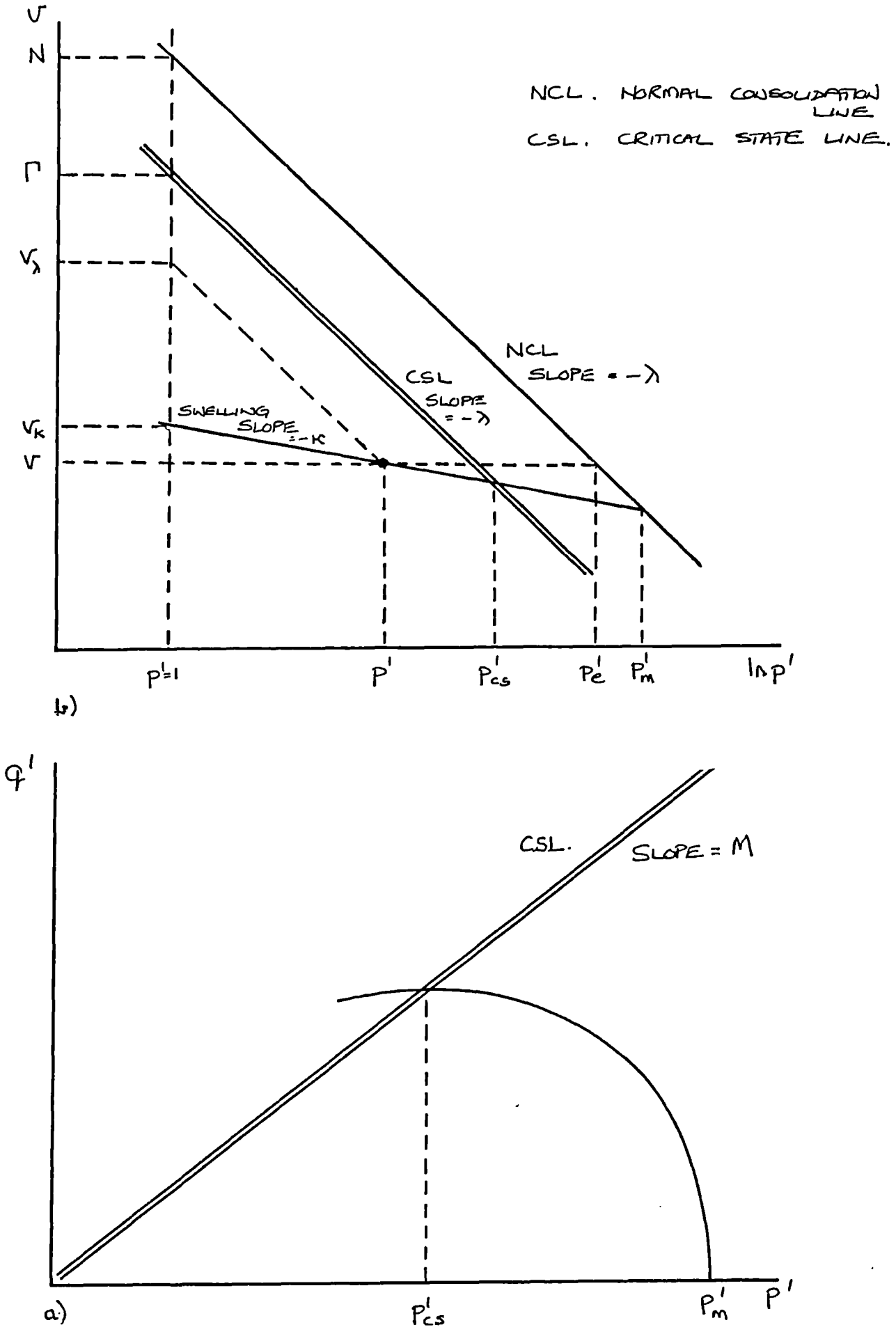

Fig 3.4 Definitions of critical state model constants.

a) ln q', p' space.
b) ln v , lnp' space.

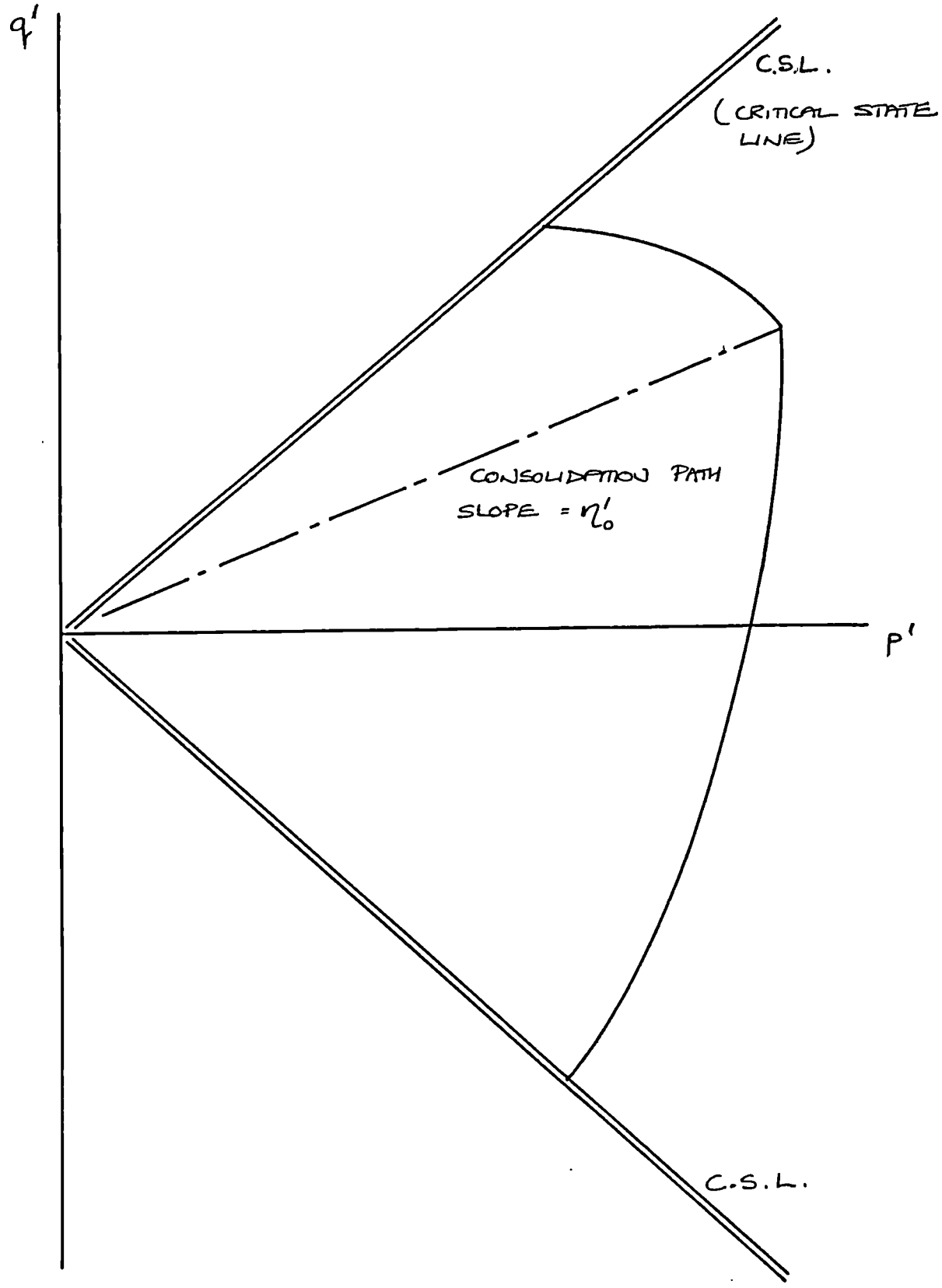

Fig 3.5 A state boundary surface for a soil anisotropically consolidated with a stress ratio of η'_o.

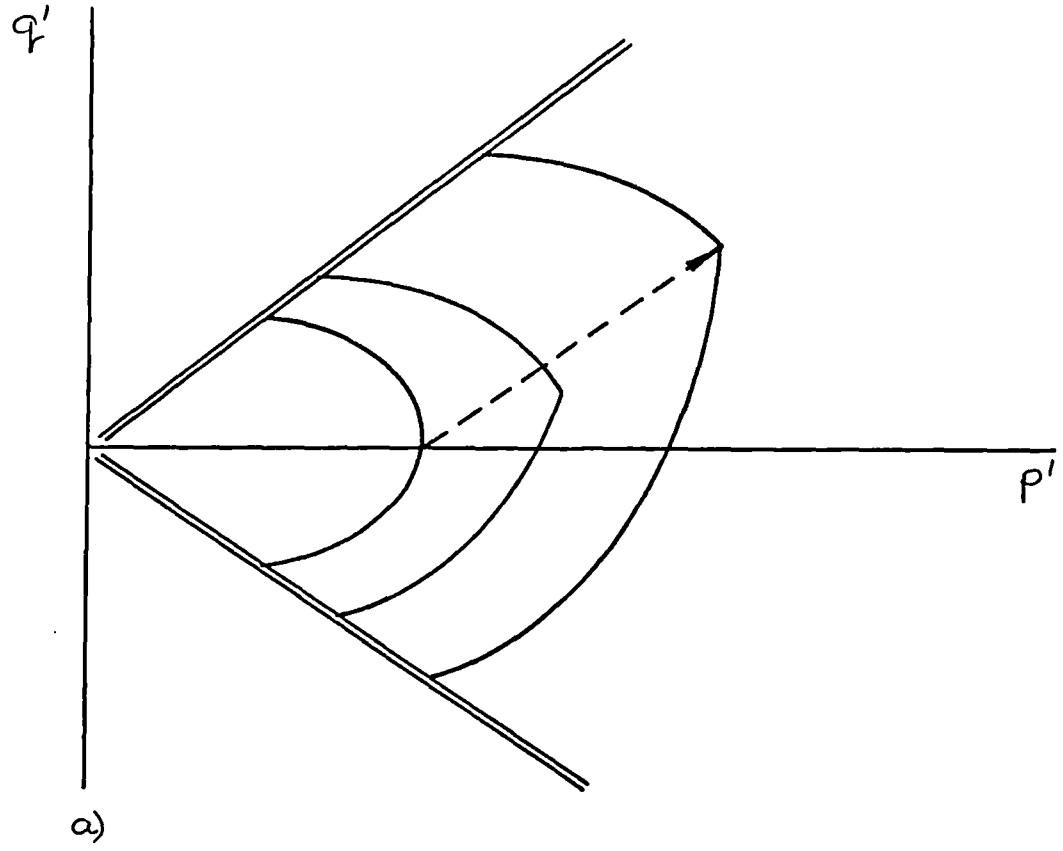

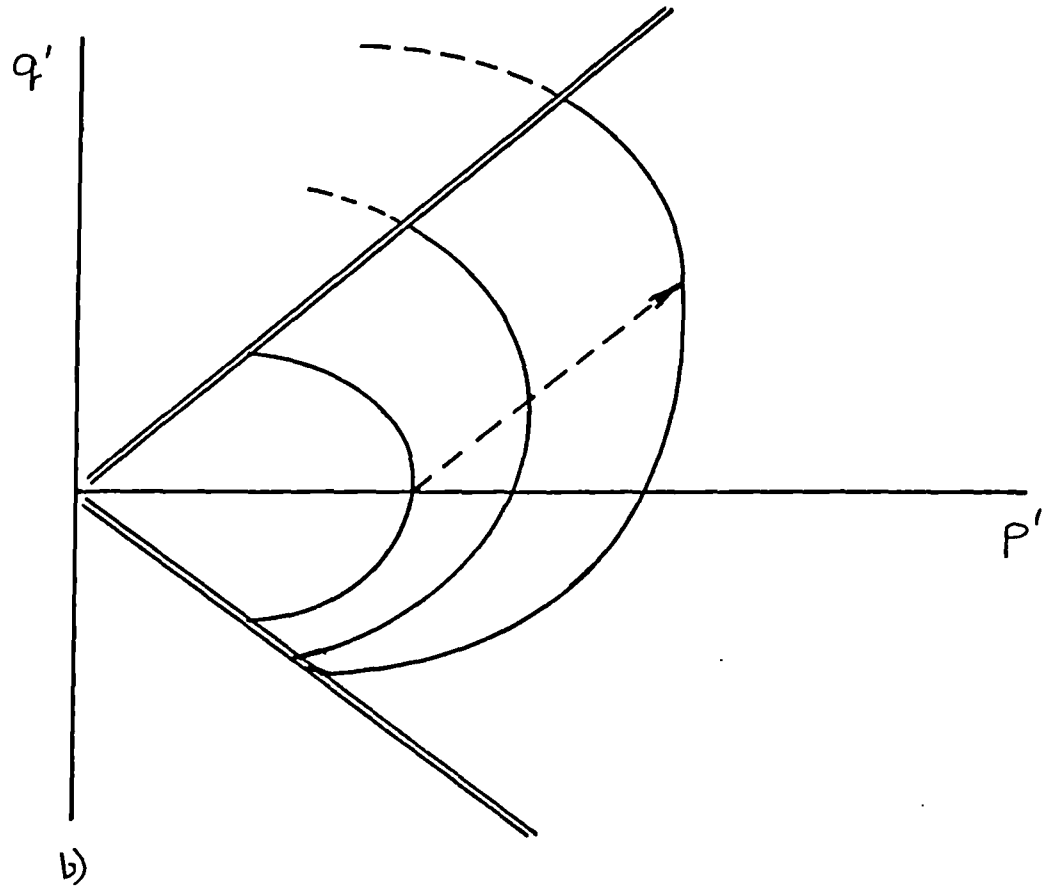

Fig 3.6 a) Rotational hardening of the state boundary surface.
b) Kinematic hardening of the state boundary surface.

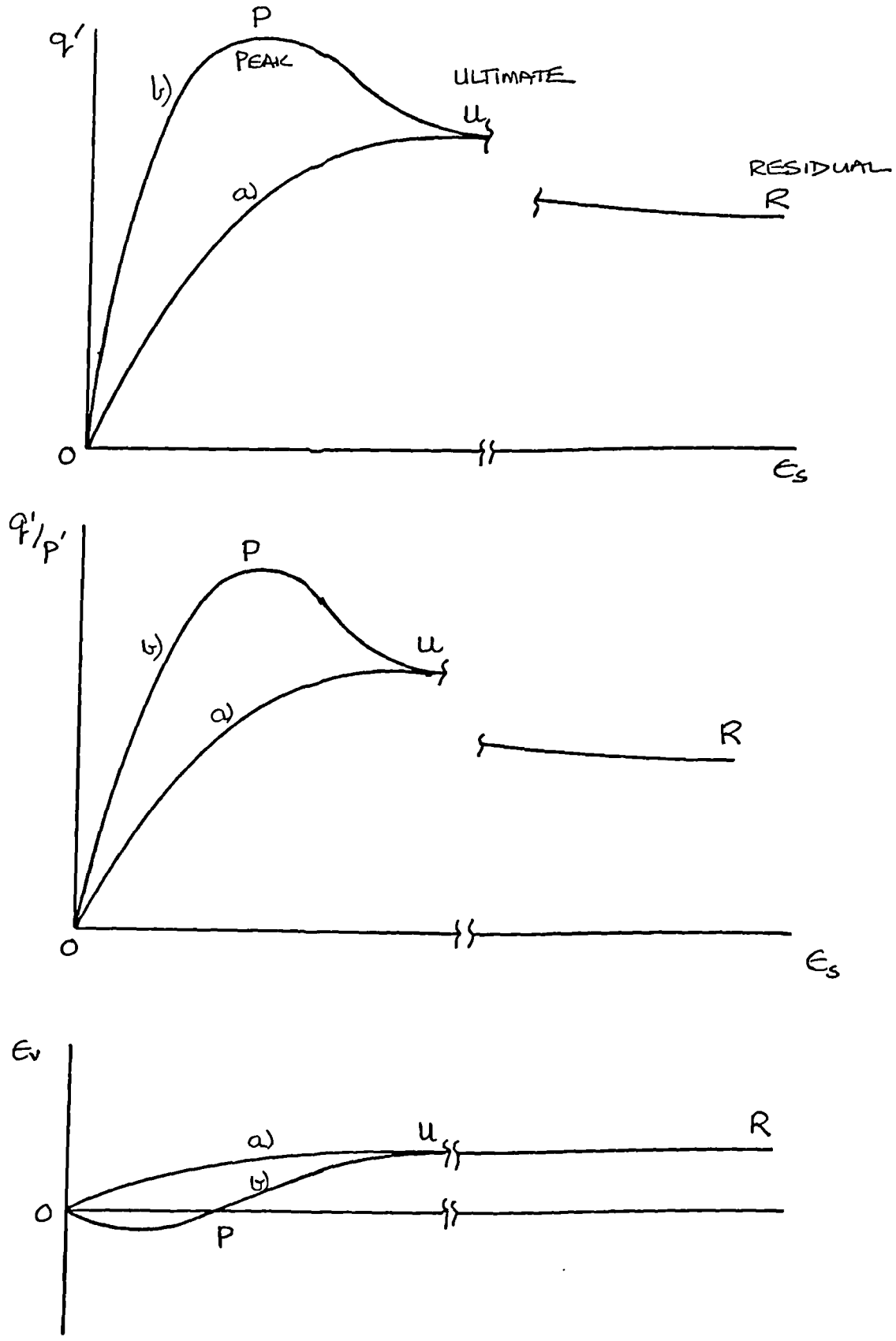

Fig 3.7 Drained failure of soil samples.
a) Normally consolidated.
b) Overconsolidated.

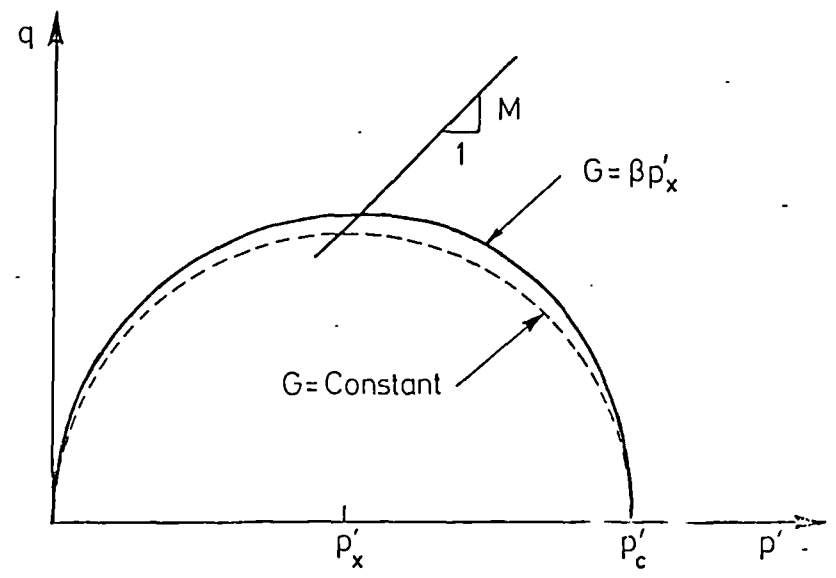

a)

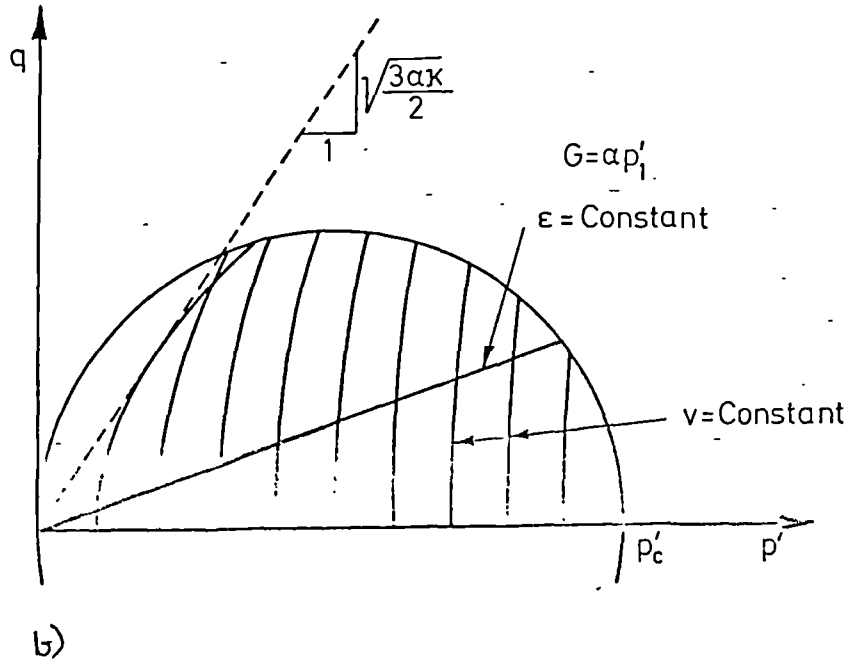

b)

Fig 3.8 Variation of stiffness moduli (Houlsby, 1981).
a) Shear modulus, G' α p'.
b) Shear modulus, G' α p'_c.

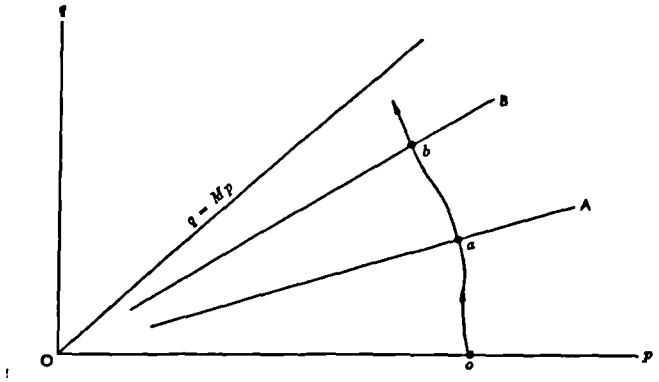

a)

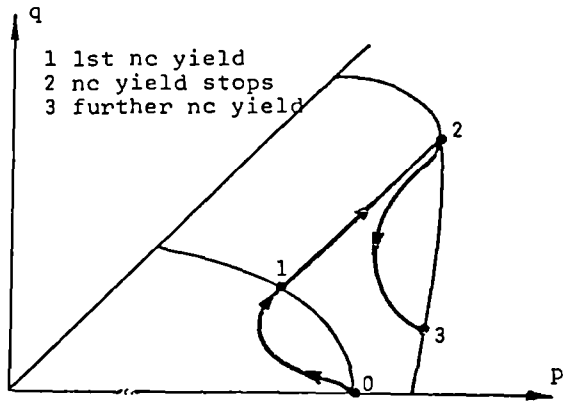

b)

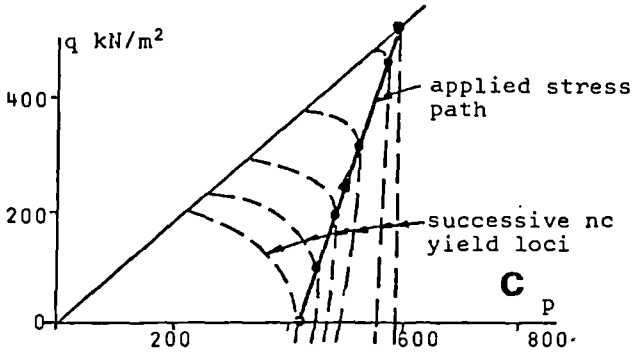

c)

Fig 3.9 a) Yield locus in Pender's model (Pender, 1978).
b) Anisotropic yield locus in Pender's model (Pender, 1977).
c) Changing shape of yield locus with loading (Pender, 1977).

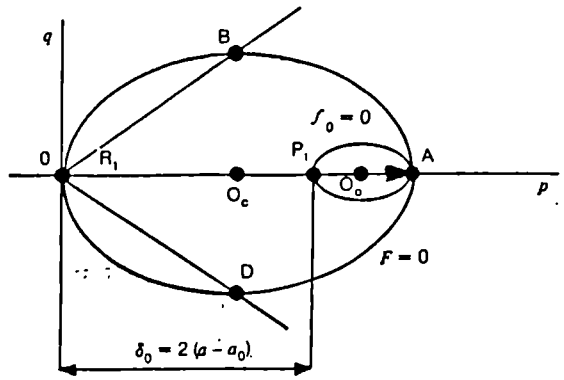

a)

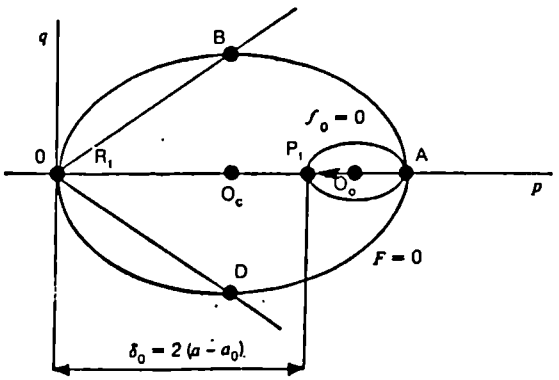

b)

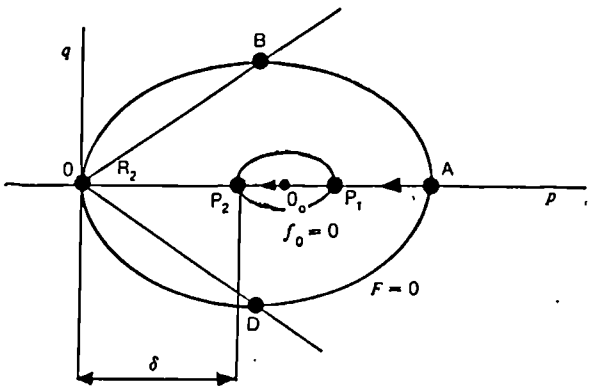

c)

Fig 3.10 A model incorporating kinematic hardening (Mroz et al, 1979).

a) Position of K.Y.S. while state is on the consolidation surface at A.
b) State at P_1 moving off the consolidation surface into the K.Y.S.
c) Initial movement of the K.Y.S. (State point P_2).
d) Effect of change in direction of loading (to P_3) below the consolidation surface.
e) Definition of size of the kinematic yield surface.

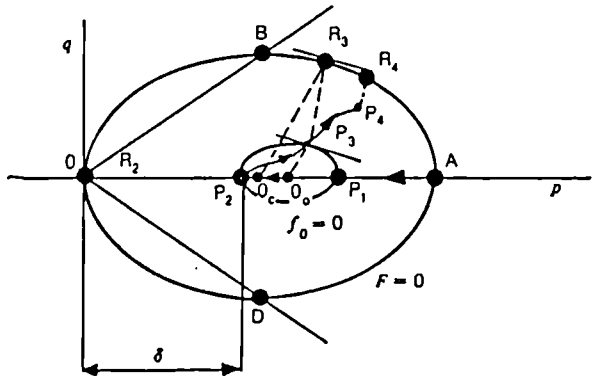

d)

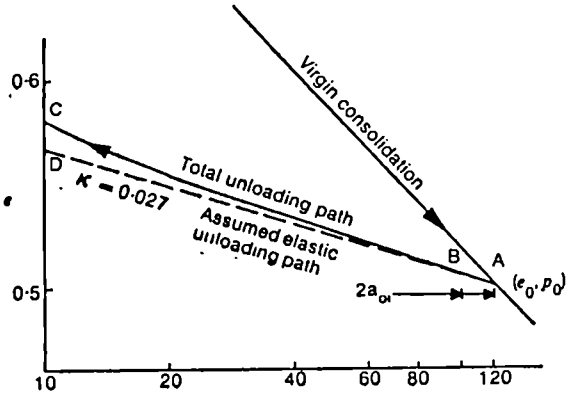

e)

FIG 3·10

Title as page 358.

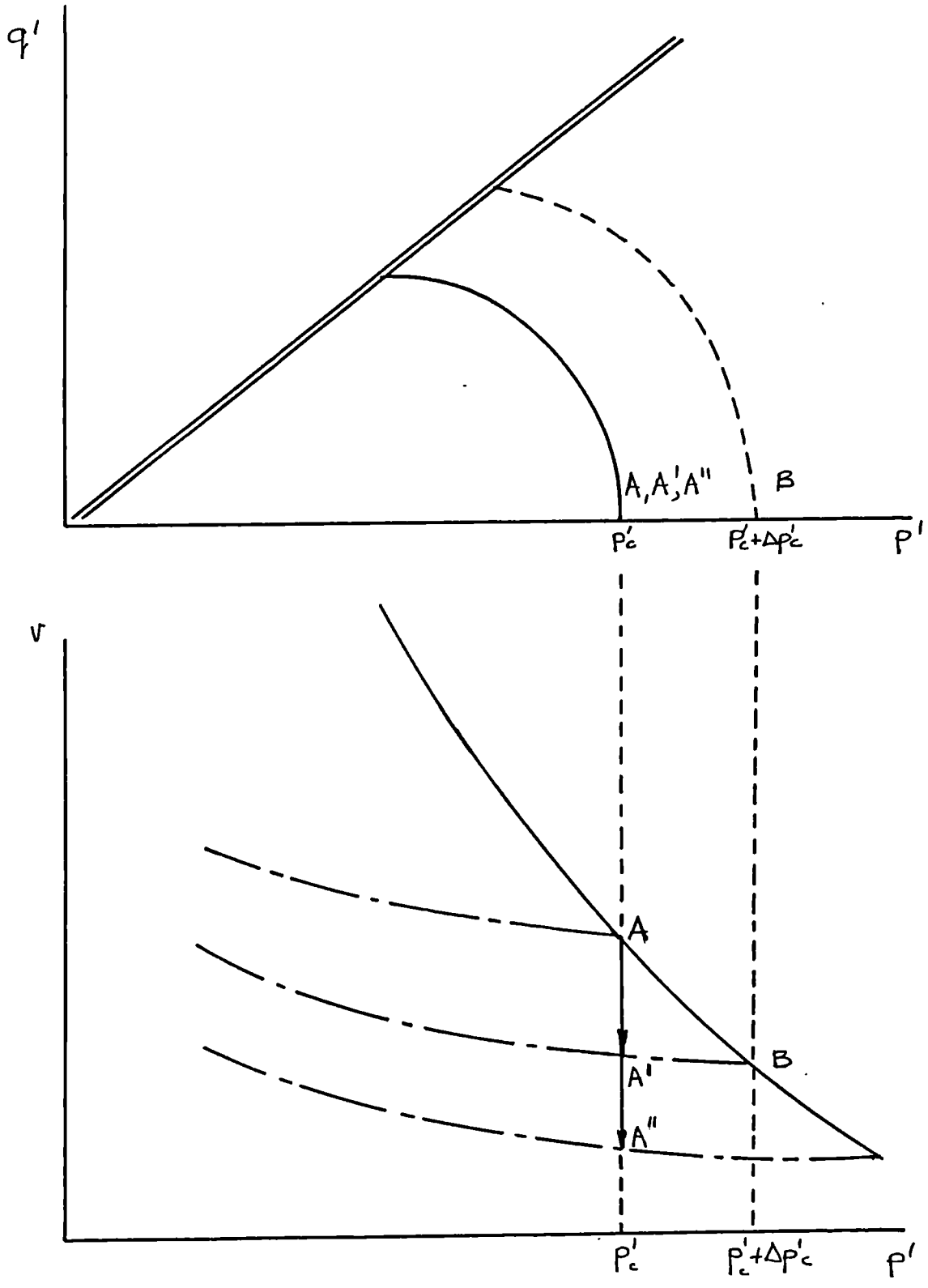

Fig 3.11 Effect of time on the position of the consolidation surface.
a) Effect on the q', p' plot.
b) Effect on v , p' plot.

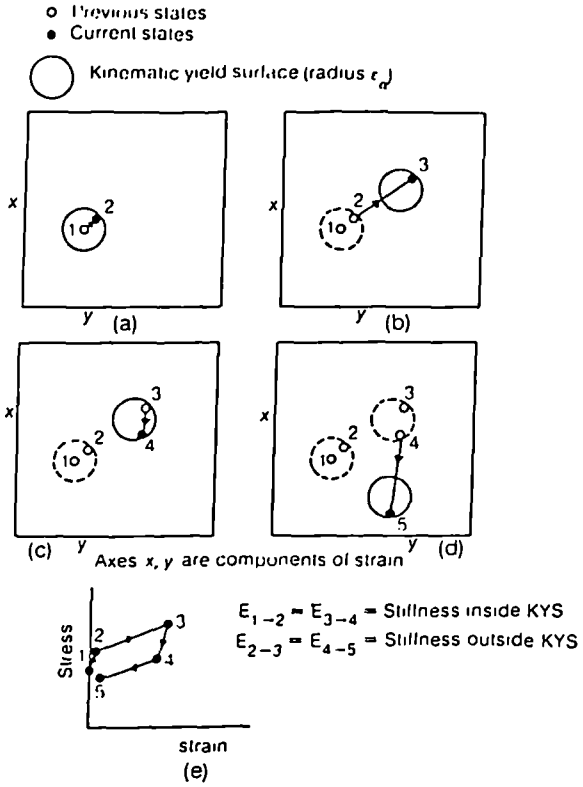

a) Initial state inside the kinematic yield surface (K.Y.S.).

b) KYS moves as straining proceeds.

c) State moves inside KYS with change of strain path.

d) KYS moves as straining proceeds.

e) Stress strain diagram for stages a) to d).

Fig 3.12 The use of the kinematic yield surface in model L.C. (Simpson et al, 1979).

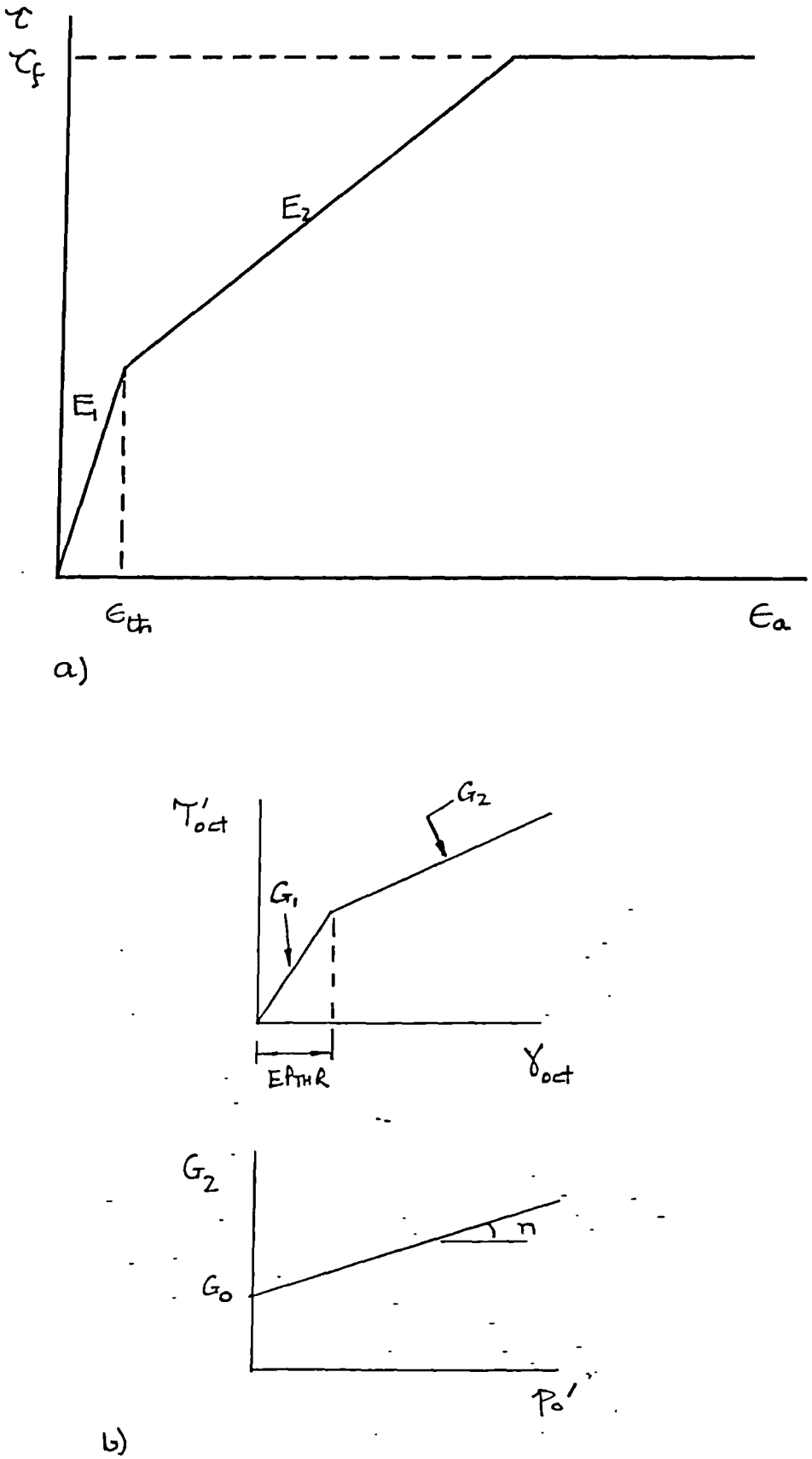

Fig 3.13 Bi-linear elastic models (Leach, 1984).
a) Bi-linear elastic perfectly plastic model.
b) Modified Cam Clay including a threshold range.

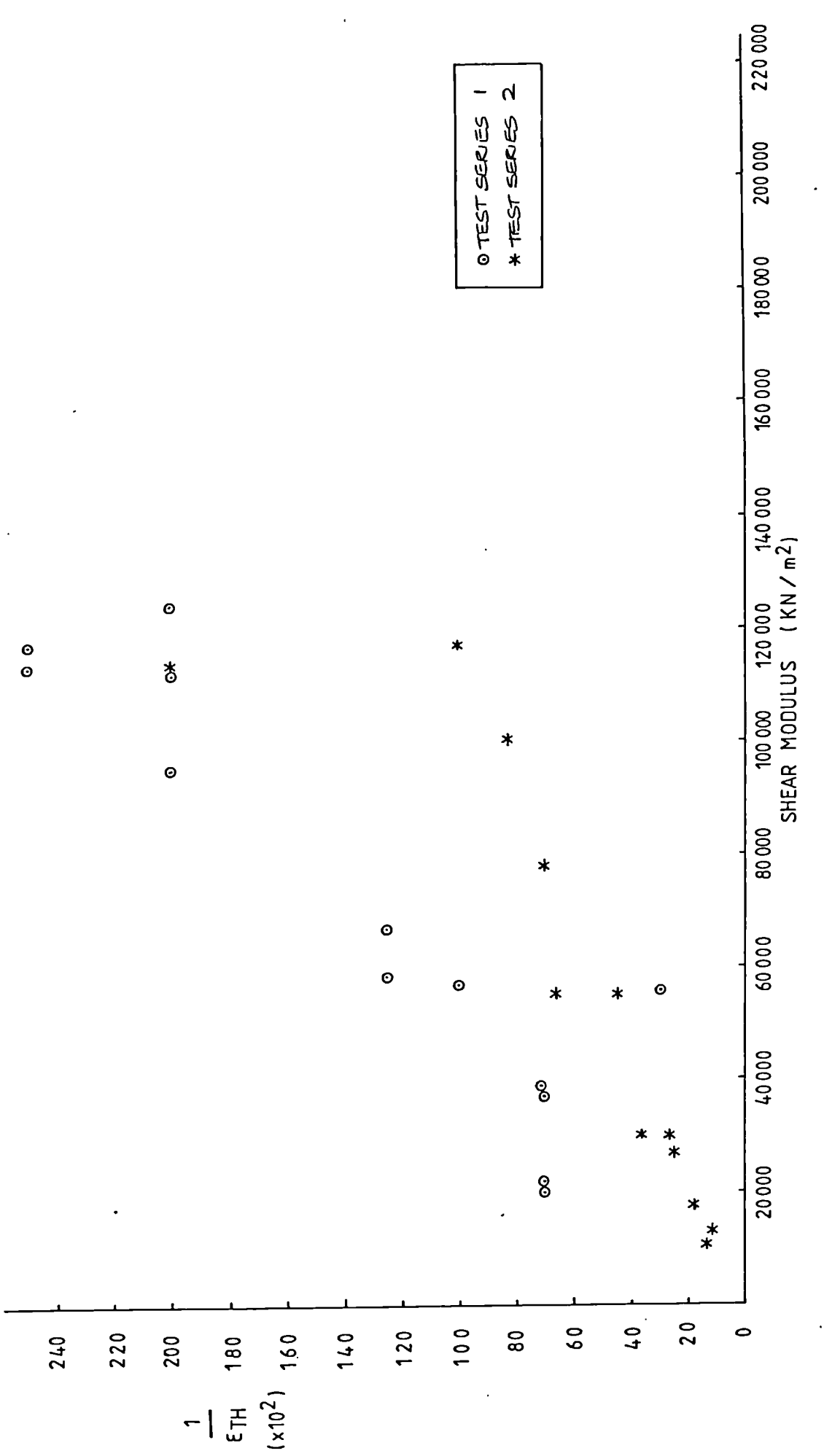

Fig 3.14 Data for the threshold range in London Clay (Leach, 1986).

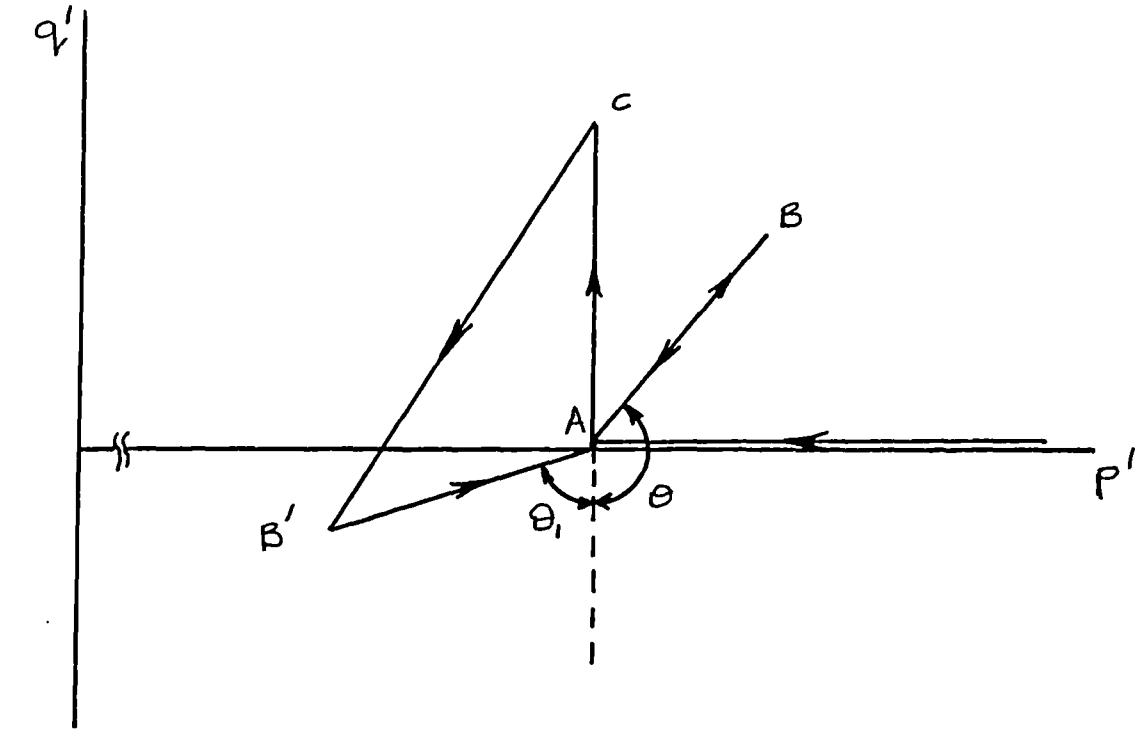

Fig 4.1 Test paths to assess the effect of changes in direction of effective stress path.

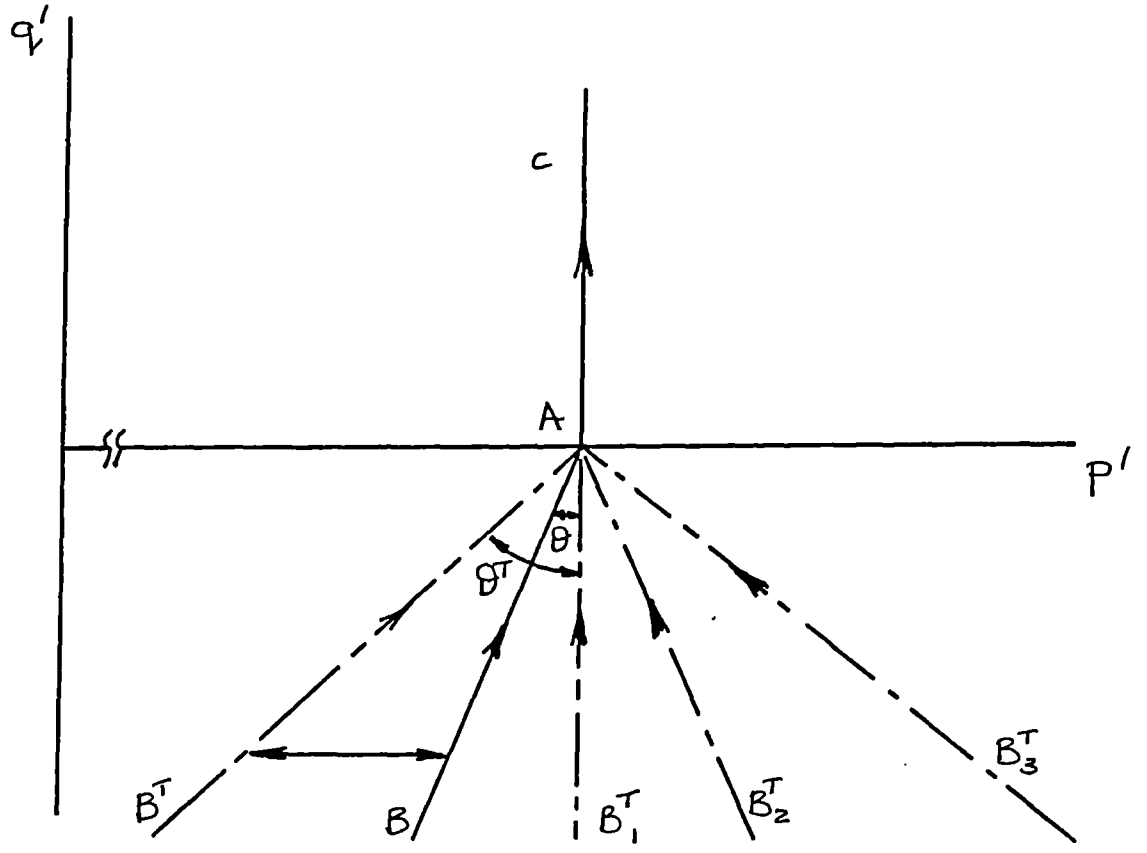

Fig 4.2 Test paths to assess the effect of changes in direction of total stress path.

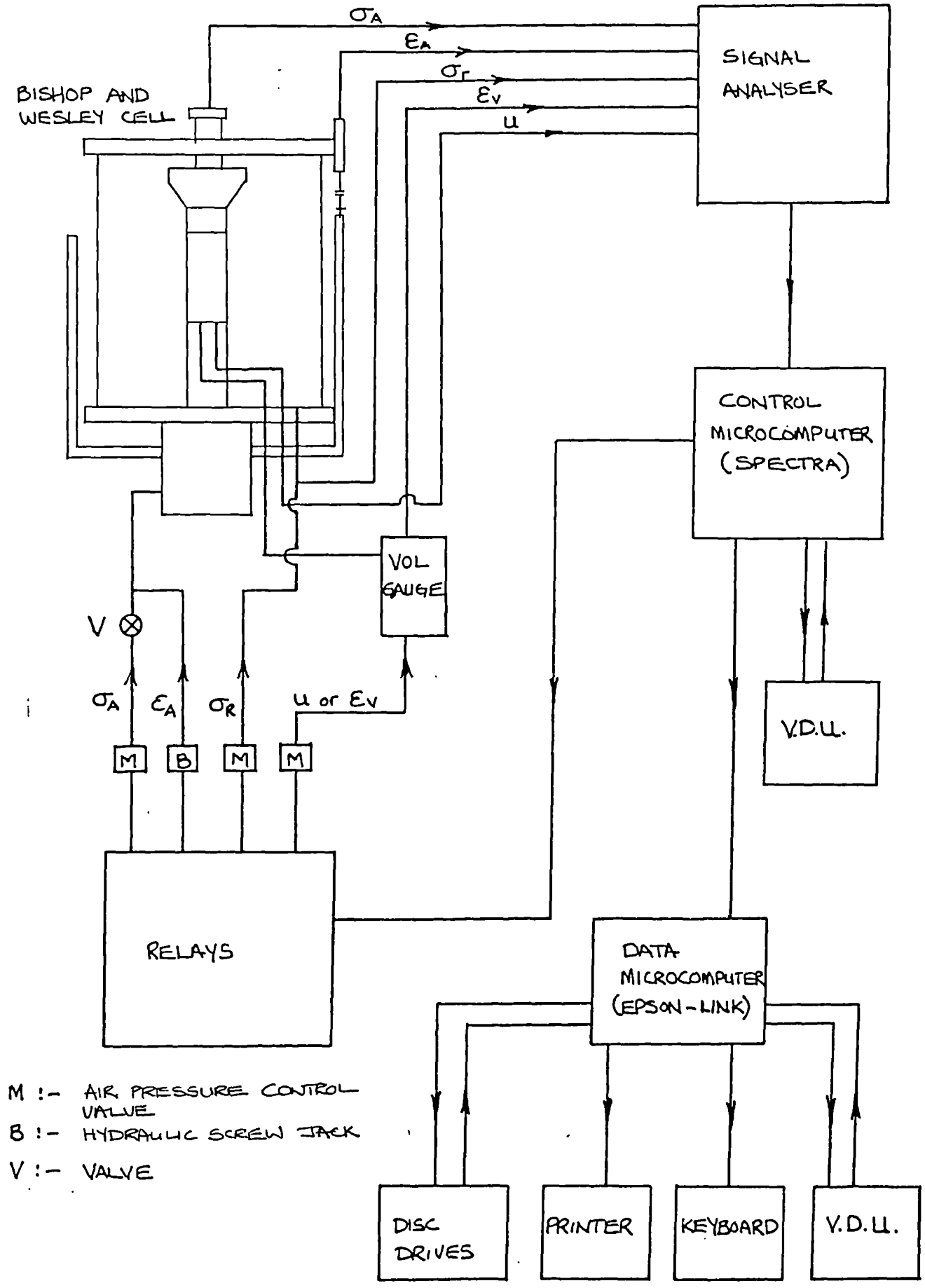

Fig 5.1 General arrangement of the Bishop and Wesley Spectra / Epson control system.

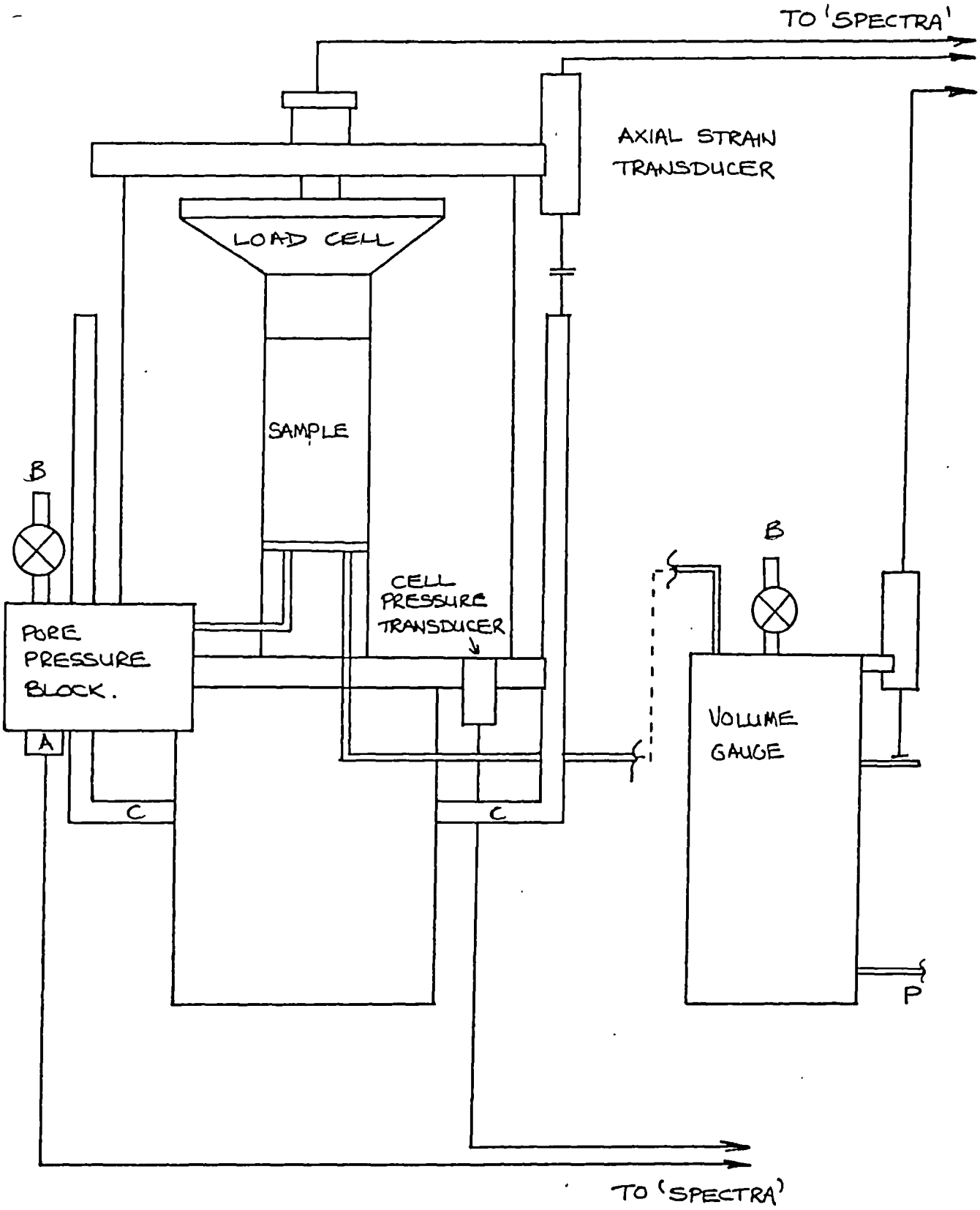

A PORE PRESSURE TRANSDUCER
B BLEED VALVES
C CROSSHEAD
P TO BACK PRESSURE SUPPLY

Fig 5.2 Diagrammatic view of sample and instrumentation in the Bishop and Wesley cell.

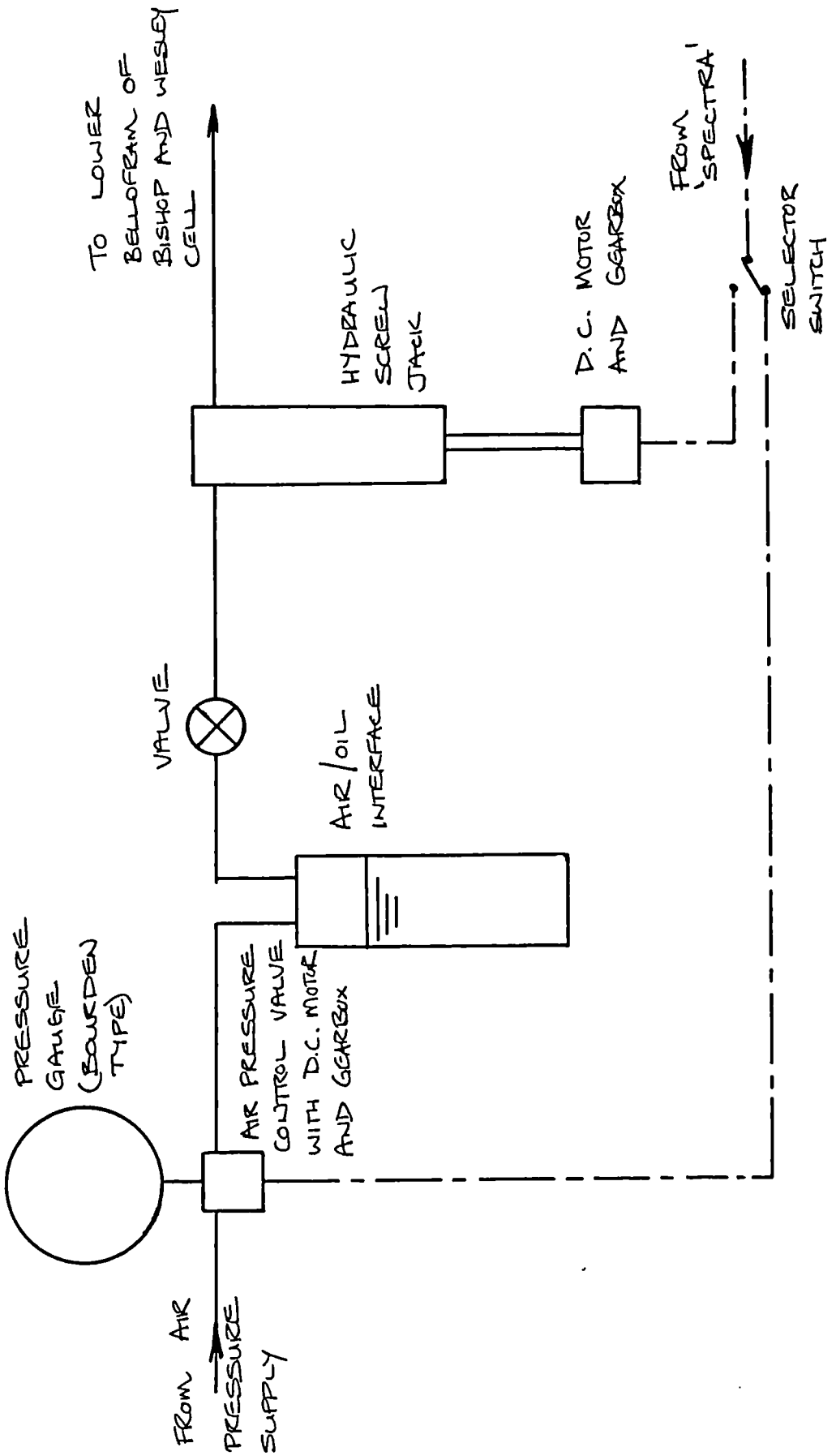

Fig 5.3 Axial strain control system.

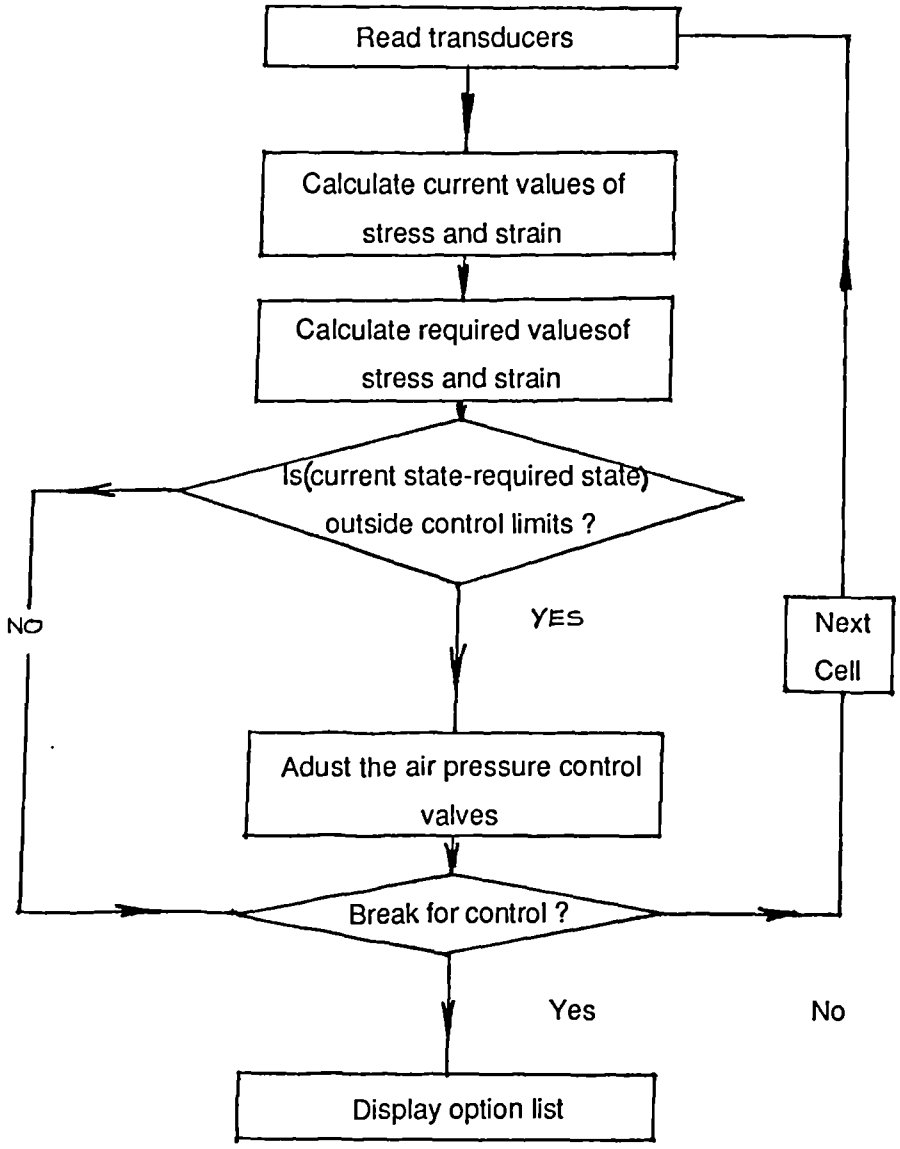

Fig 5.4 SPCTRA control program loop.

0	Return control
1	Enter test data
2	Zero pressure readings
3	Set initial pressures
4	Zero strain readings
5	Start a test stage
6	End a test stage
7	Display current state
8	Display records in store
9	Print records in store
10	Test relays
11	Calibrate transducers
12	Enter calibration data
13	Time check

Fig 5.5 The SPCTRA option list.

THE CITY UNIVERSITY : CIVIL ENGINEERING DEPARTMENT
GEOTECHNICAL ENGINEERING DIVISION
STRESS-PATH TESTING FACILITY

Test Data (Option 1) Form 2

Cell No: [ ]

Job : [ ]

Test No: and Stage No: [,]

Initial Length and Diameter [,]

Control Data

	Control Code	Start	Values Increment per hour	Finish	Limit
σ_a or ε_a	[ ]	[,]	[,]	[,]	
u or ε_v	[ ]	[,]	[,]	[,]	[,]
σ_r or ε_r	[ ]	[,]	[,]	[,]	[,]

Fig 5.6 Specimen Spctra data sheet.

SPCTRA

THE CITY UNIVERSITY : CIVIL ENGINEERING DEPARTMENT
GEOTECHNICAL ENGINEERING DIVISION
STRESS-PATH TESTING FACILITY

Calibration Data (Option 12) Form 1

Cell No: [ ]

Transducer Data

	Channel No:	Range	Calibration Constant (+ve load)	Calibration Constant (-ve load)
Load cell ( )	,	,	,	
(u)	,	,		
(σ_r)	,	,		
(ΔL)	,	,		
(Δv)	,	,		

DOP Unit No: [ ]

DOP Channels

Test	Motor 1		Motor 2		Motor 3	
on/off	on/off	fwd/rev	on/off	fwd/rev	on/off	fwd/rev
,	,	,	,	,	,	

Fig 5.7 Specimen Spctra transducer calibration data sheet.

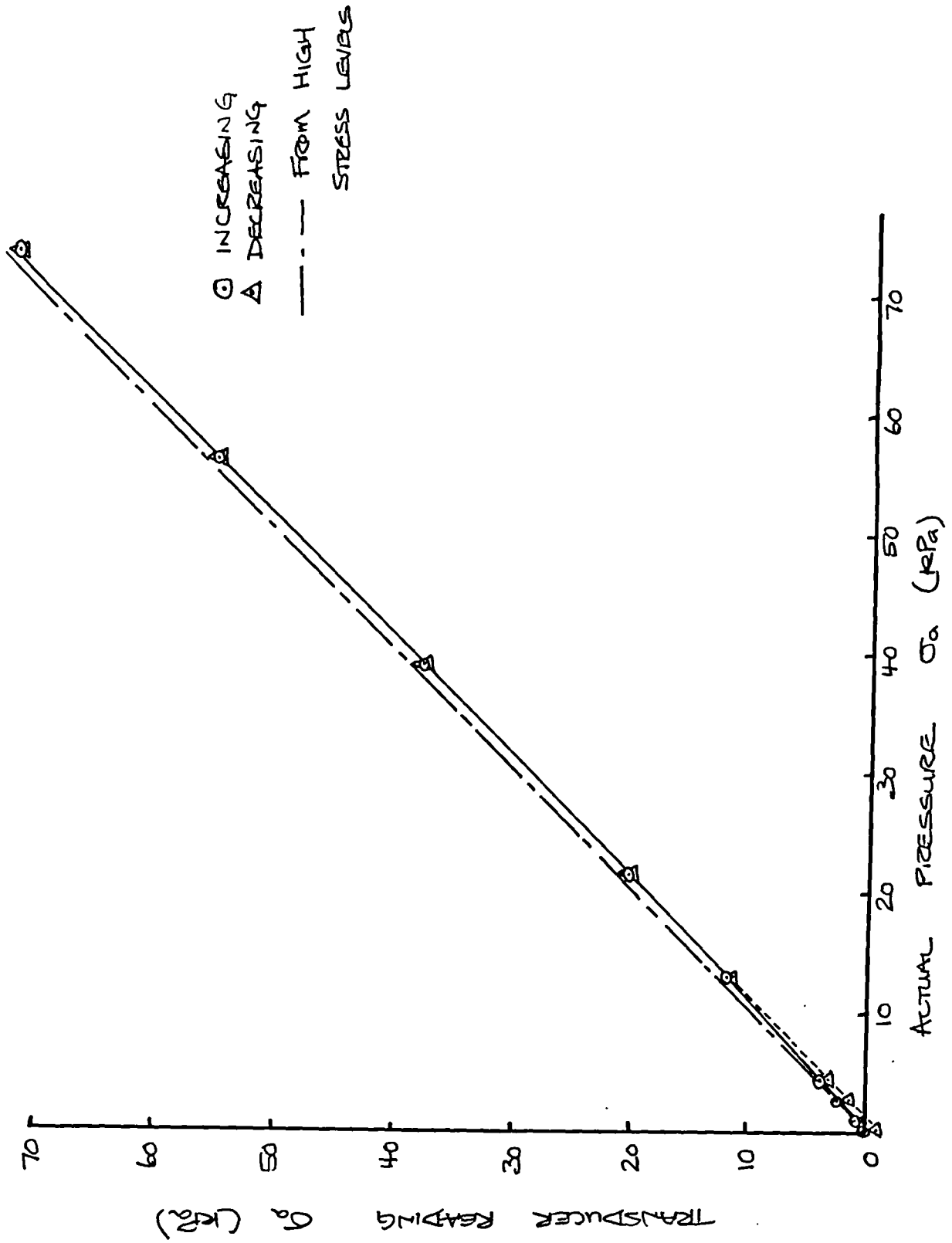

Fig 6.1 Typical load cell calibration.
a) At low stress levels.
b) At high stress levels.

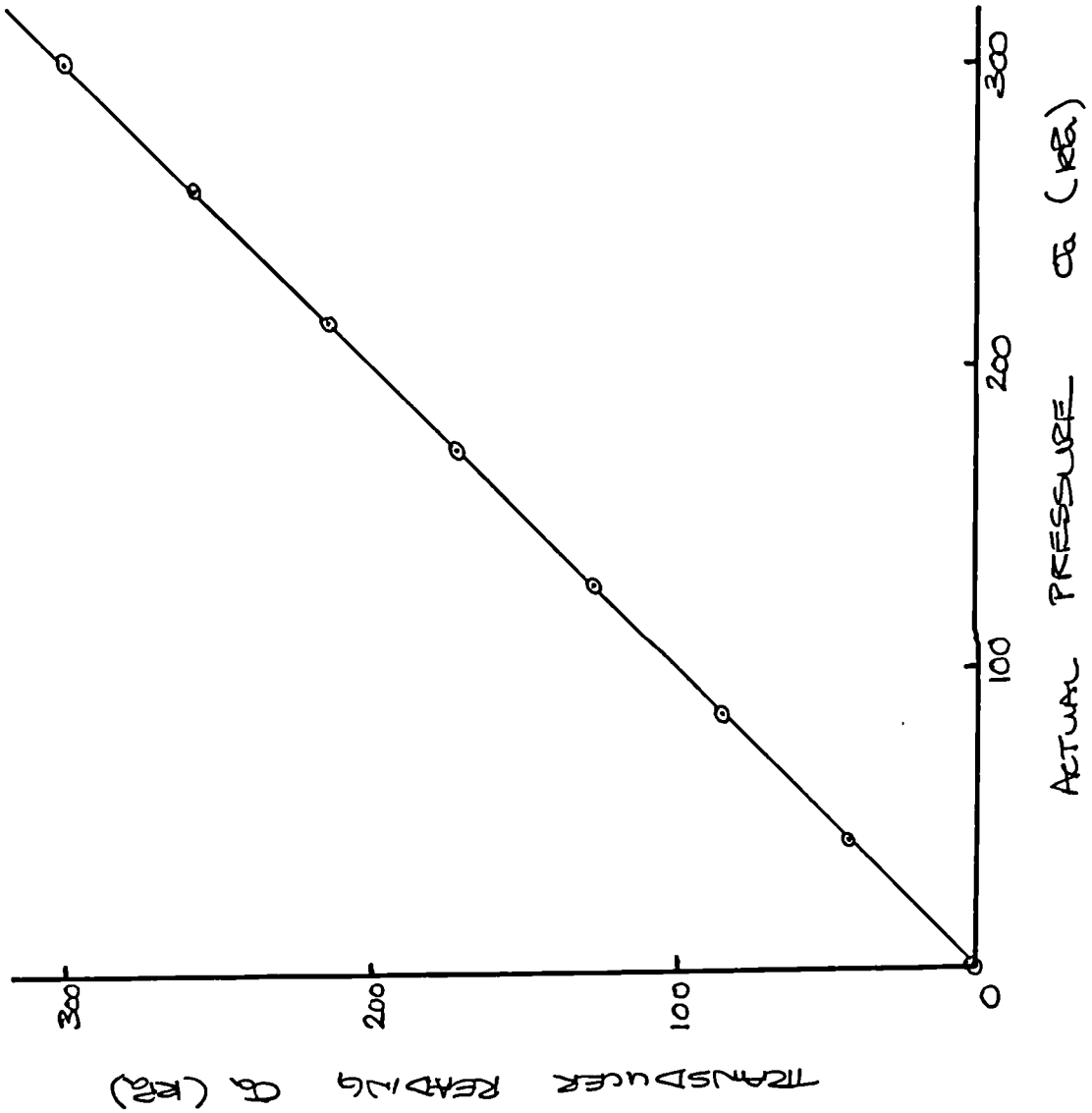

FIG 6·16
Title as page 372

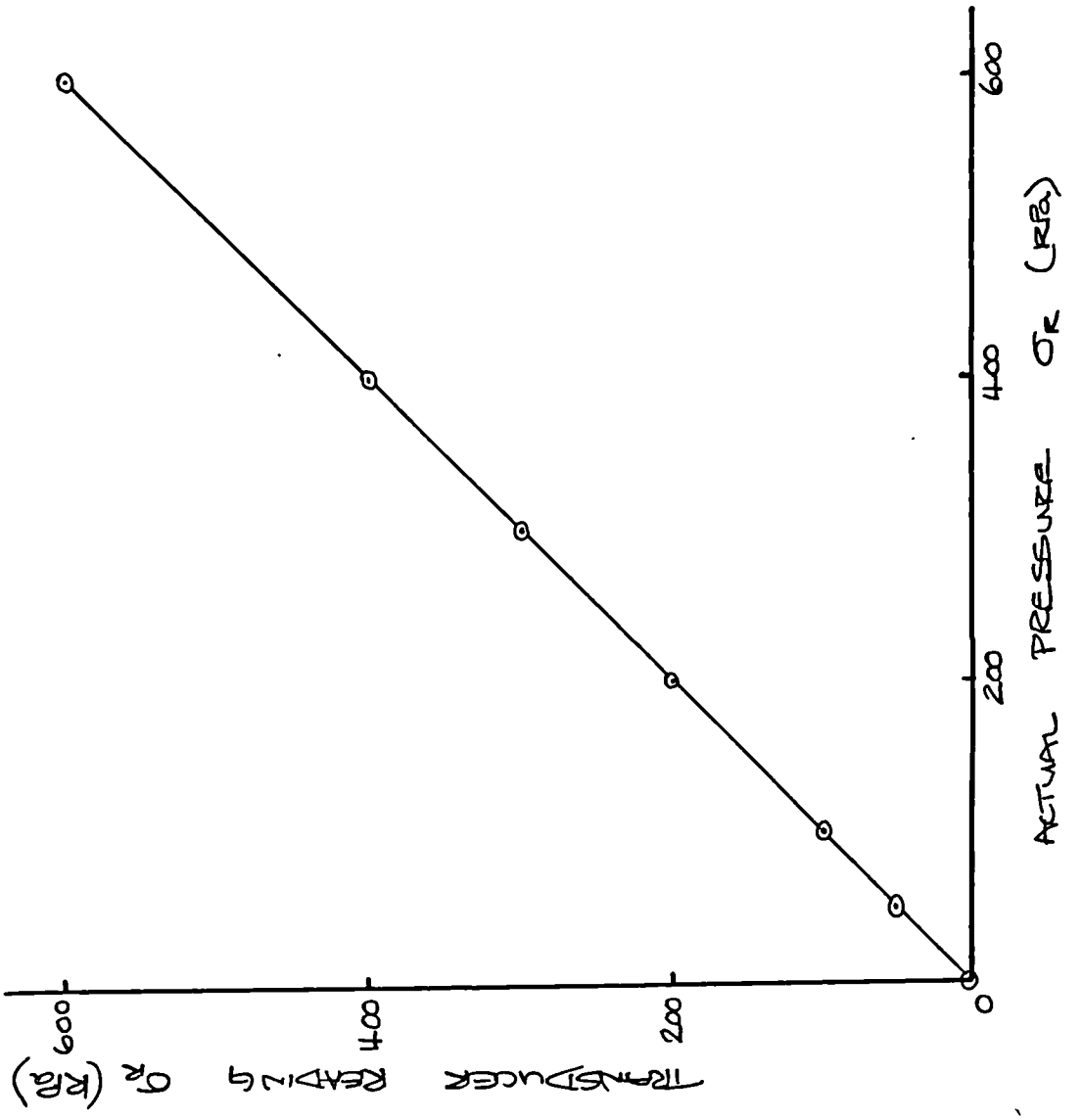

Fig 6.2 Typical calibration curve for the cell pressure transducer.

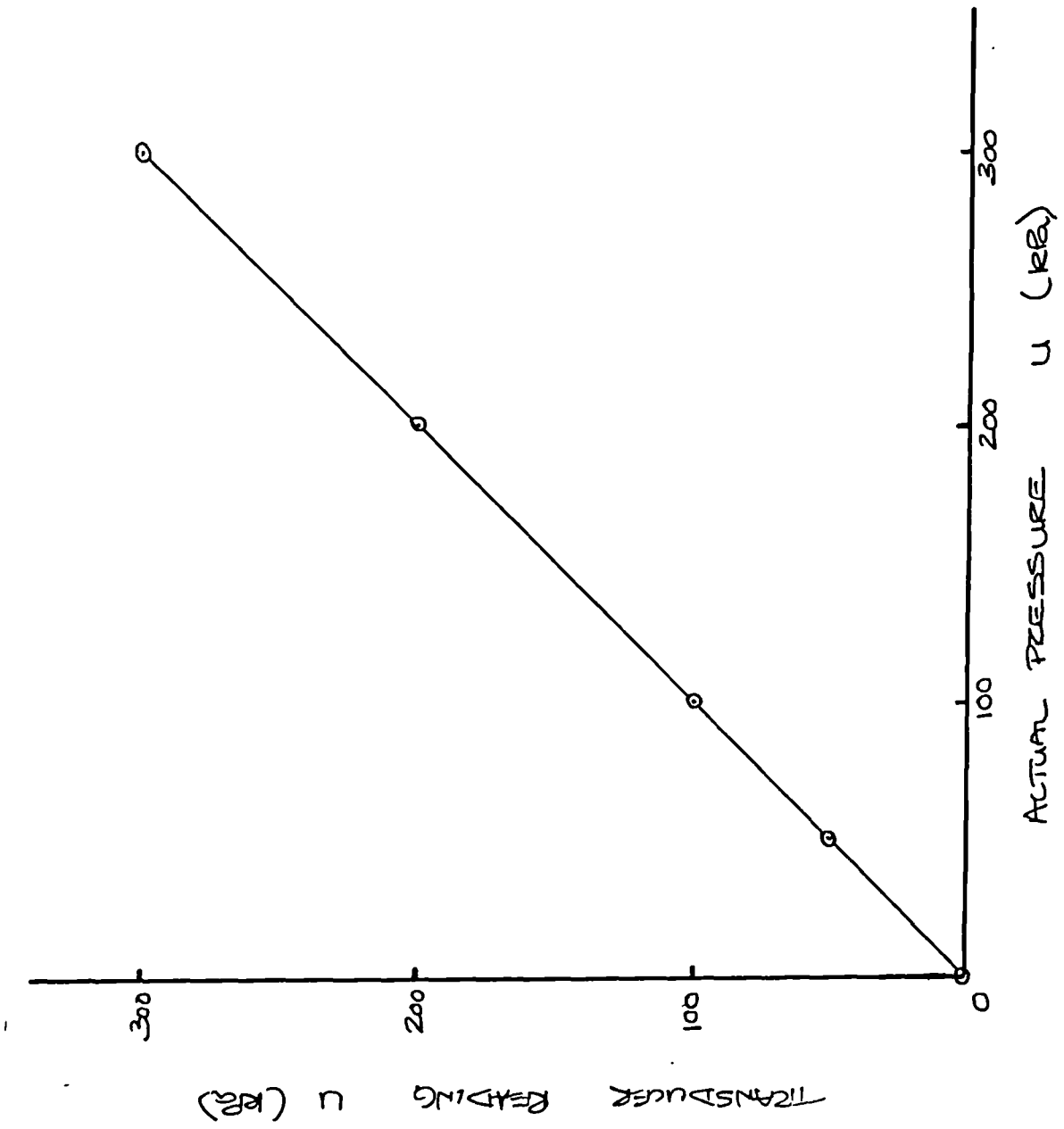

Fig 6.3 Typical calibration curve for the pore pressure transducer.

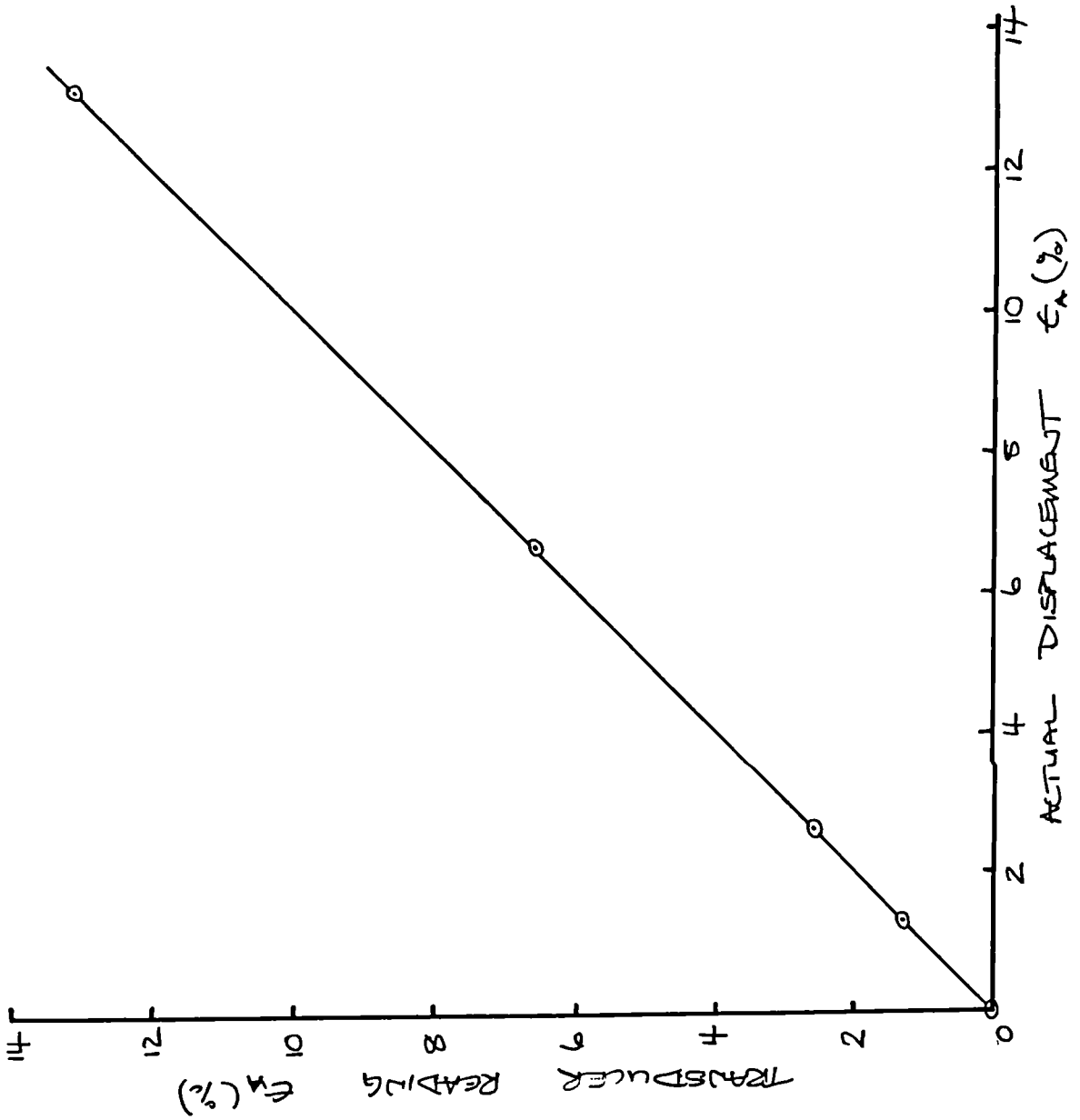

Fig 6.4 Typical calibration curve for the axial strain transducer.

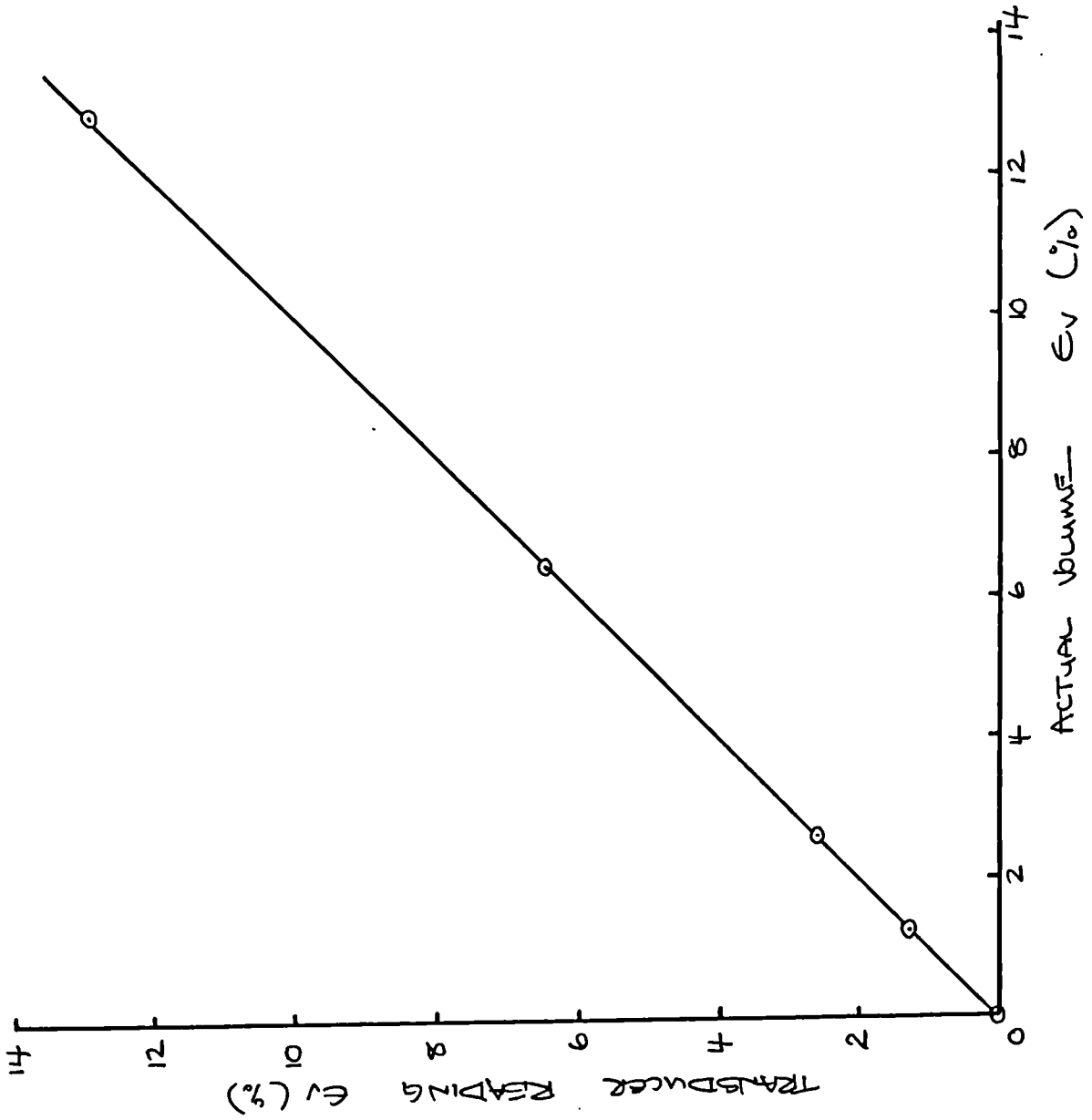

Fig 6.5 Typical calibration curve for the volume gauge.

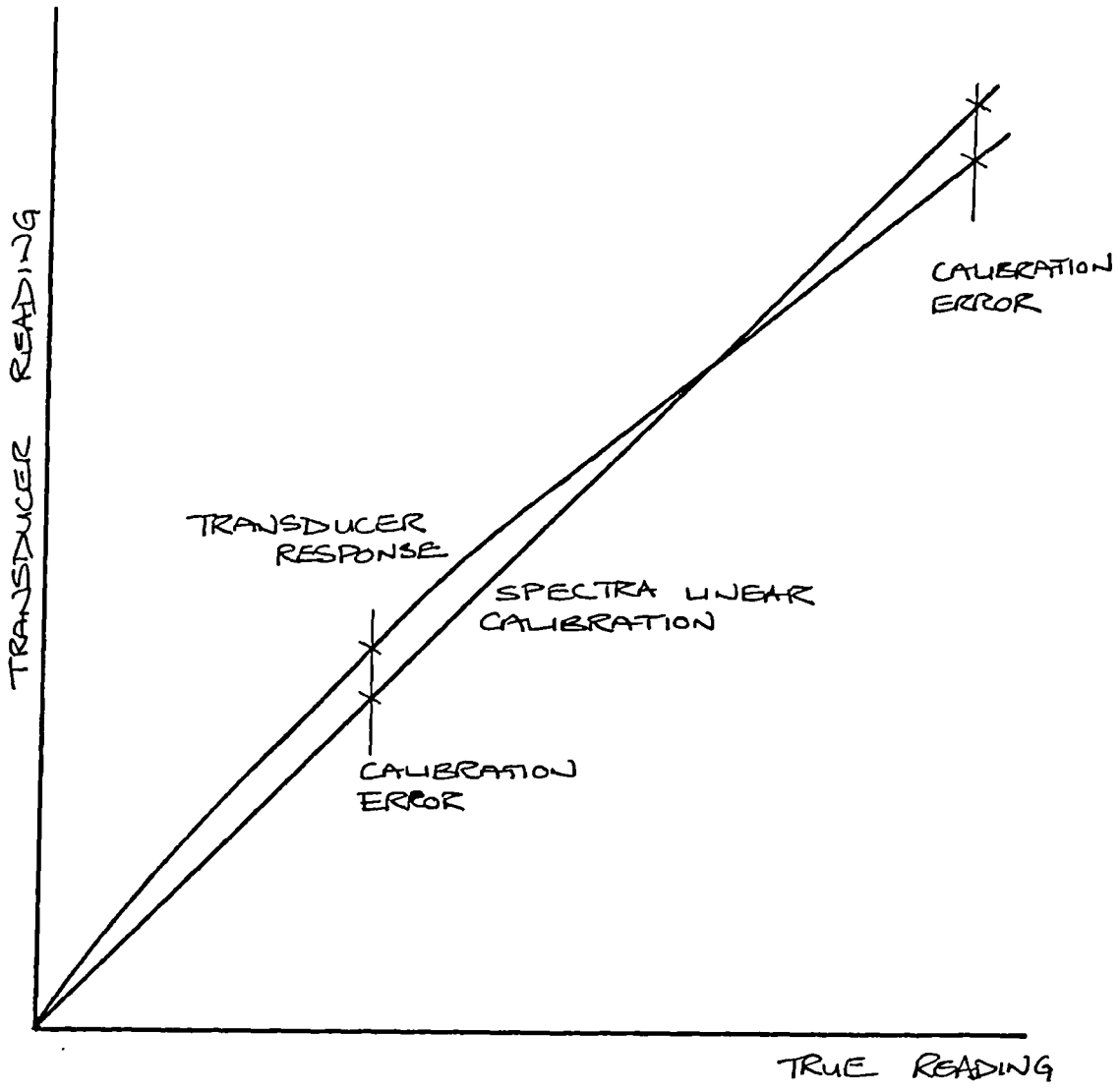

Fig 6.6 Exaggerated diagram of calibration errors.

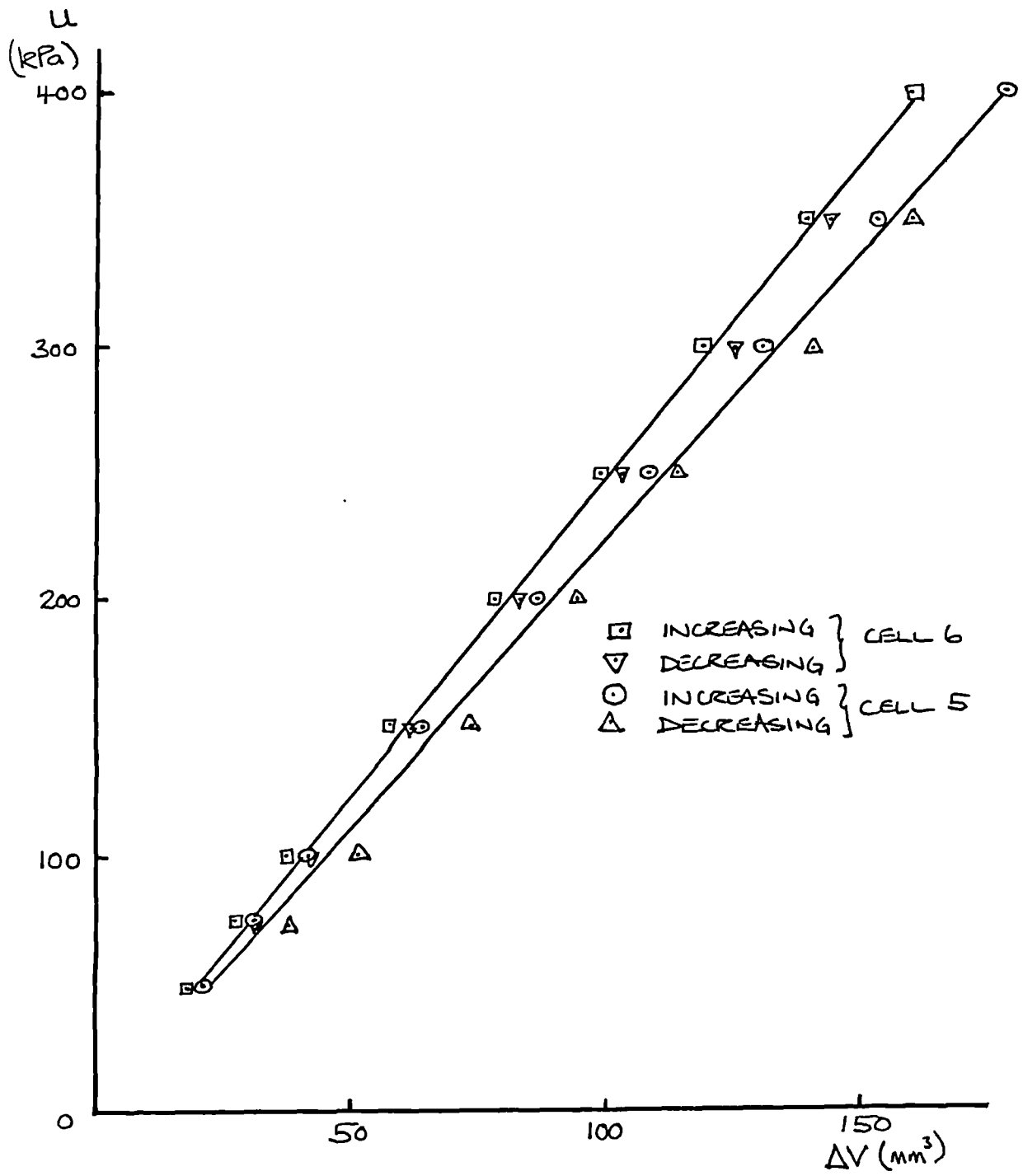

Fig 6.7 Calibration of the volume gauge expansion.

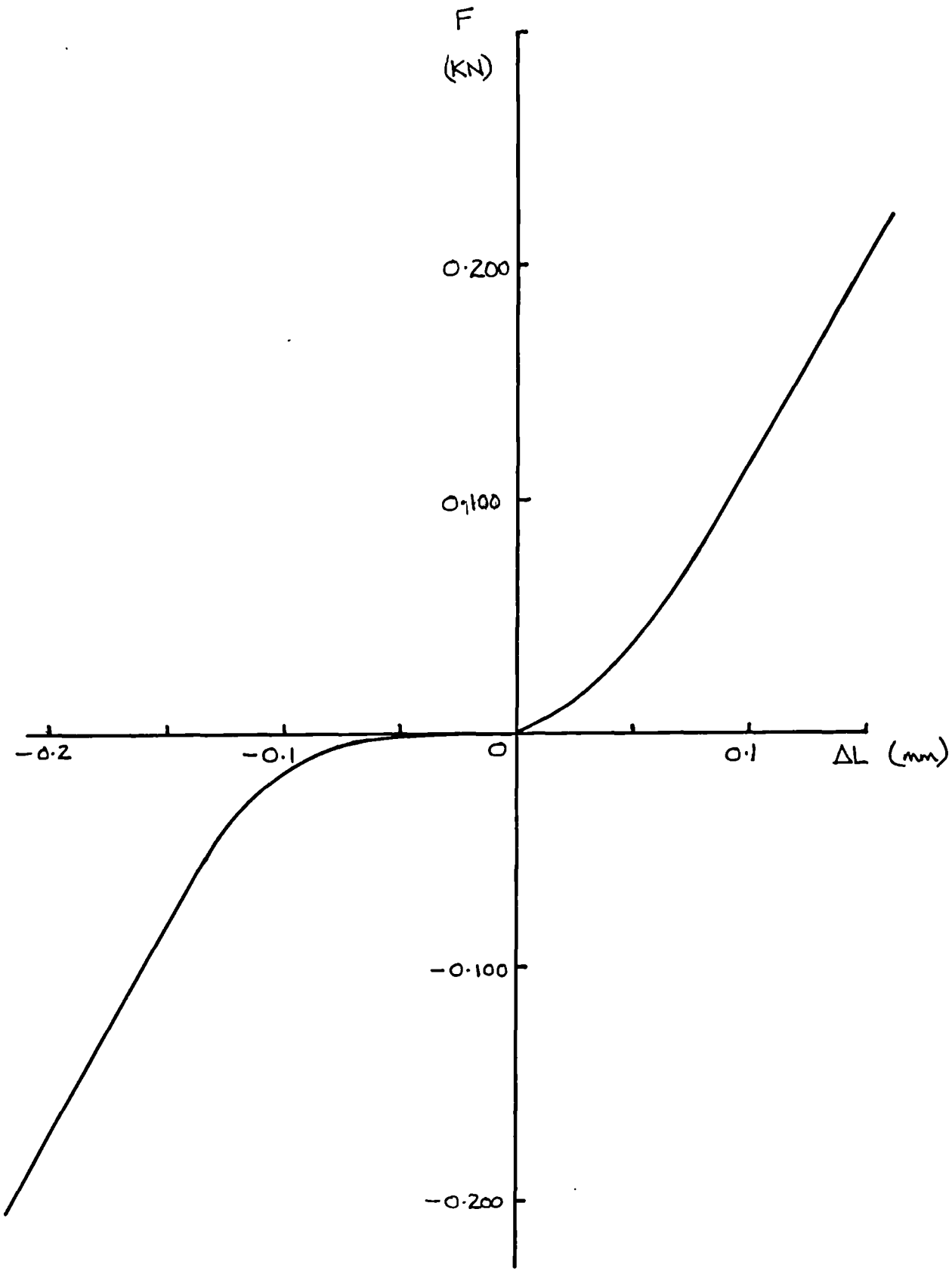

Fig 6.8 Calibration of the load cell compressibility, cell 5.

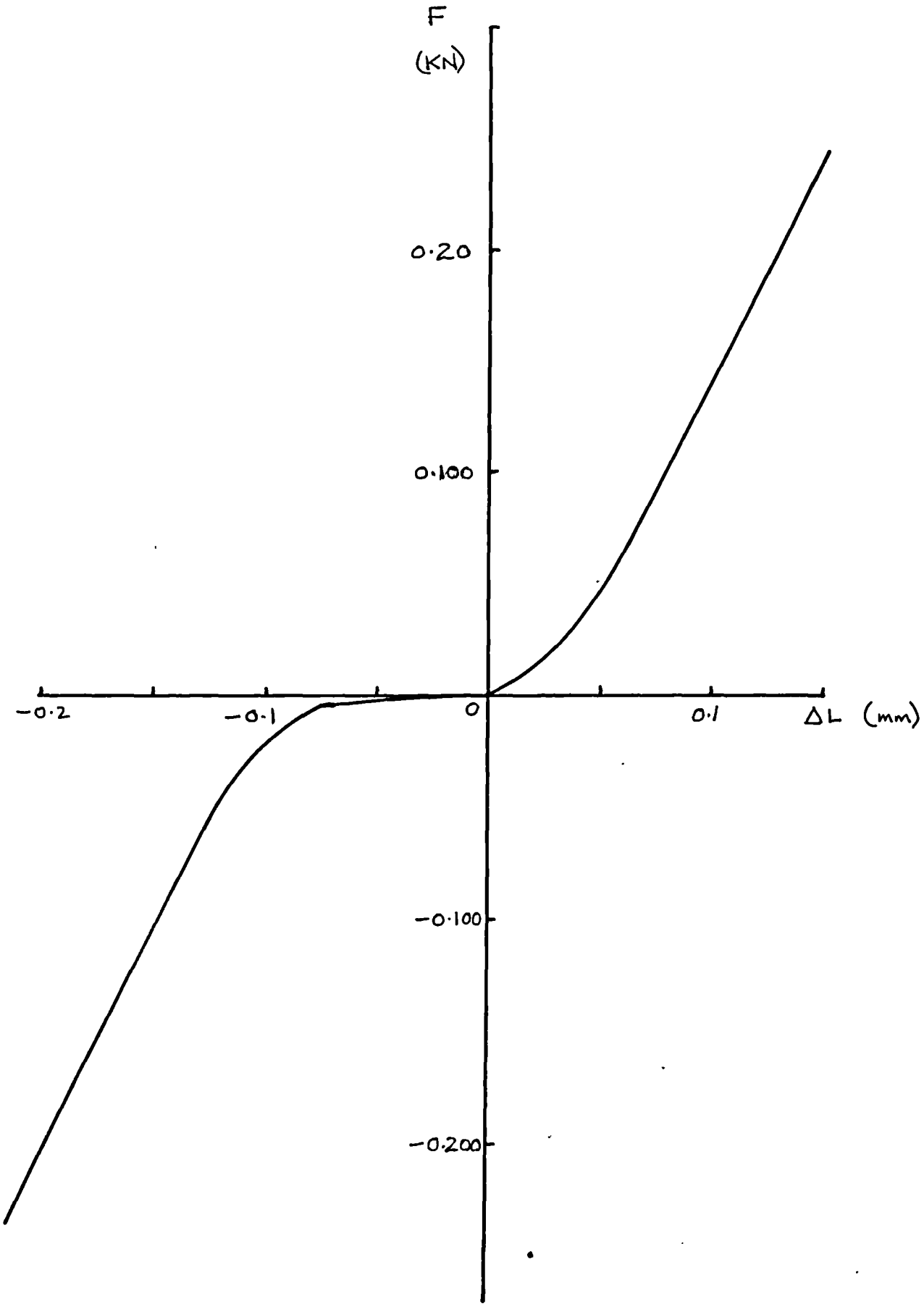

Fig 6.9 Calibration of the load cell compressibility, cell 6.

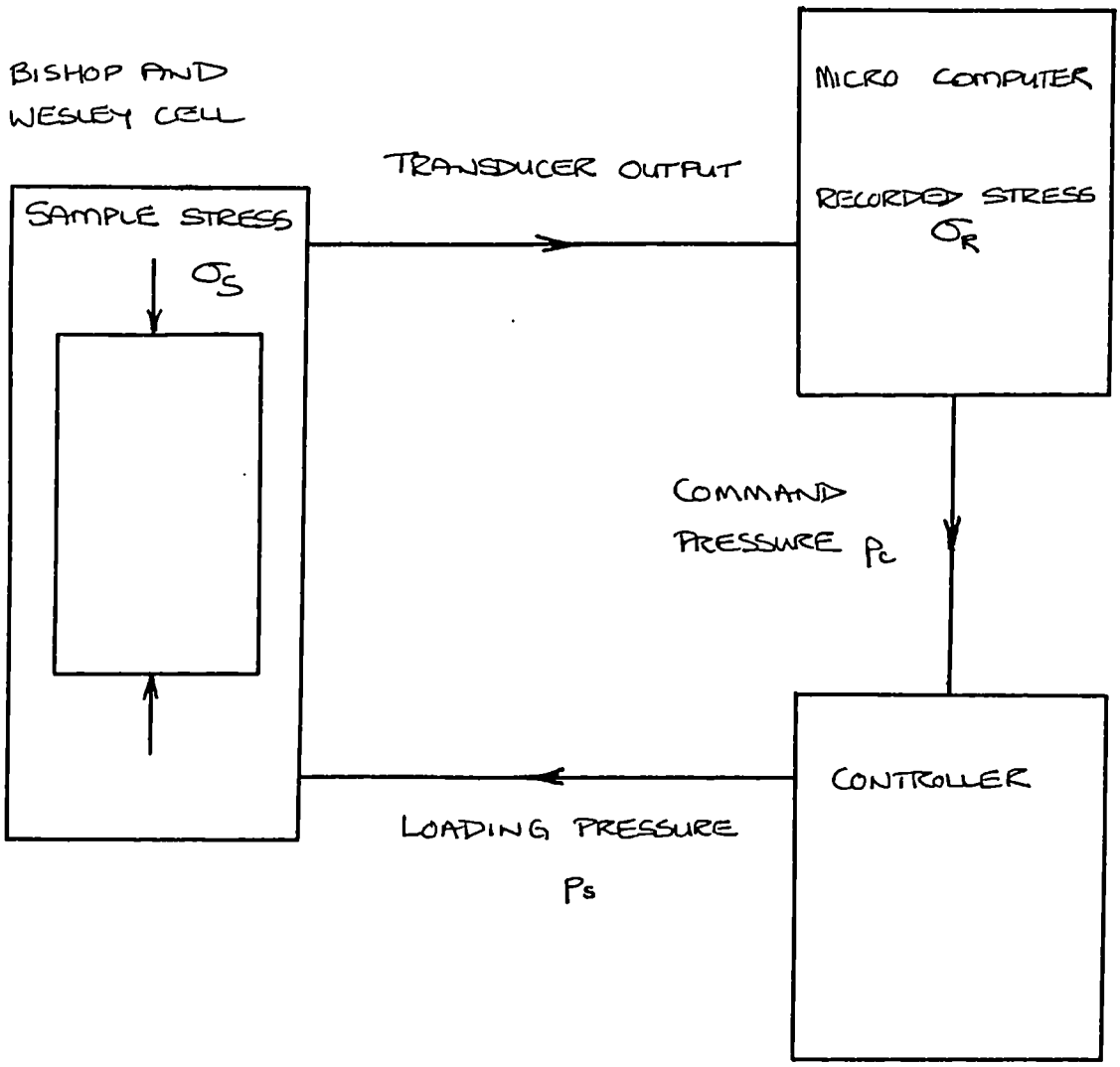

Fig 6.10 Precision of control in the Spectra system.

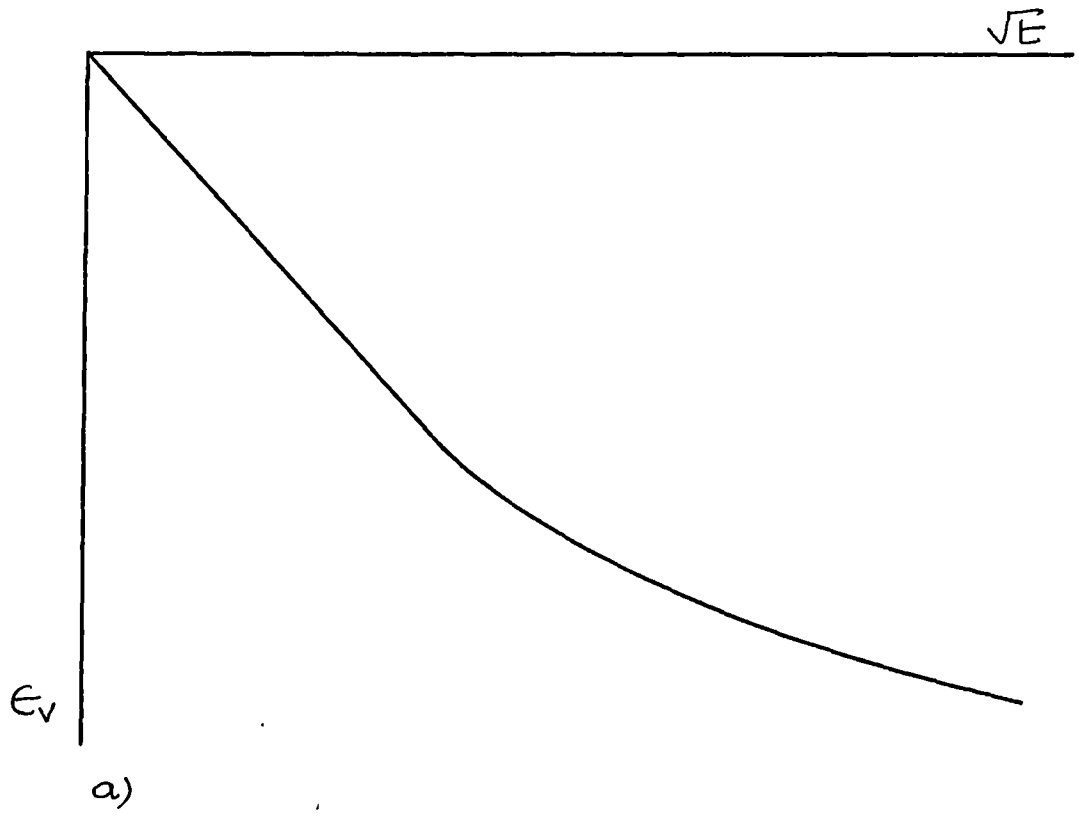

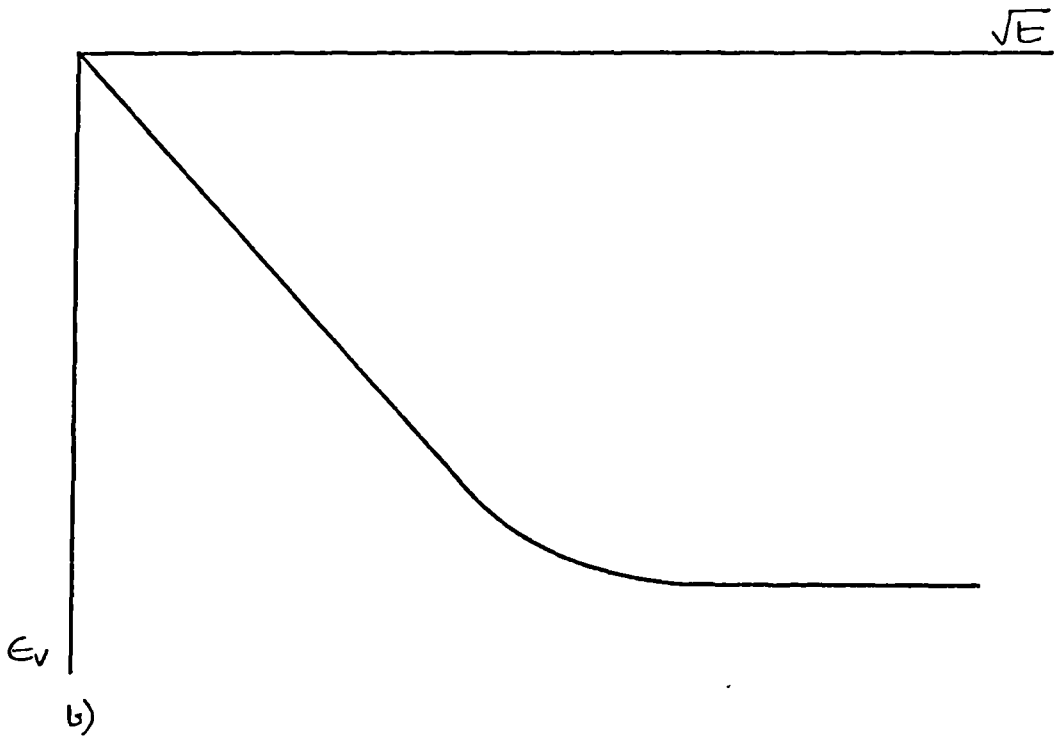

Fig 7.1 Plot of volumetric strain against square root of time.
a) Unsuitable soil for testing.
b) Suitable soil for testing.

7.1

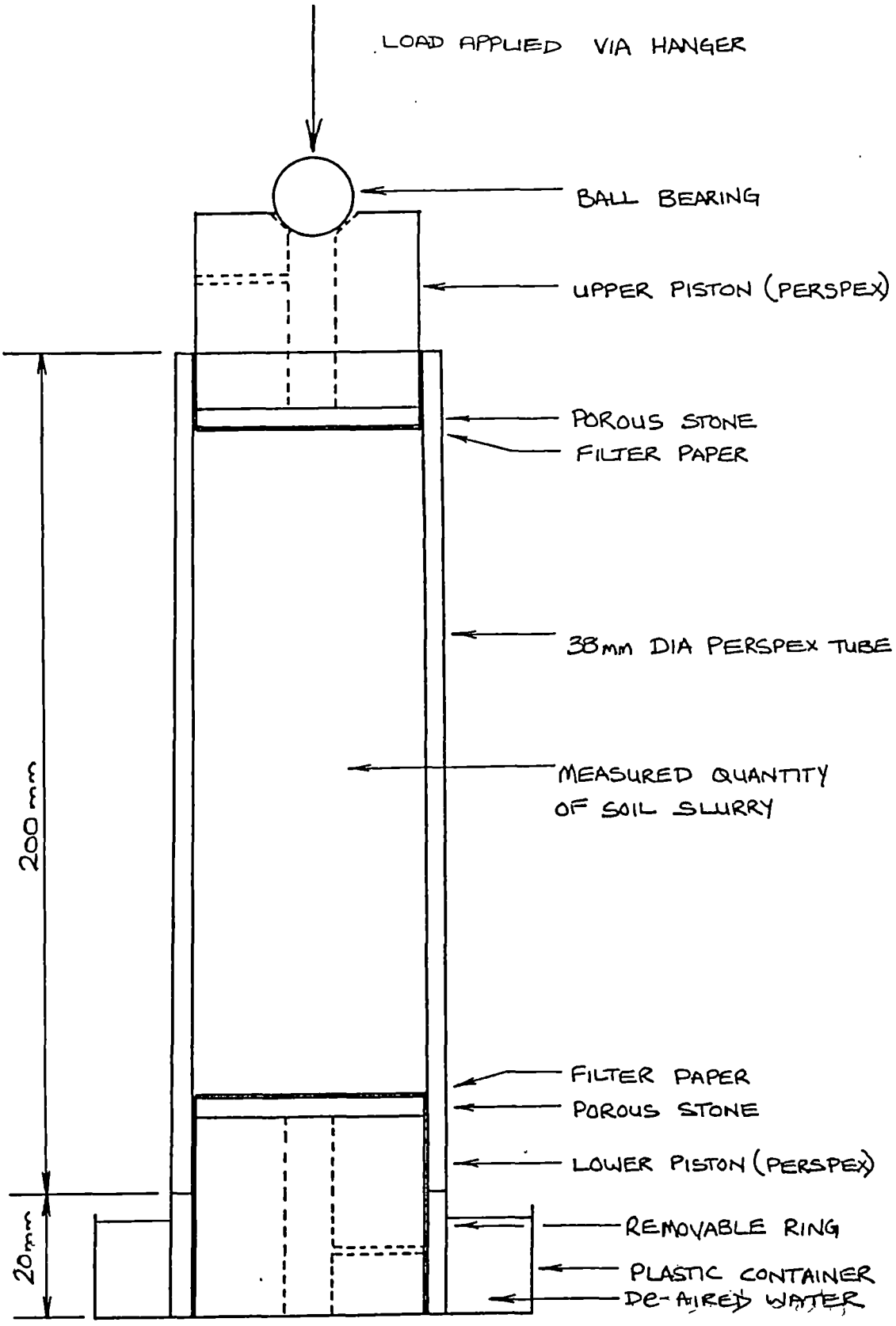

Fig 7.2 Diagram of sample presses.

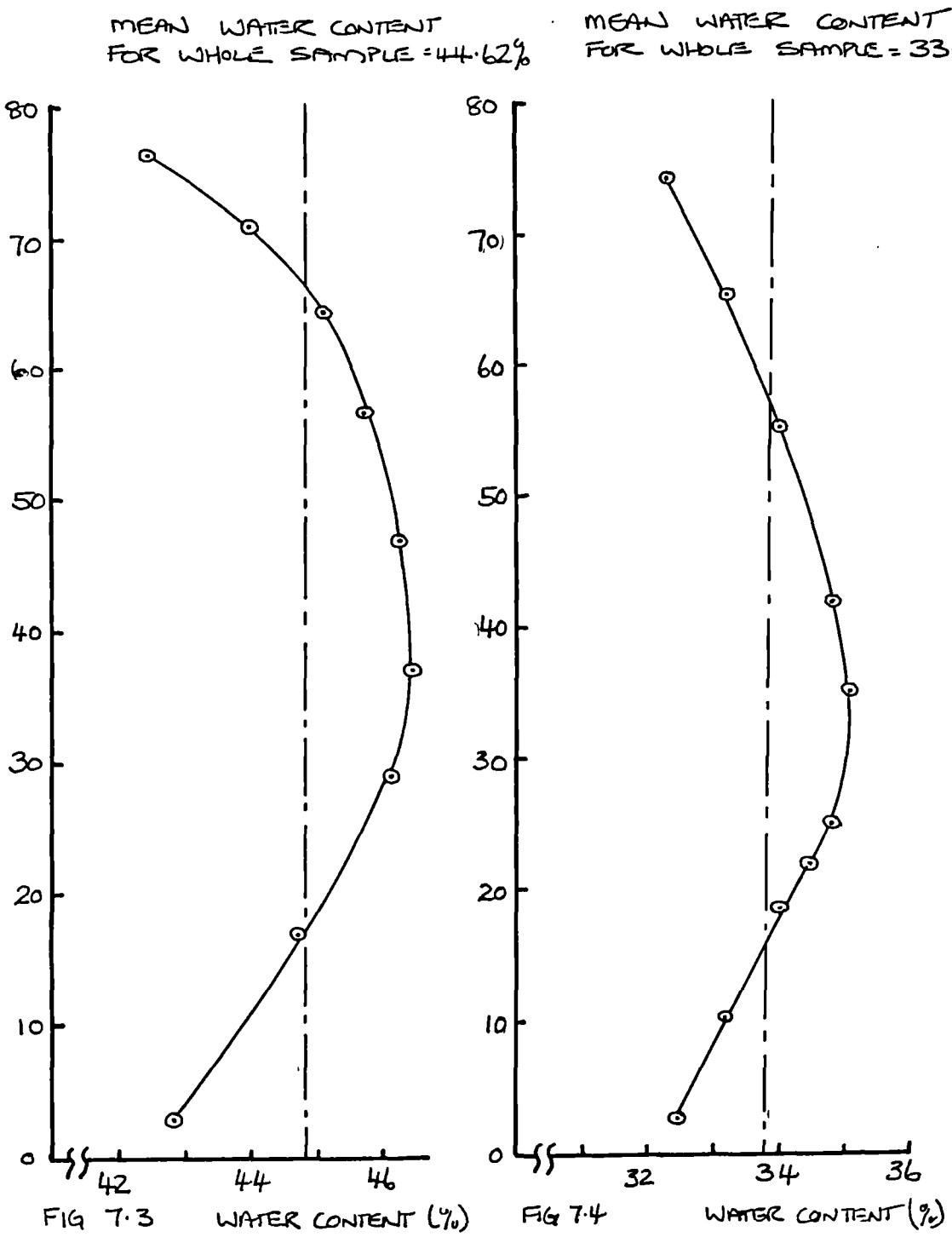

FIG 7·3 FIG 7·4

Fig 7.3 Initial water content profile in London Clay samples.

Fig 7.4 Initial water content profile in Ware till samples.

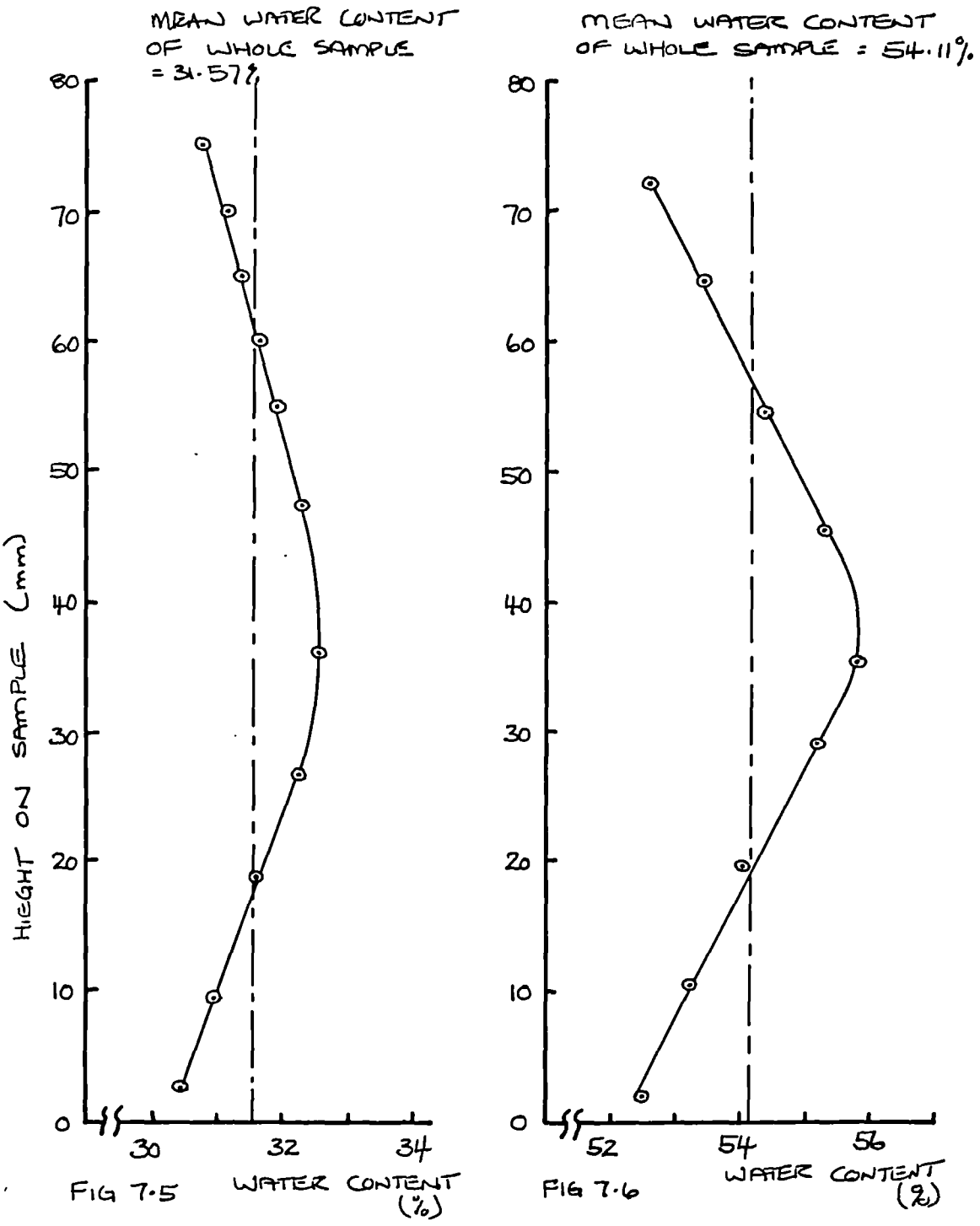

Fig 7.5 Initial water content profile in Cowden till samples.

Fig 7.6 Initial water content profile in Speswhite kaolin samples.

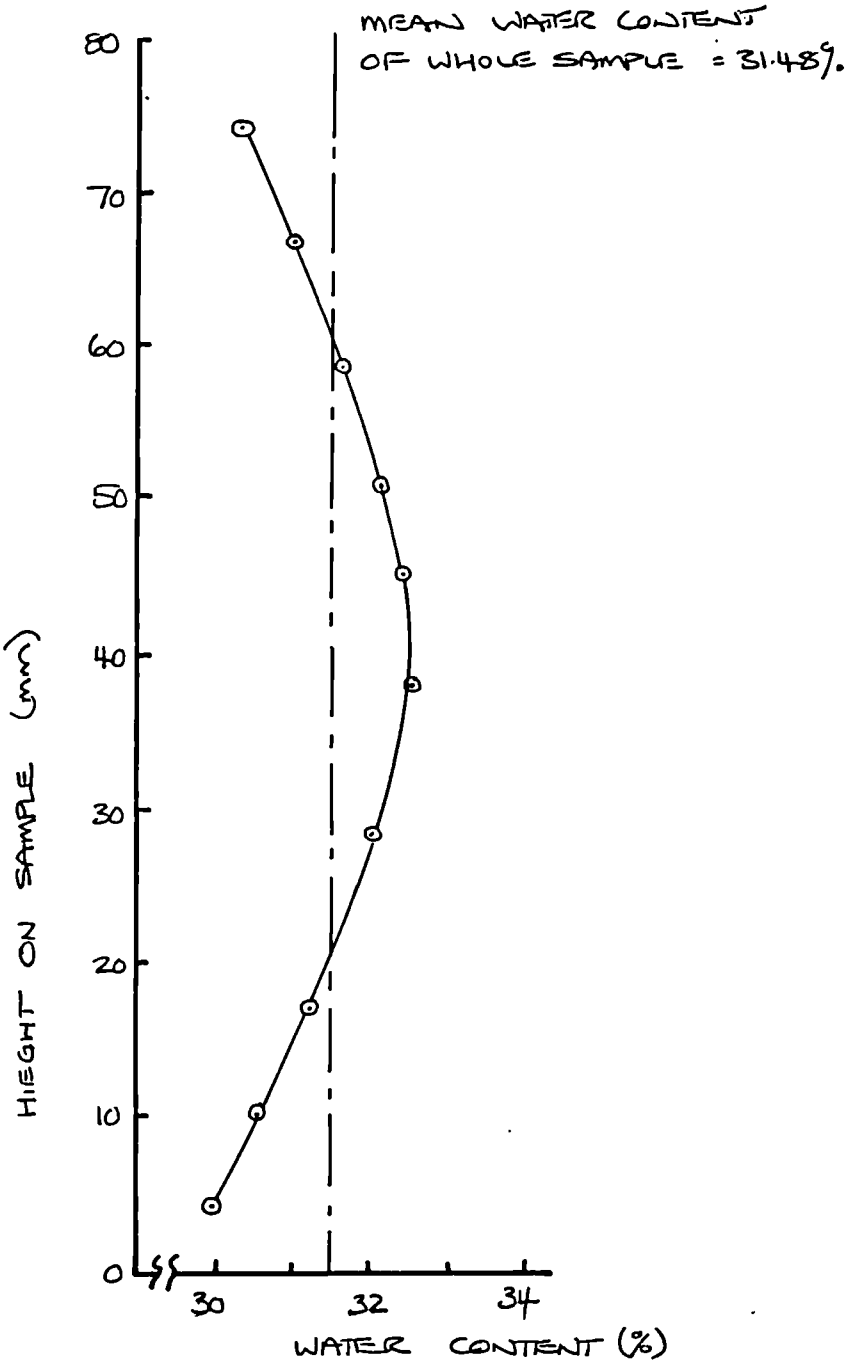

Fig 7.7 Initial water content profile in Slate dust samples.

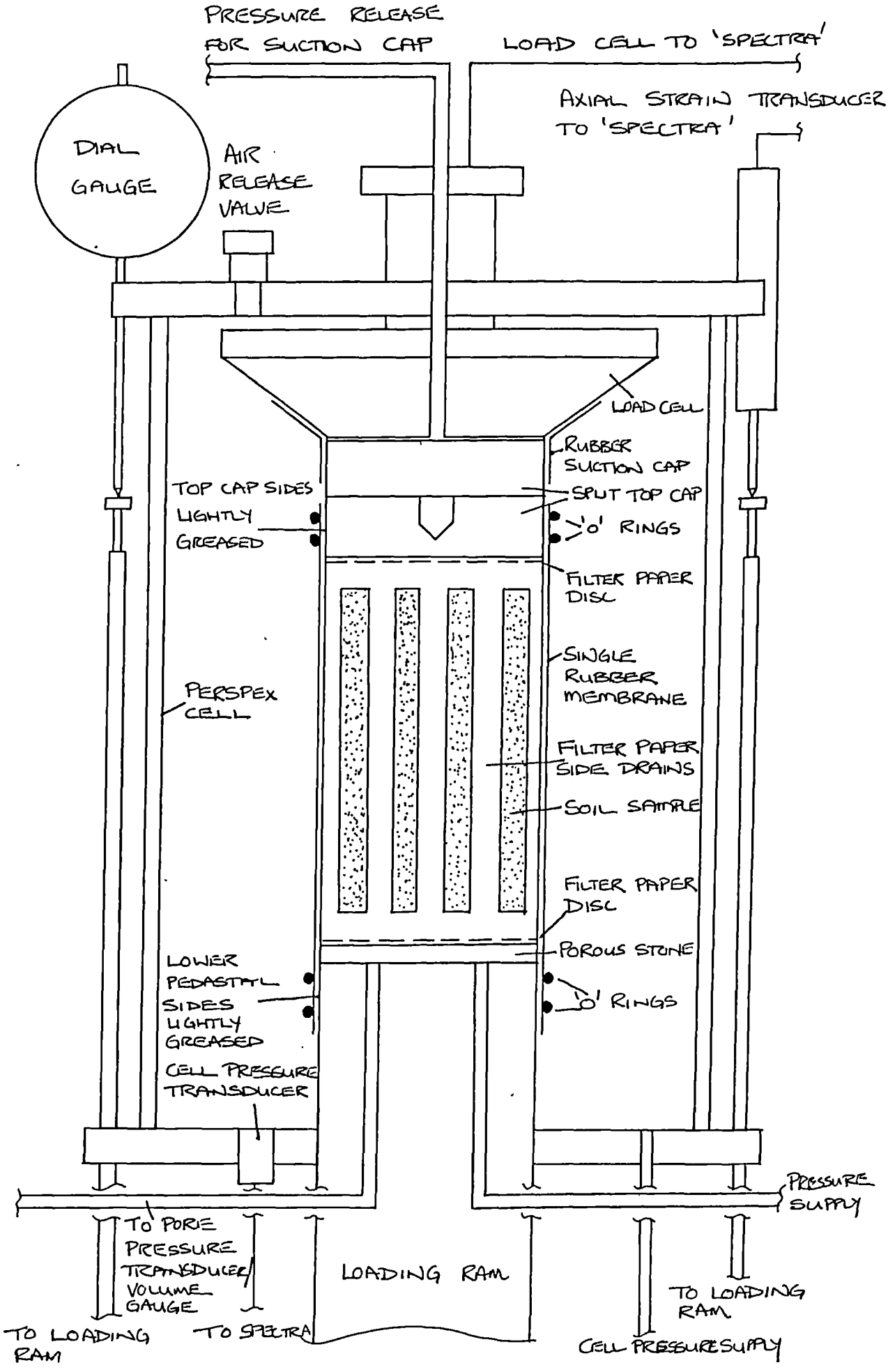

Fig 7.8 Diagrammatic view of sample set up in the triaxial cell.

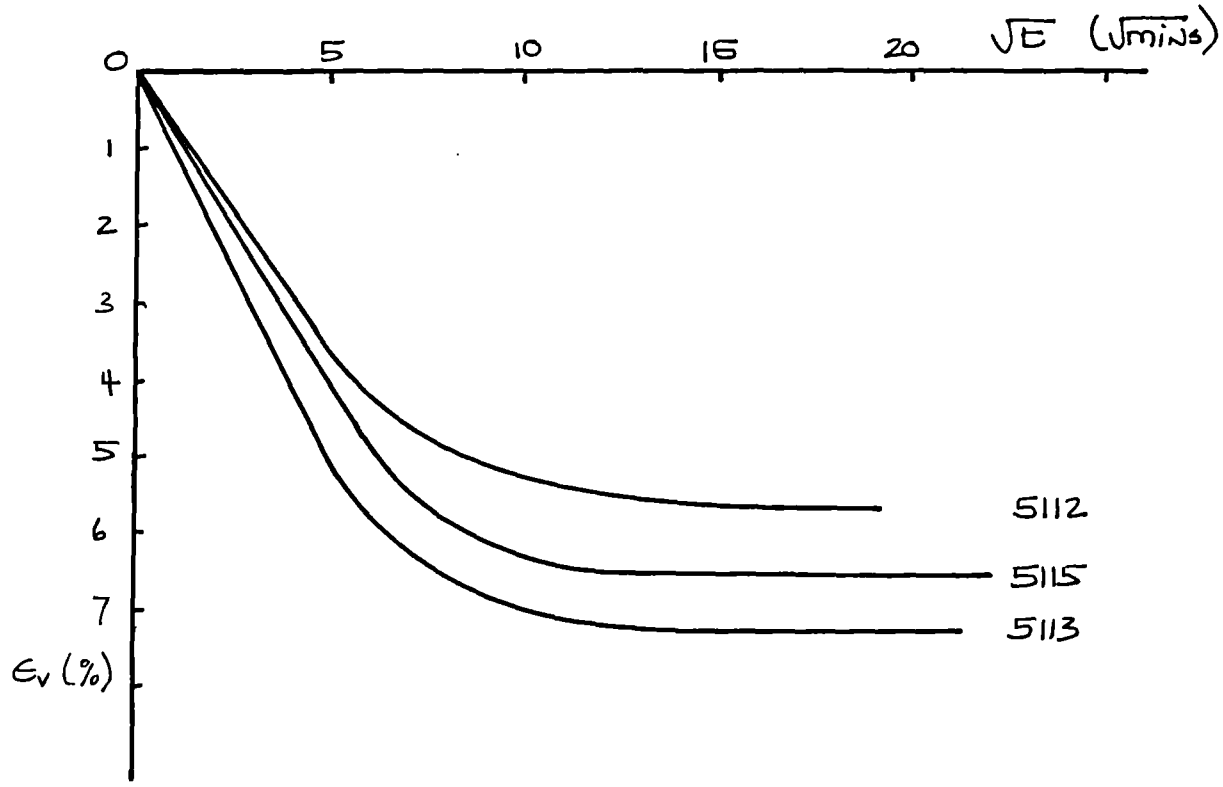

Fig 7.9 ε_v against $\sqrt{t}$ for London Clay, initial compression by Method A.

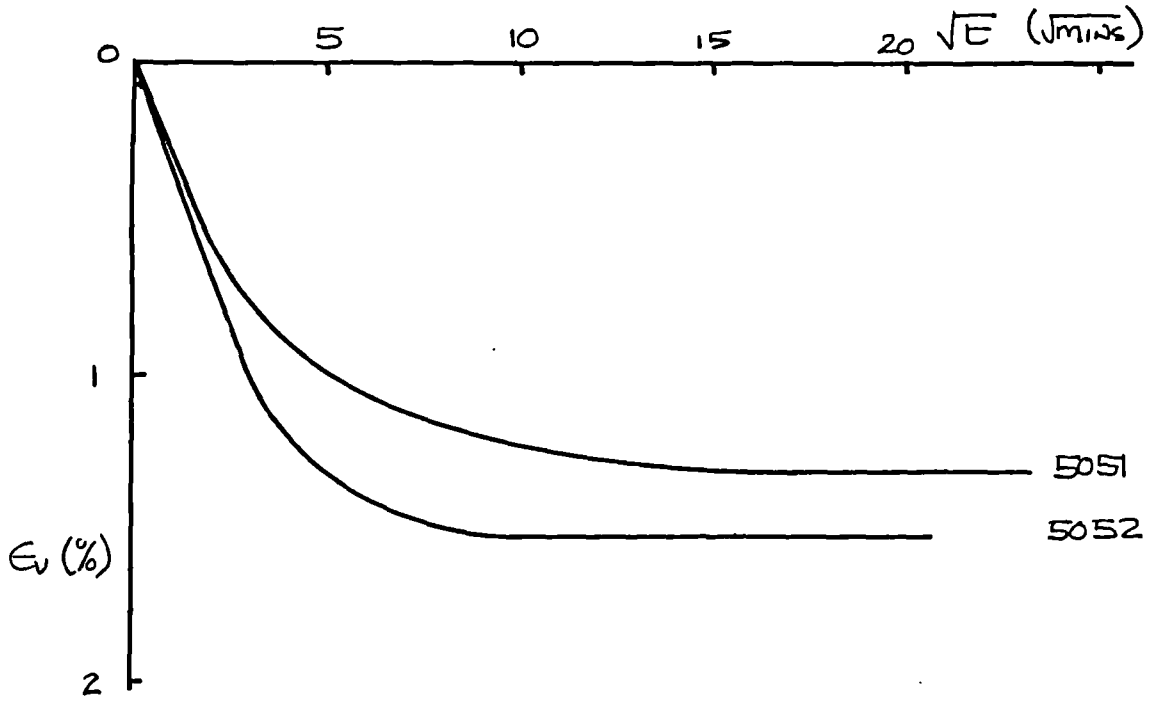

Fig 7.10 ε_v against $\sqrt{t}$ for Ware till, initial compression by Method A.

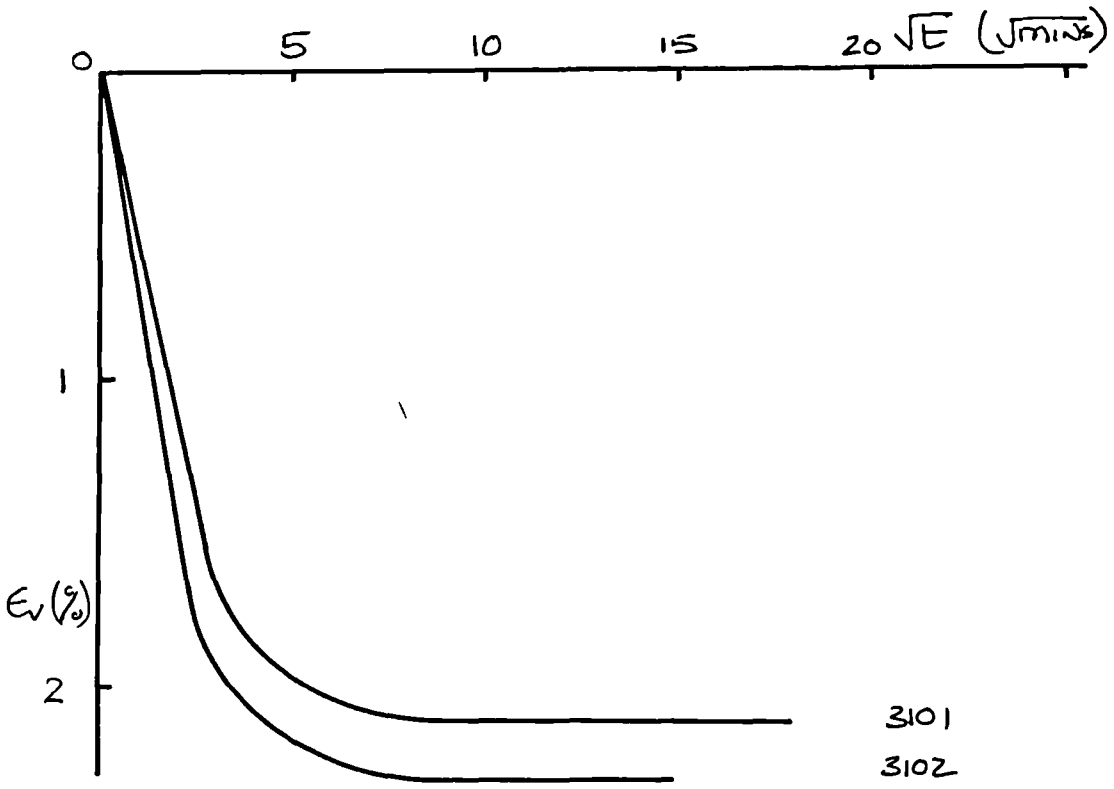

Fig 7.11 ε_v against $\sqrt{t}$ for Speswhite kaolin, initial compression by Method A.

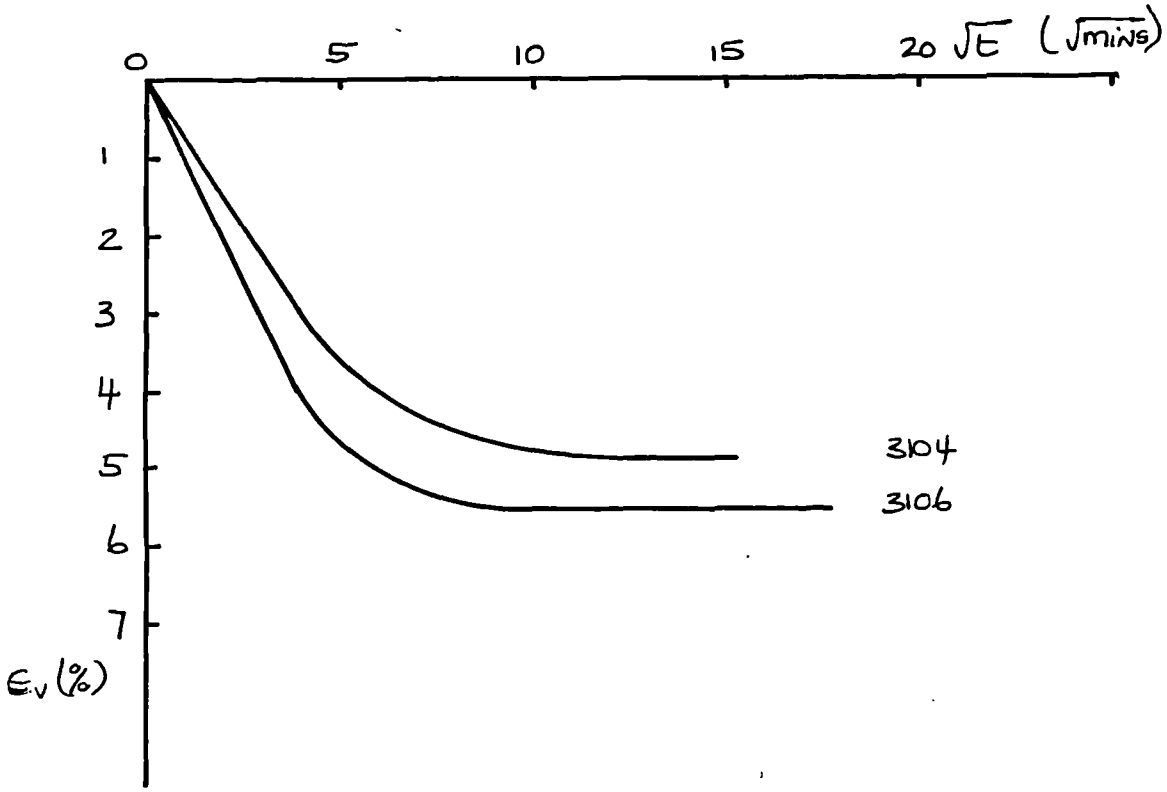

Fig 7.12 ε_v against $\sqrt{t}$ for Cowden till, initial compression by Method A.

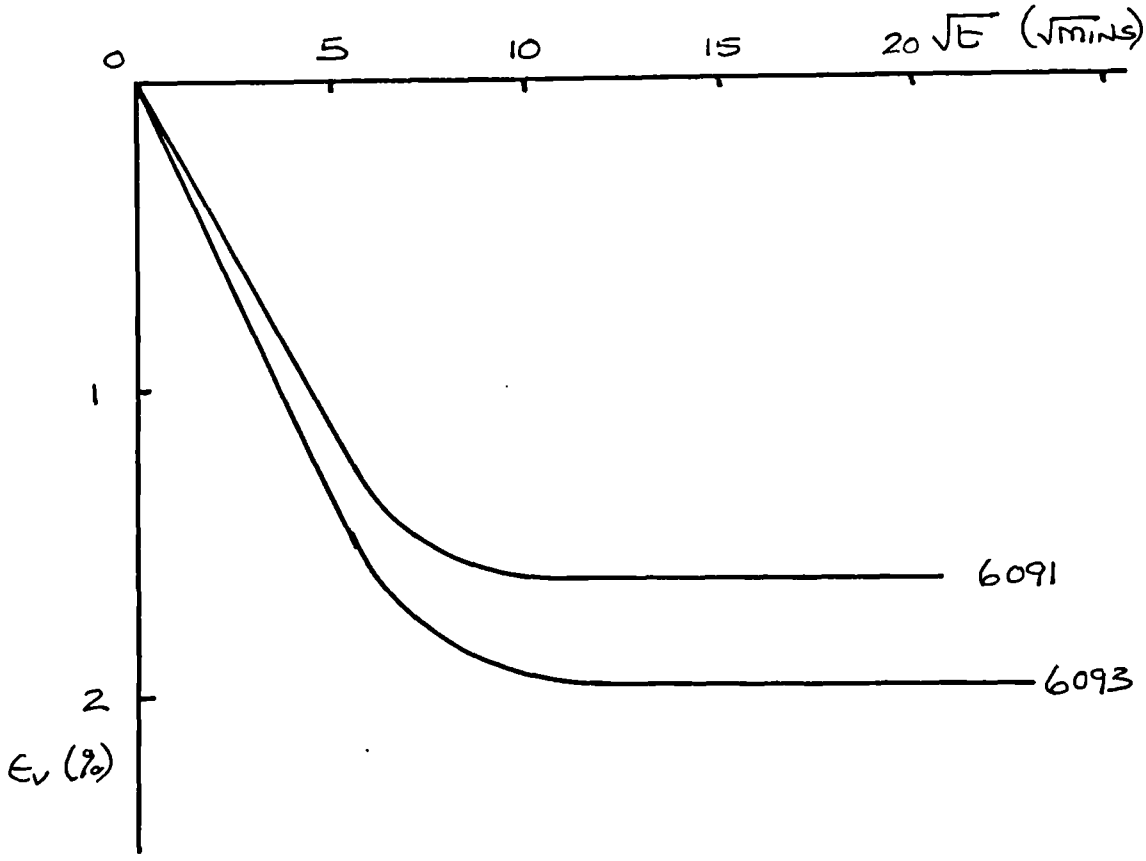

Fig 7.13 ε_v against $\sqrt{t}$ for Slate dust, initial compression by Method A.

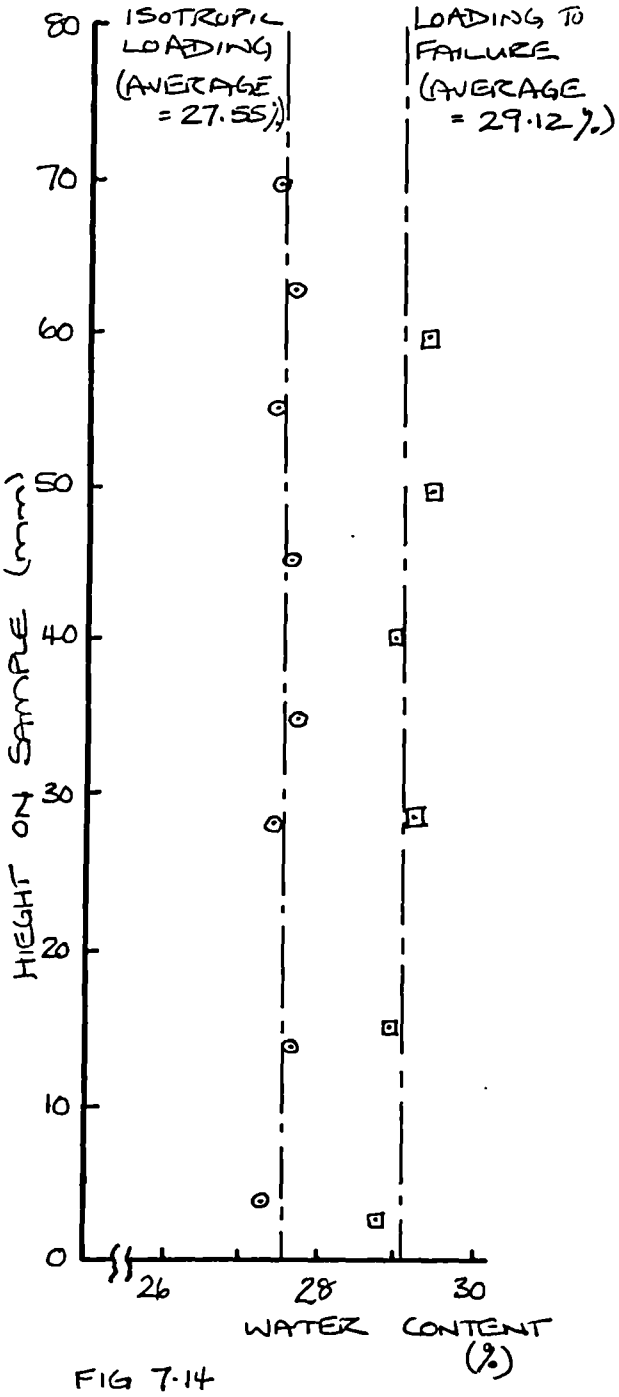

FIG 7·14

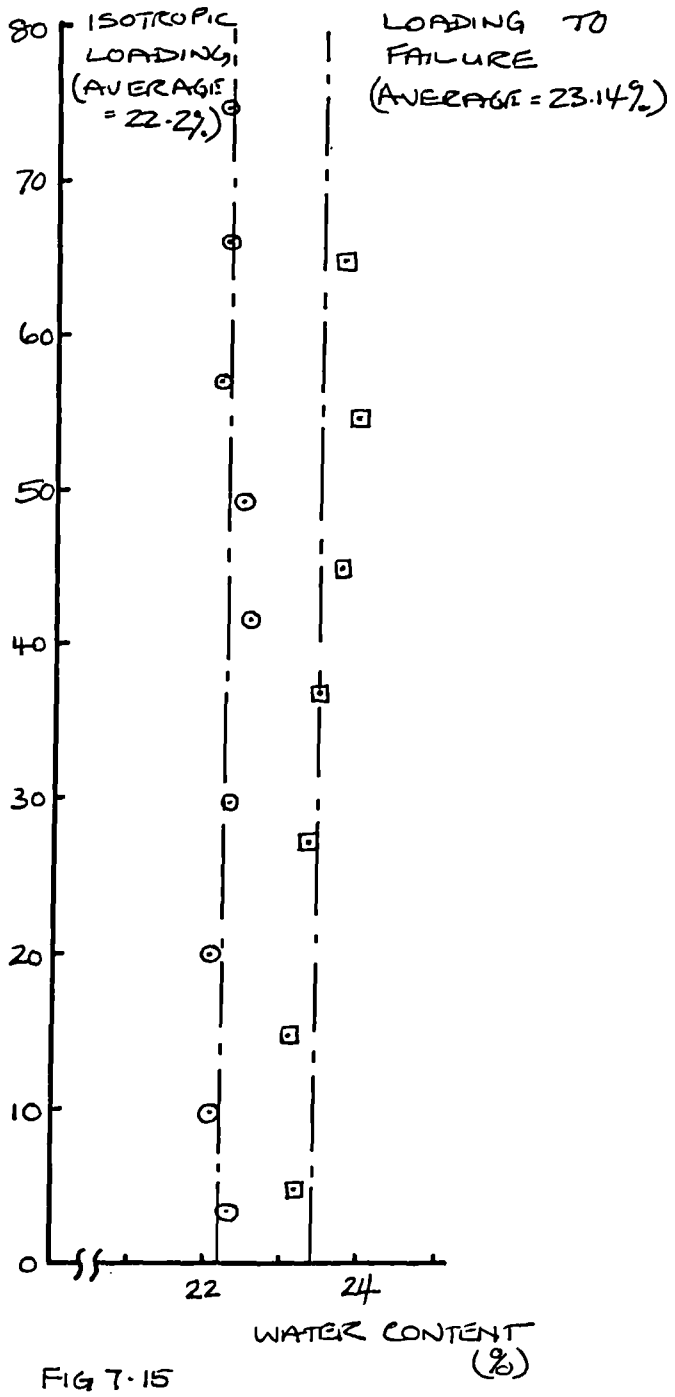

FIG 7·15

Fig 7.14 Final water content profile at the end of tests on London Clay samples.

Fig 7.15 Final water content profile at the end of tests on Ware till samples.

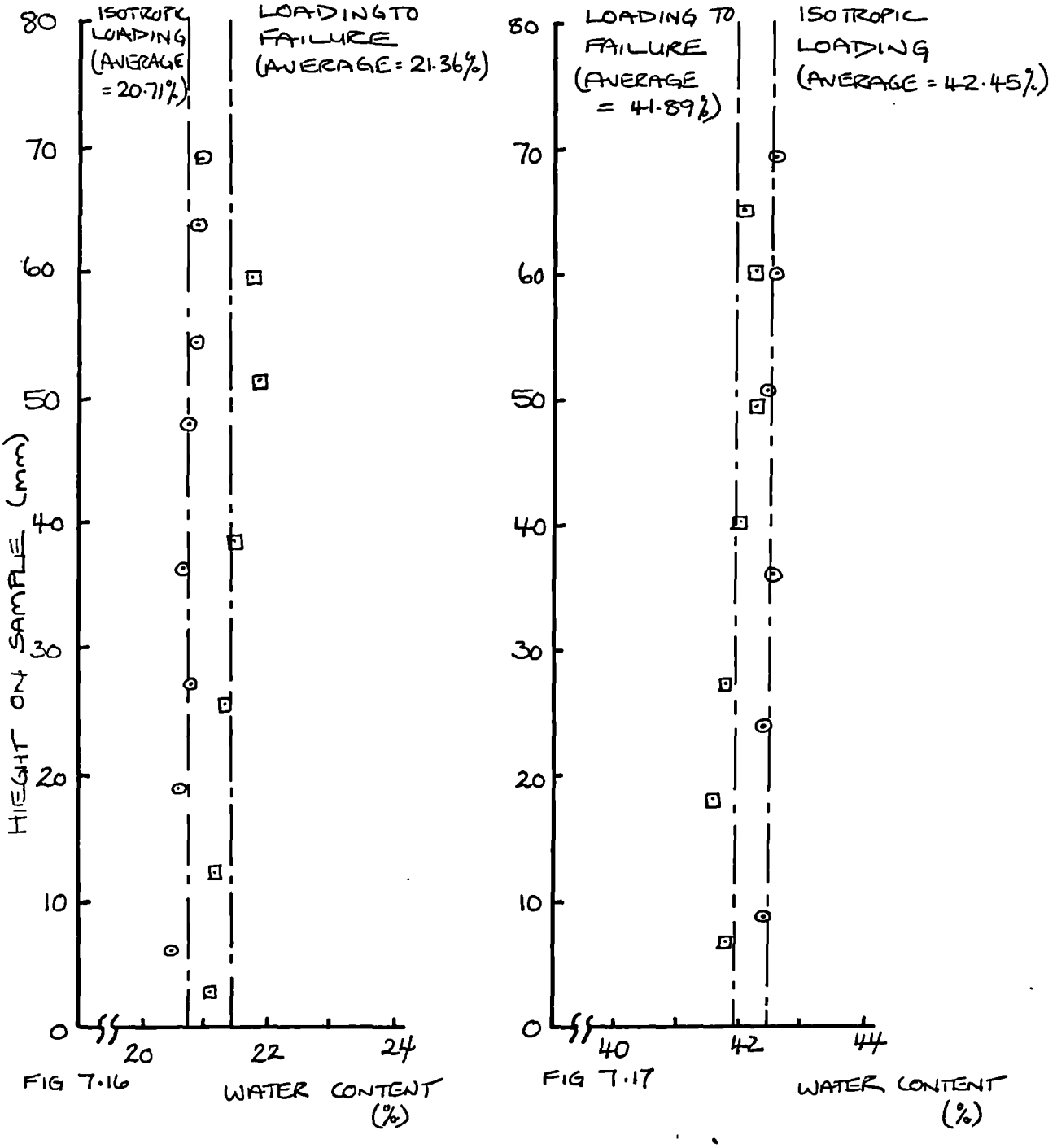

Fig 7.16 Final water content profile at the end of tests on Cowden till samples.

Fig 7.17 Final water content profile at the end of tests on Speswhite kaolin samples.

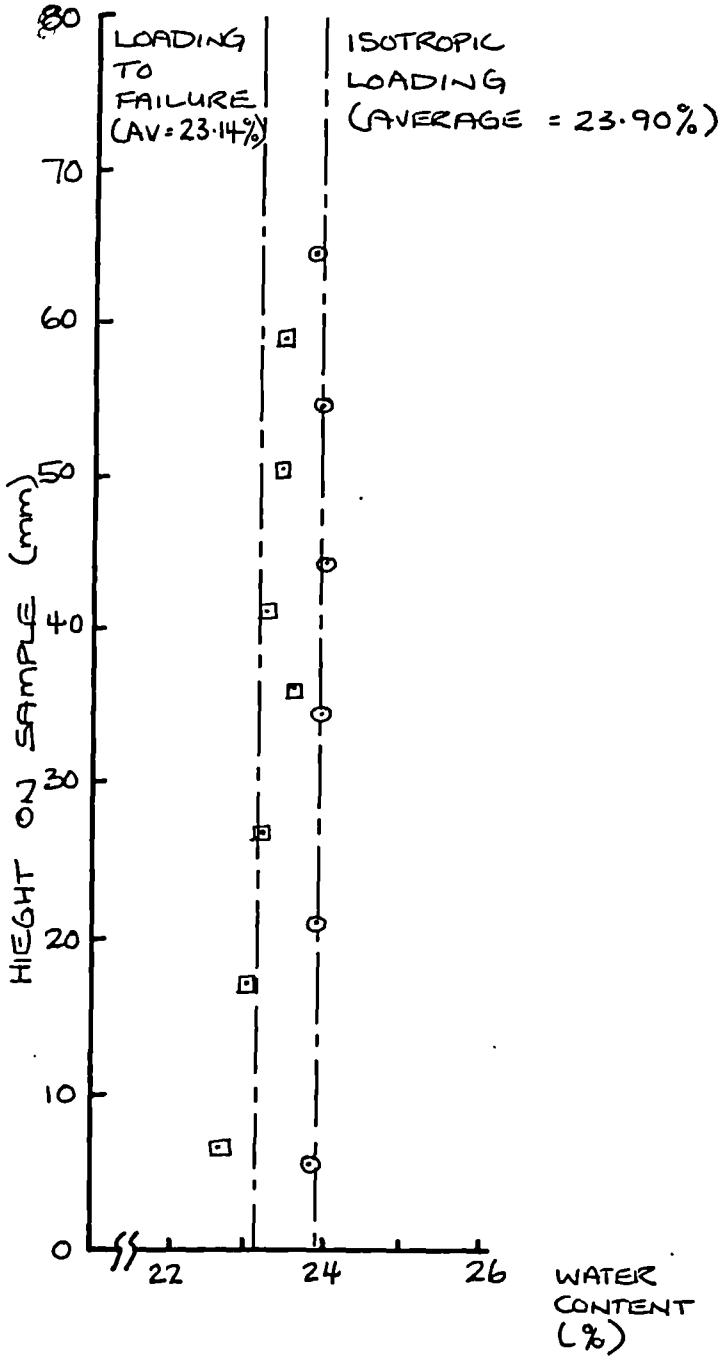

Fig 7.18 Final water content profile at the end of tests on Slate dust samples.

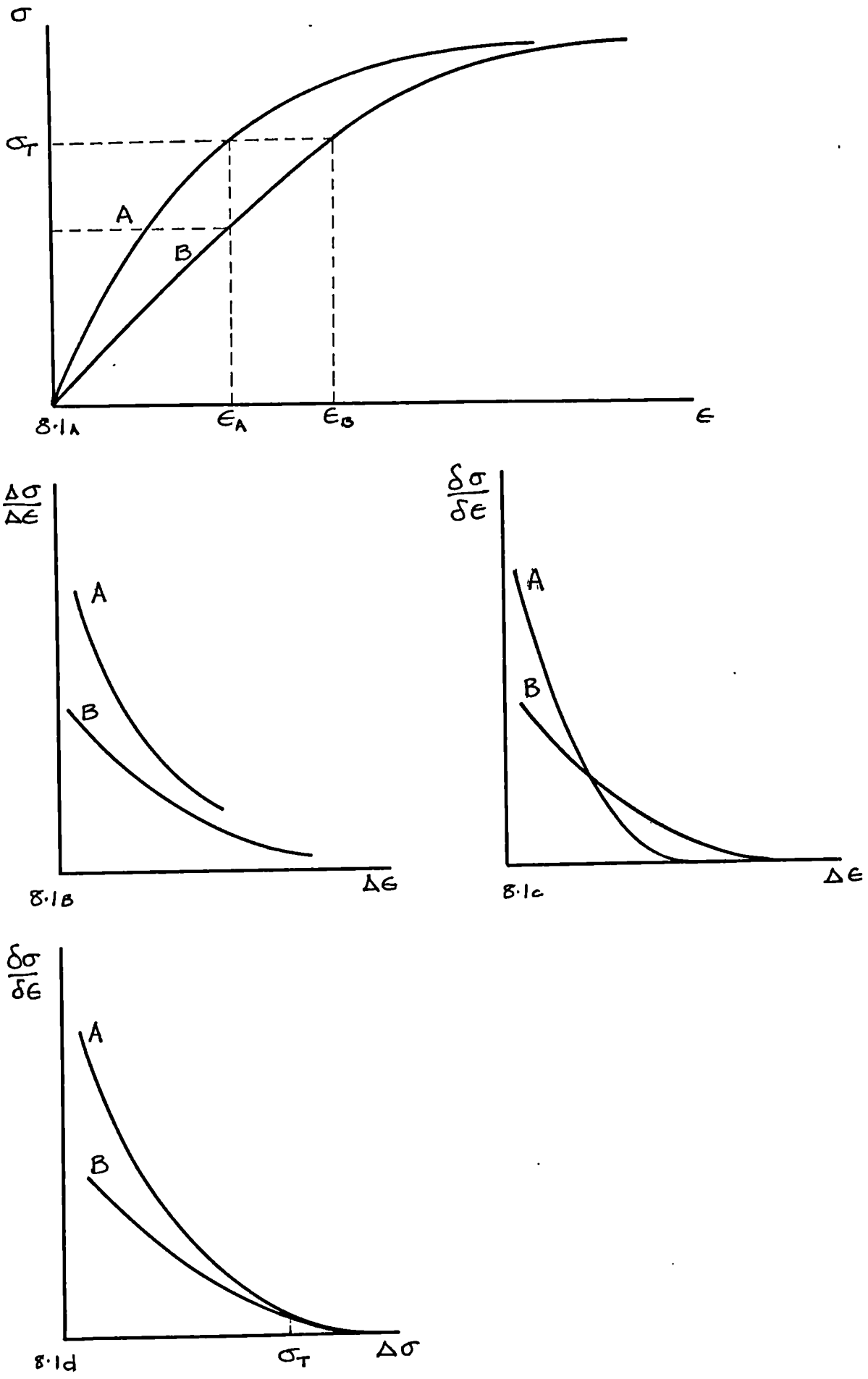

Fig 8.1 Selection of stiffness definition.

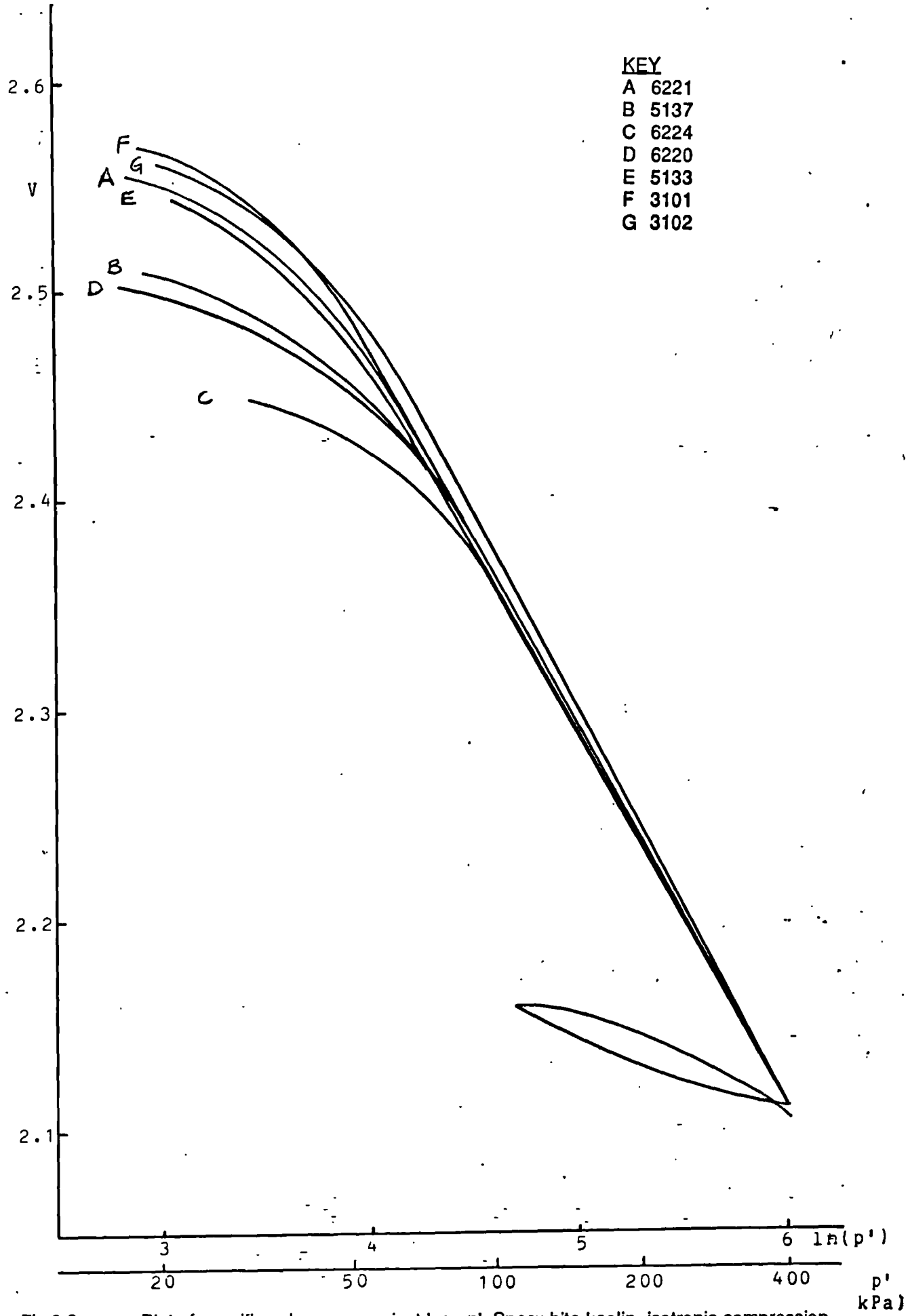

Fig 8.2 Plot of specific volume, v, against log $_e$p'. Speswhite kaolin, isotropic compression and swelling.

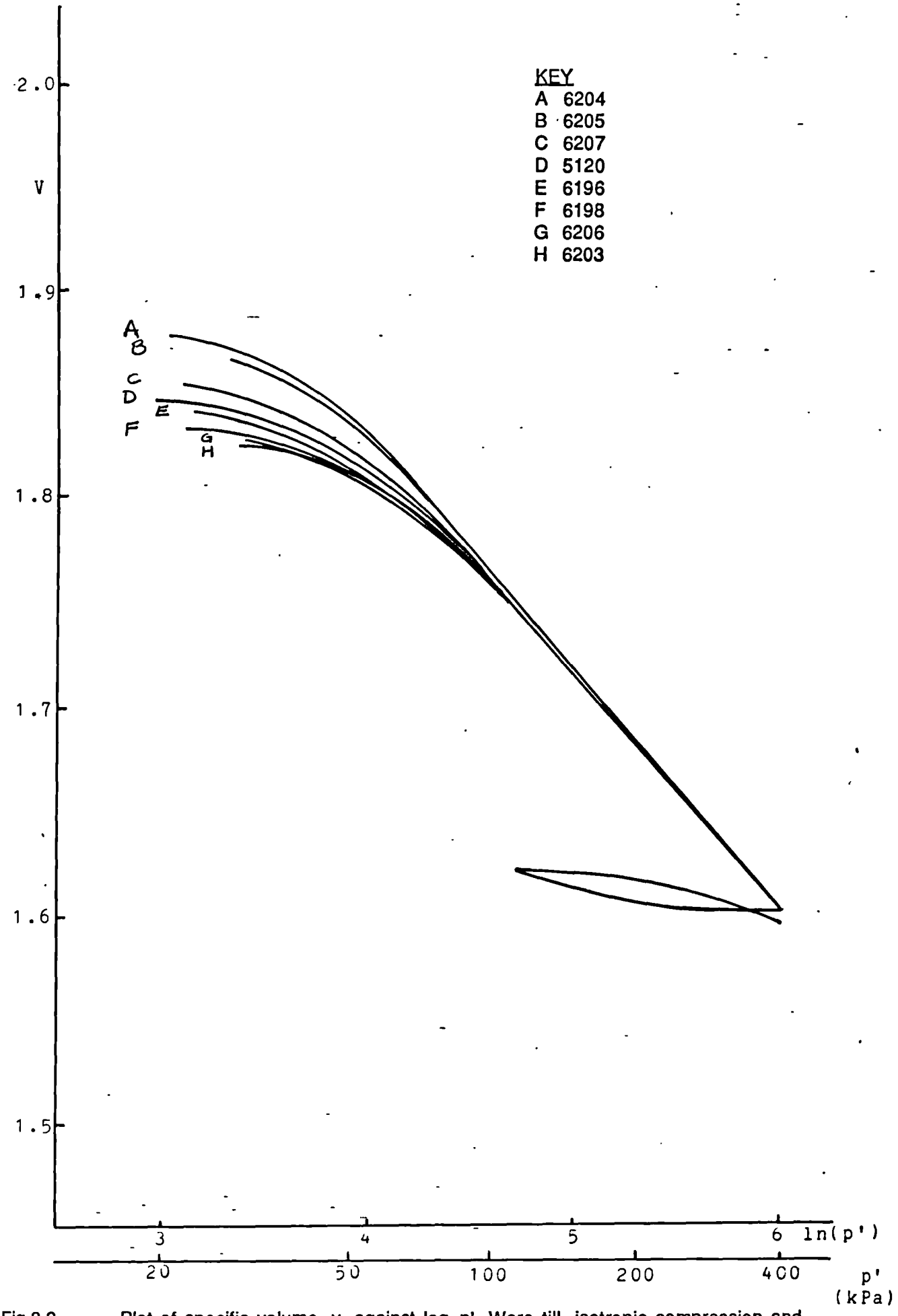

Fig 8.3 Plot of specific volume, v, against $\log_e p'$. Ware till, isotropic compression and swelling.

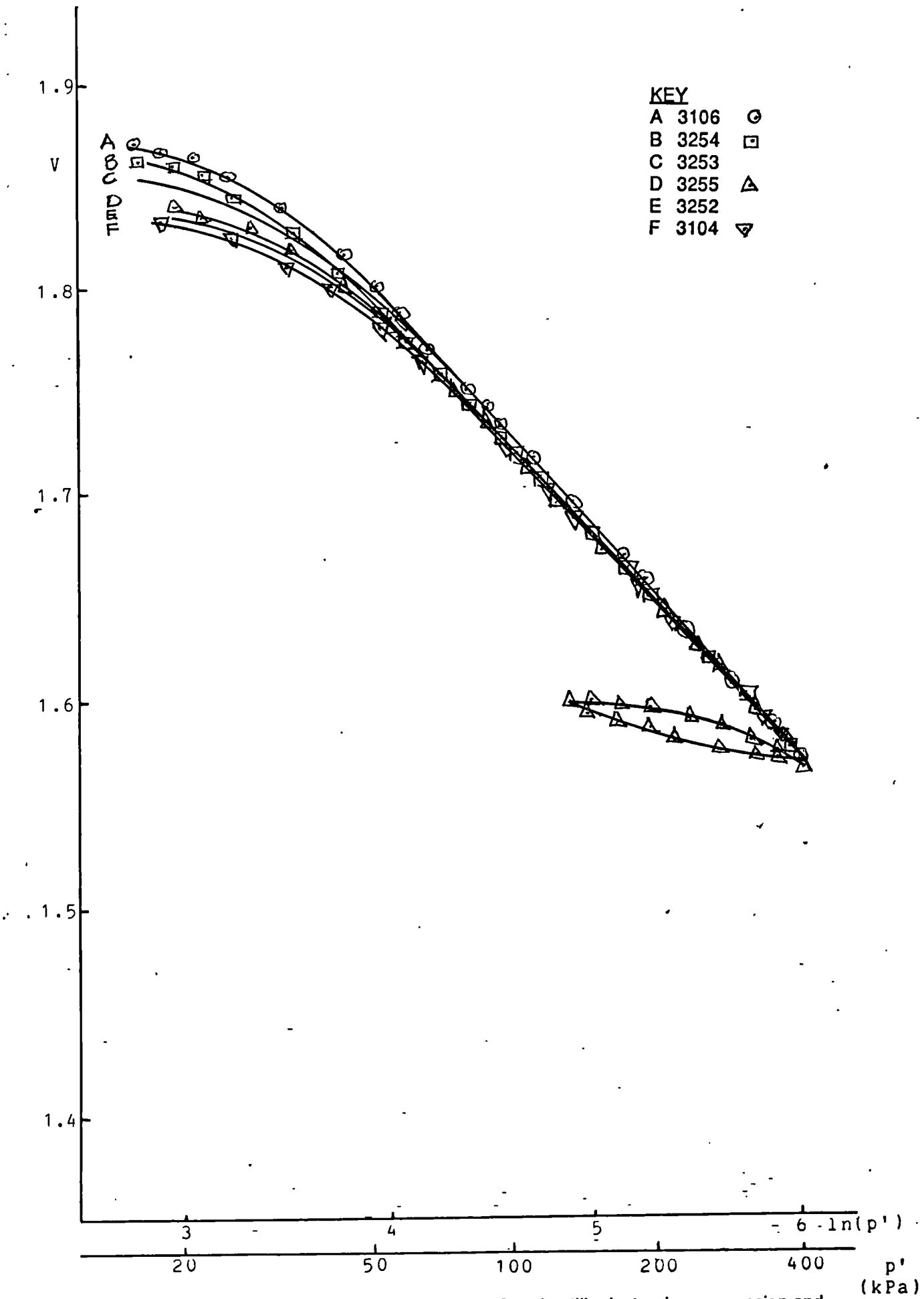

Fig 8.4 Plot of specific volume, v, against $\log_e$ p'. Cowden till , isotropic compression and swelling.

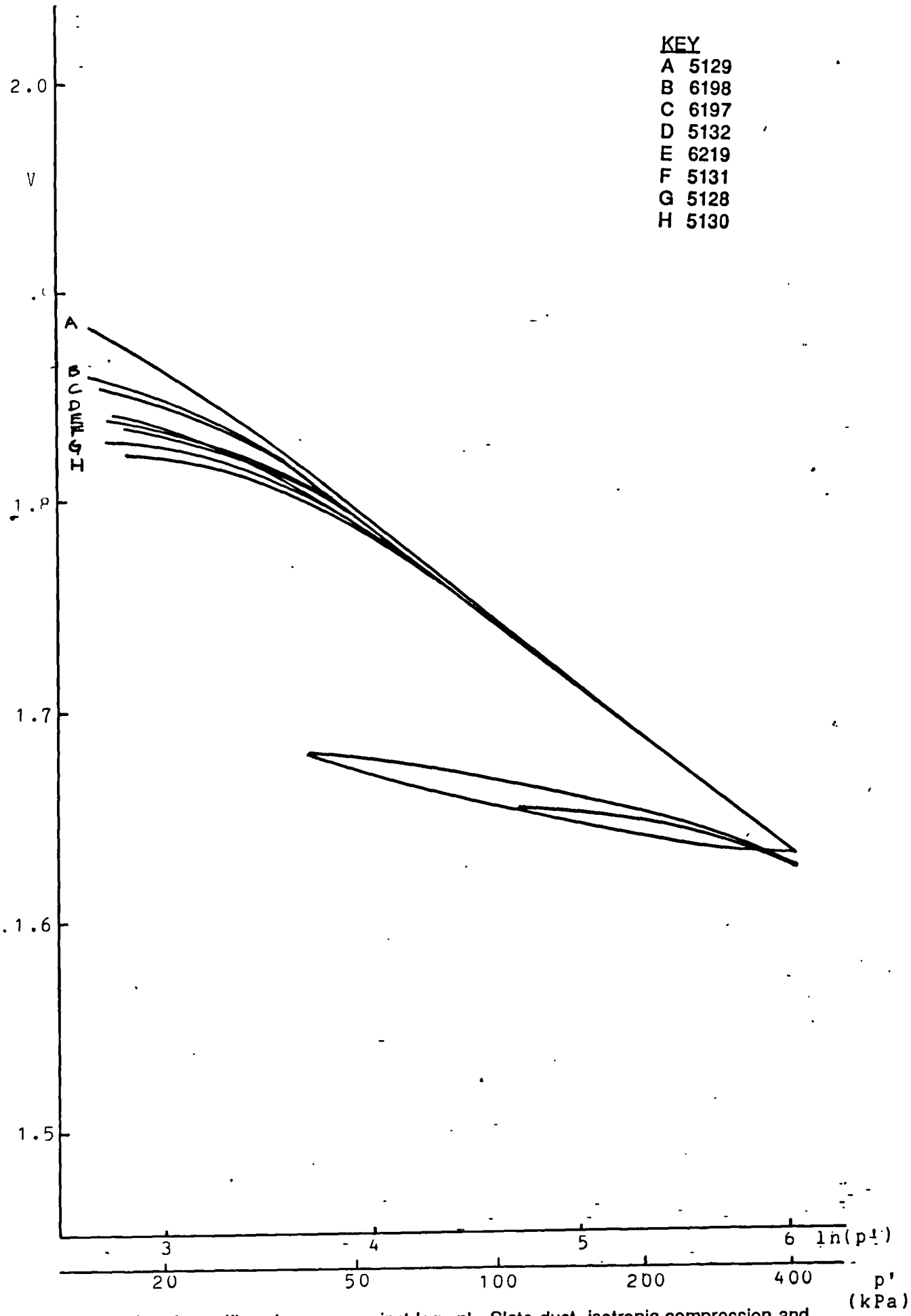

Fig 8.5 Plot of specific volume, v, against $\log_e p'$. Slate dust, isotropic compression and swelling.

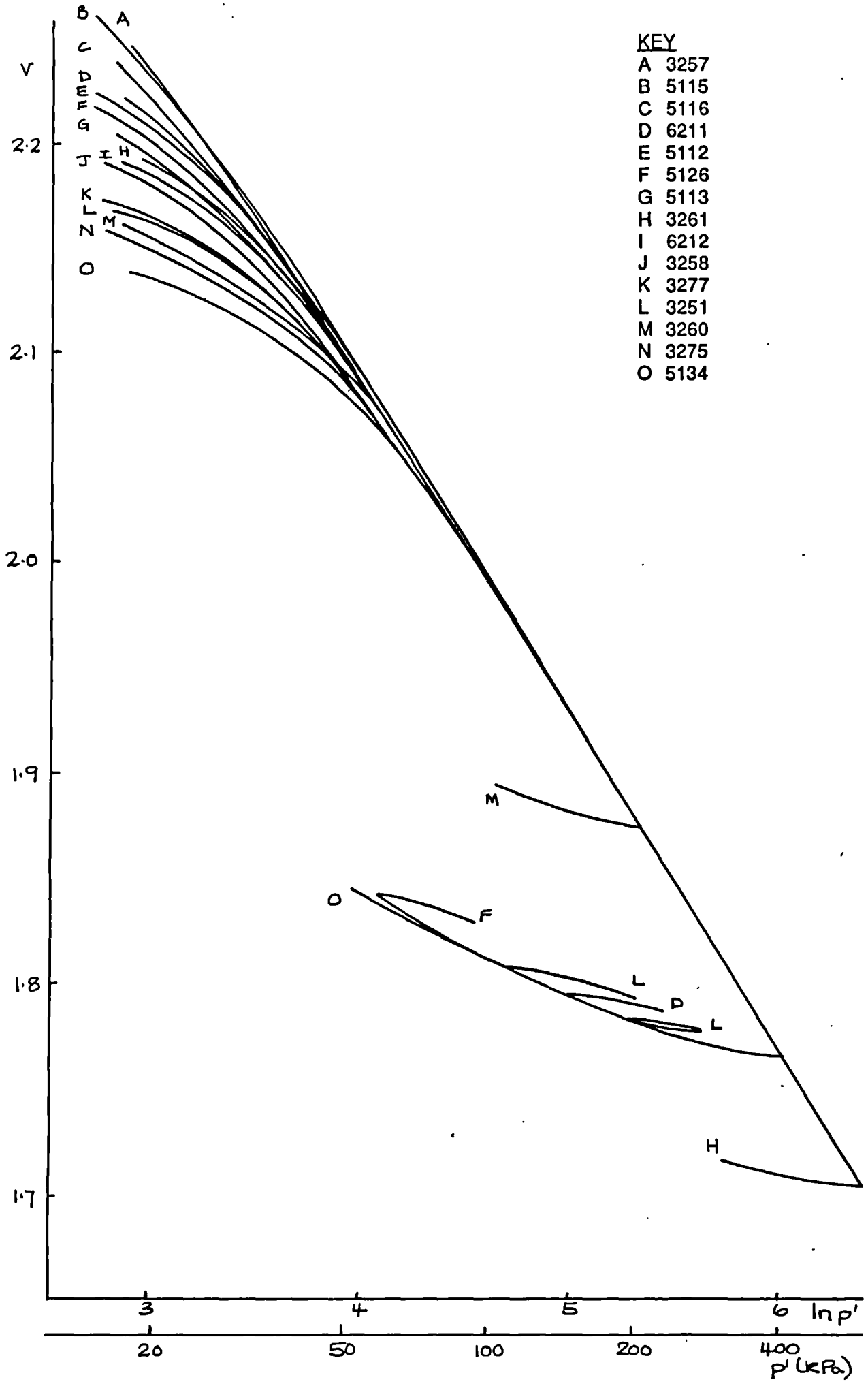

Fig 8.6a Plot of specific volume, v, against $\log_e$ p'. London Clay. Isotropic compression and swelling.

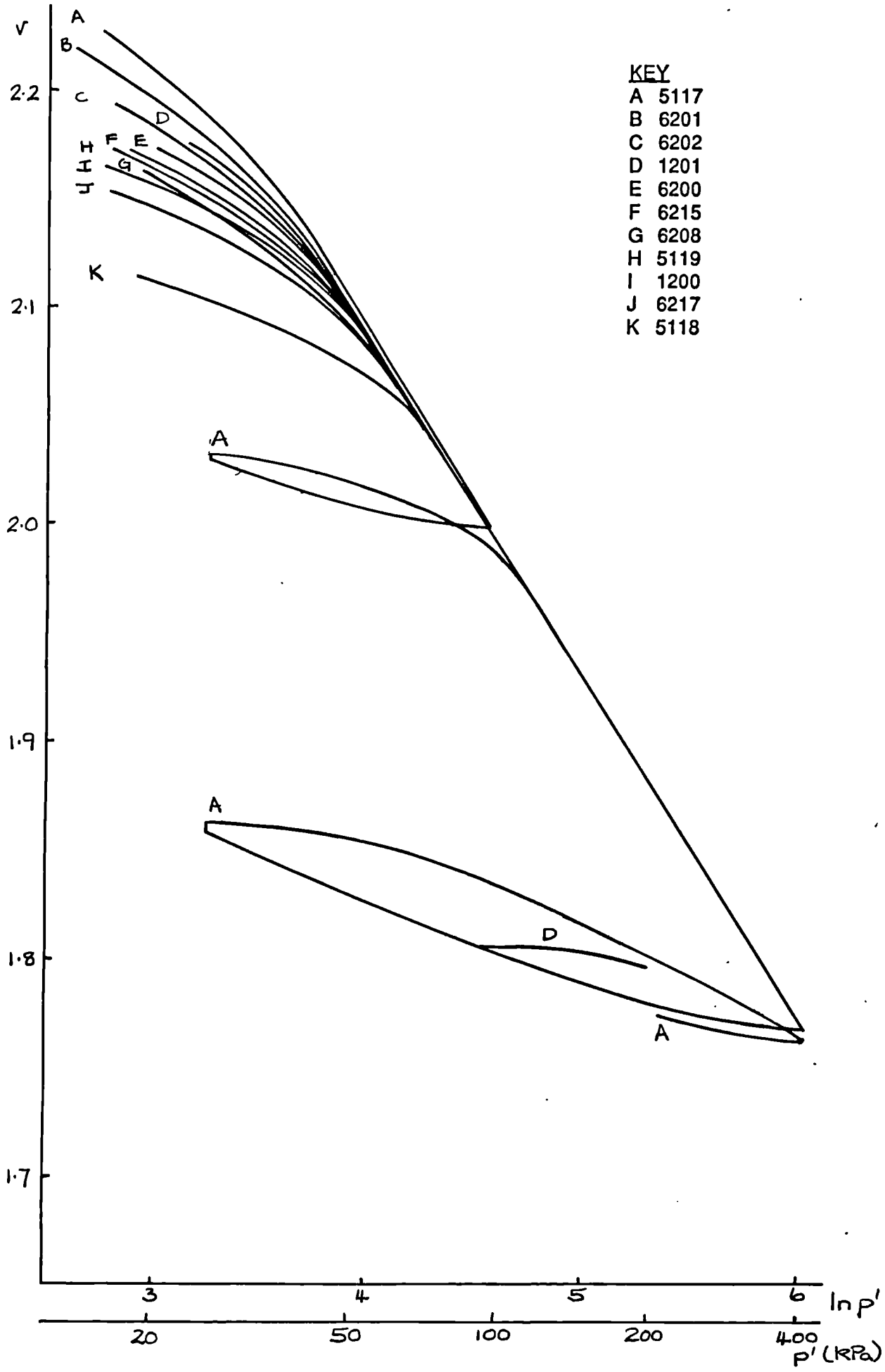

Fig 8.6b Plot of specific volume, v, against $\log_e$ p'. London Clay. Isotropic compression and swelling.

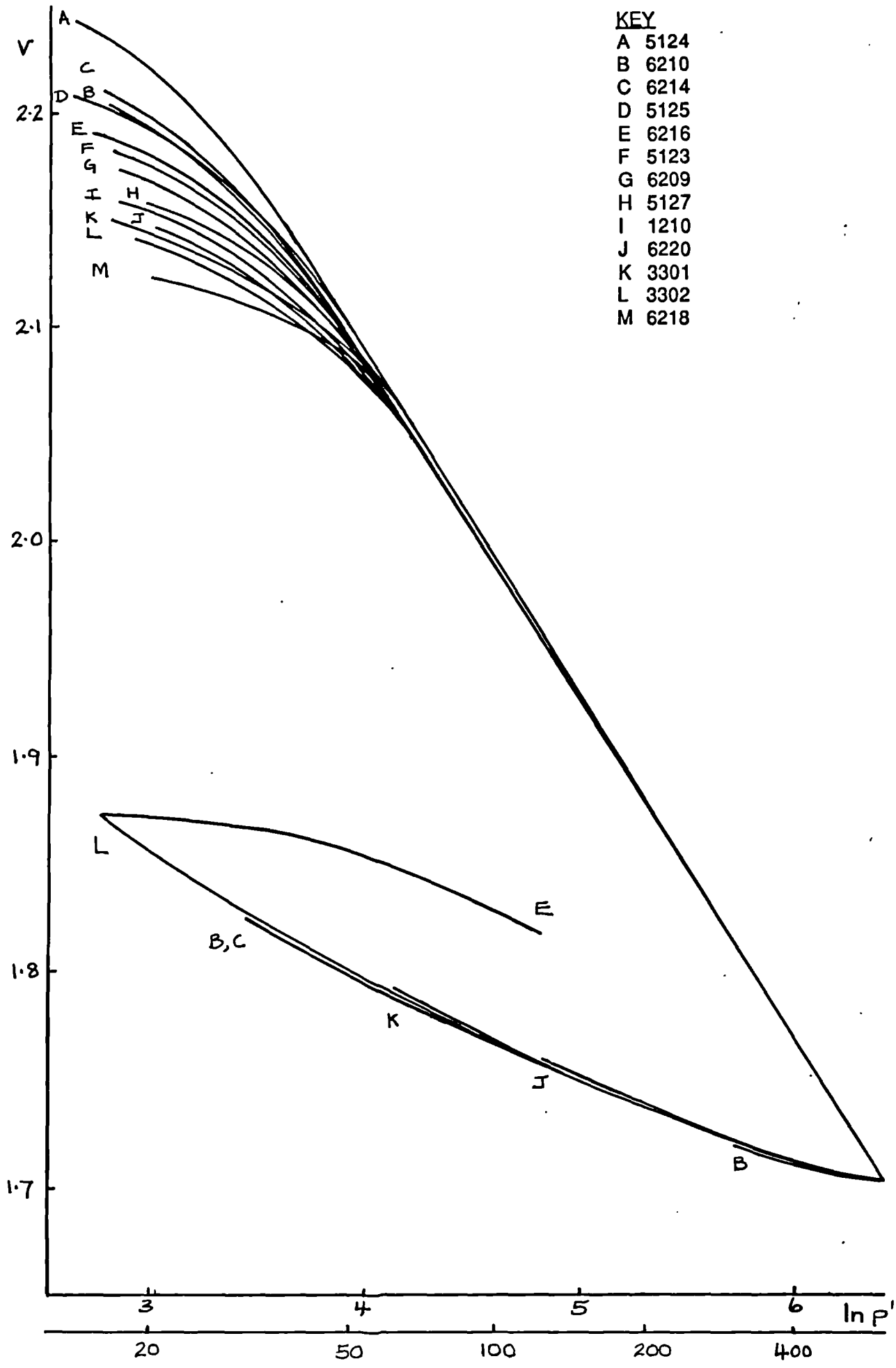

Fig 8.6c Plot of specific volume, v, against $\log_e$ p'. London Clay. Isotropic compression and swelling.

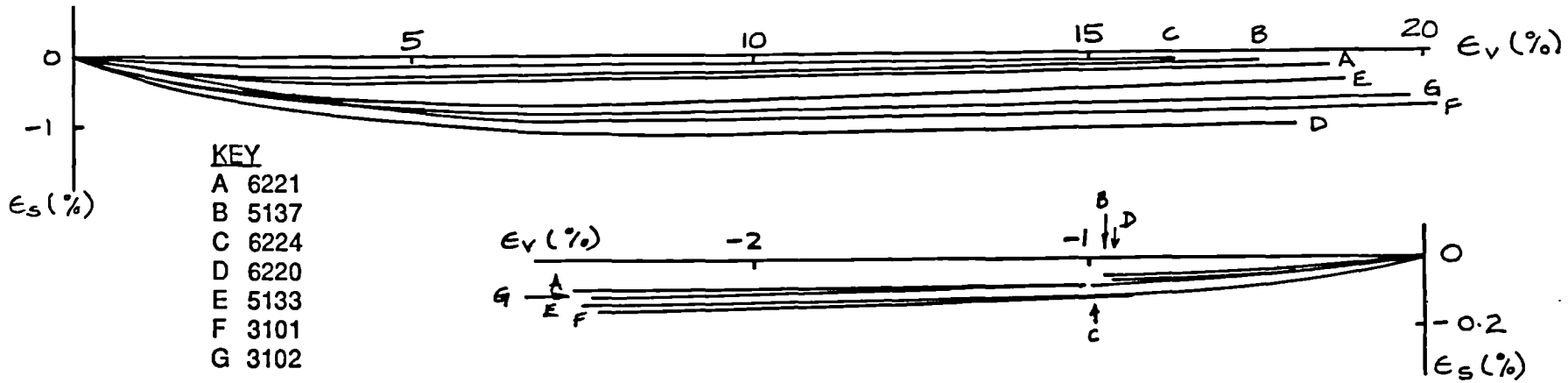

Fig 8.7 Plot of shear strain, ε_s , against volumetric strain, ε_v .Speswhite kaolin. Isotropic compression and swelling.

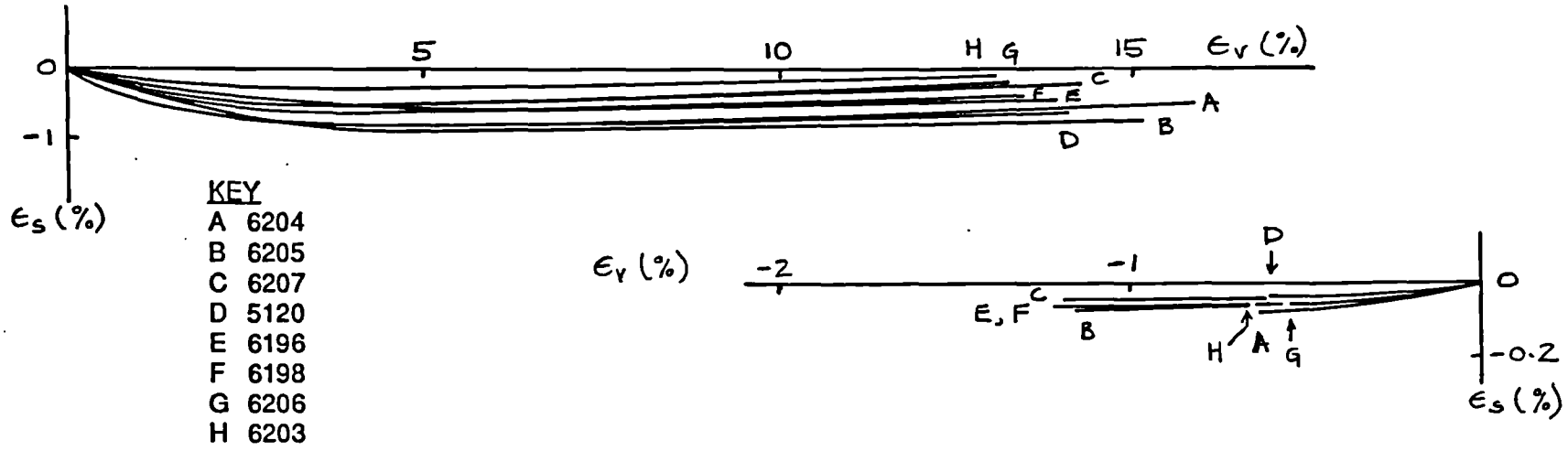

Fig 8.8 Plot of shear strain, ε_s , against volumetric strain, ε_v .Ware till. Isotropic compression and swelling.

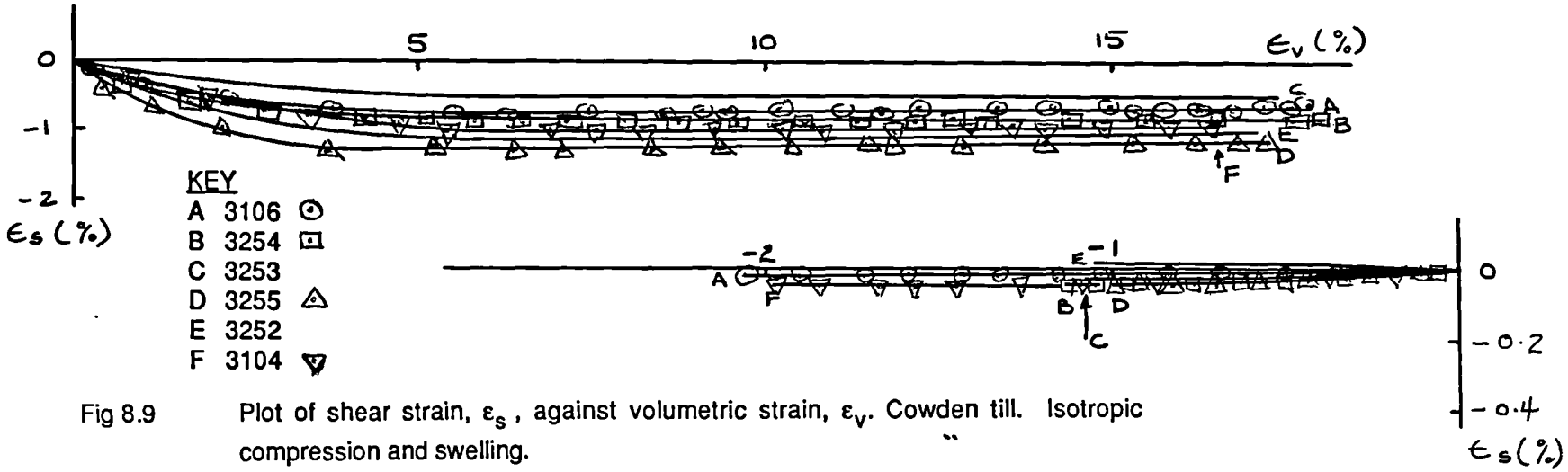

Fig 8.9 Plot of shear strain, ε_s, against volumetric strain, ε_v. Cowden till. Isotropic compression and swelling.

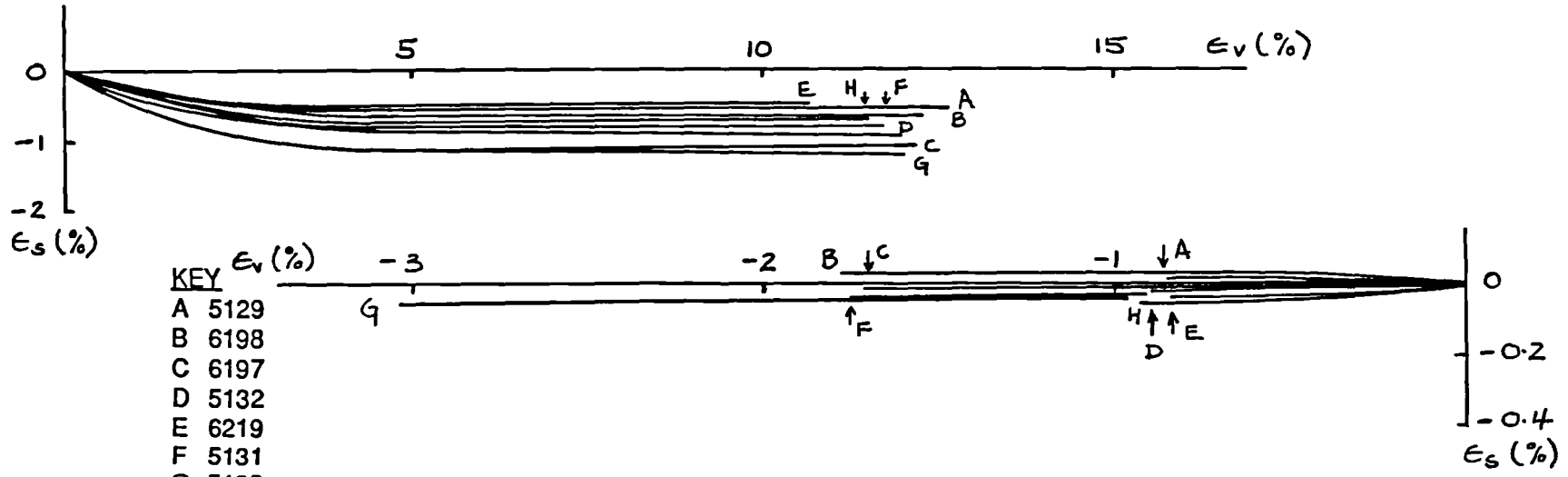

Fig 8.10 Plot of shear strain, ε_s, against volumetric strain, ε_v. Slate dust. Isotropic compression and swelling.

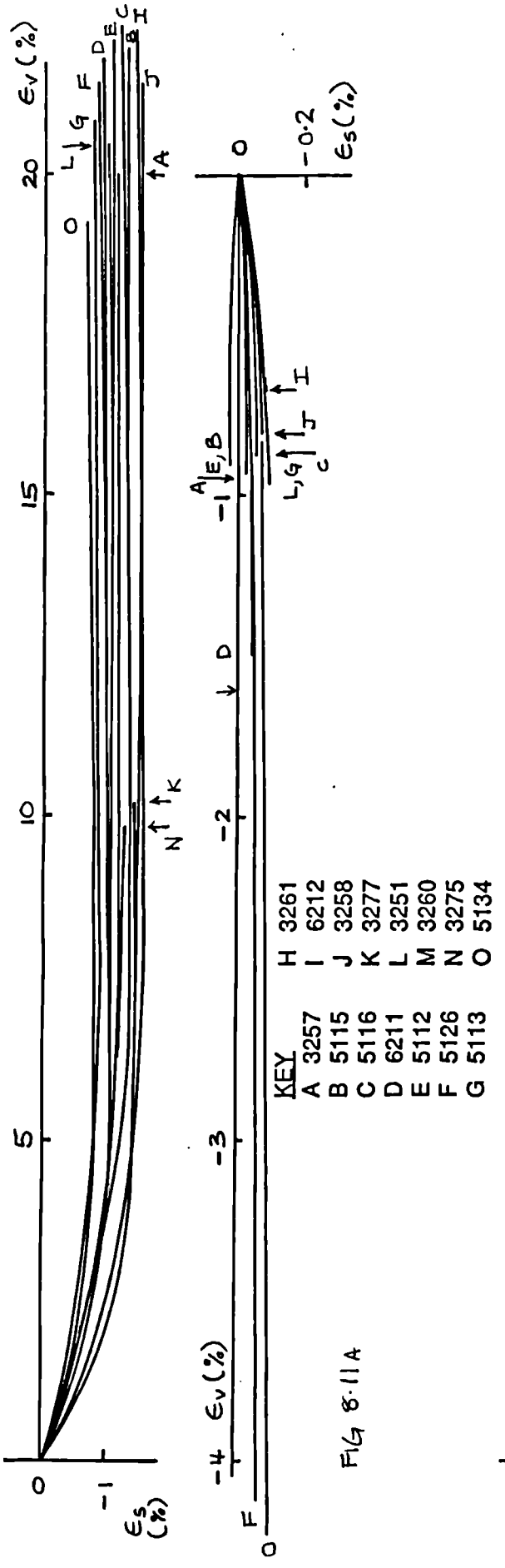

Fig 8.11a

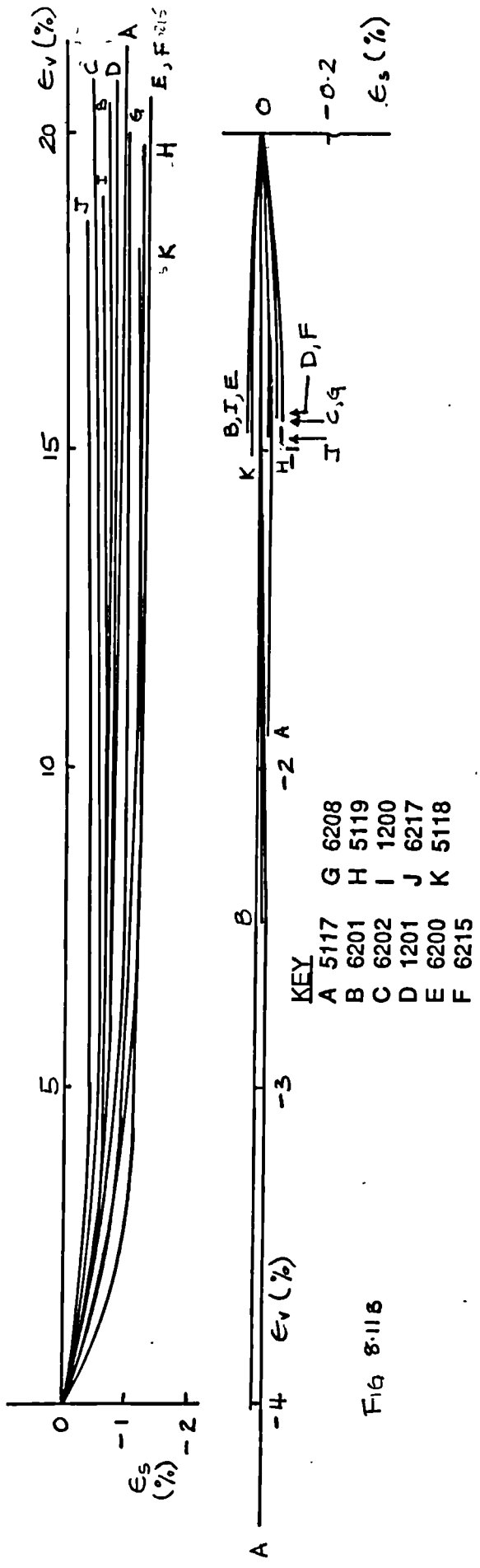

Fig 8.11b

Fig 8.11a Plot of shear strain, ε_s, against volumetric strain, ε_v. London Clay, Isotropic compression and swelling.

Fig 8.11b Plot of shear strain, ε_s, against volumetric strain, ε_v. London Clay. Isotropic compression and swelling.

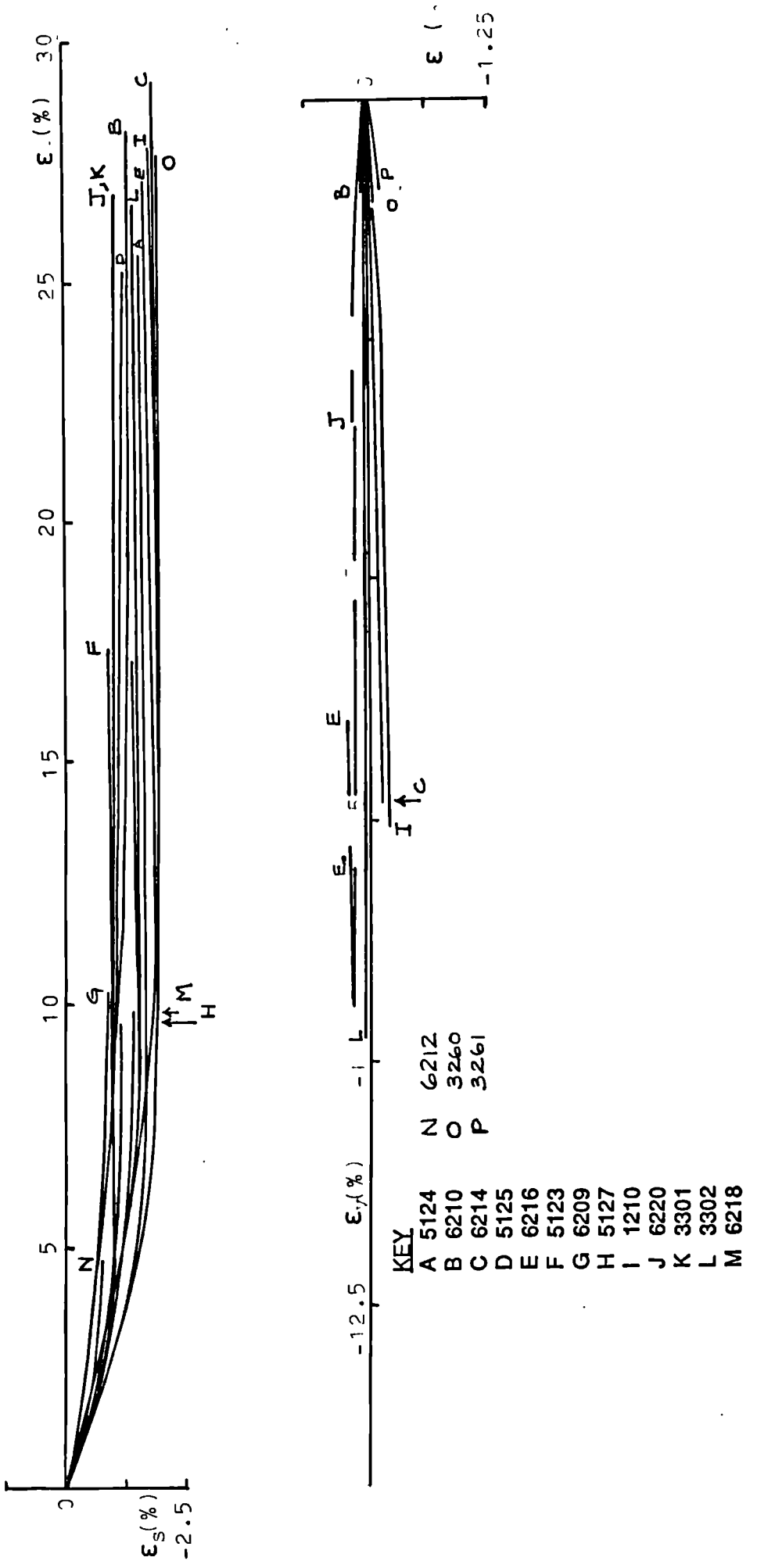

FIG 8·11c. Plot of shear strain, ϵ_s, against volumetric strain, ϵ_v, London Clay. Isotropic compression and swelling.

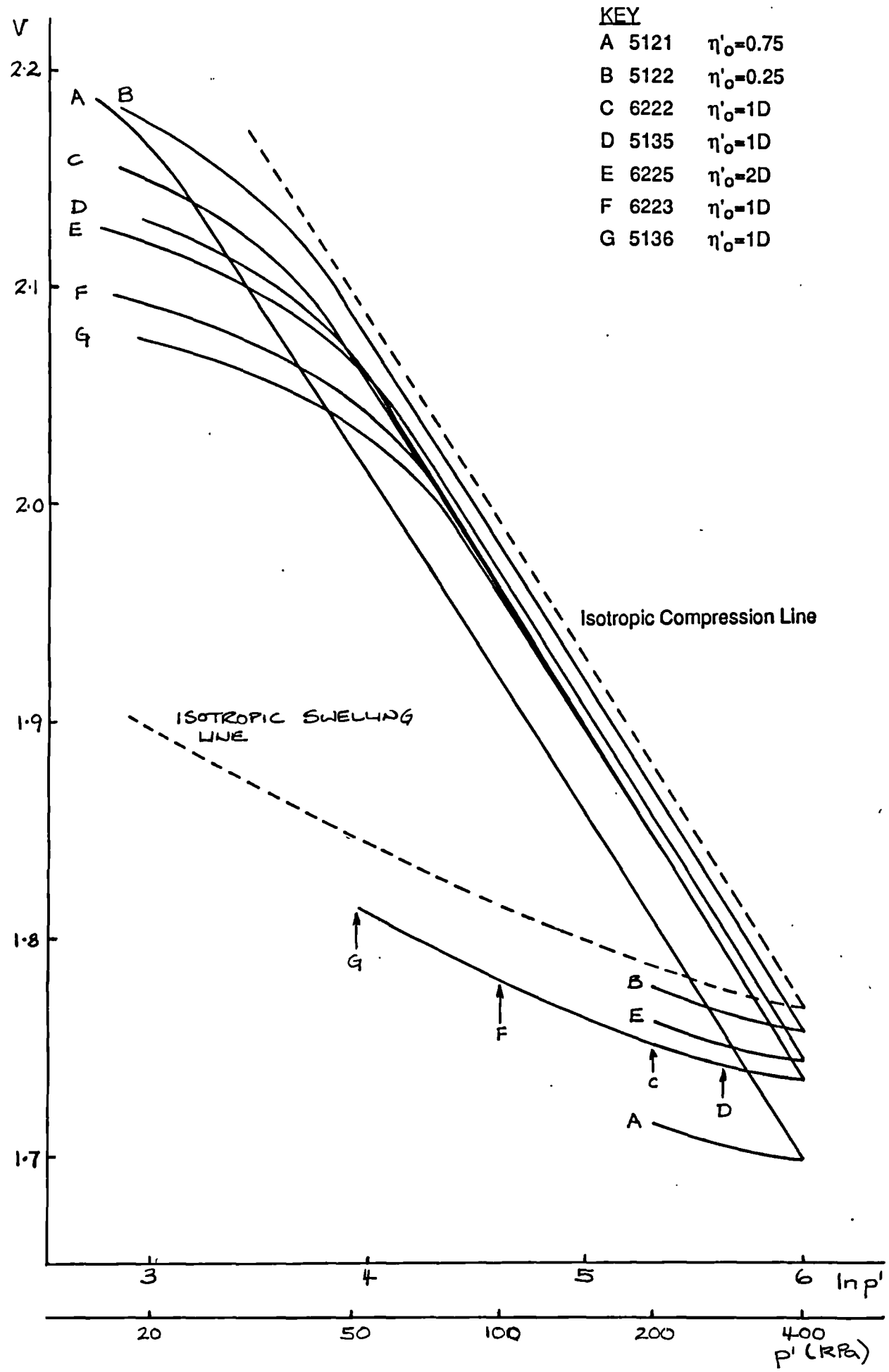

Fig 8.12 Plot of specific volume, v , against $\log_e$ p'. All stress histories (excluding isotropic) London Clay.

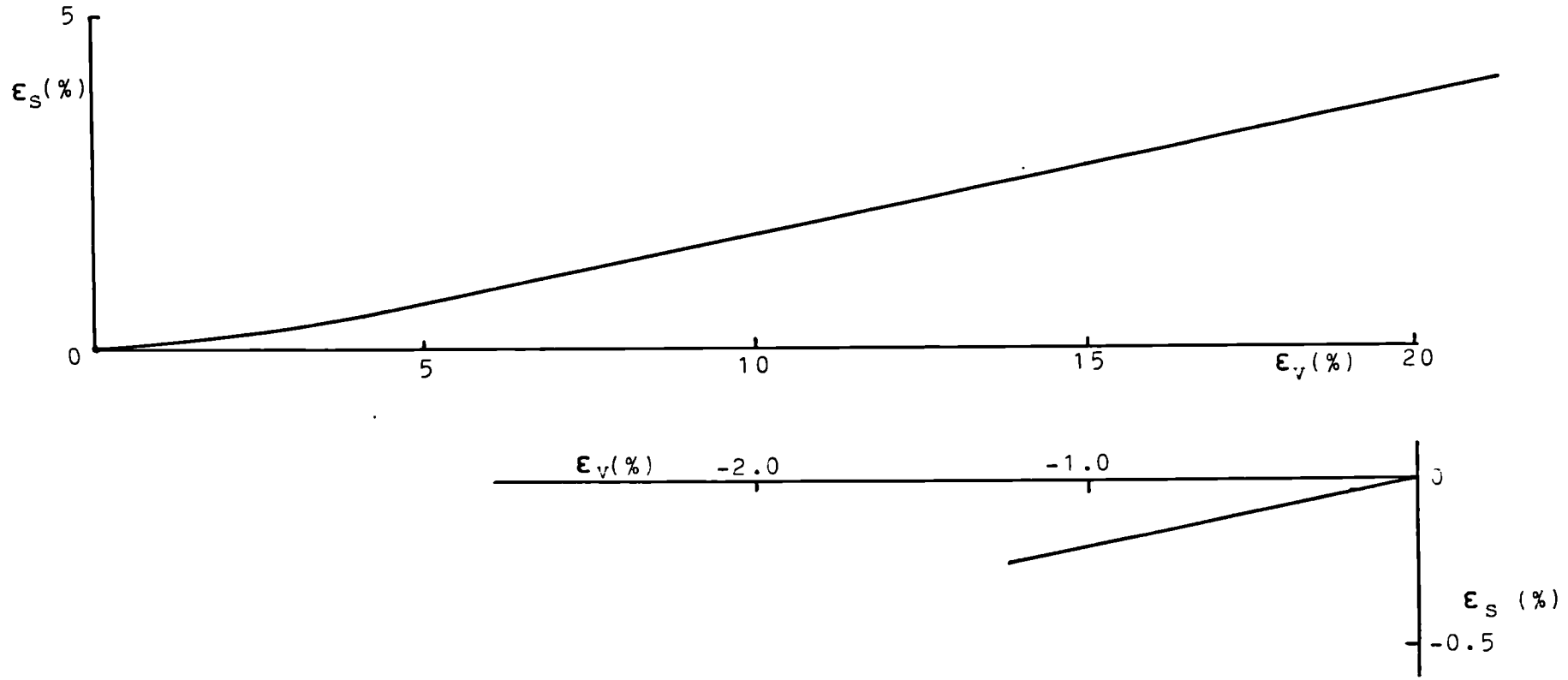

Fig 8.13 Plot of shear strain, ε_s, against volumetric strain, ε_v. London Clay compression and swelling, $\eta'_o = 0.25$.

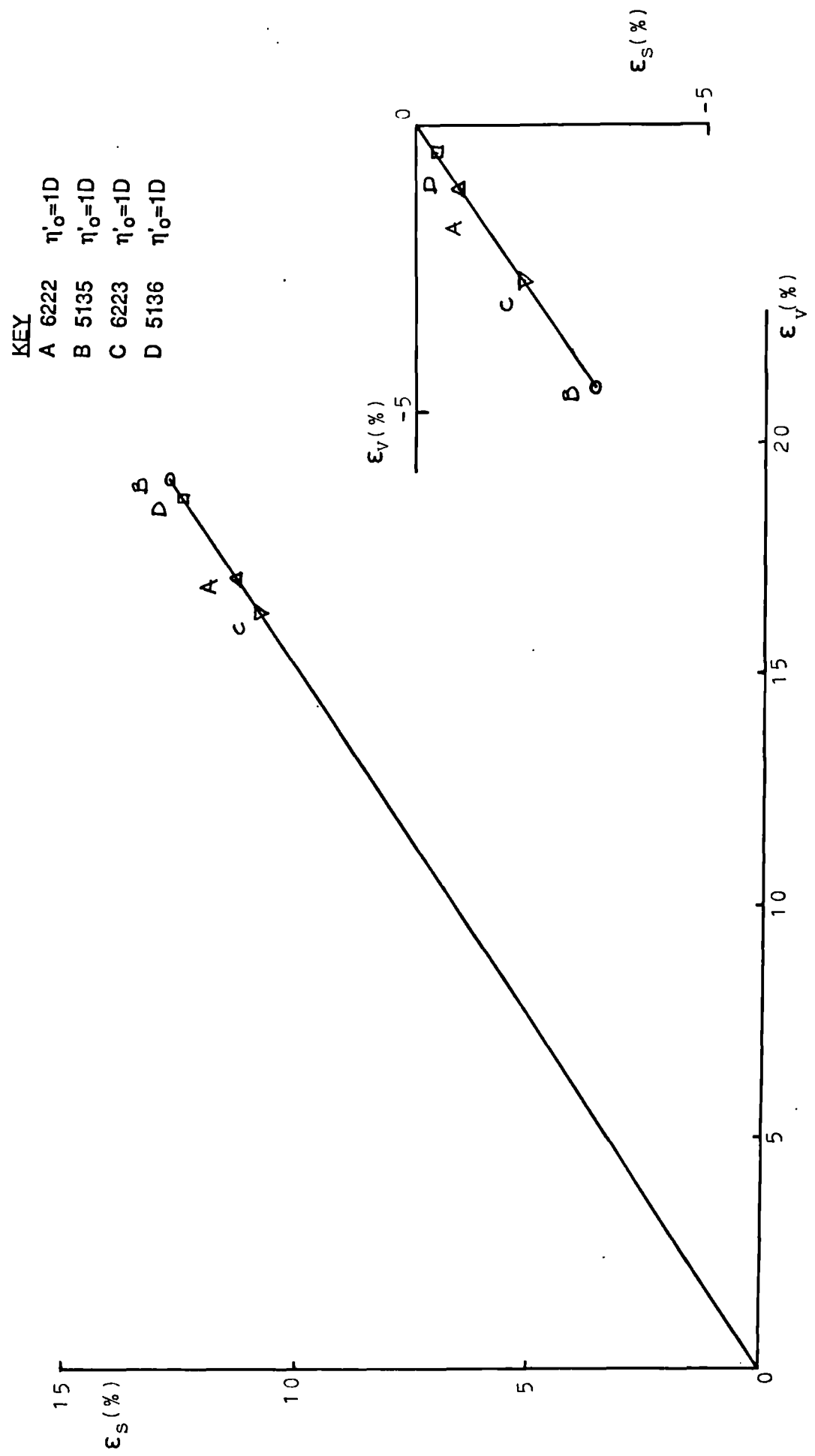

Fig 8.14 Plot of shear strain, ε_s, against volumetric strain, ε_v. London Clay one-dimensional compression and swelling.

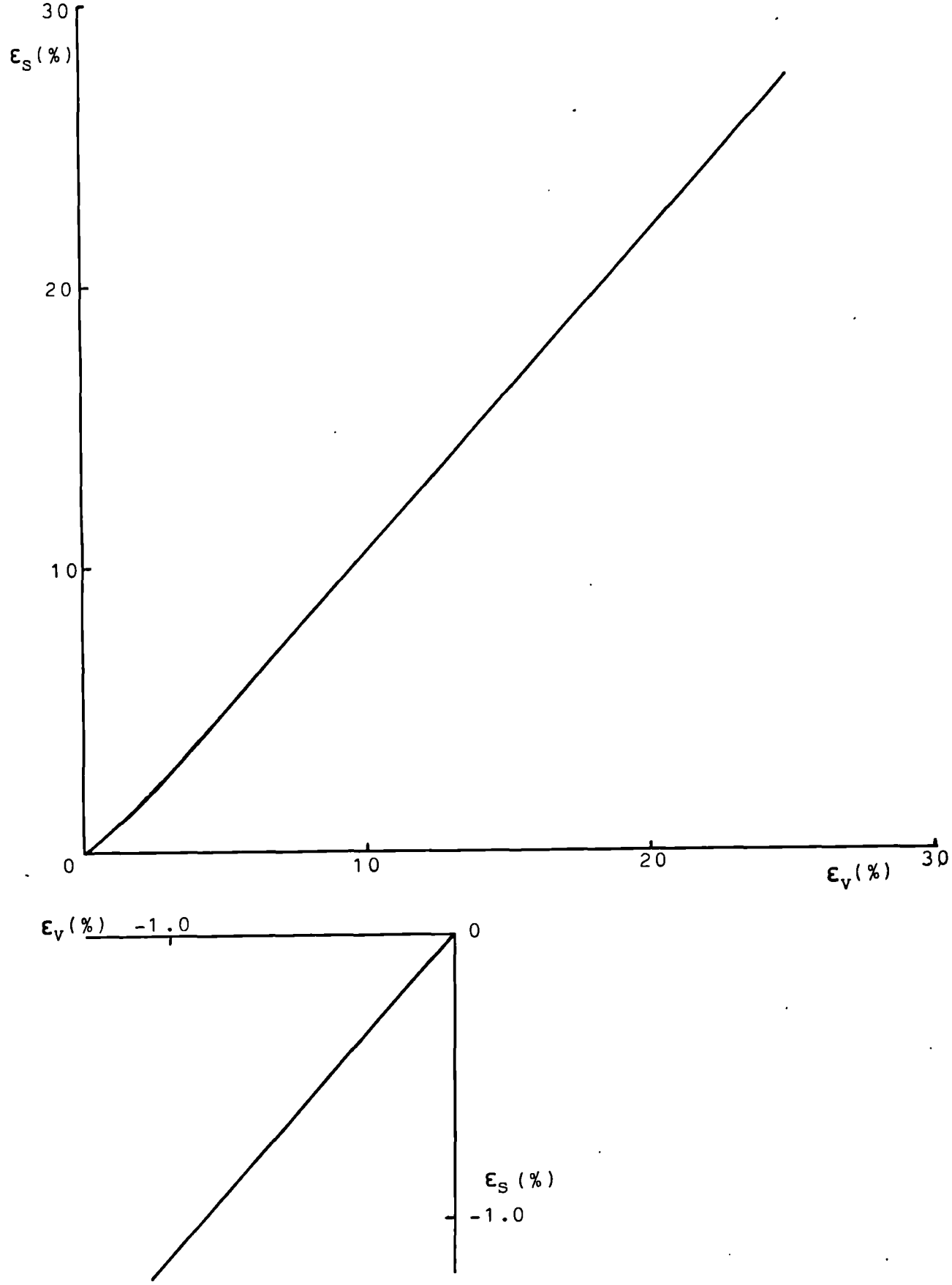

Fig 8.15 Plot of shear strain, ε_s, against volumetric strain, ε_v. London Clay. Compression and swelling, $\eta'_o = 0.75$.

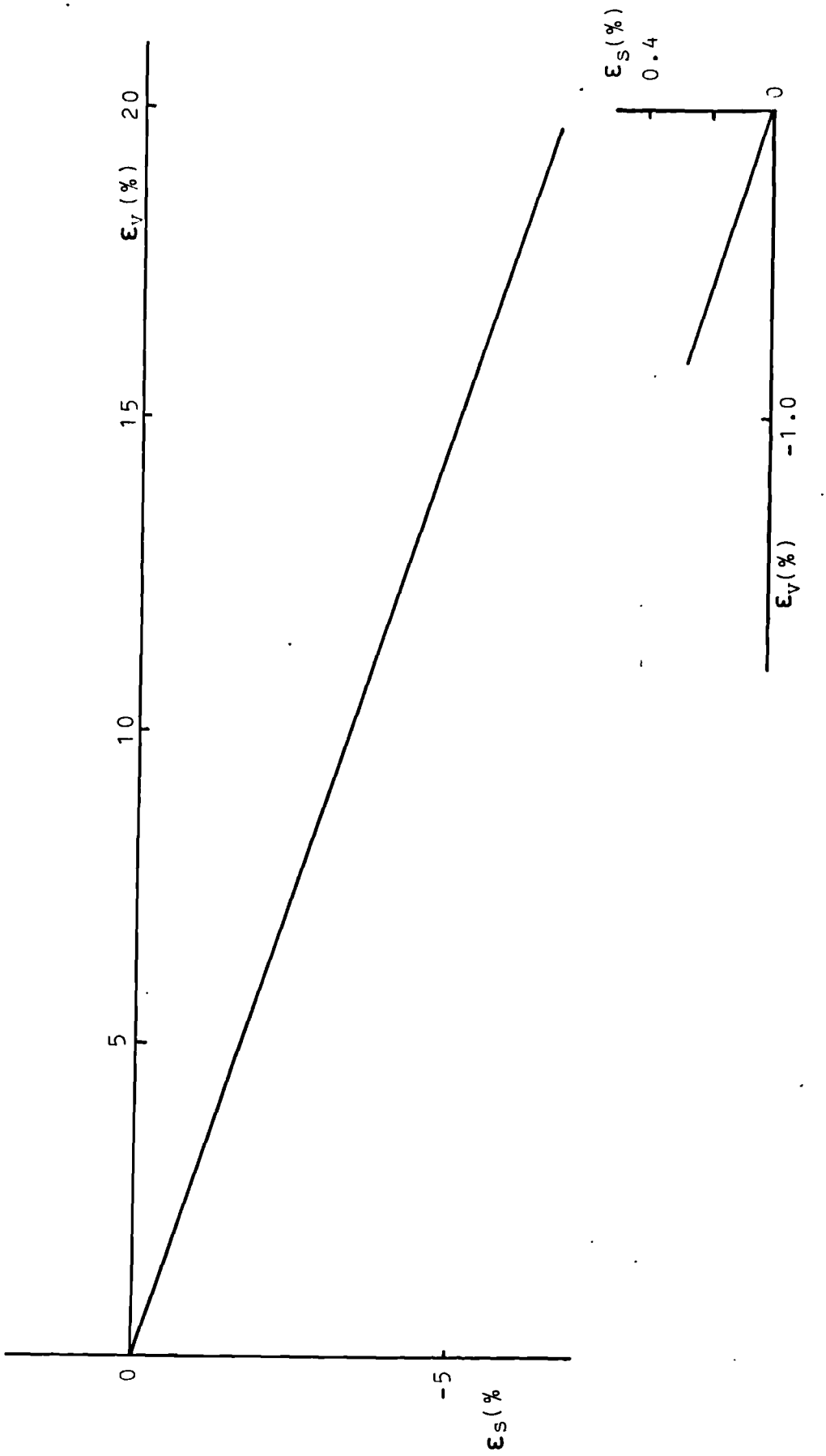

Fig 8.16 Plot of shear strain, ε_s, against volumetric strain, ε_v. London Clay. .Two-dimensional compression and swelling.

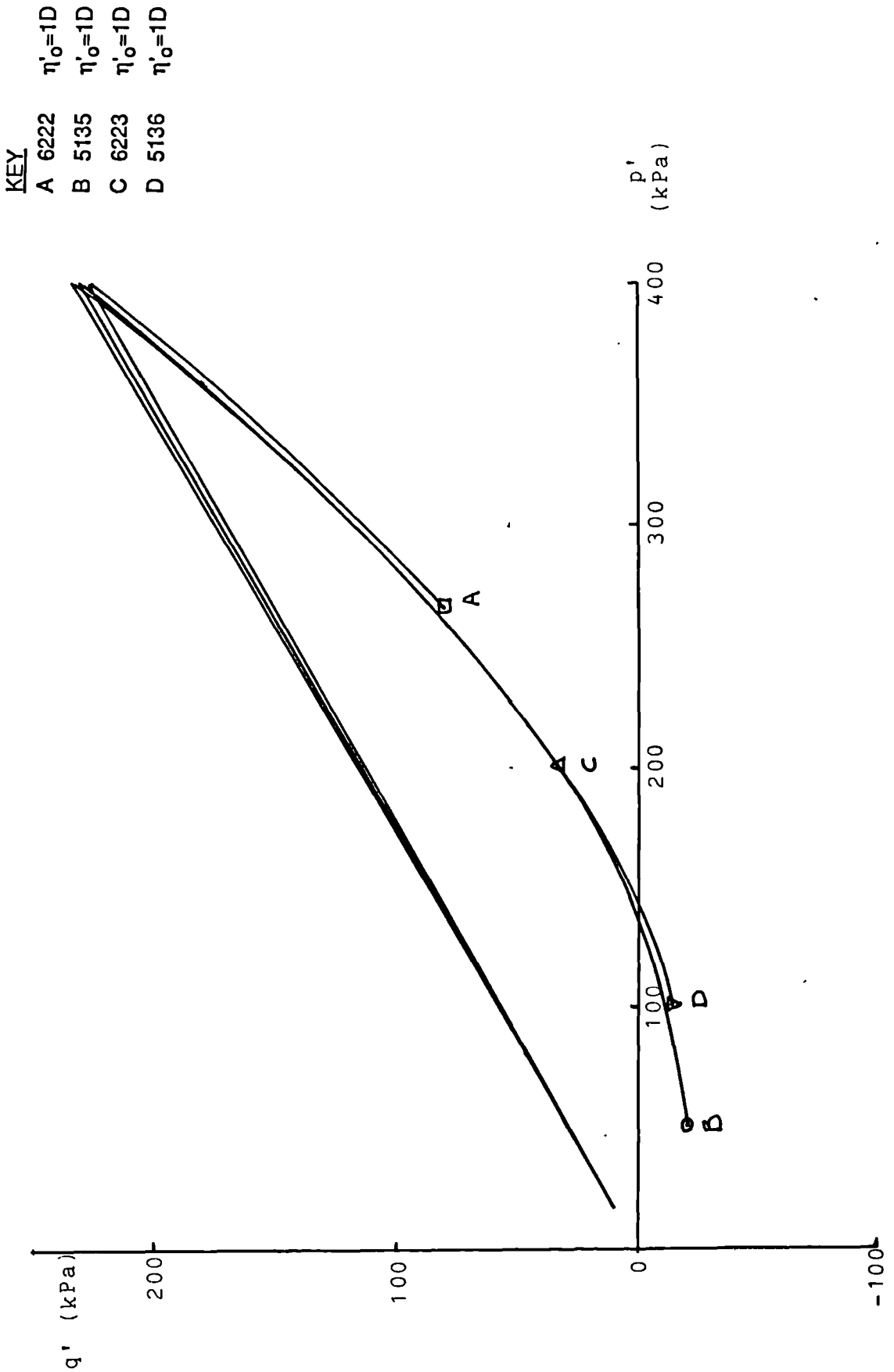

Fig 8.17 Stress paths,q' against p', for one-dimensionally compressed London Clay.

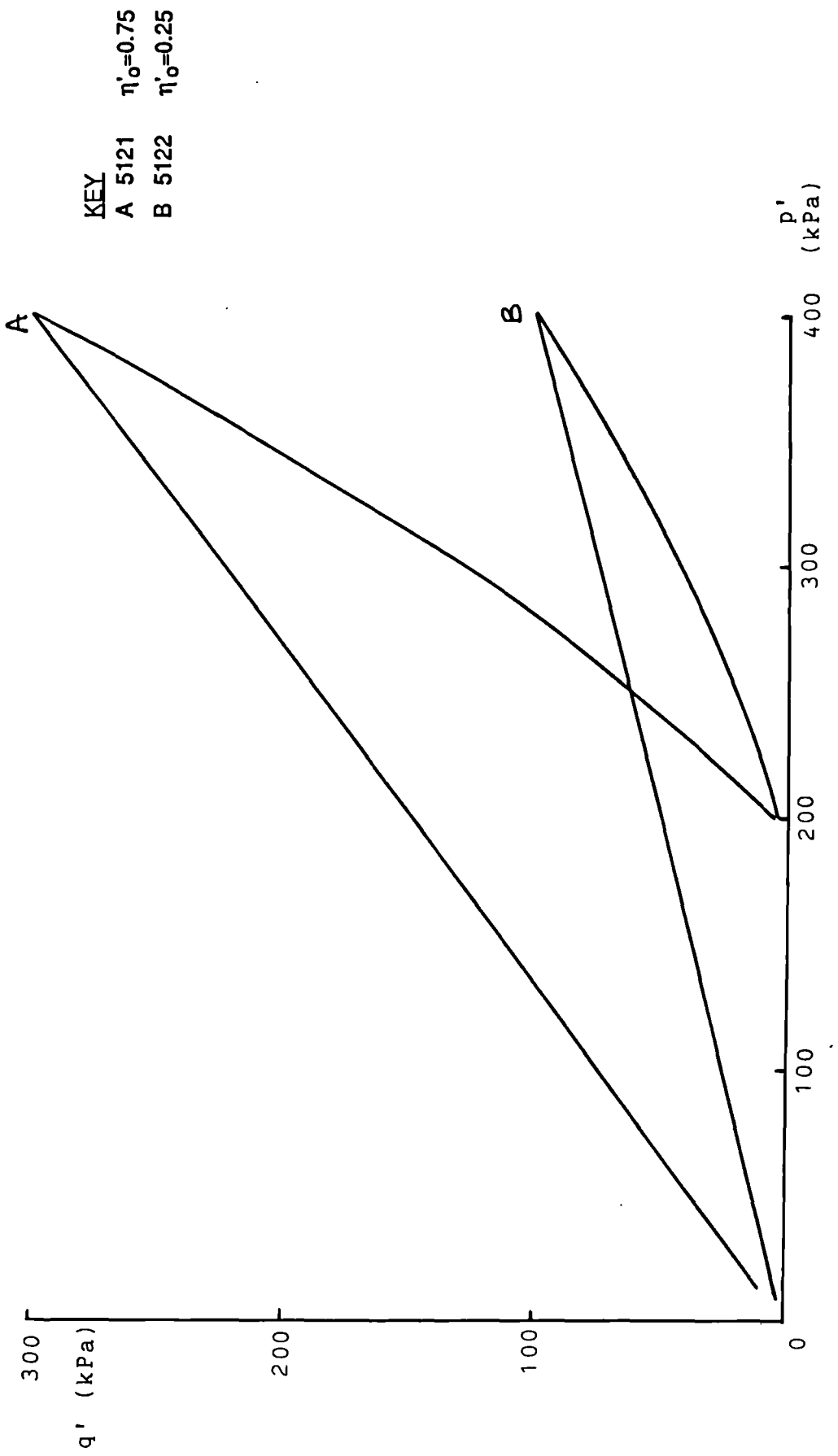

Fig 8.18 Stress paths, q' against p', for London clay. $\eta'_o = 0.75$ and $\eta'_o = 0.25$. Compression and swelling.

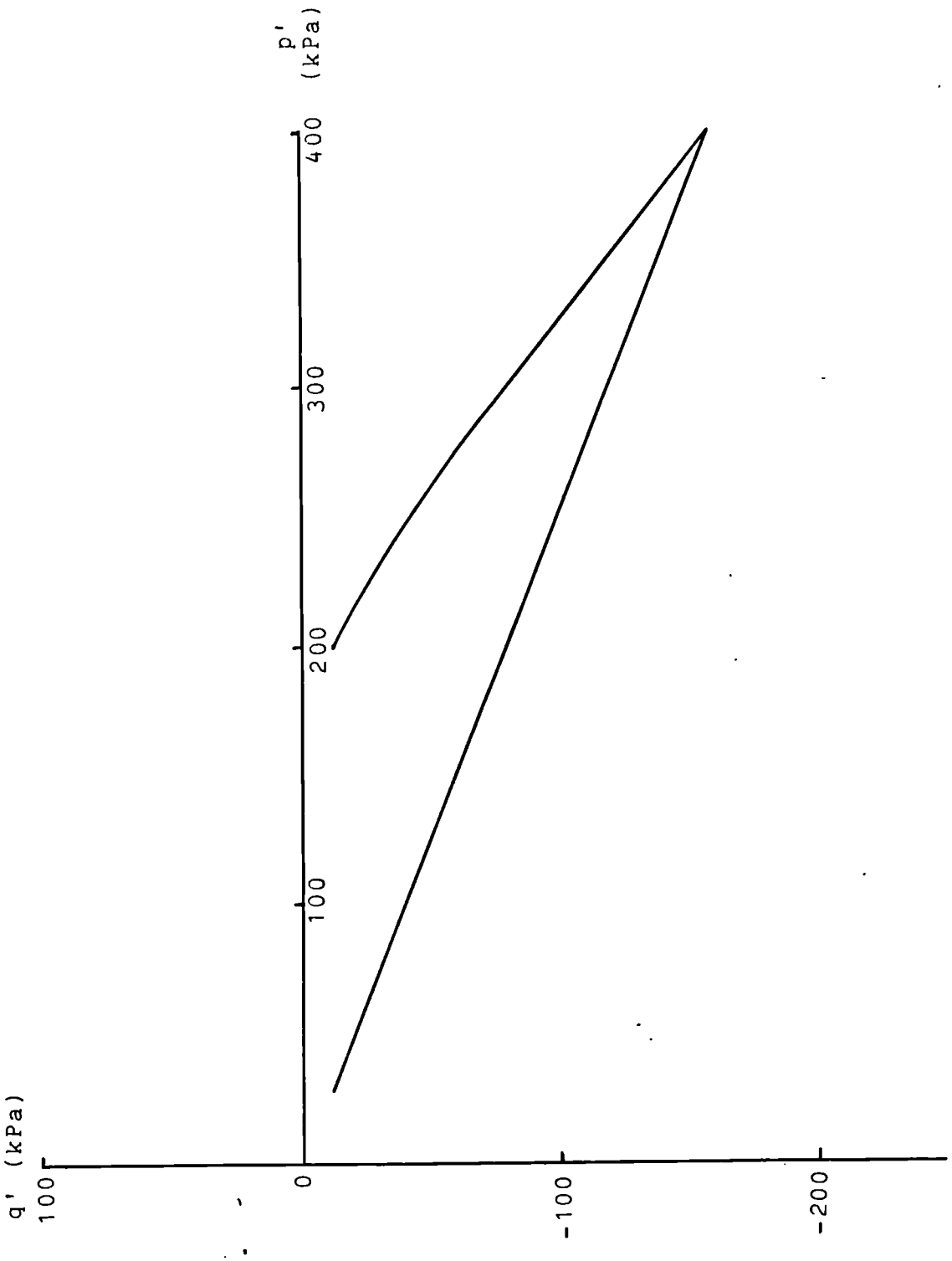

Fig 8.19 Stress paths , q' against p', for two dimensionally compressed London clay.

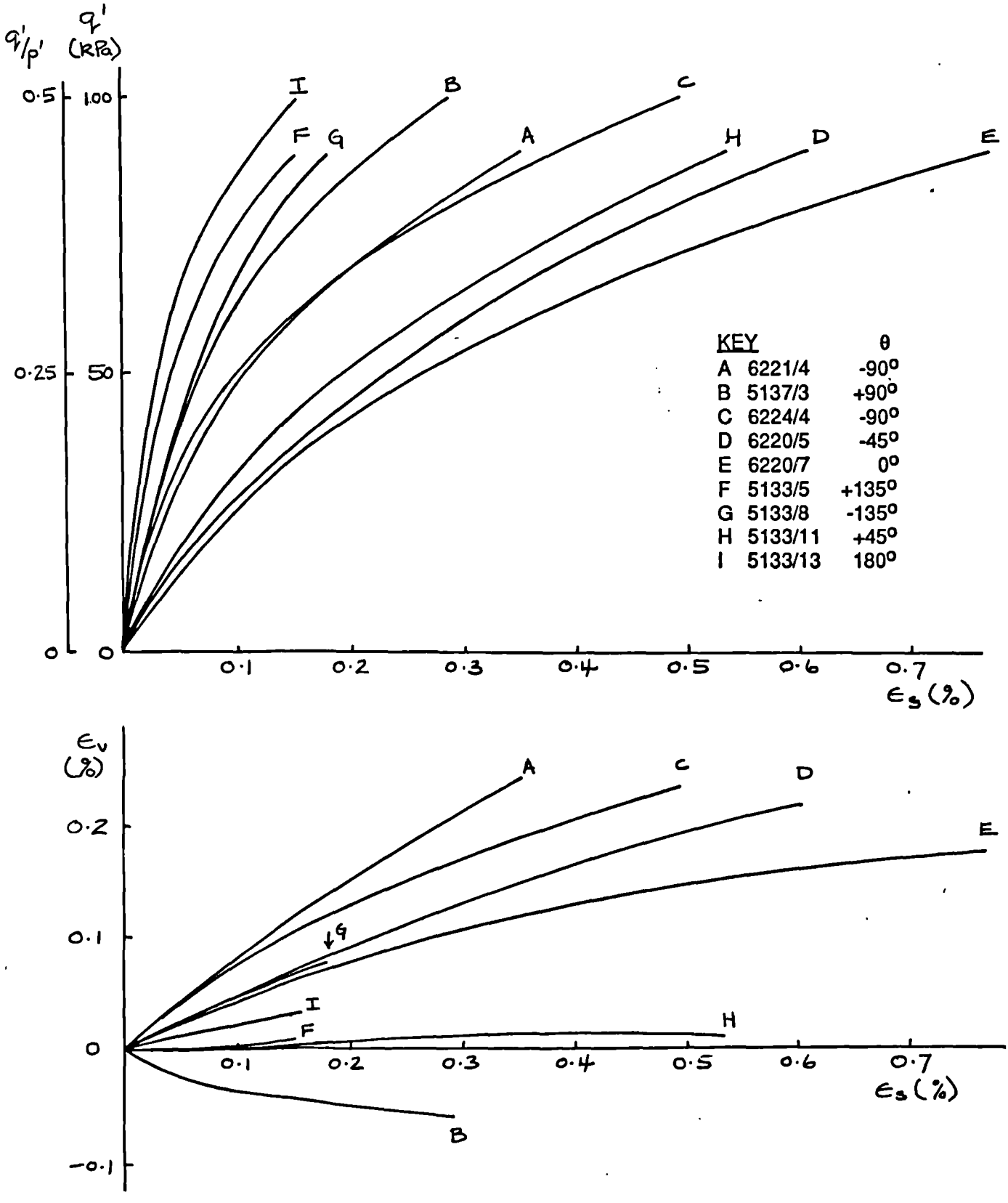

Fig 8.20 Plots of q' against ε_s and ε_v against ε_s .Speswhite kaolin, isotropically compressed, OCR = 2, p' = 200kPa, constant p' path.

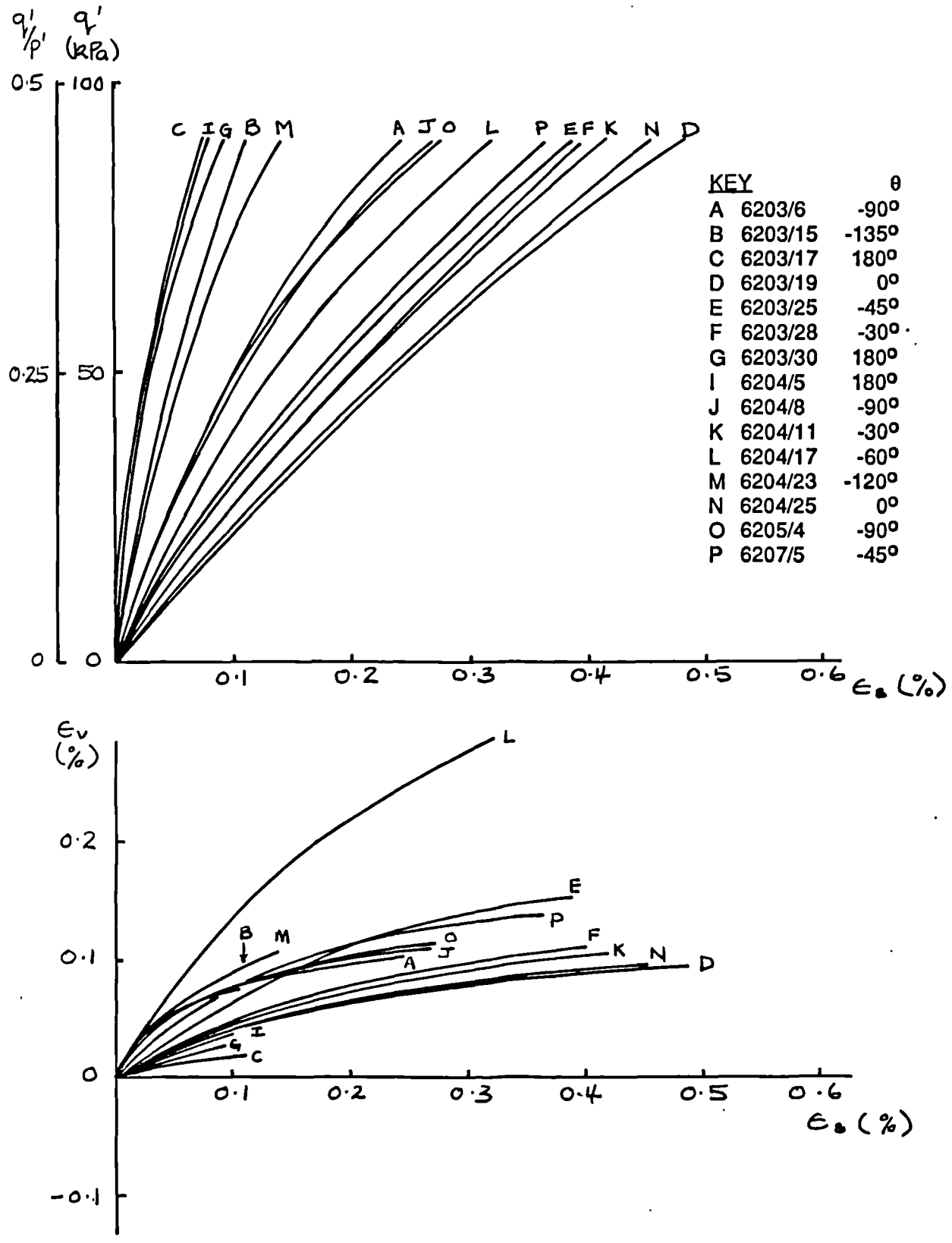

Fig 8.21a Plots of q' against ε_s and ε_v against ε_s . Positive deviations of stress path Ware till, isotropically compressed, OCR = 2, p' = 200kPa, constant p' path.

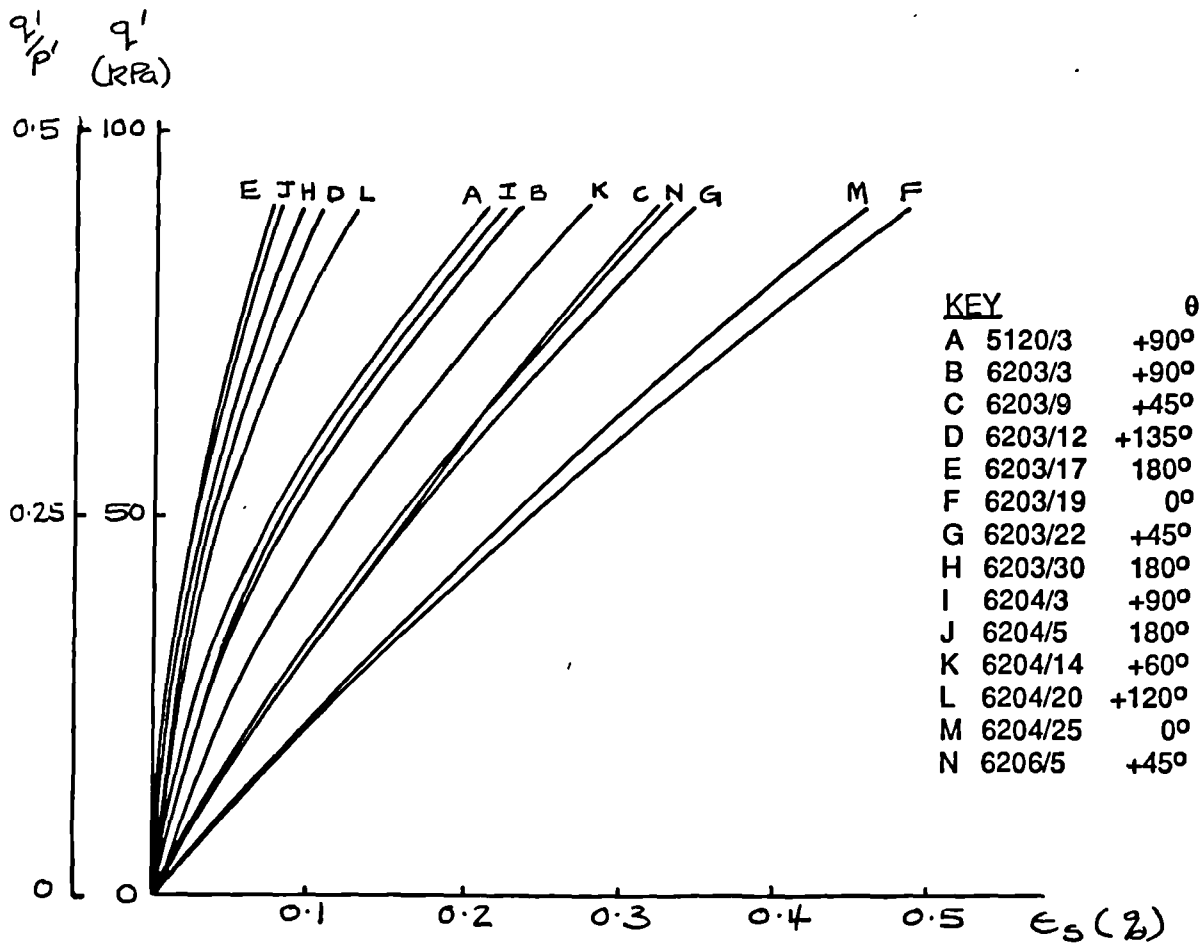

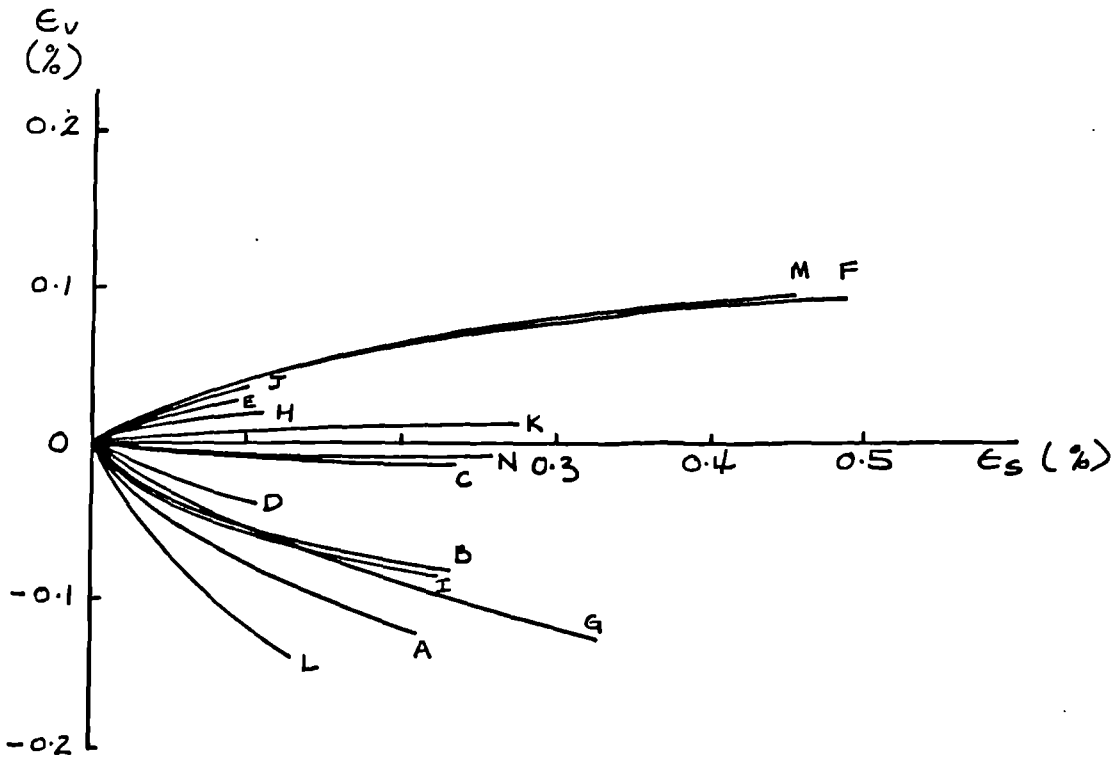

Fig 8.21b Plots of q' against ε_s and ε_v against ε_s . Negative deviations of stress path Ware till, isotropically compressed, OCR = 2, p' = 200kPa, constant p' path.

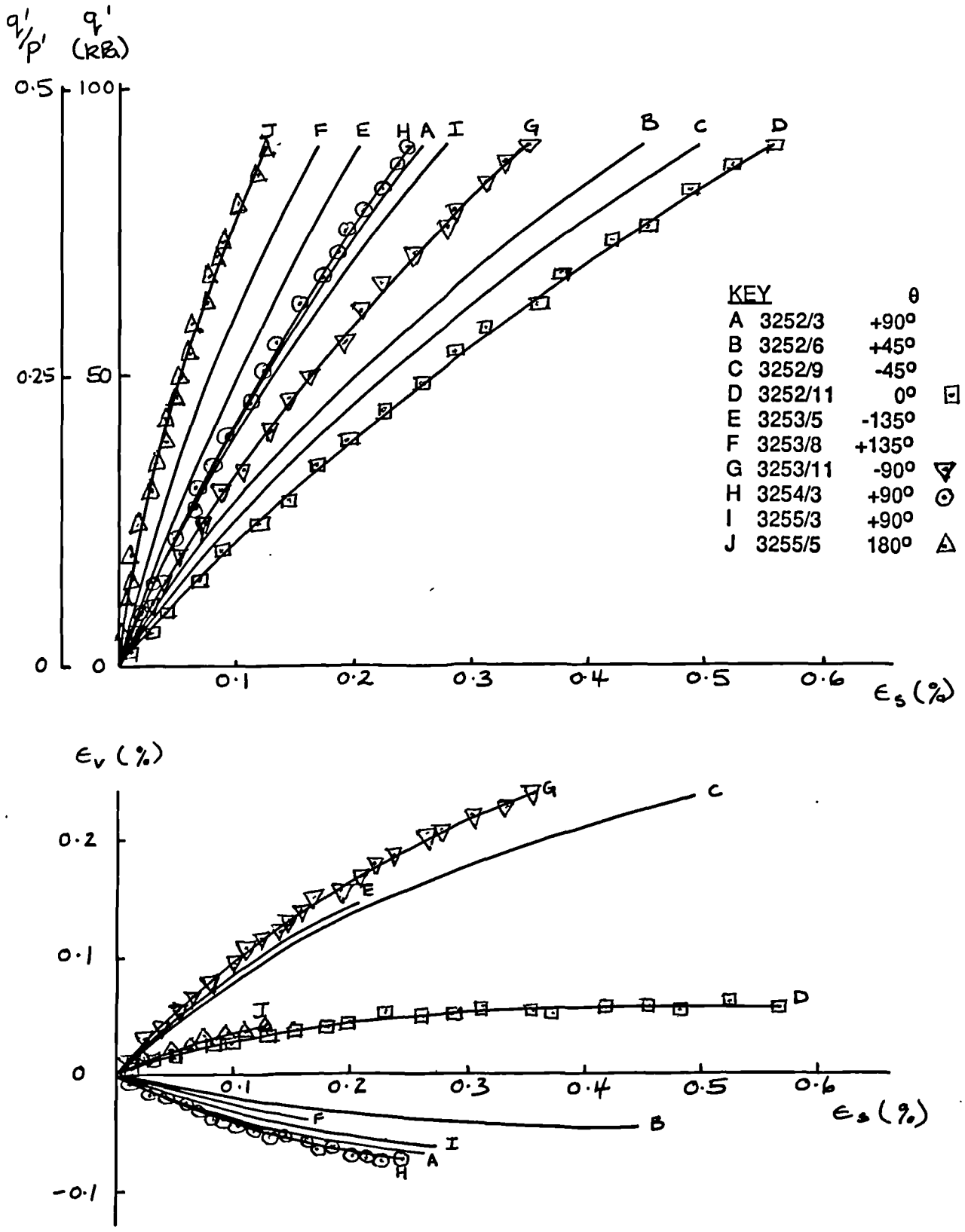

Fig 8.22 Plots of q' against ε_s and ε_v against ε_s .Cowden till, isotropically compressed, OCR = 2, p' = 200kPa, constant p' path.

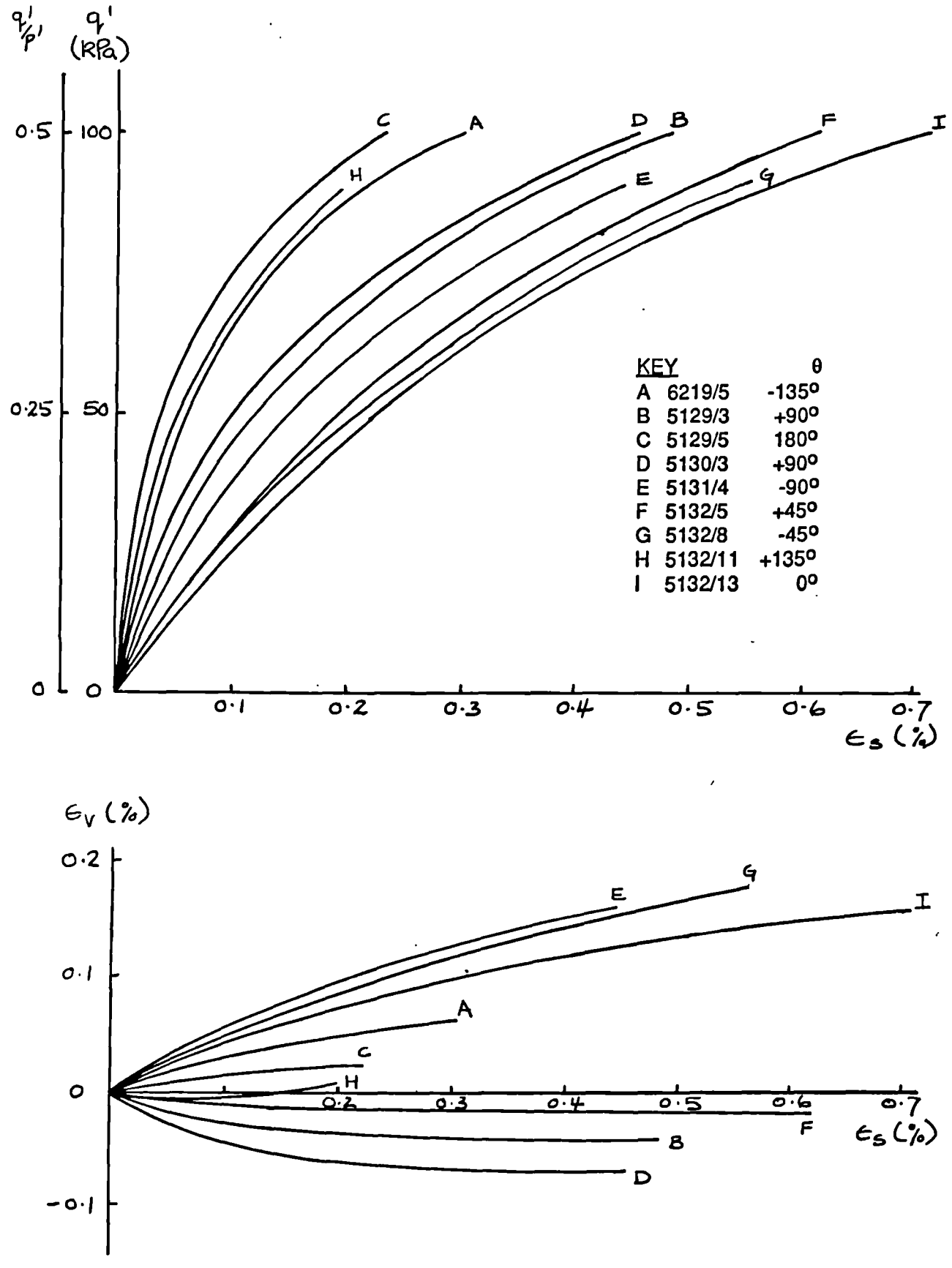

Fig 8.23 Plots of q' against ε_s and ε_v against ε_s . Slate dust, isotropically compressed, OCR = 2, p' = 200kPa, constant p' path.

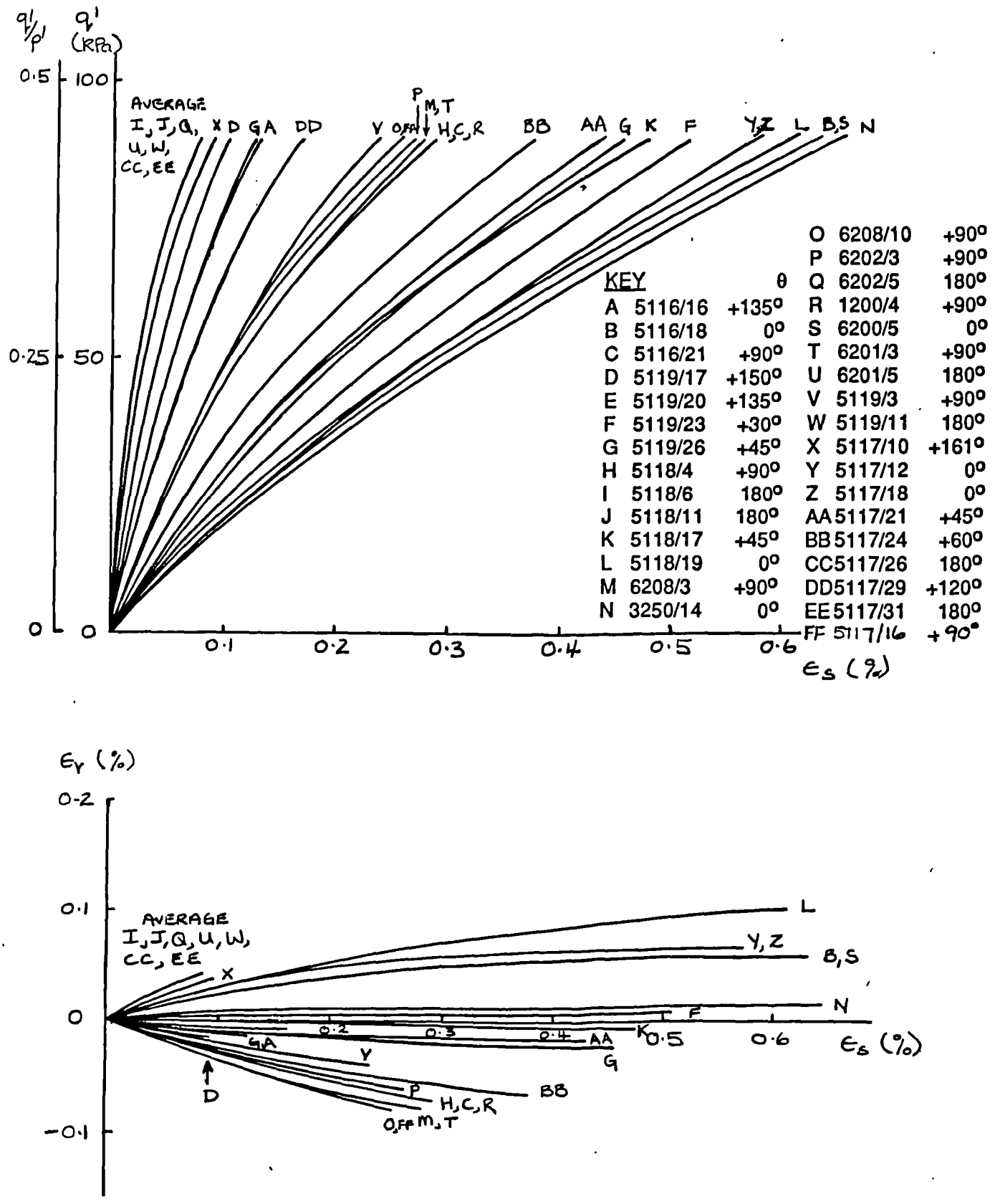

Fig 8.24a Plots of q' against ε_s and ε_v against ε_s . Positive deviations of stress path London clay isotropically compressed, OCR = 2, p' = 200kPa, constant p' path

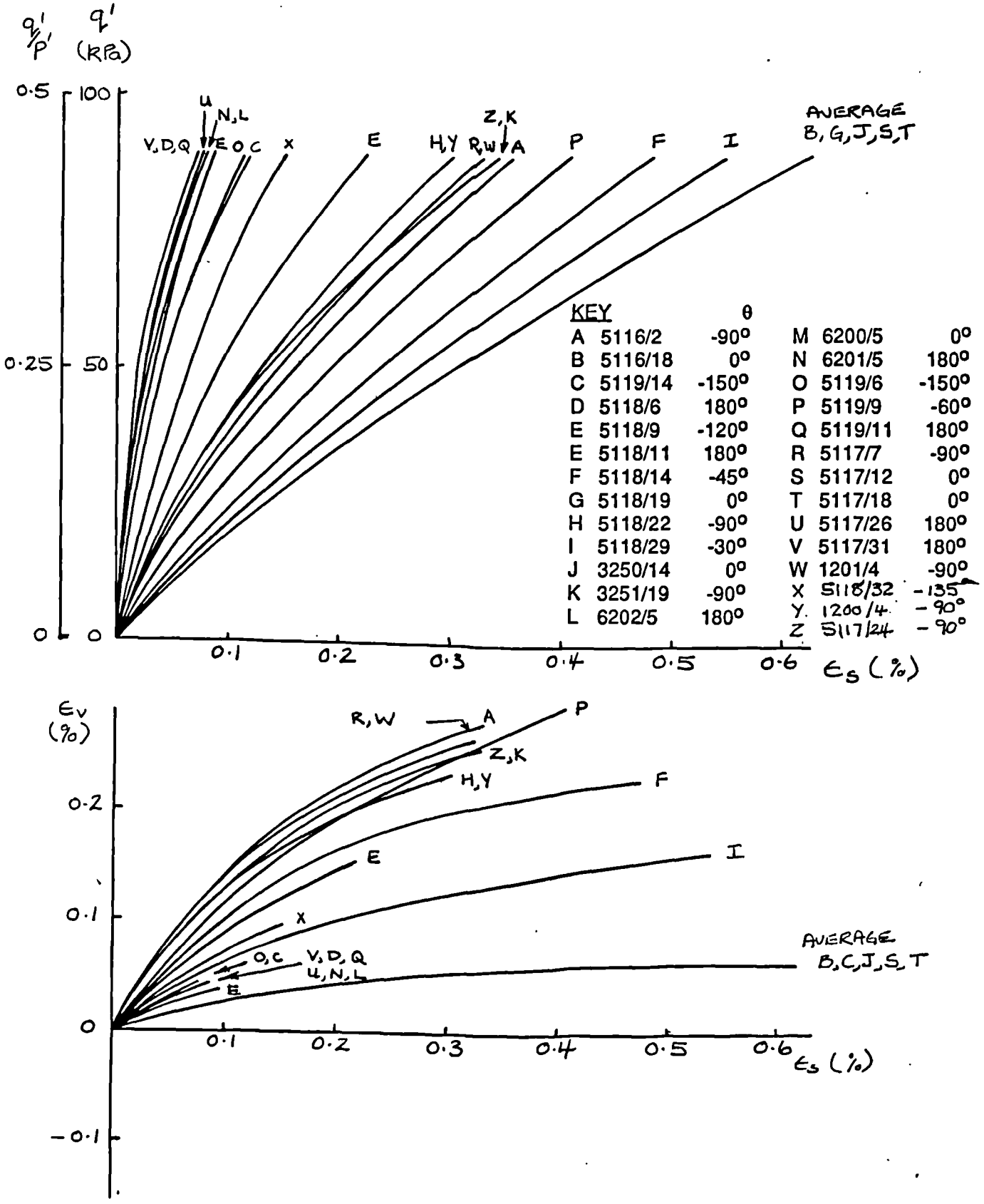

Fig 8.24b Plots of q' against ε_s and ε_v against ε_s . Negative deviations of stress path London clay, isotropically compressed, OCR = 2, p' = 200kPa, constant p' path.

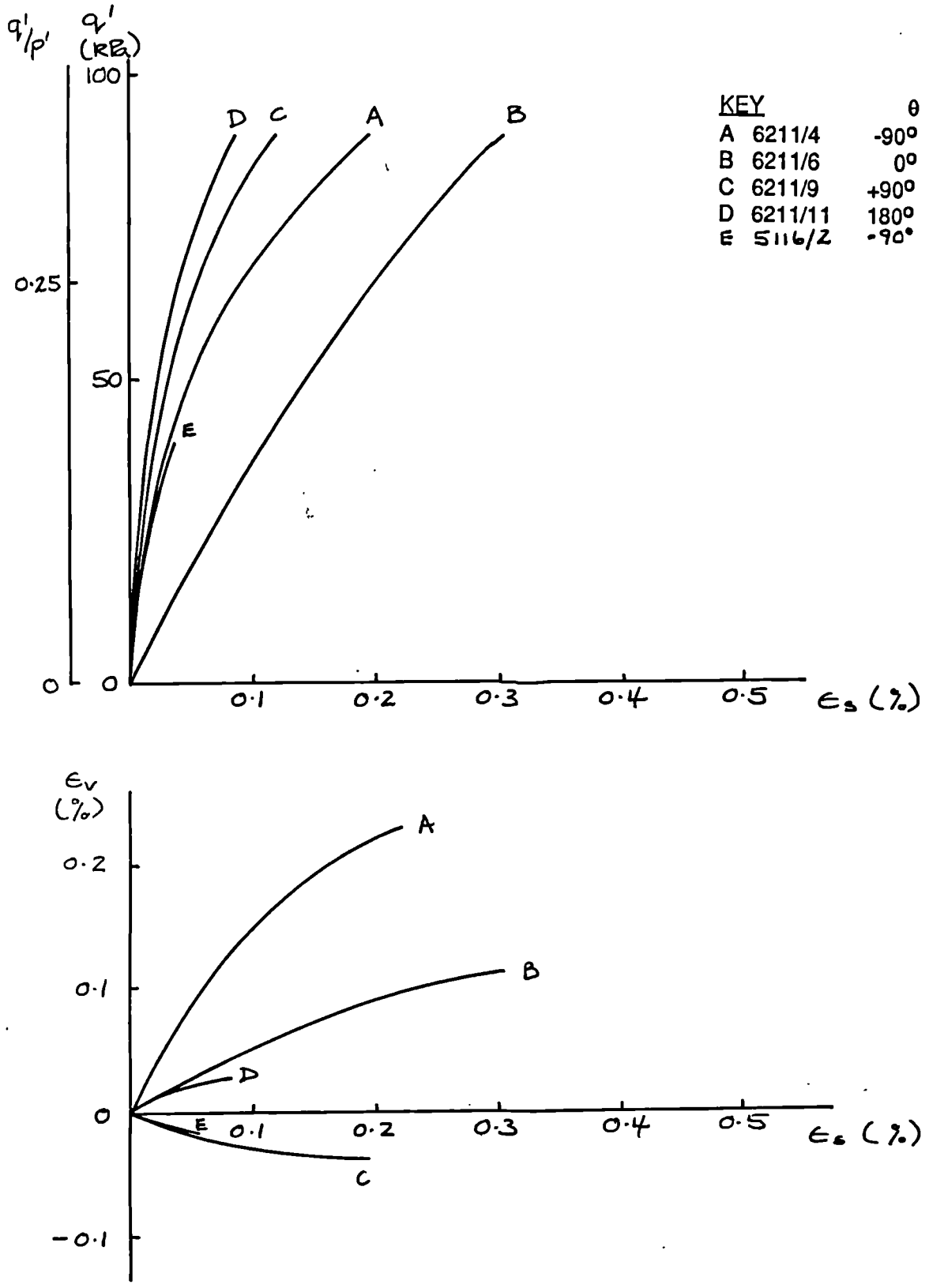

Fig 8.25 Plots of q' against ε_s and ε_v against ε_s . London clay , isotropically compressed, OCR = 1.5, p' = 267kPa, constant p' path.

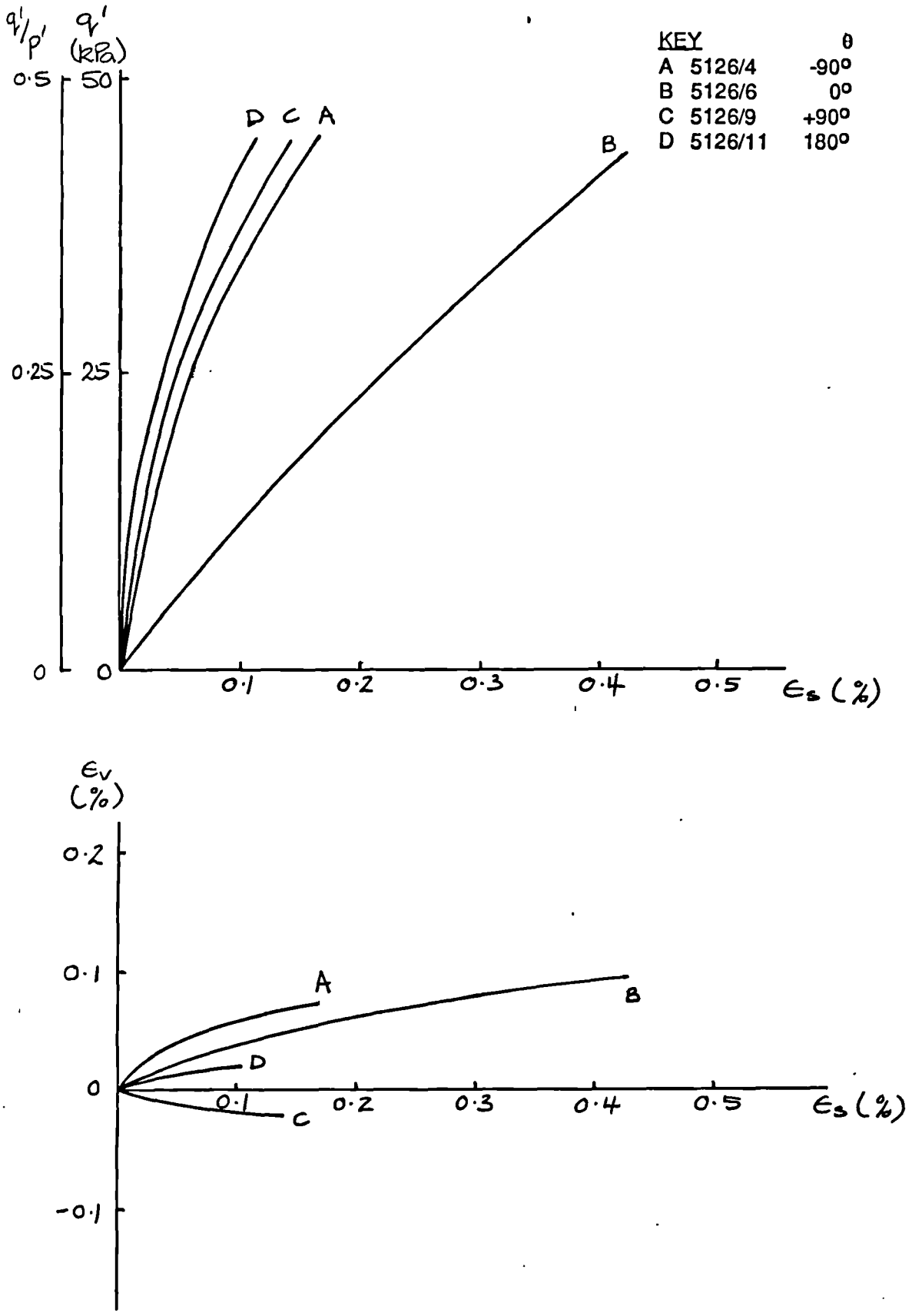

Fig 8.26 Plots of q' against ε_s and ε_v against ε_s . London clay , isotropically compressed, OCR = 4.0 , p' = 100kPa, constant p' path.

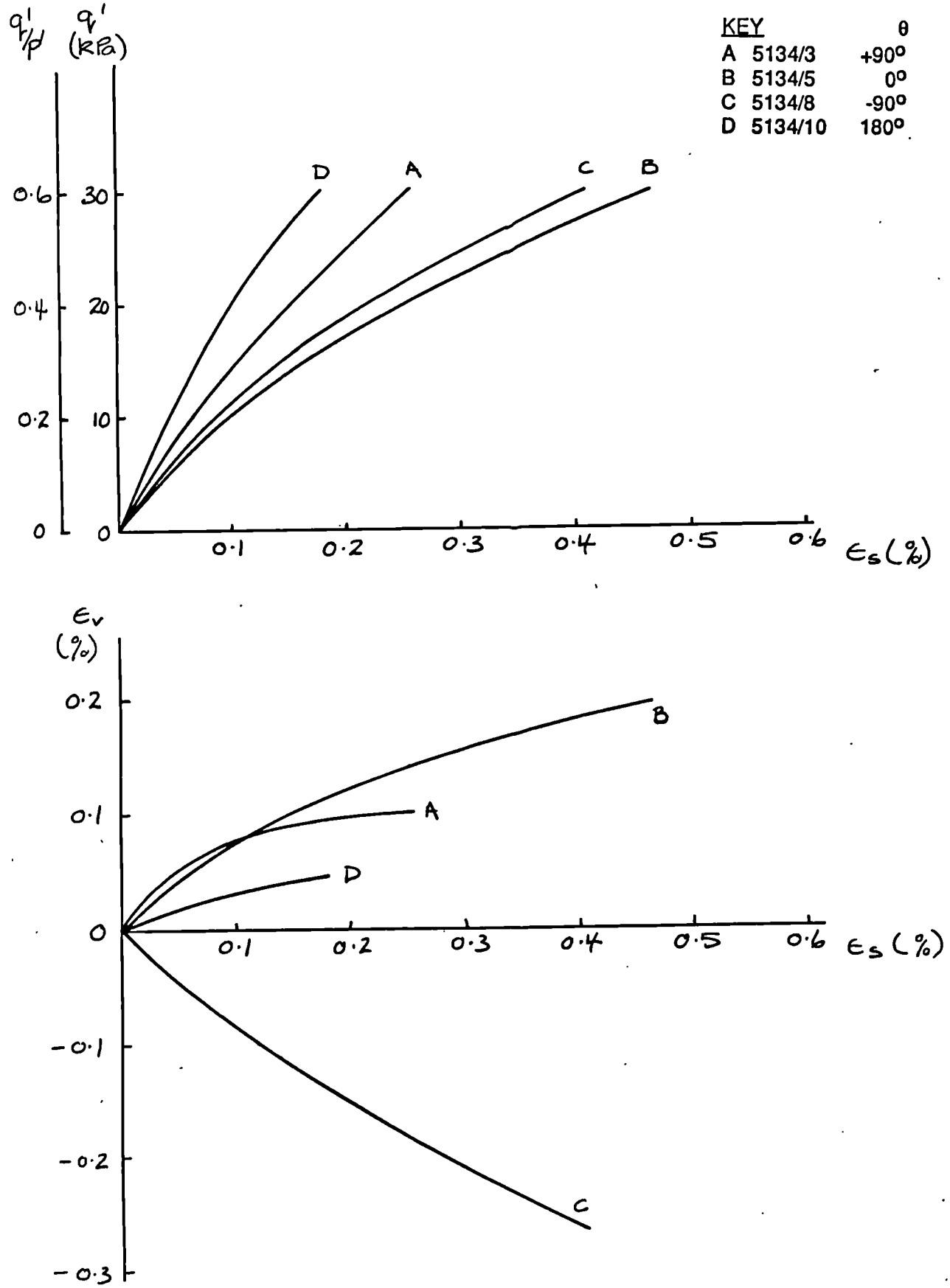

Fig 8.27 Plots of q' against ε_s and ε_v against ε_s . London clay , isotropically compressed, OCR = 8.0 , p' = 50kPa, constant p' path.

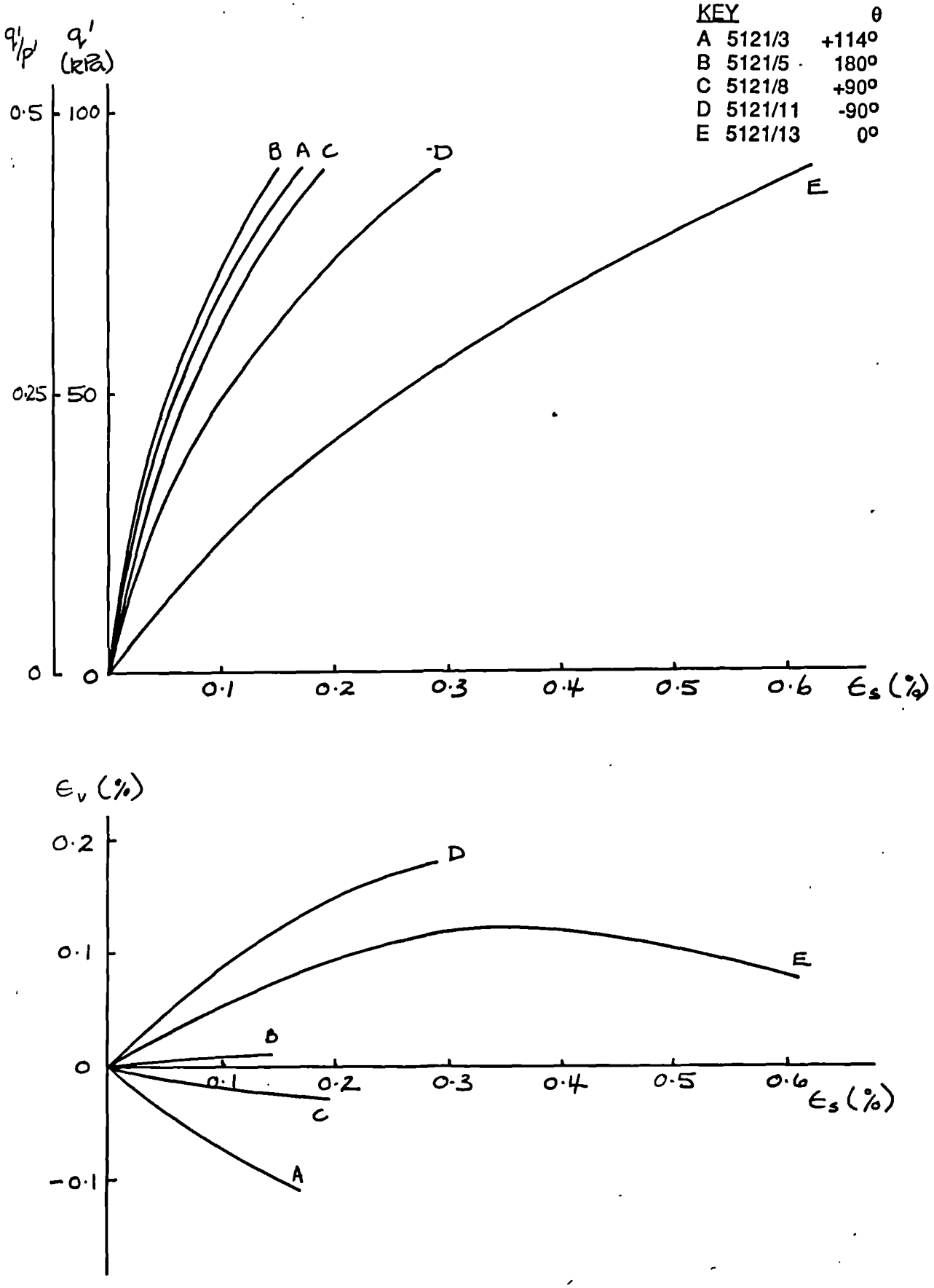

Fig 8.28 Plots of q' against ε_s and ε_v against ε_s . London clay , compressed with $\eta'_o = 0.25$, OCR = 2.0, p' = 200kPa, $q'_o = 5$kPa , constant p' path.

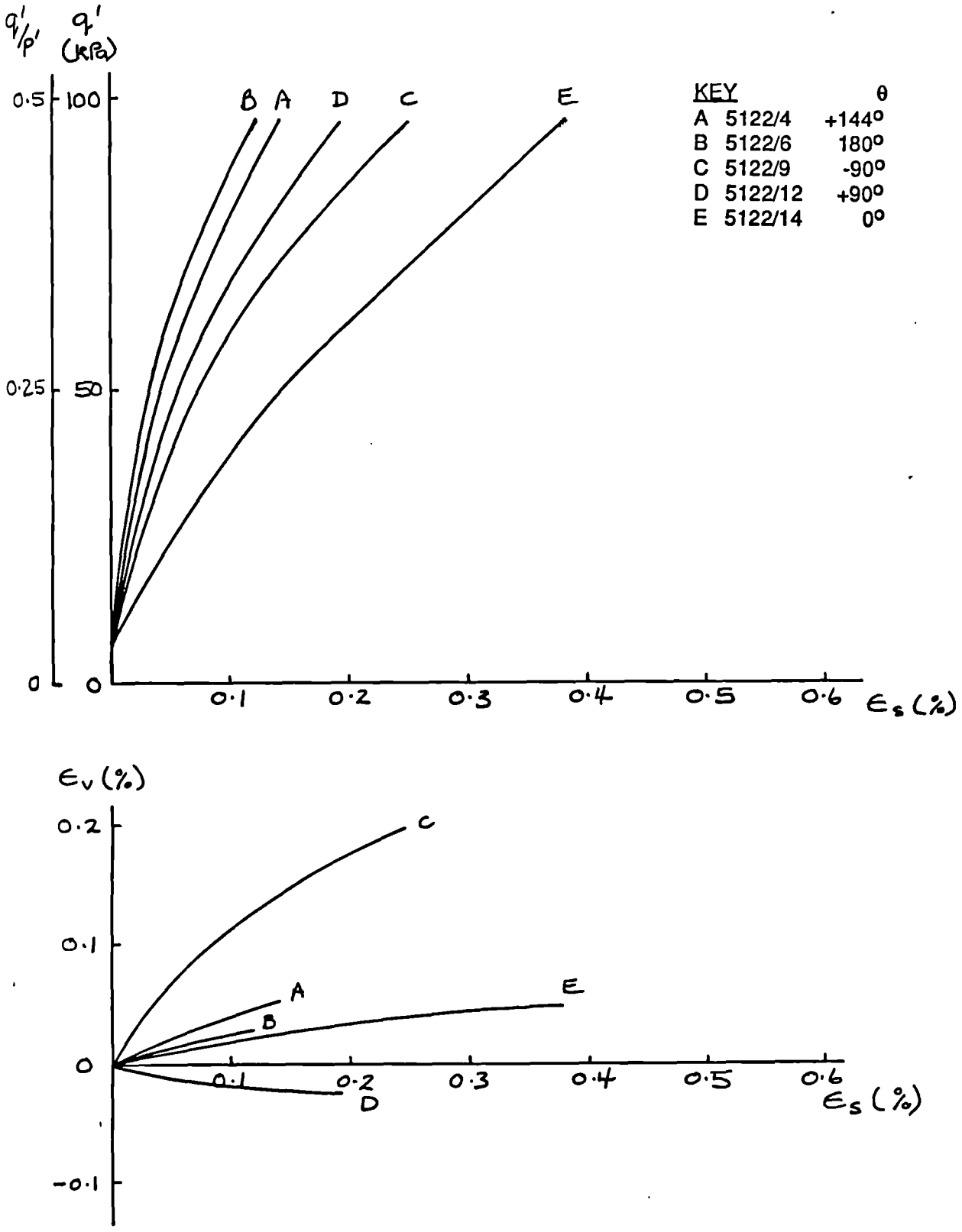

Fig 8.29 Plots of q' against ε_s and ε_v against ε_s . London clay , compressed with $\eta'_o = 0.75$, OCR = 2.0, p' = 200kPa, $q'_o = 7$kPa , constant p' path.

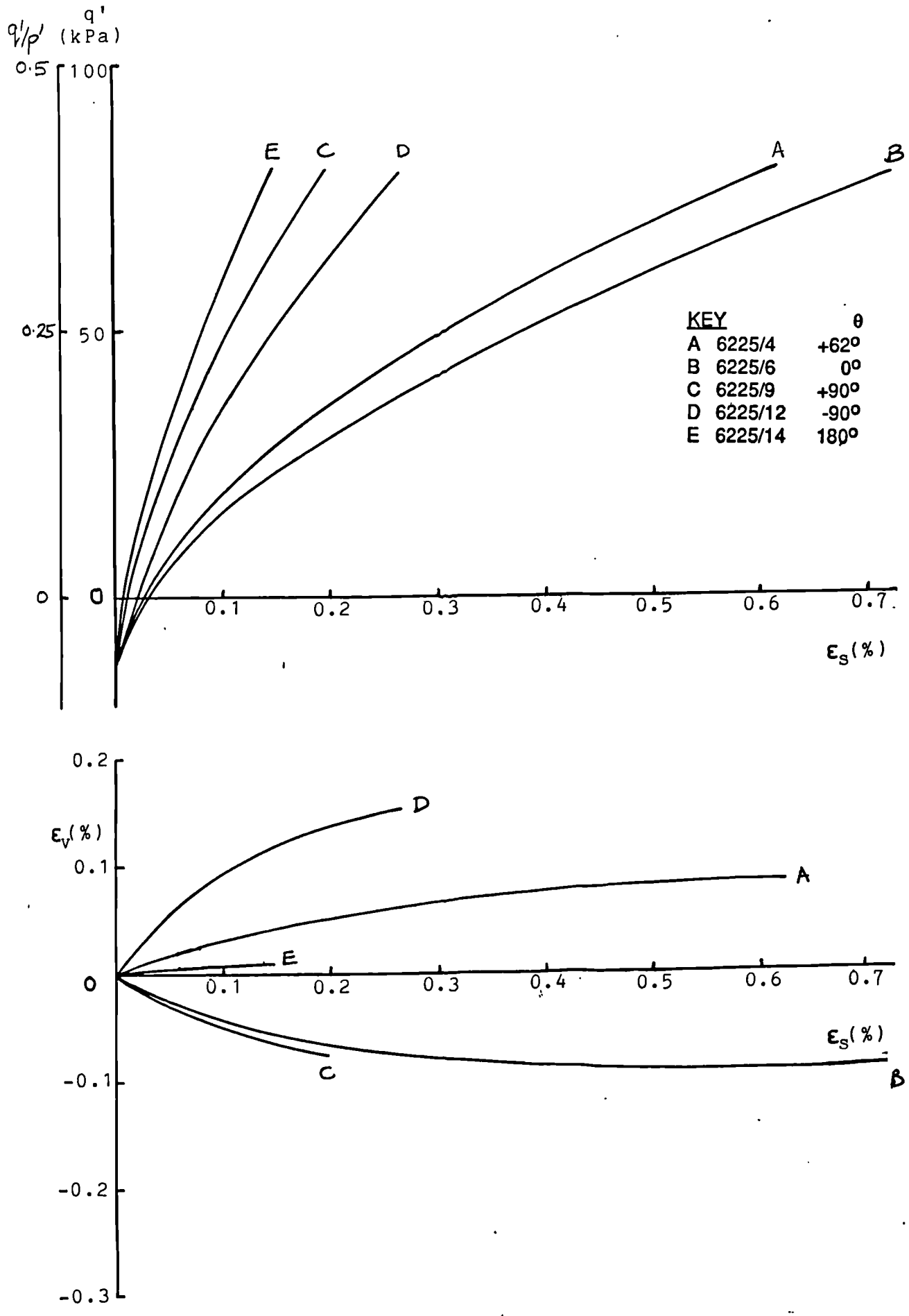

Fig 8.30 Plots of q' against ε_s and ε_v against ε_s . London clay , one dimensionally compressed , OCR = 2.0, p' = 200kPa, q'_o = -12kPa , constant p' path.

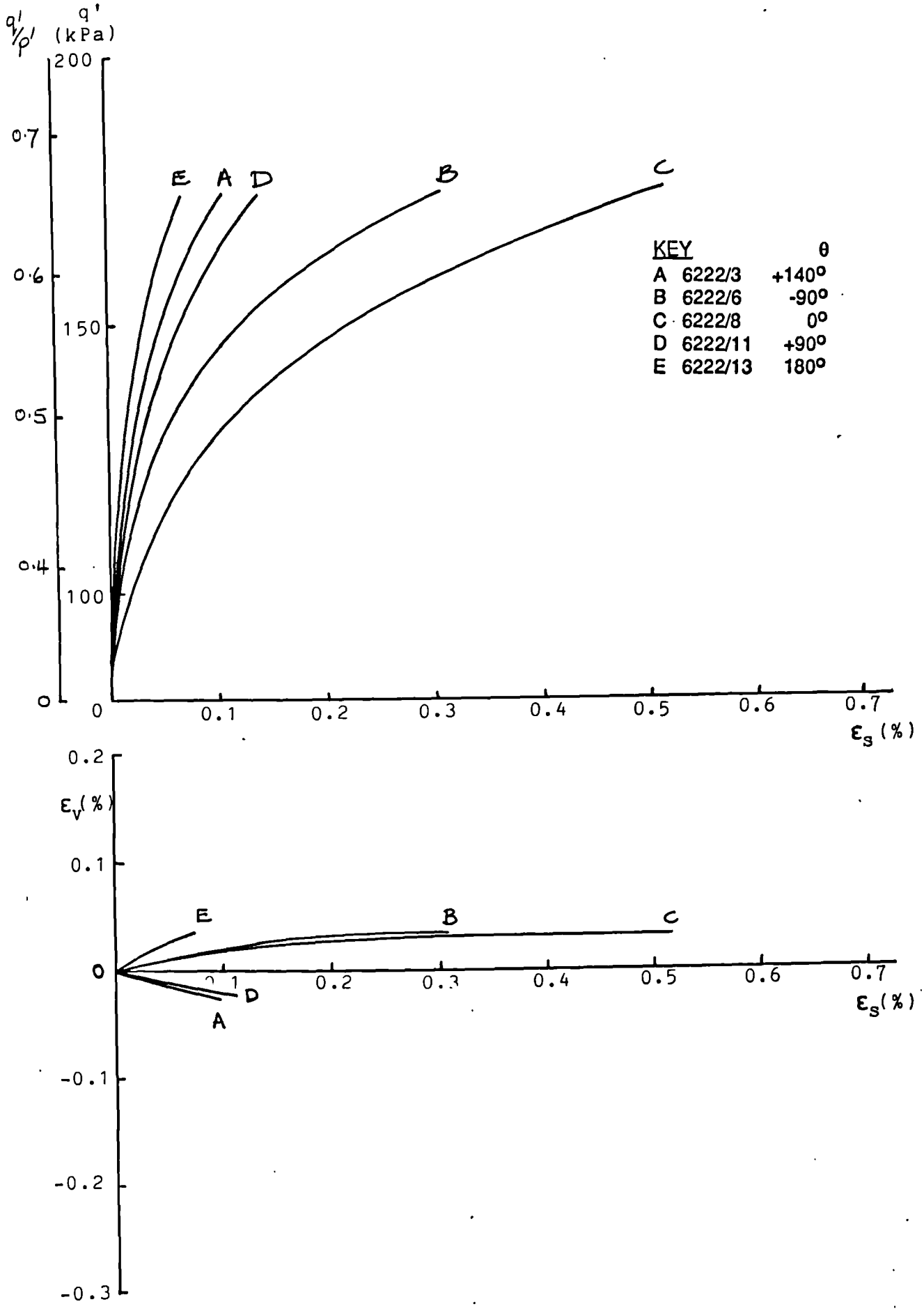

Fig 8.31 Plots of q' against ε_s and ε_v against ε_s . London clay , two dimensionally compressed , OCR = 1.5, p' = 267kPa, q'_o = 85kPa , constant p' path.

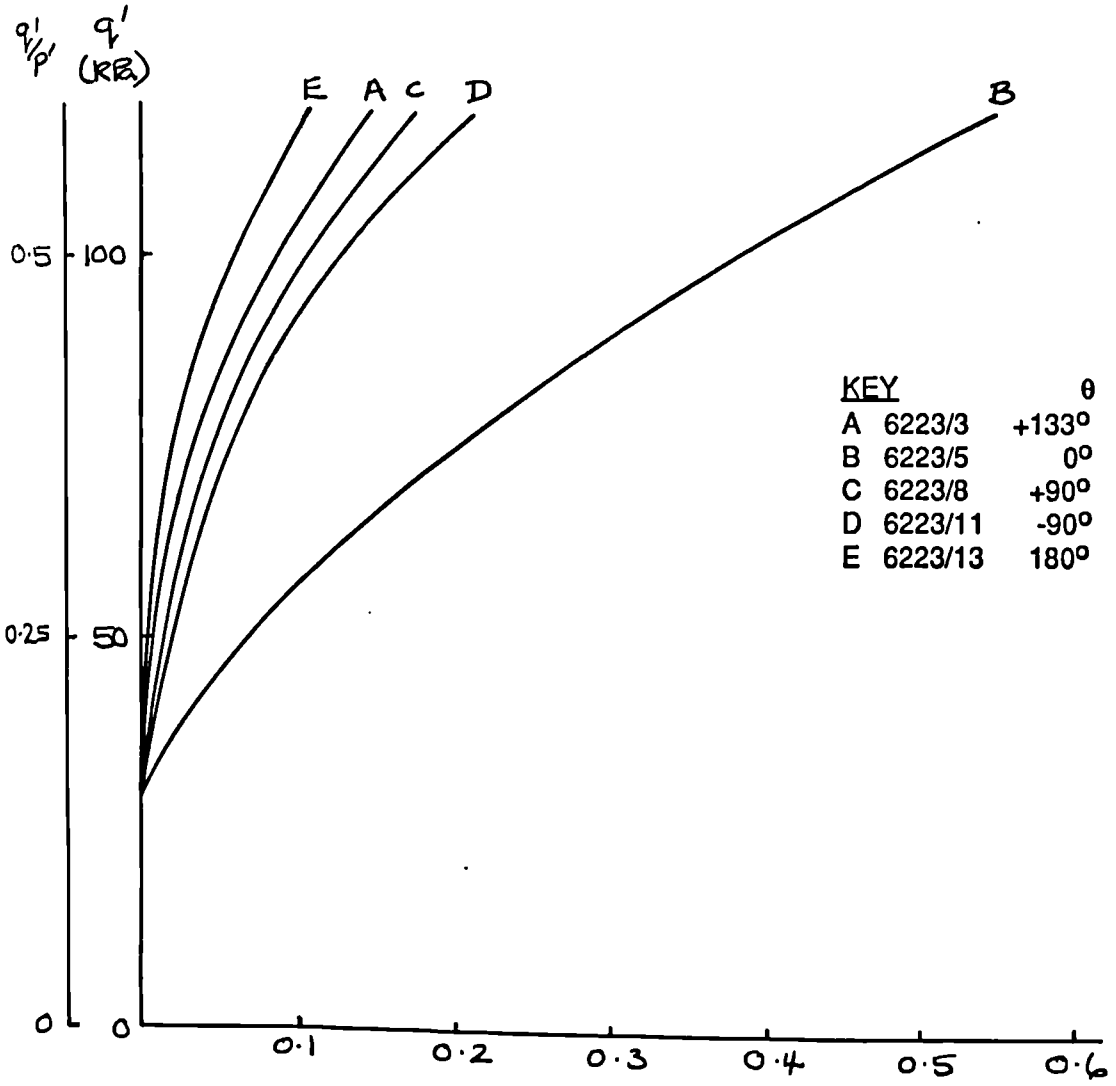

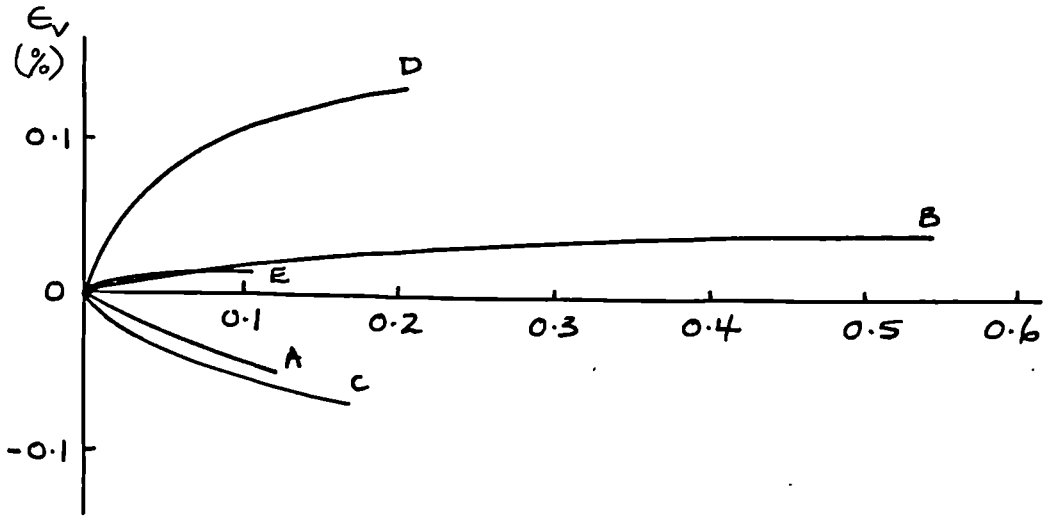

Fig 8.32 Plots of q' against ε_s and ε_v against ε_s . London clay , one dimensionally compressed , OCR = 2.0, p' = 200kPa, q'_o = 36kPa , constant p' path.

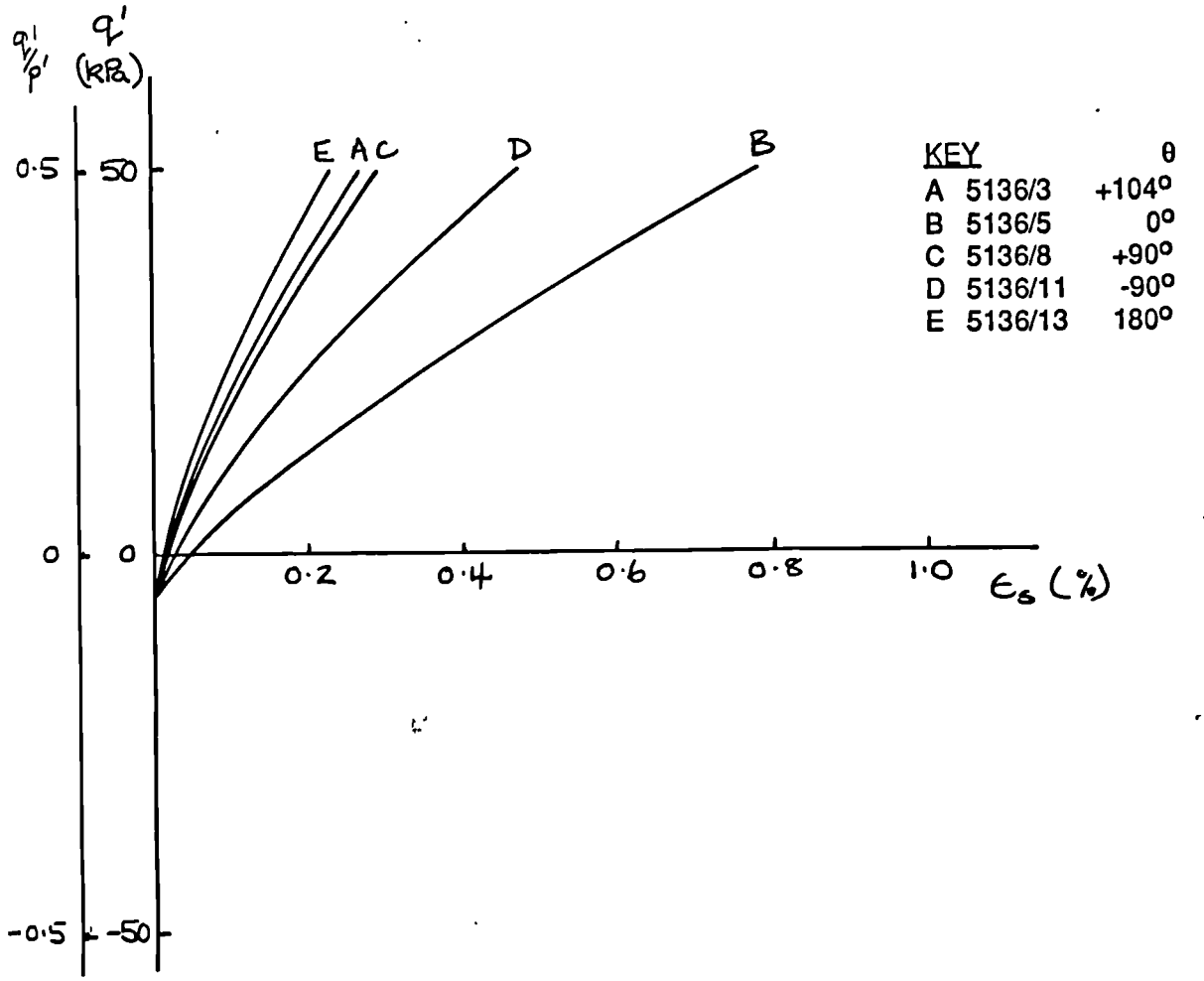

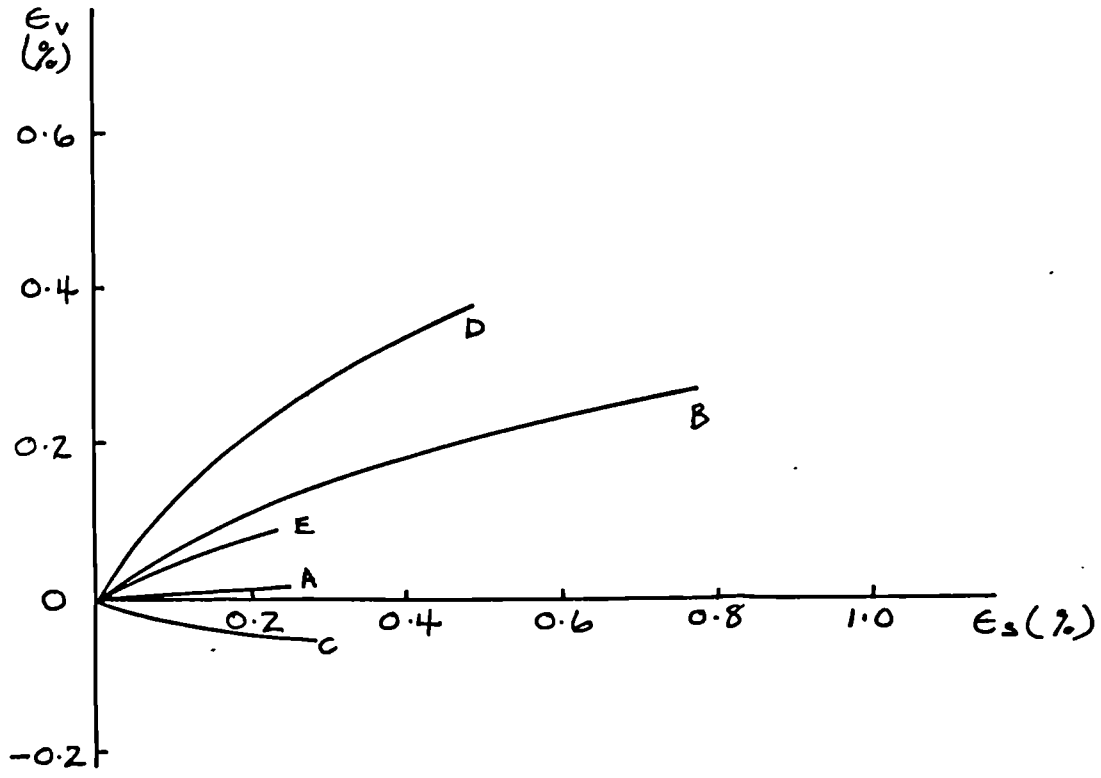

Fig 8.33 Plots of q' against ε_s and ε_v against ε_s . London clay , one dimensionally compressed , OCR = 4.0, p' = 100kPa, q'_o = -5kPa , constant p' path.

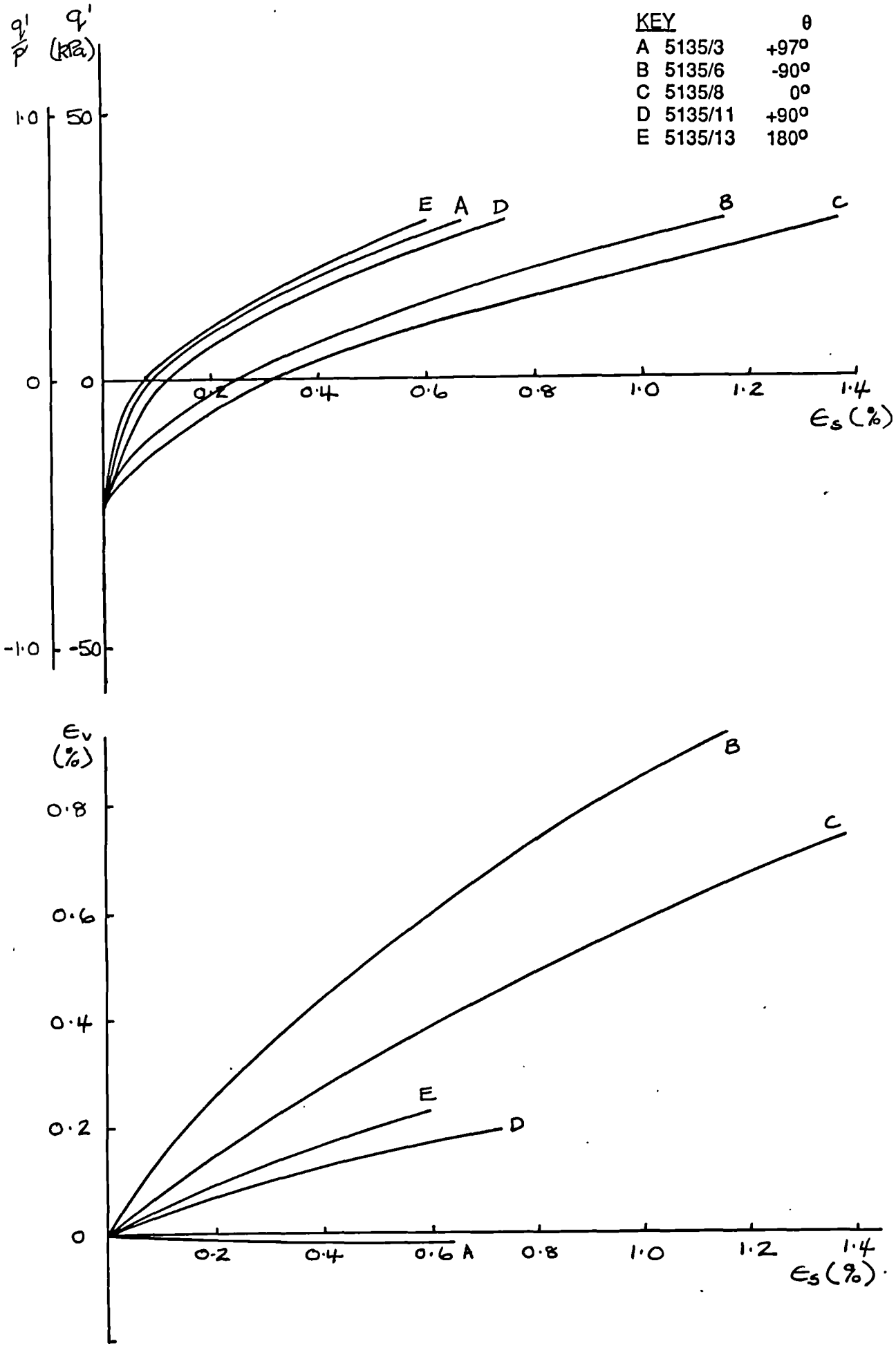

Fig 8.34 Plots of q' against ε_s and ε_v against ε_s . London clay , one dimensionally compressed , OCR = 8.0, p' = 50kPa, q'_o = -24kPa , constant p' path.

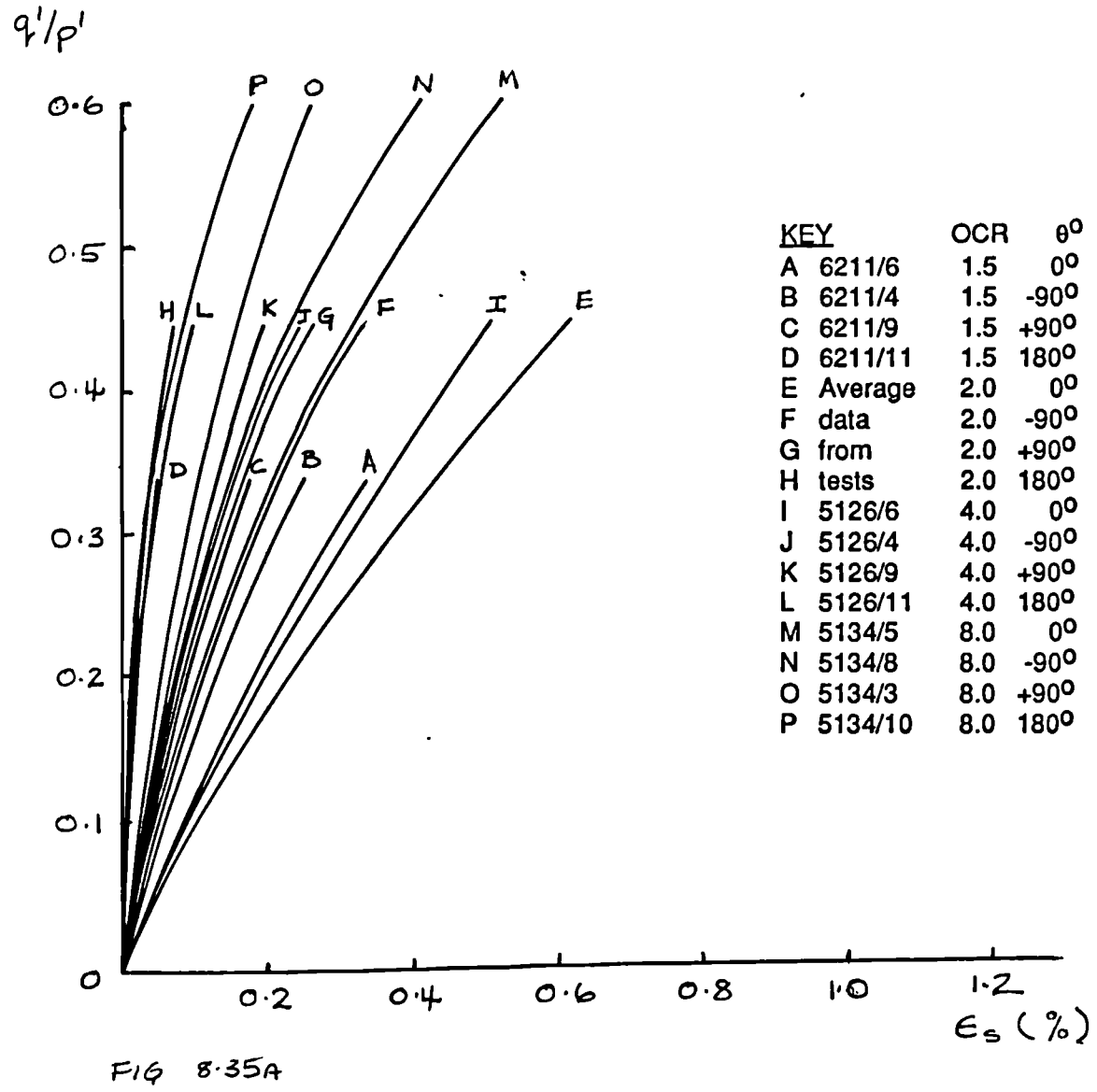

FIG 8·35A

Fig 8.35 Plots of q' / p' against ε_s for London clay at various overconsolidation ratios. constant p' paths.

a) Isotropically compressed.
b) one dimensionally compressed.

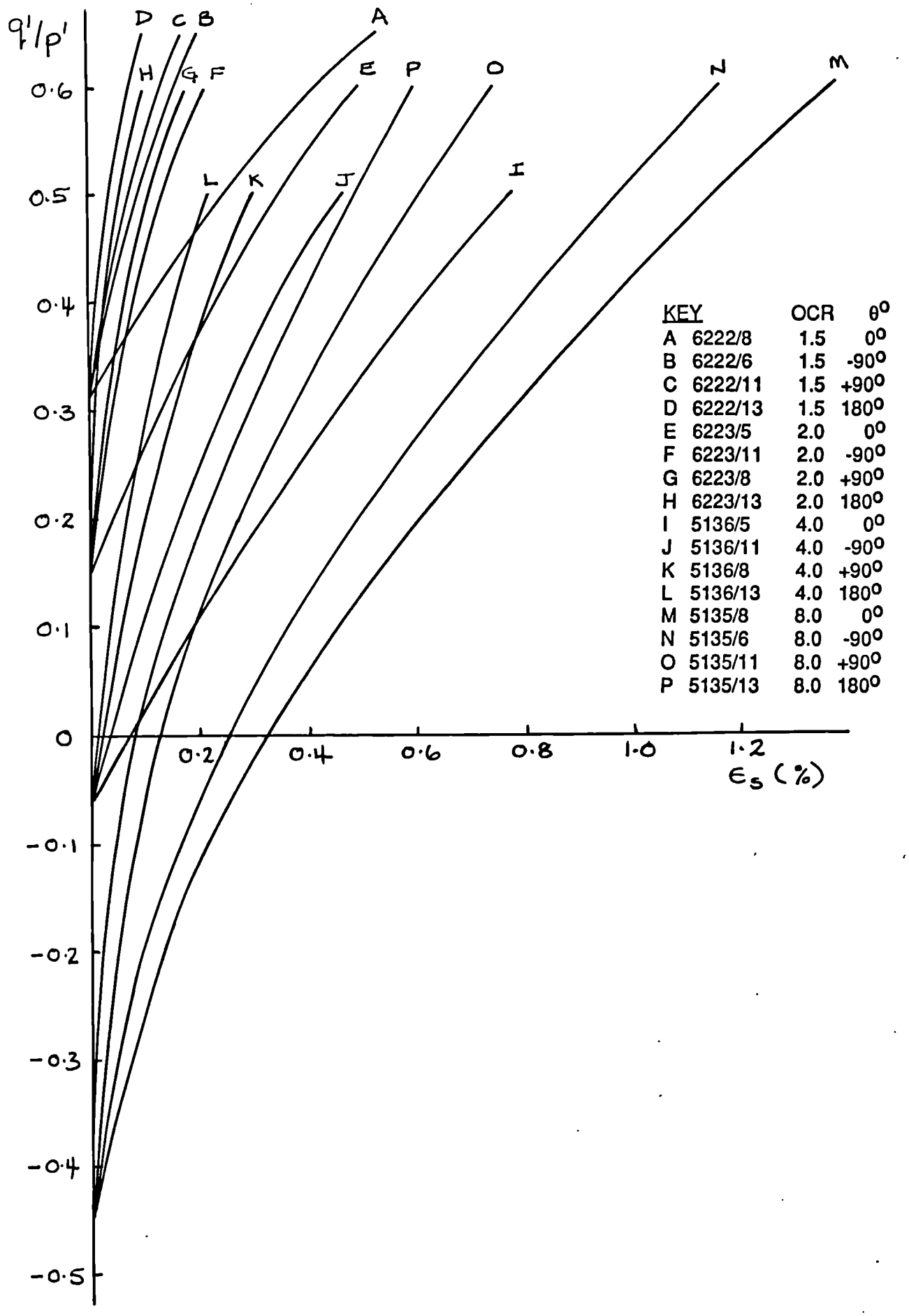

FIG 8.35B

Title as page 432

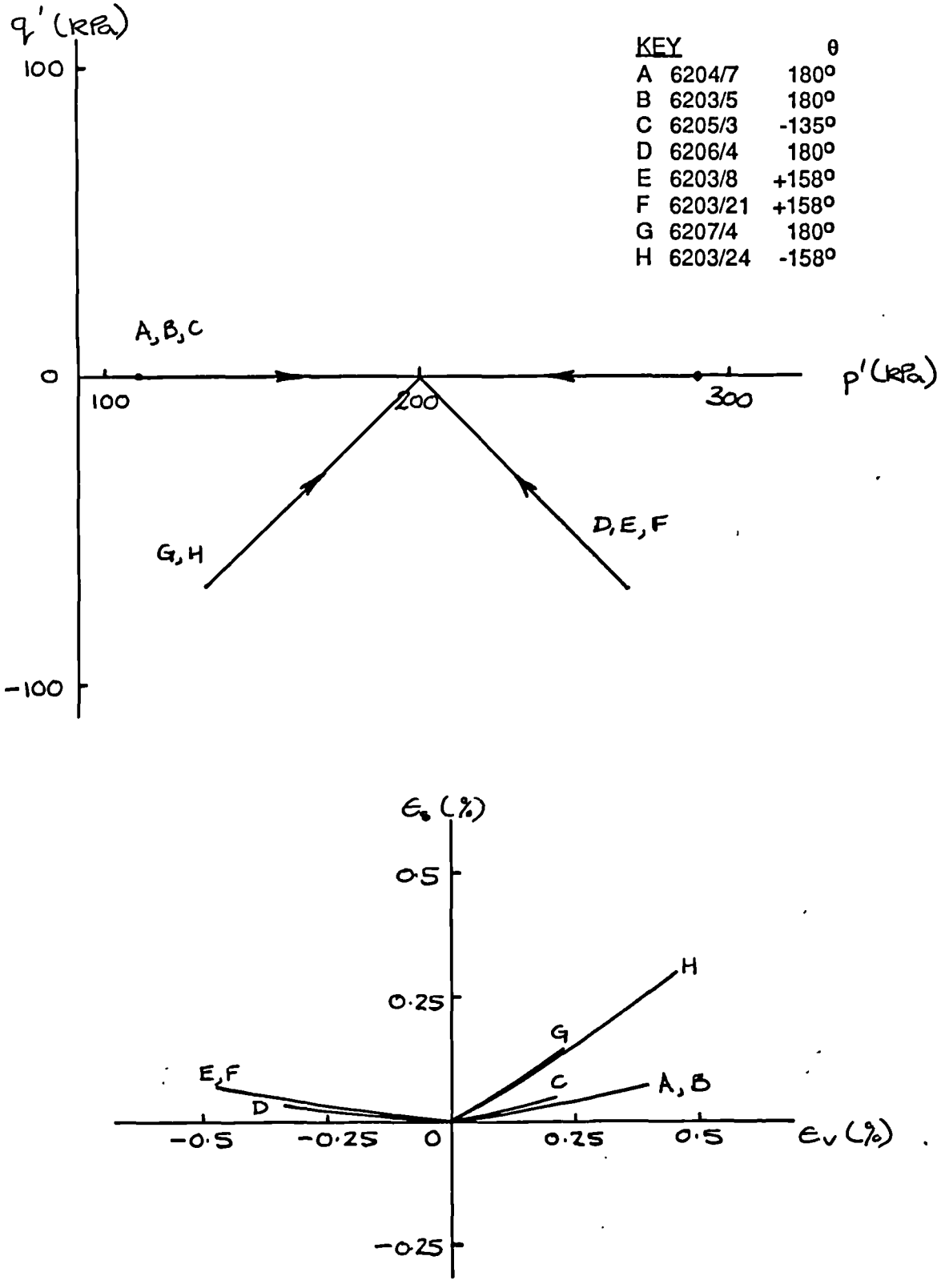

Fig 8.36 Plots of q' against p' and ε_s against ε_v. Isotropically compressed Ware till,various stress paths.

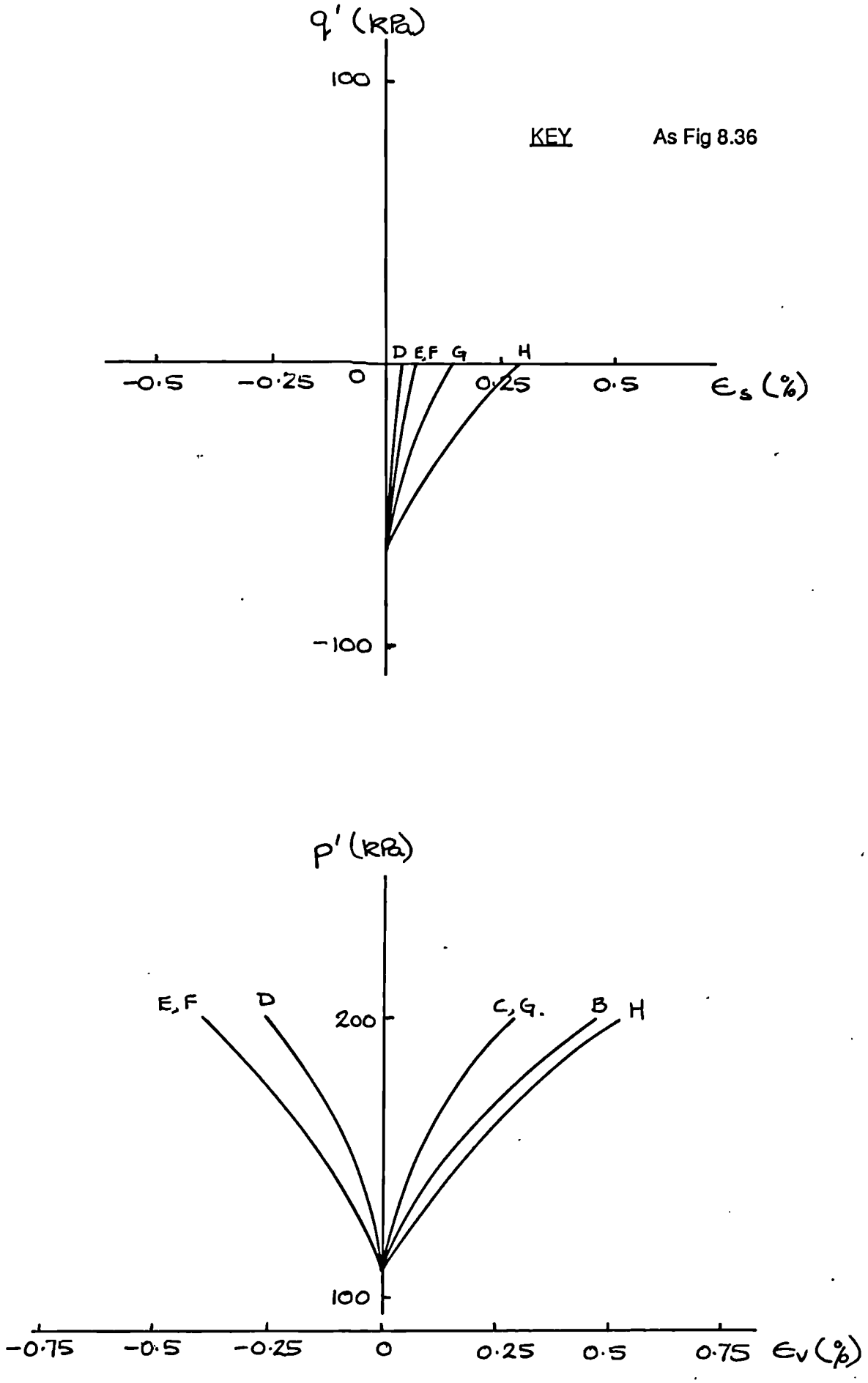

Fig 8.37 Plots of q' against ε_s and p' against ε_v . Isotropically compressed Ware till, various paths.

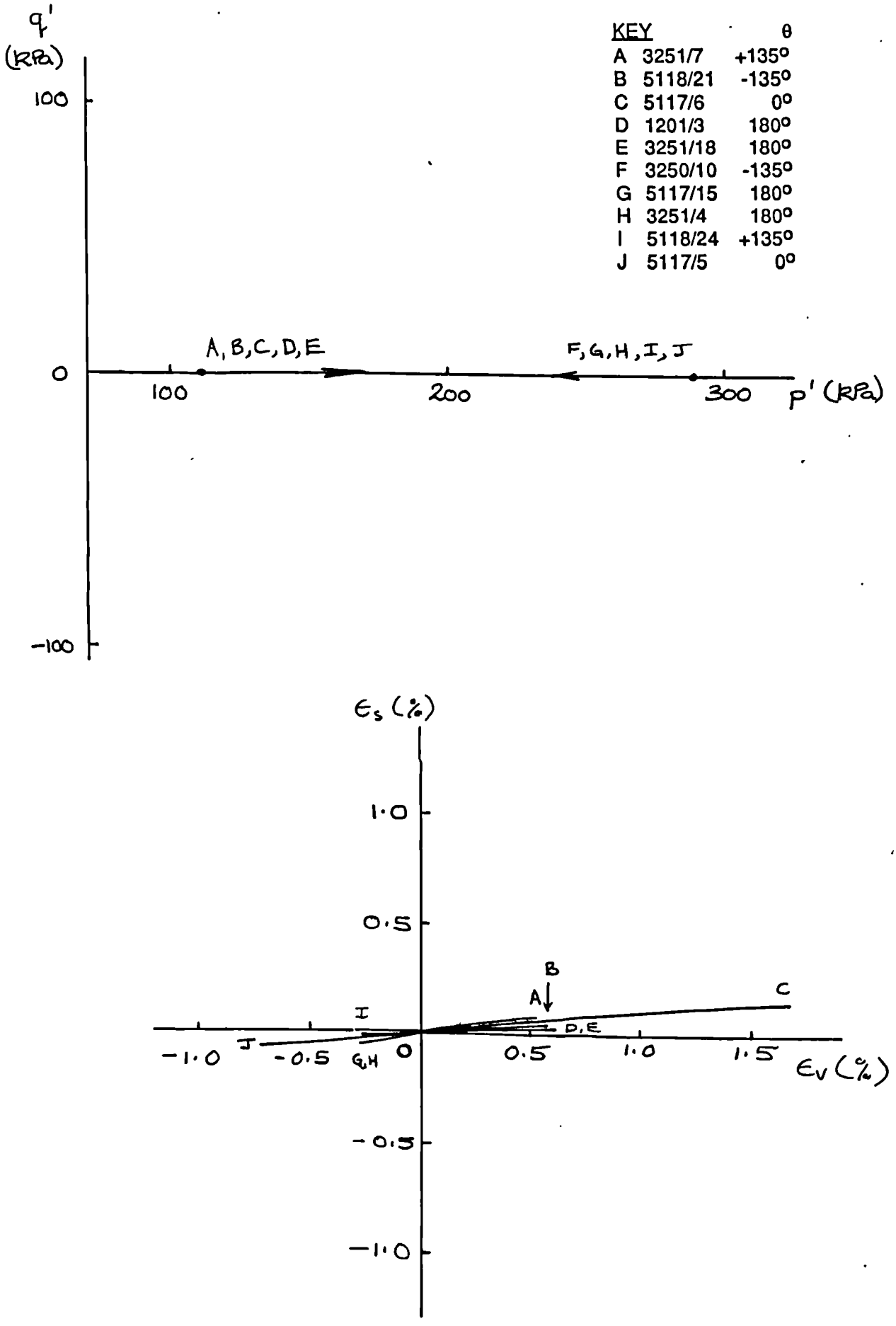

Fig 8.38 Plots of q' against p' and ε_s against ε_v. Isotropically compressed London clay, various stress paths.

KEY As Fig 8.38

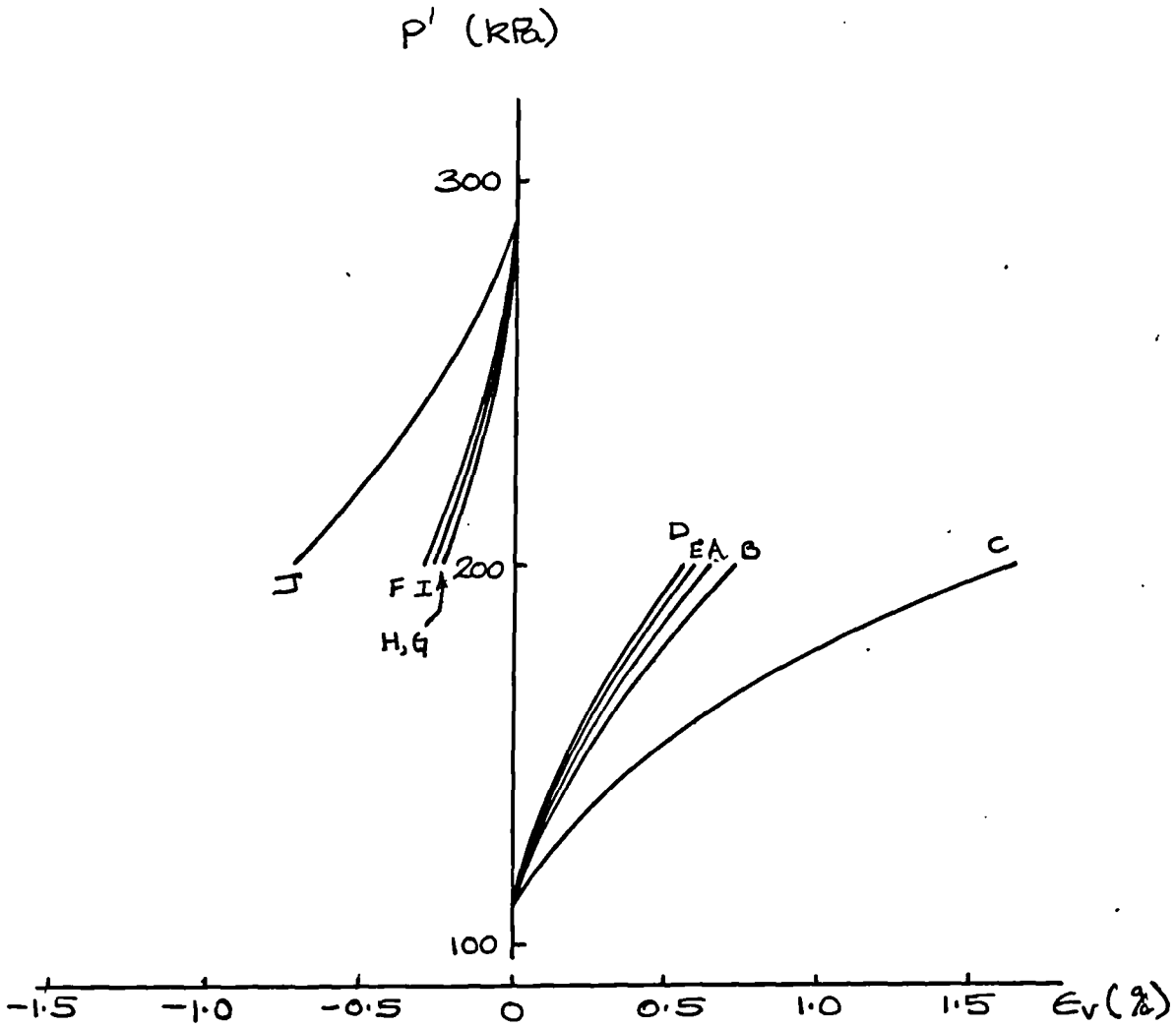

Fig 8.39 Plot of p' against ε_v. Isotropically compressed London clay, various paths.

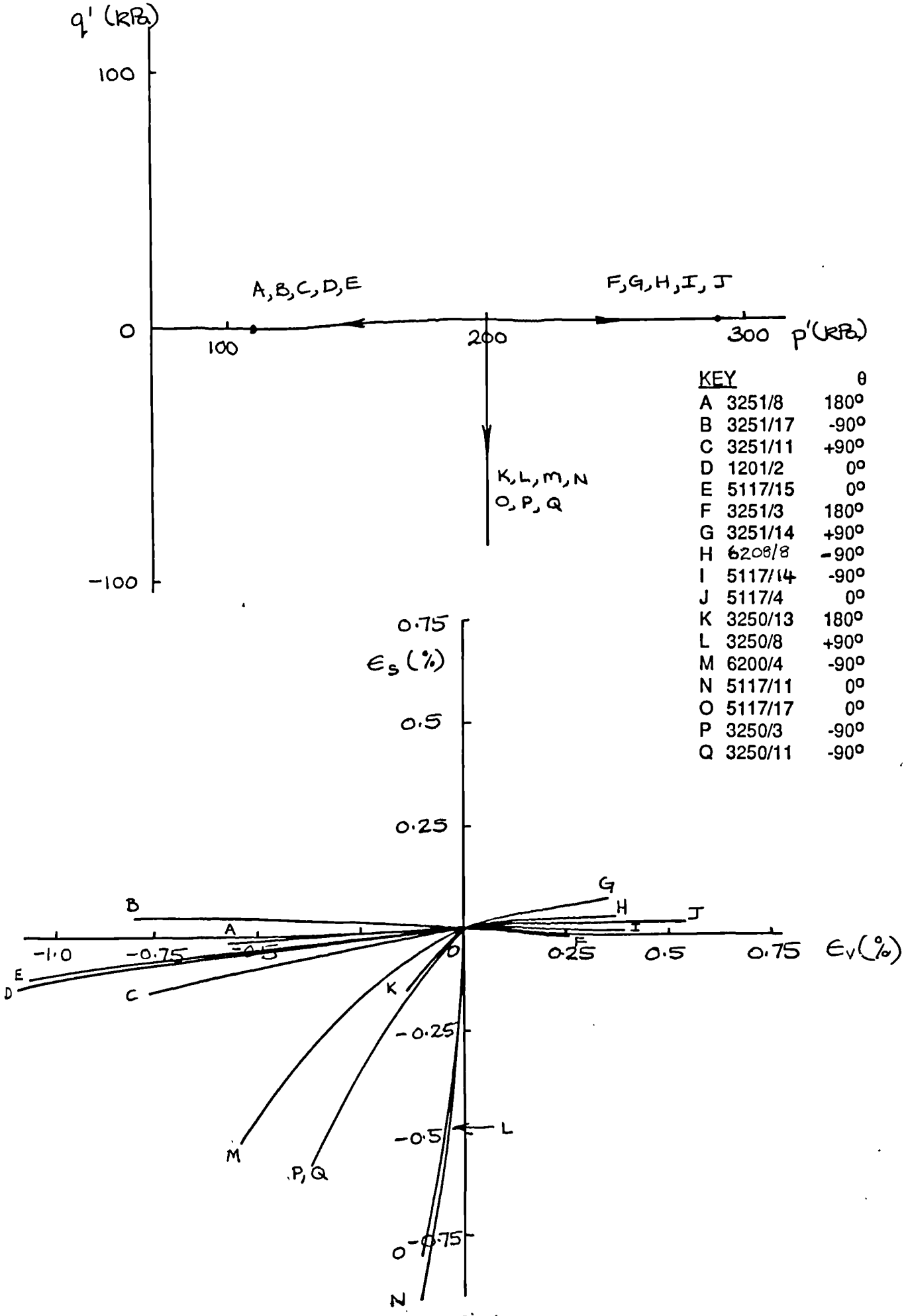

Fig 8.40 Plots of q' against p' and ε_s against ε_v. Isotropically compressed London clay various stress paths. OCR = 2.0, p' = 200kPa.

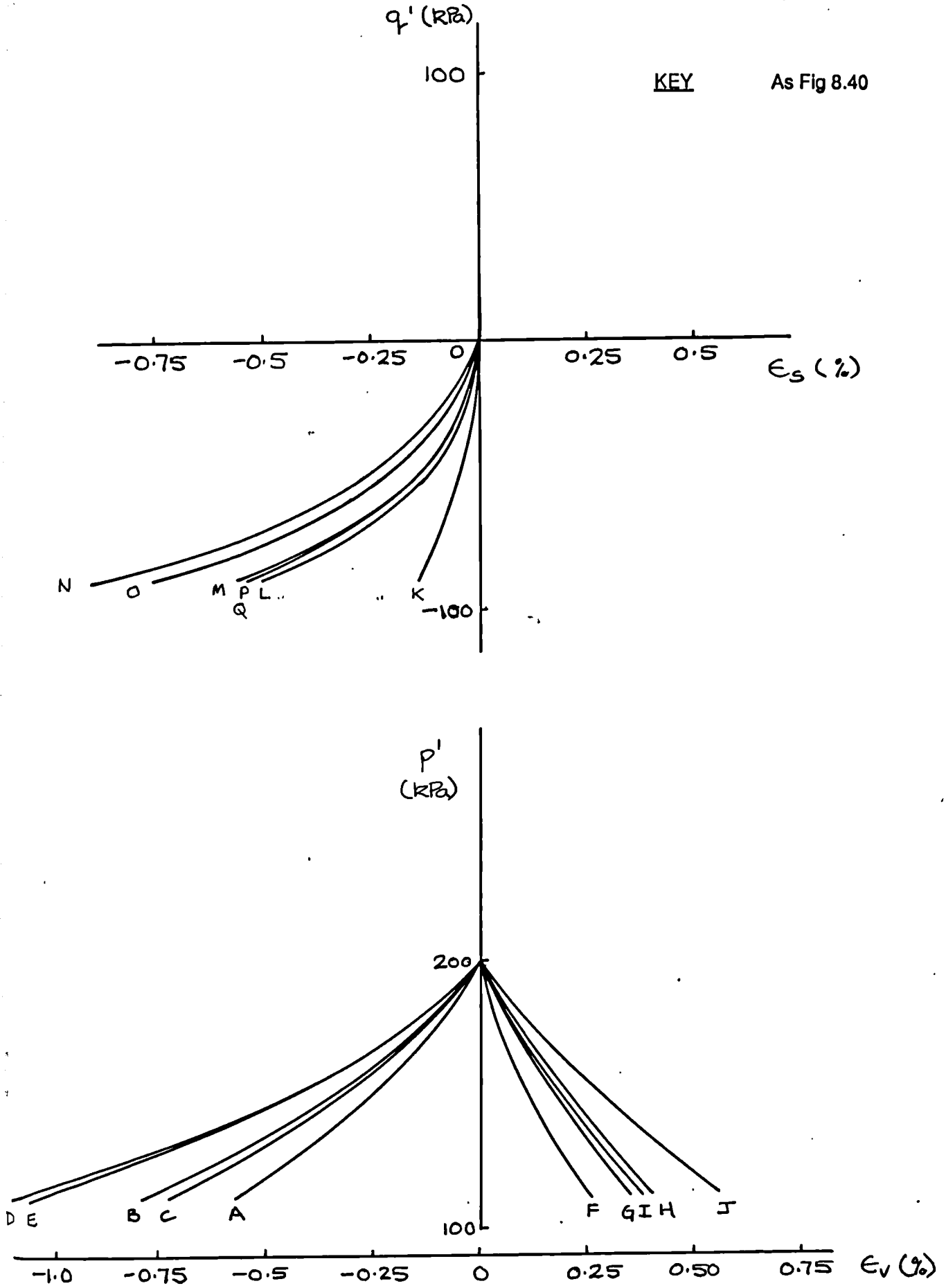

Fig 8.41 Plots of q' against ε_s and p' against ε_v . Isotropically compressed London clay, various stress paths. OCR = 2.0 ,p' =200kPa.

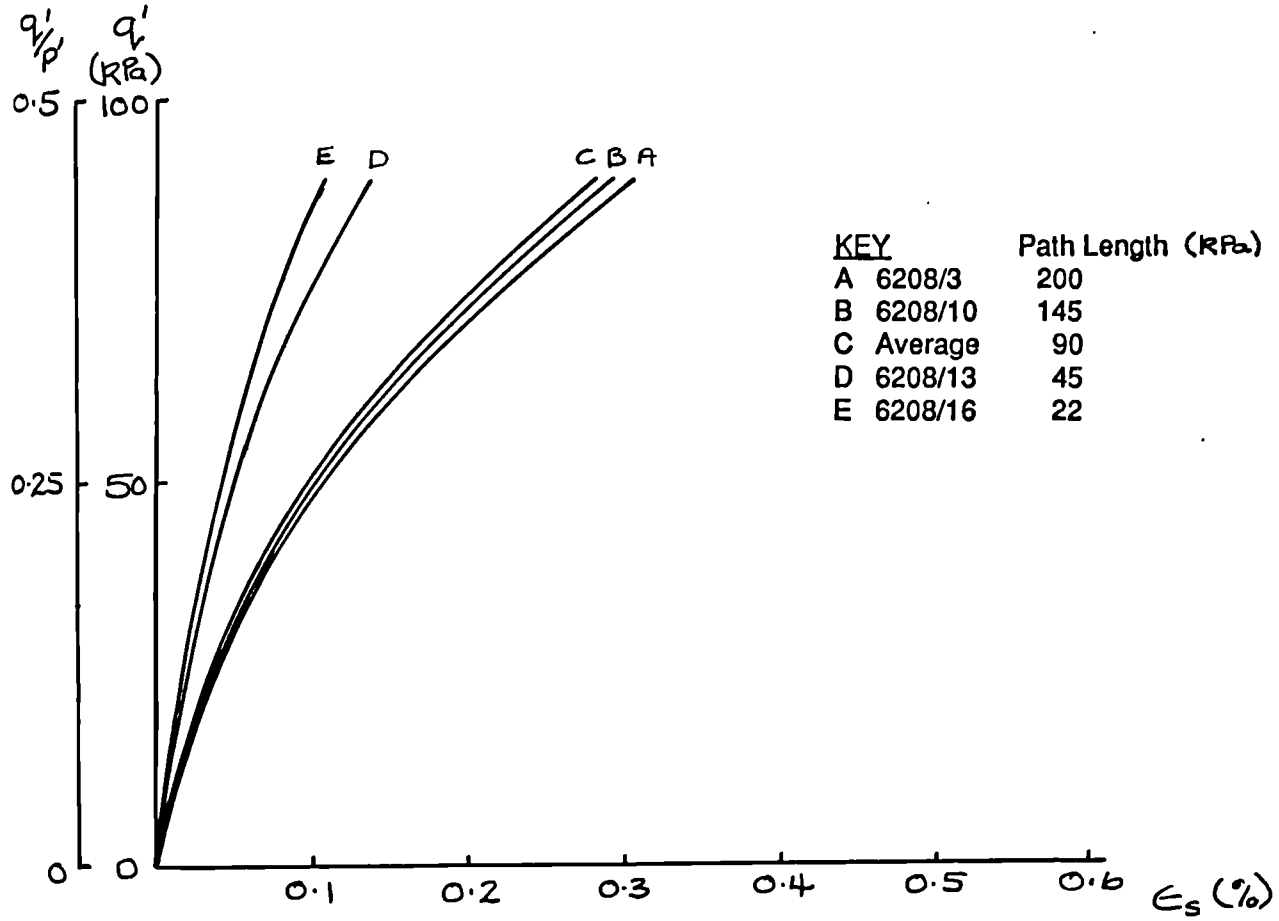

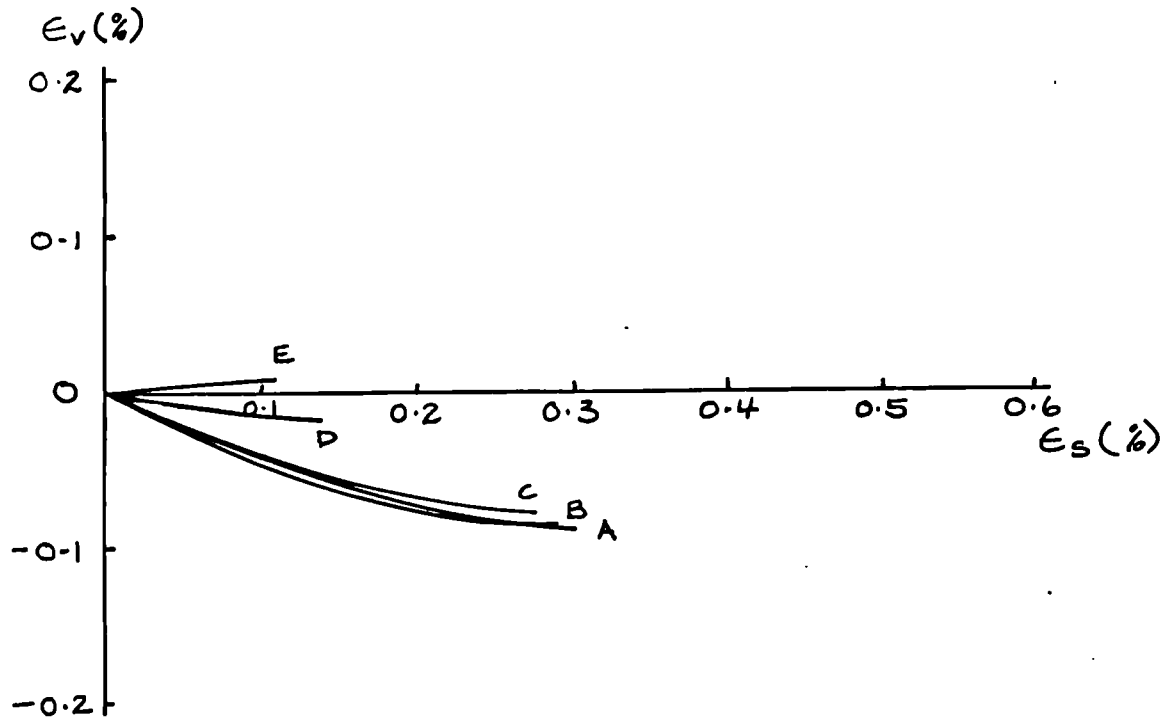

Fig 8.42 Plots of q' against ε_s and ε_v against ε_s . Isotropically compressed London clay. OCR = 2.0 ,p' =200kPa, constant p' paths. Various approach path lengths.

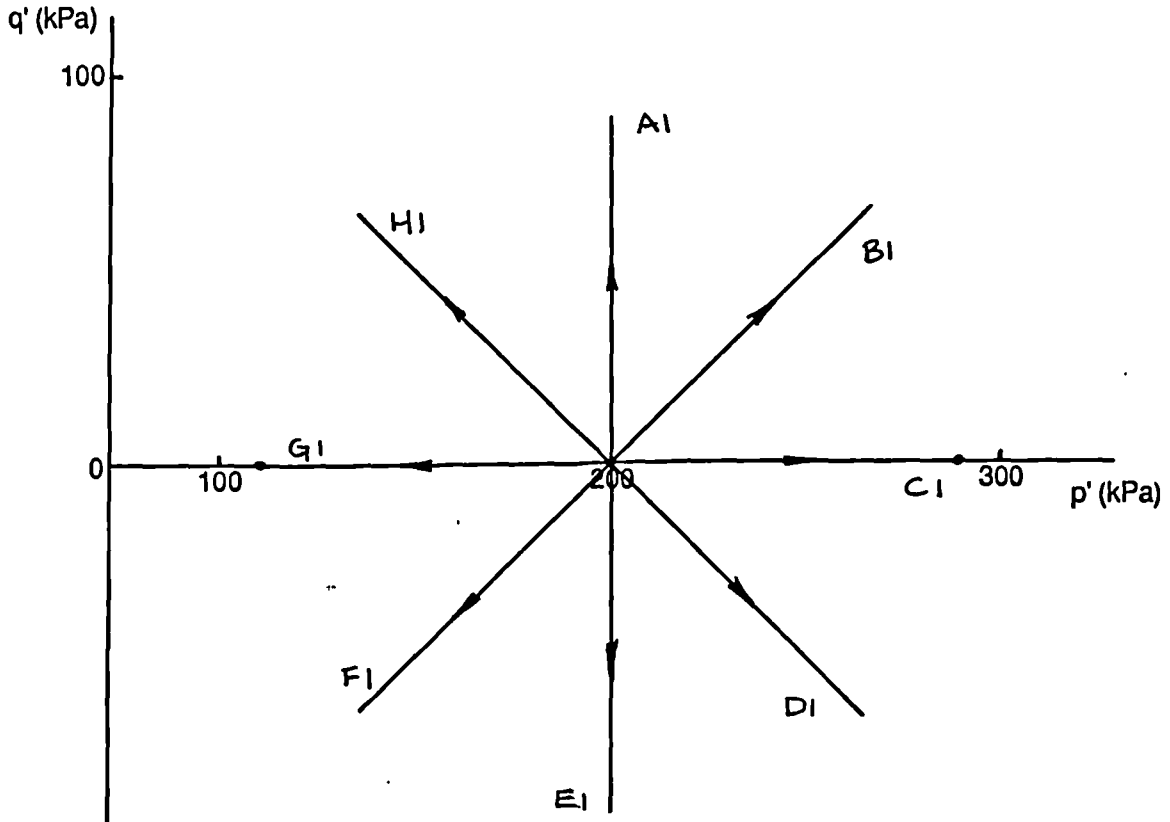

Fig 8.43 Plot of q' against p'. Stress paths followed during path dependence type one tests. $\eta'_o = 0$, OCR = 2.0. All data Figs 8.44 - 8.53.

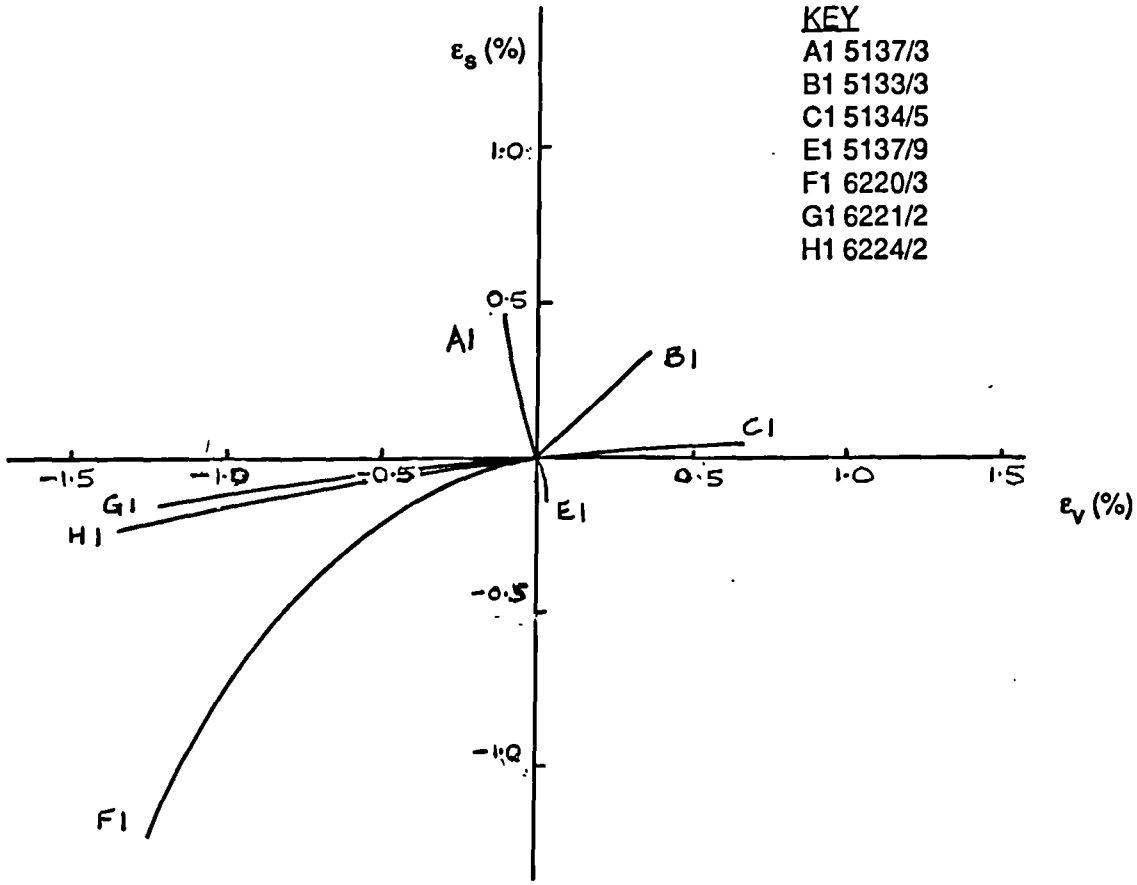

Fig 8.44 Plot of strain paths, ε_s against ε_v for type one path dependence tests on speswhite kaolin.

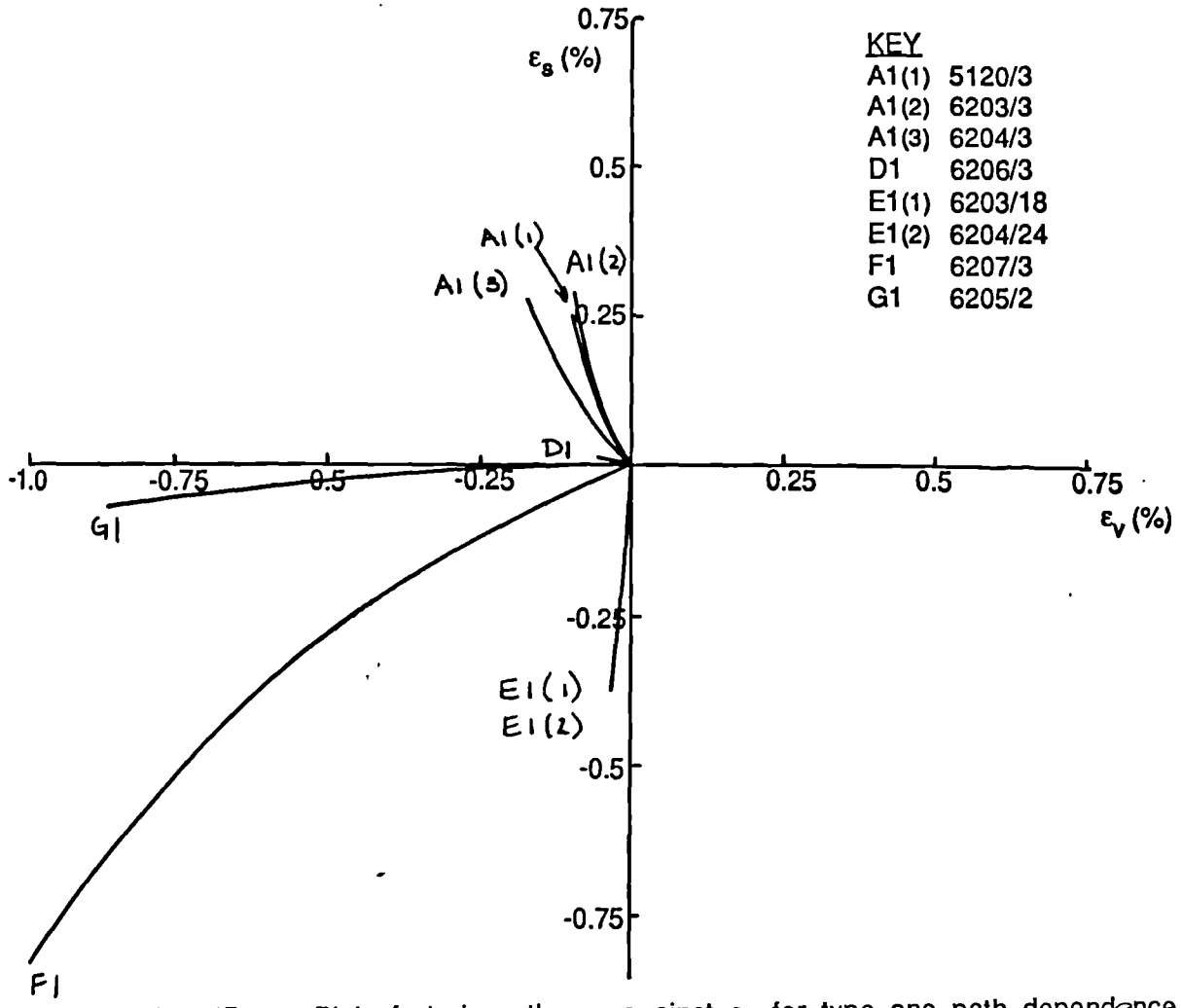

Fig 8.45 Plot of strain paths, ε_s against ε_v for type one path dependence tests on Ware till.

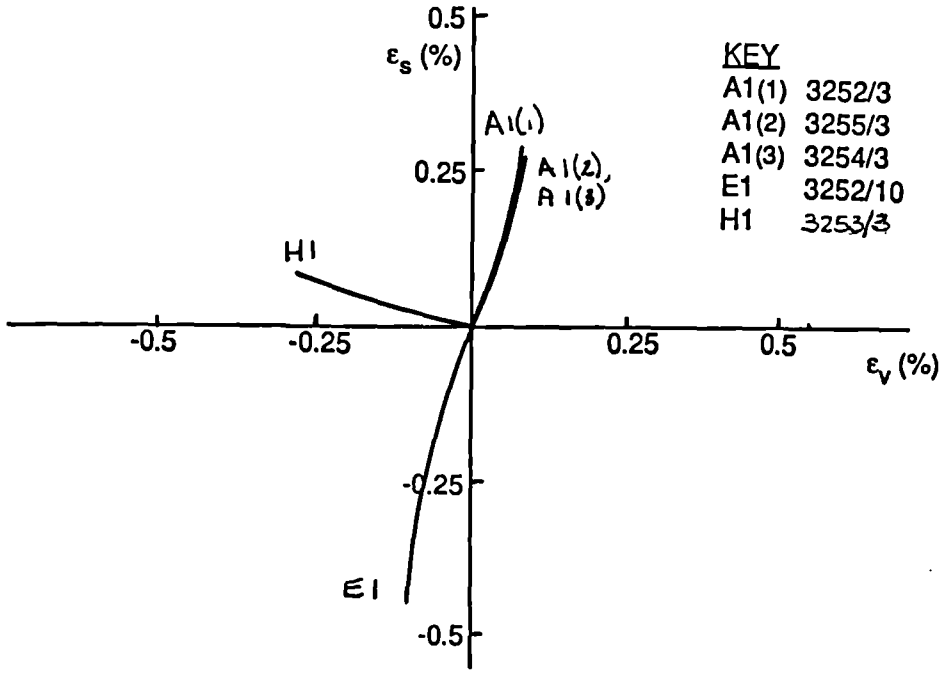

Fig 8.46 Plot of strain paths, ε_s against ε_v for type one path dependence tests on Cowden till.

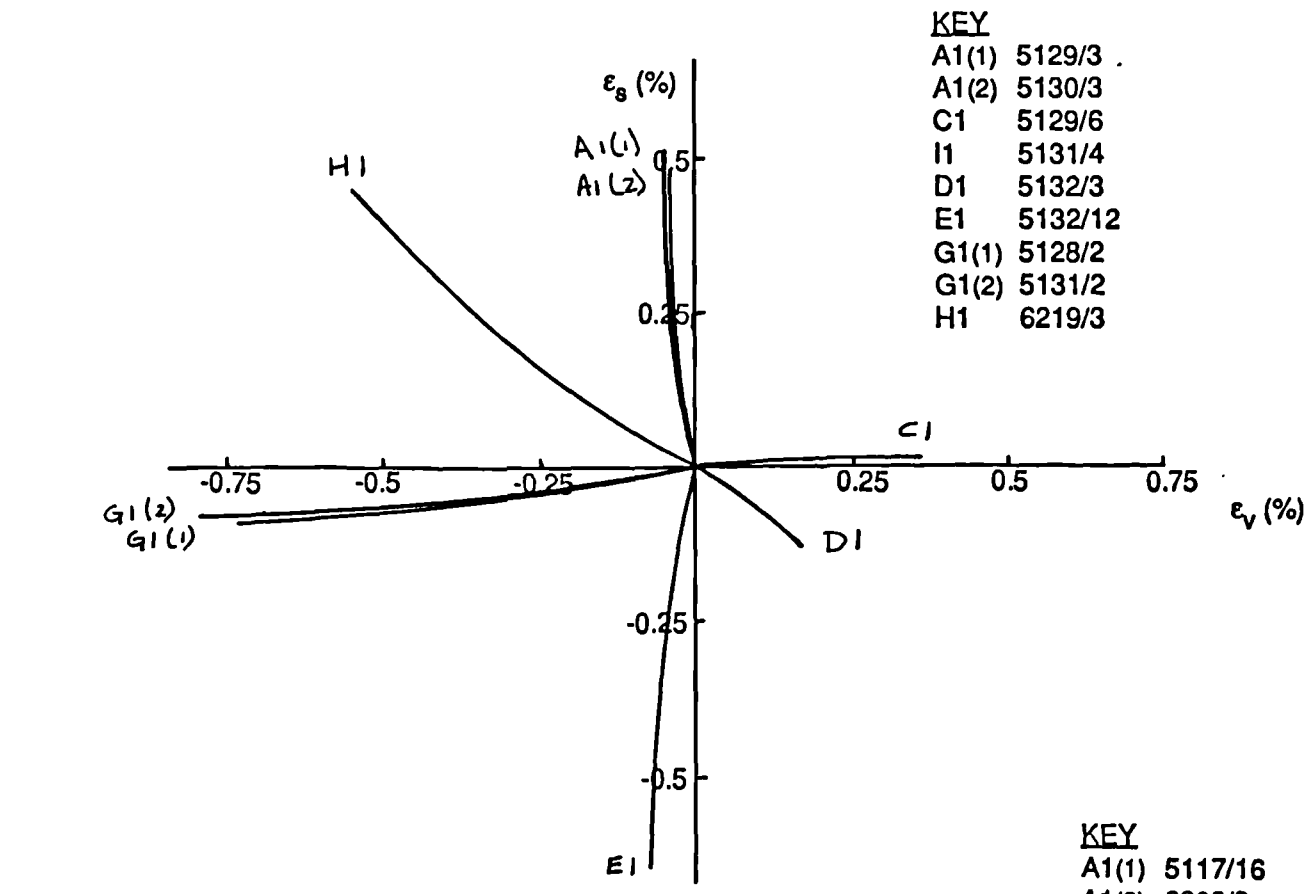

Fig 8.47 Plot of strain paths, ε_s against ε_v for type one path dependence tests on slate dust.

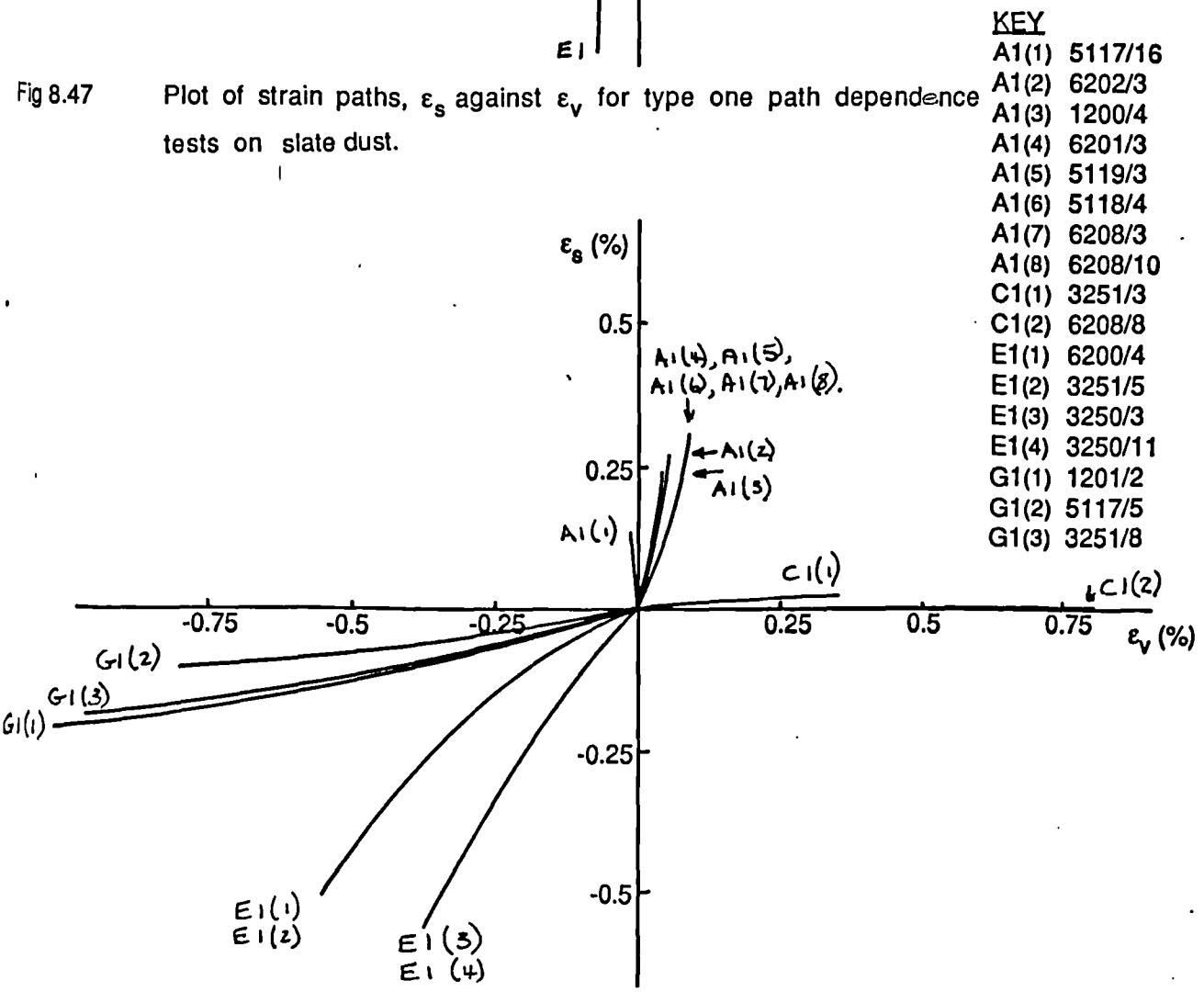

Fig 8.48 Plot of strain paths, ε_s against ε_v for type one path dependence tests on London clay.

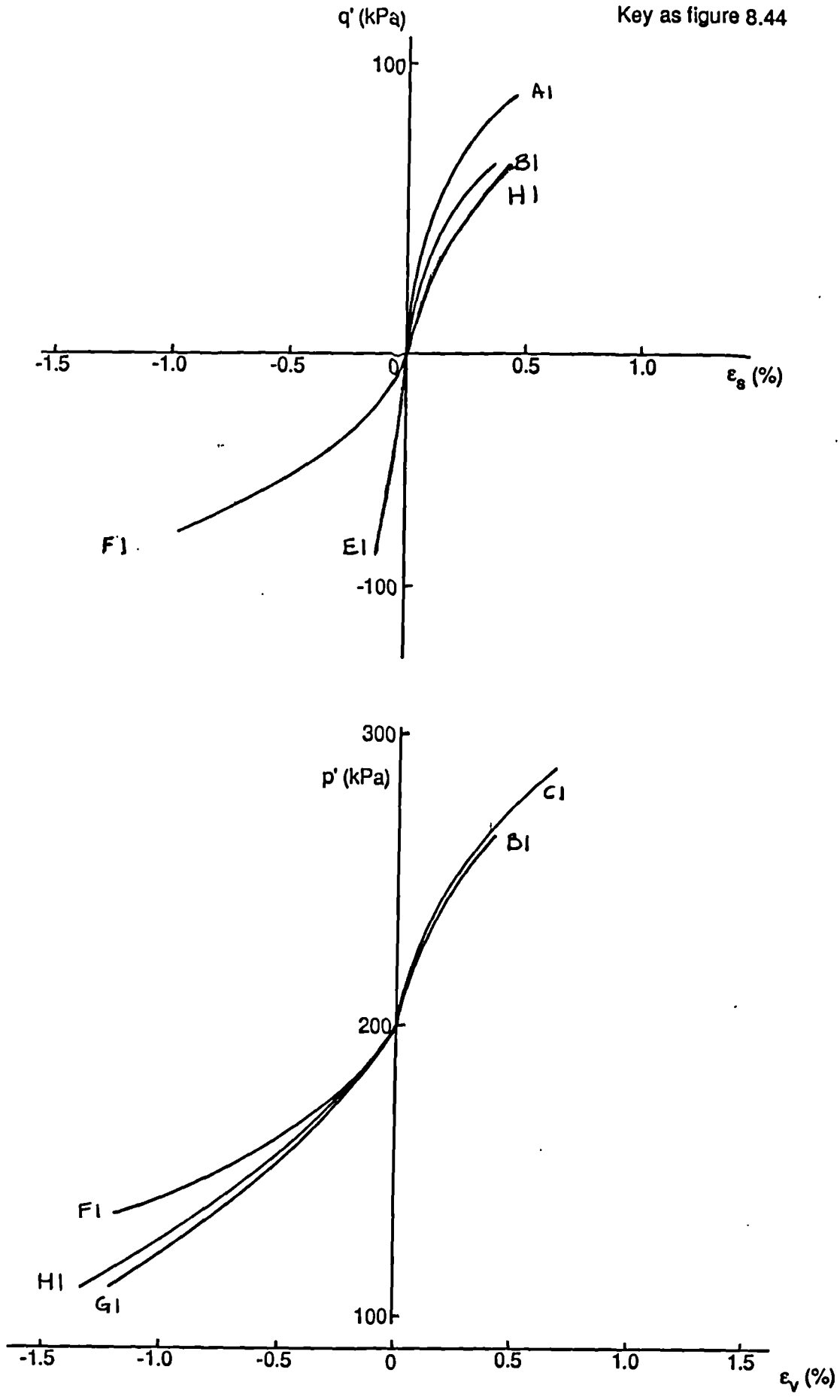

Fig 8.49 Plots of q' against ε_s and p' against ε_v for type one path dependence tests on speswhite kaolin.

Key as figure 8.46

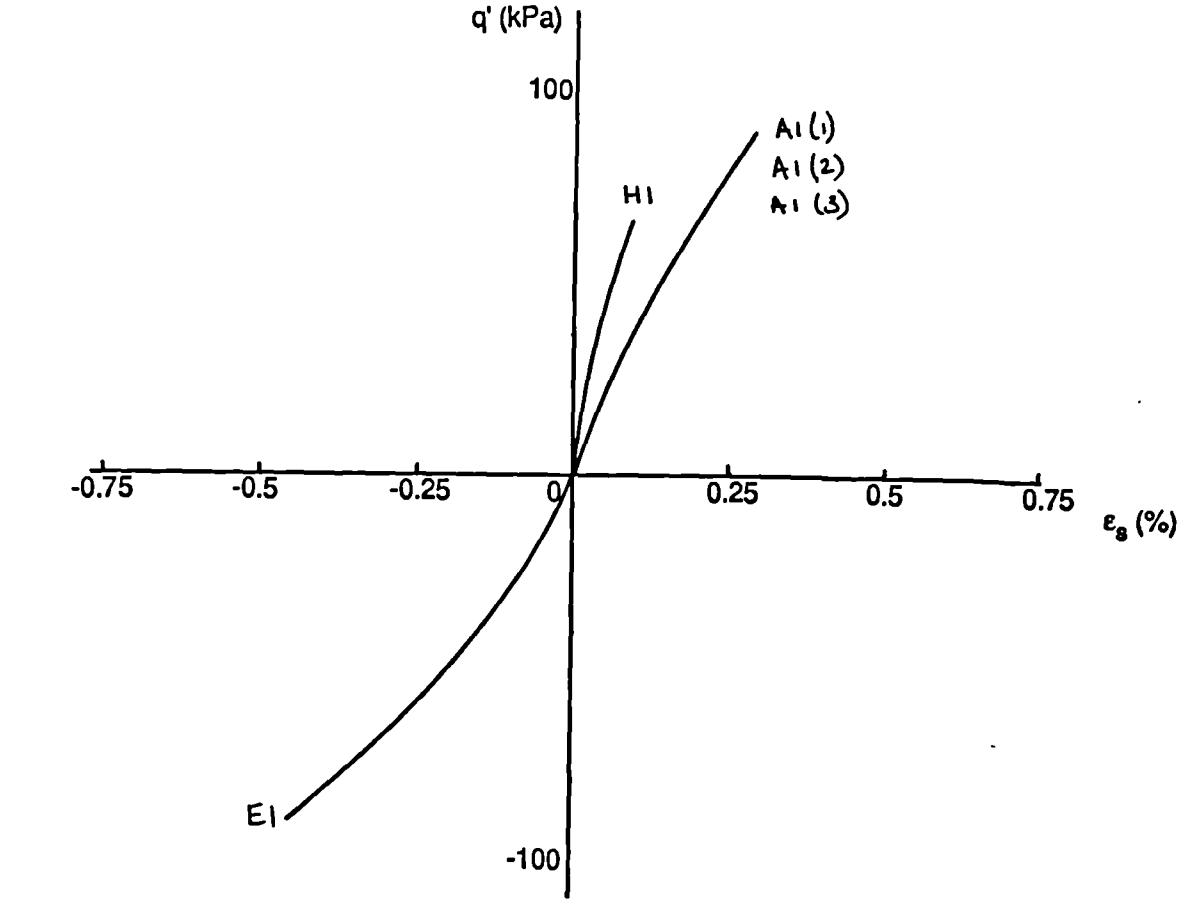

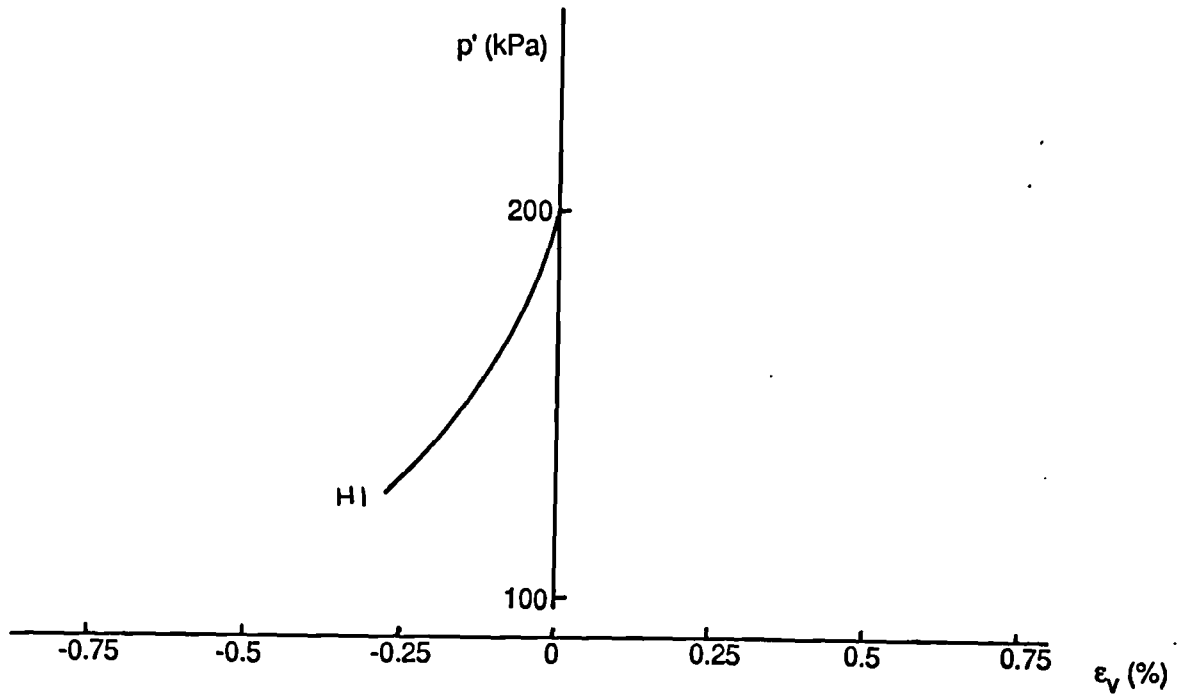

Fig 8.50 Plots of q' against ε_s and p' against ε_v for type one path dependence tests on Ware till.

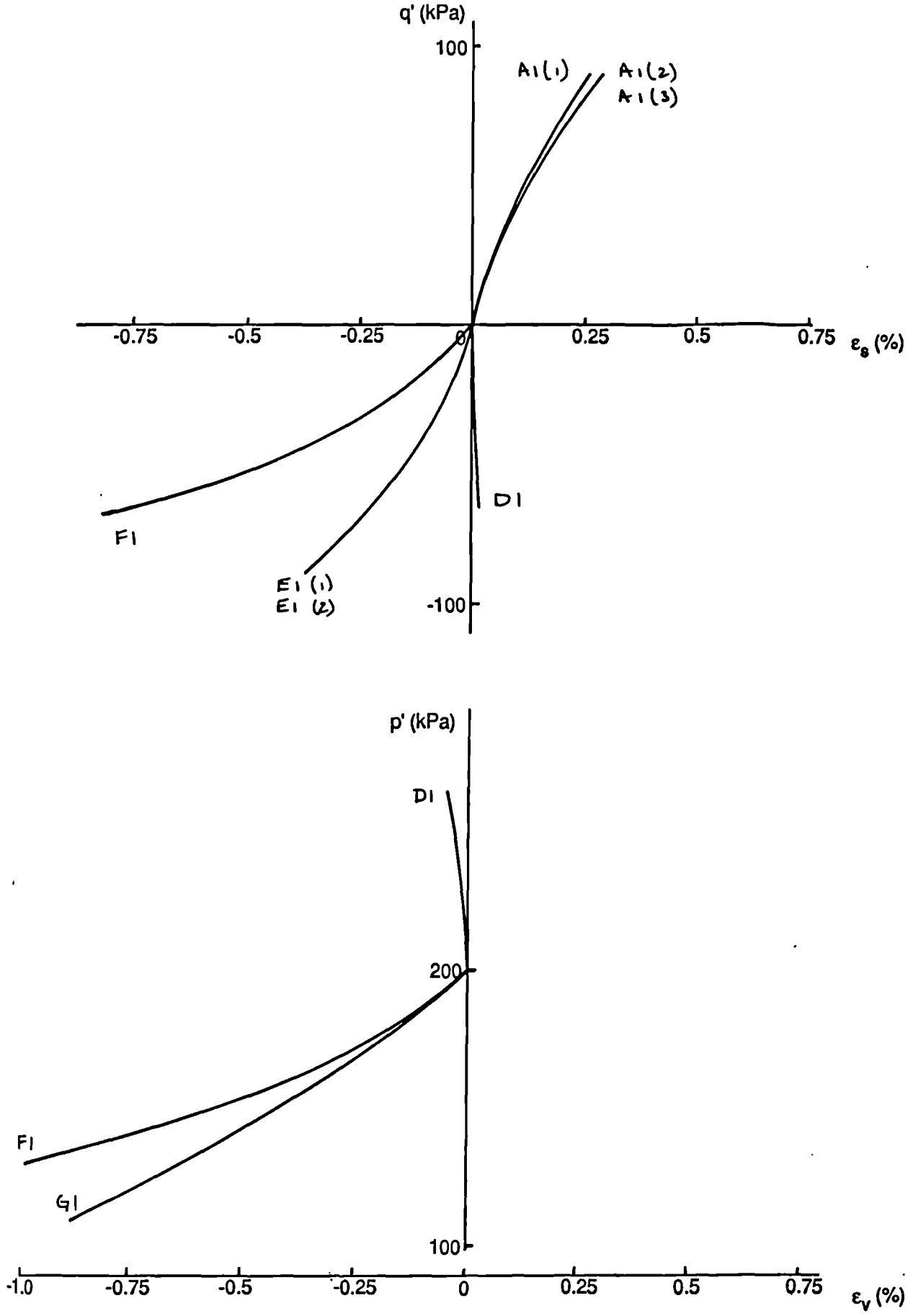

Fig 8.51 Plots of q' against ε_s and p' against ε_v for type one path dependence tests on Cowden till.

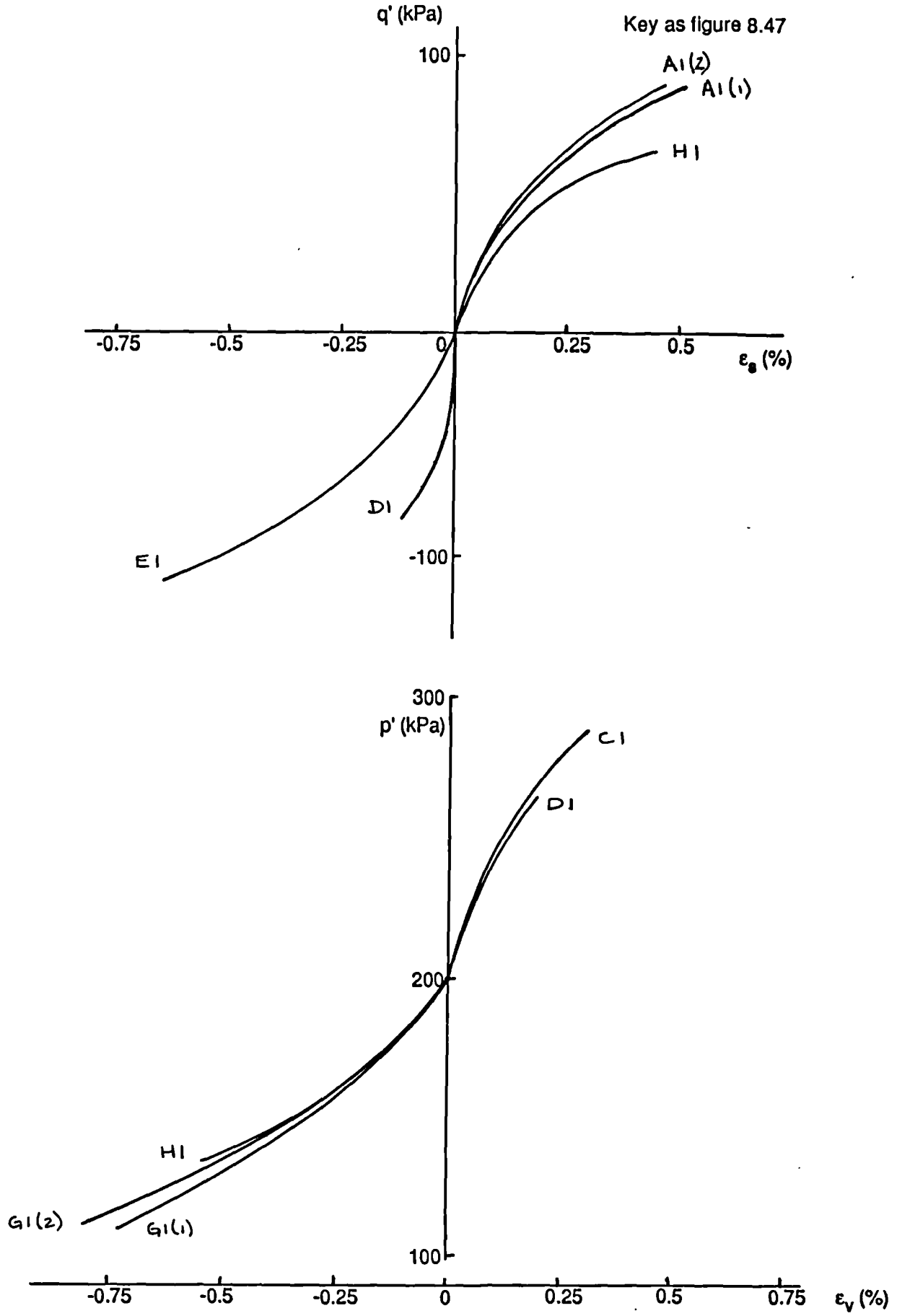

Fig 8.52 Plots of q' against ε_s and p' against ε_v for type one path dependence tests on slate dust.

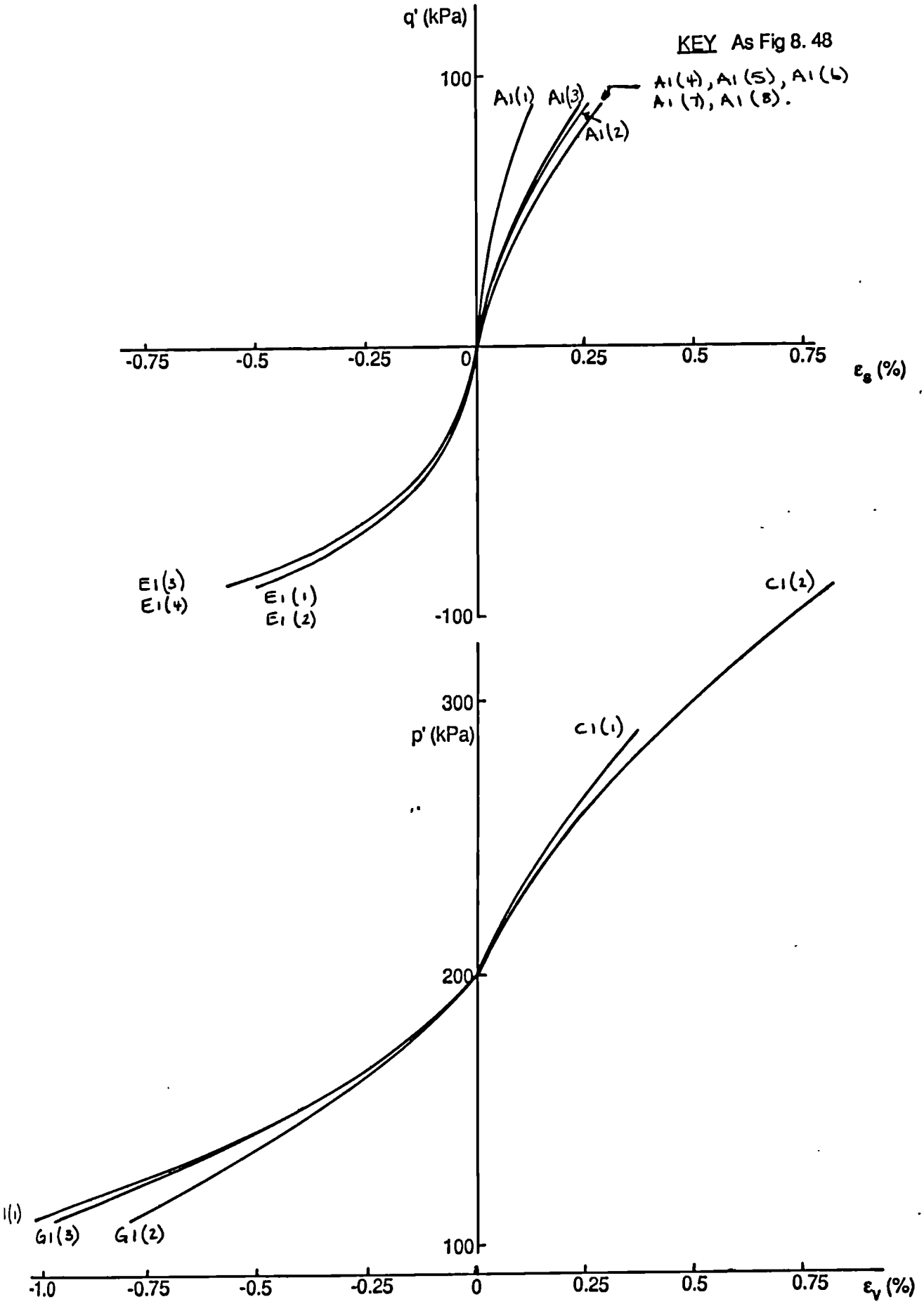

Fig 8.53 Plots of q' against ε_s and p' against ε_v for type one path dependence tests on London clay.

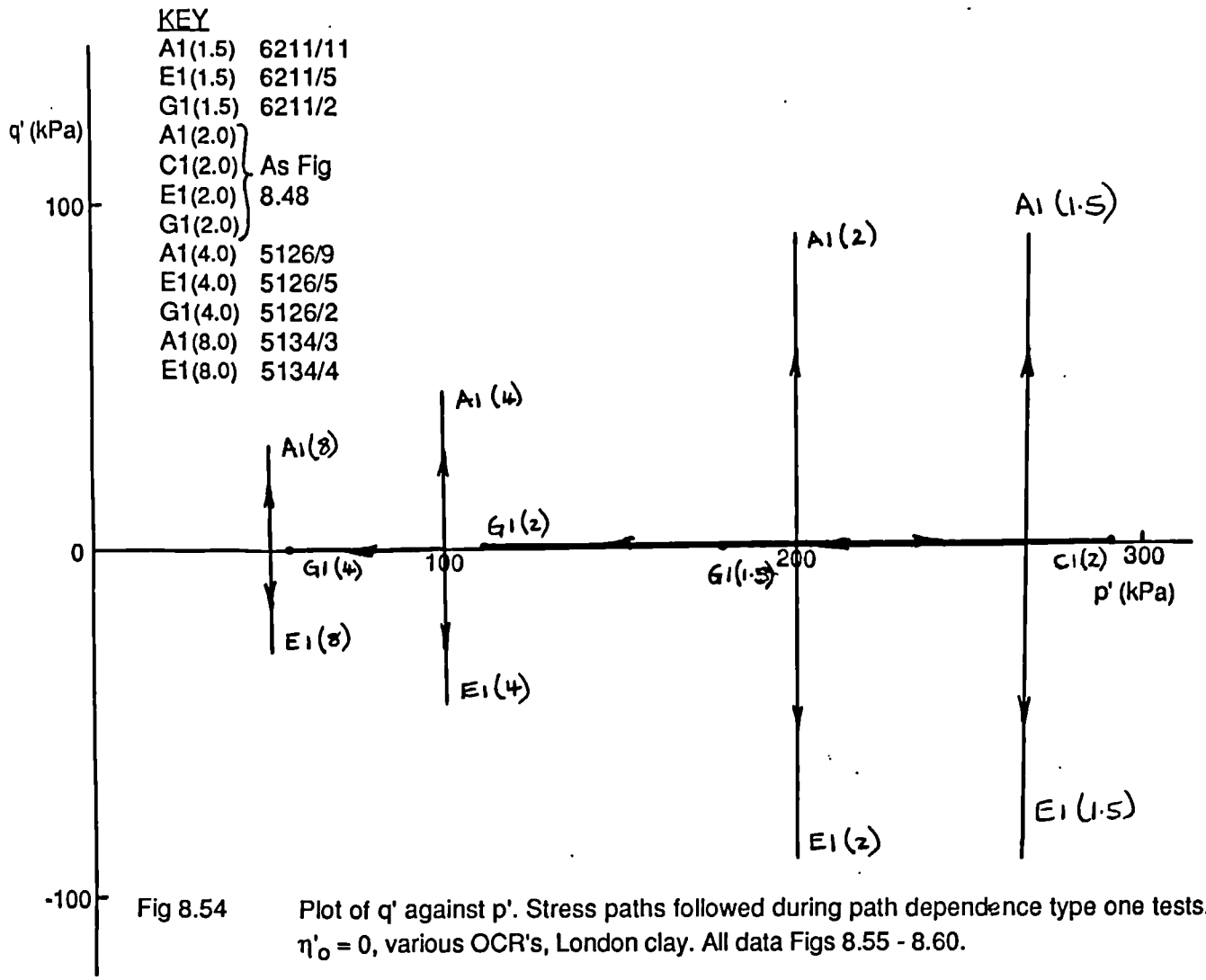

Fig 8.54 Plot of q' against p'. Stress paths followed during path dependence type one tests. $\eta'_o = 0$, various OCR's, London clay. All data Figs 8.55 - 8.60.

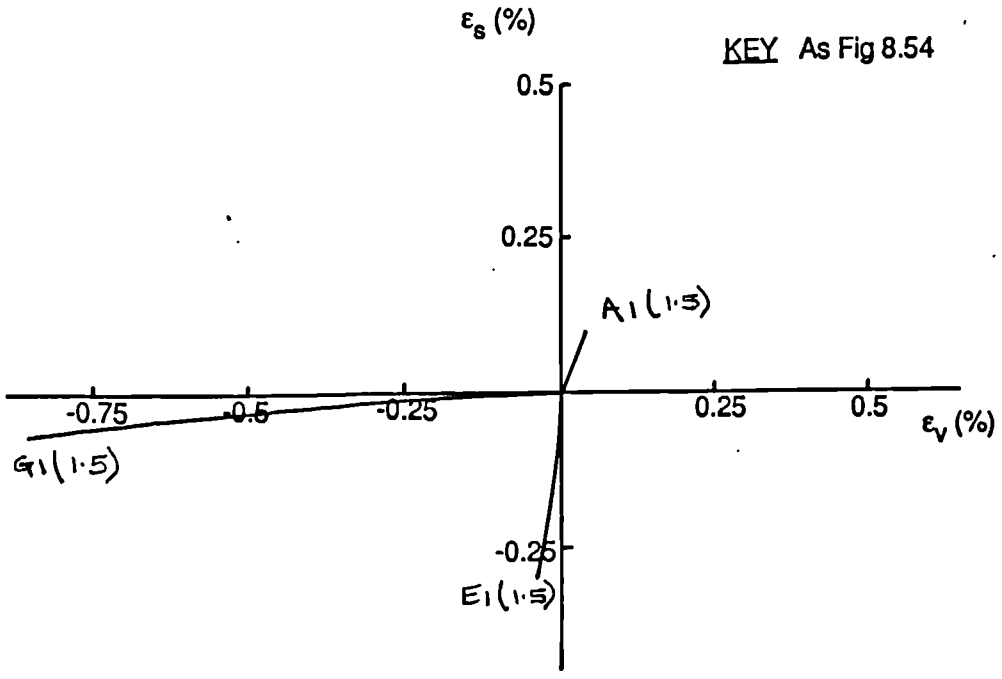

Fig 8.55 Plot of strain paths, ε_s against ε_v for type one path dependence tests o London clay, OCR = 1.5.

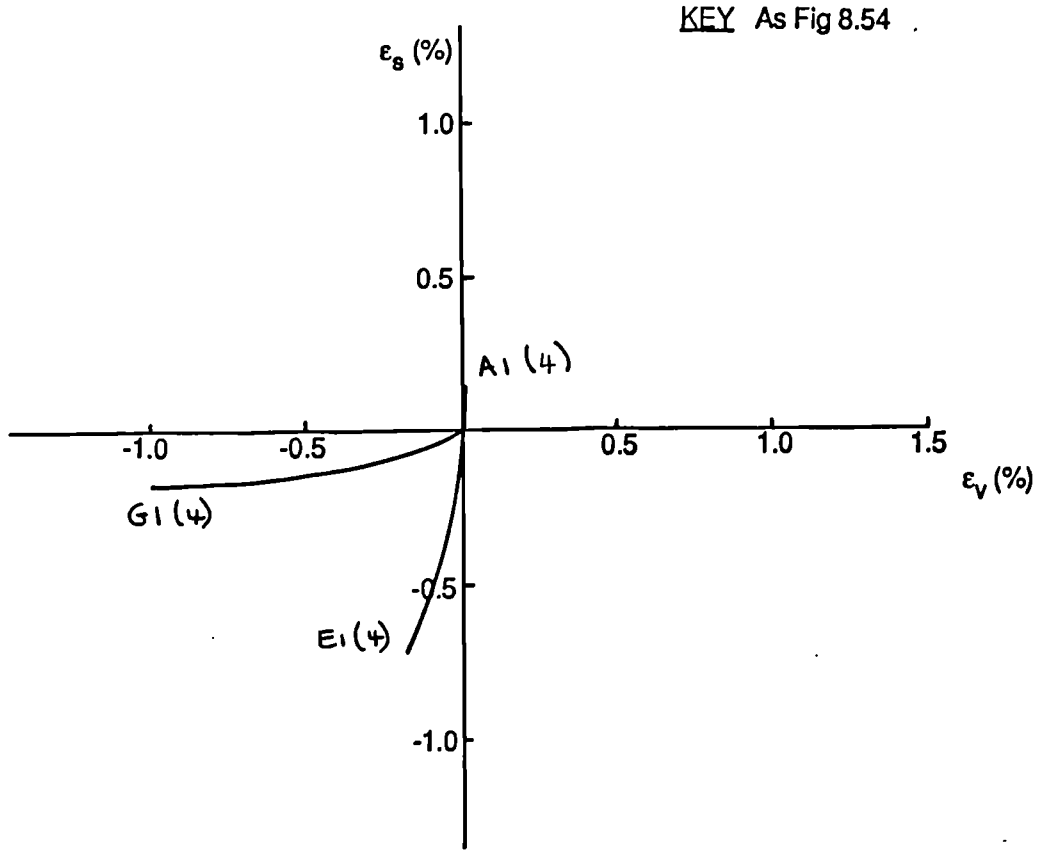

Fig 8.56 Plot of strain paths, ε_s against ε_v for type one path dependence tests on London clay, OCR = 4.0.

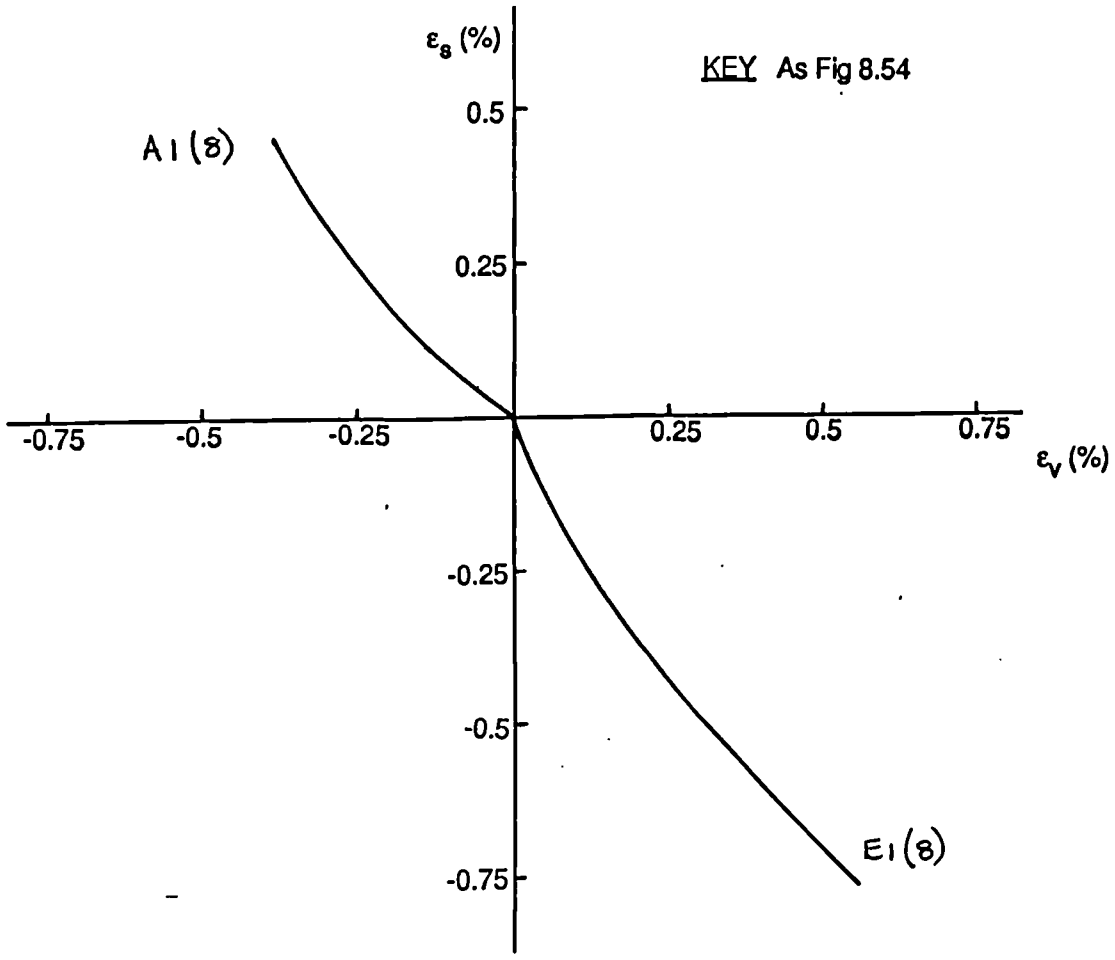

Fig 8.57 Plot of strain paths, ε_s against ε_v for type one path dependence tests on London clay, OCR = 8.

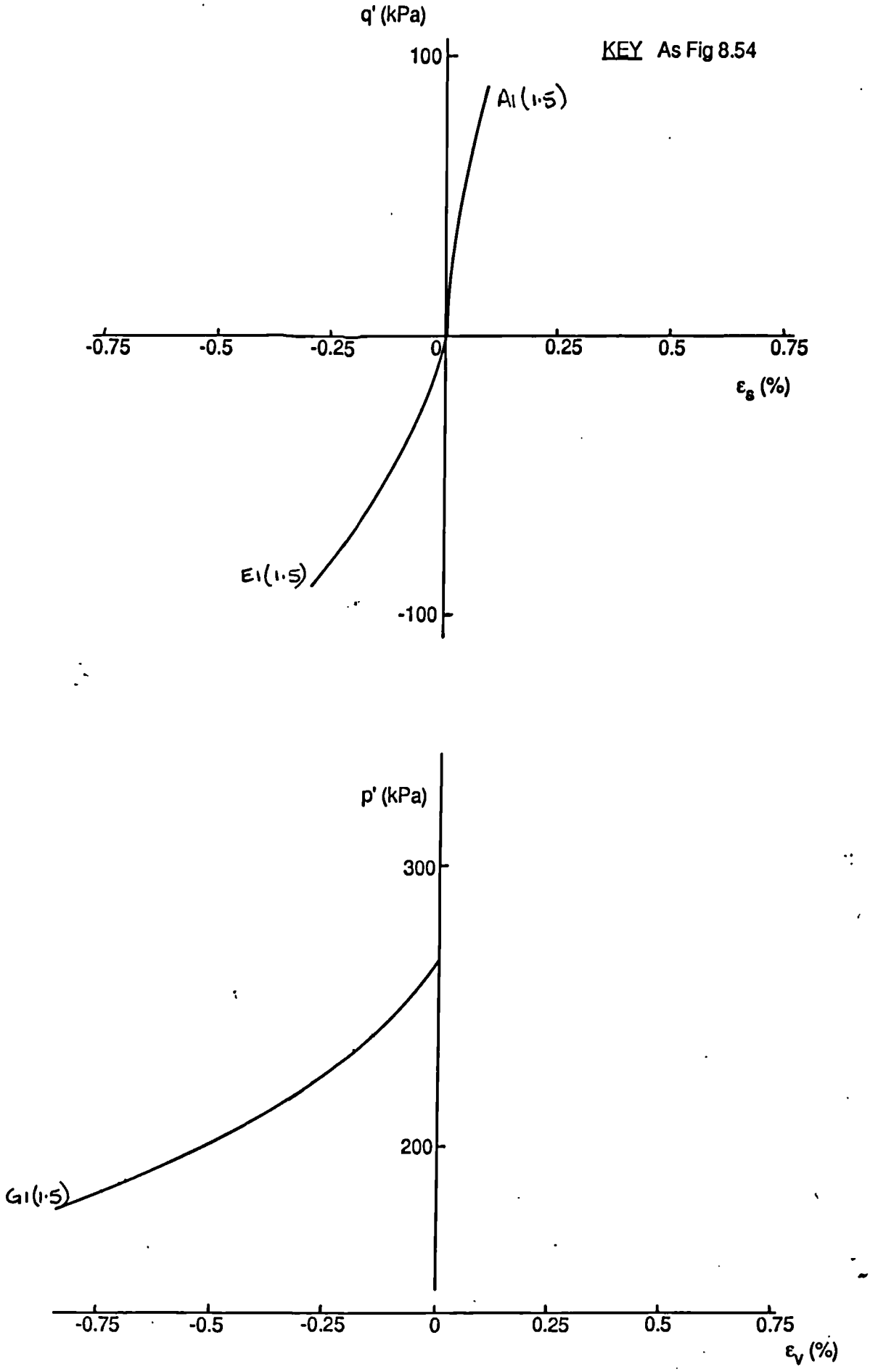

Fig 8.58 Plots of q' against ε_s and p' against ε_v for type one path dependence tests on London clay, OCR = 1.5.

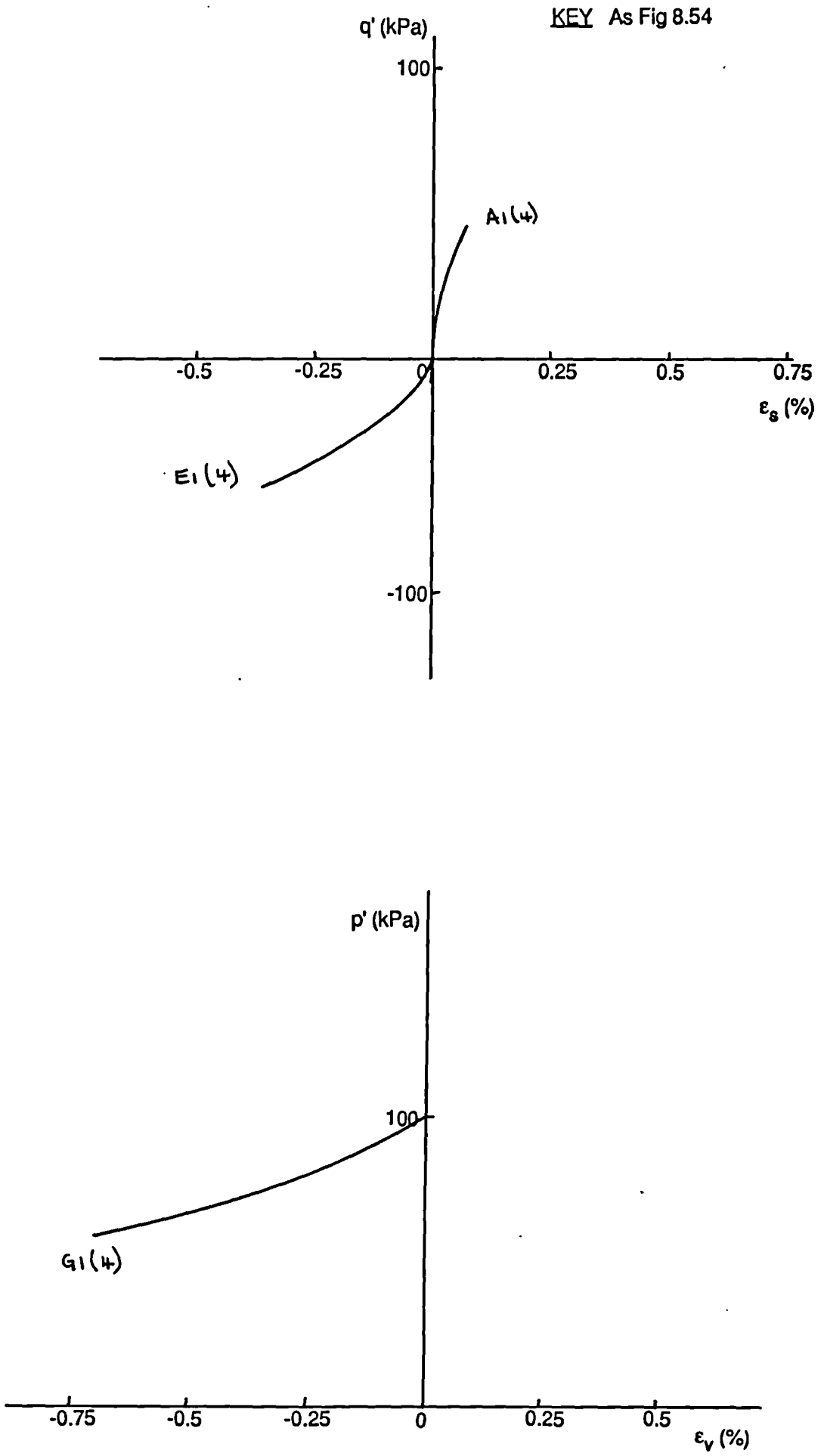

Fig 8.59 Plots of q' against ε_s and p' against ε_v for type one path dependence tests on London clay, OCR = 4.0.

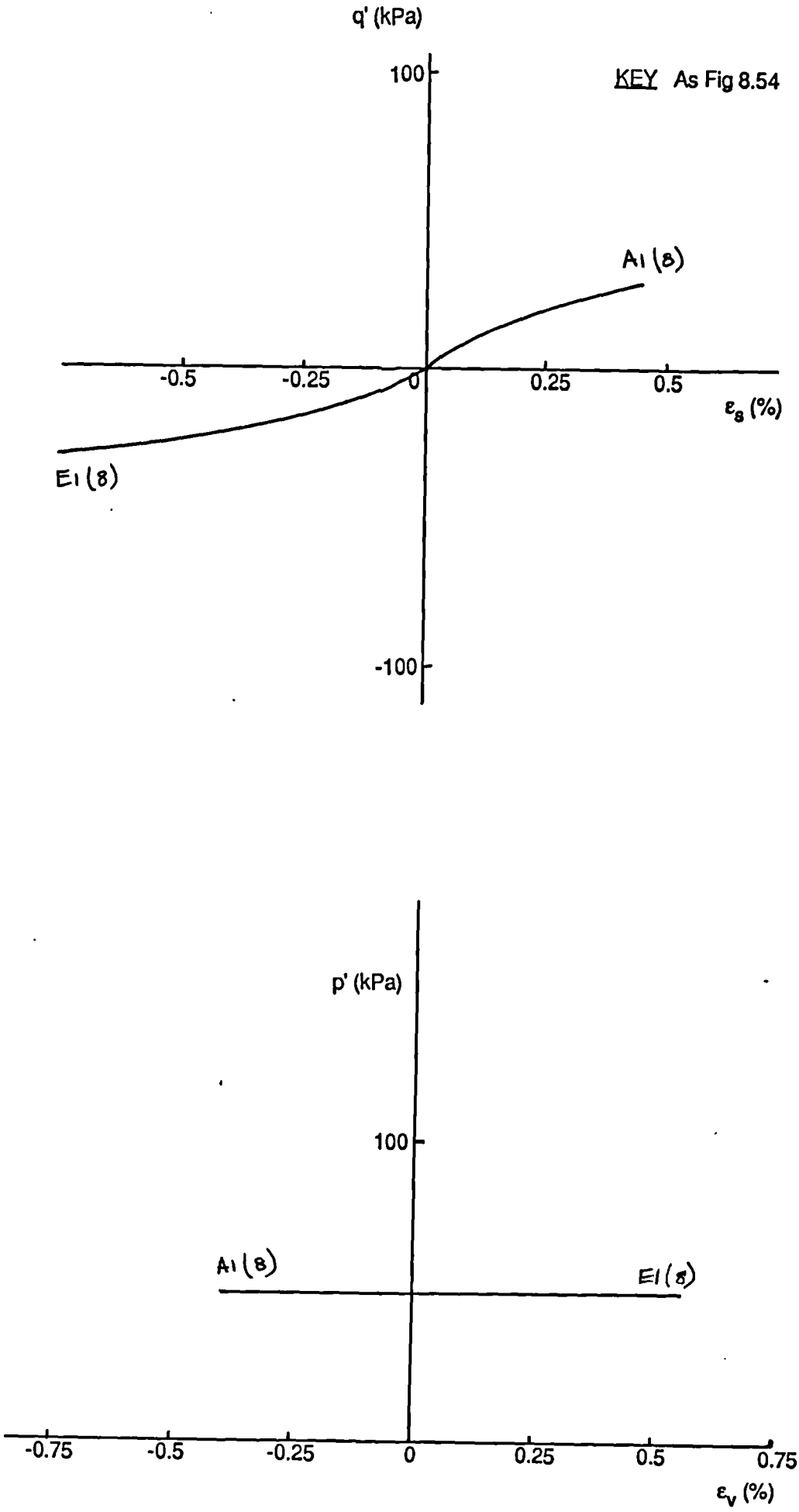

Fig 8.60 Plots of q' against ε_s and p' against ε_v for type one path dependence tests on London clay, OCR = 8.0.

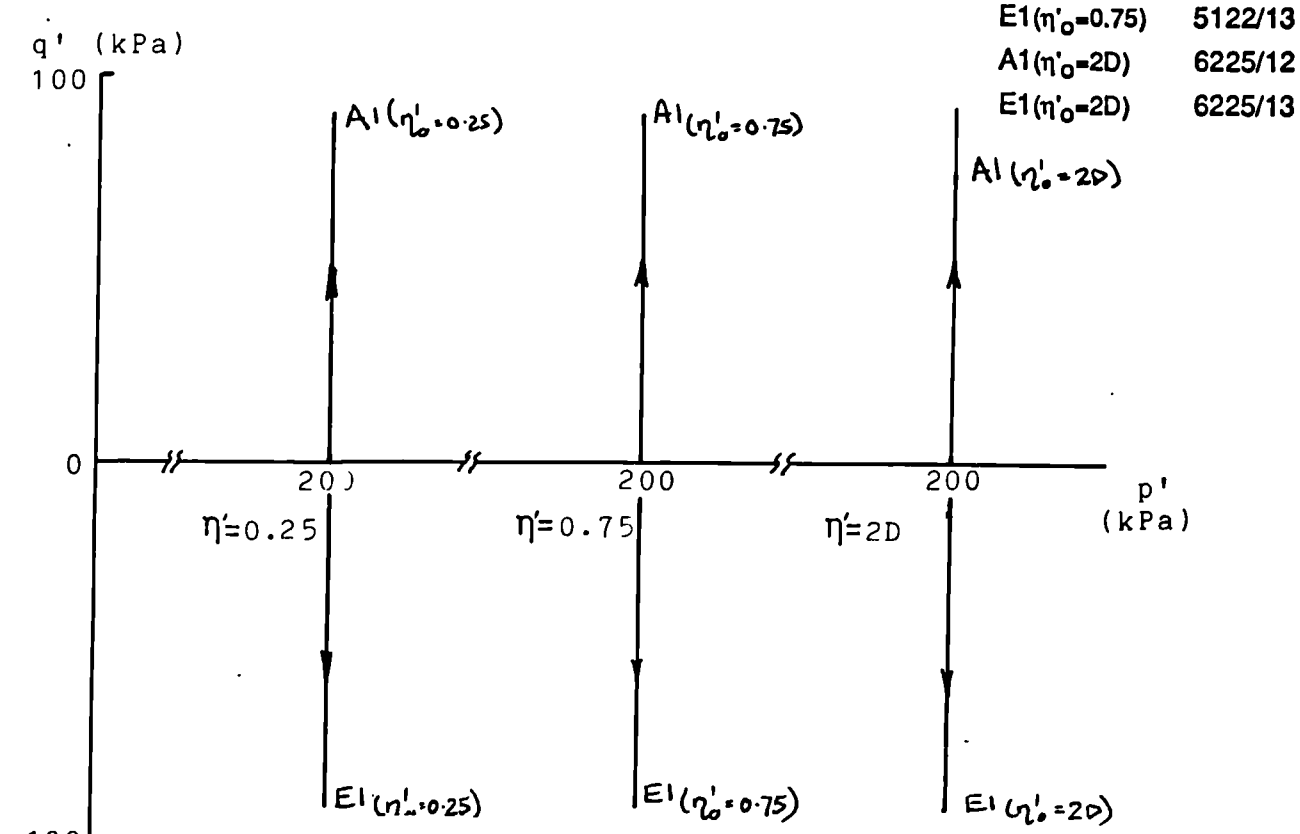

Fig 8.61 Plot of q' against p'. Stress paths followed during type one path dependence tests. Various stress histories, OCR = 2.0, p' = 200kPa. London clay . All data Figs 8.62 - 8.67.

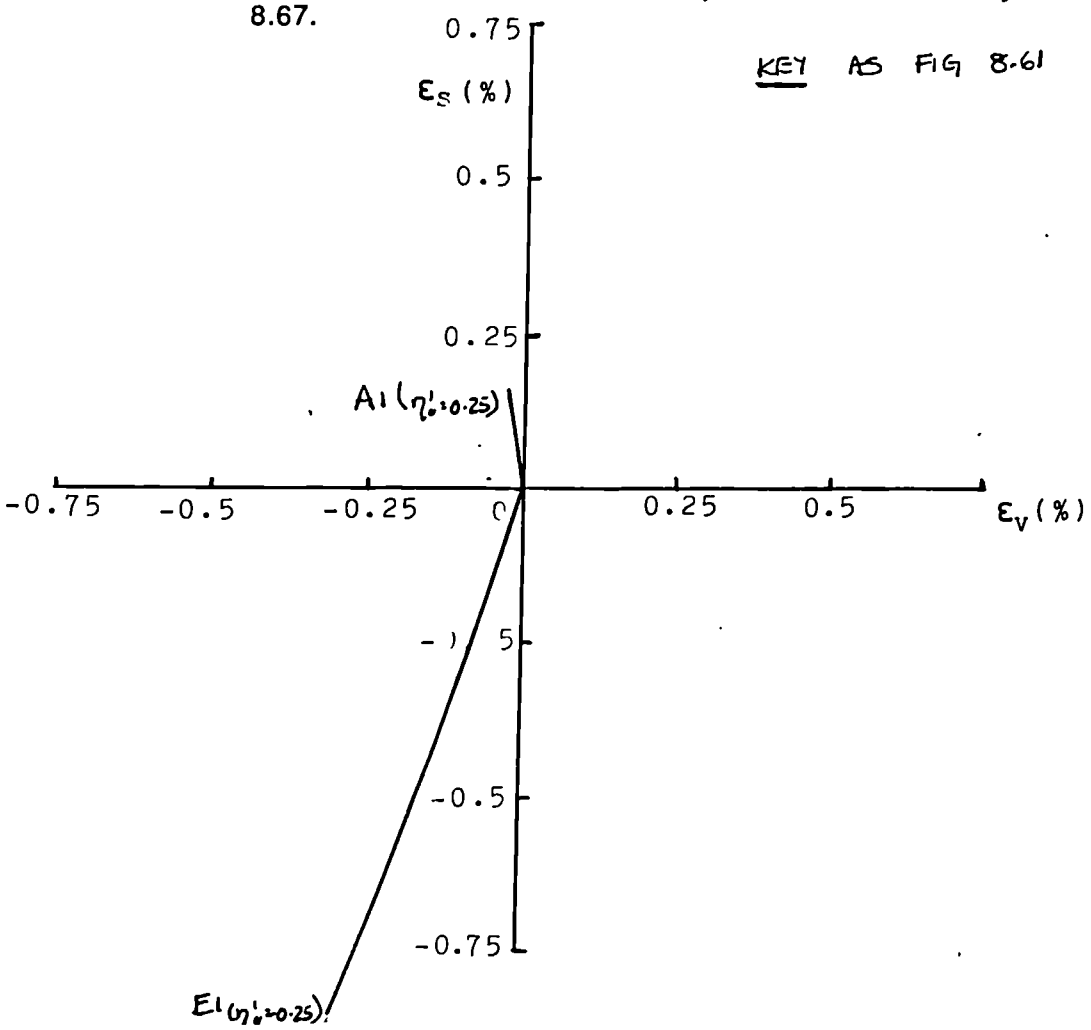

Fig 8.62 Plot of strain paths, ε_s against ε_v for type one path dependence tests on London clay, $\eta'_o = 0.25$.

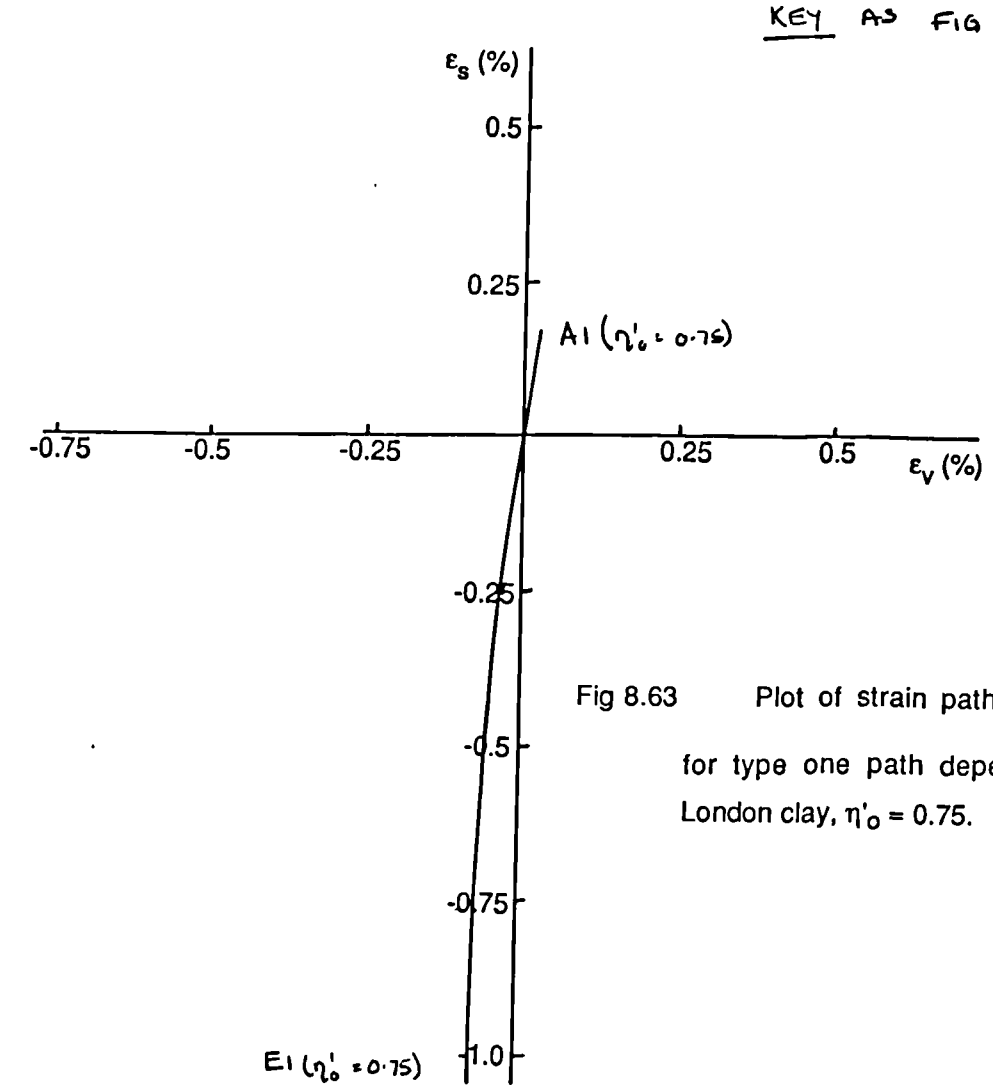

Fig 8.63 Plot of strain paths, ε_s against ε_v for type one path dependence tests on London clay, $\eta'_o = 0.75$.

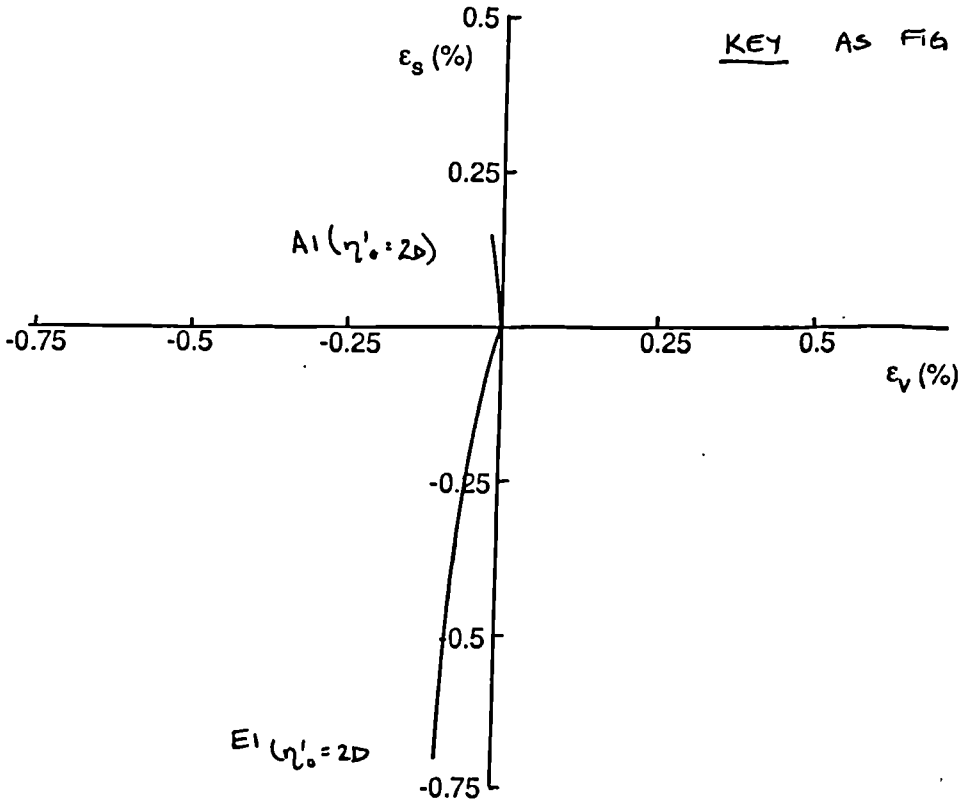

Fig 8.64 Plot of strain paths, ε_s against ε_v for type one path dependence tests on London clay, two dimensionally compressed.

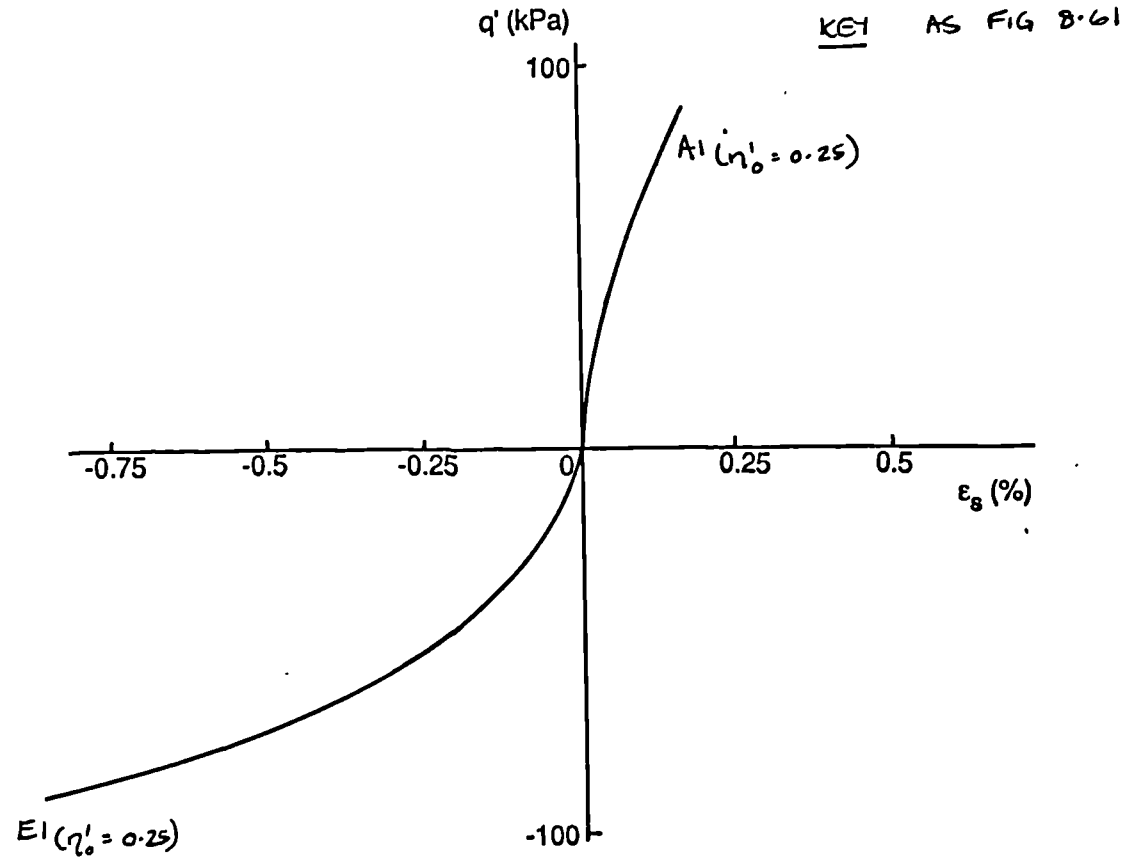

Fig 8.65 Plot of q' against ε_s for type one path dependence tests on London clay, $\eta'_o = 0.25$.

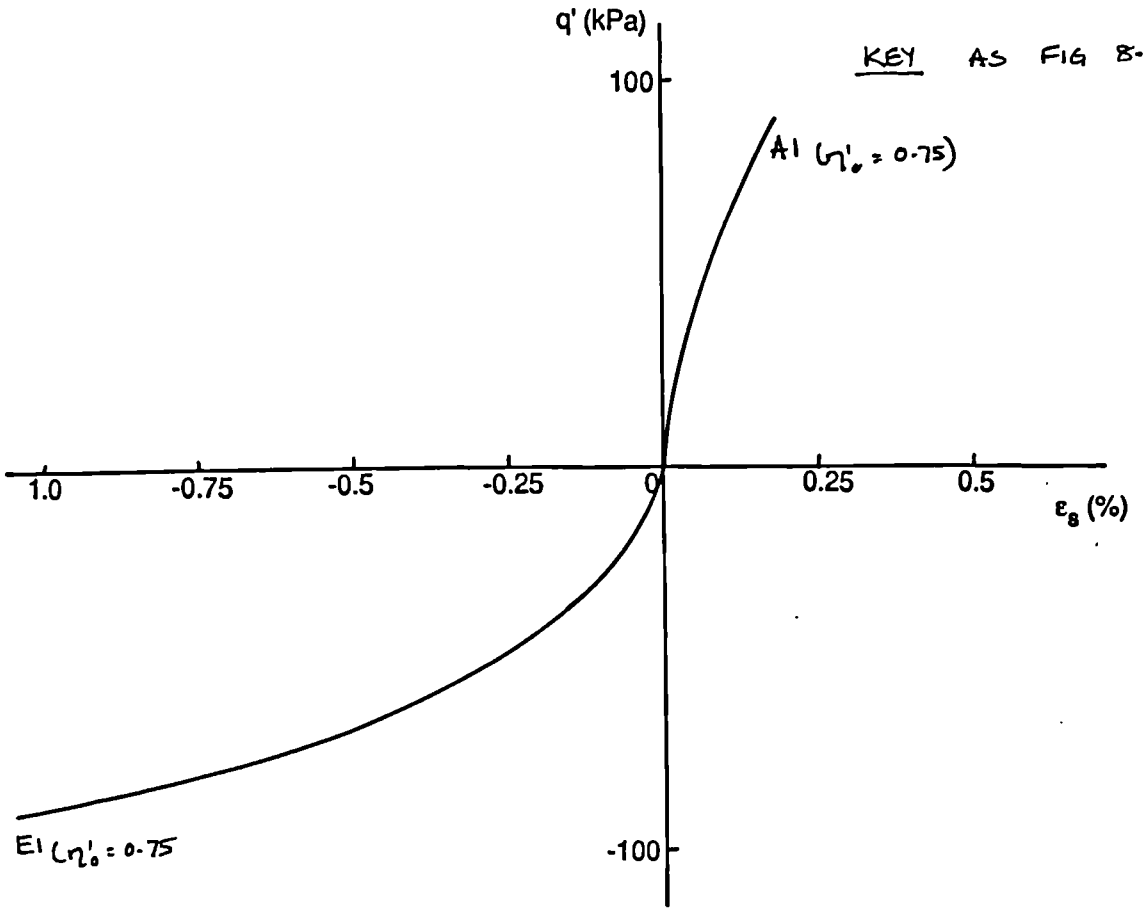

Fig 8.66 Plot of q' against ε_s for type one path dependence tests on London clay, $\eta'_o = 0.75$.

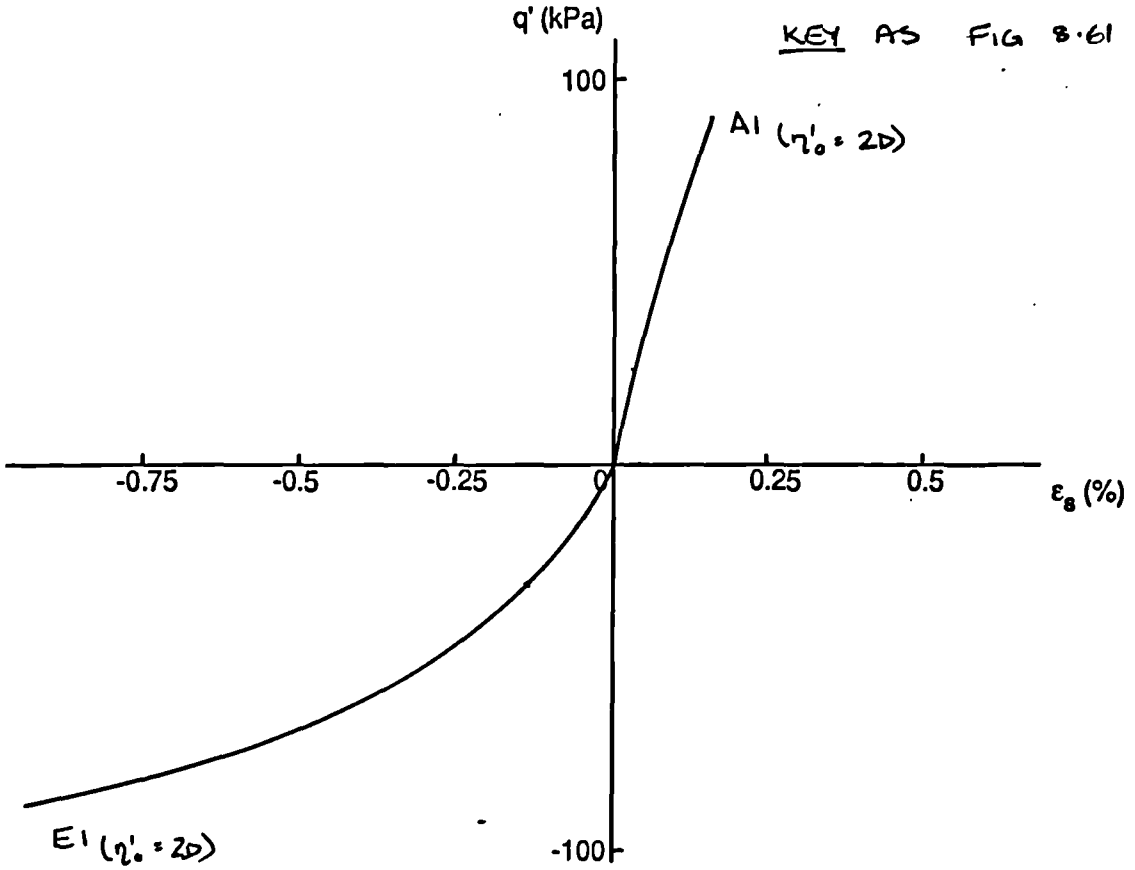

Fig 8.67 Plot of q' against ε_s for type one path dependence tests on London clay, two dimensionally compressed .

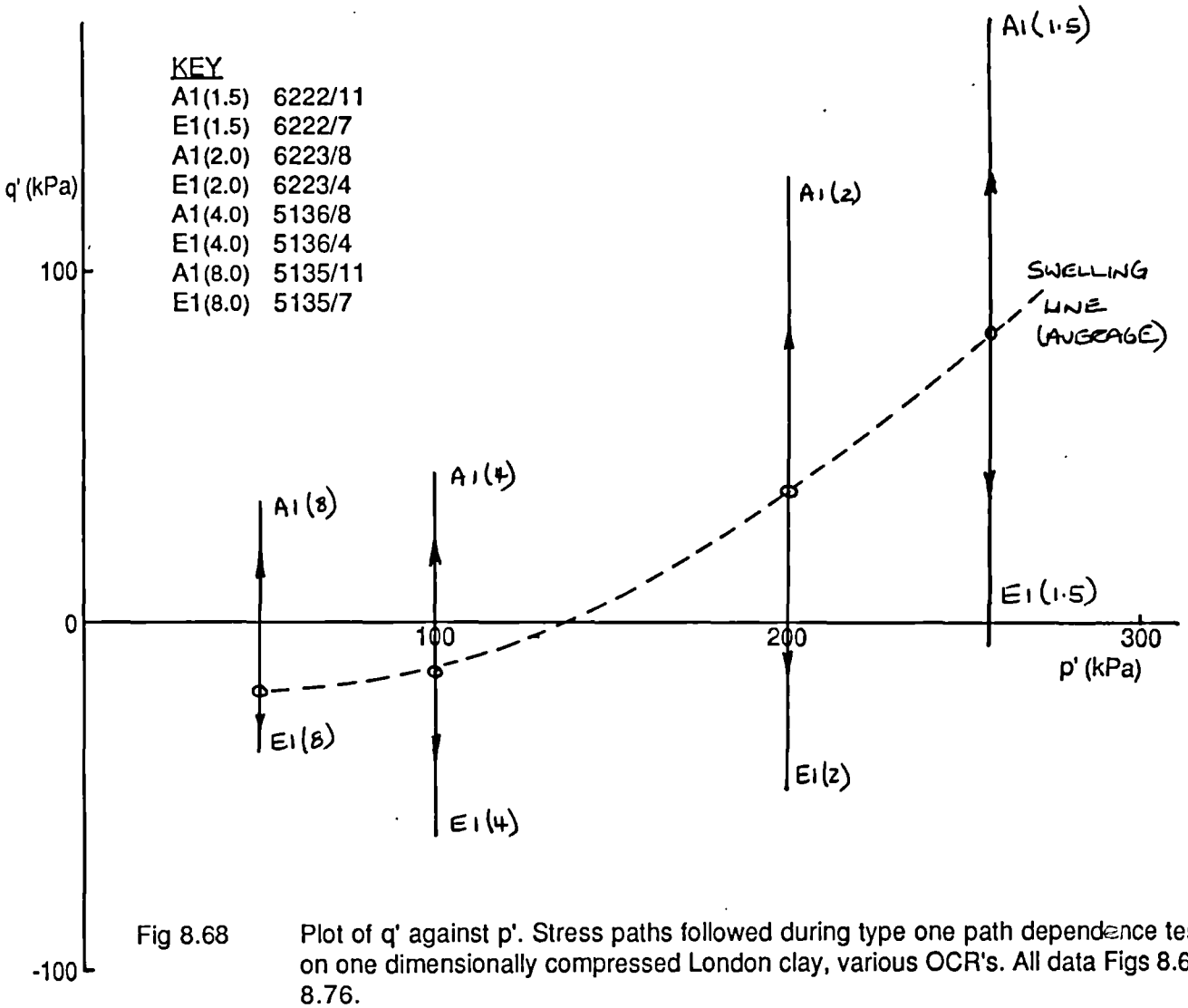

Fig 8.68 Plot of q' against p'. Stress paths followed during type one path dependence tests on one dimensionally compressed London clay, various OCR's. All data Figs 8.69 - 8.76.

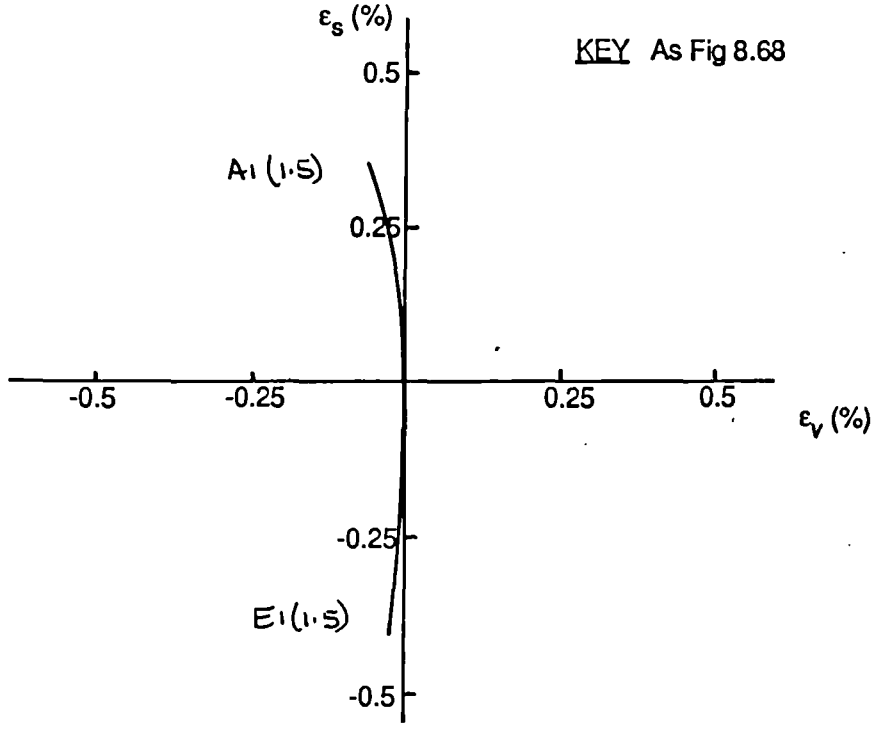

Fig 8.69 Plot of strain paths, ε_s against ε_v for type one path dependence tests on one dimensionally compressed London clay, OCR = 1.5.

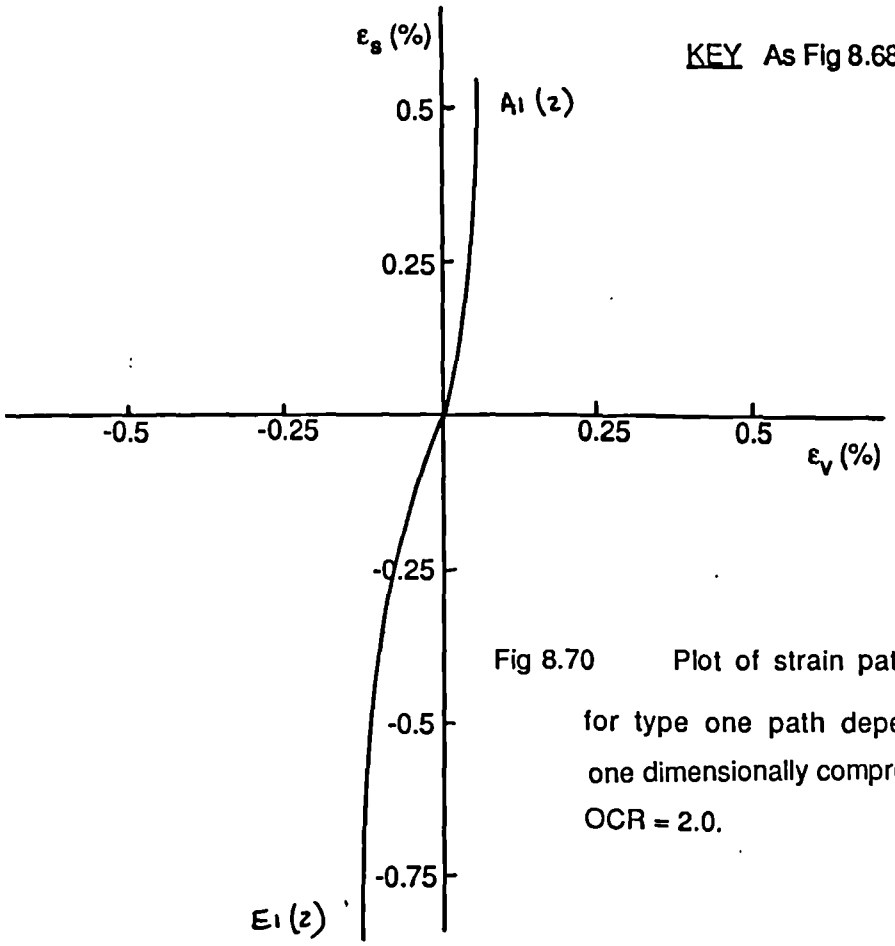

Fig 8.70 Plot of strain paths, ε_s against ε_v for type one path dependence tests on one dimensionally compressed London clay, OCR = 2.0.

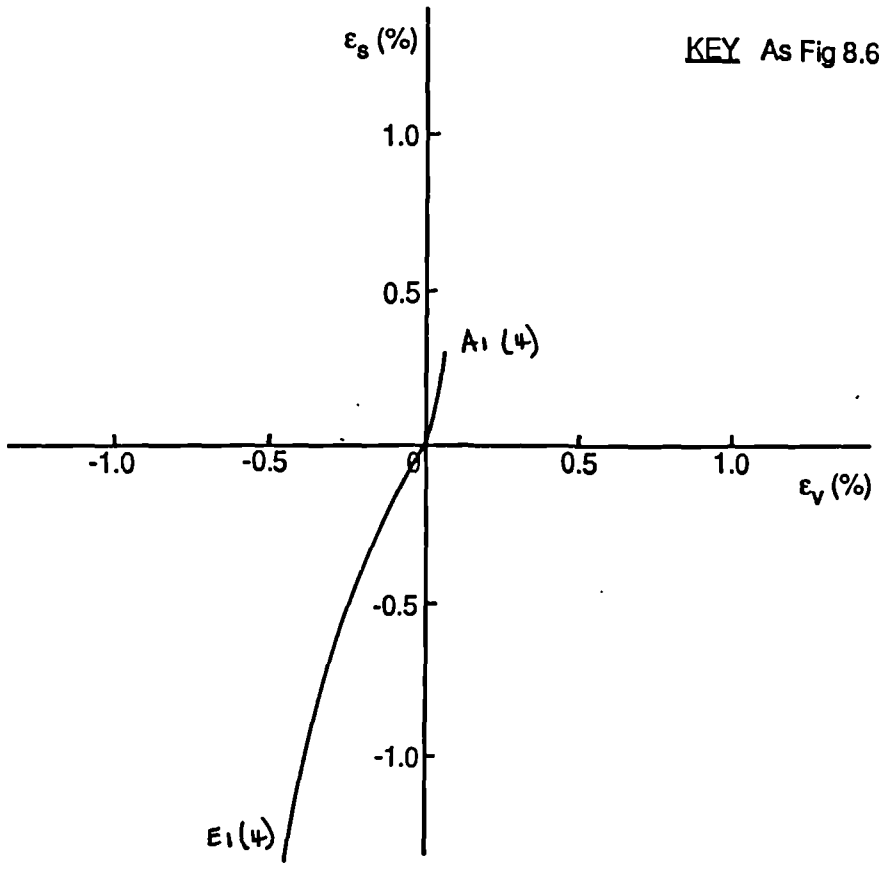

Fig 8.71 Plot of strain paths, ε_s against ε_v for type one path dependence tests on one dimensionally compressed London clay, OCR = 4.0.

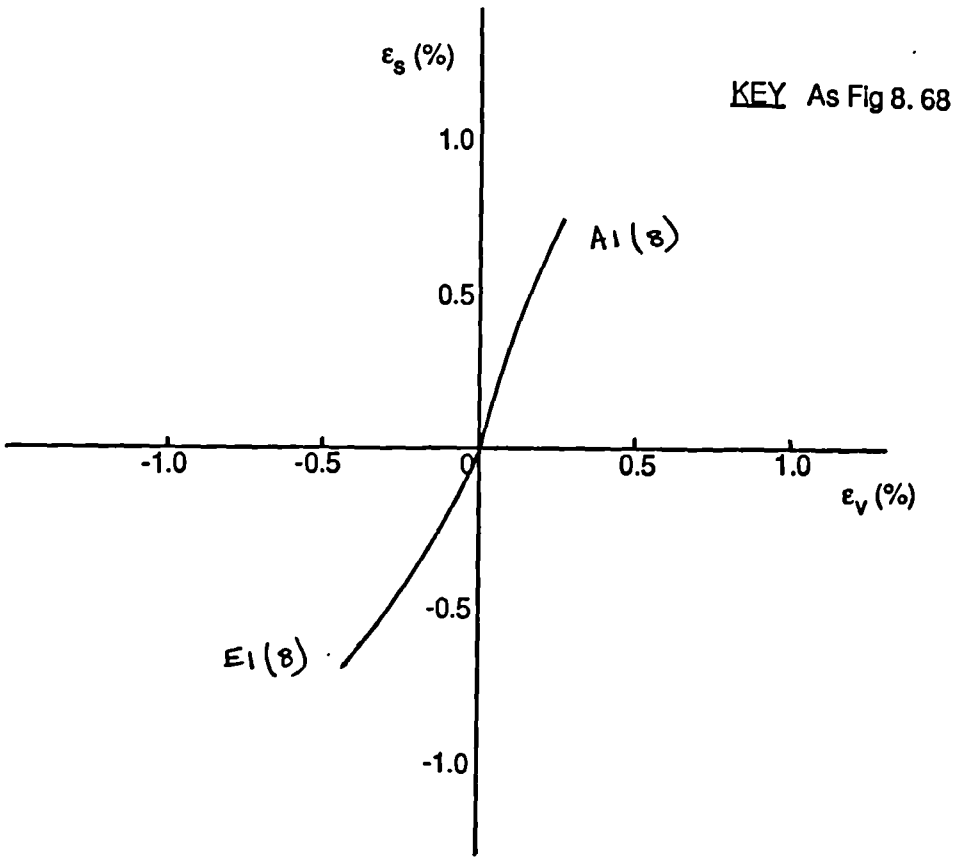

Fig 8.72 Plot of strain paths, ε_s against ε_v for type one path dependence tests on one dimensionally compressed London clay, OCR = 8.0.

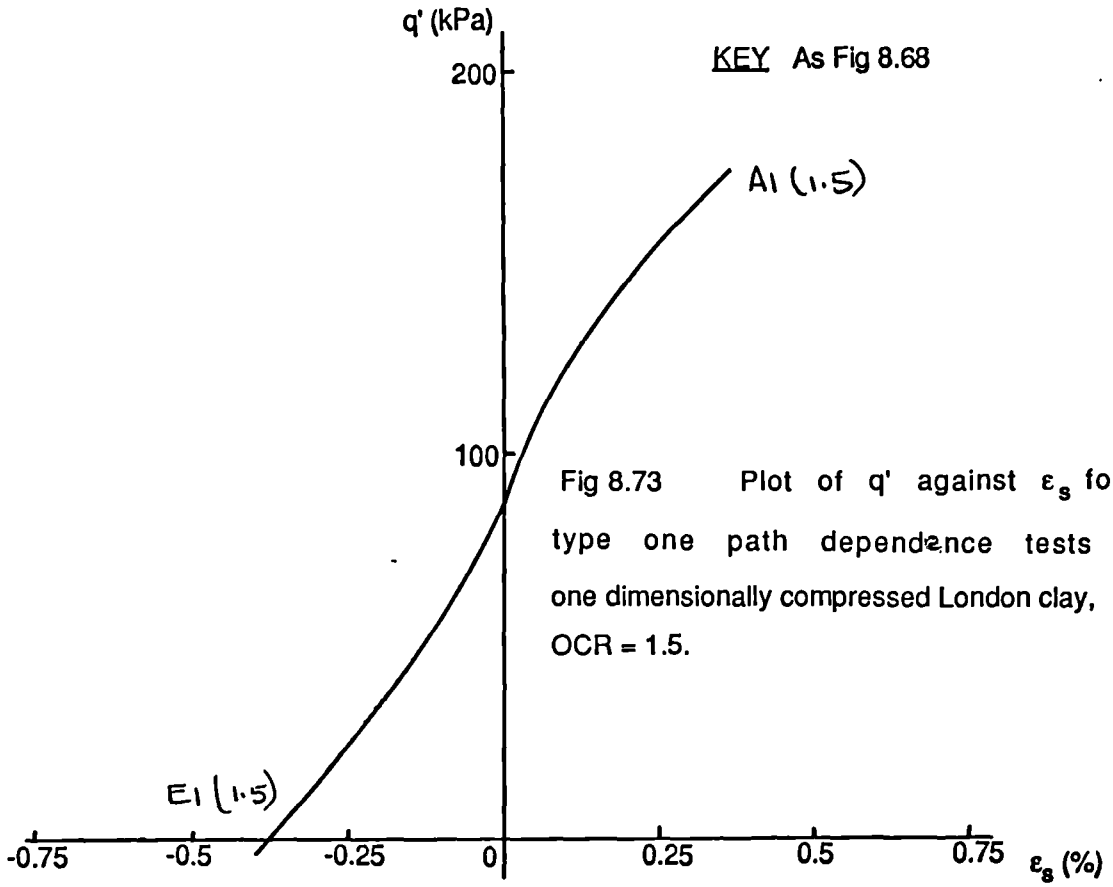

Fig 8.73 Plot of q' against ε_s for type one path dependence tests on one dimensionally compressed London clay, OCR = 1.5.

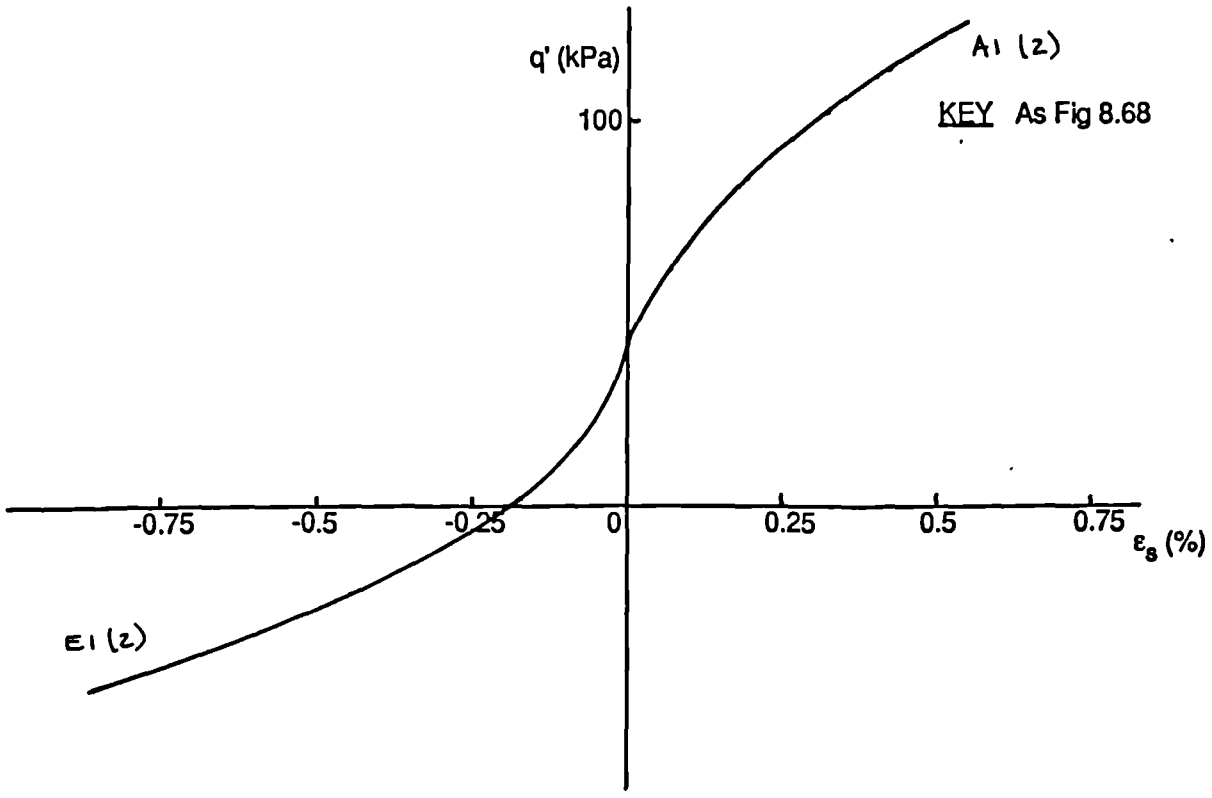

Fig 8.74 Plot of q' against ε_s for type one path dependence tests on one dimensionally compressed London clay, OCR = 2.0.

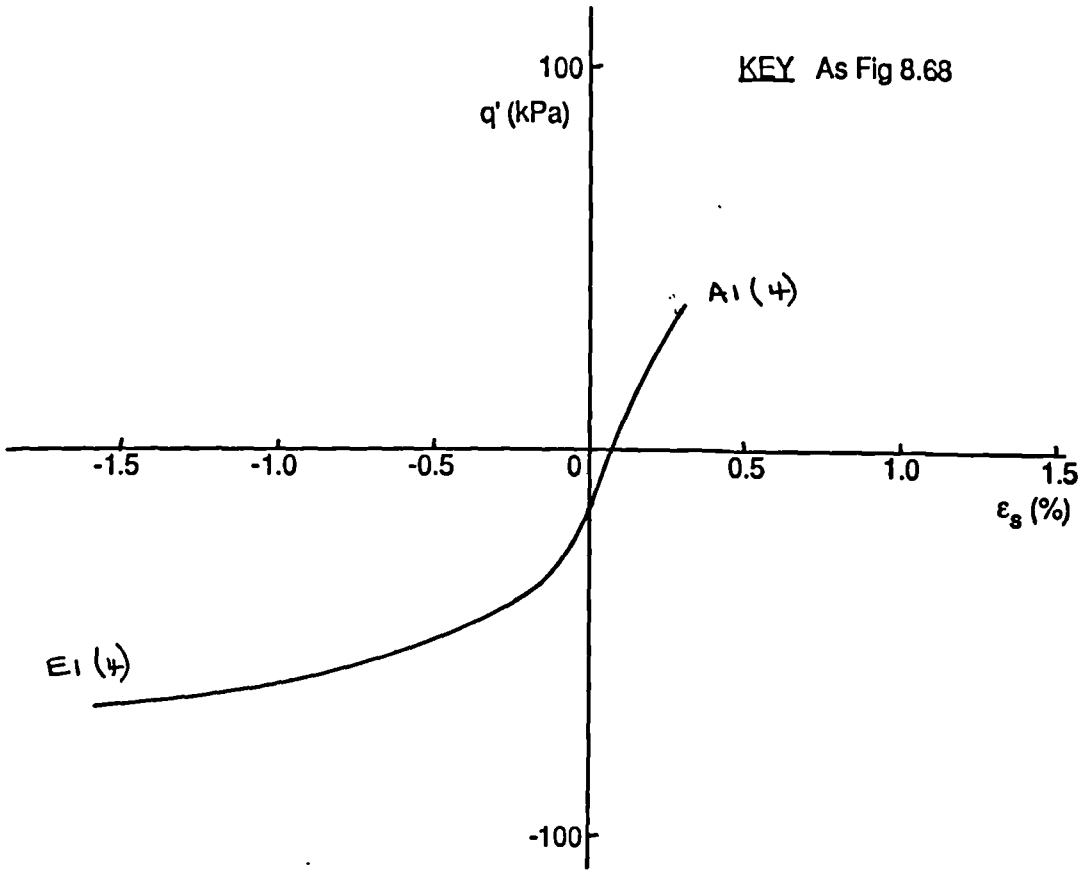

Fig 8.75 Plot of q' against ε_s for type one path dependence tests on one dimensionally compressed London clay, OCR = 4.0.

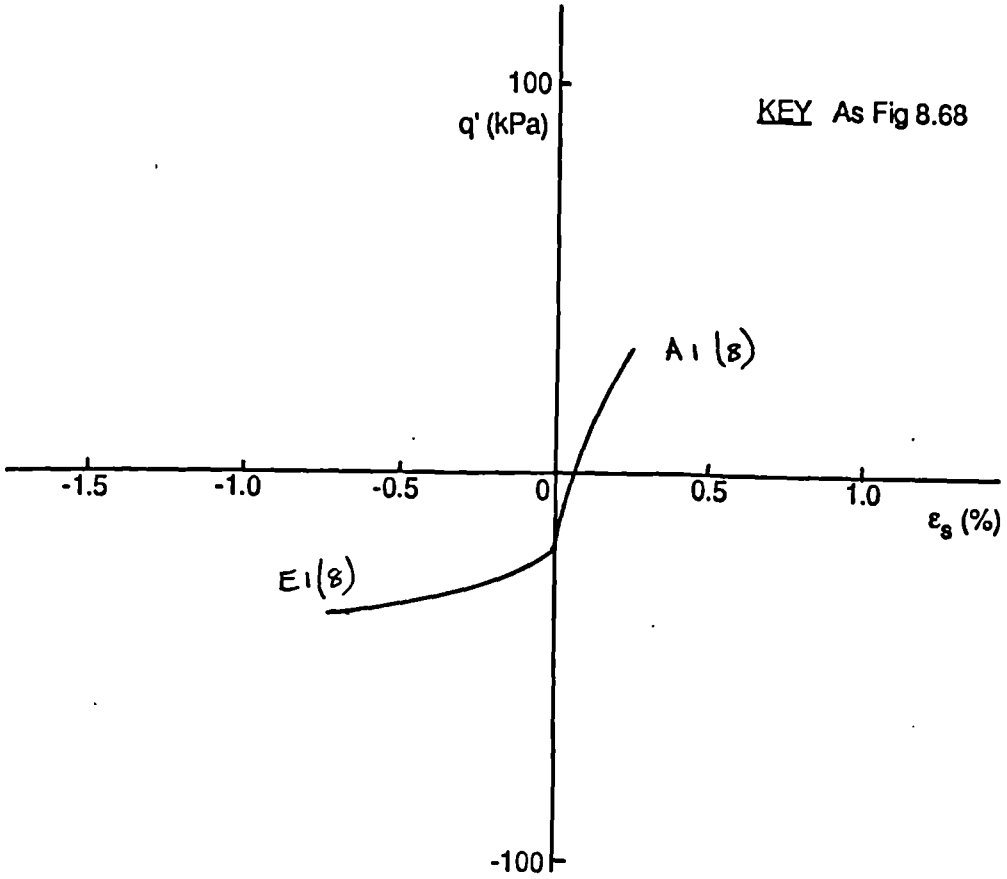

Fig 8.76 Plot of q' against ε_s for type one path dependence tests on one dimensionally compressed London clay, OCR = 8.0.

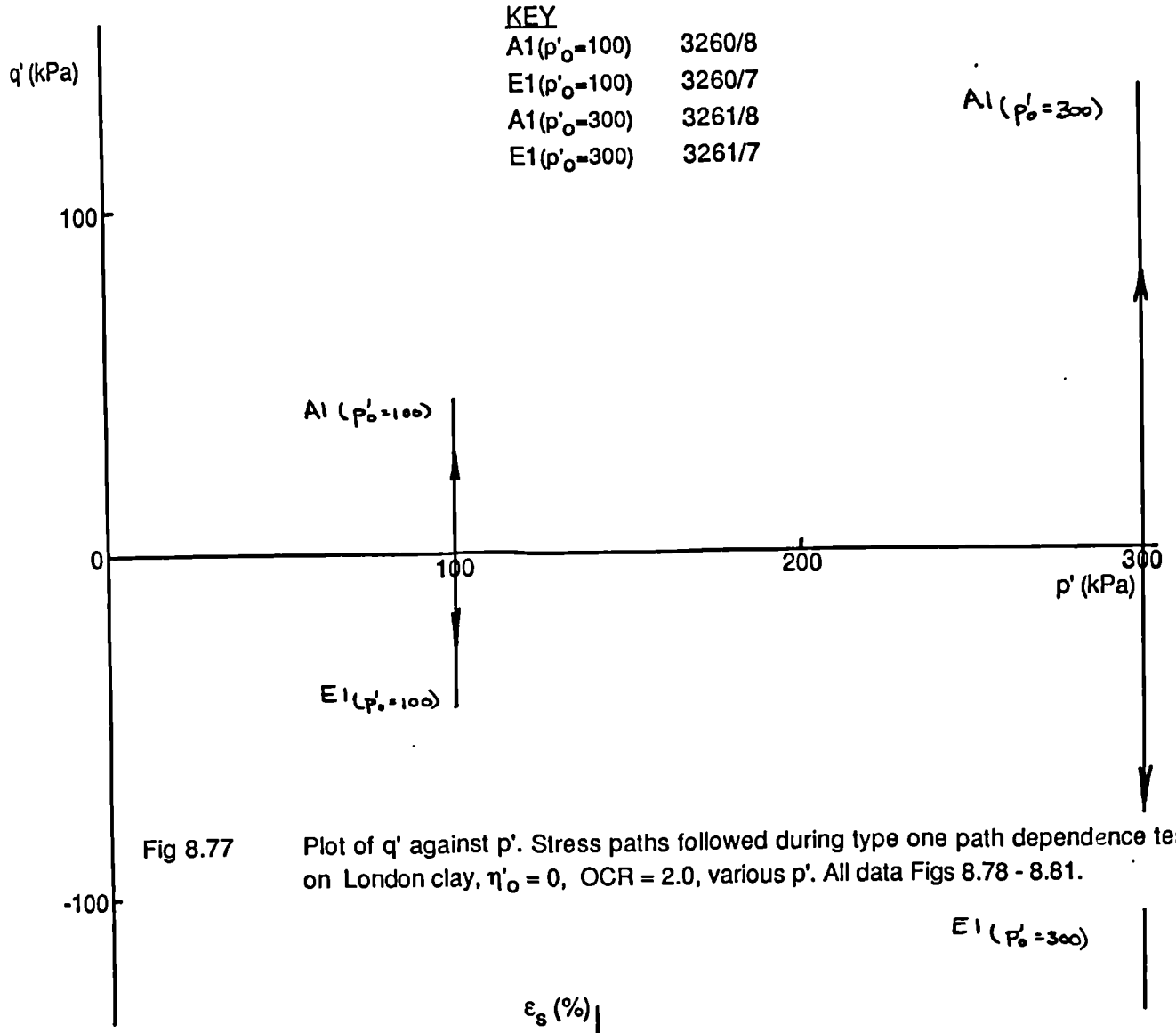

Fig 8.77 Plot of q' against p'. Stress paths followed during type one path dependence tests on London clay, $\eta'_o = 0$, OCR = 2.0, various p'. All data Figs 8.78 - 8.81.

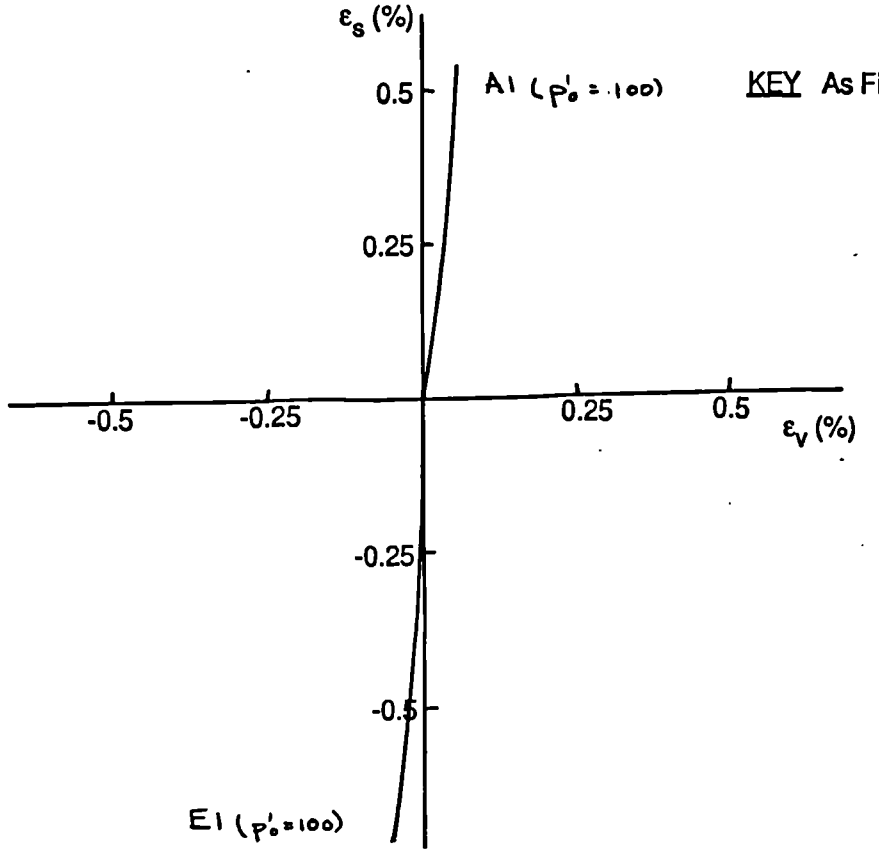

Fig 8.78 Plot of strain paths, ε_s against ε_v for type one path dependence tests on London clay, OCR = 2.0, p' = 100 kPa.

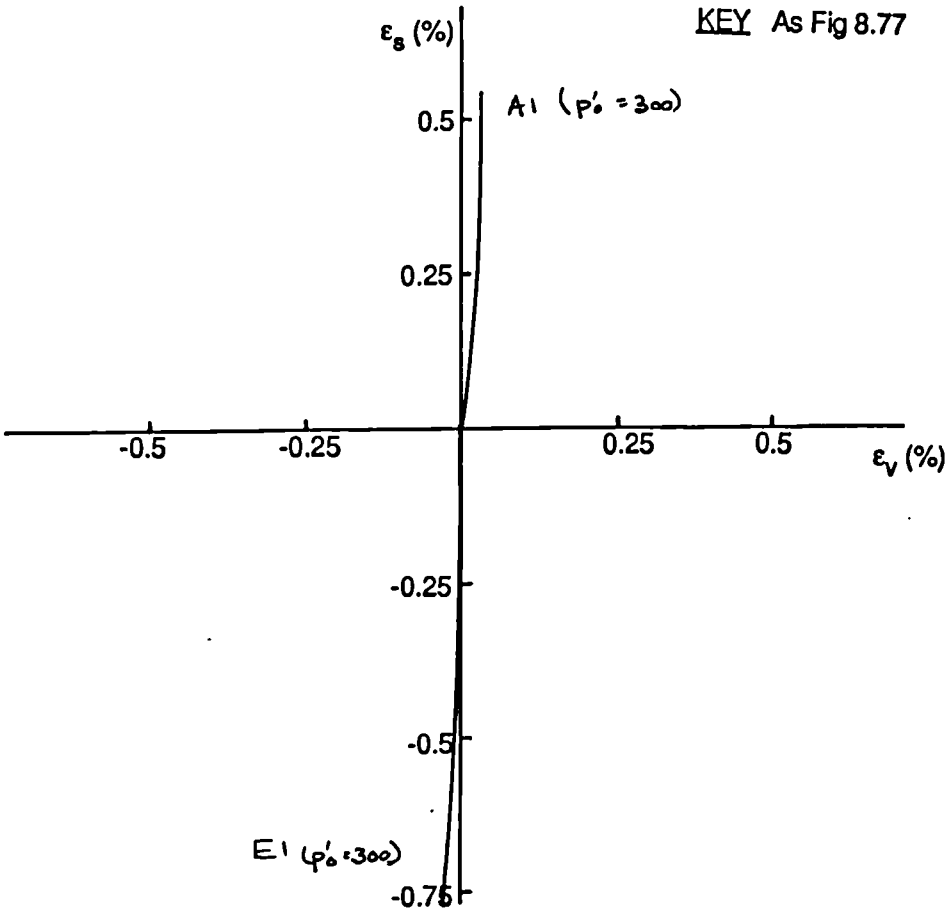

Fig 8.79 Plot of strain paths, ε_s against ε_v for type one path dependence tests on London clay, OCR = 2.0, p' = 300 kPa.

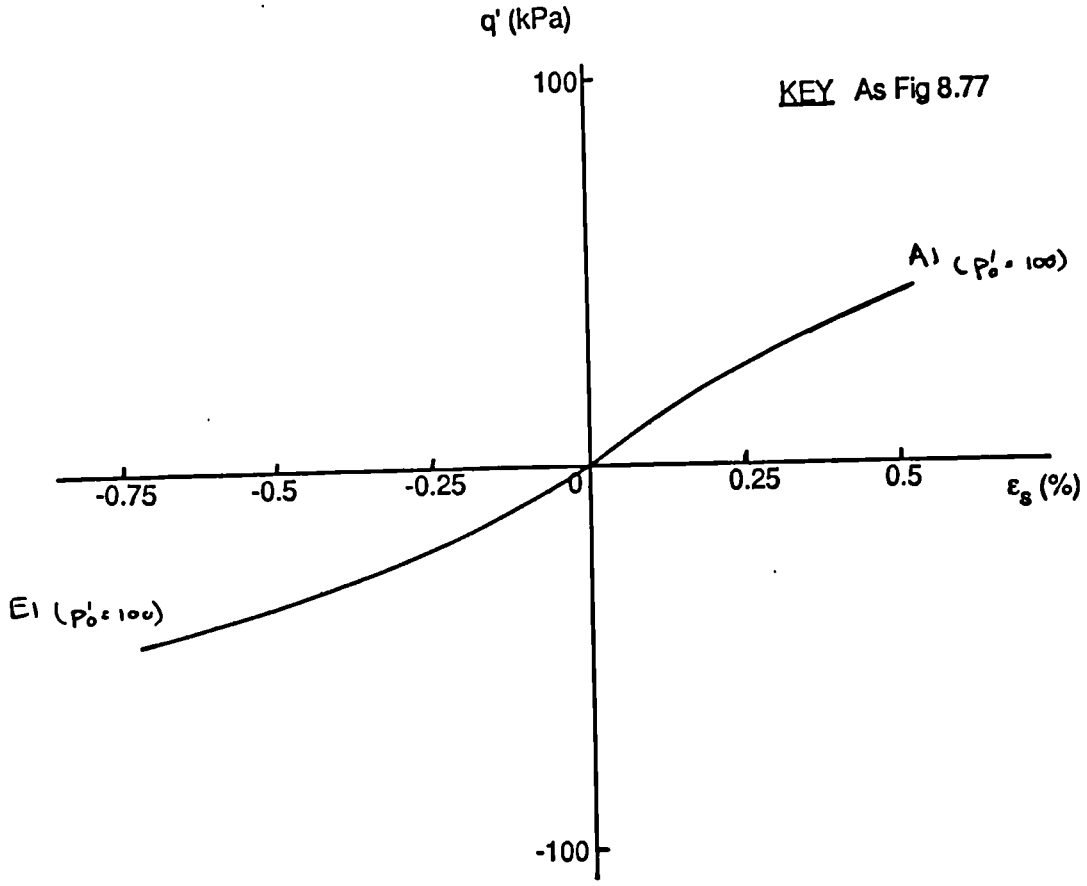

Fig 8.80 Plot of q' against ε_s for type one path dependence tests on London clay, OCR = 2.0, p' = 100kPa.

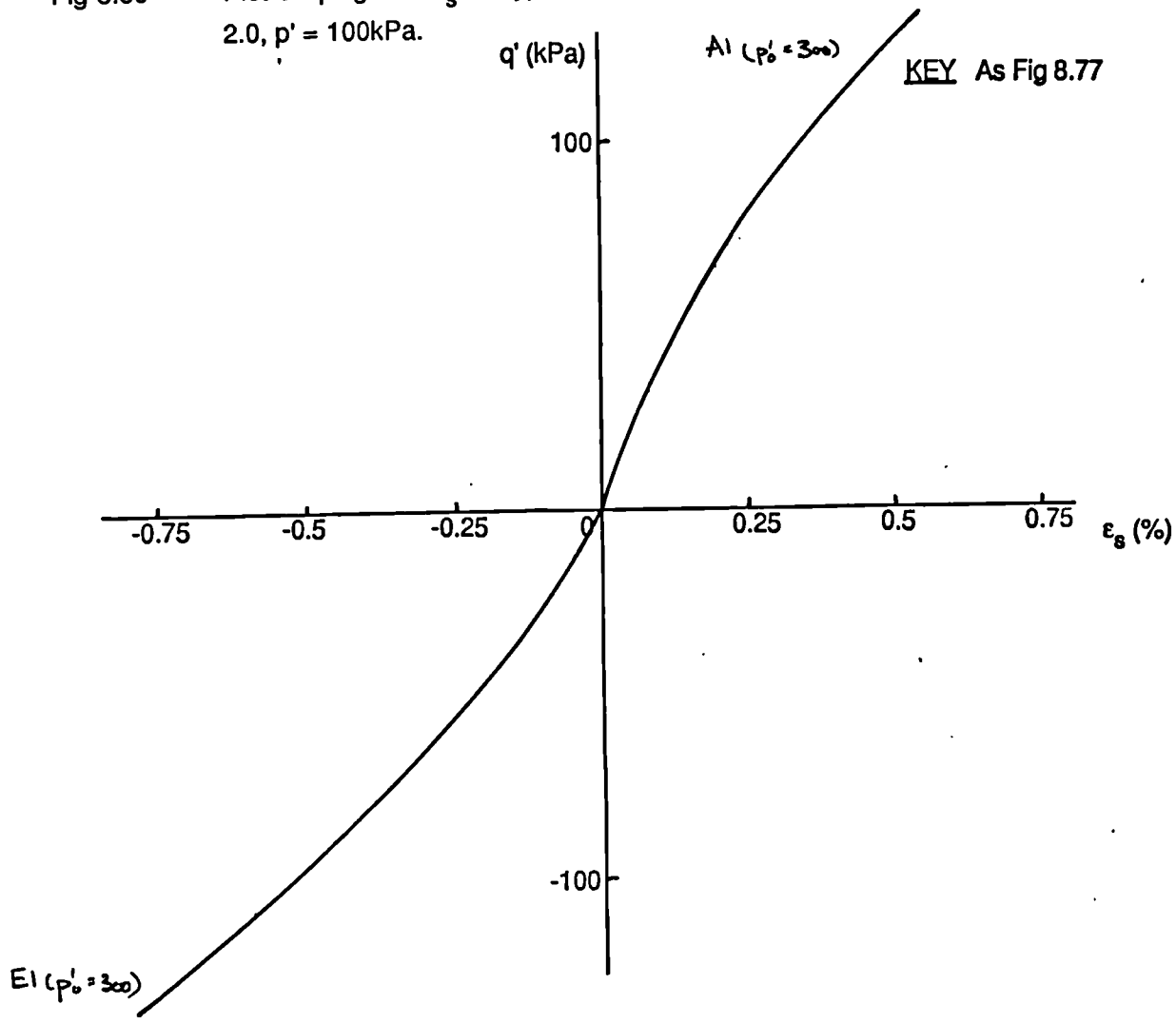

Fig 8.81 Plot of q' against ε_s for type one path dependence tests on London clay, OCR = 2.0, p' = 300kPa.

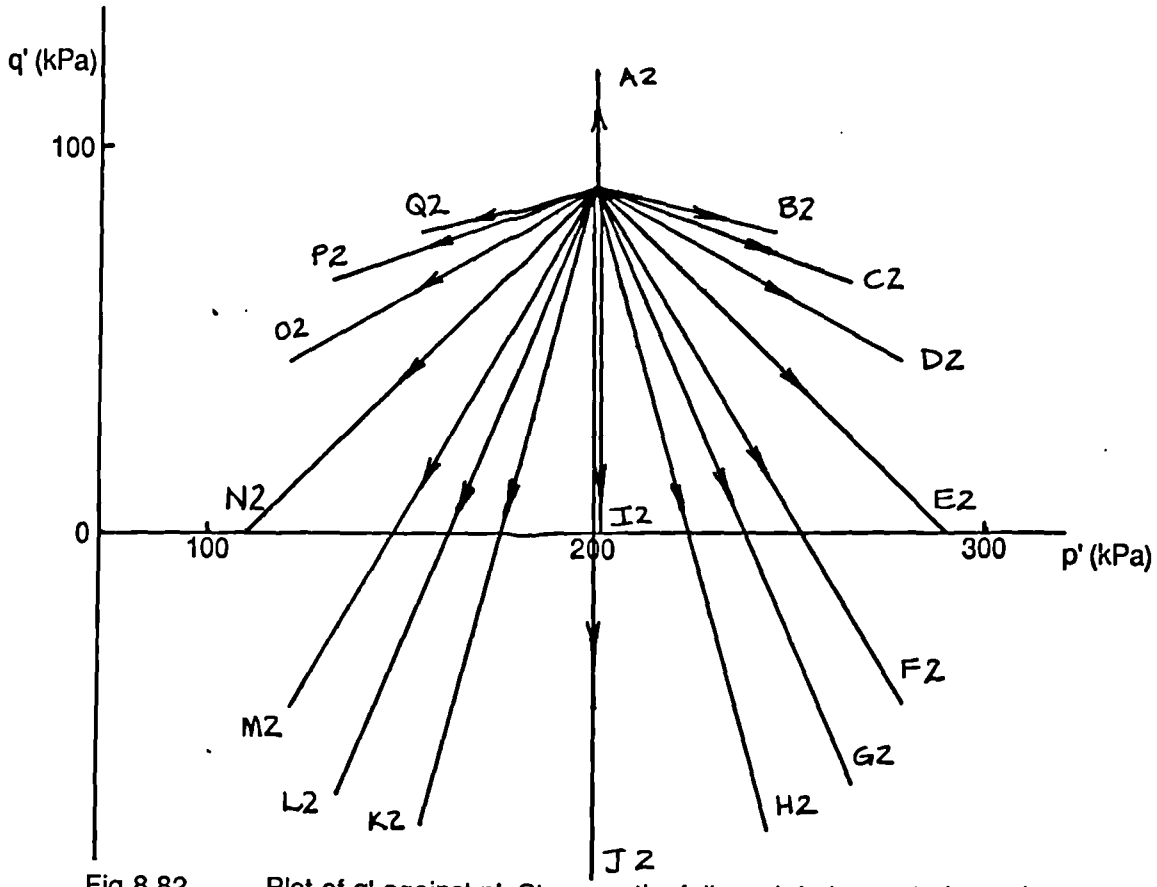

Fig 8.82 Plot of q' against p'. Stress paths followed during path dependence type two tests. $\eta'_o = 0$, OCR = 2.0. All data Figs 8.83 - 8.92.

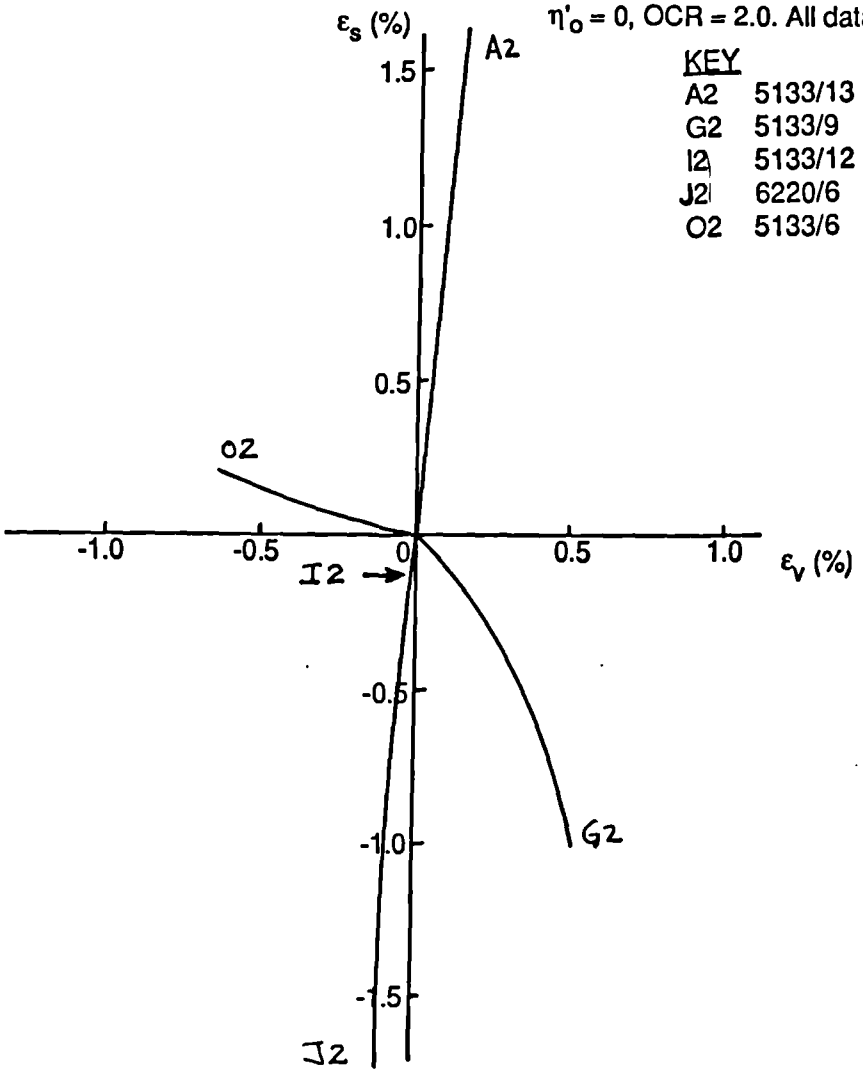

Fig 8.83 Plot of strain paths, ε_s against ε_v for type two path dependence tests on speswhite kaolin.

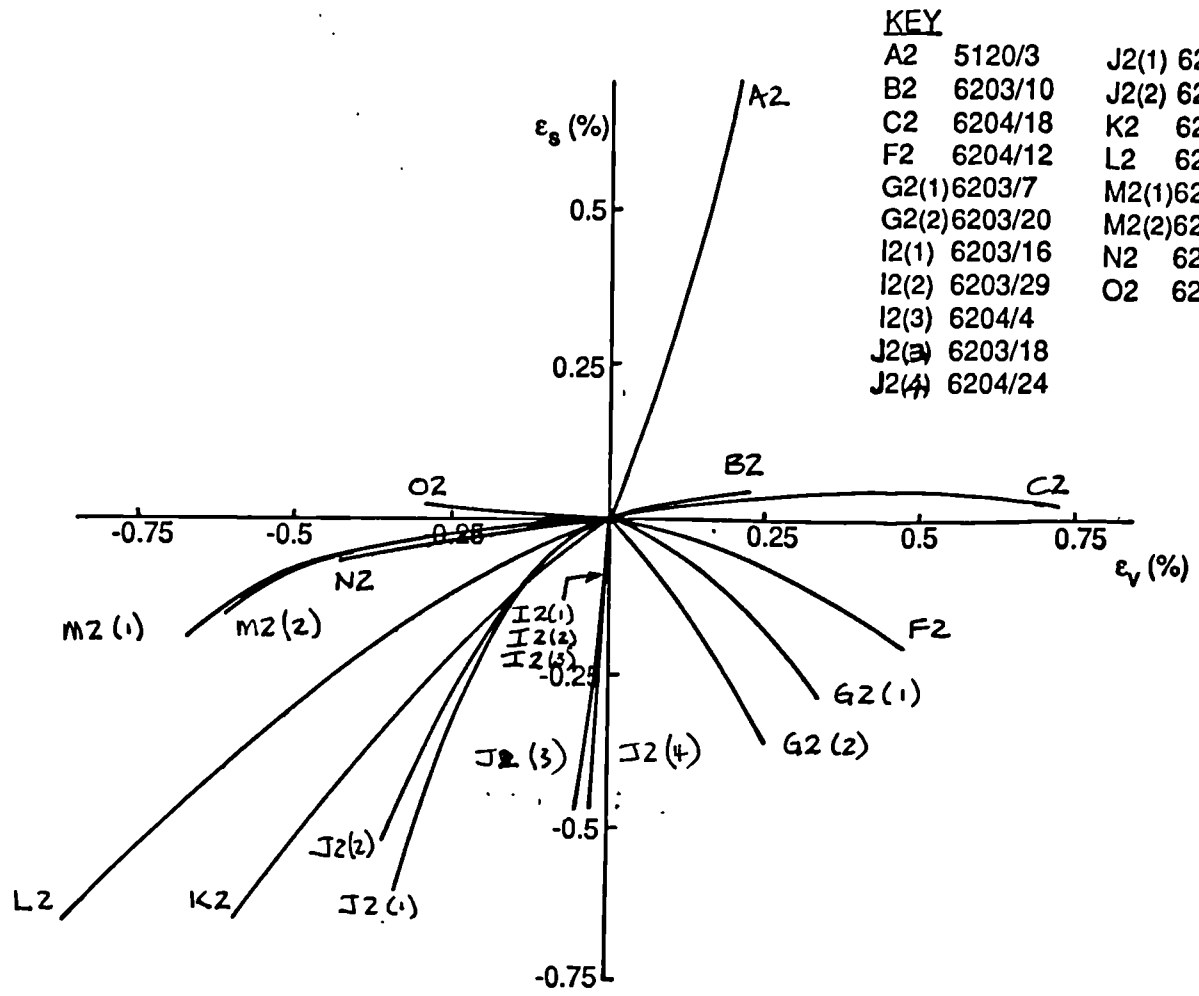

Fig 8.84 Plot of strain paths, ε_s against ε_v for type two path dependence tests on Ware till.

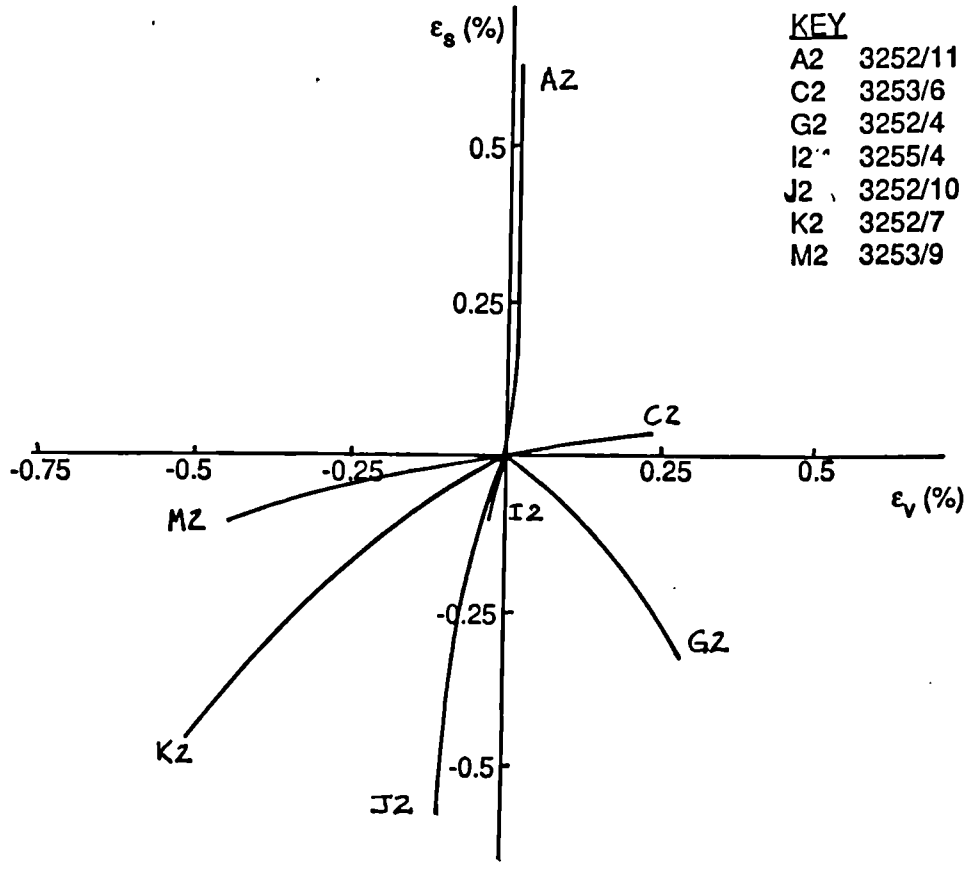

Fig 8.85 Plot of strain paths, ε_s against ε_v for type two path dependence tests on Cowden till.

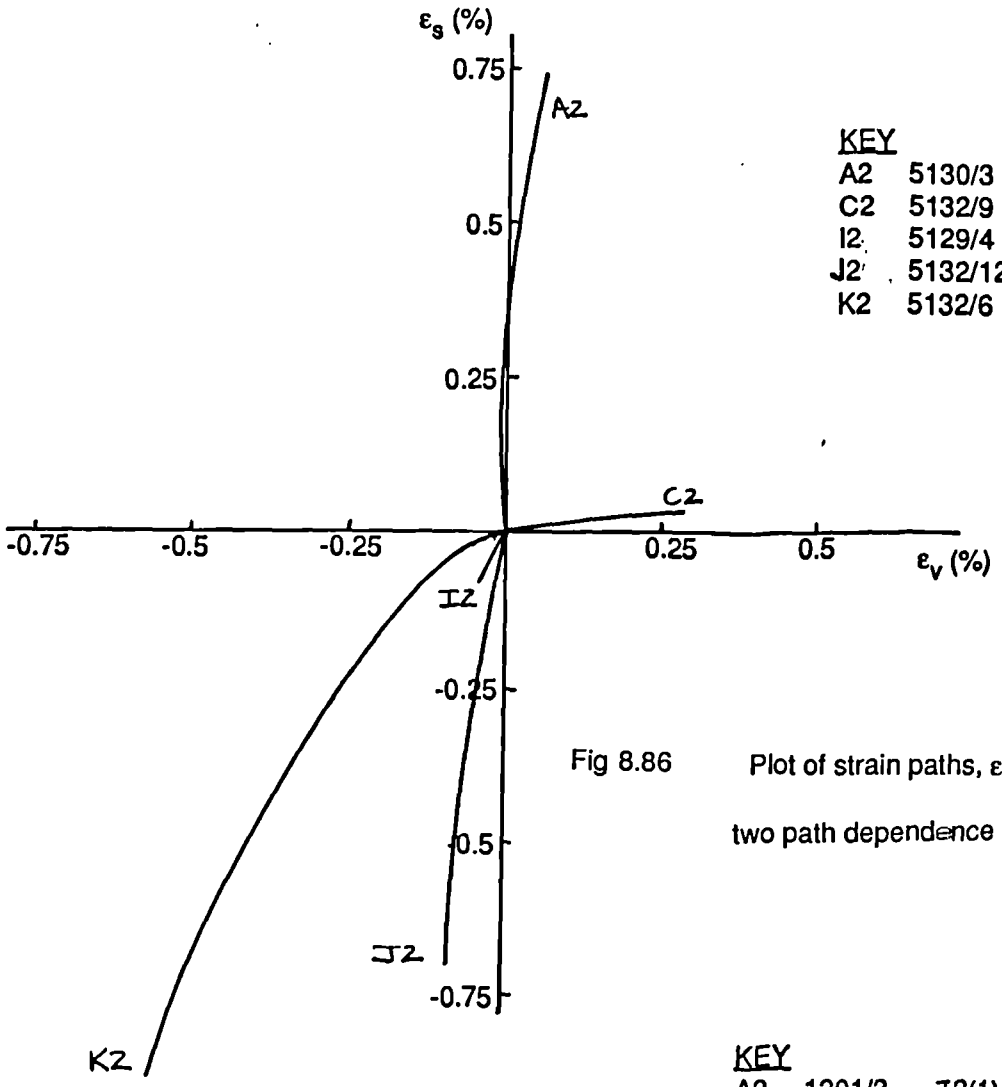

Fig 8.86 Plot of strain paths, ε_s against ε_v for type two path dependence tests on slate dust.

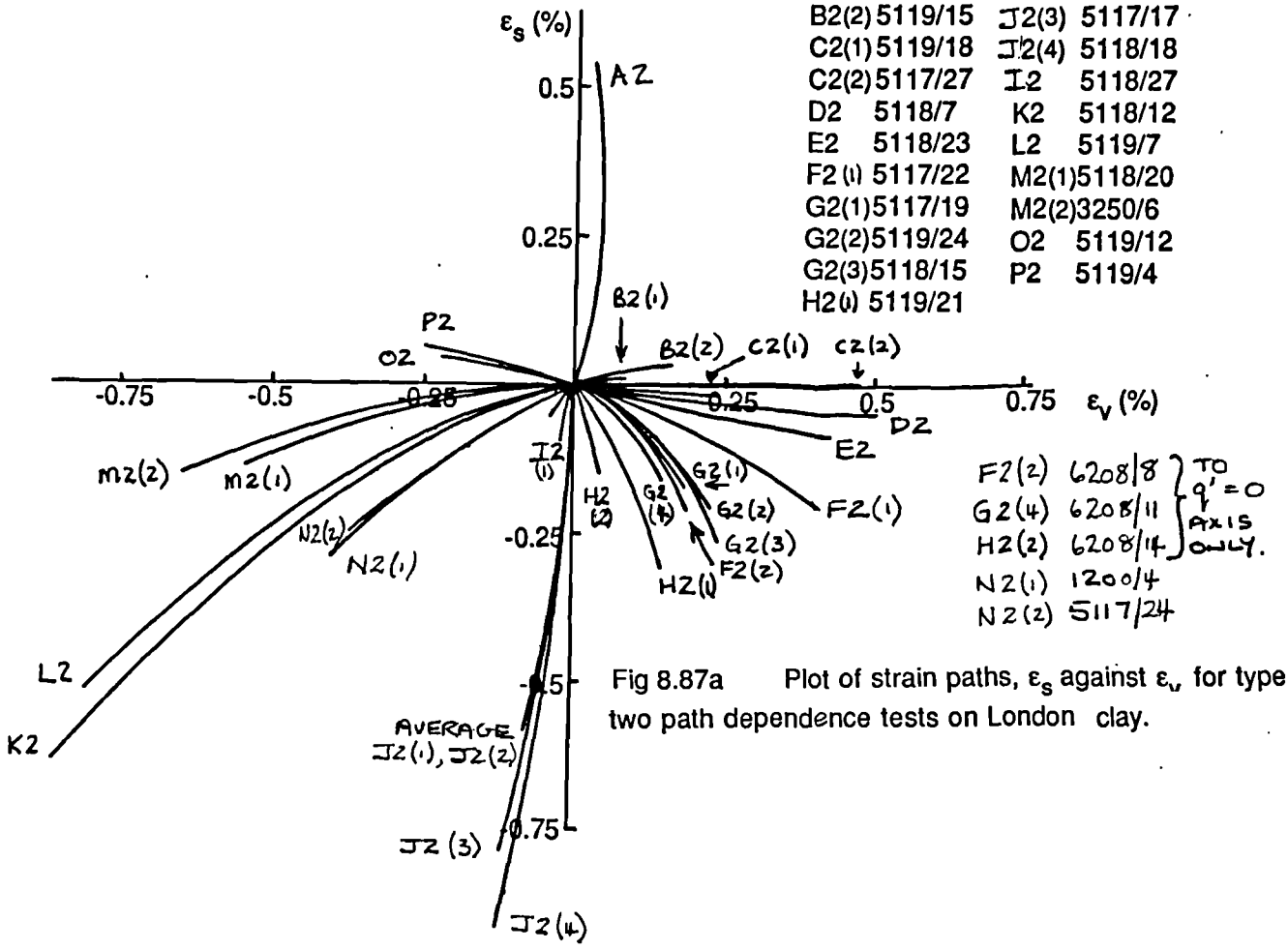

Fig 8.87a Plot of strain paths, ε_s against ε_v for type two path dependence tests on London clay.

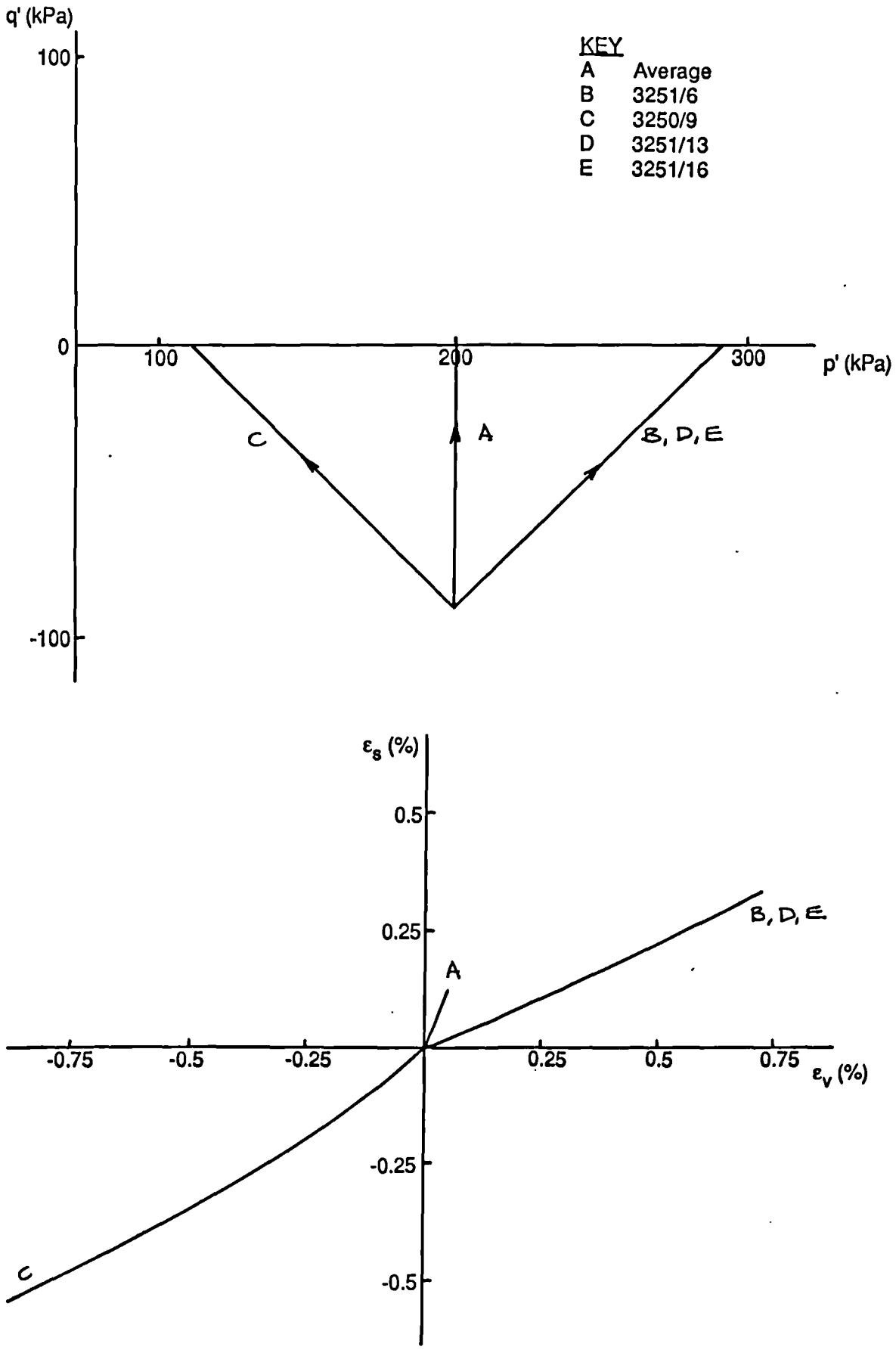

Fig 8.87b Plot of stress paths, q' against p', and strain paths followed during path dependence type two tests on London clay. η'_o = 0, OCR = 2.0, p' = 200kPa, q'=-90kPa. Data in Fig 8.92a.

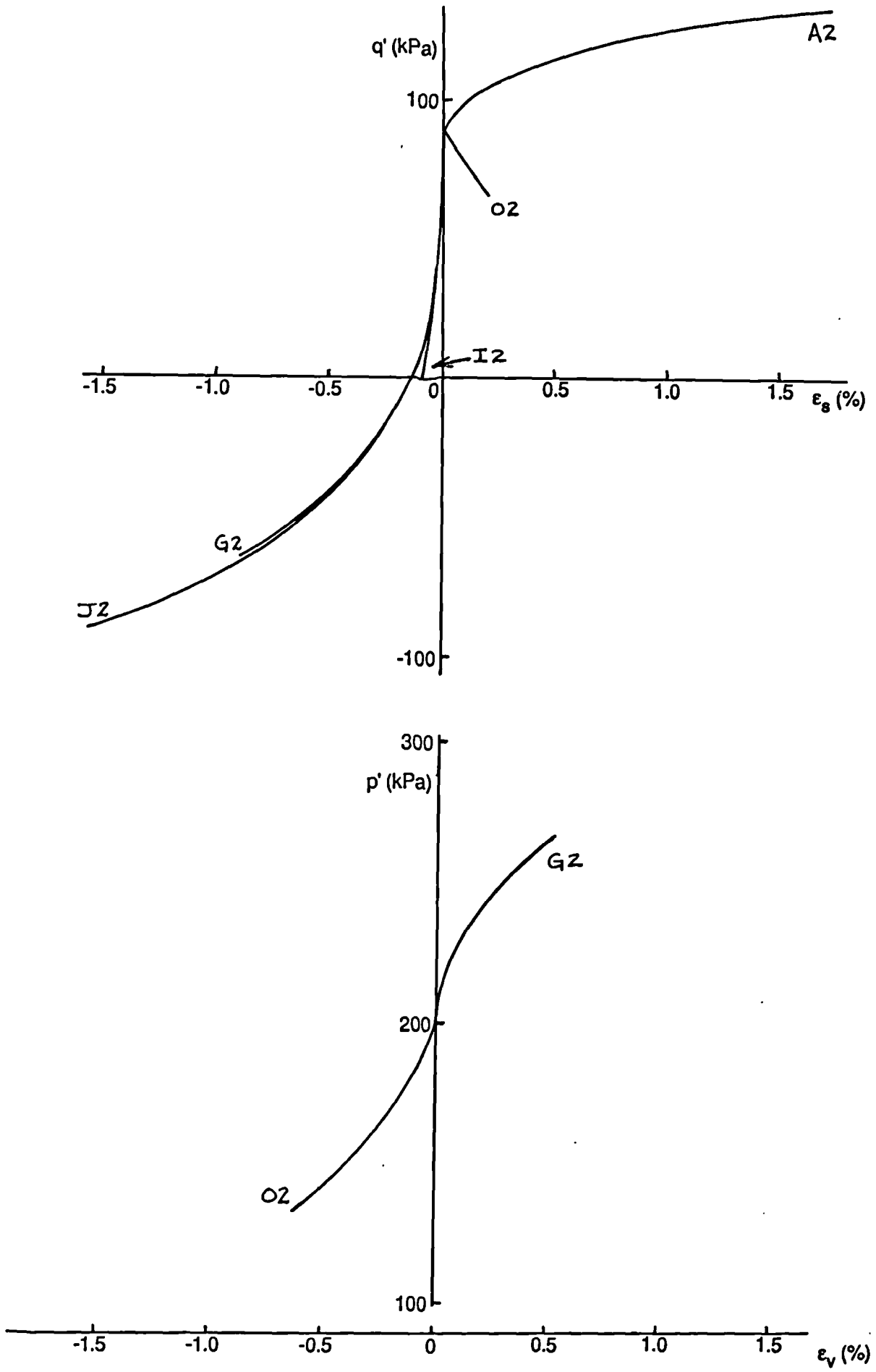

Fig 8.88 Plots of q' against ε_s and p' against ε_v for type two path dependence tests on speswhite kaolin.

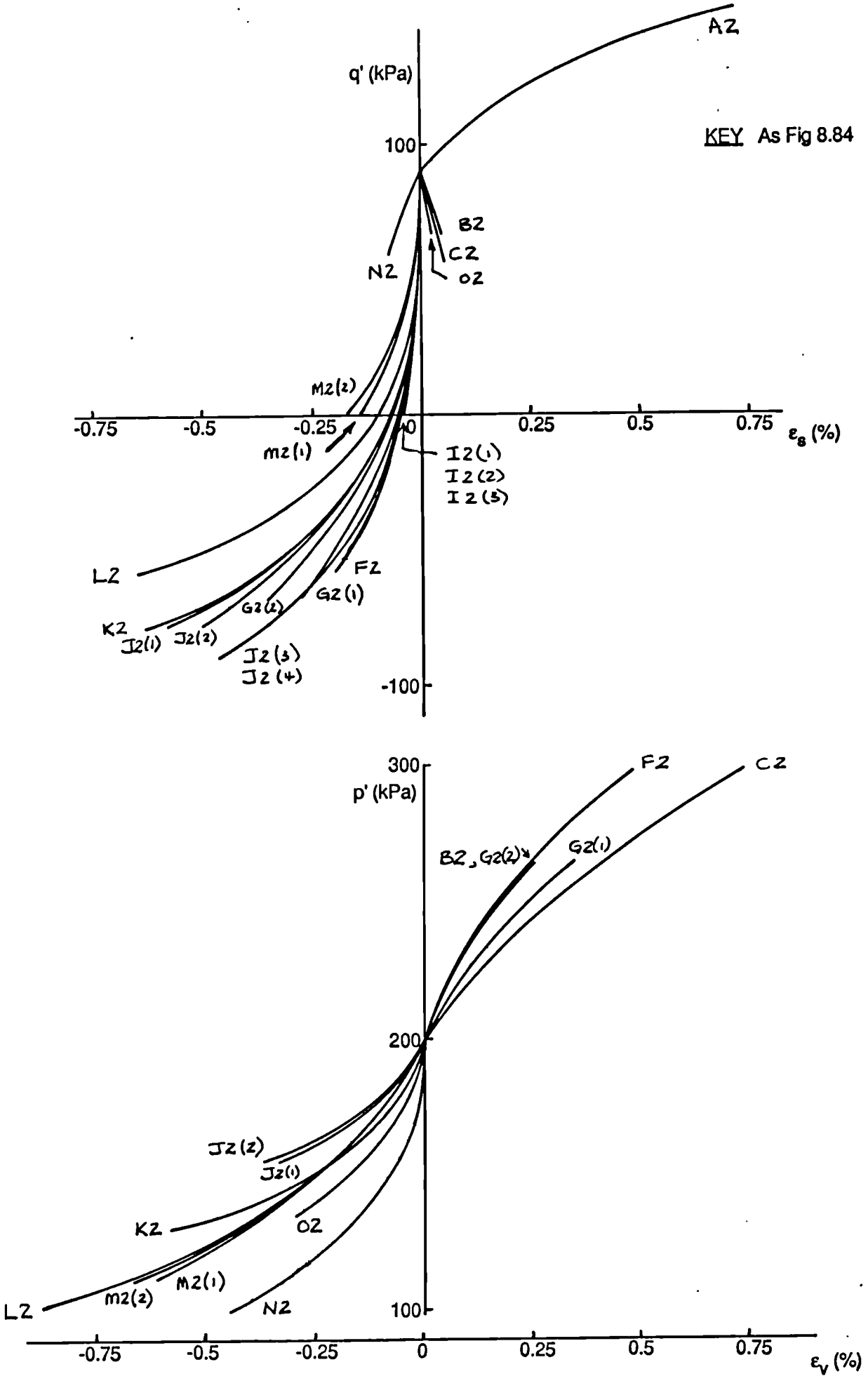

Fig 8.89 Plots of q' against ε_s and p' against ε_v for type two path dependence tests on Ware till.

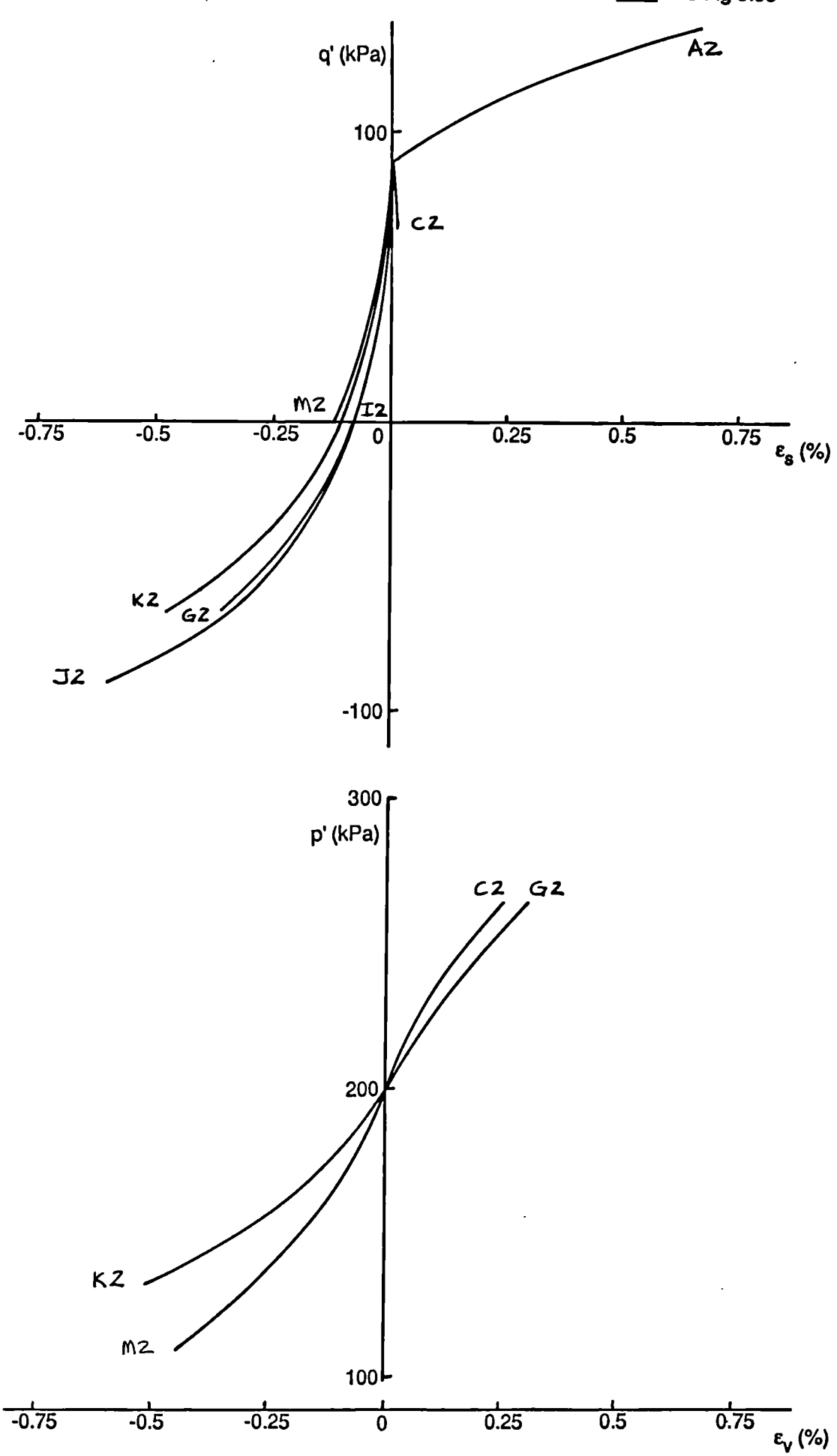

Fig 8.90 Plots of q' against ε_s and p' against ε_v for type two path dependence tests on Cowden till.

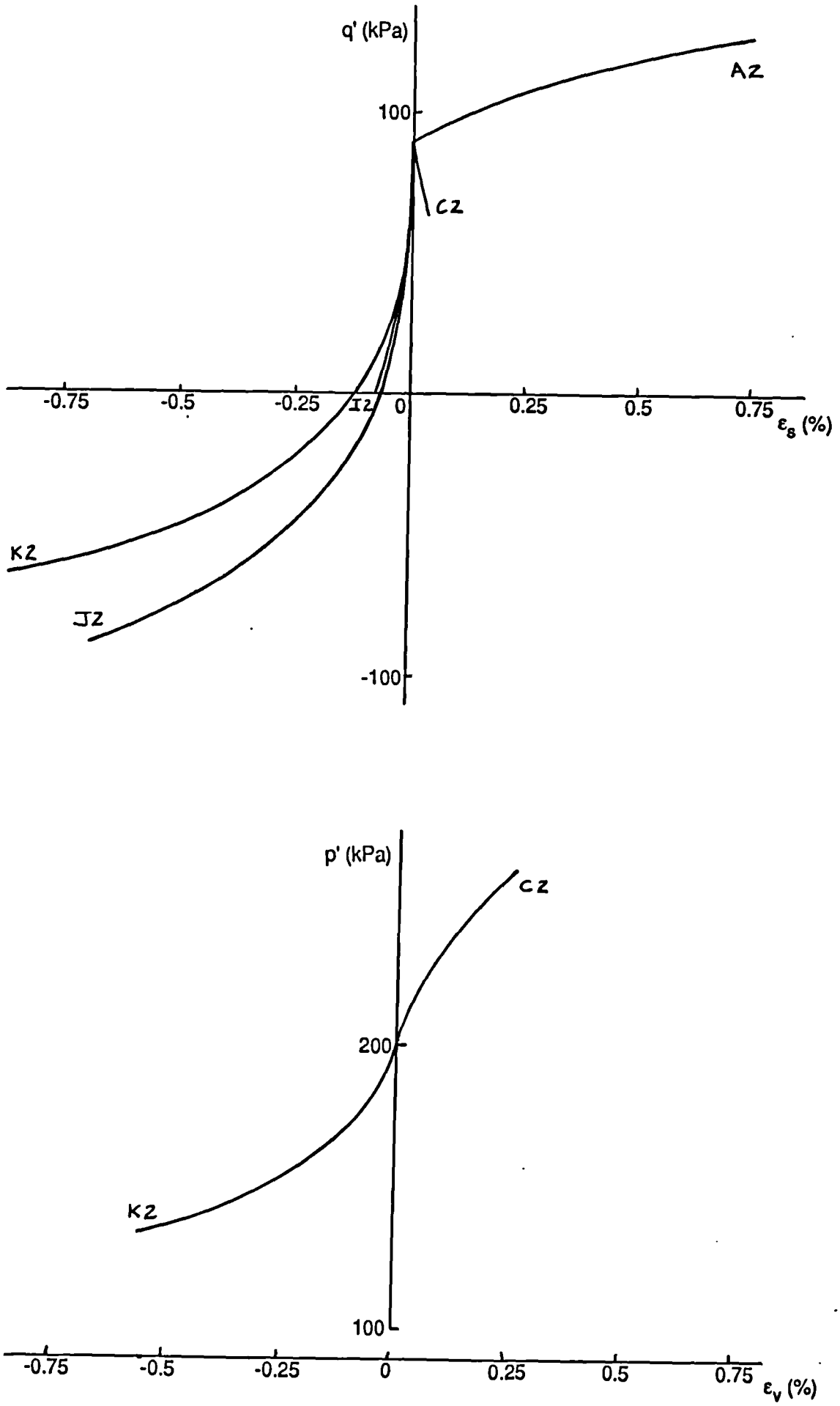

Fig 8.91 Plots of q' against ε_s and p' against ε_v for type two path dependence tests on slate dust.

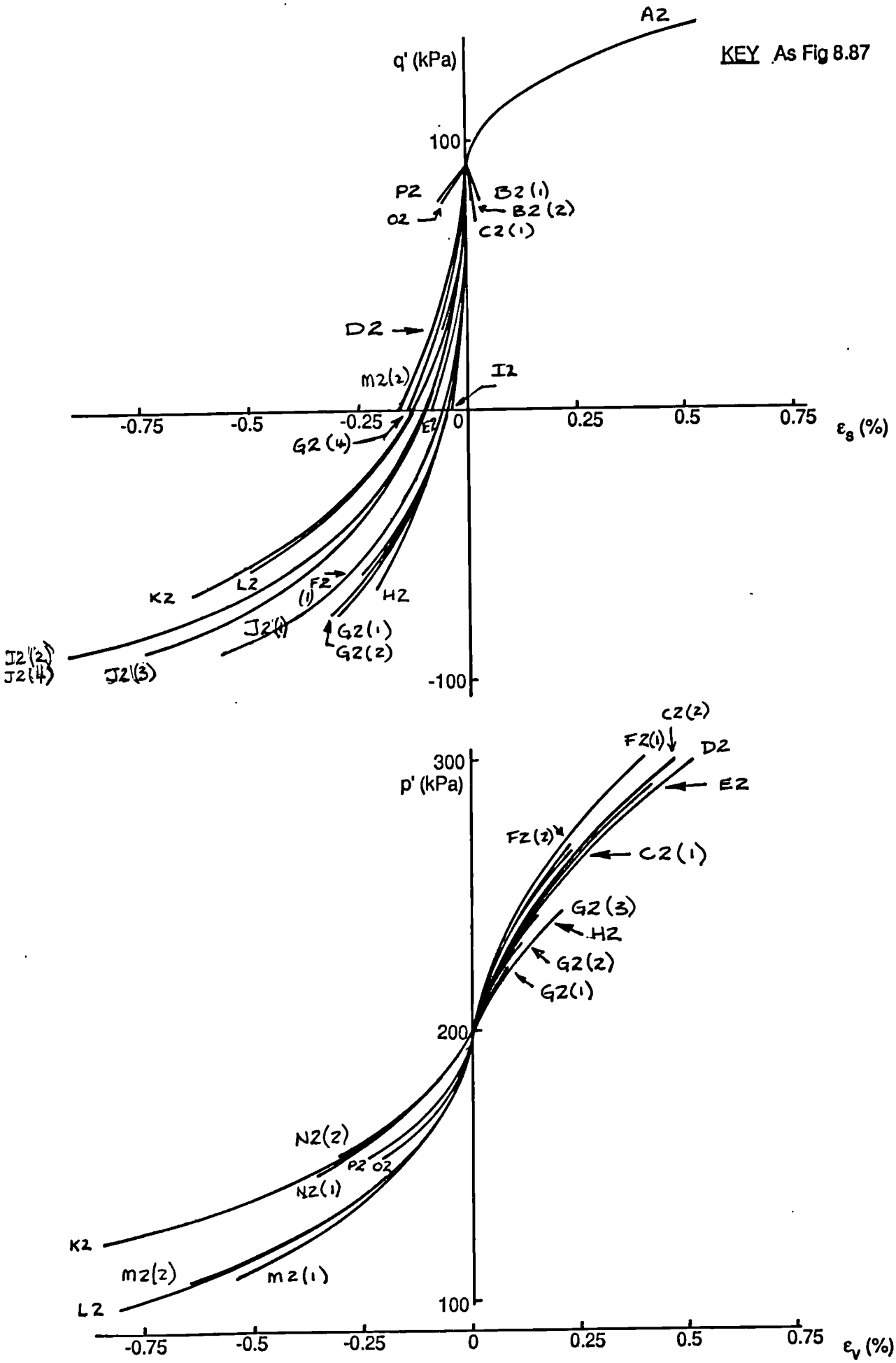

Fig 8.92a Plots of q' against ε_s and p' against ε_v for type two path dependence tests on London clay.

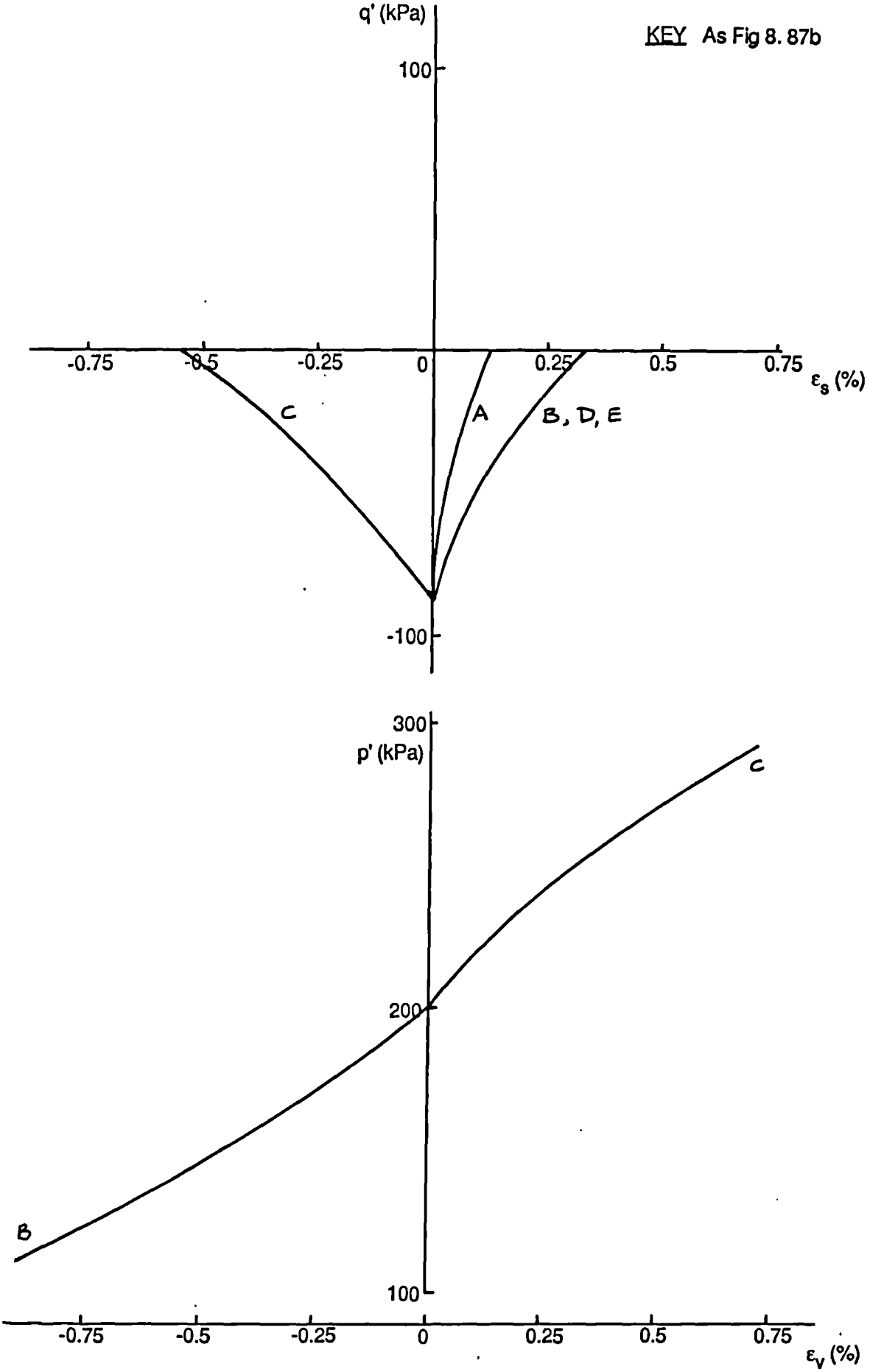

Fig 8.92b Plots of q' against ε_s and p' against ε_v for type two path dependence tests on London clay.

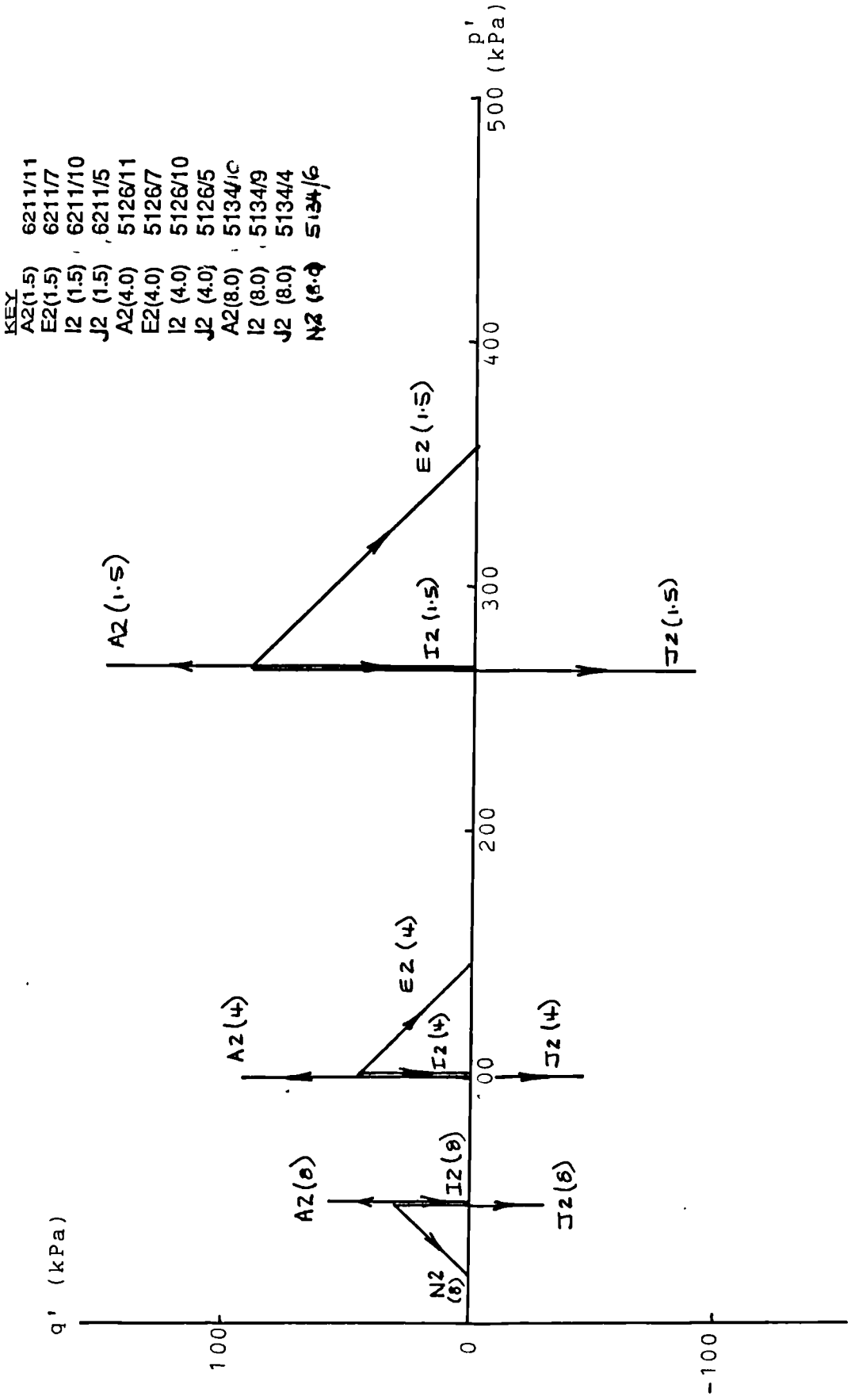

Fig 8.93 Plot of q' against p'. Stress paths followed during path dependence type two tests. $\eta'_o = 0$, various OCR's, London clay. All data Figs 8.94 - 8.99.

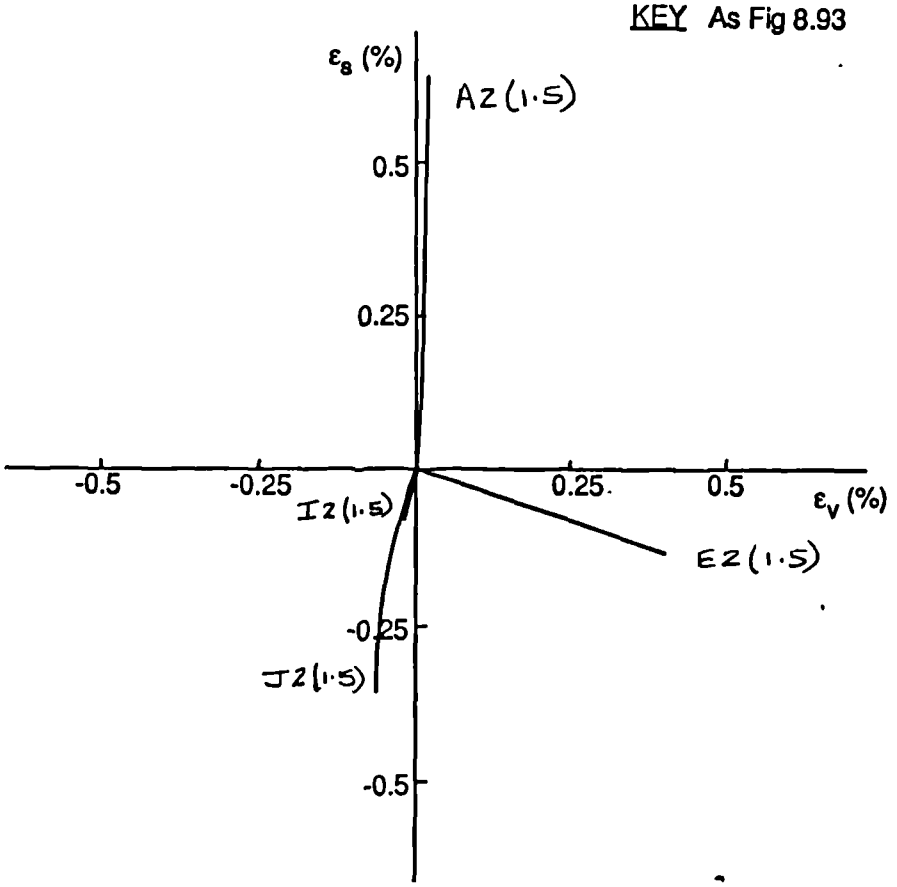

Fig 8.94 Plot of strain paths, ε_s against ε_v for type two path dependence tests on London clay, OCR = 1.5.

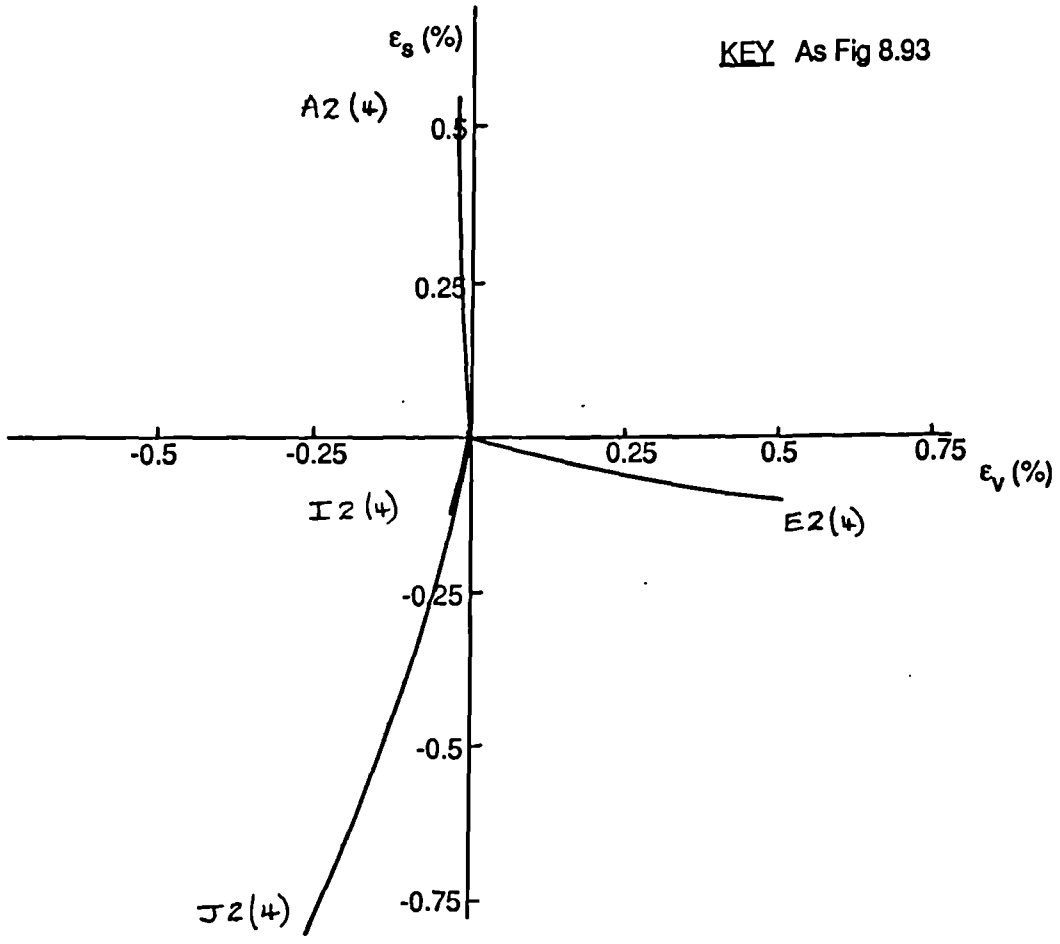

Fig 8.95 Plot of strain paths, ε_s against ε_v for type two path dependence tests on London clay, OCR = 4.0.

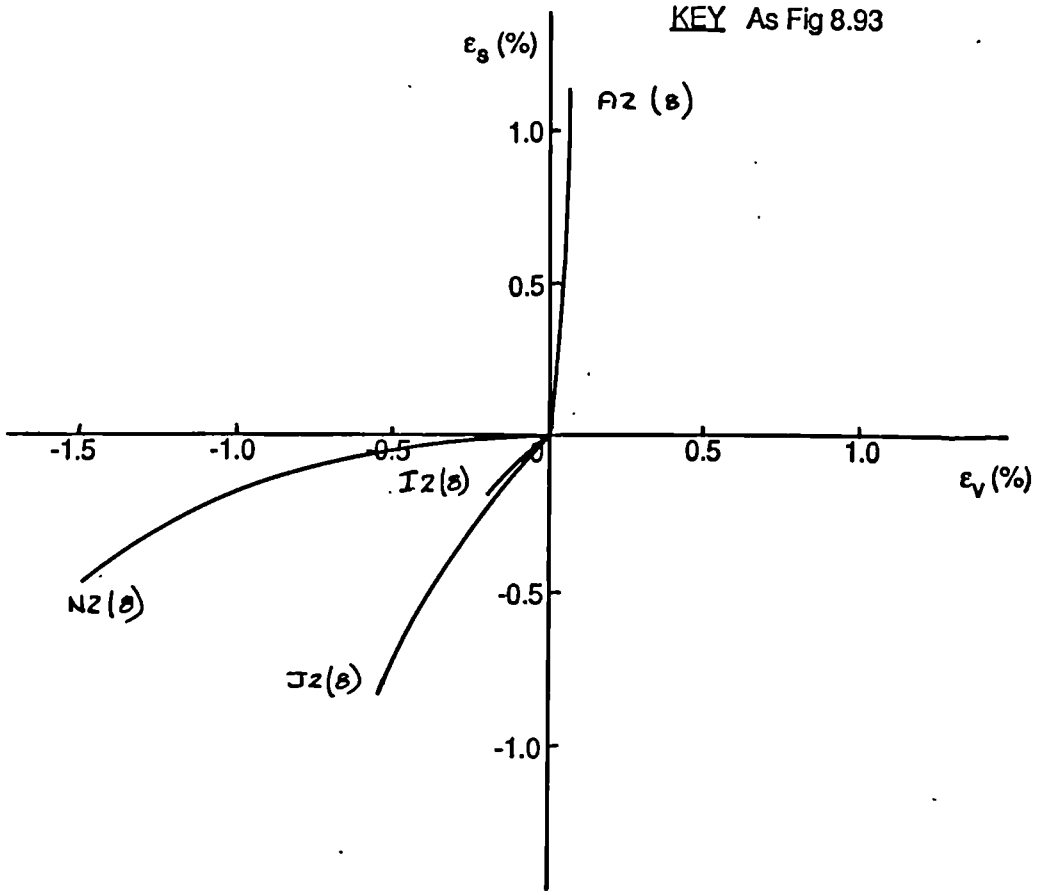

Fig 8.96 Plot of strain paths, ε_s against ε_v for type two path dependence tests on London clay, OCR = 8.

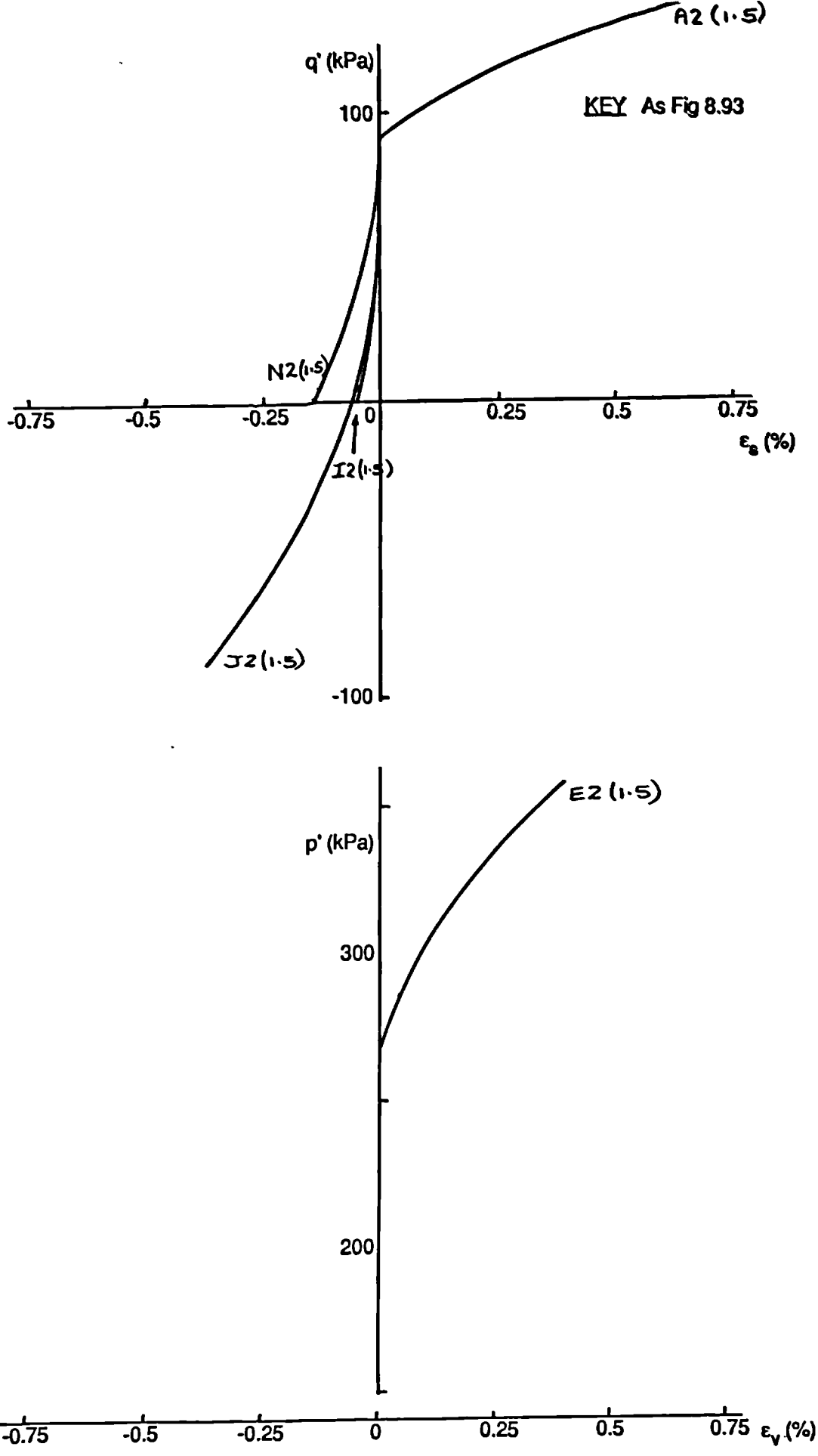

Fig 8.97 Plots of q' against ε_s and p' against ε_v for type two path dependence tests on London clay, OCR = 1.5.

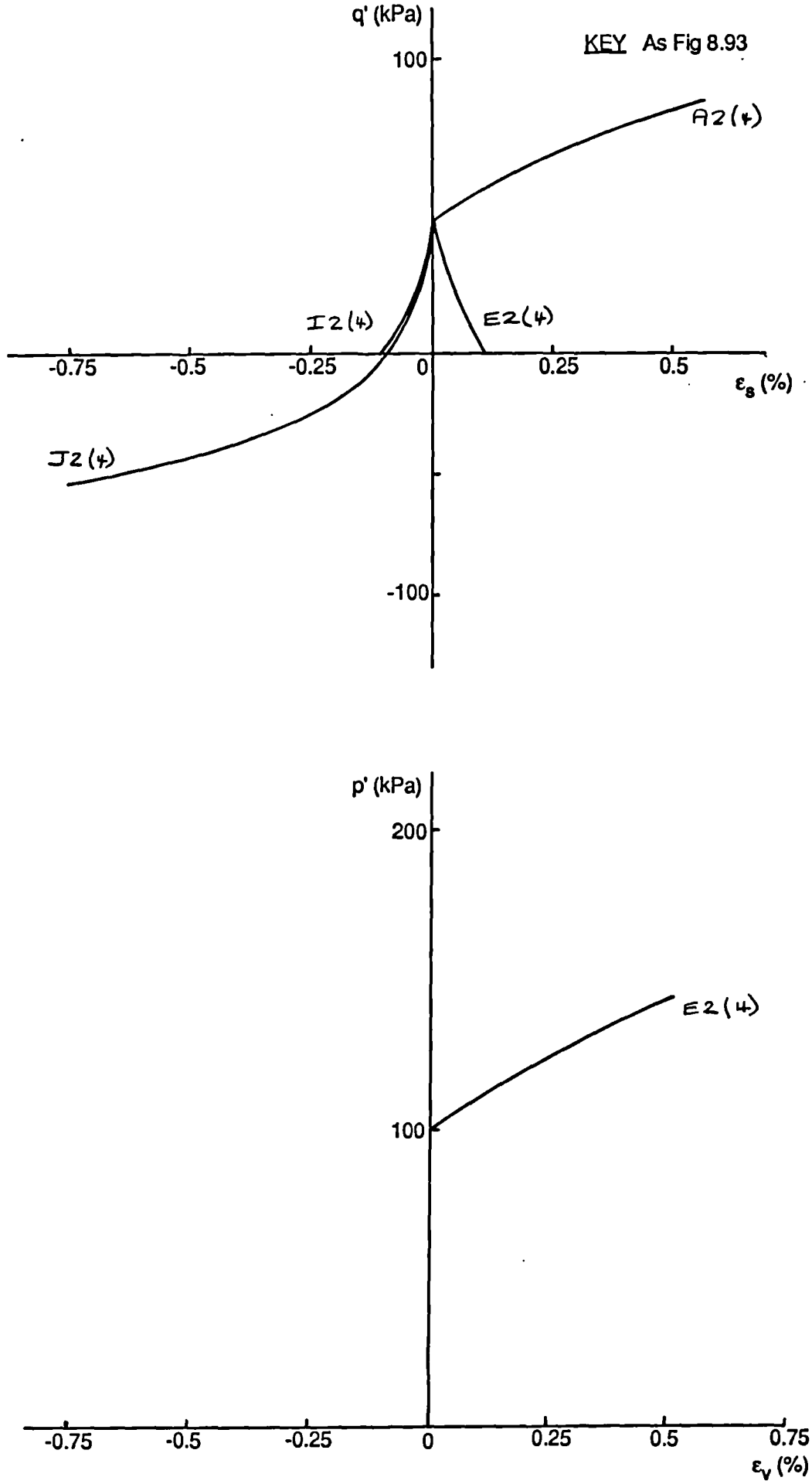

Fig 8.98 Plots of q' against ε_s and p' against ε_v for type two path dependence tests on London clay, OCR = 4.0.

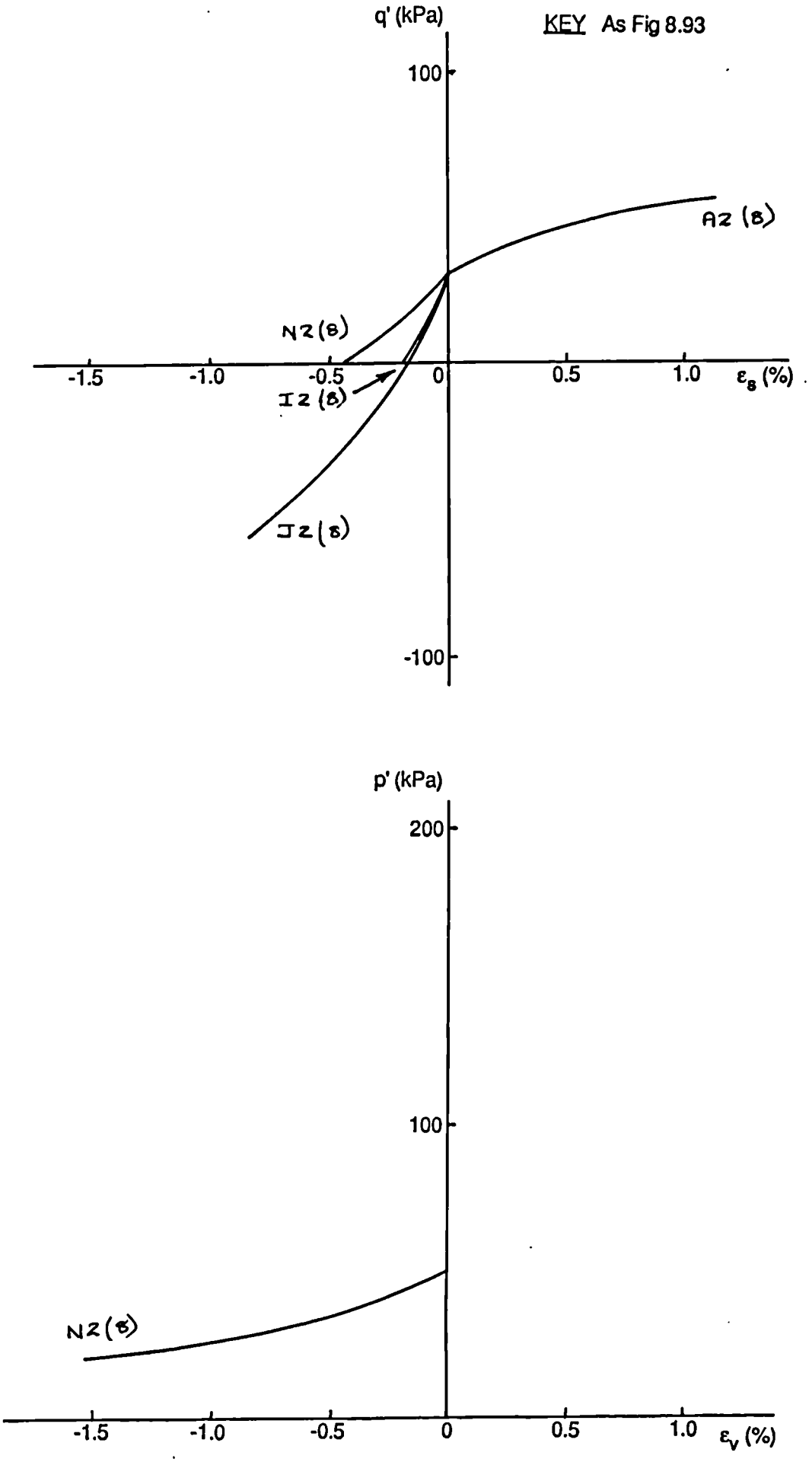

Fig 8.99 Plots of q' against ε_s and p' against ε_v for type two path dependence tests on London clay, OCR = 8.0.

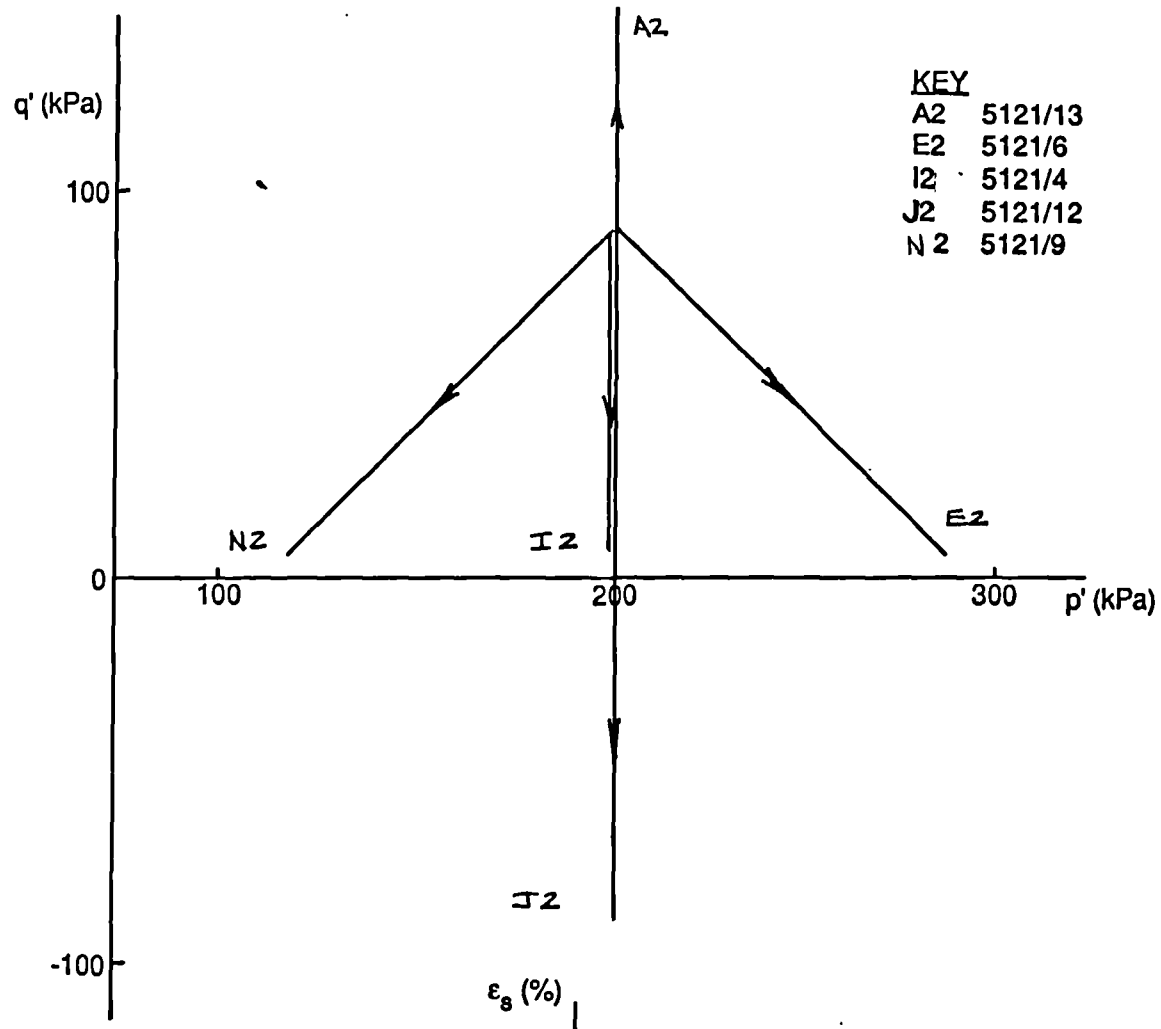

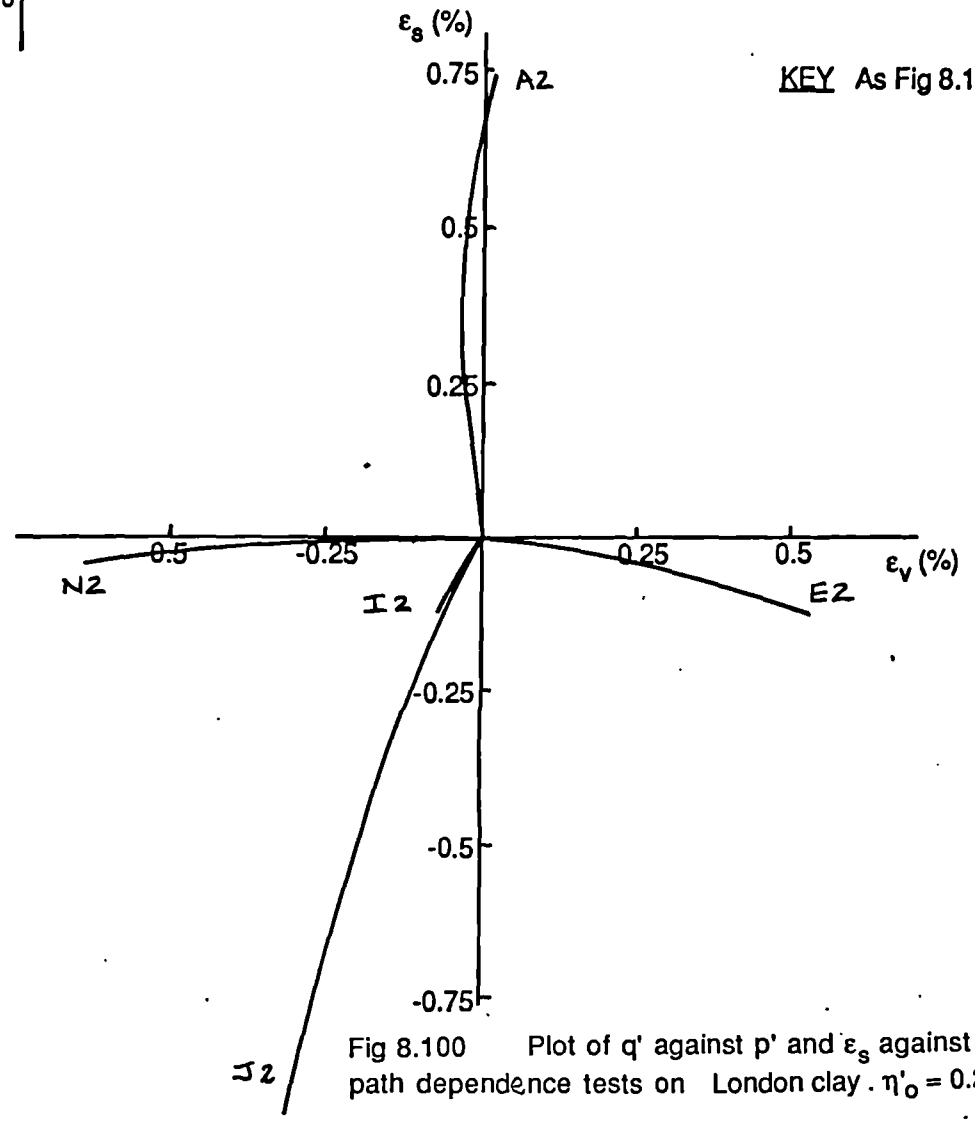

Fig 8.100 Plot of q' against p' and ε_s against ε_v for type one path dependence tests on London clay . $\eta'_o = 0.25$, OCR = 2.0.

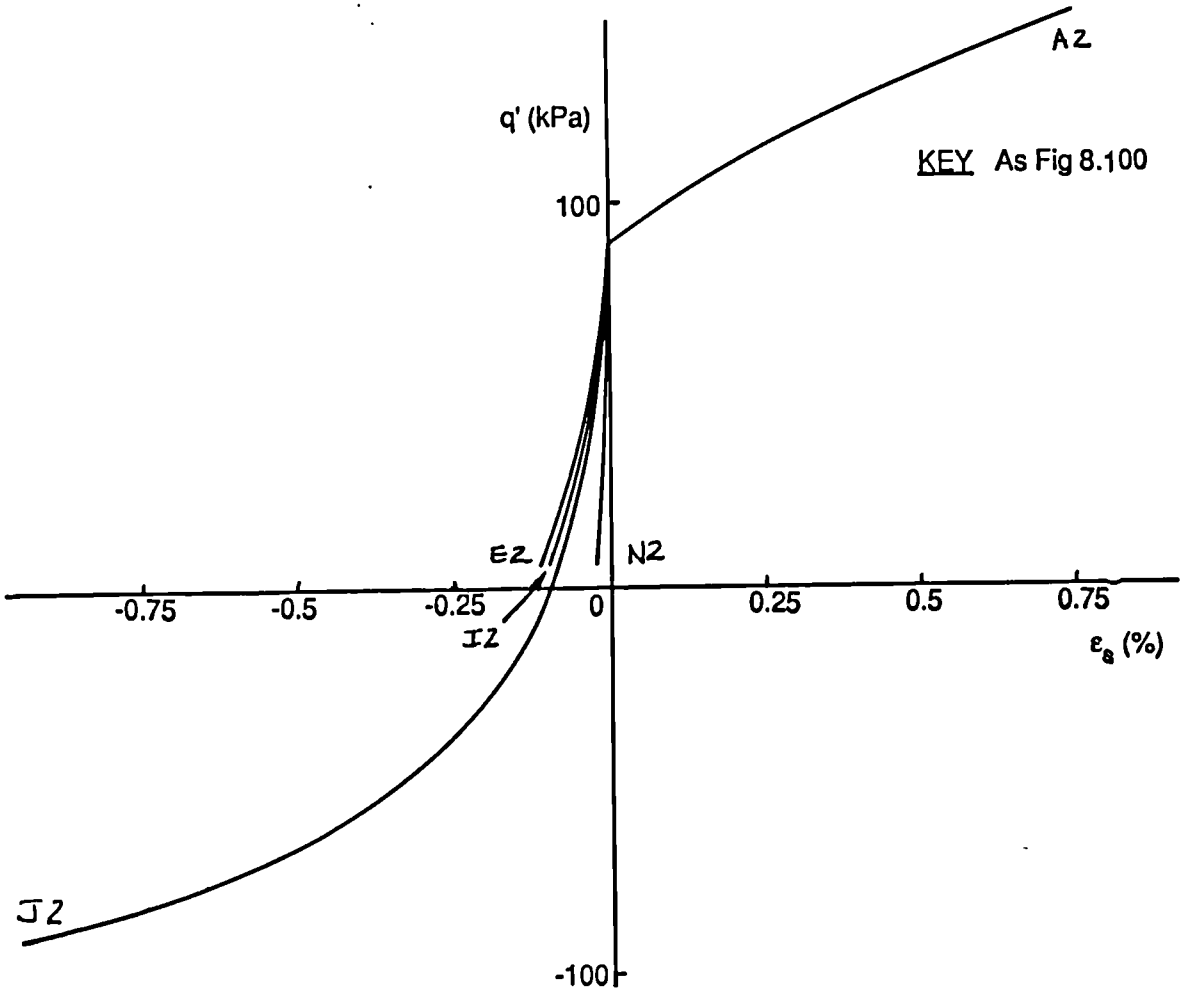

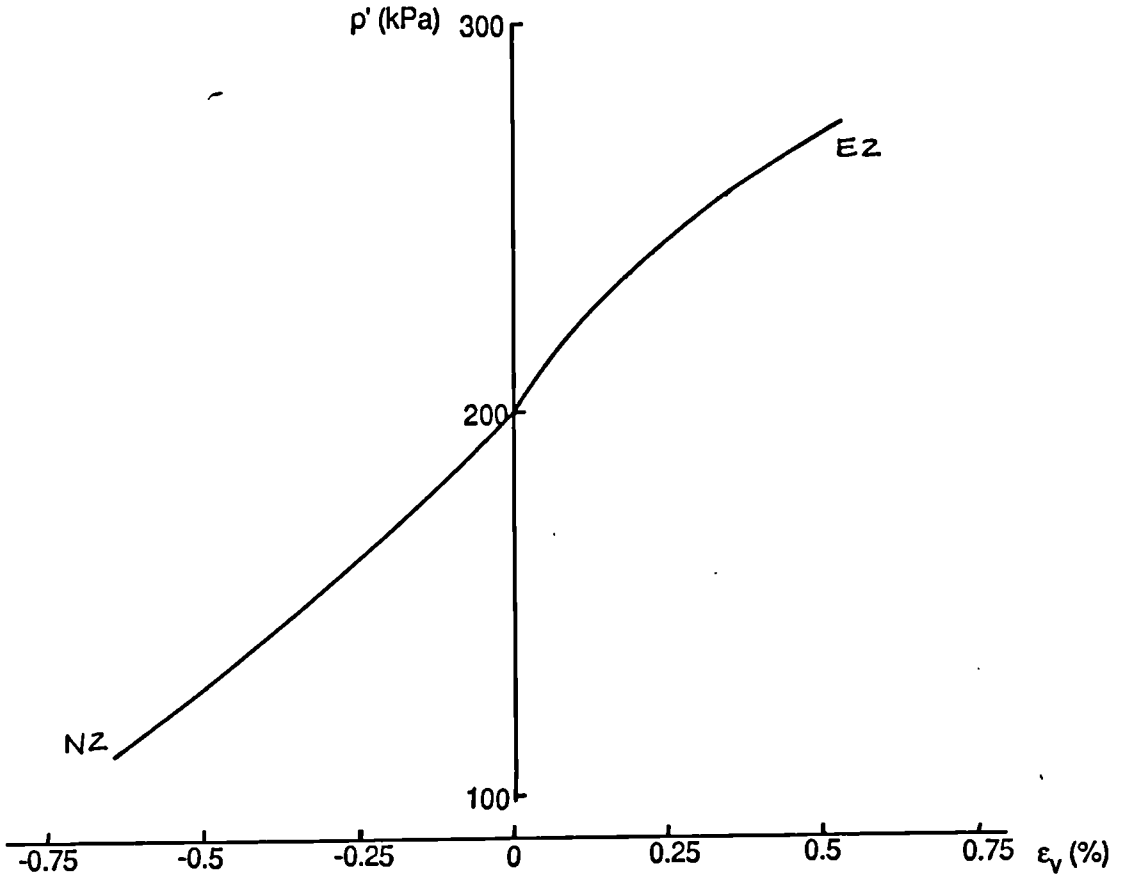

Fig 8.101 Plot of q' against ε_s and p' against ε_v for type two path dependence tests on London clay, η'_o = 0.25, OCR = 2.0.

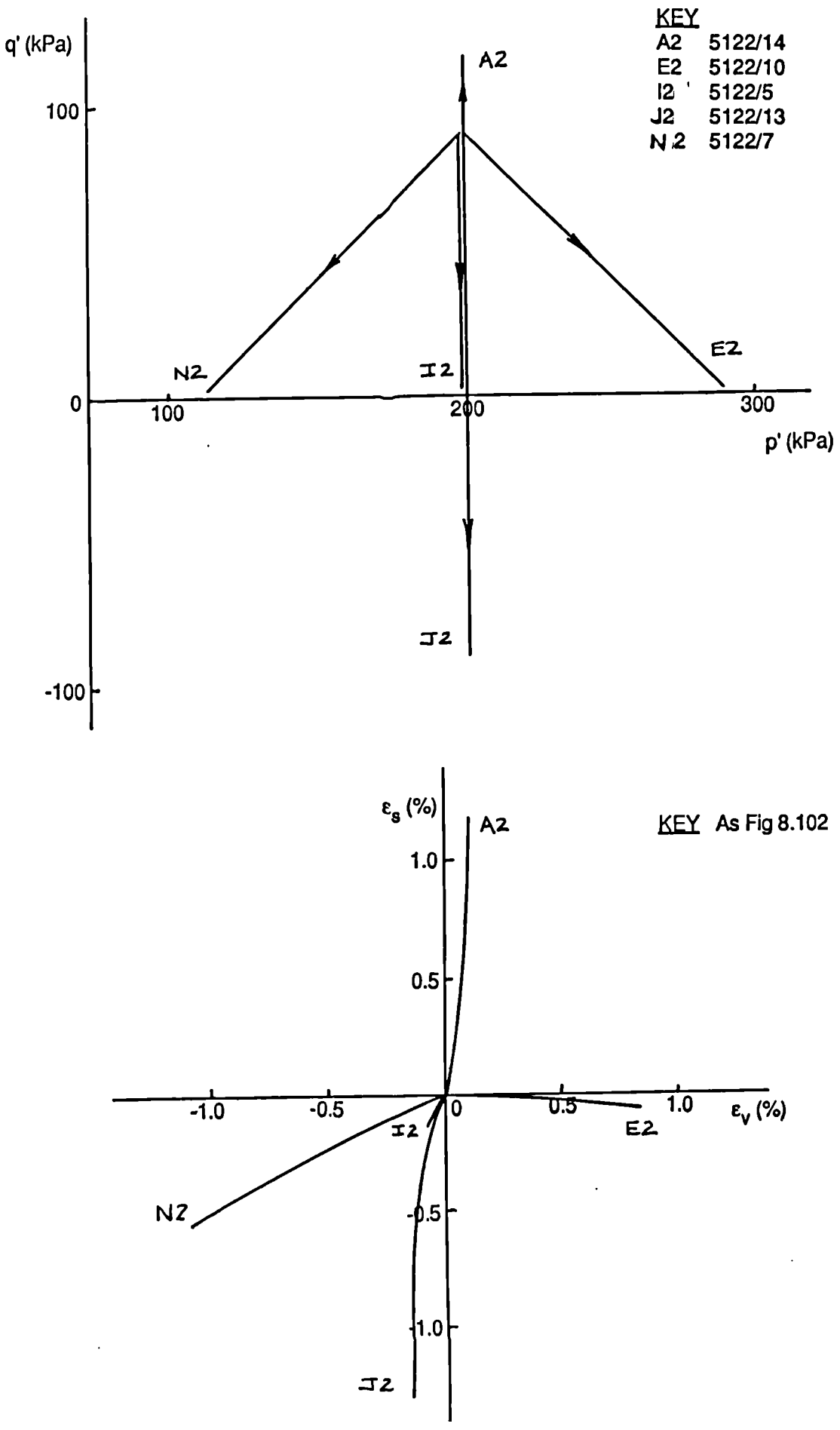

Fig 8.102 Plot of q' against p' and ε_s against ε_v for type two path dependence tests on London clay . η'_o = 0.75, OCR = 2.0.

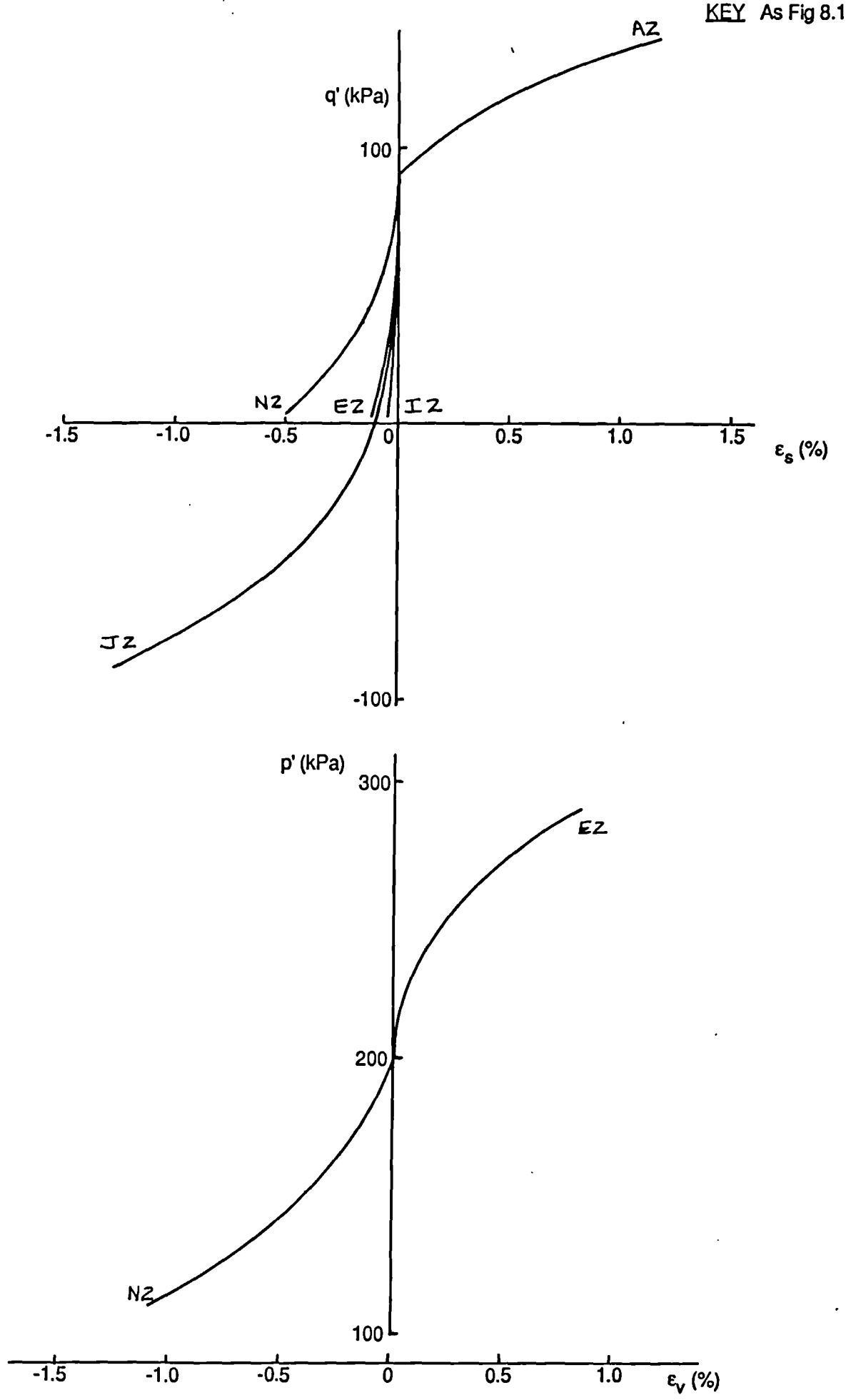

Fig 8.103 Plot of q' against ε_s and p' against ε_v for type two path dependence tests on London clay, η'_o = 0.75, OCR = 2.0.

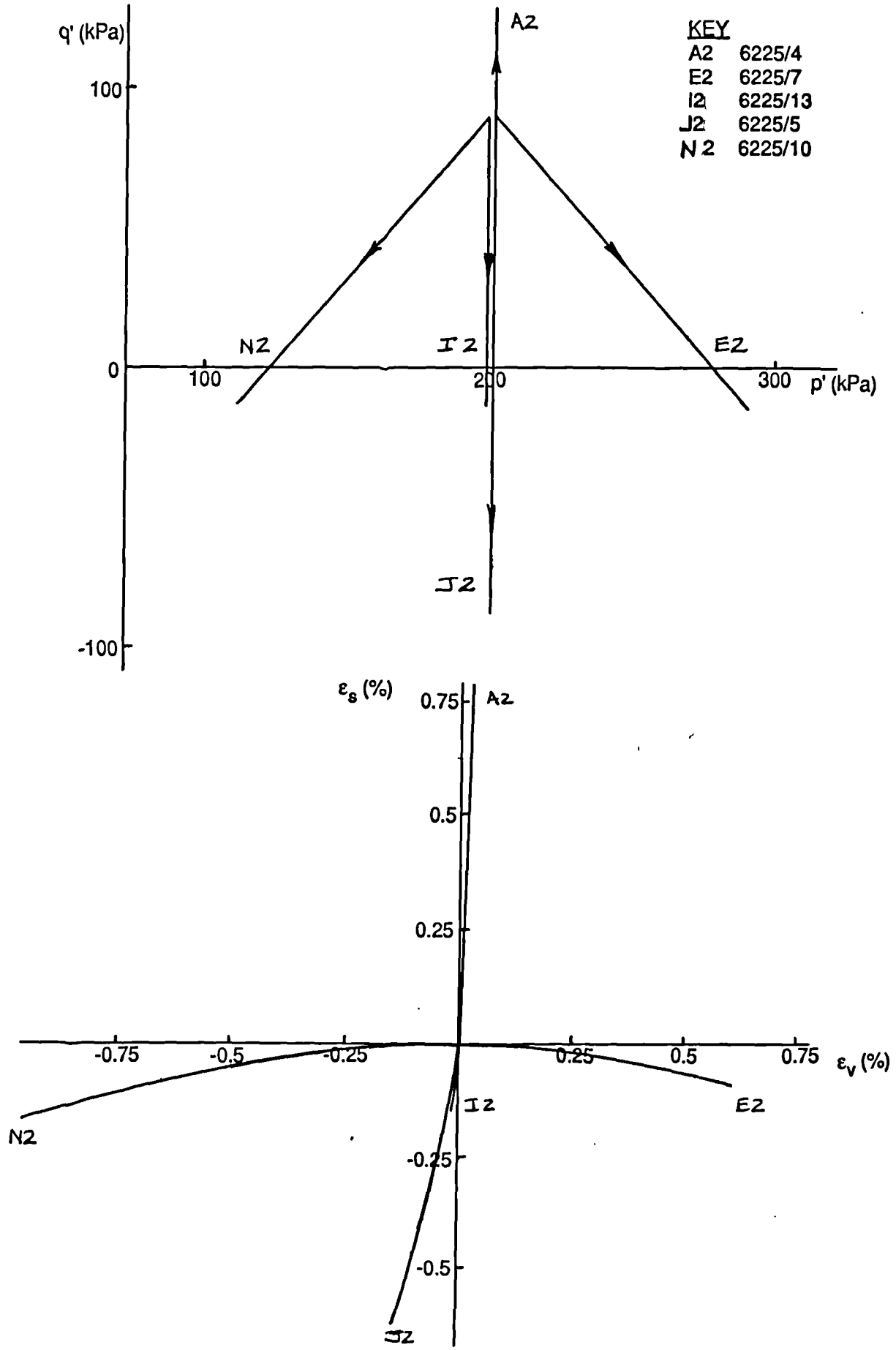

Fig 8.104 Plot of q' against p' and ε_s against ε_v for type two path dependence tests on London clay, two dimensionaly compressed, OCR = 2.0.

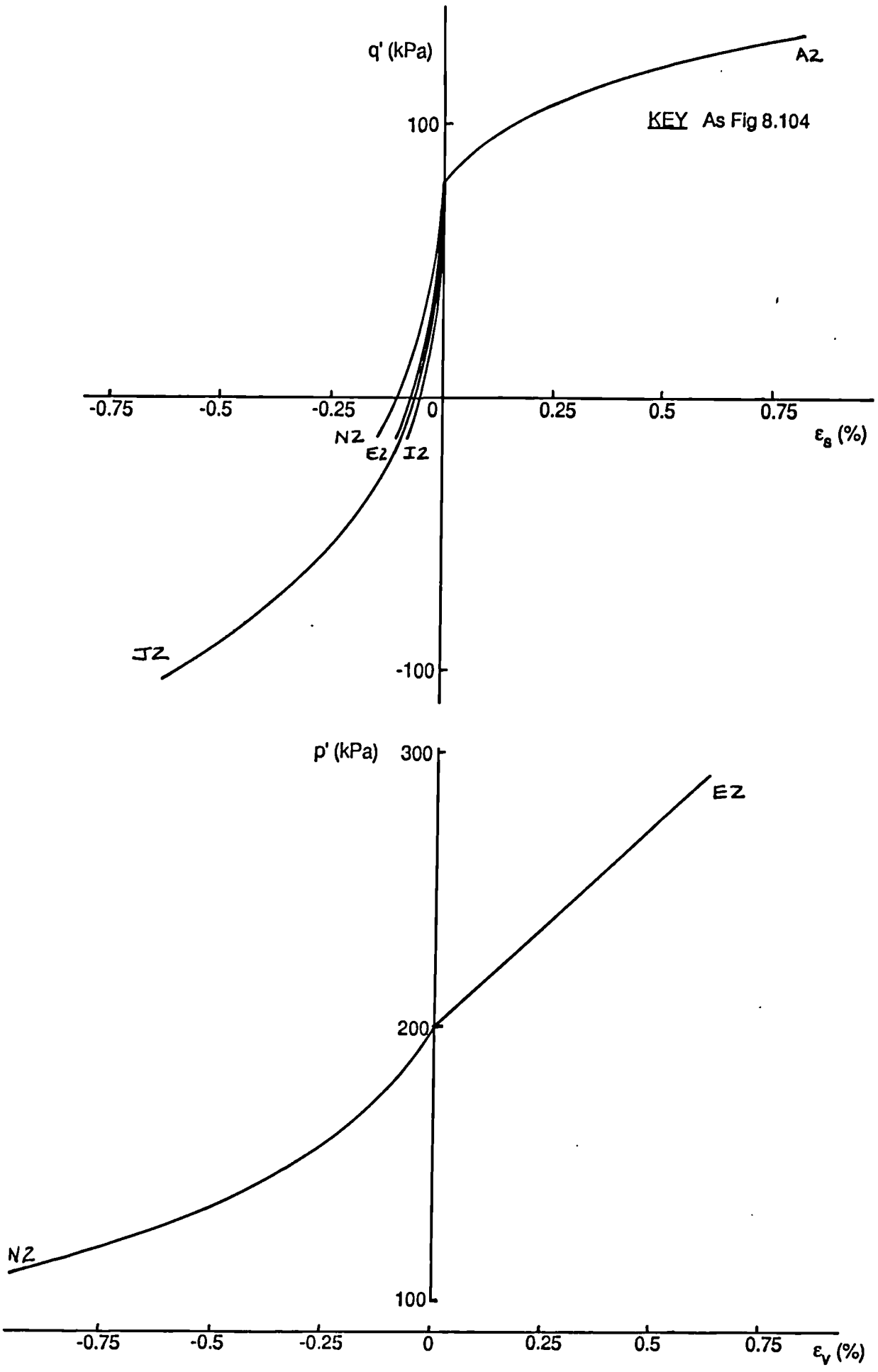

Fig 8.105 Plot of q' against ε_s and p' against ε_v for type two path dependence tests on London clay, two dimensionaly compressed, OCR = 2.0.

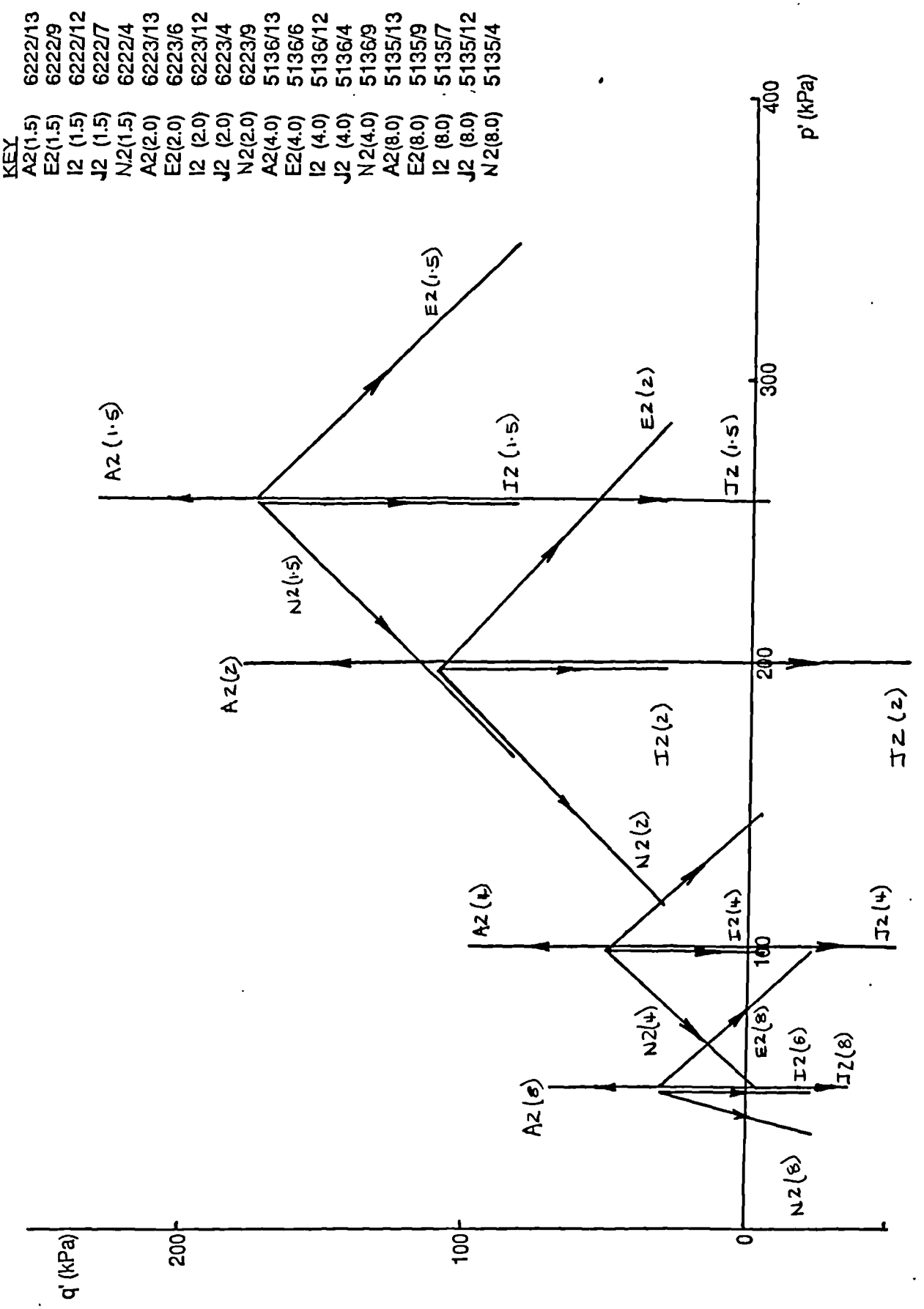

Fig 8.106 Plot of q' against p'. Stress paths followed during type two path dependence tests on London clay, one dimensionally compressed, various OCR's. All data Figs 8.107 - 8.114.

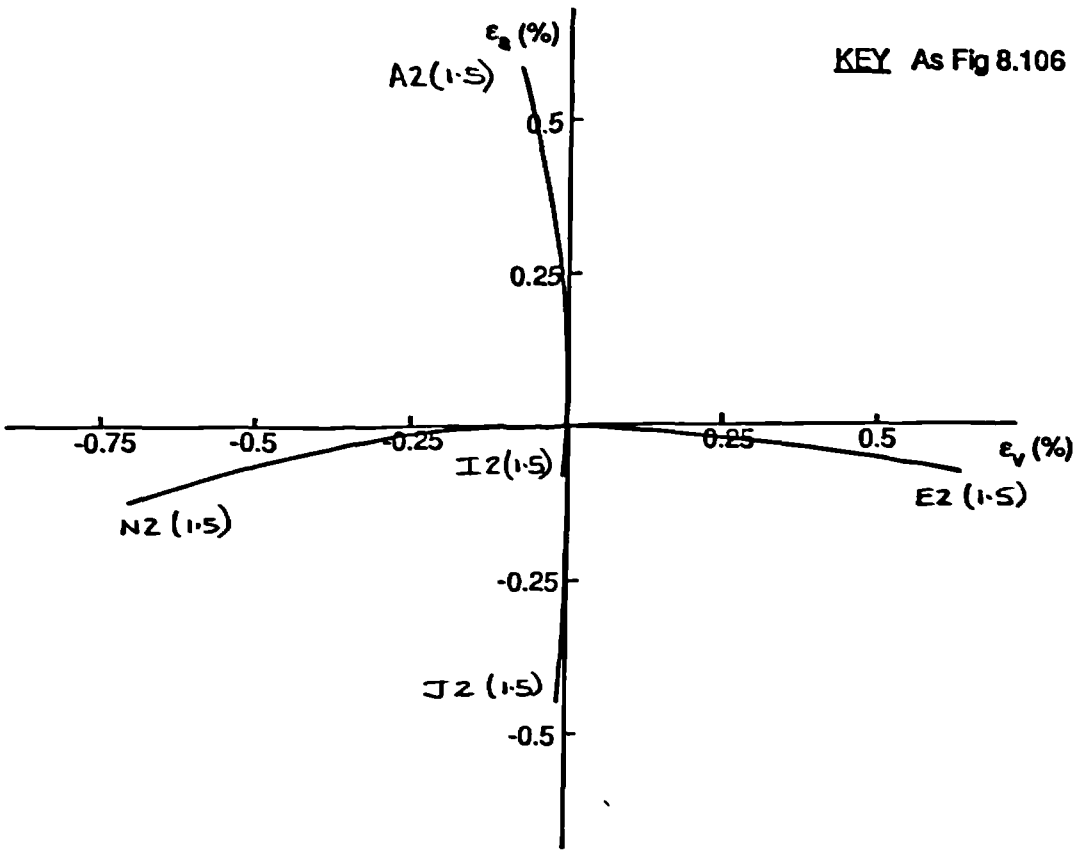

Fig 8.107 Plot of strain paths, ε_s against ε_v for type two path dependence tests on one dimensionally compressed London clay, OCR = 1.5.

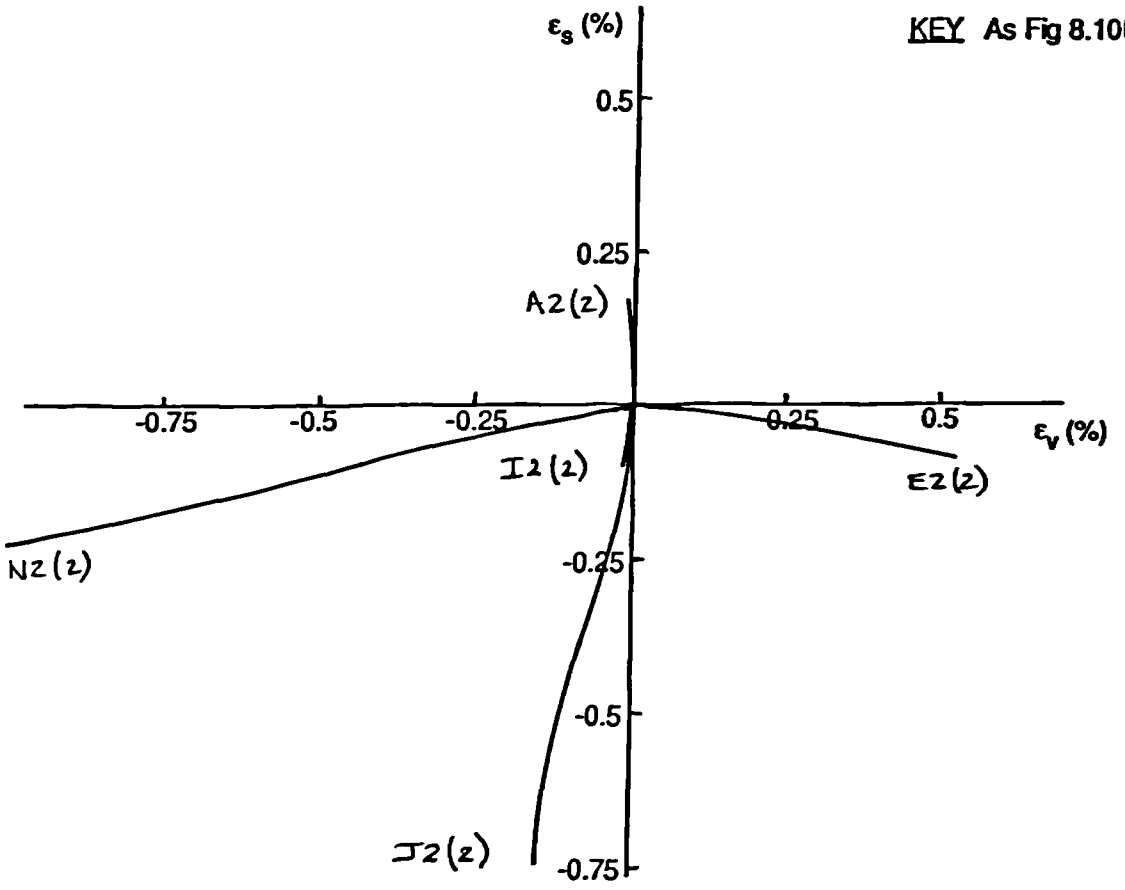

Fig 8.108 Plot of strain paths, ε_s against ε_v for type two path dependence tests on one dimensionally compressed London clay, OCR = 2.0.

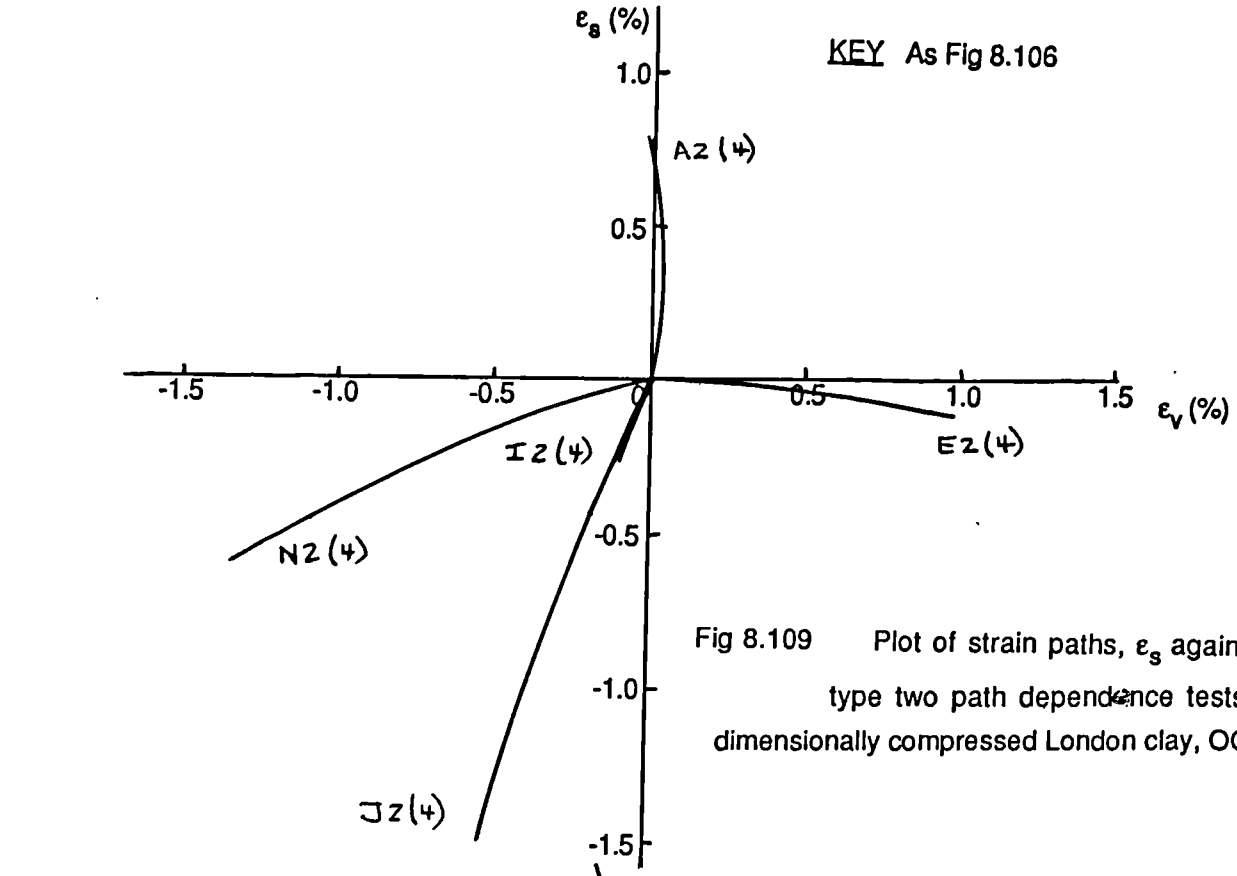

Fig 8.109 Plot of strain paths, ε_s against ε_v for type two path dependence tests on one dimensionally compressed London clay, OCR = 4.0.

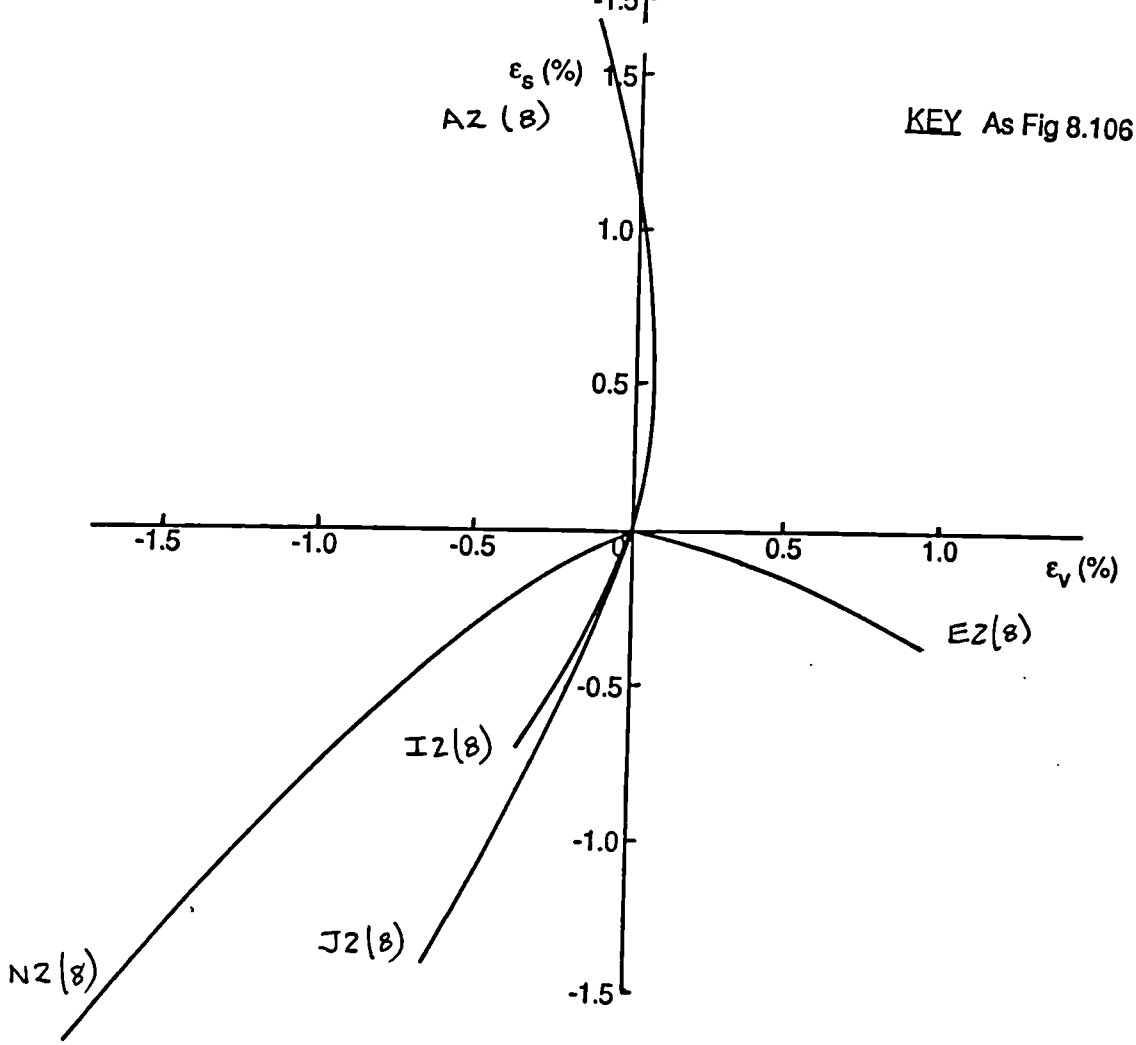

Fig 8.110 Plot of strain paths, ε_s against ε_v for type two path dependence tests on one dimensionally compressed London clay, OCR = 8.0.

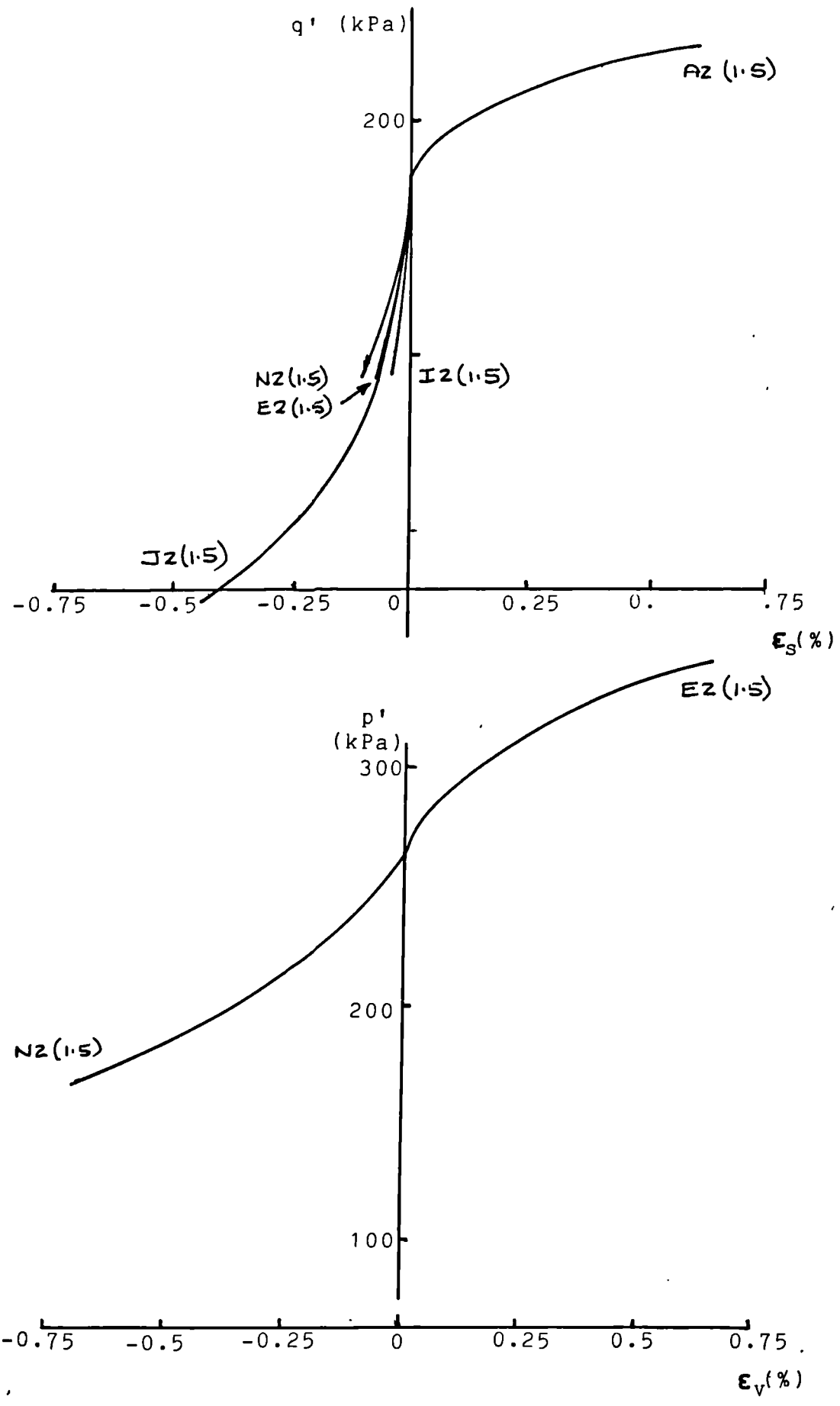

Fig 8.111 Plots of q' against ε_s and p` against ε_v for type one path dependence tests on one dimensionally compressed London clay, OCR = 1.5.

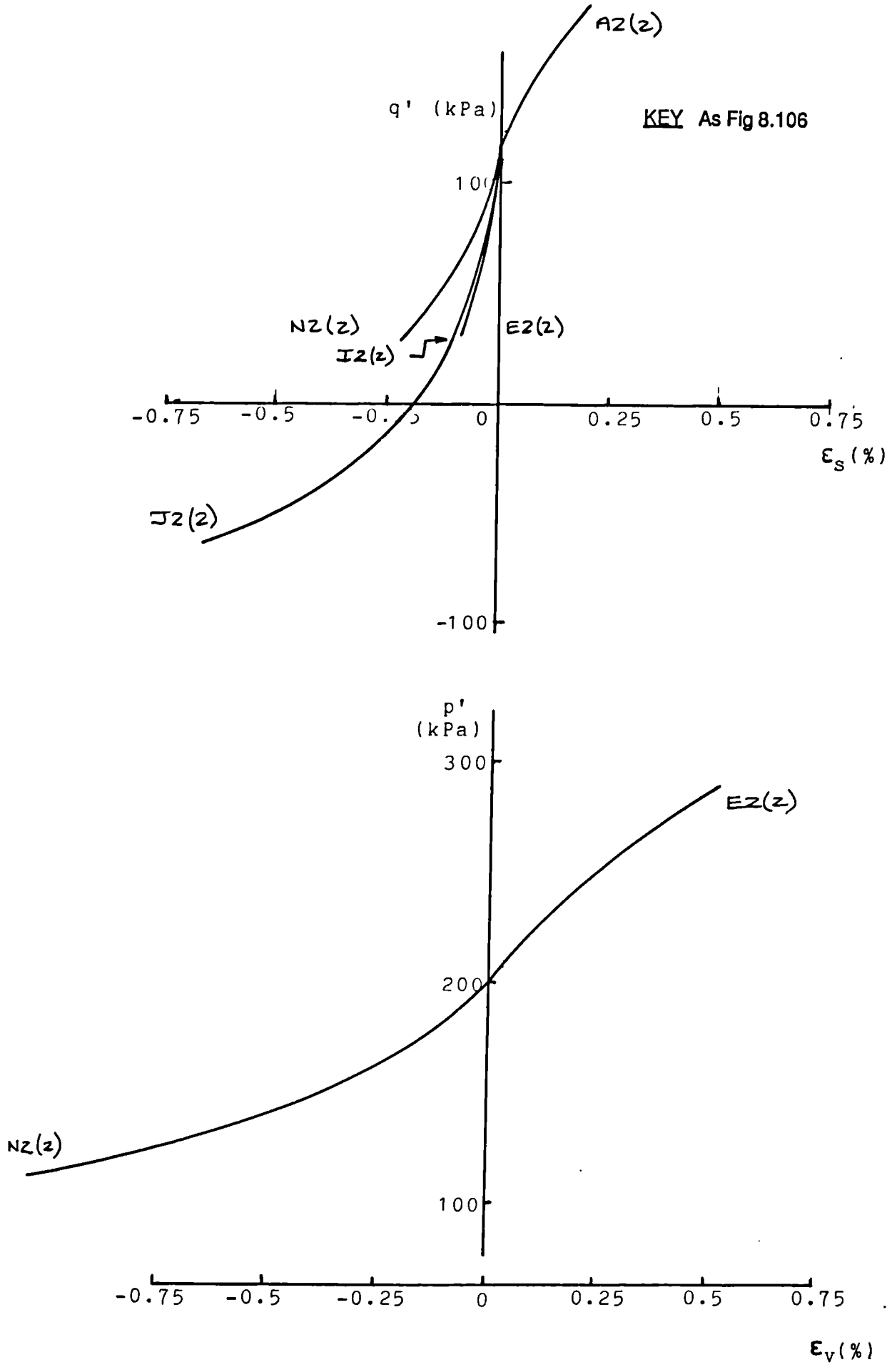

Fig 8.112 Plots of q' against ε_s and p` against ε_v for type two path dependence tests on one dimensionally compressed London clay, OCR = 2.0.

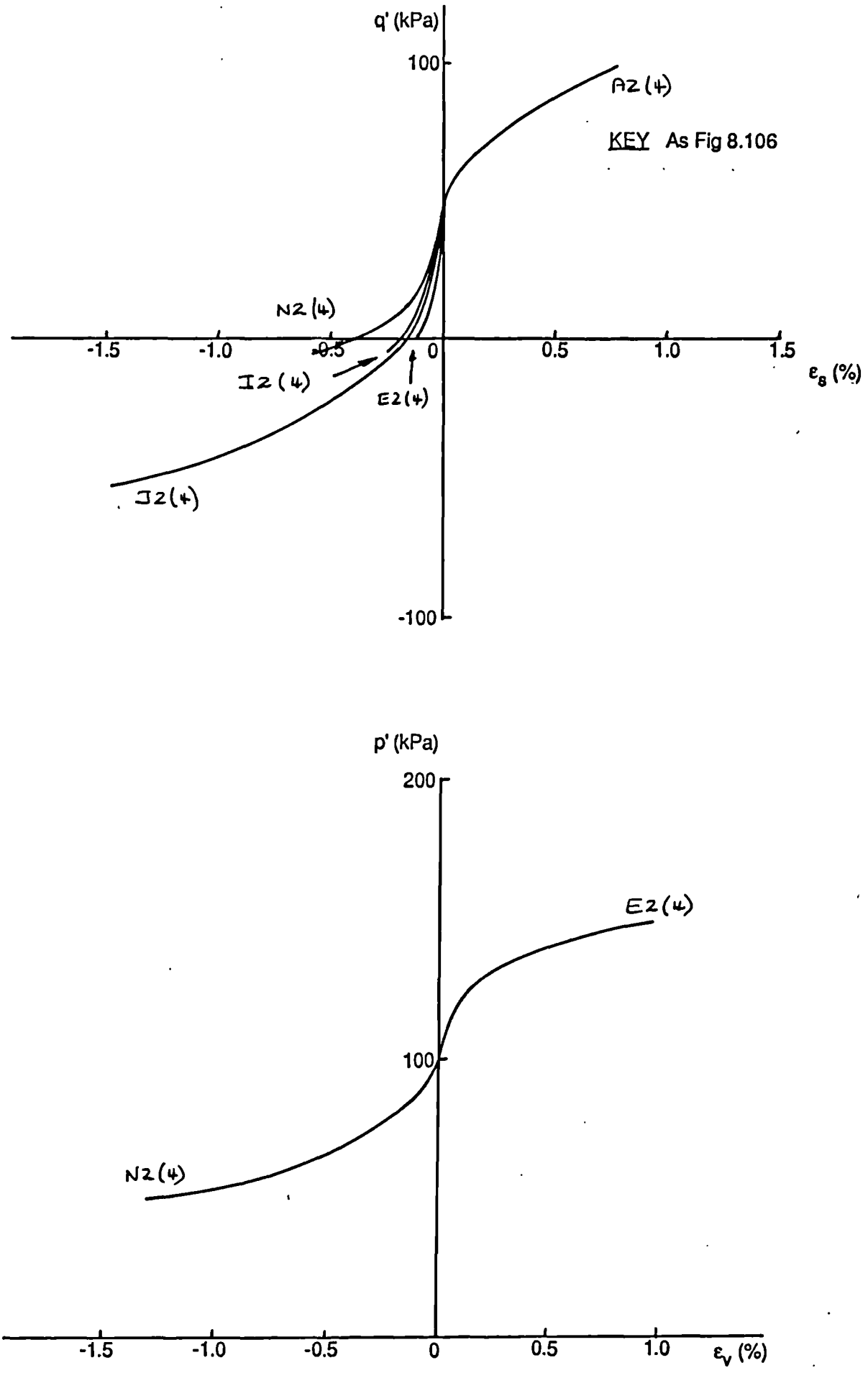

Fig 8.113 Plots of q' against ε_s and p` against ε_v for type two path dependance tests on one dimensionally compressed London clay, OCR = 4.0.

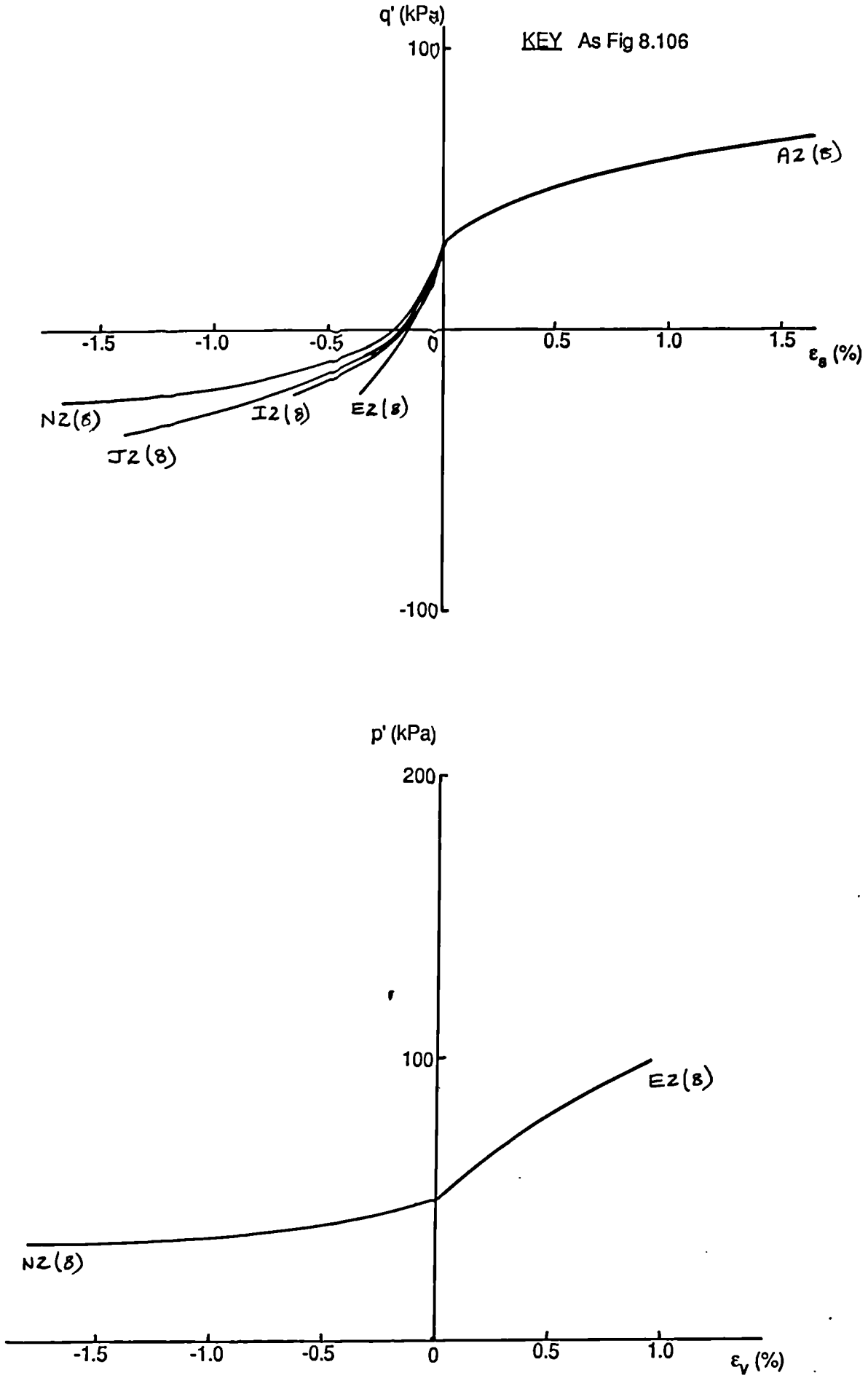

Fig 8.114 Plots of q' against ε_s and p` against ε_v for type two path dependence tests on one dimensionally compressed London clay, OCR = 8.0.

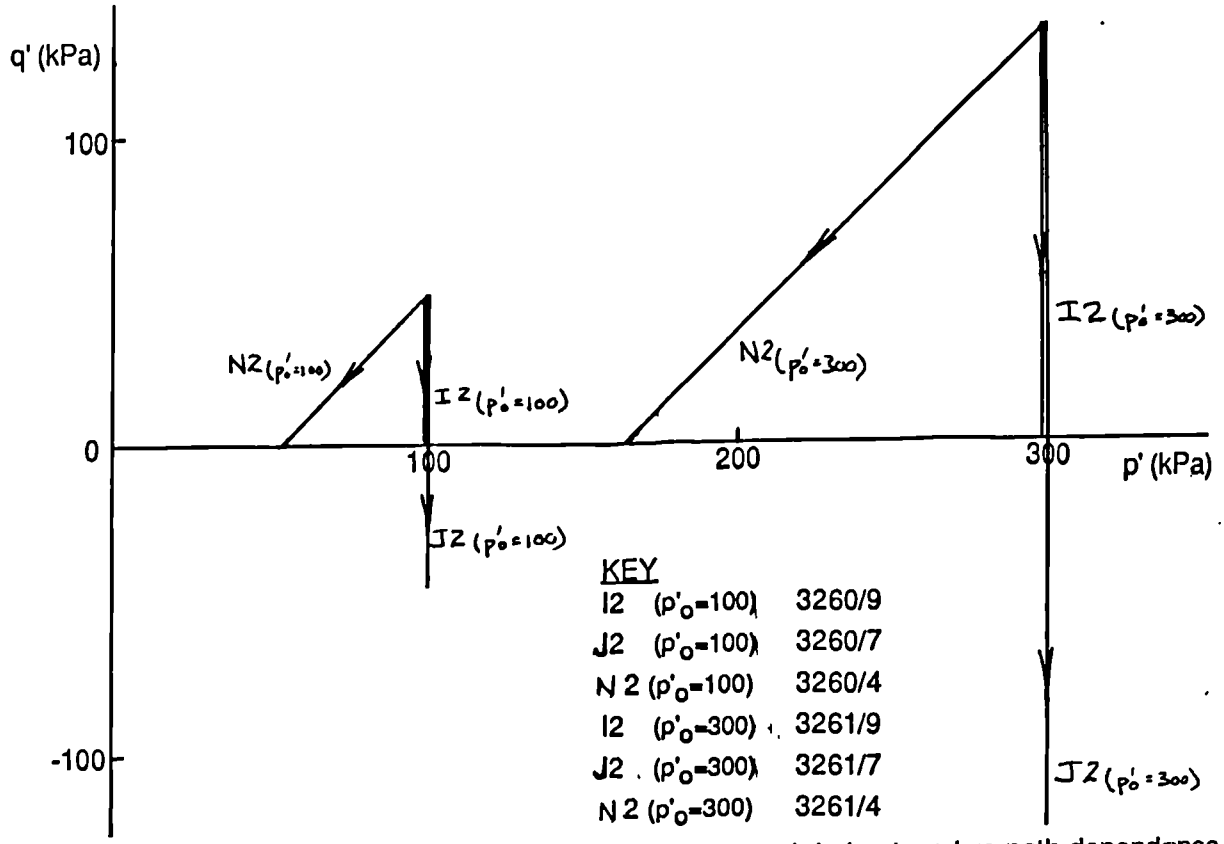

Fig 8.115 Plot of q' against p'. Stress paths followed during type two path dependence tests on London clay, $\eta'_o = 0$, OCR = 2.0, various p'. All data Figs 8.116 - 8.119.

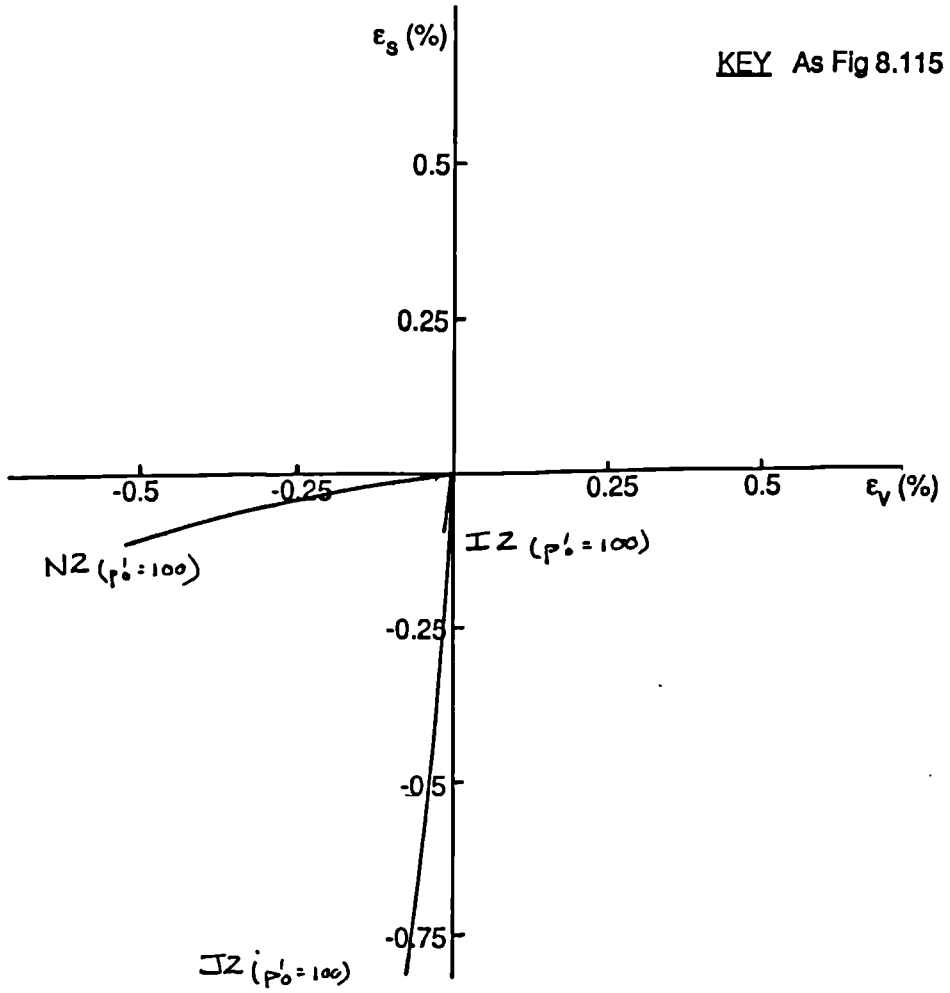

Fig 8.116 Plot of strain paths, ε_s against ε_v for type two path dependence tests on London clay, OCR = 2.0, p' = 100 kPa.

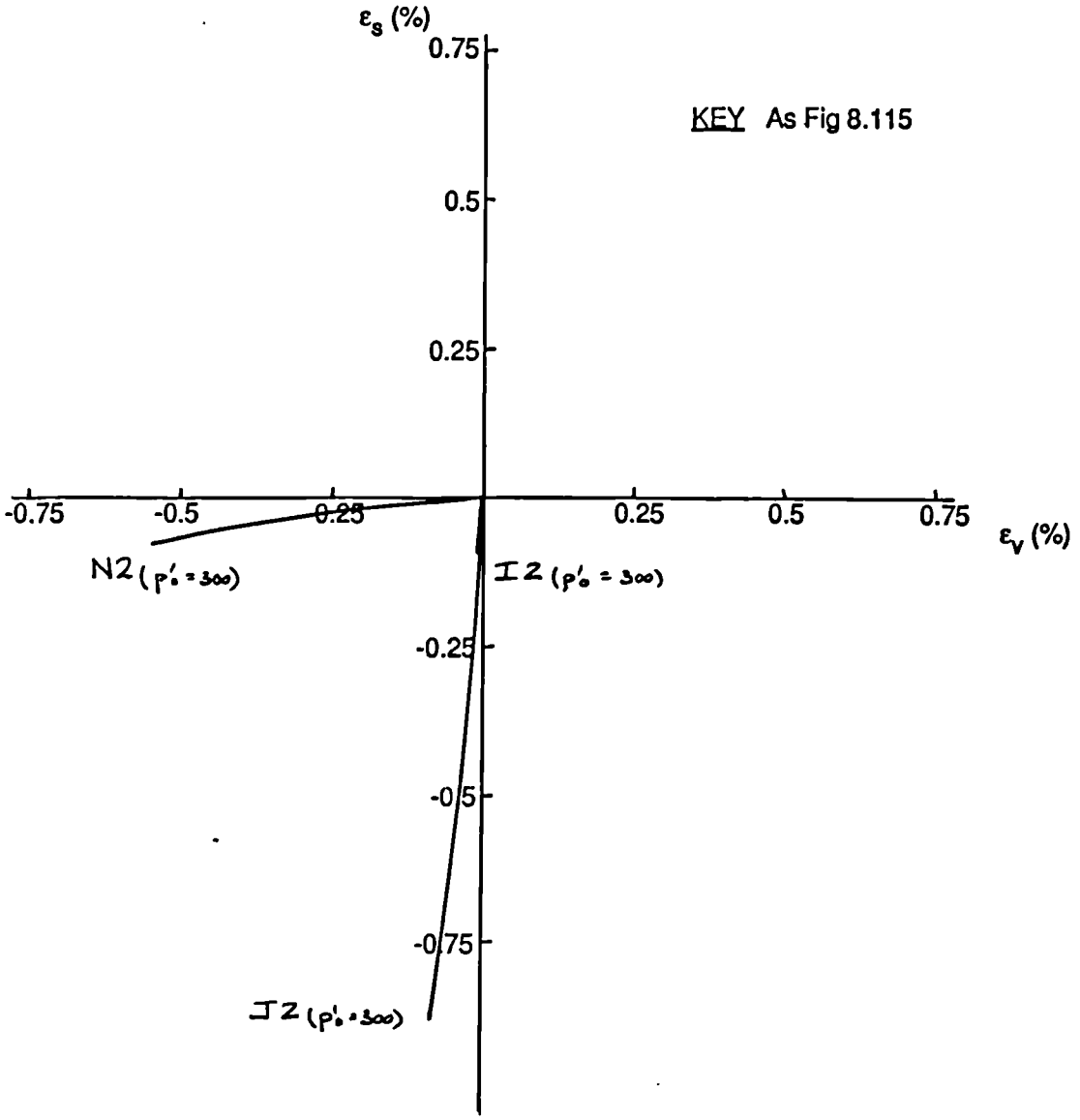

Fig 8.117 Plot of strain paths, ε_s against ε_v for type two path dependence tests on London clay, OCR = 2.0, p' = 300 kPa.

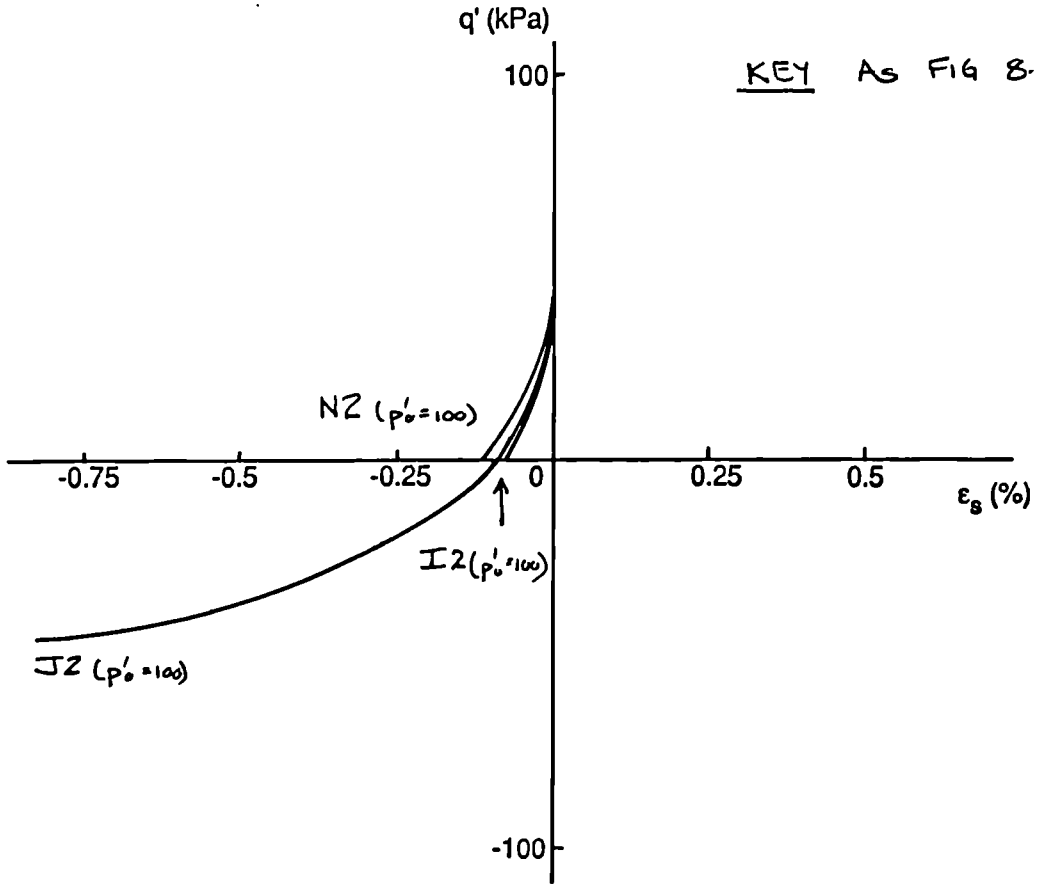

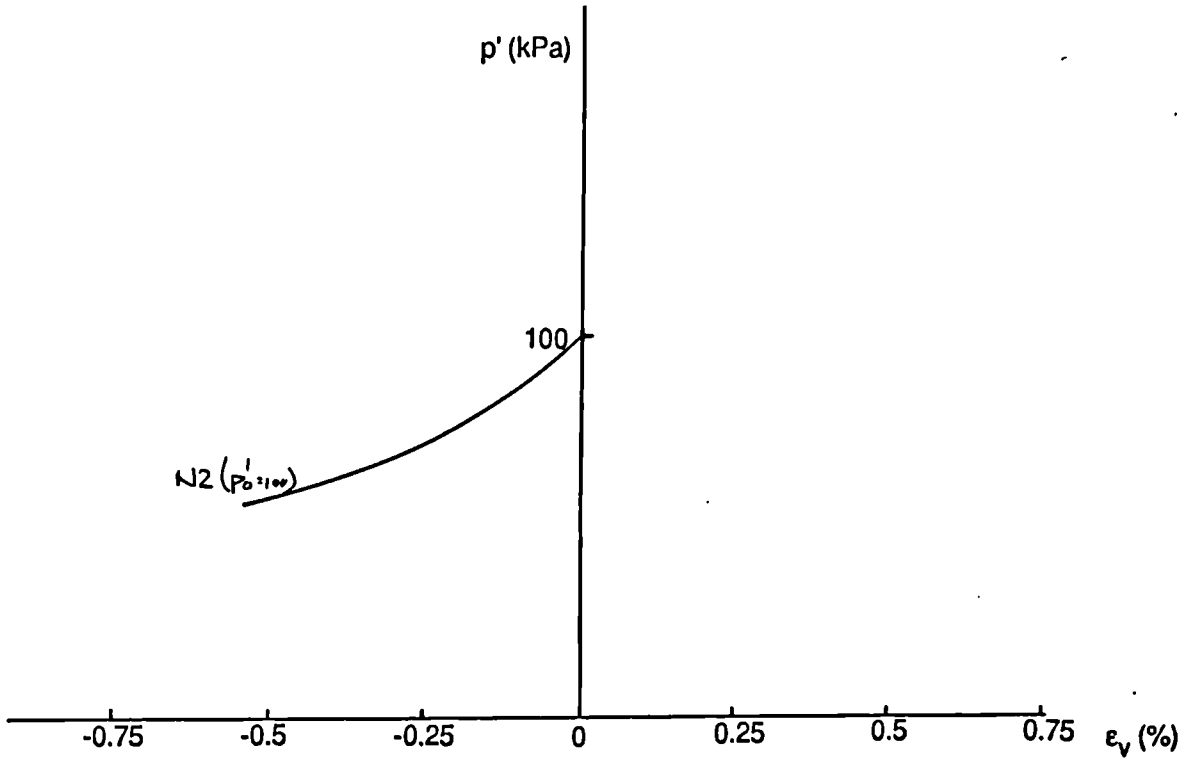

Fig 8.118 Plots of q' against ε_s and p' against ε_v for type two path dependence tests on London clay, OCR = 2.0, p' = 100kPa.

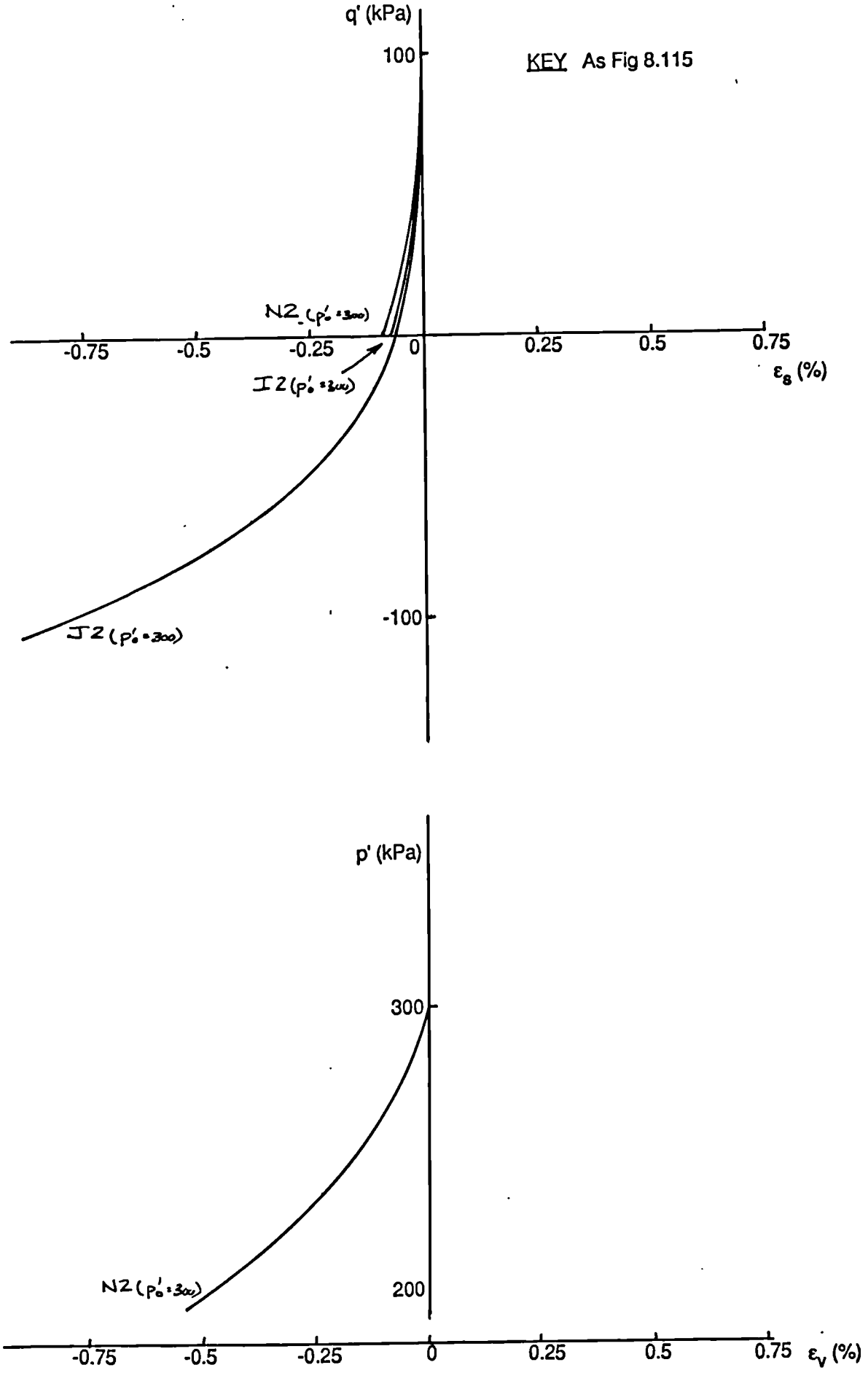

Fig 8.119 Plots of q' against ε_s and p` against ε_v for type two path dependence tests on London clay, OCR = 2.0, p' = 300kPa.

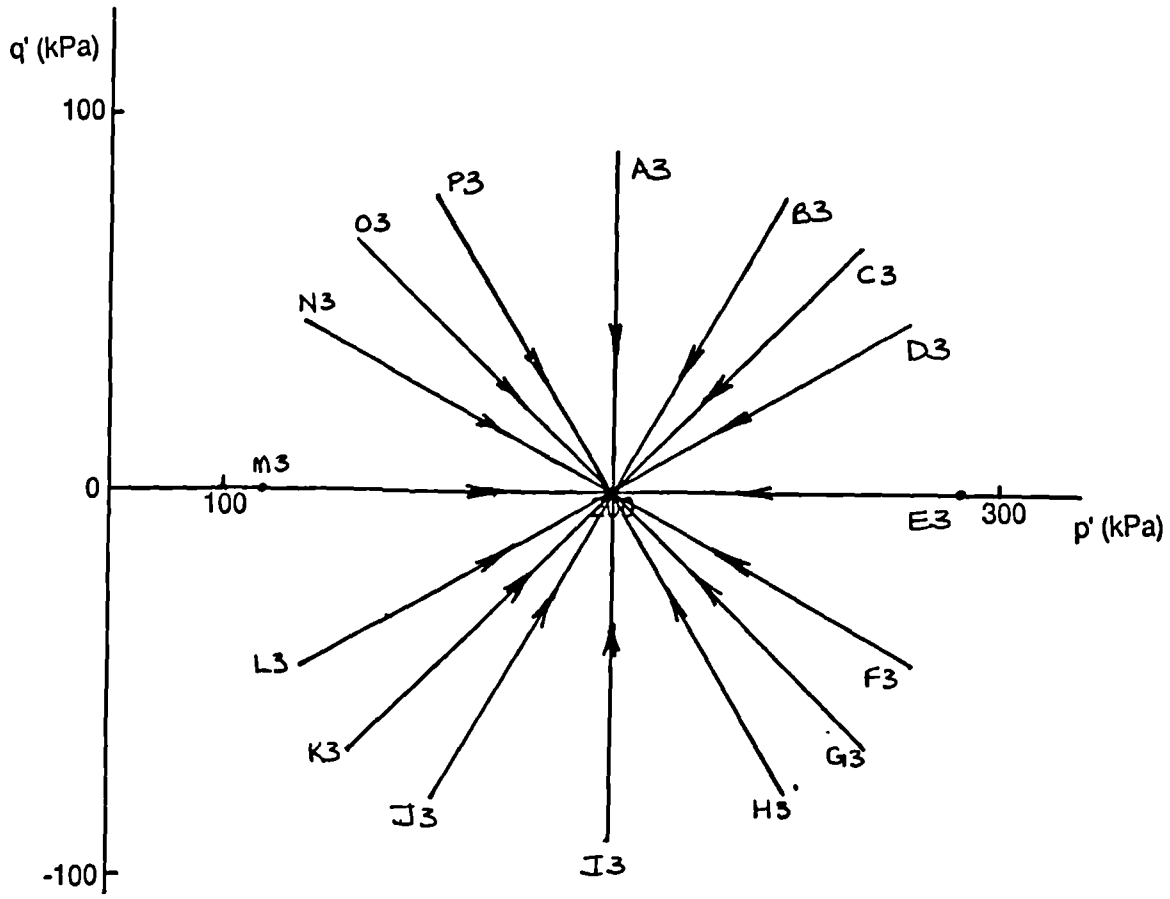

Fig 8.120 Plot of q' against p'. Stress paths followed during path dependence type three tests. $\eta'_o = 0$, OCR = 2.0. All data Figs 8.121 - 8.130b.

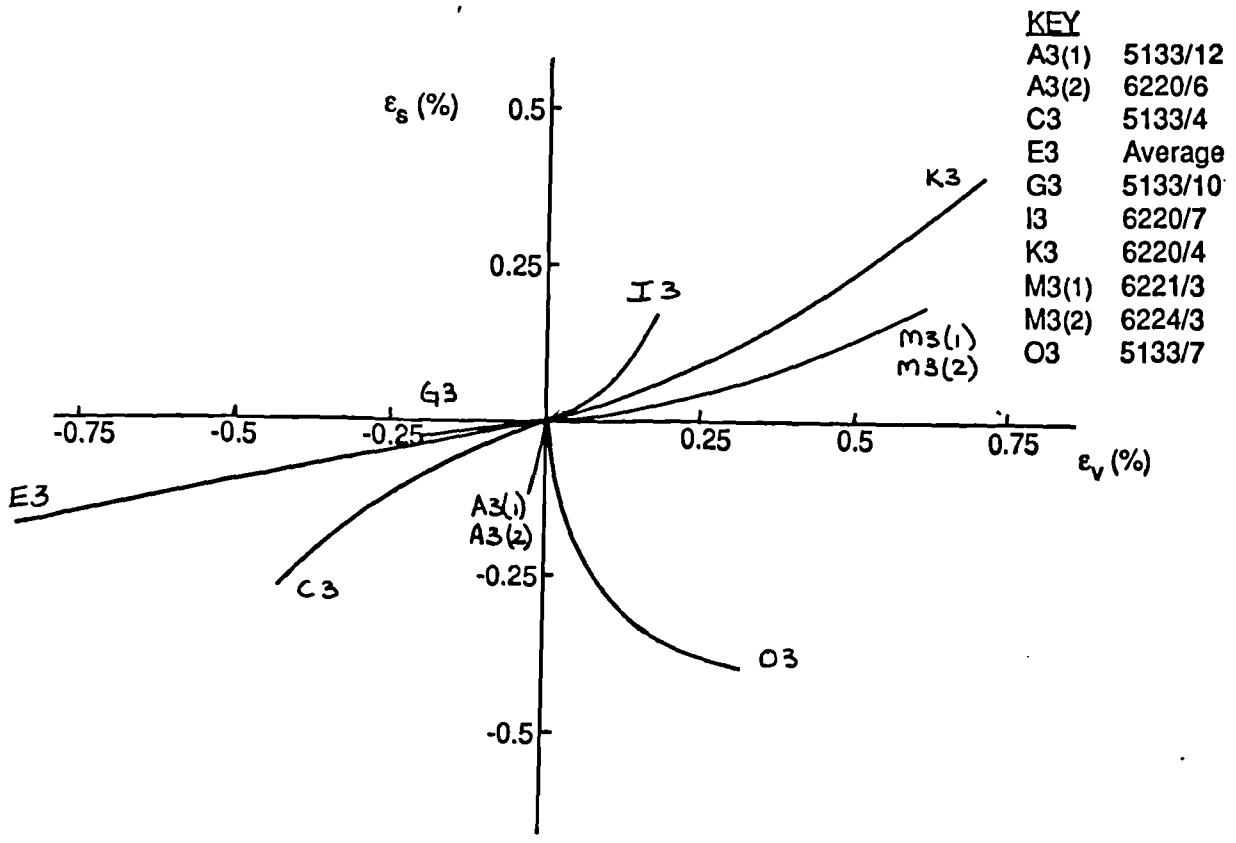

Fig 8.121 Plot of strain paths, ε_s against ε_v for type three path dependence tests on speswhite kaolin.

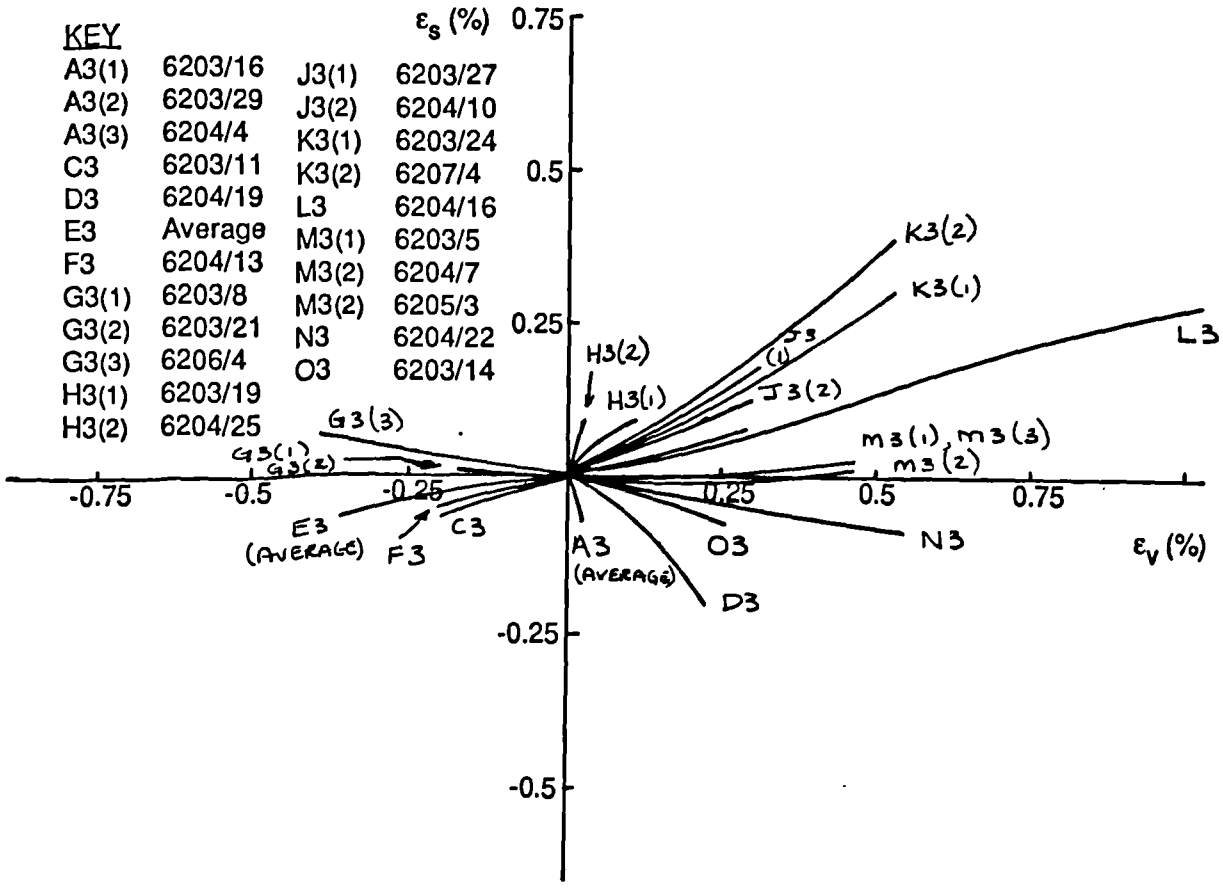

Fig 8.122 Plot of strain paths, ε_s against ε_v for type three path dependence tests on Ware till.

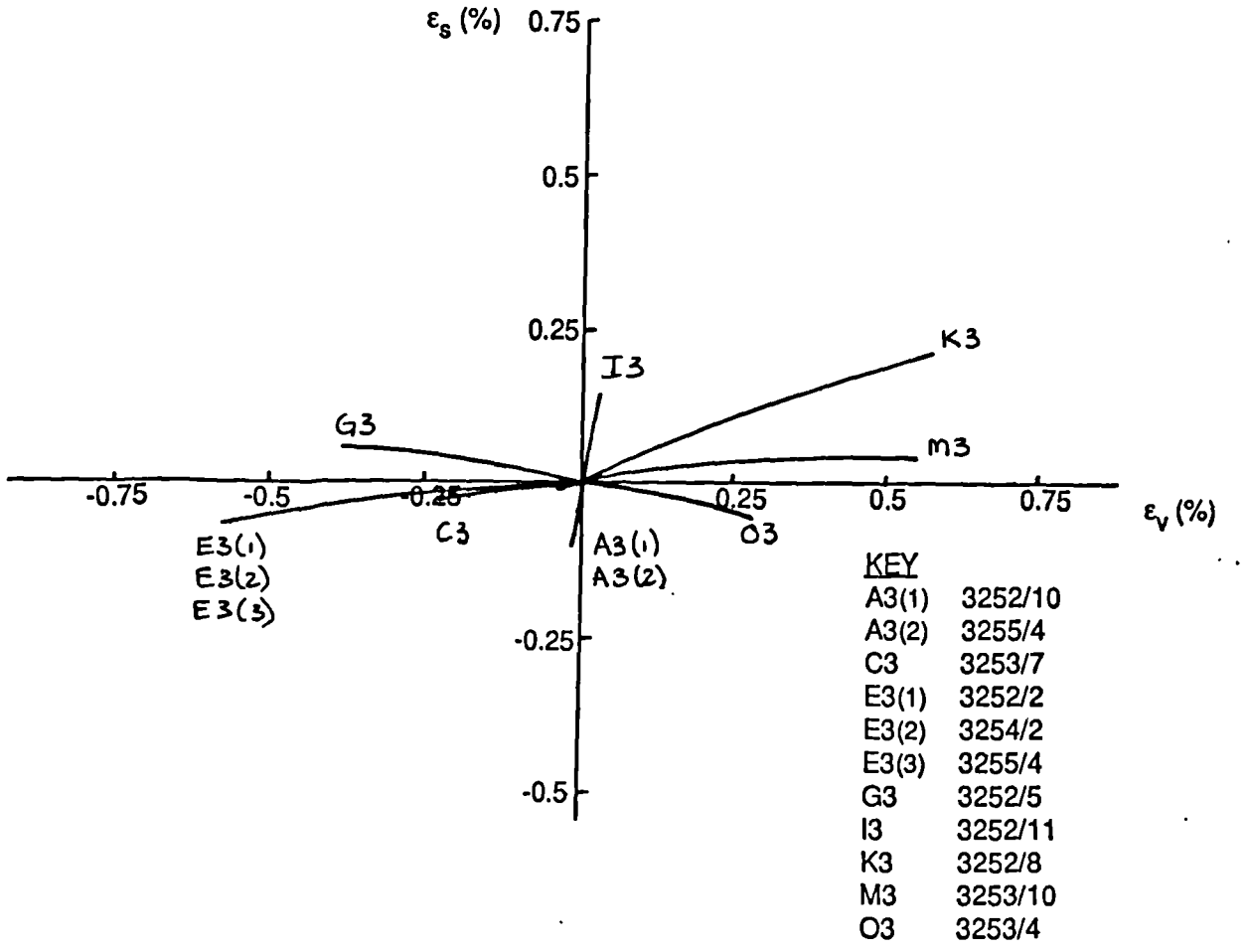

Fig 8.123 Plot of strain paths, ε_s against ε_v for type three path dependence tests on Cowden till.

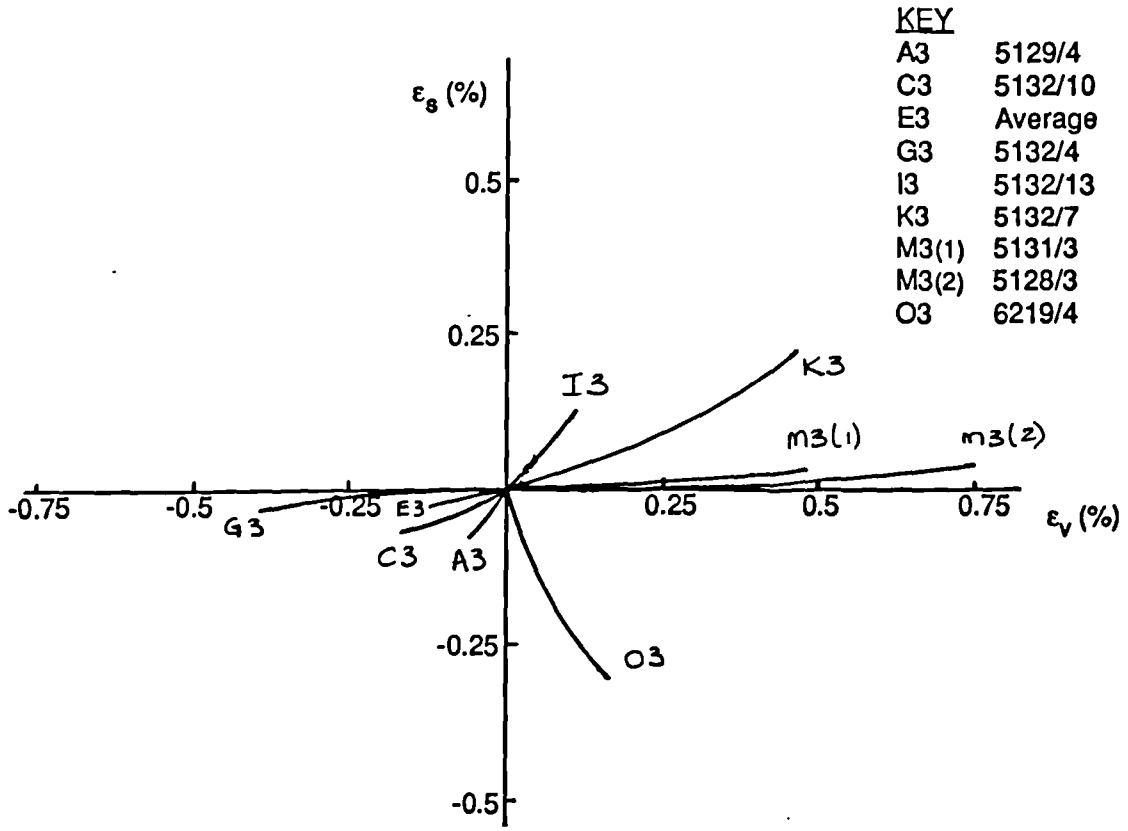

Fig 8.124 Plot of strain paths, ε_s against ε_v for type three path dependence tests on slate dust.

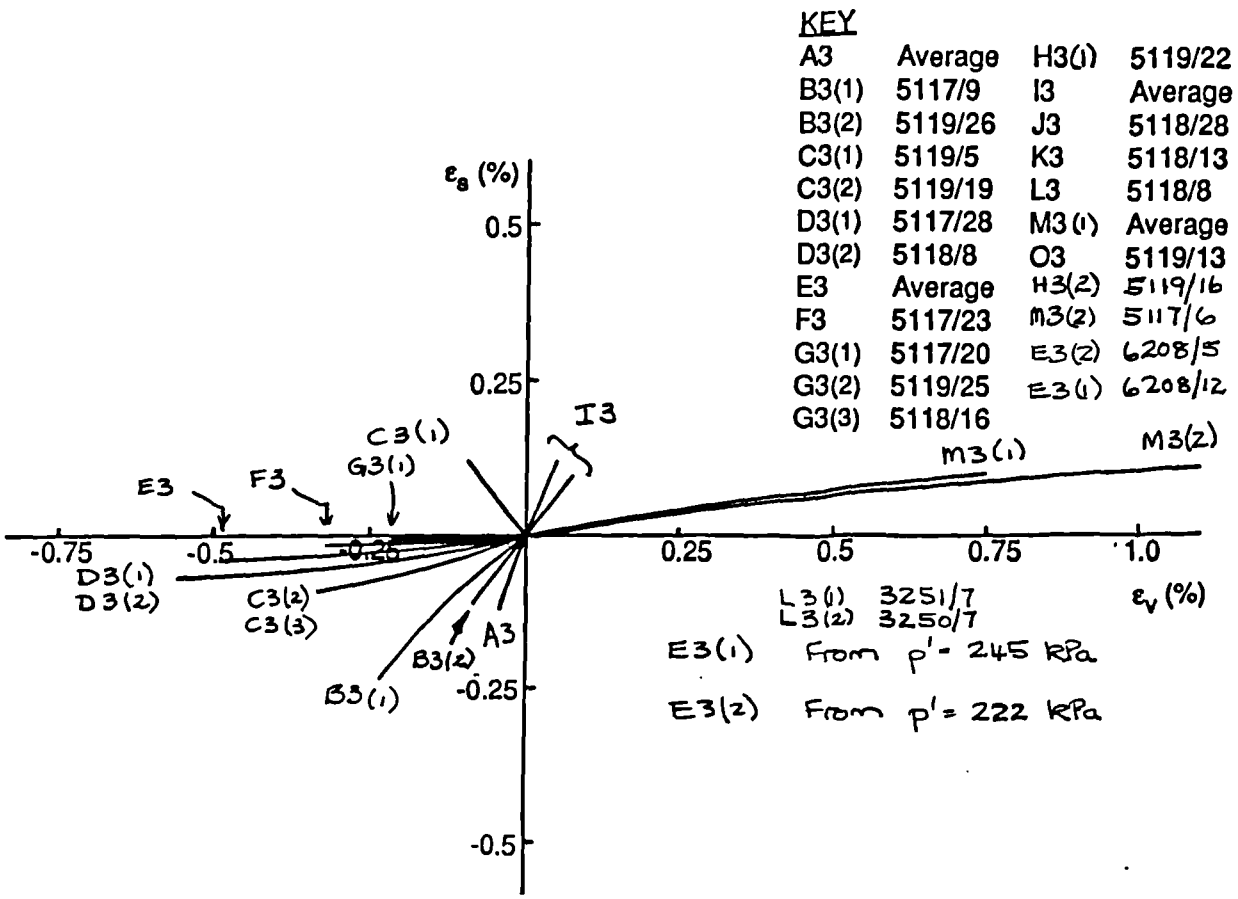

Fig 8.125a Plot of strain paths, ε_s against ε_v for type three path dependence tests on London clay.

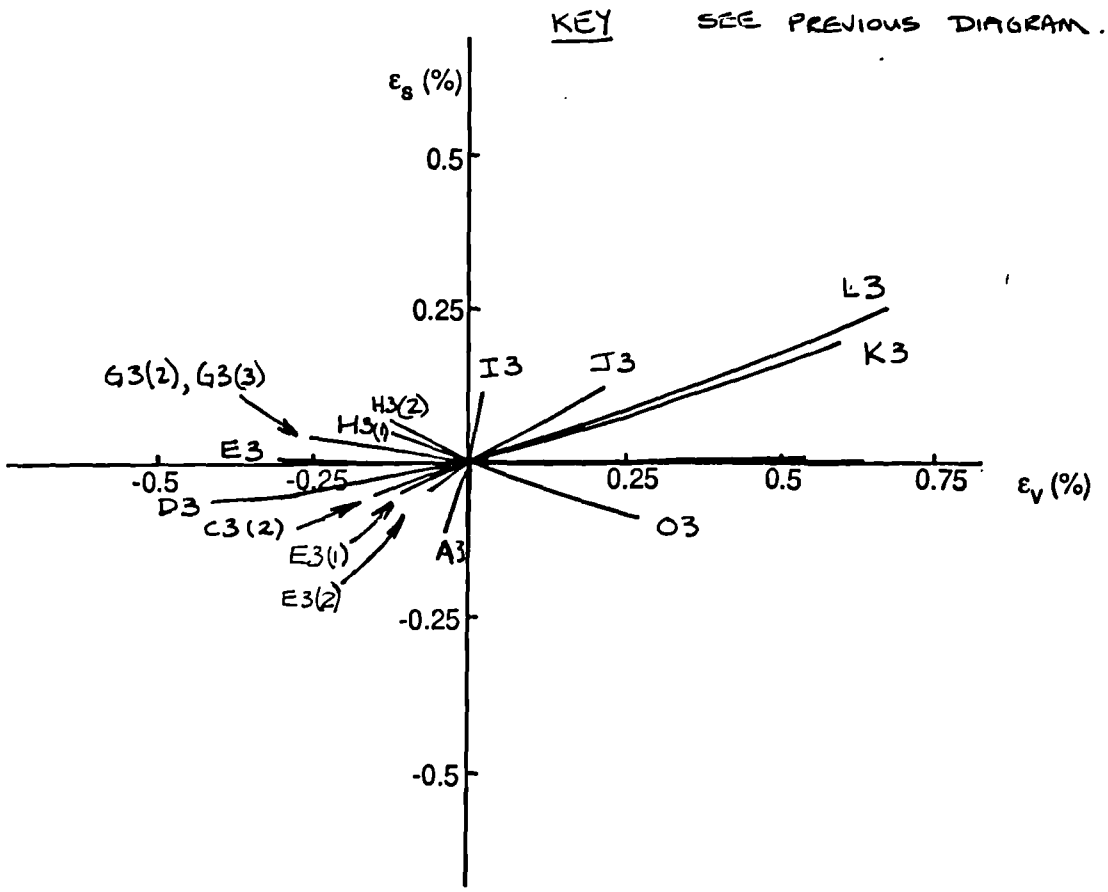

Fig 8.125b Plot of stress paths, q' against p', and strain paths followed during path dependence type three tests on London clay. $\eta'_o = 0$, OCR = 2.0, p' = 200kPa. Data in Fig 8.130b.

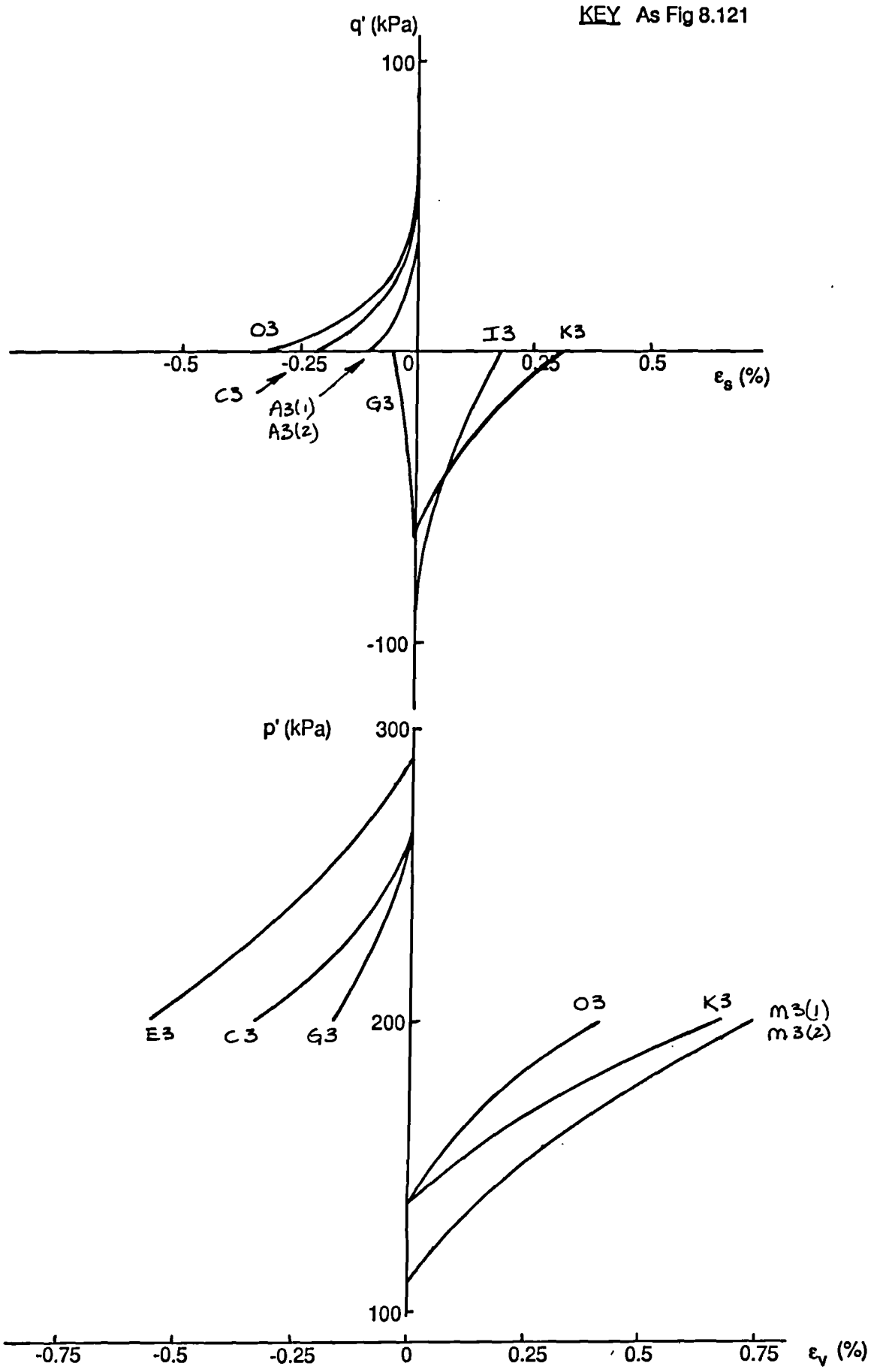

Fig 8.126 Plots of q' against ε_s and p' against ε_v for type three path dependence tests on speswhite kaolin.

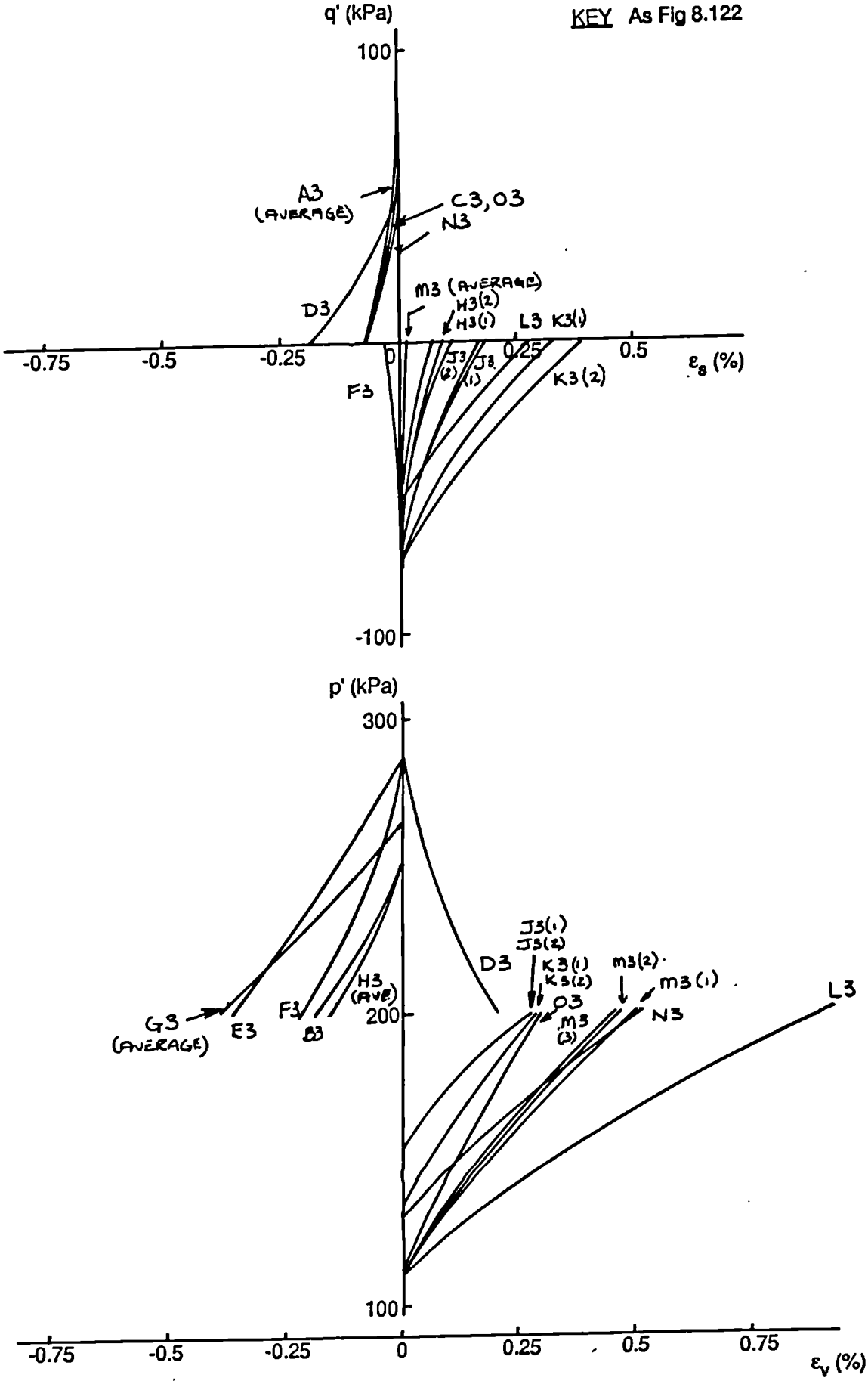

Fig 8.127 Plots of q' against ε_s and p' against ε_v for type three path dependence tests on Ware till.

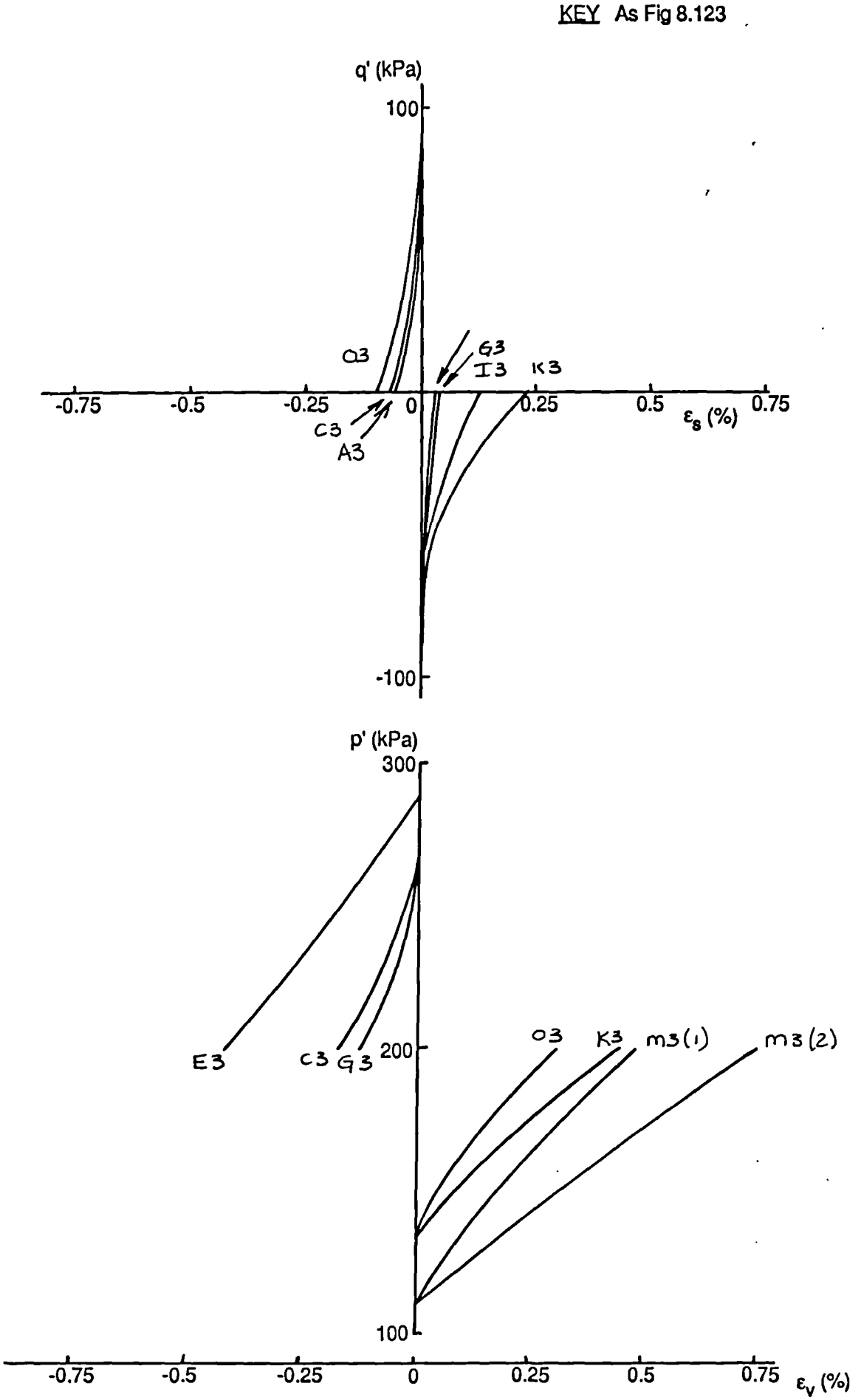

Fig 8.128 Plots of q' against ε_s and p' against ε_v for type three path dependence tests on Cowden till.

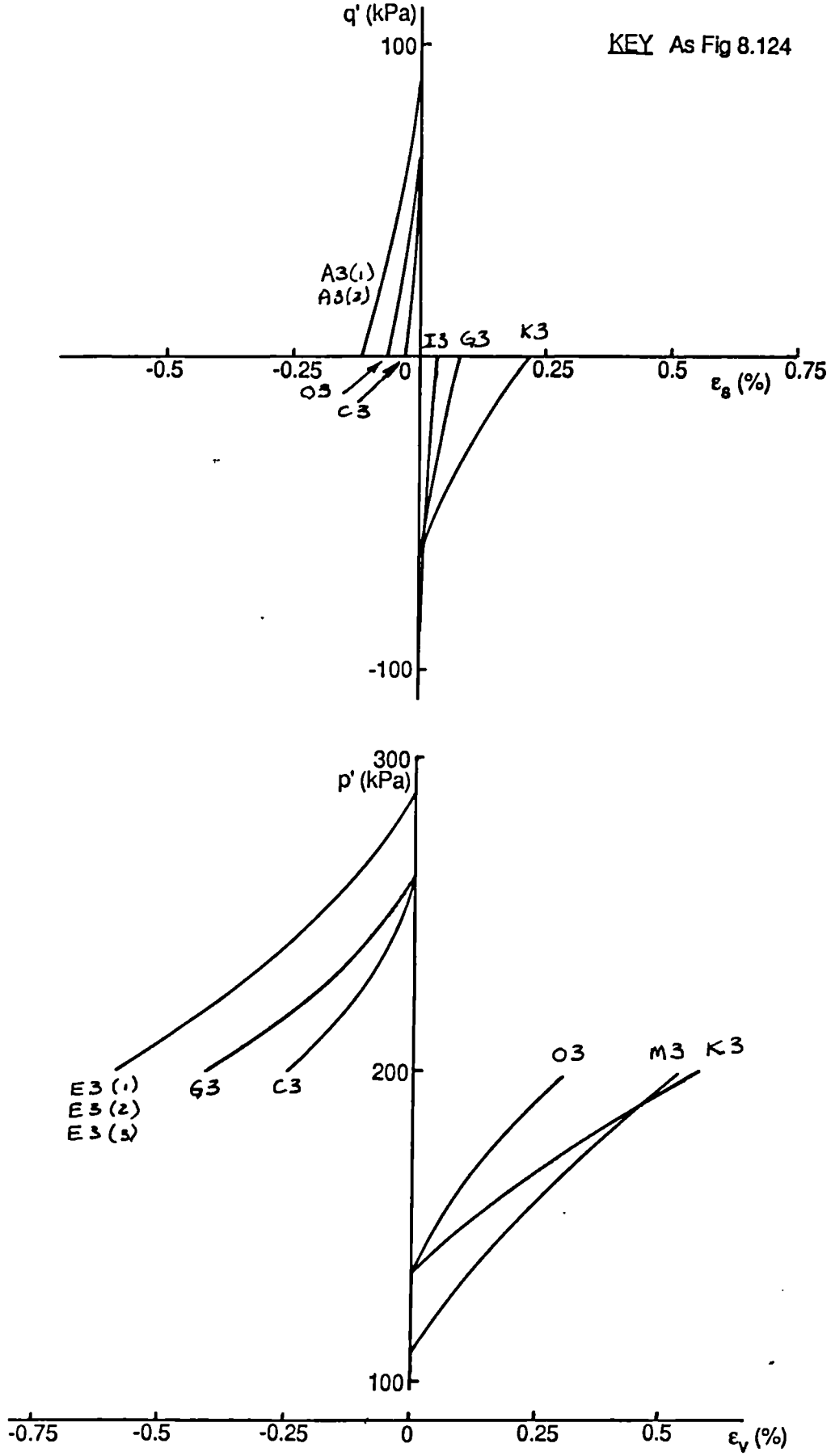

Fig 8.129 Plots of q' against ε_s and p' against ε_v for type three path dependence tests on slate dust.

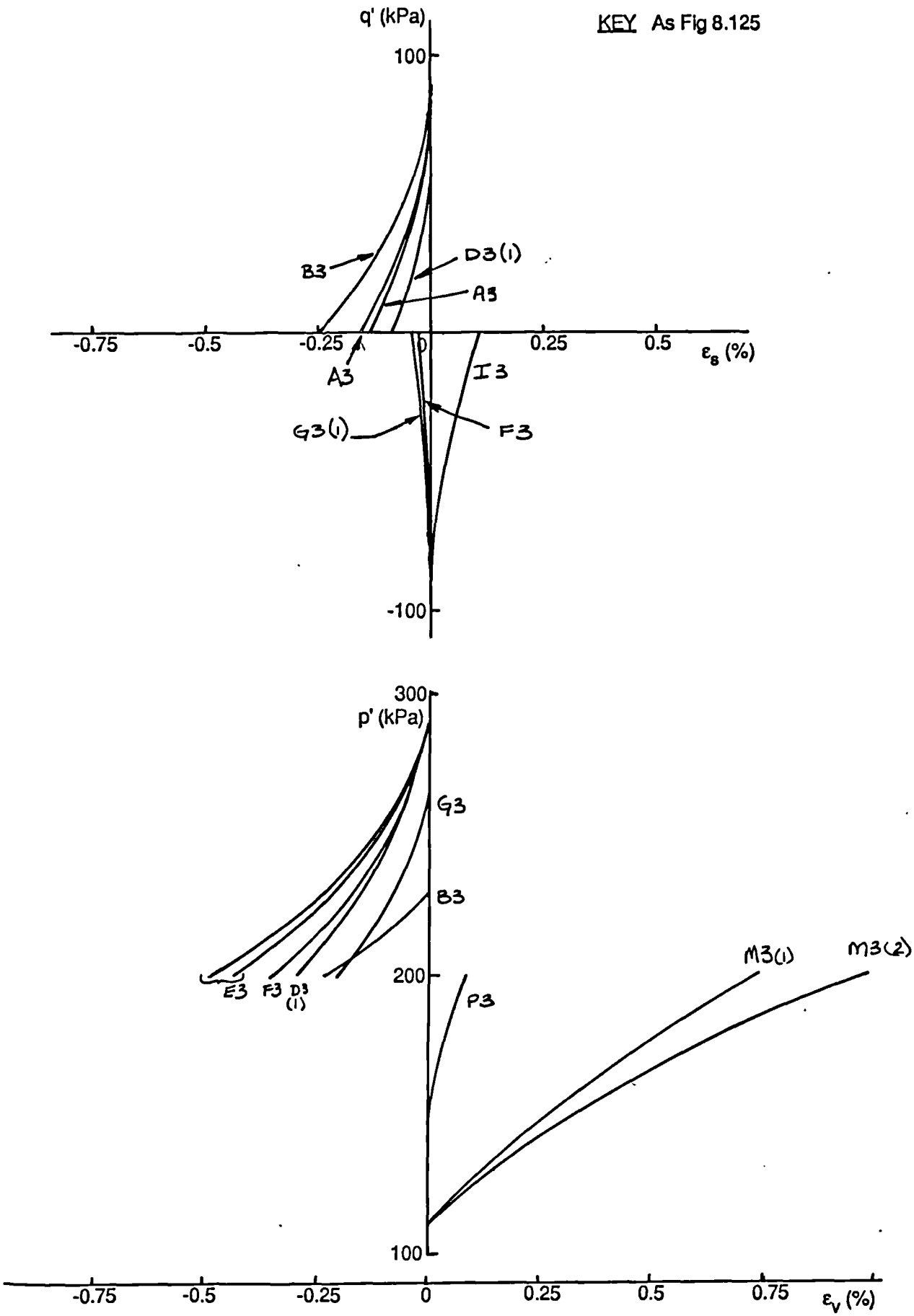

Fig 8.130a Plots of q' against ε_s and p' against ε_v for type three path dependence tests on London clay.

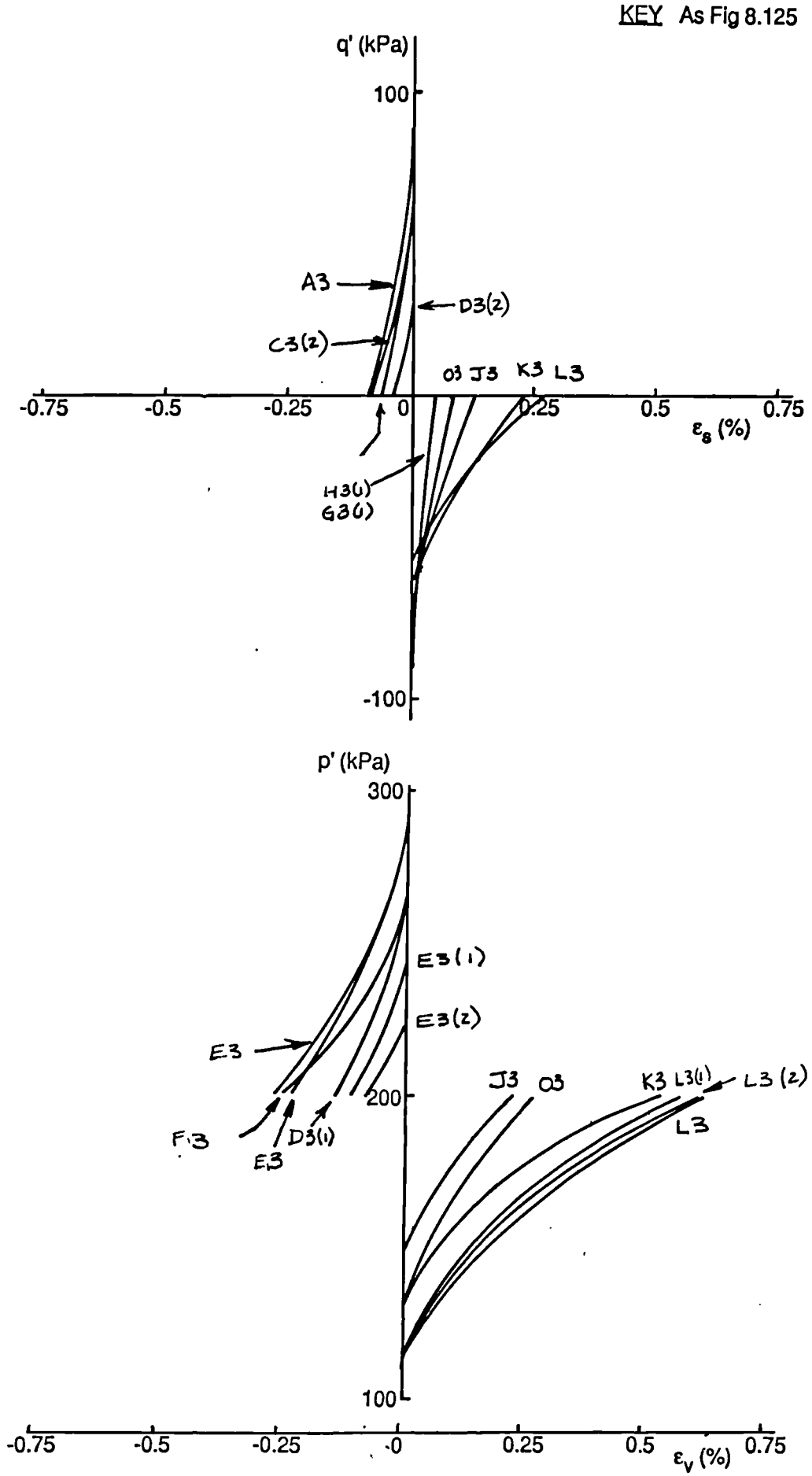

Fig 8.130b Plots of q' against ε_s and p' against ε_v for type three path dependence tests on London clay.

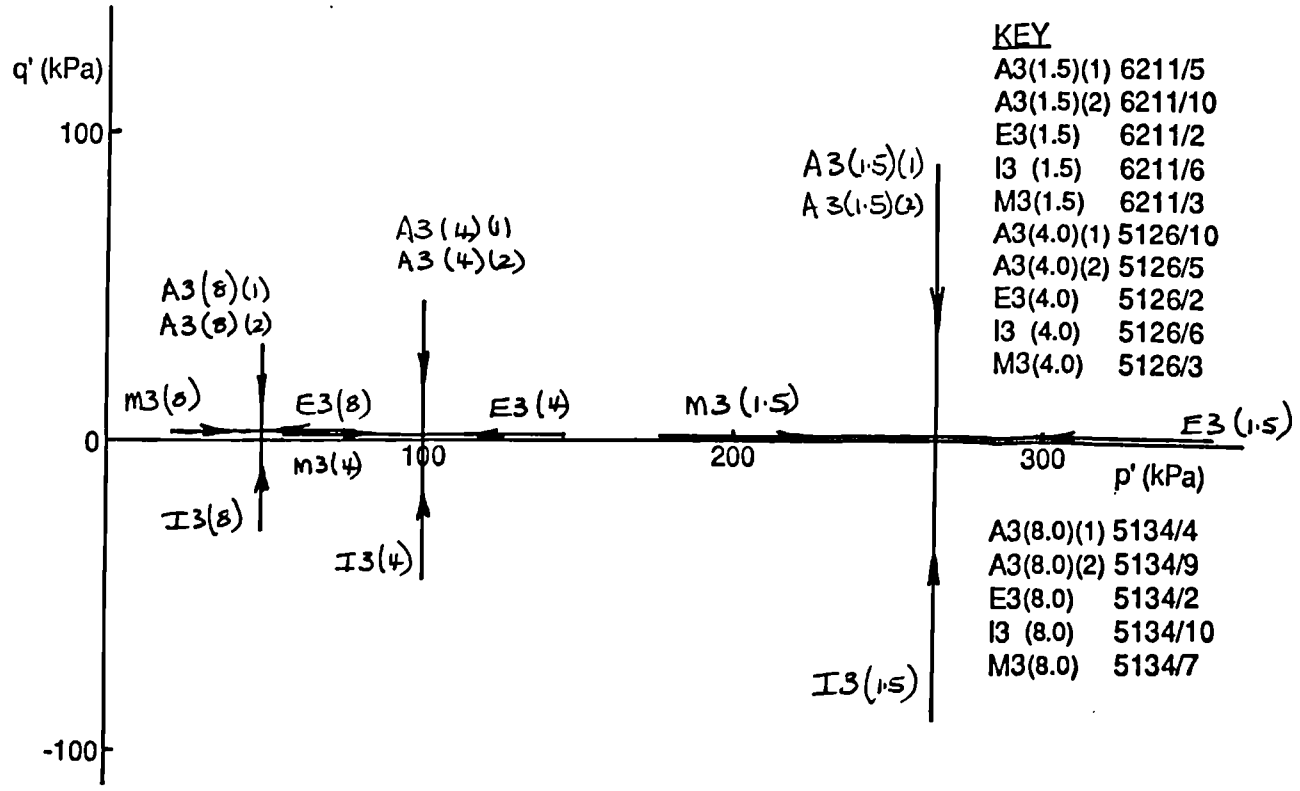

Fig 8.131 Plot of q' against p'. Stress paths followed during path dependence type three tests. $\eta'_0 = 0$, various OCR's, London clay. All data Figs 8.132 -137.

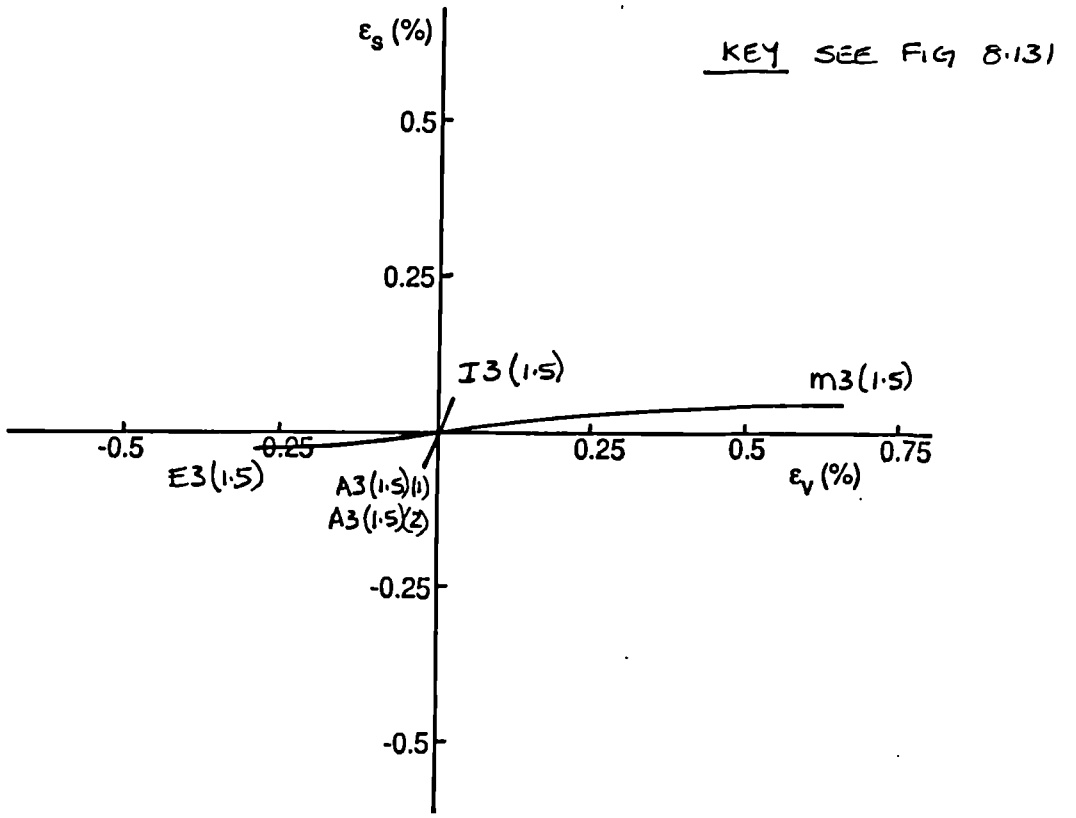

Fig 8.132 Plot of strain paths, ε_s against ε_v for type three path dependence tests on London clay, OCR = 1.5.

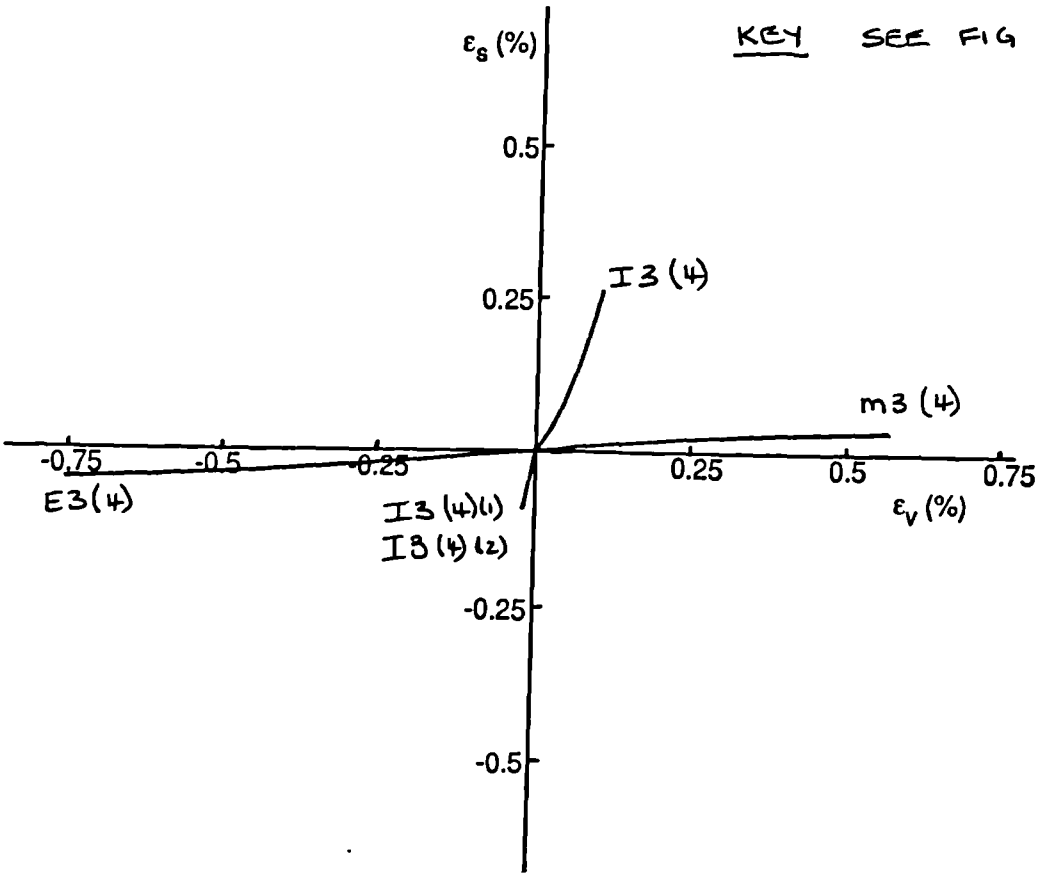

Fig 8.133 Plot of strain paths, ε_s against ε_v for type three path dependence tests on London clay, OCR = 4.0.

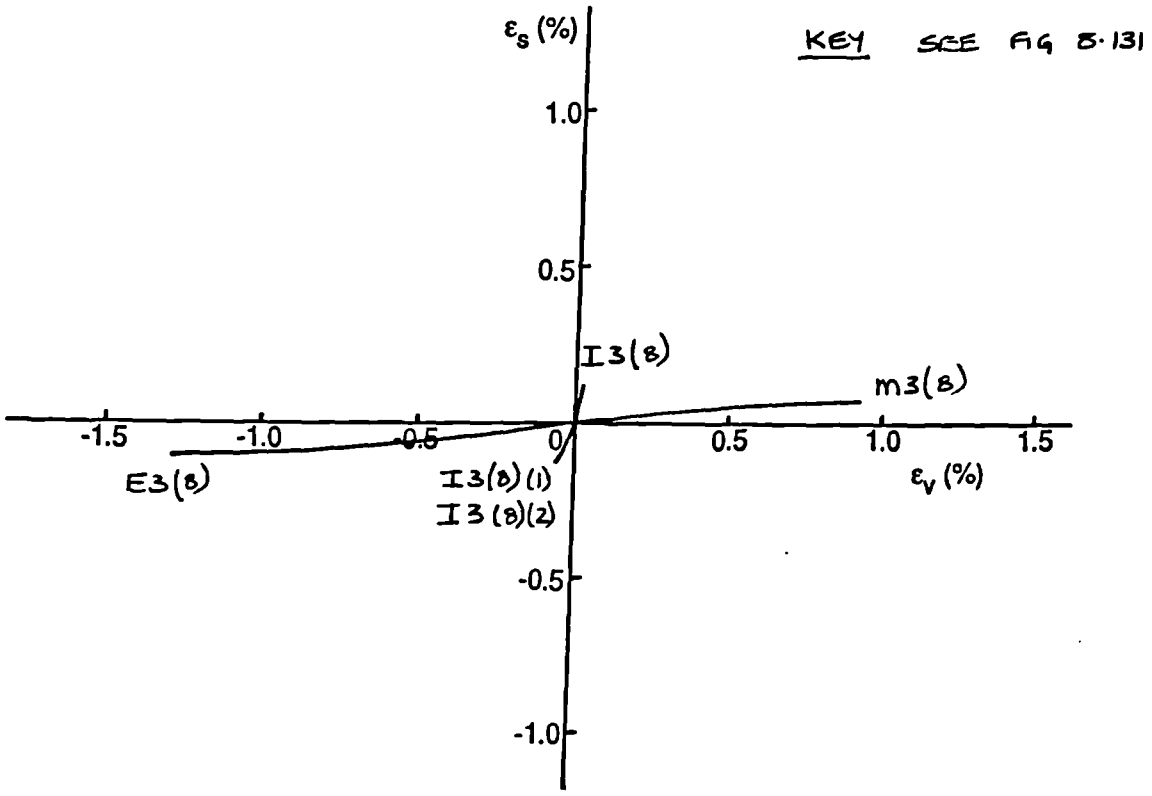

Fig 8.134 Plot of strain paths, ε_s against ε_v for type three path dependence tests on London clay, OCR = 8.

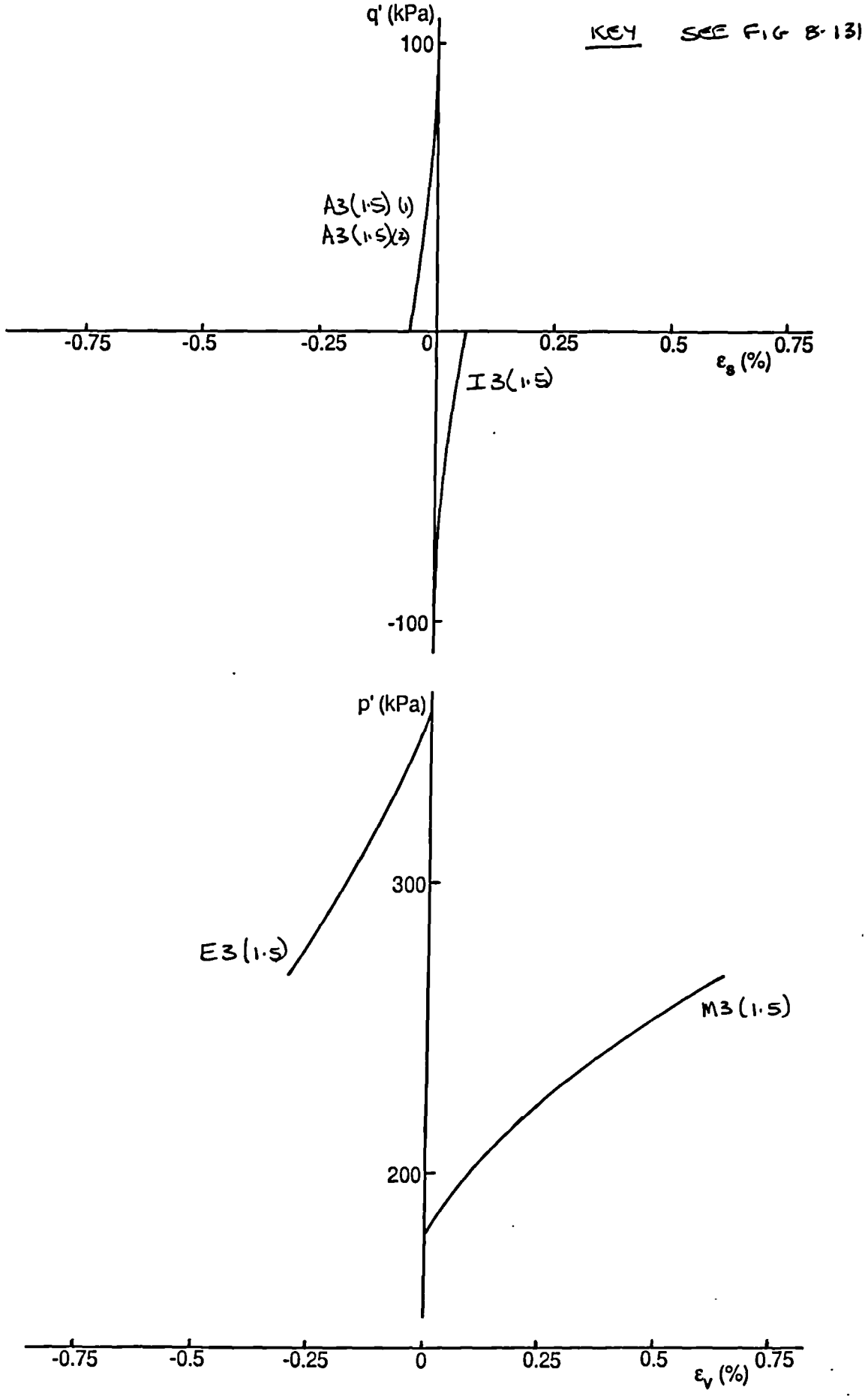

Fig 8.135 Plots of q' against ε_s and p' against ε_v for type three path dependence tests on London clay, OCR = 1.5.

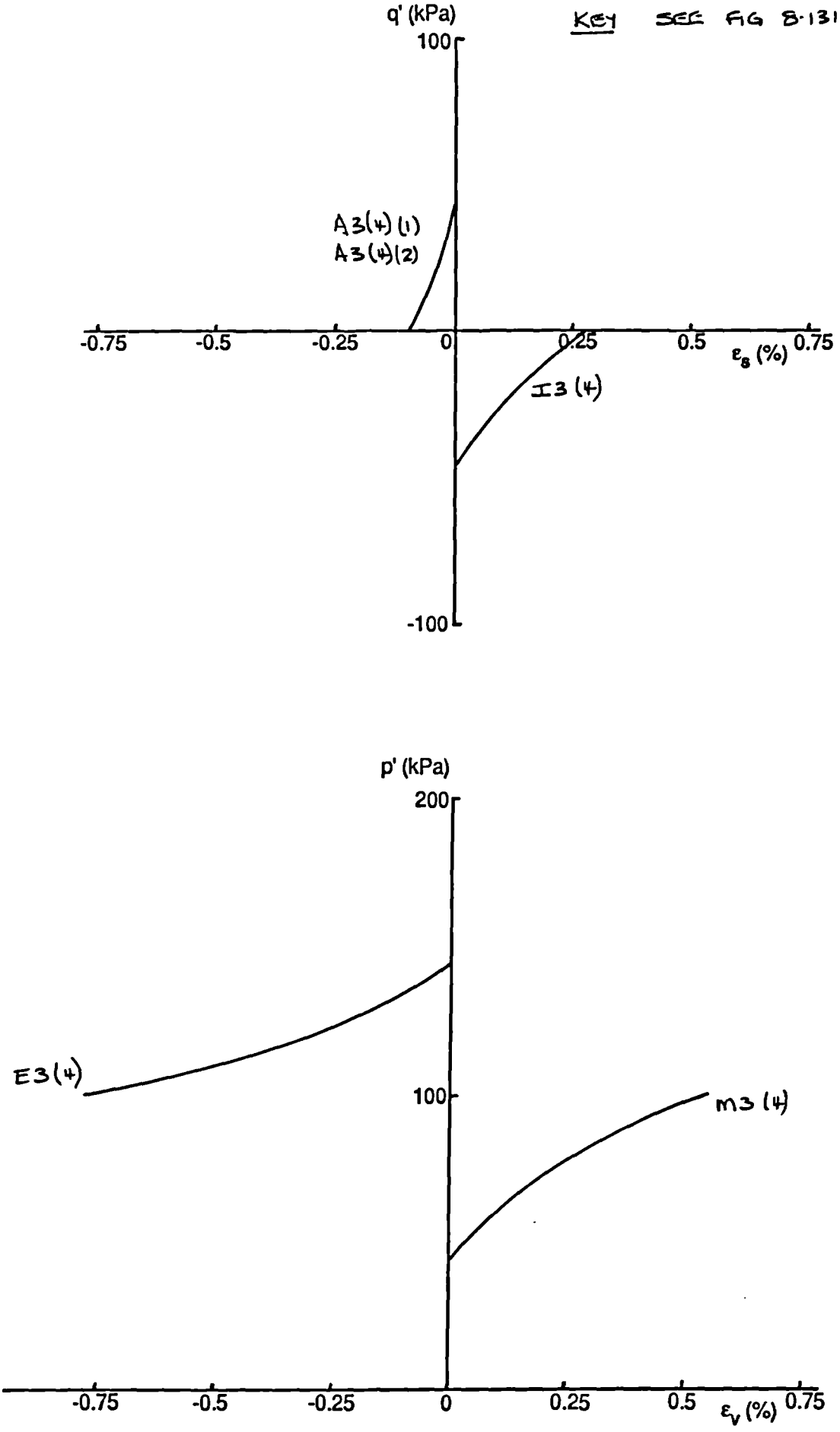

Fig 8.136 Plots of q' against ε_s and p' against ε_v for type three path dependence tests on London clay, OCR = 4.0.

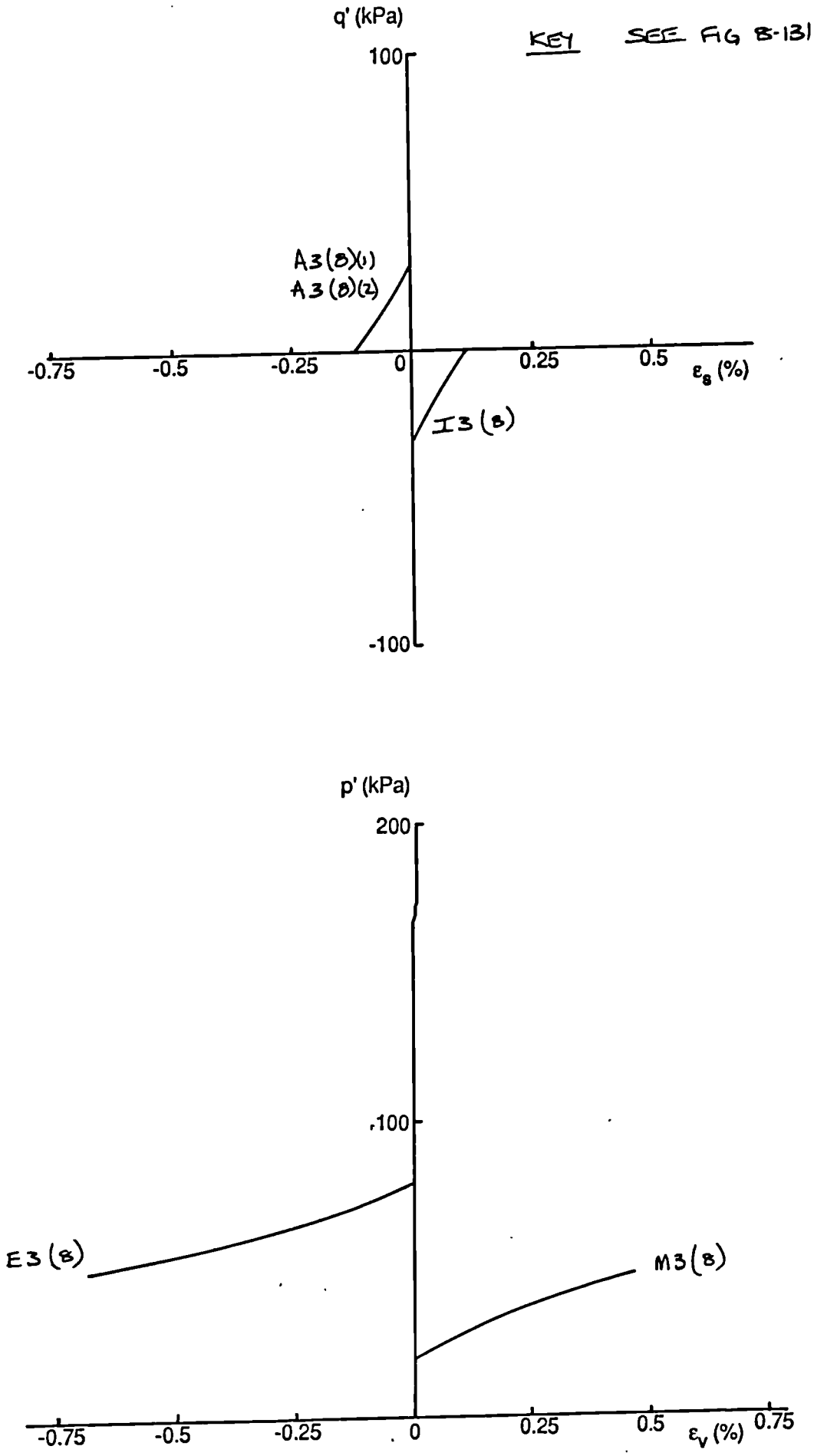

Fig 8.137 Plots of q' against ε_s and p' against ε_v for type three path dependence tests on London clay, OCR = 8.0.

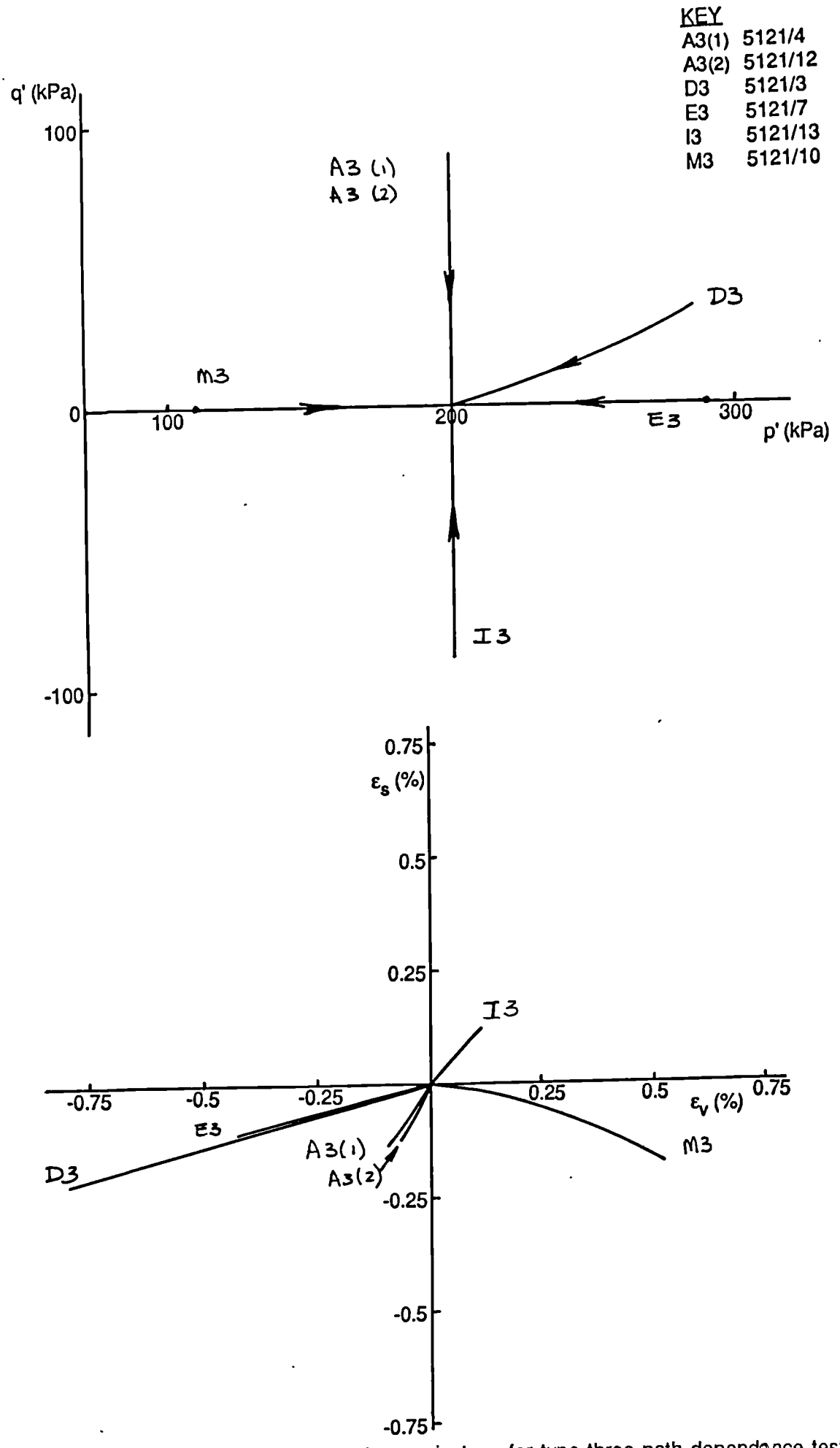

Fig 8.138 Plot of q' against p' and ε_s against ε_v for type three path dependence tests on London clay . η'_o = 0.25, OCR = 2.0.

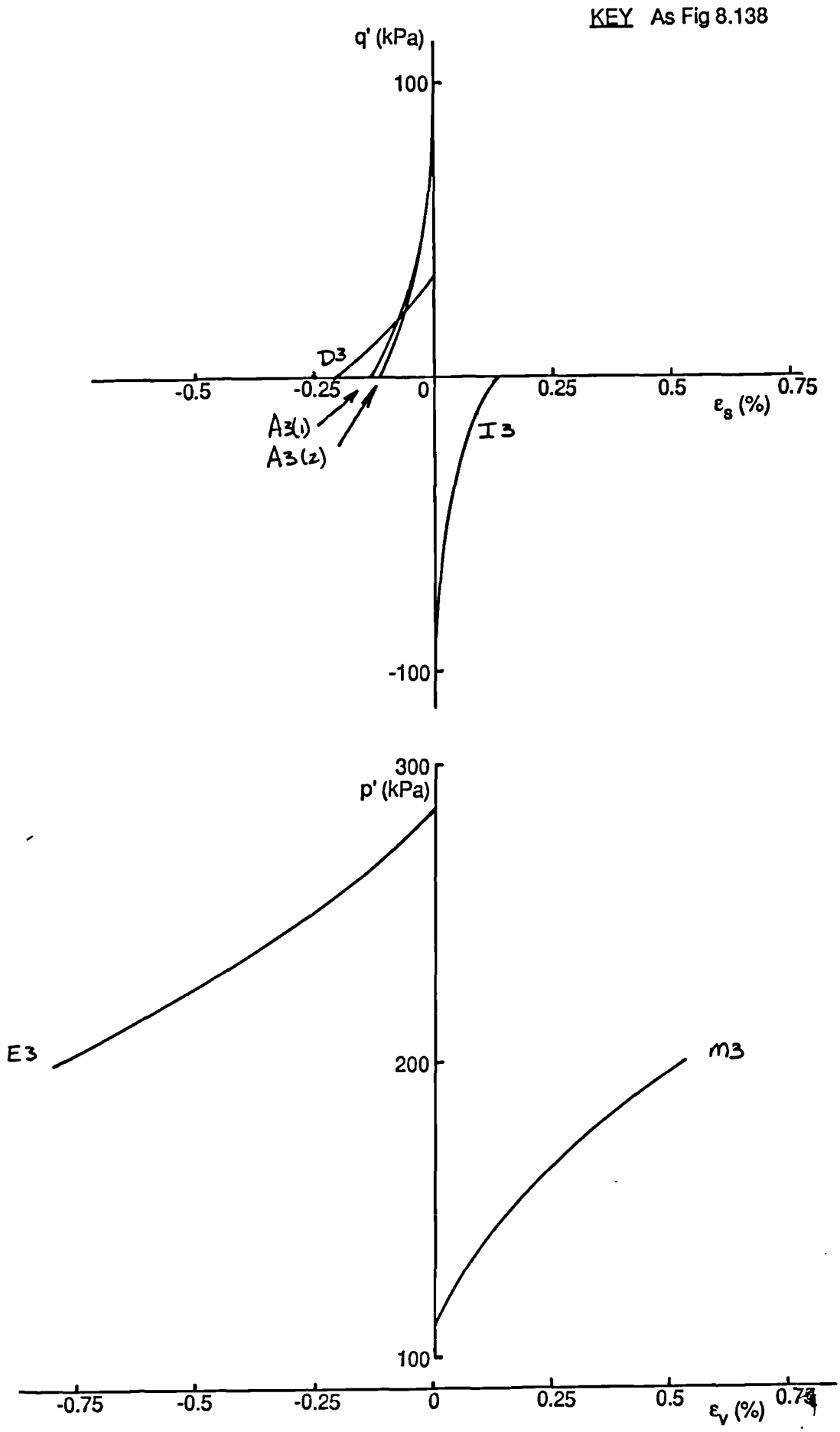

Fig 8.139 Plot of q' against ε_s and p' against ε_v for type three path dependence tests on London clay, $\eta'_0 = 0.25$, OCR = 2.0.

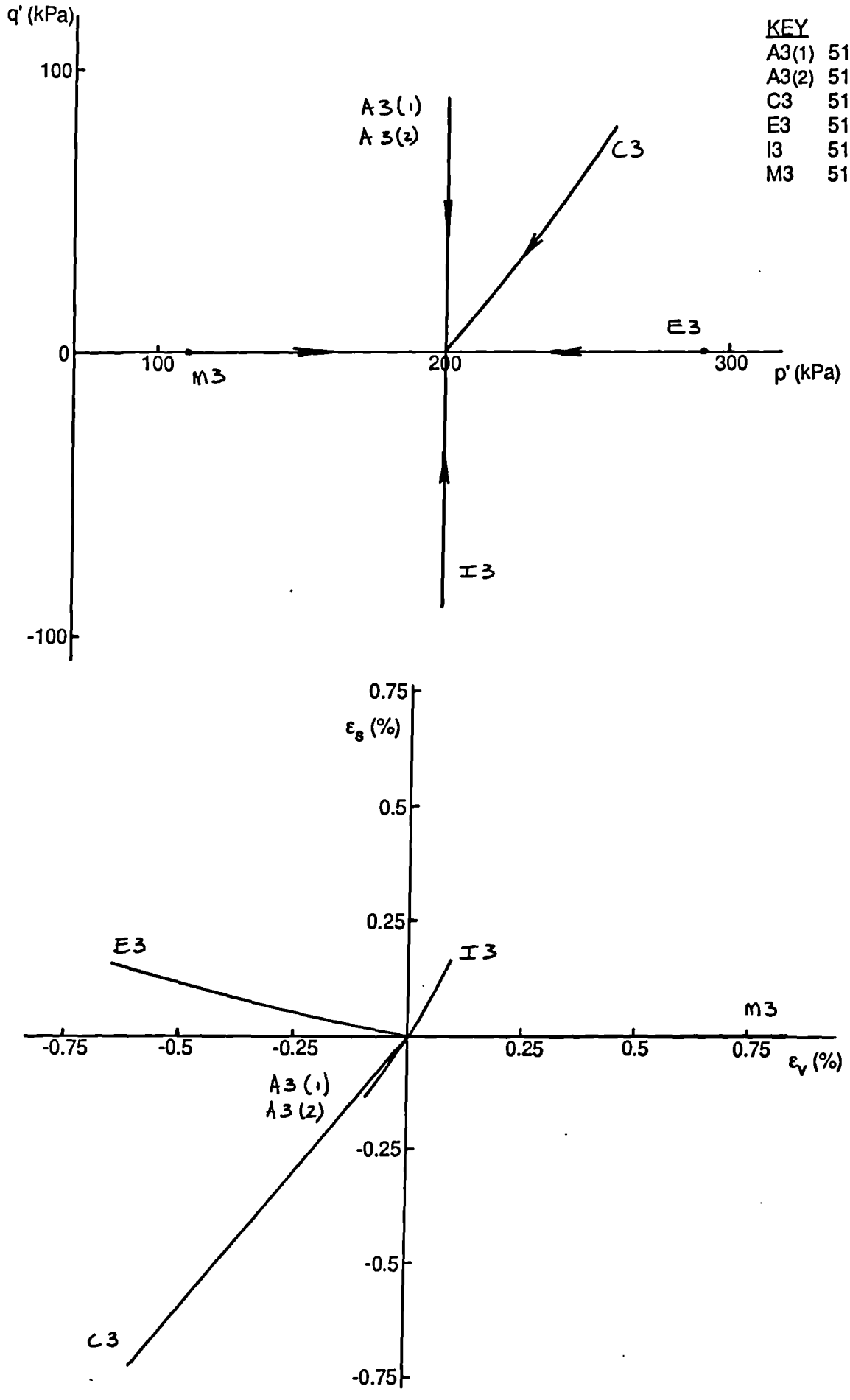

Fig 8.140 Plot of q' against p' and ε_s against ε_v for type three path dependence tests on London clay . η'_o = 0.75, OCR = 2.0.

KEY As Fig 8.140

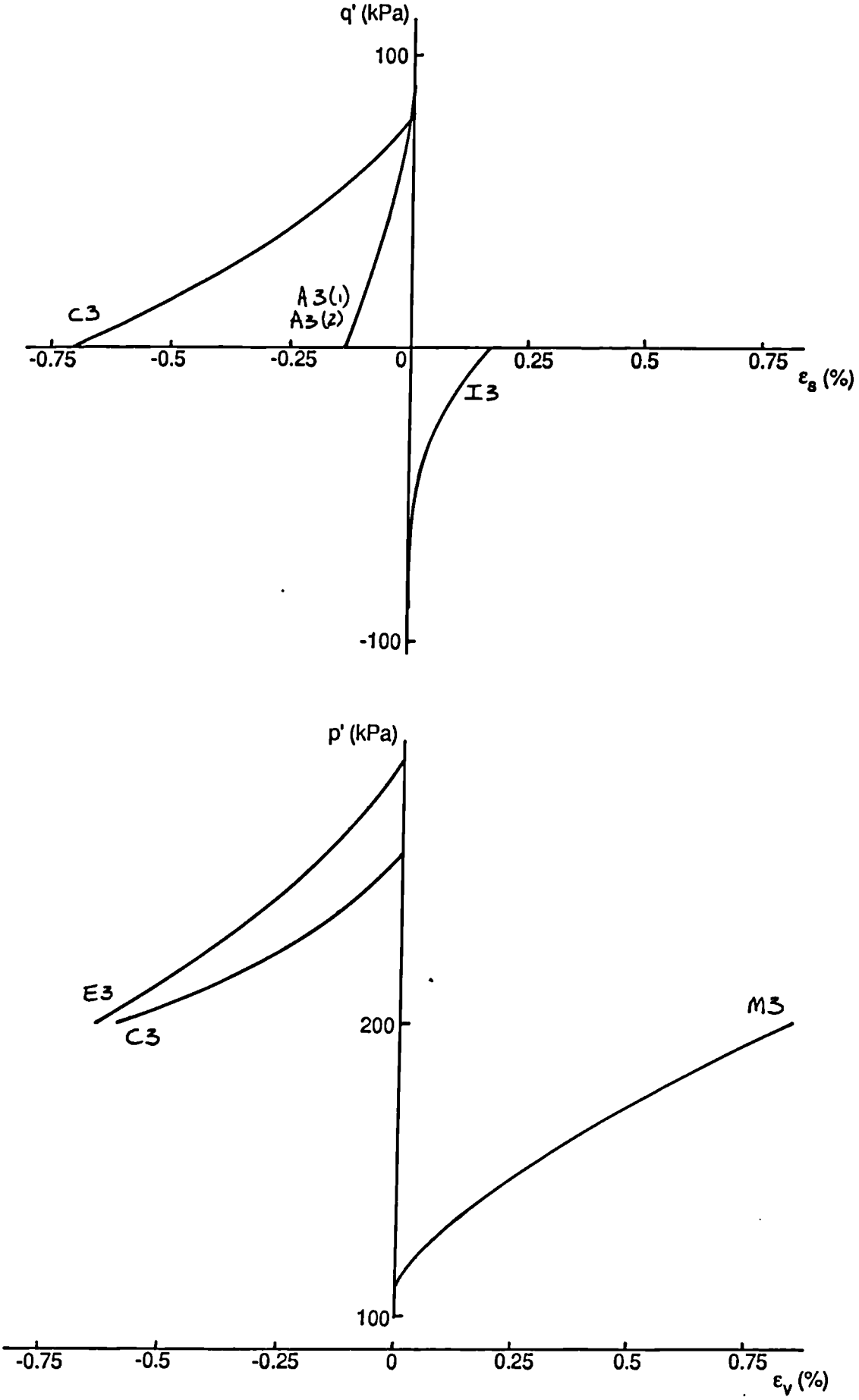

Fig 8.141 Plot of q' against ε_s and p' against ε_v for type three path dependence tests on London clay, $\eta'_0 = 0.75$, OCR = 2.0.

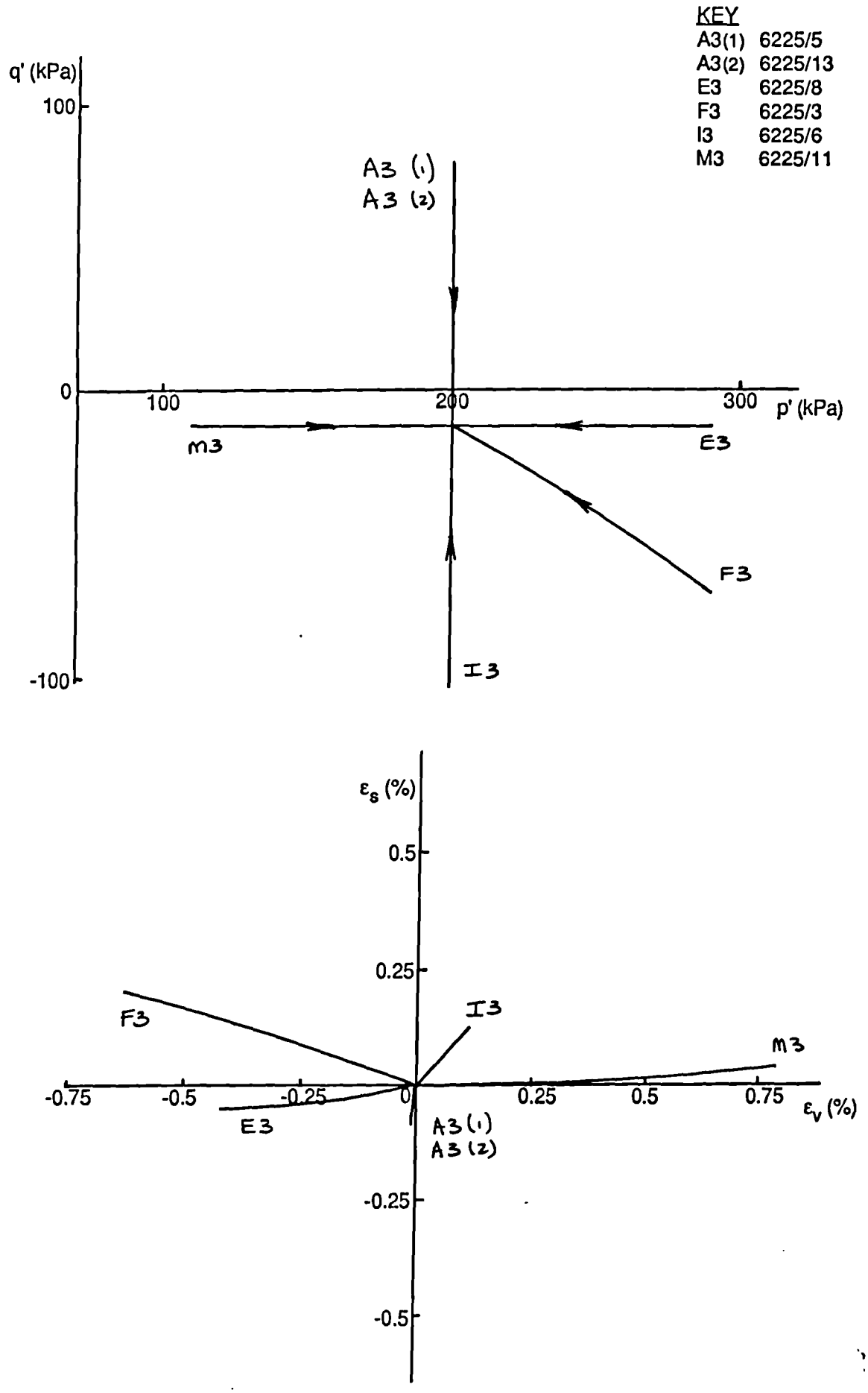

Fig 8.142 Plot of q' against p' and ε_s against ε_v for type three path dependence tests on London clay, two dimensionaly compressed, OCR = 2.0.

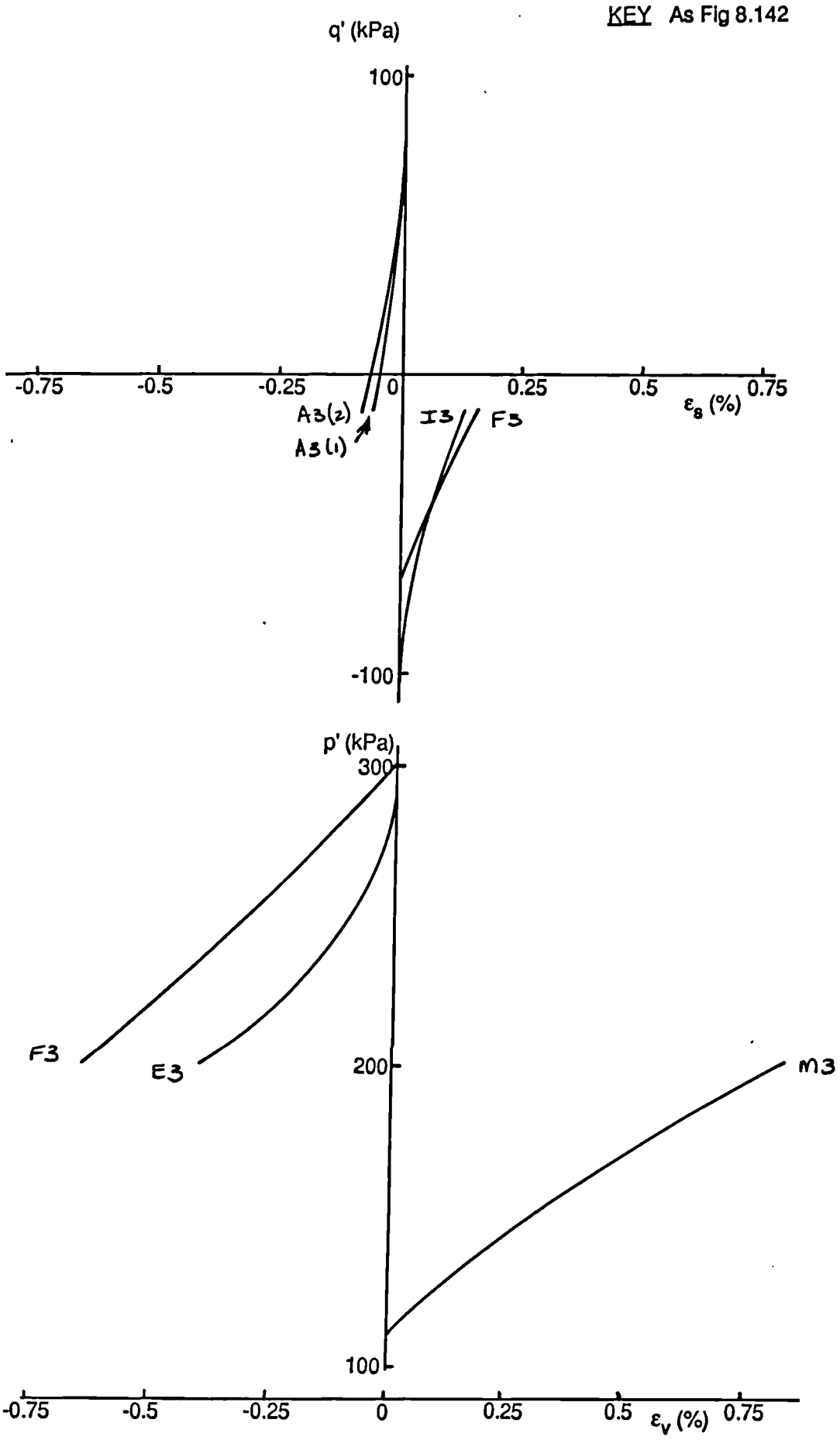

Fig 8.143 Plot of q' against ε_s and p' against ε_v for type three path dependence tests on London clay, two dimensionaly compressed, OCR = 2.0.

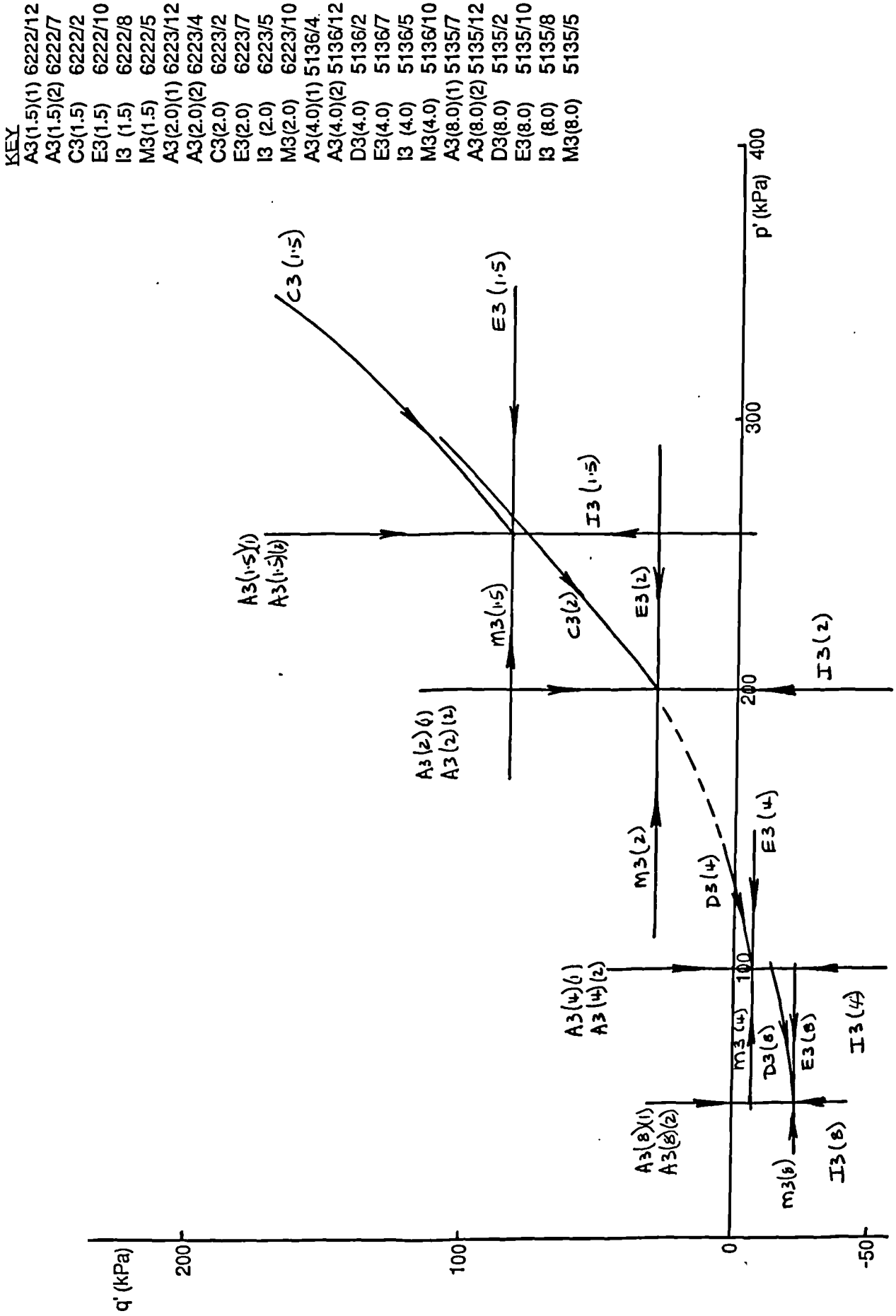

Fig 8.144 Plot of q' against p'. Stress paths followed during type three path dependence tests on London clay, one dimensionally compressed, various OCR's. All data Figs 8.145 - 8.152.

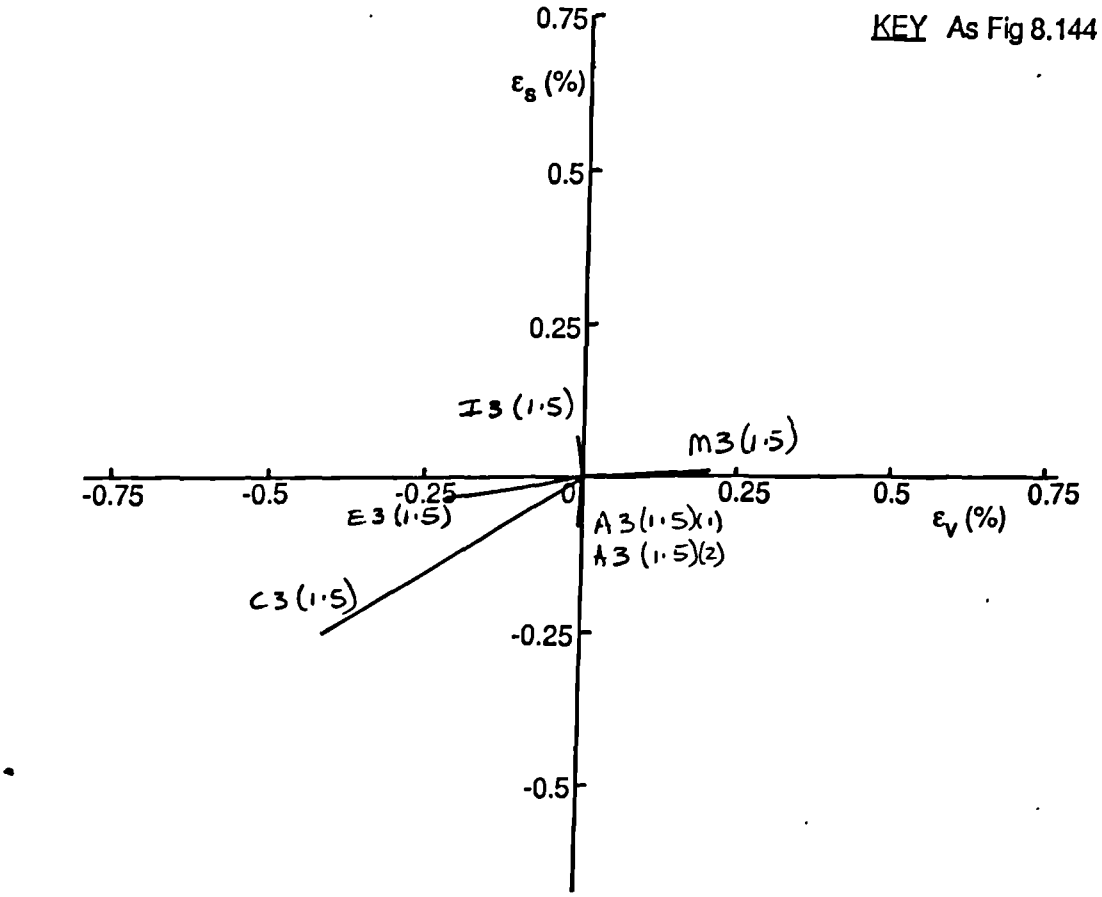

Fig 8.145 Plot of strain paths, ε_s against ε_v for type three path dependence tests on one dimensionally compressed London clay, OCR = 1.5.

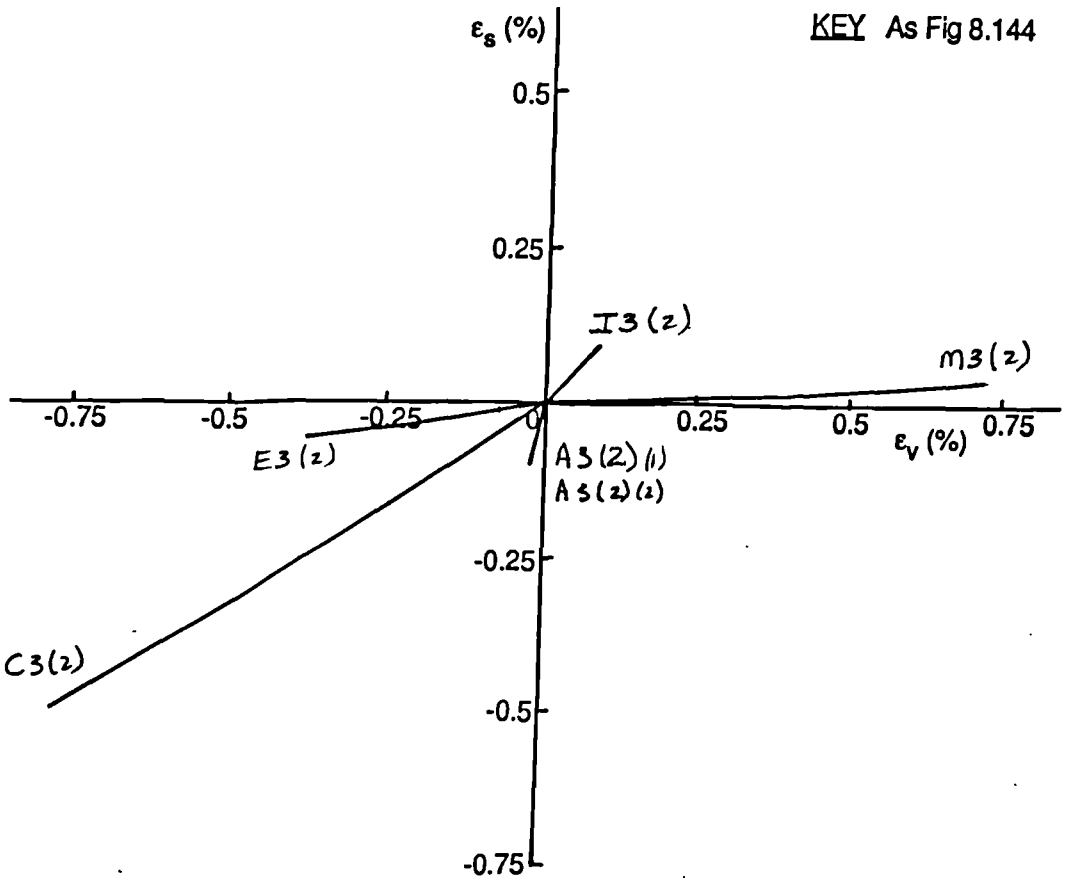

Fig 8.146 Plot of strain paths, ε_s against ε_v for type three path dependence tests on one dimensionally compressed London clay, OCR = 2.0.

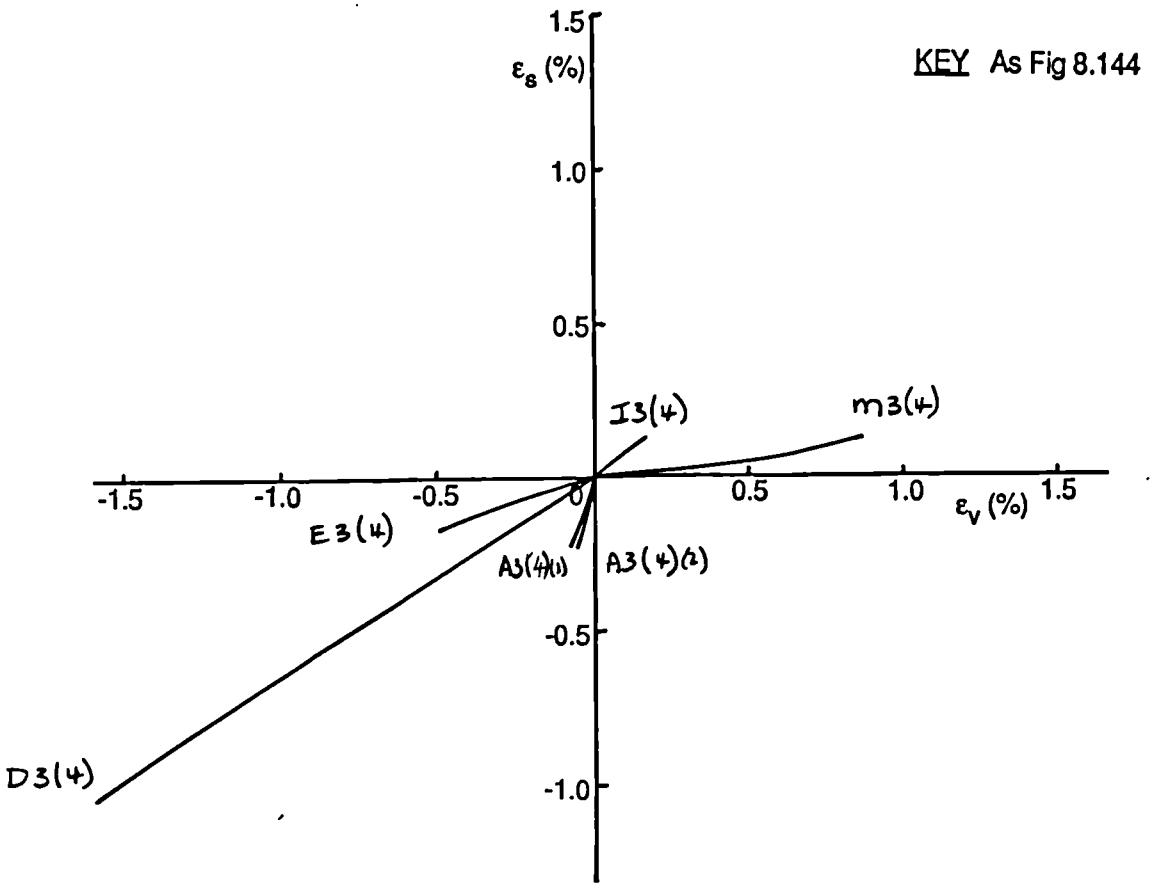

Fig 8.147 Plot of strain paths, ε_s against ε_v for type three path dependence tests on one dimensionally compressed London clay, OCR = 4.0.

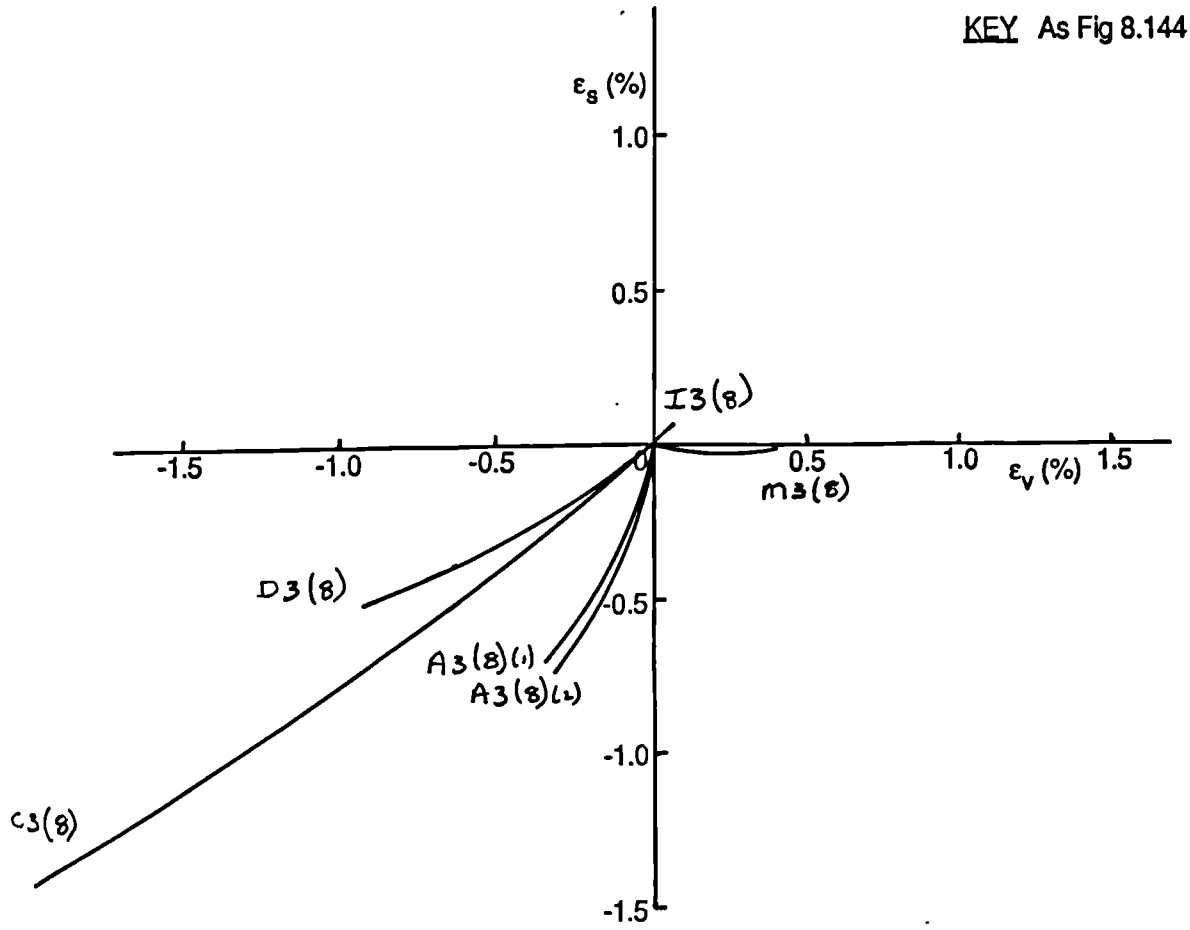

Fig 8.148 Plot of strain paths, ε_s against ε_v for type three path dependence tests on one dimensionally compressed London clay, OCR = 8.0.

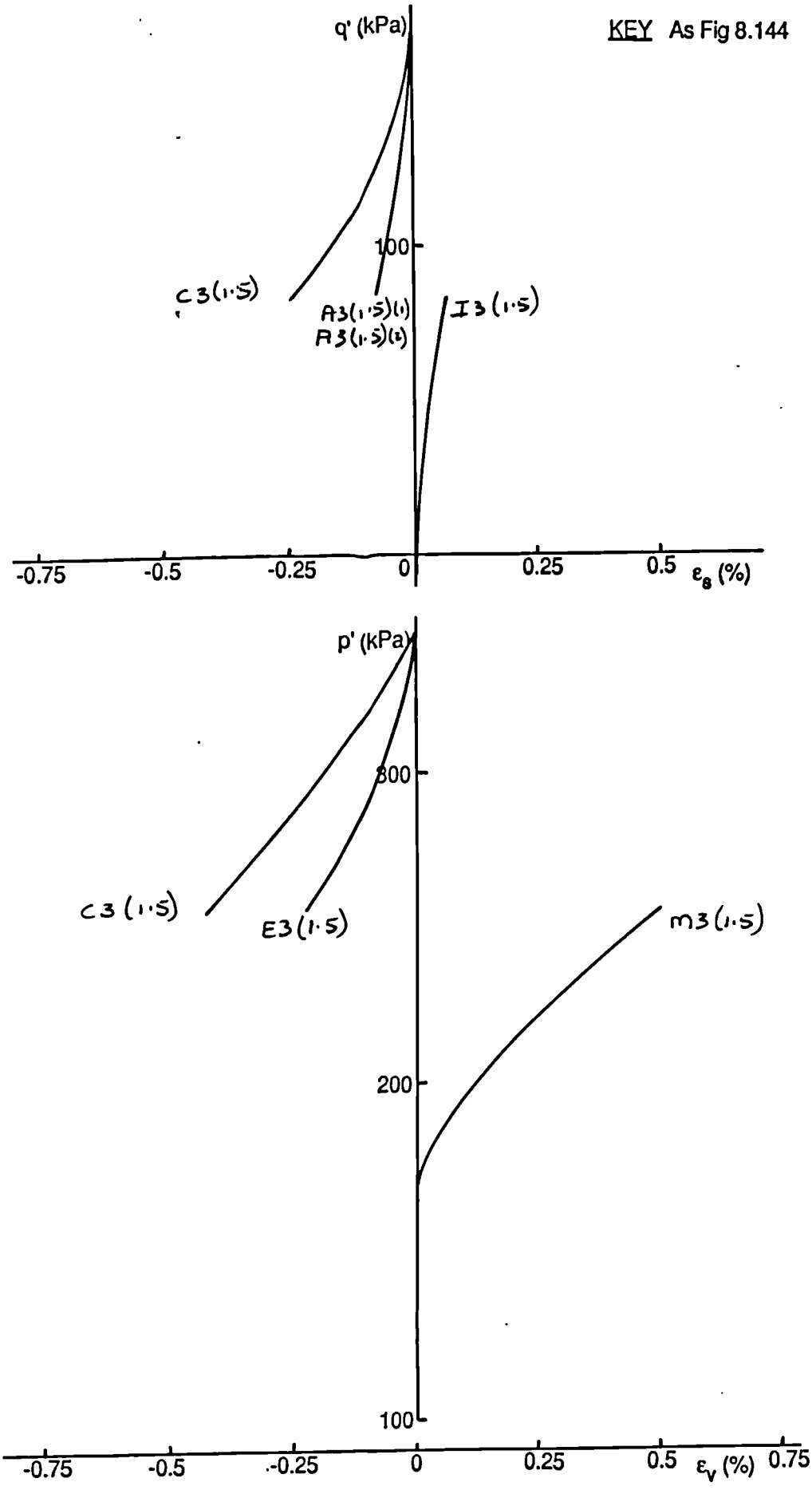

Fig 8.149 Plots of q' against ε_s and p` against ε_v for type three path dependence tests on one dimensionally compressed London clay, OCR = 1.5.

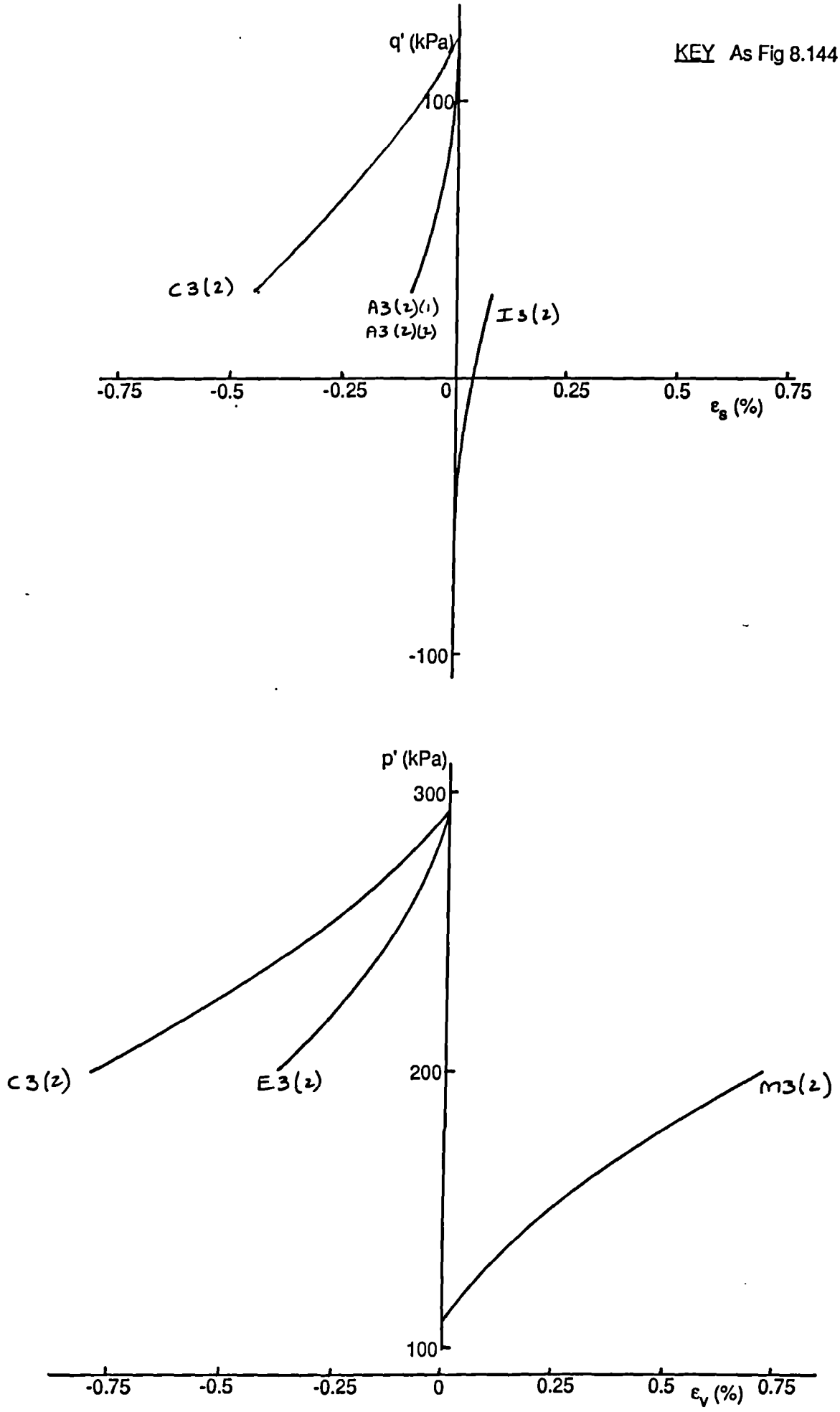

Fig 8.150 Plots of q' against ε_s and p` against ε_v for type three path dependence tests on one dimensionally compressed London clay, OCR = 2.0.

KEY As Fig 8.144

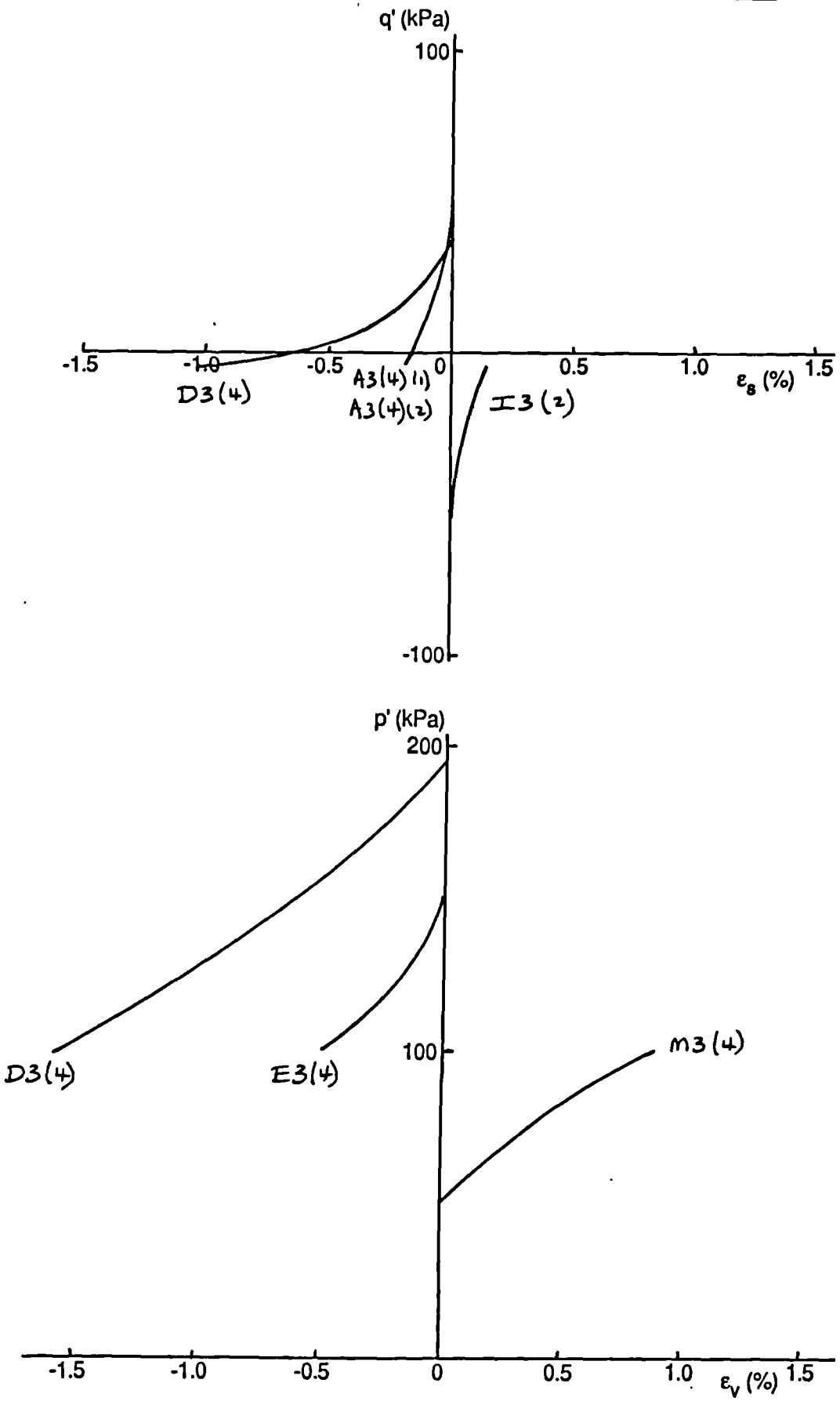

Fig 8.151 Plots of q' against ε_s and p` against ε_v for type three path dependence tests on one dimensionally compressed London clay, OCR = 4.0.

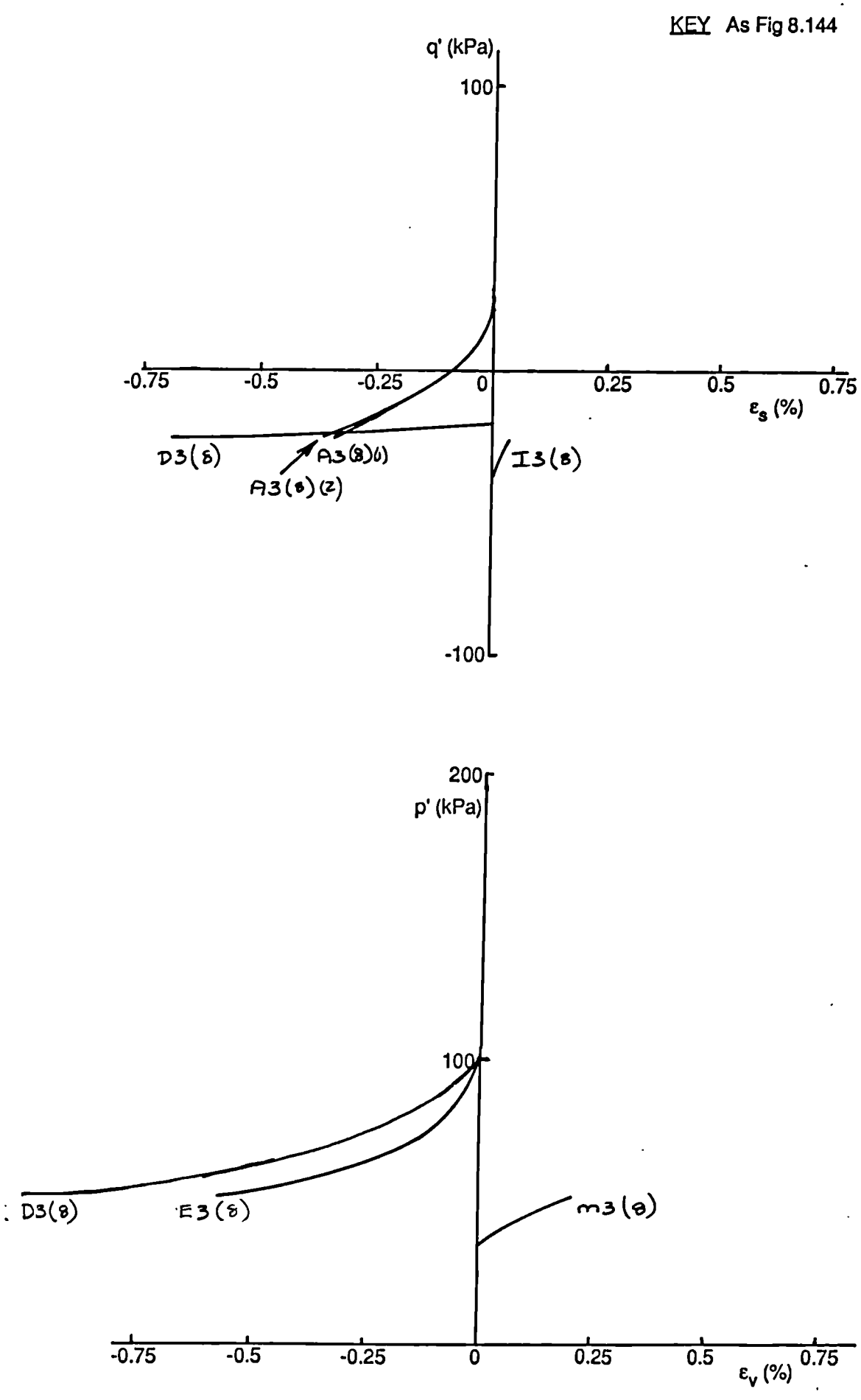

Fig 8.152 Plots of q' against ε_s and p' against ε_v for type three path dependence tests on one dimensionally compressed London clay, OCR = 8.0.

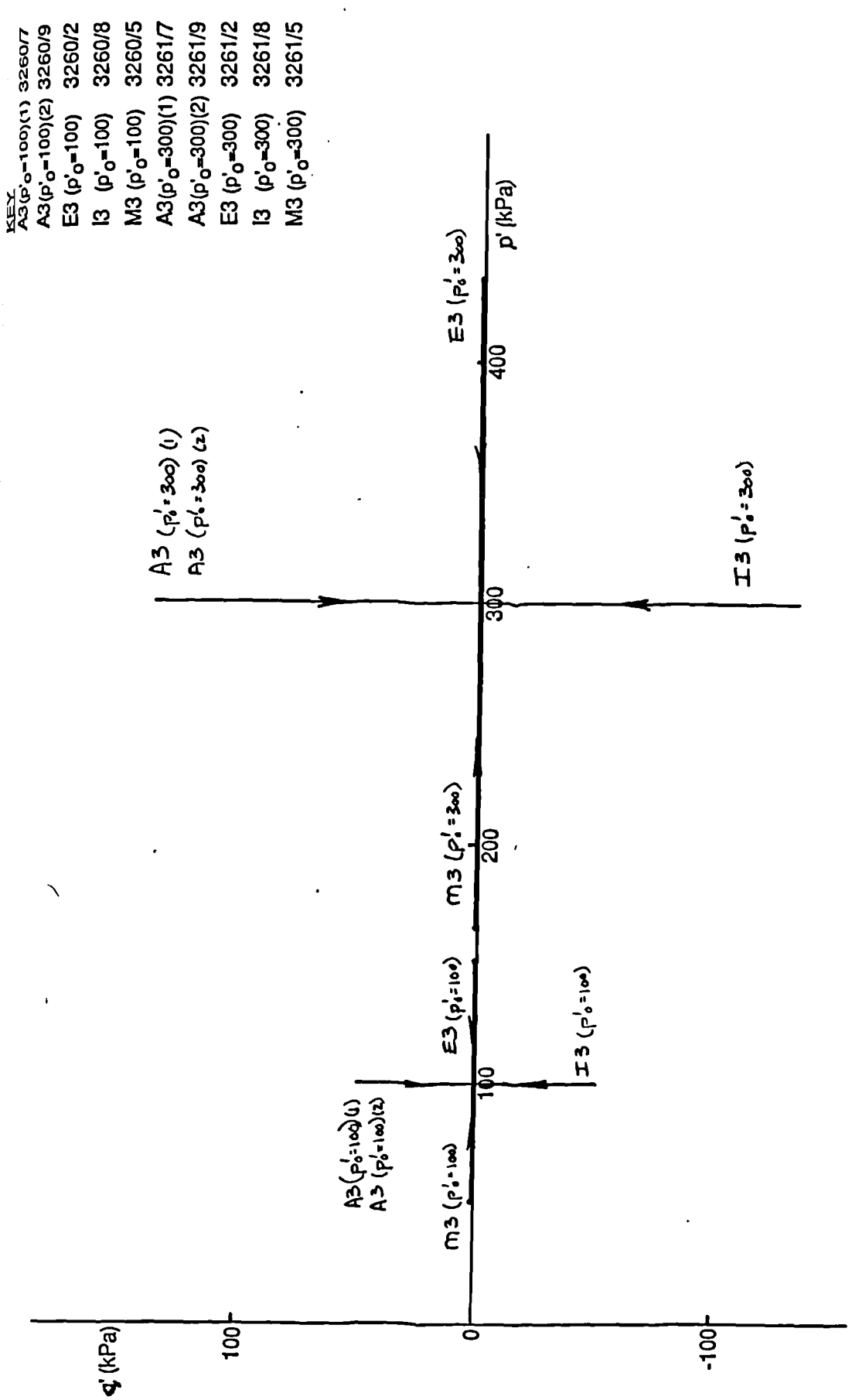

Fig 8.153 Plot of q' against p'. Stress paths followed during type three path dependence tests on London clay, $\eta'_o = 0$, OCR = 2.0, various p'. All data Figs 8.154 - 8.157.

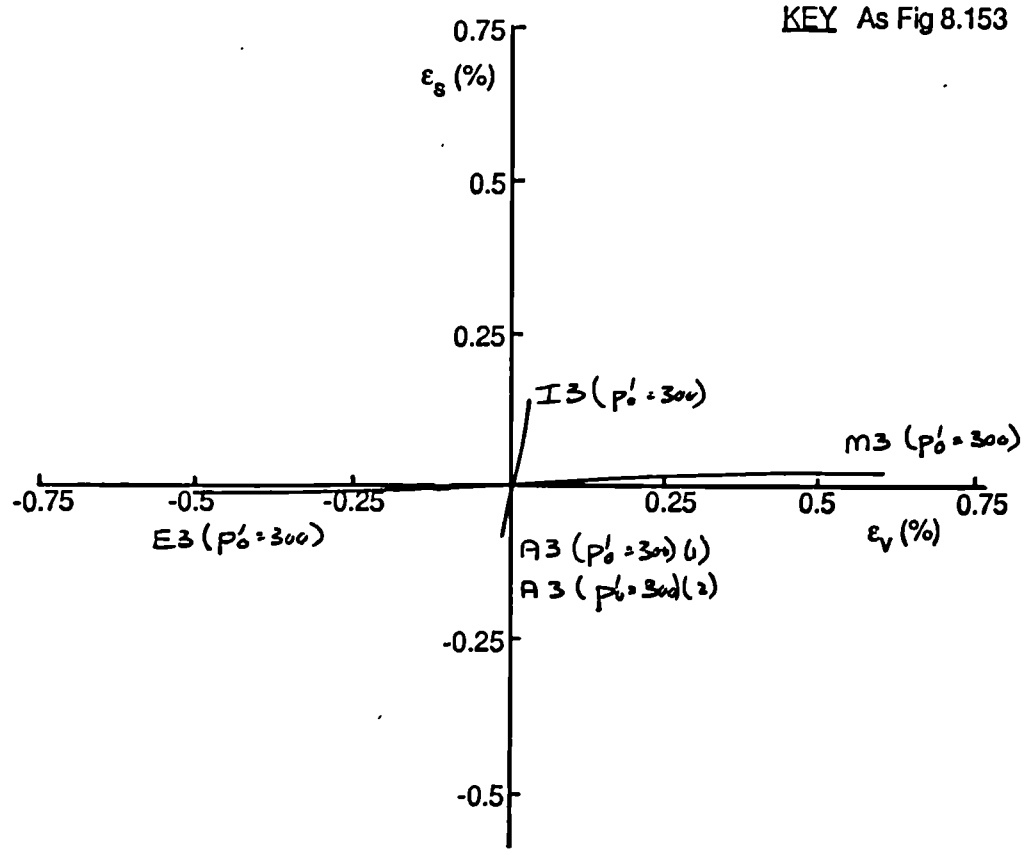

Fig 8.154 Plot of strain paths, ε_s against ε_v for type three path dependence tests on London clay, OCR = 2.0, p' = 100 kPa.

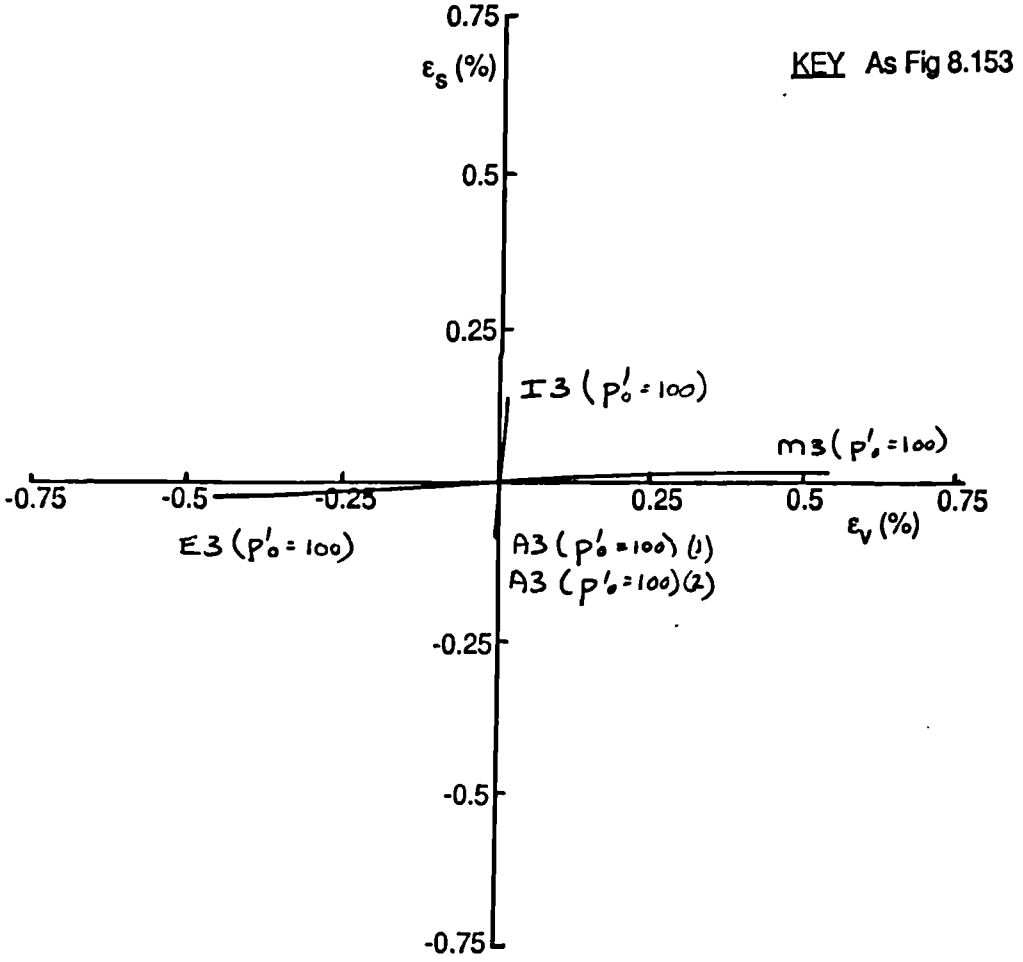

Fig 8.155 Plot of strain paths, ε_s against ε_v for type three path dependence tests on London clay, OCR = 2.0, p' = 300 kPa.

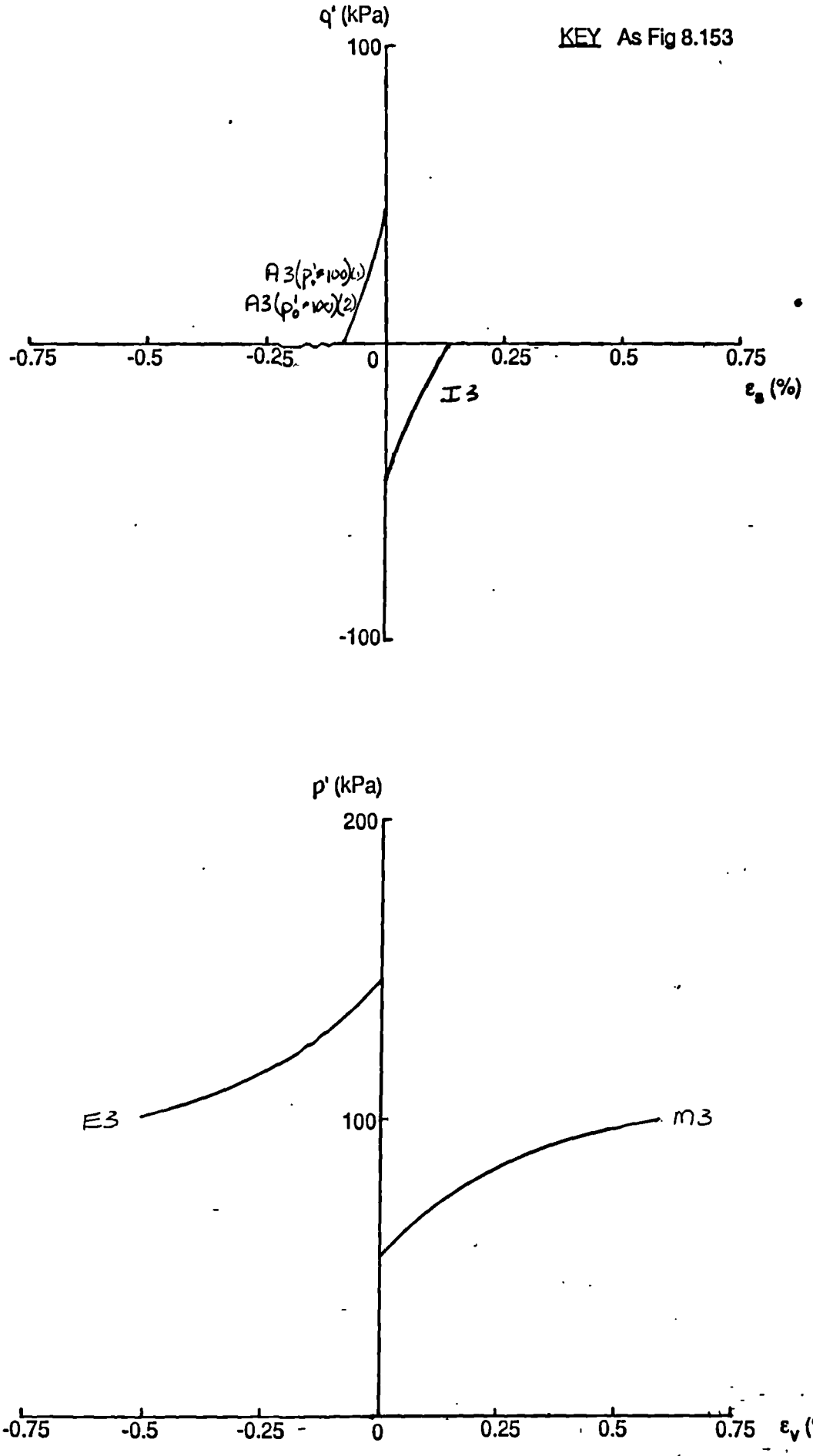

Fig 8.156 Plots of q' against ε_s and p` against ε_v for type three path dependence tests on London clay, OCR = 2.0, p' = 100kPa.

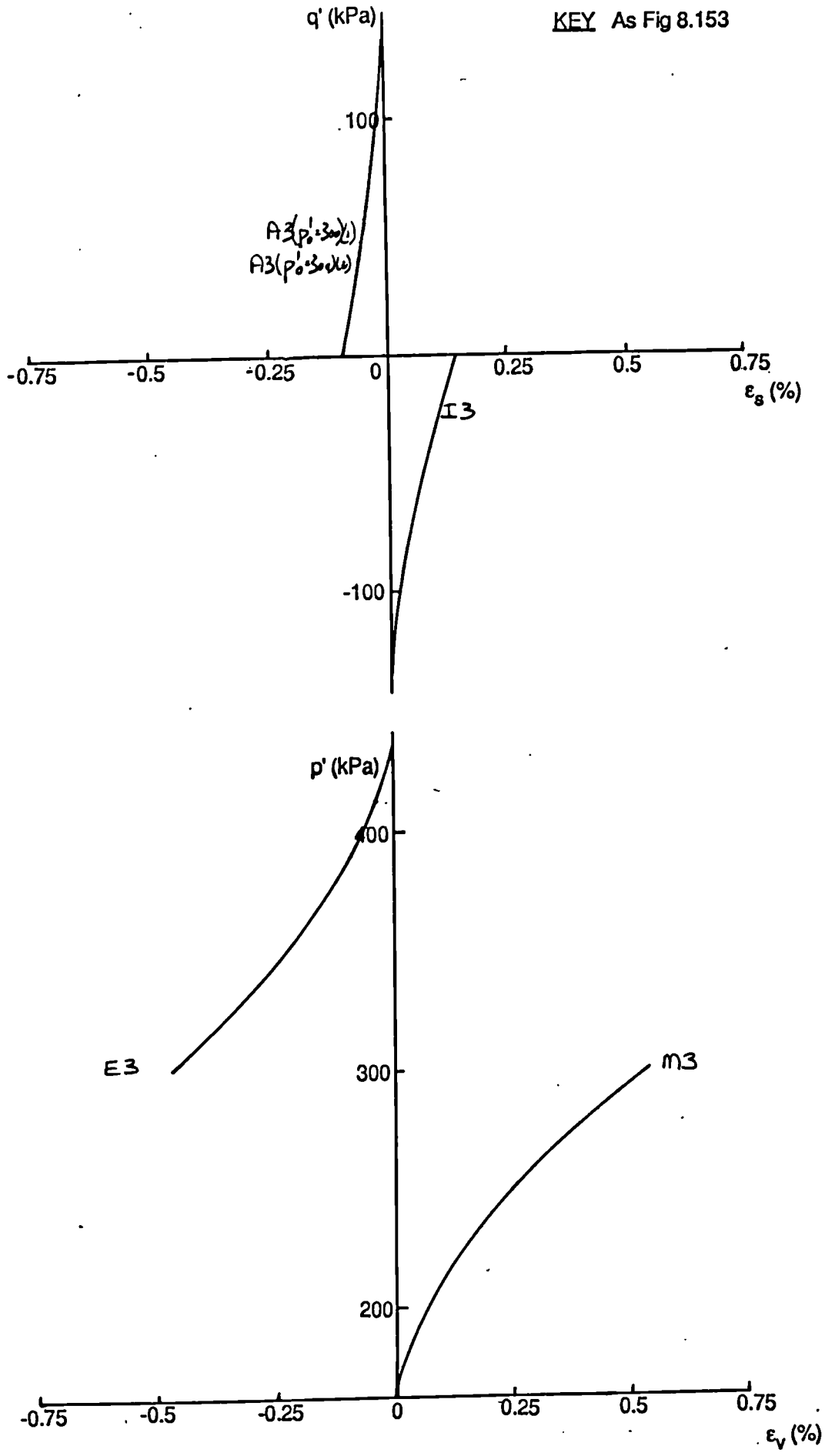

Fig 8.157 Plots of q' against ε_s and p` against ε_v for type three path dependence tests on London clay, OCR = 2.0, p' = 300kPa.

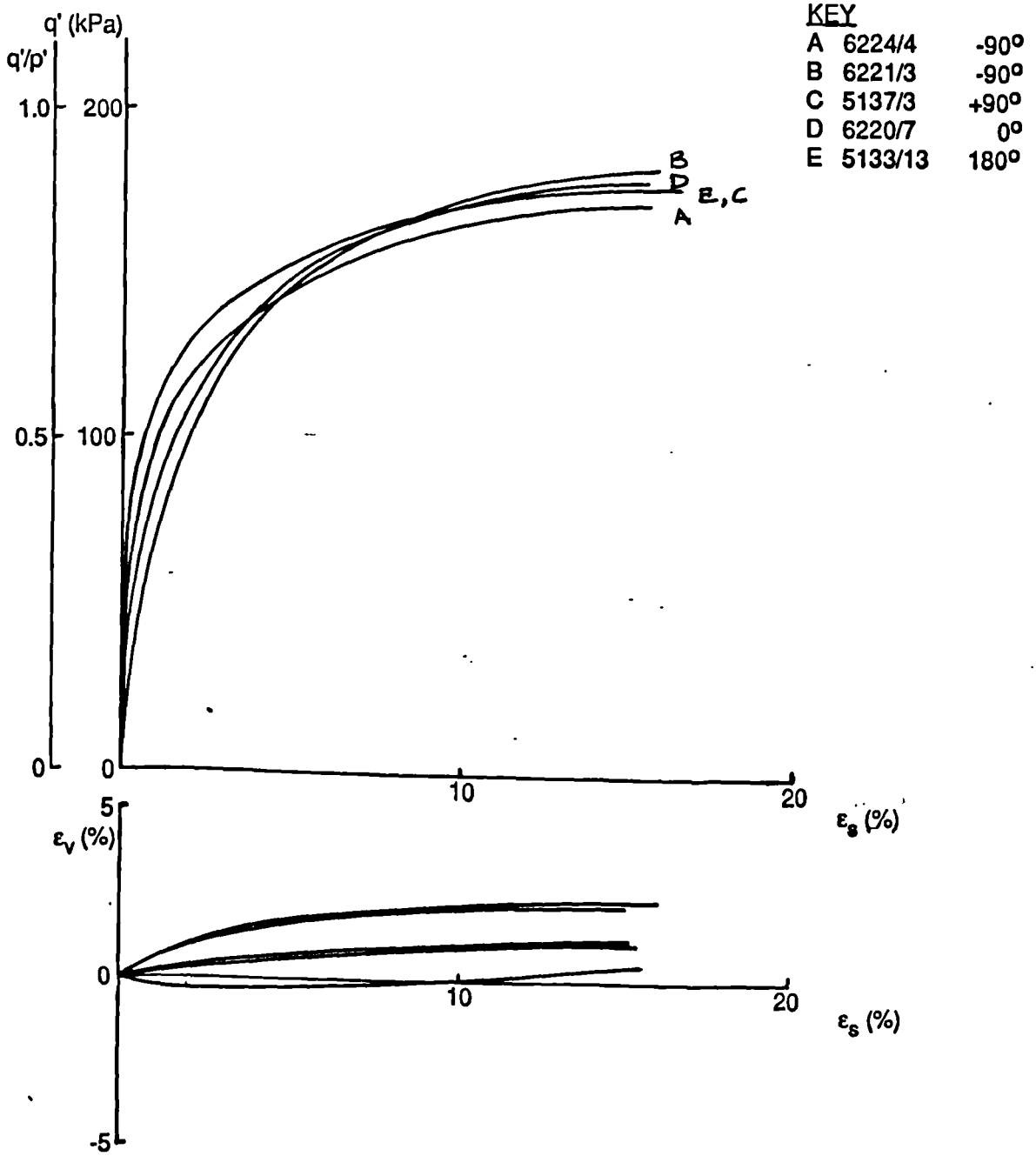

Fig 8.158 Plots of q' against ε_s ,q'/p' against ε_s and ε_v against ε_s. Threshold tests to failure. Isotropically compressed speswhite kaolin. OCR = 2.0, p' =200kPa, constant p' paths.

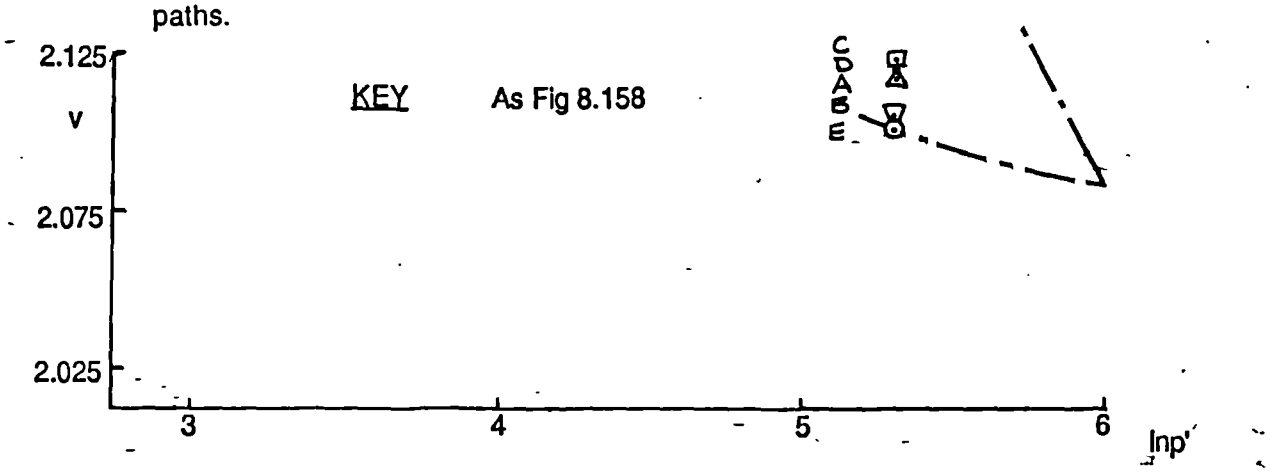

Fig 8.159 Plot of v against $\log_e$ p' for threshold tests to failure. Isotropically compressed speswhite kaolin. OCR = 2.0, p' = 200kPa, constant p' paths.

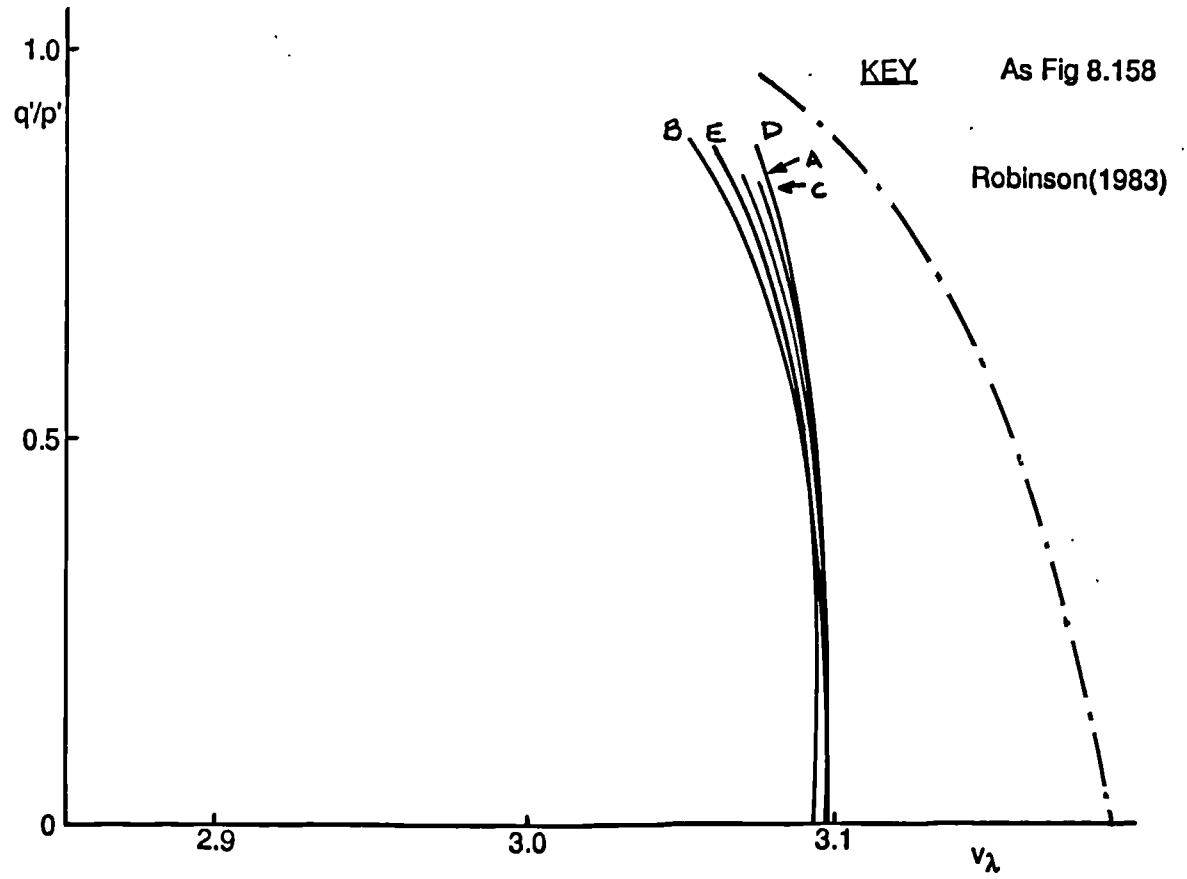

Fig 8.160 Plot of q' / p' against v_λ. Threshold tests to failure. Isotropically compressed speswhite kaolin. OCR = 2.0, p' = 200kPa, constant p' paths.

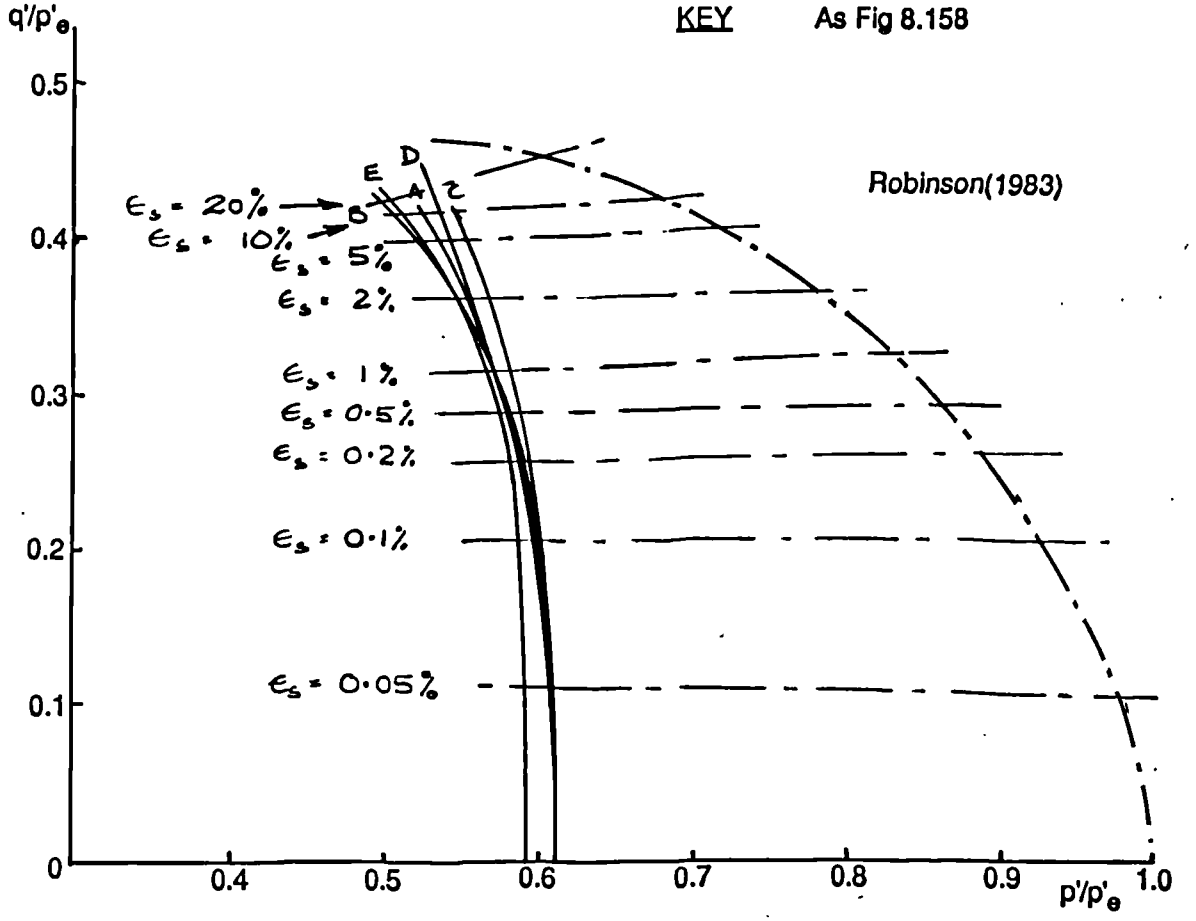

Fig 8.161 Plot of q' / p'_e against p' / p'_e. Threshold tests to failure. Isotropically compressed speswhite kaolin. OCR = 2.0, p' = 200kPa, constant p' paths.

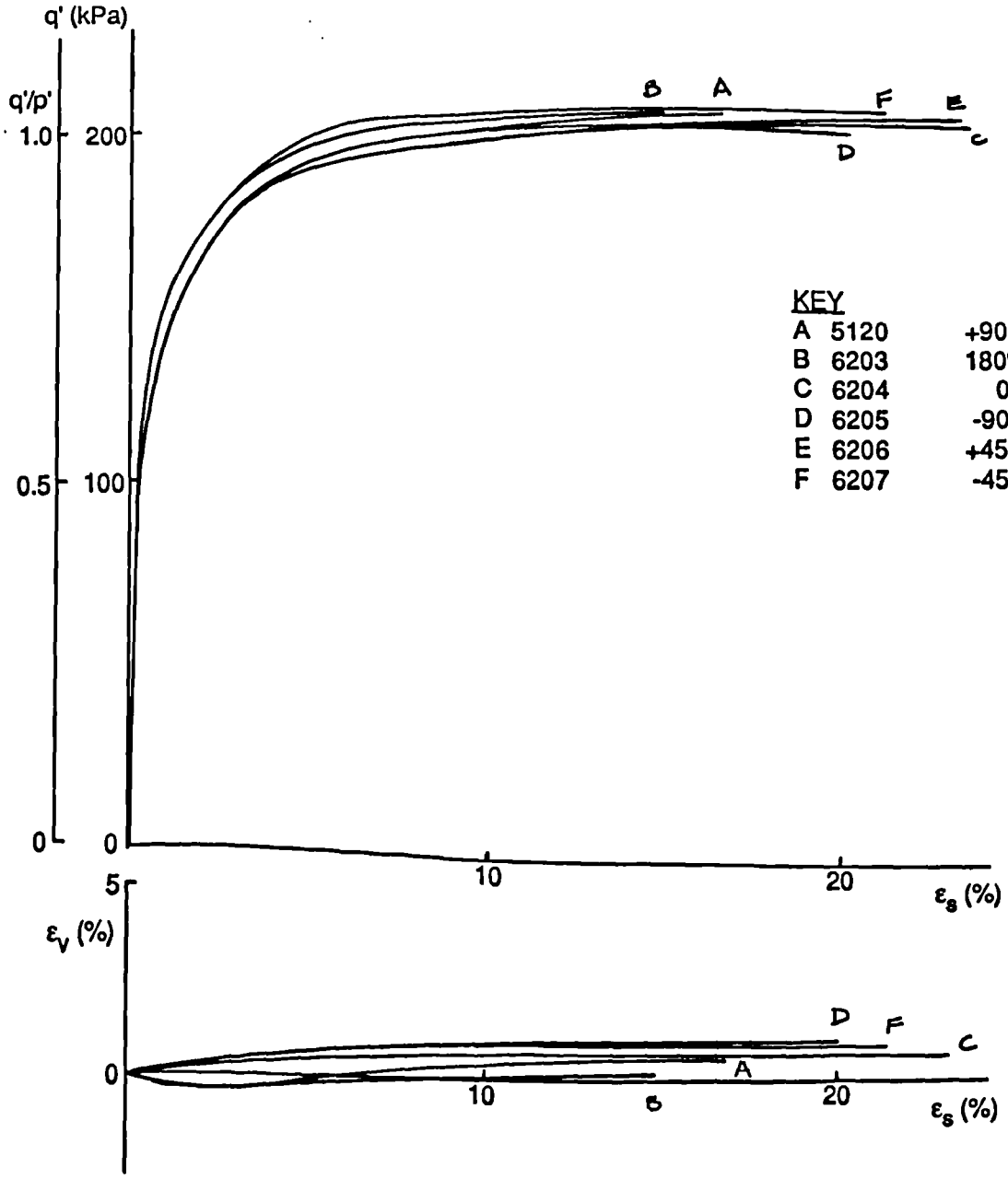

Fig 8.162 Plots of q' against ε_s ,q'/p' against ε_s and ε_v against ε_s. Threshold tests to failure. Isotropically compressed Ware till. OCR = 2.0, p' =200kPa, constant p' paths.

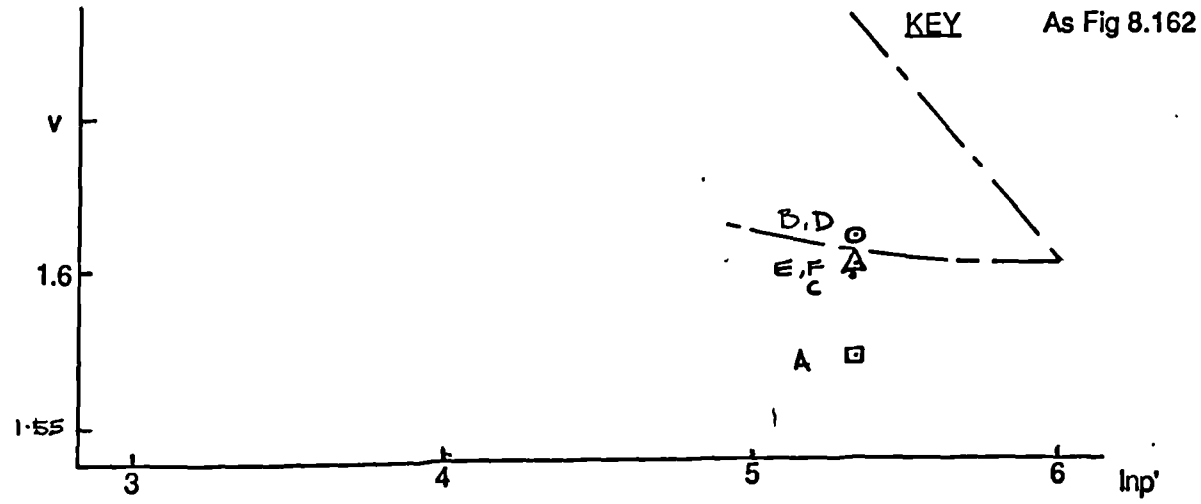

Fig 8.163 – Plot of v against $\log_e$ p' for threshold tests to failure. Isotropically compressed Ware till. OCR = 2.0, p' = 200kPa, constant p' paths.

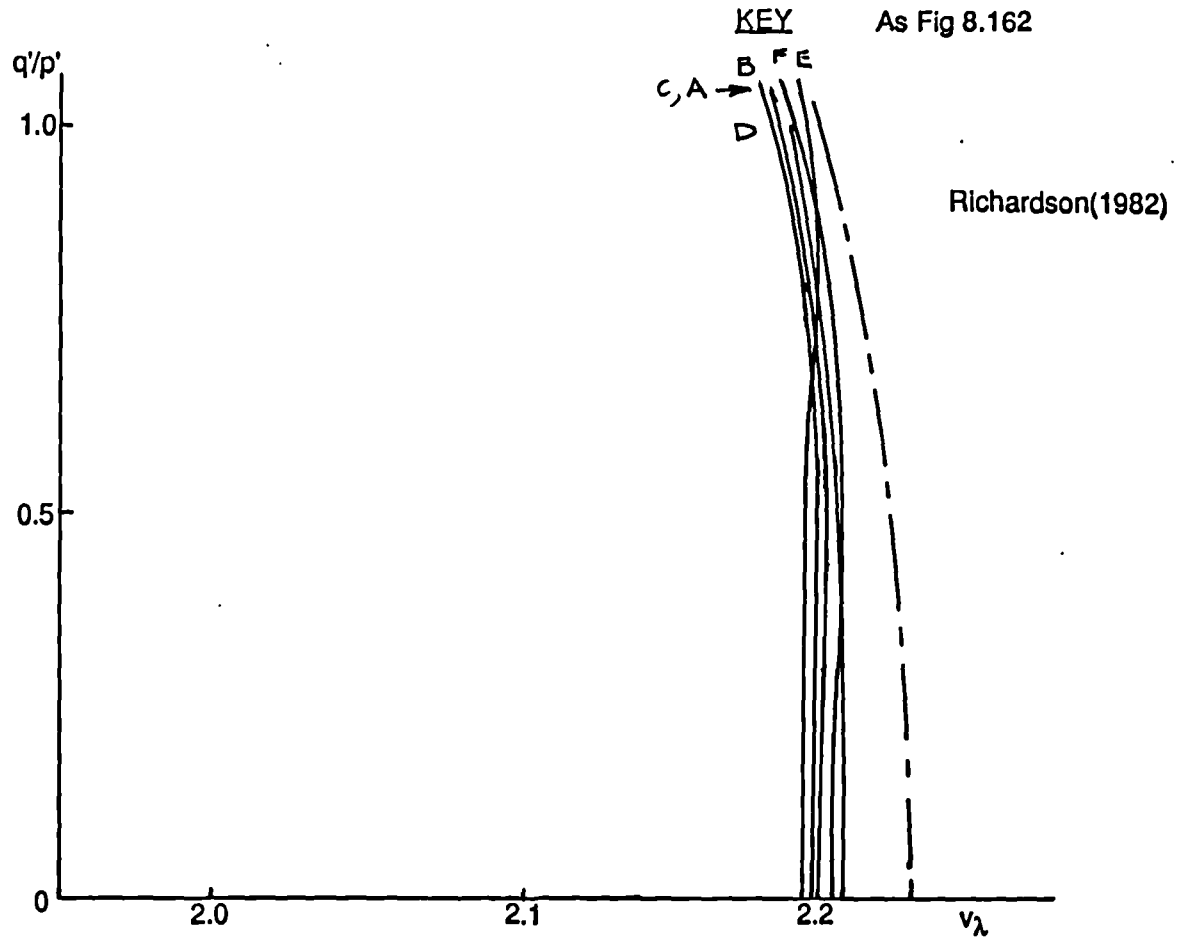

Fig 8.164 Plot of q' / p' against v_λ. Threshold tests to failure. Isotropically compressed Ware till. OCR = 2.0, p' = 200kPa, constant p' paths.

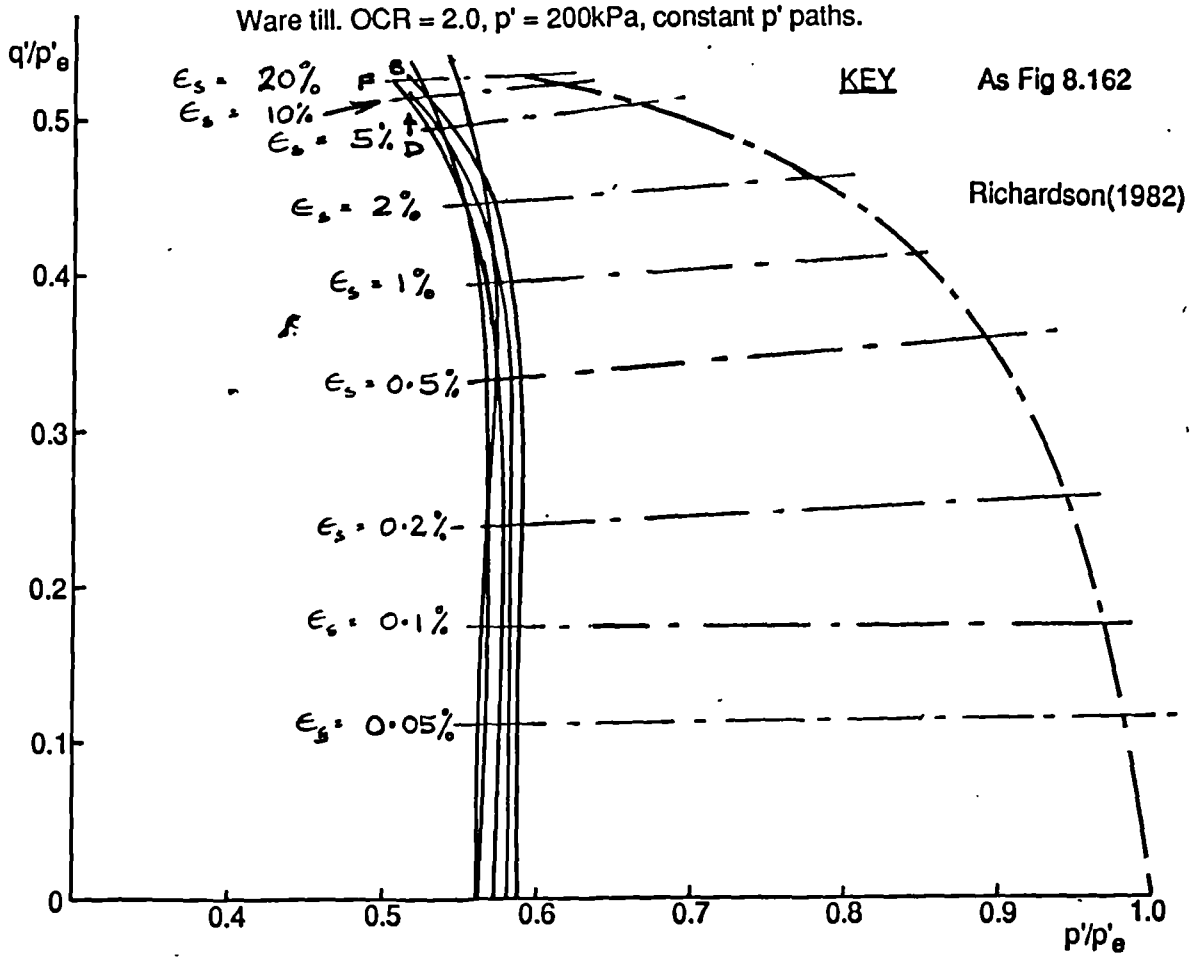

Fig 8.165 Plot of q' / p'_e against p' / p'_e. Threshold tests to failure. Isotropically compressed Ware till. OCR = 2.0, p' = 200kPa, constant p' paths.

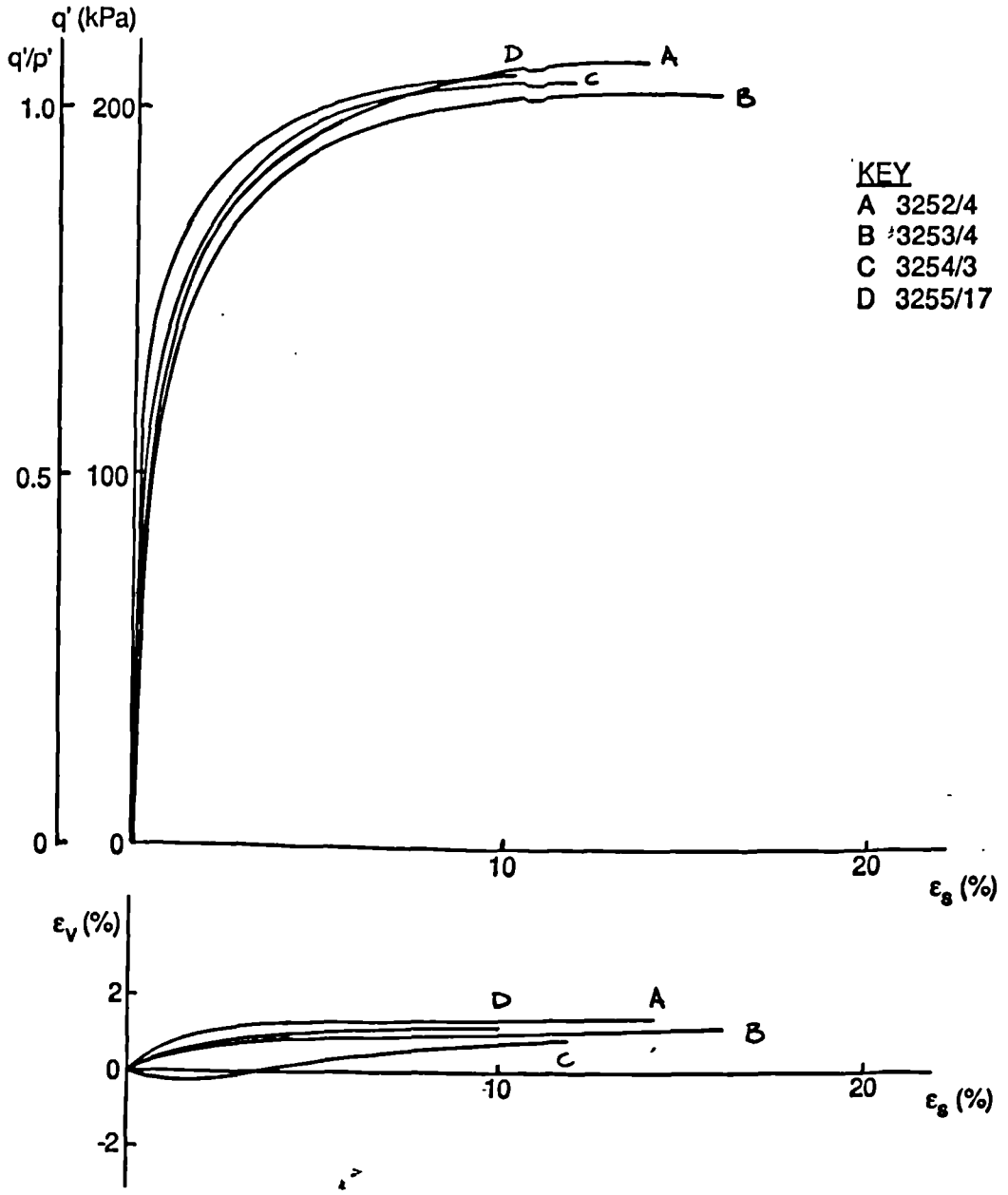

Fig 8.166 Plots of q' against ε_s ,q'/p' against ε_s and ε_v against ε_s. Threshold tests to failure. Isotropically compressed Cowden till. OCR = 2.0, p' =200kPa, constant p' paths.

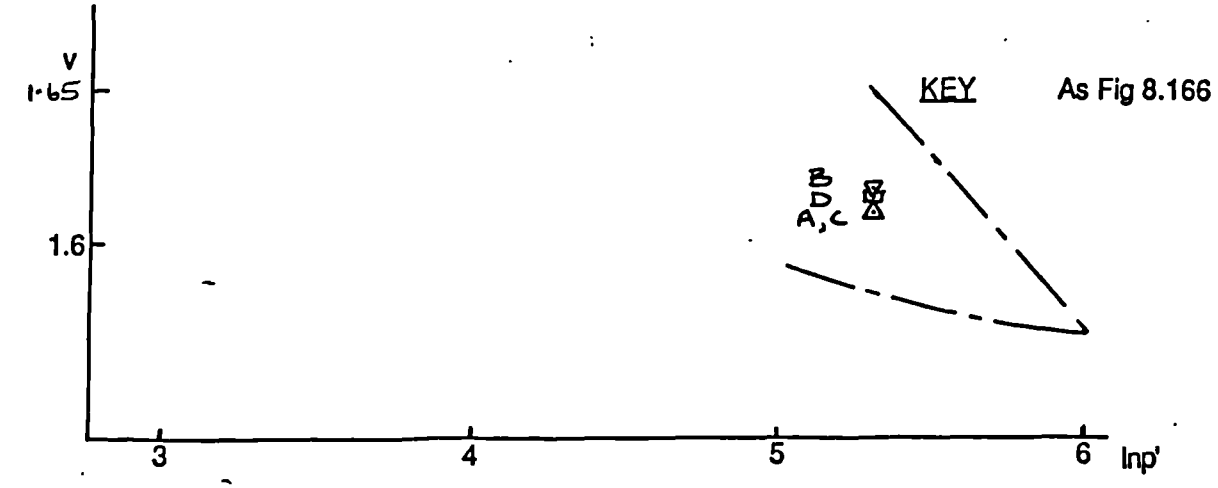

Fig 8.167 Plot of v against $\log_e$ p' for threshold tests to failure. Isotropically compressed Cowden till. OCR = 2.0, p' = 200kPa, constant p' paths.

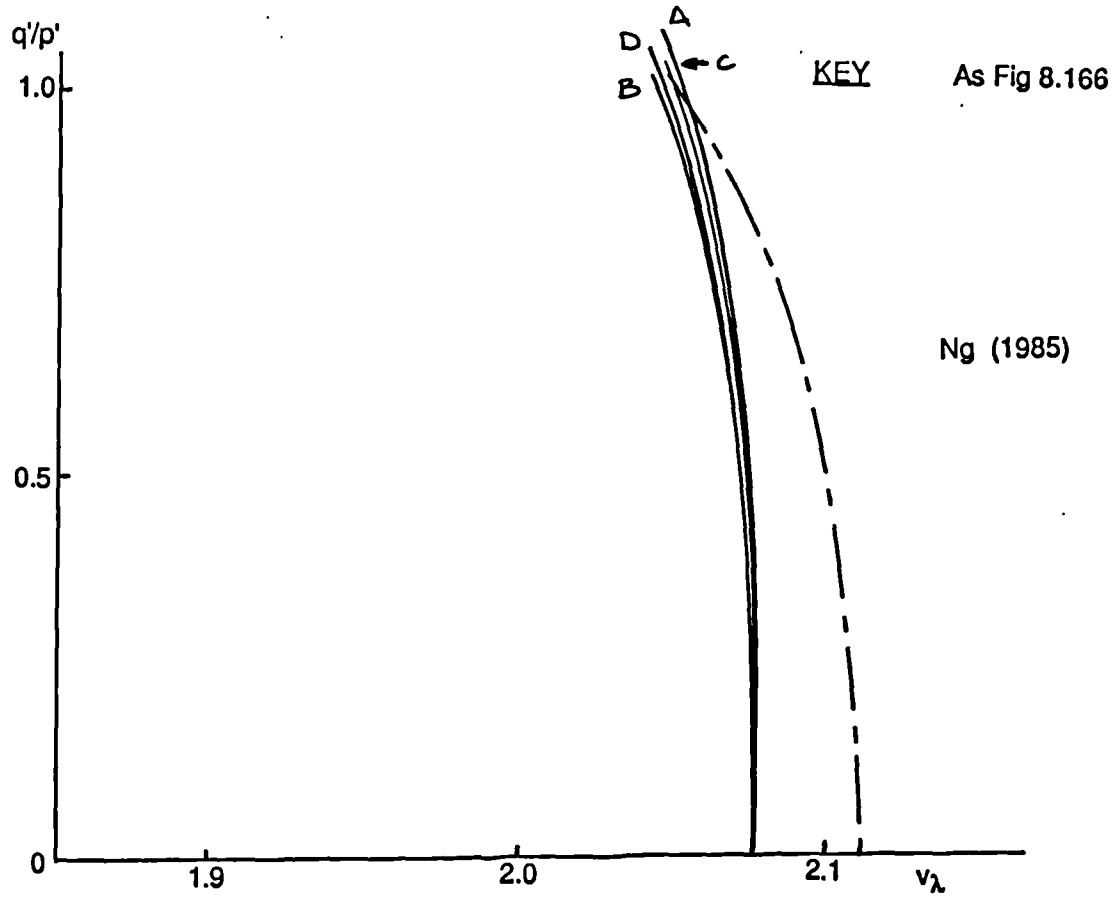

Fig 8.168 Plot of q' / p' against v_λ. Threshold tests to failure. Isotropically compressed Cowden till. OCR = 2.0, p' = 200kPa, constant p' paths.

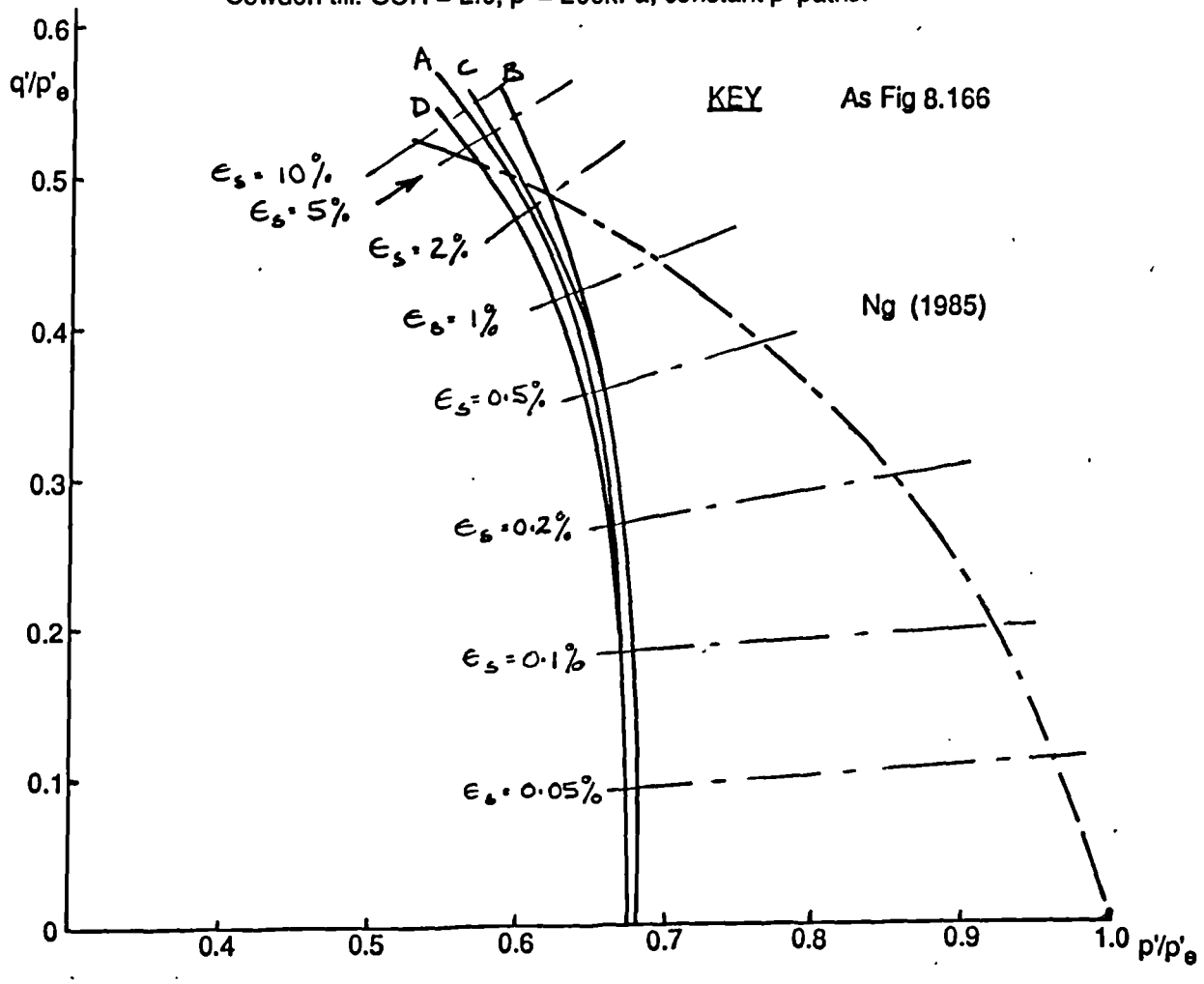

Fig 8.169 Plot of q' / p'_e against p' / p'_e. Threshold tests to failure. Isotropically compressed Cowden till. OCR = 2.0, p' = 200kPa, constant p' paths.

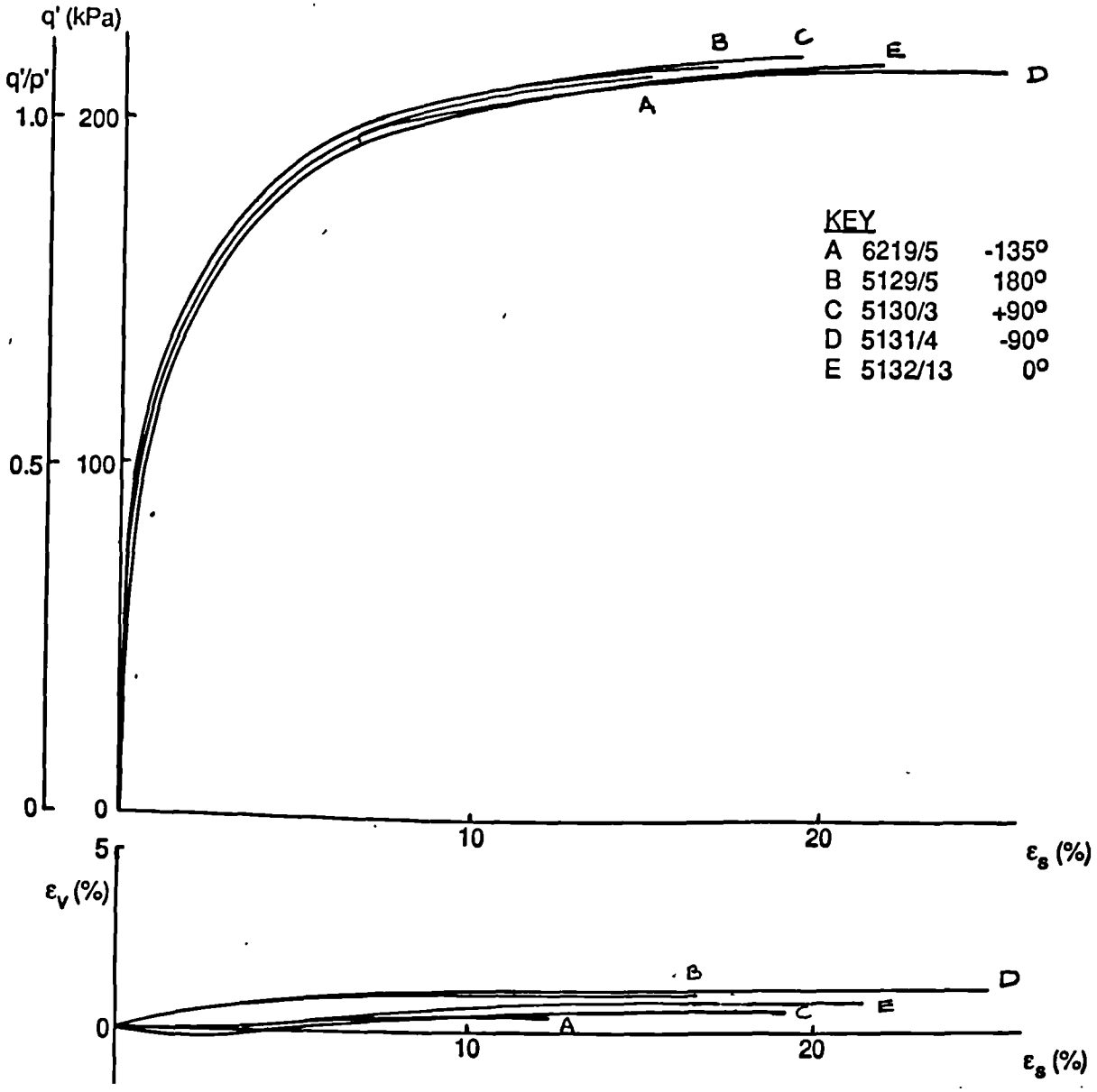

Fig 8.170 Plots of q' against ε_s ,q'/p' against ε_s and ε_v against ε_s. Threshold tests to failure. Isotropically compressed slate dust. OCR = 2.0, p' =200kPa, constant p' paths.

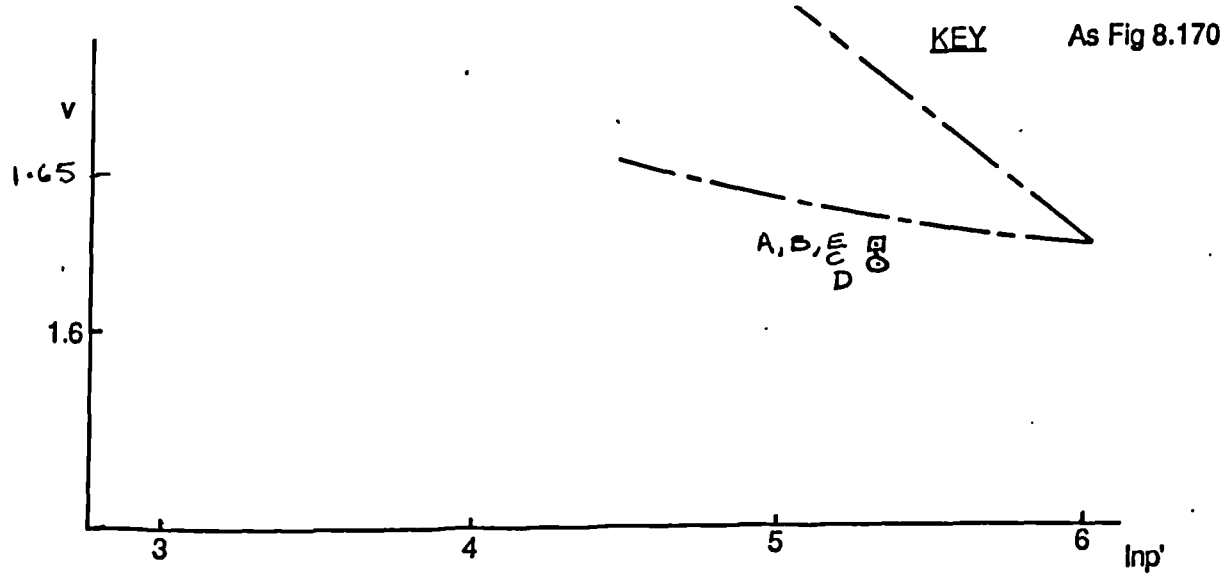

Fig 8.171 Plot of v against $\log_e$ p' for threshold tests to failure. Isotropically compressed slate dust. OCR = 2.0, p' = 200kPa, constant p' paths.

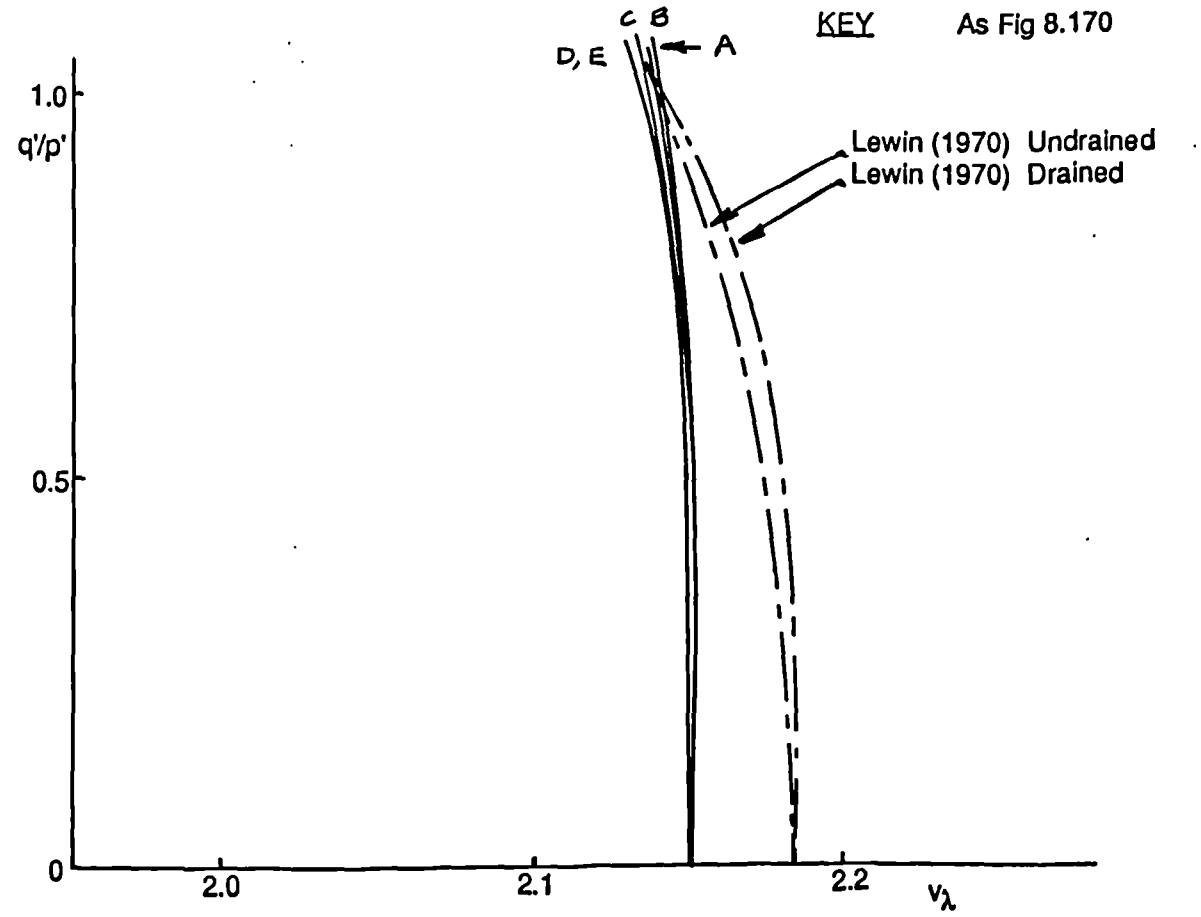

Fig 8.172 Plot of q' / p' against v_λ. Threshold tests to failure. Isotropically compressed slate dust. OCR = 2.0, p' = 200kPa, constant p' paths.

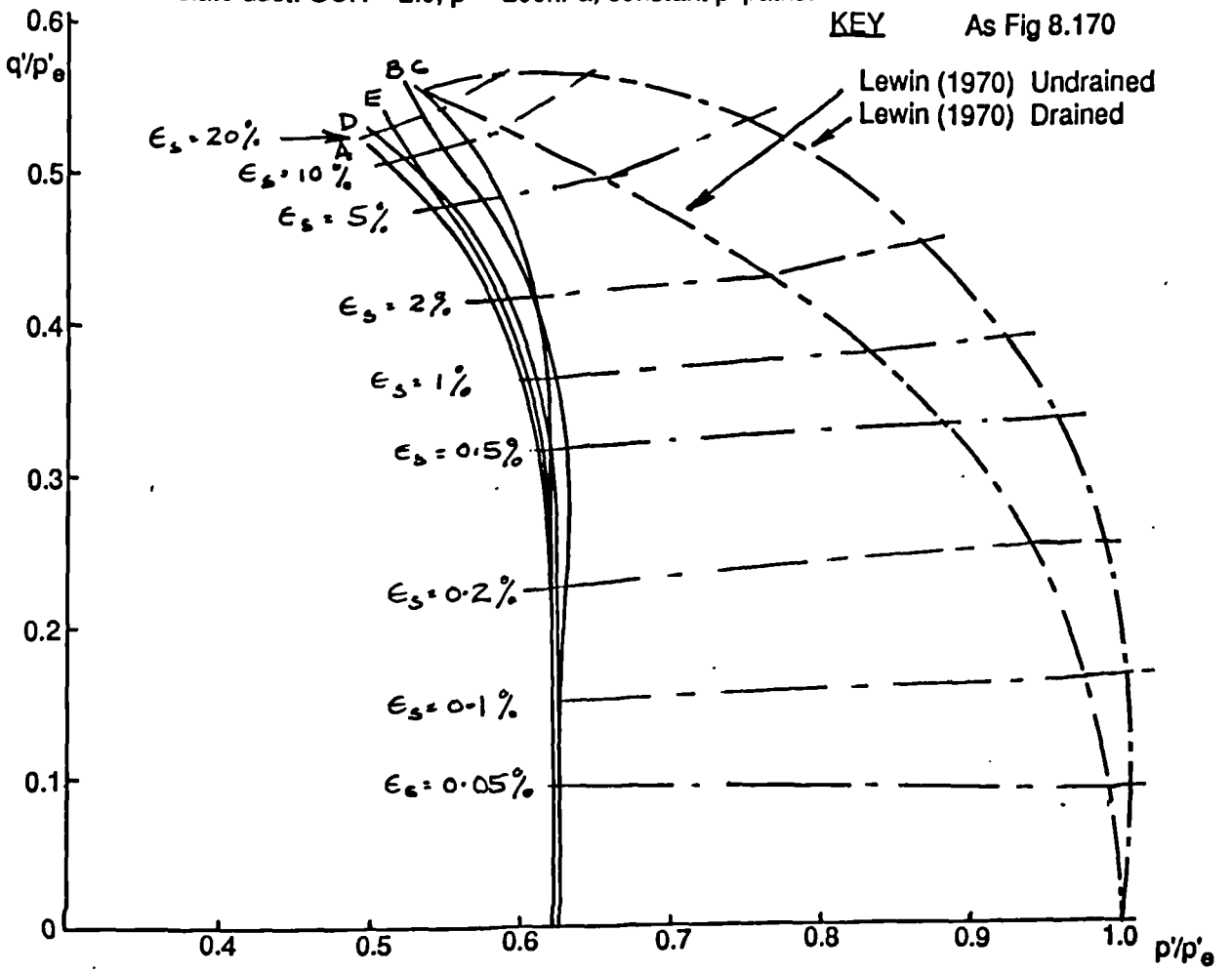

Fig 8.173 Plot of q' / p'_e against p' / p'_e. Threshold tests to failure. Isotropically compressed slate dust. OCR = 2.0, p' = 200kPa, constant p' paths.

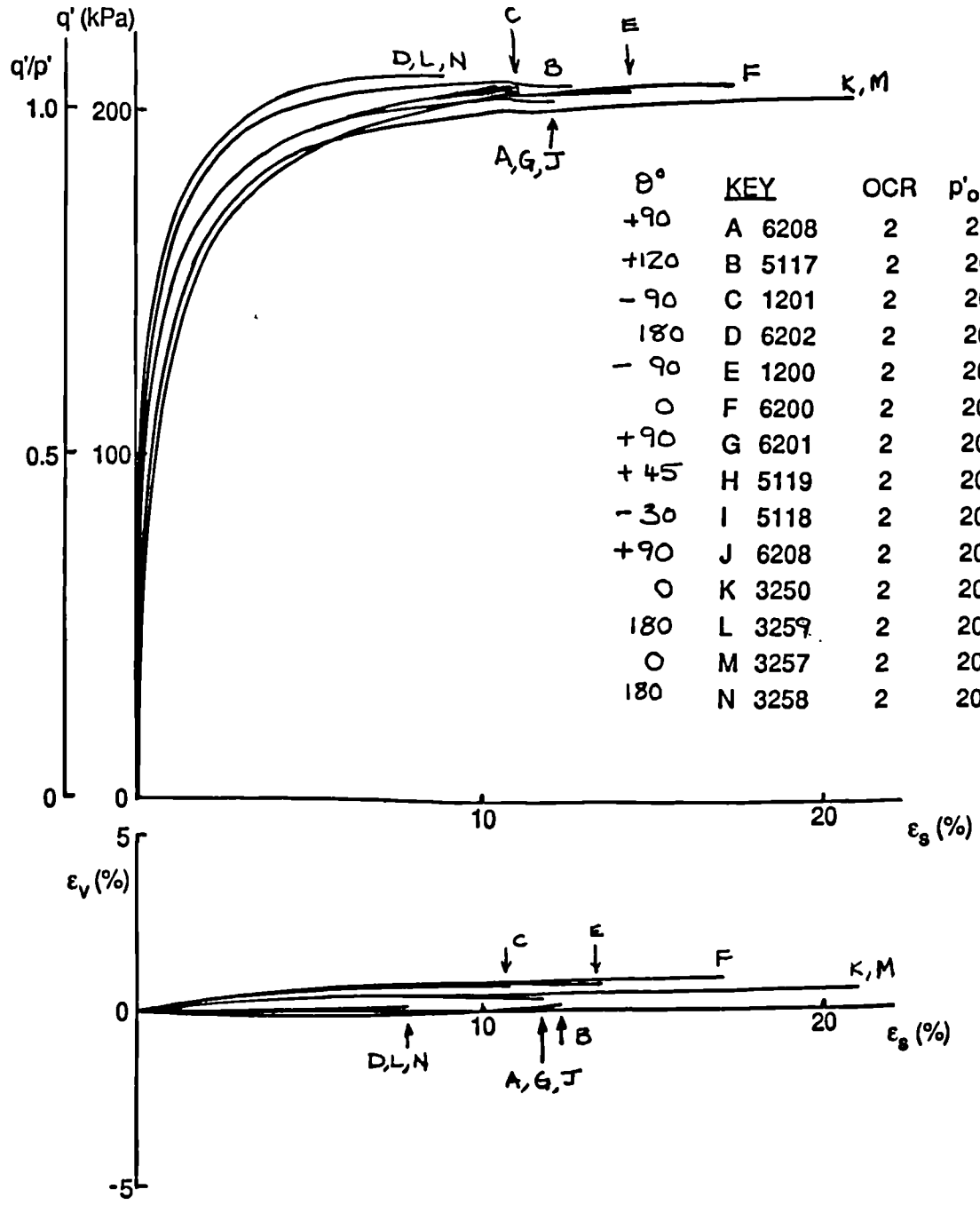

θ°	KEY	OCR	p'_o (kPa)	Test Type
+90	A 6208	2	200	$\delta p'=0$
+120	B 5117	2	200	$\delta p'=0$
−90	C 1201	2	200	$\delta p'=0$
180	D 6202	2	200	$\delta p'=0$
−90	E 1200	2	200	$\delta p'=0$
0	F 6200	2	200	$\delta p'=0$
+90	G 6201	2	200	$\delta p'=0$
+45	H 5119	2	200	$\delta p'=0$
−30	I 5118	2	200	$\delta p'=0$
+90	J 6208	2	200	$\delta p'=0$
0	K 3250	2	200	$\delta p'=0$
180	L 3259	2	200	$\delta p'=0$
0	M 3257	2	200	$\delta p'=0$
180	N 3258	2	200	$\delta p'=0$

Fig 8.174 Plots of q' against ε_s ,q'/p' against ε_s and ε_v against ε_s. Threshold tests to failure. Isotropically compressed London clay. OCR = 2.0, p' =200kPa, constant p' paths.

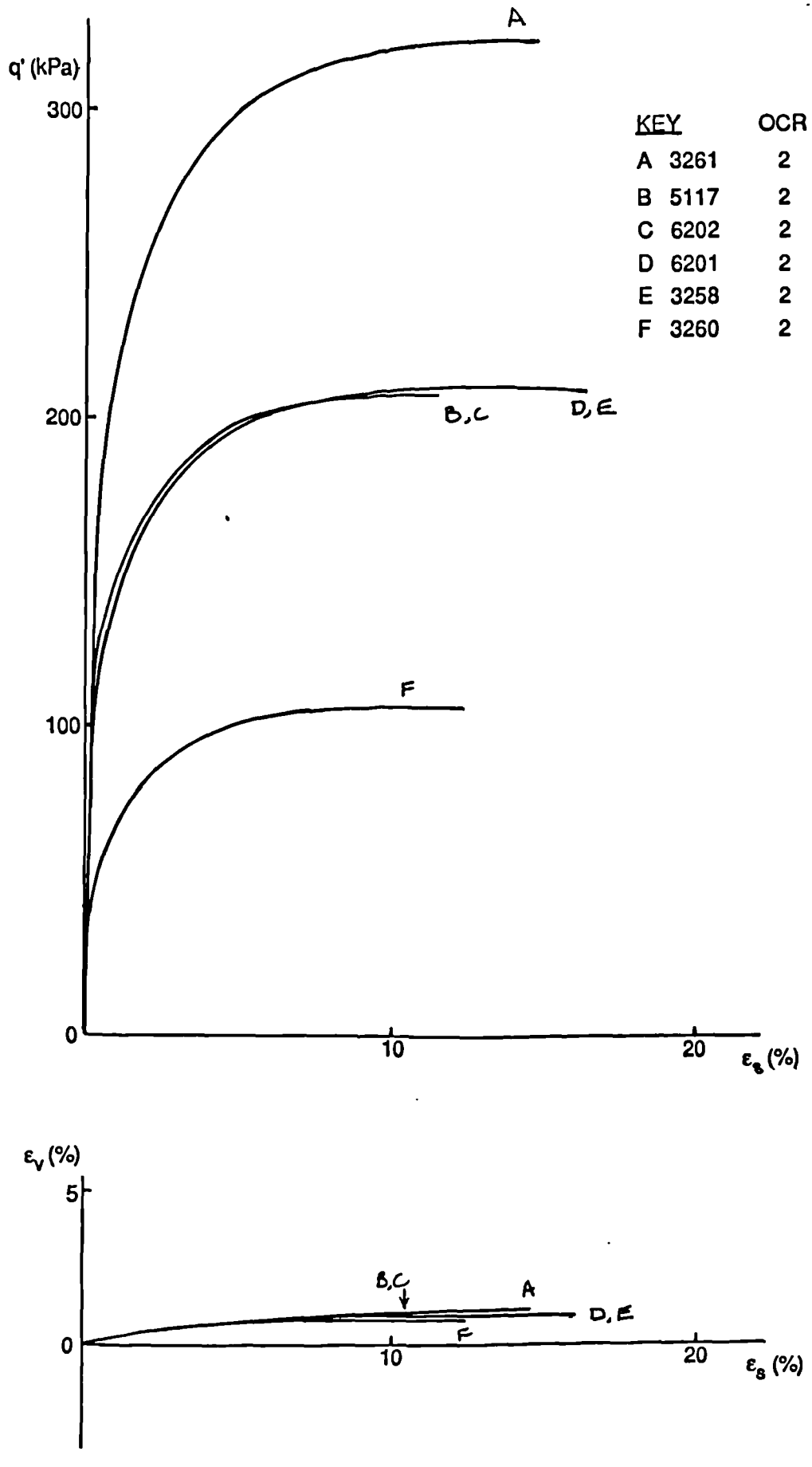

KEY	OCR	p'_o (kPa)	Test Type
A 3261	2	300	$\delta p'=0$
B 5117	2	200	$\delta p'=0$
C 6202	2	200	$\delta p'=0$
D 6201	2	200	$\delta p'=0$
E 3258	2	200	$\delta p'=0$
F 3260	2	100	$\delta p'=0$

Fig 8.175 Plots of q' against ε_s and ε_v against ε_s for threshold tests to failure. Isotropically compressed London clay. OCR = 2.0, various p', constant p' paths.

KEY	OCR	p'_o (kPa)	Test Type
A 5134/10	8	50	$\delta p'=0$
B 5126/11	4	100	$\delta p'=0$
C Average	2	200	$\delta p'=0$
D 6211/11	1.5	267	$\delta p'=0$

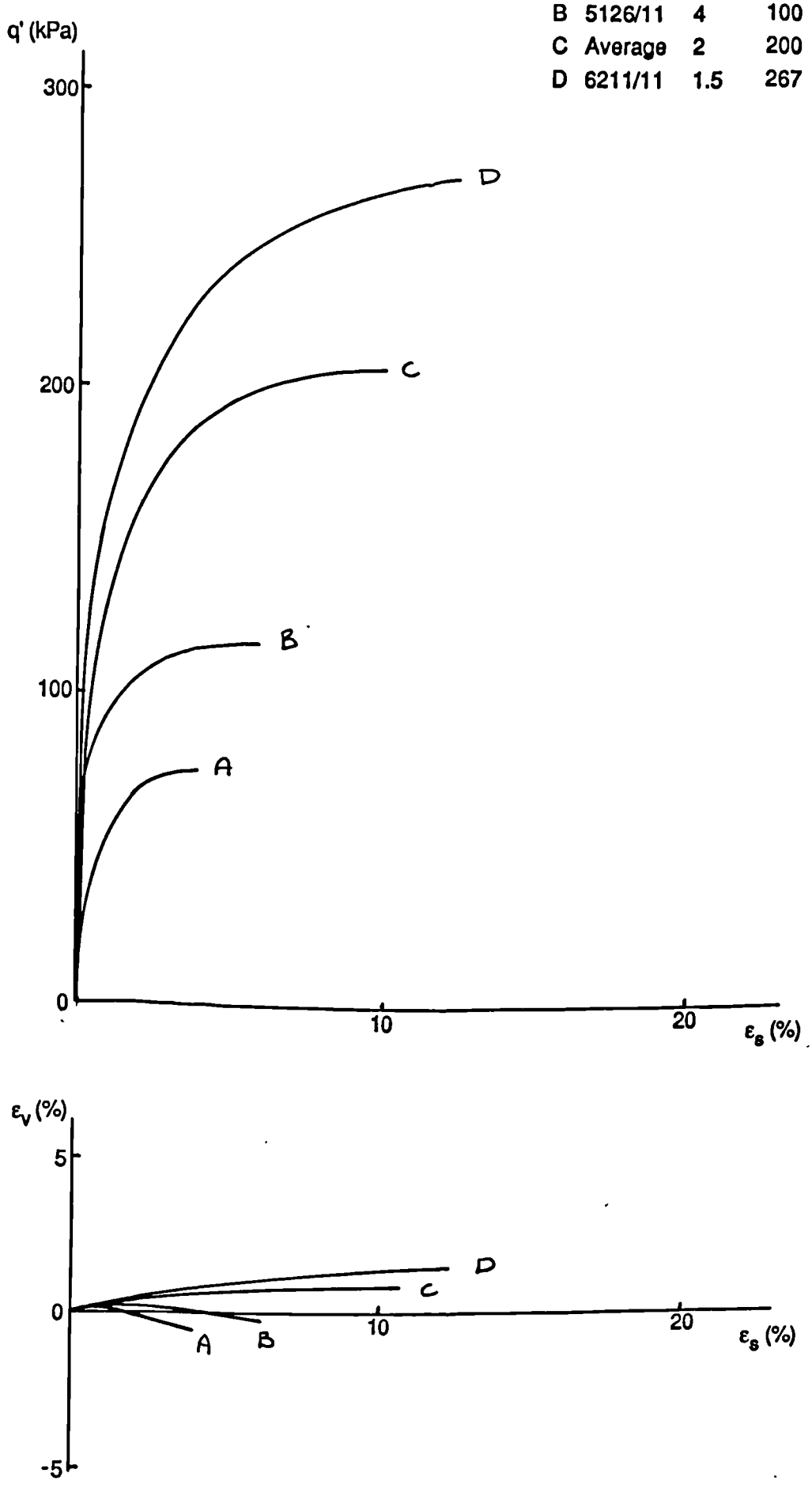

Fig 8.176 Plots of q' against ε_s and ε_v against ε_s for threshold tests to failure. Isotropically compressed London clay. various OCR's, $\theta = 180^o$. constant p' paths.

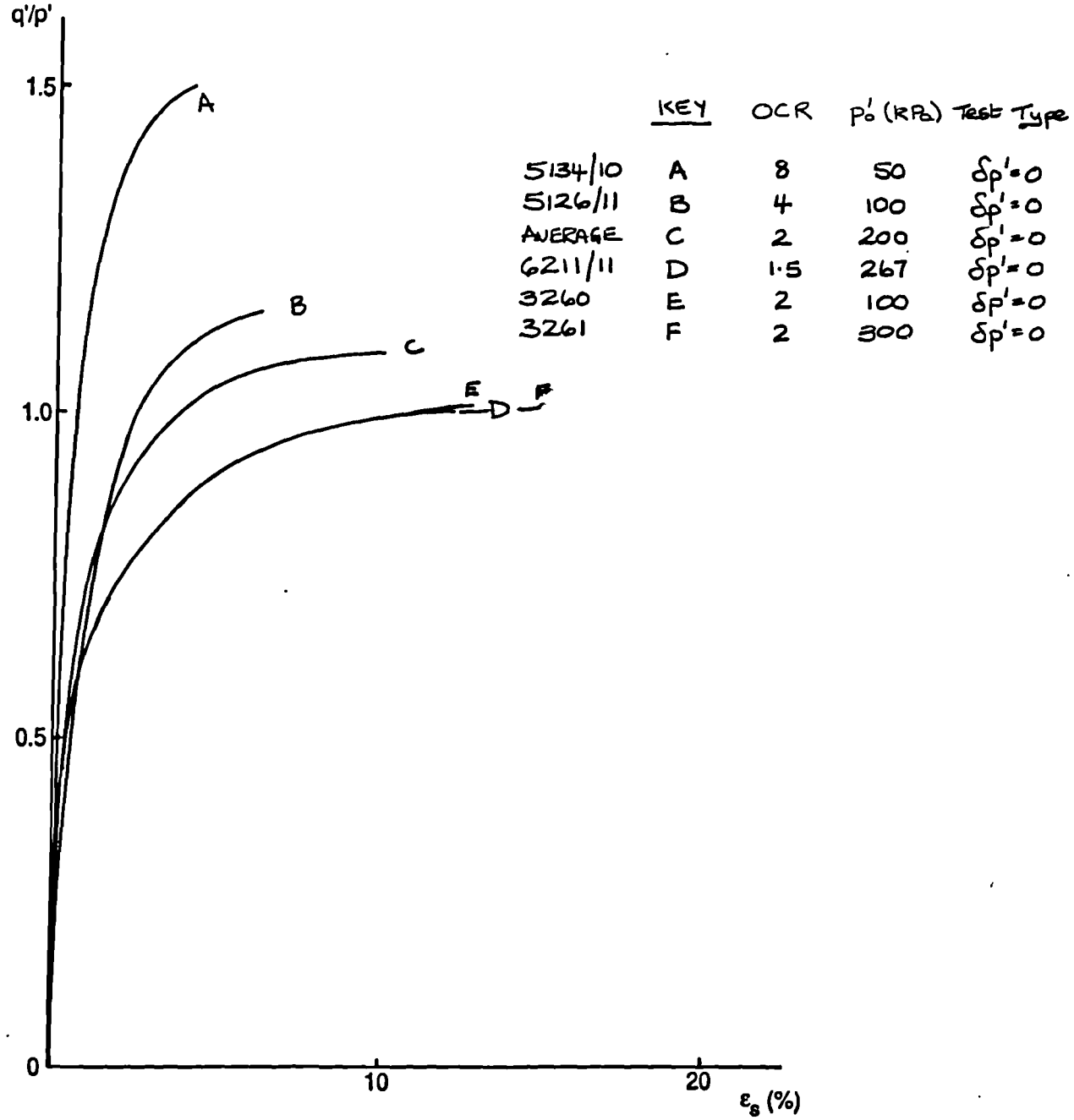

Fig 8.177 Plot of q' / p' against ε_s for threshold tests to failure. Isotropically compressed London clay. various OCR's, $\theta = 180^o$. constant p' paths.

KEY	OCR	p'_o (kPa)	Test Type
A 5134	8	50	$\delta p'=0$
B 5126	4	100	$\delta p'=0$
C 6208	2	200	$\delta p'=0$
D 5117	2	200	$\delta p'=0$
E 1201	2	200	$\delta p'=0$
F 6202	2	200	$\delta p'=0$
G 1200	2	200	$\delta p'=0$
H 6200	2	200	$\delta p'=0$
I 6201	2	200	$\delta p'=0$
J 5119	2	200	$\delta p'=0$
K 5118	2	200	$\delta p'=0$
L 6208	2	200	$\delta p'=0$
M 3250	2	200	$\delta p'=0$
N 3251	2	200	$\delta p'=0$
O 3257	2	200	$\delta p'=0$
P 3258	2	200	$\delta p'=0$
Q 3260	2	100	$\delta p'=0$
R 3261	2	300	$\delta p'=0$
S 6211	1.5	267	$\delta p'=0$

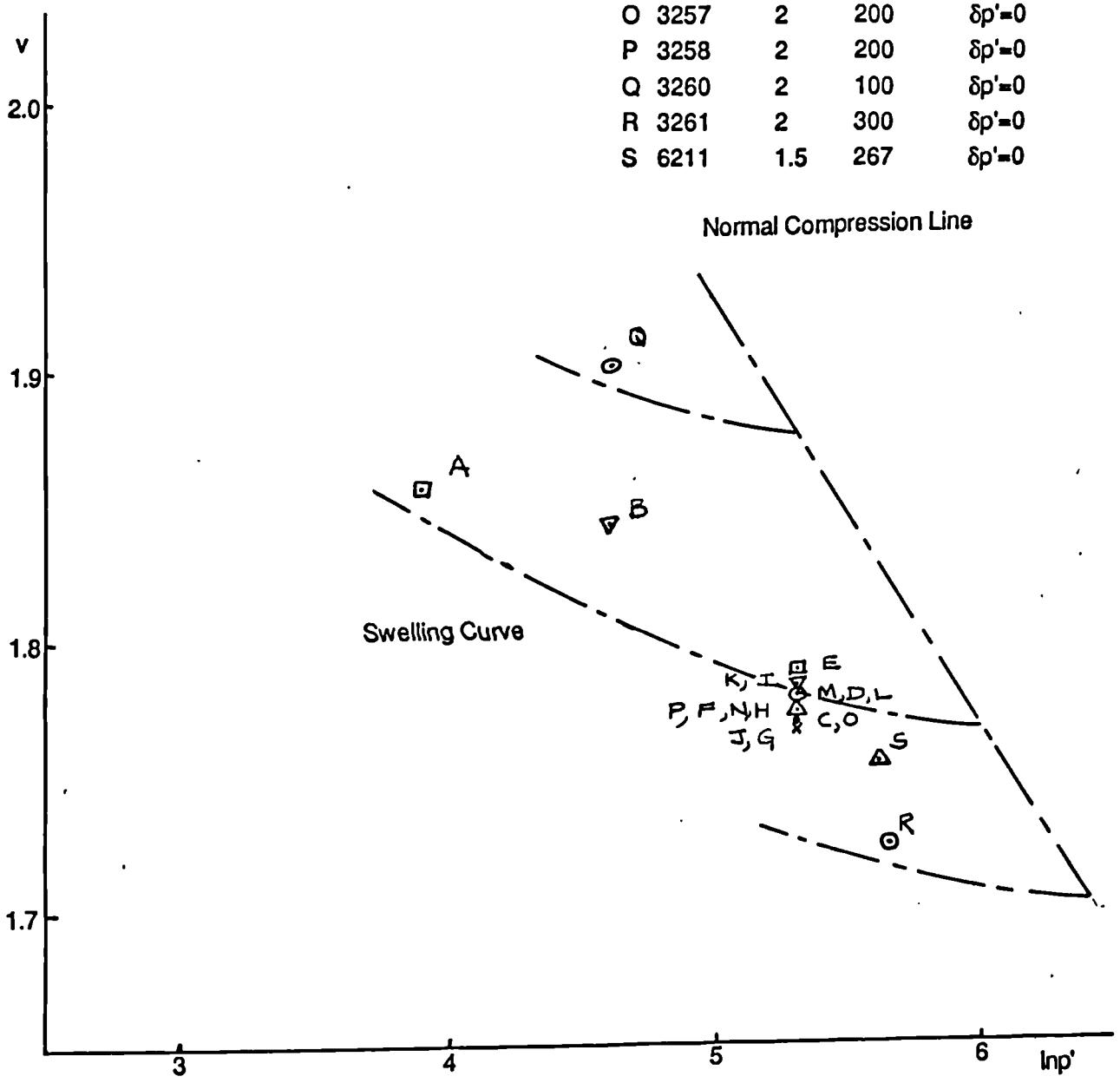

Fig 8.178 Plot of v against $\log_e p'$ for threshold tests to failure. Isotropically compressed London clay. various OCR's. constant p' paths.

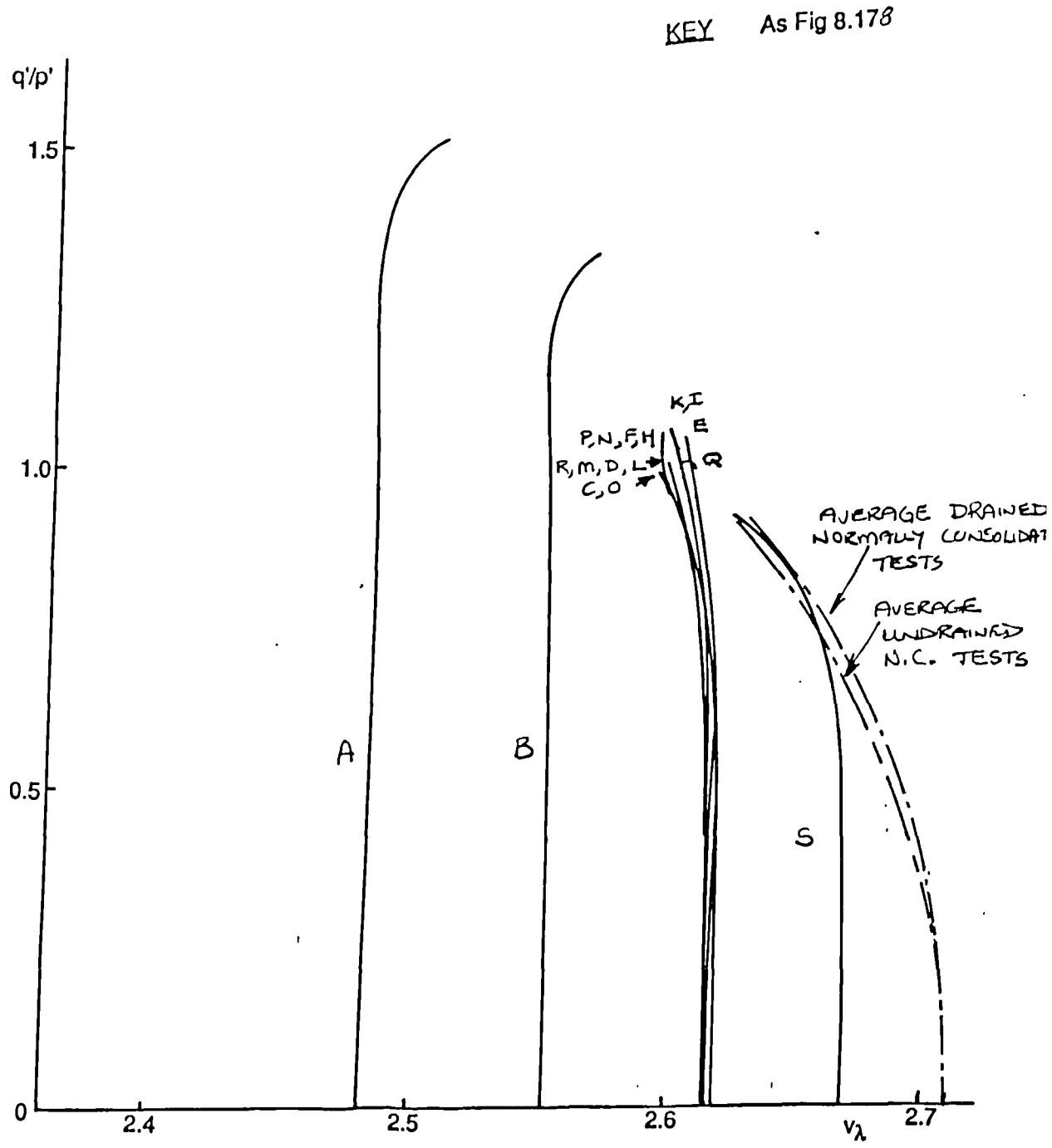

Fig 8.179 Plot of q' / p' against v_λ. Threshold tests to failure. Isotropically compressed London clay. Various OCR's, constant p' paths.

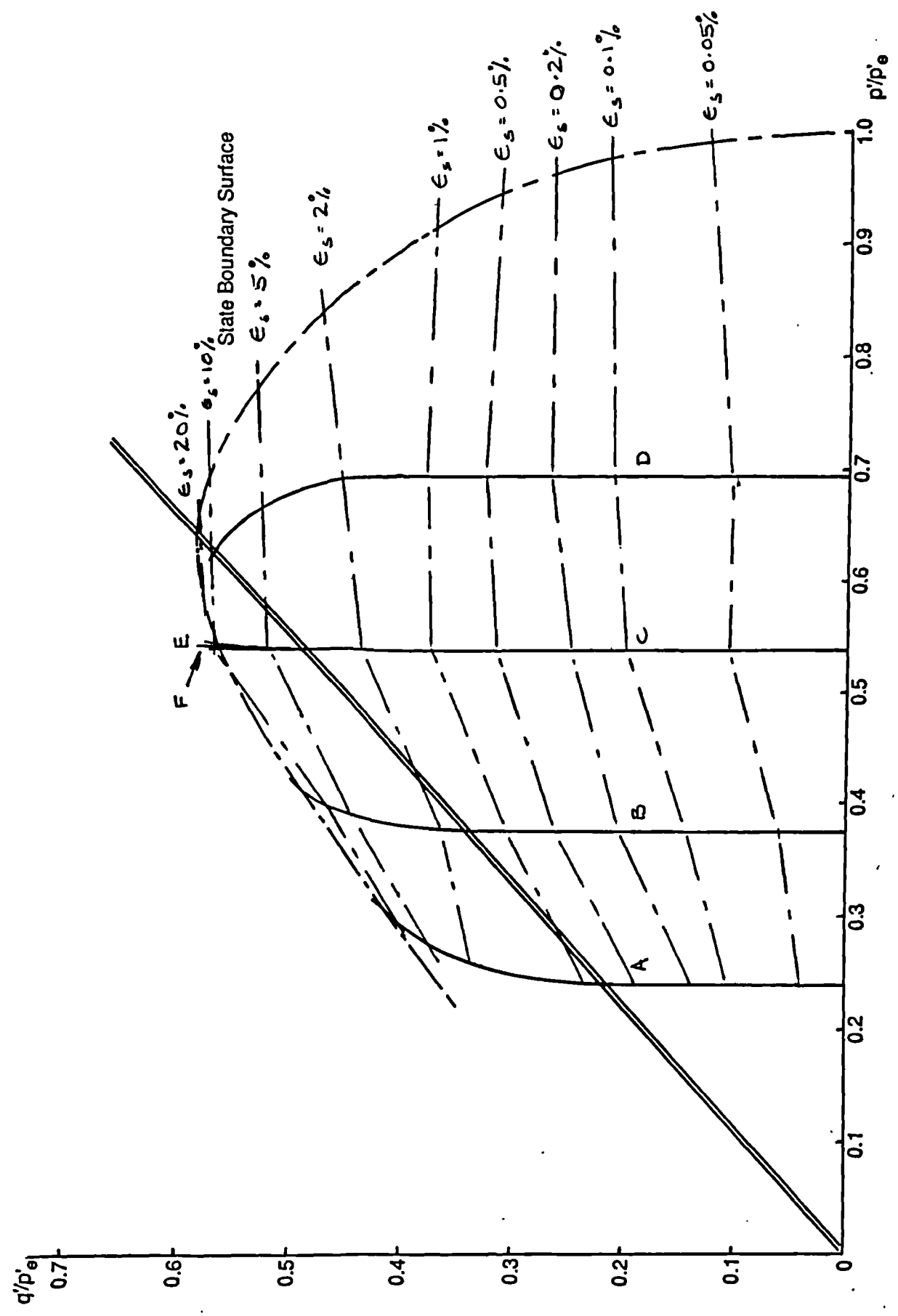

Fig 8.180 Plot of q' / p'_e against p' / p'_e . Threshold tests to failure. Isotropically compressed London clay. Various OCR's, constant p' paths.

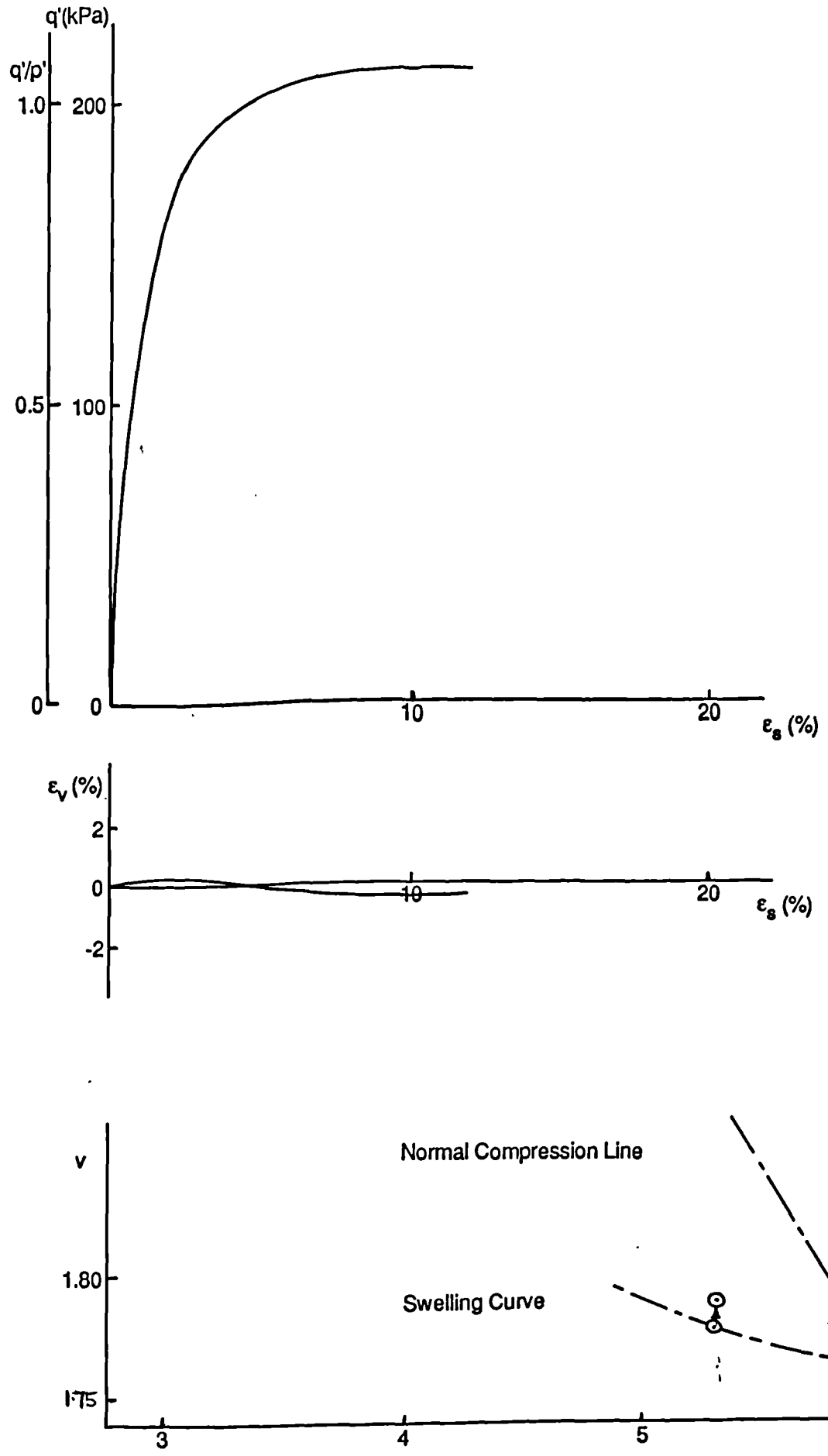

Fig 8.181 Plots of q' against ε_s ;q'/p' against ε_s , ε_v against ε_s and v against $\log_e p'$. Threshold tests to failure on London clay. η'_o = 0.25, OCR = 2.0, p' =200kPa, constant p' paths.

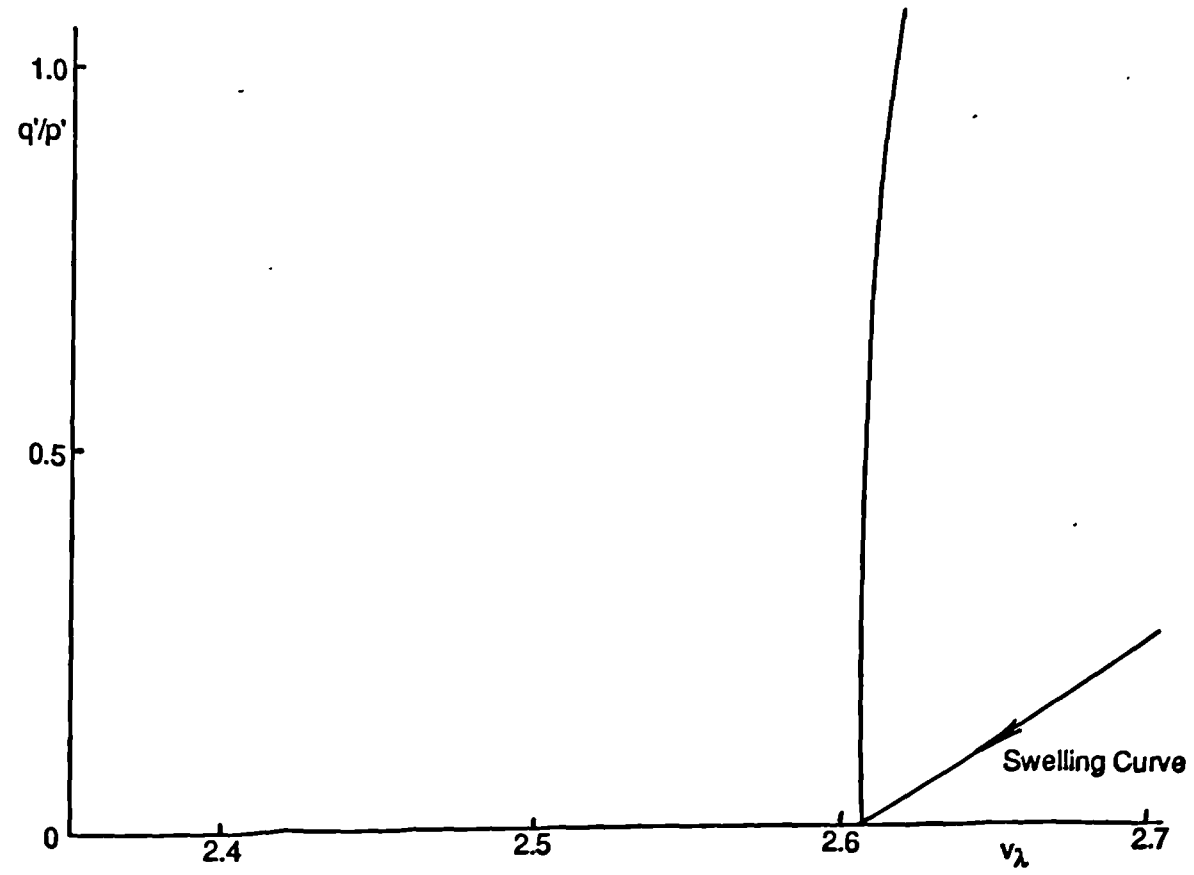

Fig 8.182 Plot of q' / p' against v_λ. Threshold tests to failure on London clay. η'_o = 0.25,OCR = 2.0, p' = 200kPa, constant p' paths.

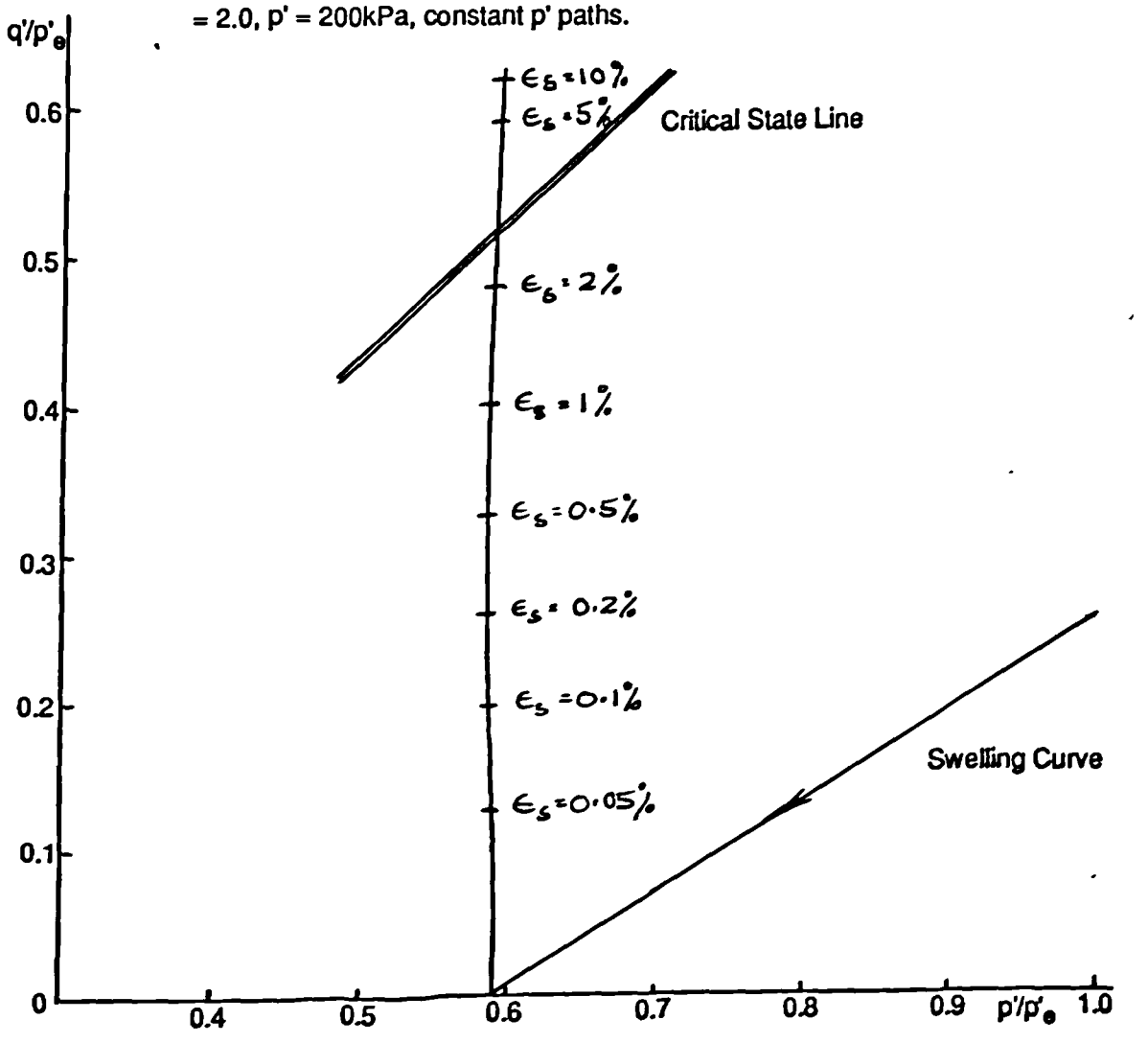

Fig 8.183 Plot of q' / p'_e against p' / p'_e. Threshold tests to failure. London clay. η'_o = 0.25, OCR = 2.0, p' = 200kPa,constant p' paths.

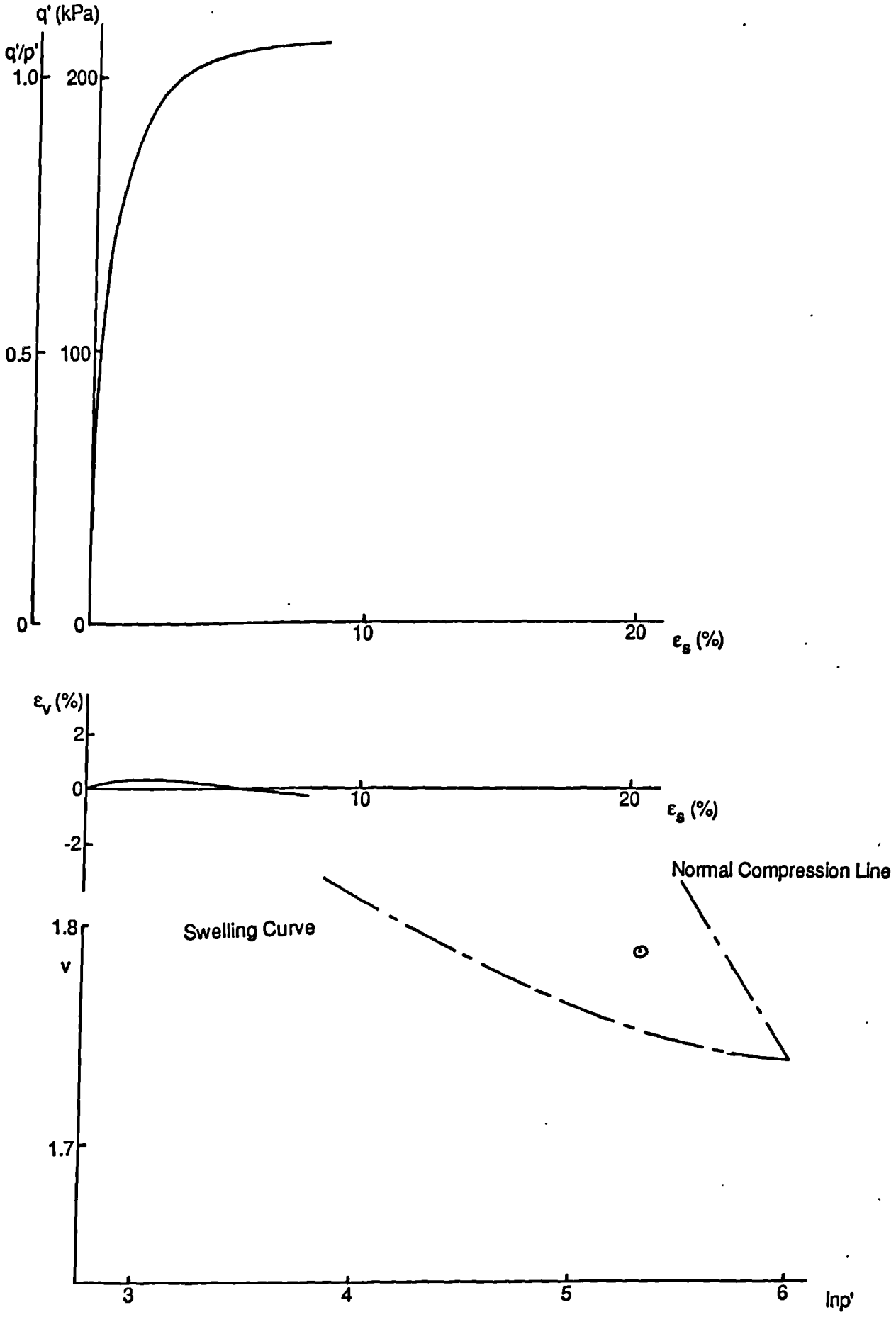

Fig 8.184 Plots of q' against ε_s ,q'/p' against ε_s , ε_v against ε_s and v against $\log_e p'$. Threshold tests to failure on London clay. One dimensionally compressed, OCR = 2.0, p' =200kPa, constant p' paths .

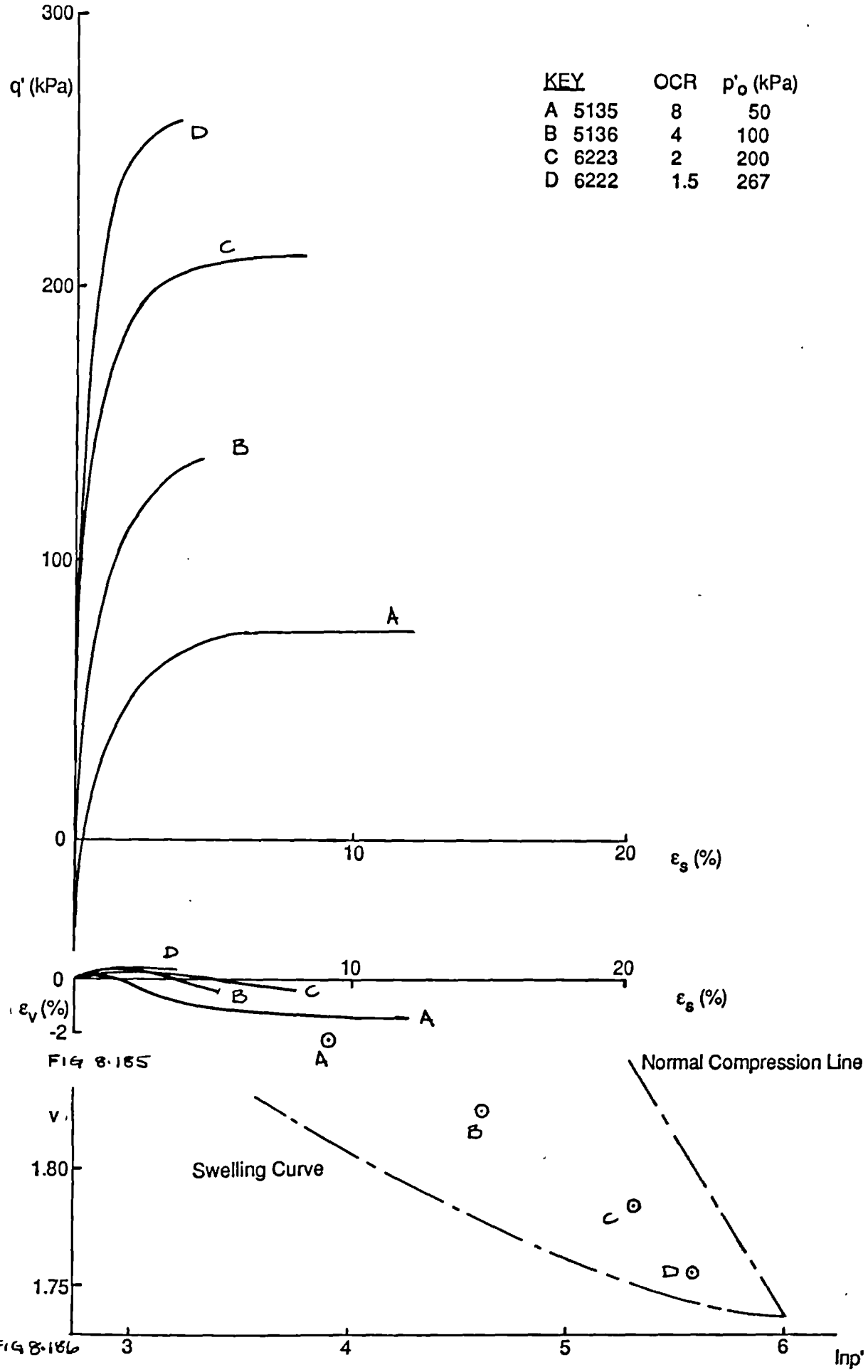

Fig 8.185

Fig 8.186

Fig 8.185 Plots of q' against ε_s and ε_v against ε_s for threshold tests to failure. One dimensionally compressed London clay. various OCR's, $\theta = 180^o$. constant p' paths.

Fig 8.186 Plot of v against $\log_e p'$ for threshold tests to failure . One dimensionally compressed London clay. Various OCR's. Constant p' paths.

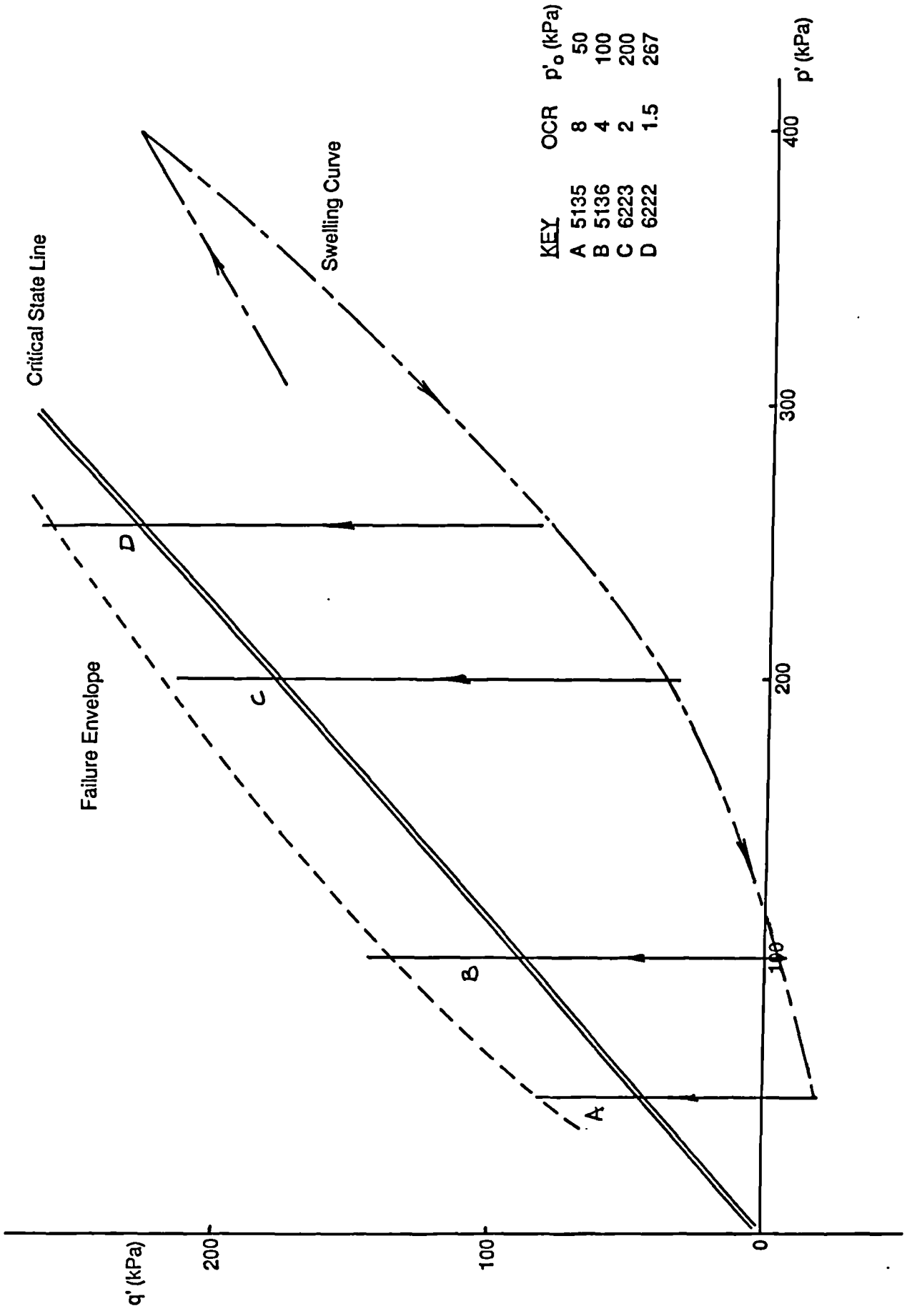

Fig 8.187 Plot of q' against p'. Stress paths to failure of one dimensionally compressed London clay. Various OCR's, constant p'.

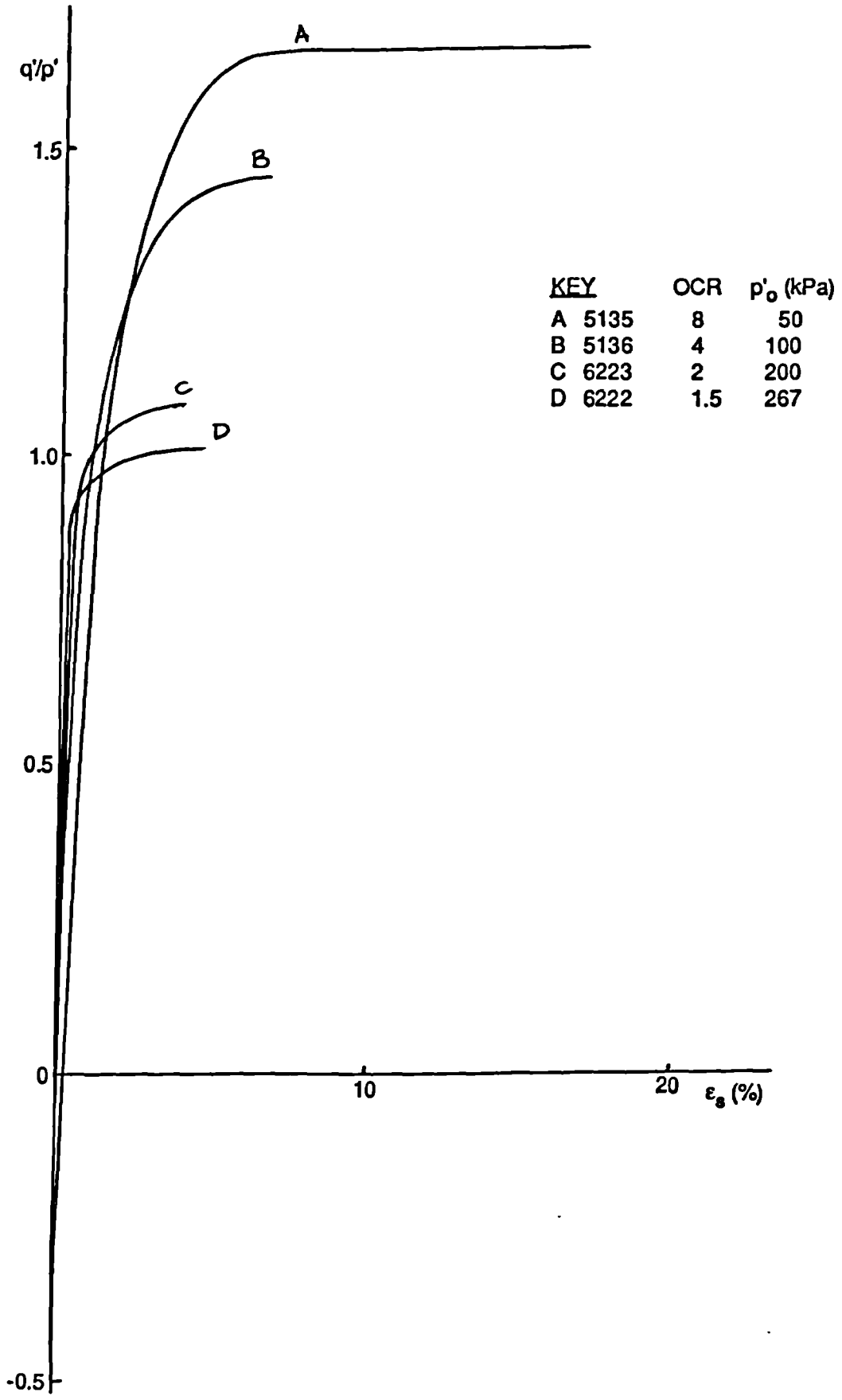

Fig 8.188 Plot of q' / p' against ε_s for threshold tests to failure. One dimensionally compressed London clay. various OCR's, $\theta = 180^o$. constant p' paths.

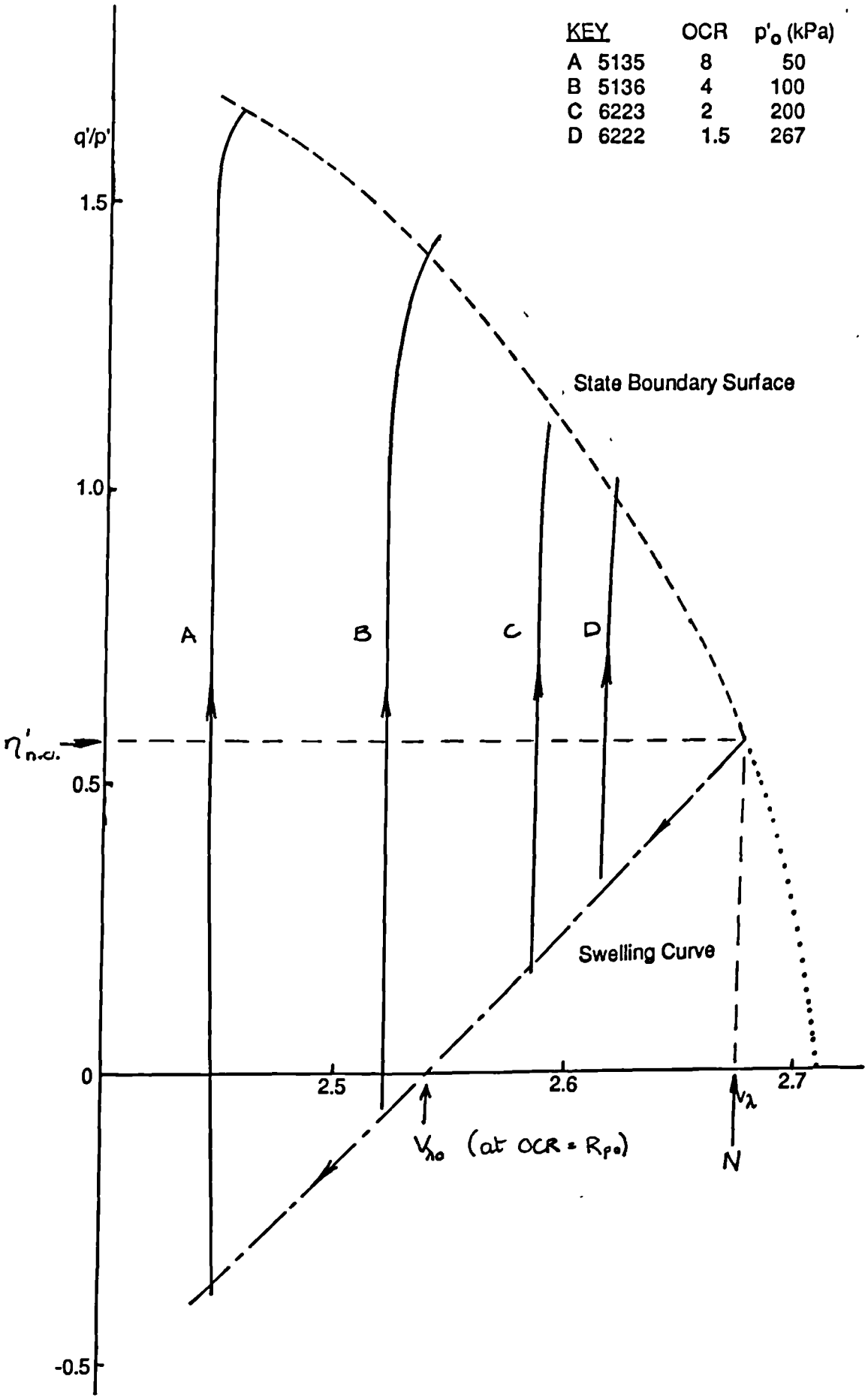

Fig 8.189 Plot of q' / p' against v_λ. Threshold tests to failure. One dimensionally compressed London clay. Various OCR's, constant p' paths.

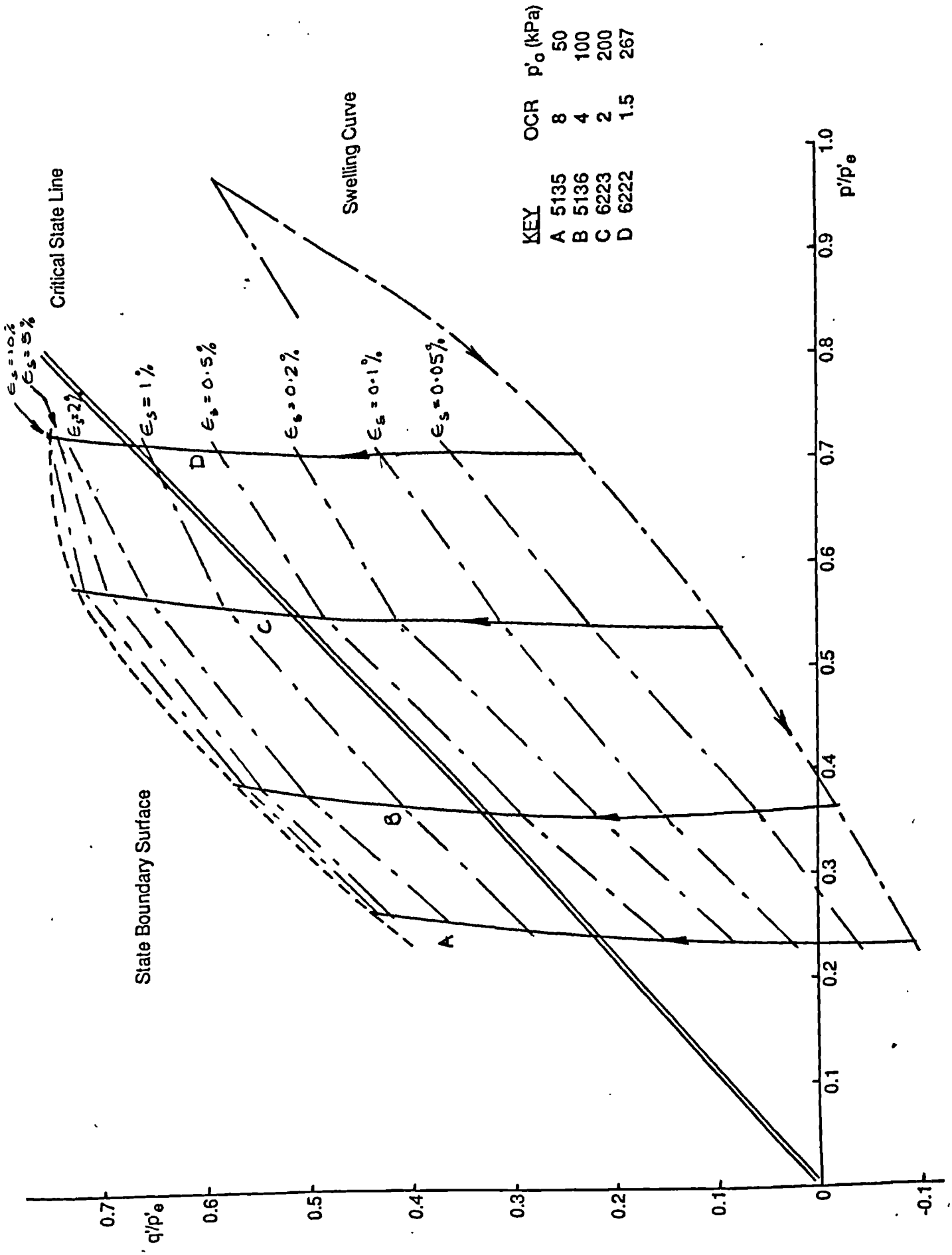

Fig 8.190 Plot of q' / p'_e against p' / p'_e . Threshold tests to failure. One dimensionally compressed London clay. Various OCR's, constant p' paths.

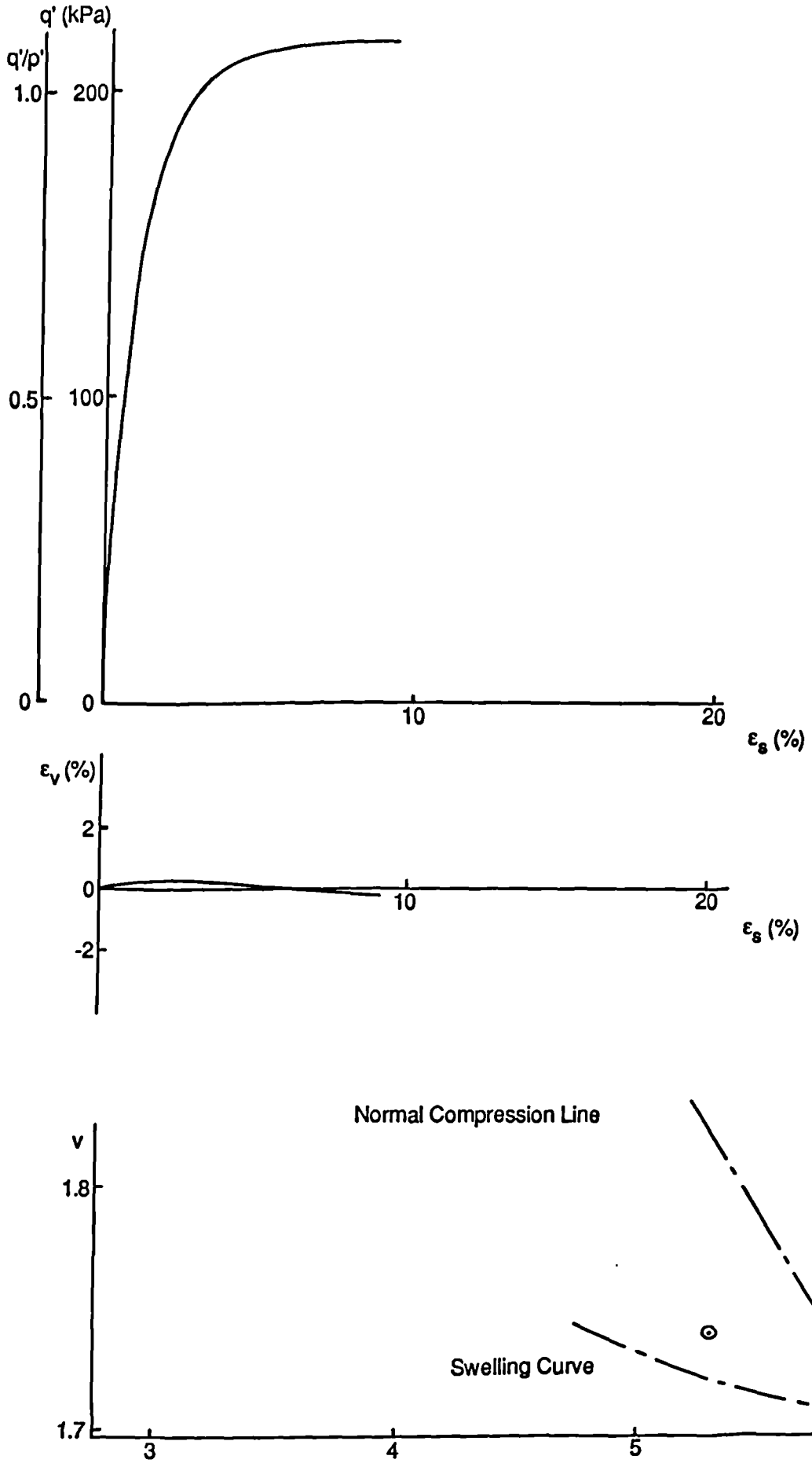

Fig 8.191 Plots of q' against ε_s ,q'/p' against ε_s , ε_v against ε_s and v against $\log_e p'$. Threshold tests to failure on London clay. η'_o = 0.75, OCR = 2.0, p' =200kPa, constant p' paths.

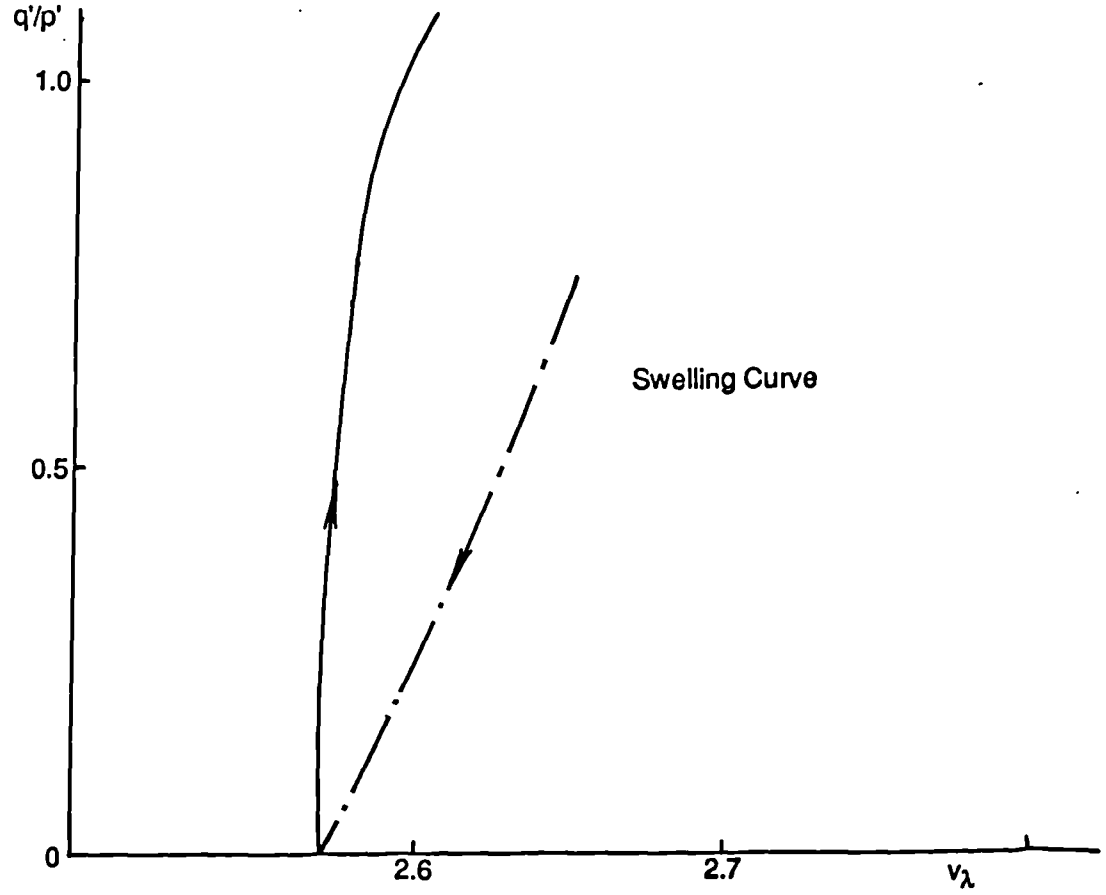

Fig 8.192 Plot of q' / p' against v_λ. Threshold tests to failure on London clay. η'_o = 0.75,OCR = 2.0, p' = 200kPa, constant p' paths.

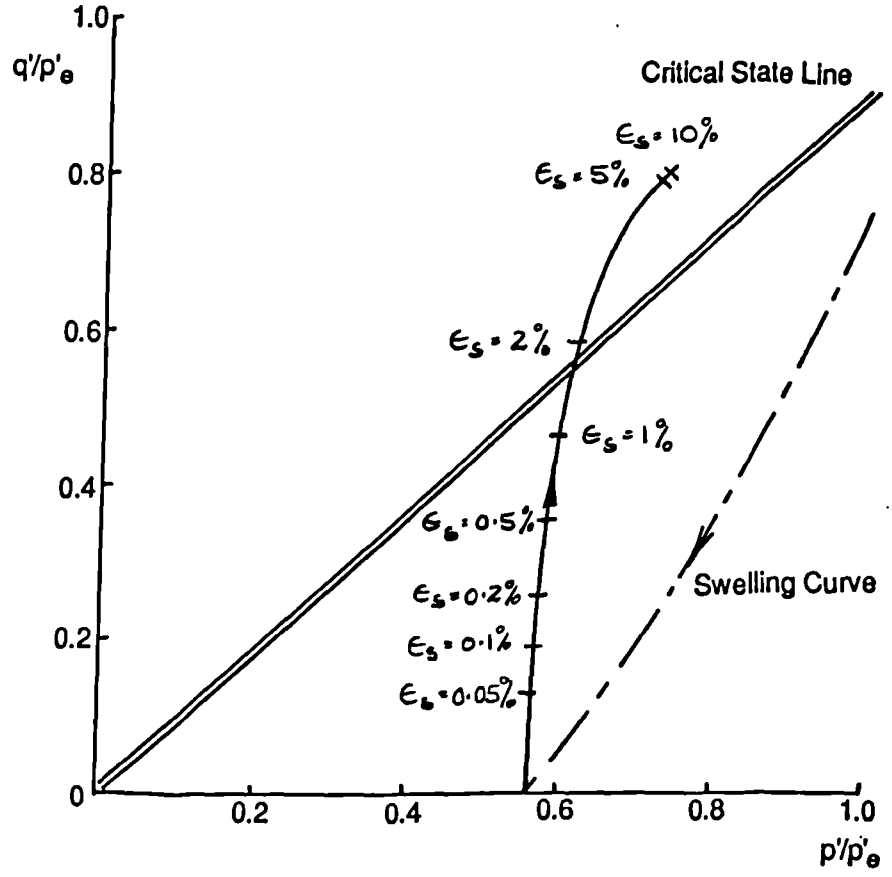

Fig 8.193 Plot of q' / p'_e against p' / p'_e. Threshold tests to failure. Isotropically compressed London clay. η'_o = 0.75, OCR = 2.0, p' = 200kPa,constant p' paths.

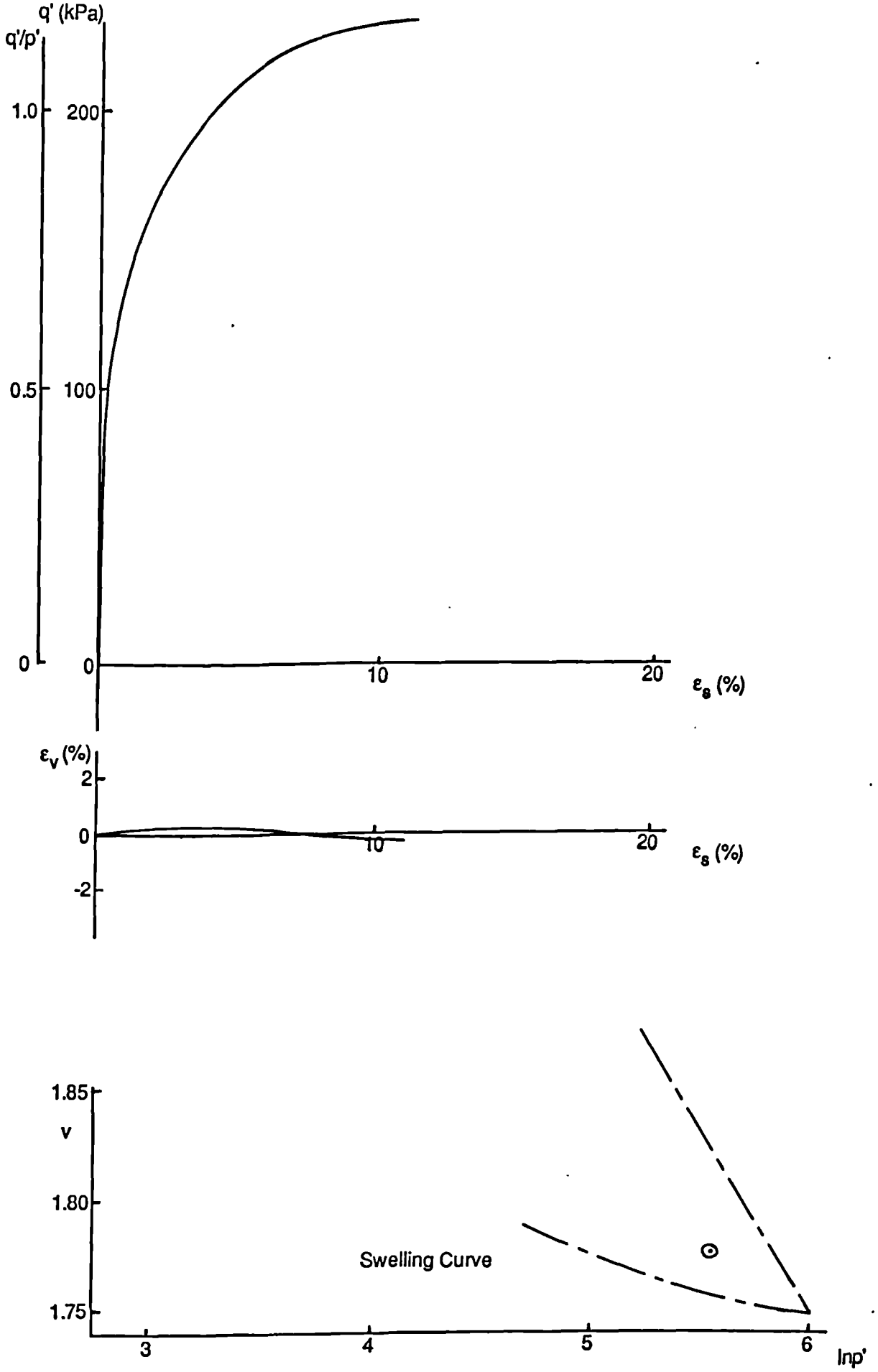

Fig 8.194 Plots of q' against ε_s ,q'/p' against ε_s , ε_v against ε_s and v against $\log_e p'$. Threshold tests to failure on London clay. Two dimensionally compressed, OCR = 2.0, p' =200kPa, constant p' paths .

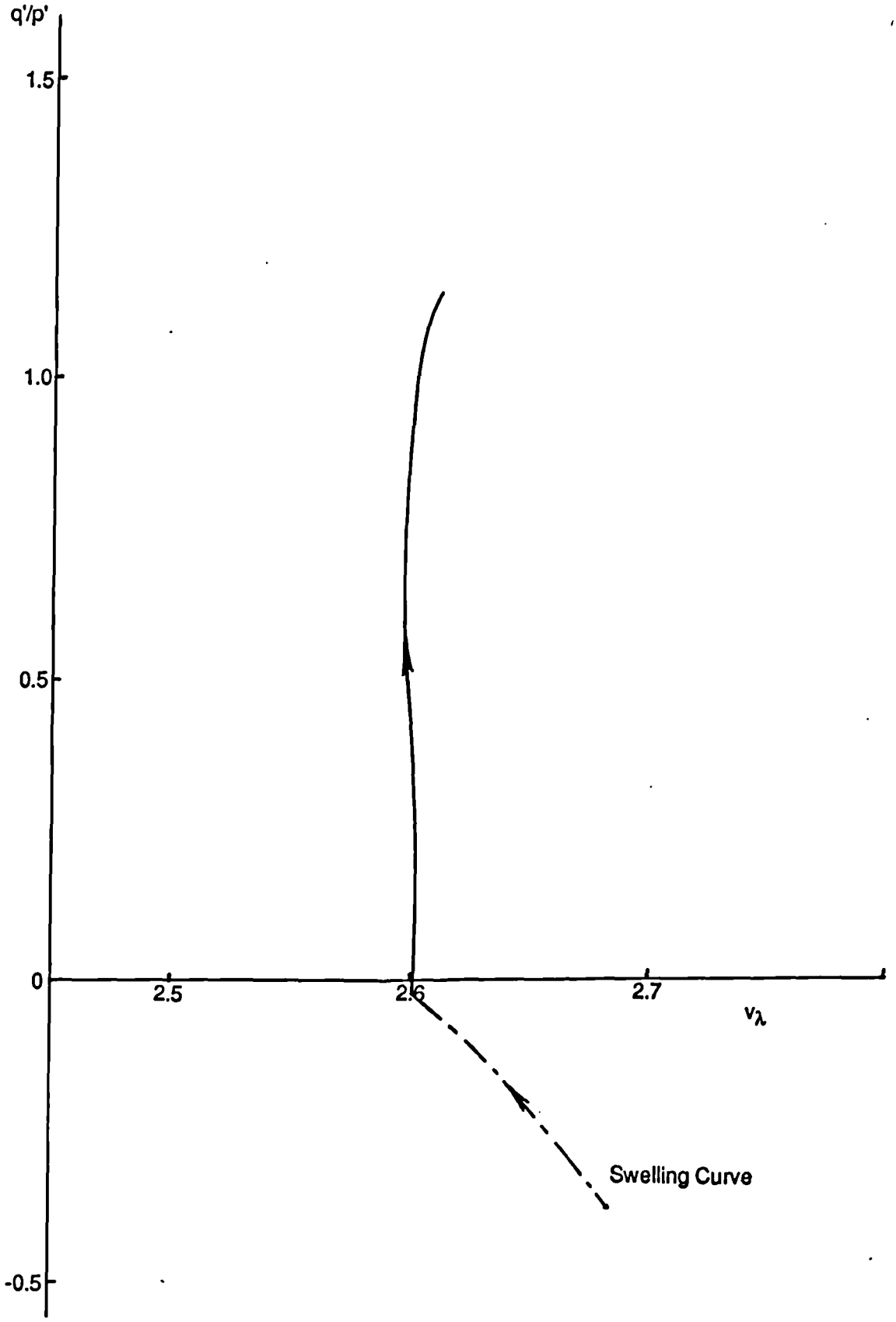

Fig 8.195 Plot of q' / p' against v_λ . Threshold tests to failure on London clay. Two dimensionally compressed , OCR = 2.0, p' = 200kPa, constant p' paths.

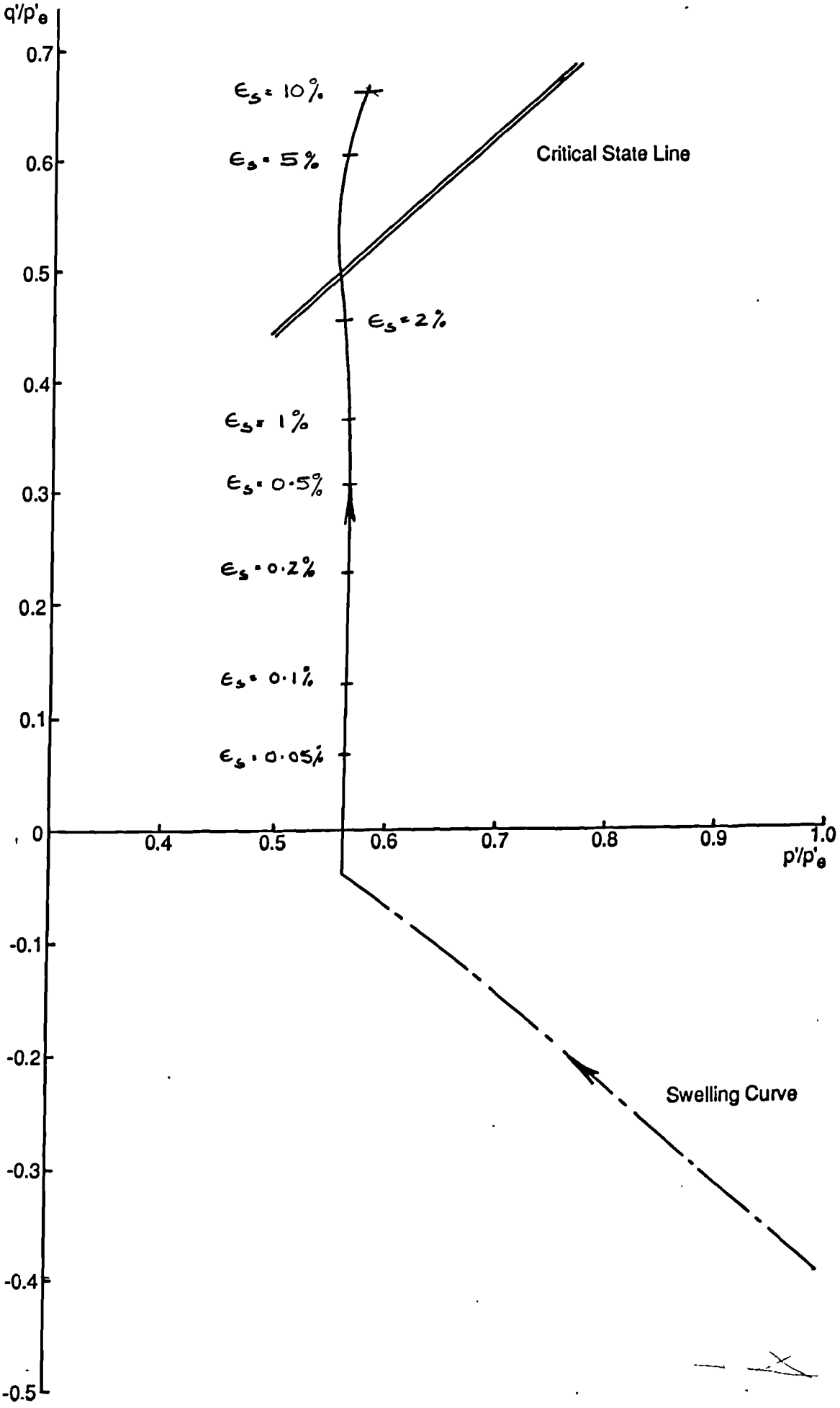

Fig 8.196 Plot of q' / p'_e against p' / p'_e . Threshold tests to failure. Isotropically compressed London clay. Two dimensionally compressed, OCR = 2.0, p' = 200kPa,constant p' paths.

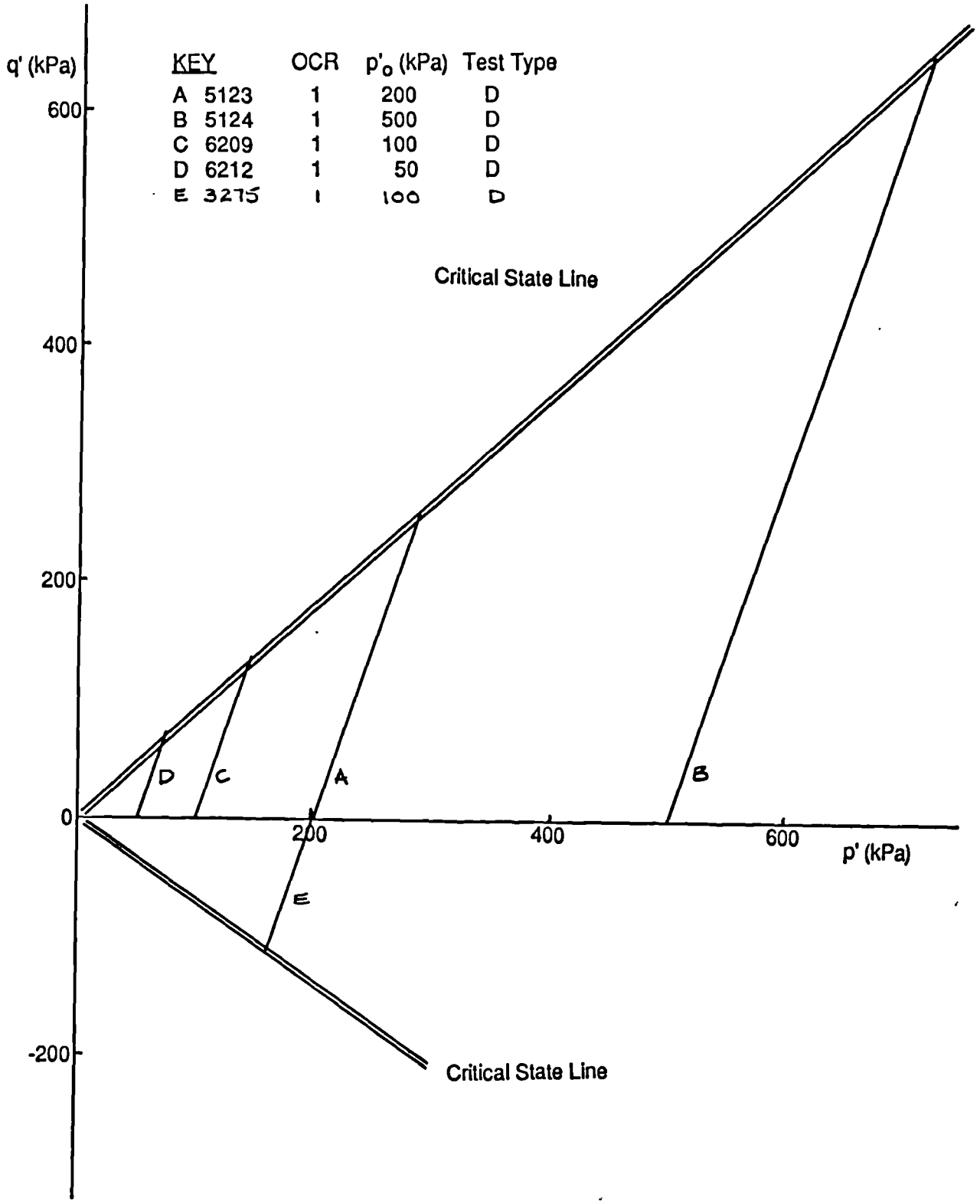

Fig 8.197a Plot of q' against p'. Drained stress paths to failure of normally consolidated London clay ($\eta'_o = 0$).

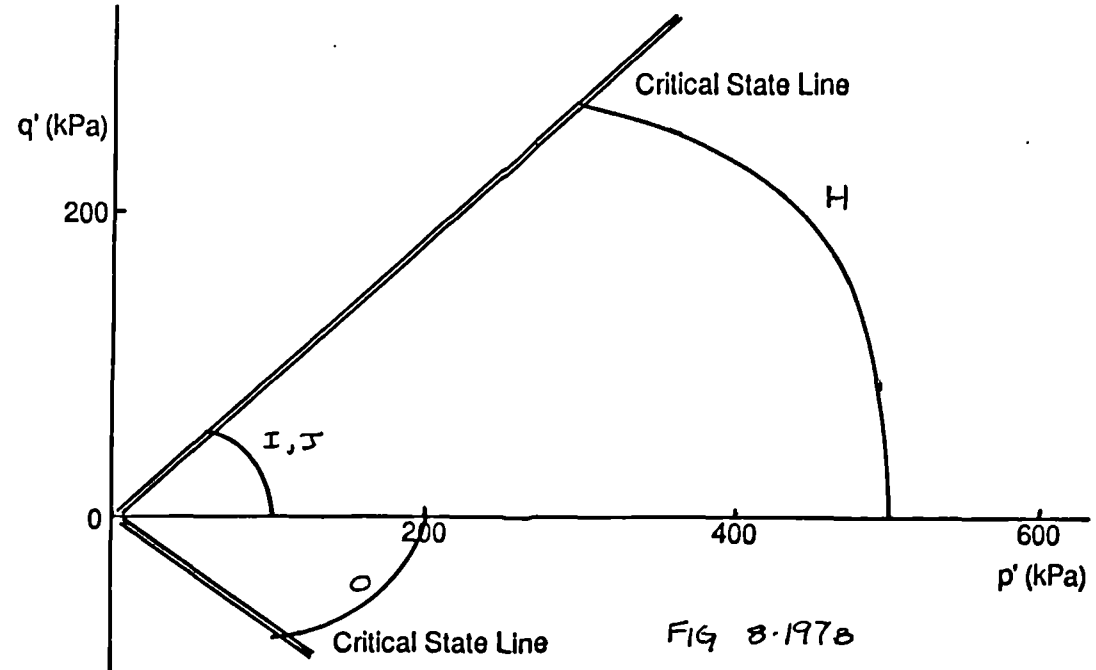

FIG 8.197b

KEY		OCR	p'_o (kPa)	Test Type
A	3302	40	15	U.D.
B	1210	20	30	U.D.
C	6214	20	30	U.D.
D	3301	10	60	U.D.
E	6220(c)	5	120	U.D.
F	6216(s)	5	120	U.D.
G	6210	2	300	U.D.
H	5125	1	500	U.D.
I	5127	1	100	U.D.
J	6218	1	100	U.D.
K	5134	8	50	$\delta p'=0$
L	5126	4	100	$\delta p'=0$
M	6208	2	200	$\delta p'=0$
N	6211	1.5	267	$\delta p'=0$
O	3211	1	200	U.D.

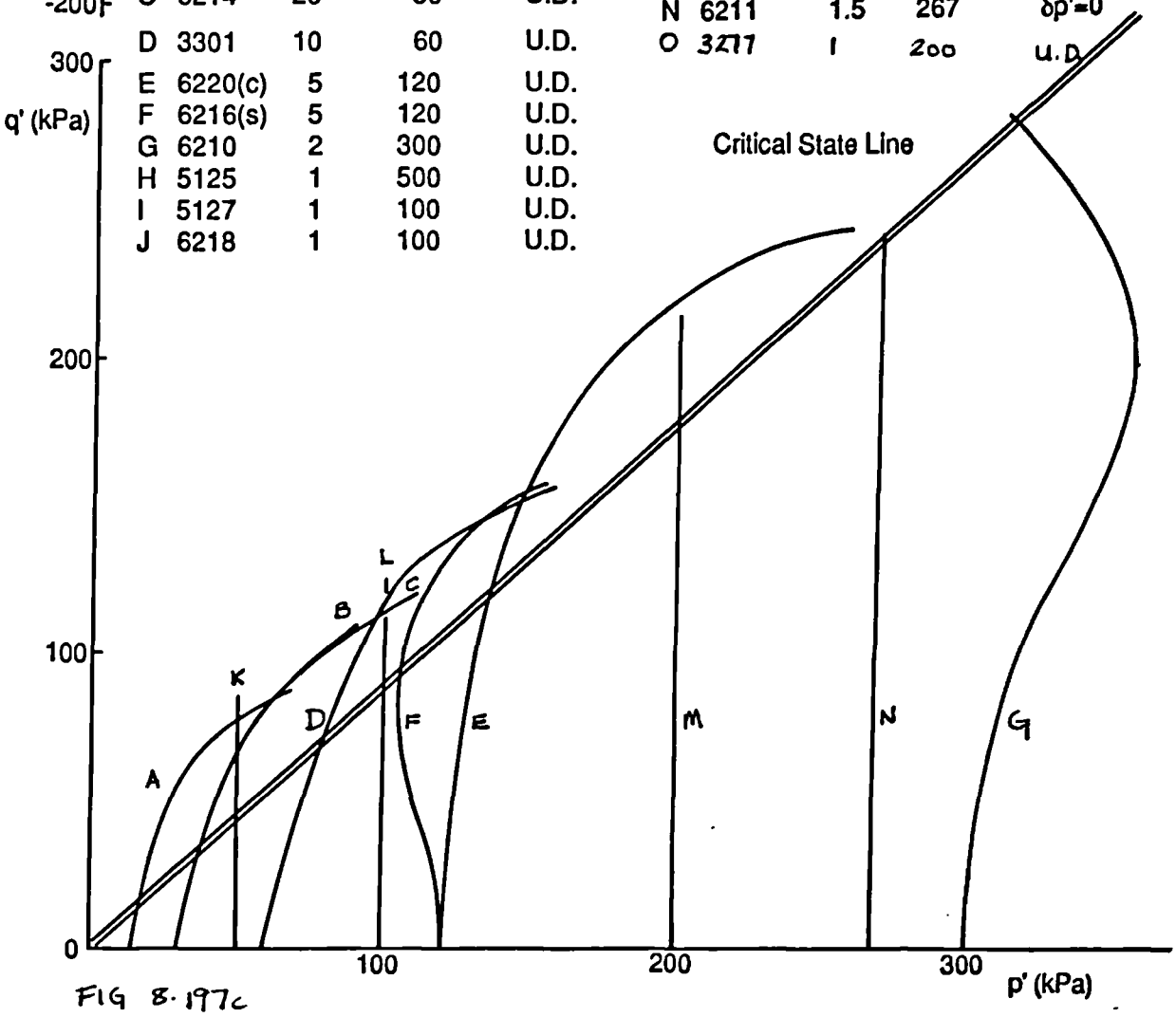

FIG 8.197c

Fig 8.197b Plot of q' against p'. Undrained stress paths to failure of normally consolidated London clay ($\eta'_o = 0$).

Fig 8.197c Plot of q' against p'. Undrained stress paths to failure of overconsolidated London clay ($\eta'_o = 0$).

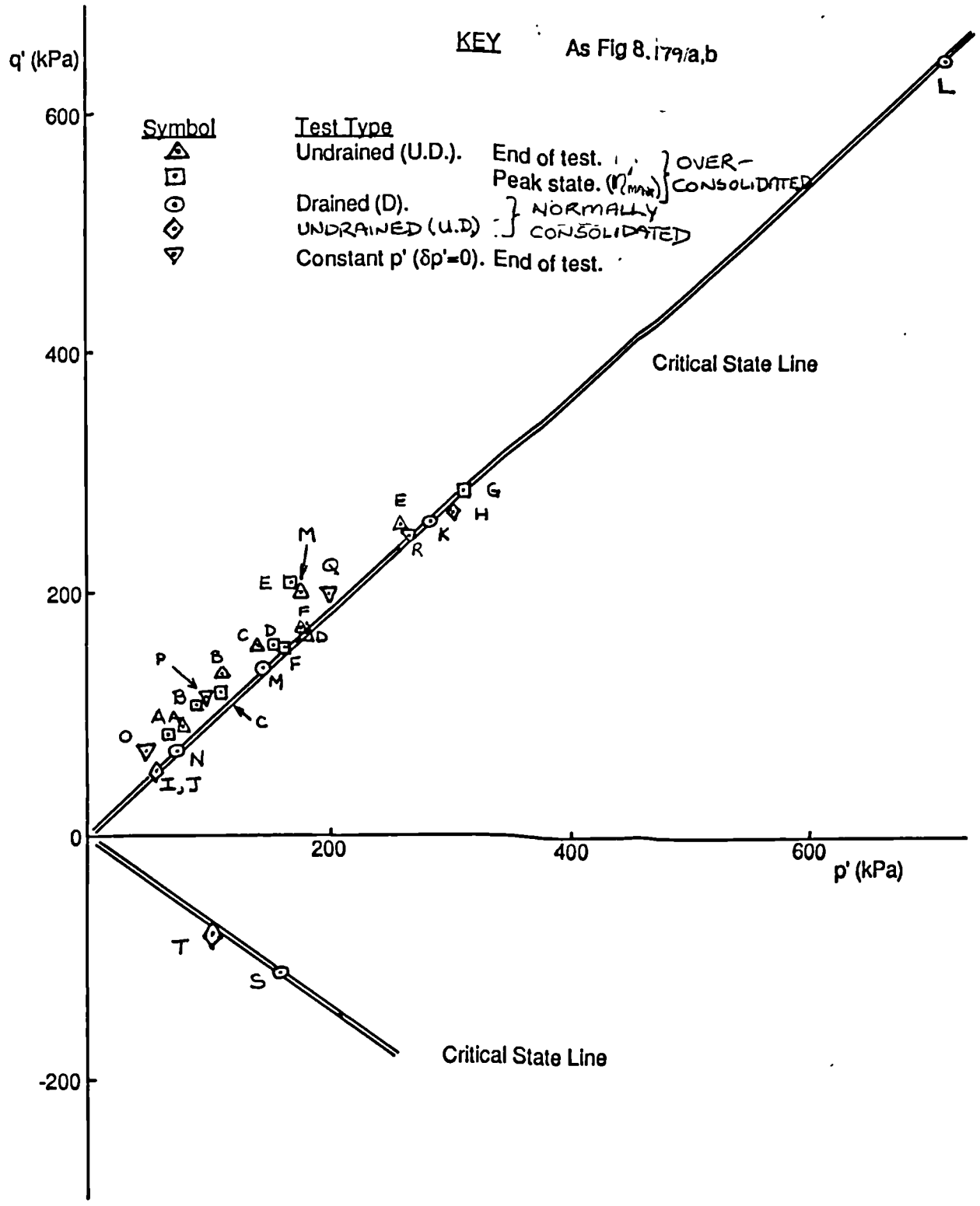

Fig 8.197d Plot of q' against p' for states at failure . Normally and overconsolidated London clay ($\eta'_o = 0$).

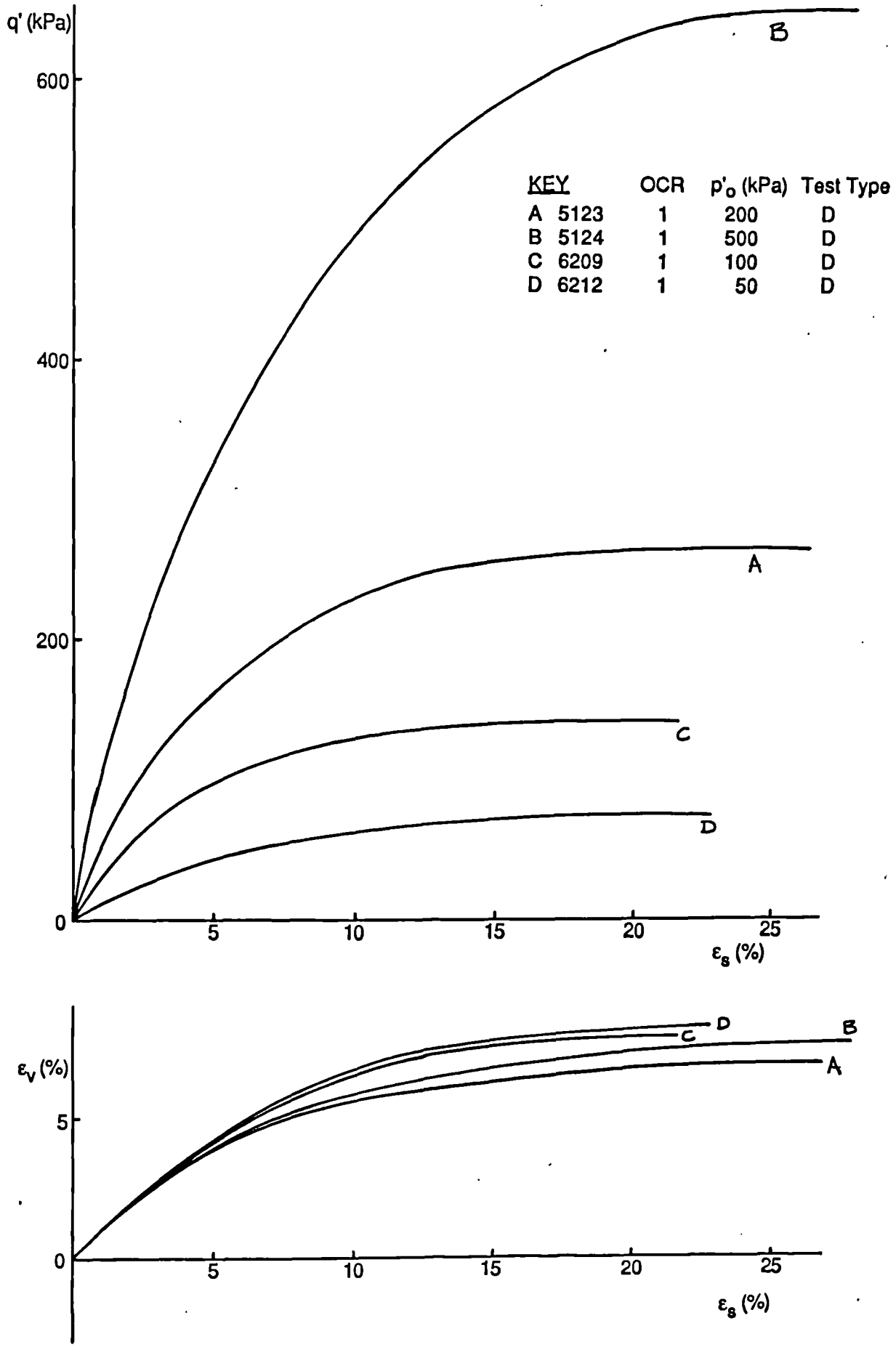

Fig 8.198 Plots of q' against ε_s and ε_v against ε_s for drained normally consolidated tests to failure on London clay ($\eta'_o = 0$).

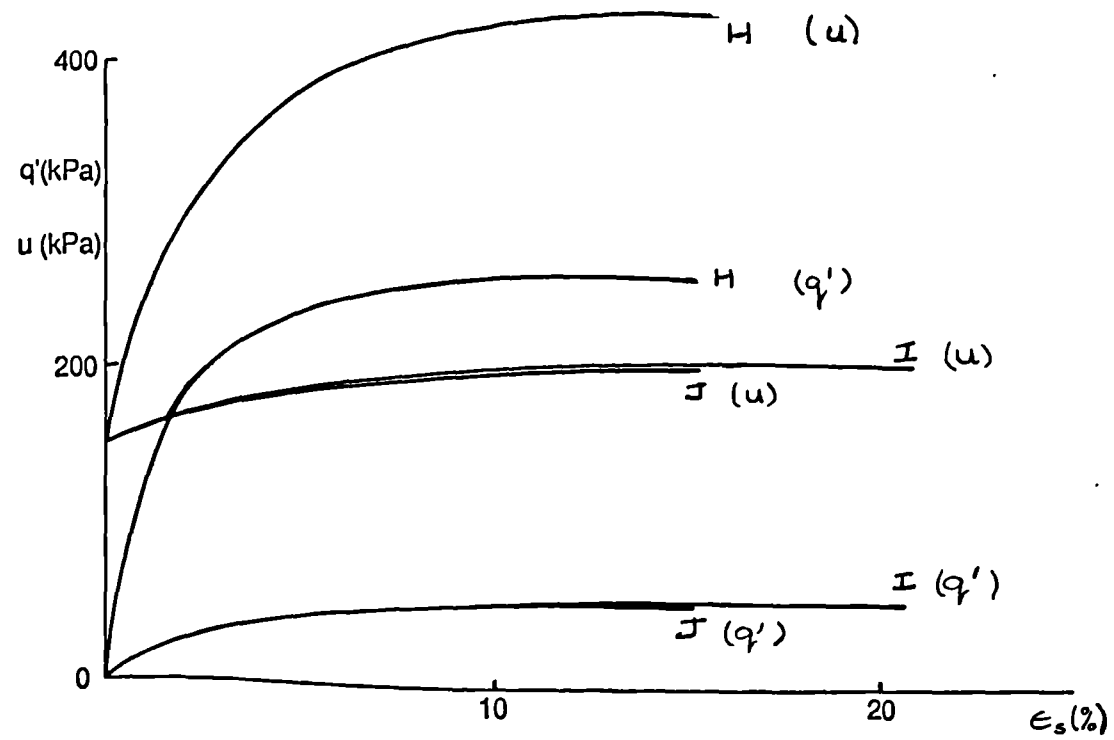

FIG 8·199a

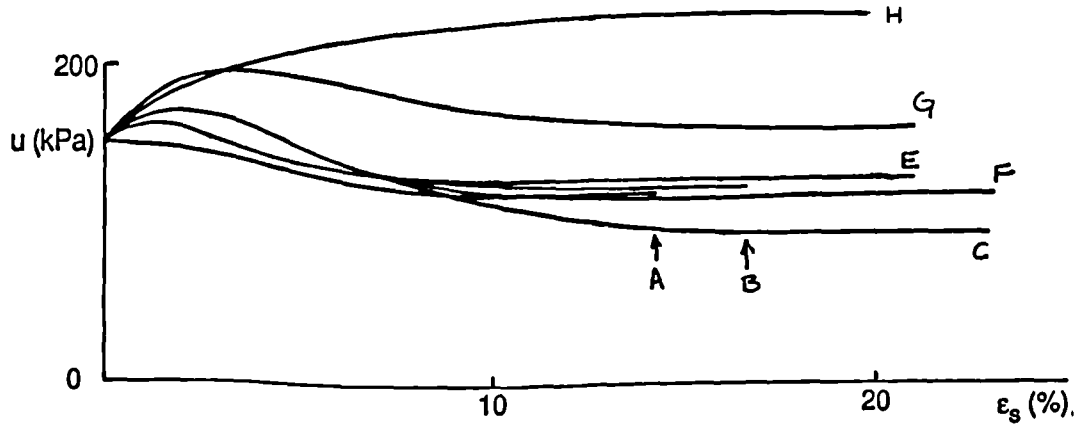

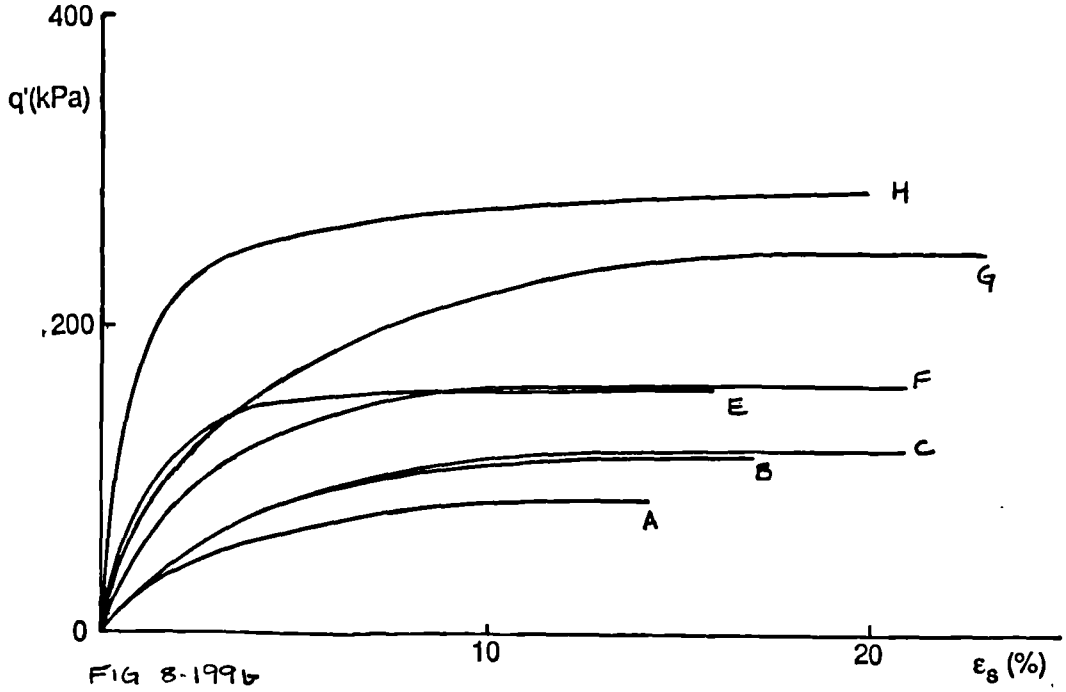

FIG 8·199b

Fig 8.199 Plots of q' against ε_s and u against ε_s for undrained tests to failure on London clay ($\eta'_o = 0$).

a) Normally consolidated.
b) Overconsolidated.

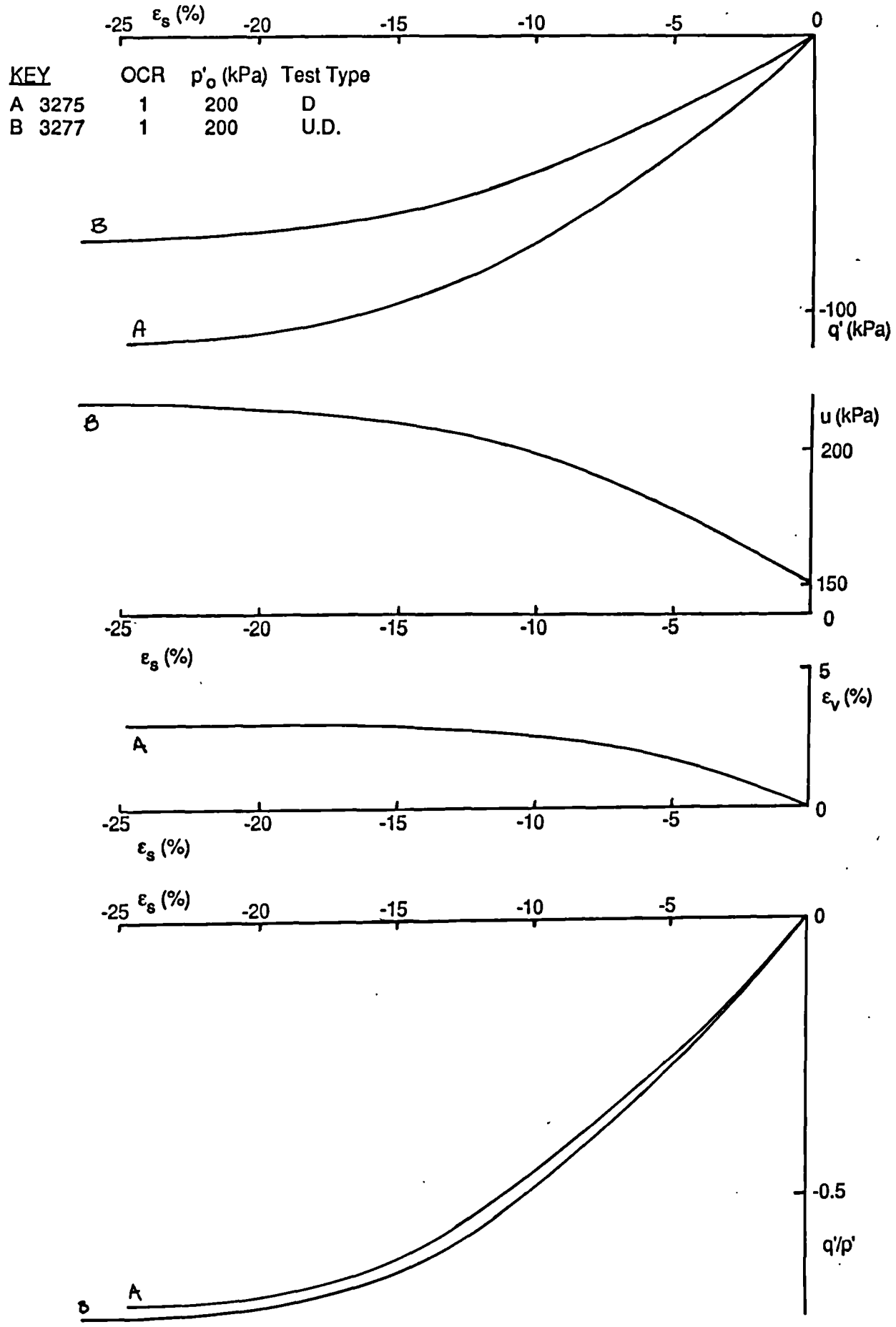

Fig 8.200 Results ofof extension tests to failure on isotropically compressed London clay drained and undrained plotted as q' against ε_s, u against ε_s, ε_v against ε_s and q'/p' against ε_s.

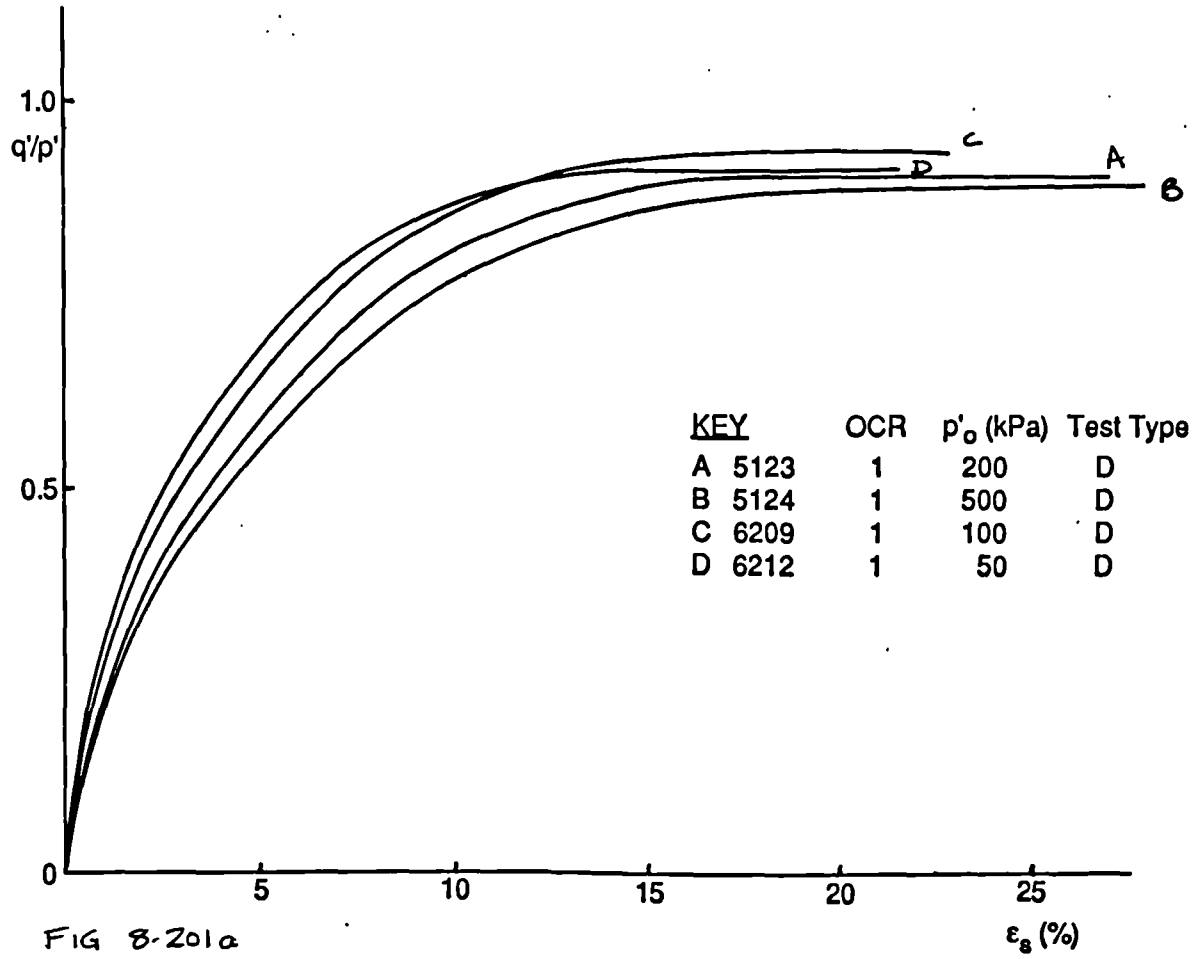

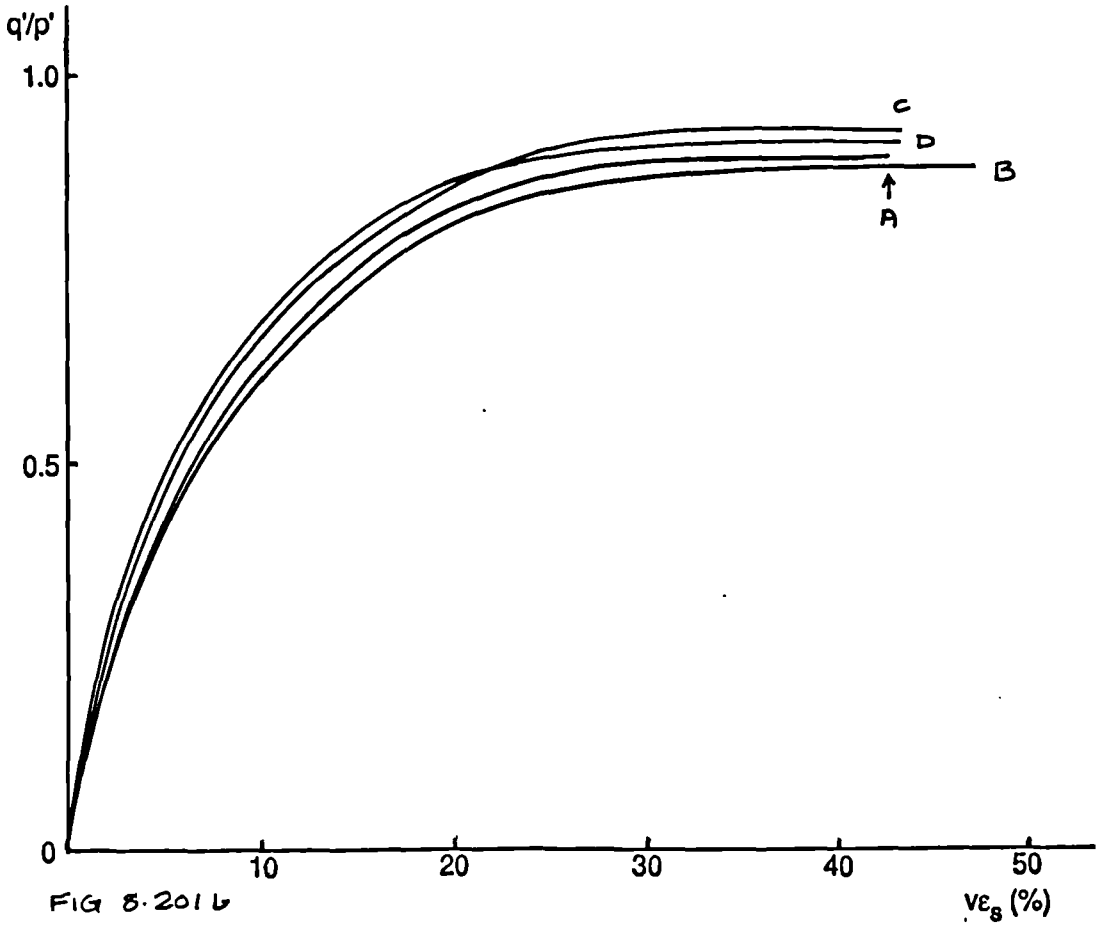

Fig 8.201 Drained tests to failure on normally consolidated London clay ($\eta'_o = 0$).

a) q' / p' against ε_s.

b) q' / p' against $v\varepsilon_s$.

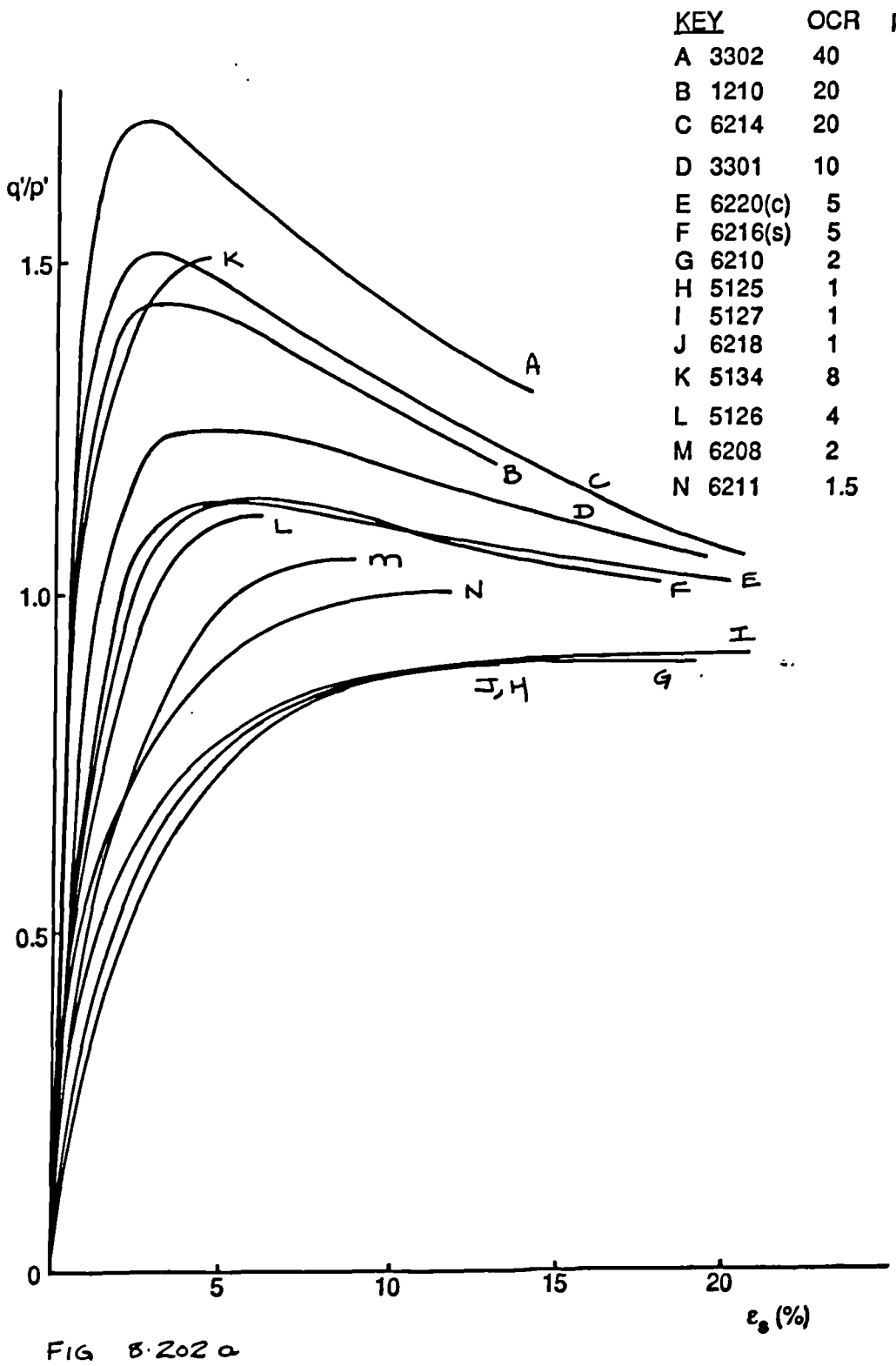

FIG 8.202a

Fig 8.202 Results of all tests to failure on London clay ($\eta'_o = 0$).

a) q' / p' against ε_s.

b) q' / p' against $v\varepsilon_s$.

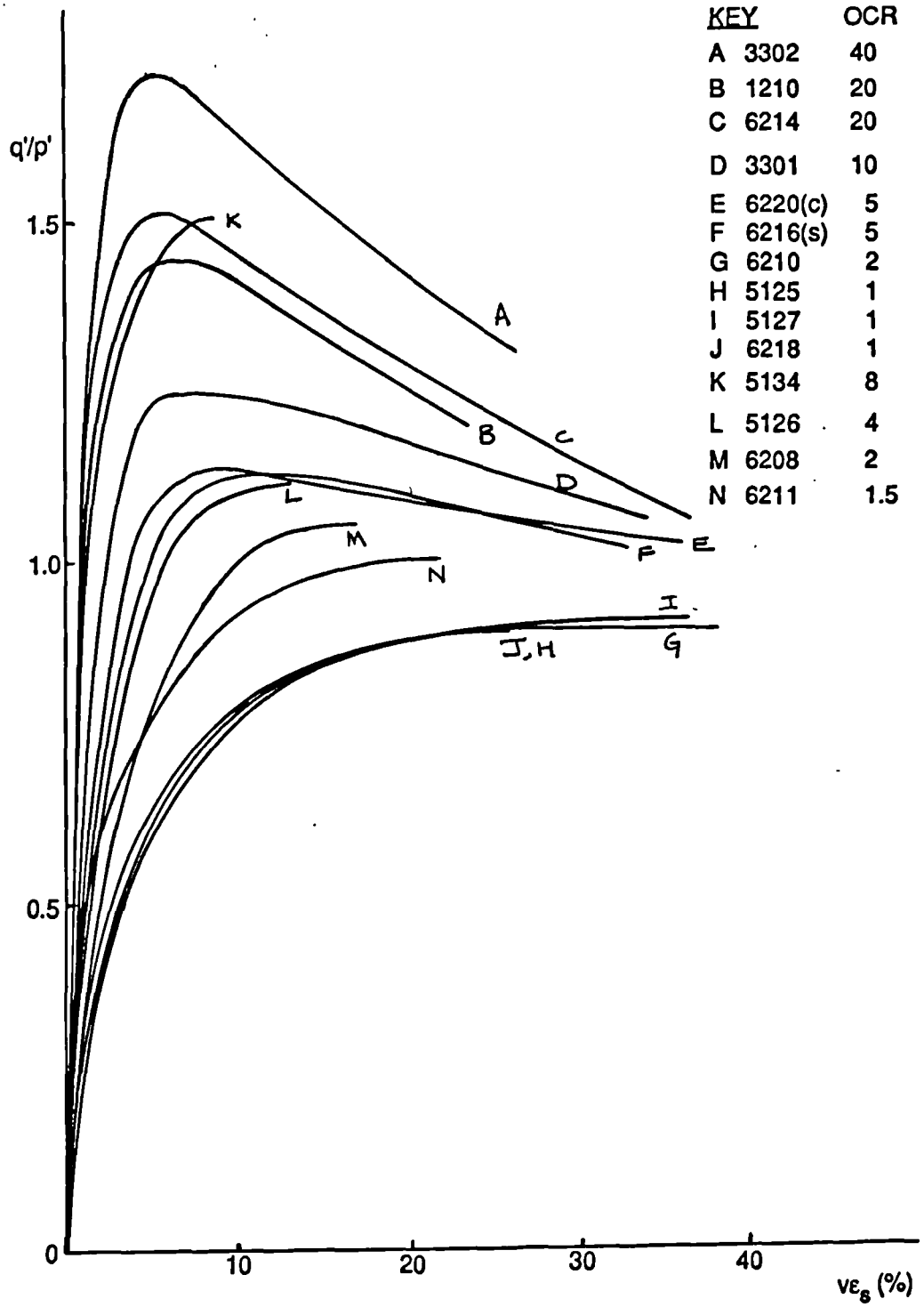

KEY	OCR	p'_o (kPa)	Test Type
A 3302	40	15	U.D.
B 1210	20	30	U.D.
C 6214	20	30	U.D.
D 3301	10	60	U.D.
E 6220(c)	5	120	U.D.
F 6216(s)	5	120	U.D.
G 6210	2	300	U.D.
H 5125	1	500	U.D.
I 5127	1	100	U.D.
J 6218	1	100	U.D.
K 5134	8	50	$\delta p'=0$
L 5126	4	100	$\delta p'=0$
M 6208	2	200	$\delta p'=0$
N 6211	1.5	267	$\delta p'=0$

FIG 8.202b

Title as page 566

KEY	OCR	p'_o (kPa)	Test Type
A 3302	40	15	U.D.
B 1210	20	30	U.D.
C 6214	20	30	U.D.
D 3301	10	60	U.D.
E 6220(c)	5	120	U.D.
F 6216(s)	5	120	U.D.
G 6210	2	300	U.D.
H 5125	1	500	U.D.
I 5127	1	100	U.D.
J 6218	1	100	U.D.
K 5123	1	200	D
L 5124	1	500	D
M 6209	1	100	D
N 6212	1	50	D
O 5134	8	50	$\delta p'=0$
P 5126	4	100	$\delta p'=0$
Q 6208	2	200	$\delta p'=0$
R 6211	1.5	267	$\delta p'=0$
S 3275	1	200	D
T 3277	1	200	U.D.

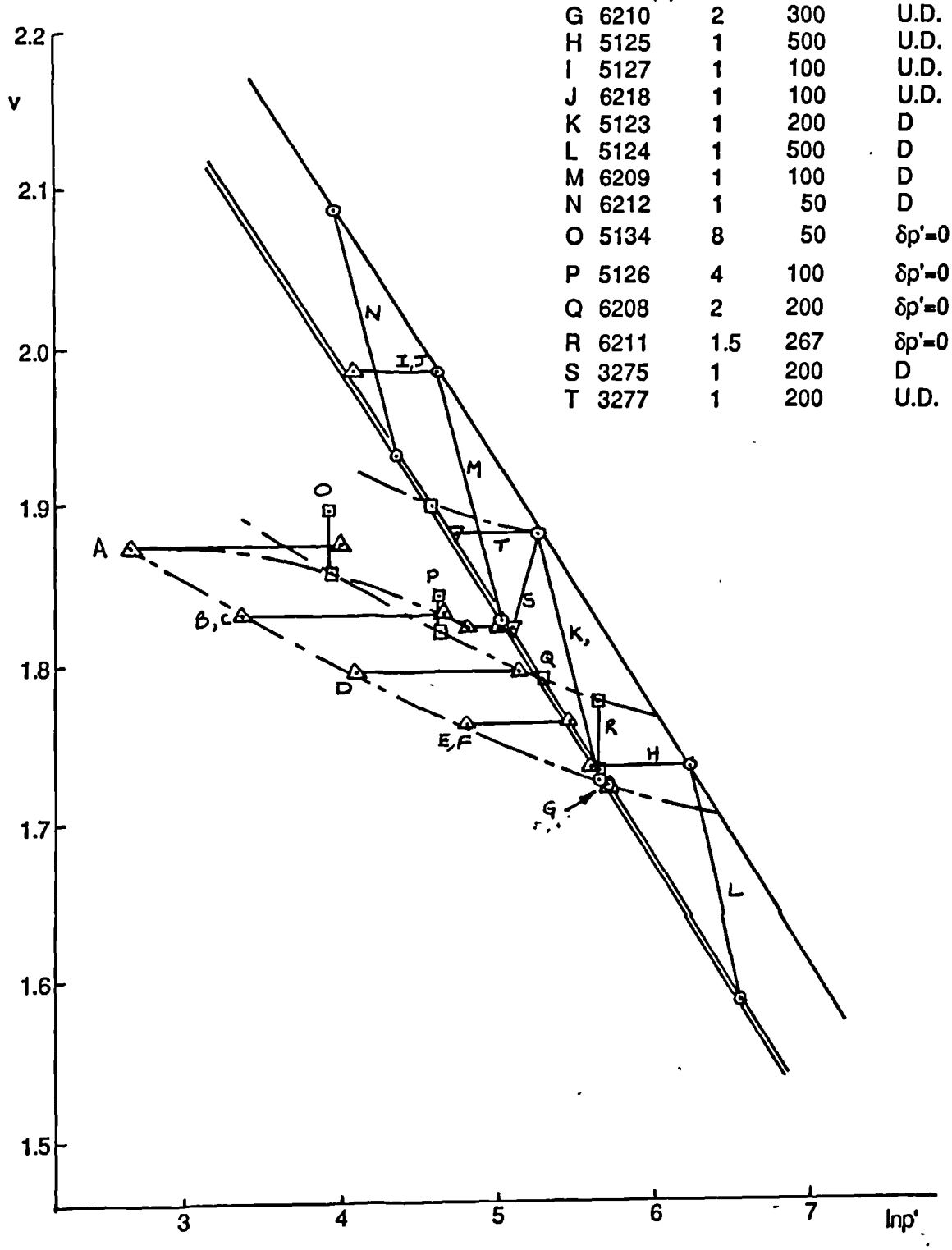

Fig 8.203 Plot of v against $\log_e p'$ all London clay tests to failure ($\eta'_o = 0$).

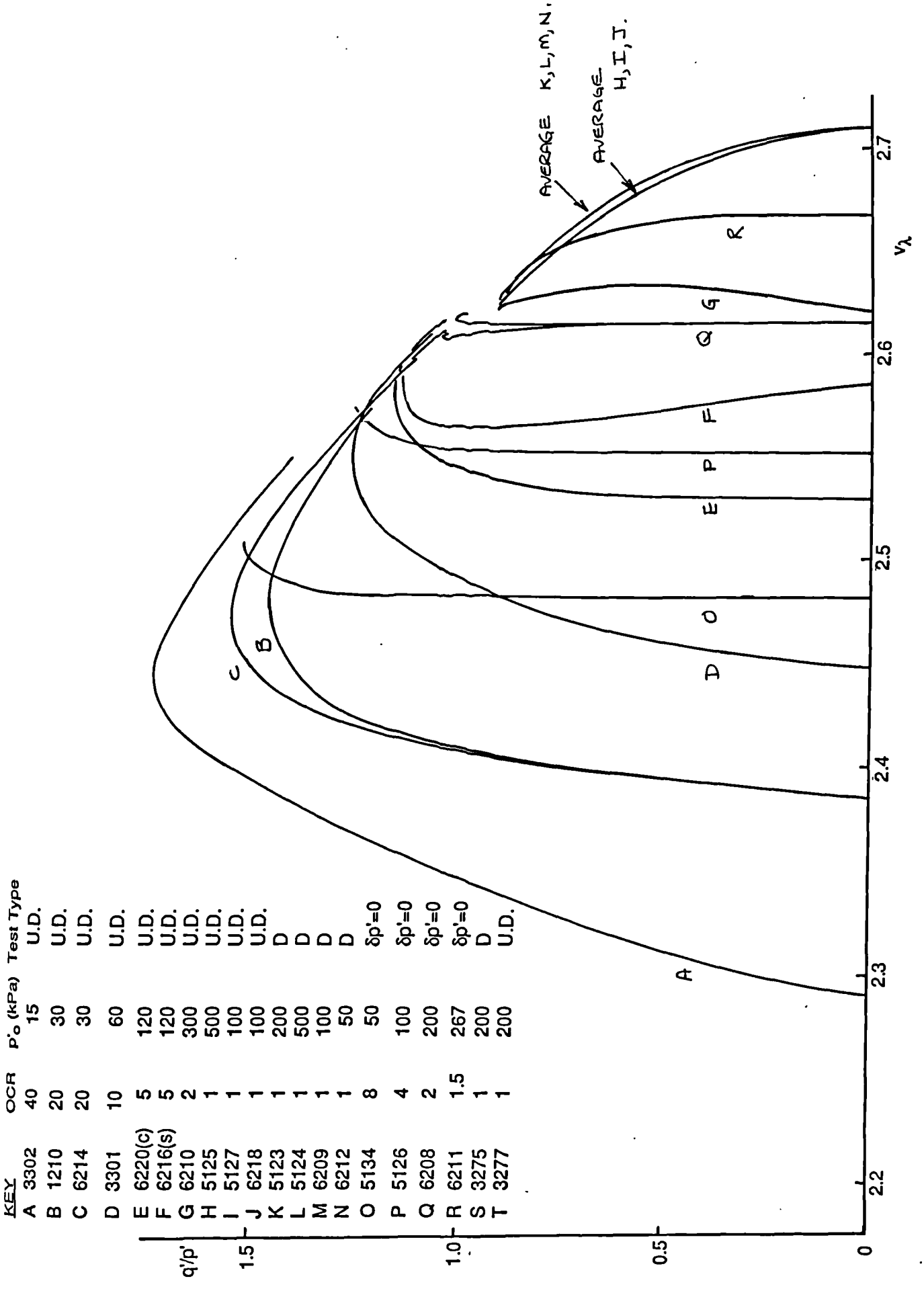

Fig 8.204 Plot of q' / p' against v_λ. For all compression tests to failure on London clay. ($\eta'_o = 0$).

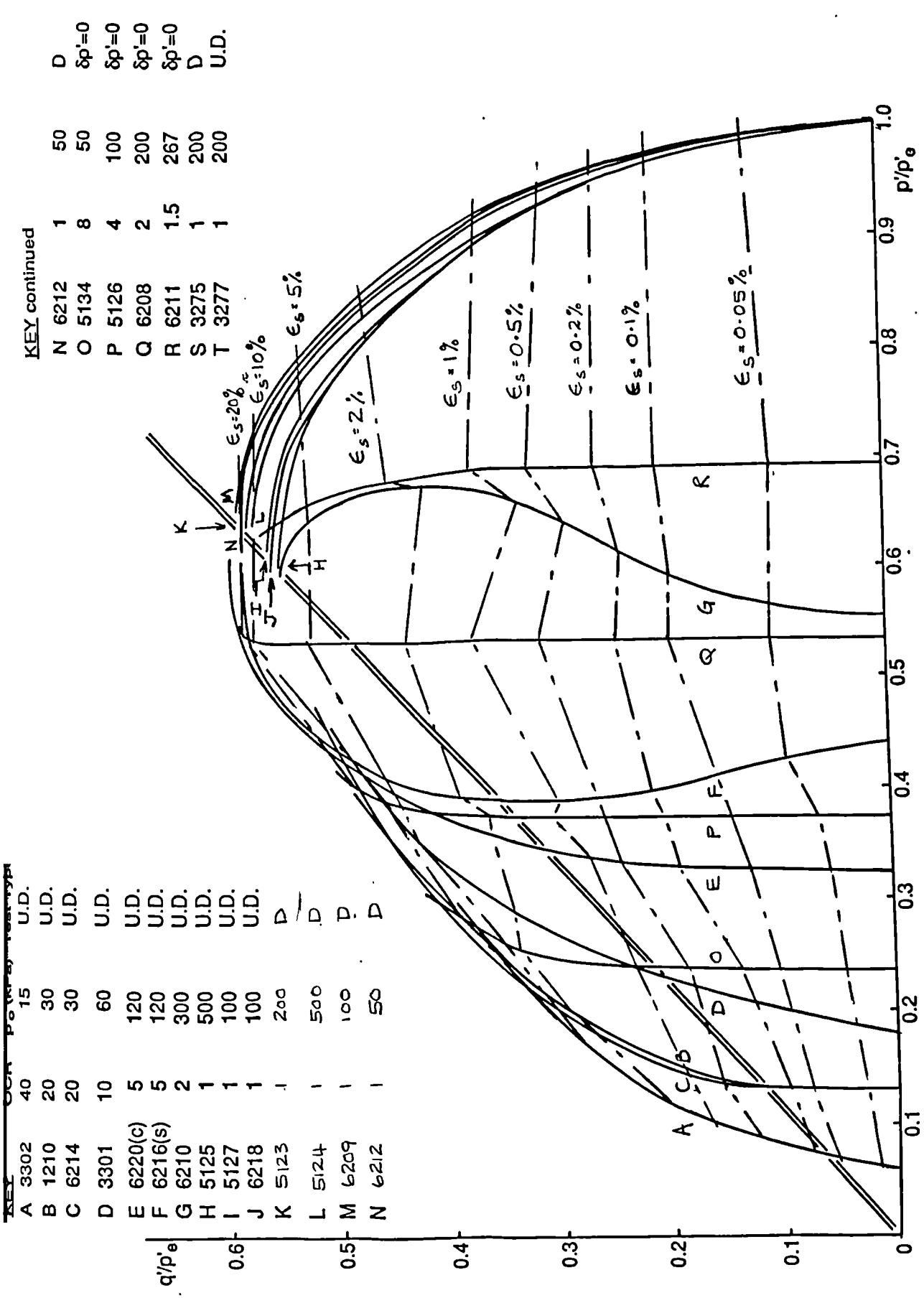

Fig 8.205 Plot of q' / p'_e against p' / p'_e .For all compression tests to failure on London clay. ($\eta'_o = 0$).

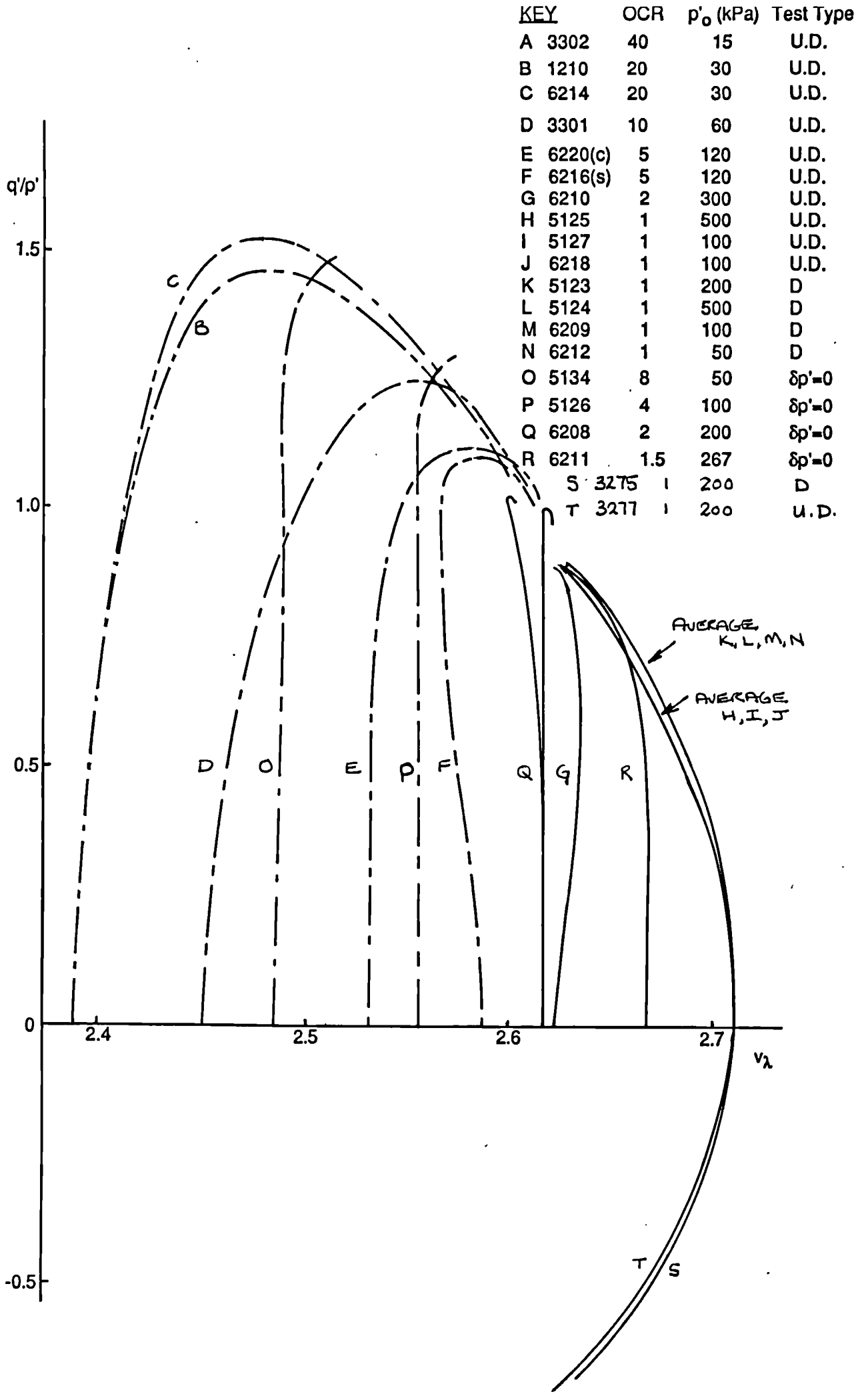

Fig 8.206 Plot of q' / p' against v_λ. For compression and extension tests to failure on London clay. ($\eta'_o = 0$).

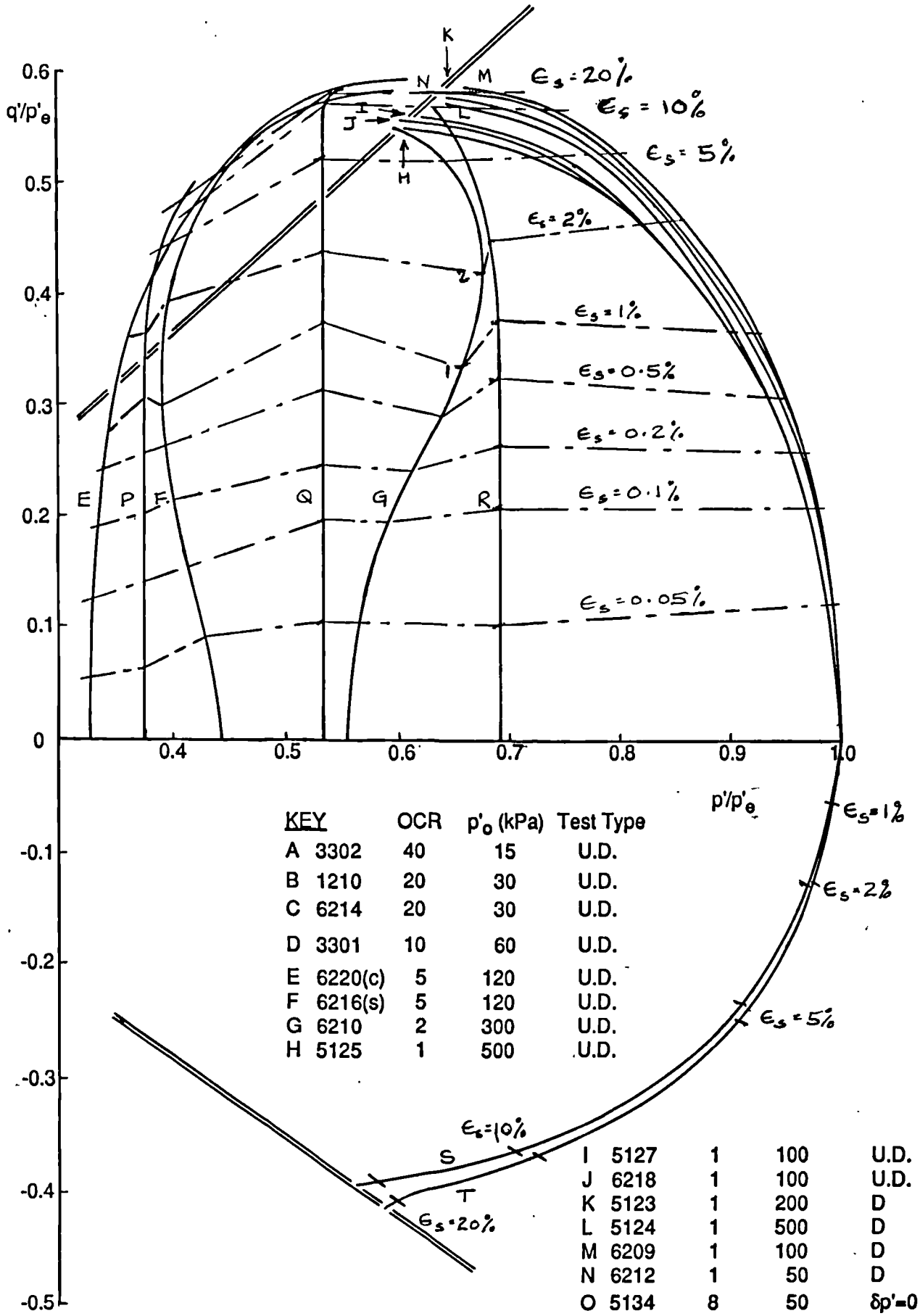

KEY	OCR	p'o (kPa)	Test Type
A 3302	40	15	U.D.
B 1210	20	30	U.D.
C 6214	20	30	U.D.
D 3301	10	60	U.D.
E 6220(c)	5	120	U.D.
F 6216(s)	5	120	U.D.
G 6210	2	300	U.D.
H 5125	1	500	U.D.
I 5127	1	100	U.D.
J 6218	1	100	U.D.
K 5123	1	200	D
L 5124	1	500	D
M 6209	1	100	D
N 6212	1	50	D
O 5134	8	50	δp'=0
P 5126	4	100	δp'=0
Q 6208	2	200	δp'=0
R 6211	1.5	267	δp'=0
S 3275	1	200	D
T 3277	1	200	U.D.

Fig 8.207 Plot of q' / p'e against p' / p'e .For compression and extension tests to failure on London clay. ($\eta'_o = 0$).

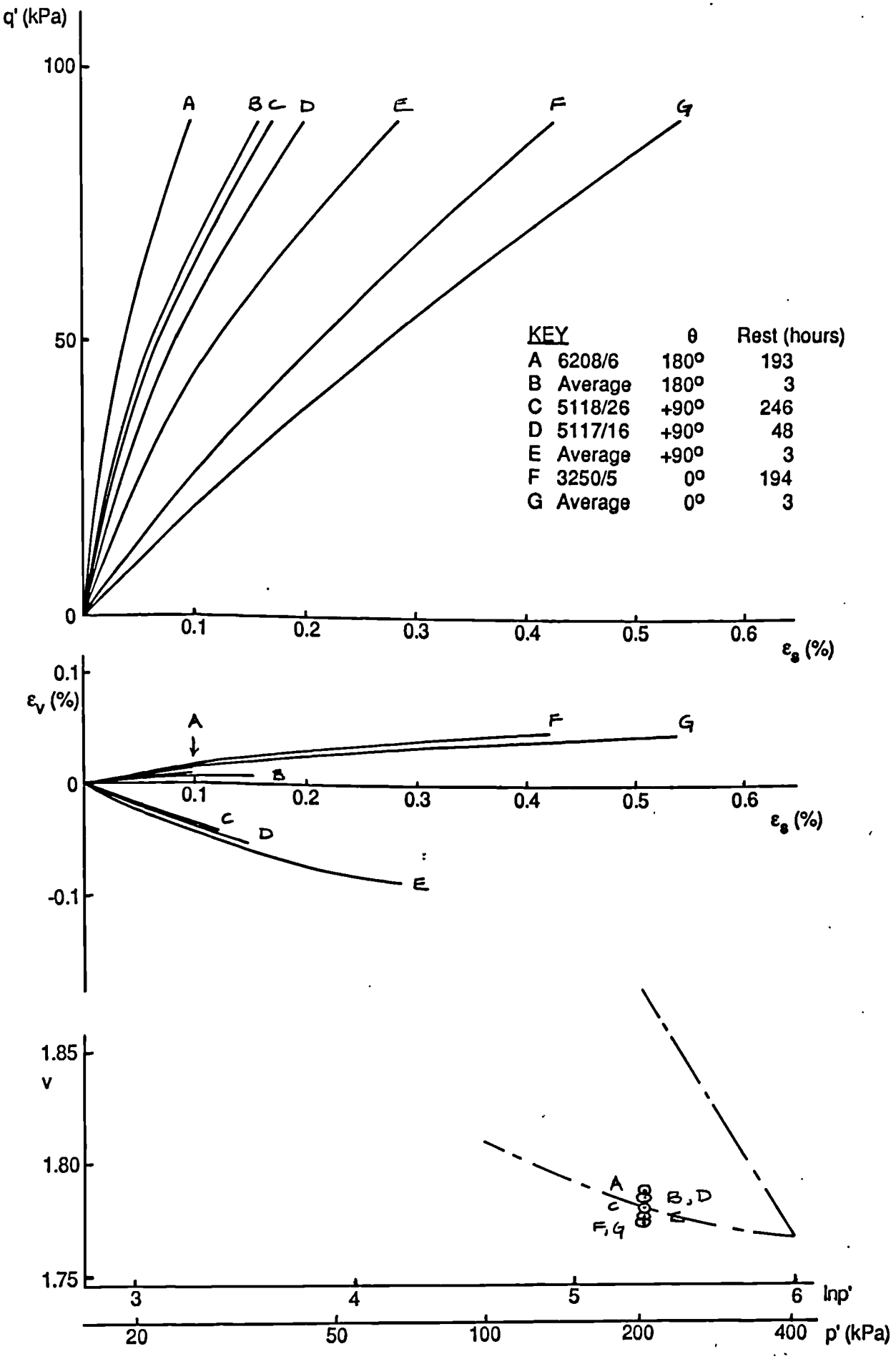

Fig 8.208 Plots of q' against ε_s, ε_v against ε_s and v against ln p'.The effect of varying the rest periods for isotropically compressed samples of London clay. OCR = 2.0, p' = 200kPa, constant p' paths.

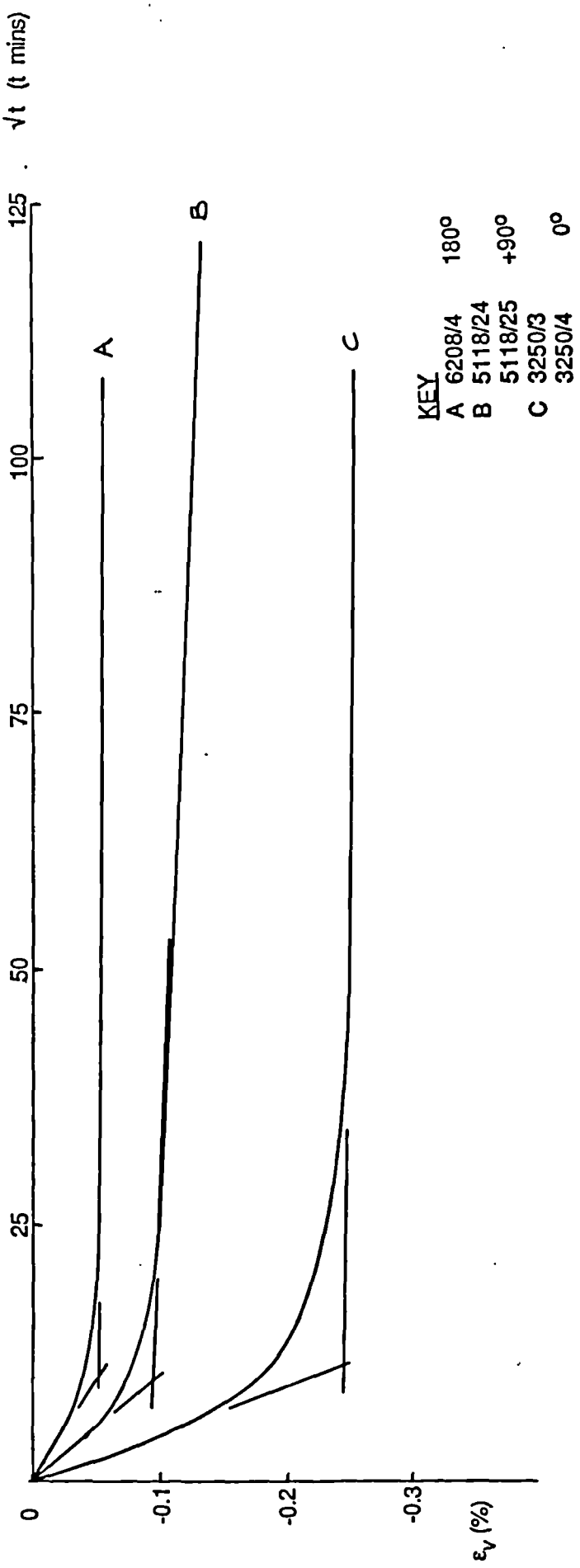

Fig 8.209 Plot of ε_v against square root of time elapsed, $\sqrt{t}$ for rest periods for London clay.

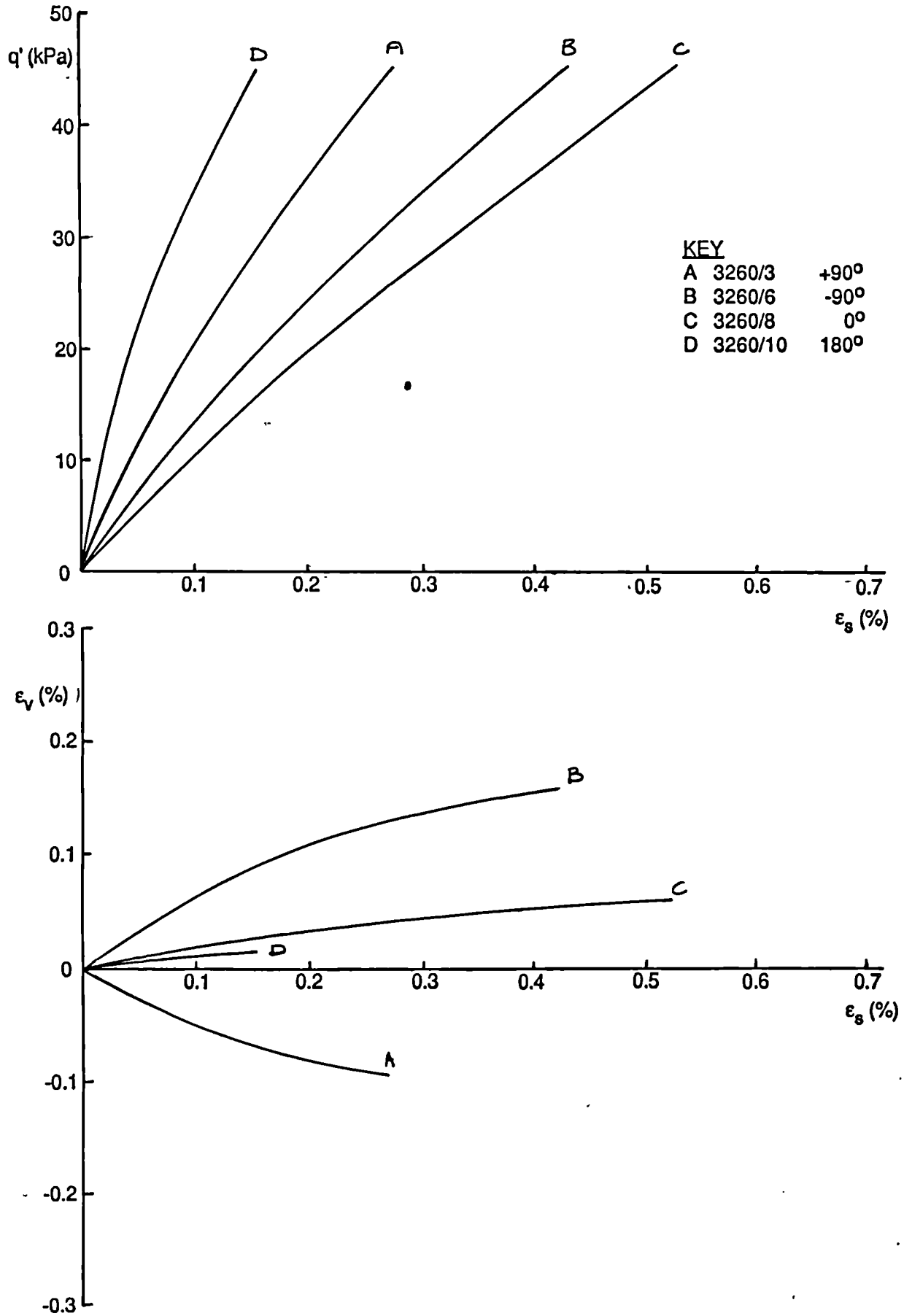

Fig 8.210 Plots of q' against ε_s and ε_v against ε_s for isotropically compressed samples of London clay. OCR = 2.0, p' = 100kPa, constant p' paths.

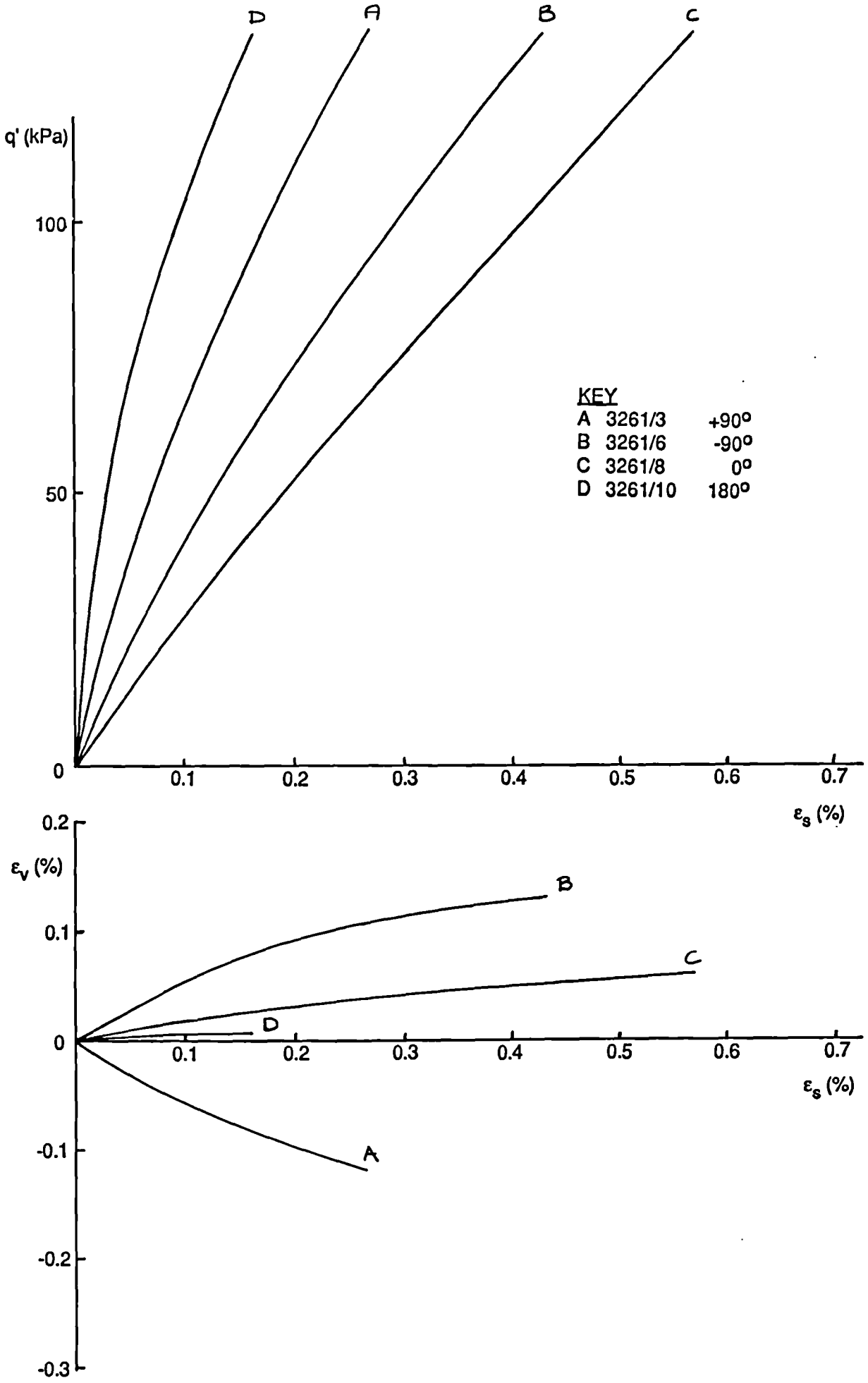

Fig 8.211 Plots of q' against ε_s and ε_v against ε_s for isotropically compressed samples of London clay. OCR = 2.0, p' = 300kPa, constant p' paths.

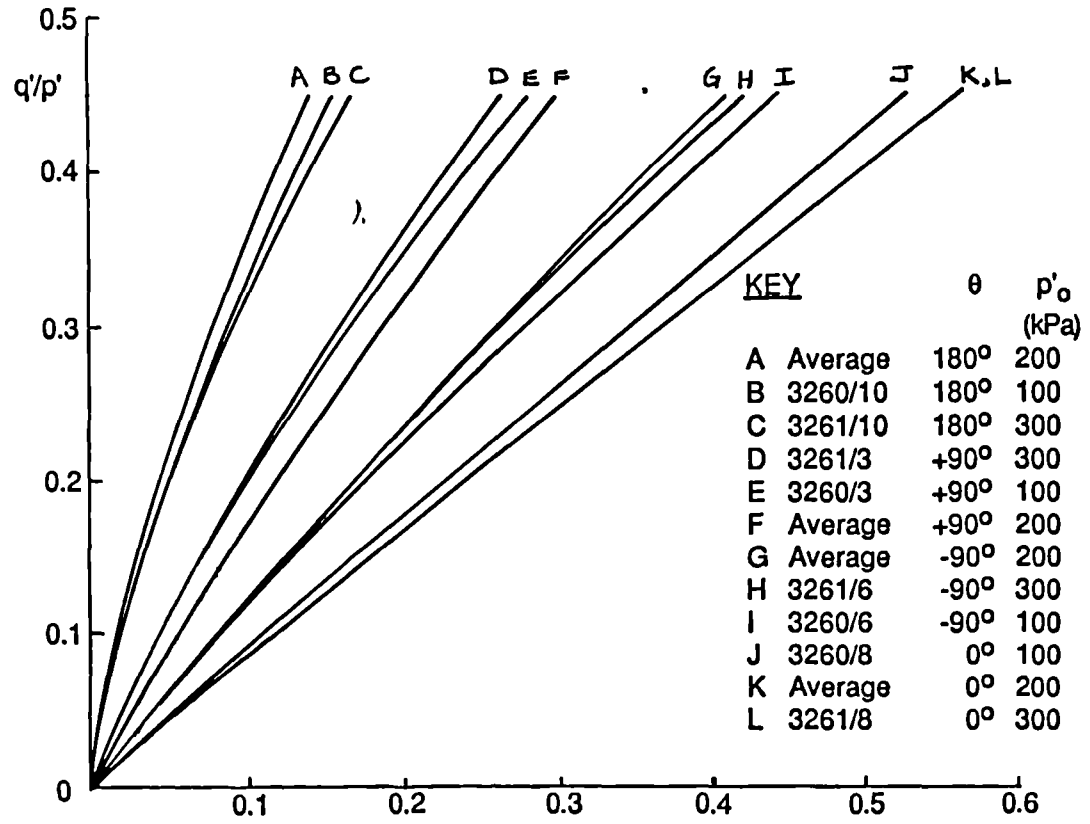

FIG 8·212 a.

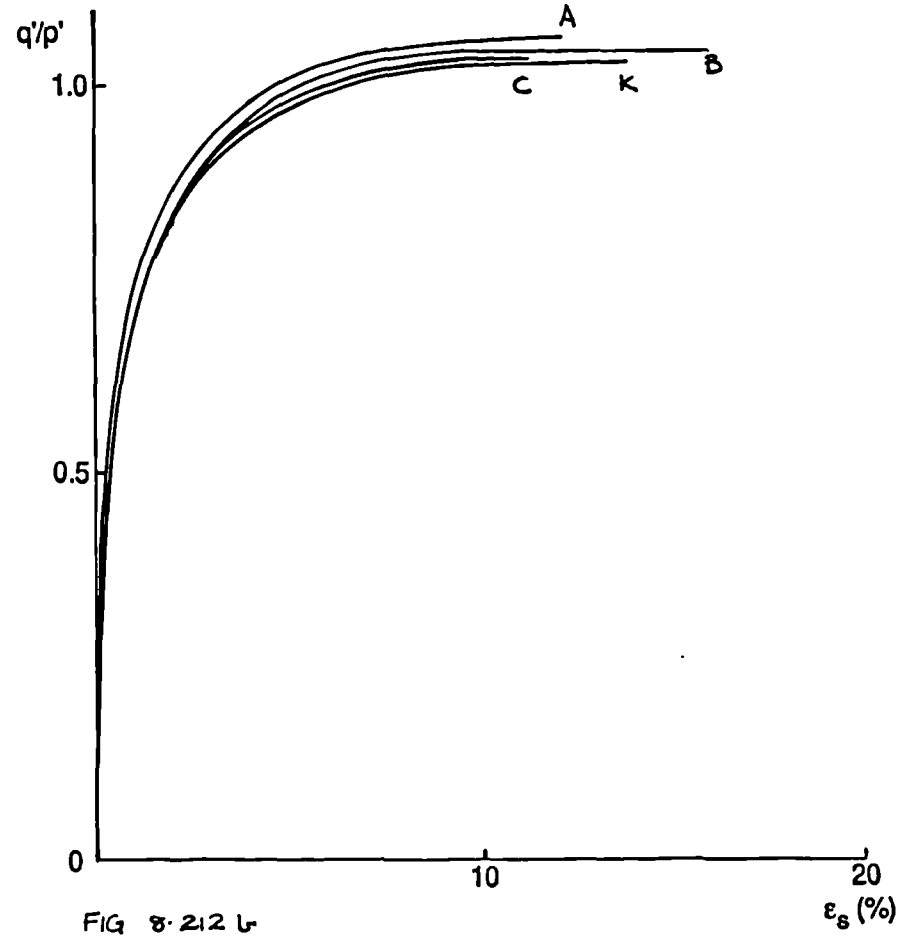

FIG 8·212 b

Fig 8.212 Plot of q' / p' against ε_s for isotropically compressed London clay. OCR = 2.0, various p', constant p' paths.

a) At low stress levels.
b) To failure.

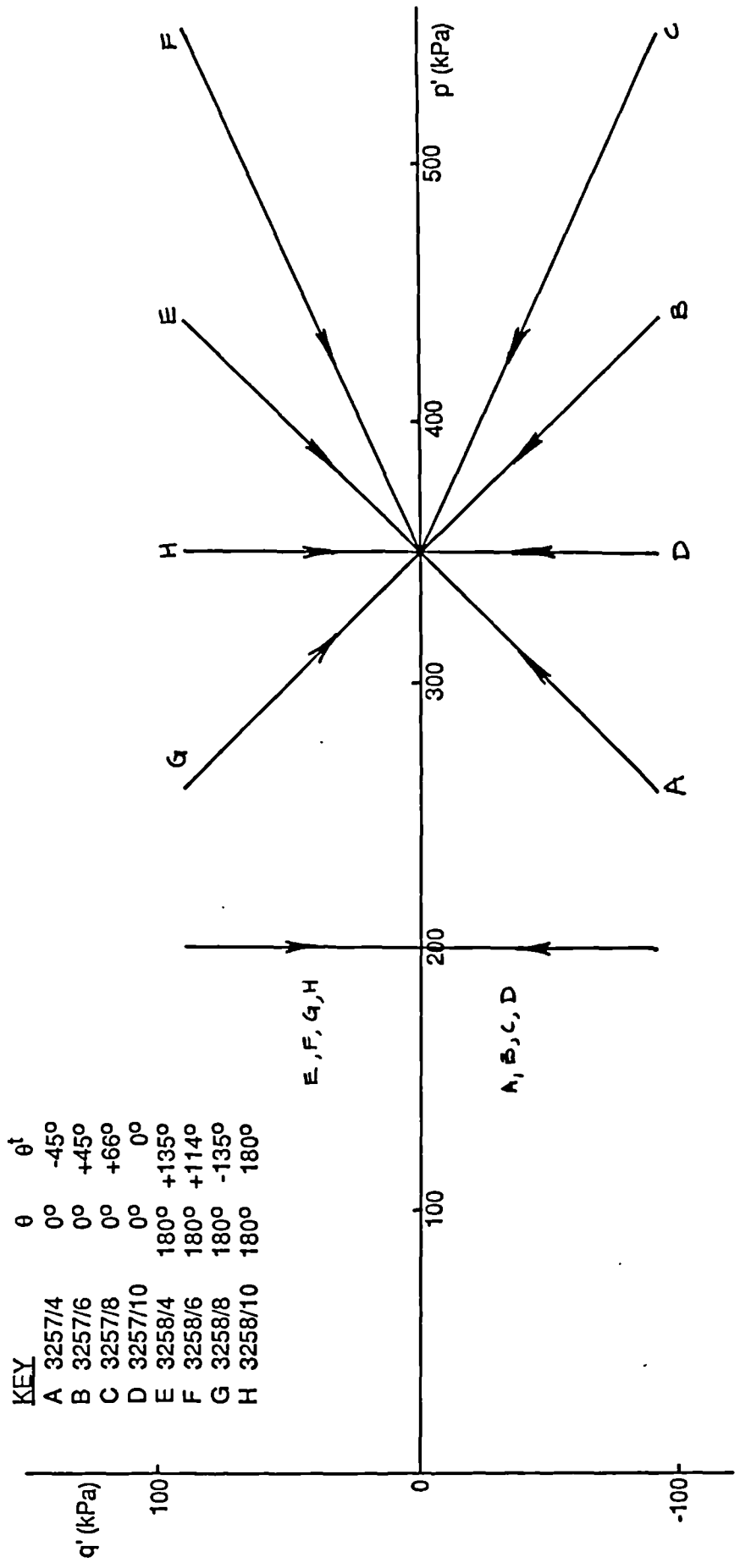

Fig 8.213 Total, q against p, and effective, q' against p', stress paths for London clay for total stress path threshold tests. $\eta'_o = 0$, OCR = 2.0.

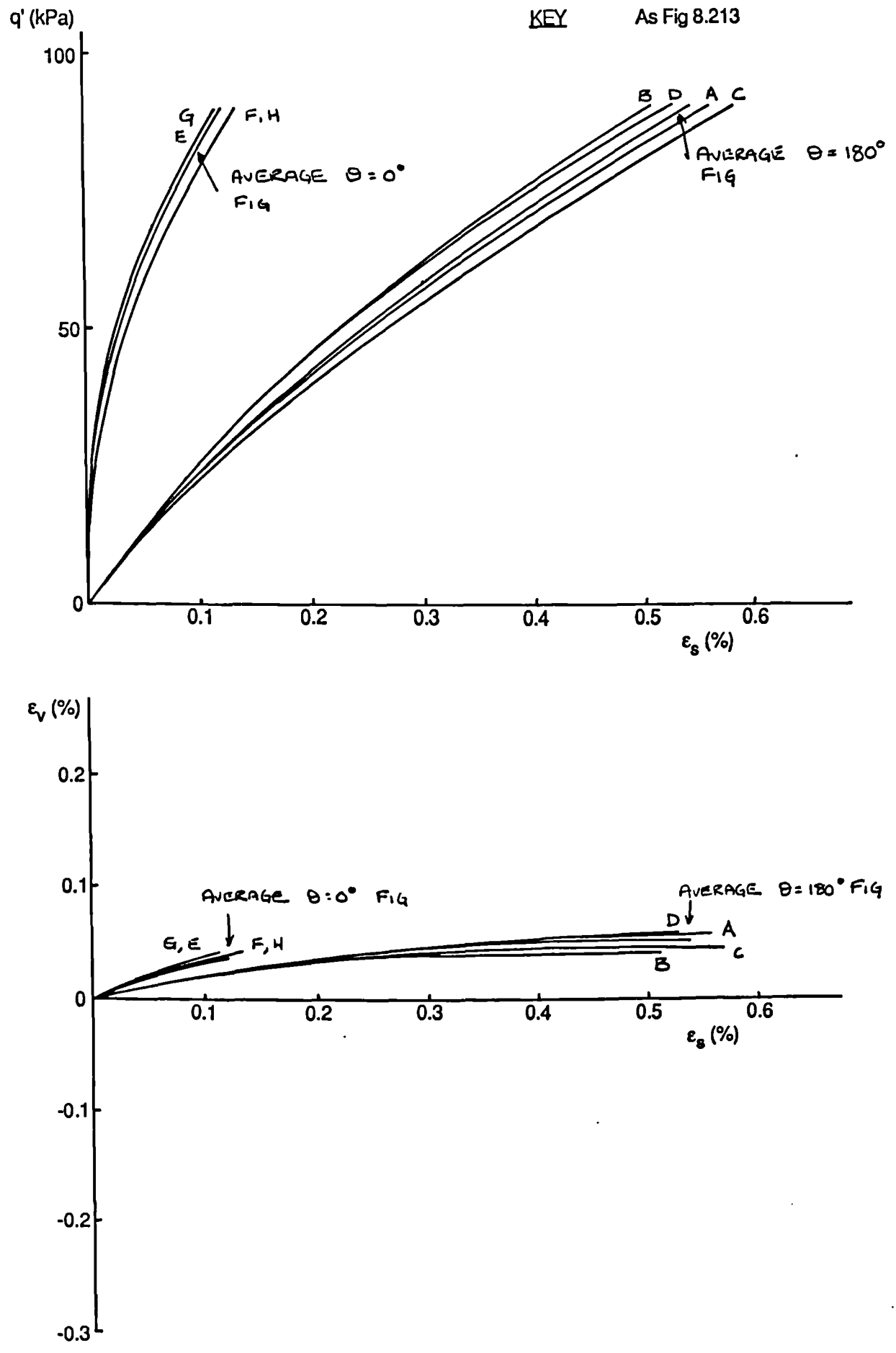

Fig 8.214 Plots of q' against ε_s and ε_v against ε_s for London clay for total stress path threshold tests. $\eta'_o = 0$, OCR = 2.0.
OCR = 2.0.

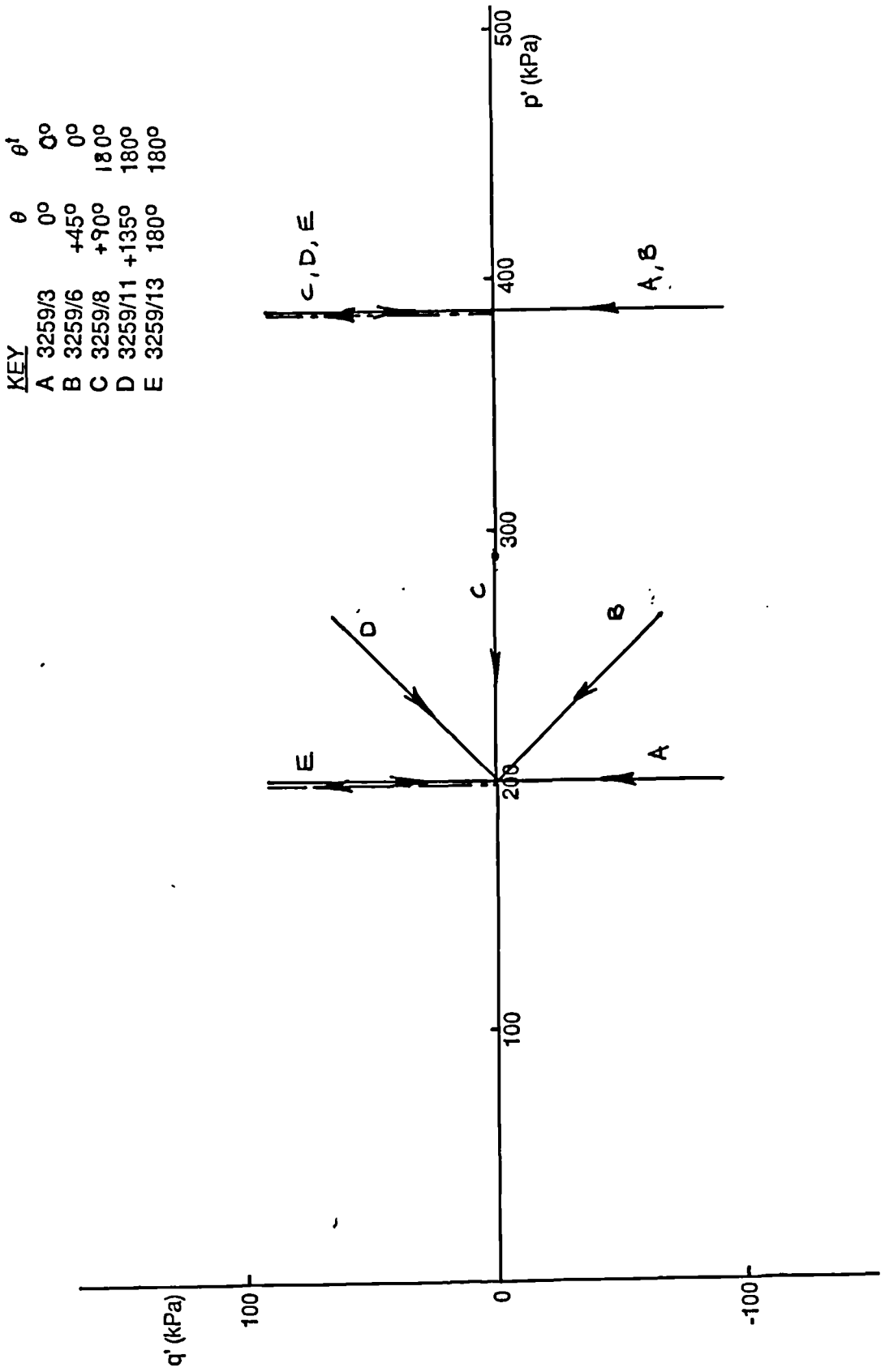

Fig 8.215 Total, q against p, and effective, q' against p', stress paths for London clay for total stress path threshold tests. $\eta'_o = 0$, OCR = 2.0.

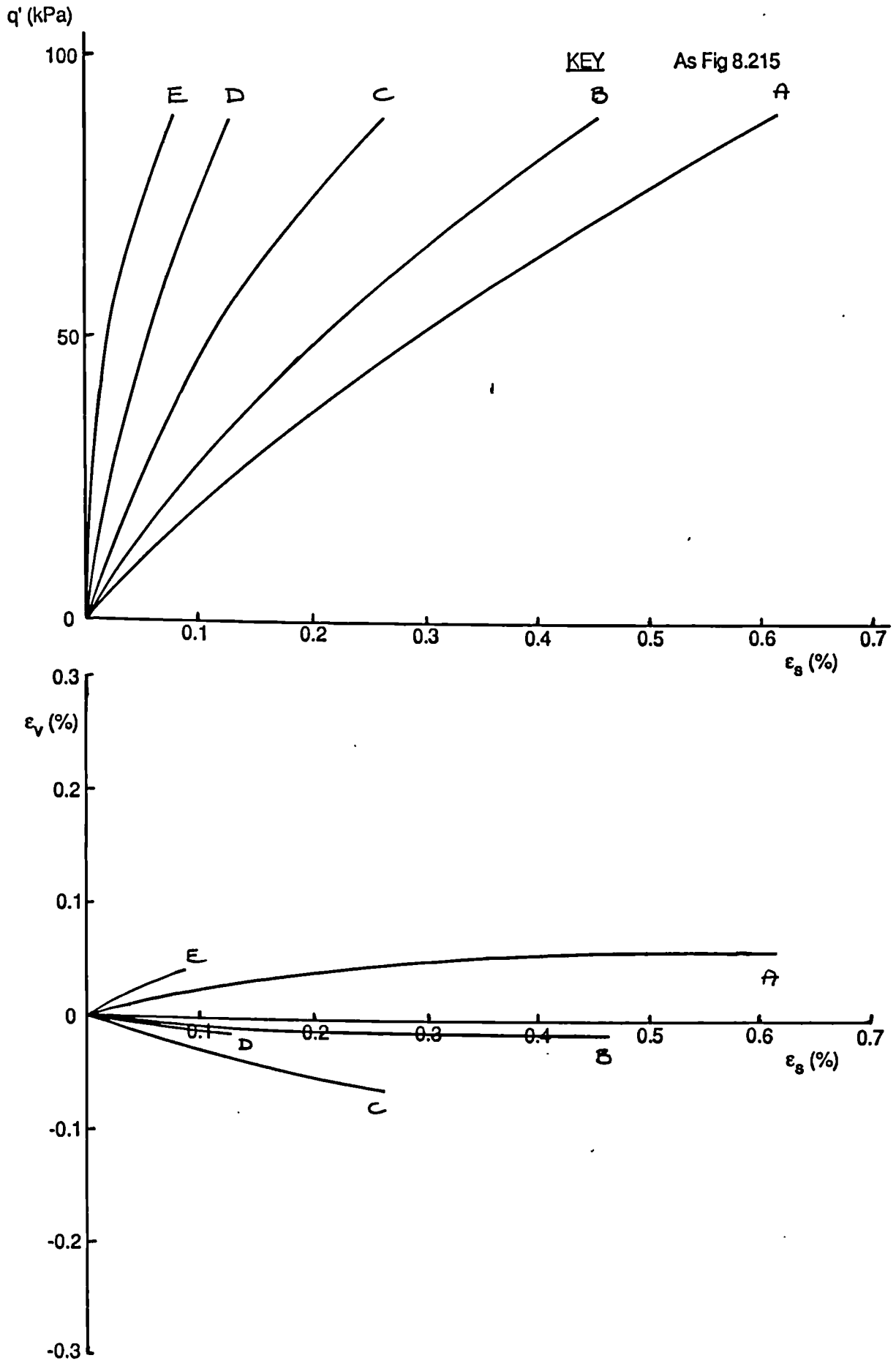

Fig 8.216 Plots of q' against ε_s and ε_v against ε_s for London clay for total stress path threshold tests. $\eta'_o = 0$, OCR = 2.0.

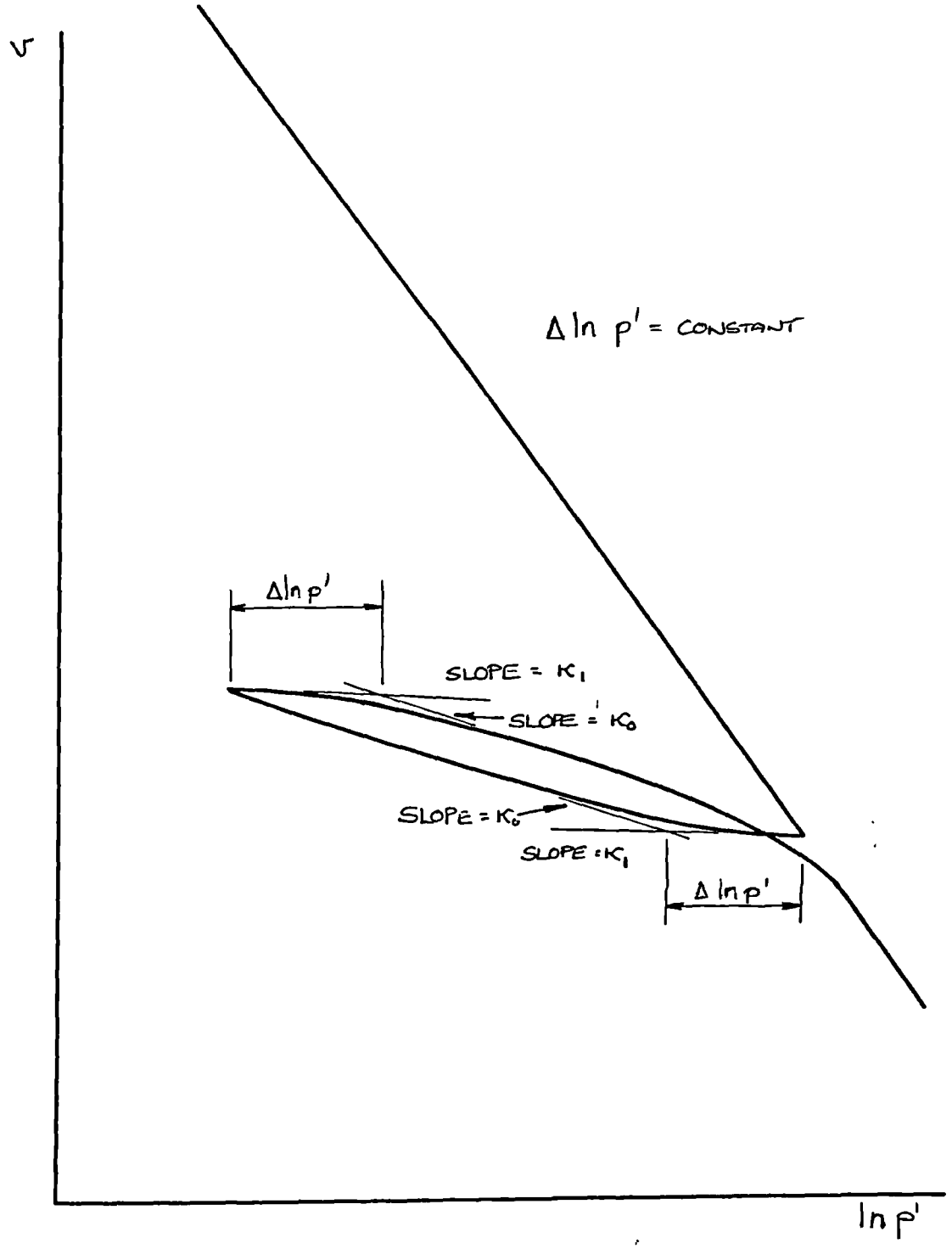

Fig 9.1 Hysteresis loops in swelling and recompression data. definitions of κ_0 and κ_1.

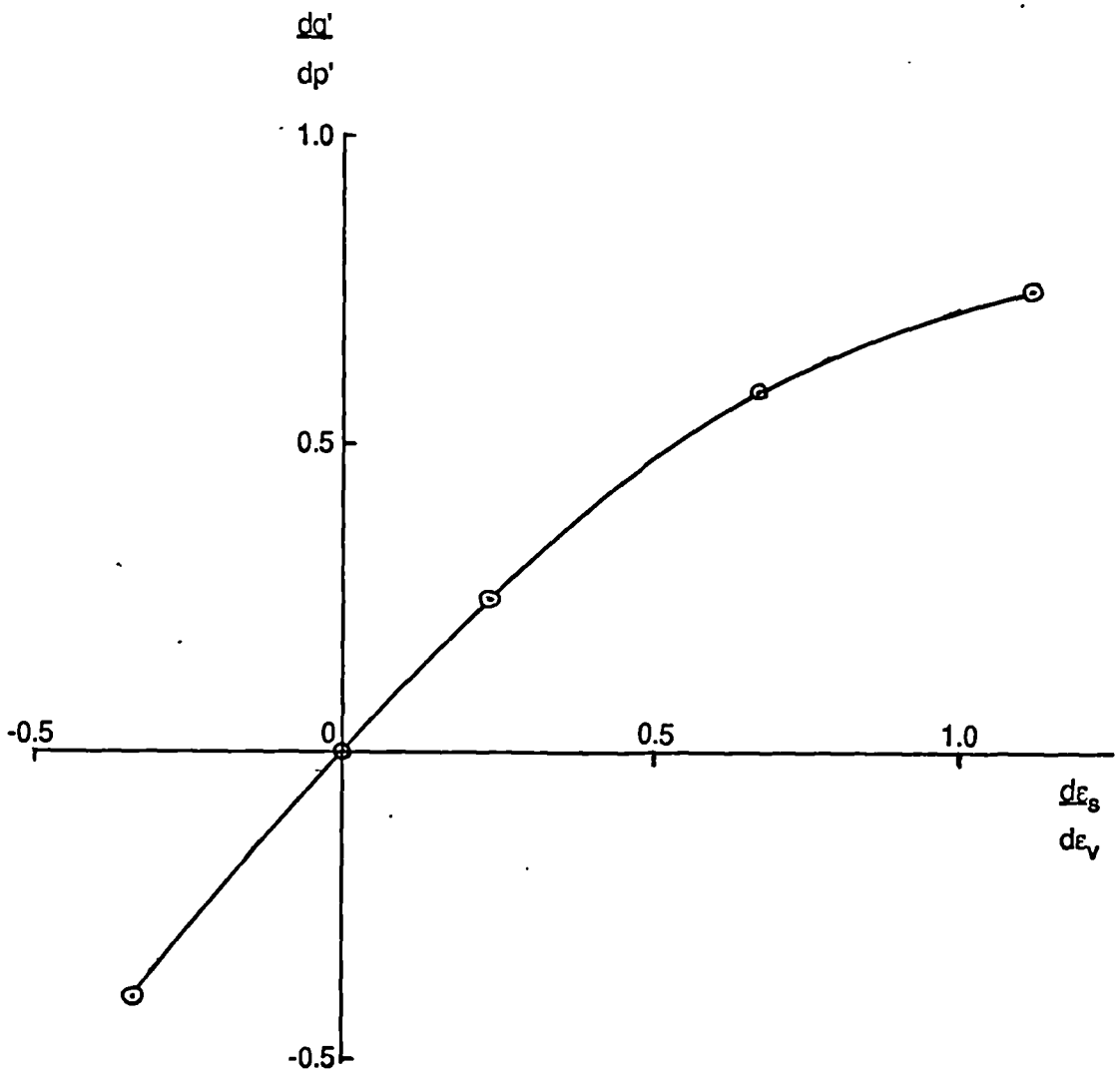

Fig 9.2 Plot of stress increment ratio, dq' / dp' against strain increment ratio $d\varepsilon_s$ / $d\varepsilon_v$ for London clay during anisotropic compression stages.

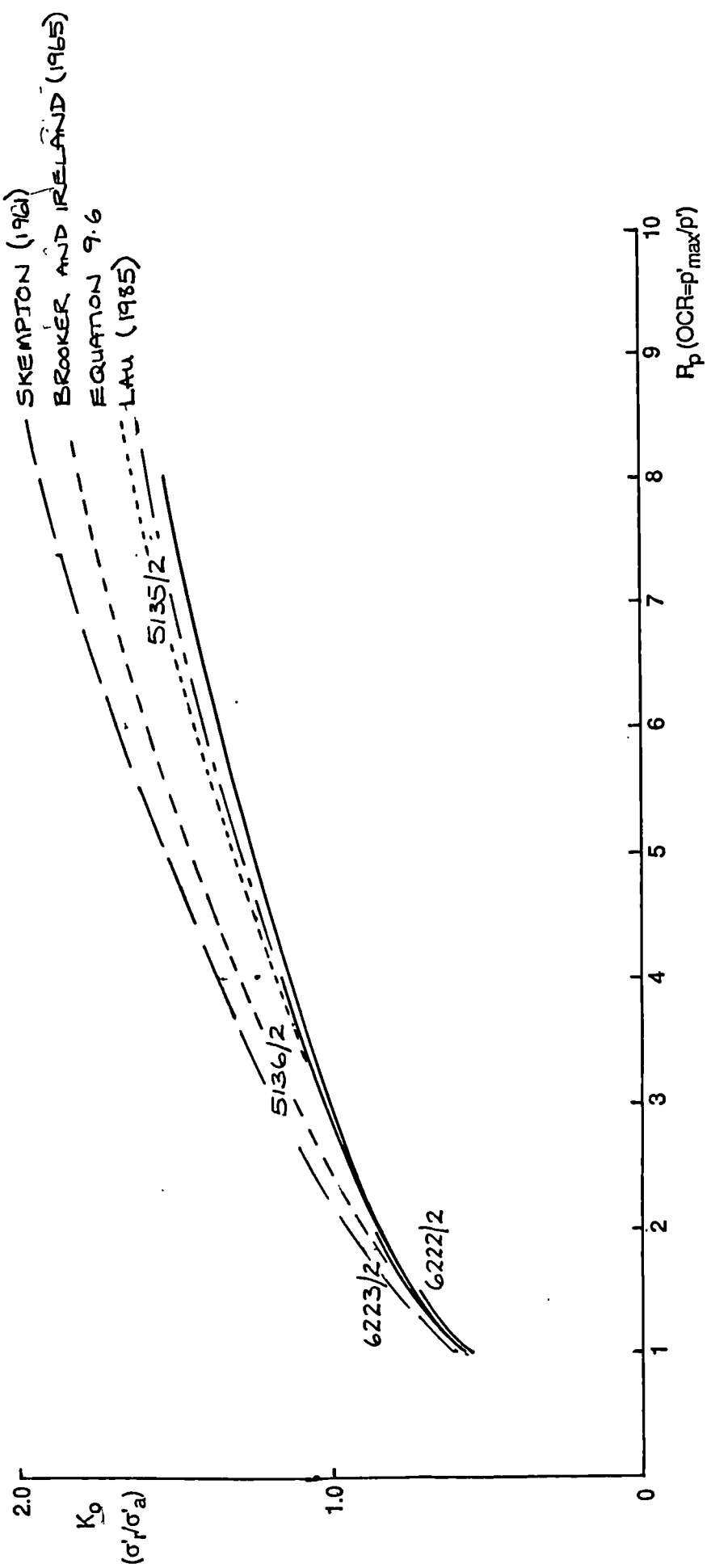

Fig 9.3 Variation of $K_o = \sigma'_r / \sigma'_a$ during one dimensional compression and swelling of London clay with overconsolidation ratio.

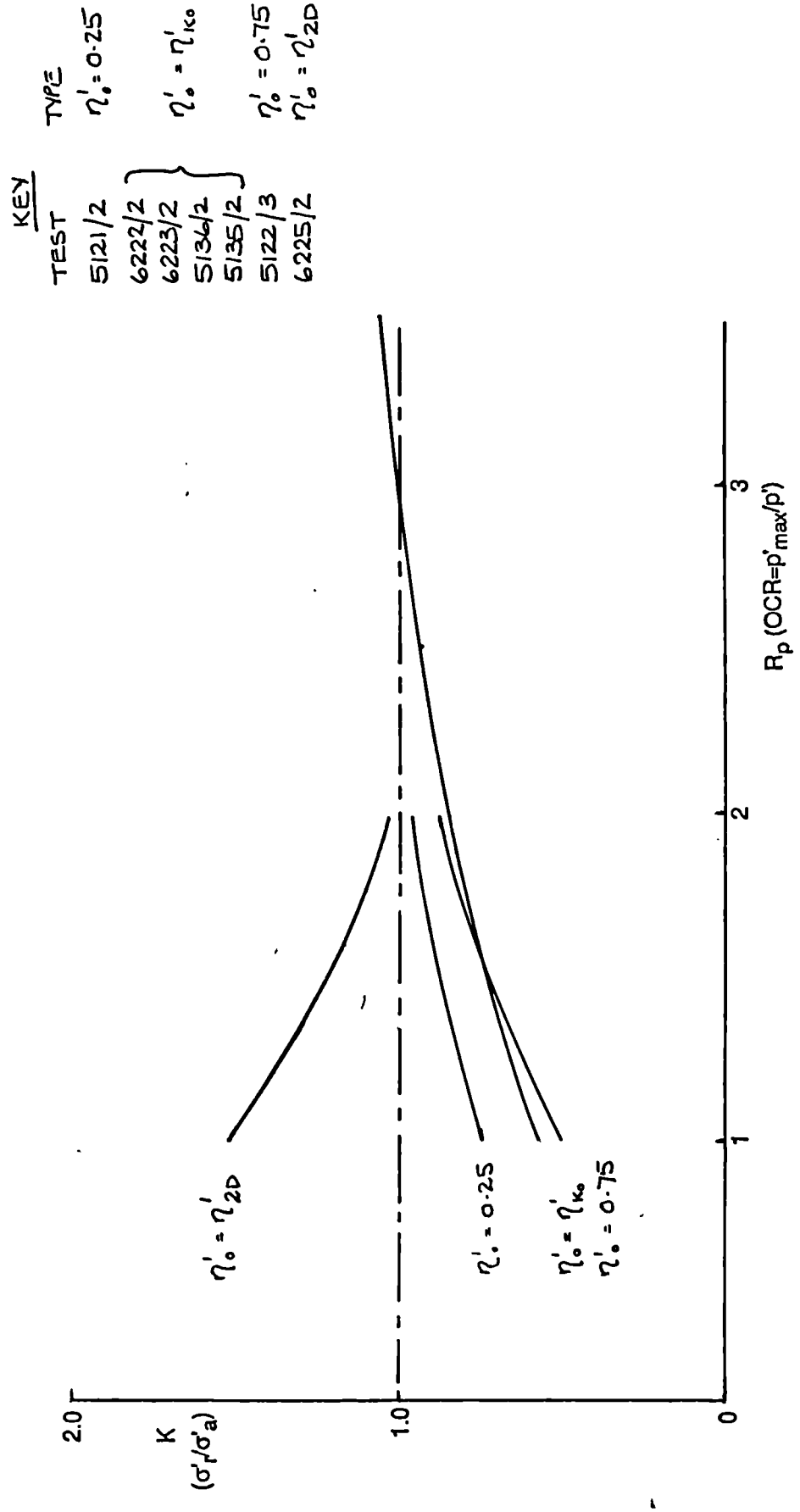

Fig 9.4 Variation of $K_{2D} = \sigma'_r / \sigma'_a$ during anisotropic compression and swelling of London clay .

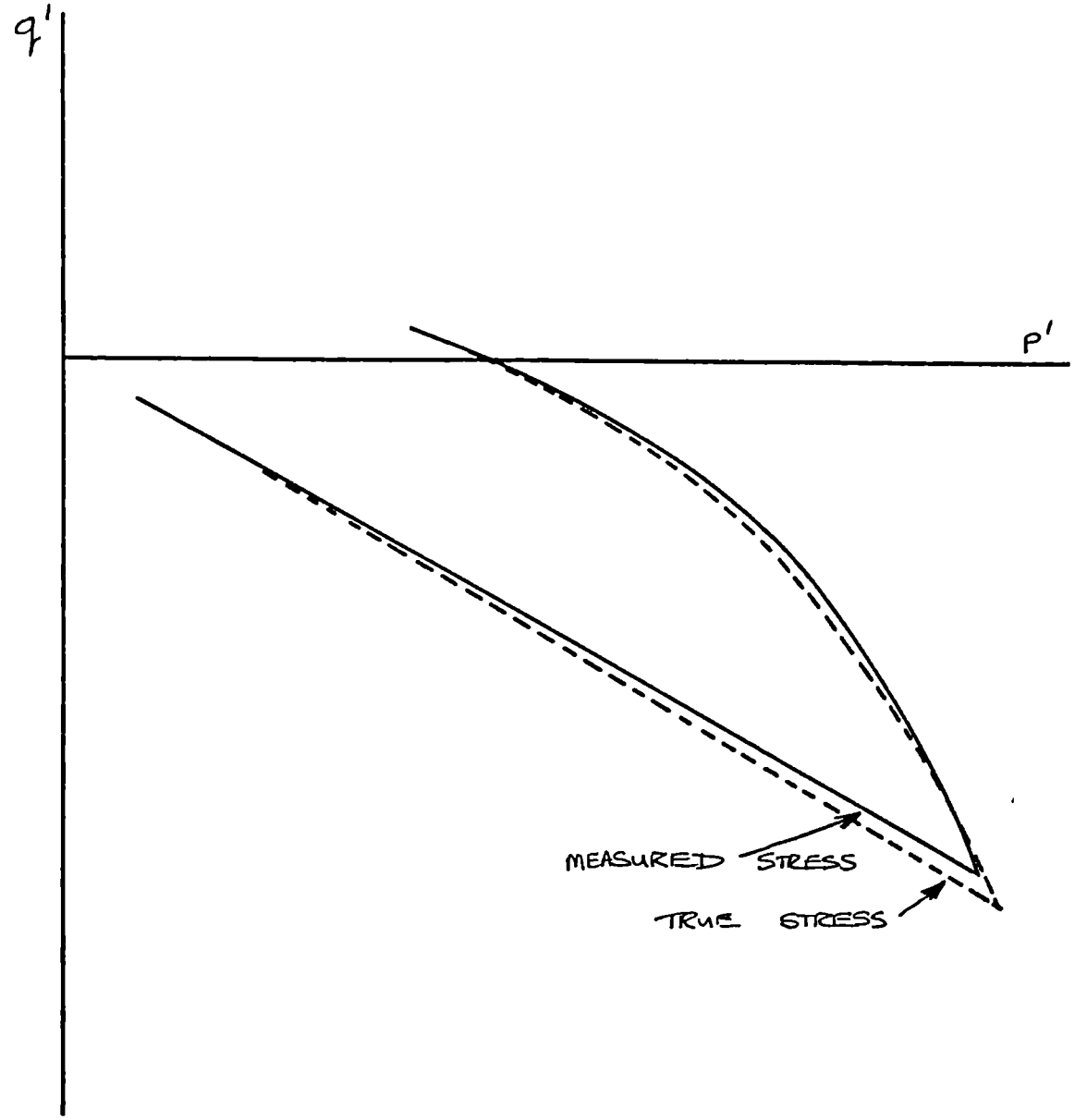

Fig 9.5 Effect of errors in control during two dimensional compression and swelling tests on London clay.

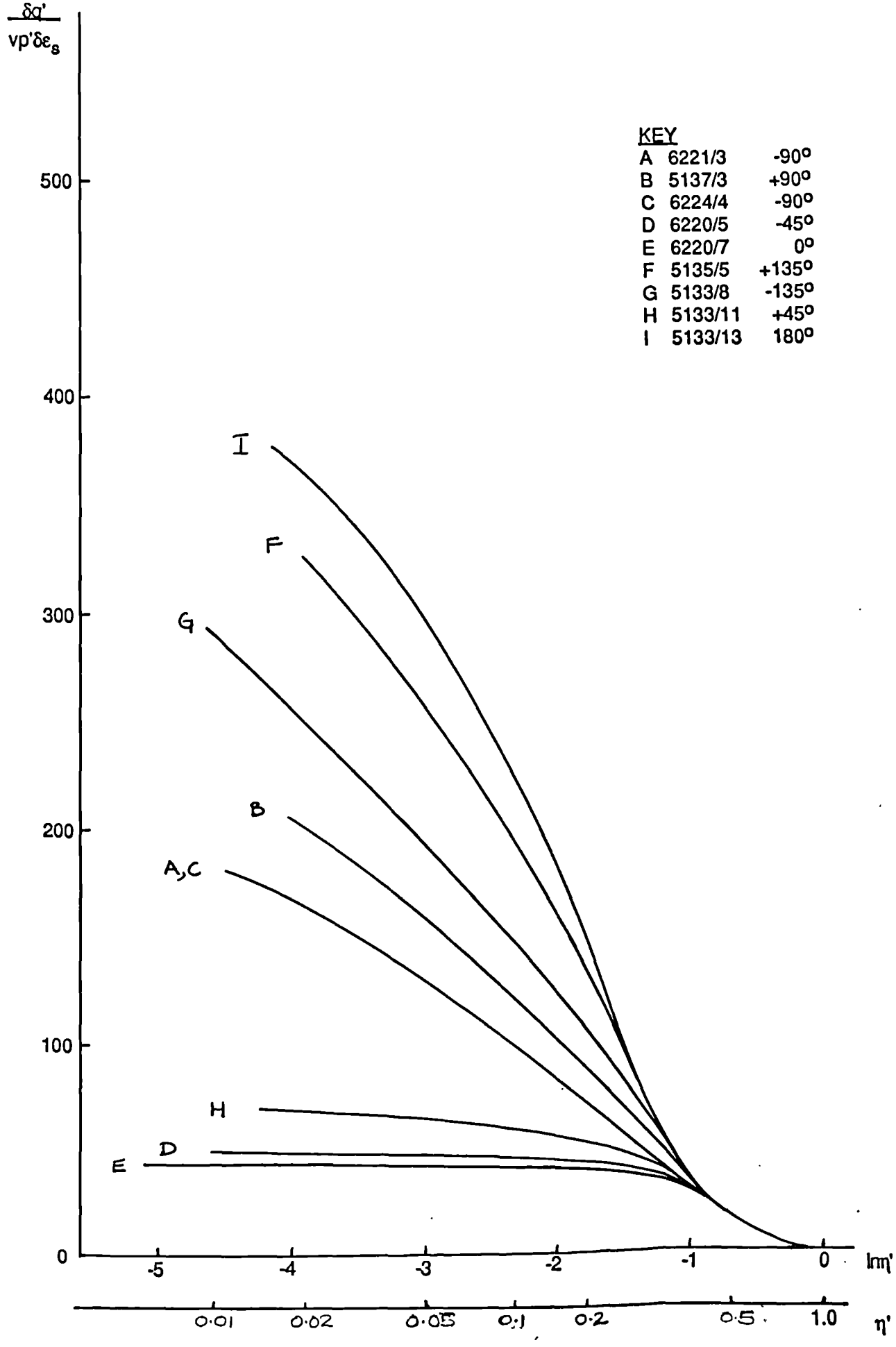

Fig 9.6 Plot of normalised stiffness $\delta q' / vp'\delta\varepsilon_s$ against $\log_e \Delta\eta'$. Speswhite kaolin isotropically compressed, OCR = 2.0, p' = 200 kPa, constant p' paths.

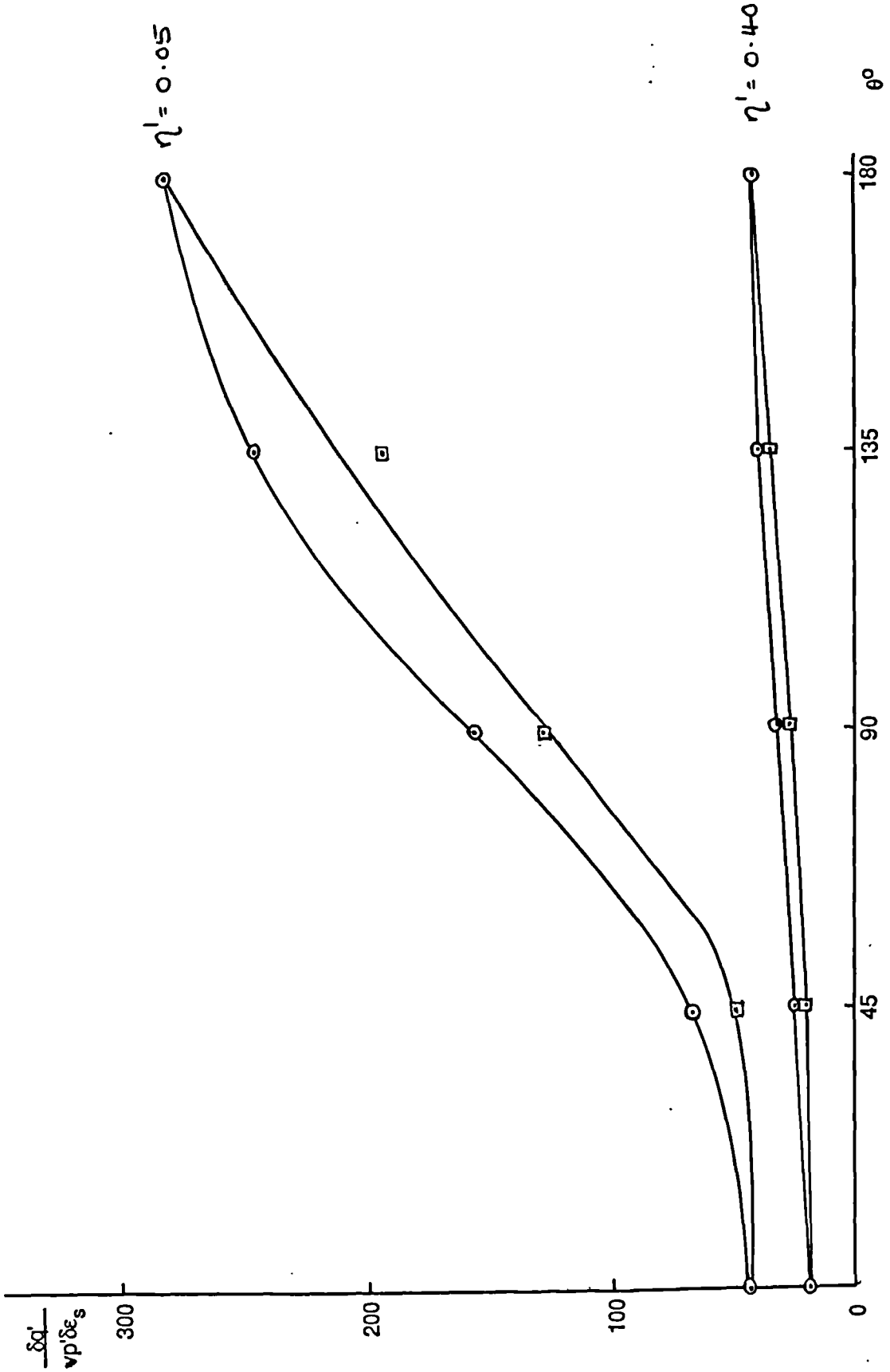

Fig 9.7 Plot of normalised stiffness $\delta q' / vp'\delta\varepsilon_s$ against deviation of stress path, θ. Speswhite kaolin isotropically compressed, OCR = 2.0, p' = 200 kPa, constant p' paths.

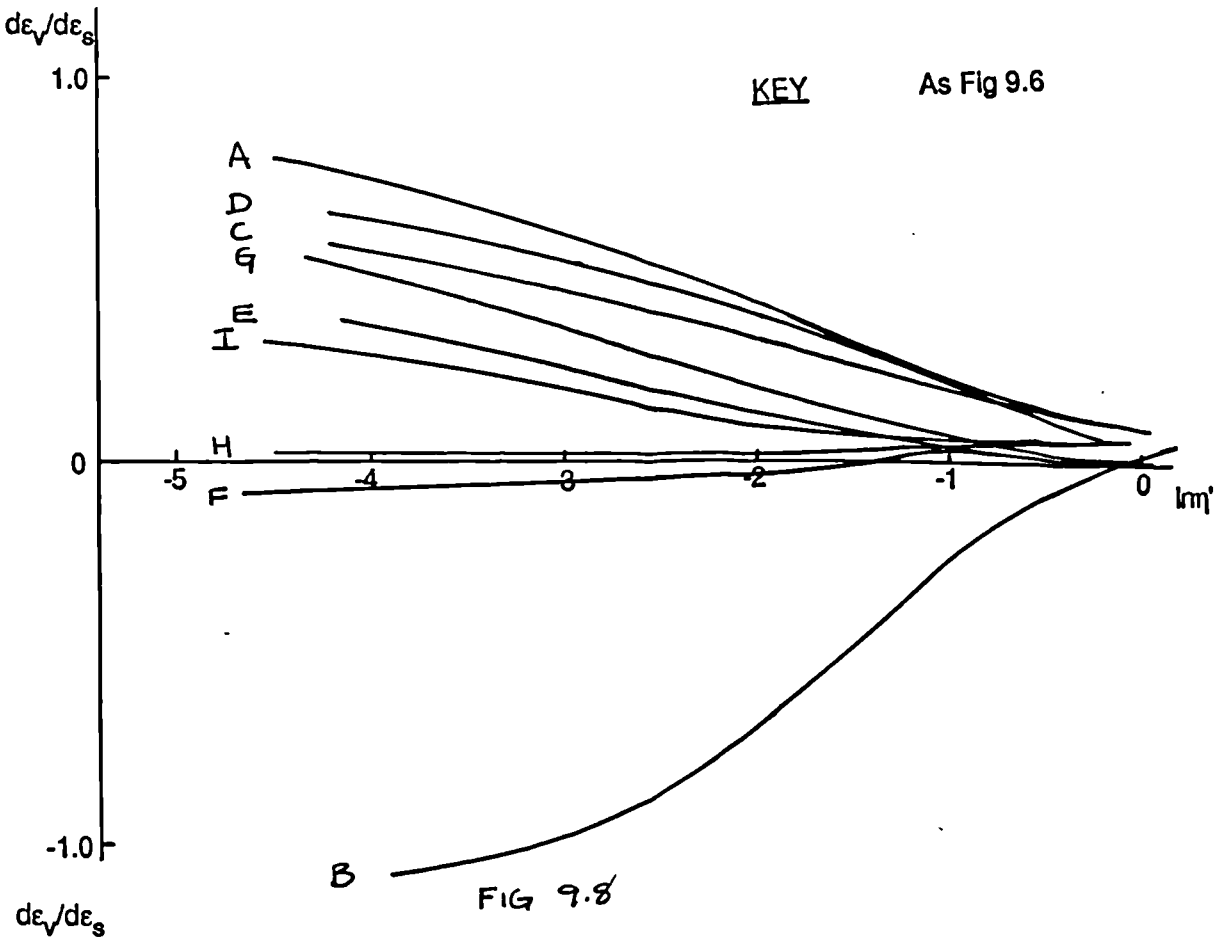

FIG 9.8

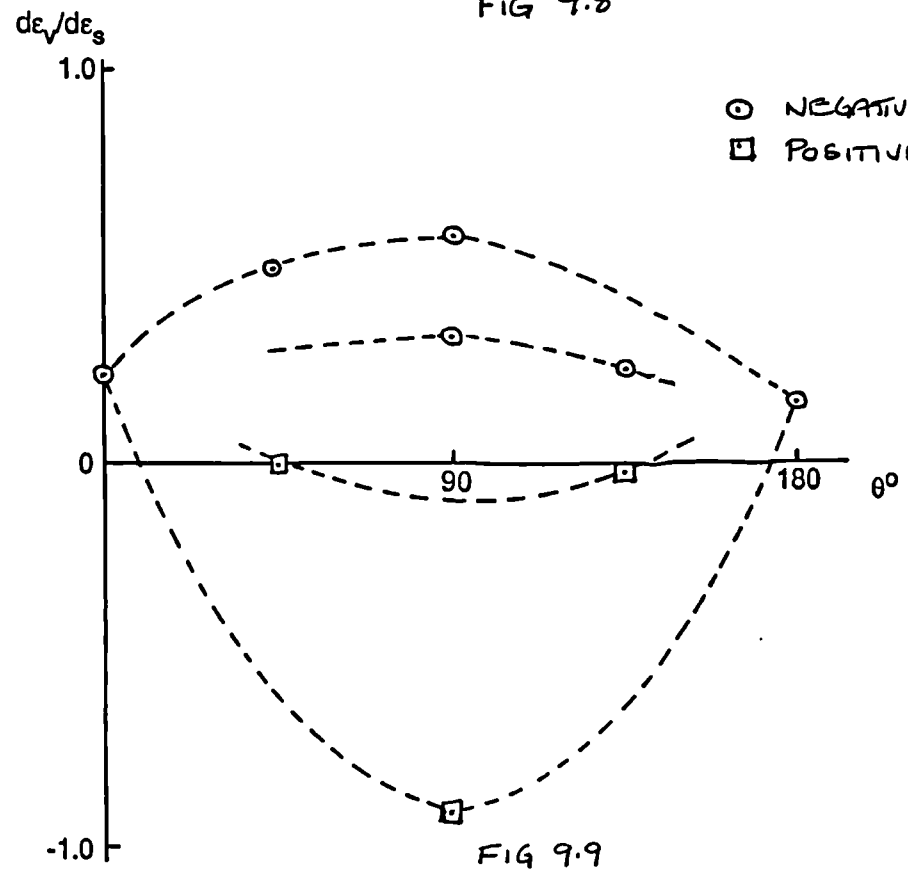

FIG 9.9

Fig 9.8 Plot of total strain increment ratio, $d\varepsilon_v / d\varepsilon_s$, against $\log\Delta\eta'$. Speswhite kaolin, isotropically compressed, OCR = 2.0, p' = 200kPa, constant p' paths.

Fig 9.9 Plot of total strain increment ratio, $d\varepsilon_v / d\varepsilon_s$, against deviation of stress path, θ. Speswhite kaolin, isotropically compressed, OCR = 2.0, p' = 200kPa, constant p' paths.

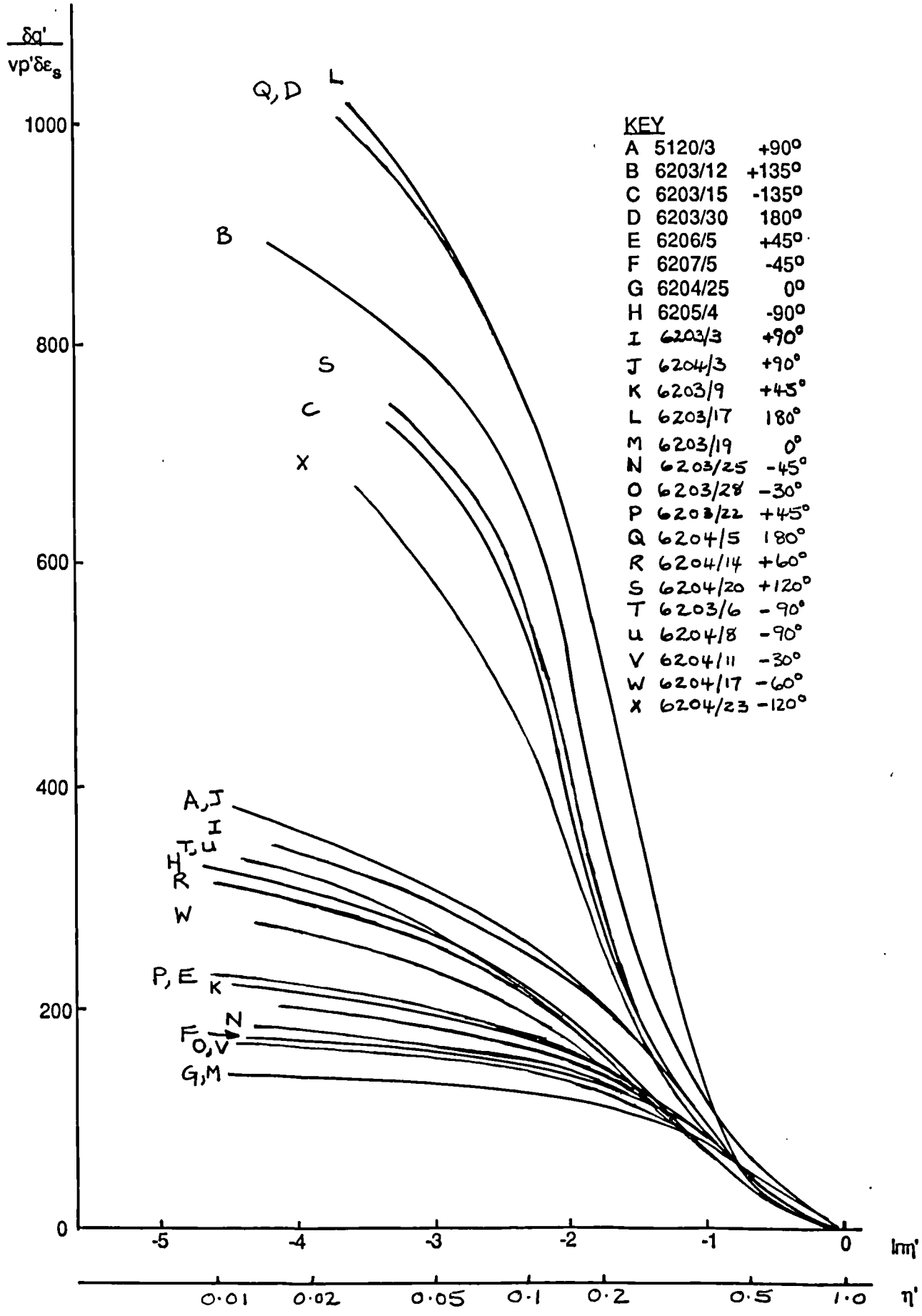

Fig 9.10 Plot of normalised stiffness $\delta q' / vp'\delta\varepsilon_s$ against $\log_e \Delta\eta'$. Ware till isotropically compressed, OCR = 2.0, p' = 200 kPa, constant p' paths.

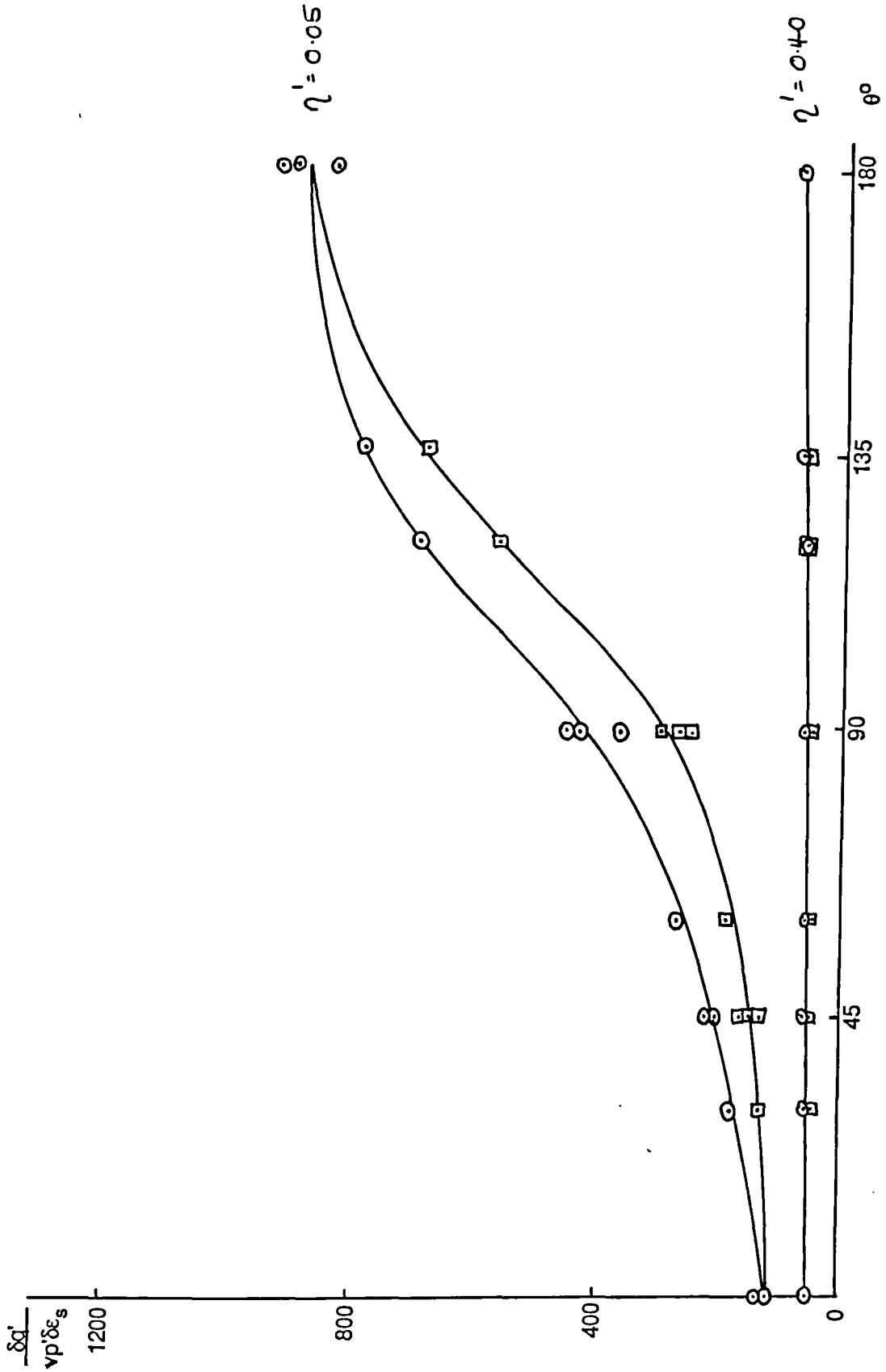

Fig 9.11 Plot of normalised stiffness $\delta q' / vp'\delta\varepsilon_s$ against deviation of stress path, θ. Ware till isotropically compressed, OCR = 2.0, p' = 200 kPa, constant p' paths.

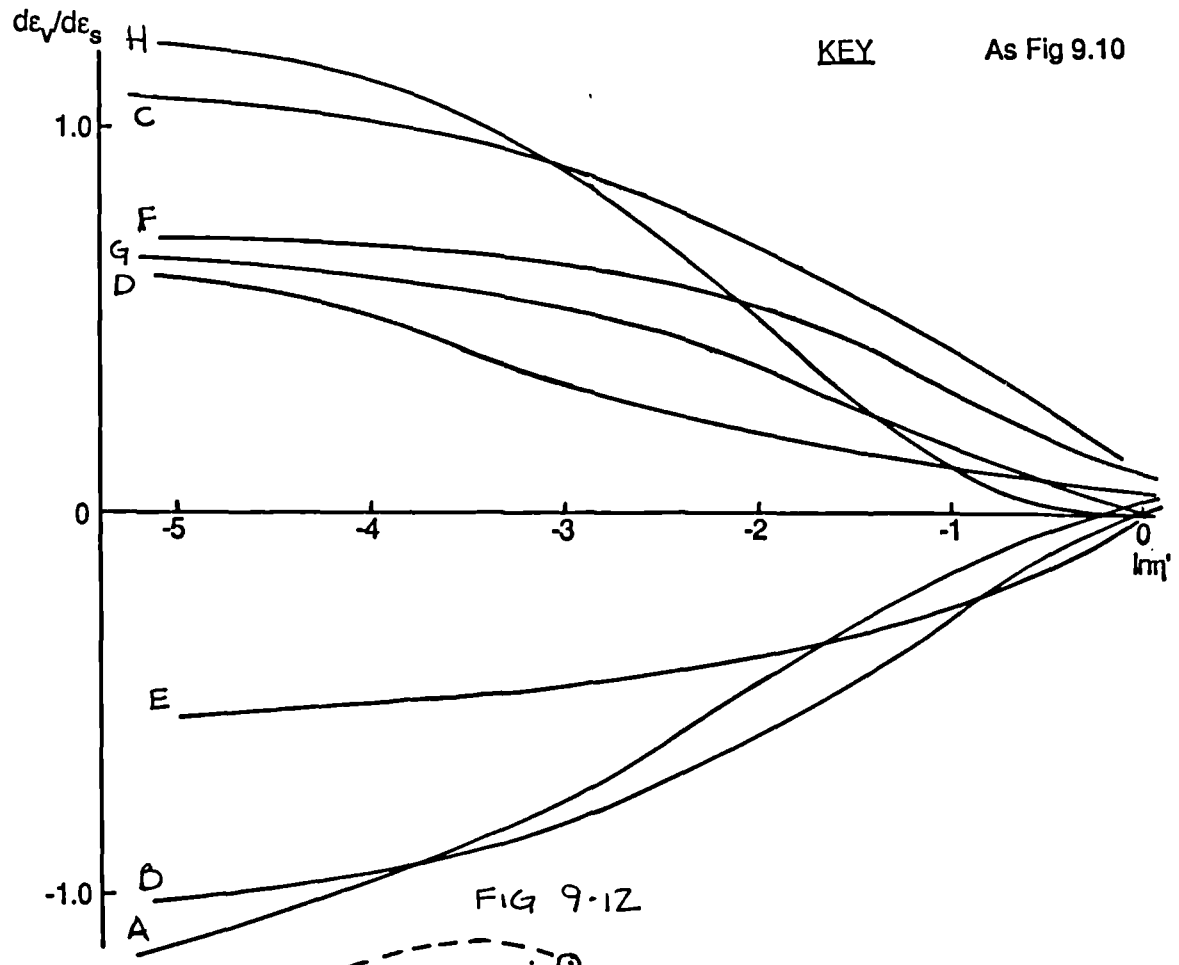

FIG 9·12

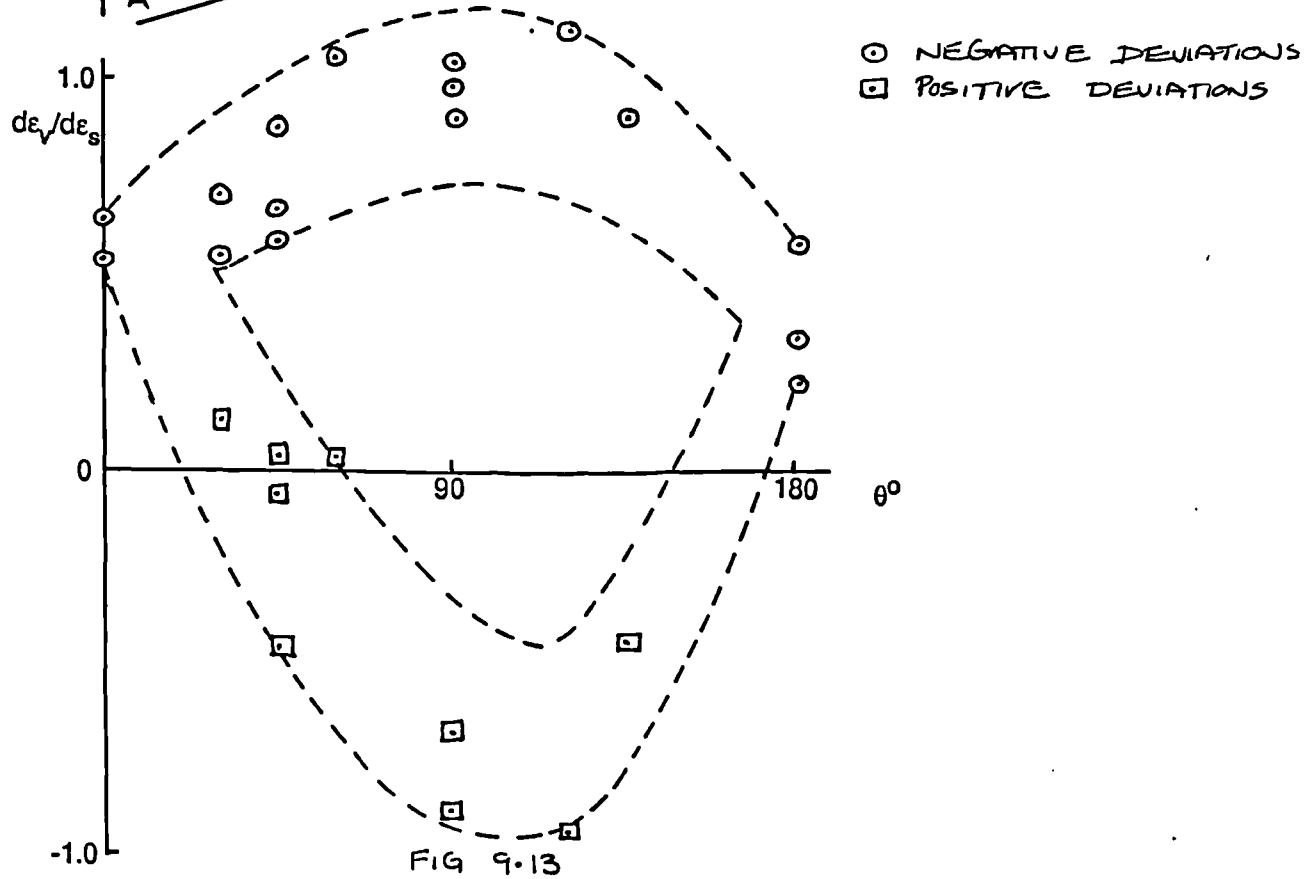

FIG 9·13

Fig 9.12 Plot of total strain increment ratio, $d\varepsilon_v / d\varepsilon_s$, against $\log\Delta\eta'$. Ware till, isotropically compressed, OCR = 2.0, p' = 200kPa, constant p' paths.

Fig 9.13 Plot of total strain increment ratio, $d\varepsilon_v / d\varepsilon_s$, against deviation of stress path, θ. Ware till, isotropically compressed, OCR = 2.0, p' = 200kPa, constant p' paths.

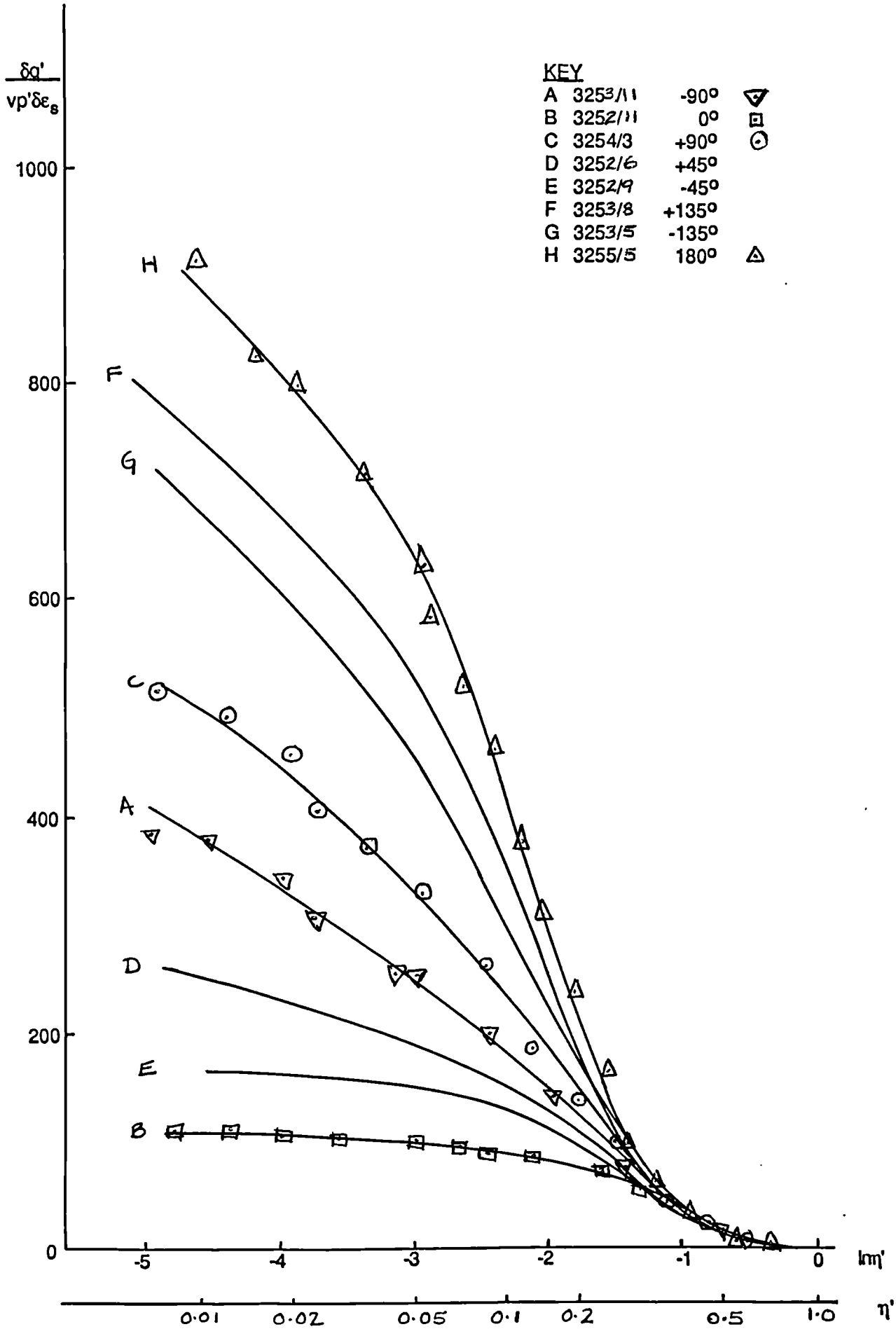

Fig 9.14 Plot of normalised stiffness $\delta q' / vp'\delta\varepsilon_s$ against $\log_e \Delta\eta'$. Cowden till isotropically compressed, OCR = 2.0, p' = 200 kPa, constant p' paths.

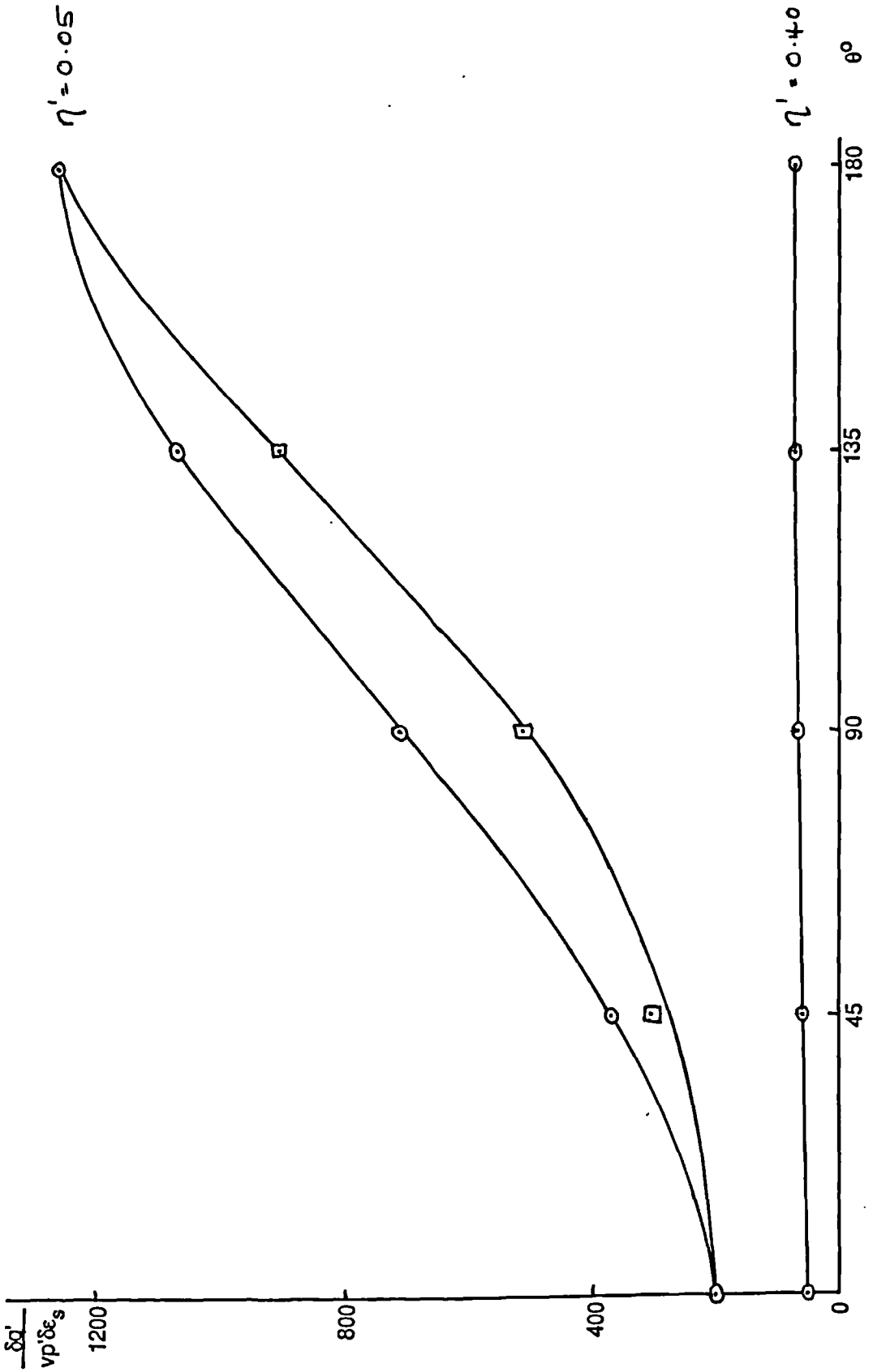

Fig 9.15 Plot of normalised stiffness $\delta q' / vp'\delta\varepsilon_s$ against deviation of stress path, θ. Cowden till isotropically compressed, OCR = 2.0, p' = 200 kPa, constant p' paths.

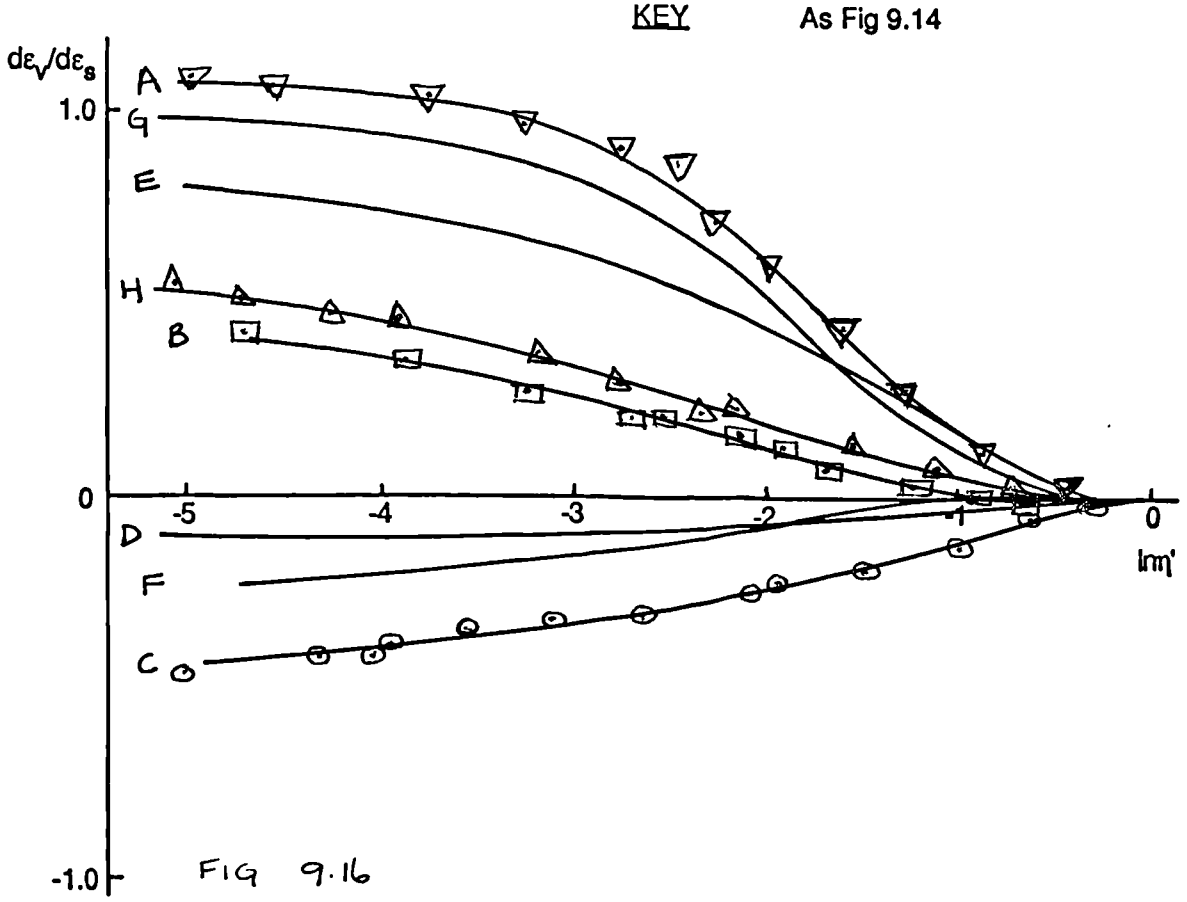

FIG 9.16

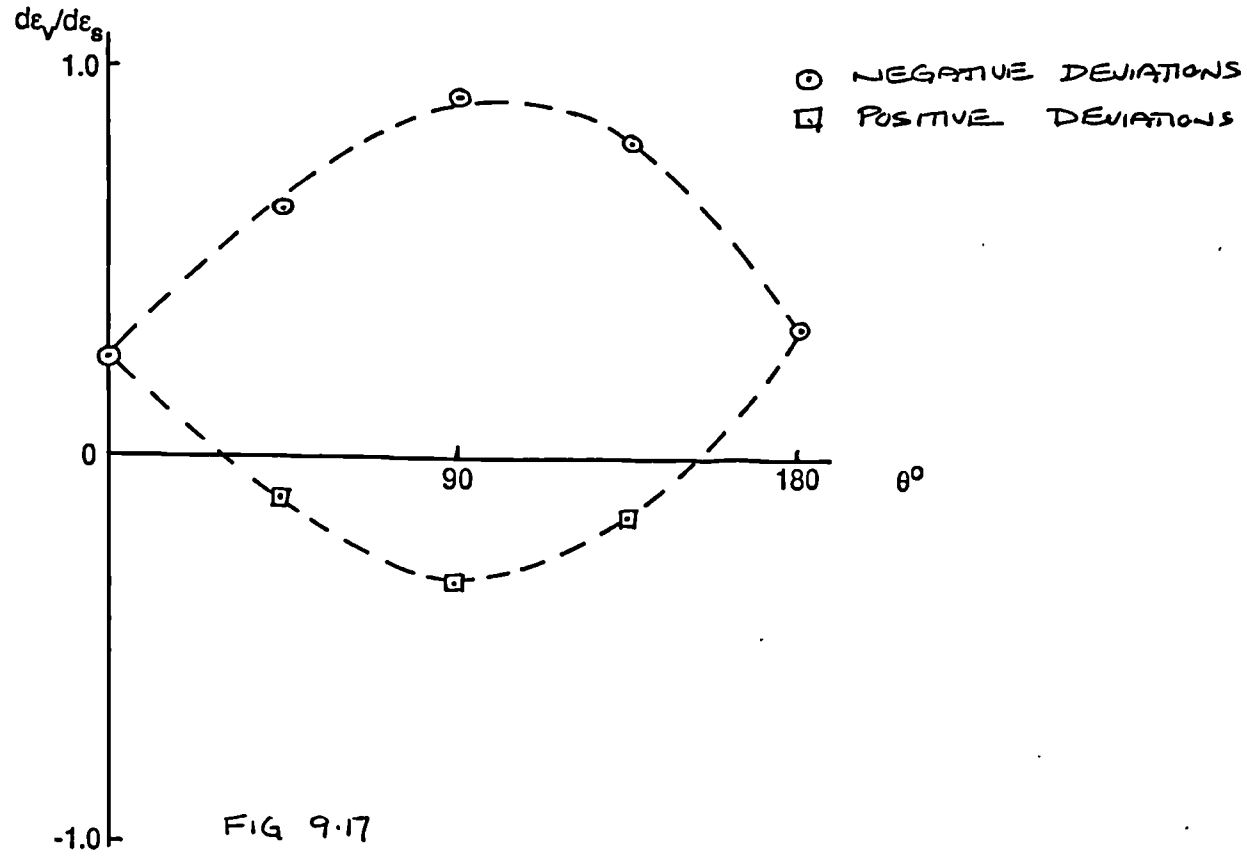

FIG 9.17

Fig 9.16 Plot of total strain increment ratio, $d\varepsilon_v / d\varepsilon_s$, against $\log\Delta\eta'$. Cowden till, isotropically compressed, OCR = 2.0, p' = 200kPa, constant p' paths.

Fig 9.17 Plot of total strain increment ratio, $d\varepsilon_v / d\varepsilon_s$, against deviation of stress path, θ. Cowden till, isotropically compressed, OCR = 2.0, p' = 200kPa, constant p' paths.

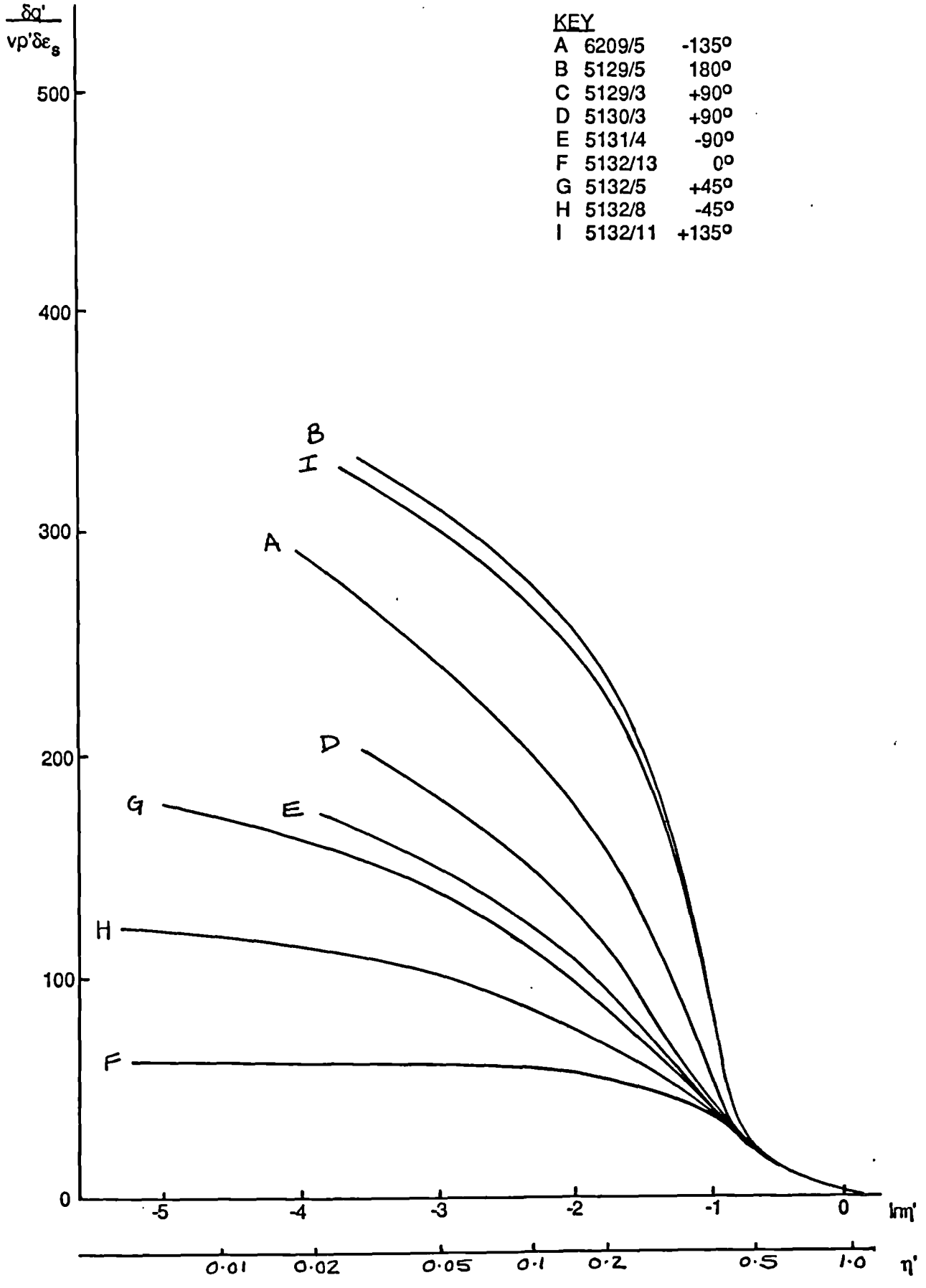

Fig 9.18 Plot of normalised stiffness $\delta q' / vp'\delta\varepsilon_s$ against $\log_e \Delta\eta'$. Slate dust isotropically compressed, OCR = 2.0, p' = 200 kPa, constant p' paths.

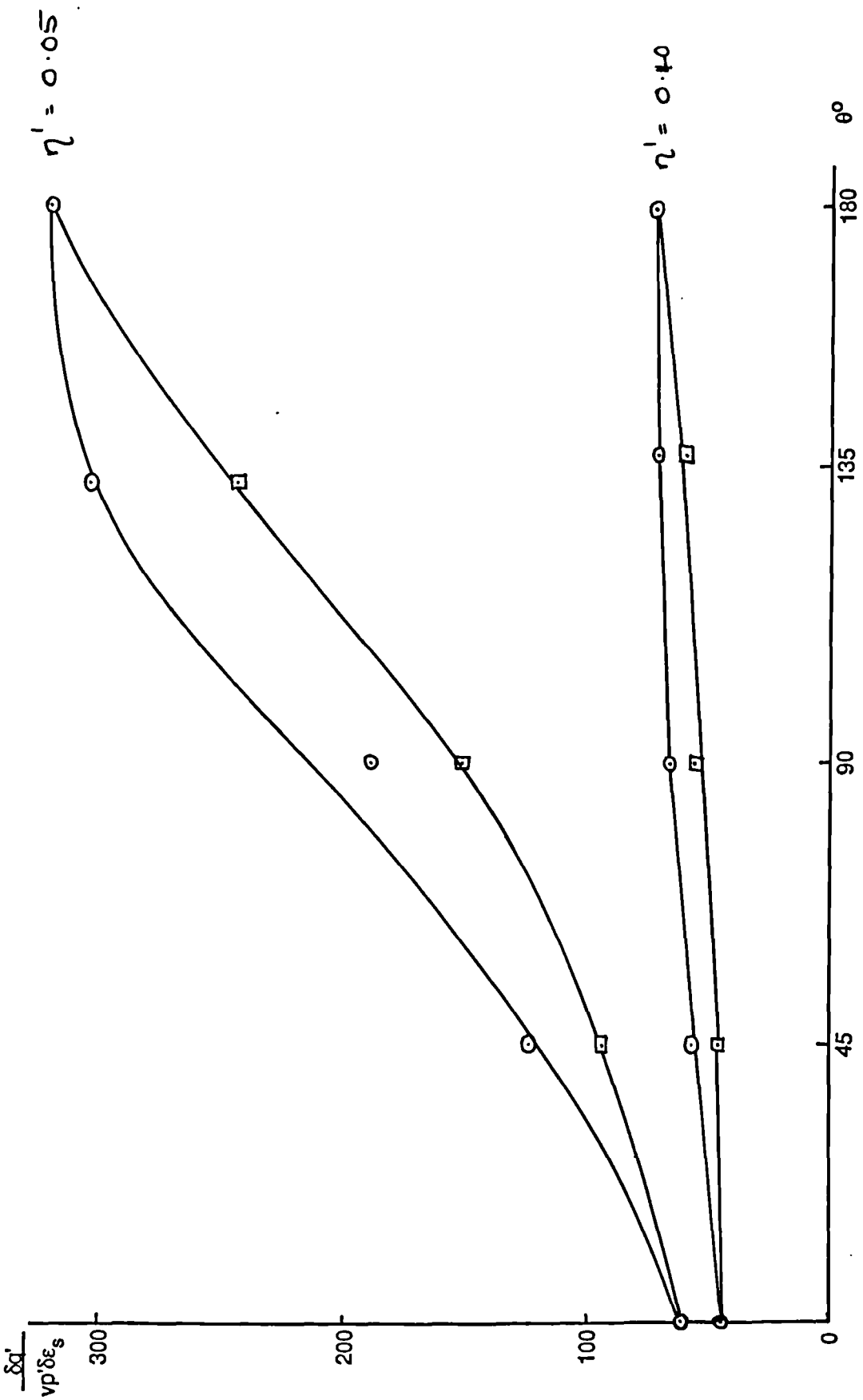

Fig 9.19 Plot of normalised stiffness $\delta q' / vp'\delta\varepsilon_s$ against deviation of stress path, θ. Slate dust isotropically compressed, OCR = 2.0, p' = 200 kPa, constant p' paths.

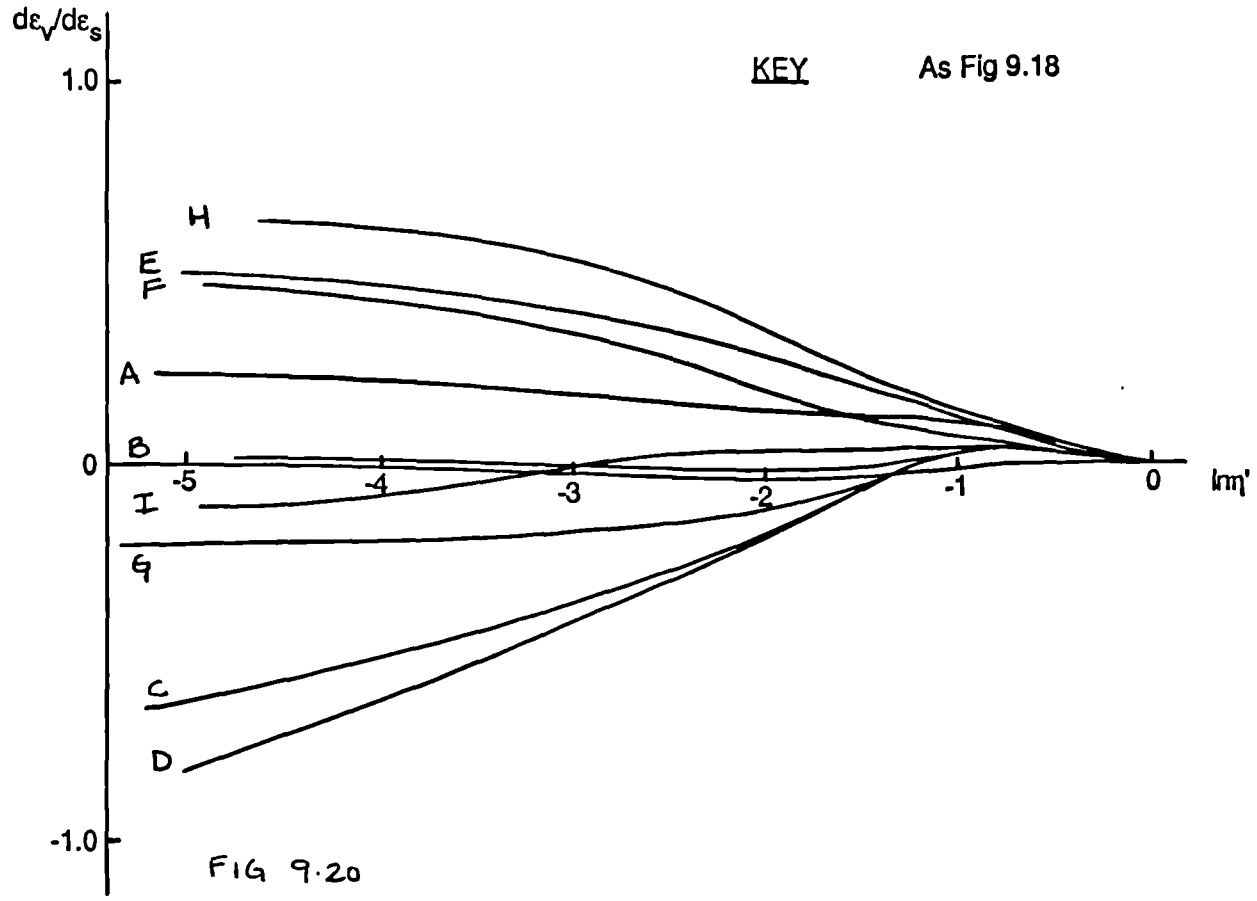

FIG 9.20

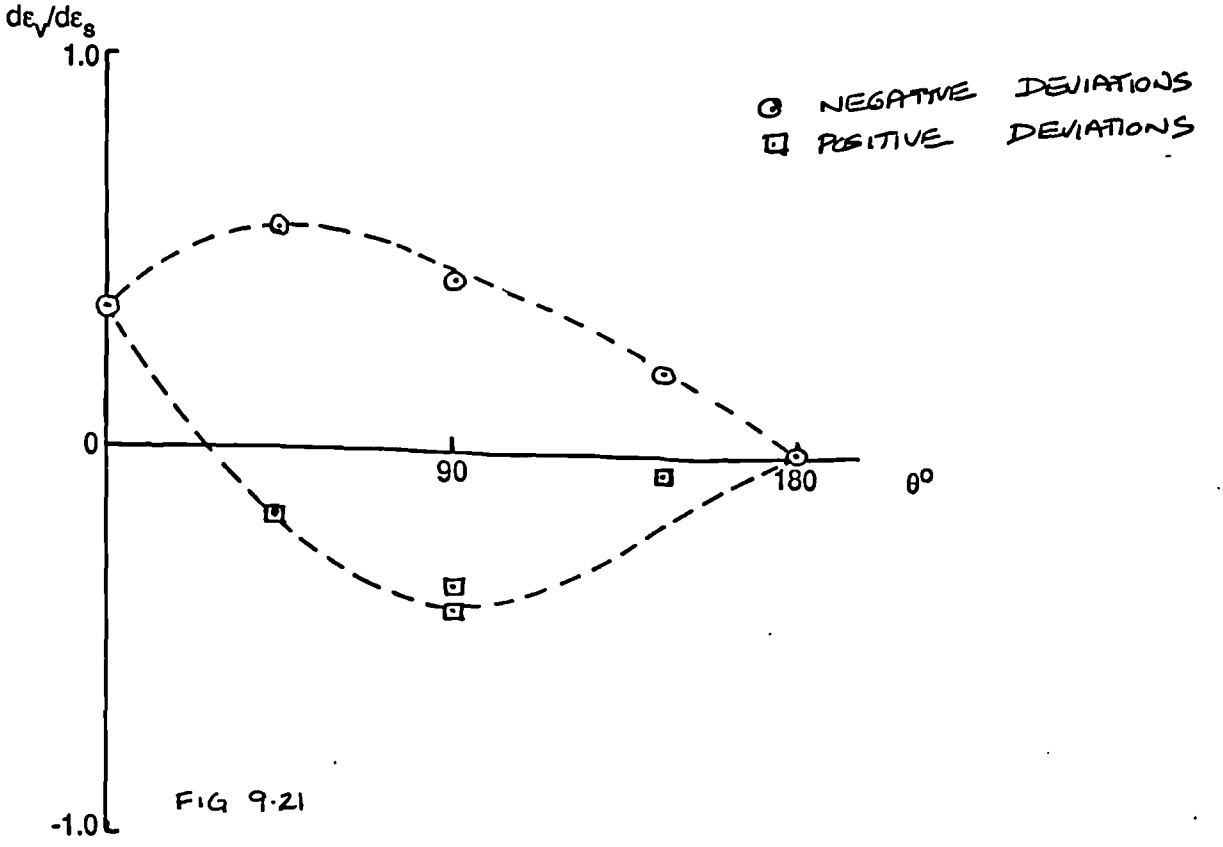

FIG 9.21

Fig 9.20 Plot of total strain increment ratio, $d\varepsilon_v / d\varepsilon_s$, against $\log\Delta\eta'$. Slate dust, isotropically compressed, OCR = 2.0, p' = 200kPa, constant p' paths.

Fig 9.21 Plot of total strain increment ratio, $d\varepsilon_v / d\varepsilon_s$, against deviation of stress path, θ. Slate dust, isotropically compressed, OCR = 2.0, p' = 200kPa, constant p' paths.

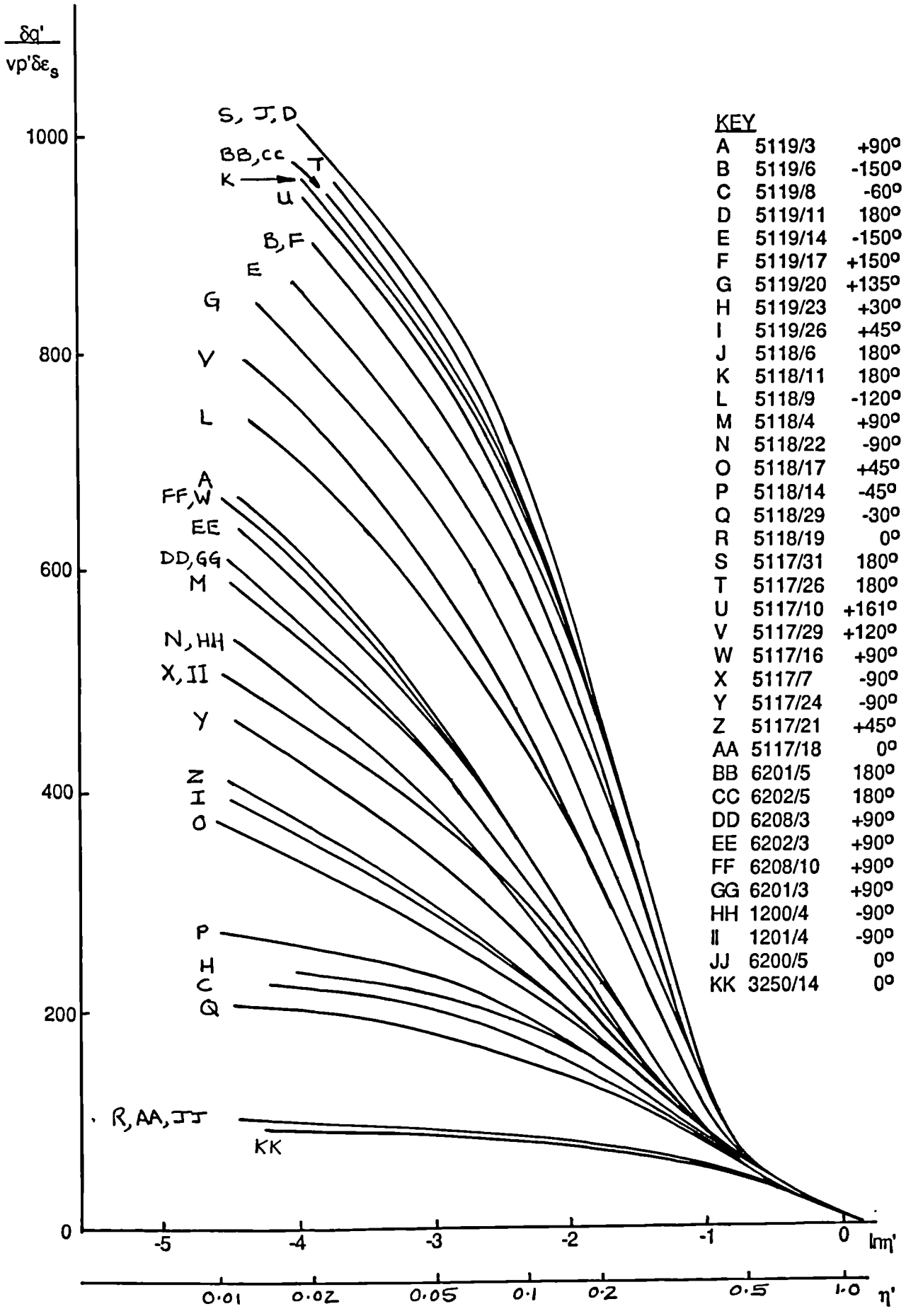

Fig 9.22 Plot of normalised stiffness $\delta q' / vp'\delta\varepsilon_s$ against $\log_e \Delta\eta'$. London clay isotropically compressed, OCR = 2.0, p' = 200 kPa, constant p' paths.

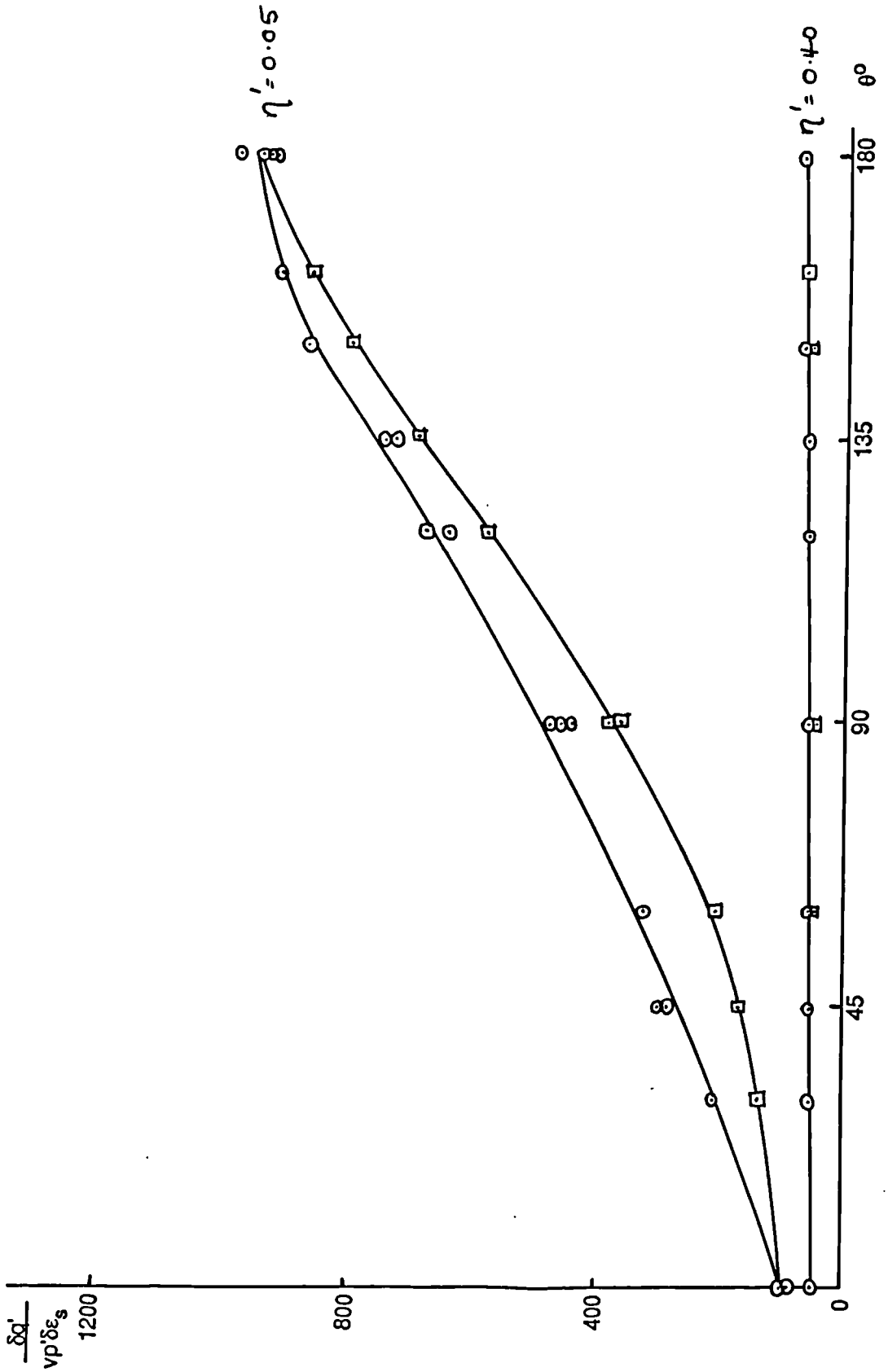

Fig 9.23 Plot of normalised stiffness $\delta q' / vp'\delta\varepsilon_s$ against deviation of stress path, θ. London clay isotropically compressed, OCR = 2.0, p' = 200 kPa, constant p' paths.

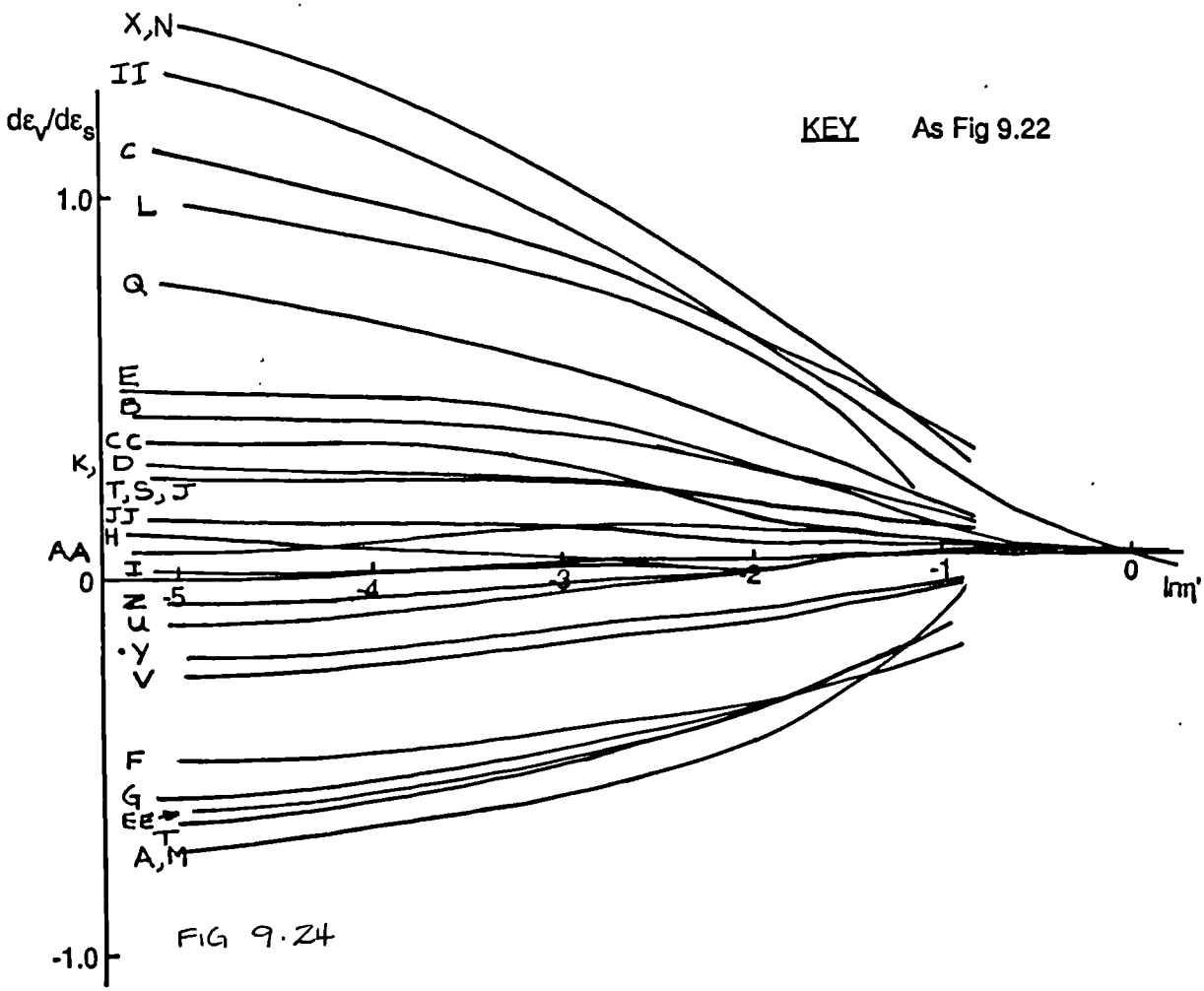

FIG 9.24

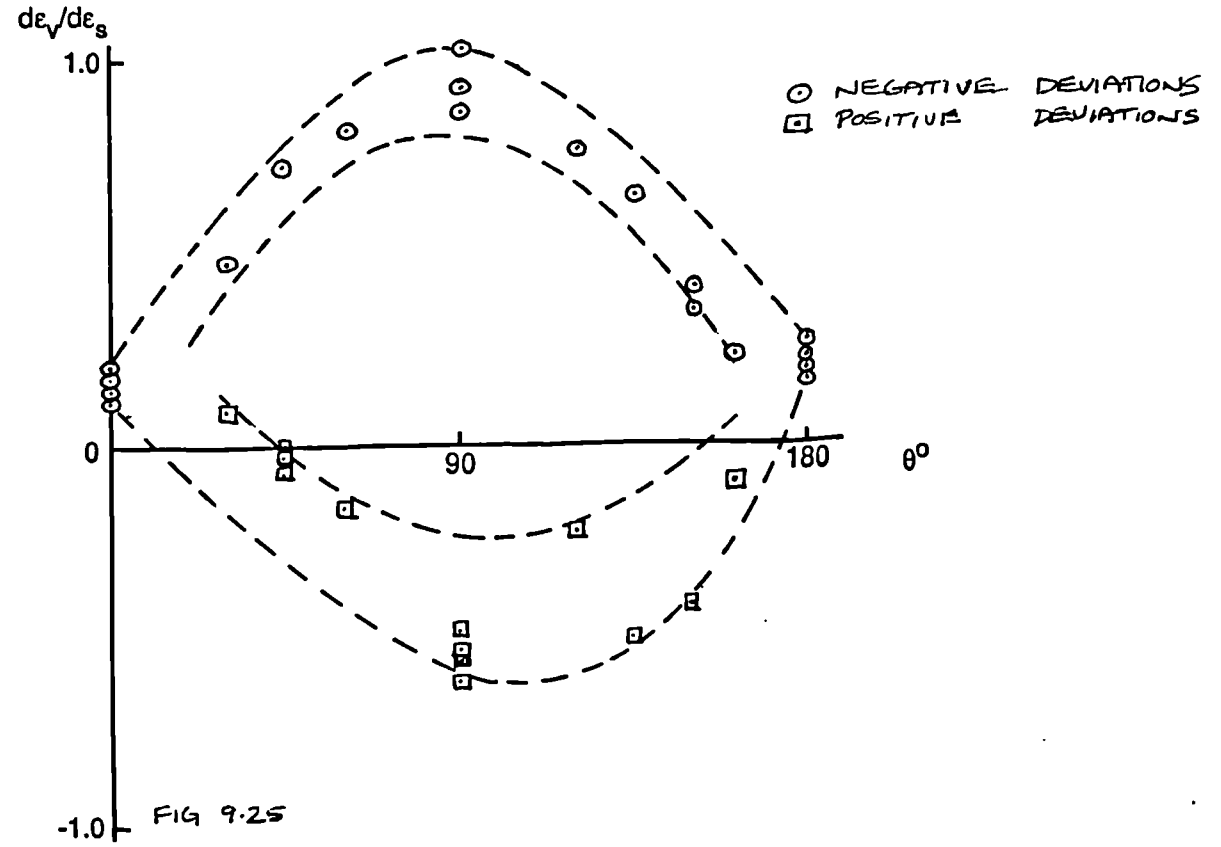

FIG 9.25

Fig 9.24 Plot of total strain increment ratio, $d\varepsilon_v / d\varepsilon_s$, against $\log\Delta\eta'$. London clay , isotropically compressed, OCR = 2.0, p' = 200kPa, constant p' paths.

Fig 9.25 Plot of total strain increment ratio, $d\varepsilon_v / d\varepsilon_s$, against deviation of stress path, θ. London clay , isotropically compressed, OCR = 2.0, p' = 200kPa, constant p' paths.

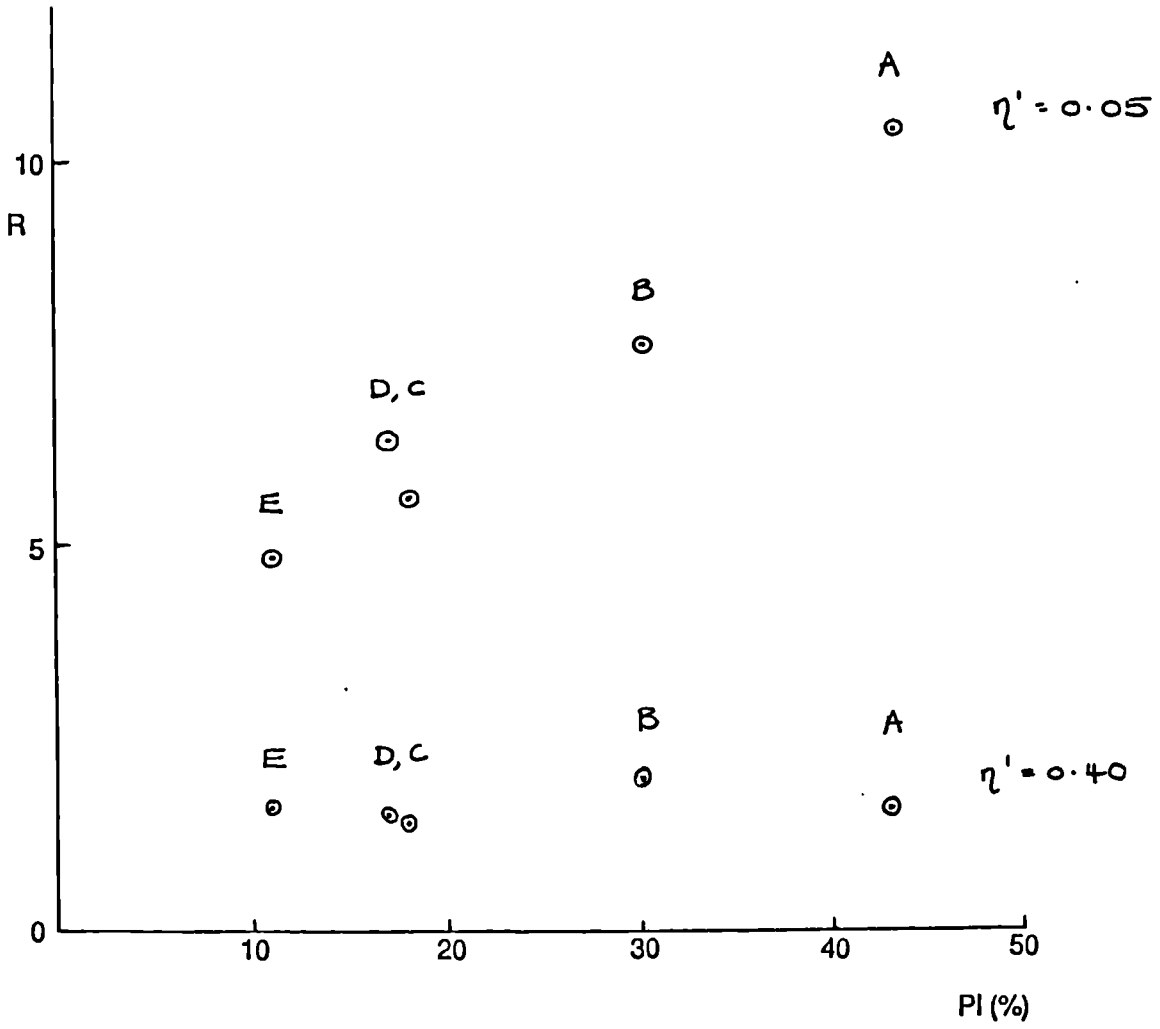

KEY
A London Clay
B Speswhite Kaolin
C Ware Till
D Cowden Till
E Slate dust

Fig 9.26 Plot showing range of stiffness, R, against plasticity index, PI, for $\Delta\eta' = 0.40$ and $\Delta\eta' = 0.05$.

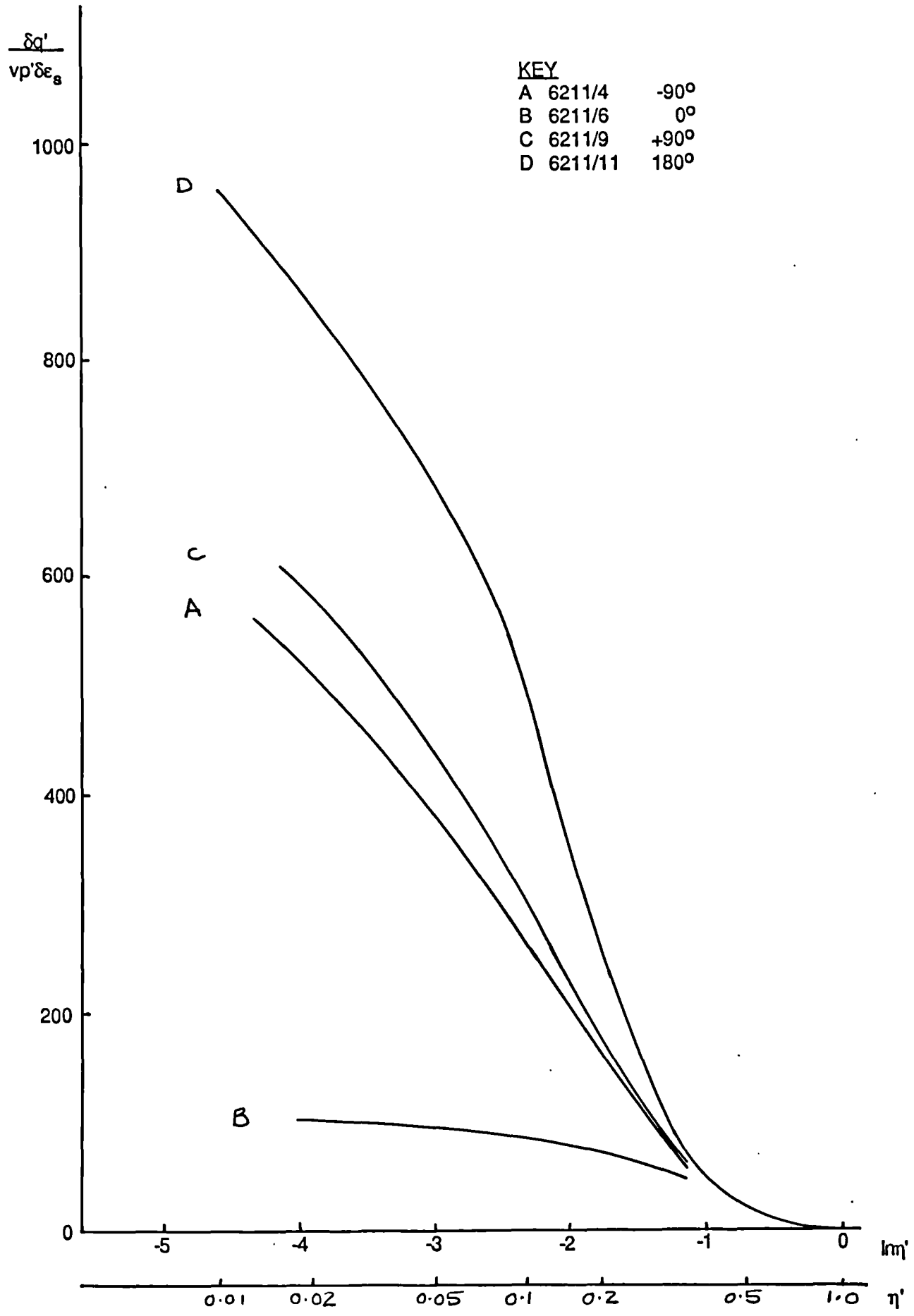

Fig 9.27 Plot of normalised stiffness $\delta q' / vp'\delta\varepsilon_s$ against $\log_e \Delta\eta'$. London clay isotropically compressed, OCR = 1.5, p' = 267 kPa, constant p' paths.

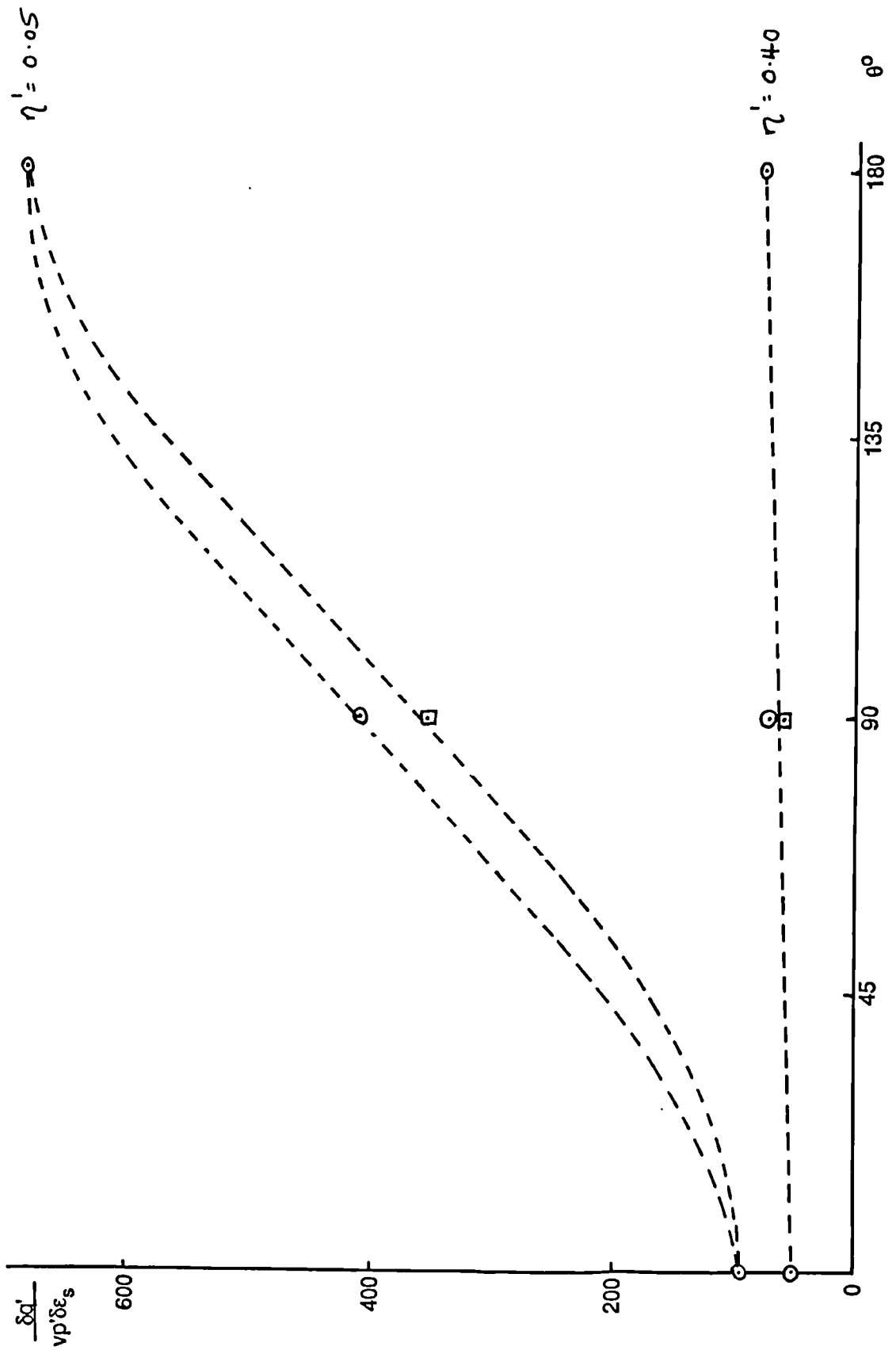

Fig 9.28 Plot of normalised stiffness $\delta q' / vp'\delta\varepsilon_s$ against deviation of stress path, θ. London clay isotropically compressed, OCR = 1.5, p' = 267 kPa, constant p' paths.

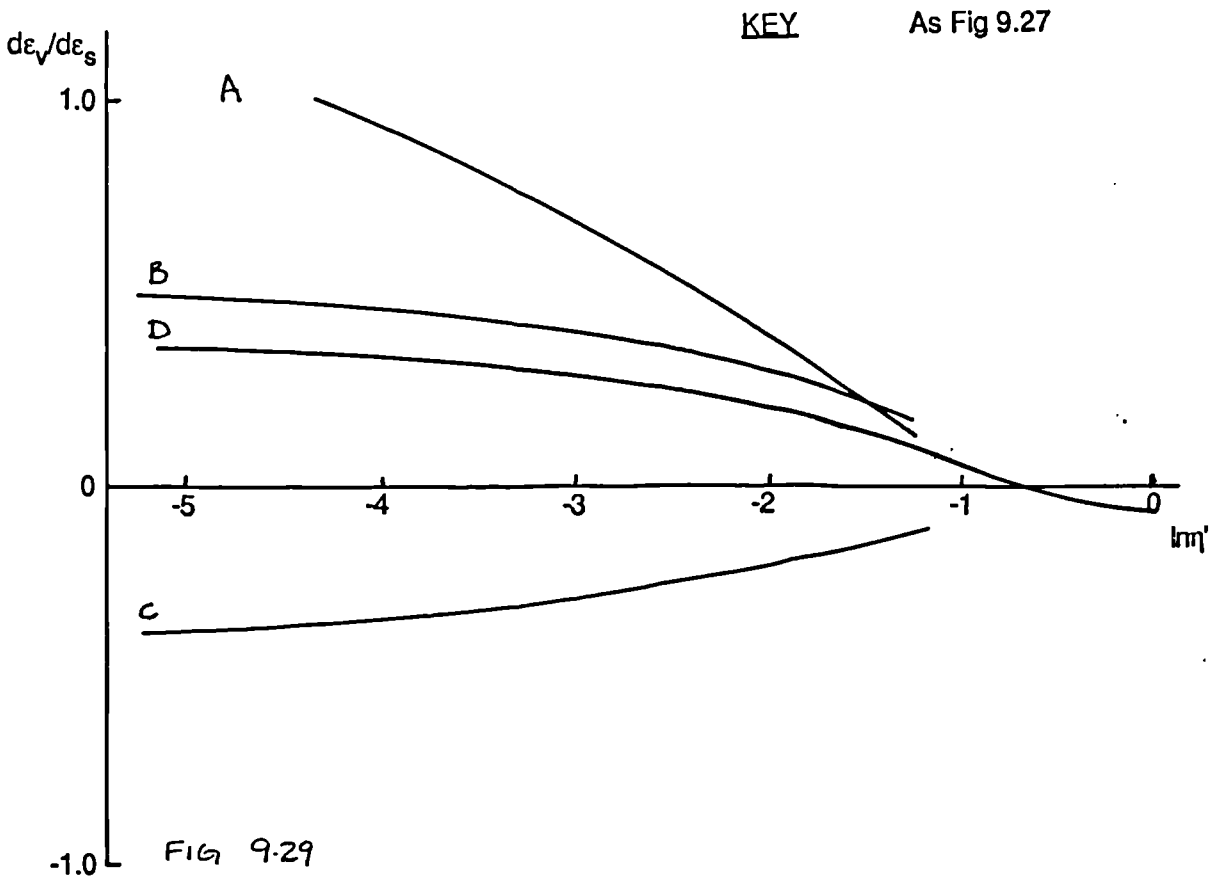

FIG 9.29

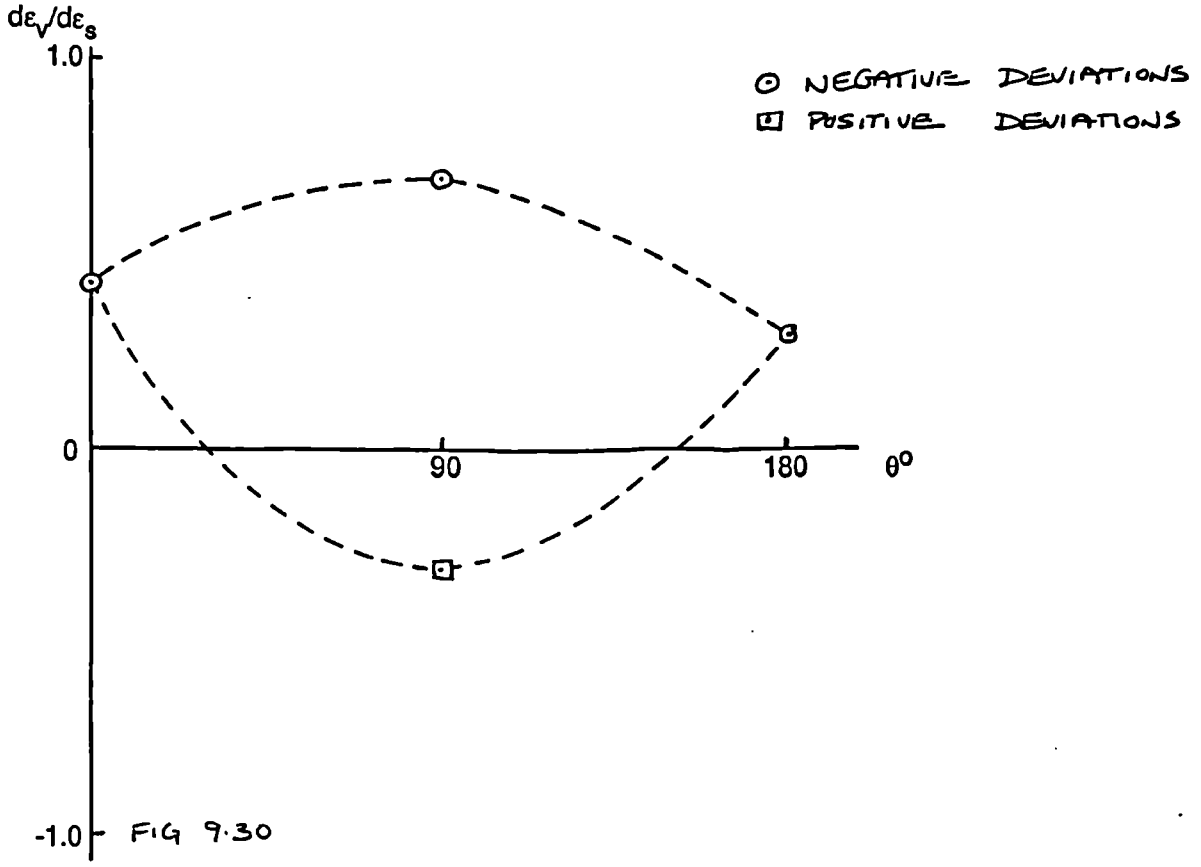

FIG 9.30

Fig 9.29 Plot of total strain increment ratio, $d\varepsilon_v / d\varepsilon_s$, against $\log\Delta\eta'$. London clay , isotropically compressed, OCR = 1.5, p' = 267kPa, constant p' paths.

Fig 9.30 Plot of total strain increment ratio, $d\varepsilon_v / d\varepsilon_s$, against deviation of stress path, θ. London clay , isotropically compressed, OCR = 1.5, p' = 267kPa, constant p' paths.

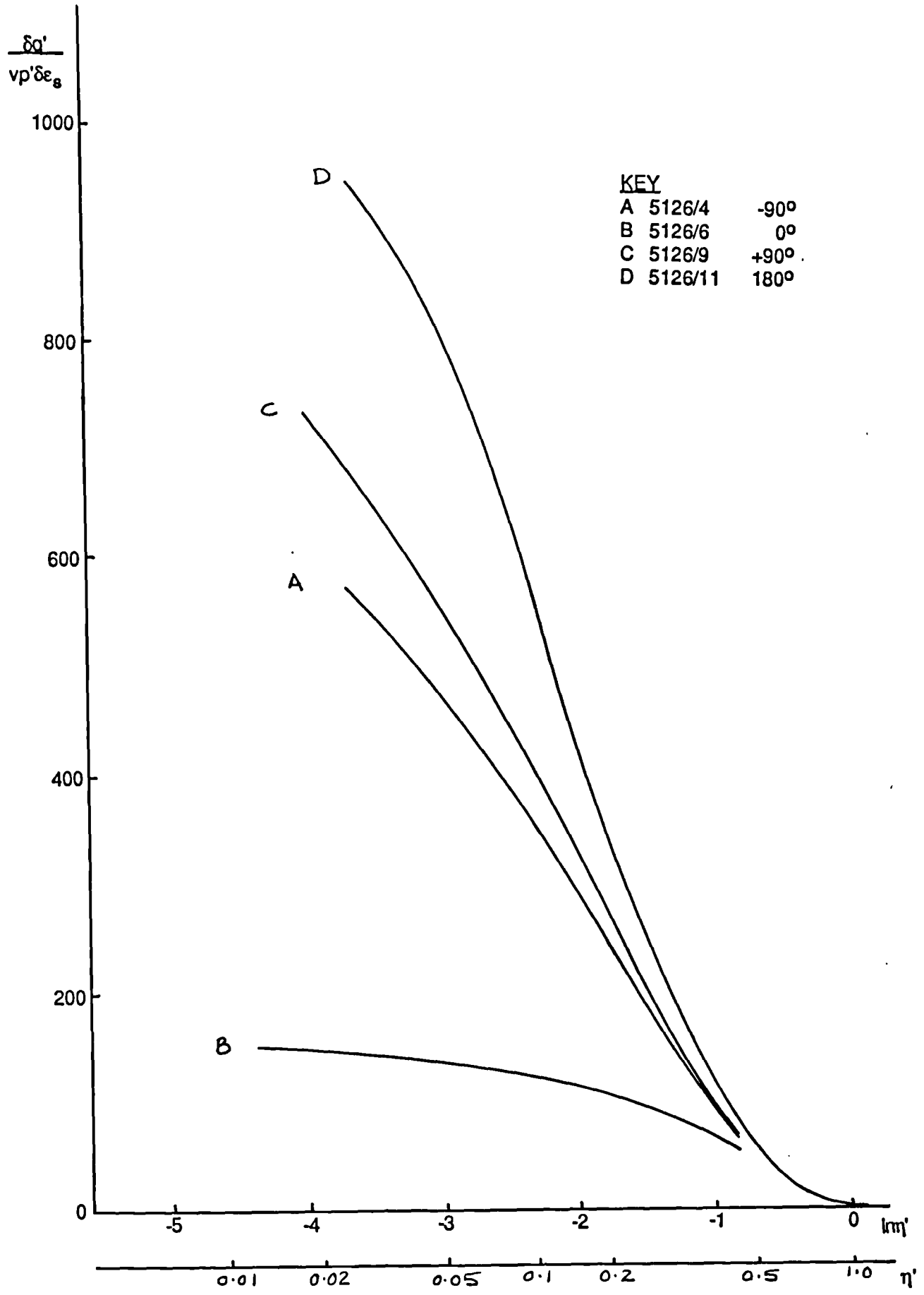

Fig 9.31 Plot of normalised stiffness $\delta q' / vp'\delta\varepsilon_s$ against $\log_e \Delta\eta'$. London clay isotropically compressed, OCR = 4.0, p' = 100 kPa, constant p' paths.

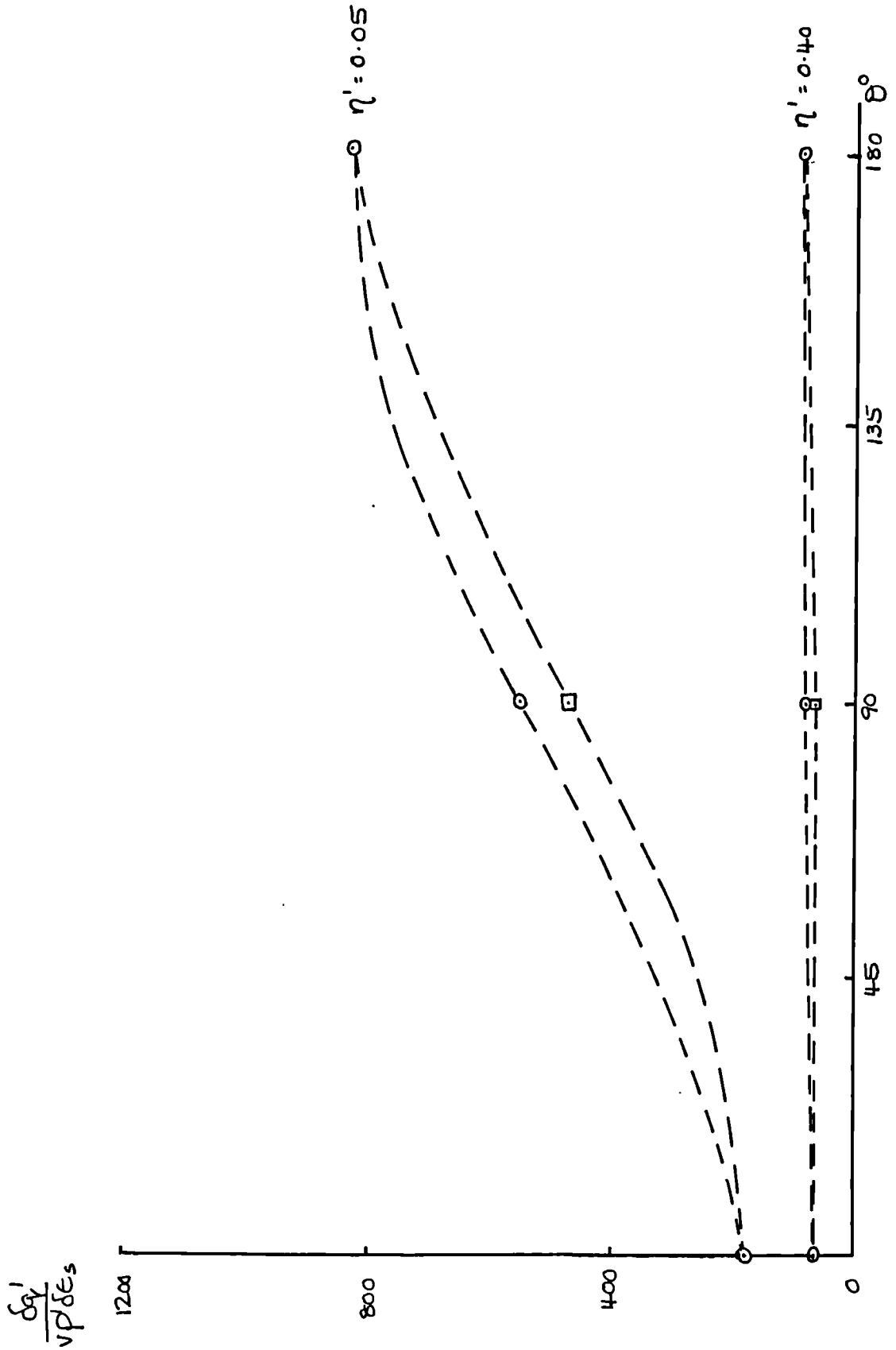

Fig 9.32 Plot of normalised stiffness $\delta q' / vp'\delta\varepsilon_s$ against deviation of stress path, θ. London clay isotropically compressed, OCR = 4.0, p' = 100 kPa, constant p' paths.

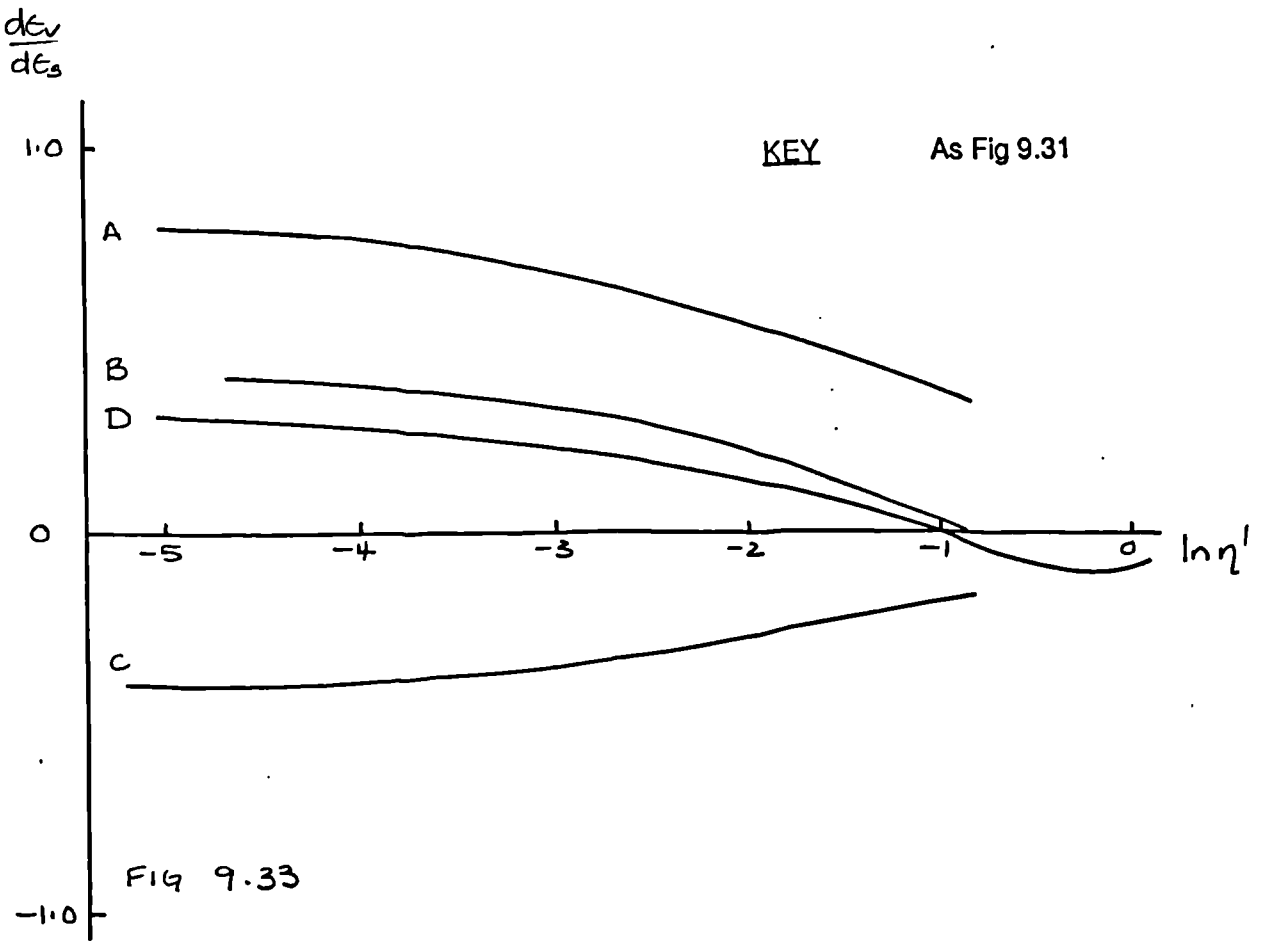

FIG 9.33

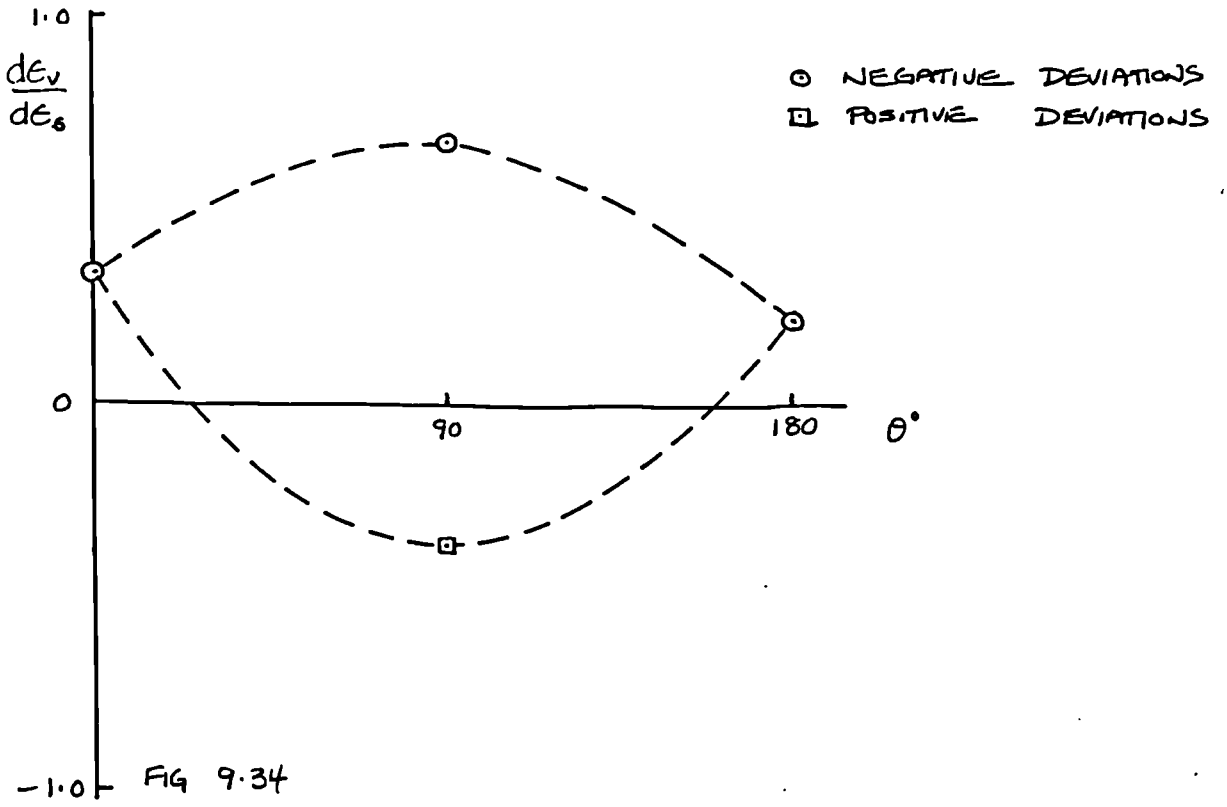

FIG 9.34

Fig 9.33 Plot of total strain increment ratio, $d\varepsilon_v / d\varepsilon_s$, against $\log\Delta\eta'$. London clay , isotropically compressed, OCR = 4.0, p' = 100kPa, constant p' paths.

Fig 9.34 Plot of total strain increment ratio, $d\varepsilon_v / d\varepsilon_s$, against deviation of stress path, θ. London clay , isotropically compressed, OCR = 4.0, p' = 100kPa, constant p' paths.

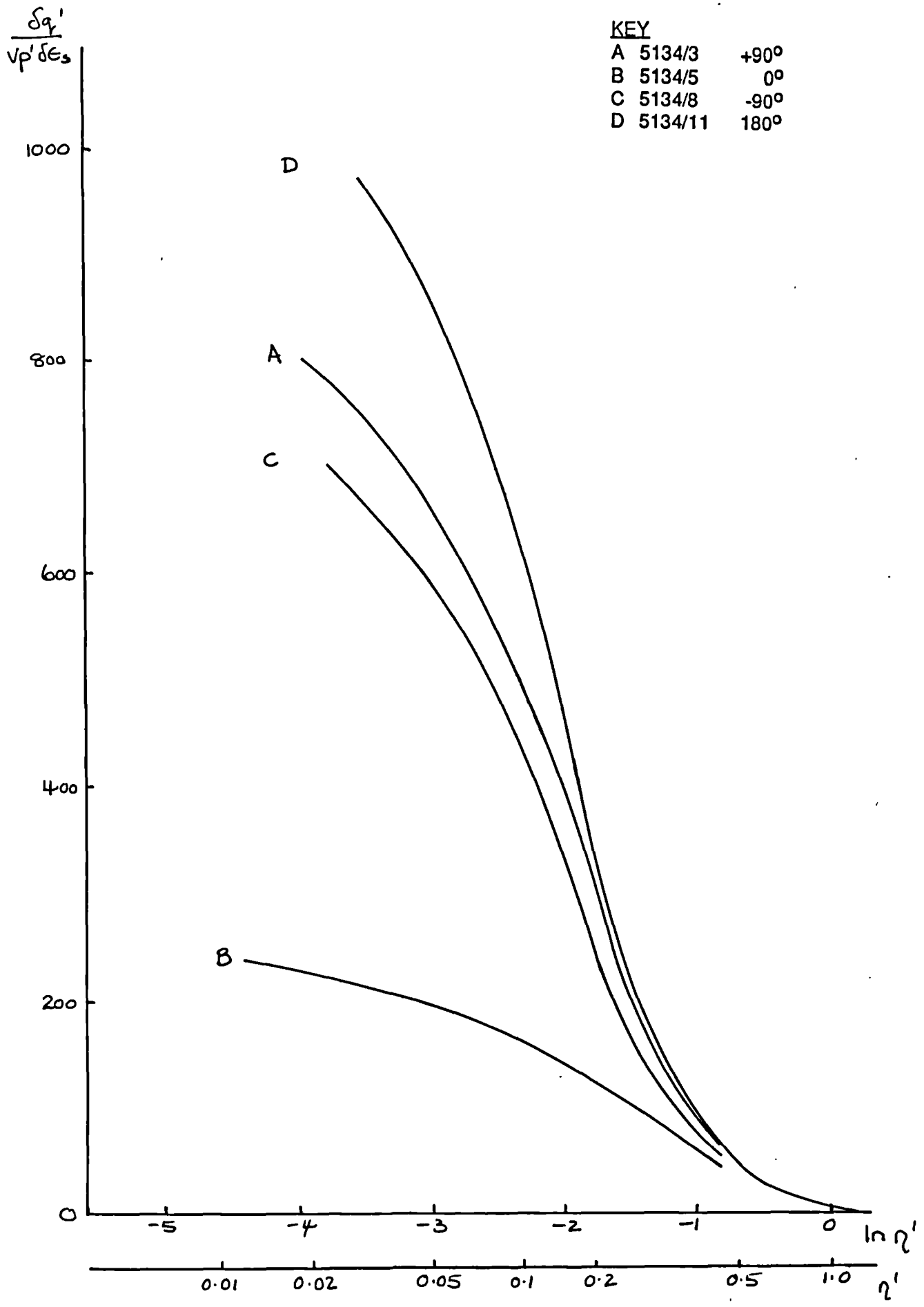

Fig 9.35 Plot of normalised stiffness $\delta q' / vp'\delta\varepsilon_s$ against $\log_e \Delta\eta'$. London clay isotropically compressed, OCR = 8.0, p' = 50 kPa, constant p' paths.

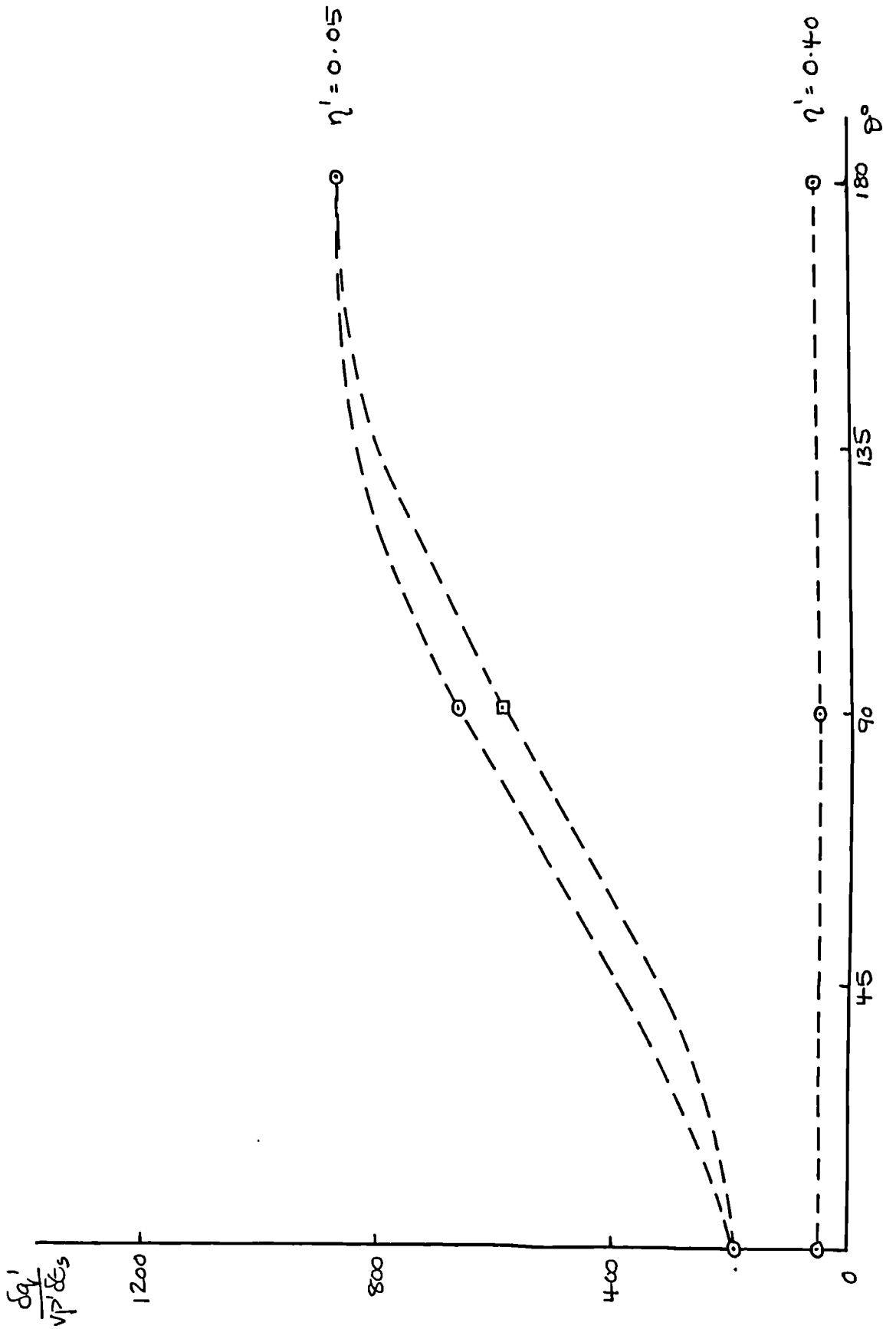

Fig 9.36 Plot of normalised stiffness $\delta q' / vp'\delta\varepsilon_s$ against deviation of stress path, θ. London clay isotropically compressed, OCR = 8.0, p' = 50 kPa, constant p' paths.

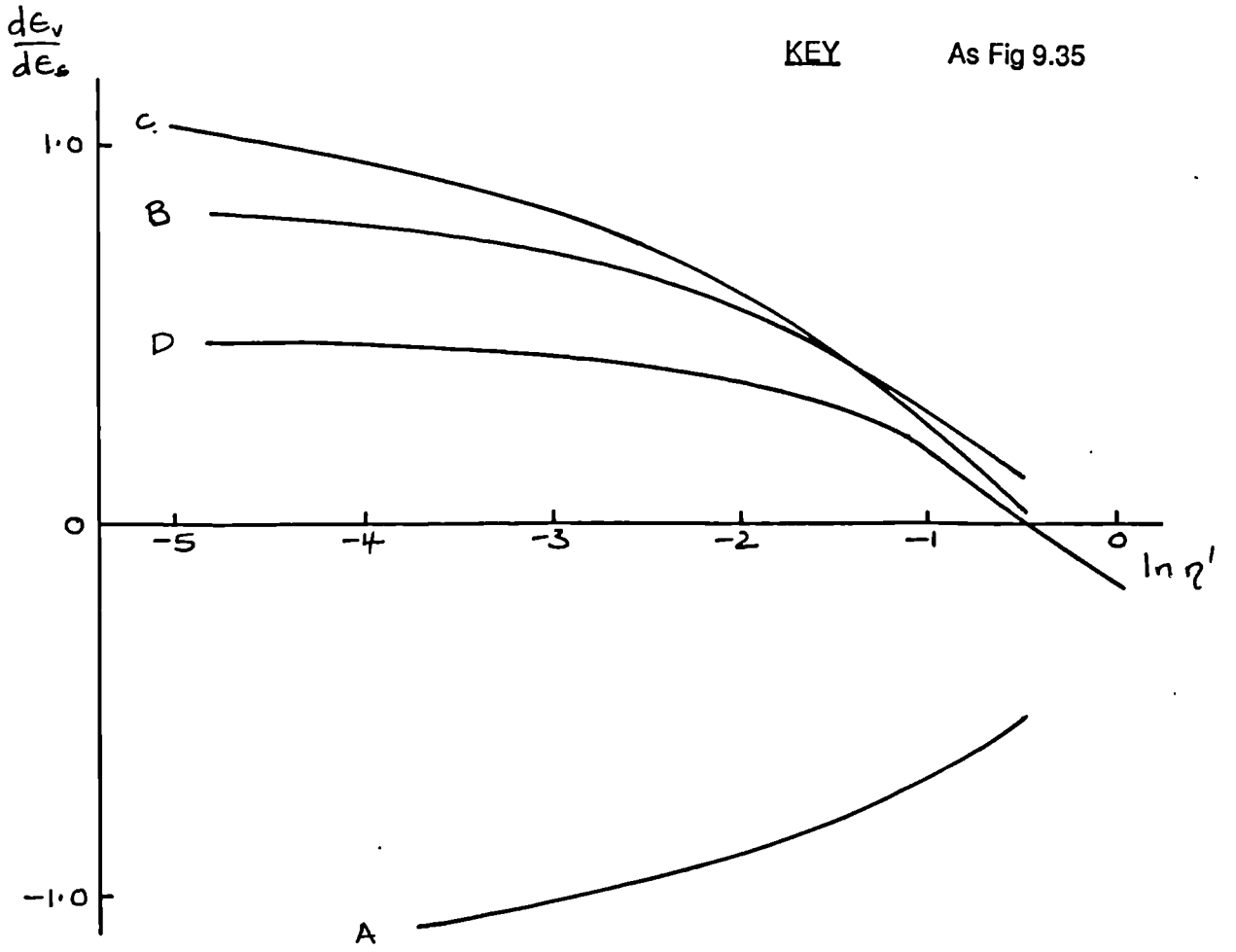

FIG 9.37

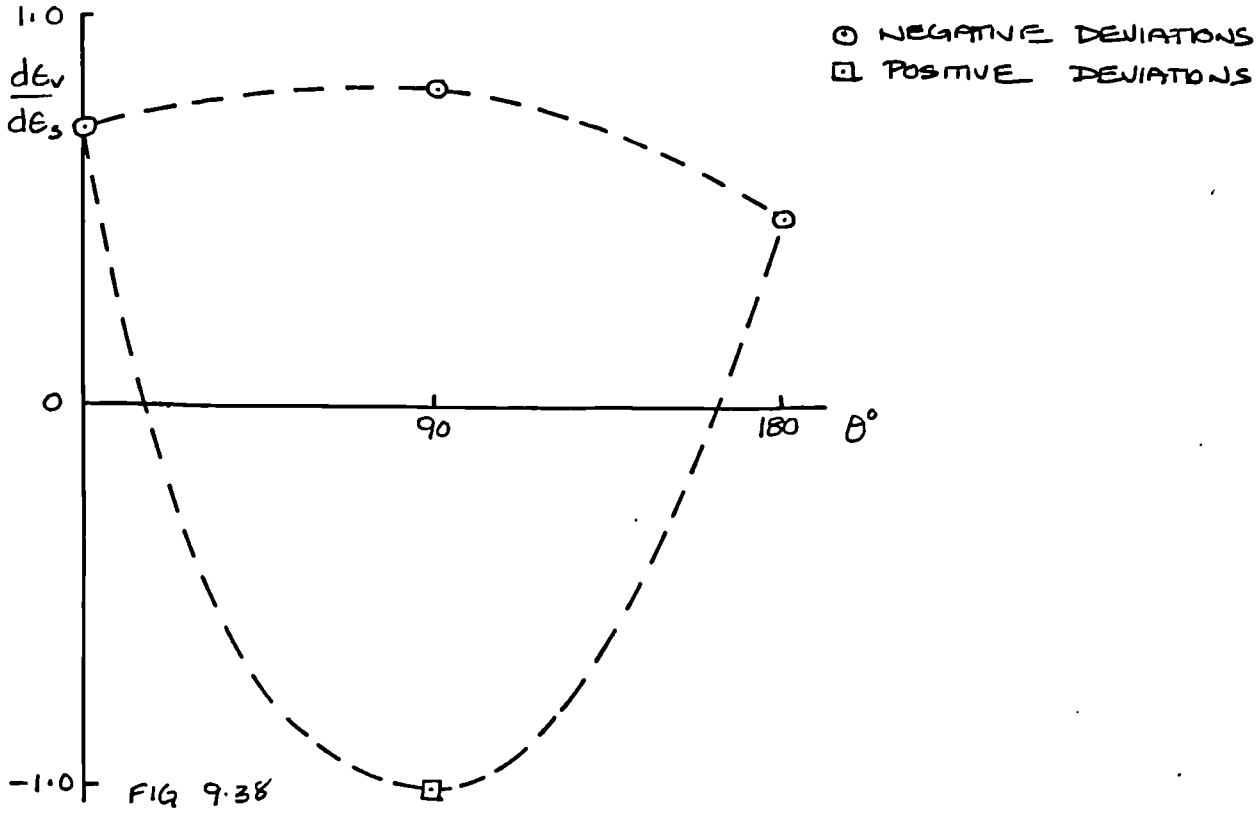

FIG 9.38

Fig 9.37 Plot of total strain increment ratio, $d\varepsilon_v / d\varepsilon_s$, against $\log\Delta\eta'$. London clay , isotropically compressed, OCR = 8.0, p' = 50kPa, constant p' paths.

Fig 9.38 Plot of total strain increment ratio, $d\varepsilon_v / d\varepsilon_s$, against deviation of stress path, θ. London clay , isotropically compressed, OCR = 8.0, p' = 50kPa, constant p' paths.

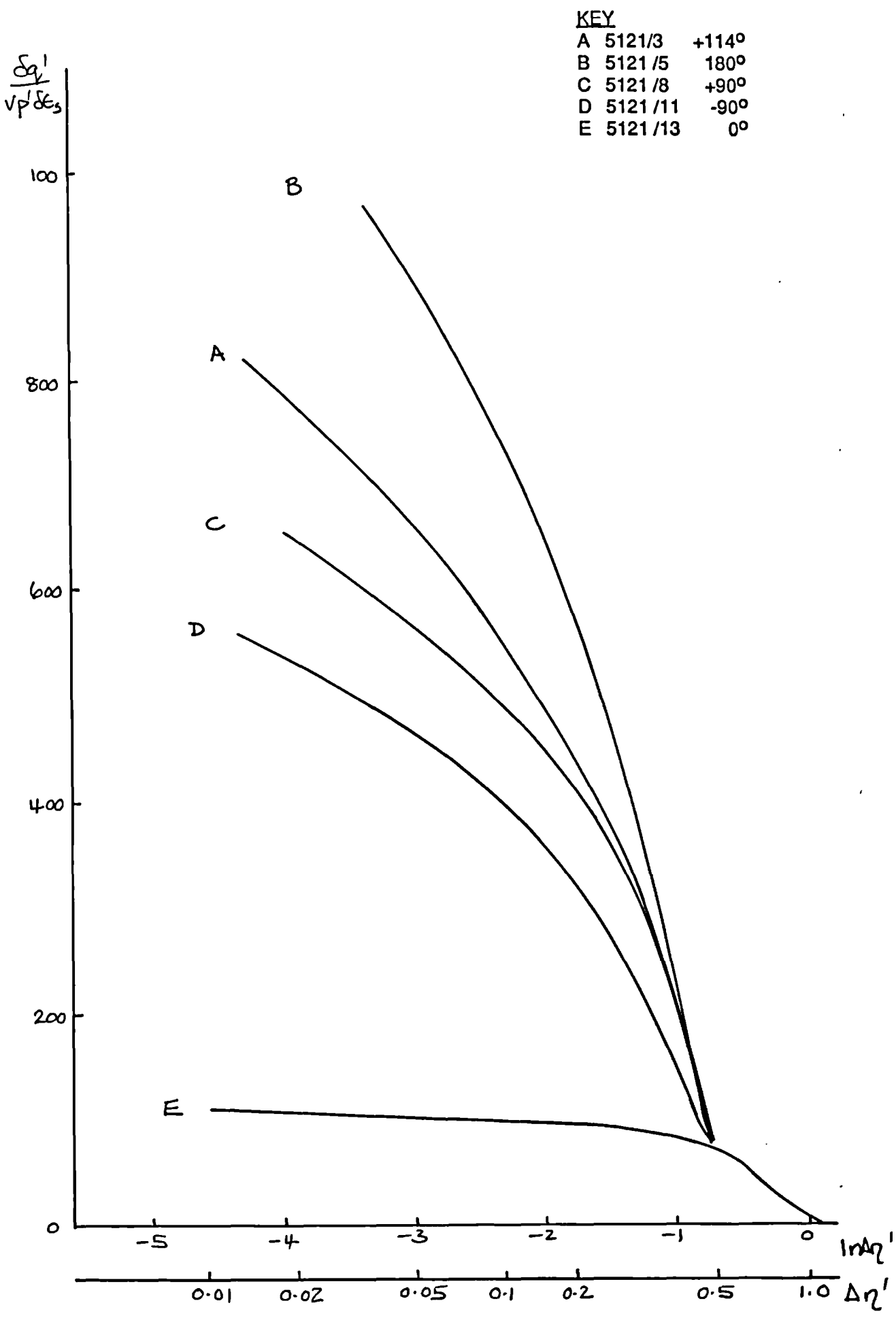

Fig 9.39 Plot of normalised stiffness $\delta q' / vp'\delta\varepsilon_s$ against $\log_e \Delta\eta'$. London clay, $\eta'_o = 0.25$, OCR = 2.0, p' = 200 kPa, constant p' paths.

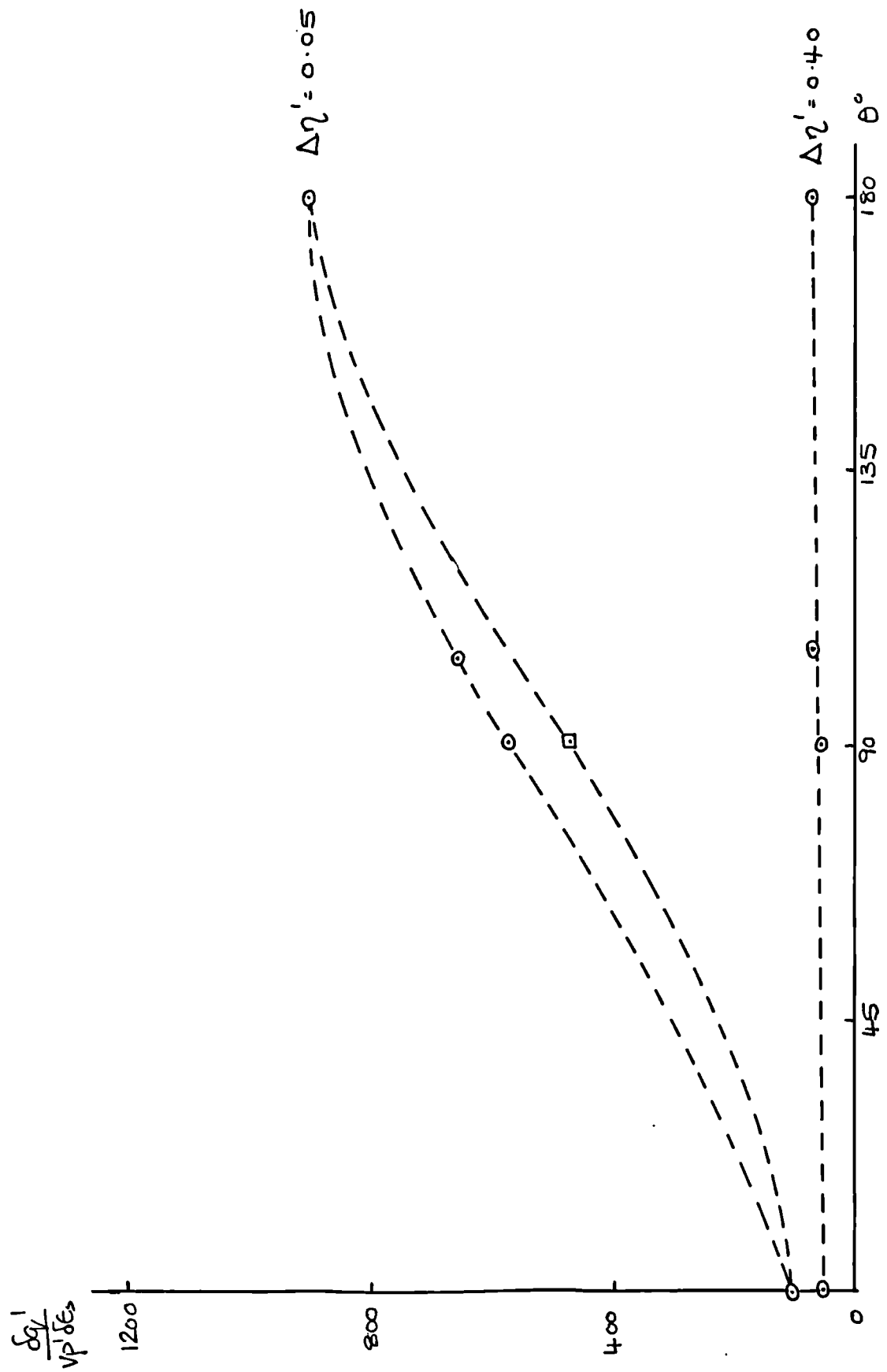

Fig 9.40 Plot of normalised stiffness $\delta q' / vp'\delta\varepsilon_s$ against deviation of stress path, θ. London clay, $\eta'_o = 0.25$, OCR = 2.0, p' = 200 kPa, constant p' paths.

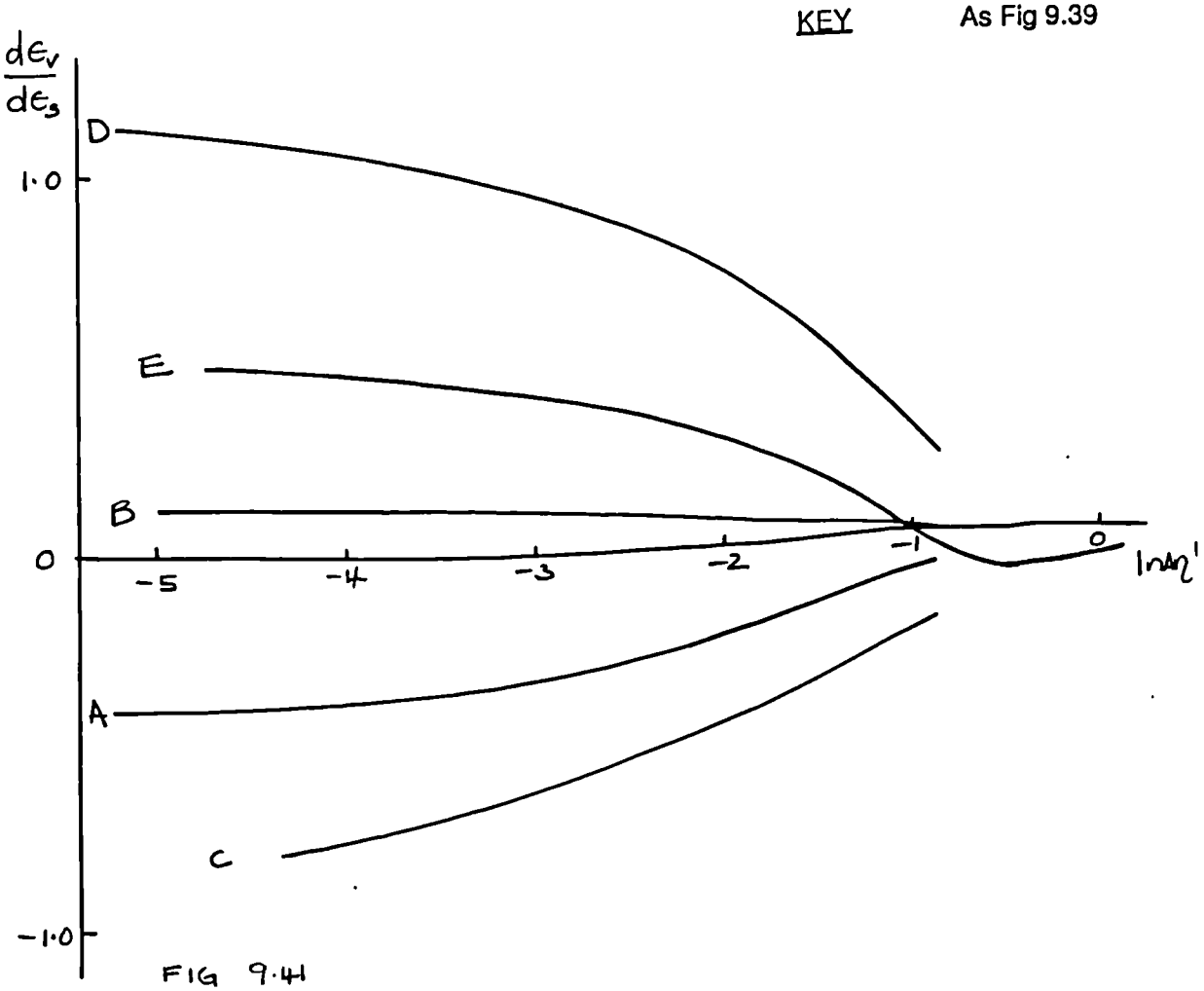

FIG 9.41

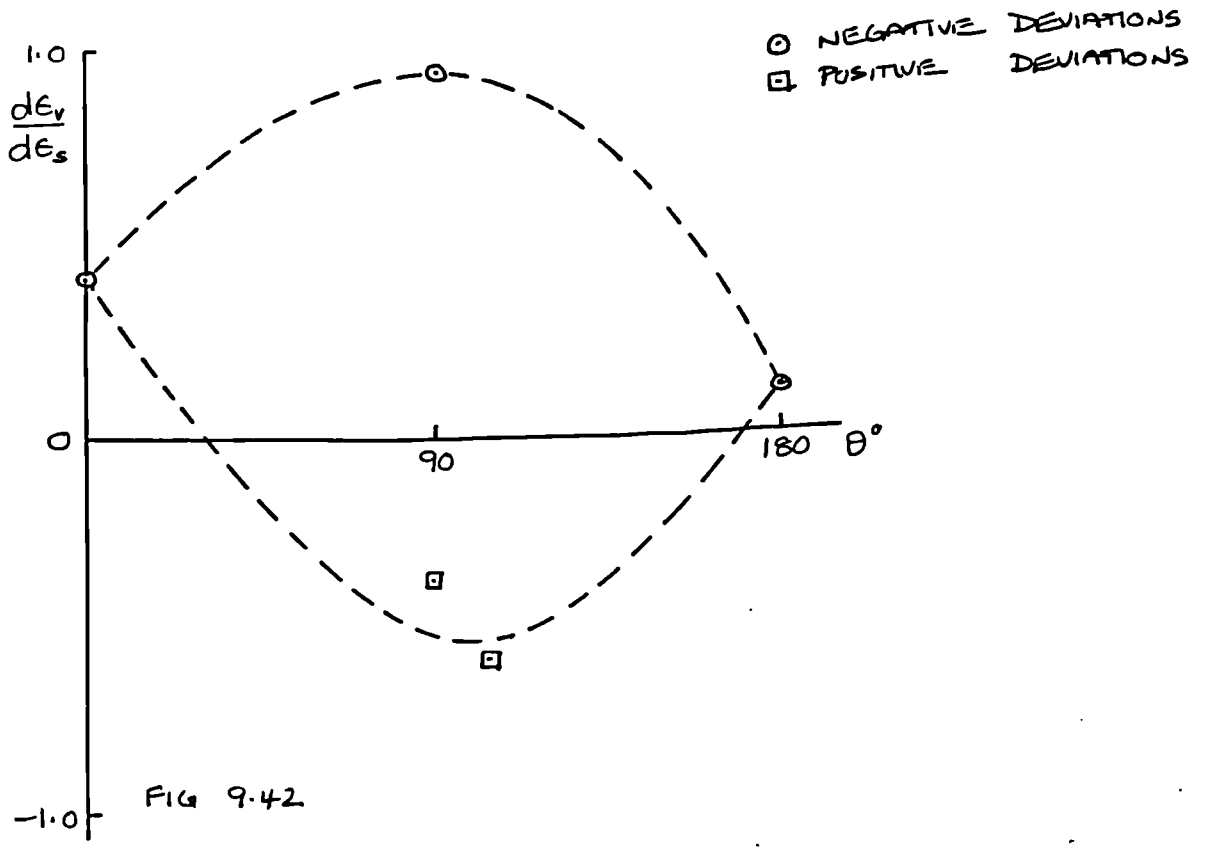

FIG 9.42

Fig 9.41 Plot of total strain increment ratio, $d\varepsilon_v / d\varepsilon_s$, against $\log\Delta\eta'$. London clay, $\eta'_o = 0.25$, OCR = 2.0, p' = 200kPa, constant p' paths.

Fig 9.42 Plot of total strain increment ratio, $d\varepsilon_v / d\varepsilon_s$, against deviation of stress path, θ. London clay, $\eta'_o = 0.25$, OCR = 2.0, p' = 200kPa, constant p' paths.

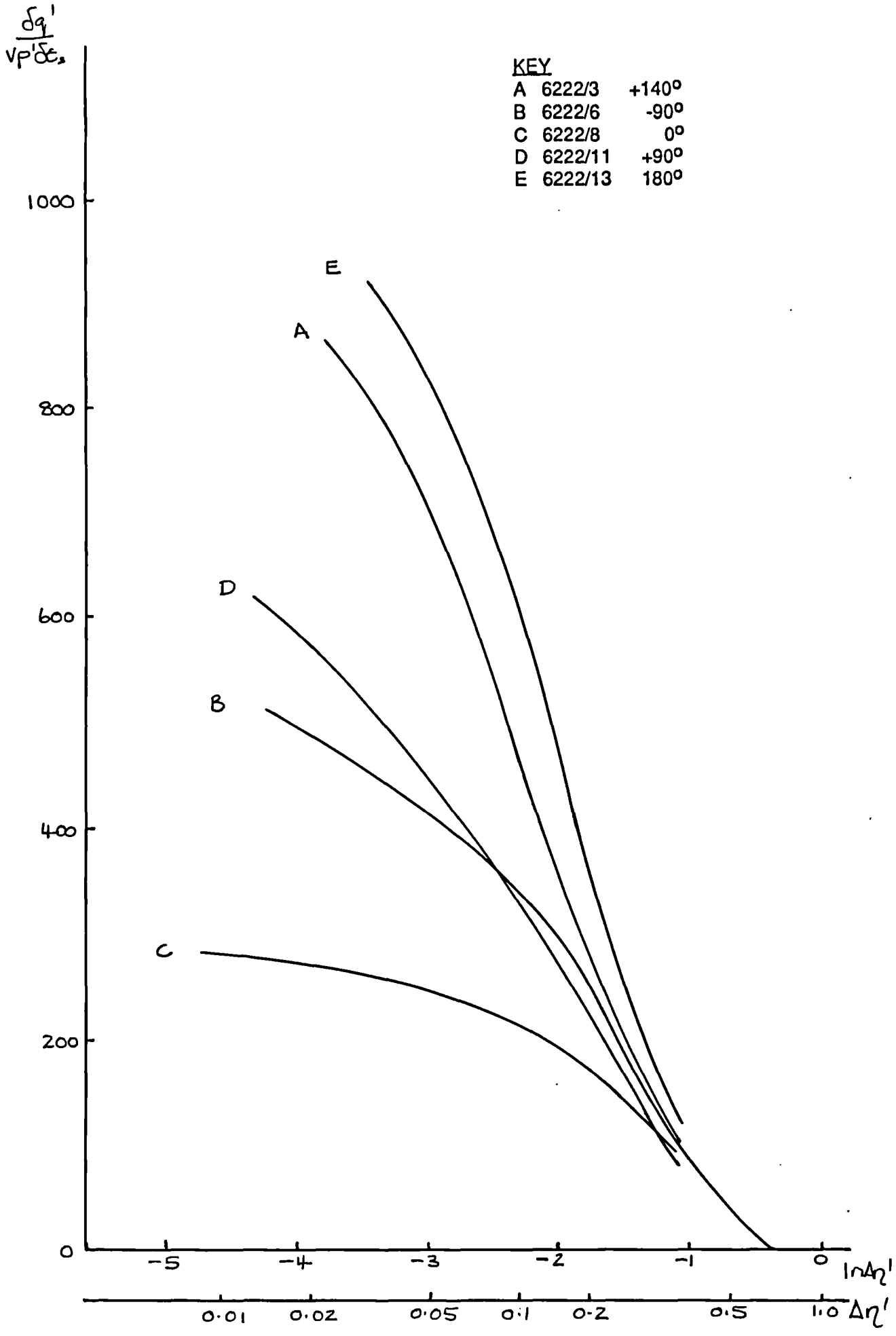

Fig 9.43 Plot of normalised stiffness $\delta q' / vp'\delta\varepsilon_s$ against $\log_e \Delta\eta'$. London clay one dimensionally compressed, OCR = 1.5, p' = 267 kPa, constant p' paths.

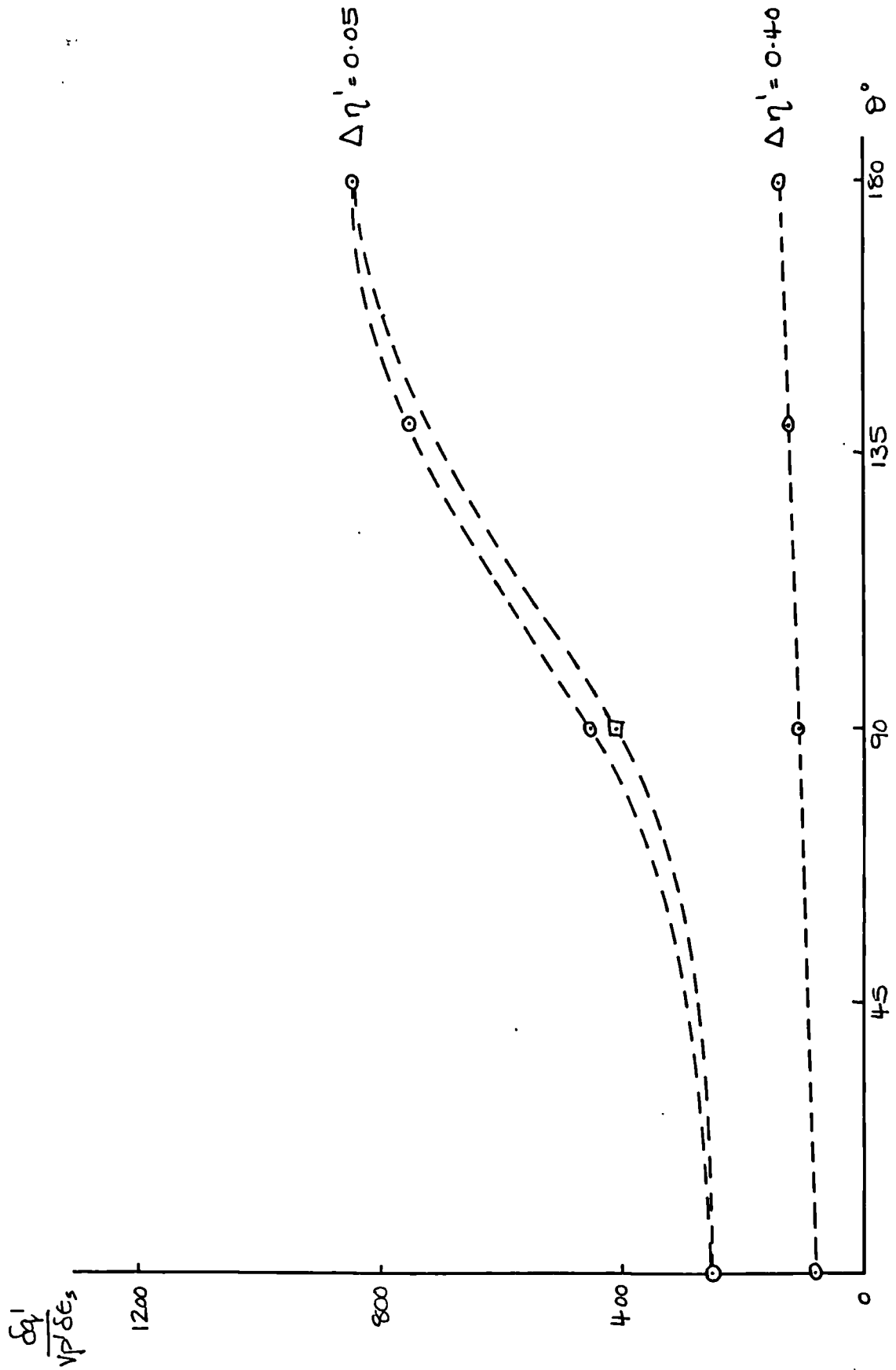

Fig 9.44 Plot of normalised stiffness $\delta q' / vp'\delta\varepsilon_s$ against deviation of stress path, θ. London clay one dimensionally compressed, OCR = 1.5, p' = 267kPa, constant p' paths.

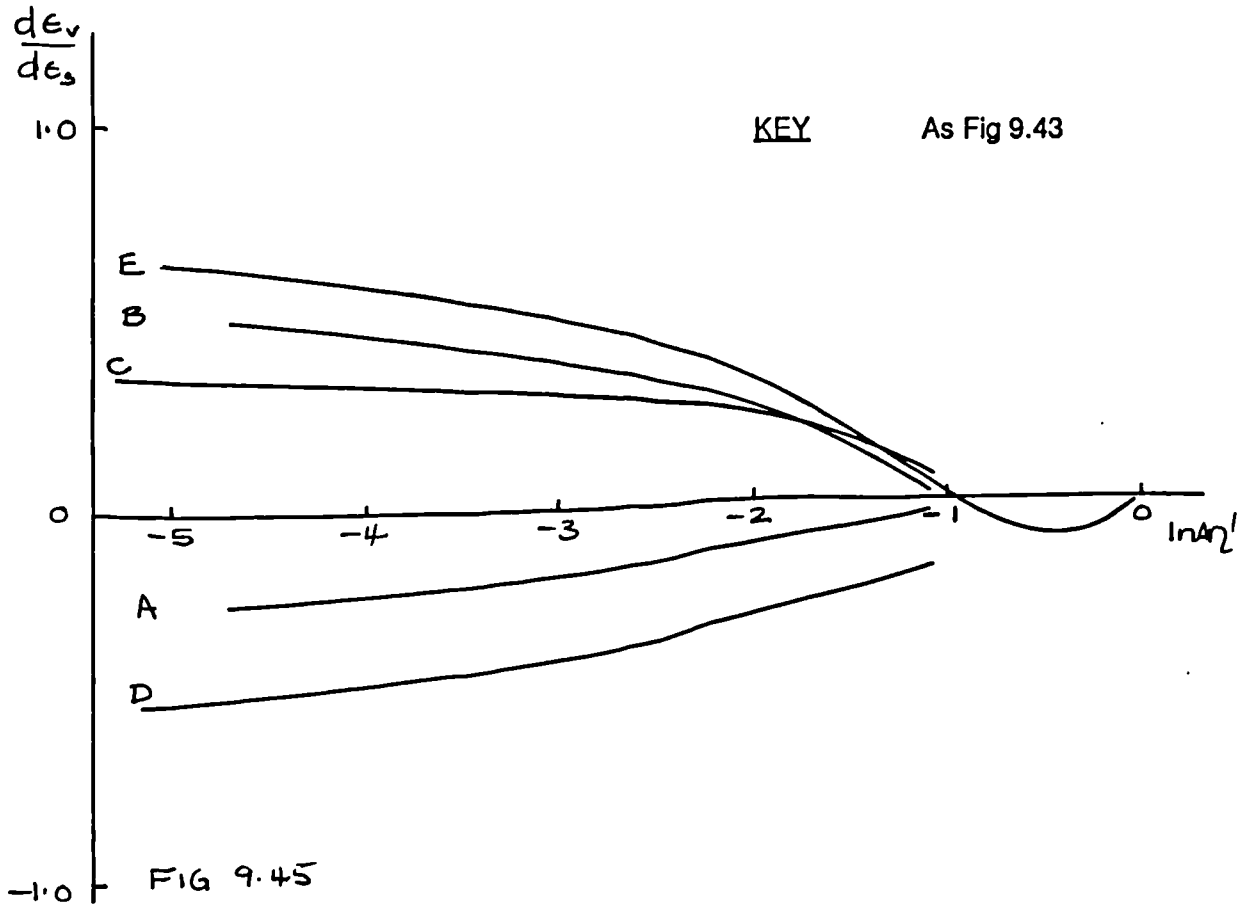

FIG 9.45

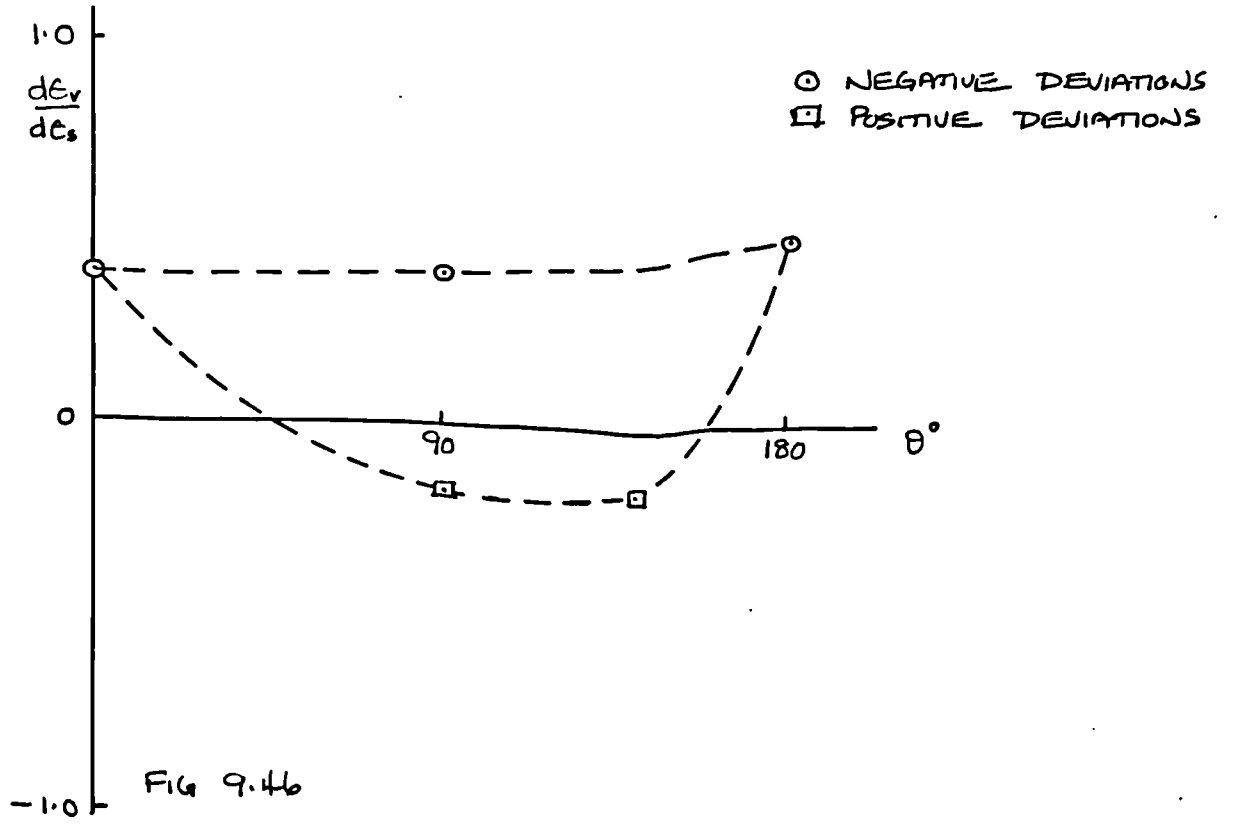

FIG 9.46

Fig 9.45 Plot of total strain increment ratio, $d\varepsilon_v / d\varepsilon_s$, against $\log\Delta\eta'$. London clay , one dimensionally compressed, OCR = 1.5, p' = 267kPa, constant p' paths.

Fig 9.46 Plot of total strain increment ratio, $d\varepsilon_v / d\varepsilon_s$, against deviation of stress path, θ. London clay , isotropically compressed, OCR = 1.5, p' = 267kPa, constant p' paths.

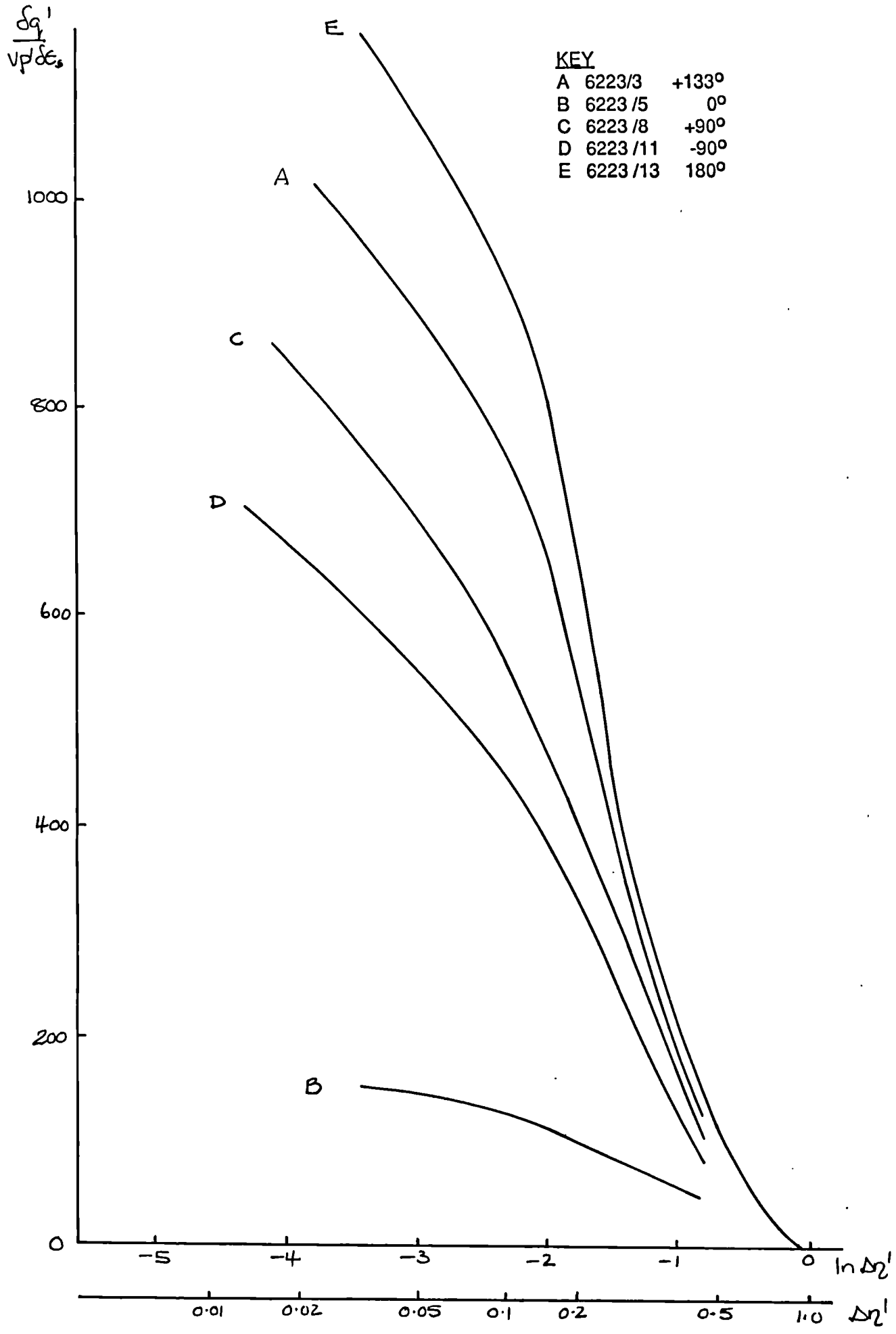

Fig 9.47 Plot of normalised stiffness $\delta q' / vp'\delta\varepsilon_s$ against $\log_e \Delta\eta'$. London clay one dimensionally compressed, OCR = 2.0, p' = 200 kPa, constant p' paths.

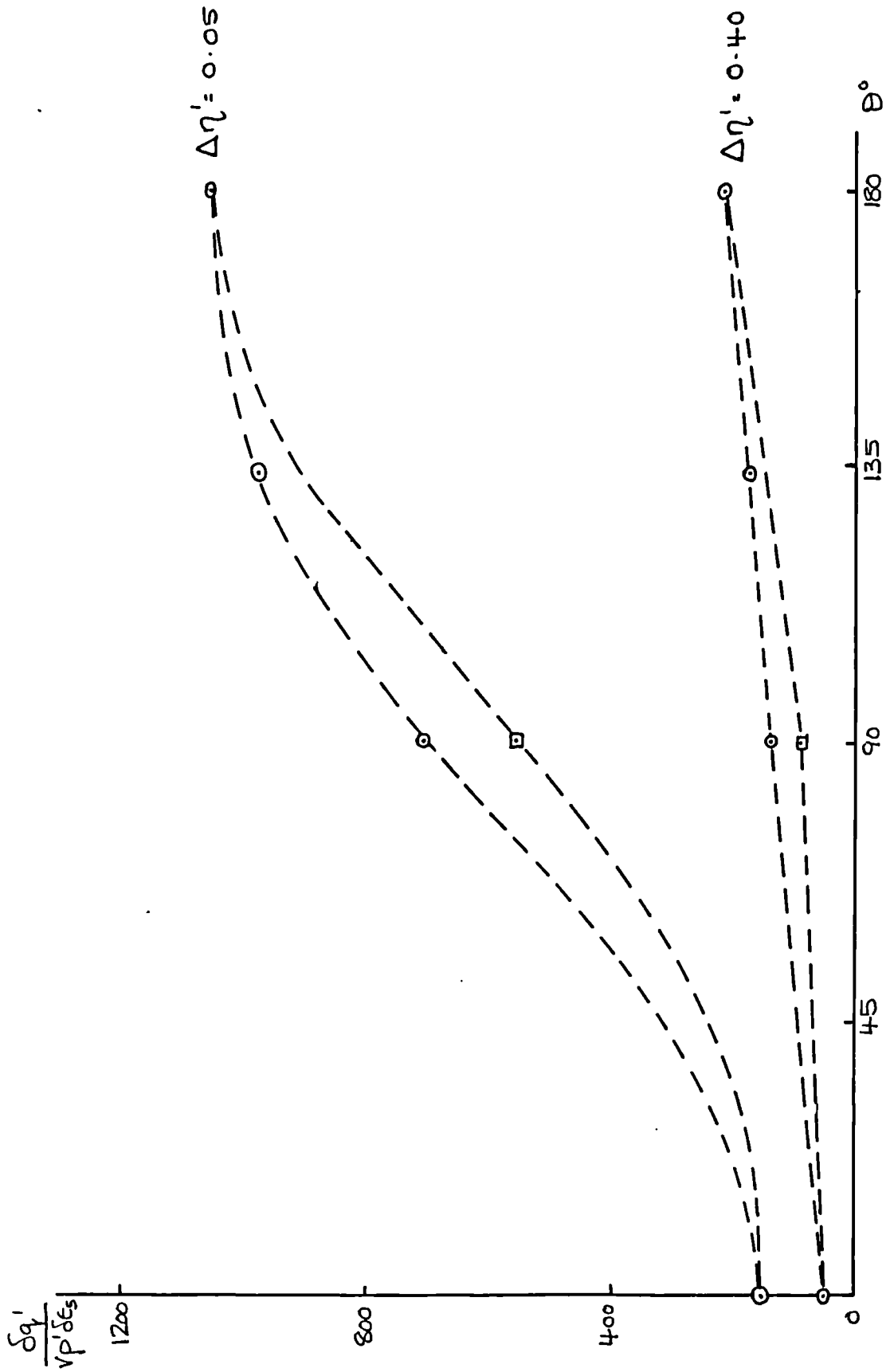

Fig 9.48 Plot of normalised stiffness $\delta q' / vp'\delta\varepsilon_s$ against deviation of stress path, θ. London clay one dimensionally compressed, OCR = 2.0, p' = 200kPa, constant p' paths.

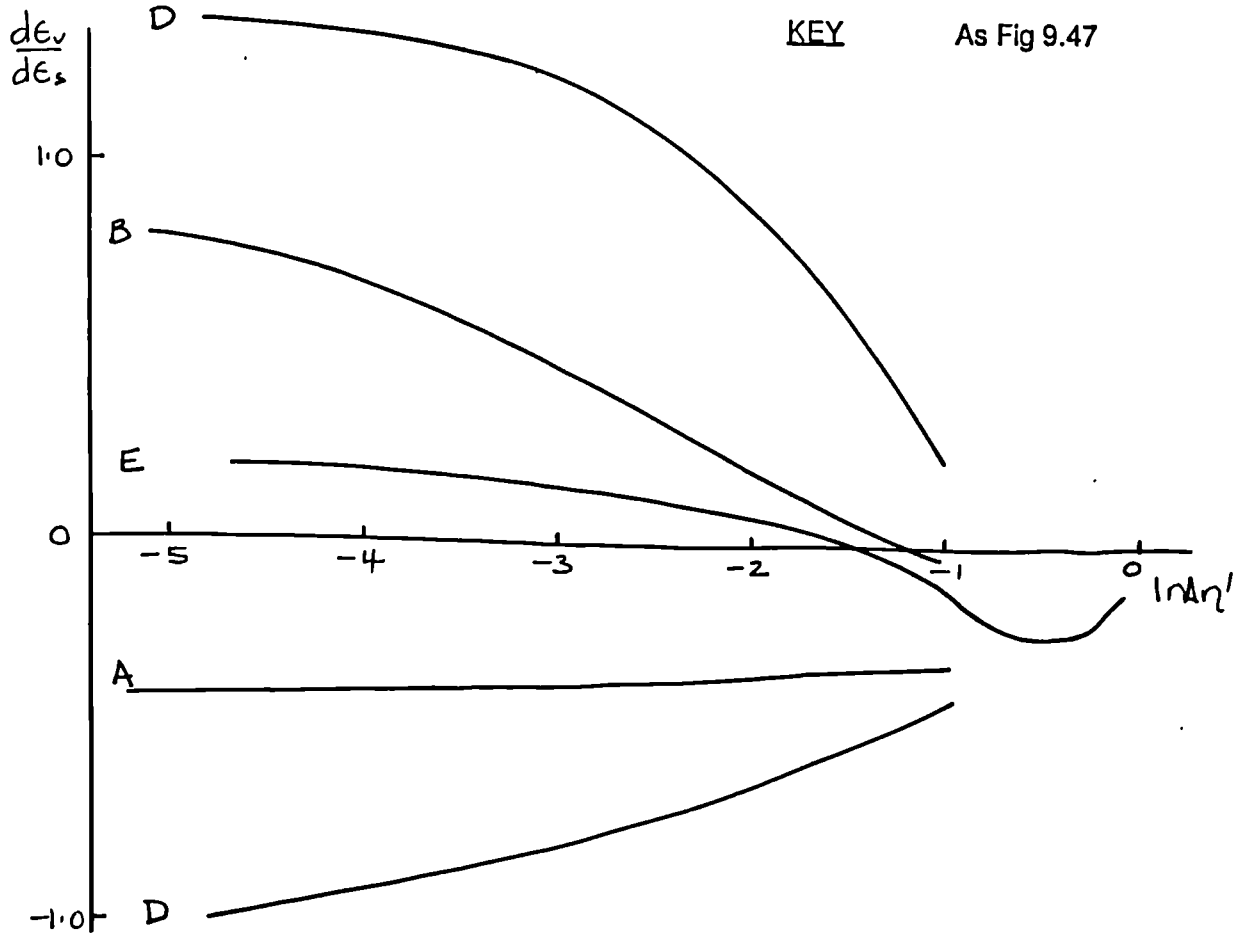

FIG 9.49

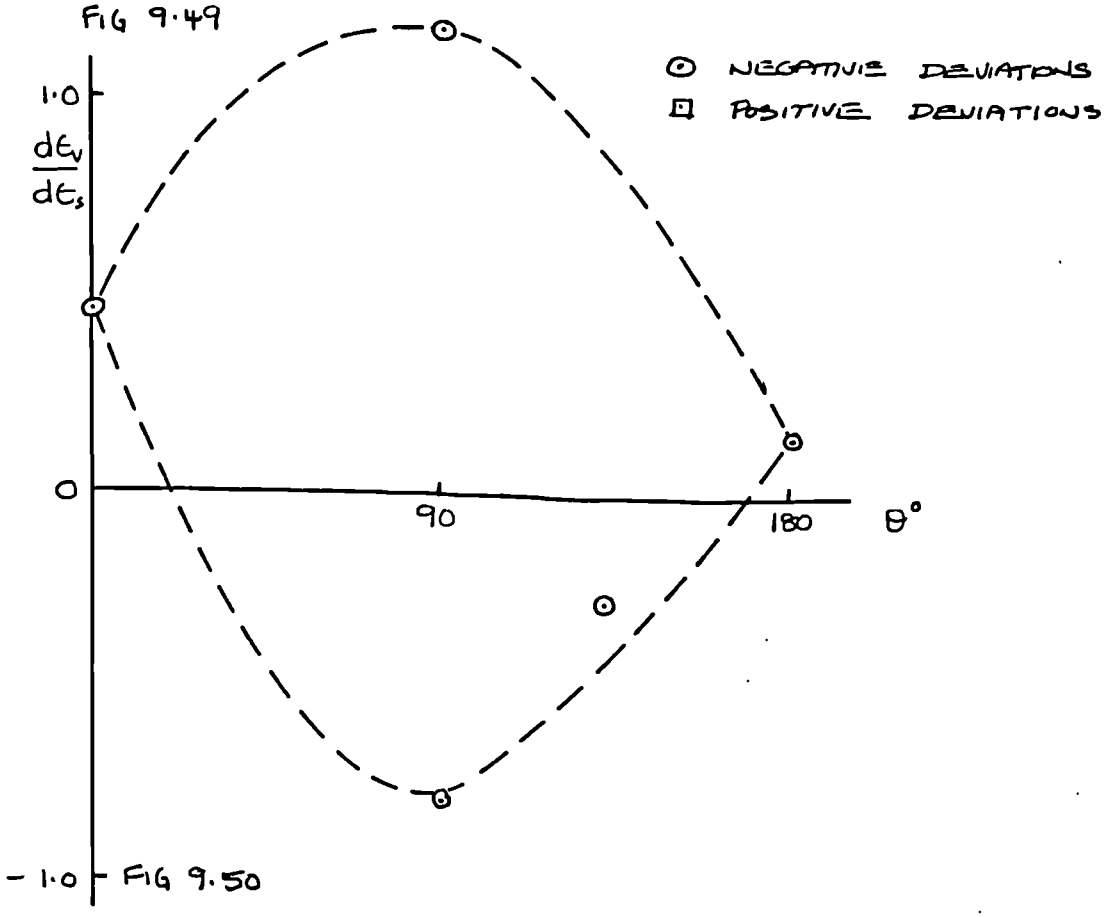

FIG 9.50

Fig 9.49 Plot of total strain increment ratio, $d\varepsilon_v / d\varepsilon_s$, against $\log\Delta\eta'$. London clay , one dimensionally compressed, OCR = 2.0, p' = 200kPa, constant p' paths.

Fig 9.50 Plot of total strain increment ratio, $d\varepsilon_v / d\varepsilon_s$, against deviation of stress path, θ. London clay , isotropically compressed, OCR = 2.0, p' = 200kPa, constant p' paths.

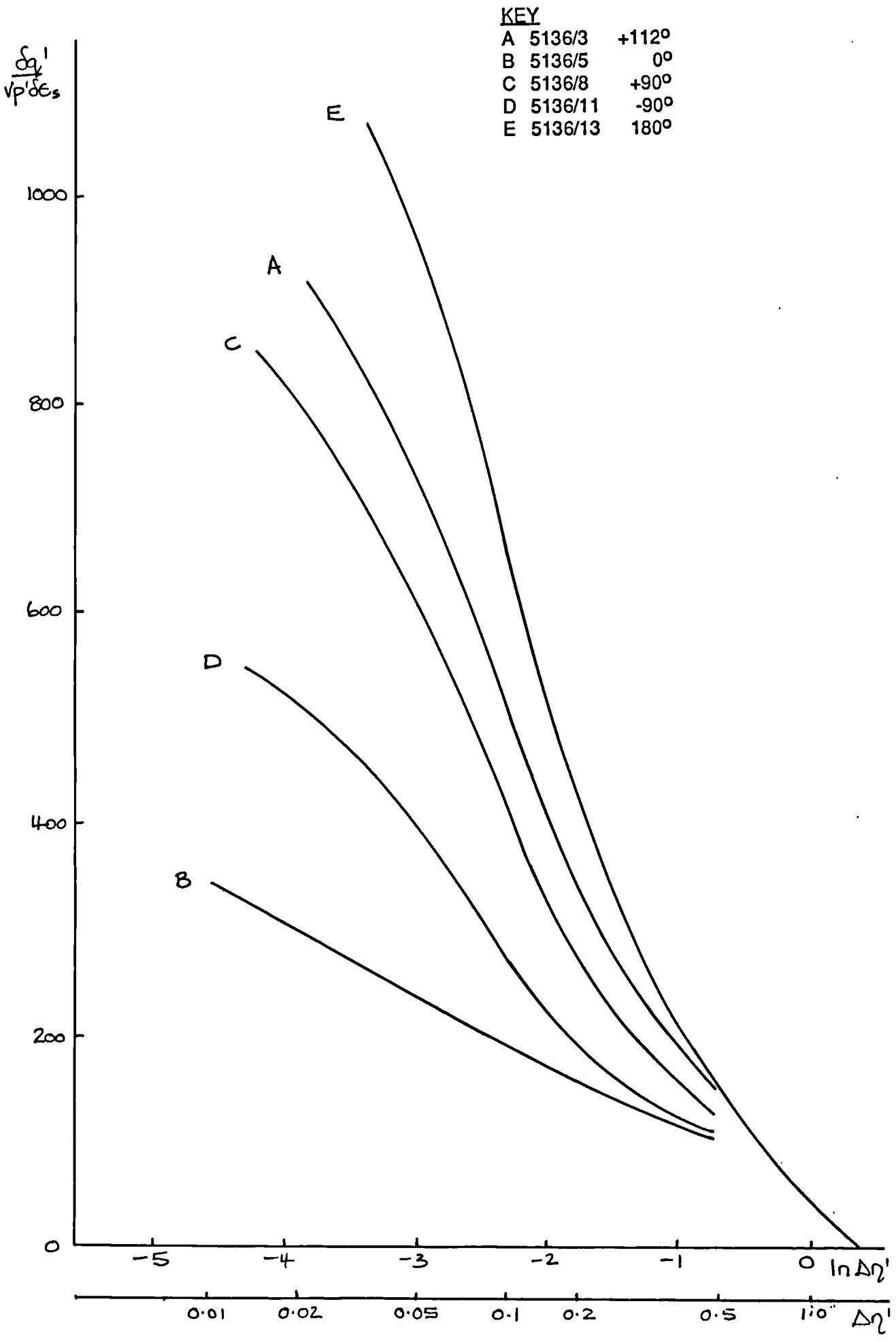

Fig 9.51 Plot of normalised stiffness $\delta q' / vp'\delta\varepsilon_s$ against $\log_e \Delta\eta'$. London clay one dimensionally compressed, OCR = 4.0, p' = 100 kPa, constant p' paths.

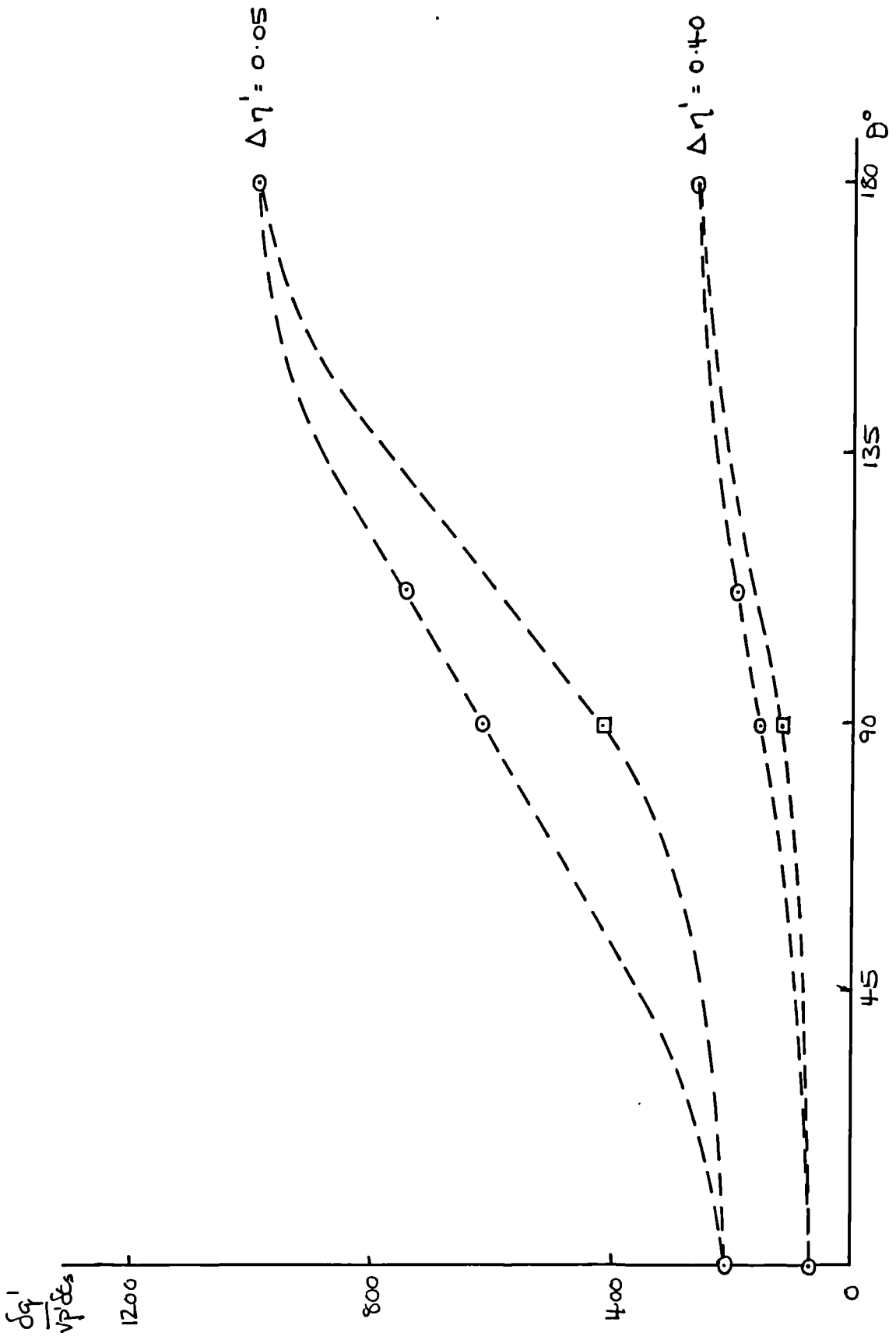

Fig 9.52 Plot of normalised stiffness $\delta q' / vp'\delta\varepsilon_s$ against deviation of stress path, θ. London clay one dimensionally compressed, OCR = 4.0, p' = 100kPa, constant p' paths.

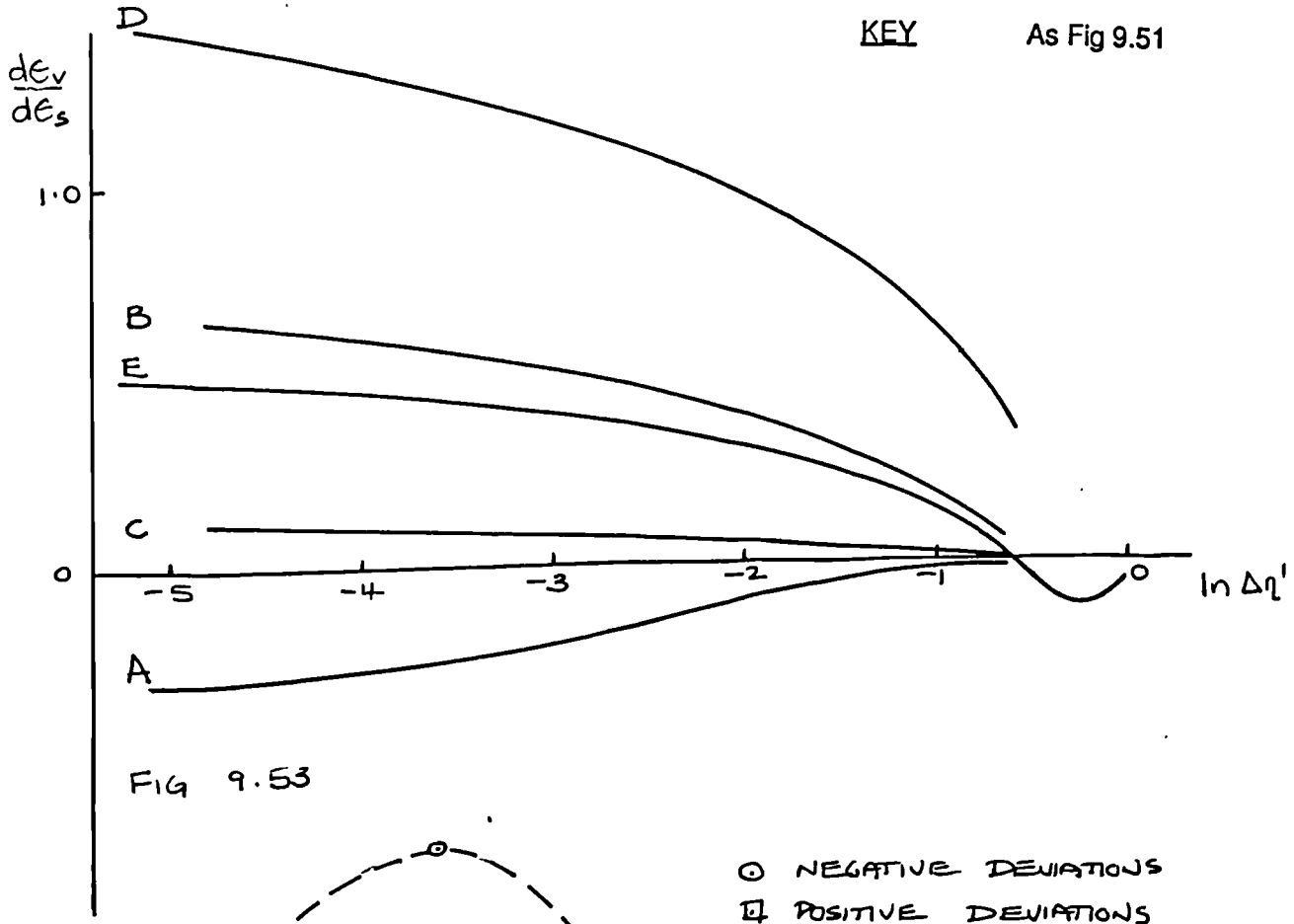

FIG 9.53

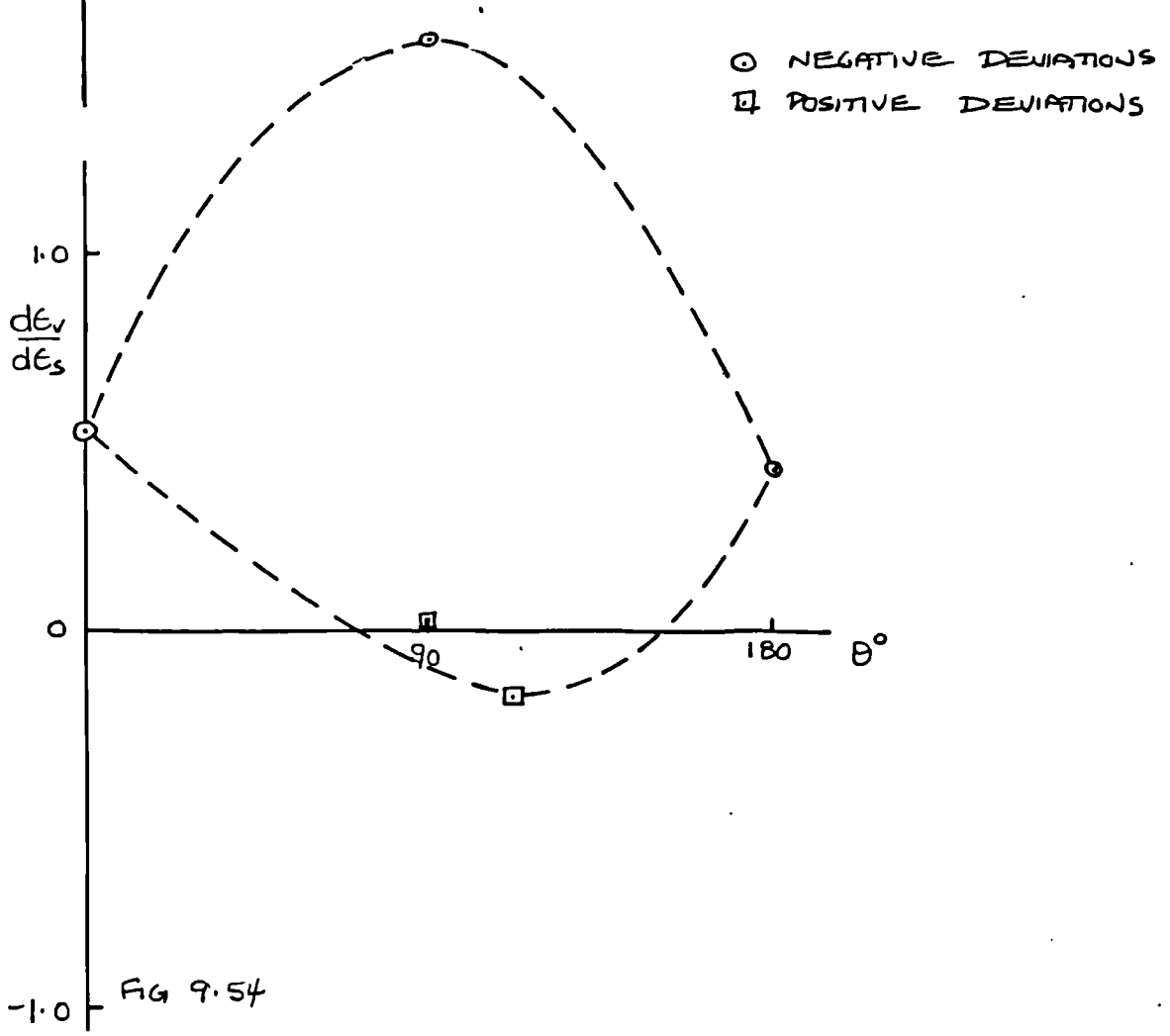

FIG 9.54

Fig 9.53 Plot of total strain increment ratio, $d\varepsilon_v / d\varepsilon_s$, against $\log\Delta\eta'$. London clay , one dimensionally compressed, OCR = 4.0, p' = 100kPa, constant p' paths.

Fig 9.54 Plot of total strain increment ratio, $d\varepsilon_v / d\varepsilon_s$, against deviation of stress path, θ. London clay , isotropically compressed, OCR = 4.0, p' = 100kPa, constant p' paths.

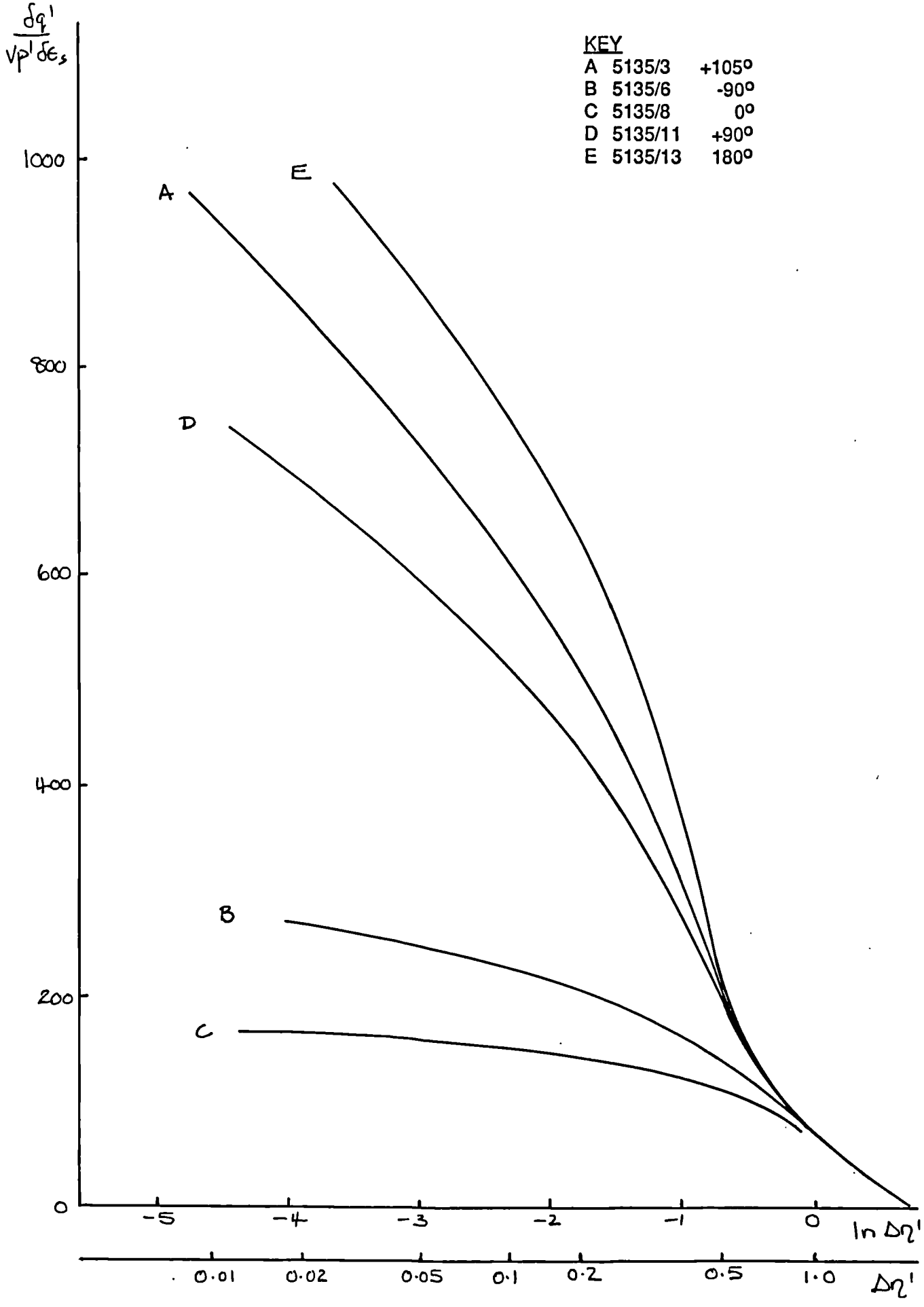

Fig 9.55 Plot of normalised stiffness $\delta q' / vp'\delta\varepsilon_s$ against $\log_e \Delta\eta'$. London clay one dimensionally compressed, OCR = 8.0, p' = 50kPa, constant p' paths.

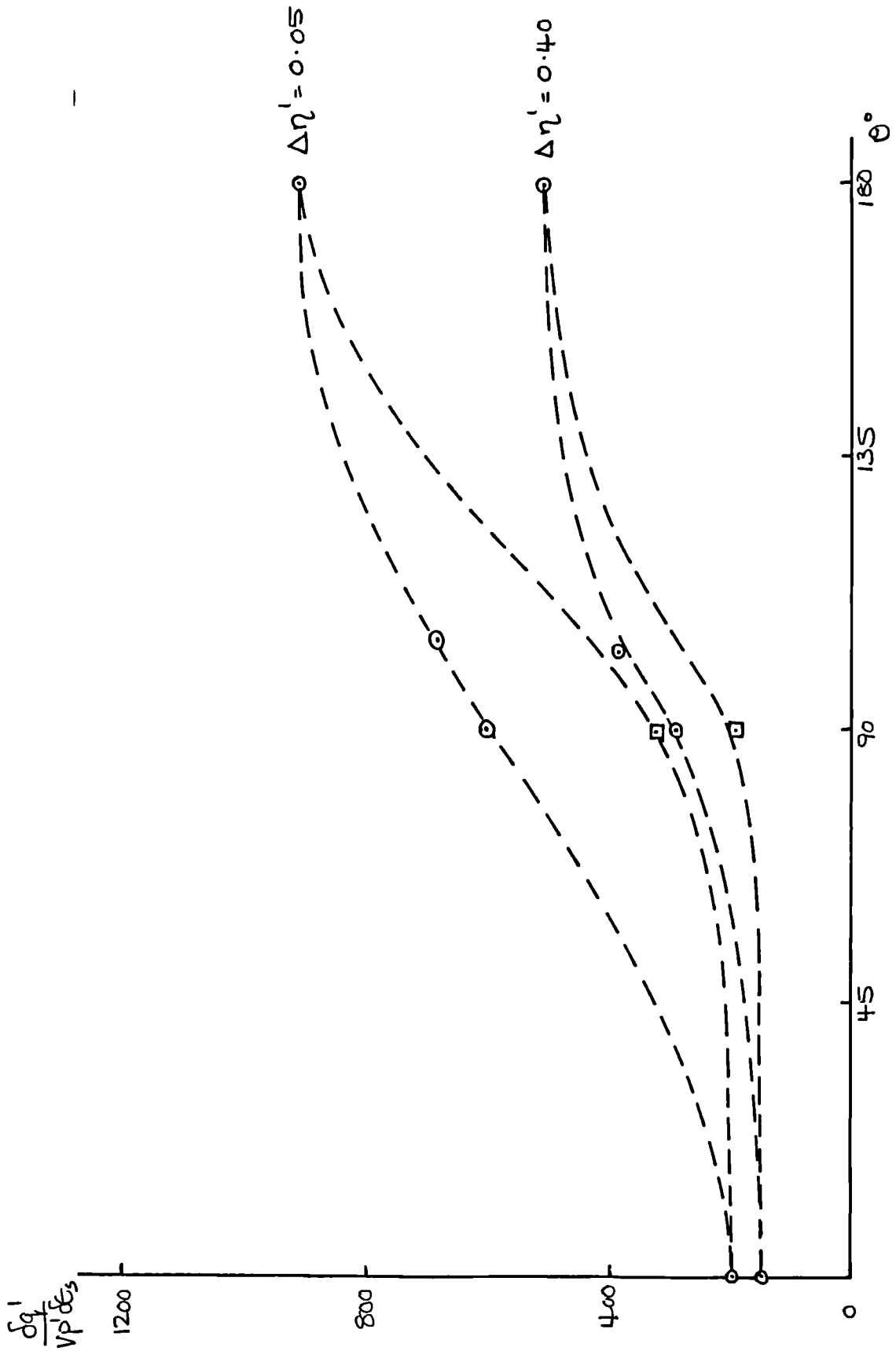

Fig 9.56 Plot of normalised stiffness $\delta q' / vp'\delta\varepsilon_s$ against deviation of stress path, θ. London clay one dimensionally compressed, OCR = 8.0, p' = 50kPa, constant p' paths.

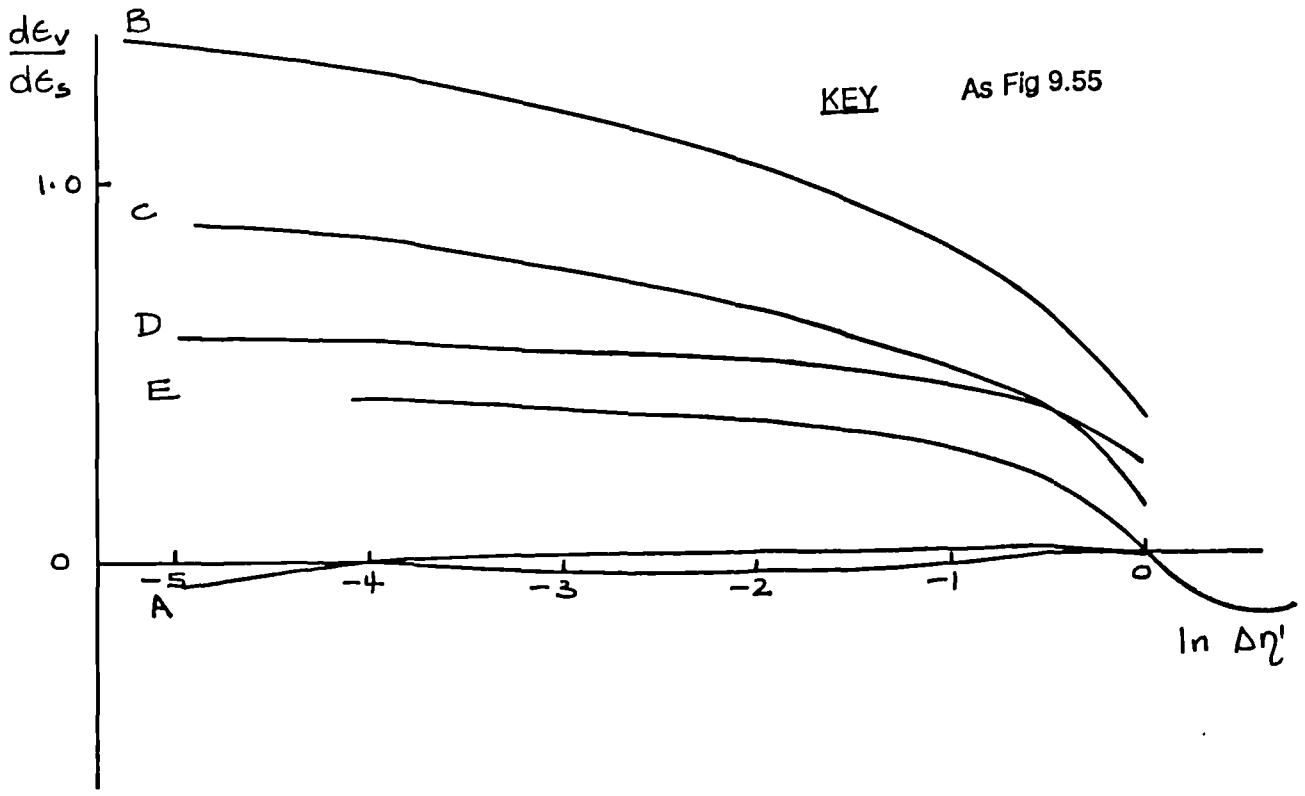

FIG 9.57

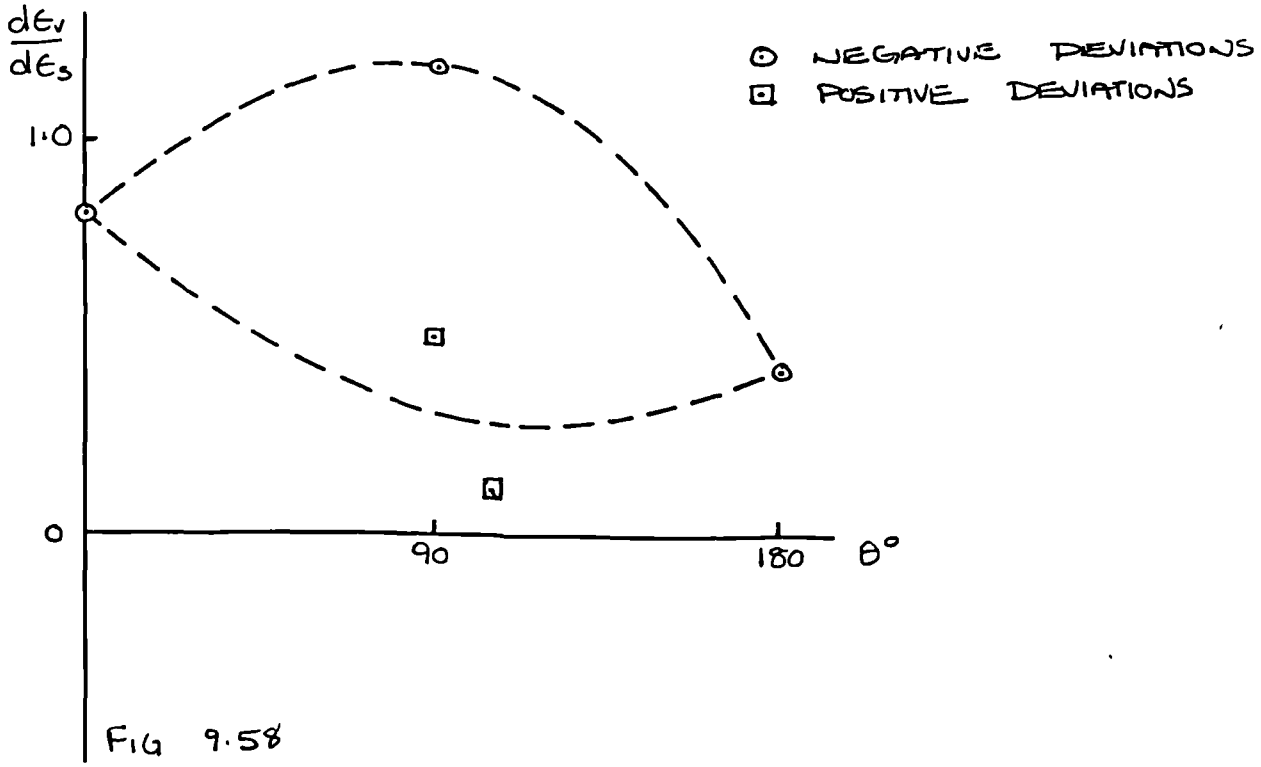

FIG 9.58

Fig 9.57 Plot of total strain increment ratio, $d\varepsilon_v / d\varepsilon_s$, against $\log\Delta\eta'$. London clay , one dimensionally compressed, OCR = 8.0, p' = 50kPa, constant p' paths.

Fig 9.58 Plot of total strain increment ratio, $d\varepsilon_v / d\varepsilon_s$, against deviation of stress path, θ. London clay , isotropically compressed, OCR = 8.0, p' = 50kPa, constant p' paths.

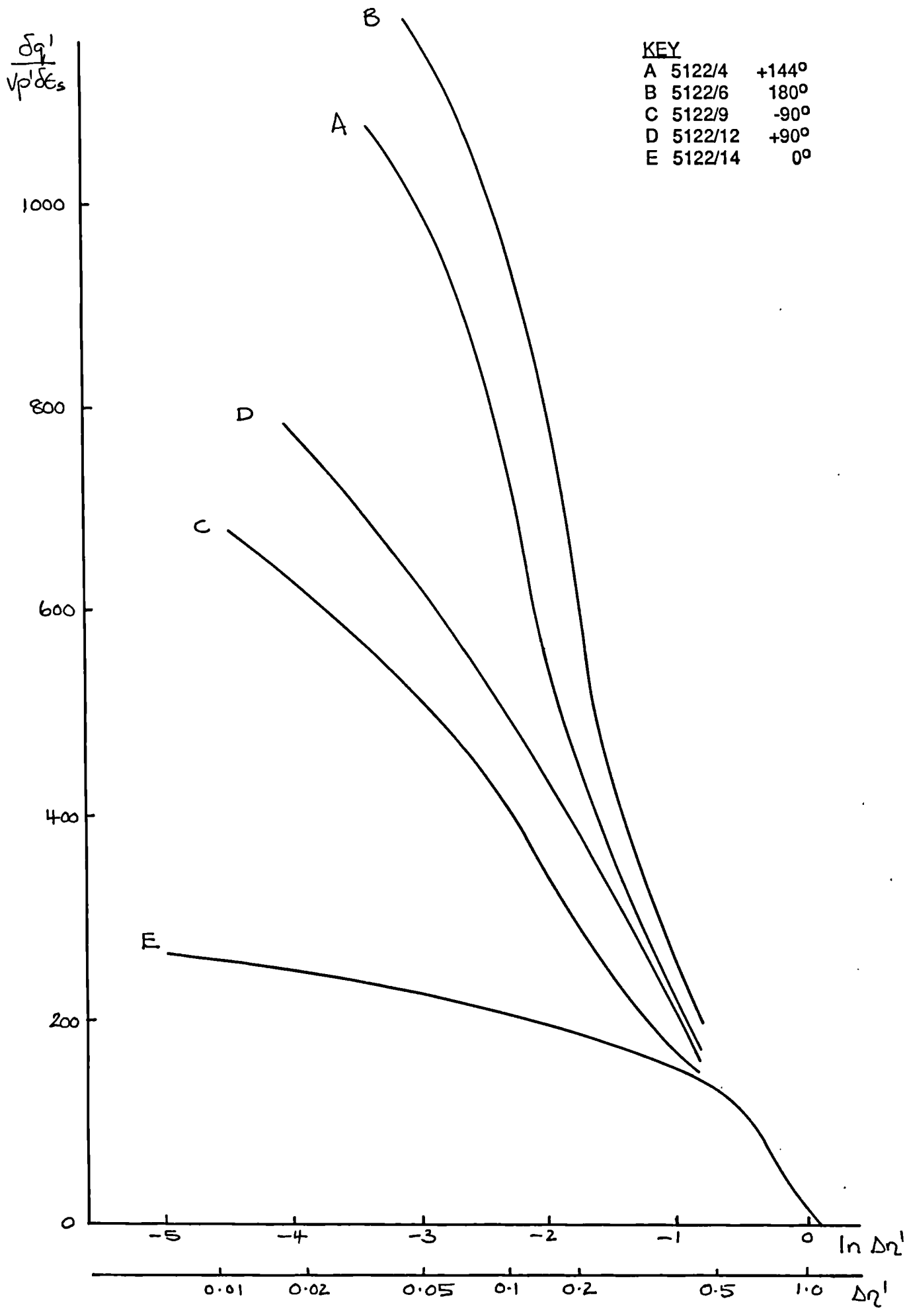

Fig 9.59 Plot of normalised stiffness $\delta q' / vp'\delta\varepsilon_s$ against $\log_e \Delta\eta'$. London clay, $\eta'_o = 0.75$, OCR = 2.0, p' = 200kPa, constant p' paths.

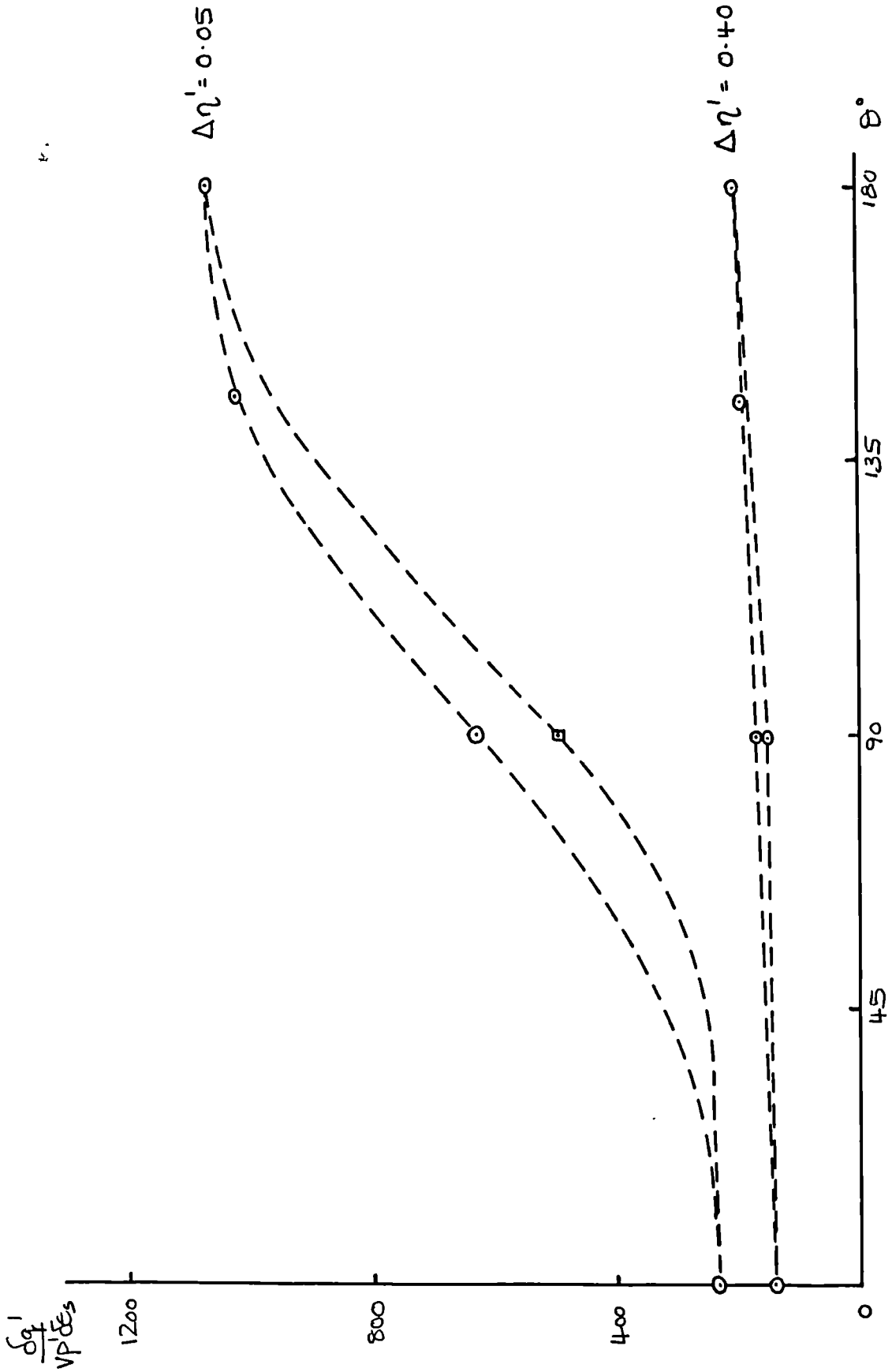

Fig 9.60 Plot of normalised stiffness $\delta q' / vp'\delta\varepsilon_s$ against deviation of stress path, θ. London clay, $\eta'_o = 0.75$, OCR = 2.0, p' = 200kPa, constant p' paths.

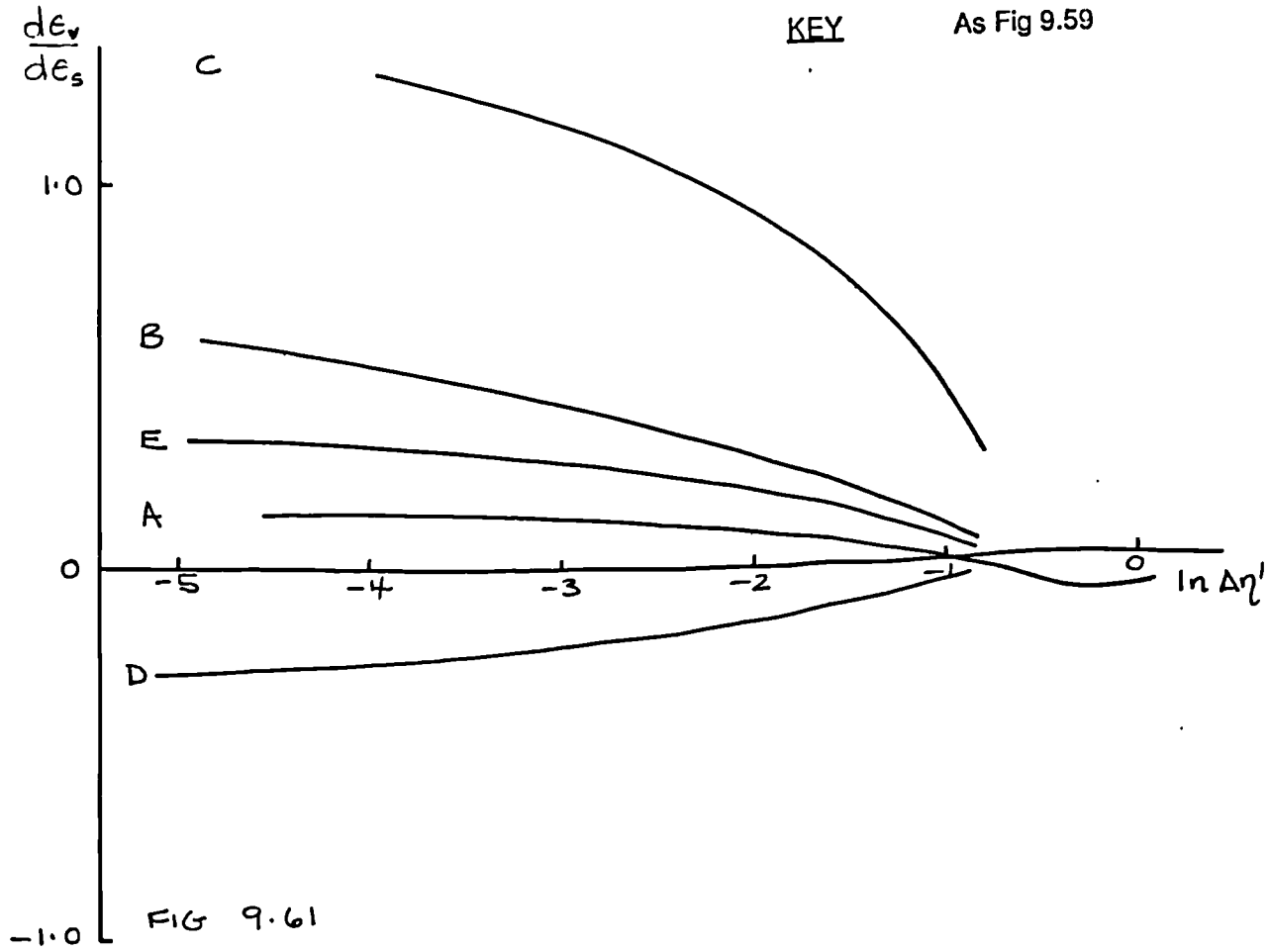

FIG 9.61

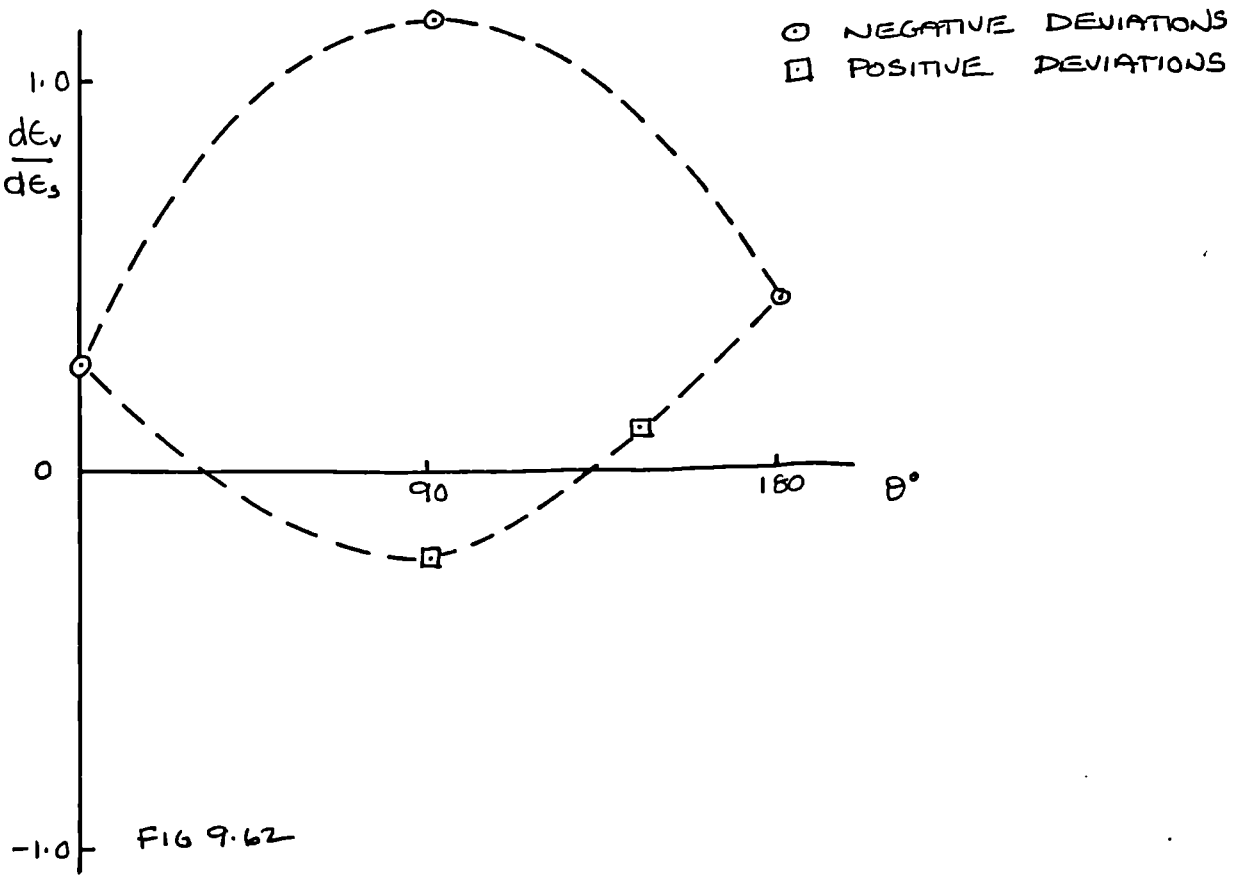

FIG 9.62

Fig 9.61 Plot of total strain increment ratio, $d\varepsilon_v / d\varepsilon_s$, against $\log\Delta\eta'$. London clay, $\eta'_o = 0.75$, OCR = 2.0, p' = 200kPa, constant p' paths.

Fig 9.62 Plot of total strain increment ratio, $d\varepsilon_v / d\varepsilon_s$, against deviation of stress path, θ. London clay, $\eta'_o = 0.75$, OCR = 2.0, p' = 200kPa, constant p' paths.

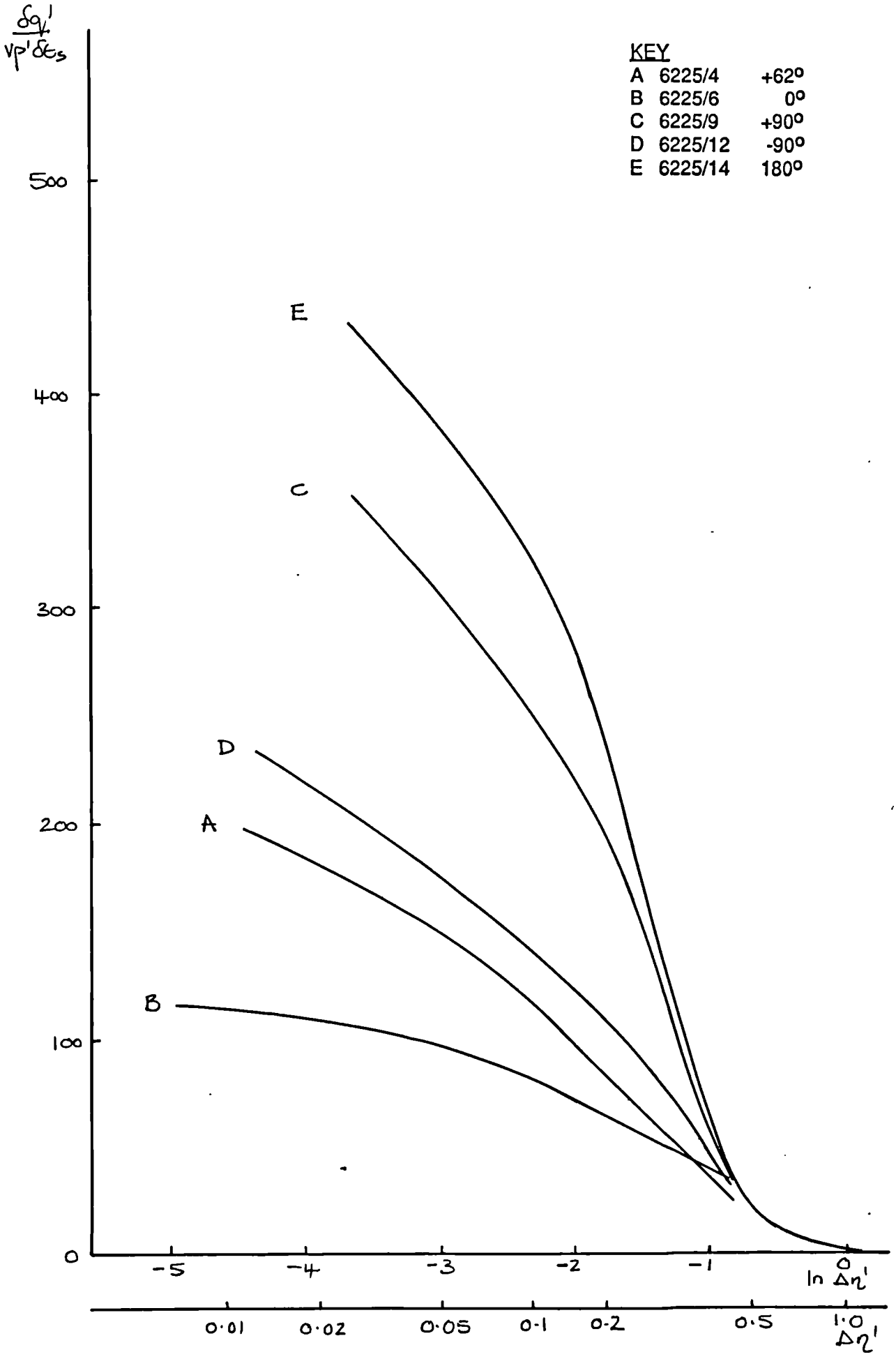

Fig 9.63 Plot of normalised stiffness $\delta q' / vp'\delta\varepsilon_s$ against $\log_e \Delta\eta'$. London clay two dimensionally compressed, OCR = 2.0, p' = 200 kPa, constant p' paths.

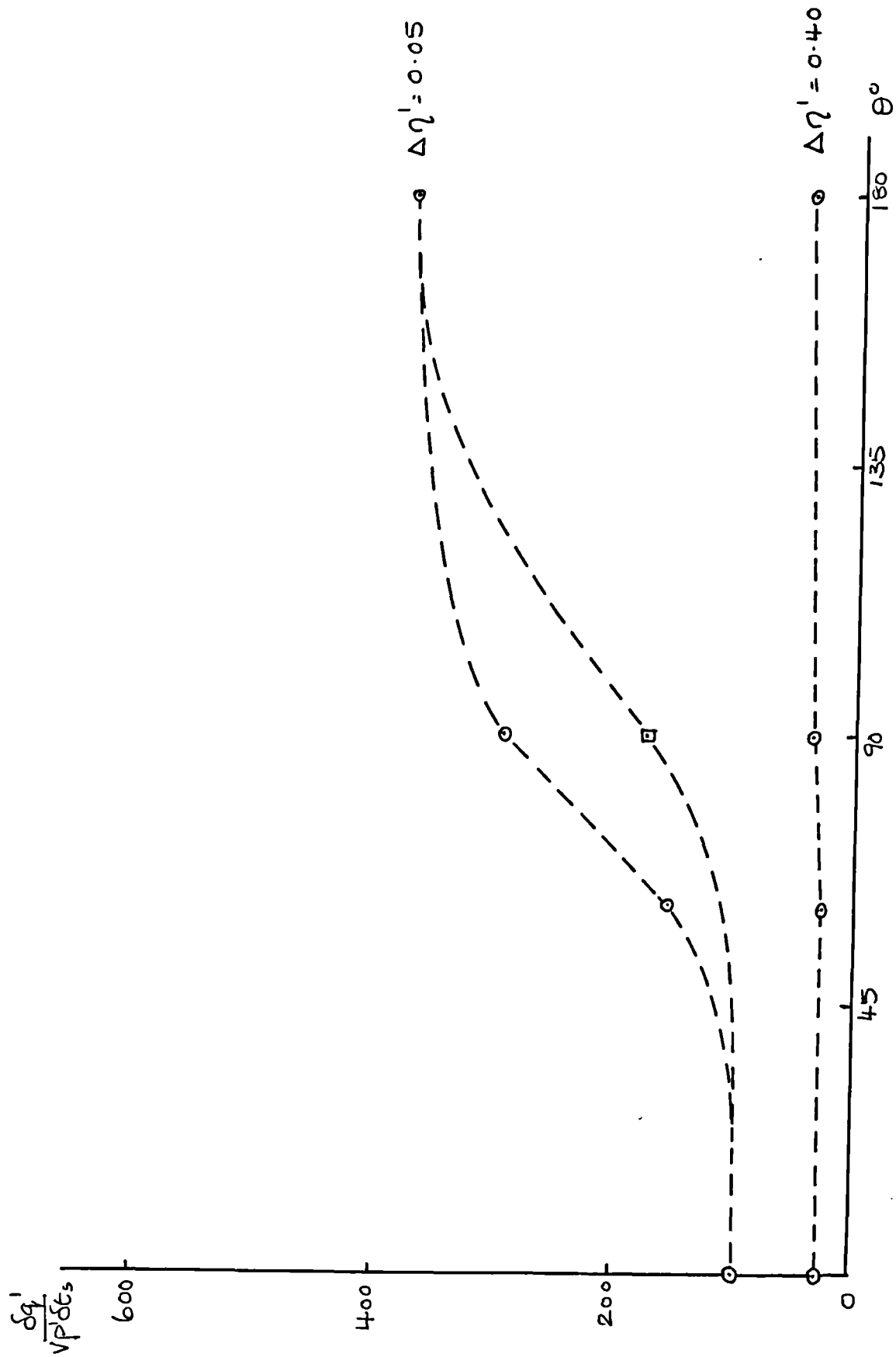

Fig 9.64 Plot of normalised stiffness $\delta q' / vp'\delta\varepsilon_s$ against deviation of stress path, θ. London clay two dimensionally compressed, OCR = 2.0, p' = 200 kPa, constant p' paths.

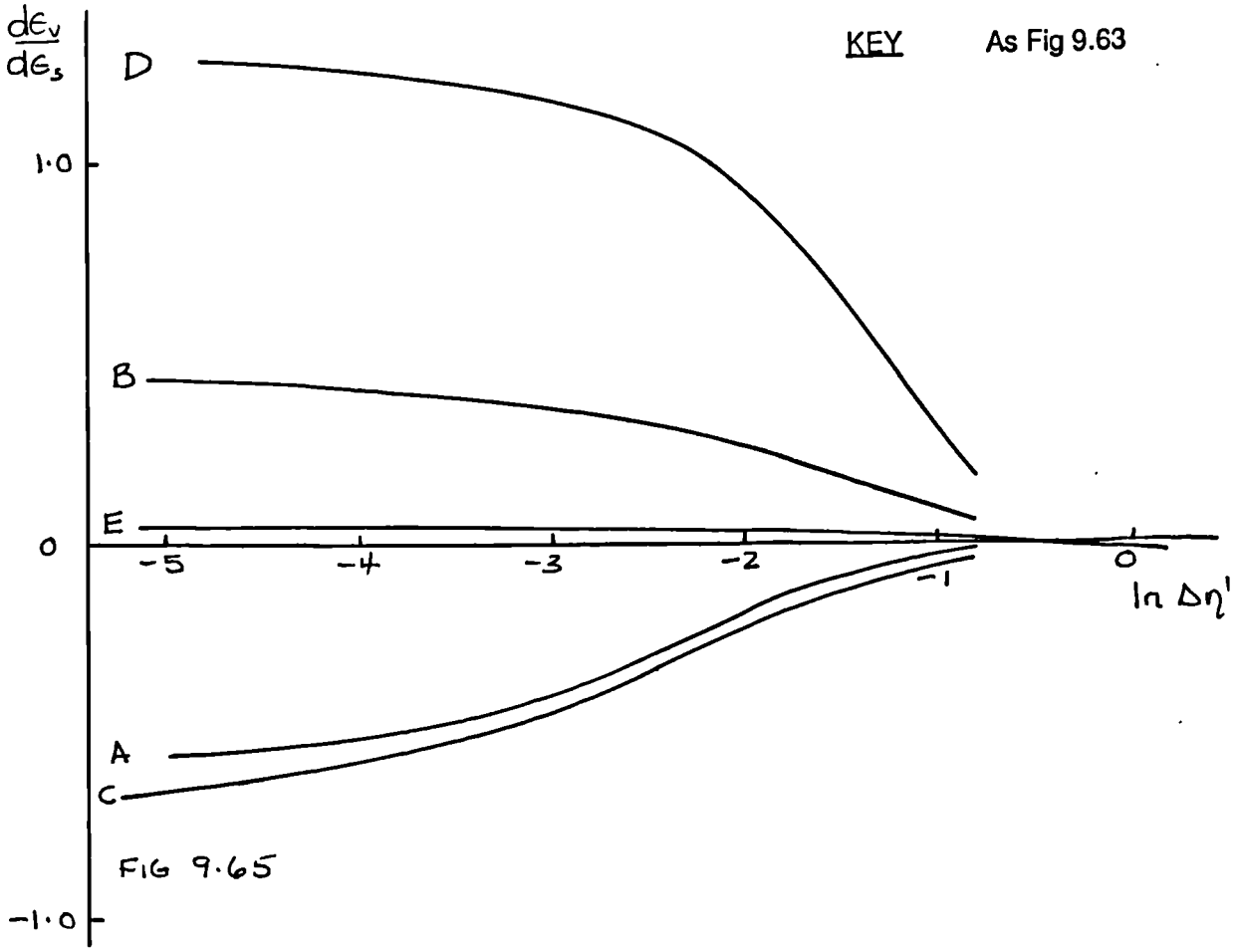

FIG 9.65

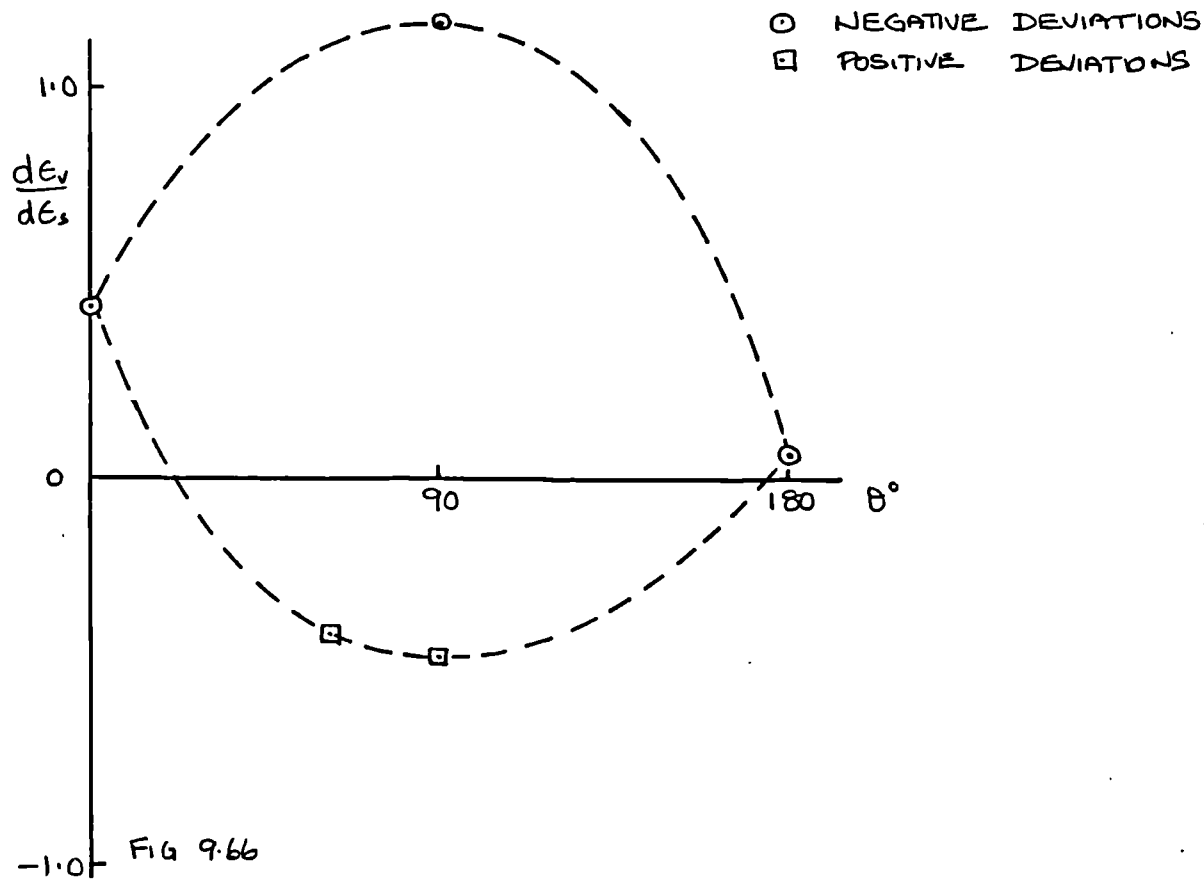

FIG 9.66

Fig 9.65 Plot of total strain increment ratio, $d\varepsilon_v / d\varepsilon_s$, against $\log\Delta\eta'$. London clay two dimensionally compressed, OCR = 2.0, p' = 200 kPa, constant p' paths.

Fig 9.66 Plot of total strain increment ratio, $d\varepsilon_v / d\varepsilon_s$, against deviation of stress path, θ. London clay two dimensionally compressed, OCR = 2.0, p' = 200 kPa, constant p' paths.

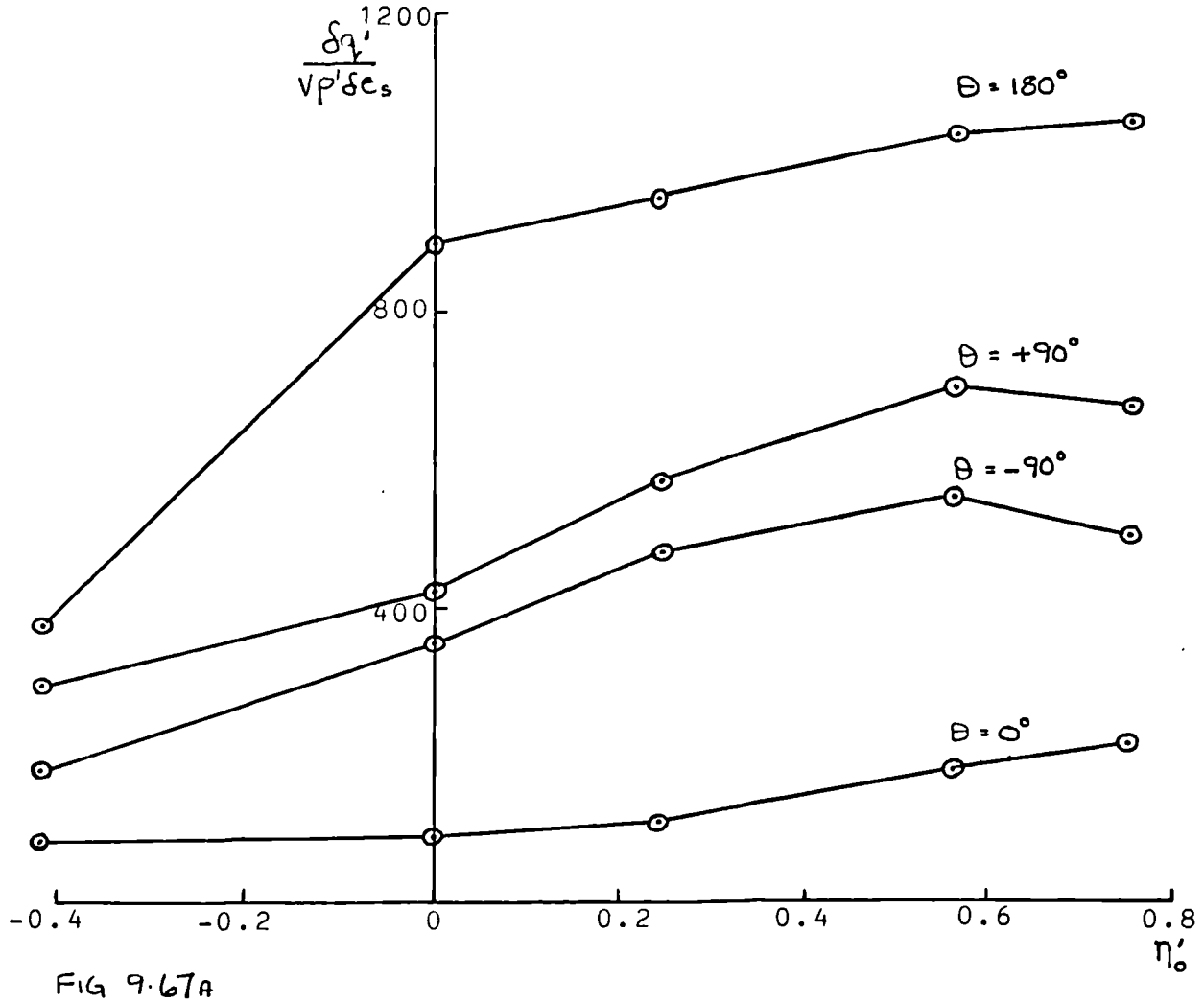

FIG 9.67A

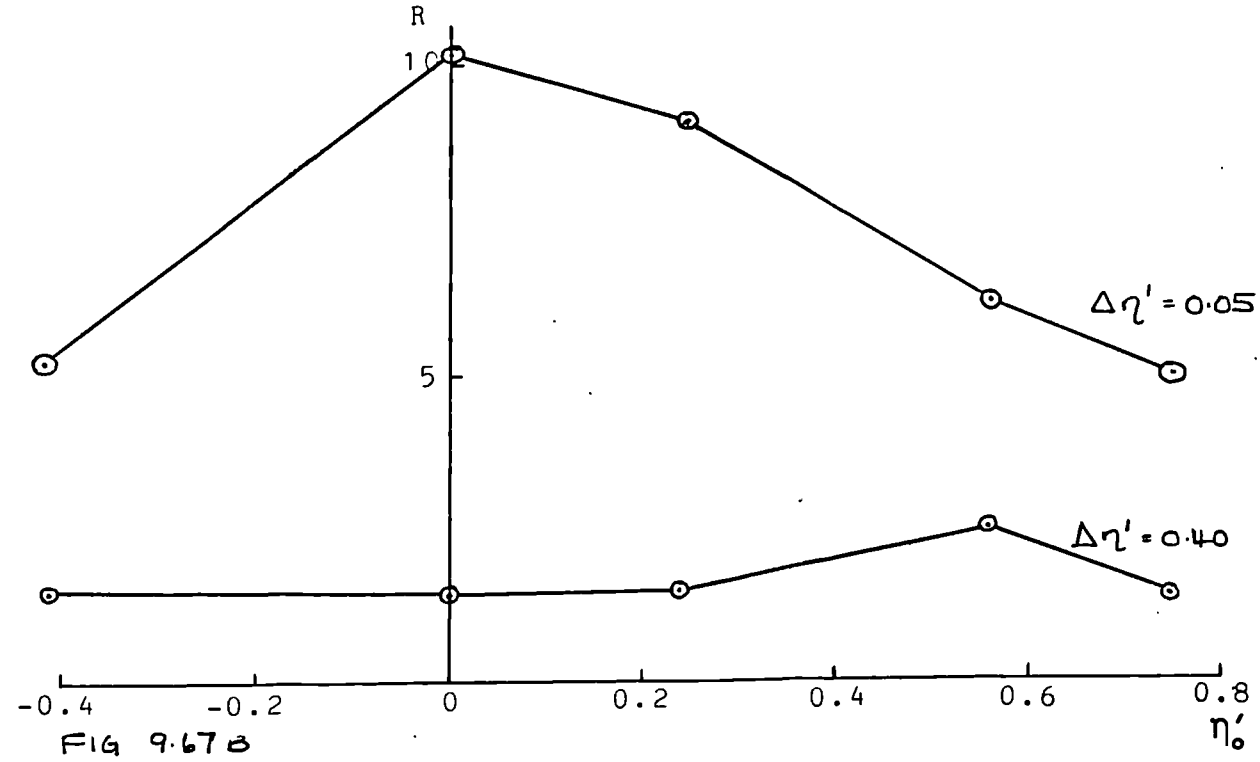

FIG 9.67B

Fig 9.67 a) Plot of normalised stiffness, $\delta q' / vp'\delta\varepsilon_s$, against stress ratio (during initial compression, η'_o), for London clay, OCR = 2.0.

b) Plot of range of stiffness observed, R, against initial stress ratio during compression, η'_o.

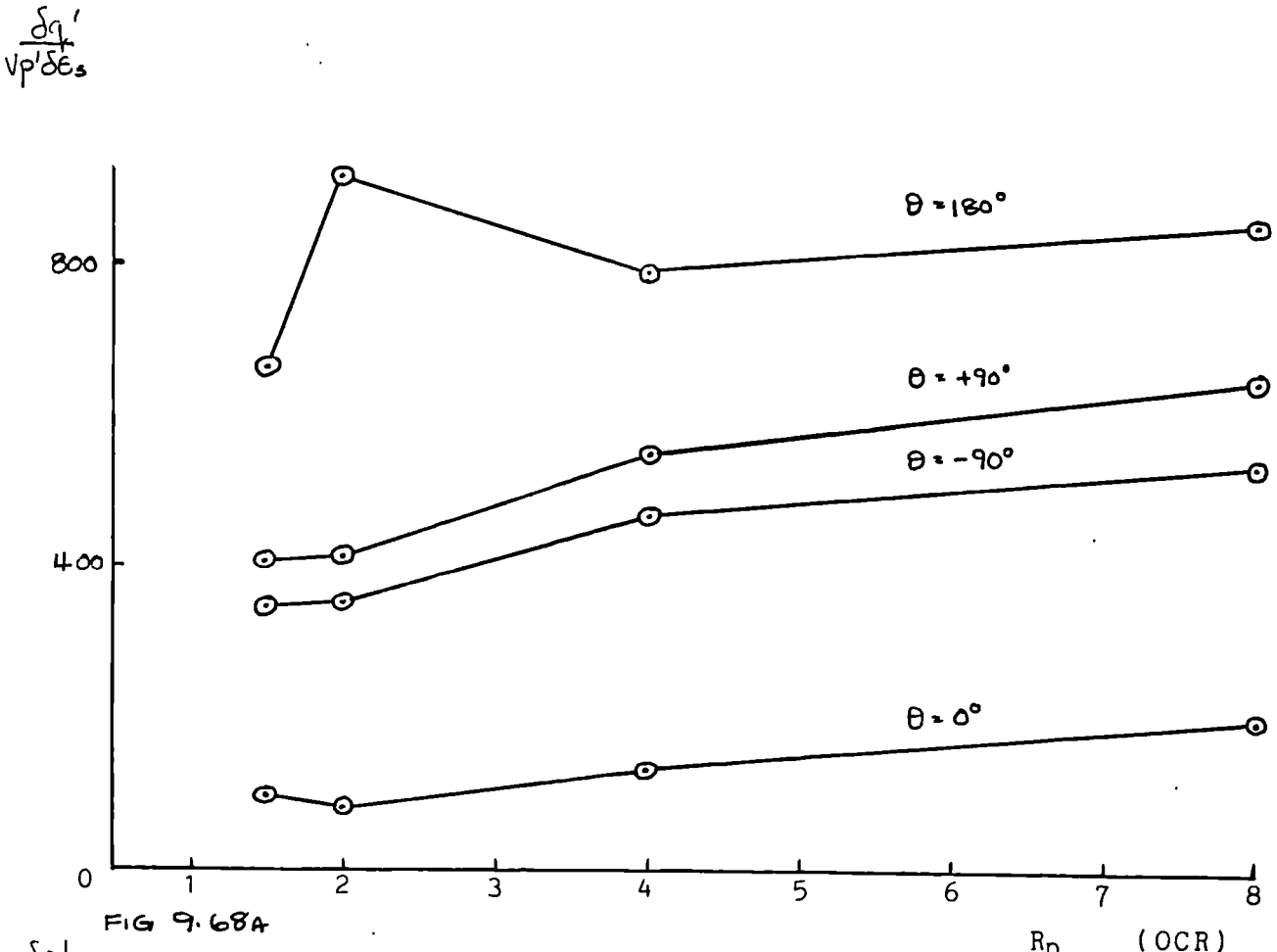

FIG 9.68A

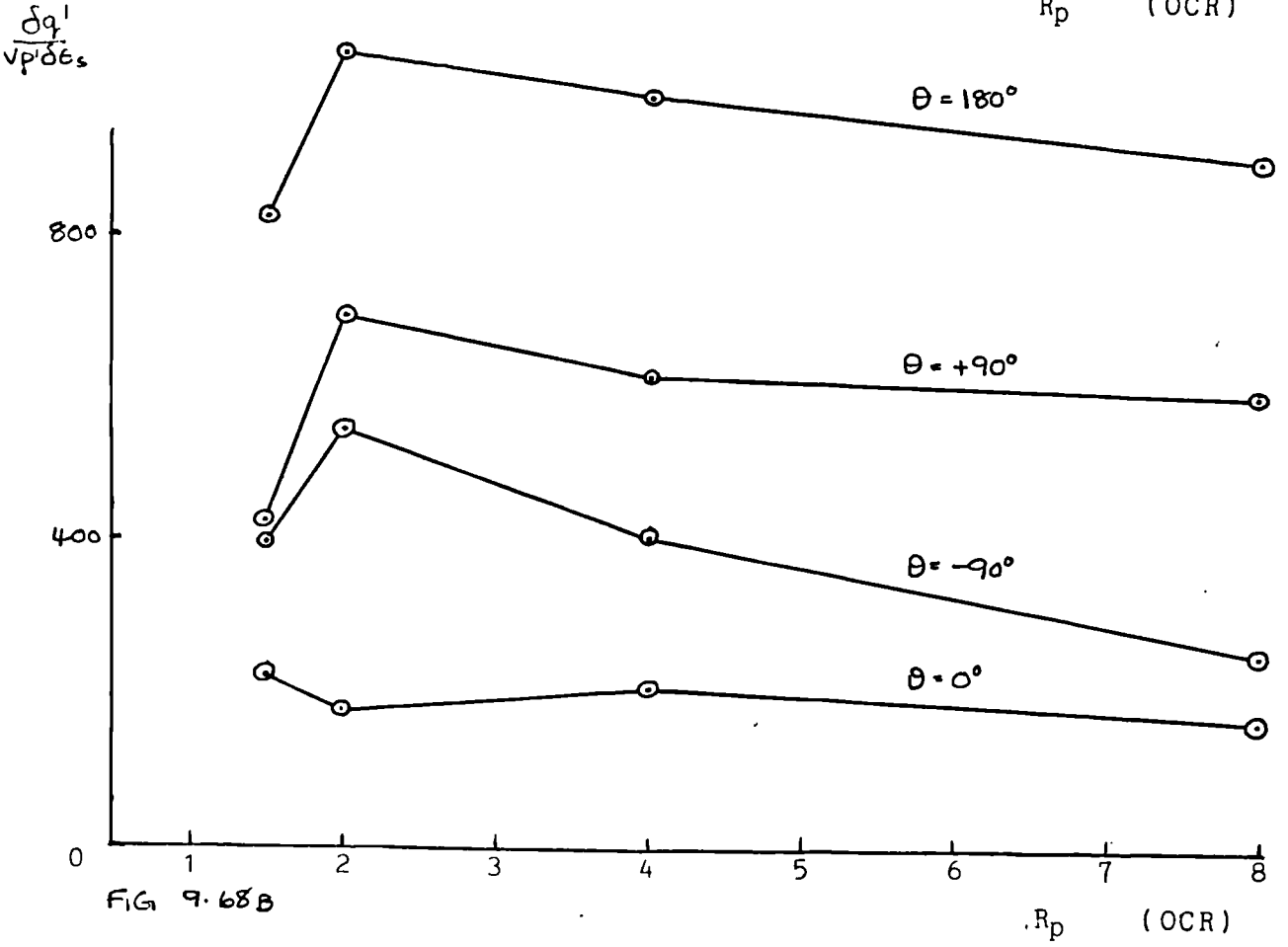

FIG 9.68B

Fig 9.68 Plot of normalised stiffness, $\delta q' / vp'\delta\varepsilon_s$, against overconsolidation ratio for isotropically compressed London clay.
a) For a given stress level. $\Delta\eta' = 0.05$
b) For a given strain level. $\Delta\varepsilon_s = 0.02\%$

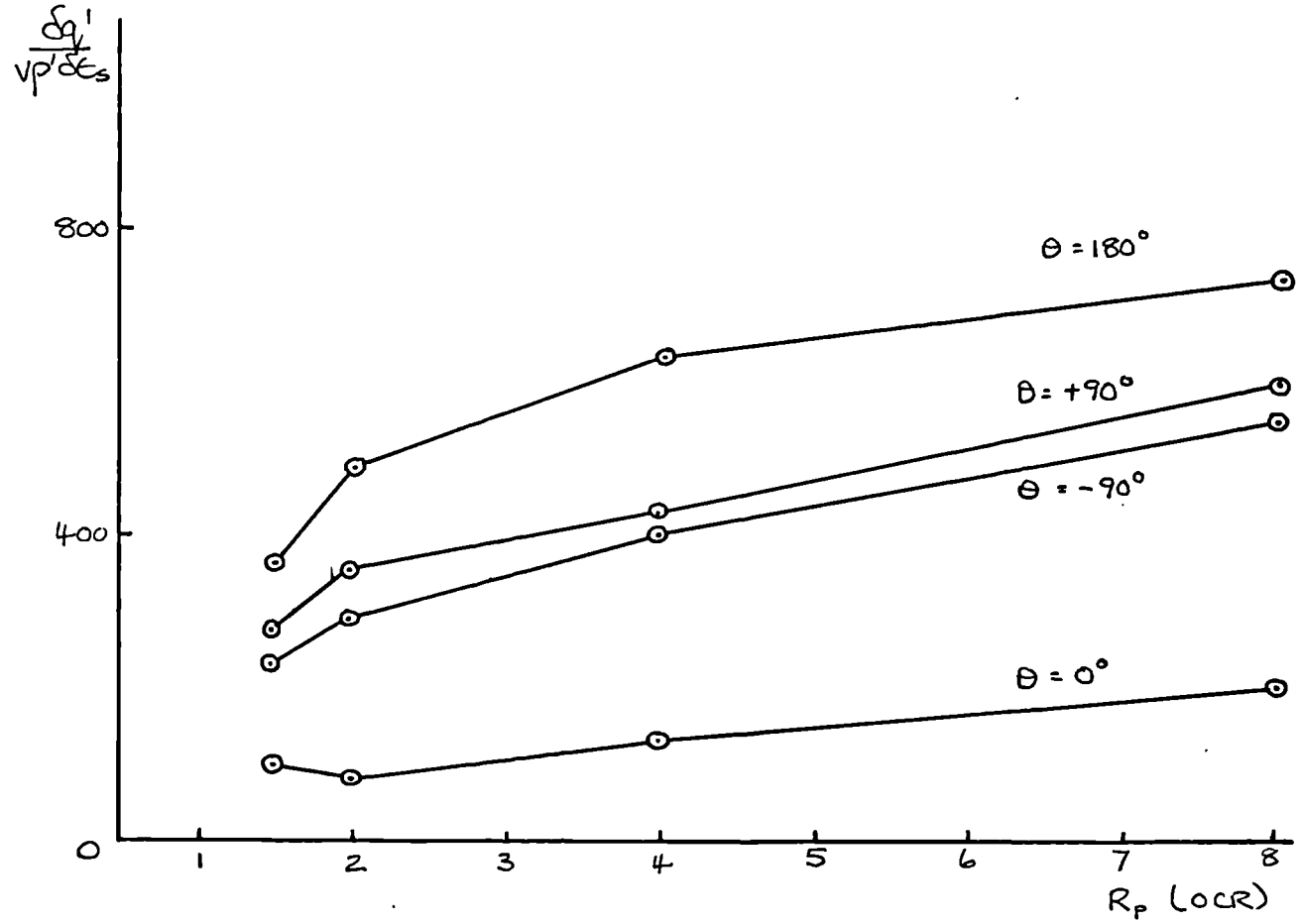

FIG 9.69A

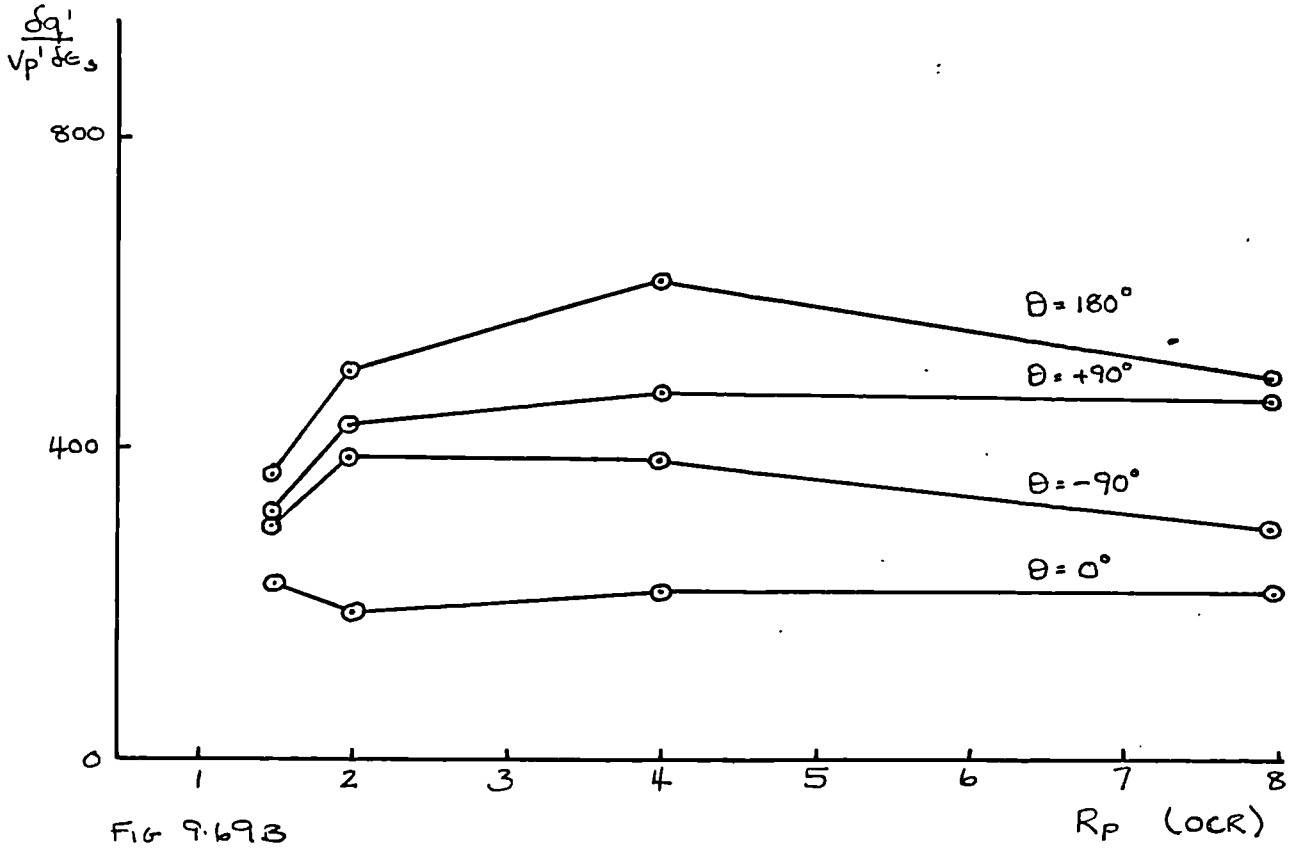

FIG 9.69B

Fig 9.69 Plot of normalised stiffness, $\delta q' / vp'\delta\varepsilon_s$, against overconsolidation ratio for one dimensionally compressed London clay.
a) For a given stress level. $\Delta\eta' = 0.05$
b) For a given strain level. $\Delta\varepsilon_s = 0.02\%$

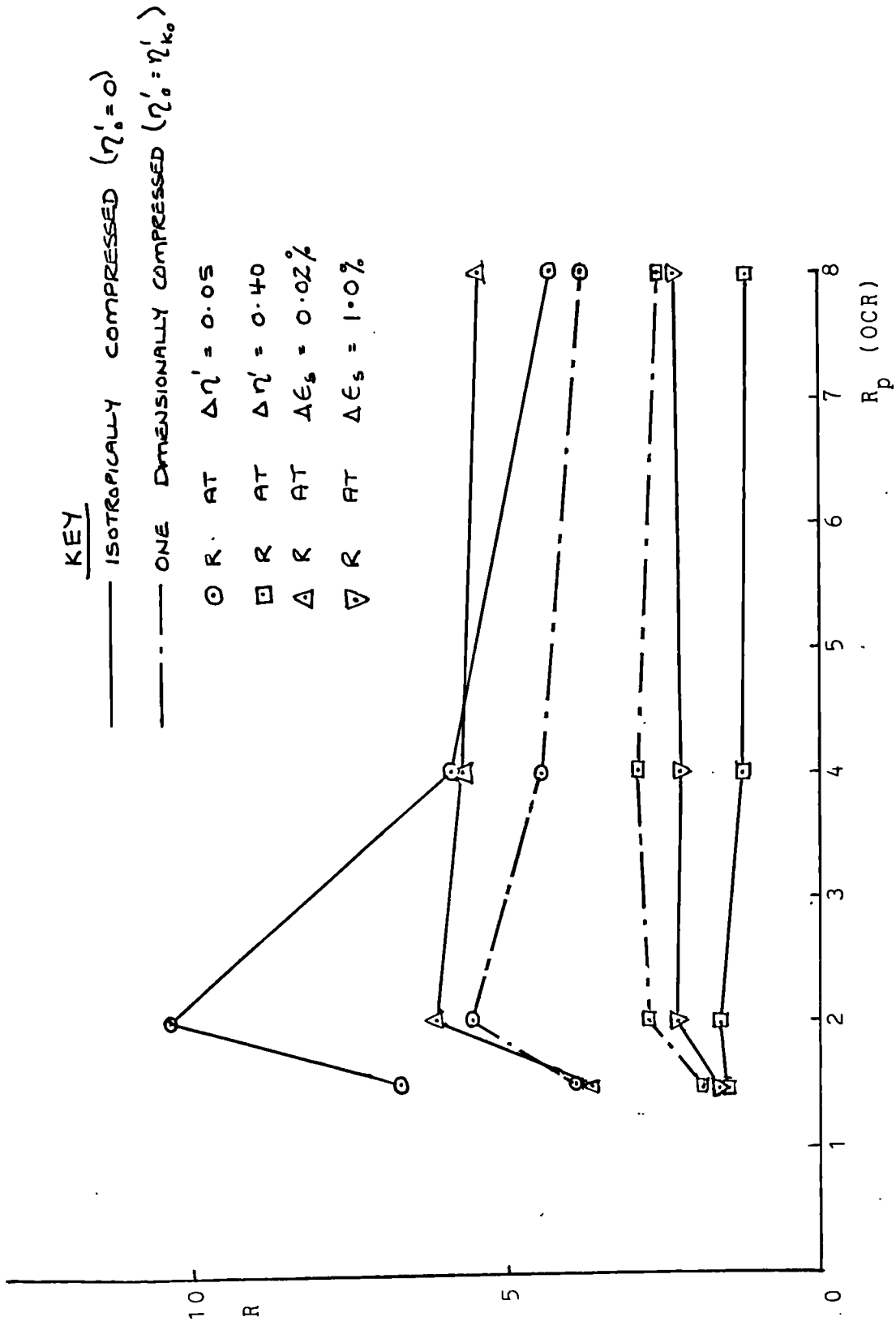

Fig 9.70 Range of stiffness, R, plotted against overconsolidation ratio for both isotropically and one dimensionally compressed London clay.

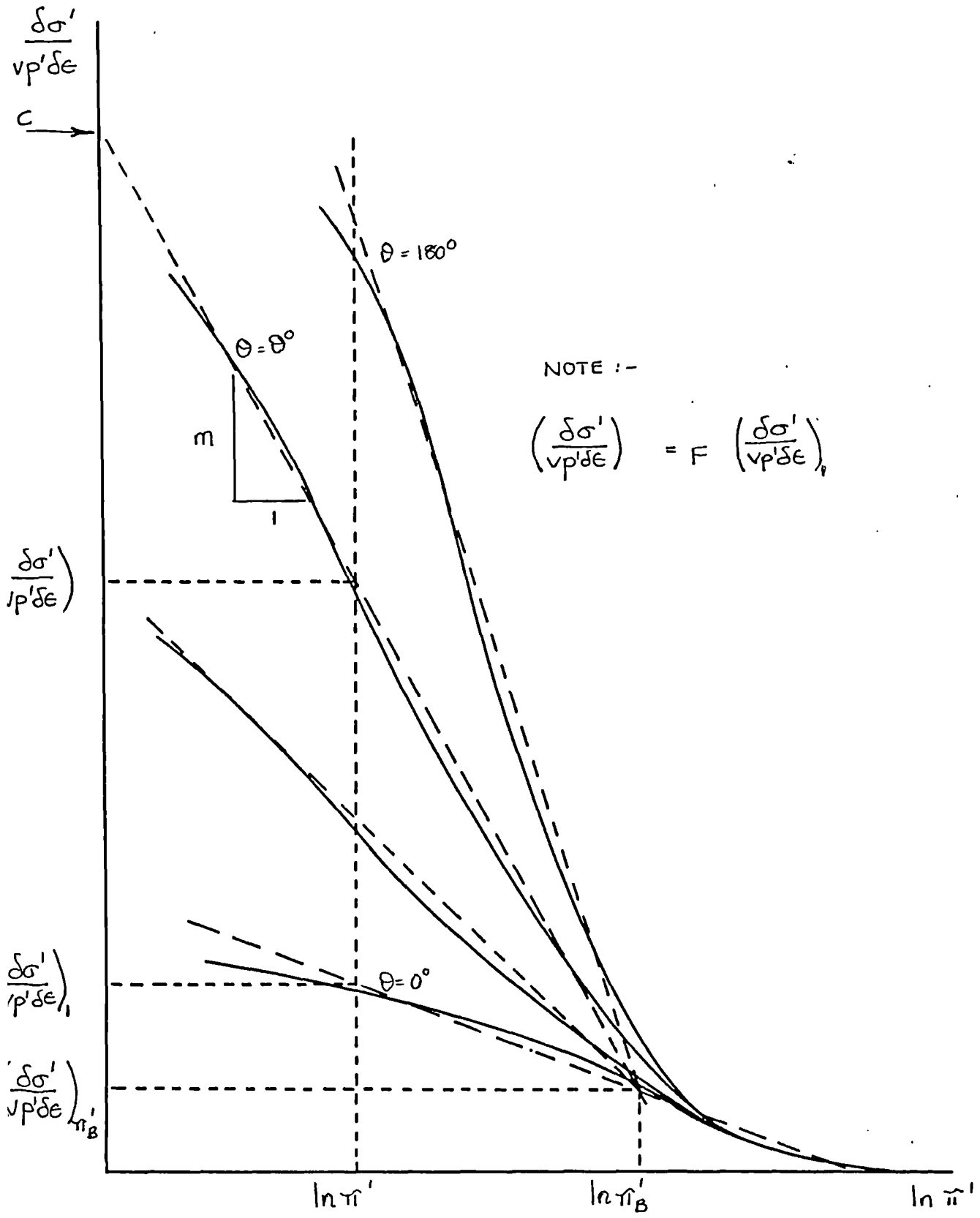

Fig 9.71 Idealised plot of normalised stiffness against $\log_e \Delta\pi'$.

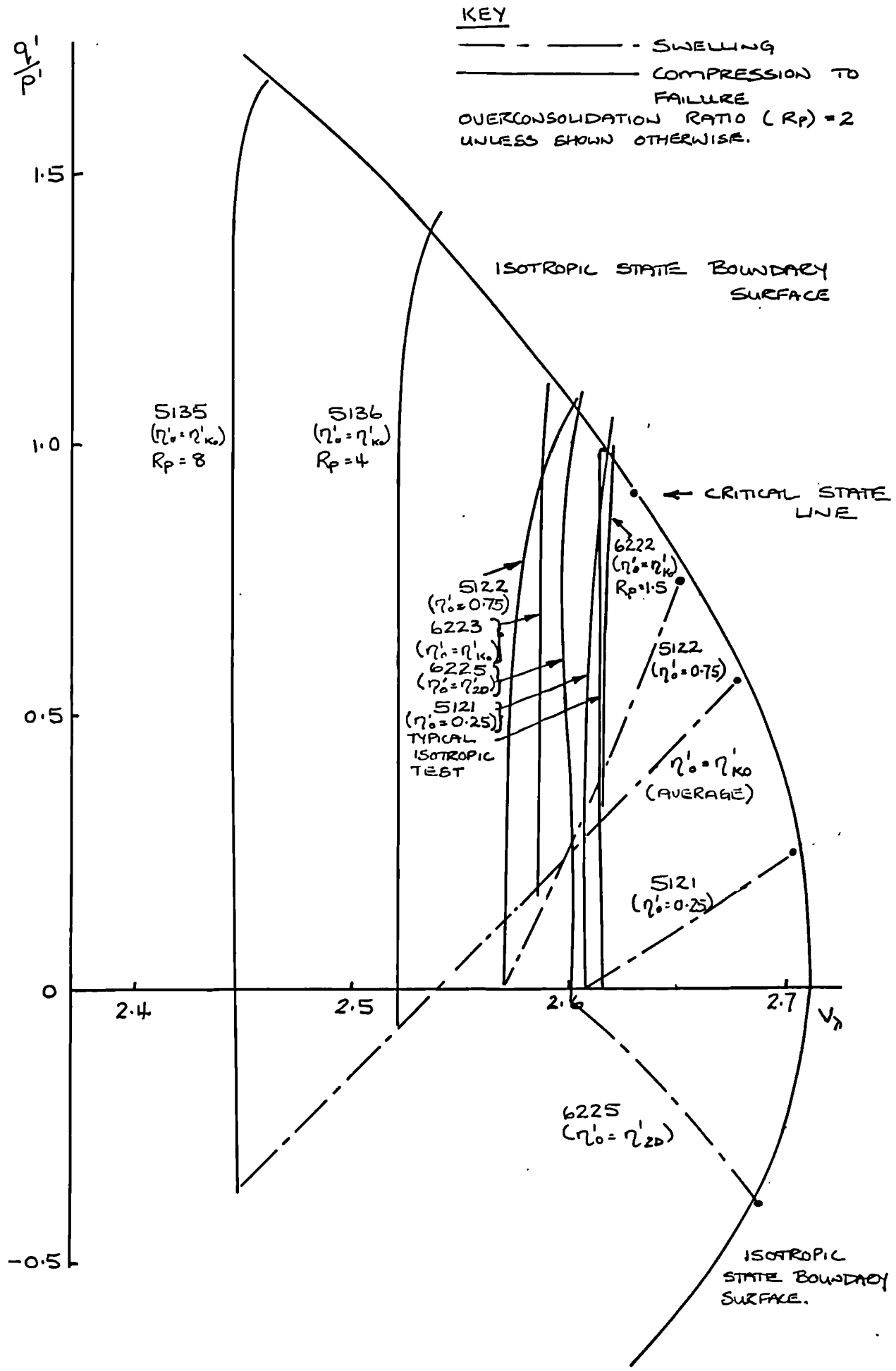

Fig 9.72 Plot of q' / p' against v_λ for samples of London clay from all initial compression histories.

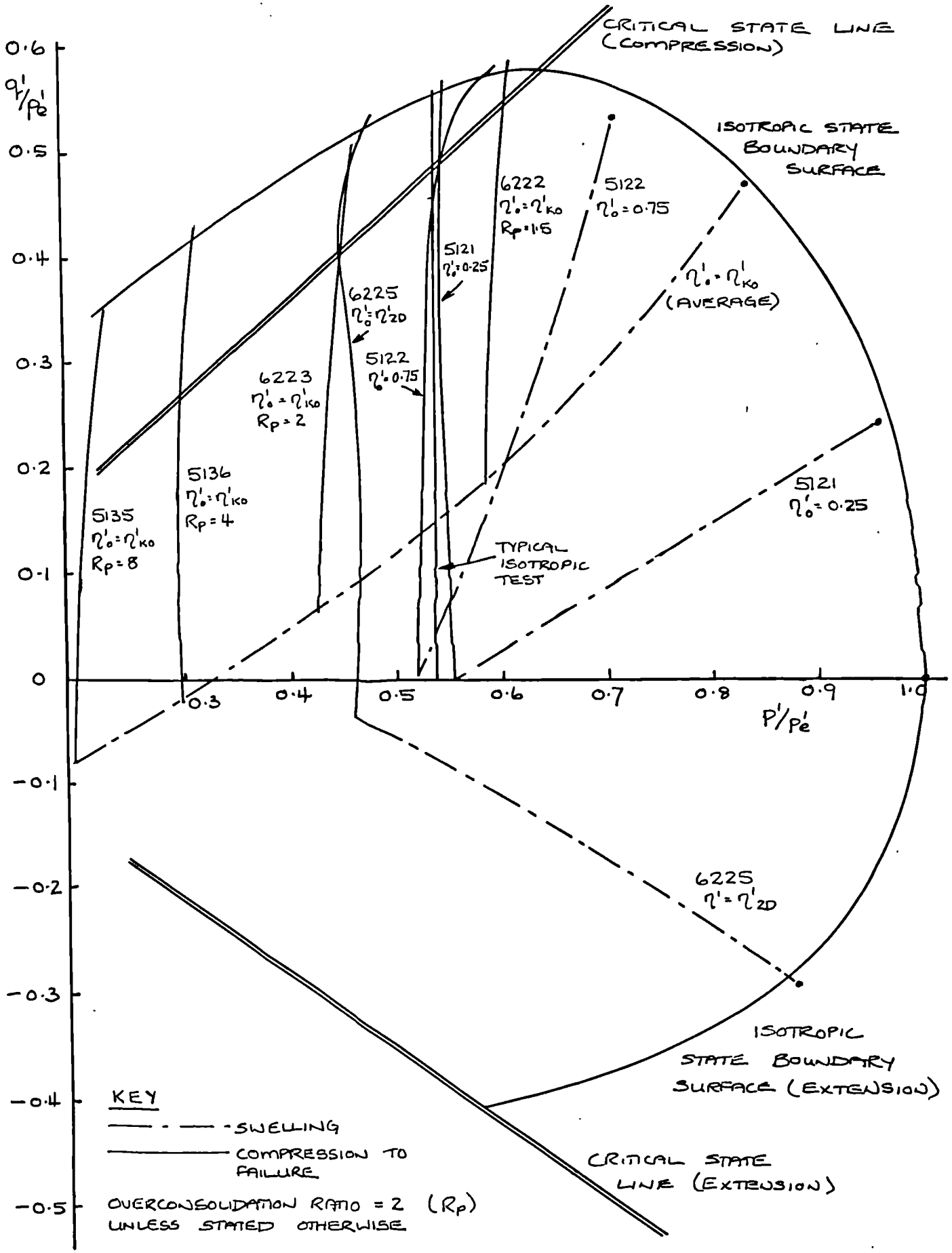

Fig 9.73 Plot of q' / p'_e against p' / p'_e for samples of London clay from all initial compression histories using a value of N from isotropic compression data.

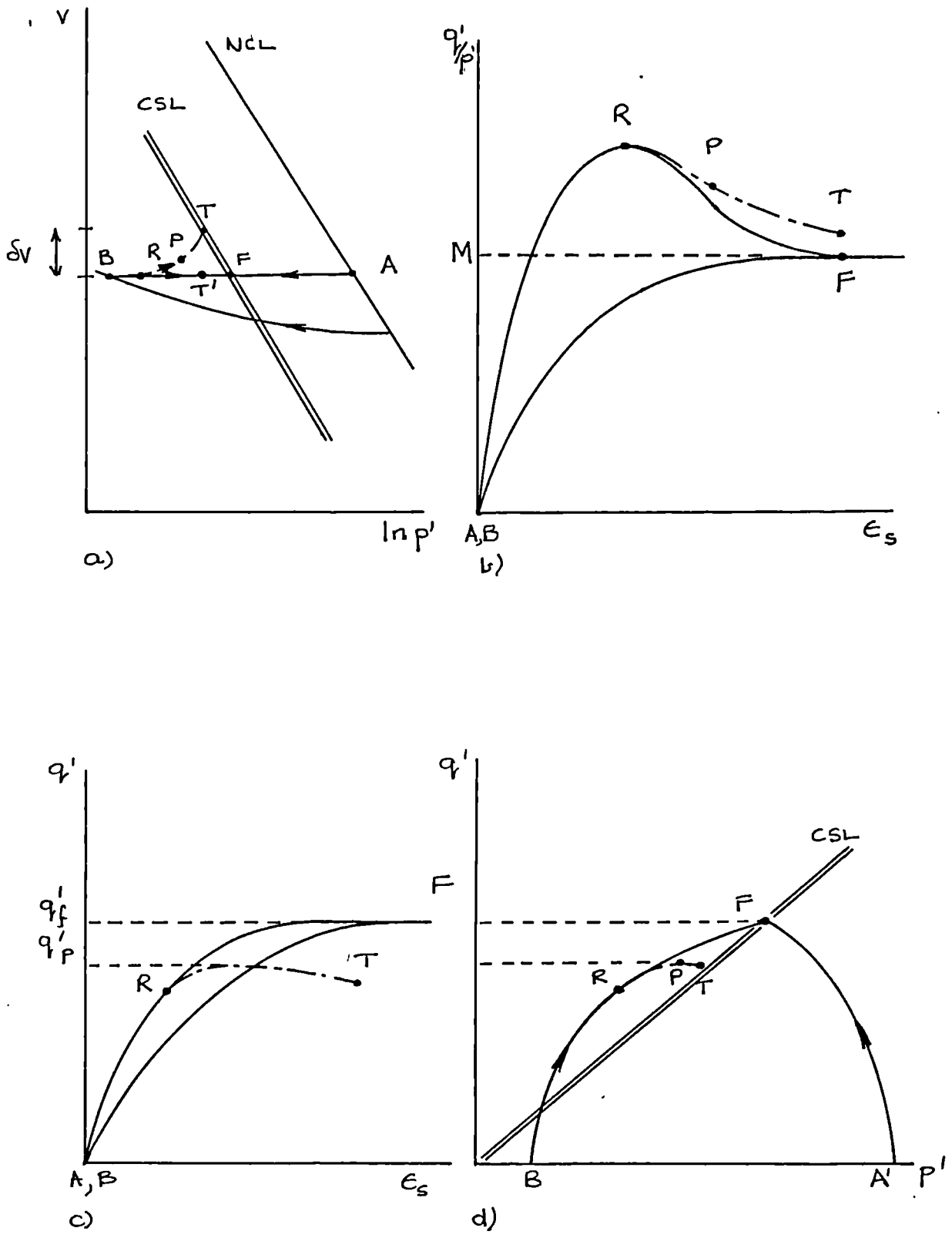

Fig 9.74 Effect of local drainage on the stress strain behaviour and failure states of samples.

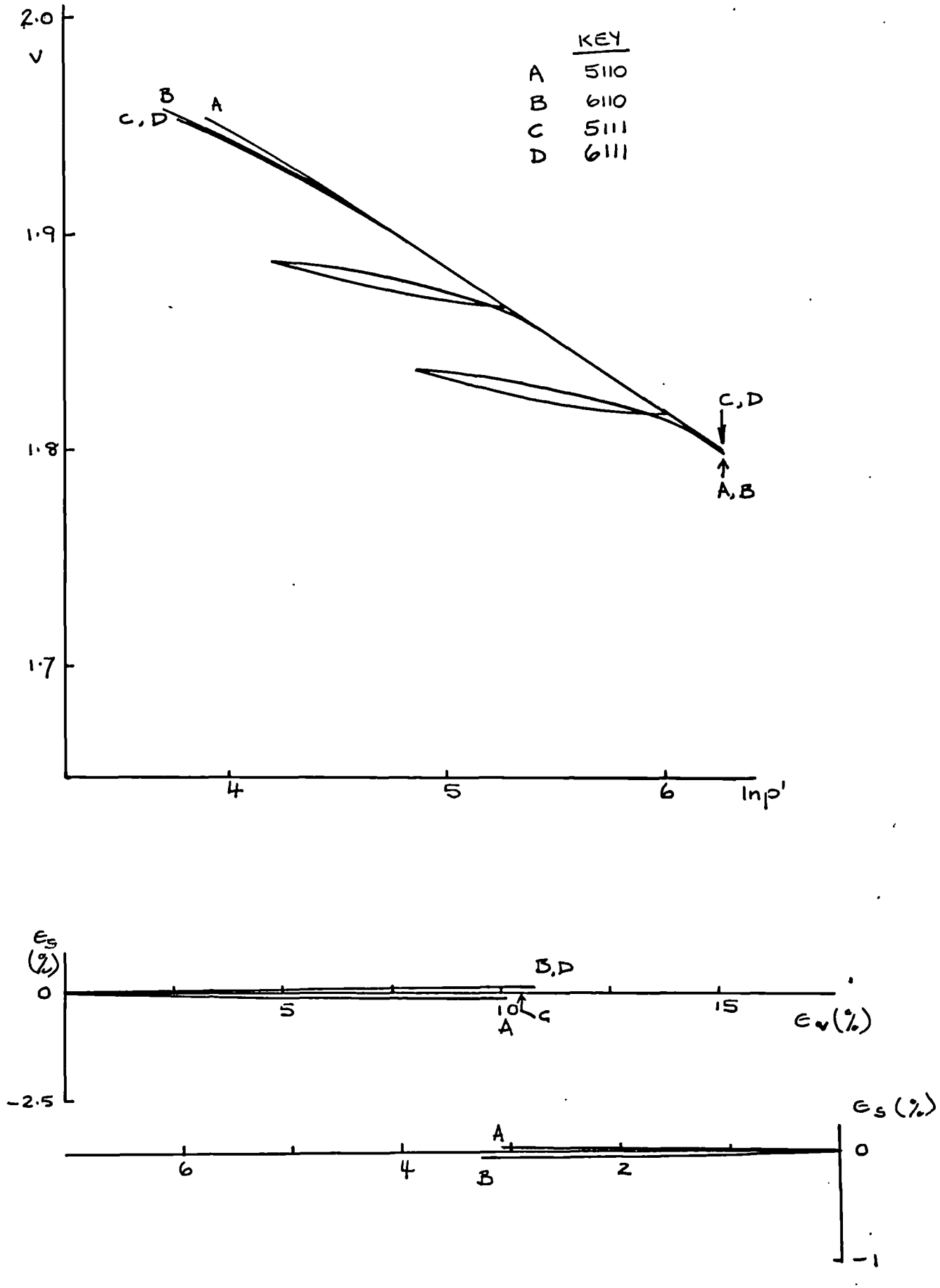

Fig 9.75 Plots of v against $\log_e p'$ and ε_s against ε_v for speswhite kaolin samples produced by the alternative method. Isotropic compression and swelling.

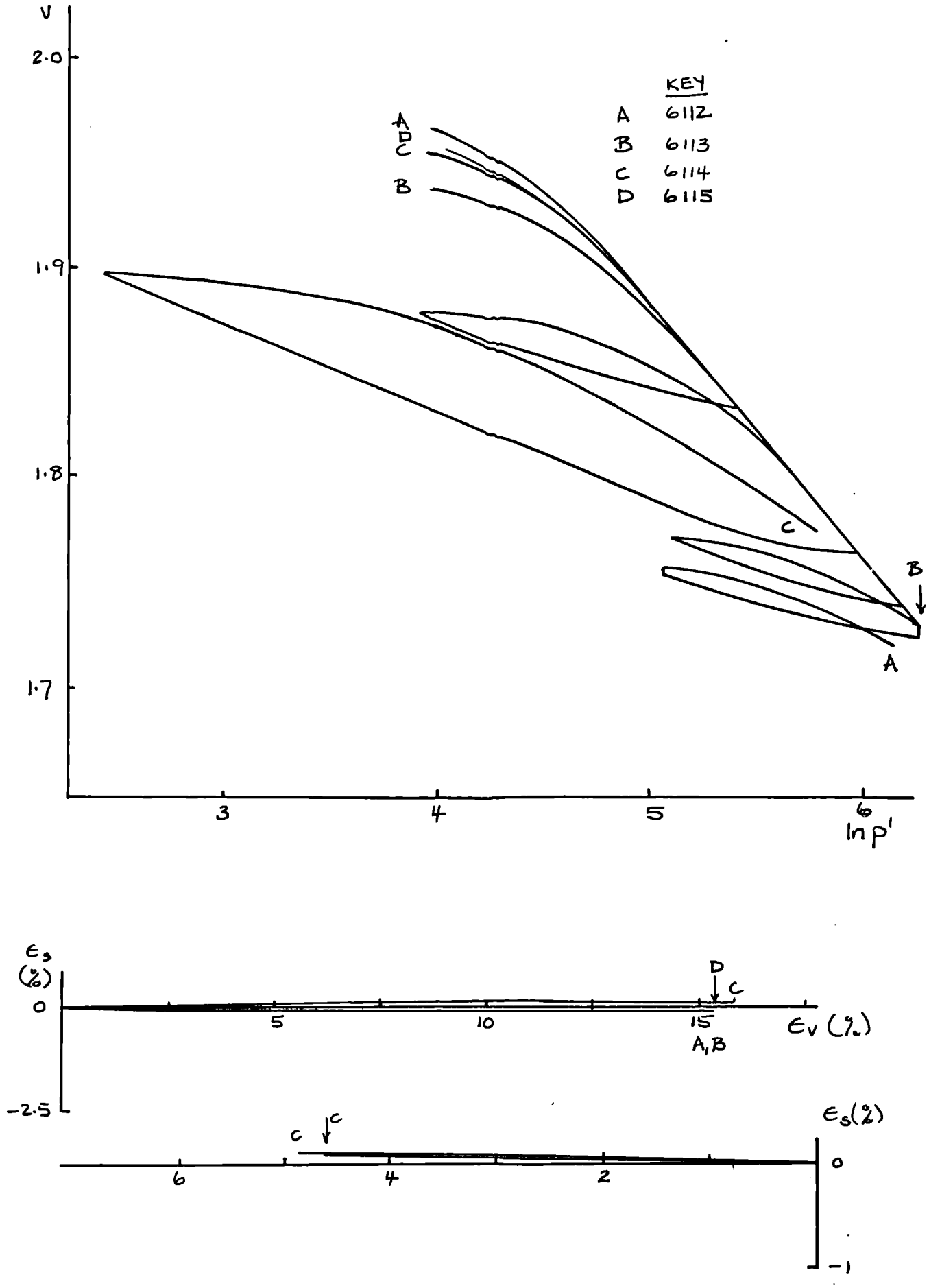

Fig 9.76 Plots of v against $\log_e p'$ and ε_s against ε_v for London clay samples produced by the alternative method. Isotropic compression and swelling.

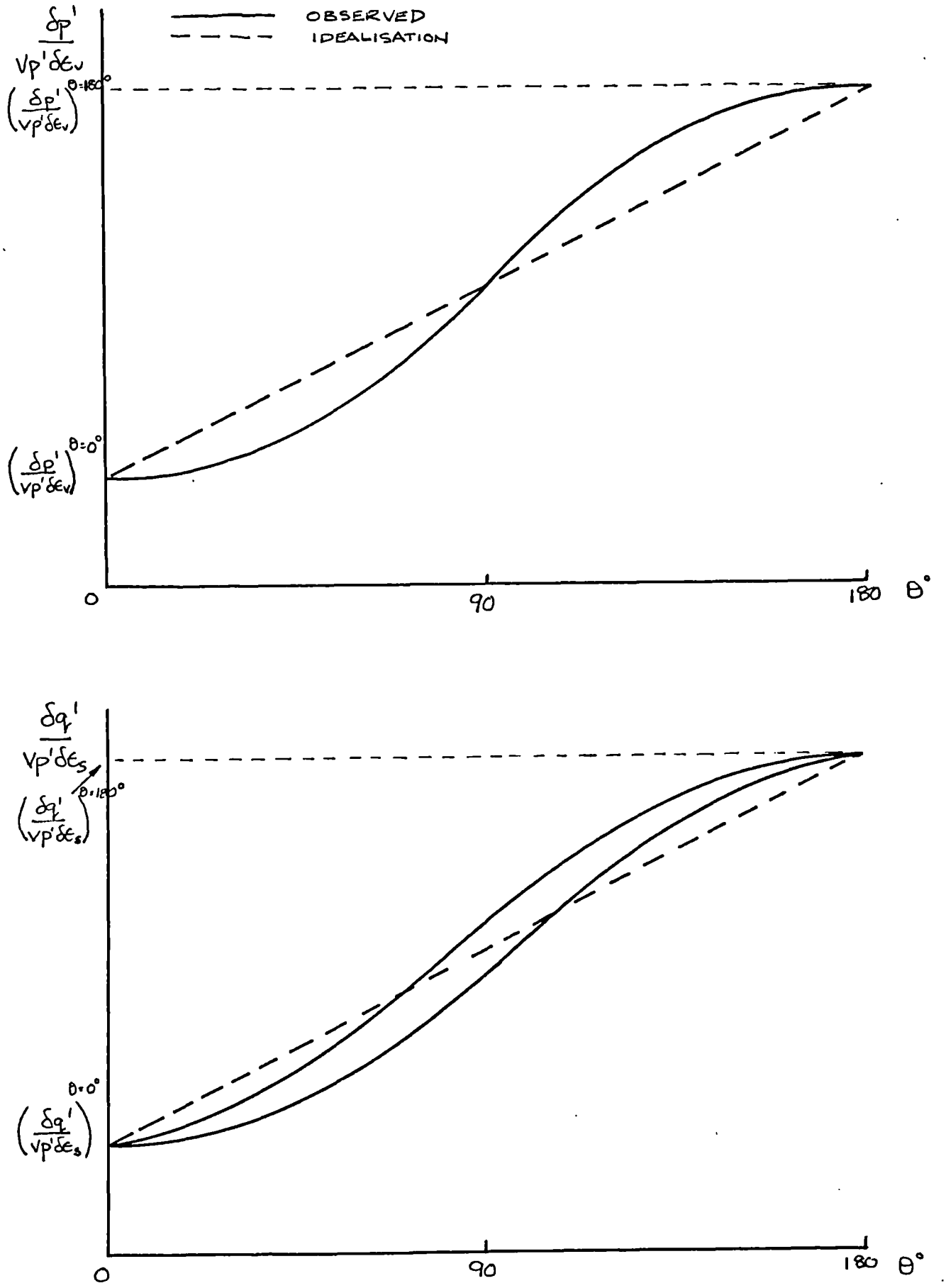

Fig 9.77 Typical form of data obtained from tests plotted as normalised stiffness against deviation of stress path.

a) Constant p' paths.
b) Constant q' paths.

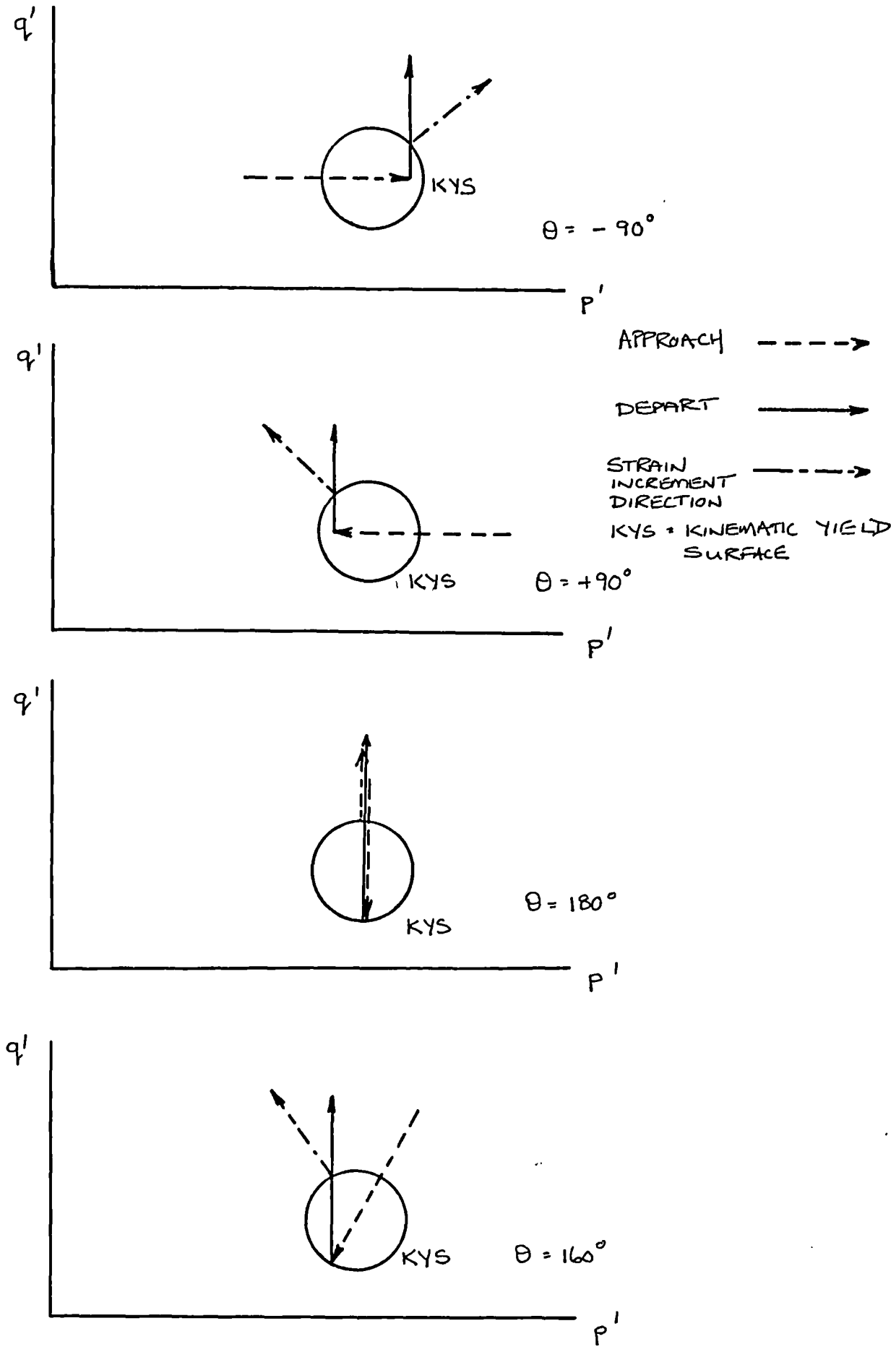

Fig 9.78 Effect of a kinematic yield surface on the behaviour of samples due to different approach paths.

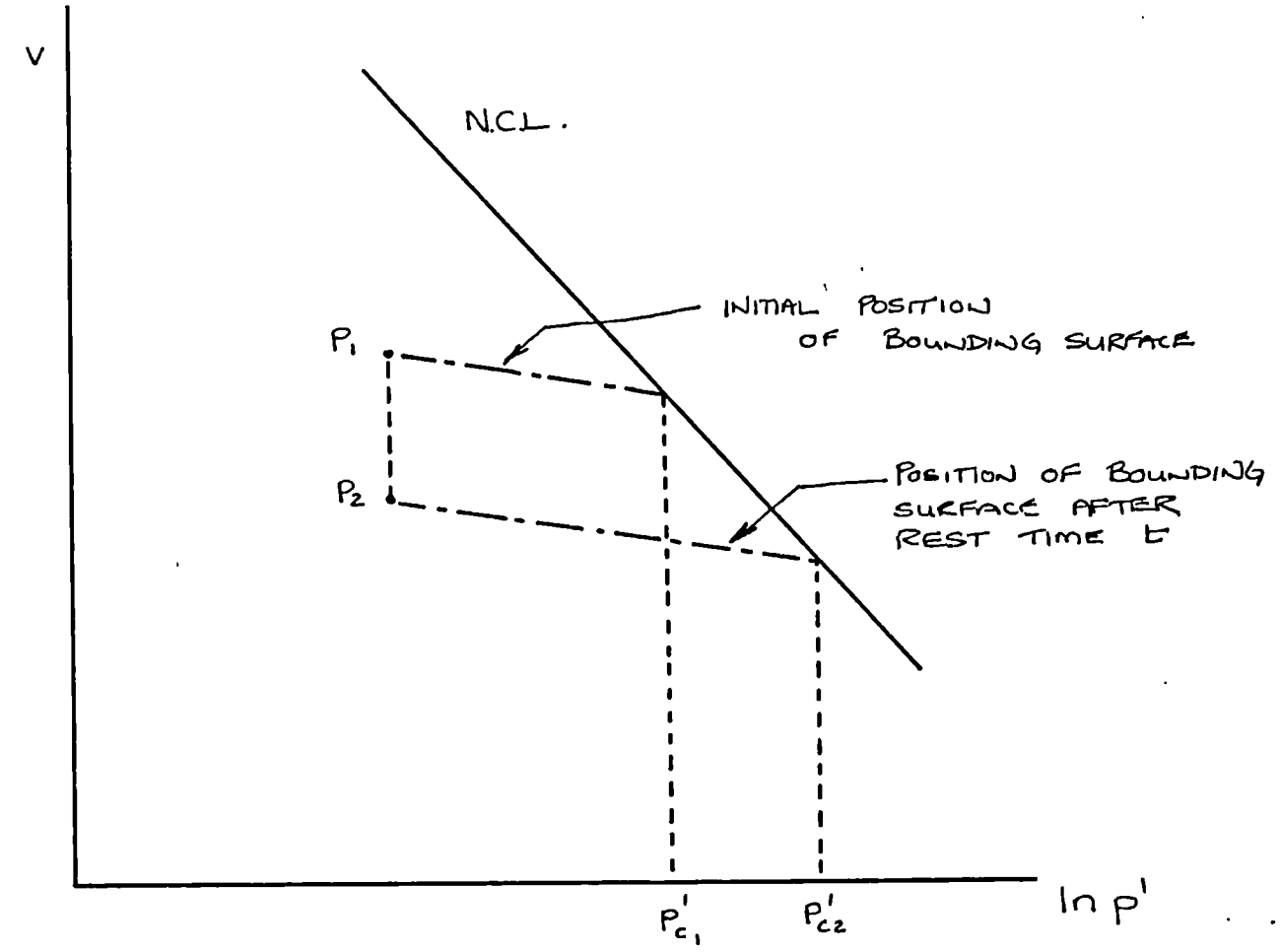

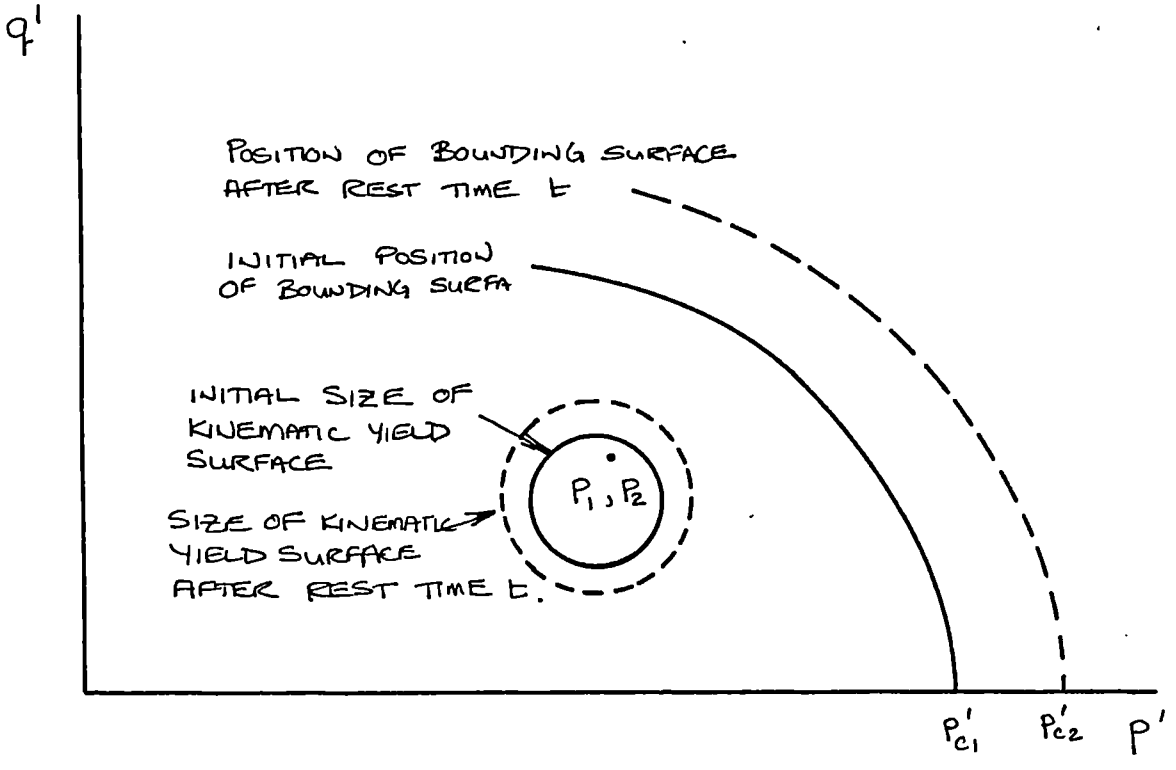

Fig 9.79 Growth of the threshold zone due to rest periods.

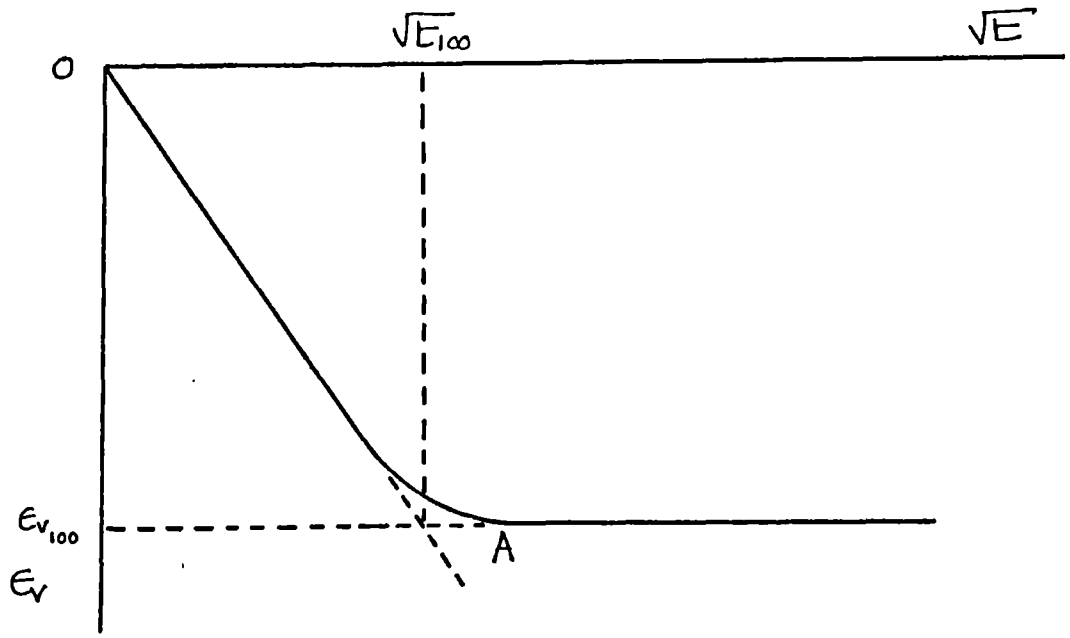

Fig A 1.1 Plot of volumetric strain against square root of time.

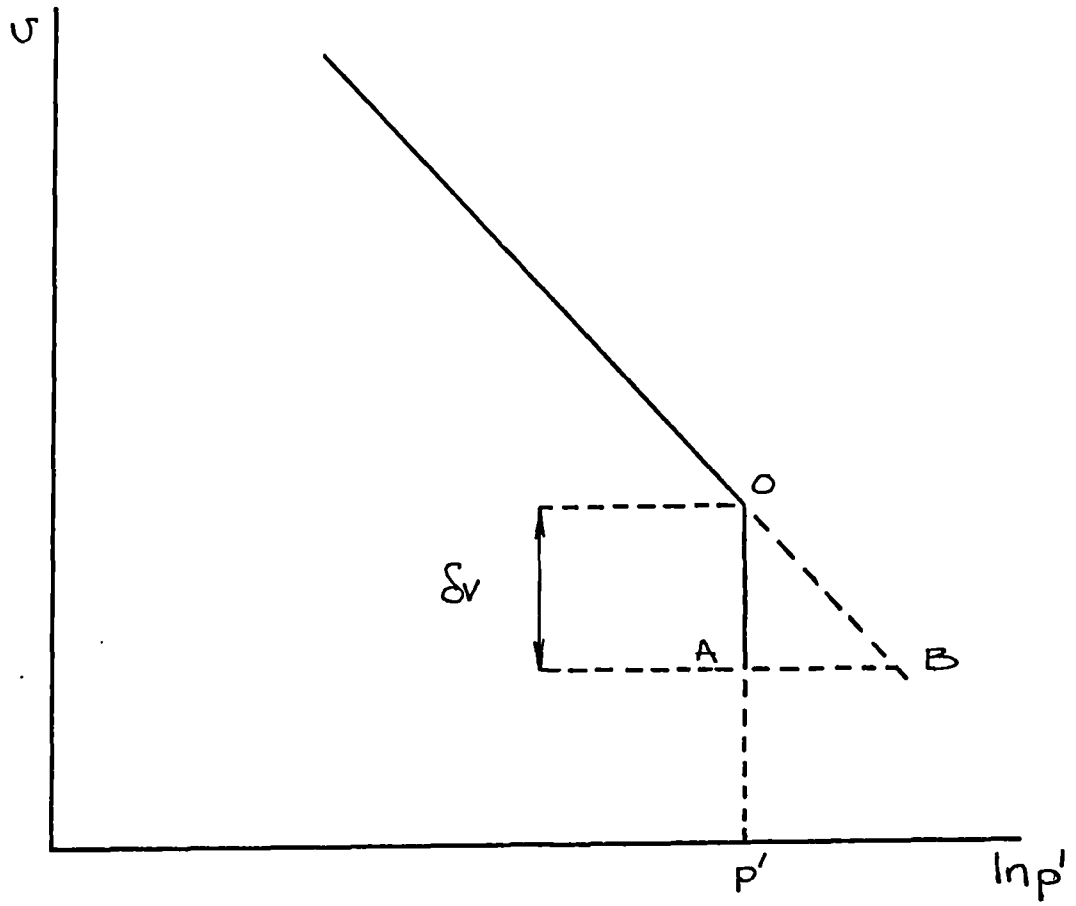

Fig A 1.2 Plot of specific volume against $\log_e p'$.

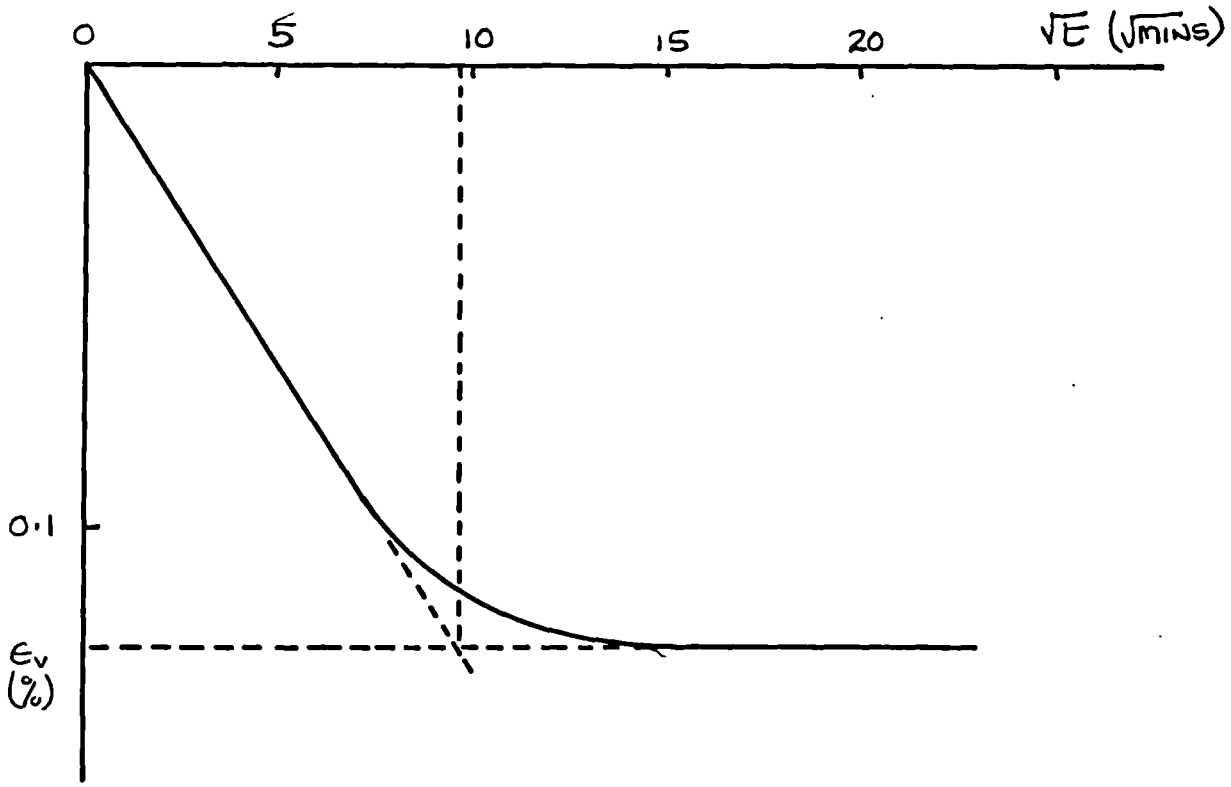

Fig A 1.3 Dissipation of excess pore pressures at the end of loading for London clay.

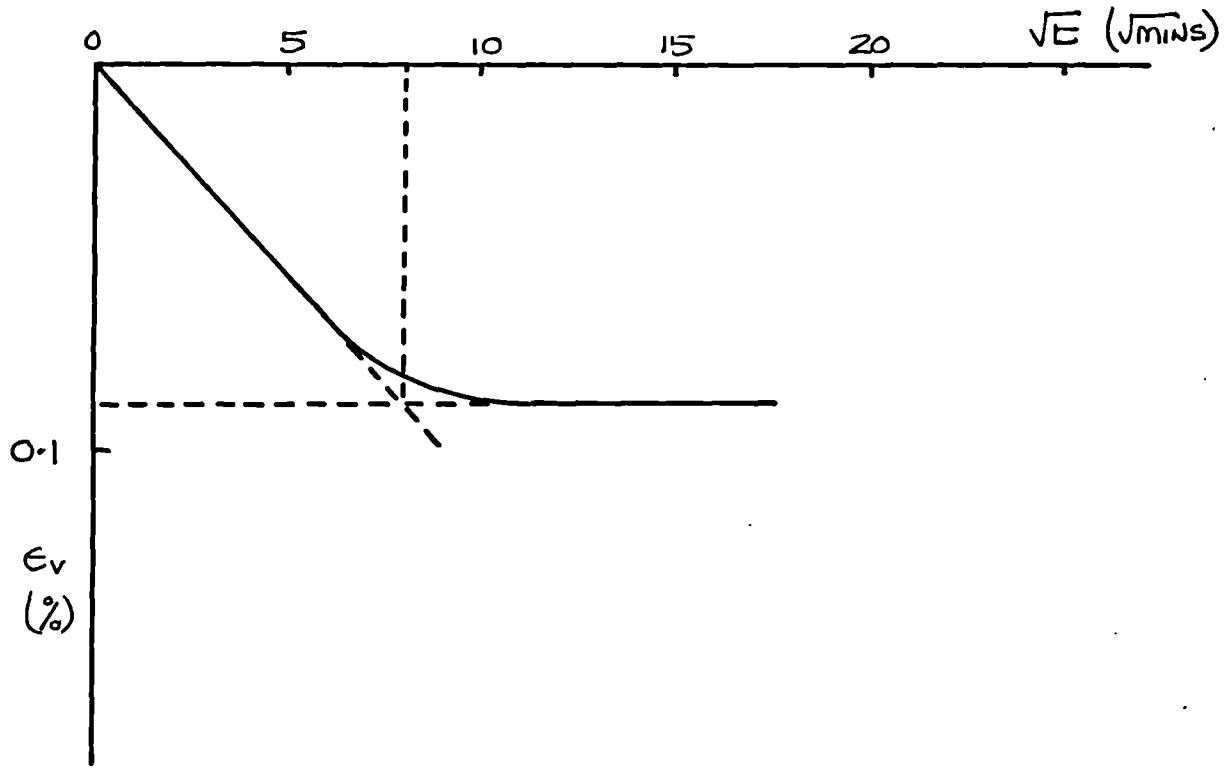

Fig A 1.4 Dissipation of excess pore pressures at the end of loading for Ware till.

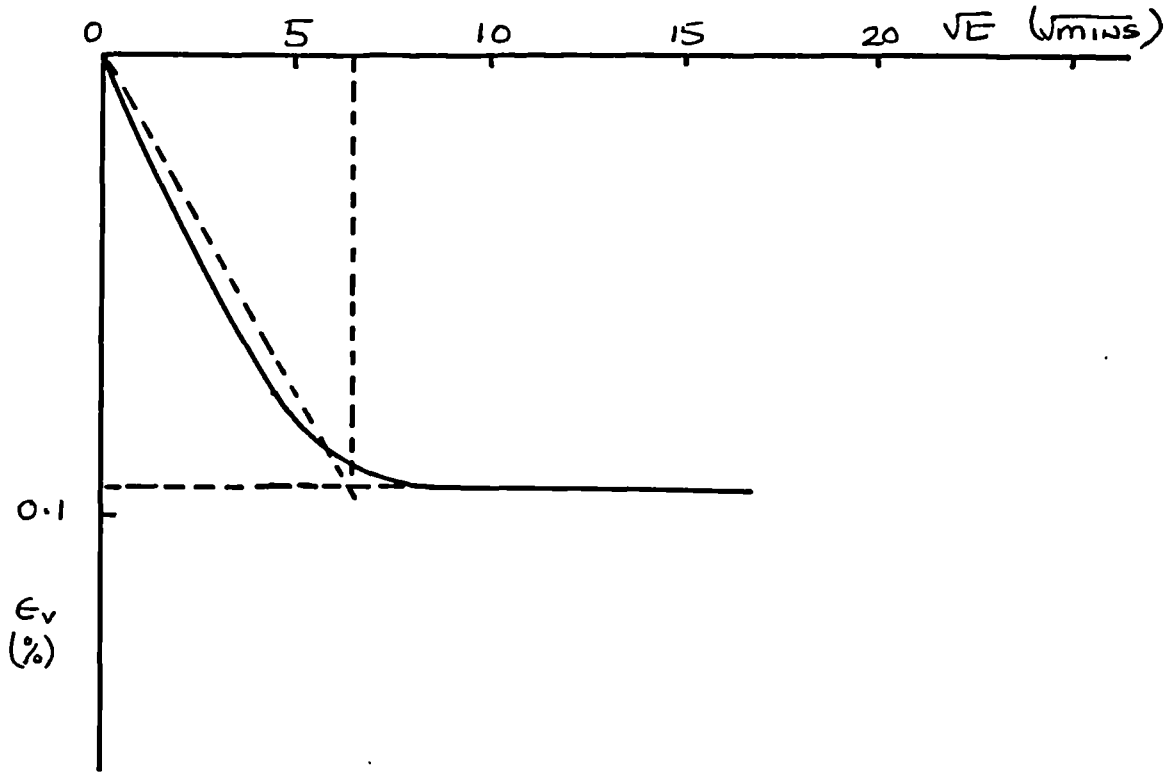

Fig A 1.5 Dissipation of excess pore pressures at the end of loading for Cowden till.

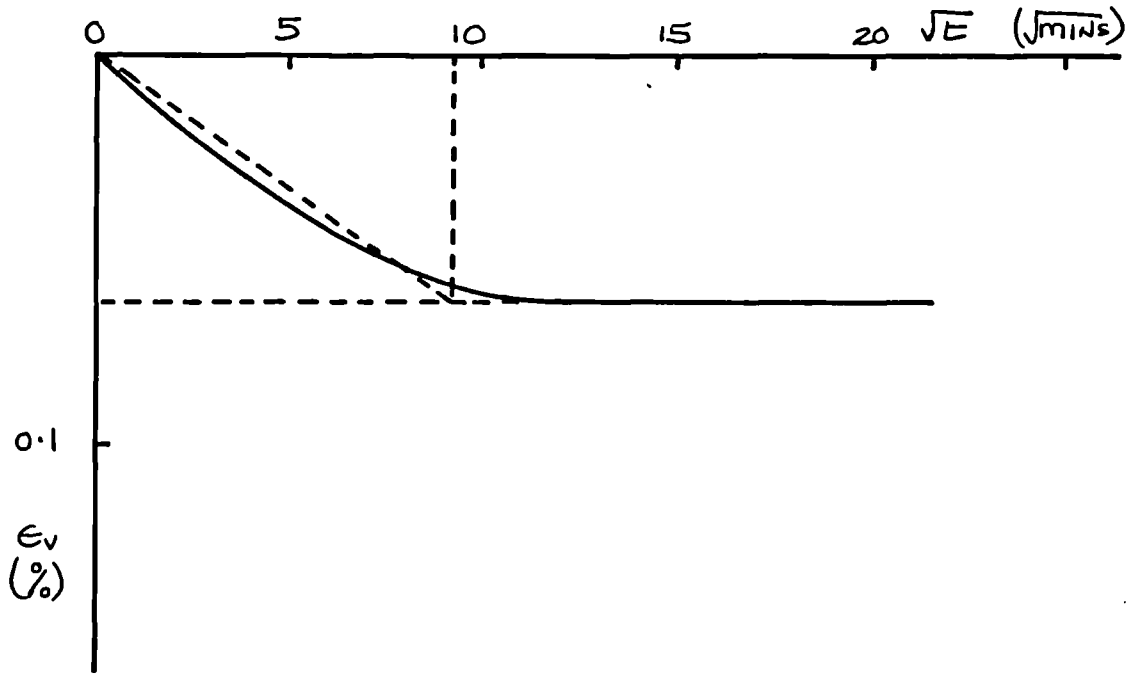

Fig A 1.6 Dissipation of excess pore pressures at the end of loading for Slate dust.

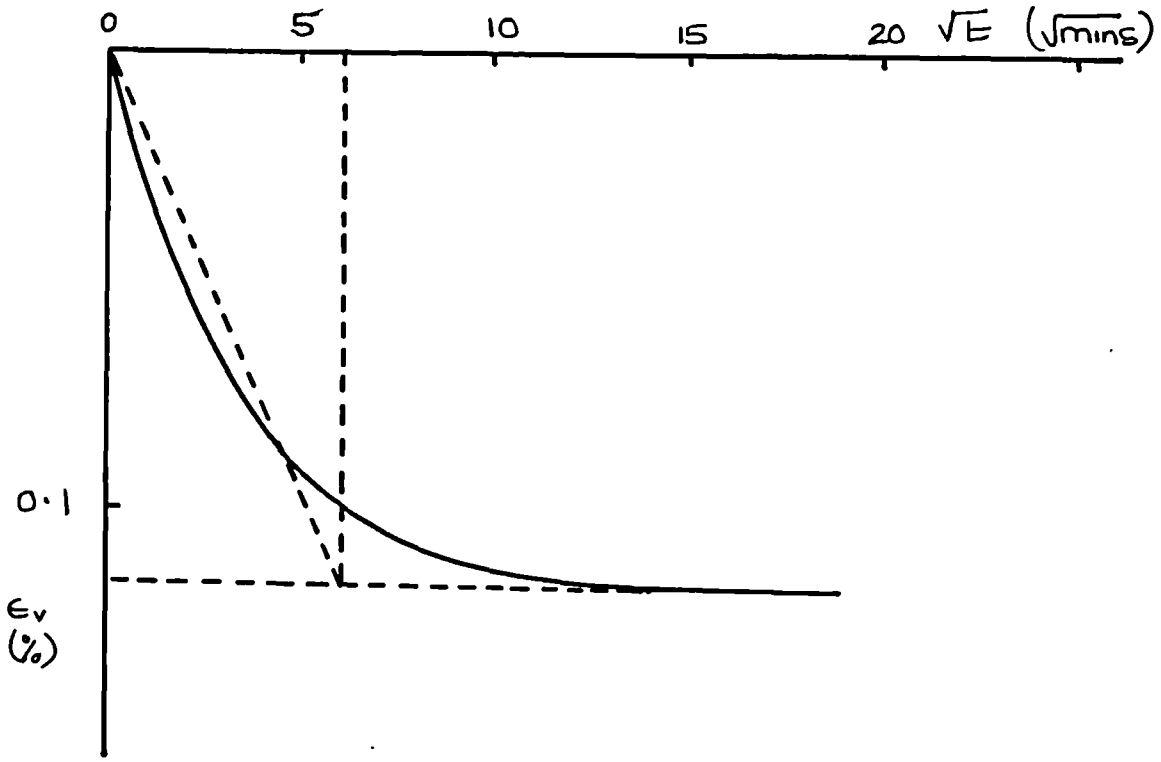

Fig A 1.7 Dissipation of excess pore pressures at the end of loading for Speswhite kaolin.

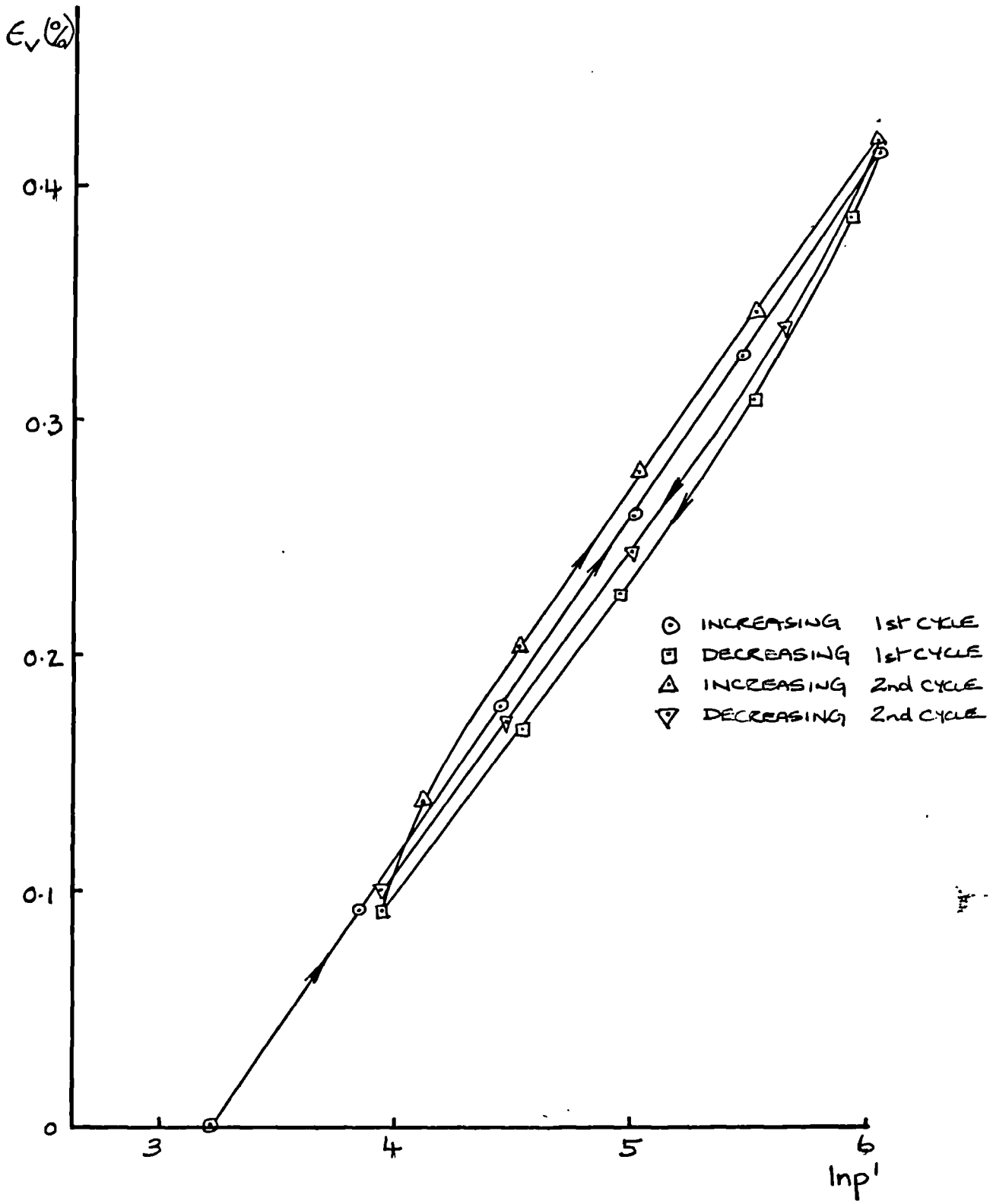

Fig A 2.1 Plot of volumetric strain against lnp' for filter paper side drains.

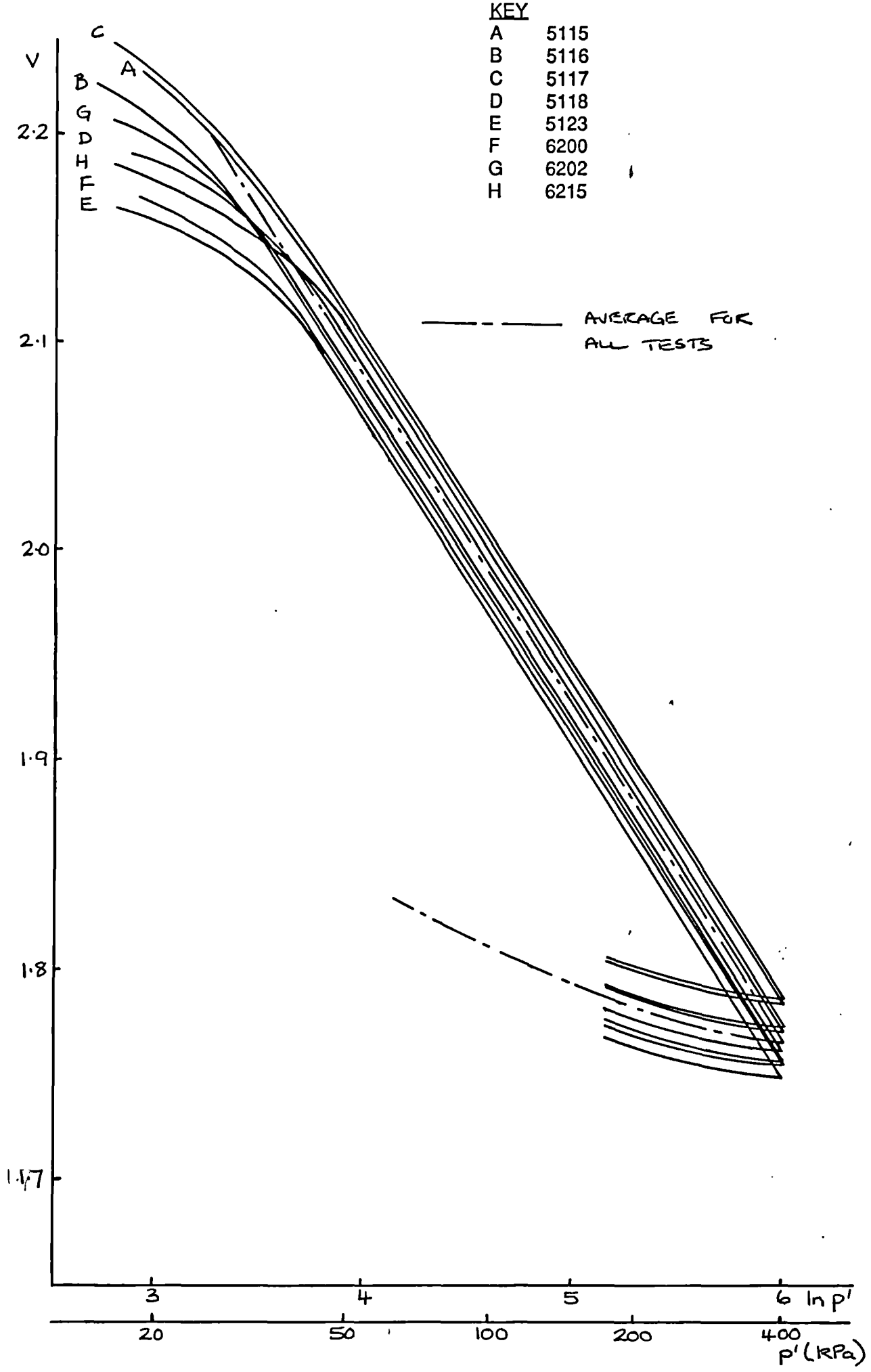

Fig A 2.2 Plot of specific volume against lnp' for isotropically compressed London clay. Initial water contents unadjusted.

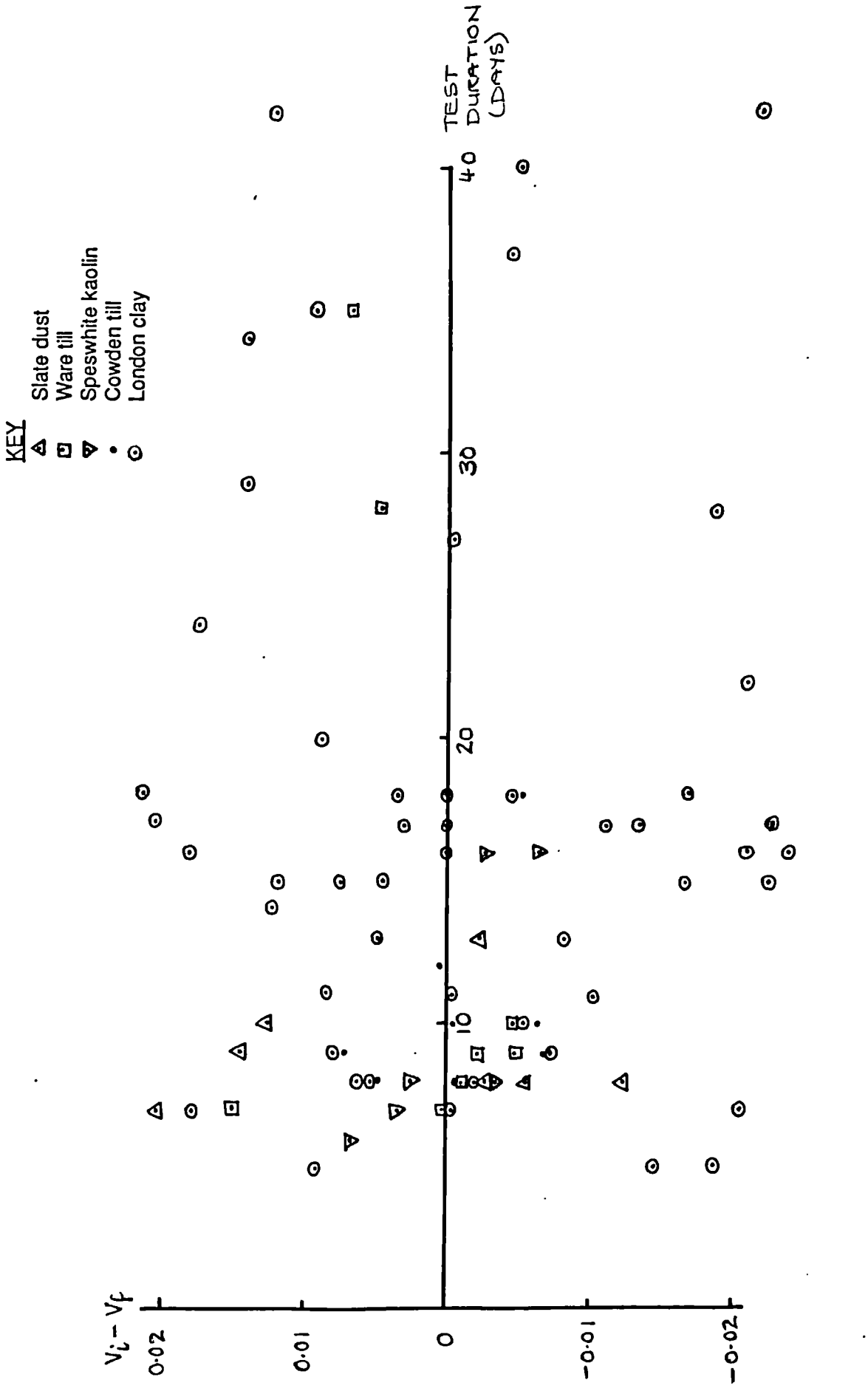

Fig A 2.3 Error in specific volume between initial and final values against duration of test.

I wish you all many happy days on the fells in the years ahead.
There will be fair winds and foul, days of sun and days of rain. But enjoy them all.
Good walking! And don't forget— watch where you are putting your feet.

AW.

Christmas. 1965.

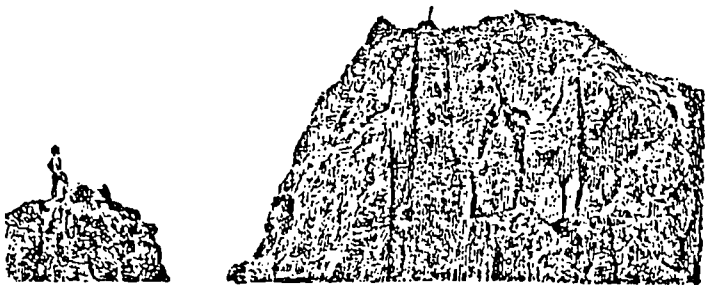

Wainwright,A.(1965). The Western Fells, Book 7. Westmorland Gazette.

So I will sign off by wishing all my readers many more happy wanderings on Lakeland's glorious fells in the years ahead, and hoping that, when they are there, they will think kindly of me sometimes.

AWainwright

Wainwright,A.(1987). Ex-Fellwanderer. Westmorland Gazette.